VROM ●

Methods for the calculation of Physical Effects

Due to releases of hazardous materials (liquids and gases)

Ministerie van VROM →
staat voor ruimte, wonen,
milieu en rijksgebouwen.
Beleid maken, uitvoeren
en handhaven.
Nederland is klein.
Denk groot.

Publicatiereeks Gevaarlijke Stoffen 2

Methods for the calculation of Physical Effects

Due to releases of hazardous materials (liquids and gases)

Ministerie van **Binnenlandse Zaken** *en* **Koninkrijksrelaties**

SZW

Ministerie van Verkeer en Waterstaat

Methods for the calculation of physical effects

– due to releases of hazardous materials (liquids and gases) –

'Yellow Book'

CPR 14E

TNO

Research performed by TNO - The Netherlands Organization of Applied Scientific Research

List of authors

Chapter 1.	General introduction	Ir. C.J.H. van den Bosch Dr. R.A.P.M. Weterings
Chapter 2.	Outflow and Spray release	Ir. C.J.H. van den Bosch Ir. N.J. Duijm
Chapter 3.	Pool evaporation	Ir. C.J.H. van den Bosch
Chapter 4.	Vapour cloud dispersion	Dr. E.A. Bakkum Ir. N.J. Duijm
Chapter 5.	Vapour cloud explosion	Ir. W.P.M. Mercx Ir. A.C. van den Berg
Chapter 6.	Heat flux from fires	dIr. W.F.J.M. Engelhard
Chapter 7.	Ruptures of vessels	Mrs. Ir. J.C.A.M. van Doormaal Ir. R.M.M. van Wees
Chapter 8.	Interfacing of models	Ir. C.J.H. van den Bosch
Annex	Physical properties of chemicals	Ir. C.J.H. van den Bosch

Contents

Preamble

When the first edition of this 'Yellow Book' was issued, it contained calculation methods to be performed on pocket calculators.

Although the second edition in 1988 presumed that personal computers would be available to perform the required calculations, only part of the report was updated. Today more powerful computers are generally available, thus enabling the use of more complex and more accurate computing models.

This third edition is a complete revision by TNO Institute of Environmental Sciences, Energy Research and Process Innovation. It is based on the use of these powerful PC's and includes the application of proven computing models. Special attention is paid to provide adequate directions for performing calculations and for the coupling of models and calculation results.

The revision of the 'Yellow Book' was supervised by a committee in which participated:

Dr. E.F. Blokker, chairman	Dienst Centraal Milieubeheer Rijnmond
Mr.Ir. K. Posthuma, secretary	Ministerie van Sociale Zaken en Werkgelegenheid
Dr. B.J.M. Ale	Rijksinstituut voor Volksgezondheid en Milieu
Drs. R. Dauwe	DOW Benelux N.V.
Ir. E.A. van Kleef	Ministerie van Binnenlandse Zaken
Mrs. Ir. M.M. Kruiskamp	Dienst Centraal Milieubeheer Rijnmond
Dr. R.O.M. van Loo	Ministerie van Volkshuisvesting, Ruimtelijke Ordening en Milieubeheer
Ing. A.J. Muyselaar	Ministerie van Volkshuisvesting, Ruimtelijke Ordening en Milieubeheer
Ing. H.G. Roodbol	Rijkswaterstaat
Drs.Ing. A.F.M. van der Staak	Ministerie van Sociale Zaken en Werkgelegenheid
Ing. A.W. Peters	Ministerie van Verkeer en Waterstaat
Ir. M. Vis van Heemst	AKZO Nobel Engineering B.V.

With the issue of this third edition of the 'Yellow Book' the Committee for the Prevention of Disasters by Hazardous Materials expects to promote the general use of standardised calculation methods of physical effects of the release of dangerous materials (liquids and gases).

The Hague, 1996

THE COMMITEE FOR THE PREVENTION OF
DISASTERS BY HAZARDOUS MATERIALS,

Drs. H.C.M. Middelplaats, chairman

Preface to the PGS 2 edition of the Yellow Book

Starting from June 1st 2004, the Advisory Council on Dangerous Substances (Adviesraad Gevaarlijke Stoffen - AGS) was installed by the Cabinet. At the same time the Committee for the Prevention of Disasters (Commissie voor de Preventie van Rampen- CPR) was abolished.

CPR issued several publications, the so-called CPR-guidelines (CPR-richtlijnen), that are often used in environmental permits, based on the Environmental Protection Law, and in the fields of of labour safety, transport safety and fire safety.

The CPR-guidelines have been transformed into the Publication Series on Dangerous Substances (Publicatiereeks Gevaarlijke Stoffen – PGS). The aim of these publications is generally the same as that of the CPR-guidelines. All CPR-guidelines have been reviewed, taking into account the following questions:
1. Is there still a reason for existence for the guideline or can the guideline be abolished;
2. Can the guideline be reintroduced without changes or does it need to be updated.

The first print (1997) of the 3rd edition Yellow Book contained typographical errors that occurred during the conversion of the Yellow Book documents from one word processing system to another. Most of these conversion errors occurred especially with formulas, leading to erroneous and non-reproducible results when calculation examples and formulas were recalculated.

This PGS 2 edition (2005) is a second print that has been thoroughly checked for errors. Every chapter starts with a condensed summary of changes to give the user an idea about what was changed and where it was changed.

Despite all effort, it might be possible that errors still persist. If this is the case, or if you have any other remarks about the Yellow Book, please send a mail to: info@infomil.nl.

Hard copies of this PGS-2 edition can be obtained from Frank van het Veld, TNO Department of Industrial & External Safety: YellowBook@tno.nl, or fax +31 55 549 3390.

Also on behalf of my colleagues at the Ministries of Transport, Social Affairs and of the Interior,
The State Secretary of Housing Spatial Planning and the Environment (VROM).

Drs. P.L.B.A van Geel

november 2005

Revision history

Date	Release	Comments
19 April 2005	3rd edition 2nd print, version 1	Please refer to the modification paragrahs of all chapters.
25 July 2005	3rd edition 2nd print, version 2	The appendix of chapter 6 was missing and has now been included. Table 6.A.2 and Figure 6.A.11 were not corresponding and has been corrected.

Chapter 1
General introduction

C.J.H. van den Bosch, R.A.P.M. Weterings

Table of contents of chapter 1

1.1 Introduction to chapter 1

For designers, manufacturers of industrial equipment, operators and responsible authorities it is essential to have models available for assessing the physical effects of accidental releases of hazardous materials.
For this purpose the handbook 'Methods for the calculation of physical effects of the release of dangerous materials (liquids and gases)', was issued by the Directorate General of Labour in 1979.
In the past decade the handbook has been widely recognised as an important tool to be used in safety and risk assessment studies to evaluate the risks of activities involving hazardous materials. Because of its yellow cover, the handbook is world-wide known as the 'Yellow Book'.

The 'Yellow Book', originating from 1979, was partially revised in 1988. However, it can be stated that the Yellow Book issued in 1988 was almost entirely based on literature published before 1979.
The current version of the Yellow Book results from an extensive study and evaluation of recent literature on models for the calculation of physical effects of the release of dangerous materials. The Committee for the Prevention of Disasters, Subcommittee Risk Evaluation started this project in June 1993 and it was completed in March 1996.

This project was carried out by TNO Institute of Environmental Sciences, Energy Research and Process Innovation, TNO Prins Maurits Laboratory and TNO Centre for Technology and Policy Studies.

The project was supervised by a steering commitee with representatives from governmental organisations and proces industries with the following members:
B.J.M. Ale, E.F. Blokker (chairman), R. Dauwe, E.A. van Kleef, Mrs. M. Kruiskamp, R.O.M. van Loo, A.J. Muyselaar, A.W. Peters, K. Posthuma (secretary), H.G. Roodbol, A.F.M. van der Staak, M. Vis van Heemst.

The revision had the following three objectives:
1. to update individual models from a scientific point of view, and to complete the book with models that were lacking,
2. to describe the interfacing (coupling) of models,
3. to meet educational requirements.

This general introduction starts with a description of the educational objectives pursued by the Yellow Book. A general description of the target groups is envisioned (in section 1.2). The differences between this edition and the previous edition are elucidated in section 1.3. Finally (in section 1.4), guidance will be given to the reader regarding how to use the Yellow Book.

1.2 Educational objectives and target groups

In the first phase of the process of developing this update of the Yellow Book, an educational framework was formulated [Weterings, 1993] and a set of educational objectives was defined. Studying the Yellow Book the reader may expect to:

a. gain knowledge of the phenomena relevant to estimating the physical effects of the release of hazardous materials,

b. gain knowledge of the models that have been developed to describe these phenomena,

c. gain understanding of the general principles of the selection of these models, and of the conditions under which these models can be applied,

d. gain understanding of the procedure according to which the selected models should be applied,

e. be able to apply the selected models in practical situations, and to interface them adequately to related models for estimating physical effects of hazardous releases, according to more complex release scenarios.

The Yellow Book has been written in such a manner as to meet the requirements of:
− chemical industry,
− technical consultancy bureaus,
− engineering contractors,
− authorities and government services (national and regional level),
− institutes for advanced research and education.

It should be kept in mind that these target groups will use the models for estimating physical effects of hazardous releases for different purposes. Table 1.1 presents some of the purposes for which specialists from industry, government agencies or consultancy may use the presented models. The number of stars gives some indication of the frequency in which the models are used in practice.

Table 1.1   Selected target groups and purposes in estimating physical effects

Purpose	Target groups		
	Companies	Authorities	Consultants
Design of installations	***	*	**
Quantified risk assessment	***	**	***
Workers safety	*	*	
Emergency planning	**	**	*

1.3 Contents of the Revised Yellow Book

1.3.1 General remarks

In the past decade, considerable progress has been made in modelling physical effects resulting from accidental releases of a hazardous material.
The current revision has been based on available data in the open literature and known state-of-the-art models, and maintains more or less the same structure as the former version:

Chapter	Author
1. General Introduction	C.J.H. van den Bosch and R.A.P.M. Weterings
2. Outflow and Spray Release	C.J.H. van den Bosch and N.J. Duijm
3. Pool Evaporation	C.J.H. van den Bosch
4. Vapour Cloud Dispersion	N.J. Duijm and E. Bakkum
5. Vapour Cloud Explosions	W.P.M. Mercx and A.C. van den Berg
6. Heat Fluxes from Fires	W.J.F.M. Engelhard
7. Ruptures of Vessels	R.M.M. van Wees and J.C.A.M. van Doormaal
8. Interfacing of Models	C.J.H. van den Bosch

The strongly increased availability of powerful (personal) computers has caused a shift in the application of analytical models and physical correlations towards complex computerised numerical models. We aimed to collect models that combine a good scientific performance with ease of application in practice.
It appears that the optimal combination of models varies for different classes of physical effect models; some models are simple correlations, many models consist of a straight forward numerical scheme, but few models are unavoidably complex as the related physical phenomena have a complex nature.
The selected models are described in a way to make computerisation by the reader possible in principle, yet prices of available software packages are relatively low.

An inventory of the applicable models available in the field of safety and hazard assessment studies has shown the 'white spots' left in this area.
Guidelines on how to deal with 'white spots' in the revised 'Yellow Book' have been based on engineering judgement, which may lead to simple rules of the thumb.

Although the Yellow Book focuses on liquids and gases, under certain conditions some models may be applied for solids. In particular, atmospheric dispersion models may be used to estimate concentrations of non-depositing dust in the atmosphere, or concentrations of volatile reaction products of burning solids.

1.3.2   Remarks on the individual chapters

Below, the major improvements and differences in this version of the Yellow Book in relation to the former edition are outlined.

In chapter 2 'Outflow and Spray Release' a rather fast model for two-phase flow in pipes is given as well as several models about non-stationary outflow from long pipe lines. Much attention is given to the dynamic behaviour of the content of vessels due to the release of material.
An adequate model for spray release is presented, explaining amongst others why 'light gases' such as ammonia can behave like a heavy gas under certain circumstances.

In chapter 3 'Pool Evaporation' a model for the evaporation of a (non-)spreading boiling and non-boiling liquid pool on land or on water is described. This model overcomes many numerical boundary problems encountered in the past, but is also quite complex. In addition a model for the evaporation of volatile solved chemicals in water is given.

Chapter 4 'Vapour Cloud Dispersion' reflects the major scientific progress that has been made on modelling heavy gas dispersion. The plume rise model has been extended for heavy gases. Also a new description is given for the atmospheric boundary layer stability.

In chapter 5 'Vapour Cloud Explosions' a new method for the prediction of blasts resulting from confined vapour cloud explosions is described. This so-called Multi-Energy-Method is an improvement to earlier methods. Although not fully developed yet, it is able to incorporate results of future experiments on vapour cloud explosions.

In chapter 6 'Heat Fluxes from Fires' a new model for gas flares and a model for confined pool fires on land and water are included.

In chapter 7 'Ruptures of Vessels' models are described for several different types of vessel ruptures leading to blast and fragmentation. Although these models are much more adequate than previous models, they are not yet able to render very accurate predictions.

In chapter 8 'Interfacing of Models' attention is given to the interfacing of the physical effect models described in the previous chapters. Often (subsequent) physical effects are involved in between the release of hazardous material and the actual impact on people and properties causing damage. So, physical effect models may have to be 'coupled', meaning that their results, i.e. the predictions of these models (output data), have to be adapted and transferred to serve as input to other subsequent

models. The procedure of adaptation and transfer of data is usually addressed by 'interfacing'.

The remainder of this chapter deals with the physical effects of BLEVE's.
A BLEVE (Boiling Liquid Expanding Vapour Explosion) causes several physical effects: heat radiation, pressure waves and fragmentation, that may cause damage. These phenomena will be treated in different chapters. In order to present an overall picture of the BLEVE an integral calculation example is given in chapter 8.

1.4   User instructions

The educational design provides a framework according to which this version of the Yellow Book has been structured. This framework defines the topics to be considered in separate sections, and reflects a causal chain of effects to be a logical argument in determining the sequence in which these topics should be addressed. As a result the Yellow Book starts with a section on outflow and spray release (chapter 2), then addresses evaporation (chapter 3) and dispersion (chapter 4), before addressing several other specific aspects, such as vapour cloud explosion (chapter 5), heat load (chapter 6) and the rupture of vessels (chapter 7). Finally a section on interfacing related models (chapter 8) illustrates how to proceed in applying a sequence of models in estimating physical effects, according to a few selected scenarios.

Using the Yellow Book, it is helpful to keep in mind that all chapters are structured in a similar manner. Each of the chapters 2 to 7 contains the following sections:
- section 1 provides an **introduction** and positions the chapter in relation to other chapters,
- section 2 provides a general introduction and defines **relevant phenomena**,
- section 3 gives a **general overview** of existing (categories) of models for the phenomena addressed,
- section 4 describes **criteria** according to which a limited number of models has been selected,
- section 5 provides a detailed **description of the selected models**: the general principles and assumptions on which they have been based, the procedure according to which these models should be applied as well as some considerations on their potential and limitations in practice,
- section 6 illustrates the practical application of the selected models by means of **calculation examples**,
- section 7 addresses relevant issues in relation to **interfacing** the selected models with other models,
- section 8 provides some **discussion** on the state-of-the art in the field addressed, which is relevant in view of assumptions and limitations of the selected models.

In conclusion, for background information the reader is referred to the sections 1 to 4 of each chapter. However, if the reader has already mastered the general principles of the selected models, it is advised to concentrate on the sections 5 and 6 – and if necessary also sections 7 and 8 – in which a detailed description is given of how to use the most relevant models for estimating the physical effects of hazardous releases.

1.5   References

YellowBook (1988),
Methods for the calculation of physical effects of the release of dangerous materials (liquids and gases) 2nd ed.,1988), published by Directorate General of Labour; English version, 1992).

Weterings (1993),
R.A.P.M. Weterings, The revised Yellow Book - educational concept,
TNO Centre for Technology and Policy Studies (STB), Apeldoorn, October 1993.

Chapter 2
Outflow and Spray release
C.J.H. van den Bosch, N.J. Duijm

Modifications to Chapter 2 (Outflow and Spray release) with respect to the first print (1997)

Numerous modifications were made concerning typographical errors. A list is given below for the pages on which errors have been corrected.

In section 2.3.4.3 on page 2.36, as well as on page 2.87 and 2.89 the term 'void fraction' has been replaced by 'vapour mass fraction (or quality)'. The void fraction is a volume fraction, while the quality is a mass fraction, on which the two-phase density is based.

In section 2.4.3.4 and further onwards the name 'LPG' used with reference to the models of Morrow and Tam has been replaced by 'propane', for which these models are derived.

In section 2.5.2.3 in equation (2.23) the erroneous = sign in front of γ has been removed.

In chapter 2 use is made of two different friction factors, viz. the Fanning factor f_F and the Darcy factor f_D, where $f_D = 4f_F$. As this has caused some confusion, f_D has replaced almost all occurrences of $4f_F$.

In section 2.5.2.5 a closing bracket has been added to equation (2.35).
In equation (2.47a) the leading and ending brackets are removed.

In section 2.5.3.2 some equations have been corrected, viz.:
− In equation (2.58) the parameter $\phi_{m,e,1}$ has been removed, because its value equals one according to the assumption of vapour outflow in step 1.
− In equation (2.59) the parameter ρ_V is incorrect and has been replaced by ρ_L.
− Equation (2.60c) denoting the surface tension has been added.
− At the right hand side of equation (2.65) the parameter $f_{\Phi v2}$ is incorrect and has been replaced by $f_{\Phi v1}$.
− In equation (2.68a) the first bracket under the square root sign has been replaced to in front of the gravitational acceleration g.
− In equation (2.98) two brackets have been added.
− On page 2.95 some correlations for the parameters C_{Ar} and C_{Br} from the TPDIS model have been added.

In section 2.5.3.6 the equations (2.118) have been modified and the constants C have been corrected. The same holds for equation (2.128b).

In section 2.5.4.2 the discharge coefficient for a ruptured pipe has been added (equation (2.197d)), as well as equation (4.198) denoting the pressure drop in a pipe.

In section 2.5.5 the equations (2.202) and (2.202a) have been modified by adding two brackets enclosing the last multiplication.

In chapter 2.6 (calculation examples) the results of some examples have been corrected.

In section 2.6.2.1 table 2.3 has been replaced.

In section 2.6.2.2 the input parameter 'Vessel volume' has been added and the resulting mass flow at t equals zero seconds has been adjusted. Furthermore table 2.4, containing incorrect and irrelevant data, has been removed.

In section 2.6.2.3 the input parameter 'Initial density' has been added and the resulting mass flows have been corrected. Furthermore all the computational steps described on page 2.132 have been corrected, i.e.

− Equation (2.24) has been added.
− Equations (2.40) and (2.41) have been corrected.
− The equation in step 6 has been corrected; two minus signs were missing in the exponents.

In section 2.6.2.4 in the equation in the first step two brackets have been added. Furthermore the results have been adjusted.

In section 2.6.3.2 the value for the surface tension has been corrected, as well as the output values. Equation (2.59) was incorrect and has been modified, cf. this equation on page 2.79. Furthermore table 2.6, containing incorrect and irrelevant data, has been removed.

In section 2.6.3.3 the resulting output values have been corrected and table 2.7 has been removed. This table presented data from a rather slow iterative calculation, while it is preferred to search for the maximum using a maximum finder e.g. the Golden Section Search method.

In section 2.6.3.4 table 2.5 has replaced the former incorrect table 2.8.

In section 2.6.3.5 table 2.6 has replaced the former incorrect table 2.9. Furthermore all calculation steps have been reviewed and the results have been corrected where appropriate. The former figure 2.13 has been removed.

Also in section 2.6.3.6 the various results in the calculation steps have been corrected.

In section 2.6.4.1 the output results have been corrected and table 2.8 has replaced the former incorrect table 2.11.

In section 2.6.4.2 the computational procedure has been modified. The former procedure tried to find the actual liquid mass flow by iterating on the Reynolds number. It is more straightforward to iterate on the mass flow itself, preferably using a root finder. The new approach has been described. Furthermore the output result has been corrected and the former table 2.12 has been removed.

List of symbols Chapter 2

A_e	exit cross-sectional area (2.1b)	m^2
A_f	jet cross-section after flashing (2.1b)	m^2
A_h	cross-sectional area hole (2.22)	m^2
A_j	jet cross-section after evaporation droplets (2.167)	m^2
A_p	cross-sectional area pipe (2.31)	m^2
A_r	area ratio (2.49)	-
A_L	normal liquid surface in the vessel (2.58)	m^2
A_R	area ratio defined by (2.134b)	-
b	radius (2.6)	m
b_{disp}	cloud radius (2.177)	m
b_e	exit radius (table 2.4)	m
b_f	jet or cloud radius after flashing (2.6)	m
b_j	jet or cloud radius after evaporation droplets (2.176)	m
c	molar or volume fraction (2.159)	-
c'	atmospheric concentration (2.214)	kg/m^3
c_{disp}	c after expansion to ambient windspeed (2.179)	-
c_j	c after evaporation droplets (2.155)	-
c_w	molar fraction of water (2.159)	-
c_{wv}	molar fraction of water vapour (2.159)	-
C	arbitrary constant (2.32)	-
C^*	arbitrary constant (2.33)	$(N/m^2) \cdot m^{3\zeta}$
C_{AA}	combined Arrhenius' and Arnolds' constant (2.67)	$kmol^{1/6} \cdot K^{1/2}/m^{1/2}$
C_{Ar}	volume ratio parameter in TPDIS (2.103)	-
C_{D1}	constant Diers model (2.59)	-
C_{D2}	constant in Diers model (2.62a)	-
C_{Bi}	polynomial constants in Morrow's model (2.129a)	-
C_{Br}	density ratio parameter in TPDIS (2.104)	-
C_{Ci}	polynomial constants in Morrow's model (2.118a)	-
C_b	blow-down correction factor (2.48)	-
C_c	contraction coefficient (2.27)	-
C_d	discharge coefficient (2.22)	-
C_{ds}	constant related to droplet size (2.143b)	-
C_f	friction coefficient (2.27)	-
C_{Lp}	artificial constant in Tam's model (2.137a)	m
C_p	specific heat at constant pressure (2.26)	$J/(kg \cdot K)$
$C_{p,L}$	specific heat liquid phase at constant pressure (2.77)	$J/(kg \cdot K)$
C_{Tam}	correction factor for initial mass flow rate (2.137b)	(-)
C_v	specific heat at constant volume (2.18)	$J/(kg \cdot K)$
C_α	constant of decay in Tam's model (2.131)	1/s
C_ε	constant (2.3)	-
$C_{C\alpha}$	subconstant in Tam's model (2.134)	1/K
$C_{\Phi v}$	auxiliary variable (2.68a)	m
$C_{\phi mf}$	constant (2.2)	-

C_σ	constant Walden's rule (2.66)	m
d_d	droplet diameter (2.143a)	m
d_h	hole diameter (2.208)	m
d_p	(inner) pipe diameter (2.31)	m
d_v	vessel diameter (2.68b)	m
d_0	droplet diameter at ground level (2.151)	m
d_M	maximum rain-out droplet (2.148)	m
d_R	radius ratio defined by (2.134a)	-
D	diffusion coefficient (2.144b)	m^2/s
D_c	toxic load (2.214)	$(kg/m^3)^n \cdot s$
f_D	Darcy friction factor defined by (2.201a)	-
f_F	Fanning friction factor (2.204)	-
F_1	function of pressure(2.118)	-
F_2	function of pressure (2.127)	N/m^2
F_3	function of pressure (2.129a)	-
F_4	function of pressure (2.128a)	N/m^2
$f_{\Phi v1}$	flow dependent parameter in Diers model (2.65)	-
$f_{\Phi v2}$	flow dependent parameter in Diers model (2.65)	-
g	gravitational acceleration (2.68A)	m/s^2
G	mass flux (2.94)	$kg/(m^2 \cdot s)$
h_f	fluid height (2.93)	m
h_h	height leak in vessel (par. 2.6.3.1)	m
h_L	liquid height (2.70)	m
$h_{L,0}$	pipe inlet height (2.96)	m
$h_{L,2}$	pipe height at end of second flow regime (2.96)	m
$h_{L,e}$	pipe outlet height (2.105)	m
$h_{L,3}$	height difference in third regime (2.105)	m
h_s	source height (2.148)	m
H	specific enthalpy (2.4)	J/kg
H_e	specific enthalpy at exit conditions (2.1a)	J/kg
H_f	specific enthalpy after flashing (2.1a)	J/kg
H_j	specific enthalpy after evaporation droplets (2.156)	J/kg
H_L	specific enthalpy of liquid (2.116)	J/kg
H_V	specific enthalpy of vapour (2.140)	J/kg
$H_{L,0}$	idem at initial storage temperature (2.116)	J/kg
H_0	specific enthalpy at initial conditions (2.5)	J/kg
Δh_L	height difference during the flow (2.96)	m
Δh_{Lp}	head loss defined by (2.202)	m
i	time-step counter	-
k_B	droplet evaporation coefficient (2.146)	m^2/s
K_i	resistance coefficient defined by (2.209)	-
l_p	pipe length (2.31)	m
l_v	length cylinder (par. 2.6.3.1)	m

L_v	heat of vaporisation (2.66)	J/kg
$L_{v,w}$	heat of vaporisation of water (2.161)	J/kg
$LN(x)$	natural logarithm of argument x	-
$^{10}LOG(x)$	common logarithm of argument x	-
Δl_i	distance along the pipe from rupture to interface (2.126)	m
n	number of moles (2.9a)	-
N_t	number of time-steps (2.12)	-
p	pressure ratio (2.47b)	-
p_{cr}	critical flow pressure ratio (2.47d)	-
p_f	final pressure ratio (2.47c)	-
P	(absolute) pressure (2.8)	N/m^2
P_a	ambient (atmospheric) pressure (2.1b)	N/m^2
P_c	critical pressure of the chemical (2.11a)	N/m^2
P_e	exit pressure in the pipe (2.1b)	N/m^2
P_h	(hydraulic) liquid pressure (2.195)	N/m^2
P_i	upstream pressure at interface (2.46)	N/m^2
P_{aL}	external pressure above liquid (2.195)	N/m^2
P_R	reduced pressure (2.11)	-
Pr	Prandtl number (2.144c)	-
P_v°	saturated vapour pressure (2.1d)	N/m^2
P_0	initial pressure (2.95)	N/m^2
P_*	corrected pressure (2.118c)	N/m^2
ΔP	pressure drop (2.29a)	N/m^2
q_S	mass flow (discharge rate) (2.14)	kg/s
$q_{S,e}$	exit flow rate (2.121)	kg/s
$q_{S,0}$	initial mass outflow (discharge) rate (2.35)	kg/s
$q_{S,\Phi m=1}$	initial mass flow rate vapour only (2.82)	kg/s
Q	(total) mass content (2.83)	kg
Q_H	heat transferred into a system (2.18a)	J/mol
Q_L	liquid mass (2.71)	kg
Q_0	initial total mass content (2.35)	kg
Q_V	vapour mass (2.72)	kg
$Q_{V,0}$	initial vapour mass (2.81)	kg
R	gas constant (2.9a)	J/(mol·K)
Re	Reynolds number (2.98)	-
RH	relative humidity (2.157)	-
s_p	circumference of a pipe (2.208)	m
S_L	specific entropy of liquid phase (2.111)	J/(kg·K)
S_V	specific entropy of vapour phase (2.111)	J/(kg·K)
t	time from the start of the outflow (2.12)	s
t_0	time when droplet reaches the ground (2.150)	s
t_v	duration vapour blown-out (2.81)	s
t_B	time constant in the Wilson model (2.35)	s
t_E	maximum time validity model (2.42)	s
Δt_E	duration release remaining liquid (2.130b)	s

T	absolute temperature (2.8)	K
T_c	critical temperature of a chemical (2.11b)	K
T_d	droplet temperature (2.146)	K
T_{disp}	temperature after expansion to ambient (2.178)	K
T_e	exit temperature (2.113)	K
T_j	temperature after evaporation droplets (2.155)	K
T_m	melting point (2.113)	K
T_{sh}	shatter temperature limit (2.3)	K
T_B	normal boiling point (2.1d)	K
T_0	initial temperature (2.39c)	K
T_R	reduced temperature (2.11)	-
T_{3p}	triple point temperature (par. 2.2.3.3)	K
$\delta T_{sc,0}$	initial sub-cooling (par. 2.3.4.4.2)	K
u	(fluid) velocity (2.6)	m/s
u_a	wind speed (2.177)	m/s
u_b	bubble rise velocity (2.59)	m/s
u_g	gas velocity (2.204a)	m/s
u_d	droplet free fall velocity (2.145)	m/s
u_e	fluid velocity at exit (2.1a)	m/s
u_f	fluid velocity after flashing (2.1a))	m/s
u_j	fluid velocity after evaporation droplets (2.166)	m/s
u_s	speed of sound (2.39a)	m/s
$u_{s,L}$	speed of sound in liquid (2.122)	m/s
$u_{s,V}$	speed of sound in vapour (2.120)	m/s
u_L	velocity liquid phase (2.114)	m/s
u_V	superficial (average) vapour velocity (2.58)	m/s
u_{VR}	dimensionless superficial velocity (2.61)	-
$u_{VR,bf}$	minimum value u_{VR} for bubbly flow (2.62a)	-
$u_{VR,cf}$	minimum value u_{VR} for churn flow (2.62c)	-
U	internal energy of the gas (2.18a)	J/mol
v	specific volume (2.8)	m³/kg
v_F	specific volume fluid (2.93)	m³/kg
$v_{F,e}$	fluid specific volume at the outlet (2.103)	m³/kg
$v_{F,i}$	specific volume at resistance site (2.108)	m³/kg
v_L	specific volume of the liquid phase (2.95)	m³/kg
v_V	specific volume vapour (2.110)	m³/kg
V_c	critical volume (2.11d)	m³/mol
V	vessel volume (2.71)	m³
V_{disp}	V after expansion to ambient windspeed (2.177)	m³
V_f	cloud volume after flashing (2.171)	m³
V_j	cloud volume after evaporation droplets (2.176)	m³
$V_{L,E}$	expanded 'liquid' volume in the vessel (2.69)	m³
$V_{L,0}$	initial liquid volume in the vessel (2.69)	m³
V_p	pipeline volume (2.136)	m³
V_R	reduced volume (2.11d)	-
We	Weber number (2.142)	-
x	length variable along the pipe (2.97)	m
x_s	distance to the source (2.210)	m
z	compressibility factor (2.10a)	-

Greek symbols

β	isothermal compressibility (2.7)	m^2/N
γ	specific heat ratio (Poisson ratio) defined by (2.26)	-
ε	wall roughness (2.40)	m
η_L	dynamic viscosity of liquid phase (2.102)	$N \cdot s/m^2$
η_V	dynamic viscosity of vapour phase (2.102)	$N \cdot s/m^2$
η_{tp}	dynamic viscosity two-phase fluid (2.101)	$N \cdot s/m^2$
λ	thermal conductivity (2.144c)	$J/(m \cdot s \cdot K)$
μ_i	molecular mass (weight) chemical i (2.9b)	kg/mol
ξ	liquid fraction in vessel (2.84)	-
ρ	density (2.9c)	kg/m^3
ρ_F	average fluid density (2.91)	kg/m^3
ρ_L	liquid density (2.59)	kg/m^3
ρ_{tp}	density two-phase fluid (2.101)	kg/m^3
ρ_V	vapour density (2.58)	kg/m^3
ρ_e	density at exit (2.1b)	kg/m^3
ρ_f	density after flashing (2.1b)	kg/m^3
ρ_j	density after evaporation droplets (2.176)	kg/m^3
σ	surface tension (2.59)	N/m
σ_x	downwind dispersion parameter (2.210)	m
ζ	constant (2.33)	-
τ_{cr}	dimensionless sonic blow-down time (2.46)	-
τ_i	specific volume ratio defined by (2.108)	-
τ_s	dimensionless subsonic blow-down time (2.47a)	-
τ_v	time constant in Weiss model (2.43)	s
υ_a	kinematic viscosity of air (2.145)	m^2/s
υ_L	liquid kinematic viscosity (2.67)	m^2/s
υ_V	vapour kinematic viscosity (2.67)	m^2/s
ϕ	filling degree vessel (2.63)	m^3/m^3
$\phi_{m,e}$	quality (mass fraction vapour) at the exit (2.58)	kg/kg
Φ_m	quality (mass fraction vapour) (2.92)	kg/kg
$\Phi_{m,f}$	quality (mass fraction vapour) after flashing (2.2)	kg/kg
Φ_v	void fraction (2.62a)	m^3/m^3
$\Phi_{v,av}$	average void fraction (2.63)	m^3/m^3
ψ	outflow coefficient (2.22)	-

Mathematical symbols

C	general constant
ΔX	change in quantity X
δX	small change in quantity X
dx	differential of X
∂X	partial differential of X

Note: the numbers between brackets refer to equations.

Glossary of terms

critical flow	The critical (choked) outflow is reached when the downstream pressure is low enough for the stream velocity of the fluid to reach the sound of speed in the mixture, which is the maximum possible flow velocity.
critical temperature	The highest temperature at which it is possible to have two fluid phases of a substance in equilibrium: vapour and liquid. Above the critical temperature there is no unambiguous distinction between liquid and vapour phase.
entropy	Thermodynamic quantity which is the measure of the amount of energy in a system not available for doing work; the change of entropy of a system is defined by $\Delta S = \int dq/T$.
enthalpy	Thermodynamic quantity that is the sum of the internal energy of system and the product of its volume multiplied by its pressure: $H = U + P \cdot V$. The increase in enthalpy equals the heat absorbed at constant pressure when no work is done other than pressure-volumetric work.
flashing or flash evaporation	Part of a superheated liquid that evaporates rapidly due to a relatively rapid depressurisation, until the resulting vapour/liquid-mixture has cooled below boiling point at the end pressure.
flow	Transport of a fluid (gas or liquid or gas/liquid-mixture) in a system (pipes, vessels, other equipment).
fluid	Material of any kind that can flow, and which extends from gases to highly viscous substances, such as gases and liquids and gas/liquid-mixtures; meaning not fixed or rigid, like solids.
head loss	A measure for pressure drop related to the hydraulic liquid height.
physical effects models	Models that provide (quantitative) information about physical effects, mostly in terms of heat fluxes (thermal radiation), blast due to explosions, and environmental (atmospheric) concentrations.
piping	Relatively short pipes in industrial plants.

pipelines	Relatively long pipes for transportation of fluid chemicals.
pressurized liquified gas (pressure liquefied gas)	
	Gas that has been compressed to a pressure equal to saturated vapour pressure at storag temperature, so that the larger part has condensed to the liquid state
quality	The mass fraction of vapour in a liquid-vapour mixture (two-phase mixture).
release (synonyms: outflow, discharge, spill)	
	The discharge of a chemical from its containment, i.e. the process and storage equipment in which it is kept.
saturation curve	Saturation pressure as function of the (liquid) temperature.
saturation pressure	The pressure of a vapour which is in equilibrium with its liquid; also the maximum pressure possible by vapour at given temperature.
source term	Physical phenomena that take place at a release of a chemical from its containment before entering the environment of the failing containment, determining:

- the amount of chemical entering the surroundings in the vicinity of the containment, and/or release rate and duration of the release;
- the dimensions of the area or space in which this process takes place, including height of the source;
- the thermodynamic state of the released chemical, such as concentration, temperature, and pressure;
- velocities of the chemical at the boundaries of the source region.

source term model	Models that provide (quantitative) information about the source term, to be input into a subsequent physical effect model.
specific volume	Volume of one kilogram of a substance; reciprocal of density ρ.
superheat	The extra heat of a liquid that is available by decreasing its temperature, for instance by vaporisation, until the vapour pressure equals that of its surroundings.

triple point	A point on a phase diagram representing a set of conditions (pressure P_{3p} and temperature T_{3p}), under which the gaseous, liquid and solid phase of a substance can exist in equilibrium. For a pure stable chemical the temperature and pressure at triple point are physical constants.
two-phase flow	Flow of material consisting of a mixture of liquid and gas, while the gas (vapour) phase is developing due to the vaporisation of the superheated liquid during the flow, caused by decreasing pressure along the hole or pipe due to the pressure drop over the resistance.
vapour	Chemical in the gaseous state which is in thermodynamic equilibrium with its own liquid under the present saturation pressure at given temperature.
void fraction	The volume fraction of vapour in a liquid-vapour mixture (two-phase mixture).

Note: Some definitions have been taken from Jones [1992], AIChE [1989] and Webster [1981].

Table of contents Chapter 2

2   Outflow and Spray release

2.1   Introduction

Many hazardous materials are stored and transported in large quantities in gaseous and, usually, in liquid form, refrigerated or under pressure.

Incidental releases of hazardous materials can arise from failures in the process or storage equipment in which the hazardous substance is kept in a safe condition.

Initiating events are either system internal or system external. Internal causes may be subdivided into those arising from departures from design condition during operation and those from human error in operation. External causes could be, for instance, failure through mechanical impact, natural causes, corrosion and domino effects which are events arising at one plant affecting another.

Releases may also be necessary for the operation of a process.

The release of a material depends on:

−   the physical properties of the hazardous material;
−   the process or storage conditions;
−   the way the (accidental) decontainment takes place, and,
−   possible subsequent mechanical and physical interaction with the environment.

The state of aggregation of a chemical is determined by its physical properties, and the process or storage conditions, i.e. pressure and temperature in the containment. For mixtures of chemicals also the composition has to be known.

The Yellow Book deals with gases and liquids, so the following process conditions are considered, as usual:

1.   compressed gas,
2.   pressurised liquefied gases,
3.   liquids.

Incidental releases from containment systems range from slow discharge through a small pinhole failure to rapid discharge resulting from a major rupture of a containment; Jones [1992].

During and after a release, the released material, gas or liquid, may interact with the immediate surroundings in its own specific way, also depending on the process conditions. These interactions have a direct effect on the (thermodynamic) state of the hazardous material entraining into the surroundings. The released material may form a liquid pool, or may be dispersed into the atmosphere or into a water body, or may be ignited immediately.

The models in this chapter 'Outflow and Spray Release' may act as a source term model to provide (quantitative) information about the so-called source term, such as:

−   the amount of material entering the surroundings in the vicinity of the failing containment;
−   the dimensions of the area or space in which this process takes place;
−   the thermodynamic state of the released chemicals: concentration, temperature, and pressure;
−   velocities of the outflowing chemical at the boundaries of the source region.

These results may be used for further calculations as input for subsequent physical effect models, described in chapter 3 'Pool evaporation', in chapter 4 'Vapour Cloud Dispersion', and in chapter 6 'Heat flux from fires'.

In the following sections, release phenomena of gases/vapours and liquids under various conditions will be addressed. Each section will treat the subject from another perspective.
Section 2.2 provides the principles and basic understanding of the phenomena of outflow and spray release. It will address the applied thermodynamics and transport laws.
Section 2.3 provides an overview of methods and models published in open literature regarding the estimation of the characteristics of releases: release rates, temperatures of the released chemical, etc.
In section 2.4 the considerations will be elucidated that have led to the selection of the recommended models.
Section 2.5 provides complete detailed descriptions of the recommended models and methods. Whenever calculations or analyses have to be made, all necessary information can be found in this chapter, except for the physical properties of the chemical.
Section 2.6 provides examples in using the selected models and methods.
In section 2.7 the interfacing of other models, i.e. the necessary transformation of the results, will be addressed.
Finally, in section 2.8 general considerations are given about the models and methods presented and present gaps in the knowledge about outflow and spray release.

2.2   Phenomenon of outflow

2.2.1   Introduction to section 2.2

Section 2.2 provides the principles and basic understanding of the phenomenon of outflow (and spray release).
The outflow through an opening in a containment is mainly controlled by:
1. The pressure in the containment and the resistance to flow through the opening, and,
2. The state of aggregation of the chemical: gas, liquid, or vapour/liquid-mixture.

The different modes of a release can be divided in:
1. Transient releases (outflow), and,
2. Instantaneous releases.

The effect of pressure and resistance is briefly addressed in subsection 2.2.2.
The influence of the aggregation state of the outflowing fluid chemical is explained in subsection 2.2.3.
In subsection 2.2.4 mainly the distinction between stationary and non-stationary outflow is addressed in detail, determining the concept of modelling.

2.2.2   Pressure and resistance

The driving force for outflow of a material from a containment is the pressure difference between the containment and the ambient.
Such overpressure may exist because of:
1. gas compression,
2. saturated vapour pressure at storage temperature, or,
3. hydraulic liquid height.

The pressure difference has to overcome the wall friction due to flow in pipes and pipe fittings. Friction causes a pressure drop depending on the roughness of the pipe wall and the shape of the pipe fittings. Friction factors relate the pressure drop caused by friction to the characteristics of the pipe, such as pipe diameter and roughness of the inner pipe wall, and the flow velocity and the viscosity of the fluid.

In general the outflow rate of fluids will increase if the pressure difference over the hole or pipe increases, and thus also the stream velocity. Flow of compressible fluids, like gases and vapour/liquid-mixtures (two-phase mixtures) may become critical.
The so-called critical (choked) outflow is reached when the downstream pressure is low enough for that the stream velocity of the fluid to reach the speed of sound in the mixture, which is the maximum flow velocity possible. For a given constant upstream stagnation state, further lowering of the downstream pressure does not increase the mass flux, but will only lead to steep pressure drops in the opening to the ambient.
When the upstream pressure increases, the critical mass flow rate (kg/s) will increase but only due to the increasing density of the outflowing chemical.

If the pressure in the outlet is higher than the ambient pressure, the flow is called choked. If these pressures are (nearly) equal, the flow is non-choked. It is customary to use 'choked flow' and 'critical flow' as synonyms.

2.2.3   Thermodynamic state of the stored chemical

The state of aggregation of a chemical is determined by its physical properties and the process or storage conditions, i.e. pressure and temperature in the containment. For mixtures of chemicals also the composition has to be known.

This book deals with gases and liquids, and so the following different process conditions are considered, as usual:
1. compressed gas,
2. pressurised liquefied gases,
3. liquids.

2.2.3.1   Gases

'State of aggregation of chemical or mixture of chemicals that is fully in the gaseous state under the present pressure and temperature; gases have neither independent shape nor volume [Webster, 1981].'

If the temperature T of a chemical is higher than its critical temperature T_c, it will be a gas. Below the critical temperature the chemical may still be a gas if the pressure P is lower than the saturated vapour pressure $P_v^°(T)$. Increasing the pressure above its saturated vapour pressure at given temperature, forces the chemical to condensate.

2.2.3.2   Liquids

'State of aggregation of a chemical or mixture of chemicals, in which it has a definite volume but no definite form except that given by its container [Webster, 1981].'

If a chemical has a temperature between its boiling point $T_B(P)$ at given (partial) pressure P and its melting point T_m, it will be in the liquid state. Often these liquids are called non-boiling liquids, to distinguish them from the liquid phase apparent in stored pressurised liquefied gases.
It must be mentioned, however, that the mere fact of boiling or not boiling of the liquid is not relevant for outflow. Just the fact that the vapour pressure of a (non-boiling) liquid may be neglected if it is less than atmospheric, is relevant.
Refrigerated liquefied gases (just) below atmospheric pressure are also non-boiling liquids.

2.2.3.3   Pressurised liquefied gases

'Chemical in the liquid state which is in thermodynamic equilibrium with its own vapour under the present saturation pressure at given temperature, higher than the atmospheric pressure.'

The usual term 'pressurised liquefied gases' refers to a state in which a liquid chemical, i.e. the condensed 'gas', is in thermodynamic equilibrium with its own vapour, and thus at saturation pressure at given temperature: $P=P_v^\circ(T)$.
The use of the terminology about 'gases' and 'vapours' used in this respect may be a little awkward, but will be maintained while commonly used in practice.

A so-called 'pressurised liquefied gas' is basically a two-phase system in which the vapour phase is in thermodynamic equilibrium with the liquid phase. This liquid-vapour equilibrium may exist along the saturation curve: the storage temperature must be between the critical temperature T_c and the triple point temperature T_{3p} of the chemical.

2.2.3.4   Influence of thermodynamic state of the stored chemical

The different thermodynamic states a chemical can have, have a major influence on the outflow in two ways. First, the magnitude of the mass outflow rate is very dependent on the aggregation state of the fluid. Secondly, the thermodynamic state of the chemical in the vessel determines to a great extent the way in which the vessel will react to the loss of material resulting from the outflow.

Mass flow rate

The diagram in figure 2.1 gives possible leak rates per unit of effective leak cross-section for (non-boiling) liquids, pressurised liquefied gases and gases over a range in pressure difference from 0.05 up to 2000 bar ($5\cdot10^3$-$2\cdot10^8$ N/m^2). The different curves clearly show the strong pressure dependence of gas flow, and the fact that liquid leaking rates are 10-20 times higher than gas mass flow rates [Pilz, 1976].
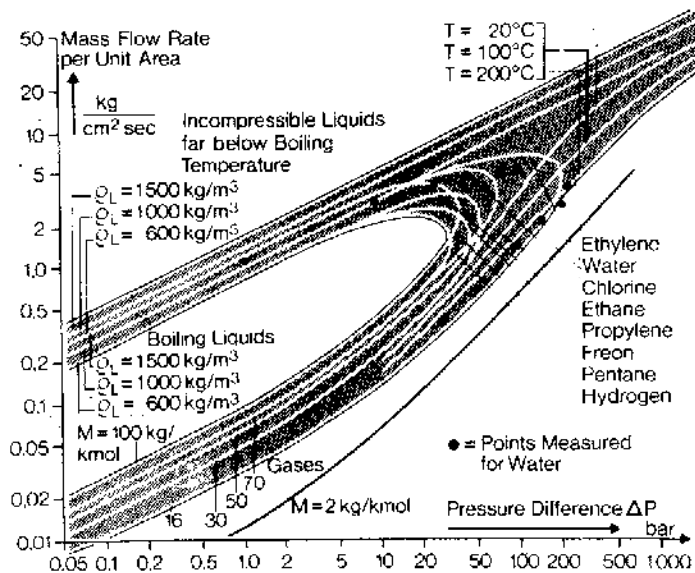
Figure 2.1   Mass flow rate versus pressure difference for flow of gases, vapours and liquids through an orifice [Pilz, 1976]

Two-phase flow

Beside gas flow and liquid flow, a so-called two-phase flow may be apparent.
In general a 'two-phase flow' is basically a fluid flow consisting of a mixture of two separate phases, for instance water and oil, or water and air.
In this chapter we consider only two-phase flows of a pure, single chemical.
Such two-phase flows may develop when a pressurised liquefied gas flows through a pipe and the local pressure in the pipe becomes lower than the saturation pressure of the flowing liquid, due to decrease of pressure along the pipe due to friction.
Then the liquid becomes superheated and a gas phase may appear due to vaporisation of the liquid.

The most important factor in the two-phase flow is the volumetric void fraction of vapour in the liquid (or its mass equivalent: quality). The quality determines to a large extent the mass flow rate and the friction in the pipe.
The largest possible discharge rate is obtained with a pure liquid phase flow. For a two-phase discharge the mass flow rate may be substantially smaller, due to the increased specific volume of the fluid.

Two-phase flow occurs if a pressurised liquefied gas is flowing in a pipe. This is a complex physical process, and a concise description of the process will be given here. Liquid, from the liquid section of the vessel filled with pressurised liquefied gas, accelerates into the pipe entrance and experiences a pressure drop. Regarding initially saturated liquids which are per definition in thermodynamic equilibrium with their vapour phase, this pressure drop creates a superheated state and nucleation bubbles are formed, when the pressure decreases below the saturation pressure.

The (rapidly) vaporising liquid (flashing) is part of a bubble formation process in which subsequently the formation of vaporisation nuclei, bubble growth and bubble transport take place. The flashing process is related to the vaporisation of liquid around nuclei and the hydrodynamics of the liquid under thermodynamic non-equilibrium conditions. Vaporisation nuclei develop under the influence of micro-cavitation at the pipe surface on the inside, as shown in figure 2.2.
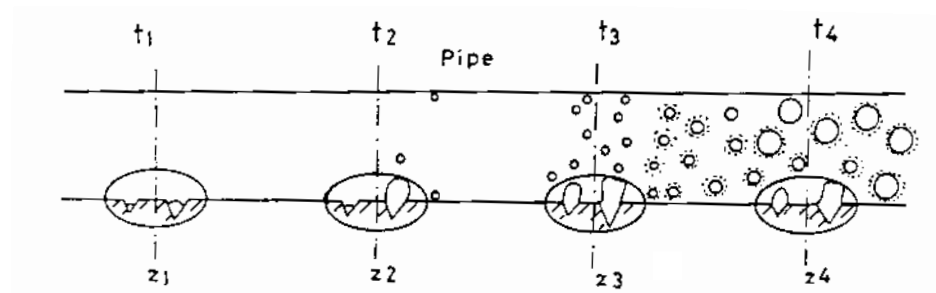
Figure 2.2   *Flash vaporisation of a pressurised liquefied gas in a pipe [Yan, 1990]*

The driving force for liquid evaporation is therefore its excessive temperature above the saturation curve corresponding to the local pressure. Evaporation is usually considered to occur at the liquid bubble interface, and bubbles may continue to form downstream. Further continuous pressure losses arise due to liquid wall friction and, more importantly, due to the evaporation process. As a result, the degree of superheat tends to increase and consequently also the evaporation rate. In addition, the expanding bubbles begin to interact and coalesce and adopt different heat and mass transfer modes: bubble flow, churn turbulent flow.
In many flows the evaporation proceeds to a point where the liquid is forced to the pipe walls and the gas occupies a rapidly moving core: annular flow.
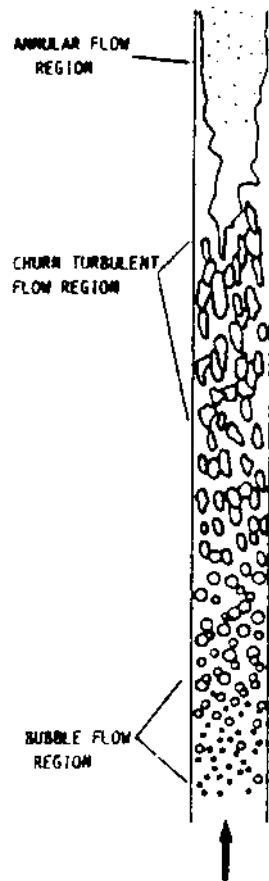
Figure 2.3   Schematic of superheated liquid pipe flow [Ewan, 1988]

In critical flows, the acceleration has progressed to the point where the flow is choked, which is characterised by very steep pressure gradients located at the pipe exit, where the pressure is above ambient.

The maximum fraction of pressurised liquefied gas that may flash (vaporise) occurs when the final pressure is equal to the atmospheric pressure. During flashing, the total entropy of the fluid is conserved. Often it is assumed that the fluid is in a saturated state initially and finally, and the fluid is initially pure liquid (quality $\Phi_{m,0} = 0$). The final temperature of the fluid leaving the pipe, is the boiling point temperature.
In choked isentropic pipe flow the vapour fraction of the fluid at the exit is always smaller than the maximum flash fraction, because the exit pressure is higher than the atmospheric pressure for choked (critical) pipe flow. Small qualities correspond to a partial flashing process in which the exit pressure is substantial.

Note that although the discharged fluid is mostly liquid on the basis of mass, it is mostly vapour on the basis of volume. The qualities of a few per cent correspond to vapour volume fractions larger than 90%. Clearly, this is due to the fact that the density of liquid is two to three hundred times higher than the density of vapour [Kukkonen, 1990].

Behaviour vessel content ('vessel dynamics')

For gases the position of the opening in the containment is irrelevant in general, although depressurising gas mixtures may partially condensate on the wall of the containment, resulting in a liquid pool at the bottom.

In case of a pressurised liquefied gas, a rapid depressurisation causes the liquid in the vessel to flash, which means that due to a relatively rapid depressurisation part of a superheated liquid evaporates rapidly until the resulting vapour/mixture is cooled below boiling point at the end pressure. Due to the development of vapour bubbles in the stored liquid ('champagne-effect') the liquid phase seems to expand, necessitating a redefinition of liquid height.
If the expanded liquid rises above the hole in the tank, a two-phase flow will be apparent through the hole in the tank.
The level swell is illustrated in figure 2.4.
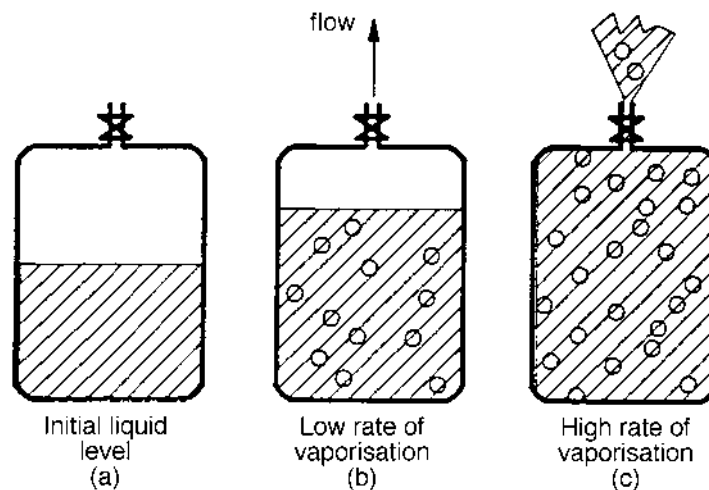
Figure 2.4   *Illustration of level swell in a depressurizing vessel filled with pressurised liquefied gas [Wilday, 1992]*

It might not be realistic to expect a homogeneous rise of the liquid level in the vessel. During the blow down of the vapour, initially apparent in the vapour section of the vessel, liquid might be dragged along through the opening.
However, little data exist for the transient void fraction in the vent line during rapid depressurisation. Experiments have been carried out in which the blow-down times were less than two seconds [Bell, 1993]. It was concluded that the quality inside the vent line, based on the calculated vessel-average values, was much less than the experimentally determined values. This effect may compensate neglected apparent

liquid dragged along with the vapour stream.

Altogether it may be concluded, that the some-what idealised approach of having a blow-off of the vapour initially apparent, until the swelled liquid has risen above the opening in the vessel, may be not too bad an approximation.

So, for pressurised liquefied gases the relative height of the liquid level above the outflow opening in the containment is a crucial factor in determining the initial quality of the outflowing material from the vessel:

1. (Small) hole in vapour space of the vessel
   well above liquid level: →   vapour outflow
2. Hole in vapour space just above liquid level: →   two-phase flow
3. Hole in liquid space well below liquid level: →   liquid outflow

In case of pressurised liquefied gases and non-boiling liquids the shape of the vessel should be taken into account for estimation of the liquid height. This height might be of importance for the relative height of the hole or pipe connection and the hydraulic pressure.

Liquids will flow out as long as the liquid level is higher than the opening.

2.2.4   Release modes

Incidental releases from containment systems range from slow discharge through a small pinhole failure to rapid discharge resulting from a major rupture of a containment [Jones,1992].

In case a vessel has been damaged to a minor extent, this results in a small opening to the environment leading to relatively small outflow rates compared to the total amount of hazardous material in the process. This opening could be a crack or hole in the vessel wall, or could be a rupture of connected piping with a relatively small diameter. Depending on the ratio between the (initial) transient outflow rate and the total mass of chemical stored, a transient outflow has to be regarded as non-stationary or as (quasi-)stationary.

In general for outflow from vessels through a hole and through piping, the flow can be considered to be stationary, meaning that the outflow is (fully) controlled by the (stagnant) upstream pressure and the downstream pressure.

If the conditions upstream are changing gradually in time, the flow may be considered quasi-stationary, meaning that the outflow rate is changing in time only because the conditions upstream are changing.

The vessel can also be ruptured totally. This causes the content, at least the larger part of it, to be released into the environment in a relatively short time. This type of release may be regarded as instantaneous. Instantaneous releases of pressurised liquefied gases will be considered in the paragraph dealing with spray release. Different release types are illustrated in figure 2.5.
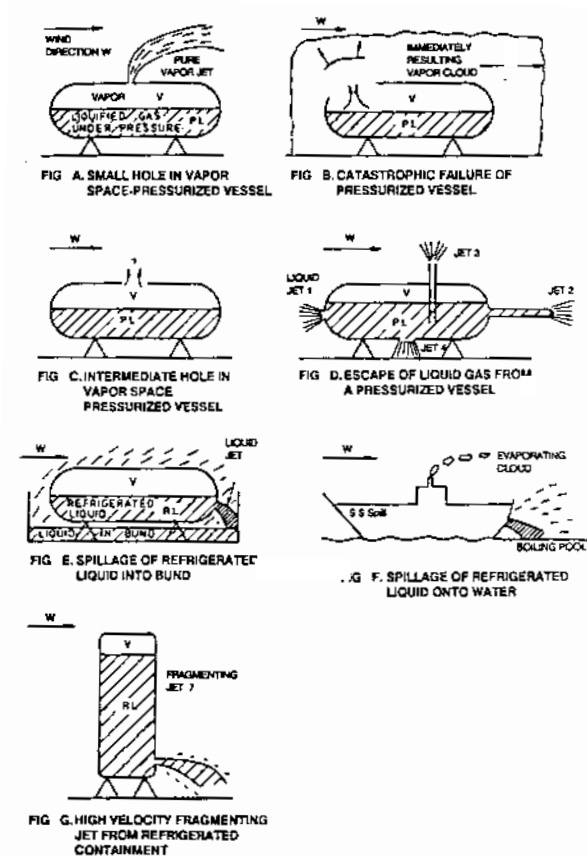
*Figure 2.5   llustration of some conceivable
           release mechanisms [Kaiser, 1988]*

In case of ruptured pipelines the flow in the pipeline will not be stationary during the larger part of the outflow, meaning that the outflow is not being controlled by the (stagnant) conditions of both pipe ends only, but will also be a function of time after the rupture itself.

2.3　General overview of existing models

2.3.1　Introduction to section 2.3

Section 2.3 provides an overview of methods and models for estimation of the characteristics of releases: release rate and thermodynamic state of the released chemical.

In the previous section the following different process conditions have been considered:
1. compressed gas,
2. pressurised liquefied gases,
3. (non-boiling) liquids.
The main structure of this section will be along this classification.

In the previous section also the following release modes have been distinguished:
1. outflow from vessels,
2. outflow from pipelines,
3. total rupture of vessels.
For each process condition these three different release modes have to be addressed.

While the way of modelling of the different release modes is typical for every process condition, the general features of the approaches concerning the different release modes will be explained in subsection 2.3.2 first.
In subsection 2.3.3 the outflow of compressed gases will be explained, in subsection 2.3.4 the outflow of pressurised liquefied gases and in subsection 2.3.5 the outflow of (non-boiling) liquids.
In general physical properties are required to perform the calculations. For the calculations of the mass flow rate for flow in pipes, friction factors are required. Finally, in subsections 2.3.6 and 2.3.7 these two topics will be briefly addressed.

2.3.2　Release modes

2.3.2.1　Quasi-stationary flow from vessels

For outflow through relatively small holes in a vessel wall or in piping the flow may be considered to be quasi-stationary, as the vessel conditions change relatively gradually. Transient conditions in the hole or pipe may be neglected.
The flow of a chemical out of a containment with a large capacity relative to the outflow rate, can be described by two coupled independent sub-models:
1. a sub-model 'vessel dynamics' that describes the dynamic behaviour of the material stored in the containment,
2. a sub-model 'outflow' that predicts the outflow rate and the conditions of the outflowing material as function of the conditions in the containment.

The independency of the 'outflow' and the 'vessel dynamics', makes it possible to estimate the change of the vessel conditions, regardless whether:
1. the outflow of materials goes through piping or through a hole in the vessel wall,
2. the gas outflow is critical or sub-critical (choked or non-choked),
3. the loss of containment is due to a one-phase outflow through a hole in the vessel wall or a two-phase flow in a pipe, etc.

The sub-model 'vessel dynamics' covers the changes of pressure, temperature, and mass content in the vessel caused by the outflow of material.
The changes of the conditions in the vessel may be estimated for small steps, i.e. sufficiently short periods of time, assuming the outflow rate and physical properties of the stored material to be constant.
This approach accommodates handling of discontinuities in the behaviour of the vessel content, like the 'sudden' drop of the liquid level under the vessel hole or pipe connection. In case the outflow rate effects the dynamic behaviour in the tank then for every time-step an iterative solution is still required.
The dependency of physical properties of temperature and pressure in the vessel can easily be taken into account, avoiding analytical approximations.
Usual assumptions made are thermodynamic equilibrium, isentropic processes, and homogeneous liquid and vapour or gas phases in the vessel.
A process is called isentropic when it is adiabatic and thermodynamic reversible. The assumption of adiabatic process may be a good approximation for relatively badly isolated systems when the quantity of mass flowing through is so big that any heat exchange can be neglected.

2.3.2.2 Non-stationary flow from pipelines

In case of a rupture of a pipeline the flow in the pipe itself is non-stationary. The flow is controlled by the initial conditions in the pipeline apparent before the rupture, the ambient conditions, and the time passing after the rupture.
The models may be distinguished according to the different process conditions
1. gas pipelines,
2. liquid pipelines,
3. pipelines with pressurised liquefied gases.
For non-stationary flows the usual assumptions regarding thermodynamic equilibrium can not be made without careful examination.

2.3.2.3 Total rupture of vessels: instantaneous releases

The physical phenomena playing a roll with instantaneous release of gases and (non-boiling) liquids are incorporated in 'subsequent' models, respectively vapour cloud dispersion (chapter 4) and pool evaporation (chapter 3), and will not be addressed in this chapter.
The instantaneous release of pressurised liquefied gases is not trivial and independent modelling exist. This topic will be addressed in the subsection 2.3.4.7

2.3.3   Compressed gases

2.3.3.1   Introduction to compressed gases

The (out-)flow of gases through holes and in pipes, and the dynamic behaviour of a (adiabatic) expansion of a compressed gas in a vessel, have been well established for many years. The governing equations can be found in any handbook on this matter.

2.3.3.2   Vessel dynamics compressed gas

Due to the outflow of gas out of a containment (vessels or pipelines), the remaining gas rapidly depressurises and will expand. This inevitably leads to a reduction in the temperature of the gas and the vessel itself. In case of gas mixtures less volatile components may condensate [Haque, 1990].

Applying the first law of thermodynamics, using the definition of volumetric work done by an expanding gas and of equations of state for (non-)perfect gases, enables the prediction of the decrease of pressure and temperature during the outflow.
This will result in an adequate description of the vessel dynamics as will be described in section 2.5.

2.3.3.3   Gas flow through holes and piping

Well-known relations for the stationary outflow through orifices and through pipes exist. In the previous edition [YellowBook,1988] models for critical and non-critical gas flow through holes have been given, together with laminar and turbulent flow of fluids (i.e. gases and liquids). These models will be described in section 2.5.

Vapour flow

The models for outflow of gas through holes and through piping are also valid for pure vapour flowing out of the vapour section in the containment for vaporising pressurised liquefied gases.

2.3.3.4   Non-stationary gas flow in pipelines

Non-stationary gas flow after a full bore pipeline rupture

The previous edition of the YellowBook [1988] describes an approximate solution of the set differential equations governing the non-stationary gas flow after a full bore pipeline rupture by linearisations and applying perfect gas law. The time-dependency

of the outflow is treated by assuming a so-called expansion zone which, after full bore rupture, starts moving with the speed of sound in the pipeline in the opposite (upstream) direction. This model has not been validated.

Both Olorunmaiye [1993] and Lang [1991] describe two rather complex models with corresponding numerical solution procedures. Assumptions made are: one-dimensional flow, friction term as in steady flow, isothermal or adiabatic flow, perfect gas.
Lang [1991] describes the flow in the gas pipeline after breakage by solving the mass balance and momentum differential equation using the spectral method with Legrendre-polynomials.
Olorunmaiye [1993] recognises the conservation equations for mass and momentum to form a set of hyperbolic partial differential equations, and solves them with a numerical method of characteristics.

Hanna [1987] gives the empirical correlation of Bell, as reformulated by Wilson. The Wilson model predictions for the mass flow rate of methane from a pipeline are quite similar to those of the Gasunie-model.

Non-stationary gas flow in pipelines through small holes

In Weiss [1988] an empirical correlation has been given for small leakages in pipelines, which has been validated against complex models.
This correlation for small holes in pipelines is the only model found in open literature.

2.3.4   Pressurised liquefied gases

2.3.4.1   Introduction to pressurised liquefied gases

After a (sudden) depressurisation the liquid in the vessel will flash, and due to the presence of vapour bubbles in the tank the liquid section will expand ('champagne effect'), necessitating a redefinition of liquid height.
When the expanded liquid rises above the hole in the tank a two-phase flow will be apparent through the opening in the tank, in stead of a pure vapour outflow.
Qualitatively the following situations for outflow of pressurised liquefied gases from a vessel may occur:
1. (small) hole in vapour space of the vessel well
    above liquid level: vapour outflow
2. hole in vapour space near initial liquid level: two-phase flow
3. hole in liquid space (well) below liquid level: liquid outflow

So, for pressurised liquefied gases the height of the liquid level relative to the outflow opening in the containment, is an important factor determining the initial state of the outflowing material from the vessel, and thus the behaviour of the vessel content ('vessel dynamics'). In order to determine which flow type will initially be at hand, the rise of the boiling liquid due to the bubble formation relative to the position of the opening in the vessel should be estimated first.

Furthermore, the outflow from the vessel may be through a hole or short pipe, or through a pipe.

In the scheme below a survey is given of the possible situations concerning the outflow of pressurised liquefied gas from a containment. The description of the various situations will be according to this diagram.

Diagram 2.1   Different situations concerning the outflow of pressurised liquefied gas from containment

---

I) Quasi-stationary outflow from vessel:

      1) Vapour outflow (2.3.4.2.3):

            a) Through hole in vessel wall

            b) Through piping

      2) Two-phase outflow (2.3.4.2.4):

            a) Through hole in vessel wall

            b) Through piping

      3) Liquid outflow (2.3.4.2.5):

            a) Through hole in vessel wall

            b) Through piping

II) Non-stationary outflow from pipeline (2.3.4.5):

      a) Due to full bore rupture

      b) Through hole in pipe wall
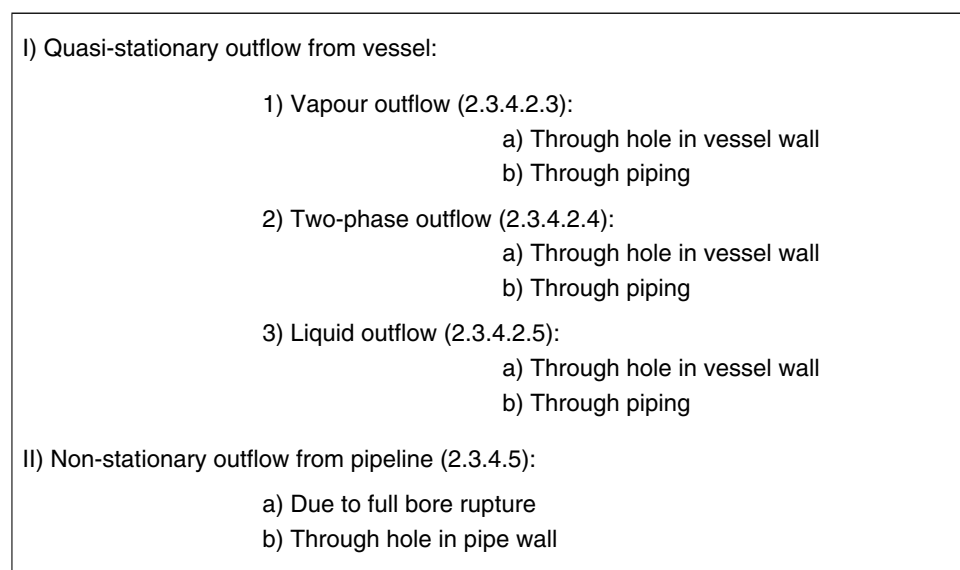
In the following section the vessel dynamics of stored pressurised liquefied gases for the different outflow types will be addressed first in paragraph 2.3.4.2.

The outflow through holes and piping for each of the different flow types, will be addressed in paragraphs 2.3.4.3 and 2.3.4.4 respectively.

In paragraph 2.3.4.5 the two-phase flow in pipelines will be addressed.

2.3.4.2   Vessel dynamics pressurised liquefied gases

2.3.4.2.1 Flow type inside the vessel

Fauske [1988] gives simple criteria that may determine whether there exists a two-phase flow inside the vessel or not. Fauske has presented simple vapour disengagement rules for determining the release type of non-foamy materials.

Especially if the liquid is viscous (e.g. greater than 500 cP) or has a tendency to foam, two-phase flow in the containment will be apparent [AIChE, 1989].

Melhem [1993] describes a refined DIERS-method that distinguishes different ways of boiling in case of top venting, and relations to estimate the quality in the outflow opening for vertical vessels. From Sheppard [1993] it appears that the analytical

solution of the DIERS-model validates the Fauske correlation. This analytical solution has been shown to hold for varying cross-sectional vessels.

The DIERS-model SAFIRE [Skouloudis, 1990] is a complex model requiring extensive thermophysical data [AIChE, 1989]. However, in Sheppard [1994] it has been concluded that the numerical DIERS-model underpredicts the void fraction for vertical vessels for bubbly flow.

2.3.4.2.2 Void fraction in the vessel

The expansion of a rapid boiling liquid depends on the ratio of the outflow rate and the size of the vaporisation area of the boiling liquid.
Belore [1986] gives the correlation of Mayinger to estimate the void fraction in the expanded liquid. The void fraction or hold-up in a flashing liquid due to depressurisation is calculated using Viecenz experimental correlation, as published by Mayinger in 1981 [Belore, 1986].

For large atmospheric containers the liquid swell may be principally due to the boiling two-phase boundary layer, in the absence of vapour carry-under, so the major part of the bulk liquid remains bubble free. The two-phase flow effects for non-foamy substances can be ignored as long as liquid entrainment at the interface is prevented ensuring low vapour velocities. However, the present state of knowledge about the effects of bulk liquid sub-cooling on mitigating the liquid swell permits only case by case numerical solutions involving sizeable computer programs [Sallet, 1990,3].

The depressurisation of a pressurised liquefied gas causing bubble formation in the liquid and thus expansion of the boiling liquid is a rather complex phenomenon.
A large computer model has been presented by Haque [1992]. Although it deals with gas-oil-water mixtures, it demonstrates the complexity of the process by showing the various factors that influence the behaviour of the boiling liquid in the vessel.
For instance, the heat flux between the different phases and between the vessel and the surroundings, are taken into account. During a 'blow-down' large temperature gradients in the vessel may be apparent.

2.3.4.2.3 Vessel dynamics vapour outflow (quality=1)

Vessel dynamics are mainly controlled by the evaporation of the pressurised liquefied gas, which is assumed to be at saturated vapour pressure initially.
Due to the outflow of vapour the vessel depressurises. This causes the liquefied gas to evaporate, and subsequently the temperature will decrease and so will the saturated vapour pressure. More details can be found in section 2.5.

2.3.4.2.4 Vessel dynamics two-phase outflow (0<quality<1)

The model for two-phase outflow from a vessel is similar to the one for outflow of only vapour. Additional assumptions are that the two-phase mixture in the

vessel is considered to be homogeneous, and that the quality of the outflowing material is identical to that of the vessel. More details can be found in section 2.5.

The quality in the vessel, and so the ratio between the vapour and liquid mass, changes due to the evaporation of liquid in the vessel caused by the depressurisation. Sumathipala [1990] states that the average void fraction is not representative of the local void fraction in the vessel. The void fraction in the top of the vessel venting may be much higher than the average value. This is demonstrated in the figure 2.6.
Also Bell [1993] concludes that the void fraction in the vent line is much higher than in the vessel. This corresponds to a lower mass flow rate and also to a higher volumetric flow rate. This criticism can only be coped with by applying very complicated models.
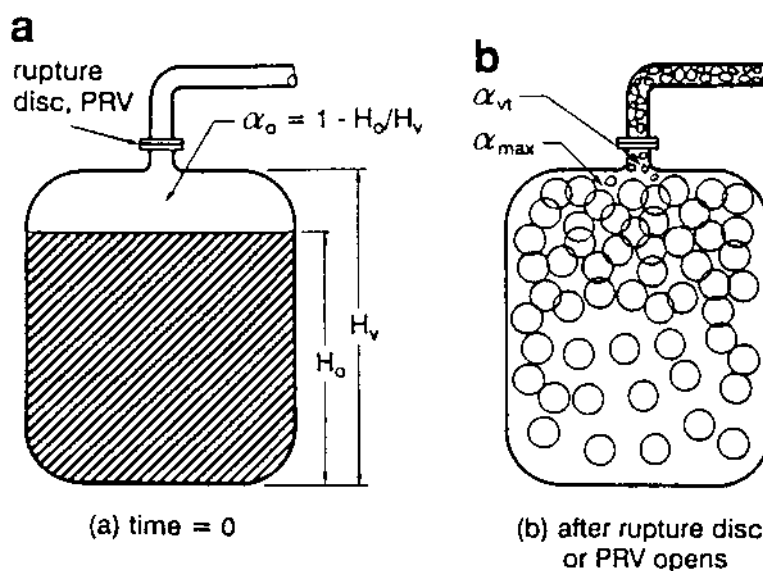
Figure 2.6   Top venting with flashing fluid [Bell, 1993]

2.3.4.2.5 Vessel dynamics of liquid outflow (quality=0)

In this case vessel dynamics are mainly controlled by saturated vapour pressure of the liquid at vessel temperature.
Due to the outflow of liquid the vessel depressurises. While the density of the vapour is much lower than the liquid, a relatively small amount of liquid has to evaporate in order to maintain the pressure, and the temperature drop will be relatively small.
The model for liquid outflow from a vessel filled with pressurised liquefied gas is quite similar to the one for outflow of only vapour. Here it is assumed that the change of vapour mass in the vessel is caused by evaporation of liquid only.
The estimation of the vessel conditions is similar to the model for the vapour outflow. In addition, the new liquid height has to be estimated as a function of the remaining liquid mass.
More details can be found in section 2.5.

2.3.4.3 Outflow of pressurised liquefied gas through a hole in vessels

Vapour outflow

The models for outflow of gas through holes are valid for pure vapour flowing out of the vapour section in the containment from vaporising pressurised liquefied gases.

Two-phase outflow through a hole: champagne outflow

In the previous edition of the [YellowBook, 1988] the outflow of a two-phase mixture through a hole has been described assuming a fluid having a density based on the vapour mass fraction or quality. This approach is commonly applied, WorldBank [1988].
As a matter of fact the model is a particular solution for a two-phase flow, with the following conditions:
1. the two-phase flow is 'frozen' (see next paragraph),
2. the outflow quality equals the quality in the vessel,
3. the two-phase flow may be treated like a common liquid,
4. the pipe length is zero.

Liquid outflow through a hole

The same approach as for champagne flow can be applied. The well-known relations for pure liquid flow through a hole can be applied, see paragraph 2.3.5.1.

2.3.4.4 Outflow of pressurised liquefied gas through piping

2.3.4.4.1 Vapour flow

The models for outflow of gas through piping are valid for pure vapour flowing out of the vapour section in the containment for vaporising pressurised liquefied gases.

2.3.4.4.2 Two-phase flow

If a pure liquid is flowing out of a vessel through a pipe, then due to the pressure drop along the pipe caused by friction, the pressure will decrease below the saturated vapour pressure, and part of the liquid will vaporise. The most important factor in the two-phase flow model is the volumetric void fraction of vapour in the liquid (or its mass equivalent: quality). The quality to a large extent determines the mass flow rate and the friction in the pipe.

Survey of models for two-phase flow in pipes

Much research has been carried out in the (recent) past on the subject of two-phase flows through pipes. The following list has been taken from Melhem [1993] and Giot [1992]:
− Fauske's model
− Ogasawara's model
− Separated phases model
− Henry's model
− Chrisholm's correlation
− Leung and Grolmes (DIERS)
− Sallet's correlation
− DISP [Kukkonen,1990]
− Moody's model
− Levy's model
− AIChE-DIERS
− Lackmé's model
− ENEA
− Flinta's model
− Yan's model

Giot et al. have carried out a benchmark on two-phase-flow models, within the European Union program 'Major Technological Hazards', on the basis of selected well-documented and reliable data sets [Giot, 1992].
A model classification has been made, based on the 3 criteria corresponding with different physical regimes:

* l_p/d_p < 50   or > 50
* $\Phi_{m,0}$ < 0.01   or > 0.01
* $\delta T_{sc,0}/T$ < 0.1   or > 0.1

with

l_p = pipe length   [m]
d_p = pipe diameter   [m]
$\Phi_{m,0}$ = initial vapour fraction   [-]
$\delta T_{sc,0}$ = initial sub-cooling   [K]

In general most models from the list above are valid only for a specific physical regime, i.e. one combination of criteria (l_d/d_p, $\Phi_{m,0}$, $\delta T_{sc,0}/T$).

Note that the pressurised liquefied gas is sub-cooled when the (vapour) pressure is higher than the saturation pressure; this may be the case if the pressurised liquefied gas is under pump pressure.

The following classifications put some order in the large number of models found in the open literature.

In general the following categories of two-phase pipe flow models exist, based on different physical assumptions:

1. Quasi-one-phase models
    The two-phase-flow is being approximated by (standard) relations for liquid flow, taking into account an average density related to the vapour fraction.

2. Homogeneous equilibrium models (HEM)
    HEM assume equal flow velocities of both phases as well as thermodynamic equilibrium between the liquid and vapour phase. This means that the quality (vapour mass fraction) can be estimated by thermodynamic relations only.

3. Non-homogeneous models
    Non-homogeneous models do not assume equal flow velocities of liquid and vapour phases, but account for phase slip.

4. 'Frozen' models
    'Frozen' models assume equal flow velocities of both phases as well as a constant ratio between the vapour and liquid fraction of the flowing fluid.

The following classes of two-phase pipe flow models exist, based on different mathematical treatment [Giot, 1994]:

A. 'Critical flow' correlations.
    These models are hybrids in which theoretical inferred relations have been fitted by empirical correlations to improve the reproduction of experimental data.

B. 'Critical flow' models.
    These models consist of or are based on sets of differential equations, to describe the variation of physical flow quantities along the pipe. The models in this category vary considerably in complexity [Nijsing, 1988].

Some categories of models for two-phase flow in pipes in more detail

1. 'Homogeneous Equilibrium Models'

Homogeneous Equilibrium Models (HEMs) are generally accepted and are widely used [Kukkonen, 1990].
The expert opinions about the predictive abilities of the mass flow rate by HEMs are quite diverse. Nyren [1987], Leung [1990], Leung and Nazario [1990], Morris [1990] and Nielsen [1991] report good agreement between HEM and experimental data.
Many others emphasise underprediction by HEMs. For instance, in Nielsen [1991] underprediction of about 10% has been reported for those situations HEM is supposed to be valid. More recently in Giot [1994] considerable underprediction has been reported.
However according to Giot [1996] HEMs will give reasonable predictions if the quality Φ_m is larger than 1%, else HEMs will underpredict. Small vapour fractions may occur in case of sub-cooled liquid at the pipe inlet, or in case of relatively short pipes. Ewan [1988], Kukkonen [1990] and Melhem [1993] state that after 100 millimetres pipe length, thermodynamic equilibrium between vapour phase and liquid phase exists in the pipe. So, in case of saturated liquid upstream and pipes much longer than 0.1 metre, HEMs may be applied.

Also in Leung [1989] underprediction has been reported, but this paper deals with designs of nozzles. Clearly the assumption of thermodynamical equilibrium, in case of a minimum pipe length of 0.1 metre, is not valid here.

The computer model TPDIS [Kukkonen, 1990] is a complete model including the required thermodynamics supplied in the form of correlations for some chemicals.

Nyren and Winter [Nyren, 1983] have done field experiments, using liquefied ammonia and sulphur dioxide, the objective being to test the TPDIS model experimentally. As reported in these references, the experimental results and model predictions were compatible within a reasonable accuracy. However, this comparison was based on a fairly limited set of data. Fletcher and Johnson have presented more extensive experimental data in 1984, based on the studies of several investigators. The data include results of laboratory experiments using superheated refrigerant-ll, and laboratory and large-scale experiments using superheated water. Suitable data for other substances are sparse.

TPDIS predicts mass flow rates of about 10% higher than TRAUMA [Wheatley, 1987].

In Ramskill [1987] a HEM has been presented to predict the maximum two-phase outflow rate in pipes, neglecting the flow resistance.

2. Non-homogeneous models

In [anonymus] a model is given for the prediction of the maximum two-phase outflow rate in pipes, neglecting the flow resistance, based on the work of Fauske.

This model takes into account the phase slip. In general the model predicts mass flow rates that are about 1.4 higher than the HEM predictions.

3. 'Frozen flow'

The relevancy of the 'frozen flow model' is emphasised in Sallet [1990,1] for the estimation of the mass flow rate through 'nozzles' and 'valves'. In that case, the flow velocities are so high that the time is simply to short to reach thermodynamic equilibrium, and 'frozen flow' may be assumed, meaning constant quality of the two-phase flow.

In the model for champagne outflow described in the previous edition of the [YellowBook, 1988] the frozen flow assumption has been made implicitly.

4. 'Critical flow' correlations

Sallet pleads clearly for the use of correlations instead of flow rate models [Sallet, 1990,2]. His arguments are as follows. In general the calculation of the critical mass flux (G_{cr}) is a cumbrous task. The numerical procedure is necessary iterative, because a priori the pressure in the pipe at the location where the mass flux G_{cr} becomes critical, is unknown. Furthermore, thermodynamic data for most chemicals are insufficient to be able to make reasonably accurate estimations [Sallet, 1990,2]. These inaccuracies may lead to deviations of 50-150% in the critical heat flux G_{cr} by HEMs. Sallet constructed generalised correlations for 10 industrial commodities.

However, these correlations deal with the release of pure vapour through vents, assuming that the phases are separated in the vessels, and no liquid flow through the valve [Giot, 1996].

5. 'Critical flow' models

Within the European Union program 'Major Technological Hazards' the computer model FLIERS has been developed for two-phase flows in pipes.

Differential equations describe the conservation of mass, energy and momentum over the two-phases, the behaviour of the bubbles, etc. The model is capable, besides estimation of the critical mass flow rate, to calculate axial pressure and quality profiles in the pipe. The so-called Yan's model [Giot, 1994] relates the flashing process with the vaporisation of liquid around nuclei and the hydrodynamics of the liquid under thermodynamic non-equilibrium conditions. It accounts for the development of vaporisation nuclei under the influence of micro-cavitation at the inside pipe surface. This model seems very complete from a theoretical scientific point, but requires large computational efforts, and may only run on 'main frames' requiring long response-times nevertheless. Yan's model demonstrates clearly the dominating physical phenomena along the pipe length, but also shows its limitations concerning application in practical situations.

Similar developments are reported by Riznic [1989], where a new flashing model is demonstrated based on the bubble formation process: vaporisation nuclei, bubble growth and bubble transport. These theories are under development, and obviously non-HEM.

Influence of pipe length

l_p/d_p-models

In earlier studies the flow type has been commonly correlated with the ratio of the pipe length and the pipe diameter (l_p/d_p). The flow is assumed to be pure liquid for sufficiently small l_p/d_p ratios, and two-phase fluid in equilibrium for sufficiently large l_p/d_p ratios. For intermediate values of l_p/d_p, a two-phase fluid in disequilibrium may exist. Based on their experimental results with Freon 12, Fletcher and Johnson found that the mass flux density [$kg/(s \cdot m^2)$] of a two-phase pipe flow depends on the pipe length, but not on the pipe diameter. They concluded that the flow types should be distinguished on the basis of the absolute length l_p rather than the ratio l_p/d_p, [Kukkonen, 1990].

Two-phase flow in short piping

The rapid initial depressurisation during pipe flow may cause thermal and hydrodynamic non-equilibrium; these effects may be particularly important for short pipe lengths. In certain two-phase flow regimes the temperature and velocity are different for the vapour and the liquid phases, and the two-phase fluid is non-homogeneous. These effects may be important if the interfacial area of the phases is small, i.e., for high-quality flow [Kukkonen, 1990].

As mentioned before, for two-phase pipe flows no thermodynamic equilibrium exists for pipe lengths shorter than 100 millimetres [Melhem, 1993], [AIChE, 1989]. Apparently, the release path must be sufficiently long to enable some degree of interphase mass transfer and equilibration. In Ewan [1988] a numerical flow model has been presented for two-phase flows for short pipes. In this paper it is advised to use specific correlations [AIChE, 1989], or to interpolate between the prediction of

the one-phase-liquid approximation and HEM prediction.

In Hardekopf [1988] the influence of other parameters than the pipe length, is demonstrated. An interesting survey is given regarding the effect of geometry on the critical mass flux.

2.3.4.5 Non-stationary two-phase flow in pipelines

The previous edition of the [YellowBook, 1988] describes an approximate solution of the set differential equations governing the non-stationary two-phase flow after a full bore pipeline rupture by linearisations, applying perfect gas law and approximating thermodynamic relations.

The time-dependency of the outflow is treated by assuming a so-called evaporation zone that, after the rupture, starts moving with the speed of sound in the pipeline in the opposite (upstream) direction. No thermodynamic equilibrium and homogeneous flow has been assumed, but the kinetic energy of the flow near the vaporisation zone is maximised. The model has been taken from 'LPG a study', TNO [1983].

The model has not been validated. The numerical solution has appeared to be non-stable. So, the approach is more or less the same as the previous approach for non-stationary gas flow in pipelines, for which its bad performance has been shown (paragraph 2.3.3.4). Altogether the model is expected to give doubtful predictions because two-phase flow is much more complex than gas flow.

Morrow [1983] describes a model specific for LPG pipelines, using an iterative numerical procedure. The model is used for the entire region of two-phase flow within the pipeline. At the point of pipe rupture, the upstream and downstream end of the pipe are assumed to be totally separated so that the flow rates coming from the upstream and downstream pipe regions, are independent.

The initial outflow is determined based on the assumption of choked flow at the pipe exit. As time progresses the flow rate diminishes until choking (equivalent to sonic flow in a perfect gas discharge) no longer occurs.

The Fauske model for critical flow at the exit G_{cr} of a full pipe break is used. Away from the point of rupture, the frictional pressure drop in the pipeline is given by the well-known Darcy-Weisbach equation.

An analysis of two-phase flow pressure gradient and void fraction (vapour volume) was developed to provide the mass depletion in the pipe as a function of exit flow rate and pressure. These correlations for exit flow and pipe flow together allow correlations for exit flow versus time after rupture.

Although the authors had no opportunity to make detailed comparisons of methods and accuracy assessments of the models, it is believed that these models will give slightly conservative results.

Large-scale experimental data have been used to compare and derive simple mathematical models to describe the transient release rate of pressurised liquid petroleum gas (LPG) from a ruptured pipeline if the fluid supply upstream of the rupture location has been stopped [Tam,1990]. A simple exponential correlation has been fitted against experiments with 100 metre LPG pipeline. The model is valid for small leaks as well as for a full bore rupture.

2.3.4.6   Finite duration spray release

Statement of the problem

This section considers releases from liquefied gases stored under pressure at a temperature above normal boiling point. If a breach or puncture in the containment occurs, the pressurised liquefied gas will flow out and 'flash', i.e. part of the liquid phase will evaporate, extracting heat from the liquid phase, until the vapour/liquid mixture is cooled below boiling point. (The difference between storage temperature and boiling point is often called 'superheat'). Flashing may (partly) occur upstream the release (e.g. in a long pipe between vessel and breach) or just downstream the release. Flashing before the release and its consequences for the release rate are dealt with in sections 2.3.3.2 and 2.3.3.3.

After flashing, either a vapour jet with a droplet spray or a liquid jet with vapour bubbles develops.

A droplet laden vapour jet will entrain air and the droplets in the jet evaporate. A part of the droplets may fall on the ground and form an (evaporating) liquid pool.

A liquid jet with vapour bubbles will form an (evaporating) pool, and the flashed vapour in the bubbles has to be dealt with as originating from the pool.

Evaporation from the pool is dealt with in chapter 3; the atmospheric dispersion of the single-phase jet and the vapour evaporating from a pool can be described using the models provided in chapter 4, Dispersion.

In order to describe the whole evolution of the two-phase jet, separate descriptions or models are needed for the following phenomena taking place in the jet:
- the flashing of the liquid phase after release, leading to the vapour mass fraction and temperature in the jet;
- the droplet size of the liquid fraction, the evaporation during sedimentation of the droplets and the fraction deposited on the ground (rain-out fraction);
- the evolution of velocity, concentration and width of the two-phase jet; and,
- the evaporation of droplets in the two-phase jet due to air entrainment and the thermodynamic state (temperature, density) of the mixture.

Hereafter, the emphasis will be on droplet-laden vapour jets. The treatment of liquid jets is straightforward in that they will form a (spreading) pool.

Figure 2.7 presents a schematic view of a two-phase jet. The jet shows three parts, divided by three cross-sections. Flashing occurs after the exit until the mixture is cooled to the boiling point. Then air is entrained, droplets may rain-out and/or evaporate due to the heat brought to the jet by air. Water vapour in the jet may condense. Finally all chemical droplets evaporate and a single-phase jet, which still might contain condensed water vapour, remains. The single-phase jet will be described in chapter 4, Vapour Cloud Dispersion; here emphasis is on the first two parts of the jet. The relevant phenomena are summarised in Diagram 2.2. The first two lines refer to the first part of the jet, the other three lines refer to the second part of the jet. Models and descriptions of these phenomena are discussed in the following sections.
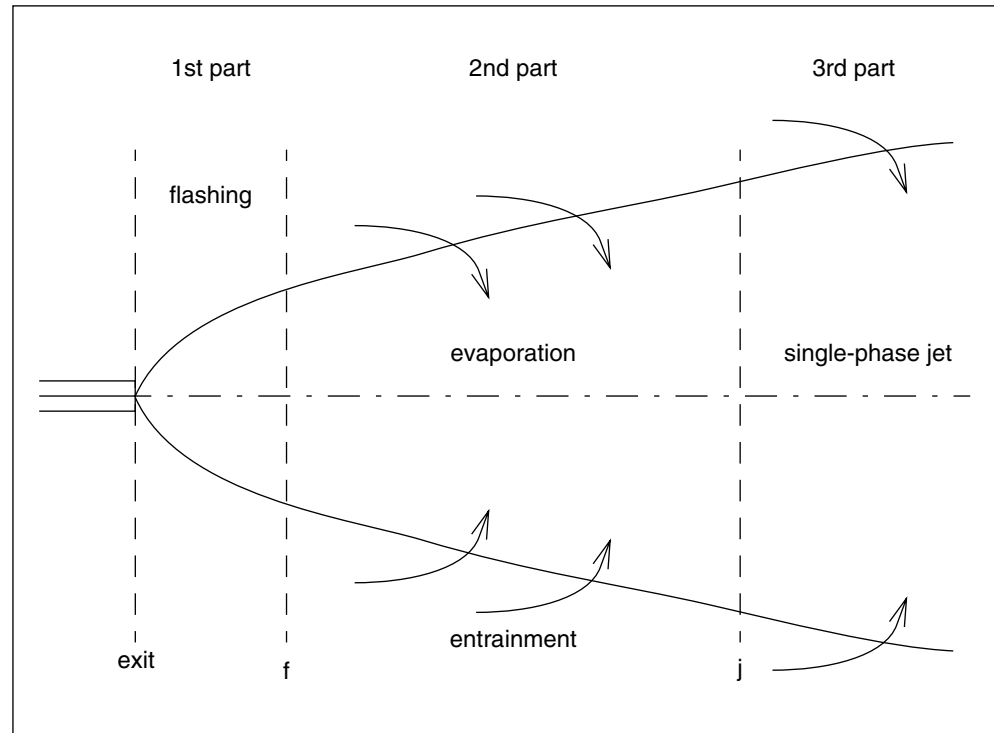
Figure 2.7   Schematic view of a two phase-jet

Diagram 2.2   Phenomena of two-phase jets

Expansion and flashing at atmospheric pressure

Droplet diameter after flashing

Droplet diameter after flashing

Jet dispersion

Evaporation of the droplets in the jet

Expansion and flashing in the atmosphere

It is common practice to neglect entrainment during the flashing stage.
Furthermore, except for Computational Fluid Dynamics approaches, it is assumed
that vapour and droplets have the same velocity (no slip between phases). Under
these assumptions the flash fraction (and other quantities) at the end of the flashing
stage can be calculated from the exit conditions by

−   conservation of enthalpy: $H_e + 0.5\ u_e^2 = H_f + 0.5\ u_f^2$ (J/kg)   (2.1a)

−   conservation of momentum: $\rho_e\ u_e^2\ A_e + A_e\ (P_e - P_a) = \rho_f\ u_f^2\ A_f$ (N)   (2.1b)

−   conservation of mass: $\rho_e\ u_e\ A_e = \rho_f\ u_f\ A_f$ (kg/s)   (2.1c)

- T_B is the boiling temperature; $P_v^°$ $(T_B) = P_a$ $\qquad$ (N/m^2) (2.1d)

- an equation of state relating density to pressure, temperature, and quality. The vapour density is a function of pressure and temperature (e.g. the perfect gas law), and the density of the liquid phase is a function of temperature alone.

- data on the enthalpies H_e and H_f as a function of pressure, temperature and quality.

This approach is in principle used in the Yellow Book [1988] and by many other authors, e.g. Wheatley [1987]. In his case he used the perfect gas properties and the Clausius-Clapeyron relations in order to define the equation of state, the saturation pressure and the enthalpies (assuming isentropic evaporation to give a higher bound on the flash fraction).

Often, e.g. Yellow Book [1988] and Kukkonen [1990], the flash fraction is calculated using entropy relations.

In addition to the 'conventional' approach described above, some authors, e.g. Woodward [1993], state that equilibrium flash fractions are not established for orifice discharge or short nozzles and pipes. Instead one should use:

$$\Phi_{m,f} = C_{\Phi mf} \times \Phi_{m,f,equilibrium} \qquad (-) \qquad (2.2)$$

with

$$\begin{cases} C_{\Phi mf} = \Phi_{m,f,e}/0.14 & \text{if} \quad \Phi_{m,f,e} \leq 0.14 \\ C_{\Phi mf} = 1.0 & \text{if} \quad \Phi_{m,f,e} > 0.14 \end{cases}$$

However other authors, e.g. Wheatley [1987], argue that the important parameter in reaching equilibrium is the path length of the flow since nucleation, and this can not, according to Wheatley, be estimated by simple expressions such as those mentioned above.

Some alternative approaches towards determination of flash fractions and the conditions after flashing can be found. One such an alternative model is presented by Woodward [1993]. This model, which includes determination of critical flow rate, see 'outflow', is based on similarity of the two-phase discharge with underexpanded single-phase jets. The differences with the 'conventional' approach are considerable (higher jet velocities, less diameter expansion). Woodward [1993] states that experiments are necessary to decide which of the approaches is better.
Another alternative is proposed by Vandroux-Koenig et al. [1991]. They estimate the diameter and velocity after flashing on isotropic increase of bubble size. Also in that case the jet velocity is higher and droplet diameters smaller than when using the conventional approach, but the momentum balance is neglected.

Droplet diameters after flashing

A liquid jet (either or not flashing) may break-up into droplets due to:
− the size of the nozzle (capillary break-up);
− aerodynamic break-up of the jet;
− shattering by flashing.

For capillary break-up and aerodynamic break-up the literature provides a number of models and descriptions. Most of these descriptions are quite similar, (Tilton & Farley [1990], Wheatley [1987]). The summary of drop size correlations is provided by Tilton and Farley [1990]. This summary includes also correlations for the length before break-up (relevant to determine which process starts first, e.g. a sub-cooled jet may break-up aerodynamically before being shattered by flashing, causing larger drops).

The initial drops formed in the jet may break further by aerodynamic forces. The maximum stable drop size can be determined using a critical Weber number. The values of critical Weber numbers vary, and may be dependent on parameters not included in the Weber number, between 5 and 100, [Wierzba, 1990] but often used values are between 10 and 20 [Tilton & Farley, 1990], Kocamustafaogullari et al., [1994], Wheatley [1987], Appleton [1984].

Application of the above-mentioned correlations leads to a single number for the drop size, not allowing for the variation of droplet sizes within a jet. Alternatively, Vandroux-Koenig et al. [1991] suggest assuming a droplet population using an upper log-normal distribution of which the median is the largest hydro-dynamically stable drop size.
With respect to the effect of shattering, Appleton [1984] and Hague and Pepe [1990] conclude that shattering of the jet by flashing occurs if the exit temperature exceeds a 'shatter' temperature T_{sh}, which obeys

$$\frac{T_{sh} - T_B}{T_{sh}} = C_\varepsilon \qquad\qquad (-) \qquad\qquad (2.3)$$

Here T_B is the boiling temperature and C_ε is 0.07 - 0.1 (Appleton) or 0.1 (Hague and Pepe).
Estimates of drop size due to shattering are provided by Tilton & Farley [1990], Appleton [1984] and Vandroux-Koenig [1991]. The approach used by Vandroux-Koenig et al. [1991] requires an estimate of the rate of depressurisation in the flashing jet, which is not easy to obtain.

Most authors however, determine the drop size after flashing by using the critical Weber number for aerodynamical break-up. In this way effects of coalescence of droplets (droplet growth) do not have to be dealt with separately and the method explains the experimental (low) fractions of rain-out satisfactorily.

Droplet evaporation and rain-out on the ground

Droplets will settle by gravity and they can fall on the ground, forming an (evaporating) pool.

The calculation of the trajectory of droplets is generally performed by assuming that the horizontal velocity of the droplet equals the horizontal jet velocity, and the vertical velocity (settling velocity) follows from the aerodynamic drag force.

The evaporation of droplets has been given much attention in recent research. In view of differences in complexity, one has to distinguish between

1. evaporation of a pure, single component droplet,
2. evaporation of a binary (or multi) component droplet.

The first approach is more simple and leads to more analytic or simple definite conclusions.

A simple approximate expression for the droplet diameter d_m for which drying time and settling time to the ground are equal, has been derived by Kukkonen et al. [1989]. Only droplets larger than d_m will fall on the ground. Expressions describing the change of droplet mass up to the moment the droplet falls on the ground can be derived using the basic model principles.

The same principles are used by Papadourakis et al. [1991] and Woodward & Papadourakis [1991]. Droplet evaporation is combined with calculations of the droplet trajectory in differential form. The calculations are combined with an integral plume trajectory model, and the difference between jet trajectory and droplet trajectory defines the 'ambient' droplet conditions for evaporation and drag. All evaporated chemical is fed 'back' into the jet/plume model.

The evaporation of binary component droplets is described by Vesala [1990], Vesala & Kukkonen [1992] and Pattison [1992].

Pattison attempts to include the binary component model in a jet/plume model frame work comparable to Woodward & Papadourakis [1991] as described above, see also Hewitt & Pattison [1992]. This leads to an extensive set of coupled ordinary differential equations.

In order to obtain some information about the relevance of the binary component model compared to the single component droplet evaporation model, the evolution of droplets was investigated by Vesala and Kukkonen [1992]: in 100% humid air, 20 ˚C ambient temperature, initial diameter 100 μm, the 'drying' time of a binary ammonia/water droplet is reduced by a factor 1.5 compared to a single component ammonia droplet in dry air (and thus ignoring 'binary' effects).

Jet dispersion

A droplet-laden two-phase jet is assumed to behave like a pure vapour jet. According to Wheatley [1987], Kukkonen [1990], Webber et al. [1991], entrainment rates identical to those for pure vapour jets can be used. The jet model allows for prediction the change of concentration, velocity and radius of the jet along the jet axis. The following section will address droplet evaporation in the jet.

Evaporation of the droplets in the jet

The rate of evaporation of droplets in the jet is dominated by the amount of entrained air and the amount of heat brought into the jet by the entrained air. The calculation of droplet evaporation in the jet can be made by the enthalpy balance at any point in the jet.

A rigorous derivation of concentration, phase balance and enthalpy balance in differential form, i.e. changes in properties related to small increases of entrained air in the jet, is provided by Webber et al. [1991]. Webber considers different possibilities:
1. Two-phase chemical dispersing in dry air.
2. Two-phase chemical which is immiscible with water dispersing in moist air.
3. Two-phase chemical which forms an ideal solution in water (i.e. the partial vapour fraction of the chemical is linear to the molar fraction of chemical solved in water) dispersing in moist air.
4. NH_3 dispersing in moist air.
5. HF dispersing in moist air.

However, it is not always necessary to use a differential approach. In some cases it is possible to make use of enthalpy- and phase balances at arbitrary positions in the jet without needing to solve differential equations. Examples of these methods are provided by Kukkonen [1990], who treats the 2nd possibility from above, Wheatley [1987] (possibility 4), and Webber and Brighton [1989] (possibilities 2 to 4).

The latter calculate the temperature after entrainment by evaluating the enthalpy changes when a certain amount of moist air at T_a is mixed with chemical at flashing conditions (X_f, T_B). The nett change of enthalpy is zero:

$$0 = \Delta H = \Delta H_{chemical} + \Delta H_{dry\ air} + \Delta H_{water\ vapour} \qquad (J/kg) \qquad (2.4)$$

The individual enthalpy changes include the temperature change, both of liquid and vapour, and the heat of evaporation and/or condensation.
If the chemical is soluble in water, the scheme remains the same, but the liquid phase will be mixed. It also means that in most cases, if the chemical does not form an ideal solution in water, an additional term ΔH_{mixing} has to be added to the enthalpy balance above to account for the fact that chemicals dissolving in water produce heat (e.g. ammonia). Also the saturated vapour pressures of both water and chemical change and become dependent on the mixture fraction in the droplet.
Methods to calculate the mixing enthalpy and saturation pressures for ammonia/water mixtures are provided on an empirical way by Wheatley [1987] and in a more general way by Vesala & Kukkonen [1992]
If one is only interested in the situation at cross-section 'j' after complete evaporation of the chemicals, the nett mixing enthalpy equals zero.

The above-described approach assumes liquid and vapour to have the same temperature, and no velocity difference between the phases. This is the so called 'homogeneous equilibrium' theory (HE). According to Kukkonen [1990], a temperature difference, i.e. the 'temperature depression', is necessary to drive evaporation. By comparison with advanced models, Kukkonen [1993] concludes that at least in clouds, HE theory can be used for droplets up to 100 μm. It is not necessarily valid in the jet region where high entrainment occurs. Furthermore, it appeared that the results were not very sensitive to the thermodynamic properties, i.e. the differences between Wheatley's [1990] and Vesala & Kukkonen's [1992] expression.

2.3.4.7 Instantaneous releases pressurised liquefied gases

Statement of the problem

This section considers the release following a complete failure of a vessel containing liquefied gases stored under pressure at a temperature above normal boiling point. After failure, the liquid will flash and expand in all directions until the vapour/liquid mixture is cooled below boiling point.

After flashing, the cloud will expand further and entrain ambient air. The entrained air will cause further evaporation of liquid droplets in the cloud. Part of the droplets may fall on the ground and form an evaporating pool.

For consequence analysis it is necessary to be able to describe the evolution of the cloud size and the concentration in the cloud after the release, before atmospheric dispersion takes over, and the fraction of the release that remains in the air compared to the fraction that will form an evaporating liquid pool.

In order to describe the evolution of the instantaneous release, separate descriptions or models are needed for the following phenomena taking place in the expanding two-phase cloud:
- the flashing of the liquid phase after release, leading to the vapour mass fraction and temperature in the two-phase cloud;
- the evolution of the size, expansion velocity and concentration of the two-phase cloud;
- the fraction deposited of liquid droplets on the ground (rain-out fraction);
- the evaporation of droplets in the two-phase cloud due to air entrainment and the thermodynamic state (temperature, density) of the mixture.

A division in three stages, similar to that used for continuous releases, can be made. First, the liquid flashes and expands without entrainment. Secondly, air is entrained, droplets may rain-out and/or evaporate due to entrained air. Finally all chemical droplets disappear and a single-phase cloud remains.

Again, emphasis will be on the first two stages. The phenomena are also summarised in Diagram 2.3. The first two boxes refer to the first stage, the last two boxes to the second stage. Models and descriptions of the phenomena in Diagram 2.3 are discussed in the following sections. A number of methodologies described in section 2.3.4.6 (continuous releases) will also be applicable to instantaneous releases.

Diagram 2.3   Phenomena of instantaneous releases of pressurised liquefied gases

Flashing and initial cloud expansion
Droplet size and rain-out on the ground
Expansion of the two-phase cloud during the entrainment phase
Evaporation of the droplets in the cloud

The study of instantaneous releases is far less developed than the study of continuous (jet) releases. The largest scale experiments reported are those by British Gas [Johnson et al., 1990], involving a commercial storage vessel of 5.7 m^3 filled with 2 tonnes of butane (fill ratio 77% by volume). For this test only visual and LIDAR-data of the expanding cloud is available.

Other rather large-scale experiments are those of Hardee and Lee [1975] regarding 450 kg of welding gas 'MAPP' and propane, and Giesbrecht et al. [1981] involving 435 kg of propylene.

Small-scale tests have been performed using refrigerants (Nolan et al. [1991] 1 litre, Schmidli et al. [1992] 2 litres, and HSE, Webber et al. [1991] 20 litres) and propane (Schmidli et al. [1992] 2 litres).

With respect to the use and importance of small-scale experiments, Nolan et al. [1991] point out that a rigorous analysis of scaling aspects is necessary, but has not as yet been performed, in order to translate small-scale experiments to reality. Especially the rain-out behaviour of small-scale experiments is difficult to extrapolate to large-scale, and the older large-scale experiments provide no information on rain-out.

Flashing and initial cloud expansion

For the flashing stage immediately after the loss of containment it is reasonable to assume that no ambient air will entrain into the cloud, Webber et al. [1991].

The conditions in the cloud just after complete flashing can be described by the enthalpy balance, taking into account the kinetic energy of the expanding cloud and the work performed on the atmosphere [Melhem & Croce, 1993], [Nolan et al., 1991]:

$$H_0 = \{\Phi_{m,f} H_{V,f} + (1-\Phi_{m,f}) H_{L,f}\} + 0.5 \ u_f^2 + (P_0 - P_a)/\rho_0 \qquad (J/kg) \qquad (2.5)$$

In order to calculate the unknown flash fraction $\Phi_{m,f}$ and the expansion velocity u_f, the thermodynamic path between H_0 and H_f needs to be known. Assuming an isentropic evaporation, an upper boundary for u_f and a lower boundary for $\Phi_{m,f}$ can be obtained.

From experiments [Nolan et al., 1991], [Schmidli et al., 1992], [Webber et al., 1991] it is obvious that the expansion velocity is smaller than it would be by assuming isentropic evaporation and using the above mentioned enthalpy balance, but the differences in results and conclusions are large. Some researchers [Schmidli et al., 1992], [Webber et al., 1991] find expansion velocities of only 10% - 30% of the theoretical, isentropic values. However the data from Nolan et al. [1991] leads to expansion velocities which are about 60% - 80% of the theoretical, isentropic values (see also the analysis of Nolan et al.'s data by Melhem and Croce [1993]).

The reasons for lower-than-theory expansion velocities are that part of the kinetic energy is transformed into turbulent kinetic energy, the evaporation and expansion process is not isentropic and during the flashing stage no equilibrium state is reached (Webber et al. [1991] describe non-equilibrium between temperature and pressure during the HSE-experiments).

Nevertheless, no simple relation between 'theoretical' and real expansion velocities can be derived.

Droplet size and rain-out on the ground

In order to estimate the possibility of liquid rain-out on the ground there is an interest in describing the droplet size in the aerosol cloud after flashing.
Measurement and analysis of droplet size are reported by Nolan et al. [1991] and Schmidli et al. [1992]. Observed droplet sizes are (much) smaller than the maximum stable droplet diameter, using a critical Weber-number and the expansion velocity of the cloud (cf. section 2.3.4.6). No other droplet size theories have been published.

No physically sound models have been found to describe rain-out and droplet evaporation in instantaneous releases.
The settling of aerosols depends on the height to which droplets are carried, and the rate at which ambient air is mixed in the cloud in order to evaporate the droplet. It is reasonable to assume a dependence on the size of the release for droplet settling.
Moreover, rain-out occurs not only by settling of aerosol in the cloud, but also by impingement of droplets by the energy of the expanding cloud in the early stages of expansion.

Cavanaugh et al. [1994] suggest the assumption that all liquid will be emitted as aerosol if the storage temperature exceeds the boiling temperature by 10 K. For boiling temperatures between 200-250 K, this corresponds to a 'shattering' criterion (see formula (2.3), section 2.3.4.6) in which C_ε is less than 0.05. However, Cavanaugh's assumption is supported neither by physical reasoning nor experimental data.

Only Schmidli et al. [1992] provide quantified experimental information on the amount of rain-out and pool formation for Refrigerants 12 and 114. Even for releases exceeding the 'shattering' criterion with $C_\varepsilon=0.1$, a significant amount of mass remains in the pool. Impact of liquid on the ground during the early stage of expansion seems to be the major cause. A reduced liquid fill level leads to increased pool formation as the vapour above the liquid forces the liquid downwards during expansion.
It is common practice to assume that twice the amount of the flashing liquid remains airborne. This assumption provides a rough but reasonable approximation of the result of Schmidli et al. Of course, such a simple rule does not account for probable dependency of rain-out on droplet diameter, release size or fill level.

Expansion of the aerosol cloud during the entrainment phase

No generally accepted model for the expansion of an instantaneous aerosol cloud exists. The models published by Giesbrecht et al. [1981] and Hardee & Lee [1975] for the expansion after flashing are very different in their approach.
The model included in the Yellow Book [1988] and the 'Worldbank' model are based on the work by Giesbrecht et al. [1981]. Webber et al. [1991], however, criticize the Yellow Book [1988] model as it fails to reproduce the HSE experiments.
The model by Hardee & Lee [1975] for the expansion rate of the cloud is based on conservation of momentum, but they assume no expansion in vertical direction, and the release is not purely instantaneous, but a large puncture in a vessel.
The simplest approach, using Hardee & Lee's ideas, is to assume that during flashing the expansion velocity is constant and that it can be calculated using formula (2.5), possibly with a correction for non-isentropy and turbulence. Afterwards an expanding cloud with a uniform concentration is assumed. The momentum which is contained

in a segment of the (hemi-) spherical cloud at the moment when flashing is complete, will be conserved. From this and from neglecting the density difference between the cloud and the ambient air, one derives the uniform radial velocity in the cloud, which is also assumed to be the expansion velocity:

$$u(t) = u_f \, (b_f/b(t))^3 \qquad\qquad\qquad (m/s) \qquad (2.6)$$

Here, b_f is the cloud radius at the moment when flashing is complete, and b the cloud radius at any moment thereafter. By stating u = db/dt, one can derive the evolution of the cloud size with time.

The expansion rate according to this simple model agrees fairly well with the experimental results of Giesbrecht et al. [1981], assuming expansion in a hemispherical cloud at ground level.

The model applies until the expansion velocity is of the same magnitude as the ambient wind speed.

Evaporation of the droplets in the cloud

All statements made in section 2.3.4.6 for droplet evaporation in continuous releases are applicable to the expanding aerosol cloud. No research is known towards the applicability of the HE-assumptions for instantaneous clouds. In the later stage of the cloud, the expansion velocities become small and the HE approach may probably be applied.

2.3.5 Liquids

The models for (non-boiling) liquids neglect the vapour pressure of the liquid, being not higher than atmospheric.

Non-boiling liquids are liquids that have a normal boiling point higher than the ambient temperature, or refrigerated liquefied gases at (nearly) atmospheric pressure.

2.3.5.1 Introduction to liquids

In general the hydraulic pressure of the liquid is the driving force of a flow of a non-boiling liquid out of a vessel.

In case a liquid has been pressurised, the hydraulic pressure may be much smaller than the storage pressure, and the effect of the decreasing liquid level may be negligible. This is also true if pressurised liquefied gas has been set under pressure higher than the saturated vapour pressure.

The flow of liquids in orifices and in pipes, and the rather simple behaviour of liquid in a vessel, have been well established for many years. In the previous edition of the [YellowBook, 1988] models for liquid outflow through holes have been given, and so have laminar and turbulent flows of fluids in pipes (i.e. gases ánd liquids).

2.3.5.2 Vessel dynamics liquids

Applying the basic law of conservation of mass, and taking into account the hydraulic pressure of a liquid column, will suffice for an adequate description of the vessel dynamics.
The hydraulic pressure determining the mass flow rate depends on the liquid level in the tank. The only slightly complicating factor may be the estimation of the liquid level as function of the filling degree and geometry of the vessel. For simple geometries (sphere, cylinders) relations $h_L=F(V_L)$ exist.

2.3.5.3 Liquid flow through holes and piping

Well-known relations for the stationary outflow through orifices and through pipes exist. In the previous edition [YellowBook, 1988] models for laminar and turbulent flow of fluids have been given. More details can be found in section 2.5.

Simple analytical expressions exist for predicting the outflow rate through small holes in the vessel wall (punctures), as functions of time, in case the vessel has a simple geometric form. In Foster [1981], Lee [1987], Woodward [1991], Crowl [1993] and Sommerveld [1993], analytical expressions are inferred to compute the time it takes to empty vessels of different shapes: vertical cylinders, cone, horizontal cylinders, spheres, and other. In Hart [1993], equations are given to estimate liquid discharge amounts and rates from a flow opening at any arbitrary elevation. In figure 2.8 some examples of these models have been given.

Vertical cylinder

$$t = \frac{\pi D^2 \sqrt{h}}{\sqrt{8}\, C_d\, A_n\, \sqrt{g}}$$

Cone

$$t = \frac{\sqrt{2}\,\pi\, \tan^2\theta\, h^{5/2}}{5\, C_d\, A_n\, \sqrt{g}}$$

Horizontal cylinder

$$t = \frac{\sqrt{8}\, L\, (D^{3/2}-(D-h)^{3/2})}{3\, C_d\, A_n\, \sqrt{g}}$$

Sphere

$$t = \frac{\sqrt{2}\,\pi\, h^{3/2}(D-3/5h)}{3\, C_d\, A_n\, \sqrt{g}}$$

A_n = orifice area, ft² C_d = 0.61 for sharp-edged orifice
g = 32.2 ft/s²   = 0.80 for short, flush-mounted tube
t = time to empty, s   = 0.98 for rounded orifice
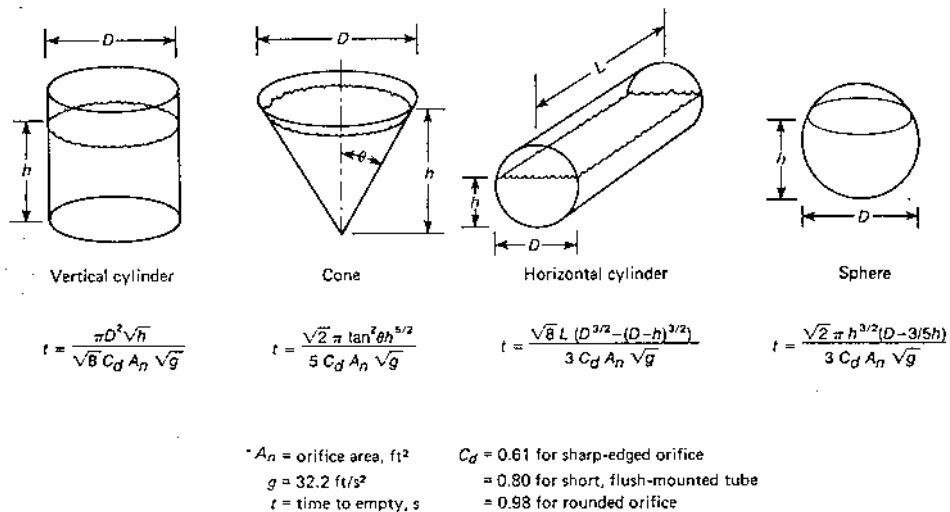
Figure 2.8   Time required to empty a vessel [Foster, 1981]

2.3.5.4 Non-stationary liquid flow in pipelines

No model has been found in open literature except the model in the previous edition of the [YellowBook, 1988]. This model is an approximate solution of the mass balance (continuity equation) and the momentum balance governing the liquid flow in a horizontal pipeline. It has been assumed that after the full bore rupture of the pipeline, a decompression wave is travelling upstream into the pipe. The liquid flow is assumed to be stationary between this upstream moving wave and the downstream pipe end.

The average isothermal compressibility of liquids between 1 and 1000 bar (10^5-10^8 N/m^2) is about:

$$\beta = 1.0 \times 10^{-9} \text{ m}^2/\text{N}$$

with

$$\beta = -1/V \times (\partial V/\partial P)_T \qquad (2.7)$$

This means that with pipe pressure below 200-300 bar ($2\text{-}3 \times 10^7$ N/m^2), the liquid volume has been compressed to a volume which is only a few percent smaller.
Due to the minor compressibility of liquids in general, it is advised to set the mass flow rate equal to the pump flow rate in case of a full bore rupture, taking into account less friction due to a smaller pipe length until the breakage. In case of a relatively small hole in the pipe wall, the outflow rate may be based on the initial pressure in the pipeline.

2.3.6 Friction factors

Friction factors have been given in the previous edition [YellowBook, 1988]. Additional information can be found in, for instance Melhem [1993] and Radford [1990].
The models for outflow through pipes have been developed for a pipe with no bends, reductions of cross-section or branches. If such fittings are present, they can be accounted for by introducing either an equivalent pipe length or extra resistance coefficients. In section 2.5 we put them together.

2.3.7 Physical properties of chemicals

Fluid flow and the vaporisation of liquids are controlled by thermodynamic laws and laws governing physical transport phenomena. Relations for thermophysical properties have been given for well-known commodities in many publications.

Pressure, volume, temperature (PVT) relationships for gases and liquids, and also solids would preferably all be summarised in the form of equations of state of the general type:

$$v = f(P,T) \qquad\qquad (m^3/mol) \qquad (2.8)$$

where

v	= specific volume	[m^3/mol]
P	= absolute pressure	[N/m^2]
T	= absolute temperature	[K]

In theory it is possible to derive the thermodynamic properties from an equation of state, like:

T_{fl}	= flash point	[K]
C_p	= specific heat	[J/(kg·K)]
ρ	= liquid density	[kg/m^3]
$P°$	= vapour pressure	[N/m^2]
H	= enthalpy	[J/kg]
S	= entropy	[J/(kg·K)]
L_v	= heat of vaporisation	[J/kg]

Only in the case of gases there has been much progress in the development of these state equations. They are obtained by correlation of empirical PVT data, and also from theoretical considerations based on atomic and molecular structure. The equation of state of gases will be addressed in more detail in section 2.5.

For compressible chemicals, gases and two-phase mixtures with vapour, the density depends strongly on pressure and temperature.
The physical properties of condensate phases, liquefied gases, liquids and solids, as well as the other physical properties of gases do not vary much as a function of pressure P at moderate pressures, and may be expressed as functions of temperature only. Temperature-dependent thermodynamic and physical transport properties of pure chemicals will be addressed in the annex to this Yellow Book.

Multi-component systems that act as a multi-phase system at given pressure, temperature and composition will not be addressed because they demand specific treatment.
Mono-phase multi-component mixtures can be treated as quasi one-component systems only in case of ideal mixing, meaning using average values for the physical properties proportional to the weight fractions of the chemical in the mixture.

2.4 Selection of models

2.4.1 Introduction to section 2.4

In section 2.4 the considerations which have led to the selection of the models that are included in section 2.5, are explained. In section 2.5 these models will be described in detail. In general the selection is based on the following considerations.

Safety studies and hazard assessment require models that are reasonably accurate, demand little computational effort and not too much input.
Larger computational demands of the model are acceptable only if the accuracy of the predictions will be much greater and/or when the model has a (much) wider range of applicability.
Needless complicated models that mainly make an additional scientific contribution should be avoided, yet we must not close our eyes to future developments.

Leaving all models relying on computational fluid dynamics (CFD) behind, two main practical approaches may be distinguished:

1. Simple models, such as approximating analytical expressions and empirical correlations, meant for predictions of maximum and averaged flow rates and duration of the outflow.

2. Numerical procedures without approximating sub-models, meant for predictions of the outflow rate as function of time.

The analytical equations may be used to get a quick estimate of the magnitude of the outflow rate. These models are based on simplifying assumptions like: perfect gas behaviour, constant physical properties, and unchanged boundary conditions.
A numerical approach takes into account changes of the physical properties as a function of temperature and pressure, non-perfect gas and liquid behaviour, and 'sudden' changes in boundary conditions.

The (specific) considerations that have lead to the selection of the models to be described in section 2.5, are presented as follows:
− sub-section 2.4.2 addresses models for gases;
− sub-section 2.4.3 addresses models for releases of pressurised liquefied gases, including spray releases;
− sub-section 2.4.4 addresses models for releases of (non-boiling) liquids.

2.4.2 Gases

The well-known relations for the stationary critical and non-critical outflow of gases through orifices and through pipes are as in the previous edition of the YellowBook [1988].

There is not much discussion about applying standard thermodynamics for the description of vessel dynamics, as will be described in section 2.5.
We have opted for numerical models, because these models are still relatively simple, and are able to cope with varying physical properties and sudden changes in constraints.

The model for non-stationary gas flow in pipelines in the previous edition of the [YellowBook, 1988] was not validated, has a bad performance, and seems numerically unsound. The Wilson correlation has good performance and is rather simple [Hanna, 1987]. This model will be described in section 2.5.

The Weiss correlation [Weiss, 1988] for small holes in pipelines is the only model found in open literature. Therefore it will be described in chapter 2.5.

No model to cope with crater formation, in case of leaks from buried pipelines, is publicly available, therefore no model can be included in section 2.5.

Vapour outflow

The models for outflow of gas through holes and piping are valid for pure vapour flowing out of the vapour section in the containment for vaporising pressurised liquefied gases.

2.4.3   Pressurised liquefied gases

2.4.3.1   Vessel dynamics pressurised liquefied gases

The depressurising of a pressurised liquefied gas causes bubble formation in the liquid and thus expansion of the boiling liquid is a rather complex phenomenon.
A large computer model has been given in Haque [1992].
Because other models are much more complex and obviously do not have a (much) better performance, it would be advisable to use the Fauske correlation to determine whether there exists a two-phase flow inside the vessel or not [Fauske, 1988]. This model is simple and based on experimental data for horizontal cylinders and spheres. In Melhem [1993] a refined DIERS-method has been described that distinguishes different ways of boiling for top venting and relations to estimate the quality in the outflow opening for vertical vessels. In Sheppard [1993] it appears that this analytical solution of the DIERS-method validates the Fauske correlation, but this analytical solution is also able to predict disengagement, regardless of vessel shape.
So the DIERS-method is to be preferred, being more generally applicable and not much more complicated. In chapter 2.5 the analytical DIERS-method is described.

A comparison of the results of both models in Haque [1992] shows that the correlation of Mayinger [Belore, 1986] may well be used for the estimation of the void fraction in relatively small vessels. The present state of knowledge about the effects of bulk liquid sub-cooling on mitigating the liquid swell, permits only case by case numerical solutions involving sizeable computer programs [Sallet, 1990,3].

Therefore, due to lack of a better and also manageable model, it is advised to apply the correlation of Mayinger, also for larger vessels.

The fact that the void fraction in the top of the vessel venting may be much higher than the average value, can only be coped with by applying very complicated models. Although the behaviour of a depressurising pressurised liquefied gas is a complex process, we choose to describe a model based on standard thermodynamics, taking into account the criteria of DIERS and Mayinger.

We have opted for a numerical model, instead of analytical solutions, because these models are still relatively simple, but are able to cope with varying physical properties and sudden changes in constraints, predicted by the criteria of DIERS and Mayinger. This approach will be described in section 2.5.

2.4.3.2   Stationary outflow of vapour through holes and piping

The well-known relations for the stationary critical and non-critical outflow of gases through orifices and through pipes are valid for one-phase vapour flow, and will be described in section 2.5.

2.4.3.3   Two-phase outflow through holes and piping

Giot et al. have carried out a benchmark on two-phase-flow models, within the European Union program 'Major Technological Hazards', on the basis of selected well-documented and reliable data sets [Giot, 1992].

The benchmark has led to the conclusion that most models presented in open literature have a limited validity range.

The main conclusions are:
1. Only Flinta's model has a acceptable performance on all ranges,
2. 'Homogeneous Equilibrium Models' (HEMs) generally underpredict.

However, a very limited number of data points related to fluids other than water were included in the database and have been used for model validation [Giot,1992].

The TPDIS-model has been selected because of:
1. HEM is broadly accepted, and according to Giot [1996] HEMs will give reasonable predictions if the quality $\phi_{m,e}$ is larger than 1%,
2. TPDIS is a complete model, well-described in open literature.

Flinta's model has not been selected because of:
1. Its general applicability has not been proven,
2. Some quantities in the required formulae cannot be easily obtained or derived.

It is advised to use TPDIS and other HEMs for those situations for which they have been validated.

2.4.3.4 Non-stationary two-phase flow in pipelines

Having presumably a low accuracy and a not very robust numerical solution procedure, and not being validated, any simpler and validated model is to be preferred to the previous Yellow Book model.

A generally applicable model is necessary. Therefore the model given in Morrow [1983] will be described in section 2.5. This model has been derived for propane, but could be generalised by using appropriate physical properties.

While propane is often transported in pipelines, the specific correlation given in Tam [1990] will also be described in this section.

2.4.3.5 Finite duration spray releases

Expansion and flashing at atmospheric pressure

The selected model to calculate the conditions after flashing is based on the conventional, generally accepted model using the equations (2.1a-d) provided in section 2. No correction is applied for non-equilibrium flash fractions because of lack of consensus on this subject.

Droplet diameter after flashing

The proposed model for initial droplet size is based on the work by Appleton [1984] and presented by Wheatley [1987]. These expressions are relatively simple to use and Appleton [1984] compared the proposed dropsize correlations with available experimental data. He concludes (for his case, a water/steam mixture at 192 ˚C, 0.8 mm orifice) that there is reasonable agreement between the correlations and experimental data.
The correlations are different for shattered and non-shattered jets. The criterion for shattering follows the suggestions by Appleton with $C_\varepsilon = 0.1$.

Droplet evaporation and rain-out on the ground

The proposed methodology to predict droplet rain-out from a two-phase jet is:
1. To refrain from the description of binary droplet evaporation in view of uncertainty in exit droplet size and the moderate reductions in drying times according to Vesala [1990];
2. First to determine whether droplets at the end of the flashing zone will reach the ground using Kukkonen's [1990] limiting radius;
3. If the droplets in the jet exceed the limiting droplet radius, then calculate the evaporated mass fraction until the droplet hits the ground. The deposited mass fraction is subtracted from the liquid mass entering the vapour jet, and will form an evaporating pool. For these evaporation calculations, use is made of the expressions by Kukkonen [1990] assuming evaporation in pure air. Only velocity differences between droplet and air due to settling are considered, the horizontal velocity of the jet and the droplet are assumed to be the same.

Jet dispersion

It is assumed that the two-phase jet after flashing can be treated as a single-phase jet with respect to width, entrainment, and evolution of concentration and velocity on the jet centre line.
This leads to the conclusion that the single-phase vapour jet model as described in chapter 4 is applicable, using the jet diameter after flashing as the exit condition.

Evaporation of the droplets in the jet

The evaporation of droplets remaining in the jet due to the heat brought into the jet by entrained air is relevant to determine the density of the jet. In order to calculate the conditions in the jet after evaporation of the aerosols, use will be made of the homogeneous equilibrium model. It has been demonstrated that the homogeneous equilibrium model may be used for droplets less than 100 μm in clouds. The essence of the homogeneous equilibrium method is the use of the integral balance for the enthalpy in the jet (2.4) in section 2.3.4.6, and neglecting temperature differences between the two-phases.

2.4.3.6   Instantaneous release of pressurised liquefied gas

Flashing and initial cloud expansion

The flash fraction is calculated assuming isentropic flashing. The expansion velocity is calculated using the enthalpy balance (2.5), but multiplied by 0.8 to account for turbulence and non-isentropy. This factor is justified by the available experimental data.

Expansion of the aerosol cloud during the entrainment phase

For the evolution of cloud size the simple model as presented in section 2.3.4.7 is selected because there is no evidence that more complex and advanced models provide better results compared to the scarce data. The concentration in the cloud is assumed to be uniform.

Droplet size and rain-out on the ground

By absence of alternatives and considering an instantaneous airborne vapour cloud to give conservative results, it is assumed that a total mass of twice the isentropic flash fraction (in addition to the initial vapour mass in storage) will remain airborne.
This simple model makes no use of droplet diameter, so no model for calculating the droplet diameter after flashing has been selected.

Evaporation of the droplets in the cloud

The conditions in the cloud at the moment when all aerosols have evaporated, are calculated by using exactly the same methods as included in the two-phase jet model (section 2.3.4.6).
The self-driven expansion of the cloud is assumed to have ended when all aerosols have evaporated **and** the expansion velocity is equal to the ambient wind speed at the height of the initially expanded cloud just before entrainment starts.

2.4.4   Liquids

Since there is not much discussion about which models to apply for liquid flow through holes and pipes, and the behaviour of liquid vessels, the standard approach will be followed in section 2.5.

Most analytical models for liquid vessel dynamics suffice, although the expressions are not always simple to calculate and integral tables might be needed. We have opted for numerical models for the description of vessel dynamics in order to be able to maintain the same approach as in the previous paragraphs.

A specific model for non-stationary liquid flow in pipelines is not considered relevant.

2.5 Description of models

2.5.1 Introduction to section 2.5

Section 2.5 provides descriptions of the recommended models for releases of compressed gases, pressurised liquefied gases and (non-boiling) liquids.
It contains all necessary information to perform the calculations. For background of the models the reader may refer to section 2.3.
Section 2.5 provides detailed descriptions of the models and methods for the following releases:
− subsection 2.5.2 addresses models for releases of gases;
− subsection 2.5.3 addresses models for releases of pressurised liquefied gases, including spray releases;
− subsection 2.5.4 addresses models for releases of non-boiling liquids.
Finally, friction factors for pipe flow will be given in subsection 2.5.5.

Guide to the calculations

First, the reader must determine the state of the chemical in its containment, by means of the criteria given in subsection 2.2.3 and summarised in the diagram 2.4.

Diagram 2.4   Thermodynamic states

Thermodynamic state	Physical conditions
I. compressed gas	$T > T_c$ or $P < P_v°(T)$
II. pressurised liquefied gas	$P = P_v°(T)$
III. (non-boiling) liquid	$T_m < T < T_B(P)$

Secondly, the reader should check the failure mode of the containment.

Models are available in this section for the outflow conditions listed in the diagram below.

Diagram 2.5   Models available

Outflow condition	Paragraphs
I. compressed gas (2.5.2)	
A.1. outflow from vessel through small leak	(2.5.2.2)
a) hole in vessel wall	(2.5.2.3)
b) break of piping	(2.5.2.4)
B.1. outflow from pipeline through small leak	(2.5.2.5)
B.2. outflow from full bore ruptured pipeline	(2.5.2.5)
II. pressurised liquefied gas (2.5.3)	
A.1. outflow from vessel through small leak	(2.5.3.2/3)
a) hole in vessel wall	(2.5.3.4)
b) break of piping	(2.5.3.5)
A.2. totally ruptured vessel	(2.5.3.8)
B.1. outflow from pipeline through small leak	(2.5.3.6)
B.2. outflow from full bore ruptured pipeline	(2.5.3.6)
III. (non-boiling) liquid (2.5.4)	
A.1. Outflow from vessel through small leak	(2.5.4.1)
a) hole in vessel wall	(2.5.4.2)
b) break of piping	(2.5.4.2)

No models are available in this section for the outflow conditions listed in diagram 2.6.

Diagram 2.6   Models not available

Outflow condition
I. compressed gas (2.5.2)
A.2. totally ruptured vessel
III. (non-boiling) liquid (2.5.4)
A.2. totally ruptured vessel
B.1. outflow from pipeline through small leak
B.2. outflow from full bore ruptured pipeline

A total rupture of a vessel filled with compressed gas leads to a cloud that expands to atmospheric pressure. No models have been found to estimate the amount of air

entrained during the expansion. Most atmospheric dispersion models assume that the initial cloud has not been diluted.

A total rupture of a vessel filled with non-boiling liquid leads to a spreading pool on the ground or on a water surface. The release phenomena are taken into account in these pool spreading models.

In section 2.4.4 arguments were given for not describing models for (long) liquid pipelines. The equations given in subsection 2.5.4.2 may be used.

2.5.2 Compressed gases

2.5.2.1 Equation of state for gases

Because gases are compressible, the gas density $\rho(P)$ as a function of the gas pressure P must be known.
The equation of state of a perfect gas is given by:

$$P \times V = n \times R \times T \hspace{3cm} \text{(J)} \hspace{2cm} (2.9a)$$

or

$$v = R \times T/(P \times \mu_i) \hspace{3cm} \text{(m}^3\text{/kg)} \hspace{1cm} (2.9b)$$

note that

$$v = 1/\rho \hspace{8cm} (2.9c)$$

where

P	= absolute gas pressure	[N/m^2]
T	= absolute temperature	[K]
R	= gas constant	[J/(mol·K)]
n	= number of moles	[-]
v	= specific volume	[m^3/kg]
V	= volume	[m^3]
μ_i	= mol mass of gaseous chemical i	[kg/mol]
ρ	= density	[kg/m^3]

The perfect gas equation describes the PVT behaviour of real gases only to a first approximation.

A way of showing the deviations from ideality is to write for the real gas:

$$P \times V = z \times n \times R \times T \hspace{2.5cm} \text{(J)} \hspace{2cm} (2.10a)$$

or

$$v = z \times R \times T/(P \times \mu_i) \hspace{2.5cm} \text{(m}^3\text{/kg)} \hspace{1cm} (2.10b)$$

where

z   = compressibility factor [-]

The factor z is called compressibility factor, although this might be confusing because the factor z has no relation with the compressibility of a gas. The German term 'Realgasfaktor' is more plain [Gasunie, 1980]; the factor z expresses the departure from the perfect gas behaviour with one single factor.

The compressibility factor appears to be a universal function of the so-called reduced temperature and pressure:

$$z = f(P_R, T_R) \qquad\qquad (-) \qquad\qquad (2.11)$$

with

$$P_R = P/P_c \qquad\qquad (-) \qquad\qquad (2.11a)$$

$$T_R = T/T_c \qquad\qquad (-) \qquad\qquad (2.11b)$$

where

P_R = reduced pressure   [-]
P_c = critical pressure of the chemical   [N/m^2]
T_R = reduced temperature   [-]
T_c = critical temperature of the chemical [K]
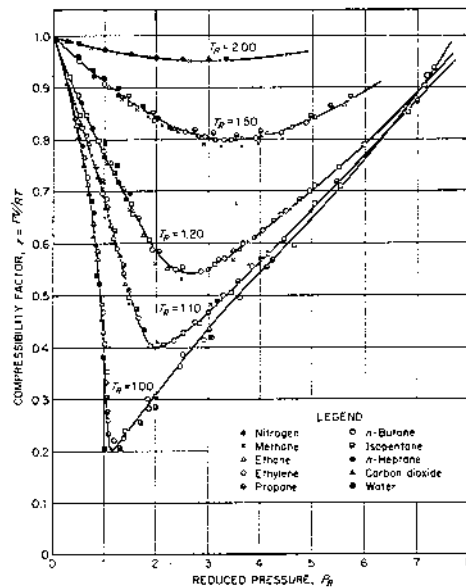
Figure 2.9   *Compressibility factor as function of reduced state variables by Gouq-Jen Su [Moore, 1972]*

For perfect gases the compressibility factor z equals unity. It is noted that most deviation from perfect gas behaviour occurs near the thermodynamic critical pressure

and critical temperature. In general for real gases the compressibility factor z is about unity for high temperature and low pressures.

Other classical equations of state for real gases are those by Van der Waals and Berthelot. The Van der Waals equation [Moore,1972] may be expressed as:

$$(P_R + 3/V_R{}^2) \times (V_R-1/3) = 8/3 \times T_R \qquad\qquad (2.11c)$$

with

$$V_R = V/V_c \qquad\qquad (\text{-}) \qquad (2.11d)$$

and

$$V_c = 3/8 \times R \times T_c/P_c \qquad\qquad (m^3/mol) \quad (2.11e)$$

where

V_c = critical volume $[m^3/mol]$
V_R = reduced volume   [-]

In Leung [1988] the Redlich-Kwong-equation of state for gases has been used.
Also viral equations may be used to represent the behaviour of gases with greater accuracy, having more adjustable coefficients.
The Starling-Han equation and chemical dependent coefficients have been presented in [Edminster, 1984]. In Morrow's model the Starling equation is used, see paragraph 2.5.3.6.

2.5.2.2   Vessel dynamics compressed gas

The modelling of the dynamics of compressed gas stored in a vessel aims at predicting the decrease of pressure and temperature due to the outflow of gas.
Due to the release of gas the remaining gas in the vessel will expand. This expansion causes cooling and depressurisation.

The model is basically an iterative numerical procedure in which the outflow of gas out of a vessel is described in small steps. These steps should be small enough to consider the conditions in the vessel to be constant during one time-step.
First, the initial condition and termination condition of the numerical procedure will be given. After this the model in the form of a numerical procedure is given. This numerical procedure has to be repeated until the termination conditions will have been satisfied.
Afterwards, the inference is given of the system equation governing the behaviour of the compressed gas in the vessel used in the model.

The initial and termination condition of the numerical procedure concerning gas outflow

The initial condition of the vessel is given by: P_1, T_1, ρ_1, meaning i=1.
The duration of δt may freely be chosen in principle, and depends of the number of

time-steps N_t. When one wishes to estimate the mass flow rate and vessel conditions at time t_{end}, then the size of time step δt is given by

$$\delta t = t_{end}/N_t \qquad \qquad \text{(s)} \qquad \text{(2.12)}$$

t   = time from the start of the outflow [s]

The larger the number of steps, the higher the accuracy of the model, but the more time needed for the calculation. The choice N_t=50 will be appropriate for most calculations.

The numerical procedures given should be repeated as long as the constraints are valid:

$$t_i < t_{end} \qquad \qquad P > P_a \qquad \qquad T > T_m \qquad \text{(2.13)}$$

The model for gas outflow: a numerical procedure

Starting every step at time t_i in the iteration with a condition in the vessel given by P_i, T_i, ρ_i, the following procedure aims at calculation of the condition in the vessel at the end of the small time-step δt, given by P_{i+1}, T_{i+1}, ρ_{i+1}.

Let us say that the outflow rate $q_{S,i}$ is given by a generalised function f, depending on whether the outflow is through a hole (see paragraph 2.5.2.3) or a pipe (see paragraph 2.5.2.4)

$$q_{S,i} = f(P_i,T_i,\rho_i,...) \qquad \qquad \text{(kg/s)} \qquad \text{(2.14)}$$

Due to the gas release in period δt, the density in the vessel decreases

$$\delta\rho = - q_{S,i}/V \times \delta t \qquad \qquad \text{(kg/m}^3\text{)} \qquad \text{(2.15)}$$

$$\rho_{i+1} = \rho_i + \delta\rho \qquad \qquad \text{(kg/m}^3\text{)} \qquad \text{(2.16)}$$

$$t_{i+1} = t + \delta t \qquad \qquad \text{(s)} \qquad \text{(2.17)}$$

These steps should be small enough to consider the conditions in the vessel to be constant during one time-step.

Due to the decrease of the gas density, the gas will expand and the gas temperature will decrease; applying the system equation (see Intermezzo below) gives

$$\delta T = P_i/(\rho_i^2 \times C_v) \times \delta\rho \qquad \qquad \text{(K)} \qquad \text{(2.18)}$$

$$T_{i+1} = T_i + \delta T \qquad \qquad \text{(K)} \qquad \text{(2.19)}$$

The change in density and temperature of the gas forces the pressure to adapt to the new conditions according to the equation of state of (non-perfect) gases given by equation (2.10b)

2.66

$$P_{i+1} = z \times \rho_{i+1} \times R \times T_{i+1}/\mu_j \qquad (N/m^2) \qquad (2.20)$$

with

$$z = z(P_{R,i}, T_{R,i}) \qquad (-) \qquad (2.21)$$

The new condition of the vessel at time t_{i+1} given by: P_{i+1}, T_{i+1}, ρ_{i+1}.
As long as the termination condition has not been fulfilled, this procedure has to be repeated.

Intermezzo: inference of the system equation (2.18) for compressed gases

The equations without a reference number in this paragraph are only part of the inference of the system equation that is required.
Applying the first law of thermodynamics and using the definition of volumetric work done by an expanding gas, gives

$$\Delta U = Q_H - \int P \times dv \qquad (J/kg) \qquad (2.18a)$$

where

ΔU	= change in internal energy of the gas	$[J/kg]$
P	= gas pressure	$[N/m^2]$
v	= specific volume of the gas	$[m^3/kg]$
Q_H	= heat transferred into 1 kg gas	$[J/kg]$

Note that the internal energy U is given per unit mass in the vessel.

Assuming reversible adiabatic outflow results in

$$\delta U = P \times \delta V \qquad (J/kg) \qquad (2.18b)$$

δX = small change in quantity X

Neglecting the internal pressure of non-perfect gases gives a relationship between the internal energy of gas and its temperature

$$\delta U = C_v(T) \times \delta T \qquad (J/kg) \qquad (2.18c)$$

C_v = specific heat at constant volume the gas $[J/(kg.K)]$

Using the definition of density ρ and combining the equations leads to the system equation that governs the behaviour of the gas in the vessel, namely

$$C_v \times \delta T = P/\rho^2 \times \delta\rho \qquad (J/kg) \qquad (2.18d)$$

ρ = density $[kg/m^3]$

2.5.2.3   Gas outflow through holes

The modelling of the outflow of gas through holes aims at predicting the mass flow rate as a function of pressure drop over the hole.

The mass flow rate for gas outflow through an orifice can be estimated by a generalised equation

$$q_S = C_d \times A_h \times \psi \times \sqrt{(\rho_0 \times P_0 \times \gamma \times (2/(\gamma + 1))^{(\gamma + 1)/(\gamma - 1)})} \quad \text{(kg/s)} \qquad (2.22)$$

The factor ψ^2 is given by equation (2.24) or (2.25) below, and depends on whether the gas outflow is choked (critical) or not.

The outflow is critical or choked when

$$P_0/P_a \geq ((\gamma+1)/2)^{(\gamma/(\gamma-1))} \qquad\qquad (-) \qquad (2.23)$$

For critical outflow

$$\psi^2 = 1 \qquad\qquad (-) \qquad (2.24)$$

and for sub-critical outflow

$$\psi^2 = 2/(\gamma-1) \times ((\gamma+1)/2)^{(\gamma+1)/(\gamma-1)} \times (P_a/P_0)^{2/\gamma} \times (1-(P_a/P_0)^{((\gamma-1)/\gamma)})$$
$$\qquad\qquad (-) \qquad (2.25)$$

with

$$\gamma = C_p/C_v \qquad\qquad (-) \qquad (2.26)$$

where

q_S	= mass flow rate	[kg/s]
C_d	= discharge coefficient	[-]
A_h	= cross-sectional area hole	[m^2]
ψ	= outflow coefficient	[-]
ρ_0	= initial gas density	[kg/m^3]
P_0	= initial gas pressure	[N/m^2]
γ	= Poisson ratio	[-]
C_p	= specific heat at constant pressure	[J/(kg·K)]
C_v	= specific heat at constant volume	[J/(kg·K)]

For most gases $1.1<\gamma<1.4$ and the outflow will be critical when $P_0/P_a > 1.9$.

$$(2.23a)$$

The discharge coefficient C_d is in fact determined by two factors: friction and contraction.

$$C_d = C_f \times C_c \qquad\qquad (-) \qquad (2.27)$$

where

C_f	= friction coefficient	[-]
C_c	= contraction coefficient	[-]

Contraction is caused by the fact that the fluid in the vessel is flowing into the opening from all directions, having a velocity component perpendicular to the axis of the opening. The flowing fluid must be bent in the direction parallel to the hole axis. The

inertia of the fluid results in the smallest cross-sectional area, with no radial acceleration, that is smaller than the area of the opening.
For sharp orifices contraction plays a part and friction is negligible;
The following value for the discharge coefficient is recommended [Beek, 1974]:

$$C_d \approx 0.62 \qquad\qquad\qquad (2.28a)$$

For rounded orifices contraction does not play a part and friction is small;
The following value for the discharge coefficient is recommended [Beek, 1974]:

$$C_d \approx 0.95 - 0.99 \qquad\qquad\qquad (2.28b)$$

Vapour outflow

The models for outflow of gas from holes are valid for pure vapour flowing out of the vapour section in the containment for vaporising pressurised liquefied gases, as long as no condensation of the vapour occurs. This means that the pressure of the vapour may not become higher than its saturation pressure at given temperature.

2.5.2.4   Gas outflow through piping

The modelling of the outflow of gas through piping aims at predicting the mass flow rate as a function of the pressure drop over the piping. This mass flow rate is mainly determined by the overpressure in the vessel and the flow resistance.

Principles of the model for gas flow in piping

The total pressure drop ΔP between the vessel and the ambient is equal to the pressure drop over the pipe and the pressure drop over the downstream opening in the pipe

$$\Delta P \quad = P_0 - P_a \qquad\qquad (N/m^2) \qquad (2.29a)$$

$$= (P_0 - P_e) - (P_e - P_a)$$

$$= \Delta P_{pipe} - \Delta P_{hole}$$

with

$$\Delta P_{hole} = P_e - P_a \qquad\qquad (N/m^2) \qquad (2.29b)$$

$$\Delta P_{pipe} = P_0 - P_e \qquad\qquad (N/m^2) \qquad (2.29c)$$

where

ΔP_{pipe} = pressure drop in the pipe $\qquad$ [N/m^2]
ΔP_{hole} = pressure drop in the hole $\qquad$ [N/m^2]
P_e $\quad$ = the (unknown) pressure at the downstream end
$\qquad$ of the pipe, just before the outflow opening $\qquad$ [N/m^2]
P_0 $\quad$ = stagnant (initial) pressure at the upstream end
$\qquad$ of the pipe, in the vessel $\qquad$ [N/m^2]
P_a $\quad$ = atmospheric pressure $\qquad$ [N/m^2]

The pressure P_e at the end in the pipe just before the pipe opening to the atmosphere is initially unknown.
The mass flow through the pipe $q_{S,pipe}$ is controlled by the pressure drop over the pipe and the mass flow through the pipe opening $q_{S,hole}$ is controlled by the pressure drop over the pipe opening. The law of conservation of mass requires the mass flow through the pipe $q_{S,pipe}$ to be equal to the mass flow through the hole $q_{S,hole}$ (or pipe opening). Thus, the condition that must be fulfilled is given by

$$q_{S,pipe}(\Delta P_{pipe}) = q_{S,hole}(\Delta P_{hole}) \qquad \text{(kg/s)} \qquad (2.30)$$

In conclusion, in the estimation of the mass flow through the pipe, the pressure just inside the pipe P_e must be determined. The governing set of equations can be solved by trial and error, by guessing the internal pressure in the pipe just before the pipe opening P_e.

The model for gas flow in piping: a numerical procedure

1. Guess the internal pressure P_e at the downstream end of the pipe, just before the outflow opening: $P_a < P_e < P_0$

2. Calculate the mass flow through a pipe opening or a hole in the pipe wall, with respect to the condition formulated by equations (2.29a-c).
   The mass flow rate $q_{S,hole}$ in the opening in the pipe can be estimated by using the equations in paragraph 2.5.2.3. In case of a full bore pipe rupture the mass flow rate in the pipe opening $q_{S,hole}$ can be estimated by assuming the pipe opening having the diameter of the pipe; then a discharge coefficient $C_d = 1.0$ is advised to be used in the calculation, Beek [1974]. For smaller holes the standard model for outflow through an orifice is valid, and a value for discharge coefficient $C_d = 0.62$ is recommended.

3. Calculate the mass flow rate through the pipe $q_{S,pipe}$ by equation (2.31) and related equations, as has been derived in the following subparagraph.

The mass flow rate through a pipe as function of the pressure at both pipe ends can be calculated by (see Intermezzo)

$$q_S = A_p \sqrt{\frac{2 \times \int_{P_0}^{P_e} \rho(P) \times dP}{4f_F \times l_p/d_p}} \qquad \text{(kg/s)} \qquad (2.31)$$

2.70

with

$$\rho = C \times (P/z)^{1/\zeta} \qquad\qquad (kg/m^3) \qquad (2.32)$$

$$\zeta = 1 + z \times R/(C_v \times \mu_i) \qquad\qquad (\text{-}) \qquad (2.33)$$

where

C = constant

Note that for perfect gas behaviour (z=1)

$$\zeta = \gamma \qquad\qquad (\text{-}) \qquad (2.33b)$$

The integral may be solved simply by numerical methods, but also analytically assuming constant compressibility factor, for instance $z = 1$, and constant specific heat at constant volume C_v:

$$\int_{P_0}^{P_E} \rho(P) \times dP \approx P_o \times \rho_o \times (\zeta/(1+\zeta)) \times ((P_e/P_o)^{((1+\zeta)/\zeta)} - 1)$$

$$(kg^2/(m^4 \cdot s^2)) \; (2.31a)$$

4. Compare those two mass flow rates $q_S(\Delta P_{pipe})$ and $q_S(\Delta P_{hole})$. If not equal repeat procedure.

A more convenient way to solve equation (2.30) is to use a root finding procedure by defining

$$F(P_e) \quad = q_{S,pipe}(\Delta P_{pipe}) - q_{S,hole}(\Delta P_{hole}) \qquad\qquad (kg/s)$$

$$= q_{S,pipe}(P_0\text{-}P_e) - q_{S,hole}(P_e\text{-}P_a) \qquad\qquad (kg/s) \qquad (2.30a)$$

The principle is still the same, but the determination of the right P_e is much quicker.

Intermezzo: inference of the equation (2.31) describing the mass flow rate of gas flow in a pipe

The total pressure drop for a stationary fluid flow (gases and fluids) in piping can be estimated by the well-known Darcy-Weisbach equation

$$\Delta P \quad = f_D \times \rho_g/2 \times u_g^2 \times l_p/d_p \qquad\qquad (N/m^2) \qquad (2.198a)$$

This relation does not account for the effect of the pressure drop on the density of the gas, which consequently will expand. In the following the equation will be inferred which relates the mass flow rate q_S of a gas in a pipe to the pressure drop in the pipe. Reformulated for the local pressure drop along the pipe the relation gives

$$\delta P/\delta l_p = f_D \times \rho_g/2 \times u_g^2/d_p \qquad\qquad (N/m^3) \qquad (2.198b)$$

where

f_D = Darcy friction factor [-]
ρ_g = gas density [kg/m³]
u_g = gas velocity [m/s]
l_p = pipe length [m]
d_p = pipe diameter [m]
ΔP = total pressure drop over the pipe [N/m²]

The Darcy friction factor f_D is a function of the inside wall roughness of the pipeline and the Reynolds number (see section 2.5.5).
The gas velocity u is determined by the mass flow rate in the pipe by

$$u_g = q_S / (\rho_g \times A_p) \qquad \text{(m/s)}$$

Integrating over the pipe length results in

$$\int_{P_0}^{P_e} \rho(P) \times dP = f_D \times l_p / d_p \times (q_s / A_p)^2 / 2 \qquad \text{(kg}^2/(\text{m}^4 \cdot \text{s}^2)) \qquad (2.34)$$

The calculation of the integral on the left-hand side of equation (2.34) requires an expression for the gas density as a function of the local pressure in the pipe: $\rho(P)$.

When the equation of state of a non-perfect gas is given by equation (2.10a) and (2.11)

$$P \times V = z(P_R, T_R) \times R \times T \qquad \text{(J)}$$

Then, an adiabatic expansion of a non-perfect gas may be described by

$$P \times V^\zeta / z \approx C^* \qquad (2.32a)$$

with

$$\zeta = 1 + z \times R / (C_v \times \mu_i) \qquad \text{(-)} \qquad (2.33)$$

where

$$C^* = \text{constant } ((\text{N/m}^2) \cdot \text{m}^{3\zeta})$$

And thus the integral on the left-hand side of equation (2.34) can be calculated using

$$\rho = C \times (P/z)^{1/\zeta} \qquad (2.32)$$

where

$$C = \text{constant}$$

The mass flow rate through a pipe as a function of the pressure at both pipe ends can now be calculated by using equations (2.33) and (2.32) and

$$q_{S,pipe} = A_p \sqrt{\frac{2 \times \int_{P_0}^{P_e} \rho(P) \times dP}{f_D \times l_p / d_p}} \qquad \text{(kg/s)} \qquad (2.31)$$

2.72

Vapour outflow

The models for outflow of gas through piping are valid for pure vapour flowing out of the vapour section in the containment for vaporising pressurised liquefied gases, as long as no condensation of the vapour occurs. This means the pressure of the vapour may not become higher than its saturation pressure at given temperature.

2.5.2.5   Non-stationary gas flow in pipelines

After a sudden rupture at one end of the pipeline, a pressure wave will start moving with the speed of sound in the pipeline in the opposite (upstream) direction.

Non-stationary gas flow in pipelines after a full bore rupture

The Wilson model of the outflow of gas through pipelines aims at predicting the mass flow rate as a function of time depending on the initial conditions.
The model assumes a compressor to trip when the decompression wave in the pipeline reaches the compressor station at the other pipe end.

The mass flow rate for a full bore ruptured pipeline according to the empirical model of Wilson [Hanna, 1987] is given by

$$q_S(t) = q_{S,0}/(1+Q_0/(t_B \times q_{S,0})) \times \{Q_0/(t_B \times q_{S,0}) \times \exp(-t/t_B) + \exp(-t \times t_B \times (q_{S,0}/Q_0)^2)\}$$
$$\text{(kg/s)} \qquad \text{(2.35)}$$

where

$q_{S,0}$ = initial mass flow (discharge) rate   [kg/s]
Q_0 = initial total gas mass in the pipeline   [kg]
t_B = time constant   [s]

1. The initial total mass Q_0 in the pipeline can be calculated by

$$Q_0 = \rho_0 \times A_p \times l_p \qquad\qquad\qquad \text{(kg)} \qquad \text{(2.36a)}$$

with

$$A_p = \pi/4 \times d_p{}^2 \qquad\qquad\qquad\qquad \text{(m}^2\text{)} \qquad \text{(2.36b)}$$

2. The initial release rate $q_{S,0}$ can be calculated by using the equations presented in paragraph 2.5.2.4

$$q_{S,0} = C_d \times A_p \times \psi \times \sqrt{(\rho_0 \times P_0 \times \gamma \times (2/(\gamma+1))^{(\gamma+1)/(\gamma-1)})} \quad \text{(kg/s)} \qquad \text{(2.37)}$$

For outflow through the pipe opening in case of a full bore rupture it is advised to use the following value for the discharge coefficient

$$C_d = 1.0 \qquad\qquad\qquad\qquad\qquad \text{(-)} \qquad \text{(2.38)}$$

3. The sonic velocity in the gas u_s, assuming adiabatic expansion ($\Delta S = 0$) is given by

$$u_s = \sqrt{(dP/d\rho)_s} \qquad\qquad \text{(m/s)} \qquad (2.39a)$$

Using the equations of state for non-perfect gases given in paragraph 2.5.2.4 results in

$$d\rho/dP = \rho/(\zeta \times P) \qquad\qquad (s^2/m^2) \qquad (2.39b)$$

which results for non-perfect gases in

$$u_s = \sqrt{(\zeta \times z \times R \times T_0 / \mu_i)} \qquad\qquad \text{(m/s)} \qquad (2.39c)$$

4. The Darcy friction factor may be calculated by the Colebrook-White equation, approximated for high Reynolds numbers, by

$$f_D = \{ 1/(-2 \times {}^{10}\log(\varepsilon/(3.715 \times d_p))) \}^2 \qquad\qquad (-) \qquad (2.40)$$

5. The time constant t_B is given by

$$t_B = 2/3 \times l_\rho / u_s \times \sqrt{(\gamma \times f_D \times l_\rho / d_\rho)} \qquad\qquad \text{(s)} \qquad (2.41)$$

6. Finally the mass flow rate $q_S(t)$ can be estimated at any time t after the full bore rupture of the pipeline by the Wilson model given by equation (2.35).

7. Check the validity of the model.
   When the pressure wave travelling upstream reaches the opposite side of the pipeline the Wilson model is not valid any more. This is the case when

$$t_E = l_p / u_s \qquad\qquad \text{(s)} \qquad (2.42)$$

The following symbols used in this paragraph have not been mentioned earlier:

d_p	= pipe diameter	[m]
l_p	= pipe length	[m]
Q_0	= initial mass content in the pipeline	[kg]
P_0	= initial (operating) pressure in pipeline	[N/m^2]
$q_{S,0}$	= initial mass flow (discharge) rate	[kg/s]
T_0	= initial temperature	[K]
t	= time after rupture	[s]
t_E	= maximum time validity model	[s]
f_D	= Darcy friction factor	[-]
γ	= specific heat ratio	[-]
ε	= wall roughness	[m]
ζ	= constant defined paragraph 2.5.2.4	[-]
μ_i	= molecular weight of substance i	[kg/mol]
ρ	= density of the gas	[kg/m^3]
ρ_0	= initial density of the gas	[kg/m^3]

Non-stationary gas outflow from pipelines through small holes

The Weiss model of the outflow of gas from pipelines through punctures (small holes) aims at the estimation of the blow-down time (and not the mass flow rate as a function of time).
The model has been developed for blow-down riser design, but can be applied to a small hole in a pipeline similarly.

The method for accurately predicting gas-pipeline blow-down times, involves application of appropriate correction factors to a simple calculation that regards the pipeline as a volume. The correction factors apply to a wide range of length/diameter values and the ratio of the main pipe area to the area of the small holes [Weiss, 1988].
It is assumed that the gas within the pipeline expands isothermally.
The effect of friction in the pipeline can have pronounced effects on the blow-down time. The cross-area of a small hole is much smaller than the cross-section of the pipeline. Consequently the gas velocities in the pipeline are moderate and the flow may be regarded as quasi-steady. In case the $(f_D \times l_p/d_p) < 40$ the pipeline may be considered as a stagnant volume neglecting the effects of flow and friction in the pipeline.
An attempt was made to formulate correction factors which could be applied to the volume model calculations in order to provide better blow-time predictions.
The result was a polynomial expression in $(f_D \times l_p/d_p)$ and pipe to hole area $(A_p/A_h \cdot C_d)$
Note that the Darcy friction factor f_D is explained in subsection 2.5.5.

Numerical procedure non-stationary blow-down time of pipelines through small holes

1. Determine the average speed of sound u_s and the Poisson ratio γ for the blow-down and calculate the time constant τ_v

$$\tau_v = V_p \times \frac{((\gamma + 1)/2)^{(\gamma + 1)/(2(\gamma - 1))}}{u_s \times A_h \times C_d} \qquad \text{(s)} \qquad (2.43)$$

$$u_s = \sqrt{(z \times \gamma \times R \times T / \mu_i)} \qquad \text{(m/s)} \qquad (2.44)$$

$$V_p = \frac{\pi}{4} \times d_p^2 \times l_p \qquad \text{(m}^3\text{)} \qquad (2.45)$$

$$\gamma = C_p/C_v \qquad \text{(-)} \qquad (2.26)$$

2. Calculate the dimensionless sonic blow-down time

$$\tau_{cr} = \ln(P_i/P_a) - (\gamma/(\gamma-1)) \times \ln((\gamma+1)/2) \qquad \text{(-)} \qquad (2.46)$$

3. Calculate the dimensionless sub-sonic blow-down time τ_s by solving the following equation by a standard numerical integration procedure (method by Simpson or Romberg)

$$\tau_s = \frac{2^{1/(\gamma - 1)} \times \sqrt{(\gamma - 1)}}{(\gamma + 1)^{(\gamma - 1)/(2 \times (\gamma - 1))}} \times \int_{P_{cr}}^{P_f} \frac{1}{p \times (p^{-2/\gamma} - p^{-(\gamma + 1)/\gamma})} \times dp \qquad \text{(-)} \qquad (2.47a)$$

with

$$p = P/P_a \qquad\qquad (-) \qquad (2.47b)$$

$$p_f = 1 \qquad\qquad (-) \qquad (2.47c)$$

$$p_{cr} = P_{cr}/P_a \qquad\qquad (-) \qquad (2.47d)$$

The dimensionless sub-sonic blow-down time τ_s can also be determined more quickly by using table 2.1 below, knowing the (average) Poisson ratio γ of the gas, yet, thereby losing some accuracy.

Table 2.1 *Some values for the dimensionless*
sub-sonic blow-down time τ_s
as function of the Poisson ratio $\gamma = C_p/C_v$ of the gas

γ	P_{cr}/P_a	τ_s
1.20	1.7716	0.7371
1.25	1.8020	0.7605
1.30	1.8324	0.7833
1.35	1.8627	0.8058
1.40	1.8929	0.8278
1.45	1.9231	0.8495
1.50	1.9531	0.8707
1.55	1.9831	0.8916
1.60	2.0130	0.9122

4. Estimate the blow-down correction factor C_b

$$C_b = a_1 + a_2 \times {}^{10}\log(f_D \times l_p/d_p) + a_3 \times ({}^{10}\log(f_D \times l_p/d_p))^2 + a_4 \times ({}^{10}\log(f_D \times l_p/d_p))^3$$
$$(-) \qquad (2.48)$$

Note that f_D is the Darcy friction factor; see paragraph 2.5.5;

with

$$A_r = A_p/(A_h \times C_d) \qquad\qquad (-) \qquad (2.49)$$

$$a_1 = b_{1,1} + b_{1,2} \times A_r + b_{1,3} \times A_r^2 + b_{1,4} \times A_r^3 \qquad\qquad (2.50)$$

$$a_2 = b_{2,1} + b_{2,2} \times A_r + b_{2,3} \times A_r^2 + b_{2,4} \times A_r^3$$

$$a_3 = b_{3,1} + b_{3,2} \times A_r + b_{3,3} \times A_r^2 + b_{3,4} \times A_r^3$$

$$a_4 = b_{4,1} + b_{4,2} \times A_r + b_{4,3} \times A_r^2 + b_{4,4} \times A_r^3$$

These coefficients have been matched with a numerical pipe model that corresponds well with experimental data.

(2.51)

$$b_{1,1} = 0.88107 \quad b_{1,2} = -0.064749 \quad b_{1,3} = 0.0067921 \quad b_{1,4} = -0.00019302$$

$$b_{2,1} = 0.82784 \quad b_{2,2} = 0.053443 \quad b_{2,3} = -0.0088474 \quad b_{2,4} = 0.00026646$$

$$b_{3,1} = -0.78302 \quad b_{3,2} = -0.0086017 \quad b_{3,3} = 0.0049027 \quad b_{3,4} = -0.00016658$$

$$b_{4,1} = 0.34043 \quad b_{4,2} = -0.032399 \quad b_{4,3} = 0.0013735 \quad b_{4,4} = -0.000023546$$

These correlations are valid for

$$4 \leq A_r \leq 16 \tag{2.52}$$

The following correlations

$$a_1 = c_{1,1} + c_{1,2} \times (1/A_r) + c_{1,3} \times (1/A_r)^2 + c_{1,4} \times (1/A_r)^3 \tag{2.53}$$

$$a_2 = c_{2,1} + c_{2,2} \times (1/A_r) + c_{2,3} \times (1/A_r)^2 + c_{2,4} \times (1/A_r)^3$$

$$a_3 = c_{3,1} + c_{3,2} \times (1/A_r) + c_{3,3} \times (1/A_r)^2 + c_{3,4} \times (1/A_r)^3$$

$$a_4 = c_{4,1} + c_{4,2} \times (1/A_r) + c_{4,3} \times (1/A_r)^2 + c_{4,4} \times (1/A_r)^3$$

with

$$c_{1,1} = 1.0319 \quad c_{1,2} = -5.2735 \quad c_{1,3} = 25.680 \quad c_{1,4} = -38.409 \tag{2.54}$$

$$c_{2,1} = -0.26994 \quad c_{2,2} = 17.304 \quad c_{2,3} = -86.415 \quad c_{2,4} = 144.77$$

$$c_{3,1} = 0.24175 \quad c_{3,2} = -12.637 \quad c_{3,3} = 56.772 \quad c_{3,4} = -88.351$$

$$c_{4,1} = -0.054856 \quad c_{4,2} = 2.6258 \quad c_{4,3} = -8.9593 \quad c_{4,4} = 12.139$$

apply to a somewhat wider validity range

$$3 \leq A_r \leq 30 \tag{2.55}$$

but may be not so good a fit in the middle range, and can best be used at the extremities of the range

$$3 \leq A_r < 4 \tag{2.56}$$

$$16 \leq A_r \leq 30$$

5. The duration of the outflow can be determined by

$$t = (\tau_{cr}+\tau_s) \times \tau_v \times C_b \qquad\qquad (s) \qquad\qquad (2.57)$$

The following symbols have been used in this paragraph:

A_p	= cross-sectional area pipeline	[m²]
A_h	= cross-sectional area hole	[m²]
C_d	= discharge coefficient hole	[-]
C_b	= blow-down correction factor	[-]
d_p	= pipeline diameter	[m]
f_D	= Darcy friction factor	[-]
γ	= Poisson ratio	[-]
l_p	= pipe length	[m]
P	= (absolute) pressure	[N/m²]
p	= pressure ratio (P/P_a)	[-]
p_{cr}	= critical flow pressure ratio	[-]
p_f	= final pressure ratio	[-]
P_a	= atmospheric pressure	[N/m²]
P_0	= initial pipeline pressure	[N/m²]
R	= gas constant	[J/(mol·K)]
T	= absolute temperature	[K]
τ_{cr}	= dimensionless sonic blow time	[-]
τ_s	= dimensionless subsonic blow time	[-]
u_s	= speed of sound	[m/s]
V	= pipeline volume	[m³]
z	= compressibility factor	[-]
ρ	= density	[kg/m³]
τ_v	= time constant	[s]

2.5.3   Pressurised liquefied gases

2.5.3.1   Introduction to pressurised liquefied gases

The modelling of the dynamics of a vessel filled with pressurised liquefied gas aims at predicting the decrease in temperature and liquid mass during outflow.

The way the content in the vessel behaves ('vessel dynamics') is very much dependent on the type of outflow initially from the vessel:
*   outflow of pure vapour $\Phi_m = 1$
*   two-phase outflow $0 < \Phi_m < 1$
*   liquid outflow $\Phi_m = 0$
Note that Φ_m is the quality or vapour mass fraction of the outflowing fluid.

In order to determine which flow type will be at hand, the swell of the boiling liquid due to the bubble formation relative to the position of the opening inside the vessel should be estimated first. The DIERS-criteria determine whether two-phase flow

inside the vessel is apparent in case of top venting. In case of a release the rise of the liquid level can be estimated by the relation of Mayinger [Belore, 1986].

The model is basically an iterative numerical procedure in which the outflow of gas and liquid from a vessel is described in small steps. These steps should be small enough to consider the conditions in the vessel to be constant during one time-step.

The outlines of the numerical procedure for the vessel dynamics concerning the release of pressurised liquefied gas is somewhat different for each flow type.
The procedure corresponding to the vessel dynamics resulting from outflow of pure vapour ($\Phi_m=1$) will be described first. The other procedures will be described as a variant of this procedure.

In the following, first the criteria for the flow type inside the vessel and the model for liquid level rise are given.
Next, the initial and termination condition of the numerical procedure will be given.
After this the model in the form of a numerical procedure is described. Every flow type is related to its own variant of the basic procedure.
The numerical procedure has to be repeated until the termination conditions will have been satisfied, and as long as the initial flow type remains.

2.5.3.2   Determination outflow type from the vessel

Flow type inside the vessel

A detailed analytical method for predicting the flow regime for two-phase flows from a vertical vessel during depressurisation was developed by the Design Institute of Emergency Relief Systems (DIERS) of the American Institute of Chemical Engineers (AIChE) [DIERS, 1986 and Melhem, 1993].

The DIERS-method proceeds as follows:

1. Determine the outflow rate $q_{s,1}$, assuming vapour outflow at the exit, by using the equations presented in paragraphs 2.5.2.3 and 2.5.2.4.

2. Calculate the superficial vapour velocity inside the vessel

$$u_V = q_{s,1}/(\rho_V \times A_L) \hspace{3cm} \text{(m/s)} \hspace{1cm} (2.58)$$

3. Calculate the bubble rise velocity

$$u_b = C_{D1} \times (g \times \sigma \times (\rho_L - \rho_V))^{0.25}/\sqrt{\rho_L} \hspace{1.5cm} \text{(m/s)} \hspace{1cm} (2.59)$$

with

C_{D1} = 1.18 for bubbly flow $\hspace{4cm}$ (-) $\hspace{1cm}$ (2.60a)

C_{D1} = 1.53 for churn flow (extensive bubble coalescence) $\hspace{0.3cm}$ (-) $\hspace{1cm}$ (2.60b)

σ $\hspace{0.3cm}$ = surface tension $\hspace{4.5cm}$ (N/m) $\hspace{0.8cm}$ (2.60c)

In figure 2.3 (page 2.24) the bubble flow region and the churn turbulent flow region have been outlined.

4. The dimensionless superficial vapour velocity is given by

$$u_{VR} = u_V/u_b \hspace{4cm} (-) \hspace{2cm} (2.61)$$

5. Calculate the characteristic dimensionless superficial velocity u_{VR} for both typical two-phase flow types.

For bubbly flow the dimensionless superficial velocity u_{VR} must be greater than

$$u_{VR,bf} = \Phi_v \times (1 - \Phi_v)^2/((1 - \Phi_v^3) \times (1 - C_{D2} \times \Phi_v)) \hspace{1cm} (-) \hspace{2cm} (2.62a)$$

with

$$C_{D2} = 1.2 \text{ for bubbly flow} \hspace{5cm} (2.62b)$$

For churn flow the dimensionless superficial velocity must be greater than

$$u_{VR,cf} = 2 \times \Phi_v/(1 - C_{D2} \times \Phi_v) \hspace{3cm} (-) \hspace{2cm} (2.62c)$$

with

$$C_{D2} = 1.5 \text{ for churn flow} \hspace{5cm} (2.62d)$$

The average void fraction $\Phi_{v,av}$ in the vessel is assumed to be given by

$$\Phi_{v,av} = 1 - \phi \hspace{4cm} (m^3/m^3) \hspace{1.5cm} (2.63)$$

6. Determination whether two-phase flow is apparent inside the vessel, if so than two phase outflow occurs.

Application of the criteria

$$u_{VR} \geq u_{VR,cf} \hspace{2cm} \rightarrow \text{two-phase churn flow} \hspace{1cm} (-) \hspace{1.5cm} (2.64a)$$

$$u_{VR} \geq u_{VR,bf} \hspace{2cm} \rightarrow \text{two-phase bubbly flow} \hspace{1cm} (-) \hspace{1.5cm} (2.64b)$$

$$u_{VR} < u_{VR,bf} \text{ and } u_{VR} < u_{VR,cf} \rightarrow \text{vapour outflow} \hspace{1cm} (-) \hspace{1.5cm} (2.64c)$$

Note that if both conditions (2.64a) and (2.64b) are satisfied that churn flow prevails.

If condition (2.64b) is satisfied while two-phase flow is in progress, disengagement is predicted.

7. If vapour outflow is predicted, then the procedure is finished. If two-phase flow is predicted, the quality for top venting $\Phi_{m,e,2}$ can be estimated by an implicit function

$$\frac{\phi_{m,e,2} \times q_{s,2}}{f_{\Phi v1} \times f_{\Phi v2} \times u_b \times \rho_v \times A_L} = \frac{1}{1 - C_{D2} \times f_{\Phi v1} \times (\rho_v/\rho_L) \times (1 - \phi_{m,e,2})/\phi_{m,e,2}}$$

(-)   (2.65)

The parameters $f_{\Phi v1}$ and $f_{\Phi v2}$ are flow dependent.
For bubbly flow:

$$f_{\Phi v1} = \Phi_{v,av}/(1 - C_{D2} \times \Phi_{v,av})$$

(-)   (2.65a)

and

$$f_{\Phi v2} = (1 - \Phi_{v,av})^2/(1 - \Phi_{v,av}^3)$$

(-)   (2.65b)

For churn flow:

$$f_{\Phi v1} = 2 \times \Phi_{v,av}/(1 - C_{D2} \times \Phi_{v,av})$$

(-)   (2.65c)

and

$$f_{\Phi v2} = 1$$

(-)   (2.65d)

Note: use the correct value for C_{D2}.

Equation (2.65) has to be solved iteratively.

The outflow rate $q_{s,2}$ in every iteration step, must be recalculated by the equations in paragraph 2.5.3.4 or 2.5.3.5, taking quality $\phi_{m,e,2}$ into account.

Where
A_L	=	vessel cross sectional area	[m²]
u_b	=	bubble rise velocity	[m/s]
u_V	=	superficial vapour velocity in vessel	[m/s]
u_{VR}	=	dimensionless superficial velocity	[-]
$u_{VR,bf}$	=	minimum dimensionless superficial velocity for bubbly flow	[-]
$u_{VR,cf}$	=	minimum dimensionless superficial velocity for churn flow	[-]
ϕ	=	filling degree of vessel	[m³/m³]
$\Phi_{m,e}$	=	quality (mass fraction vapour) at the exit	[kg/kg]
$\Phi_{v,av}$	=	average void fraction in the vessel	[m³/m³]

Rise liquid level

After a (sudden) depressurisation the liquid in the vessel will flash, and due to the presence of vapour bubbles in the tank the liquid will expand, necessitating a redefinition of liquid height.
The correlation of Mayinger [Belore, 1986] may be used for the estimation of the void fraction in the liquid phase in vessels. The procedure may also be used to determine the rise of the liquid level for outflow through the side wall of the vessel, in order to check if two-phase outflow will occur.

The void fraction or hold-up in a flashing liquid due to depressurisation is calculated using the following procedure [Belore,1986].

The superficial vapour velocity is given by

$$u_{V,0} = q_S/(\rho_V \times A_L) \qquad\qquad (m/s) \qquad (2.58)$$

The surface tension at boiling point, may be calculated using Walden's rule [Perry, 1973]:

$$\sigma = C_\sigma \times L_v(T_B) \times \rho_L \qquad\qquad (N/m) \qquad (2.66)$$

with

$$C_\sigma = 6.56 \times 10^{-7}\, m$$

The ratio of the liquid kinematic viscosity to the gas kinematic viscosity at boiling point can be calculated by using Arrhenius's relation for liquid viscosity [Perry, 1973] and Arnold's correlation for gas viscosity [Perry, 1973], resulting in

$$\upsilon_L/\upsilon_V = C_{AA} \times (\mu_i \times 10^3)^{1/6} \times \rho_V \times (T+1.47 \times T_B) \, / \, (\rho_L^{7/6} \times T^{3/2}) \; (\text{-}) \qquad (2.67)$$

with

$$C_{AA} = 37 \; [m^{-1/2}{\cdot}kmol^{1/6}\,K^{1/2}]$$

For convenience we define

$$C_{\phi v} = \sqrt{\sigma / (g \times (\rho_L - \rho_V))} \qquad\qquad (m) \qquad (2.68a)$$

The void fraction is given by

$$\Phi_v = 0.73 \times (u_{V,0}^2/(g \times C_{\Phi v}))^{0.376} \times (C_{\Phi v}/d_v)^{0.176} \times (\rho_L/(\rho_L\text{-}\rho_V))^{0.585} \times (\upsilon_L/\upsilon_V)^{0.256}$$

$$(m^3/m^3)\,(2.68b)$$

The liquid with bubbles will expand to a new volume

$$V_{L,E} = V_{L,0}/(1\text{-}\Phi_v) \qquad\qquad (m^3) \qquad (2.69)$$

The increased liquid height can be estimated by using the inverse function between liquid volume and liquid height for the specific geometry of the vessel (see paragraph 2.5.4.1), written in generalised form

$$h_{L,i} = F^{-1}(V_{L,i}) \qquad \text{(m)} \qquad (2.70)$$

Where

Φ_v	= void fraction	$[m^3/m^3]$
q_S	= discharge rate	$[kg/s]$
A_L	= normal liquid surface in the vessel	$[m^2]$
d_v	= vessel diameter	$[m]$
T	= liquid/vapour temperature	$[K]$
μ_i	= mol weight chemical i	$[kg/mol]$
ρ_L	= liquid density	$[kg/m^3]$
ρ_V	= vapour density	$[kg/m^3]$
$L_v(T_B)$	= heat of vaporisation at boiling point	$[J/kg]$
T_B	= normal boiling point	$[K]$
$u_{V,0}$	= superficial vapour velocity	$[m/s]$
σ	= surface tension	$[N/m]$
g	= gravitational acceleration	$[m/s^2]$
υ_L	= liquid kinematic viscosity	$[m^2/s]$
υ_V	= vapour kinematic viscosity	$[m^2/s]$
$V_{L,E}$	= expanded 'liquid' volume in the vessel	$[m^3]$
$V_{L,0}$	= initial liquid volume in the vessel	$[m^3]$

2.5.3.3 Vessel dynamics related to outflow type

The initial and termination conditions for all type of outflows from vessel filled with pressurised liquefied gas

The initial condition of the vessel (i=1) is given by its temperature T_1, filling degree ϕ, and vessel volume V.
The initial vapour mass $Q_{V,1}$ and liquid mass $Q_{L,1}$ in the vessel can easily be derived, given the filling degree ϕ and the storage temperature, by

$$Q_{L,1} = \phi \times V \times \rho_{L,1} \qquad \text{(kg)} \qquad (2.71)$$

$$Q_{V,1} = (1-\phi) \times V \times \rho_{V,1} \qquad \text{(kg)} \qquad (2.72)$$

with

$$\rho_{L,1} = \rho_L(T_1)$$

$$\rho_{V,1} = \rho_V(T_1)$$

The duration of δt may be chosen freely in principle, and depends of the number of time-steps N_t. When one wishes to estimate the mass flow rate and vessel conditions at time t_{end}, then the size of time step δt is given by

$$\delta t = t_{end}/N_t \qquad\qquad\qquad\qquad (s) \qquad\qquad (2.12)$$

t = time from the start of the outflow [s]

The larger the number of steps, the higher the accuracy of the model, but the more time needed for the calculation. The choice $N_t=50$ will be appropriate for most calculations.
The numerical procedures given should be repeated as long as the constraints are valid, namely

$$t_i < t_{end} \qquad\qquad P > P_a \qquad\qquad T > T_m \qquad\qquad (2.73a)$$

In case of liquid outflow, an additional constraint for the liquid level is active, namely

$$h_L > h_{hole} \qquad\qquad\qquad\qquad\qquad\qquad (2.73b)$$

Every time-step the criteria of DIERS and Mayinger should be checked. During the blow-down the amount of liquid may decrease so that the swelled liquid level will drop and pure vapour outflow may become apparent again eventually. In case of top venting the churn flow may change into bubbly flow, or the two-phase flow may disengage.

If the flow type changes during the outflow, then we have to switch to the appropriate vessel dynamics model. The calculation restarts with the vessel conditions at the moment of the switch.

1. *Vessel dynamics pure vapour outflow (quality $\Phi_m=1$)*

This version of modelling of the dynamics of a vessel with pressurised liquefied gas aims at predicting the decrease in temperature and liquid mass during outflow of only vapour. The vessel dynamics are mainly controlled by the evaporation of the pressurised liquefied gas, which is assumed to be at saturated vapour pressure initially.

In case no two-phase flow is apparent inside the vessel when top venting, or the rise of the expanded liquid is below the hole in the vessel wall, only vapour outflow will be at hand. Due to the outflow of vapour the vessel depressurises. This causes the liquefied gas to evaporate, and subsequently the temperature will decrease and so will the saturated vapour pressure.
The basic assumptions of the model are:
1. Liquid mass is removed by evaporation only.
2. The vapour phase is in thermodynamic equilibrium with its liquid phase, which means that the actual vapour pressure is equal to the saturated vapour pressure at liquid temperature.
3. The heat capacity and volumetric work done by the vapour is negligibly small relative to the heat of vaporisation.
4. The heat of vaporisation is drawn from the superheat of the pressurised liquefied gas only: the heat capacity of the vessel is neglected.
5. The vapour and liquid phase are homogeneous.
6. Pure vapour from the vapour section is flowing out of the vessel.

The invariant condition controlling the numerical solution is set by the requirement that the vapour volume and the liquid volume together equal the vessel volume. The densities of both phases and thus their temperatures at present vapour pressure have to be adapted accordingly.

Numerical procedure: pure vapour outflow

Starting every step at time t_i in the iteration with a condition in the vessel given by T_i, $Q_{L,i}$ and $Q_{V,i}$, the following procedure aims at calculation of the condition in the vessel at the end of the small time-step δt, given by T_{i+1}, $Q_{L,i+1}$ and $Q_{V,i+1}$.

Assuming thermodynamic equilibrium, the pressure in the vessel can be estimated by

$$P_i = P_v(T_i) \qquad\qquad (N/m^2) \qquad (2.74)$$

Let us say that the outflow rate $q_{S,i}$ is given by a generalised function f, depending on whether the outflow is through a hole (see paragraph 2.5.2.3) or a pipe (see paragraph 2.5.2.4)

$$q_{S,i} = f(P_i, T_i, Q_{L,i}, Q_{V,i},...) \qquad\qquad (kg/s) \qquad (2.75)$$

Guessing a new temperature T_{i+1} results in a temperature decrease of

$$\delta T = T_{i+1} - T_i \qquad\qquad (K) \qquad (2.76)$$

The law of heat conservation applied on the evaporation of liquid, results in

$$Q_{L,i+1} = Q_{L,i} \times (1 - C_{p,L}/L_v \times \delta T) \qquad\qquad (kg) \qquad (2.77)$$

Application of the law of conservation of mass gives

$$Q_{V,i+1} = (Q_{L,i} - Q_{L,i+1}) + Q_{V,i} - q_{S,i} \times \delta t \qquad\qquad (kg) \qquad (2.78)$$

The new temperature T_{i+1} for any time-step can be found by means of the invariant vessel volume.
The evaporating liquid has to supply vapour to the vapour section in such an amount that the following condition must be fulfilled

$$V = Q_{L,i+1}/\rho_L(T_{i+1}) + Q_{V,i+1}/\rho_V(T_{i+1}) \qquad\qquad (m^3) \qquad (2.79)$$

If not, another guess for temperature T_{i+1} should be made.
The set of four equations (2.76 - 2.79) mentioned above can also be solved by a root-finding procedure

$$f(\delta T) = V - Q_{L,i+1}/\rho_L(T_{i+1}) + Q_{V,i+1}/\rho_V(T_{i+1}) \rightarrow 0 \qquad (m^3) \qquad (2.79a)$$

The temperature range in which the root T_{i+1} can be found depends on the size of the time-step. If the number of time-steps $N_t=50$, a value for $\delta T \approx 10$ will suffice.

The time from the start of the release must be increased with one time-step after every pass through this numerical procedure

$$t_{i+1} = t_i + \delta t \qquad \text{(s)} \qquad (2.80)$$

The new condition of the vessel at time t_{i+1} is given by: T_{i+1}, $Q_{L,i+1}$ and $Q_{V,i+1}$

This numerical procedure has to be repeated until the termination conditions will have been satisfied. Every time-step the flow type may be checked.

2. *Vessel dynamics in case of (initially) two-phase outflow (quality $0<\Phi_m<1$)*

This version of the modelling of the dynamics of a vessel with pressurised liquefied gas aims at predicting the decrease in temperature and mass during the two-phase outflow.

In case two-phase flow is apparent inside the vessel when top venting, or the rise of the expanded liquid is above the hole in the vessel wall, see paragraph 2.5.3.2, two-phase outflow will be at hand. The two-phase outflow will start after the vent of the gas initially apparent in the vapour section. The vapour initially apparent above the liquid is assumed to be driven out by the rising liquid acting like a piston. The duration of the blow-out of the vapour can be estimated by

$$t_v = Q_{v,0}/q_{S,\Phi m=1} \qquad \text{(s)} \qquad (2.81)$$

t_v = duration vapour blowing out   [s]
$Q_{v,0}$ = initial vapour mass in vessel   [kg]

The initial mass flow rate of only vapour can be calculated by equation (2.22) for orifices and the set of equations of subsection 2.5.2.5. for pipes, based on the saturated vapour pressure $P_v^{\,\circ}$ in the vessel.

$$q_{S,\Phi m=1} = q_S(P_v^{\,\circ}) \qquad \text{(kg/s)} \qquad (2.82)$$

$q_{S,\Phi m=1}$ = initial mass flow rate vapour only   [kg/s]

The model for two-phase outflow from a vessel is quite similar to the one for outflow of pure vapour, except for the first assumption.

2a. Hole in side-wall

In case of a hole in the side-wall of the vessel the two-phase mixture inside the vessel is considered to be homogeneous, and the quality of the outflowing material is assumed to be identical to that of the vessel.
This assumption forces the quality Φ_m, i.e. vapour and liquid mass ratio, to be constant during the outflow. This leads to some additional statements to the procedure for outflow of pure vapour.

The basic assumptions of the model are:
1. the quality of the two-phase outflow just leaving the vessel corresponds to the average quality inside the vessel,
2. the vapour phase is in thermodynamic equilibrium with its liquid phase, meaning that the actual vapour pressure is equal to the saturated vapour pressure at liquid temperature,
3. the heat capacity and volumetric work done by the vapour is negligibly small relative to the heat of vaporisation,
4. the heat of vaporisation is drawn from the super heat of the pressurised liquefied gas only: the heat capacity of the vessel is neglected,
5. the expanded boiling liquid has a homogeneous void fraction.

Numerical procedure: two-phase outflow

$$Q_i = Q_{L,i} + Q_{V,i} \qquad\qquad \text{(kg)} \qquad (2.83)$$

$$\xi_i = Q_{L,i}/Q_i \qquad\qquad \text{(-)} \qquad (2.84)$$

Applying the law of conservation of mass gives simply

$$Q_{i+1} = Q_i - q_S \delta t \qquad\qquad \text{(kg)} \qquad (2.85)$$

Forcing initially the quality to be constant results in

$$Q_{L,i+1} = Q_{i+1} \times \xi_i \qquad\qquad \text{(kg)} \qquad (2.86\text{I})$$

$$Q_{V,i+1} = Q_{i+1} \times (1-\xi_i) \qquad\qquad \text{(kg)} \qquad (2.87\text{I})$$

Due to evaporation of liquid, the vapour mass fraction inside the vessel will change. The law of heat conservation applied to the evaporation of liquid results in an adaption of the earlier calculated (by equation (2.86)) liquid mass by

$$Q_{L,i+1} = Q_{L,i+1} \times (1 - C_{p,L}/L_v \times \delta T) \qquad\qquad \text{(kg)} \qquad (2.88)$$

This set of equations replaces equations (2.77) and (2.78) in the numerical procedure concerning vessel dynamics in case of a pure vapour outflow.
The mass flow rate q_S must be determined by the equations in paragraph 2.5.3.4 valid for champagne flow.
The other steps are the same as in the case of outflow of pure vapour.

2b.   Top venting

In case of top venting, the basic assumptions of the model are the same except for the first one:
1. the quality of the two-phase outflow just leaving the vessel $\Phi_{m,e}$ is determined by the outflow model.

In the numerical procedure, equations (2.83) - (2.85) are not relevant anymore, while equations (2.86) and (2.87) have to be adapted.
Applying the law of conservation of mass simply gives

$$Q_{L,i+1} = Q_{L,i} - q_s \times (1 - \Phi_{m,e}) \times \delta t \qquad\qquad \text{(kg)} \qquad (2.86\text{II})$$

$$Q_{V,i+1} = Q_{V,i} - q_s \times \Phi_{m,e} \times \delta t \qquad\qquad \text{(kg)} \qquad (2.87\text{II})$$

For this case equation (2.88) still holds.
The mass flow rate q_s must be determined by the equations in paragraph 2.5.3.4, valid for top venting.

3. *Vessel dynamics liquid outflow (quality $\Phi_m=0$)*

This version of the modelling of the dynamics of a vessel with pressurised liquefied gas aims at predicting the decrease in temperature and liquid mass during the outflow of a pressurised liquefied gas. The opening in the vessel should be under the (unexpanded) liquid level inside the vessel.

The model for two-phase outflow from a vessel is quite similar to the one for outflow of pure vapour, except for the first assumption.

The basic assumptions of the model are:
1. vapour mass is added to the vapour section by evaporation of liquid,
2. the vapour phase is in thermodynamic equilibrium with its liquid phase, which means that the actual vapour pressure is equal to the saturated vapour pressure at liquid temperature,
3. the heat capacity and volumetric work done by the vapour is negligible small relative to the heat of vaporisation,
4. the heat of vaporisation is drawn from the super heat of the pressurised liquefied gas only: heat capacity of the vessel is neglected,
5. the vapour and liquid phase are homogeneous,
6. pure liquid is flowing out of the liquid section of the vessel, i.e. the flashing of liquid takes place outside the vessel.

Numerical procedure: liquid outflow

Because the liquid volume inside the vessel decreases, the enlarging vapour section has to be refilled by vapour through evaporation of liquid

$$Q_{V,i+1} = Q_{V,i} + Q_{L,i} \times C_{p,L}/L_v \times \delta T \qquad\qquad \text{(kg)} \qquad (2.89)$$

The conservation applied to the evaporation of liquid results in an adaption of the earlier calculated liquid mass, namely

$$Q_{L,i+1} = Q_{L,1} - q_S \times \Delta t + (Q_{V,i+1} - Q_{V,i}) \qquad\qquad \text{(kg)} \qquad (2.90)$$

The changes in liquid level can be calculated with the equations given for liquids in paragraph 2.5.4.1.

These equations replace equations (2.77) and (2.78) in the numerical procedure concerning the vessel dynamics in case of a pure vapour outflow.
The mass flow rate q_S must be determined by the equations in paragraph 2.5.3.3 valid for two-phase flow in pipes (paragraph 2.5.3.4).
The other steps are the same as in the case of outflow of pure vapour.

2.5.3.4   Outflow of pressurised liquefied gas through holes

Vapour outflow

In case of pure vapour outflow from a vessel, the relation for gas flow through orifices can be applied (see paragraph 2.5.2.3).

Two-phase outflow through a hole: Champagne outflow

The standard relations for liquid flow through orifices can be applied; see paragraph 2.5.4.2. However the fluid is assumed to have a density as a function of the vapour mass fraction [WorldBank, 1988].

So the mass flow rate can be estimated by

$$q_S = C_d \times A \times \sqrt{(2(P_0 - P_a) \times \rho_F)} \qquad \text{(kg/s)} \qquad (2.91)$$

with

$$\rho_F = 1 / (\Phi_m/\rho_V + (1-\Phi_m)/\rho_L) \qquad \text{(kg/m}^3) \qquad (2.92)$$

Φ_m = quality or vapour mass fraction in the two-phase flow [-]

ρ_F = average fluid density   (kg/m^3)

In case of liquid outflow from a vessel, the standard relations for liquid flow through orifices can be applied (see paragraph 2.5.4.2).

2.5.3.5   Outflow of pressurised liquefied gas through piping

2.5.3.5.1 Vapour flow in piping

The relation for gas flow through piping can be applied (see paragraph 2.5.2.4).

2.5.3.5.2 Two-phase flow in piping: introduction

In general for those situations they have been validated for, the so-called 'Homogeneous Equilibrium Models' (HEM) are generally accepted and are widely used [Kukkonen, 1990]. In particular the homogeneous equilibrium model TPDIS [Kukkonen, 1990] will be described here in detail.

Two-phase flow in piping by HEM (TPDIS) [Kukkonen, 1990]

TPDIS is an acronym for 'Two-Phase DIScharge of liquefied gases through a pipe'. The description of the TPDIS model has been taken from 'Modelling source terms for the atmospheric dispersion of hazardous substances', Dissertations No. 34, The Finnish Society of Sciences and Letters, 1990, by Kukkonen.
The complete specification of the model will be concise and will use results that have been derived by others. References made in the original publication by Kukkonen, [Kukkonen, 1990] will not be repeated here.

The modelling of the two-phase flow in pipes aims at predicting the mass flow rate, the velocity, the mass fraction of vapour (the quality) and the thermodynamic state of the outflowing fluid as a function of the initial conditions at the upstream end of the piping.
The two-phase pipe flow model TPDIS has been generalised, in particular to allow for the influence of gravity on two-phase flow and to include a more detailed description of the flow friction at pipe walls. Especially for refrigerated and semi-refrigerated kinds of storages gravity may be an important driving term.

TPDIS: basic assumptions

In the model the flow has been divided into three flow regimes:
1. superheated liquid,
2. non-equilibrium evaporating and expanding two-phase fluid and,
3. equilibrium two-phase fluid.

When the stagnant pressure in the vessel is higher than the saturation pressure at present temperature, the (sub-cooled) liquid will not vaporise in the pipe at first.
Due to the pressure drop in the pipe the pressure will become lower than the saturation pressure at some point in the pipe. Due to nucleating delay it will take some time, and thus a certain length along the pipe, to reach thermodynamic equilibrium. Homogeneous equilibrium flow has been assumed in the third flow regime. This implies that the fluid is a homogeneous mixture of vapour and liquid, and that the phases move with the same velocity. For long pipes, the length of the third regime may be nearly equal to the pipe length.
The process is assumed to be adiabatic. This is a reasonable assumption, as the outflow is very rapid and the heat energy conducted through the pipe walls is therefore much less than the energy of the phase transitions.
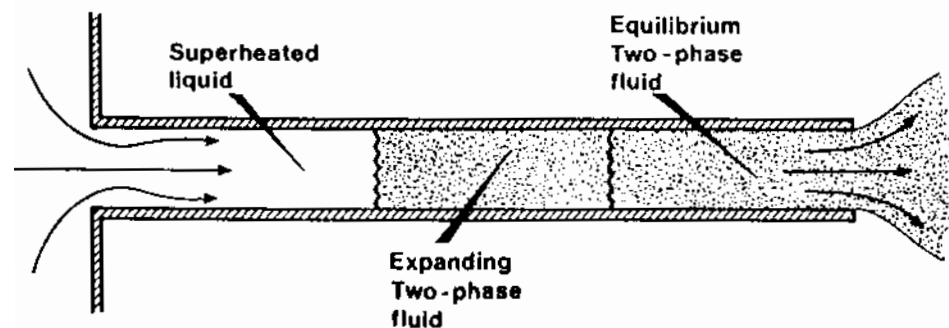
Figure 2.10   Two-phase flow regimes assumed in the discharge model (Nyren and Winter, 1987)

Note that particularly the size of regime 2 'expanding two-phase fluid' in figure 2.9 has been exagerated, and is in reality small.

Numerical procedure in case of two-phase flow in a pipe

For convenience the scheme of the numerical procedure of the TPDIS model is given before the description of the model equations.

Diagram 2.7   Numerical procedure TPDIS

> I.   The critical mass flow rate q_s at the pipe outlet may be computed by maximising numerically the right-hand side of equation (2.107) in terms of outlet pressure P_e.
>
> II. The specific volume of the fluid is computed from equations (2.110) and (2.112).
>
> III. The friction is computed by equation (2.99).
>   Friction is one of the factors determining the flow velocity in the pipe.
>   As the friction factor depends on the flow velocity and the quality, a numerical iterative procedure should to be applied.

The model requires thermodynamic data, preferably in the form of correlations of the temperature. The properties of a few chemicals: ammonia, chlorine, sulphur dioxide, propane and hydrogen fluoride, are given as a function of temperature in the saturated state in appendix 2.1. These functions have the original form from the publication of Kukkonen [1990]. The maximum deviation of the numerical correlations from the original data is approximately 2%.

TPDIS: initial flow regimes 1 and 2

In HEM the flow is usually taken to be isentropic, which means an adiabatic and reversible flow. When the conduction of heat and the friction effects can be neglected, and assuming also that the process is isentropic, we can write the Bernoulli equation in the following form

$$u^2/2 = C_d{}^2 \times (\int v_F \times dP + g \times h_f) \qquad\qquad (m^2/s^2) \qquad (2.93)$$

where

u	= fluid flow velocity	[m/s]
C_d	= discharge coefficient	[-]
v_F	= specific volume of the fluid	[m³/kg]
P	= pressure	[N/m²]
g	= gravitational acceleration	[m/s²]
h_f	= fluid height	[m]

The discharge coefficient (C_d) is a measure for pressure loss of the liquid flow at the pipe inlet (not related to the outflow at the pipe exit). The pipe is assumed to have a uniform bore.
The ratio q_S/A_p is called the mass flux G defined by

$$G = q_S/A_p = u/v_F \qquad\qquad (kg/(m^2 \cdot s)) \quad (2.94)$$

where

q_S	= mass flow rate (discharge rate)	[kg/s]
A_p	= cross-sectional area of the pipe	[m²]

For very short pipes, smaller than 0.1 m, the discharge of pressurised liquefied gases can be assumed to remain in liquid form. For liquid flow, the fluid is incompressible and the equation (2.93) reduces in flow regimes 1 and 2 to the form of

$$q_S = C_d \times A_p/v_L \times \sqrt{(2(v_L \times (P_0 - P_2) + g \times \Delta h_{L,2}))} \qquad (kg/s) \qquad (2.95)$$

where

v_L	= specific volume of the liquid phase	[m³/kg]
P_0	= initial pressure in the vessel	[N/m²]
P_2	= pressure at the end of flow regime 2	[N/m²]
$\Delta h_{L,2}$	= liquid height difference in the flow regime 2	[m]

The vertical coordinate axis is chosen to be in the upward direction, and

$$\Delta h_{L,2} = h_{L,0} - h_{L,2} \qquad\qquad (m) \qquad (2.96)$$

where

$h_{L,0}$	= liquid height pipe inlet	[m]
$h_{L,2}$	= liquid height pipe at end of flow regime 2	[m]

Equation (2.95) gives the mass flow rate at the end of the flow regime 2. This equation can also be applied in estimating liquid discharges through breaches in container wall or through very short pipes.

TPDIS: mass flux equation

In the third regime, the conservation of the total energy of the fluid gives

$$v_F \times dP + d(u^2/2) + u^2 \times f_D/(2 \times d_p) \times dx + g \times dh_L = 0 \qquad (m^2/s^2) \qquad (2.97)$$

where

d_p	= inner pipe diameter	[m]
f_D	= friction factor	[-]
x	= length variable along the pipe	[m]
v_F	= specific volume of the fluid	[m³/kg]

The first term in equation (2.97) is the energy per unit mass due to change of state of the fluid. The second term is the kinetic energy, and the third term is the energy loss due to flow friction at pipe walls and the fourth term is the potential energy.
The third term in equation (2.97) can be derived from the theory of the turbulent boundary layer flows, applied to pipes by Landau and Lifschitz. It has been assumed that the laminar friction forces are in general much smaller than the forces governing the turbulent energy dissipation.
The friction factor is a function of the roughness of the pipe divided by the pipe diameter ε/d_p, and the Reynolds number Re.
The friction factor for turbulent flow in smooth and rough pipes can be computed from the Colebrook-White law for the transition zone

$$1/\sqrt{f_D} = -2 \times {}^{10}\log(2.51/(Re \times \sqrt{f_D}) + \varepsilon/(3.715 \times d_p)) \qquad (-) \qquad (2.98)$$

Equation (2.98) is an implicit equation for f_D. Chen has shown that the following explicit equation gives the same numerical results with an accuracy greater than 0.5%

$$1/\sqrt{f_D} = -2.0 \times {}^{10}\log\left(\left(\frac{\varepsilon}{d_p}\right) \times \frac{1}{C_1} - \frac{2 \times C_2}{Re} \times {}^{10}\log\left(\left(\frac{\varepsilon}{d_p}\right)^{C_3} \times \frac{1}{C_4} + \frac{C_5}{Re^{C_6}}\right)\right)$$

$$(-) \qquad (2.99)$$

with

C_1	= 3.7065
C_2	= 2.5226
C_3	= 1.1098
C_4	= 2.8257
C_5	= 5.8506
C_6	= 0.8981

This equation is valid for $4000 < Re < 10^7$. (2.100)

The Reynolds number is given by

$$Re = u \times d_p \times \rho_{tp}/\eta_{tp} \qquad (-) \qquad (2.101)$$

where

u	= fluid flow velocity	[m/s]
d_p	= pipe diameter	[m]
ρ_{tp}	= density two-phase fluid	[kg/m^3]
η_{tp}	= dynamic viscosity two-phase fluid	[N·s/m^2]

The dynamic viscosity is given by

$$\eta_{tp} = \eta_L \times (1 - \Phi_m \times (1 - (\eta_L / \eta_V))) \qquad\qquad (-) \qquad (2.102)$$

where

η_L	=	dynamic viscosity of liquid phase	[N·s/m^2]
η_V	=	dynamic viscosity of vapour phase	[N·s/m^2]
Φ_m	=	quality or mass fraction of vapour in two-phase mixture	[-]

$\Phi_{m,e}$ can be found by equation (2.112).

In integrating equation (2.97) over the third regime, unsolvable integrals of the specific volume and the density appear. These integrals can be estimated as follows. We define the volume and density ratio parameters C_{Ar} and C_{Br}

$$\int v_F \times dx = C_{Ar} \times v_{F,e} \times l_p \qquad\qquad (m^4/kg) \qquad (2.103)$$

$$- \int \rho_F \cdot dh_L = C_{Br} \times \rho_L \times \Delta h_{L,3} \qquad\qquad (kg/m^2) \qquad (2.104)$$

with

$$\Delta h_{L,3} = h_{L,2} - h_{L,e} \qquad\qquad (m) \qquad (2.105)$$

where

$v_{F,e}$	= specific volume fluid at the outlet	[m^3/kg]
ρ_F	= density fluid	[kg/m^3]
ρ_L	= liquid density	[kg/m^3]
l_p	= pipe length	[m]
$h_{L,2}$	= height pipe at end of flow regime 2	[m]
$h_{L,e}$	= height pipe outlet	[m]
$\Delta h_{L,3}$	= height difference in third regime	[m]

The volume and density ratio parameters are measures of the rate of evaporation in the equilibrium flow regime. As the fluid is initially liquid and the specific volume of the fluid increases in the equilibrium flow regime, the following limits are obtained

$$\text{if } l_p \rightarrow 0 \text{ then } C_{Ar} \text{ and } C_{Br} \rightarrow 1.0 \qquad\qquad (2.106a)$$

$$\text{if } l_p \rightarrow \infty \text{ then } C_{Ar} \text{ and } C_{Br} \rightarrow 0.5 \qquad\qquad (2.106b)$$

The lower limits of C_{Ar} and C_{Br} are only approximative; possible values for C_{Ar} and C_{Br} are between these limits.

If there is phase equilibrium in the tank and the pipe is relatively short, let us say within a few metres, the change in the specific volume of the fluid is relatively small. Numerical estimates show that the volume ratio parameter is in the range $0.7 < C_{Ar} < 0.9$. If there is phase equilibrium in the tank and the pipe is relatively long, $0.5 < C_{Ar} < 0.7$. If there is overpressure in the tank relative to the saturation vapour pressure, $C_{Ar} \approx 1.0$. These values apply approximately also for the density ratio parameter C_{Br}. The ratio parameters C_{Ar} and C_{Br} are computed in the model from numerical correlations, based on the values mentioned above.

The following correlations are suggested:

if $\ 0 <= l_p <= 3$ $\qquad\qquad$ $C_{Ar} = C_{Br} = 1 - 0.1 \times l_p$ $\qquad\qquad$ (2.106c)

if $\ 3 < l_p <= 20$ $\qquad\qquad$ $C_{Ar} = C_{Br} = 0.7 - (l_p - 3) \times 0.2 / 17$ $\qquad$ (2.106d)

if $\ l_p > 20$ $\qquad\qquad$ $C_{Ar} = C_{Br} = 0.5$ $\qquad\qquad$ (2.106e)

Thus C_{Ar} and C_{Br} decrease linearly from 1 to 0.7 over the first three meters pipe length (2.106c) and have a constant value of 0.5 above 20 meters (2.106e). Along the intermediate region the parameters decrease linearly from 0.7 to 0.5 (2.106d).

The values of the volume ratio parameter C_{Ar} are not known precisely in the model. However, it was found that the numerical results are not sensitive to variations in this parameter; it can be shown that inaccuracies in estimating C_{Ar} cause only a few per cent error in the mass flux values. The same result also applies to variations in the density ratio parameter C_{Br}.

Equation (2.97) can now be integrated over regime 3, using the definitions (2.103) and (2.104). Finally, combination with equation (2.95) yields the following equation for the mass flux density q_S/A_p at the outlet

$$\left(\frac{q_S(P_e)}{A_p}\right)^2 = \frac{(P_0 - P_e) + \frac{g}{v_L} \times (\Delta h_{L,2} + C_{Br} \times \Delta h_{L,3})}{\left[v_{F,e}(P_e) \times \{1 + (l_p \times f_D \times C_{Ar}/(2 \times d_p)) + \Sigma(K_i \times \tau_i/2)\} - v_L(P_e)/C_d \times (1 - 1/(2 \times C_d))\right]}$$

$$(\text{kg}^2/(\text{m}^4 \cdot \text{s}^2)) \qquad (2.107)$$

with

$$\tau_i = v_{F,i}/v_{F,e} \qquad\qquad\qquad (-) \qquad\qquad (2.108)$$

where

K_i	= resistance coefficient	[-]
P_e	= pressure at the pipe exit	[N/m^2]
v_{vi}	= specific volume at resistance site pipe	[m^3/kg]
v_{ve}	= specific volume at the exit	[m^3/kg]
τ_i	= specific volume ratio	[-]

The critical mass flow rate q_s *at the pipe outlet* may be computed by numerically maximising the right-hand side of equation (2.107) in terms of the outlet pressure P_e.

The values of the resistance coefficients are determined by the geometrical structure of the pipe system. In subsection 2.5.5 resistance coefficients have been given.

The gravity term increases the mass flux for a downward flow ($h_L > 0$, $h_2 > 0$) and decreases it for an upward flow. The parameter C_{Br} describes the reduced effect of gravity on two-phase flow, due to fluid vaporisation. The effective density of the fluid in regime 3 is given by C_{Br}/v_L

The influence of gravity on two-phase pipe flow depends on the height difference during flow, on the physical properties of the chemical and on the pressure in the container. Clearly, gravity is more important for small container pressures. For instance, for chlorine releases at 15 °C, assuming pipe lengths of 1-5 m and pipe inclination angles from 10° to 20°, the effect of gravity on the mass flux is approximately 10%.

TPDIS: specific volume and the quality

The discharge rate can be solved from equation (2.107) using the critical flow condition if the specific volume of the two-phase fluid as a function of pressure $v_e(P_e)$ is known.
The mass flow rate is critical when

$$(dq_S/dP_e)_c = 0 \qquad\qquad \text{(m·s)} \qquad (2.109)$$

The critical exit pressure is less than the reservoir stagnation pressure and higher than the ambient pressure at pipe exit.
The specific volume of the two-phase fluid at the exit aperture can be written in terms of the vapour and liquid phase specific volumes by

$$v_{F,e}(P_e) = \Phi_{m,e}(P_e) \times v_{Vs}(P_e) + (1-\Phi_{m,e}(P_e)) \times v_{Ls}(P_e) \qquad \text{(m}^3\text{/kg)} \qquad (2.110)$$

where

$\Phi_{m,e}$ = vapour mass fraction (quality) at pipe outlet   [-]
$v_{F,e}$ = specific fluid volume at pipe outlet   [m^3/kg]
$v_{Vs}(P_e)$= specific saturated vapour volume at pipe outlet   [m^3/kg]
$v_{Ls}(P_e)$= specific saturated liquid volume at pipe outlet   [m^3/kg]

The compressibility of the vapour and liquid phases has also been taken into account, as the saturation state properties have been used.
The mass fraction of vapour phase at the pipe outlet can be computed using the isentropic assumption

$$S_L(T_0,P_0) = \Phi_{m,e}(P_e) \times S_{Vs}(P_e) + (1-\Phi_{m,e}(P_e)) \times S_{Ls}(P_e) \qquad \text{(J/(kg·K))} \quad (2.111)$$

where

$S_L(T_0,P_0)$ = specific entropy liquid phase at initial conditions   [J/(kg·K)]
$S_{Ls}(P_e)$ = specific entropy saturated liquid phase at pipe outlet   [J/(kg·K)]
$S_{Vs}(P_e)$ = specific entropy saturated vapour phase at pipe outlet   [J/(kg·K)]

In appendix 2.2 of this section entropy and enthalpy have been given for a few compounds as a function of temperature.

It can be shown that this yields

$$\Phi_{m,e}(P_e) = T_{e,s}(P_e)/L_{v,e}(P_e) \times (S_{Ls}(P_0)-S_{Ls}(P_e)) \qquad (-) \qquad (2.112)$$

where

$L_{v,e}$ = heat of evaporation of the liquid at pipe outlet   [J/kg]
$T_{e,s}(P_e)$ = saturated fluid temperature at pipe outlet   [K]
         at exit pressure

The saturated fluid temperature at pipe outlet at given exit pressure $T_{es}(P_e)$ can be found through the saturation curve. By the assumption of thermodynamic equilibrium the saturation pressure equals the exit pressure

$$P^\circ_v(T_{e,s}) = P_e \qquad\qquad (N/m^2) \qquad (2.113)$$

It must be stated that the TPDIS model predicts rather high exit pressures.

The influence of the pipe geometry and the fluid properties on the mass flux

Figure 2.11 shows the influence of pipe length and pipe diameter on the mass flow rate. The ambient temperature has been set at 15 ˚C.
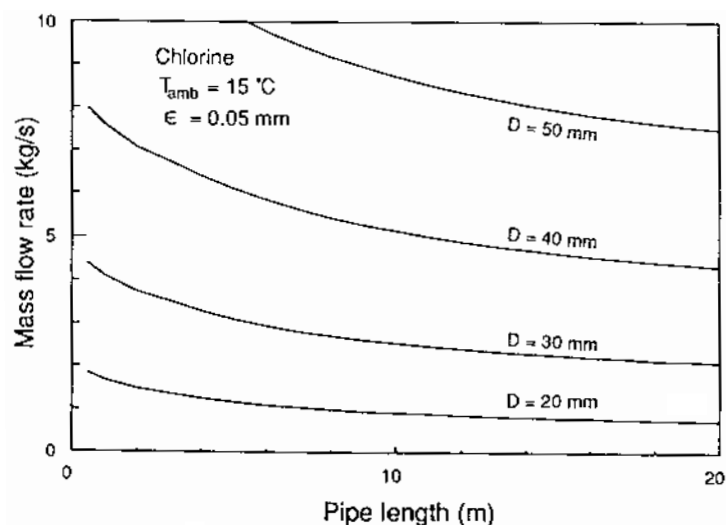
Figure 2.11   The mass flow rate versus pipe length in a chlorine discharge, for various pipe diameters [Kukkonen, 1990]

The decrease in mass flux with pipe length is mainly due to flow friction. The effect of flow friction depends on the relative roughness of the pipe wall (ε/d_p), and on the Reynolds number. The influence of flow friction on the mass flux is typically less than 10% for short pipes ($l_p<2$ m); however, its influence may be much greater for pipelines. Changing the roughness of the pipe wall in the range from 0.01 millimetre to 0.1 millimetre (the assumed value was 0.05 millimetre) causes a change of approximately 10% in the mass flow rate.

2.5.3.6   Non-stationary two-phase propane flow in pipelines

The modelling of the two-phase flow through pipelines aims at predicting the mass flow rate as a function of time depending on the initial conditions.

Transient release from full bore ruptured pipelines

The model given by Morrow [1983] has been derived for propane, but could be generalised by using appropriate physical properties.
The model has been designed for initial pipeline pressures at the location of the break that are (much) higher than the saturation pressure [Dodge, 1996].
The model estimates the mass flow rate *from one side* of the ruptured pipeline.
This model is used for the entire region of two-phase flow within the pipeline. At the point of pipe rupture, the upstream and downstream end of the pipe are assumed to be totally separated so that the flow rates coming from the upstream and downstream pipe regions are independent. Both flows are determined initially on the basis of choked flow at the pipe exit. As time progresses, the flow rate diminishes until choking (equivalent to sonic flow in a perfect gas discharge) no longer occurs.
The model of Fauske is used to determine the correlation of pressure just inside the pipe exit and flow rate during choked flow. An analysis of two-phase flow pressure gradient and void fraction (vapour volume) has been developed to provide the mass depletion in the pipe as a function of exit flow rate and pressure. These correlations for exit flow and pipe flow together allow correlations for exit flow versus time after rupture.

The basic assumptions are briefly as follows. The Fauske equation for critical flow at the exit G_{cr} of a full pipe break is used.
Away from the point of rupture, the frictional pressure drop of the pipeline is given by the Fanning equation, which has been explained in subsection 2.5.5.
The slip ratio used, i.e. the ratio of vapour velocity to liquid velocity, can be calculated using the relation of Fauske

$$u_V/u_L = \sqrt{(\rho_L/\rho_V)} \hspace{3cm} (\text{-}) \hspace{2cm} (2.114)$$

The thermodynamic properties $H_{L,0}$, H_L, L_v and v_L are relatively insensitive to changes in pressure. This makes it possible, though not necessary, to correlate some terms of the equations with a simple (intermediate) polynomial function $F_i(P)$. By doing this, computation time can be saved. For propane the coefficients of these correlations are given.

Intermezzo

The Fauske equation for critical flow at the exit G_{cr} of a full pipe break is given by equation (2.115).
Together with the subsequent equations up to and including equation (2.121) the critical flow can be estimated as a function of the unknown exit pressure P_e.

$$1/G_{cr}{}^2 = - d\Phi_m/dP \times$$

$$\{-2v_L + 2\sqrt{(v_L \times v_V)} - 4\Phi_m \times \sqrt{(v_L \times v_V)} + 2\Phi_m \times v_L + 2\Phi_m \times v_V\}$$

$$- dv_V/dP \times \{\Phi_m \times \sqrt{(v_L/v_V)} - \Phi_m{}^2 \times \sqrt{(v_L/v_V)} + \Phi_m{}^2\} \quad \left(\frac{m^4 s^2}{kg^2}\right) \qquad (2.115)$$

with

$$\Phi_m = (H_{L,0} - H_L)/L_v \qquad\qquad (-) \qquad (2.116)$$

The derative of quality Φ_m with respect to pressure is found from the derative of liquid enthalpy, latent heat and vapour specific volume, by

$$d\Phi_m/dP = - 1/L_v \times \{dH_L/dP + \Phi_m \times (dL_v/dP) + 0.5 \times \Phi_m \times u_L{}^2/v_L \times (dv_V/dP)\}$$

$$(m^2/N) \qquad (2.117)$$

The thermodynamic properties $H_{L,0}$, H_L, L_v and v_L are relatively insensitive to changes in pressure, so that

$$d\Phi_m/dP \approx - 0.5/L_v \times \Phi_m \times u_L{}^2/v_L \times (dv_V/dP) \qquad (m^2/N) \qquad (2.117a)$$

A method for expressing u_L as a function of pressure makes use of the slip ratio used by Fauske. The following equation can be inferred:

$$F_1(P) = (q_S \times v_L/(A \times u_L))^2$$

$$= \left(\frac{(L_v/(H_{L,0} - H_L)) \times \sqrt{(v_L/v_V)}}{1 + (L_v/(H_{L,0} - H_L) - 1) \times \sqrt{(v_L/v_V)}}\right)^2 \qquad (-) \qquad (2.118)$$

The value of the bracketed term is influenced primarily by $v_V(P)$, the other thermodynamic quantities are relatively insensitive to changes in pressure.
Note that the right-hand term of equation (2.118) is dimensionless.

Coefficients C_i can be calculated by the polynomial approximation of the intermediate function $F_1(P)$ which includes only thermodynamic quantities:

$$F_1(P) \approx C_{C1} + C_{C2} \times P + C_{C3} \times P^2 + C_{C4} \times P^3 \qquad (-) \qquad (2.118a)$$

For propane:

C_{C1}	=	-0.0081	[-]	(2.118b)
C_{C2}	=	3.1785×10^{-7}	[(m^2/N)]	
C_{C3}	=	1.8820×10^{-13}	[(m^2/N)^2]	
C_{C4}	=	9.4027×10^{-19}	[(m^2/N)^3]	

Equation (2.117) and (2.117a) contain a factor (dv_V/dP).
The non-stationary flow in a pipeline of a pressurized liquefied gas may be considered as an adiabatic process. This means that we are looking for a function $f(P,T)$ which satisfies the following equation

$$(dv/dP)_s = f(P,T) \qquad (m^4 \cdot s^2/kg^2) \qquad (2.119)$$

Combining equations (2.9c) and (2.39a) shows the relationship between the differential and the speed of sound in the vapour phase

$$(dv/dP)_s = -1/(\rho_V \times u_{s,V})^2 \qquad (m^4 \cdot s^2/kg^2) \qquad (2.120)$$

By equation (2.39c) the speed of sound in the vapour phase can be estimated. However, being stored as a pressurized liquefied gas the approximation by perfect gas behaviour may not be accurate. The introduction of the compressibility factor z for non-ideal gases shifts the problem towards finding an expression for $z=z(P,T)$.
In the original publication Morrow [1983] referred to Starling [1983] who presented an equation of state for several chemicals, like butane, carbon dioxide, ethane, ethene, hydrogen sulphide, methane, and propane. Data for other chemicals, like for instance ammonia, can be found in [Edminster, 1984].

The unknown exit pressure P_e can be estimated if a boundary condition for the mass flow rate at the exit $q_{s,e}$ is given, which could be a function of the exit pressure P_e too. Then it is possible to calculate the exit pressure P_e corresponding to $q_{s,e}$ by a rootfinding numerical routine, solving the following equation

$$G_{cr} - q_{S,e}/A_p = 0 \qquad (2.121)$$

Note that exit pressure P_e will be somewhere between the ambient pressure P_a and the saturation pressure $P_v^\circ(T_0)$.

Where

A_p	=	pipe cross-sectional area	[m^2]
G_{cr}	=	critical mass flux at the exit	[kg/(m$^2 \cdot$s)]
H_L	=	specific enthalpy of saturated liquid	[J/kg]
$H_{L,0}$	=	specific enthalpy of saturated liquid at initial storage temperature	[J/kg]
L_v	=	latent heat of vaporisation	[J/kg]
P	=	pressure	[N/m^2]
P_a	=	ambient pressure	[N/m^2]
P_e	=	exit pressure	[N/m^2]
$P_v^\circ(T)$	=	saturation pressure	[N/m^2]
q_s	=	mass flow rate	[kg/s]
$q_{s,e}$	=	mass flow rate at the exit	[kg/s]
u_V	=	vapour velocity	[m/s]
u_L	=	liquid velocity	[m/s]
$u_{s,V}$	=	speed of sound in vapour	[m/s]
T_0	=	initial temperature	[K]
Φ_m	=	quality	[-]
ρ_L	=	liquid density	[kg/m^3]
ρ_V	=	vapour density	[kg/m^3]
v_L	=	specific volume saturated liquid	[m^3/kg]
v_V	=	specific volume vapour	[m^3/kg]

Numerical procedure in case of two-phase propane flow from complete ruptured pipelines

1. When the initial pressure P_0 in the pipeline is much higher than the saturation pressure, the initial discharge flow rate (t = 0) at the pipe break location can be estimated by assuming sonic liquid outflow through the end of the pipe [Dodge, 1996]

$$q_{S,e,1} = A_p \times (P_0 - P_e)/u_{s,L} \qquad\qquad \text{(kg/s)} \qquad (2.122)$$

where
P_0 = initial pressure in the pipeline $\qquad$ [N/m^2]
$u_{s,L}$ = speed of sound in liquid $\qquad\qquad$ [m/s]

The initial estimate of mass flow is based on an acoustic decompression of the compressed liquid in the pipeline at the break location.

The speed of sound in chemicals that are commonly stored as a pressure liquefied gas, like propane, ammonia and chlorine, is not easily found in literature as is its pressure dependency.
The speed of sound in the liquid phase of a few chemicals stored as a pressure liquefied gas at a temperature of 288.15 K [NIST] are presented in the table:

chemical	$P_v{}^\circ(T)$ $(10^5 \cdot$ N/m^2)	$u_{s,L}$ (m/s)
propane	7.31	786.2
propene	8.91	715.1
ammonia	7.27	1361
butane	1.82	950.6

Most liquids have a speed of sound between 900 m/s and 1500 m/s, and on the average about 1250 m/s. Liquid propane and propene are both one of the exceptions. An increase of pressure will increase the speed of sound. In most cases a pressure increase of about 100 bars will increase the speed of sound in liquids about 5-15%. So, when the initial mass flow rate calculated by equation (2.121) is based on the sound speed at moderate pressures conditions, the estimate will be somewhat conservative.

Use the scheme presented in the intermezzo above, equations (2.115-2.121), to estimate the unknown exit pressure, and the initial discharge flow rate $q_{s,e,1}$ implicitly.

In case of propane outflow a better estimate for the initial mass flow rate for moderate pressures could be calculated by Tam's model, equation (2.137). For other chemicals at moderate pressures the correction factor (2.137b) could be applied.

2. Assume a lower value for the exit mass flow rate

$$q_{S,e,2} = 0.95 \times q_{S,e,1} \qquad\qquad \text{(kg/s)} \qquad (2.123)$$

3. Calculate the average flow rate at the exit

$$q_{S,e_{av}} = 0.5 \cdot (q_{S,e,1} + q_{S,e,2}) \qquad \text{(kg/s)} \qquad (2.124)$$

4. Calculate the new exit pressure P_e corresponding to $q_{S,e,2}$, by the scheme presented in the intermezzo, equations (2.115-2.121), using the following boundary condition

$$G_{cr} = q_{S,e,2}/A_p \qquad \text{(kg/(m}^2\cdot\text{s))} \quad (2.125)$$

5. Calculate the distance to the interface Δl_i, from

$$\Delta l_i = \frac{3 \times d_p \times A_p^2 \times [F_2(P_i) - F_2(P_e)]}{2 \times f_F \times v_L \times q_{S,e_2}^2} \qquad \text{(m)} \qquad (2.126)$$

with intermediate correlation F_2

$$F_2(P) = C_1 \times P + C_2/2 \times P^2 + C_3/3 \times P^3 + C_4/4 \times P^4 \qquad \text{(N/m}^2) \qquad (2.127)$$

The upstream flow rate at interface where two-phase flow starts $q_{S,us}$ is set to be zero after the pumps are shut down.

Note that the intermediate function F_2 is the integral of intermediate function F_1 given by equation (2.118a).

Where

d_p	=	inner pipe diameter	[m]
f_F	=	Fanning friction factor	[-]
u_L	=	velocity liquid phase	[m/s]
Δl_i	=	distance from rupture to interface	[m]

6. Neglecting the vapour density in comparison with liquid density, the mass removed from the pipeline $Q_{yi,2}$ can be calculated by equation

$$Q_{yi,2} = \frac{3 \times d_p \times A_p^3 \times [F_4(P_i) - F_4(P_e)]}{2 \times f_F \times v_L^2 \times q_{S,e}^2} \qquad \text{(kg)} \qquad (2.128)$$

with

$$F_4(P) \quad = C_{B1} \times P + C_{B2}/2 \times P^2 + C_{B3}/3 \times P^3 + C_{B4}/4 \times P^4 + C_{B5}/5 \times P^5$$
$$\text{(N/m}^2) \qquad (2.128a)$$

Q_{yi} = quantity of mass removed from pipeline by void formation

Note that initially $Q_{yi,1} = 0$.

The coefficients C_{Bi} can be calculated by the polynomial approximation of the intermediate function $F_3(P)$ which includes only thermodynamic quantities.

$$F_3(P) = \Phi_v \times F_1$$

$$= F_1 / [1 + (L_v/(H_{L,0}-H_L)-1) \times \sqrt{(v_L/v_V)}] \qquad (-) \qquad (2.129)$$

$$F_3(P) \approx C_{B1} + C_{B2} \times P + C_{B3} \times P^2 + C_{B4} \times P^3 + C_{B5} \times P^4 \qquad (-) \qquad (2.129a)$$

The intermediate function F_4 is the integral of intermediate function F_3.
Note that the right-hand term of equation (2.129) is dimensionless.
The value of the bracketed term is influenced primarily by $v_V(P)$.

For propane:

$$
\begin{array}{llll}
C_{B1} & = & -5.5695 \times 10^{-3} & [-] \\
C_{B2} & = & 2.94896 \times 10^{-7} & [(m^2/N)] \\
C_{B3} & = & -1.27218 \times 10^{-13} & [(m^2/N)^2] \\
C_{B4} & = & 1.34158 \times 10^{-18} & [(m^2/N)^3] \\
C_{B5} & = & -1.8414 \times 10^{-24} & [(m^2/N)^4]
\end{array}
\qquad (2.128b)
$$

7. Calculate the time increment in step i for mass removed

$$\Delta t_i = (Q_{yi,2} - Q_{yi,1})/q_{S,e,av} \qquad (s) \qquad (2.130)$$

8. The exit mass flow rate at the beginning of the next time step $q_{s,e,1}$ must be set equal to the exit mass flow rate at the end of the previous time step $q_{s,e,2}$.

    Repeat the numerical procedure for each new time-step by starting again with step 2, until the distance to the interface Δl_i is larger than the pipelength L_p or if time t is smaller than the specified time for which the outflow rate or the conditions in the pipeline must be estimated.

Note that the time after the rupture is given by

$$t = \Sigma \Delta t_i \qquad (s) \qquad (2.130a)$$

By comparing the initial mass content in the pipeline with the mass removed $Q_{yi,2}$ it may appear that the pipeline is not empty after the last time step. If so, it is recommended to continue the predicted mass flow rate of the last time step until all remaining mass will be removed. The duration of this stage of the release is given by

$$\Delta t_E = (\rho_0 \times A_p \times L_p - Q_{yi,2}) / q_{s,e,2} \qquad (s) \qquad (2.130b)$$

where

$$
\begin{array}{llll}
\Delta t_E & = & \text{duration release remaining liquid} & [s] \\
\rho_0 & = & \text{initial liquid density} & [kg/m^3]
\end{array}
$$

Remark

If the pipeline has been ruptured in the middle ('double' guillotine break), then the overall mass flow rate from the pipeline is twice the calculated value by this model.

In case the rupture is near one of the pipe ends or an isolation valve, both parts of the original pipeline should be regarded as two independent sources.

The way Morrow accounted for pumping rate in the pipeline apparent before the break, is not correct.
Dodge [1996] has given several useful comments on Morrow's model, amongst others on how to cope with a pumping rate in the pipeline.
In case of a 'double' guillotine break to the first order the pumping rate does not influence the venting rate, and to account for the pumping rate to consider second order effects would make the computational model much more complicated. In case of a guillotine break the fluid vents from both the upstream and downstream sides of the guillotine break.
On the upstream side, the pumping rate (which is in the same direction as the venting flow) adds to the initial estimate of the venting rate, and thus it will increase all the subsequent computations of upstream venting rate from Fauske's model. On the downstream side, the pumping rate (which is in the opposite direction as the venting flow) subtracts from the initial estimate of the venting rate, and thus it will decrease all the subsequent computations of downstream venting rate from Fauske's model. The net effect is that the pumping rate tends to cancel out of the venting rate calculations (but not quite) when the upstream and downstream venting rates are added together.
For this reason the pumping rate for the 'double' guillotine break case can be neglected, certainly at the early stages of the release.

Transient release from leaking or (partially) ruptured propane pipelines

A simple exponential correlation has been fitted against experiments with 100 metre propane pipeline of 0.150 m diameter and 0.05 m diameter orifice plate [Tam, 1990]. A characteristic of the transient releases in the test data was found to be that the total mass of propane inside the test line decreases exponentially with time after a period of flow establishment. The flow establishment lasted from less than 1 to about 5 seconds, depending on the size of the test orifice. The release rate does not decay exponentially in this period. In the experiments the duration of the established flow was 20 seconds or more, again depending on the orifice size.

The model for the transient releases rate is given by

$$d\, Q(t)/dt = -C_\alpha \times Q(t) \qquad\qquad \text{(kg/s)} \qquad (2.131)$$

where

C_α = constant of decay [1/s]
Q = mass content pipeline [kg]
t = time from the start of the release [s]

While by definition the mass flow rate from the pipe is given by

$$q_S(t) = - d\ Q(t)/dt \qquad\qquad \text{(kg/s)} \qquad (2.132)$$

the following equation can be inferred from the model as formulated by Tam [1990]

$$q_S(t) = C_\alpha \times Q_0 \times e^{-C_\alpha \cdot t} \qquad\qquad \text{(kg/s)} \qquad (2.133)$$

q_S = mass flow rate [kg/s]

The main factors which affect the value of the exponential decay constant were assessed using statistical analysis. These factors were the initial fluid conditions, such as fluid temperature, and the test line configurations, such as pipe length and orifice area. The following regression was obtained from the data set

$$C_\alpha = d_R{}^{0.25} \times (0.22 \times A_R - 0.13 \times A_R^{1.5} + C_{C\alpha} \times (T_0 - 288.15))$$
$$\text{(1/s)} \qquad (2.134)$$

with

$$d_R = d_p[m]\ /\ 0.05\ [m] \qquad\qquad \text{(-)} \qquad (2.134a)$$

$$A_R = A_h/A_p \qquad\qquad \text{(-)} \qquad (2.134b)$$

and

$$C_{C\alpha} = 0.00068\ [K^{-1}] \qquad\qquad (2.134c)$$

Where
A_h	= cross-sectional area hole	[m²]
A_p	= cross-sectional area pipe	[m²]
A_R	= area ratio	[-]
d_p	= pipe diameter	[m]
d_R	= radius ratio	[-]
T_0	= initial (absolute) temperature fluid	[K]

The deviation between the predictions and the measured results is less than 20%. The experiments did not result in any significant correlation between the initial pressure and the value of the decay constant.

Range of experimental parameters:

Initial pressure	P_0 [N/m²]	$7.5 \cdot 10^5$ - $22 \cdot 10^5$
Initial temperature	T_0 [K]	287.15 - 297.15
Pipe diameter	d_p [m]	0.05 - 0.15
Area ratio	A_R [m²/m²]	0.04 - 1.0

Although the variation in length of the pipeline has been recognised by Tam as a factor governing the exponential decay of the transient release rate, no correlation between the mass flow rate and the pipe length was given.

Note that equations (2.131) and (2.132) imply that the initial mass flow rate seems to depend on the initial mass content of the pipe, and thus on the length of the pipeline, since

$$q_0 = q(t=0)$$

$$= C_\alpha \times Q(t=0) \qquad\qquad\qquad \text{(kg/s)} \qquad (2.135)$$

with

$$Q_0 = Q(t=0)$$

$$= \rho_L(T_0) \times V_p$$

$$= \rho_{L,0} \times \pi/4 \times d_p{}^2 \times L_p \qquad\qquad \text{(kg)} \qquad (2.136)$$

where

Q_0	= initial mass content pipeline	[kg]
L_p	= length pipeline	[m]
V_p	= pipeline volume	[m^3]
$\rho_{L,0}$	= density propane at initial temperature T_0	[kg/m^3]

This can not be true, which means that the model can not be used for pipe lengths other than 100 m.
However, the model can give a good impression of the magnitude of the initial flow rate after the flow establishment region by

$$q_0 = C_\alpha \times C_{Lp} \times \rho_{L,0} \times \pi/4 \times d_p{}^2 \qquad\qquad \text{(kg/s)} \qquad (2.137)$$

with somewhat artificially

$$C_{Lp} = 100 \text{ m} \qquad\qquad\qquad\qquad\qquad\qquad (2.137a)$$

It must be mentioned however, that the duration of the flow establishment will be a function of the length of the pipeline.

In an engineering approach we could define a (general) correction factor C_{Tam} by

$$C_{Tam} = q_{0,Tam}/q_{0,L} \qquad\qquad\qquad\qquad \text{(-)} \qquad (2.137b)$$

with

$q_{0,Tam}$	= propane mass flow rate estimated by equation (2.137)
$q_{0,L}$	= propane mass flow rate estimated by equation (2.199)

This correction factor can be used to improve the estimation of the initial mass flow rate for any pressure liquefied gas assuming pure liquid outflow.
The latter two quantities should be calculated for the same conditions.

2.5.3.7 Finite duration spray releases

This section provides the models to describe the behaviour of the two-phase jets into the atmosphere from pressurised liquefied gases. First, the effects associated with the depressurisation of the release to atmospheric pressure are described. Secondly, the possibility of rain-out of droplets to the ground (forming an evaporating pool) is addressed. Therefore, the droplet size is estimated and the evaporation of a droplet falling through the air. Finally the effects of the evaporation of the droplets remaining in the air are described, leading to an effective density and concentration of the vapour/air mixture that will disperse in the atmosphere. The methodologies are presented stepwise in Diagram 2.8.

Diagram 2.8   Stepwise overview of models to describe two-phase jets

Step 1	Calculate the conditions in the jet after flashing in the atmosphere is complete: – flash fraction – jet velocity – radius and density of flashed jet
Step 2	Calculation of the droplet diameter after flashing
Step 3	Droplet evaporation and rain-out on the ground: First determine if droplets may reach the ground; If so, calculate the liquid mass fraction that will reach the ground.
Step 4	Calculate the conditions in the jet after evaporation of all airborne droplets: – concentration – jet velocity – radius and density of the single-phase jet

In this section extensive use is made of thermodynamical properties of chemicals. Knowledge is required of the following material properties: density of liquid and vapour as a function of temperature and pressure, enthalpy as a function of temperature, kinematic viscosity of the liquid phase, latent heat, surface tension of the liquid-vapour interface, molar weight, saturation pressure as a function of temperature and the binary diffusion coefficient of the vapour in air. For a number of chemicals these data are collected in the Annex of this Yellow Book. In some cases e.g. (the binary diffusion coefficient) approximate values are presented in the text.

Step 1 - Calculate the conditions in the jet after flashing

The outflow conditions can be characterised by the following quantities:
− the pressure at the exit P_e [N/m^2],
− the temperature at the exit T_e (K),
− the effective cross-section of the exit opening A_e [m^2],
− the total mass flow rate $q_{S,e}$ [kg/s], which is the product of exit cross-section A_e [m^2] and mass flux [kg/(m^2·s)], and
− the vapour mass fraction (or 'quality') at the exit $\Phi_{m,e}$ (kg vapour per kg two-phase mixture).

In case of outflow through a hole in a vessel wall the exit conditions are identical to the (bulk) conditions in the vessel.

In case of outflow from piping or pipeline the exit conditions refer to the conditions in the pipe before the outflow opening.

The density at the exit ρ_e [kg/m^3] can be calculated from the vapour density $\rho_{V,e}$ at P_e and T_e, the liquid density $\rho_{L,e}$ at T_e and the quality $\Phi_{m,e}$:

$$\frac{1}{\rho_e} = \frac{(1 - \Phi_{m,e})}{\rho_{L,e}} + \frac{\Phi_{m,e}}{\rho_{V,e}} \qquad \text{(m}^3\text{/kg)} \qquad (2.138)$$

After the exit the flow will depressurise to atmospheric pressure and liquid will flash to vapour until the two-phase mixture is at boiling temperature. From conservation of momentum and conservation of mass the jet velocity after flashing can be calculated:

$$u_f = \frac{(P_e - P_a)A_e}{q_{s,e}} + u_e \qquad \text{(m/s)} \qquad (2.139)$$

Here P_a is the ambient pressure, and u_e is the velocity in the exit which follows from the exit density ρ_e and the mass flux. From the conservation of total energy the quality after flashing can be calculated:

$$\Phi_{m,f} = 1 - \frac{H_{V,f} - H_{V,e} + (1 - \Phi_{m,e})L_{v,e} + \frac{1}{2}(u_f^2 - u_e^2)}{L_{v,f}} \qquad \text{(-)} \qquad (2.140)$$

Here, $H_{V,e}$ and $H_{V,f}$ are the vapour enthalpies [J/kg] for the exit temperature and boiling temperature, respectively. $L_{v,e}$ and $L_{v,f}$ are the latent heat of evaporation at exit conditions and after flashing, respectively. The average jet density after flashing ρ_f is calculated using (2.138) by changing in this formula lower index e by lower index f. Now the increase of the jet cross-section A_f and jet radius b_f can be calculated from conservation of mass:

$$A_f = \frac{\rho_e u_e}{\rho_f u_f}A_e \qquad b_f = \sqrt{\frac{A_f}{\pi}} \qquad \text{(m}^2\text{; m)} \qquad (2.141)$$

Step 2 - Calculation of the droplet diameter after flashing

In order to estimate the possibility of rain-out (droplets from the jet falling to the ground and not contributing directly to the amount of pollutant in the jet), it is necessary to calculate the droplet diameter after flashing.

In reality, all droplets have different diameters. Here, we only calculate a single droplet diameter which will be assumed to be representative of all droplets.

The droplet diameter depends on jet velocity, jet size, viscosity and surface tension. Therefore, use is made of two dimensionless numbers, the Reynolds number Re_f and the Weber number We_f. The Reynolds number characterises the balance between momentum and kinematic viscosity ν, the Weber number characterises the balance between momentum and surface tension σ_s:

$$\text{Re}_f = \frac{2b_f u_f}{\upsilon_L} \qquad \text{We}_f = \frac{2b_f u_f^2 \rho_{L,f}}{\sigma_s} \qquad\qquad (\text{-};\text{-}) \qquad (2.142)$$

Here, b_f is the jet radius and u_f is the jet velocity after flashing, $\rho_{L,f}$ is the density and υ_L is the kinematic viscosity of the liquid after flashing, and σ_s is the surface tension between the liquid and the vapour.

The droplet size can now be estimated by the following correlations:

− If $\text{We}_f < \text{Re}_f^{-0.45} \times 10^6$ **and** $T_e < 1.11 T_B$ (where T_B is the normal boiling temperature), then:

$$d_d = 3.78 b_f \sqrt{\left(1 + 3\frac{\text{We}_f^{\frac{1}{2}}}{\text{Re}_f}\right)} \qquad\qquad (\text{m}) \qquad (2.143a)$$

− Else:

$$d_d = C_{ds}\frac{\sigma_s}{u_f^2 \rho_a} \qquad\qquad (\text{m}) \qquad (2.143b)$$

Here ρ_a is the density of air (ambient gas).
In the literature values for the constant C_{ds} vary between 10 and 20. Here a value of 15 is recommended.
Large droplets falling to the ground will break-up according to the second of the above correlations, inserting the free fall velocity u_d for u_f. This requires an iterative solution using the above correlation and formula (2.145) for u_d in the following section.

Step 3 - Droplet evaporation and rain-out on the ground

In this section, first an estimate is made whether droplets originating from the flashing can fall to the ground. If this is the case, the total mass fraction that will fall on the ground is calculated.
The droplets are assumed to have the same diameter: the evolution of the single droplet diameter due to evaporation is therefore assumed to be representative of all droplets.
Estimation of droplet rain-out requires calculation of the rate of evaporation of individual droplets. The evaporation is restricted by a heat flux from the ambient air to the droplet and by the mass flux from the droplet surface into the ambient air. Therefore, the problem depends on convection and diffusion of heat and mass in air. The relevant dimensionless numbers are the Reynolds number Re_d, based on the relative velocity of the droplet through the air, the Schmidt number Sc, the ratio of viscosity to mass diffusion, and the Prandtl number Pr, the ratio between viscosity and heat diffusion. These numbers will be used in the following calculations. The latter two numbers only depend on the properties of air and the released chemical:

$$\text{Re}_d = \frac{u_d d_d}{\upsilon_a} \qquad\qquad \text{Sc} = \frac{\upsilon_a}{D} \qquad\qquad \text{Pr} = \frac{C_p \rho_a \upsilon_a}{\lambda} \qquad\qquad (\text{-};\text{-};\text{-}) \quad (2.144a,b,c)$$

In these definitions, u_d is the relative velocity of the droplet in surrounding air. In the following formulae, it is assumed that u_d equals the free fall velocity of the droplet. ν_a is the kinematic viscosity of the ambient air, d_d is the droplet diameter. D is the binary diffusion coefficient of the vapour through air. C_p is the specific heat, ρ_a the density and λ is the conductivity of heat of the ambient air. For the Prandtl number in air at about 288 K one can use Pr=0.71. If no data on the binary diffusion constant D are available, one can also assume Sc≈0.7.

The velocity u_d is assumed to be the final free fall velocity. For small droplets, use can be made of Stokes' flow regime which is strictly valid for $Re_d < 1$, but the results are not sensitive to this assumption:

$$u_d \ = \ \frac{\rho_{L,f} g}{18 \upsilon_a \rho_a} d_d^2 \qquad \text{(m/s)} \qquad (2.145)$$

Here $\rho_{L,f}$ is the density of the droplet at boiling temperature (i.e. the condition after flashing), and g is the acceleration of gravity (g≈9.8ms^{-2}).
For the calculation of the evaporation from the droplet, first a coefficient k_B is defined which governs the evaporation at the droplets' surface:

$$k_B \ = \ \frac{4\mu_i D P_a}{\rho_{L,f} R T_a} \ln\left(1 - \frac{P_s(T_d)}{P_a}\right) \qquad \text{(m}^2\text{/s)} \qquad (2.146)$$

Here, μ_i is the molar weight of the released chemicals, P_a is the ambient pressure, R the universal gas constant (R = 8.31434 J × mol^{-1}K^{-1}), T_a is the ambient temperature, and $P_v^\circ(T_d)$ is the saturation pressure of the released chemical at the droplet temperature.

Now, first the temperature difference between the ambient air and the droplet needs to be calculated. This so-called temperature depression maintains the required heat flux from the air to the droplet in order to enable the evaporation. This requires the iterative solution of the following equation. The solution needs to be iterative as the saturation pressure P_v° as included in the evaluation of k_B, is strongly dependent on the droplet temperature T_d. It is not necessary to evaluate the droplet density ρ_L and the Reynolds number Re_d for each iteration:

$$T_d \ = \ T_a - \frac{L_{v,d} k_B \rho_{L,f}\left[1 + 0.28 Re_d^{\frac{1}{2}} Sc^{\frac{1}{3}}\right]}{4\lambda\left[1 + 0.28 Re_d^{\frac{1}{2}} Pr^{\frac{1}{3}}\right]} \qquad \text{(K)} \qquad (2.147)$$

It is now possible to approximate the maximum diameter of a droplet that will rain-out from a release height h_s above the ground:

$$d_M \ = \ 2\left[\frac{9\rho_a \upsilon_a k_B h_s}{2\rho_{L,f} g}\left[1 - 0.204 Sc^{\frac{1}{3}}\left[\frac{\rho_{L,f} g}{18\rho_a \upsilon_a^2}\right]^{\frac{1}{2}}\left[\frac{72\rho_a \upsilon_a k_B h_s}{\rho_{L,f} g}\right]^{\frac{3}{8}}\right]^{-1}\right]^{\frac{1}{4}}$$

$$\text{(m)} \qquad (2.148)$$

This approximation is applicable if Re_d (based on d_M) < 4. Rain-out will only occur if the droplet size after flashing d_d is larger than the maximum rain-out droplet d_M. If d_d is smaller than d_M, and Re_d (based on d_M) < 4, one may skip to the next section.

If d_d is larger than d_M or Re_d > 4, the total mass that will rain-out and the mass that remains in the air need to be calculated. Therefore, a numerical integration needs to be performed of the evolution of the diameter of the droplet as it evaporates while falling down. The evolution of the droplet diameter $d_d(t)$ can be calculated from the differential equation:

$$\frac{d}{dt}d_d = -\frac{k_B}{d_d}\left[1 + 0.28Re_d^{\frac{1}{2}}Sc^{\frac{1}{3}}\right] \qquad \text{(m/s)} \qquad (2.149)$$

Here Re_d depends on the droplet diameter according to (2.144) and (2.145). The height above the ground of the droplet is calculated by integrating the velocity u_d, which also varies with time according to (2.145), over time. It is assumed that the release is horizontal, and that there is no initial vertical velocity component. The integration is performed until the droplet hits the ground, i.e. $h(t_0)=0$. Therefore, t_0 follows implicitly from the following expression:

$$0 = h(t_0) = h_s - \int_0^{t_0} u_d dt \qquad \text{(m)} \qquad (2.150)$$

In practice, as u_d depends on the droplet size, (2.149) and (2.150) are simultaneously numerically integrated until z=0.
By comparing the droplet size d_0 when the droplet hits the ground to the initial droplet size after flashing, d_d, the evaporated mass fraction while falling to the ground, can be calculated. This in turn will lead to the nett mass released to the air by the jet:

$$q_{s,\,nett,air} = \Phi_{m,\,f}q_{s,\,e} + (1 - \Phi_{m,\,f})\left(1 - \left[\frac{d_0}{d_d}\right]^3\right)q_{s,\,e} \qquad \text{(kg/s)} \qquad (2.151)$$

Here, $q_{S,e}$ is the mass flow rate through the release opening, and $\Phi_{m,f}$ the vapour mass ratio or quality after flashing. The first term refers to the vapour initially in the jet while the second term refers to the vapour released while the droplets fall to the ground. The latter process leads to a cooling of the air entrained in the vapour/aerosol cloud. This cooling process will be described in the following section, but it requires the redefinition for the quality and the jet cross-section after flashing in case rain-out occurs, i.e.:

$$\Phi_{m,\,f,\,rainout} = \frac{\Phi_{m,\,f}}{\Phi_{m,\,f} + (1 - \Phi_{m,\,f})\left(1 - \left[\frac{d_0}{d_d}\right]^3\right)} \qquad \text{(-)} \qquad (2.152)$$

$$A_{f,\,rainout} = A_f\frac{q_{s,\,nett,air}}{q_{s,\,e}} \qquad b_{f,\,rainout} = \sqrt{\frac{A_{f,\,rainout}}{\pi}} \qquad \text{(m}^2\text{; m)} \qquad (2.153)$$

In case rain-out occurs, in the following sections $\Phi_{m,f}$, A_f, and $q_{S,e}$ should be replaced by $\Phi_{m,f,\,rainout}$, $A_{f,\,rainout}$, and $q_{S,nett,air}$.

Step 4 - **Calculate the conditions in the jet after evaporation of all airborne droplets**

The evolution of a two-phase jets in terms of air entrainment, width, concentration decay and velocity decay is the same as the evolution of single-phase jets as described in chapter 4.

In order to perform subsequent dispersion modelling using dispersion models which do not account for two-phase effects in the plume or cloud, this section provides the technique to calculate the cooling of the single-phase jet after all airborne droplets have evaporated. More details about coupling are provided in section 2.7.2.2.

The concentration in the jet corresponding to the amount of air which has to be entrained into the jet in order to evaporate all aerosols, has to be calculated in an iterative way from the enthalpy balance. The total changes in enthalpy due to temperature change, evaporation of aerosol or condensation of ambient humidity, need to be zero:

$$\Delta(H_{chemical}) + \Delta(H_{dry\ air}) + \Delta(H_{water\ vapour}) = 0 \qquad \text{(J/mol)} \qquad (2.154)$$

The terms in the foregoing enthalpy balance will be evaluated separately below.

The molar fraction c_j of the vapour in the jet is equal to the partial vapour pressure. As long as droplets are present up to the moment when all liquid has just evaporated, the partial vapour pressure equals the saturation pressure at the jet temperature T_j:

$$c_j = \frac{P_v^o(T_j)}{P_a} \qquad \text{(-)} \qquad (2.155)$$

If all liquid aerosol has evaporated, the quality or vapour mass fraction $\Phi_{m,j}$ is zero. In that case the enthalpy change of the released chemical since flashing follows from:

$$\Delta(H_{chemical}) = c_j\mu_s[-(1 - \Phi_{m,f})L_{v,f} + H_f - H_j] \qquad \text{(J/mol)} \qquad (2.156)$$

Here, μ_s is the molar mass of the released chemical, $L_{v,f}$ is the latent heat of evaporation, and H_f and H_j the specific enthalpies at boiling temperature and jet temperature, respectively.

The enthalpy changes of air depend on the humidity of the air. The mass fraction of water vapour in the ambient dry air (it is assumed no water droplets or mist are present in the ambient air) is given by:

$$\frac{m_w}{m_{da}} = \frac{RH_a P_{v,w}^o(T_a)}{(R/\mu_w)T_a\rho_a} \qquad \text{(-)} \qquad (2.157)$$

Here, RH_a is the ambient relative humidity, $P_{s,w}(T_a)$ is the saturation pressure of water at ambient temperature T_a, R is the gas constant, μ_w is the molar weight of water, and ρ_a is the density of ambient air.

After the air in the jet has cooled down to jet temperature T_j, part of the water vapour may condense. The remaining mass fraction of vapour is calculated by:

$$\frac{m_{wv}}{m_{da}} = \frac{T_a P^o_{v,w}(T_j)}{RH_a T_j P^o_{v,w}(T_a)} \qquad\qquad (-) \qquad (2.158)$$

The molar fraction of water vapour to dry air at ambient temperature and jet temperature, respectively, are:

$$c_w = \frac{m_w \mu_a}{m_{da} \mu_w} \qquad c_{wv} = \frac{m_{wv} \mu_a}{m_{da} \mu_w} \qquad\qquad (-) \qquad (2.159)$$

Here μ_a and μ_w are the molar weights of (dry) air and water, respectively ($\mu_a = 28.96 \cdot 10^{-3}$ kg/mol, $\mu_w = 18.02 \cdot 10^{-3}$ kg/mol.
The enthalpy change of entrained dry air can now be calculated by:

$$\Delta(H_{dry,air}) = \frac{(1-c_j)}{(1+c_{wv})} C_p \mu_a (T_a - T_j) \qquad\qquad (J/mol) \qquad (2.160)$$

Here C_p is the specific heat of air.
The enthalpy change of the water entrained with the air is:

$$\Delta(H_{water\ vapour}) = \frac{(1-c_j)}{(1+c_{wv})} \mu_w [C_{p,w}(T_a - T_j)]$$
$$\qquad\qquad (J/mol) \qquad (2.161)$$

Here, $L_{w,j}$ is the latent heat of water at jet temperature, and $C_{p,w}$ is the specific heat of water vapour.
The jet temperature and molar fraction or volume concentration c_j can be calculated iteratively from the expressions above. First, an initial temperature T_j is chosen for which the molar fraction c_j can be calculated using (2.155). Then the contributions T to the enthalpy balance can be evaluated and the total sum can be calculated from (2.154). By means of an iterative procedure (Regula Falsi) new values of T_j can be selected in order to minimise the sum of enthalpy changes.
The situation in the jet just after complete evaporation of the liquid aerosols of released material (note water aerosols are likely to be present), is relevant in order to calculate the total (negative) buoyancy released to the air. The density of the jet can be calculated as follows. First, the equivalent molar mass of the vapour mixtures is calculated:

$$\mu_{jd} = c_j \mu_s + \frac{(1-c_j)}{(1+c_{wv})} (\mu_a + c_{wv} \mu_w) \qquad\qquad (kg/mol) \qquad 2.162)$$

The density of the vapour only follows from the perfect gas law:

$$\rho_{jd} = \frac{P_a \mu_{jd}}{R\ T_j} \qquad\qquad (kg/m^3) \qquad (2.163)$$

In order to account for the condensed water vapour, the additional water liquid molar fraction is calculated:

$$c_{jL} = \frac{(1-c_j)}{(1+c_{wv})} (c_w - c_{wv}) \frac{\mu_w}{u_{jd}} \qquad\qquad (-) \qquad (2.164)$$

Now the density follows from:

$$\rho_j = \frac{1 + c_{jL}}{\dfrac{1}{\rho_{j,d}} + \dfrac{c_{jL}}{\rho_{w,L}}} \qquad (kg/m^3) \qquad (2.165)$$

Here, $\rho_{w,L}$ is the density of liquid water at jet temperature.

One can define an equivalent single-phase source to be used for any jet model or dispersion model by a uniformly distributed velocity u_j over an area A_j. The initial volume concentration in this volume flow rate is c_j:

$$u_j = \frac{u_f}{1 + \dfrac{(1 - c_j)\mu_a}{c_j \; \mu_s}} \qquad (m/s) \qquad (2.166)$$

$$A_j = \frac{\rho_f u_f}{\rho_j u_j} A_f \qquad b_j = \sqrt{\frac{A_j}{\pi}} \qquad (m^2; \; m) \qquad (2.167)$$

2.5.3.8   Instantaneous release of pressurised liquefied vapours

This section provides models to describe the behaviour of pressurised liquefied vapours after complete loss of containment. First, the effects associated with the sudden depressurisation of the release to atmospheric pressure are described. Secondly, the rain-out of liquid on the ground is estimated. Thirdly, the growth of the expanding cloud while entraining air, is described. Finally, the effects of droplet evaporation on the cloud density are described.

The methodologies are presented stepwise in Diagram 2.9.

Diagram 2.9   Overview of steps to describe instantaneous two-phase releases

Step 1	Calculate the conditions after depressurisation to atmospheric pressure: − flash fraction − expansion velocity − cloud radius and density
Step 2	Calculate the rain-out fraction to the ground
Step 3	Calculate the expansion of the cloud during the entrainment phase
Step 4	Calculate the conditions in the cloud after evaporation of all airborne droplets: − concentration − expansion velocity − cloud radius and density

In general the same material properties as in section 2.5.3.7 are required.

Step 1 - **Calculate the conditions in the cloud after depressurisation**

The storage conditions as they prevail in the containment prior to the release will be assumed to be input for the calculations.

These conditions are:

Storage temperature T_0 (K)
Pressure P_0 (N/m)
Total mass stored Q (kg)
Vapour mass fraction $\Phi_{m,0}$ (-)
(to be derived from the fill level of the vessel)

The expansion to atmospheric pressure leads to flashing and evaporation of liquid. After flashing, the temperature T_B equals the normal boiling temperature of the released chemical.
The vapour mass fraction $\Phi_{m,f}$ after flashing can be calculated assuming isentropic flashing:

$$\Phi_{m,f} = \frac{\Phi_{m,0}\dfrac{L_{v,0}}{T_0} + S_{0,L} - S_{f,L}}{\dfrac{L_{v,f}}{T_f}} \qquad\text{(-)} \qquad (2.168)$$

Here $L_{v,0}$ and $L_{v,f}$ are the latent heat of the chemical at storage and boiling temperature, respectively, and $S_{0,L}$ and $S_{f,L}$ are the entropy of the liquid chemical at storage temperature and pressure and boiling temperature and ambient pressure, respectively. If no detailed data on entropies are available, this can be approximated by:

$$\Phi_{m,f} = \Phi_{m,0}\frac{T_f}{T_0} + \frac{T_f}{L_{v,f}}\,C_{p,L}\ln\frac{T_0}{T_f} \qquad\text{(-)} \qquad (2.169)$$

Here $C_{p,L}$ is the specific heat of the liquid.
It is assumed that the stored chemical is initially at rest. During flashing the liquid/vapour cloud will expand with a velocity which follows from the conservation of total energy during flashing. This energy balance also includes the work performed on the ambient air. The real expansion velocity will be about 20% lower than the value which follows directly from the energy balance because part of the kinetic energy will be transferred to turbulence and the flashing process will probably not be isentropic. So the expansion velocity u_f is approximated by:

$$u_f = 0.8\sqrt{2\left(H_{0,V} - H_{f,V} + (1 - \Phi_{m,f})L_{v,f} - (1 - \Phi_{m,0})L_{v,0} - \frac{P_0 - P_a}{\rho_0}\right)} \qquad\text{(m/s)} \qquad (2.170)$$

Here $H_{0,V}$ and $H_{f,V}$ are the vapour enthalpy of the released chemical at storage temperature and boiling temperature, respectively. ρ_0 is the average density of the

chemical in the vessel, which can be calculated by (2.138), thereby changing index e to index 0.

The total volume V_f after flashing follows from

$$V_f = \frac{Q}{\rho_f} \qquad\qquad\qquad (m^3) \qquad (2.171)$$

Here ρ_f is calculated by (2.138) thereby changing index e to index f. For a vessel on the ground the expanding cloud will be a hemisphere. After flashing the radius of the hemisphere will be:

$$b_f = \left(\frac{3V_f}{2\pi}\right)^{1/3} \qquad\qquad\qquad (m) \qquad (2.172)$$

Step 2 - Calculate the rain-out fraction to the ground

The amount of liquid raining out from the cloud depends on the flash fraction. If $\Phi_{m,f} < 0.5$, twice the initial flash fraction will remain airborne, i.e.:

$$Q_{nett,air} = 2\Phi_{m,f}Q \qquad\qquad\qquad (kg) \qquad (2.173)$$

If $\Phi_{m,f} > 0.5$, no rain-out is assumed. If rain-out occurs, the vapour mass fraction in the cloud needs to be redefined. From the calculation of $Q_{nett,air}$ it follows that in that case always $\Phi_{m,f,rainout}=0.5$. It is also necessary to redefine the cloud density ρ_f (formula 2.138 using $\Phi_{m,f,rainout}$), V_f and b_f. In the following sections one should replace Q, $\Phi_{m,f}$ ρ_f, V_f and b_f by these redefined values if rain-out occurs.
The fraction of total mass not remaining in the air will form an evaporating pool on the ground.

Step 3 - Calculate the expansion of the cloud during the entrainment phase

It is assumed that after flashing air is entrained in the cloud. The concentration of air and released chemical in the cloud are uniform throughout the cloud.
If we define t_f to be the time when flashing is complete, i.e. when the radius b equals b_f, the evolution with time after flashing of the radius and expansion velocity of the cloud can be calculated by:

$$b(t) = \left[4u_f b_f^3(t-t_f) + b_f^4\right]^{\frac{1}{4}} \qquad\qquad (m) \qquad (2.174)$$

$$u(t) = u_f\left(\frac{b_f}{b(t)}\right)^3 \qquad\qquad\qquad (m/s) \qquad (2.175)$$

Step 4 - **Calculate the conditions in the cloud after evaporation of all airborne droplets**

In order to calculate the extent of the two-phase cloud and to enable coupling with dispersion models which need an initial cloud size, this section provides the method to determine the size of the cloud when all aerosol has evaporated and the expansion velocity is reduced to the wind velocity at the cloud height after flashing b_f.

The determination of the amount of entrained air needed to evaporate all liquid aerosol (except condensed water from the water vapour contained in the air), or, in other words, the required concentration c_j, is performed as described in section 2.5.3.7, (2.154) to (2.165), reading 'cloud' for 'jet'. These formulae also provide the averaged cloud density ρ_j.

The cloud volume V_j and radius b_j at the moment all aerosol has evaporated are approximately:

$$V_j = \frac{Q}{c_j \rho_{s,j}} \qquad b_j = \left(\frac{3\,V_j}{2\pi}\right)^{\frac{1}{3}} \qquad\qquad (m^3; m) \qquad (2.176)$$

Here $\rho_{s,j}$ is the density of the vapour of **pure released chemical** (i.e. it is not the cloud averaged density) at the cloud temperature T_j. The initial volume concentration in this cloud is c_j.

Subsequent dispersion modelling can now take place if the expansion velocity u_j is lower than the wind speed u_a at the cloud height after flashing b_f. u_j can be calculated using (2.175) if b_j is inserted for $b(t)$.

If $u_j > u_a(b_f)$, the radius of the cloud b_{disp} and the volume V_{disp} (input for dispersion modelling) can be calculated from:

$$b_{disp} = b_f \left(\frac{u_f}{u_a(b_f)}\right)^{\frac{1}{3}} \qquad V_{disp} = \frac{2}{3}\pi b^3_{disp} \qquad\qquad (m; m^3) \qquad (2.177)$$

Assuming that the averaged molar specific heat of the cloud after evaporation is equal to the molar specific heat of air, the temperature T_{disp} of the cloud of volume V_{disp} can be calculated by:

$$T_{disp} = \frac{T_a}{1 - \dfrac{V_j}{V_{disp}}\left(1 - \dfrac{T_a}{T_j}\right)} \qquad\qquad (K) \qquad (2.178)$$

The molar or volume concentration c_{disp} at this stage of the cloud is:

$$c_{disp} = c_j \frac{V_j\,T_{disp}}{V_{disp}\,T_j} \qquad\qquad (-) \qquad (2.179)$$

The cloud density ρ_{disp} can be estimated (neglecting the effect of water vapour or droplets) by formulae (2.162) and (2.163) (section 2.5.3.7), assuming $c_{wv} = 0$ and inserting T_{disp} and c_{disp} for T_j and c_j, respectively.

The initial clouds V_j or V_{disp} (depending on whether the cloud expansion velocity u_j exceeds the windspeed) can be used as initial conditions for dispersion models.

2.5.4 Liquids

2.5.4.1 Vessel dynamics liquid

The modelling of the dynamics of a vessel filled with (non-boiling) liquid aims at predicting the decrease of liquid mass during the outflow of liquid.

The hydraulic pressure driving the mass flow rate depends on the liquid level in the tank; a constant pressure P by compression with inert gas may be taken into account.

Applying the basic law of conservation of mass, and taking into account the hydraulic pressure of a liquid column, will suffice for an adequate description of the vessel dynamics.

The model is basically an iterative numerical procedure in which the outflow of liquid out of a vessel is described in small steps. These steps should be small enough to consider the conditions in the vessel to be constant during one time-step.

First, the initial condition and termination condition of the numerical procedure will be given. Next, the model in the form of a numerical procedure is given. This numerical procedure has to be repeated until the termination conditions have been satisfied.
Finally, equations relating the liquid height to the liquid volume in the vessel for few vessel shapes are given.

Initial conditions and termination procedure (non-boiling) liquid outflow from a vessel

The initial condition of the vessel (i=1) is given by its filling degree ϕ, constant temperature and vessel volume.
The liquid mass in the vessel can easily be calculated given the (initial) filling degree ϕ, by

$$Q_{L,1} = \phi \times V \times \rho_L(T) \qquad \qquad \text{(kg)} \qquad (2.180)$$

where

$Q_{L,1}$ = liquid mass initially in the vessel $\qquad$ [kg]
ϕ = filling degree $\qquad$ [m^3/m^3]
V = vessel volume $\qquad$ [m^3]
ρ_L = liquid density at storage temperature $\quad$ [kg/m^3]

The initial liquid volume can be estimated by

$$V_{L,1} = Q_{L,1}/\rho_L \qquad \qquad \text{(m}^3\text{)} \qquad (2.181)$$

The initial liquid height can be estimated by using the inverse function between liquid volume and liquid height for the given geometry of the vessel (see next sub-paragraph: eq. (2.193a), (2.193b), (2.193c), expressed by

$$h_{L,1} = F^{-1}(V_{L,1}) \qquad\qquad (m) \qquad (2.182)$$

The duration of δt may be chosen freely in principle, and depends of the number of time-steps N_t. The choice $N_t = 50$ will be appropriate for most calculations. If one wishes to estimate the mass flow rate and vessel conditions at time t_{end}, then the size of time-step δt is given by

$$\delta t = t_{end}/N_t \qquad\qquad (s) \qquad (2.12)$$

The numerical procedures given should be repeated as long as the constraints are valid

$$t_i < t_{end} \qquad\qquad h_L > h_{hole} \qquad\qquad (2.183)$$

The larger the number of steps, the higher the accuracy of the model, but the more time needed for the calculation. The choice $N = 50$ will be appropriate, for most calculations.

Numerical procedure non-boiling liquid outflow from a vessel

Starting every step at time t_i in the iteration with a condition in the vessel given by $Q_{L,i}$ the following procedure aims at calculation of the condition in the vessel at the end of the small time-step δt, given by $Q_{L,i+1}$.

Let us say that the outflow rate $q_{S,i}$ is given by a generalised function f, depending on whether the outflow is through a hole or a pipe (see paragraph 2.5.4.2)

$$q_{S,i} = f(h_{L,i}, P,...) \qquad\qquad (kg/s) \qquad (2.184)$$

The conservation of mass leads very simply to

$$\delta Q = - q_{S,i} \times \delta t \qquad\qquad (kg) \qquad (2.185)$$

The liquid content will decrease with

$$\delta V_L = \delta Q / \rho_L \qquad\qquad (m^3) \qquad (2.186)$$

thus

$$V_{L,i+1} = V_{L,i} + \delta V_L \qquad\qquad (m^3) \qquad (2.187)$$

For simple geometries equations are available to calculate the liquid volume and the size of the liquid area as a function of the liquid level.
In general the following formulation holds

$$A_{L,i} = f(h_{L,i},...) \qquad\qquad (m^2) \qquad (2.188)$$

Then the new liquid level can be calculated by

$$\delta h_L \quad = \delta V_L/A_{L,i} \qquad\qquad (m) \qquad (2.189)$$

$$h_{L,i+1} = h_{L,i} + \delta h_L \qquad\qquad (m) \qquad (2.190)$$

The time from the start of the release must be increased by one time-step after every pass through this numerical procedure

$$t_{i+1} = t_i + \delta t \qquad\qquad (s) \qquad (2.191)$$

The new condition of the vessel at time t_{i+1} is given by: $Q_{L,i+1}$ or $h_{L,i+1}$.
This numerical procedure has to be repeated until the termination conditions have been satisfied.

Liquid height as a function of liquid volume

For simple geometries equations are available to calculate the liquid volume V_L and the size of the liquid surface in the vessel A_L as a function of the liquid level h_L, in the generalised form expressed by

$$A_L = F(h_L) \qquad\qquad (m^2) \qquad (2.192)$$

$$V_L = F(h_L) \qquad\qquad (m^3) \qquad (2.193)$$

For instance, the following relations hold for a few geometries

* sphere

$$A_L = \pi \times (r^2-(r-h_L)^2) \qquad\qquad (m^2) \qquad (2.192a)$$

$$V_L = \pi/3 \times h^2_L f \times (3 \times r-h_L) \qquad\qquad (m^3) \qquad (2.193a)$$

* horizontal cylinder

$$A_L = 2 \times L \times \sqrt{((2 \times r-h_L) \times h_L)} \qquad\qquad (m^2) \qquad (2.192b)$$

$$V_L = L \times [r^2 \times \mathrm{acos}(1-h_L/r) - (r-h_L) \times \sqrt{((2 \times r-h_L) \times h_L}] \qquad (m^3) \qquad (2.193b)$$

* vertical vessel

$$A_L = A_{base} \qquad\qquad (m^2) \qquad (2.192c)$$

$$V_L = A_L \times h_L \qquad\qquad (m^3) \qquad (2.193c)$$

2.120

Where

A_L = liquid surface inside vessel $[m^2]$
A_{base} = base vertical cylinder $[m^2]$
h_L = liquid height $[m]$
V_L = liquid volume in vessel $[m^3]$
r   = radius of the sphere or cylinder $[m]$

2.5.4.2   Liquid outflow through holes and piping

The modelling of the outflow of liquid through holes and piping aims at predicting the mass flow rate as a function of the pressure drop.

Liquid flow through holes or orifices

For liquids flowing through an orifice the Bernoulli equation can be applied. Neglecting the initial liquid velocity in the vessel, the mass flow rate can be estimated by

$$q_s = C_d \times A_h \times \sqrt{(2(P - P_a) \times \rho_L)} \qquad\qquad (kg/s) \qquad (2.194)$$

with

$$P = P_h + P_{aL} \qquad\qquad (N/m^2) \qquad (2.195)$$

and

$$P_h = \rho_L \times g \times h_L \qquad\qquad (N/m^2) \qquad (2.196)$$

A_h = cross-sectional area of the hole $[m^2]$
C_d = discharge coefficient $[-]$
g   = gravitational acceleration $[m/s^2]$
h_L = (relative) liquid height $[m]$
P   = total pressure at opening $[N/m^2]$
P_h = (hydraulic) liquid pressure $[N/m^2]$
P_{aL} = external pressure above liquid $[N/m^2]$
P_a = atmospheric pressure $[N/m^2]$
q_S = mass flow rate $[kg/s]$
ρ_L = liquid density $[kg/m^3]$

The following values for the discharge coefficients are recommended; Beek [1975].

For sharp orifices

$$C_d = 0.62 \qquad\qquad (-) \qquad (2.197a)$$

for straight orifices

$$C_d = 0.82 \qquad\qquad (-) \qquad (2.197b)$$

for rounded orifices

$$C_d = 0.96 \qquad\qquad\qquad\qquad (-) \qquad (2.197c)$$

and for a pipe rupture

$$C_d = 1.0 \qquad\qquad\qquad\qquad (-) \qquad (2.197d)$$

Liquid flow through pipes

The pressure drop for a stationary fluid flow in piping can be estimated by the well-known Darcy-Weisbach equation.

$$\Delta P = f_D \times \rho_f/2 \times u_f^2 \times l_p/d_p \qquad\qquad (N/m^2) \qquad (2.198)$$

Using this equation, an expression for the (average) liquid flow velocity in the pipe can be inferred

$$u_L = \sqrt{(2 \times \Delta P / l_p \times d_p / (f_D \times \rho_L))} \qquad\qquad (m/s) \qquad (2.199)$$

The mass flow rate in the pipe can be calculated by

$$q_S = \rho \times u_L \times A_{pipe} \qquad\qquad\qquad (kg/s) \qquad (2.200)$$

where

d_p	= pipe diameter	[m]
f_D	= Darcy friction factor	[-]
l_p	= pipe length	[m]
u_L	= liquid flow velocity	[m/s]
ΔP	= pressure over the pipe	[N/m²]
ρ_L	= liquid density	[kg/m³]

According to the equations above, the mass flow rate through a pipe depends on the friction in the pipe.
In general the friction factor is a function of the Reynolds number (see paragraph 2.5.5).
The Reynolds number, depending on the flow velocity in the pipe, can be expressed as a function of the mass flow rate

$$Re = f(q_S) \qquad\qquad\qquad\qquad\qquad (2.201)$$

For circular pipes

$$Re = (4/\pi) \times q_S/(d_p \times \eta) \qquad\qquad (-) \qquad (2.201a)$$

This means that the mass flow rate in the pipe has to be calculated by iteration.

2.5.5   Friction factors

Fluid flows in pipes and pipe fittings are associated with friction. The friction causes a pressure drop depending on the roughness of the pipe wall and on the shape of the pipe fitting.

Friction in straight pipes

The Colebrook-White law yields the friction factor as a function of pipe diameter, roughness of the inner pipe wall, flow velocity and viscosity.
If used in combination with the Darcy-Weisbach equation, the two equations are considered by many authorities as the best equations available for determining the head loss for turbulent flow in commercial pipes, as stated by Ackers in 1963 [Radford,1990].

The Darcy friction factor f_D can be predicted by the Colebrook-White law for the transition zone

$$1/\sqrt{f_D} = -2 \times {}^{10}\log(\varepsilon/(3.715 \times d_p) + 2.51/(Re \times \sqrt{f_D})) \qquad (-) \qquad (2.202)$$

The Reynold's number characterises the flow of fluids and is given by

$$Re = \rho \times u \times d_p/\eta \qquad\qquad (-) \qquad (2.101)$$

Equation (2.201) can be solved by applying a root finding procedure, and defining an auxiliary function

$$F(f_D) = 1/\sqrt{f_D} + 2 \times {}^{10}\log(\varepsilon/(3.715 \times d_p) + 2.51/(Re \times \sqrt{f_D})) \quad (-) \qquad (2.202a)$$

The auxiliary function $F(f_D)$ equals zero for that f_D which is the solution of equation (2.201), where

f_D	= Darcy friction factor	[-]
d_p	= pipe diameter	[m]
ε	= wall roughness	[m]
Re	= Reynolds number	[-]
u_f	= fluid flow velocity	[m/s]
ρ_f	= fluid density	[kg/m^3]
η	= dynamic viscosity	[N·s/m^2]

The Darcy-Weisbach equation also predicts the head loss in the pipe

$$\Delta h_{Lp} = f_D \times l_p \times u_f^2/(2 \times g \times d_p) \qquad\qquad (m) \qquad (2.198a)$$

Where

g	= gravitational acceleration	[m/s^2]
Δh_{Lp}	= head loss	[m]
l_p	= pipe length	[m]

The head loss Δh_{Lp} and pressure drop are simply related

$$\Delta P = \rho_f \times g \times \Delta h_{Lp} \qquad\qquad (N/m^2) \qquad (2.203)$$

As apparent from equation (2.202) the Darcy factor is a function of the Reynolds number and the relative wall roughness (the ratio between the wall roughness and the pipe diameter). For the wall roughness the values in the table below can be used.

Table 2.2   Some values for wall roughness for pipes

Material	Wall roughness ε
Bronze, lead, glass	1.5 μm
Commercial steel, wrought-iron	45 μm
Cast iron	250 μm

The pressure drop for a stationary fluid flow in piping is also often estimated by the Darcy Weisbach equation in which the Fanning friction factor is used

$$\Delta P = 4 \times f_F \times \rho_f/2 \times u_f^2 \times l_p/d_p \qquad\qquad (N/m^2) \qquad (2.204)$$

where

f_F = Fanning friction factor for flow in pipes   [-]

From the equations, (2.198) and (2.204) it easy to conclude that the Fanning friction factor is four times smaller than the Darcy friction factor

$$4 \times f_F = f_D \qquad\qquad (m) \qquad (2.205)$$

When applying the equations from literature one should check which factor is referred to.

For the Darcy friction other equations and graphics are well-known.
For laminar flow

$$f_D = 64/Re \qquad\qquad \text{if } Re < 2000 \qquad (-) \qquad (2.206)$$

For turbulent flow and smooth pipe the Blasius equation holds

$$f_D = 0.3164 \times Re^{-0.25} \qquad\qquad \text{if } 4000 < Re < 10^5 \qquad (-) \qquad (2.207)$$

Friction is one of the factors determining the flow velocity in the pipe. As the friction factor depends on the Reynolds number being a function of velocity, in general an iterative procedure should to be applied to estimate the mass flow rate in the pipe. However, according to figure 2.12 'Friction factor for flow in pipes' it appears that the friction factor is virtually constant for sufficiently high Reynolds numbers.
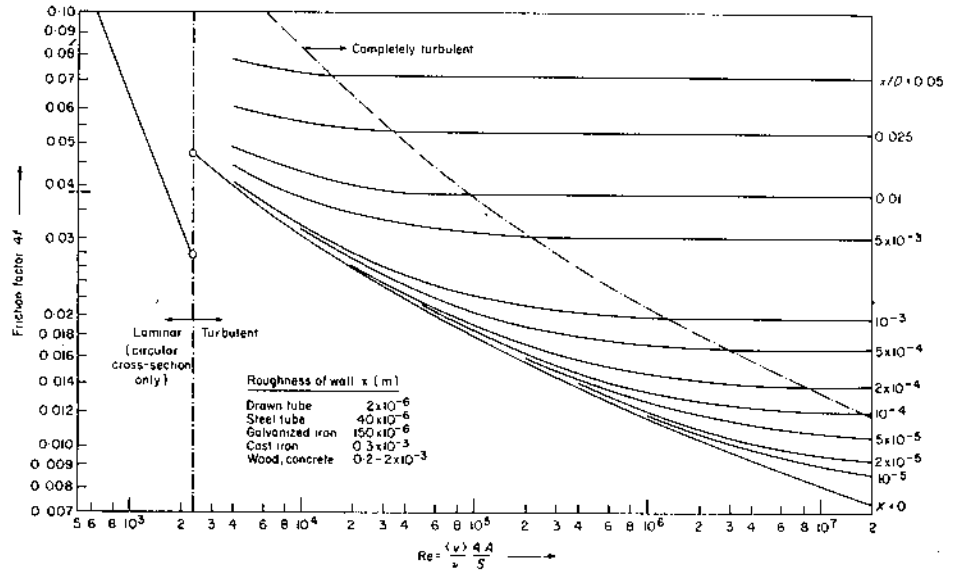
Figure 2.12   Friction factor for flow in pipes by Moody [YellowBook, 1988]

Non-circular pipes

For non-circular pipes the so-called hydraulic diameter may be used which is defined as

$$d_h = 4 \times A_p/s_p \hspace{4cm} \text{(m)} \hspace{1cm} (2.208)$$

where

A_p = cross-sectional area the pipe $[m^2]$
s_p = wetted perimeter of the pipe $[m]$

Note that for circular tubes the hydraulic diameter is equal to the pipe diameter.

The use of Hazen-Williams and Manning relations should be discouraged, but empirical equations are quoted in text books and many people working in the field of hydraulic engineering still prefer them [Radford, 1990].
Additional information can be found in for instance Melhem [1993] and Radford, [1990].

Frictional pressure drop in pipe fittings

The models for outflow through pipes are developed for a pipe with no bends, reductions of cross-section or branches. If such elements are present, they can be accounted for by introducing an extra resistance coefficient.

The relation between the pressure drop and the kinetic energy per element of volume of the transported product is called the friction or resistance coefficient

$$K_i = \Delta P/(1/2 \times \rho_f \times u^2) \hspace{4cm} \text{(-)} \hspace{1cm} (2.209)$$

where

K_i = resistance coefficient $[-]$
ΔP = pressure drop due to friction $[N/m^2]$
ρ_f = density of the fluid $[kg/m^3]$
u = flow velocity of the fluid $[m/s]$

For pipe elements the resistance coefficient K_i has the following values

45˚-bend   : 0.35
90˚-bend   : 0.75
open spherical valve   : 6.4
half-open spherical valve   : 9.5
inlet piece with sharp edges   : 0.5

2.6 Application of the selected models: calculation examples

2.6.1 Introduction to section 2.6

The models presented in this chapter can be divided into iterative models and non-iterative models.
Non-iterative models facilitate predictions by applying a set of equations once. For this type of model calculation examples have been worked out step by step.

Iterative models facilitate predictions only by repeating a (complex) numerical procedure a (great) number of times. A step-by-step approach would not be practical. For this type of model the final results will be given only as a function of specified input.

2.6.2 Compressed gases

2.6.2.1 Hydrogen outflow from a vessel through a hole in the vessel wall

The hydrogen outflow from of a vessel through a hole in the vessel wall can be calculated by the models presented in paragraphs 2.5.2.2 and 2.5.2.3.

Input:

Initial pressure	P_0	=	50	bar
Initial temperature	T_0	=	288.15	K
Vessel volume	V	=	100	m^3
Leak size	d_h	=	0.1	m
(cross-sectional area hole	A_h	=	$7.854 \cdot 10^{-3}$	m^2)
Discharge coefficient	C_d	=	0.62	-
Time from start release	t	=	30	s
Thermodynamic model	Adiabatic			

Output:

Mass flow at 30 sec	q_S	=	4.65	kg/s
Gas pressure at 30 sec	P	=	12.417	bar
Gas temperature at 30 sec	T	=	193	K

Procedure

The number of time-steps N_t has been set to equal 50.
By equation (2.22) the mass flow rate $q_{s,i}$ at the beginning of every time-step can be calculated. Because the pressure in the vessel is much larger than about $1.9 \cdot P_a$, the gas flow is critical initially.

Using the equations (2.14) and (2.20) subsequently and assuming perfect gas behaviour (z=1), the variation of the vessel conditions (P_i, T_i, ρ_i) due to the outflow can be calculated.

In table 2.3 the variations in the physical quantities have been given.

Table 2.3

Time after rupture [s]	Flowrate [kg/s]	Hole pressure [bar]	Gas temperature [°C]	Total mass release [kg]
0.00	15.31	50.000	15.00	0,00
0.60	14.92	48.494	12.47	9.07
1.20	14.53	47.037	9.97	17.90
1.35	14.44	46.681	9.35	20.07
1.50	14.34	46.328	8.74	22.23
1.80	14.16	45.630	7.51	26.51
2.10	13.98	44.945	6.29	30.73
2.40	13.80	44.271	5.08	34.89
2.70	13.62	43.609	3.87	39.00
3.00	13.45	42.959	2.67	43.06
3.30	13.27	42.319	1.48	47.07
3.60	13.10	41.690	0.30	51.03
3.90	12.94	41.072	-0.87	54.93
4.20	12.77	40.464	-2.04	58.79
4.50	12.61	39.867	-3.20	62.60
4.80	12.45	39.280	-4.35	66.36
5.10	12.30	38.702	-5.49	70.07
5.40	12.14	38.135	-6.63	73.74
5.70	11.99	37.576	-7.76	77.36
6.00	11.84	37.027	-8.88	80.93
6.30	11.69	36.488	-10.00	84.46
6.60	11.55	35.957	-11.11	87.95
6.90	11.40	35.435	-12.21	91.39
7.20	11.26	34.922	-13.30	94.79
7.50	11.12	34.417	-14.39	98.14
7.80	10.98	33.920	-15.47	101.46
8.10	10.85	33.432	-16.55	104.73
8.40	10.72	32.952	-17.61	107.97
8.70	10.58	32.479	-18.67	111.16
9.00	10.45	32.015	-19.73	114.32
9.30	10.33	31.558	-20.78	117.43
9.60	10.20	31.108	-21.82	120.51
9.90	10.08	30.666	-22.85	123.55
10.20	9.95	30.230	-23.88	126.56
10.50	9.83	29.802	-24.90	129.53
10.80	9.71	29.381	-25.92	132.46
11.10	9.60	28.967	-26.93	135.35
11.40	9.48	28.559	-27.93	138.22
11.70	9.37	28.158	-28.93	141.04
12.00	9.25	27.763	-29.92	143.83
12.30	9.14	27.375	-30.90	146.59
12.60	9.03	26.993	-31.88	149.32
12.90	8.92	26.617	-32.86	152.01

Time after rupture [s]	Flowrate [kg/s]	Hole pressure [bar]	Gas temperature [°C]	Total mass release [kg]
13.20	8.82	26.247	-33.82	154.68
13.50	8.71	25.882	-34.78	157.31
13.80	8.61	25.524	-35.74	159.90
14.10	8.51	25.171	-36.69	162.47
14.40	8.41	24.824	-37.63	165.01
14.70	8.31	24.482	-38.57	167.52
15.00	8.21	24.146	-39.51	169.99
15.30	8.11	23.815	-40.43	172.44
15.60	8.02	23.489	-41.35	174.86
15.90	7.93	23.168	-42.27	177.25
16.20	7.83	22.852	-43.18	179.62
16.50	7.74	22.541	-44.09	181.95
16.80	7.65	22.235	-44.99	184.26
17.10	7.56	21.934	-45.88	186.55
17.40	7.47	21.637	-46.77	188.80
17.70	7.39	21.345	-47.66	191.03
18.00	7.30	21.057	-48.54	193.23
18.30	7.22	20.774	-49.41	195.41
18.60	7.14	20.495	-50.28	197.57
18.90	7.05	20.221	-51.14	199.69
19.20	6.97	19.951	-52.00	201.80
19.50	6.89	19.684	-52.86	203.88
19.80	6.81	19.422	-53.71	205.93
20.10	6.74	19.164	-54.55	207.97
20.40	6.66	18.910	-55.39	209.98
20.70	6.59	18.659	-56.22	211.96
21.00	6.51	18.413	-57.05	213.93
21.30	6.44	18.170	-57.88	215.87
21.60	6.36	17.931	-58.70	217.79
21.90	6.29	17.695	-59.51	219.69
22.20	6.22	17.463	-60.33	221.57
22.50	6.15	17.234	-61.13	223.42
22.80	6.08	17.009	-61.93	225.26
23.10	6.02	16.787	-62.73	227.07
23.40	5.95	16.569	-63.52	228.87
23.70	5.88	16.354	-64.31	230.64
24.00	5.82	16.141	-65.10	232.40
24.30	5.75	15.932	-65.88	234.13
24.60	5.69	15.727	-66.65	235.85
24.90	5.63	15.524	-67.42	237.54
25.20	5.56	15.324	-68.19	239.22
25.50	5.50	15.127	-68.95	240.88
25.80	5.44	14.933	-69.71	242.52
26.10	5.38	14.742	-70.46	244.15
26.40	5.32	14.553	-71.21	245.75
26.70	5.27	14.368	-71.96	247.34
27.00	5.21	14.185	-72.70	248.91
27.30	5.15	14.005	-73.43	250.47
27.60	5.10	13.827	-74.17	252.00
27.90	5.04	13.652	-74.90	253.52
28.20	4.99	13.479	-75.62	255.03
28.50	4.93	13.309	-76.34	256.52

Time after rupture [s]	Flowrate [kg/s]	Hole pressure [bar]	Gas temperature [°C]	Total mass release [kg]
28.80	4.88	13.142	-77.06	257.99
29.10	4.83	12.977	-77.77	259.44
29.40	4.77	12.814	-78.48	260.88
29.70	4.72	12.653	-79.19	262.31
30.00	4.67	12.495	-79.89	263.72

2.6.2.2 Carbon monoxide flow through hole in a pipe

The carbon monoxide outflow from a vessel through a pipe can be calculated by the model presented in paragraph 2.5.2.4.

Input:

Vessel volume	V	=	100	m^3
Constant pressure upstream	P_0	=	15	bar
Initial temperature	T_0	=	288.15	K
Pipe length	l_p	=	1000	m
Pipe diameter	d_p	=	0.254	m
Internal wall roughness pipe	ε	=	$4.5 \cdot 10^{-5}$	m
Leak size	d_h	=	0.1	m
(cross-sectional area hole	A_h	=	$7.854 \cdot 10^{-3}$	m^2)
Discharge coefficient	C_d	=	0.62	-

Output:

Mass flow at t = 0 s	q_S	=	15.615	kg/s

Procedure

The four steps of the numerical procedure given in paragraph 2.5.2.4. have to be repeated several times. By using equation (2.30a) the number of iterations can be limited by a root finding procedure.

2.6.2.3   Non-stationary natural gas (methane) outflow from full bore ruptured MTH-1 pipeline

The non-stationary methane outflow can be calculated by the models presented in paragraph 2.5.2.5. In particular, the Wilson model for the outflow of gas from a full bore ruptured pipeline aims at predicting the mass flow rate as a function of time depending on the initial conditions.

Input:

Initial pressure	P_0	=	68.5	Bar
Initial temperature	T_0	=	288.15	K
Initial density	ρ_0	=	45.8	kg/m^3
Pipe length	l_p	=	$100 \cdot 10^3$	m
Pipe diameter	d_p	=	1.219	m
Internal wall roughness pipe	ε	=	$3.0 \cdot 10^{-5}$	m

Output:

Mass flow at t =	0 s	q_S =	13829	kg/s
	10 s	=	10335	kg/s
	20 s	=	7793	kg/s
	50 s	=	3623	kg/s
	100 s	=	1543	kg/s
	200 s	=	1017	kg/s
	226 s	=	999	kg/s

Procedure

The rather trivial steps in the set of equations in subsection 2.5.2.5 have to be followed.

1. The initial total mass Q_0 in the pipeline can be calculated by

$$A_p = \pi/4 \times d_p^{\,2} \qquad\qquad (2.36b)$$

$$= 1.167 \text{ m}^2$$

$$Q_0 = \rho_0 \times A_p \times l_p \qquad\qquad (2.36a)$$

$$= 5.345 \times 10^6 \text{ kg}$$

2. The initial release rate $q_{S,0}$ can be calculated by using the equations presented in paragraph 2.5.2.4

$$q_{S,0} = 13831 \text{ kg/s} \qquad\qquad (2.37)$$

For outflow through the pipe opening in case of a full bore rupture it is advised to use the following value for the discharge coefficient

$C_d = 1.0$ (2.38)

and $\psi^2 = 1$ (2.24)

3. The sonic velocity in the gas u_s, assuming adiabatic expansion ($\Delta S = 0$), is given for perfect gases ($z = 1$, $\zeta = \gamma = 1.31$) and for methane ($\mu_i = 16 \cdot 10^{-3}$ kg/mol) by

$$u_s = \sqrt{(\zeta \times z \times R \times T_0 / \mu_i)}$$ (2.39c)

$$= 442.9 \text{ m/s}$$

4. The Darcy friction factor may be calculated by the Von Karman equation

$$f_D = \{1./(-2 \times {}^{10}\log(\varepsilon/(3.715 \times d_p)))\}^2$$ (2.40)

$$= 9.32 \cdot 10^{-3}$$

5. The time constant t_B is given by

$$t_B = 2/3 \times l_p / u_s \times \sqrt{(\gamma \times f_D \times l_p / d_p)}$$ (2.41)

$$= 4764 \text{ sec}$$

6. Finally the mass flow rate $q_S(t)$ can be estimated at any time t after the full bore rupture of the pipeline by the Wilson model given by equation (2.35).

The mass flow rate for a full bore ruptured pipeline according to the model of Wilson at t=100

$$q_S(t) = q_{S,0}/(1 + Q_0/(t_B \times q_{S,0})) \times \{Q_0/(t_B \times q_{S,0}) \times \exp(-t/t_B) + \exp(-t \times t_B \times (q_{S,0}/Q_0)^2)\}$$

$$= 12793 \text{ kg/s} \times \{7.944 \cdot 10^{-2} + 4.118 \cdot 10^{-2}\}$$

$$= 1543 \text{ kg/s}$$

7. Check the validity of the model.

When the pressure wave travelling upstream reaches the opposite side of the pipeline the Wilson model is not valid any more. This occurs after

$$t_E = l_p / u_s$$ (2.42)

$$= 1.00 \cdot 10^5 \text{ m} / 442.9 \text{ m/s}$$

$$= 225.8 \text{ s}$$

2.6.2.4 Non-stationary gas flow in pipelines through a small hole

Non-stationary natural gas outflow can be calculated by the models presented in paragraph 2.5.2.5. In particular, the Weiss model for the outflow of gas from pipelines through punctures (small holes) aims at the estimation of the blow-down time.

Estimate the total blow-down time for 25 km of 1.0 metre pipeline which contains natural gas at 60 bar (60×10^5 N/m^2) at 0 °C, with a wall roughness of 30 μm, in which a crack has been created with an area of 0.1 m^2 and a discharge coefficient of 0.62.

Input:

Initial temperature	T	=	273.15	K
Initial pressure	P_i	=	$60.0 \cdot 10^5$	N/m^2
Length of pipeline	l_p	=	$25 \cdot 10^3$	m
Pipeline diameter	d_p	=	1.0	m
Cross-sectional area crack	A_h	=	0.1	m^2
Discharge coefficient	C_d	=	0.62	
Speed of sound	u_s	=	431	m/s
Poisson ratio at 0 °C methane	γ	=	1.31	
Wall roughness	ε	=	$30 \cdot 10^{-6}$	m
Ambient pressure	P_a	=	$1.00 \cdot 10^5$	N/m^2
Molecular weight methane	μ_i	=	$16 \cdot 10^{-3}$	kg/mol

Output:

Blow out time	t	=	100	minutes

Procedure

1. Estimate the time constant by equation (2.43)

$$\tau_v = V \times ((\gamma+1)/2)^a / (u_s \times A_h \times C_d) \qquad \text{note: } a = (\gamma+1)/(2(\gamma-1))$$
$$= 1256 \text{ s} \qquad\qquad\qquad\qquad\qquad\qquad = 3.726$$

Note

$$V = \pi/4 \times d_p{}^2 \times l_p$$
$$= 19635 \text{ m}^3$$

and equation (2.26):

$$\gamma = C_p/C_v$$

2. Calculate the dimensionless sonic blow-down time by equation (2.46)

$$P_i = 60 \text{ bar } (60 \times 10^5 \text{ N/m}^2)$$
$$P_a = 1 \text{ bar } (1 \times 10^5 \text{ N/m}^2)$$

So,

$$\tau_{cr} = \ln(P_i/P_a) - (\gamma/(\gamma-1)) \times \ln((\gamma+1)/2)$$

$$= 3.485$$

3. Calculate the dimensionless sub-sonic blow-down time by interpolating table 2.1

γ = 1.31

So,

τ_s = 0.79

4. Estimate the blow-down correction factor C_b by equations (2.48), (2.49), (2.50) and (2.51)

f_D = 0.0964 (pipe wall roughness $\varepsilon=0.00003$)
$f_D \times l_p/d_p$ = 241
A_p = $\pi/4 \times d_p^2$
     = 0.785 m^2
$A_p/(A_h \times C_d)$ = 12.67

So,

C_b = 1.12

5. Calculate the total blow-down time by equation (2.57)

t = $(\tau_{cr}+\tau_s) \times \tau_v \times C_b$
  = $(3.485+0.79) \times 1256 \times 1.12$
  = 100 minutes

2.6.3   Pressurised liquefied gases

2.6.3.1   Champagne release of propane through a hole in the side-wall of vertical cylinder

Input:

Vessel volume	V_v	=	4.7	m^3
Length cylinder	l_v	=	2.0	m
Filling degree	ϕ	=	0.95	m^3/m^3
Initial temperature	T_0	=	303.15	K
Leak size	d_h	=	0.1	m
Leak height	h_h	=	1.95	m
Discharge coefficient	C_d	=	0.62	

2.134

Output:

Initial void fraction expanded boiling liquid	Φ_v	=	0.101	m^3/m^3
Initial height expanded boiling liquid	$h_{Le,0}$	=	2.11	m
Initial height of liquid level	$h_{L,0}$	=	1.90	m
Mass flow at t=5 s	q_S	=	127.25	kg/s
Vapour mass fraction (quality) at t=5 s	Φ_m	=	0.02	kg/kg
Vessel pressure at t=5 s	P_v°	=	$8.261 \cdot 10^5$	N/m^2
Vessel temperature at t=5 s	T	=	292.71	K
Mass of liquid at t= 5 s	Q_L	=	1526.38	kg
Mass of vapour at t=5 s	Q_V	=	24.88	kg
Filling degree at t=5 s	ϕ	=	0.65	m^3/m^3
Total mass released at t=5 s	Q	=	643.32	kg

Procedure

While it is assumed that the hole is in the side-wall of the cylinder, e,g. the equations of Mayinger are applied to estimate the rise of the liquid level, i.e. equations (2.58) and equations (2.66) to (2.69).

In the first 0.32 seconds the initial vapour blow-out takes place.
The number of time-steps N_t has been set equal to 50.
This means that the duration of the time-step is: $\Delta t = 4.68/50$ s=0.0936 s.

While the liquid has risen above the leak just after initial vapour blow-out, champagne flow will occur. The mass flow rate $q_{S,i}$ at the beginning of every time-step will be calculated by equations (2.91) and (2.92).

By applying equations (2.76), (2.83) to (2.88), and (2.79) or (2.79a), the conditions at the end of every time-step Δt can be calculated.

In table 2.4 the variations in the physical quantities have been given.

Remarks

In theory the expanded boiling liquid level has decreased below the leak, at 5 seconds after the start of the release:

Void fraction expanded boiling liquid at t=5 s	Φ_v	=	0.0934	m^3/m^3
Height expanded boiling liquid at t=5 s	h_{Le}	=	1.10	m

However, 5 seconds is a fairy short time in which it may not be expected that disengagement of the two-phase flow has already taken place.

Table 2.4

t	q_S	T	$\Phi_{m,e}$	ϕ	Q_L	Q_V	$P_v^{\circ}(T)$
(s)	(kg/s)	(K)	(kg/kg)	(m³/m³)	(kg)	(kg)	(N/m²)
0.00	13.92	303.15	0.0003	0.9500	2168.94	4.29	$10.79 \cdot 10^5$
0.32	131.60	294.55	0.0017	0.9223	2165.26	3.68	$8.67 \cdot 10^5$
0.41	131.27	294.40	0.0017	0.9155	2150.47	6.18	$8.64 \cdot 10^5$
0.51	131.00	294.37	0.0029	0.9101	2137.81	6.58	$8.63 \cdot 10^5$
0.60	130.89	294.35	0.0031	0.9046	2125.16	6.97	$8.62 \cdot 10^5$
0.69	130.84	294.32	0.0033	0.8992	2112.51	7.37	$8.62 \cdot 10^5$
0.79	130.78	294.29	0.0035	0.8937	2099.88	7.76	$8.61 \cdot 10^5$
0.88	130.72	294.27	0.0037	0.8883	2087.24	8.15	$8.61 \cdot 10^5$
0.97	130.67	294.24	0.0039	0.8828	2074.62	8.55	$8.60 \cdot 10^5$
1.07	130.61	294.21	0.0041	0.8774	2062.00	8.94	$8.59 \cdot 10^5$
1.16	130.55	294.19	0.0043	0.8719	2049.38	9.33	$8.59 \cdot 10^5$
1.25	130.49	294.16	0.0045	0.8665	2036.78	9.72	$8.58 \cdot 10^5$
1.35	130.43	294.13	0.0047	0.8611	2024.18	10.11	$8.58 \cdot 10^5$
1.44	130.37	294.10	0.0050	0.8556	2011.58	10.49	$8.57 \cdot 10^5$
1.54	130.31	294.08	0.0052	0.8502	1998.99	10.88	$8.56 \cdot 10^5$
1.63	130.24	294.05	0.0054	0.8448	1986.41	11.27	$8.56 \cdot 10^5$
1.72	130.18	294.02	0.0056	0.8393	1973.84	11.65	$8.55 \cdot 10^5$
1.82	130.12	293.99	0.0059	0.8339	1961.27	12.04	$8.54 \cdot 10^5$
1.91	130.05	293.96	0.0061	0.8285	1948.71	12.42	$8.54 \cdot 10^5$
2.00	129.99	293.93	0.0063	0.8231	1936.16	12.81	$8.53 \cdot 10^5$
2.10	129.92	293.90	0.0066	0.8177	1923.61	13.19	$8.52 \cdot 10^5$
2.19	129.86	293.87	0.0068	0.8123	1911.07	13.57	$8.52 \cdot 10^5$
2.28	129.79	293.84	0.0071	0.8069	1898.54	13.95	$8.51 \cdot 10^5$
2.38	129.72	293.80	0.0073	0.8015	1886.01	14.33	$8.50 \cdot 10^5$
2.47	129.65	293.77	0.0075	0.7961	1873.49	14.71	$8.50 \cdot 10^5$
2.57	129.58	293.74	0.0078	0.7907	1860.98	15.09	$8.49 \cdot 10^5$
2.66	129.51	293.71	0.0080	0.7853	1848.48	15.46	$8.48 \cdot 10^5$
2.75	129.44	293.68	0.0083	0.7799	1835.98	15.84	$8.47 \cdot 10^5$
2.85	129.37	293.64	0.0086	0.7745	1823.50	16.21	$8.47 \cdot 10^5$
2.94	129.30	293.61	0.0088	0.7691	1811.02	16.59	$8.46 \cdot 10^5$
3.03	129.22	293.57	0.0091	0.7638	1798.55	16.96	$8.45 \cdot 10^5$
3.13	129.15	293.54	0.0093	0.7584	1786.08	17.33	$8.44 \cdot 10^5$
3.22	129.07	293.51	0.0096	0.7530	1773.63	17.70	$8.44 \cdot 10^5$
3.31	129.00	293.47	0.0099	0.7477	1761.18	18.07	$8.43 \cdot 10^5$
3.41	128.92	293.43	0.0102	0.7423	1748.74	18.44	$8.42 \cdot 10^5$
3.50	128.84	293.40	0.0104	0.7369	1736.31	18.81	$8.41 \cdot 10^5$
3.60	128.76	293.36	0.0107	0.7316	1723.89	19.18	$8.40 \cdot 10^5$
3.69	128.68	293.32	0.0110	0.7262	1711.47	19.54	$8.40 \cdot 10^5$
3.78	128.60	293.29	0.0113	0.7209	1699.07	19.91	$8.39 \cdot 10^5$
3.88	128.52	293.25	0.0116	0.7155	1686.67	20.27	$8.38 \cdot 10^5$
3.97	128.43	293.21	0.0119	0.7102	1674.28	20.63	$8.37 \cdot 10^5$
4.06	128.35	293.17	0.0122	0.7049	1661.91	20.99	$8.36 \cdot 10^5$
4.16	128.26	293.13	0.0125	0.6995	1649.54	21.35	$8.35 \cdot 10^5$
4.25	128.18	293.09	0.0128	0.6942	1637.18	21.71	$8.35 \cdot 10^5$
4.34	128.09	293.05	0.0131	0.6889	1624.83	22.07	$8.34 \cdot 10^5$
4.44	128.00	293.01	0.0134	0.6836	1612.49	22.42	$8.33 \cdot 10^5$
4.53	127.91	292.97	0.0137	0.6783	1600.15	22.78	$8.32 \cdot 10^5$
4.63	127.82	292.93	0.0140	0.6729	1587.83	23.13	$8.31 \cdot 10^5$
4.72	127.73	292.88	0.0144	0.6676	1575.52	23.48	$8.30 \cdot 10^5$
4.81	127.64	292.84	0.0147	0.6623	1563.22	23.83	$8.29 \cdot 10^5$
4.91	127.54	292.80	0.0150	0.6570	1550.93	24.18	$8.28 \cdot 10^5$
5.00	127.45	292.75	0.0154	0.6517	1538.65	24.53	$8.27 \cdot 10^5$

2.136

2.6.3.2 Outflow quality when top venting propane from vertical vessel through a hole

The outflow quality when top venting pressure liquefied propane from vertical vessel can be calculated by DIERS' method presented in paragraph 2.5.3.2.

Input

Filling degree vessel	ϕ	=	0.5	m^3/m^3
Liquid surface	A_L	=	10	m^2
Leak size	d_h	=	0.1	m
Discharge coefficient	C_d	=	0.62	
Vessel temperature	T	=	288.15	K
Vapour pressure	P_v°	=	$7.309 \cdot 10^5$	N/m^2
Surface tension	σ	=	$0.8155 \cdot 10^{-2}$	N/m
Liquid density	ρ_L	=	509.3	kg/m^3
Vapour density at $P=P_v^\circ$	ρ_V	=	13.42	kg/m^3
Poison coefficient	γ	=	1.13	
Atmospheric pressure	P_a	=	101325	N/m^2

Output

Actual outflow rate	$q_{s,2}$	=	50.01	kg/s
Exit quality	$\phi_{m,e,2}$	=	0.1378	kg/kg

Procedure

1. The vapour outflow rate q_s is estimated by using the equation (2.22) for an orifice

$$q_{s,1} = C_d \times A_h \times \psi \times \sqrt{(\rho_0 \times P_0 \times \gamma \times (2/(\gamma + 1))^{(\gamma + 1)/(\gamma - 1)})} \qquad (2.22)$$

$$= 9.68 \text{ kg/s}$$

2. Calculate the superficial vapour velocity inside the vessel

$$u_V = q_{s,1}/(\rho_v \times A_L) \qquad (2.58)$$

$$= 0.0721 \text{ m/s}$$

3. Calculate the bubble rise velocity, for bubbly flow

$$u_b = 1.18 \times (g \times \sigma \times (\rho_L - \rho_V))^{0.25}/\sqrt{\rho_L} \qquad (2.59) \text{ and}$$

$$= 0.131 \text{ m/s} \qquad (2.60a)$$

and for churn flow

$$u_b = 1.53 \times (g \times \sigma \times (\rho_L-\rho_V))^{0.25}/\sqrt{\rho_L} \qquad \text{(2.59) and}$$

$$= 0.170 \text{ m/s} \qquad (2.60b)$$

4. The dimensionless superficial vapour velocity is given by

$$u_{VR} = u_V/u_b \qquad (2.61)$$

So, for bubbly flow

$$u_{VR} = 0.549 \text{ m/s}$$

and for churn flow

$$u_{VR} = 0.424 \text{ m/s}$$

5. Calculate the characteristic dimensionless superficial velocity u_{VR} for both typical two-phase flow types.

The void fraction in the vessel can be calculated by

$$\Phi_v = 1 - \phi \qquad (2.63)$$

$$= 0.5 \text{ m}^3/\text{m}^3$$

$$u_{VR,bf} = \Phi_v \times (1-\Phi_v)^2/((1-\Phi_v^3) \times (1-1.2 \times \Phi_v)) \qquad (2.62a,b)$$

$$= 0.357 \text{ m/s}$$

$$u_{VR,cf} = 2 \times \Phi_v/(1-1.5 \times \Phi_v) \qquad (2.62c,d)$$

$$= 4.00 \text{ m/s}$$

6. Determination whether two-phase flow is apparent inside the vessel

Application the of criteria

$$u_{VR} < u_{VR,cf} \rightarrow \text{no churn flow} \tag{2.64c}$$

$$u_{VR} \geq u_{VR,bf} \rightarrow \text{two-phase bubbly flow} \tag{2.64b}$$

7. The exit quality and outflow rate can be calculated by solving the set of equations (2.65), (2.65a) and (2.65b). The iteration can be carried out by a root finding procedure.

For two-phase flow through a hole, the outflow rate can be calculated by

$$q_{s,2} = C_d \times A \times \sqrt{(2(P_0 - P_a) \times \rho_{av})} \tag{2.91}$$

with
$$\rho_{av} = 1 / (\Phi_m/\rho_V + (1-\Phi_m)/\rho_L) \tag{2.92}$$

The actual outflow rate $q_{s,2}$ is given above at "Output".

2.6.3.3 Stationary two-phase propane flow through full bore ruptured pipe

The stationary outflow of two-phase propane flow from a pipeline can be calculated by the TPDIS model presented in paragraph 2.5.3.5.

Input:

Pipe length	l_p	=	100.0	m
Pipe diameter	d_p	=	0.1	m
Wall roughness pipe	ε	=	$4.5 \cdot 10^{-5}$	m
Constant up-stream temperature	T_0	=	288.15	K
Discharge coefficient	C_d	=	1.0	

Output:

Mass flow rate	q_S	=	16.35	kg/s
Vapour mass fraction (quality)	$\Phi_{m,e}$	=	0.0621	kg/kg
Exit temperature	T_e	=	279.4	K
Constant up-stream pressure	$P_v^{\circ}(T_0)$	=	$7.309 \cdot 10^5$	N/m^2

Procedure

The critical mass flow rate $q_s(P_e)$ at the pipe outlet may be computed by numerically maximising the right-hand side of equation (2.107) in terms of outlet pressure P_e. The specific volume of the liquid is computed by equations (2.110) and (2.112). The friction is computed by equation (2.99), using the mass flow rate estimated in the previous step.
Note that $S_L(P_0) = 4.39 \cdot 10^3$ J/(kg·K), and the values for the following parameters: $C_{Ar}=0.5$, $C_{Br}=0.5$.

2.6.3.4   Non-stationary two-phase flow in pipelines

The modelling of the two-phase flow through pipelines aims at predicting the mass flow rate as a function of time depending on the initial conditions.

Transient release from full bore ruptured pipelines

Non-stationary two-phase outflow through pipelines can be calculated by the models presented in paragraph 2.5.3.6.
Morrow's model can be used to estimate the mass flow rate caused by a full bore ruptured propane-pipeline as a function of time.

Problem

A pipeline filled with propane is ruptured in the middle. Calculate the transient mass flow rate as a function of time after the rupture.

Input:

Initial pipeline pressure	P_0	=	$60 \cdot 10^5$	N/m^2
Initial temperature	T_0	=	288.15	K
Pipe length	L_p	=	$50 \cdot 10^3$	m
Pipe diameter	d_p	=	0.254	m
(cross-sectional area	A_p	=	0.05067	m^2)
Sound speed in propane liquid	$u_{s,L}$	=	864.9	m/s

Output:

Mass flow at 0 sec	$q_{S,e}$	=	672.3	kg/s
Quality at 0 sec	Φ_m	=	0.195	kg/kg
Mass flow at 4990 sec	$q_{S,e}$	=	70.37	kg/s
Quality at 4990 sec	Φ_m	=	0.298	kg/kg

Procedure

Guillotine breakage is assumed. Because the rupture is in middle of the pipeline, the effective length of the pipeline is set at $L_p/2 = 25000$ m. The mass flow rate $q_{S,e}$ and the mass removed $Q_{yi,2}$ estimated by Morrow's model are *multiplied by a factor 2*. The pumping rate is neglected.

The polynomials fitted by Morrow are used in the calculations. The friction factor is taken constant: $f_F = 0.003$, and the ambient pressure P_a is set equal to 1 atmosphere (101325 N/m^2).

The initial pressure in the pipeline P_0 is high, hence the initial mass flow rate based on sonic liquid outflow is used (equation 2.122). For sound speed in propane liquid at 60 bars overpressure, a more accurate estimation is used here [NIST]. The scheme defined by equations (2.115-2.121) is used to estimate the initial mass flow rate ($t = 0$), because the initial exit pressure is unknown.

For the estimation of the mass flow rate $q_{S,e,2}$ as a function of time, step 1 to step 8 are repeated, until the distance to the interface Δl_i exceeds the half length of the pipe line.

In table 2.5 the variation in time of some physical quantities are presented.

Table 2.5

i [-]	t_i [s]	q_s [kg/s]	quality [kg/kg]	Δl_i [m]	$Q_{iy,2}$ [kg]	P_e [bar]
0	0.00	670.23	15.127	0.00	0	2.7994
1	7.84	636.72	20.004	141.72	2561	2.7126
2	8.75	604.88	20.488	155.24	2843	2.627
3	9.80	574.64	20.972	170.00	3155	2.5427
4	11.03	545.90	21.457	186.10	3498	2.4599
5	12.45	518.61	21.941	203.68	3876	2.3785
6	14.09	492.68	22.425	222.87	4291	2.2988
7	16.00	468.04	22.908	243.82	4749	2.2206
8	18.21	444.64	23.389	266.69	5253	2.1442
9	20.76	422.41	23.870	291.67	5807	2.0695
10	23.73	401.29	24.348	318.96	6417	1.9965
11	27.16	381.23	24.824	348.77	7088	1.9253
12	31.13	362.16	25.299	381.35	7827	1.856
13	35.73	344.06	25.770	416.96	8639	1.7884
14	41.06	326.85	26.239	455.89	9532	1.7227
15	47.23	310.51	26.706	498.46	10515	1.6588
16	54.37	294.98	27.169	545.01	11597	1.5967
17	62.65	280.24	27.630	595.94	12787	1.5364
18	72.23	266.22	28.087	651.66	14096	1.4779
19	83.33	252.91	28.541	712.65	15537	1.4212
20	96.19	240.27	28.991	779.42	17122	1.3662
21	111.09	228.25	29.438	852.52	18867	1.313
22	128.35	216.84	29.882	932.58	20788	1.2615
23	148.35	206.00	30.322	1020.30	22902	1.2117
24	171.52	195.70	30.758	1116.40	25230	1.1635

i [-]	t_i [s]	q_s [kg/s]	quality [kg/kg]	Δl_i [m]	$Q_{iy,2}$ [kg]	P_e [bar]
25	198.39	185.91	31.191	1221.70	27792	1.117
26	229.52	176.62	31.620	1337.10	30614	1.072
27	265.61	167.79	32.045	1463.70	33722	1.0286
28	309.17	159.40	32.198	1614.80	37285	1.0133
29	361.01	151.43	32.198	1789.20	41313	1.0133
30	421.47	143.86	32.198	1982.50	45776	1.0133
31	491.99	136.66	32.198	2196.70	50721	1.0133
32	574.23	129.83	32.198	2434.00	56201	1.0133
33	670.16	123.34	32.198	2697.00	62273	1.0133
34	782.05	117.17	32.198	2988.30	69000	1.0133
35	912.55	111.31	32.198	3311.20	76454	1.0133
36	1064.80	105.75	32.198	3668.90	84714	1.0133
37	1242.30	100.46	32.198	4065.30	93866	1.0133
38	1449.30	95.44	32.198	4504.50	104010	1.0133
39	1690.80	90.67	32.198	4991.10	115240	1.0133
40	1972.50	86.13	32.198	5530.30	127690	1.0133
41	2301.10	81.83	32.198	6127.70	141490	1.0133
42	2684.20	77.73	32.198	6789.70	156770	1.0133
43	3131.20	73.85	32.198	7523.30	173710	1.0133
44	3652.50	70.16	32.198	8336.00	192480	1.0133
45	4260.50	66.65	32.198	9236.60	213270	1.0133
46	4969.60	63.32	32.198	10234.00	236310	1.0133
47	5796.70	60.15	32.198	11340.00	261840	1.0133
48	6761.40	57.14	32.198	12565.00	290130	1.0133
49	7886.50	54.29	32.198	13923.00	321470	1.0133
50	9198.90	51.57	32.198	15427.00	356200	1.0133
51	10730.00	48.99	32.198	17093.00	394680	1.0133
52	12515.00	46.54	32.198	18940.00	437320	1.0133
53	14597.00	44.22	32.198	20986.00	484570	1.0133
54	17026.00	42.01	32.198	23253.00	536910	1.0133
55	19858.00	39.90	32.198	25766.00	594920	1.0133

Transient release from leaking or (partially) ruptured propane pipelines

Non-stationary two-phase propane outflow through pipelines can be calculated by the models presented in paragraph 2.5.3.6.
Tam's model may be used to give an approximation of the initial mass flow rate from a crack in a pipeline.

Problem

Estimate the initial mass flow rate of a 10 inch propane pipeline after a crack in the pipe wall with a area of about 10% of the cross-section of the pipeline.

Input:

Pipe diameter (10")	d_p	=	0.254	m
Initial temperature	T_o	=	288.15	K
Area ratio	A_R	=	0.1	-

2.142

Output:

Initial mass flow q_S =   69.4   kg/s

Procedure

The density of propane at initial temperature T_0=15 ˚C (288.15 K) is

$\rho_{L,0}$ = 509.5 kg/m^3

The radius ratio d_R is given by

d_R = d_p[m] / 0.05 m

= 0.254m / 0.05 m

= 5.08

The area ratio has been given

A_R = 0.1

So, the decay coefficient can be estimated by

C_α = $d_R^{0.25} \times (0.22 \times A_R - 0.13 \times A_R^{1.5} + 0.00068 \times (T_0-288.15))$ (2.134)

= $(5.08)^{0.25} \times (0.22 \times 0.1 - 0.13 \times 0.1^{1.5} + 0.)$

= 0.0269 s^{-1}

The (artificially) constant is set at

C_{Lp} = 100 m   (2.137a)

The initial flow rate is given by

q_0 = $C_\alpha \times \rho_{L,0} \times \pi/4 \times d_p^2 \times C_{Lp}$ (2.137)

= $0.0269 \times 509.5 \times \pi/4 \times 0.254^2 \times 100$

= 69.4 kg/s

2.6.3.5   Finite duration spray releases

In order to demonstrate the calculation of a finite duration flashing release, the following situation has been selected: A 1000 m^3 vessel is filled (fill level 50%) with butane at ambient temperature (288.15 K). At the bottom of the vessel a 3"

pipeline (76.2 mm diameter) is connected. 10 cm from the vessel connection, this pipeline breaks off completely. The breach is 1 m above the ground. This results in a release of butane at a mass flow of about 41 kg s^{-1}. The discharge coefficient is 0.8, so the effective exit area is 0.00365 m^2. The flashing in the short pipe is negligible, so pure liquid flows out which flashes in the atmosphere. For the ambient humidity a value of 63% is assumed. The input data and intermediate and final results are summarised in Table 2.6.

Table 2.6   Input and output of the finite duration spray release example

Input	Source height	h_s	1	m
	Effective exit area	A_e	0.00363	m^2
	Exit radius	b_e	0.034	m
	Mass flow rate	$q_{S,e}$	41.34	kg/s
	Vapour mass fraction	$\Phi_{m,e}$	0%	
	Exit temperature	T_e	288.15	K
	Exit pressure	P_e	174549	Pa
	Liquid density	$\rho_{e,L}$	584.49	kg/m^3
	Vapour density	$\rho_{e,V}$	4.233	kg/m^3
	Averaged density	ρ_e	584.49	kg/m^3
	Exit velocity	u_e	19.475	m/s
	Boiling temperature	T_B	272.7	K
	Latent heat	$L_{v,e}$	362140	J/kg
		$L_{v,f}$	376740	J/kg
	Vapour enthalpy	$H_{e,V}$	473622	J/kg
		$H_{f,V}$	428806	J/kg
	Ambient humidity	RH	63%	
	Ambient temperature	T_a	288.15	K
After flashing	Vapour mass fraction	$\Phi_{m,f}$	0.15732	
	Jet velocity	u_f	25.91	m/s
	Liquid density	$\rho_{f,L}$	600.72	kg/m^3
	Vapour density	$\rho_{f,V}$	2.5964	kg/m^3
	Averaged density	ρ_f	16.13	kg/m^3
	Jet area	A_f	0.099	m^2
	Jet radius	b_f	0.177	m
Droplet diameter	Dynamic viscosity liquid	ν_L	0.000197	N.s/m^2
	Surface tension	σ_s	0.0159	N/m
	Jet Reynolds number	Re_f	46648	
	Jet Weber number	We_f	9012339	
	Droplet diameter	d_d	0.29	mm
Rain-out	Kinematic viscosity air	ν_a	1.71·10^{-5}	m^2/s
	Prandtl number for air	Pr	0.87	
	Schmidt number for butane	Sc	0.7	
	Droplet Reynolds number	Re_d	22.25	
	Free fall velocity	u_d	1.313	m/s
	Droplet temperature	T_d	215.09	K
	Evaporation coefficient	k_B	2.87·10^{-8}	m^2/s
	Nett mass released to the air	$q_{S,nett,air}$	41.34	kg/s
	Nett vapour mass fraction	$\Phi_{m,rainout}$	0.15732	
	Nett jet area	$A_{f,rainout}$	0.099	m^2
	Nett jet radius	$b_{f,rainout}$	0.177	m
Conditions after evaporation	Concentration after evaporation	c_j	0.138	
	Temperature after evaporation	T_j	227.3	K
	Molar fraction of water vapour at ambient temperature	c_w	10.61	
	Molar fraction of water vapour at jet temperature	c_{wv}	1.158	
	Molar fraction of condensed water	c_{jL}	2.44	
	Jet density after evaporation	ρ_j	5.127	kg/m^3
	Jet velocity after evaporation	u_j	6.29	m/s
	Jet area after evaporation	A_j	1.28	m^2
	Jet radius after evaporation	b_j	0.64	m

The input listed in Table 2.6 includes the thermodynamic properties at the storage and boiling temperature: latent heat and the enthalpies (only enthalpy differences between two temperatures and pressure levels are essential) as well as the densities.

Step 1 - **Calculate the conditions in the jet after flashing**

The outflow conditions P_e, T_e, $q_{S,e}$ and $\Phi_{m,e}$ are listed in the Table 2.6. The density at the exit follows from formula (2.138) (this formula will be used frequently to calculate the density of two-phase mixtures at various stages throughout the jet):

$$\frac{1}{\rho_e} = \frac{(1 - \Phi_{m,e})}{\rho_{L,e}} + \frac{\Phi_{m,e}}{\rho_{v,e}} \qquad (m^3/kg)$$

$\rho_e = 584.49 \text{ kg/m}^3$

The jet velocity after flashing is calculated by formula (2.139):

$$u_f = \frac{(P_e - P_a)A_e}{q_{s,e}} + u_e \qquad (m/s)$$

$u_f = 25.91$ m/s.

The vapour mass fraction after flashing is calculated by formula (2.140):

$$\Phi_{m,f} = 1 - \frac{H_{V,f} - H_{V,e} + (1 + \Phi_{m,e})L_{v,e} + \frac{1}{2}(u_f^2 - u_e^2)}{L_{v,f}} \qquad (-)$$

$\Phi_{m,f} = 0.15732$

The jet cross section A_f and jet radius b_f can be calculated from (2.141).
Here we need the averaged density ρ_f in the vessel, which can be calculated by formulae (2.138) from the vapour and liquid densities and the vapour mass fraction after flashing.

$$A_f = \frac{\rho_e u_e}{\rho_f u_f} A_e \qquad b_f = \sqrt{\frac{A_f}{\pi}} \qquad (m^2; m)$$

$A_f = 0.099 \text{ m}^2$; $b_f = 0.177$ m.

Step 2 - Calculation of the droplet diameter after flashing

Next, the droplet diameter after flashing is calculated. First, the jet Reynolds number and the jet Weber number are evaluated using formula (2.142):

$$\text{Re}_f = \frac{2b_f u_f}{\nu_L} \qquad \text{We}_f = \frac{2b_f u_f^2 \rho_{L,f}}{\sigma_s} \qquad\qquad (\text{-} ; \text{-})$$

$\text{Re}_f = 46648$
$\text{We}_f = 9012339$

Then the droplet diameter is calculated by formulae (2.143a-b). It appears that in this case the second option (b) has to be used:

$$d_d = 15 \frac{\sigma_s}{u_f^2 \rho_a} \qquad\qquad (\text{m})$$

$d_d = 0.29$ mm

Step 3 - Droplet evaporation and rain-out on the ground

Knowing the droplet diameter, it is possible to determine whether the droplets will fall on the ground. Therefore the free fall velocity of the droplet is estimated by formula (2.145).

$$u_d = \frac{\rho_{L,f} g}{18 \nu_a \rho_a} d_d^2 \qquad\qquad (\text{m/s})$$

$u_d = 1.313$ m/s

This allows to evaluate the droplet Reynolds number Re_d.

$\text{Re}_d = u_d d_d / \nu$
$\text{Re}_d = 22.25$

Table 2.6 presents the values for the Schmidt and Prandtl numbers which depend on the properties of butane and air only.
In order to determine the evaporation coefficient k_B (2.146), it is necessary to determine the droplet temperature T_d (2.147) in an iterative process using intermediate values of k_B at each iteration step. This results in $T_d = 215$ K, $k_B = 2.87 \cdot 10^{-8}$ m^2/s.
The approximate formula (2.148) for the maximum droplet diameter d_M results in a maximum droplet of 47 mm. However, this is not a useful result, as the corresponding Reynolds number using the free fall velocity, is 3671, which exceeds the range of validity ($\text{Re}_d < 4$).
Therefore it can not be avoided to integrate the differential equation (2.149) for the evolution of the droplet radius together with the descent of the droplet from the release height to the ground (2.150):

$$\frac{d}{dt}d_d = -\frac{k_B}{d_d}[1 + 0.28 \; Re_d^{1/2}Sc^{1/3}] \qquad (m/s)$$

$$0 = h(t_0) = h_s - \int_0^{t_o} u_d dt$$

And found is that all droplets have evaporated before reaching the ground.

By means of formulae (2.151) to (2.153) the values of the airborne mass flow rate, vapour mass fraction, jet area and jet radius can be corrected for rain-out:

$$q_{s, nett, air} = \Phi_{m, f} \; q_{s, e} + (1 - \Phi_{m, f})\left(1 - \left[\frac{d_0}{d_d}\right]^3\right) q_{s, e} \qquad (kg/s)$$

$q_{S,nett,air} = 41.34$ kg/s

$$\Phi_{m, f, rainout} = \frac{\Phi_{m, f}}{\Phi_{m, f} + (1 - \Phi_{m, f})\left(1 - \left[\frac{d_0}{d_d}\right]^3\right)} \qquad (-)$$

$\Phi_{m,f,rainout} = 0.15732$

$$A_{f, rainout} = A_f \frac{q_{s, nett, air}}{q_{s, e}} \qquad (m^2)$$

$A_{f,rainout} = 0.099$ m^2

$b_{f,rainout} = 0.177$ m

Step 4 - Calculate the conditions in the jet after evaporation of all airborne droplets

Finally, the effects of evaporation of droplets by entrained air on the bulk properties of the jet are calculated. Therefore, the enthalpy changes corresponding to the temperature change and droplet evaporation of butane. The temperature change of entrained air and the enthalpy change of ambient water, both due to condensation and temperature change, need to be calculated. This has to be done iteratively. Therefore an initial value of the jet temperature T_j is selected. A partial vapour pressure of butane corresponds to this temperature, and this leads to the molar fraction of butane in the jet by formula (2.155). Here we used:

$$\log\{P_s(T_j)\} = 6.80896 - 935.860/(T_j + 238.73)$$

With this information the enthalpy change of butane is calculated by (2.156). The latent heat after flashing $L_{v,f}$ is listed in Table 2.6. The vapour enthalpy is calculated from $C_p \cdot T$, with:

$$C_p = -1.779 + 0.386961 \times T - 193.255 \times 10^{-6} \times T^2 + 348.326 \times 10^{-10} \times T^3$$

Ambient humidity is transferred into a water mass fraction by using the relation between the saturation pressure of water as a function of temperature:

$$\frac{m_w}{m_{da}} = \frac{RH_a P_{v,w}^0(T_a)}{(R/\mu_w)T_a \rho_a} \qquad (-)$$

$$c_w = \frac{m_w \mu_a}{m_{da} \mu_w} \qquad (-)$$

$$c_w = 10.61$$

At the selected jet temperature this may lead to condensation: the remaining water vapour is calculated by means of (2.158). Now the enthalpy changes of dry air and water can be calculated using (2.160) and (2.161), respectively. This process needs to be repeated until a jet temperature is reached at which the sum of the enthalpy changes is approximately zero. In this case one should find $T_j = 227.3$ K. Table 2.6 presents the results as well as some thermodynamic properties at the final result for T_j in this case.

Knowing the molar concentration, the amount of condensed water and the temperature, it is possible to calculate jet density, jet velocity and jet dimensions by formulae (2.162) through (2.167):

$$c_{jL} = \frac{(1-c_j)}{(1+c_{wv})}(c_w - c_{wv})\frac{\mu_w}{\mu_{jd}} \qquad (-)$$

$$c_{jL} = 2.44$$

$$\mu_{jd} = c_j \mu_s + \frac{(1-c_j)}{(1-c_{wv})}(\mu_a + c_{wv}\,\mu_w) \qquad (kg/mol)$$

$$\rho_{jd} = \frac{P_a\,\mu_{jd}}{RT_j} \qquad (kg/m^3)$$

$$\rho_j = \frac{1 + c_{jL}}{\dfrac{1}{\rho_{j,d}} + \dfrac{c_{jL}}{\rho_{w,L}}} \qquad (kg/m^3)$$

$\rho_j = 5.127$ (using $\rho_{j,L} = 1000$ kg/m^3)
The initial volume concentration in the volume flow rate is $c_j = 0.138$:

$$u_j = \frac{u_f}{1 + \dfrac{(1-c_j)\mu_a}{c_j}\dfrac{}{\mu_s}} \qquad (m/s)$$

$u_j = 6.29$ m/s

$$A_j = \frac{\rho_f u_f}{\rho_j u_j} A_f \qquad b_j = \sqrt{\frac{A_j}{\pi}} \qquad\qquad (m^2; m)$$

$A_j = 1.28$ m^2
$b_j = 0.64$ m

2.6.3.6   Instantaneous release

In order to demonstrate the calculation of an instantaneous flashing release, the following situation has been selected: A vessel is filled (fill level about 94%) with 6 tonnes of propane at ambient temperature (291 K). This vessel fails completely. The ambient conditions are wind speed at 10 m height: 4 m/s, roughness length 0.03 m (Flat land) and Monin-Obukhov length -21.7 m (sunny weather, slightly unstable: this meteorological condition is described in chapter 4, section 4.6.2.1). For the ambient humidity a value of 63% is assumed. The input data and intermediate and final results are summarised in Table 2.7.

Table 2.7   Input and output of the instantaneous release example

Input	Total mass	Q	6000	kg
	Vapour mass fraction	$\Phi_{m,0}$	0.002	
	Storage temperature	T_0	291	K
	Storage pressure	p_0	784189	Pa
	Liquid density	$\rho_{0,L}$	504.98	kg/m^3
	Vapour density	$\rho_{0,V}$	14.29	kg/m^3
	Averaged density	ρ_0	472.53	kg/m^3
	Boiling temperature	T_B	230.9	K
	Latent heat	$L_{v,0}$	343486.3	J/kg
		$L_{v,f}$	426134.8	J/kg
	Specific heat (liquid)	$C_{p,L}$	2413.51	J/(kg·K)
	Vapour enthalpy	$H_{0,V}$	483471.9	J/kg
		$H_{f,V}$	383620.9	J/kg
	Windspeed at 10 m		4	m/s
	Monin Obukhov length		-21.7	m
	Roughness length (Flat land)		0.03	m
	Ambient humidity	RH	63%	
	Ambient temperature	T_a	291	K
Intermediate results	Vapour mass fraction after flashing	$\Phi_{m,f}$	0.304	
	Expansion velocity	u_f	258.4	m/s
	Liquid density	$\rho_{f,L}$	584.3	kg/m^3
	Vapour density	$\rho_{f,V}$	2.327	kg/m^3
	Averaged density	ρ_f	7.584	kg/m^3
	Cloud volume	V_f	791.18	m^3
	Cloud radius	b_f	7.23	m
	Wind speed at cloud height	u_a	3.76	m/s
Final results	Airborne mass	$Q_{(nett)}$	3649	kg
	Vapour mass fraction after rain-out	$\Phi_{m,f,nett}$	0.5	
	Nett averaged density	$\rho_{f,nett}$	4.636	kg/m^3
	Cloud volume	$V_{f,nett}$	787.16	m^3
	Cloud radius	$b_{f,nett}$	7.21	m
	Concentration after evaporation	c_j	0.2647	
	Cloud temperature after evaporation	T_j	204.74	K
	Cloud volume after evaporation	V_j	5252	m^3
	Cloud radius after evaporation	b_j	13.59	m
	Expansion velocity after evaporation	u_j	38.72	m/s
	Cloud density	ρ_j	1.25	kg/m^3
	Cloud radius at ambient wind	b_{disp}	25.1	m
	Cloud volume at ambient wind	v_{disp}	33070	m^3
	Concentration at ambient wind	c_{disp}	0.06	
	Temperature at ambient wind	T_{disp}	291.1	K

The input listed in Table 2.7 includes the thermodynamic properties at the storage and boiling temperature: latent heat, specific heat and the enthalpies (only enthalpy differences between two temperature and pressure levels are essential) as well as the densities.

Step 1 - Calculate the conditions in the cloud after depressurisation

The vapour mass fraction after flashing $\Phi_{m,f}$ can be calculated by formula (2.168) or (2.169) in section 2.5.3.8. As no details about entropy are available, formula (2.169) is selected:

$$\Phi_{m,f} = \Phi_{m,0}\frac{T_f}{T_0} + \frac{T_f}{L_{v,f}}C_{p,L}\ln\frac{T_0}{T_f} \qquad\qquad (-)$$

$\Phi_{m,f} = 0.304$

The expansion velocity u_f is calculated by formula (2.170). Here we need the averaged density ρ_0 in the vessel which can be calculated by formula (2.138) (section 2.5.3.7) from the vapour and liquid densities and the vapour mass fraction, $\rho_0 = 472.53$ kg/m^3:

$$u_f = 0.8\sqrt{2H_{0,V} - H_{f,V} + (1 - \Phi_{m,f})L_{v,f} - (1 - \Phi_{m,0})L_{v,0} - \frac{P_0 - P_a}{\rho_0}}$$

$u_f = 258.4$ m/s

The cloud density ρ_f after flashing is calculated similarly as ρ_0. By means of formulae (2.171) and (2.172) the cloud volume V_f and cloud radius b_f (assuming a hemisphere close to the ground) are determined:

$$V_f = \frac{Q}{\rho_f} \qquad\qquad (m^3)$$

$V_f = 791.18$ m^3

$$b_f = \left(\frac{3V_f}{2\pi}\right)^{1/3} \qquad\qquad (m)$$

$b_f = 7.23$ m

By means of the methodologies provided in chapter 4 one can calculate the wind speed at the cloud height b_f. This velocity is found to be 3.76 m/s.

Step 2 - Calculate the rain-out fraction to the ground

Next the rain-out fraction is determined. As the flash fraction is 0.304, the amount of propane remaining in the air is twice as high, i.e. 0.608 times the total contents of the vessel or 3649 kg. It is then necessary to redefine the flash fraction (0.5), the averaged cloud density (similarly to ρ_0 using $\Phi_m = 0.5$; $\rho_{f,nett} = 4.636$ kg/m^3) and the cloud dimensions ($V_{f,nett} = Q_{nett}/\rho_{f,nett} = 787.16$ m^3, $b_{f,nett} = 7.21$ m).

Steps 3/4   Calculate the expansion of the cloud during the entrainment phase and calculate the conditions in the cloud after evaporation of all airborne droplets

The amount of air that needs to be entrained in order to evaporate all propane droplets in the cloud, is now calculated iteratively by means of formulae (2.154) to (2.161) from section 2.5.3.7. This will give the molar fraction of propane in the cloud c_j, the cloud temperature T_j and the mass fraction of water droplets due to condensation of ambient humidity. From this, one can also calculate the cloud density ρ_j by formulae (2.162) to (2.167). This procedure has already been demonstrated more extensively in the foregoing section. The results are presented in Table 2.7.

In order to calculate the cloud volume it is necessary to calculate the vapour density of the chemical at temperature T_j, $\rho_{s,j}$. In this case at 204.74 K the density of propane is assumed to be 2.625 kg/m^3. The cloud volume and radius follow from:

$$V_j = \frac{Q}{c_j\,\rho_{s,j}} \qquad b_j = \left(\frac{3V_j}{2\pi}\right)^{1/3} \qquad\qquad (\text{m}^3;\ \text{m})$$

$V_j = 5252 \text{ m}^3$; $b_j = 13.59 \text{ m}$

The expansion velocity of the cloud after evaporation follows from formula (2.175):

$u_j \quad = u_f\,(b_f/b_j)^3$
$u_j \quad = 38.72 \text{ m/s}$

It appears that after evaporation the expansion velocity exceeds the ambient wind speed (38.72 m/s compared to 3.76 m/s). Therefore the cloud dimensions are calculated when the expansion velocity equals the ambient wind speed by:

$$b_{disp} = b_f \left(\frac{u_f}{u_a(b_f)}\right)^{1/3} \qquad V_{disp} = \frac{2}{3}\pi b_{disp}^3 \qquad (\text{m};\ \text{m}^3)$$

$b_{disp} = 25.1 \text{ m}$; $v_{disp} = 33070 \text{ m}^3$

After the cloud has expanded to these dimensions, the temperature in the cloud T_c is approaching the ambient temperature according to:

$$T_{disp} = \frac{T_a}{1 - \dfrac{V_j}{V_{disp}}\left(1 - \dfrac{T_a}{T_j}\right)} \qquad\qquad (\text{K})$$

$T_{disp} = 291.1 \text{ K}$

The molar or volume concentration c_{disp} at this stage of the cloud is:

$$c_{disp} = c_j\,\frac{V_j\,T_{disp}}{V_{disp}\,T_j} \qquad\qquad (\text{-})$$

$c_{disp} = 0.06$

The cloud density, calculated by means of (2.162) and (2.163) from section 2.5.3.4, is 1.25 kg/m^3, which is about equal to the density of air at 15˚C (288.15 K).

2.6.4   Liquids

2.6.4.1   Stationary Acrylonitrile liquid outflow from a vessel through a hole in the vessel wall

The liquid outflow from of a vessel through a hole in the vessel wall can be calculated by the models presented in paragraphs 2.5.4.1 and 2.5.4.2.

Input:

Vessel volume	V	= 6600	m^3
Vessel type		vertical cylinder	
Length cylinder	l_v	= 14	m
Filling degree	ϕ	= 0.8	-
Pressure above liquid	p	= 101325	N/m^2
Leak size	d_h	= 0.1	m
Height of leak	h_h	= 0	m
Initial temperature	T_0	= 288.15	K
Discharge coefficient	C_d	= 0.62	-

Output:

Mass flow liquid at 500 sec	q_S	= 58.44	kg/s
Filling degree at 500 sec	ϕ	= 0.795	-
Height of liquid at 500 sec	h_L	= 11.12	m
Total mass released at 500 sec	Q	= 29416	kg

Procedure

The number of time-steps N_t has been set equal to 50.
By equation (2.194), the mass flow rate $q_{s,i}$ at the beginning of every time-step can be calculated.

Using the equations (2.185) to (2.191) subsequently, the variation of the vessel conditions (Q_i, $h_{L,i}$) due to the outflow can be calculated.
Note that the initial liquid mass in the tank is Q_0, and that at a temperature of T=15 ˚C (288.15) the density ρ_L of acrylonitrile are respectively

$Q_0(t=0)$ = 4290000 kg

ρ_L = 812.5 kg/m^3

In table 2.8 the variations in the physical quantities have been given.

Table 2.8

Time after rupture [s]	Mass flow rate [kg/s]	Filling degree [%]	Total mass release [kg]	Liquid level in the vessel [m]
0	60.915	80	0	11.20
2013	60.075	77.8	121790	10.89
4698	58.955	74.9	281550	10.49
7382	57.835	72.1	438300	10.10
10066	56.714	69.3	592050	9.71
12751	55.594	66.6	742790	9.33
15435	54.474	64.0	890520	8.96
18119	53.353	61.4	1035200	8.59
20804	52.233	58.8	1177000	8.23
23488	51.112	56.3	1315700	7.89
26172	49.991	53.9	1451400	7.54
28857	48.871	51.5	1584100	7.21
31541	47.750	49.2	1713700	6.88
34226	46.629	46.9	1840400	6.56
36910	45.508	44.7	1964100	6.25
39594	44.387	42.5	2084700	5.95
42279	43.266	40.4	2202400	5.65
44963	42.145	38.3	2317000	5.36
47647	41.023	36.3	2428600	5.08
50332	39.902	34.3	2537300	4.81
53016	38.780	32.4	2642900	4.54
55700	37.659	30.6	2745500	4.28
58385	36.537	28.8	2845000	4.03
61069	35.415	27.0	2941600	3.79
63753	34.293	25.4	3035200	3.55
66438	33.171	23.7	3125700	3.32
69122	32.049	22.1	3213300	3.10
71806	30.926	20.6	3297800	2.89
74491	29.803	19.2	3379300	2.68
77175	28.680	17.7	3457800	2.48
79860	27.557	16.4	3533300	2.29
82544	26.434	15.1	3605700	2.11
85228	25.310	13.8	3675200	1.93
87913	24.186	12.6	3741600	1.77
90597	23.062	11.5	3805000	1.61
93281	21.938	10.4	3865400	1.45
95966	20.813	9.3	3922800	1.31
98650	19.687	8.4	3977200	1.17
101330	18.562	7.4	4028500	1.04
104020	17.435	6.6	4076800	0.92
106700	16.308	5.7	4122100	0.80
109390	15.181	5.0	4164400	0.70
112070	14.053	4.3	4203600	0.60
114760	12.923	3.6	4239800	0.50
117440	11.793	3.0	4273000	0.42
120120	10.661	2.5	4303100	0.34
122810	9.528	2.0	4330200	0.27
125490	8.393	1.5	4354300	0.21
128180	7.255	1.1	4375300	0.16
130860	6.113	0.8	4393200	0.11

Time after rupture [s]	Mass flow rate [kg/s]	Filling degree [%]	Total mass release [kg]	Liquid level in the vessel [m]
133550	4.967	0.5	4408100	0.07
136230	3.812	0.3	4419900	0.04
138920	2.644	0.2	4428500	0.02
141600	1.442	0.0	4434000	0.01

2.6.4.2 Acrylonitrile liquid outflow from a pipe

The liquid outflow from a vessel through a pipe can be calculated by the models presented in paragraphs 2.5.4.2 and 2.5.5.

Input:

Vessel volume	V	= 6600	m^3
Vessel type		vertical cylinder	
Length cylinder	l_v	= 14	m
Filling degree	ϕ	= 0.8	-
Pressure above liquid	P	= 101325	Pa
Pipe length	l_p	= 100	m
Pipe diameter	d_p	= 0.1	m
Wall roughness pipe	ε	= $4.5 \cdot 10^{-5}$	m
Leak size	d_h	= 0.1	m
Height of leak	h_h	= 0	m
Initial temperature	T_0	= 288.15	K
Discharge coefficient	C_d	= 1.0	-

Output:

Mass flow liquid at t = 0 s	q_S	= 22.33	kg/s

Procedure

1. Calculate the total pressure at the opening using equations (2.195) and (2.196).
2. Estimate the mass flow rate by equation (2.194). This value represents the maximum of the mass flow rate, as frictional pressure loss is not taken into account.
3. Calculate the Reynolds number using equation (2.201a).
4. Calculate the Darcy friction factor f_D by equation (2.202) or (2.207), or any other suitable explicit formula.
5. Calculate the frictional pressure loss using equation (2.198).
6. Due to this pressure loss the total pressure at the opening in equation (2.195) is decreased and consequently the mass flow rate as obtained by equation (2.194).
7. Hence the above steps 2 up to and including 6 should be repeated until the difference between the updated mass flow rate and its previous value is sufficiently small.

The above procedure is most conveniently applied by using a suitable root finding procedure, assuming a minimum mass flow rate of zero and a maximum value according to step 2.

2.7 Interfacing to other models

2.7.1 Introduction to section 2.7

The results from model predictions in this chapter 'Outflow and Spray Release' may be used for further calculations as input for subsequent physical effect models, described in:

    chapter 3 'Pool evaporation',
    chapter 4 'Vapour cloud dispersion', and
    chapter 6 'Heat flux from fires'.

The models in this chapter 'Outflow and Spray Release' may act as a source term model to provide (quantitative) information about:

− the amount of material entering the surroundings in the vincinity of the failing containment,
− the dimensions of the area or space in which this process takes place,
− the thermodynamic state of the released chemicals, such as concentrations, temperature, and pressure,
− velocities of the outflowing chemicals at the boundaries of the source region.

Interfacing to relevant models in chapter 3 'Pool evaporation' and chapter 6 'Heat flux from fires' is dealt with in those chapters

Interfacing to relevant models in chapter 4 'Vapour cloud dispersion', will be addressed in the following subsections.

2.7.2 Interfacing to vapour cloud dispersion models

2.7.2.1 Introduction

Most dispersion models given in chapter 4 'Vapour cloud dispersion' assume the source to be (semi-)continuous. In general the outflow models predict a time-varying mass flow rate.
This brings up the problem how to translate the time-varying mass flow rate into a semi-continuous source strength.

According to equation 4.64a in chapter 4 'Vapour Cloud Dispersion', time-varying mass flow rates may be regarded as an instantaneous source for the estimation of the atmospheric concentration c at a distance x_s and larger distances to the source, where

$$\sigma_x(x_s) > 1.3 \times u_a \times t_s \qquad\qquad (m) \qquad (2.210)$$

with

σ_x = down-wind dispersion parameter   [m]
x_s = distance to the source   [m]
u_a = windspeed   [m/s]
t_s = duration of the outflow or source duration   [s]

This means that at a distance to the source x_s which fulfils the requirement (2.210), the variations of the mass flow rate within a period t_s can not be detected.
So, the time-varying mass flow rate may always be averaged over a time period $t_{av,s}$ given by

$$t_{av,s} = \sigma_x(x_s) / 1.3 \times u_a \qquad\qquad\qquad \text{(s)} \qquad (2.211)$$

Note that $t_{av,s}(x_s)$ is a function of the distance to the source.

If the actual duration of the source t_s is greater than $t_{av,s}$, a conservative estimate of the atmospheric concentration $c(x_s)$ at distance to the source x_s may be given by using the maximum averaged mass flow rate at any time-averaged over a period $t_{av,s}$, so

$$<q_s>_{max} = MAX \int_{t - t_{av,s}/2}^{t + t_{av,s}/2} q_s(t) \times dt \qquad\qquad \text{(kg/s)} \qquad (2.212)$$

q_s =   mass flow rate of the source   [kg/s]

$<q_s>_{max}$ =   maximum averaged mass flow rate at any   [kg/s]
                      time-averaged over a period $t_{av,s}$

The total mass released can be kept the same and consequently the duration of the source must be adapted by

$$t_{s,2} = q_s/<q_s>_{max} \times t_s \qquad\qquad\qquad \text{(s)} \qquad (2.213)$$

where

$t_{s,2}$ = adapted semi-continuous source duration [s]

This method also holds for conservative estimates of the dose D_c if the exponent n is larger than unity

$$D_c = \int c'(x,t)^n \times dt \qquad\qquad\qquad ((\text{kg/m}^3)^n \cdot \text{s}) \quad (2.214)$$

c' = atmospheric concentration   [kg/m^3]
D_c = toxic load   [(kg/m^3)^n × s]
n   = chemical dependent exponent   [-]
t   = exposure time   [s]

Note, that toxic load is usually given in non SI-units: [(mg/m^3)^n·min].

In case the actual time of arrival and departure of the cloud is of importance, then a (rather) conservative estimate can be made by keeping the actual duration of the outflow t_s as input for the dispersion model, and not replacing it by $t_{s,2}$.

2.7.2.2 Compressed gases

The dispersion models: *free jet model, SLAB, model by Britter and McQuaid* described in chapter 4 'Vapour Cloud Dispersion' assume the gas(-mixture) from the source to be incompressible, meaning that the static and dynamic pressure of the gases are more or less equal to the ambient atmosphere.

For unchoked conditions the source diameter input to the jet model will be the physical source size or, if necessary, modified by a discharge coefficient.
Most operational jet models are based on uniform atmospheric pressure throughout. Several methods exist in the literature that address the problem of determining the input for a jet-dispersion model for a choked, underexpanded single-phase jet.
In Britter [1994] an overview of methods has been given and it has been concluded that little consistency exists among them.

However, for underexpanded jets the jet pressure is not atmospheric. There is a need for the determination of a pseudo-source which is consistent with the jet model and may be used to replace the complex flow when the jet expands to ambient pressure after the release from the containment (vessel or pipe).
In general, the pseudo-source area A_{Sa} is different from that of the physical break A_0, i.e. pipe or vessel hole diameter. Also the pseudo-source gas velocities will be larger than the speed of sound in the gas, but this is only for reasons of consistency.
The jet models normally assume that there is no entrainment of ambient air prior to the jet expansion to ambient pressure. All models in the literature allow expansion of the jet pressure to ambient conditions.

Usually three positions are considered:

	Index used
1. The storage reservoir	X_0
2. The exit plane	X_e
3. The ambient external state	X_{Sa}

Note for outflow from a pipe that the initial conditions should in fact be based on the conditions at the end of the pipe before the pipe opening in stead of the conditions in the storage reservoir.

The quantities in the plane where the gas jet has expanded to ambient pressure q_S, u_{sA}, T_{sA} or ρ_{sA}, and A_{Sa} or d_{Sa} are sufficient information about a gas release for any dispersion model, except for the source height.

A_{Sa}	= cross-sectional area of the jet	$[m^2]$
d_{Sa}	= diameter of the jet	$[m]$
u_{Sa}	= average gas velocity	$[m]$
ρ_{Sa}	= gas density	$[kg/m^3]$
T_{Sa}	= gas temperature	$[K]$

In the absence of any frictional effects, all models assume an isentropic (reversible and adiabatic) expansion:

$$P_e = P_0 \times (2/(\gamma+1))^{\gamma/(\gamma-1)} \qquad\qquad (N/m^2) \qquad (2.215a)$$

$$T_e = T_0 \times (2/(\gamma+1)) \qquad\qquad (K) \qquad\qquad (2.215b)$$

where

P_e	= gas pressure in the jet at the exit plane	$[N/m^2]$
P_0	= initial gas pressure	$[N/m^2]$
T_e	= temperature in the jet at the exit plane	$[K]$
T_0	= initial gas temperature	$[K]$
γ	= specific heat ratio (Poisson ratio)	$[-]$

All models take the conditions at the orifice plane to be sonic conditions, so for perfect gases

$$u_e = \sqrt{(\gamma \times R \times T_e/\mu_i)} \qquad\qquad (m/s) \qquad\qquad (2.44)$$

where

u_e	= average gas velocity in the jet at the exit plane	$[m/s]$
R	= gas constant	$[J/(mol \cdot K)]$
μ_i	= molecular mass of the gaseous chemical i	$[kg/mol]$

Note that the compressibility factor z has been taken equal to unity in equation (2.44).

The above equations are consistent with the steady flow energy equation for perfect gases

$$H + u^2/2 = \text{constant} \qquad\qquad (m^2/s^2) \qquad (2.216a)$$

or

$$C_p \times T_e + 0.5 \times \gamma \times R \times T_e/\mu_i = C_p \times T_0 \qquad\qquad (J/kg) \qquad (2.156b)$$

where

H	= specific enthalpy	$[J/kg]$
u	= average gas velocity	$[m/s]$
C_p	= specific heat at constant pressure	$[J/(kg \cdot K)]$

Note that the enthalpy terms $C_p \cdot T$ used in equation (2.216b) are approximations:

$$H_0 - H_e \approx C_p \times T_e - C_p \times T_0 \qquad\qquad (J/kg) \qquad (2.216c)$$

2.160

The accurate formulation is given by

$$H_0 - H_e \approx \int_{T_0}^{T_e} C_p(T) \times dT \qquad \text{(J/kg)} \qquad (2.216d)$$

A better approximation would be

$$H_0 - H_e \approx C_{p,av} \times (T_0 - T_e) \qquad \text{(J/kg)} \qquad (2.216e)$$

with

$$C_{p,av} = \frac{1}{T_e - T_0} \int_{T_0}^{T_e} C_p(T) \times dT \qquad \text{(J/(kg·K))} \qquad (2.216f)$$

$$\approx (C_p(T_0) + C_p(T_e))/2$$

where

$C_{p,av}$ = average C_p [J/(kg·K)]

The exit area can be estimated by

$$A_e \approx C_d \times A_0 \qquad \text{(m}^2\text{)} \qquad (2.217)$$

when assuming negligible friction

$$C_f \approx 1 \qquad \text{(-)} \qquad (2.218a)$$

and consequently by equation (2.27)

$$C_c \approx C_d \qquad \text{(-)} \qquad (2.218b)$$

where

A_e = exit area   [m²]
A_0 = area physical break   [m²]
C_c = contraction coefficient   [-]
C_d = discharge coefficient   [-]
C_f = friction coefficient   [-]

The pseudo-source distinguishes between the jet expansion to ambient pressure and the entrainment of ambient liquid. The following relates to the jet expansion to ambient pressure only.

To set up a pseudo-source the relevant steady flow mass equation

$$\rho_e \times A_e \times u_e = \rho_{Sa} \times A_{Sa} \times u_{Sa} \qquad \text{(kg/s)} \qquad (2.219)$$

the momentum equation

$$\rho_e \times A_e \times u_e^2 - \rho_{Sa} \times A_{Sa} \times u_{Sa}^2 = (P_e - P_a) \times A_e \qquad (N) \qquad (2.220)$$

and the energy equations must be satisfied. Only in case of reversible and frictionless flow, the following equation holds

$$H_0 + u_0^2 = H_e + u_e^2/2 = H_a + u_a^2/2 \qquad (m^2/s^2) \qquad (2.216h)$$

Note that for outflow from vessels it may be assumed that the initial flow velocity is negligible $u_0 \approx 0$.

The steady flow momentum equation determines the velocity u_{Sa} unambiguously with no need for reference to any thermodynamic arguments or assumptions [Britter, 1994].

ρ_e = gas density in the jet in the exit plane   [kg/m^3]
P_a = ambient atmospheric pressure   [N/m^2]
H_{Sa} = specific enthalpy jet at ambient pressure   [J/(kg $\times$ K)]
H_e = specific enthalpy jet in exit plane   [J/(kg $\times$ K)]
H_0 = initial specific enthalpy jet   [J/(kg $\times$ K)]

The quantities u_e, P_e, T_e, and A_e can be estimated by equations (2.215a), (2.215b), (2.44) and (2.217). Gas densities can be estimated by applying the perfect gas law, so

$$\rho_e = P_e \times \mu_i/(R \times T_e) \qquad (kg/m^3) \qquad (2.221)$$

where

μ_i = molecular mass gaseous chemical i [kg/mol]

The average gas velocity in the plane where the jet has expanded to ambient pressure u_{Sa} can be calculated by the following equation, resulting from combining conservation of mass and momentum

$$u_{aS} = u_e + (P_e-P_a)/(\rho_e \times u_e) \qquad (m/s) \qquad (2.222)$$

In case friction and the initial gas velocities are neglected, combining equations (2.226c) and (2.226h) gives the gas temperature T_{Sa} in the plane where the jet has expanded to ambient pressure

$$T_{Sa} = T_0 - u_{Sa}^2/(2 \times C_p) \qquad (K) \qquad (2.227a)$$

If the initial gas velocities are not neglected, then

$$T_{Sa} = T_0 - (u_{Sa}^2-u_0^2)/(2 \times C_p) \qquad (K) \qquad (2.223b)$$

The cross-sectional area and diameter of the jet at ambient pressure are given by

$$A_{Sa} = q_S/(\rho_{Sa} \times u_{Sa}) \qquad (m^2) \qquad (2.224a)$$

and

$$d_{Sa} = \sqrt{(4 \times A_{Sa}/\pi)} \qquad\qquad \text{(m)} \qquad (2.224b)$$

with

$$\rho_{Sa} = P_a \times \mu_i/(R \times T_{Sa}) \qquad\qquad \text{(kg/m}^3\text{)} \qquad (2.225)$$

where

q_S = mass flow rate [kg/s]

This model will produce a jet with a velocity u_{Sa} larger than u_e and an associated reduction in enthalpy, the reduction being brought about by a reduction in temperature.

Birch Model

However, Birch et al. in 1987 [Britter,1994] and experiments carried out by TNO (confidential) point out that the temperature of the jet after the expansion is nearly equal to the ambient temperature, quite contrary to equations (2.223a) and (2.223b)

$$T_{Sa} = T_0 \qquad\qquad \text{(K)} \qquad (2.226)$$

This means that the friction can not be neglected or equivalently the expansion is not reversible; apparently mechanical energy is converted into heat in the expansion zone of the jet.

Maintaining the conservation of mass and momentum and taking into account the discharge coefficient, the following equations have been inferred by Birch.

The gas velocity of the pseudo source can be estimated by

$$u_{Sa} = u_e \times (C_d + (1-(P_a/P_0) \times (2/(\gamma+1))^{-\gamma/(\gamma-1)})/(\gamma \times C_d)) \qquad \text{(m/s)} \qquad (2.227)$$

Note that also in this model u_{Sa} may be larger or smaller than u_e, larger at relatively high storage pressure.

The diameter of the pseudo-source is given by

$$d_{Sa}/d_0 = C_d \times (P_0/P_a) \times (2/(\gamma+1))^{1/(\gamma-1)} \times u_e/u_{Sa} \qquad \text{(-)} \qquad (2.228)$$

with

$$d_0 = \sqrt{(4 \times A_0/\pi)} \qquad\qquad \text{(m)} \qquad (2.229)$$

and of course

$$A_{Sa} = \pi/4 \times d_{Sa}{}^2 \qquad\qquad \text{(m}^2\text{)} \qquad (2.230)$$

where

d_0 = (equivalent) diameter physical break [m]

If the discharge coefficient is approximately equal to unity $C_d \approx 1$ and the Poisson ratio is $\gamma \approx 1.4$, which holds for many gases, then

$$d_{Sa}/d_0 \approx \sqrt{(0.264 \times P_0/P_a)} \qquad\qquad (-) \qquad\qquad (2.228a)$$

The mass flow rate q_S can be calculated by the appropriate outflow models given in this chapter, and is required as input for dispersion models.

The other quantities characterising the pseudo source: u_{sA}, T_{sA}, ρ_{sA}, and A_{Sa} or d_{Sa} should be estimated by the model developed by Birch, formulated by equations (2.217), (2.226), (2.220), (2.230) and (2.228) in this paragraph.

2.7.2.3   Pressurised liquefied gases

2.7.2.3.1 Introduction

If the outflow to the atmosphere is a two-phase outflow, then the results of the outflow model have to be interfaced to the spray release model first. If the vapour mass fraction is negligible, the same approach as for compressed gases can be followed.

2.7.2.3.2 Interfacing of spray release model for finite duration release of pressurised liquefied gases

Note that in this section reference is made to symbols defined in chapters 2 and 4.

The two-phase jet model can be interfaced with:
− the free jet model (section 4.5.4.1);
− the Gaussian Plume model (section 4.5.3);
− the dense gas model of Britter and McQuaid (section 4.5.5.1);
− the dense gas model SLAB (section 4.5.5.2).

The free jet model

The free jet model can be applied after flashing is complete. Therefore, in formulae 4.76, 4.77, 4.81 and 4.82 b_0 should be replaced by $b_{f,rainout}$ which results from (2.153), section 2.5.3.7. However, for the evaluation of the Froude-number (4.72), the properties after complete evaporation should be used (during evaporation the total buoyancy of the jet is not conserved, see section 4.2.7.1 for an explanation). So in formula (4.72) ρ_0 should be replaced by ρ_j from (2.165), u_0 by u_j from (2.166) and

b_o by b_j from (2.167), section 2.5.3.7. The validity of the free jet model beyond the position in the jet where evaporation of all droplets is complete, follows from (4.73). Note that the two-phase model is only valid for horizontal jets.

The Gaussian Plume Model

The Gaussian plume model (GPM, see section 4.5.3) can be applied if after evaporation of the droplets the cloud or plume is neutrally or positively bouyant, i.e. if ρ_j from (2.165), section 2.5.3.7, is less than or equal to ρ_a.
The input for the Gaussian Plume Model can be limited to the mass flow rate. Therefore the release rate q in (4.51) needs to be replaced by $q_{S,nett,air}$ according to (2.151). Then, use is made of (4.53a) and (4.57a). The initial size of the jet after evaporation can be included in the GPM by replacing b_{oy} in (4.53b) and b_{oz} in (4.57b) by b_j from (2.167).

The dense gas model of Britter and McQuaid

If the density after evaporation $\rho_j > \rho_a$ a dense gas dispersion model is needed. The simplest model is the continuous release model by Britter and McQuaid, see section 4.5.5.1. The input of this model is the effective gravity at the source, g'_o and the volume flow rate v_o. The effective gravity needs to be calculated by replacing ρ_o in the definition (section 4.3.5.1) by ρ_j from (2.175), and the volume flow rate v_o needs to be calculated by multiplying u_j with A_j, from (2.166) and (2.167), respectively.

SLAB model

Another dense gas dispersion model, SLAB, is described in section 4.5.5.2. This model accounts for the evaporation of droplets. The source conditions are therefore the conditions just after flashing and after accounting for rain-out. The following list presents the input data that should be extracted from the spray release model, using the SLAB notations (see e.g. Table 4.21):
− initial liquid mass fraction of the material CMEDO: $\Phi_{m,f,rainout}$ according to (2.152);
− temperature of the source material TS: boiling temperature T_B;
− mass flow rate of the source QS: $q_{S,nett,air}$ according to (2.151);
− area of the source AS: $A_{f,rainout}$ according to (2.153).
For this case only the horizontal jet option should be applied, i.e. IDSPL=2

2.7.2.3.3 Interfacing of spray release model for instantaneous release of pressurised liquefied gases

Note that in this section reference is made to symbols defined in chapters 2 and 4.

2.8 Discussion of outflow and spray release models

2.8.1 Introduction to section 2.8

In this section some general considerations on the models related to pool evaporation presented in this chapter are given and gaps in the descriptions of (out)flow and spray release are indicated.

2.8.2 General remarks

The standard approach for single-phase flows has been described, as well as models for non-stationary gas outflow through long pipelines. A rather fast model for stationary two-phase flow in pipes has been presented.
Much attention has been given to the dynamic behaviour of vessels due to the release of material.
An adequate model for the spray release is presented, explaining for instance why 'light gases' like ammonia can behave like a heavy gas under certain circumstances.

Two types of models have been described:
1. analytical or numerical models that are (mainly) based on physical laws,
2. models consisting mainly on mathematical correlations of experimental data.

Also in the field of (out)flow and vessel dynamics, there is a tendency to develop more complex (numerical) models. However, analytical equations may be used to get a quick estimate of the order of magnitude of the outflow rate. These models are based on simplifying assumptions like: ideal gas behaviour, constant physical properties, and unchanged boundary conditions.
A numerical approach accommodates to take into account changes of the physical properties as a function of temperature and pressure, non-ideal gas and liquid behaviour, and 'sudden' changes in boundary conditions.

A weakness of the chapter is that it has to rely for many situations on correlations, while other manageable models are lacking. Difficulties arise when predictions are required outside the validity ranges of the correlations based on limited experimental data. That is the reason why models based on general physical laws are generally favoured.

Analytical or numerical physical models have been presented for:
− gas outflow,
− liquid outflow,
− stationary two-phase pipe flow [Kukkonen, 1990],
− non-stationary two-phase pipe flow [Morrow, 1983],
− vessel dynamics.

The correlations have been presented for:
- non-stationary gas outflow from small holes in pipelines [Weiss, 1988],
- non-stationary gas outflow from full bore ruptured pipelines [Hanna, 1987],
- the void fraction in the expanded liquid, as described by Mayinger [Belore, 1986],
- transient releases rate of pressurized liquid propane from a ruptured pipeline [Tam, 1990],
- the critical mass flux for two phase flow as a function only of the pressure and temperature upstream of the pipe, as described by Flinta [Giot, 1992],
- estimating the two-phase flow in a vessel, and the quality at the exit in case of top venting for vertical vessels, as described by DIERS [Melhem, 1993].

No model to cope with crater formation, caused by ruptures or leakages of underground pipelines, appeared to be publicly available.

2.8.3   Single-phase (out)flow and vessel dynamics

The well-known relations for the stationary critical and non-critical outflow of gases through orifices and through pipes for gases and vapours are as in the previous edition [YellowBook, 1988].
There is not much discussion about applying standard thermodynamics for the description of the behaviour of vessels filled with pressurized gas or (non-boiling) liquid only. For liquid flow through holes and pipes and the behaviour of liquid vessels the standard approach has been followed.

2.8.4   Pressurized liquified gases

Although the behaviour of a depressurizing pressurized liquified gas is a complex process, we have choosen to describe a model based on standard thermodynamics, but have taken into account the criteria of DIERS [Melhem, 1993] and Mayinger [Belore, 1986].

Much research on two-phase (out)flow modelling has been carried out, but the models appear only to be valid for specific situations. 'Homogeneous Equilibrium Models' (HEMs) can successfully be applied if the quality of the flow is larger than 0.01 [Giot, 1996]. So, in case of saturated liquid entering the pipe and pipelines much longer than 0.1 meter, HEMs may be applied, but not in the case of sub-cooled liquid upstream and/or relatively short pipelines.

The model for non-stationary two-phase flow in pipelines has been worked out for propane only, but can be generalized to other chemicals [Morrow, 1983]. Morrow's model lacks extensive validation. The correlation by Tam is valid only for propane, and has limited validity within the range of the experiments [Tam, 1990].

No model for gas flow in pipes has been described that take into account the difficulties that may arise if the gas temperature decreases below its critical temperature due to depressurization, and condensation might occur. This may happen for chemicals with critical temperatures around the ambient temperature, like for instance ethene.

2.8.5   Spray release mode to reacting chemicals

The models to describe the evolution of two-phase jets and the evaporation of droplets do not account for chemical reactions, e.g. like hydrogen fluoride (HF) forming oligomers in humid air. The evolution of chemically reacting two-phase jets can only be treated by using a differential approach of the jet evolution in small steps along the flow direction, as described by Webber et al. [1991].

The common practice to assume that twice the flash fraction remains airborne in case of instantaneous releases of pressurized liquefied gas, provides a rough approximation of Schmidli et al.'s results, but these are based on small-scale experiments only [Schmidli, 1992].

2.8.6   'Epilogue'

The correlations should be replaced by practical models based on sound physical laws.

The modelling of non-stationary releases of pressurized liquified gases from pipelines requires additional research.

It is recommended to develop practical models for crater formation, caused by ruptures or leakages of underground pipes.

2.9 References

AIChE (1989),
Chemical Process Quantitative Risk Analysis - guidelines for -,
Center for Chemical Process Safety of the American Institute of Chemical Engineers,
1989.

Appleton, P.R. (1984),
A study of axi-symmetric two-phase flashing jets,
SRD report R 303, U.K. A.E.A., Culcheth, Warrington, Cheshire, U.K.

Beek (1975),
W.J. Beek and K.M.K. Mutzall
Transport Phenomena
Wiley, New York, 1975

Bell (1993),
K. Bell, S.D. Morris and R. Oster,
Ventline void fractions and mass flow rates during top venting of high viscosity fluids,
J. Loss Prev. Process Ind., 1993, Vol 6, No 1.

Belore (1986),
R. Belore and I. Buist, A computer model for predicting leak rates of chemicals from
damaged storage and transportation tanks,
S.L. Ross Environmental Research Lim. Ottawa, Ontario, Canada,1986.

Britter (1994),
R.E. Britter, Dispersion of two phase flashing releases - FLADIS Field Experiment,
The modelling of a pseudo source for complex releases, CERT Ltd. Cambridge.

Carter (1991),
Aspects of risk assessments for hazardous pipelines containing flammable substances,
J. Loss Prev. Process Ind.,1991, Vol. 4, January.

Cavanaugh II, T.A., Siegell, J.H., Steinberg, K.W. (1994),
Simulation of vapor emissions from liquid spills, J. of Hazardous Materials,
38 pp 41-63.

Commissie Preventie van Rampen door gevaarlijke stoffen (1988),
Methoden voor het berekenen van fysische effekten, CPR-14.

Crowl (1993),
D.A. Crowl, Liquid discharge from process and storage vessels,
J. Loss Prev. Process Ind., 1993, Vol. 6, No 1.

DIERS (1986)
Technology Summary
Emergency Relief Systems for Runaway Chemical Reactions and Storage Vessels:
A Summary of Multiphase Flow Models
AIChE/DIERS Publication, New York, 1986.

Dodge (1996),
Personal communication with Dr. F.T. Dodge,
South West Research Institute, San Antonio, Texas, USA 78228.

Edminster (1984),
W.C. Edminster, B.I. Lee, Applied hydrocarbon thermodynamics, volume 1, second
edition, 1984.

Ewan (1988),
B.C.R. Ewan, K. Moodie and P.J. Harper,
A study of two phase critical pipe flow models for superheated liquid releases,
J. of Hazardous Materials, 20,1988) 273-286.

Fauske (1988),
H.K. Fauske and M. Epstein,
Source term considerations in connection with chemical accidents and vapour cloud
modelling,
J. Loss Prev. Process Ind.,1988, Vol. 1, April.

Foster (1981),
T.C. Foster, Time to empty a Vessel,
Chemical Engineering May 4 1981.

Gasunie (1980),
Basisgegevens aardgassen,
N.V. Nederlandse Gasunie, 1980.

Giesbrecht, H., Hess, K., Leuckel, W., Maurer, B. (1981),
Analysis of explosions hazards on spontaneous release of inflammable gases into the
atmosphere,
Ger. Chem. Eng. 4, pp 305-314.

Giot (1992),
M. Giot and A. Fritte,
Preparation of a comprehensive computer program to predict choked multiphase
flows through simple and complex geometries,
Final report E.U. Environmental Research program EV4T0001-B(EDB), 1992.

Giot (1992),
M. Giot et all.,
Overall and detailed calculations of two-phase choked flows (FLIERS),
Conference The Safe Handling of Pressure Liquefied Gases, 26/27 November 1992,
London.

Giot (1994),
M. Giot et all.,Two-phase releases,
J. Loss Prev. Process Ind.,1994, Vol. 7, Number 2.

Giot (1996),
M. Giot, Personal communication.

Hague, W.J., Pepe, W. (1990),
Flow chamber simulations of aerosol formation and liquid jet breakup for pressurised
releases of hydrogen fluoride,
Plant/Operations Progress 9/2, pp 125-127.

Hanna (1987),
S.R. Hanna and P.J. Drivas,
Vapor Cloud Dispersions Models, CCPS, 1987.

Hardee, H.C., Lee, D.O. (1975),
Expansion of clouds from pressurised liquids,
Accid. Anal. & Prev. 7, pp 91-102.

Hardekopf (1988),
F. Hardekopf and D. Mewes, Critical ratio of two-phase flows,
J. Loss Prev. Process Ind.,1988, Vol. 1, July.

Hart (1993),
P.W. Hart and J.T. Sommerveld, Fluid discharge resulting from puncture of
spherical process vessels,
J. of Hazardous Materials, 33, 1993, 295-305.

Haque (1990),
A. Haque, S. Richardson, G. Saville, G. Chamberlain, Rapid depressurization of
pressure vessels,
J. Loss Prev. Process Ind.,1990, Vol. 3, January.

Haque (1992),
M.A. Haque, S.M. Richardson and G. Saville, Blow-down of pressure vessels,
I. Computer Model, Trans IChemE, Vol. 70, Part B, February 1992.

Heuven (1985),
J.W. van Heuven, Afblaassystemen voor chemische reactoren,
TNO-rapport PML 1985-C-31.

Hewitt, G.F., Pattison, M.J. (1991),
Modelling of release and flow of two-phase jets, presented at The safe handling of
pressure liquefied gases (IBC),
London, 26-27 Nov. 1992.

Johnson, D.M., Pritchard, M.J., Wickens, M.J. (1990),
Large scale catastrophic releases of flammable liquids, British Gas Report under
contract CEC EV4T.0014.UK(H), Midlands Research Station, Solihull, West
Midlands, U.K.

Jones (1992),
D. Jones, Nomenclature for hazard and risk assessment in the process industries,
second edition 1992, Institution of Chemical Engineers U.K.

Kaiser (1988),
G.D. Kaiser, A review of models for predicting the dispersion of ammonia in the

atmosphere,
AIChE Ammonium Symposium Safety in Ammonia and Related Facilities,
Denver, Colorado, August 1988.

Kocamustafaogullari, G., Smits, S.R., Razi, J. (1994),
Maximum and mean droplet sizes in annular two-phase flow, Int. J. Heat Mass
Transfer, 37/6 pp 955-965.

Kukkonen, J., Vesala, T., Kulmala, M. (1989),
The interdependence of evaporation and settling for airborne freely falling droplets,
J. Aerosol Sci. 20/7, pp 749-763

Kukkonen, J. (1990),
Modelling source terms for the atmospheric dispersion of hazardous substances,
Commentationes Physico-Mathematicae 115/1990, Finnish Society of Sciences and
Letters, Helsinki.

Kukkonen, J., Kulmala, M., Nikmo, J., Vesala, T., Webber, D.M., Wren, T. (1993),
Aerosol cloud dispersion and the suitability of the homogeneous equilibrium
approximation, report AEA/CS/HSE R1003/R, AEA Technology, Warrington,
Cheshire, U.K.

Lang (1991),
E. Lang, Gas flow in pipelines following a rupture computed by a spectral method,
Journal of Applied Mathematics and Physics (ZAMP) Vol. 42, March 1991.

Lee (1987),
K.S. Lee, J.T. Sommerfeld, Maximum leakage times through puncture holes for
process vessels of various shapes,
J. of Hazardous Materials, 14, 1987) 365-386.

Leung (1987),
J.C. Leung, M.A. Grolmes, The Discharge of Two-phase Flashing Flow in a
Horizontal Duct,
AIChE Journal March 1987 Vol. 33, No. 3

Leung (1988),
J.C. Leung and M. Epstein, A Generalized Critical Flow Model for Non-ideal Gases,
AIChE Journal Vol. 34, No. 9 September 1988.

Leung (1989),
J.C. Leung and H.G. Fisher, Two-Phase flow venting from reactor Vessels,
J. Loss Prev. Process Ind., 1989, Vol. 2, April.

Leung (Jan. 1990),
J.C. Leung, Two-phase discharge in nozzles and pipes - a unified approach,
J. Loss Prev. Process Ind.,1990, Vol. 3, January

Leung and Nazario (1990),
J.C. Leung and F.N. Nazario, Two-phase flow methods and comparisons,
J. Loss Prev. Process Ind.,1990, Vol. 3, April.

Leung (May 1990),
J.C. Leung, Similarity between Flashing and Non-flashing Two-Phase Flows,
AIChE Journal May 1990 Vol. 36, No. 5

Leung (1991),
J.C. Leung and M. Epstein, Including the Effects of Non-condensible Gases,
Journal of Heat Transfer, February 1991, Vol. 113

Melhem (1993),
G.A. Melhem, and P.A. Croce, Advanced Consequence Modelling Emission,
Dispersion, Fires, and Explosions, second draft July, 1993, A.D. Little.

Melhem, G.A., Croce, P.A. (1993),
Advanced consequence modelling: emission, dispersion, fires and explosions, 2nd
draft, Van Nostrand Reinhold Inc., New York, USA.

Moore (1972),
W.J. Moore, Physical Chemistry, fifth edition, Prentice-Hall, Inc.,
New Jersey.

Morris (1990),
S.D. Morris, Flashing flow through relief lines, pipe breaks and cracks,
J. Loss Prev. Process Ind.,1990, Vol. 3, January.

Morrow (1983),
T.B. Morrow, R.L. Bass, J.A. Lock., A LPG Pipeline Break Flow Model,
Journal of Energy Resources Technology, September 1983, Vol. 105.

Nielsen (1991),
D.S. Nielsen, Validation of two-phase outflow model,
J. Loss Prev. Process Ind.,1991, Vol. 4, July.

Nijsing (1988),
R. Nijsing, Treatment of moving phase boundaries and mixture-density
discontinuities in axial two phase flow,
Paper presented at the 1988 European Two Phase Flow Group Meeting at Brussels
30 May-1 June, 1988.

NIST (1993),
NIST Thermodynamic Properties of Refrigerants and Refrigerant Mixtures,
Version 5.0,
National Institute of Standards and Technology 221/A320, Gaithersburg,
MD 20897, USA.

Nolan, P.F., Hardy, N.R., Pettitt, G.N. (1991),
The physical Modelling of two phase releases following the sudden failure of
pressurised vessels,
Int. Conf. and Workshop on modelling and mitigating the consequences of accidental
releases of hazardous materials (AIChE), pp 125-146.

Nyren (1983),
K. Nyren and S. Winter, Two phase discharge of liquefied gases through pipes, field experiments with ammonia and theoretical model,
Symposium Series of the IChemE, Symposium on Loss Prevention, Harrogate, England, 1983.

Nyren (1987),
K. Nyren and S. Winter, Discharge of condensed sulfur dioxide: a field test study of the source behaviour with different release geometries,
J. of Hazardous Materials, 14, 1987, 365-386.

Olorunmaiye (1993),
J.A. Olorunmaiye and N.E. Imide, Computation of natural gas pipeline rupture problems using the method of characteristics,
J. of Hazardous Materials, 34,1993, 81-98.

Papadourakis, A., Caram, H.S., Barner, C.L. (1991),
Upper and lower bounds of droplet evaporation in two-phase jets,
J. Loss Prev. Process Ind., 4, pp 93-101.

Pattison, M.J. (1992),
The behaviour of binary droplets, report MPS/15, CLOUD/1, Imperial College of Science, Technology and Medicine,
Dept. of Chem. Eng. and Chem. Techn., London.

Perry (1973),
R.H. Perry and C.H. Chilton, Chemical Engineers'Handbook, fifthe edition,
McGraw-Hill Kogakusha LTD, 1973.

Pilz (1976),
V. Pilz and W. van Herck, Chemical Engineering Investigations with respect to the safety of large chemical plants,
Third symposium on large chemical plants, European Federation of Chemical Engineering, Antwerp, 1976.

Prins (1996),
Personal communications with J. Prins at the Technical University of Delft, Holland.

Radford (1990),
M.D. Radford, A comprehensive list of pipe coefficients of friction for the Hazen-Williams and Manning formulae derived from the Darcy-Weisbach formula and Colebrook-White transition law for roughness values (k),
Water SA Vol. 16 No.4 October 1990.

Ramskill (1987),
P.K. Ramskill, Discharge rate calculation methods for use in plant safety assessment,
SRD R352, February 1987.

Riznic (1989),
J.V. Riznic and M. Ishii, Bubble number density and vapor generation in flashing flow, Int. J. Heat Mass Transfer, No. 10.

Sallet (1990,1),
D.W. Sallet, Subcooled and saturated liquid flow through valves and nozzles,
J. of Hazardous Materials, 25, 1990,2 181-191.

Sallet (1990,2),
D.W. Sallet, Critical two-phase mass flow rates of liquefied gases,
J. Loss Prev. Process Ind.,1990, Vol. 3, January, page 38-42.

Sallet (1990,3),
D.W. Sallet, On the prevention of two-phase fluid venting during safety valve action,
J. Loss Prev. Process Ind.,1990, Vol. 3, January, page 53-58.

Schmidli, J., Yadigaroglu, G., Banerjee, S. (1992),
Sudden release of superheated liquids, HTD-Vol. 197,
Two-phase flow and heat transfer 1992, ASME, pp 207-214.

Sheppard (1993),
C.M. Sheppard, DIERS churn-turbulent disengagement correlation extended to
horizontal cylinders and spheres,
J. Loss Prev. Process Ind.,1993, Vol. 6, Number 3.

Sheppard (1994),
C.M. Sheppard, DIERS bubbly disengagement extended to horizontal cylinders and
spheres,
J. Loss Prev. Process Ind.,1994, Vol. 7, Number 1.

Skouloudis (1990),
A.N. Skouloudis, K. Bell, M. Kottowski, Venting of vessels containing reacting
fluids: a parametric study with SAFIRE and DEERS,
J. Loss Prev. Process Ind.,1990, Vol. 3, January.

Sommerfeld (1993),
J.T. Sommerfeld and M.P. Stallybrass, Elliptic integral solutions for fluid discharge
rates from puncture holes horizontal cylindrical vessels,
J. Loss Prev. Process Ind., 1993, Vol. 6, No 1.

Starling (1973),
K.E. Starling, Fluid Thermodynamic Properties for Light Petroleum Systems,
Gulf Publishing Company, Houston, 1973.

Sumathipala (1990),
K. Sumathipala, J.E.S. Venart and F.R. Steward, Two-Phase Swelling and
entrainment during pressure relief valve discharges,
J. of Hazardous Materials, 25, 1990, 219-236.

Tam (1990),
V.H.Y. Tam and R.B. Higgins, Simple Transient release rate models for releases of
pressurised liquid petroleum pipelines,
J. of Hazardous Materials, 25,1990, 193-203.

Tilton, J.N., Farley, C.W. (1990),
Predicting liquid jet breakup and aerosol formation during the accidental release of
pressurised hydrogen fluoride,
Plant/Operations Progress 9/2, pp 120-124

TNO (1983),
LPG a study, May 1983, TNO, Apeldoorn, The Netherlands.

Vandroux-Koenig, S., Berthoud, G., Cordero, D., Kahn, H., Mercier, P. (1991),
Modelling of multiphase jets in the immediate vicinity of a containment breach:
application to a propane reservoir,
note technique STR/LML/91-21, C.E.A Centre d'Etudes Nucleaires de Grenoble.

Vesala, T. (1990),
Binary evaporation Report series in aerosol science No 13, Finnish association for
aerosol research/University of Helsinki, Dept. of physics, Helsinki

Vesala, T., Kukkonen, J. (1992),
A model for binary droplet evaporation and condensation, and its application for
ammonia droplets in humid air, Atmospheric Environment, 26A/9 pp 1573-1581.

Webber, D.M., Brighton, P.W.M. (1989),
Generalisation of the two-phase jet model TRAUMA to other substances than
ammonia, report SRD/HSE/R494, SRD, Culcheth, Cheshire, U.K.

Webber, D.M., Tickle, G.A., Wren, T., Kukkonen, J. (1991),
Mathematical modelling of two-phase release phenomena in hazard analysis,
AEA Technology, Culcheth, Cheshire, U.K., report SRD/CEC/22939/01.

Webster (1981),
Websters' Third New International Dictionary, 1981.

Weiss (1988),
M.N. Weiss, K.K. Botros, W.M. Jungowski, Simple method predicts gas-line blow-
down times,
Oil&Gas Journal, Dec. 12, 1988.

Wheatley, C.J. (1987),
Discharge of liquid ammonia to moist atmospheres - survey of experimental data and
model for estimating initial conditions for dispersion calculations, SRD, Culcheth,
Cheshire, U.K., report SRD/HSE/R 410.

Wheatley (1987),
C.J. Wheatley, A users guide to TRAUMA, SRD/HSE-report R394,
April 1987.

Wierzba, A. (1990),
Deformation and breakup of liquid drops in a gas stream at nearly critical Weber
numbers,
Experiments in Fluids 9, pp 59-64.

Wilday (1992),
A.J. Wilday, Pressure relief systems, Conference The Safe Handling of Pressure Liquefied gases,
26/27 November 1992, London.

Woodward, J.L. (1993),
Expansion zone modelling of two-phase and gas discharges,
J. of Hazardous Materials, 33 pp 307-318.

Woodward, J.L., Papadourakis, A. (1991),
Modelling of droplet entrainment and evaporation in a dispersing jet,
Int. Conf. and Workshop on modelling and mitigating the consequences of accidental releases of hazardous materials.

Woodward (1991),
J.L. Woodward and K.S. Modan, Liquid and gas discharge rates through holes in process vessels,
J. Loss Prev. Process Ind.,1991, Vol. 4, April.

Worldbank (1988),
Techniques for Assessing Industrial Hazards - A manual -,
World Bank Technical Paper number 55, by Technica Ltd.

Yan (1990),
F. Yan, M.Giot, L. Bolle, Modelling of flashing during adiabatic release through pipes, Unité Thermodynamique et Turbomachines, Université Catholique de Louvain, Louvain-la-Neuve, Belgium.

Yellow Book (1988),
Methods for the calculation of physical effects of the escape of dangerous materials,
CPR-14E, Ministery of Social Affairs and Employment, The Netherlands.

Appendix 2.1 Some properties of chemicals used in the TPDIS model [Kukkonen, 1990]

Physical properties of air, water, ammonia, chlorine, sulphur dioxide, propane, hydrogen fluoride and water are given as a function of temperature, in the original form created by Kukkonen. The relations are based on data from Landolt and Bornstein [1960], CRC Handbook [1984-85], Chlorine Institute [1981], Reid et al. [1987].

Subscripts:

x_A : physical property x of ammonia
x_{Air} : physical property x of air
x_{Ch} : physical property x of chlorine
x_{HF} : physical property x of hydrogen fluoride
x_P : physical property x of propane
x_{SD} : physical property x of sulpher dioxide
x_W : physical property x of water

x_V : vapour phase
x_L : liquid phase

The temperature values referred to by T, are given in degrees Kelvin. The following notations are used:

τ = T - 223.15

Saturation vapour pressure [Pa]:

P_A = exp(23.32 - (2831/T))

P_{CH} = exp(21.757 - (2446.3/T))

P_{SD} = exp(23.164 - (3065/T))

P_P = $98.04 \times 10^3 \times$ exp(9.959 - (2293/T))

P_{HF} = $133.3 \times 10^{(8.3804-1952.6/(62.37+T))}$

P_W = exp(77.345 - (7235/T) - $8.2 \times$ ln(T) + $0.005711 \times$ T)

The density of the vapour phase in saturated state [kg/m^3]:

$\rho_{V,A}$ = 1 / ($-0.7974 \times 10^{-5} \times \tau^3 + 0.001472 \times \tau^2 - 0.09552 \times \tau + 2.373$)

$\rho_{V,C}$ = 1 / ($-0.143 \times 10^{-5} \times \tau^3 + 0.000271 \times \tau^2 - 0.0185 \times \tau + 0.508$)

$\rho_{V,SD}$ = 1 / ($-0.5043 \times 10^{-5} \times \tau^3 + 0.0009981 \times \tau^2 - 0.07006 \times \tau + 1.849$)

$$\rho_{V,P} = -0.586 \times 10^{-6} \times T^3 + 0.00371 \times T^2 - 1.57 \times T + 174$$

$$\rho_{V,HF} = 22.29 \times (P_{HF}(T)/(R \times T) + 33.7)$$

$$R = 8.31434 \text{ J/(mol} \times \text{K)}$$

The density of the liquid phase in saturated state [kg/m^3]:

$$\rho_{L,A} = -14.25 \times 10^{-5} \times \tau^3 + 0.01386 \times \tau^2 - 1.613 \times \tau + 704.7$$

$$\rho_{L,Ch} = 10^6 / (18.23 \times 10^{-6} \times \tau^3 + 1.836 \times 10^{-3} \times \tau^2 + 0.9873 \times \tau + 625.6)$$

$$\rho_{L,SD} = 9.050 \times 10^{-5} \times \tau^3 - 0.01713 \times \tau^2 - 1.642 \times \tau + 1549$$

$$\rho_{L,P} = 0.624 \times 10^{-6} \times T^3 - 0.00395 \times T^2 + 0.635 \times T + 639.0$$

$$\rho_{L,HF} = 3.125 \times 10^{-3} \times (\tau-50)^2 - 2.2625 \times (\tau-50) + 1002$$

The entropy of the vapour phase in saturated state [J/(kg · K)]:

$$S_{V,A} = 1.407 \times 10^{-4} \times \tau^3 + 0.05444 \times \tau^2 - 19.31 \times \tau + 6156$$

$$S_{V,Ch} = -0.688 \times 10^{-4} \times \tau^3 + 0.02130 \times \tau^2 - 3.98 \times \tau + 3090$$

$$S_{V,SD} = -6.575 \times 10^{-5} \times \tau^3 + 0.01612 \times \tau^2 - 5.486 \times \tau + 1834$$

$$S_{V,P} = -8.163 \times 10^{-7} \times T^3 + 5.173 \times 10^{-3} \times T^2 - 4.670 \times T + 6540$$

$$S_{V,HF} = 5.192 \times T + 7106$$

The entropy of the liquid phase in saturated state [J/(kg · K)]:

$$S_{L,A} = 1.491 \times 10^{-4} \times \tau^3 - 0.04481 \times \tau^2 + 20.09 \times \tau - 197.0$$

$$S_{L,Ch} = -0.1567 \times 10^{-4} \times \tau^3 - 0.008123 \times \tau^2 + 4.297 \times \tau + 1764$$

$$S_{L,SD} = -1.122 \times 10^{-4} \times \tau^3 + 0.01232 \times \tau^2 + 4.992 \times \tau - 52.73$$

$$S_{L,P} = -2.202 \times 10^{-7} \times T^3 - 1.359 \times 10^{-3} \times T^2 + 10.16 \times T + 1576$$

$$S_{L,HF} = 8.981 \times T + 1092$$

The heat of vaporisation in saturated state [J/kg]:

$$L_{v,A} = -0.03238 \times \tau^3 - 6.131 \times \tau^2 - 2700 \times \tau + 1418 \times 10^3$$

$$L_{v,Ch} = -0.00639 \times \tau^3 - 0.631 \times \tau^2 - 547 \times \tau + 296 \times 10^3$$

$$L_{v,SD} = 0.02126 \times \tau^3 - 9.951 \times \tau^2 - 450.8 \times \tau + 421.0 \times 10^3$$

$$L_{v,P} = 5.862 \times 10^{-4} \times T^3 - 3.689 \times T^2 + 583.8 \times T + 481.5 \times 10^3$$

$$L_{v,HF} = 374 \times 10^3$$

The enthalpy of the vapour phase in saturated state [J/kg]:

$$H_{V,A} = 0.9139 \times \tau^3 - 140.9 \times \tau^2 + 7685 \times \tau + 1298 \times 10^3$$

$$H_{V,Ch} = -0.005212 \times \tau^3 - 0.4526 \times \tau^2 - 417.9 \times \tau + 518.1 \times 10^3$$

$$H_{V,SD} = -0.02733 \times \tau^3 - 1.753 \times \tau^2 + 557.8 \times \tau + 410.3 \times 10^3$$

$$H_{V,P} = -6.187 \cdot 10^{-5} \times T^3 + 0.3908 \times T^2 + 951.3 \times T + 87.92 \times 10^3$$

$$H_{V,HF} = L_{v,HF}(T) + 1.272 \times T^2 + 1712 \times T$$

Note: the liquid phase enthalpy is given by

$$H_L = H_V - L_v$$

Specific heat capacities at constant pressure are approximately constant in the temperature range considered

$$C_{p,W} = 1860 \; J/(kg \times K)$$

$$C_{p,air} = 1005 \; J/(kg \times K)$$

Appendix 2.2 Relations for changes in enthalpy and entropy

The following statements are valid for systems that perform pressure-volumetric work ($P \cdot \Delta V$) only; it may contain liquids, vapours and gases.

Changes in enthalpy

The change in enthalpy of any system is given by

$$dH = C_p \times dT - [T \times (\partial v/\partial T)_p - v] \times dP \qquad \text{(J/kg)}$$

Changes in enthalpy *at constant pressure* for any system is given by

$$dH_p = C_p \times dT \qquad \text{(J/kg)}$$

It can easily be inferred that for ideal gas the term between brackets is equal to zero. So, for ideal gases the following expression is valid for *any change*

$$dH_v = C_{p,v} \times dT \qquad \text{(J/kg)} \qquad \text{(A.2.1)}$$

which means that

$$\Delta H_v = C_{p,v,av} \times (T_2 - T_1) \qquad \text{(J/kg)} \qquad \text{(A.2.2)}$$

For real gases and vapours this relation may hold approximately.

The difference in enthalpy between the liquid and vapour phase at temperature T is always equal to the negative heat of evaporation at that temperature, so

$$H_L(T) = H_v(T) - L_v(T) \qquad \text{(J/kg)} \qquad \text{(A.2.3)}$$

Mostly we are only interested in changes of enthalpy. The expressions above lead to the following expression for the change of enthalpy of a liquid

$$\Delta H_L = \Delta H_v - \Delta L_v$$

$$\approx C_{p,v,av} \times (T_2 - T_1) - (L_v(T_2) - L_v(T_1)) \qquad \text{(J/kg)} \qquad \text{(A.2.4)}$$

Changes in entropy

The change in entropy of any system is given by

$$dS = C_p/T \times dT - (\partial v/\partial T)_p \times dP \qquad \text{(J/(kg·K))}$$

Changes in entropy *at constant pressure* for any system is given by

$$dS_p = C_p/T \times dT \qquad \text{(J/(kg·K))}$$

It can easily be inferred that for ideal gas the following expression is valid for *any change* of system

$$dS_v = C_{p,v}/T \times dT - R/P \times dP \qquad (J/(kg \cdot K))$$

which means that

$$\Delta S_v = C_{p,v,av} \times \ln(T_2/T_1) - R \times \ln(P_2/P_1) \qquad (J/(kg \cdot K)) \quad (A.2.5)$$

For real gases and vapours this relation may hold approximately.

The difference in entropy between the liquid and vapour phase at temperature T is always equal to

$$S_L(T) = S_v(T) - L_v(T)/T \qquad (J/(kg \cdot K)) \quad (A.2.6)$$

Mostly we are only interested in changes in enthalpy. The expressions above lead to the following expression for the change in entropy of a liquid

$$\Delta S_L = \Delta S_v - \Delta(L_v/T) \qquad (J/(kg \cdot K)) \quad (A.2.7)$$

$$\approx C_{p,v,av} \times \ln(T_2/T_1) - R \times \ln(P_2/P_1) - (L_v(T_2)/T_2 - L_v(T_1)/T_1)$$
$$(J/(kg \cdot K)) \quad (A.2.8)$$

Where

C_p	= specific heat at constant pressure	$[J/(kg \times K)]$
$C_{p,av}$	= temperature average C_p	$[J/(kg \times K)]$
H	= enthalpy	$[J/kg]$
H_v	= enthalpy of vapour or gas	$[J/kg]$
H_L	= enthalpy of liquid	$[J/kg]$
$L_v(T)$	= heat of vaporisation at temperature T	$[J/kg]$
P_1	= start pressure of a system	$[K]$
P_2	= end pressure of a system	$[K]$
S	= entropy	$[J/(kg \times T)]$
T_1	= start temperature of a system	$[K]$
T_2	= end temperature of a system	$[K]$
v	= specific volume	$[m^3/kg]$

Chapter 3
Pool evaporation
C.J.H. van den Bosch

Modifications to Chapter 3 (Pool Evaporation) with respect to the first print (1997)

Numerous modifications were made concerning typographical errors. A list is given below for the pages on which errors have been corrected.

Page 3.19:	Several symbols have been added in between the text to clarify the equations on this page.
Page 3.20:	Correction for the proper use of the english language in the first sentence.
Page 3.22:	Correction of the equations 3.7, 3.8 and 3.8a
Page 3.23:	Correction of the symbol T_a in T_w in the last sentence.
	Page 3.25: Correction of the equation 3.10d and in the explanation of the symbols. The explanation of the symbol D_a has been added.
Page 3.30:	The symbol c_i has been added in the text for clarification, and the equation 3.14 has been corrected.
Page 3.34:	The symbols in the text on this page have been better indicated for clarification.
Page 3.35:	Correction of equation 3.18a (more scientific notation).
Page 3.39:	The symbol c_i has been added in the text for clarification.
Page 3.40:	On this page, for the symbol of the radius of the liquid pool is now used r_p.
Page 3.47 – 3.57:	No modifications have been made to the User Manual of GASP.
Page 3.58:	Correction of the symbol Tq_s in the equations 3.77 and 3.79.
Page 3.62:	Correction of the symbol for the subsoil surface temperature.
Page 3.66:	Page number added for the chapter on "Vapour Cloud Dispersion"
Page 3.67:	Corrections made to the equations 3.120 and 3.122b.
Page 3.68:	Correction in the equation 3.123 (more scientific notation).
Page 3.69:	Correction in the equation 3.128 (more scientific notation).
Page 3.72:	Corrections for the proper use of the english language.
Page 3.76:	Correction in the equation 3.140 (more scientific notation), First setence below equation 3.140 was corrected, equation 3.122a has been extended and in Table 3.5 (last column) should read a_s x 10^{-7}.
Page 3.78:	Corrected for the reference to the heat balance in equation 3.4, updated the symbol T_p in equation 3.142a.
Page 3.79:	Corrections in the equations 3.144, 3.145a and 3.145b (more scientific notation). Updated the symbol T_p in equation 3.145a and 3.145b.
Page 3.88:	Updated $NH_{3(l)} + H_2O_{(l)} = NH_4^+{}_{(aq)} + OH^-{}_{(aq)}$.
Page 3.92:	Thermal diffusivity $a_s = 11$ x 10^{-7} m^2/s.

List of symbols Chapter 3

a	thermal diffusivity (3.6)	m^2/s
a_{gr}	thermal diffusivity gravel (3.128)	m^2/s
a_s	thermal diffusivity of subsoil (3.97)	m^2/s
a_{si}	intrinsic permeability of soil (3.21b)	m^2
a_v	thermal diffusivity of vapour (3.132)	m^2/s
a_w	thermal diffusivity of water (3.137)	m^2/s
A	total liquid pool area (3.1)	m^2
A_s	cross-sectional area river (3.154)	m^2
A_{top}	liquid top area (3.29)	m^2
Ar	Archimedes number (3.110)	-
b	half width of the river (3.146c)	m
c_*	limiting concentration (3.160)	kg/m^3
c_i	concentration component i (3.2)	kg/m^3
$c_{i,max}$	maximum concentration (3.162)	kg/m^3
C	Constant (3.64)	-
C_A	Antoine coefficient (3.85)	K
C_B	Antoine coefficient (3.85)	K
C_C	Antoine coefficient (3.85)	K
C_{DE}	constant defined by (3.156a)	$m^{1/6}$
C_{d1}	first order decay rate coefficient (3.146b)	1/s
C_f	turbulent friction coefficient (3.70)	-
C_F	frictional resistance term (3.62)	m/s^2
C_{FL}	laminar expression for C_F (3.64)	m/s^2
C_{FT}	turbulent expression for C_F (3.70)	m/s^2
C_H	correlation coefficient (3.26)	$kg/(s \cdot m^2 \cdot k)$
$C_{m\&m}$	mass transfer coefficient of MacKay & Matsugu (3.24) $(m^{0.33}/s^{0.22})$	
C_{MRF}	Manning roughness factor (3.151)	-
$C_{p,a}$	air specific heat (3.6a)	$J/(kg \cdot K)$
$C_{p,L}$	liquid specific heat (3.4)	$J/(kg \cdot K)$
$C_{p,s}$	specific heat of subsoil (3.121)	$J/(kg \cdot K)$
$C_{p,ss}$	specific heat of sand (3.20)	$J/(kg \cdot K)$
$C_{p,v}$	vapour specific heat (3.111)	$J/(kg \cdot K)$
$C_{p,w}$	specific heat of water (3.130a)	$J/(kg \cdot K)$
C_R	correction factor defined by (3.124)	-
C_s	arbitrary spreading constant (3.15)	m/s^{Es}
C_{u*}	constant defined by (3.151a)	$m^{1/6}$
D	dispersion coefficient (3.155)	m^2/s
D_a	diffusion coefficient of air (3.10e)	m^2/s
D_v	diffusion coefficient vapour in air (3.13)	m^2/s
D_x	dispersion coefficient in downstream direction (3.146a)	m^2/s
D_y	dispersion coefficient in cross-stream direction (3.146a)	m^2/s
D_z	dispersion coefficient in depth direction (3.146a)	m^2/s

E_s	arbitrary spreading exponent (3.13)	-
$erfc_*$	a modified complementary error function (3.102)	-
f	factor for the effect of radial water flow under pool (3.67)	-
f_T	function of temperature (3.135b)	-
f_0	constant (3.84b)	-
f_1	constant (3.84c)	-
f_2	constant (3.84d)	-
f_3	constant (3.84e)	-
F_1	function defined by (3.114)	-
F_2	function defined by (3.115)	-
F_N	function implicitly, defined by (3.88)	-
Fo	Fourier number (3.8c)	-
Fr	modified Froude number (3.44)	-
Fr_{rad}	Froude number for radial spread (3.74)	-
F_x	function (3.146b)	-
F_y	function (3.146c)	-
F_z	function (3.146d)	-
g	acceleration due to gravity (3.11)	m/s^2
$g_{g/gr}$	g or reduced g (3.34)	m/s^2
$G(e^x)$	Green's function (3.80) defined in (3.84a)	-
G_*	Green's function defined by (3.103) $(m \cdot s)^{-1}$	-
Ga	Galileo number (3.109)	-
h	mean liquid pool depth (3.4)	m
$h_{c, \infty}$	minimum depth spreading vaporising pool (3.11)	m
h_d	river depth (3.147a)	m
h_e	mean dynamic liquid pool depth (3.38)	m
h_f	liquid pool depth at the edge (3.42)	m
h_{gr}	height gravel layer (3.128)	m
h_p	mean puddle depth (3.38)	m
h_r	roughness scale (3.54)	m
$h_{0,max}$	= max $(h_{\sigma,f}, h_{c,\infty})$ (3.49)	m
$h_{\sigma,f}$	frontal pool depth (3.48)	m
H	heat flux (3.20)	$J/(m^2 \cdot s)$
H_a	convected heat flux from air (3.4)	$J/(m^2 \cdot s)$
H_c	heat flux by conduction from the (3.5) subsoil or convected from water body	$J/(m^2 \cdot s)$
$H_{c,n}$	heat flux in the nucleate boiling regime (3.130a)	$J/(m^2 \cdot s)$
$H_{c,m}$	heat flux in the metastable boiling regime (3.135a)	$J/(m^2 \cdot s)$
$H_{c,f}$	heat flux in the film-boiling regime (3.132)	$J/(m^2 \cdot s)$
H_{c1}	1-D approximation of H_c (3.97)	$J/(m^2 \cdot s)$
H_{c3}	3-D formulation of H_c (3.105)	$J/(m^2 \cdot s)$
H_{cr}	critical heat flux for film-boiling (3.116)	$J/(m^2 \cdot s)$
H_r	total heat flux radiated into the pool (3.96)	$J/(m^2 \cdot s)$
H_{rl}	long-wave solar radiated heat flux (3.4)	$J/(m^2 \cdot s)$
H_{rs}	solar radiated heat flux (3.4)	$J/(m^2 \cdot s)$
$H_{s/w}$	heat flux from surface beneath (3.4)	$J/(m^2 \cdot s)$
H_w	heat flux by heat transfer from water (3.9)	$J/(m^2 \cdot s)$

$j(s)$	function (3.46)	-
j_k	clay volume fraction (3.126a-c)	m^3/m^3
k_H	heat transfer coefficient (3.99)	$J/(m^2 \cdot s \cdot K)$
$k_{H,a}$	heat transfer coefficient to the atmosphere (3.10a)	$J/(m^2 \cdot s \cdot K)$
$k_{H,w}$	heat transfer coefficient on water (3.9)	$J/(m^2 \cdot s \cdot K)$
$k_{H,f}$	film-boiling heat transfer coefficient (3.112)	$J/(m^2 \cdot s \cdot K)$
k_m	mass transfer coefficient related to concentration (3.2)	m/s
$k_{m,P}$	mass transfer coefficient related to partial pressure (3.164)	s/m
K_0	hydraulic conductivity soil at saturated conditions (3.21a)	m/s
l_c	film-boiling critical length-scale (3.108)	m
l_p	length pool along-wind direction (3.23a)	m
l_σ	capillary depth parameter (par. 3.5.2.4)	m
L	characteristic length of the spill (3.168c)	m
$L_v(T)$	heat of vaporisation at temperature T (3.4)	J/kg
L_{vR}	dimensionless heat of evaporation (3.111)	-
$m_{w,ms}$	weight (mass) fraction moist in subsoil (3.124)	kg/kg
$m_{w,NH3}$	mass fraction solved ammonia in water (3.186)	kg/kg
m_m	molar fraction solved chemical in water (3.159)	mol/mol
m_{m*}	limiting molar fraction solved chemical in water (3.172)	mol/mol
$m_{m,v}$	mole fraction of vapour above liquid pool (3.80)	mol/mol
n	wind profile index (3.80) defined by (3.87)	-
N	function (3.52)	-
Nu	Nusselt number (3.10b)	-
N_{steps}	number of steps in iteration (par. 3.6.4.6)	-
P_a	atmospheric pressure (3.86)	N/m^2
P_v	vapour pressure (3.13)	N/m^2
$P_{v,i}$	partial vapour pressure chemical i (3.164)	N/m^2
$P_{v,NH3}$	partial vapour pressure ammonia (3.186)	N/m^2
$P_{v,H2O}$	partial vapour pressure water (3.186)	N/m^2
$P_v^\circ(T)$	saturated vapour pressure at temperature T (3.3)	N/m^2
Pr_a	Prandtl number of air (3.10b)	-
Pr_v	Prandtl number of vapour (3.113)	-
q_{ch}	characteristic evaporation rate (3.174)	-
q_d	mass rate of spray deposition (3.187)	kg/s
q_D	drainage rate (3.32)	kg/s
$q_{nett,air}$	mass flow rate remaining airborne (3.188a)	kg/s
q_R	dimensionless evaporation rate (3.178)	-
q_S	liquid source discharge rate (3.11)	kg/s
q_v	liquid evaporation rate (3.1)	kg/s
q''_v	(mean) vaporisation mass flux (3.1)	$kg/(m^2 \cdot s)$
Q	mass (3.31)	kg
Q_d	mass deposited spray (3.189)	kg
Q_L	mass of liquid spilt (3.1)	kg
$Q_{nett,air}$	mass remaining airborne spray (3.189)	kg

Q_v	mass of vapour evolved (3.177)	kg
Q_{ch}	characteristic vapour mass (3.177)	kg
Q_R	dimensionless mass of evolved vapour (3.177)	-
Q''_H	total amount of heat conducted into the pool (3.7a)	J/m^2
r	liquid pool radius (3.10c)	m
r_a	semi-axis of the elliptic region on the water surface (3.160)	m
r_b	semi-axis of the elliptic region on the water surface (3.161)	m
r_{body}	radius of the heat conducting body (3.8a)	m
r_d	drop radius (3.12)	m
r_{gr}	(average) radius gravel stones (3.128)	m
r_h	hydraulic radius defined by (3.148d)	m
r_i	inner radius of annular liquid pool (3.45)	m
R	gas constant (3.13)	J/(mol·K)
Re	Reynold's number $Re = \rho \times u \times (2 \times r)/\eta$ (3.10b)	-
Re_{oa}	ambient roughness Reynolds number (3.92)	-
s	depth profile shape factor (3.42)	-
Sc	Schmidt number $Sc = \upsilon/D$ (3.14a)	-
Sc_t	turbulent Schmidt number (3.80)	-
Sc_L	laminar Schmidt number $Sc_L = \upsilon_L/D_a$ (3.82)	-
Sh	Sherwood's number (3.22)	-
t	time after the start of the release (3.1)	s
t_c	time noticeable concentrations near river banks (3.152)	s
$t_{c<lim}$	time beyond which chemical concentration (3.163) everywhere is less than the limiting concentration	s
t_H	horizontal conduction time-scale (3.104)	s
t_I	validity period for dispersion model (3.153)	s
t_{sp}	arbitrary duration pool spreading (3.145)	s
t_z	time of liquid penetration (3.21a)	s
t_0	heat transfer time-scale (3.100)	s
T	liquid pool temperature (3.4)	K
T_0	initial liquid pool temperature (par. 3.6.2)	K
T_a	ambient temperature (3.10a)	K
T_A	a temperature scale constant (3.27)	K
T_b	(normal) boiling point liquid (3.20)	K
T_c	critical temperature spilt chemical (3.134)	K
$T_{gr,0}$	initial gravel temperature (3.128)	K
T_L	liquid temperature (3.130a)	K
T_s	subsoil surface temperature (3.99)	K
$T_{s,0}$	initial subsoil temperature (3.120)	K
T_{q_s}	liquid source temperature (3.77)	K
T_{ps}	liquid temperature at pool surface (3.13)	K
$T_{p,a}$	T or T_a (3.99)	K
$T_{ss,0}$	initial sand temperature (3.20)	K
T_v	vapour temperature (3.133)	K
T_w	water temperature (3.9)	K

$\Delta T_{f,min}$	minimum temperature difference film boiling (3.134)	K
$\Delta T_{n,max}$	maximum temperature difference nucleate boiling (3.131)	K
u	radial liquid velocity at liquid pool edge (3.16)	m/s
$u_{a,10}$	wind velocity at 10 metres height (par. 3.2.6)	m/s
$u_{d,\infty}$	terminal velocity of deformable drops (3.12)	m/s
u_f	jet velocity after flashing (3.188)	m/s
u_p	penetration velocity in the sand (3.20)	m/s
u_{rA}	liquid surface regression rate (3.29)	m/s
u_s	mean stream velocity (3.146b)	m/s
u_*	shear or friction velocity defined by (3.150)	m/s
u_{*p}	friction velocity above liquid pool (3.80)	m/s
u_{*a}	ambient friction velocity (3.89)	m/s
u_w	wind speed (3.10d)	m/s
$u_{w,10}$	wind speed at standard 10 metres height (3.14)	m/s
v_o	volume flow rate (3.191)	m/s
V	volume of liquid in pool (3.32)	m^3
V_d	volume of liquid discharged (3.28)	m^3
V_e	dynamic volume of liquid in liquid pool (3.39)	m^3
V_E	volume of vaporised liquid (3.29)	m^3
V_i	initial spill volume (3.169)	m^3
We	Weber number (3.12)	-
x	coordinate in wind or downstream direction (3.146b)	m
$x_{c<lim}$	distance downstream beyond which concentration everywhere is less than the limiting concentration (3.185)	m
y	coordinate cross-stream direction (3.146c)	m
y_{sp}	distance spill centre to river middle (3.146c)	m
z	coordinate in the depthwise or vertical direction (3.2)	m
z_p	depth of liquid penetration (3.21a)	m
$z_{p,H}$	heat penetration depth (3.8)	m
$z_{0,p}$	aerodynamic roughness of liquid pool (3.89)	m
$z_{0,a}$	aerodynamic roughness pool surroundings (3.90)	m
z_{10}	standard height for meteorological measurements (3.91)	m

Greek symbols

α_w	thermal expansivity of water (3.138)	1/K
$\alpha(s)$	a profile factor (3.71)	-
β	function of Sc_L and Sc_t (3.83)	-
$\beta(s)$	a profile factor (3.64)	-
β_1	intermediate (3.126a)	J/(m·s·K)
β_2	intermediate (3.126a)	J/(m·s·K)
β_3	intermediate (3.126c)	-
γ	Euler's constant (3.81a)	-

ε_p	porosity (void fraction) sand (3.20)	-
ε	$8 \times u^2/(g \times a)$ (3.55)	-
η_L	dynamic liquid viscosity (3.21b)	N·s/m^2
η_a	dynamic air viscosity (3.10d)	N·s/m^2
η_w	dynamic water viscosity (3.69)	N·s/m^2
κ	von Karman's constant (3.80)	-
λ	thermal conductivity (3.5)	J/(m·s·K)
λ_a	thermal conductivity of air (3.10c)	J/(m·s·K)
λ_{gr}	thermal conductivity of gravel (3.128)	J/(m·s·K)
λ_L	thermal conductivity of liquid (3.130)	J/(m·s·K)
λ_s	thermal conductivity of subsoil (3.97)	J/(m·s·K)
$\lambda_{s,s}$	thermal conductivity of (dry) sandy subsoil (par. 3.6.4.1)	J/(m·s·K)
λ_v	thermal conductivity of vapour (3.112)	J/(m·s·K)
λ_w	thermal conductivity of water (3.137)	J/(m·s·K)
μ_i	molecular weight of substance i (3.13)	kg/mol
μ_L	molecular weight of spilt liquid (3.159)	kg/mol
μ_w	molecular weight of water (3.159)	kg/mol
υ_a	kinematic air viscosity (3.10e)	m^2/s
υ_L	kinematic viscosity liquid chemical (3.11)	m^2/s
υ_v	kinematic vapour viscosity (3.14a)	m^2/s
υ_w	kinematic water viscosity (3.69)	m^2/s
ξ	function (3.68)	-
ρ_a	air density (3.10d)	kg/m^3
ρ_L	liquid density (3.4)	kg/m^3
ρ_s	density of subsoil (3.121)	kg/m^3
$\rho_{s,s}$	density of sand (3.20)	kg/m^3
ρ_V	vapour density (3.108)	kg/m^3
$\rho_{V,0}$	vapour density at the source (3.192)	kg/m^3
ρ_w	density of water (3.12)	kg/m^3
σ	liquid pool surface tension (3.12)	N/m
τ	dimensionless time (3.176)	-
τ_0	wall shear stress (3.150)	N/m^2
Φ_r	reduced temperature variable (3.27)	-
$\Phi(s)$	function of s (3.63)	-
Φ_T	function of temperature $T(t)$-T_a (3.98)	K
$\Phi_1(\varepsilon)$	function (3.54)	-
$\Phi_2(\varepsilon)$	function (3.58)	-
$\Phi_3(\varepsilon)$	function (3.59)	-
χ_{Sc}	argument of (3.80) defined for U_{rA} (3.81)	-
χ_{Pr}	argument of (3.118) defined for H_a (3.118a)	-

ψ	auxiliary variable (3.97)	s
ω	temperature smoothing factor (3.79)	-

Mathematical symbols

dX/dx	differential of quantity X to x
∂X/∂x	partial differential of quantity X to x
δx	small change in quantity x
Δx	change in quantity x

Note: the numbers between brackets refer to equations.

Glossary of terms

flash	Part of a superheated liquid which evaporates rapidly due to a relative rapid depressurisation until the resulting vapour/liquid-mixture has cooled below boiling point at the end pressure.
heat transfer	Transport of heat due to difference in temperature caused by (a combination of) transport mechanism(s), such as conduction, convection, and radiation.
liquid pool	Layer of liquid on a subsoil or water surface
physical effects models	Models that provide (quantitative) information about physical effects, mostly in terms of heat fluxes (thermal radiation), blast due to explosions, and environmental (atmospheric) concentrations.
pressurised liquefied gas	Gas that has been compressed to a pressure equal to saturated vapour pressure at storage temperature, so that the larger part has condensed to the liquid state.
quality	The mass fraction of vapour in a liquid vapour mixture (two-phase mixture).
rain out	Dropping of the small liquid drops from that fraction of the flashing liquid that remains initially suspended in the atmosphere.
regression rate	The rate of decrease in depth of a liquid pool
source term	Physical phenomena that take place at a release of a chemical from its containment before entering the environment of the failing containment, determining:

source term (continued):
- the amount of chemical entering the surroundings in the vicinity of the containment,
- the dimensions of the area or space in which this process takes place,
- the thermodynamic state of the released chemical, like concentration, temperature, and pressure,
- velocities of the outflowing chemical at the boundaries of the source region.

source term model | Models that provide (quantitative) information about the source term, to be input into a subsequent physical effect model.

specific volume | Volume of one kilogram of a substance (chemical); reciprocal of density.

two-phase flow | Flow of material consisting of a mixture of liquid and gas, while the gas (vapour) phase is developing due to the vaporisation of the superheated liquid during the flow caused by decreasing pressure along the hole or pipe due to the pressure drop over the resistance.

vapour | Chemical in the gaseous state which is in thermodynamic equilibrium with its own liquid under the present saturation pressure at given temperature.

void fraction | The volume fraction of vapour in a liquid-vapour mixture (two-phase mixture).

Note: some definitions have been taken from [Jones, 1992], [AIChE, 1989], Webster [1981]

Table of Contents

3   Pool evaporation

3.1   Introduction

Many hazardous chemicals are stored and transported as liquids. Gases may be liquefied by pressurisation, like Liquefied Natural Gas (LNG) and Liquefied Petroleum Gas (LPG), or by refrigeration, like ammonia (NH_3).
A release of volatile or cryogenic liquid may be hazardous to people outside the plant because the released liquid will evaporate while the evolving vapour will disperse into the atmosphere and may reach population centres. Near the source released flammable liquid may be ignited leading to a pool fire.
In case of sudden release of a pressurised liquefied gas, part of the flashing liquid may rain out and form a liquid pool on the subsoil or on water surface. Then, the evolvement of vapour will be additive to the relative large amount of vapour resulting from the fast evaporation of liquid droplets in the air caused by the flashing of the liquid. This topic is described in chapter 2 'Outflow and Spray release'.

The principal purpose of liquid pool evaporation models is to give estimates of the evaporation rate, the duration of the vapour development and the maximum amount of vapour that can evolve. The pool evaporation models will act as a source term for subsequent dispersion models or pool fire models.
Evaporation models require definition of the spill rate, pool area for spills on subsoil and also subsoil density and thermal properties, roughnesses of the subsoil, and subsoil temperature, water temperature and size and depth of the water body for spill onto water, atmospheric conditions like ambient temperature, wind speed and solar radiation. Furthermore, several physical properties of the spilt chemical like vapour pressure as function of temperature, heat capacity, heat of vaporisation, liquid density, viscosity and emissitivity are needed as input, [AIChE, 1989].

In the following sections pool evaporation phenomena will be addressed. Each section will treat the subject from another perspective.
Section 3.2 provides the principles and basic understanding of the phenomenon of pool vaporisation. It will address relevant thermodynamics and transport laws.
Section 3.3 provides an overview of methods and models published in open literature, for the estimation of the characteristics of evaporating pools.
In section 3.4 the considerations which have led to the selection of the recommended models will be elucidated.
Section 3.5 provides complete detailed descriptions of the recommended models and methods. Whenever calculations or analyses have to be made, all necessary information can be found in this chapter, except for the physical properties of the chemical.
Section 3.6 provides examples in using the selected models and methods.
In section 3.7 the interfacing to other models, i.e. the necessary transformation of the results, will be addressed.
Finally, in section 3.8 general considerations are given regarding the models presented and present gaps in the knowledge about pool evaporation.

Other evaporation phenomena that play a roll, for instance in two-phase pipe flows or in spray releases, will be treated in chapter 2 'Outflow and Spray Release'.

3.2 Phenomenon of pool evaporation

3.2.1 Introduction to section 3.2

A liquid spilt onto the subsoil or water surface will spread. Depending on the properties of the liquid and ambient conditions, the pool will evaporate rapidly or slowly.
In case the pool is confined to a bund, the surface area A of the pool is limited.
If this is not the case (transport accidents), the liquid pool will spread and the surface area of the pool A(t) will be a function of time too.
The larger the pool surface, the higher the emission rate, [Melhelm, 1993]. Once the evaporation of liquefied gases per unit of time and per unit of area has been established, then the evaporation of the spreading pool can be calculated.

The decreasing liquid mass Q_L of an evaporating pool is depending on the mean local evaporation flux q''_v and the (time-dependent) surface area A(t) of the liquid pool

$$dQ_L/dt = q_v \qquad\qquad (kg/s) \qquad (3.1)$$
$$= q''_v \times A(t)$$

The mean local vaporisation flux q''_v and the changing pool area A(t) due to spreading, can be considered almost independent, as is the common approach.
The mean local vaporisation flux q''_v is depending on the mass transfer coefficient k_m and the atmospheric concentration c_i just at the liquid pool surface

$$q''_v = k_m \times c_i \ (z = 0) \qquad\qquad (kg/(m^2 \cdot s)) \qquad (3.2)$$

The atmospheric concentration at the surface of the pool is depending on the saturated vapour pressure $P_v°(T)$ and, therefore, on the liquid pool temperature

$$c_i \ \sim \ P_v°(T) \qquad\qquad (kg/m^3) \qquad (3.3)$$

where
A(t)	=	surface area of the pool as a function of time	[m²]
c_i	=	concentration component i	[kg/m³]
k_m	=	mass transfer coefficient related to concentration	[m/s]
$P_v°(T)$	=	saturated vapour pressure at temperature T	[N/m²]
q_v	=	liquid evaporation rate	[kg/s]
q''_v	=	(mean) local vaporisation flux	[kg/(m²·s)]
Q_L	=	mass of liquid spilt	[kg]
t	=	time after the start of the release	[s]
T	=	liquid pool (surface) temperature	[K]
z	=	coordinate in vertical direction	[m]

Summarising, this means that the crucial factors determining the vaporisation rate of an evaporating liquid pool are:
1. average liquid pool temperature T, governed by the heat balance over the liquid pool;
2. liquid pool surface area A(t);
3. mass transfer coefficient k_m.

In the following sections the three crucial factors will be addressed in detail.
Subsection 3.2.2 addresses the heat balance and possible heat sources to the liquid pool. Subsection 3.2.3 addresses the spreading of liquid on subsoil, and floating on water and mixing or sinking into water.
In subsection 3.2.4 the (limiting) mass transfer to the atmosphere will be explained.

3.2.2   Heat balance

The evaporation of a liquid requires heat. Heat will be drawn from the surroundings and also from the heat content of the pool itself, tending to decrease the average liquid pool temperature. The general case which must be considered, is that of a liquid pool spreading on subsoil or on water surface, and of which the temperature is changing. We therefore need to calculate the heat flux transferred into such a pool.

For spills on subsoil the initial stage of vaporisation is usually controlled by the heat conduction from the subsoil, especially for spills of liquids with boiling points far below ambient temperature, under cryogenic conditions.
Later on, other heat sources will prevail, such as solar heat flux and heat transfer from the atmosphere.

The general formulation of laws of conservation is given by

    change content = input - output + production - consumption

So, the conservation of energy, neglecting all mechanical friction terms, applied to an evaporating pool, gives the following heat balance per unit area:

$$\frac{d(h \times \rho_L \times C_{p,L} \times T)}{dt} = H_{s/w} + H_a + H_{rl} + H_{rs} - q''_v \times L_v \quad (J/(m^2 \cdot s)) \qquad (3.4)$$

where
$C_{p,L}$	=	specific heat liquid	[J/(kg·K)]
h	=	pool depth	[m]
$H_{s/w}$	=	heat flux from surface beneath (subsoil/water)	[J/(m²·s)]
H_a	=	convected heat flux from air	[J/(m²·s)]
H_{rl}	=	long-wave solar radiated heat flux	[J/(m²·s)]
H_{rs}	=	solar radiated heat flux	[J/(m²·s)]
L_v	=	latent heat of vaporisation	[J/kg]
q''_v	=	evaporation flux	[kg/(m²·s)]
t	=	time after the start of the spill	[s]
T	=	temperature of the liquid pool	[K]
ρ_L	=	liquid density	[kg/m³]
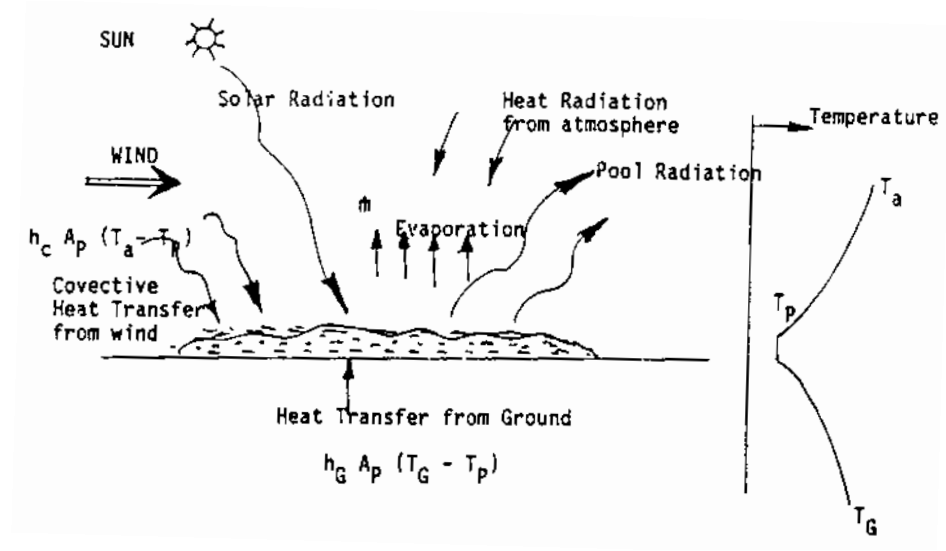
Figure 3.1   Heat transfer to a liquid pool; taken from [Raj,1987]

Heat flux from the subsoil

In case of an instantaneous spill on a solid subsoil, heat will immediately be transferred to the relatively cold evaporating pool from the relatively warm subsoil by heat conduction.
The resulting heat flow can be estimated by means of the Fourier equation based on the heat penetration theory into a semi-infinite medium (body).
The heat balance over the body has to take into account the change of temperature (heat content) of the body and the heat conduction in the body described by Fourier's law

$$H_c = -\lambda \times dT/dz \qquad\qquad (J/(m^2{\cdot}s)) \qquad (3.5)$$

H_c	=	heat flux by conduction	$[J/(m^2{\cdot}s)]$
T	=	(local) temperature	[K]
z	=	depth (coordinate)	[m]
λ	=	thermal conductivity	$[J/(m{\cdot}s{\cdot}K)]$

After some manipulations of the equations the heat balance can mathematically be expressed by

$$\frac{\partial T}{\partial t} = a \times \frac{\partial^2 T}{\partial z^2} \qquad\qquad (K/s) \qquad (3.6)$$

with

$$a = \lambda/(\rho \times C_p) \qquad\qquad (m^2/s) \qquad (3.6a)$$

where

a   = thermal diffusivity $[m^2/s]$

C_p = specific heat $[J/(kg \cdot K)]$

Assuming the following conditions:

a. the body is initially at uniform temperature T_0;
b. resulting from a sudden fixed change in temperature at the outside to temperature T_1;
c. due to the fact that the heat conducting medium is considered semi-infinite, the temperature will not change at a very long (infinite) distance from the outside;

summarised mathematically:

    a) initial condition: $T(z,t) = T_0$ for $z \geq 0$ at $t = 0$

    b) boundary condition: $T(z,t) = T_1$ at $z = 0$ for $t \geq 0$

    c) boundary condition: $T(z,t) = T_0$ at $z \rightarrow \infty$ for $t > 0$

where

T_0 = initial temperature   [K]

T_1 = new temperature   [K]

By doing this the actual dimensions of finite heat conducting bodies are neglected, which leads to the remarkably simple analytical solution given by Fourier.

Applied to the problem at hand this results in the time-dependent heat flux $H_c(t)$ from the subsoil into the evaporating pool, and is given by

$$H_c(t) = -\lambda \times dT/dt \big|_{z=0} = \frac{\lambda \times (T_0 - T_1)}{\sqrt{(a \times \pi \times t)}} \qquad (J/(m^2 \cdot s)) \qquad (3.7)$$

The total amount of heat conducted into the pool per square meter during the period until time t, is given by

$$Q''_H = 2 \times H_c(t) \times t \qquad\qquad (J/m^2) \qquad (3.7a)$$

The denominator of the quotient $\sqrt{(a \times \pi \times t)}$, with dimension length, is often called 'heat penetration depth', see Figure 3.2,

$$z_{p,H} = \sqrt{(a \times \pi \times t)} \qquad\qquad (m) \qquad (3.8)$$

This penetration depth plays a roll in case the heat source can not be regarded as semi-infinite. In general the heat penetration theory may be applied if

$$z_{p,H} = \sqrt{(a \times \pi \times t)} \ll r_{body} \qquad\qquad (m) \qquad (3.8a)$$

or

$$Fo < 0.2 \qquad\qquad (-) \qquad (3.8b)$$

with

$$Fo = a \times t/r_{body}{}^2 \qquad\qquad (-) \qquad (3.8c)$$

Fo   = Fourier number   [-]
r_{body} = radius of the heat conducting body   [m]

It must be mentioned that the time-dependent boundary condition at the subsoil surface (given by equation (3.7)) makes the heat balance over the evaporating pool a complex problem to solve.
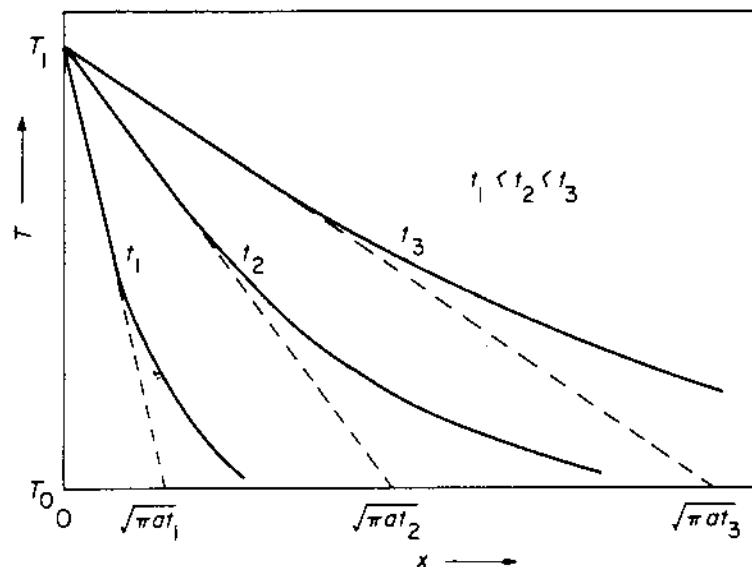
Figure 3.2   Penetration of heat into a semi-infinite medium; taken from [Beek, 1975]

The boiling-rate of spilt cryogens is mainly controlled by the rate at which heat can get into the liquid. For cryogen spilt onto land, the heat conduction from the subsoil is the prevailing heat source in the initial stages.
In experiments carried out recently by Takeno [1994], it has been reported that for spills of liquid oxygen and hydrogen, the evaporation rates were inversely proportional to the square root of time, except in the early stage just after the start of vaporisation.

It must be mentioned that the approach above is valid for flat solid surfaces. When the subsoil is permeable, for instance like (dry) sand and gravel, the heat penetration theory has to be modified.

Heat flux from the water body

In case of a cold pool floating on water, the heat transfer into the pool will depend on convection currents within the water. It can be assumed that these are sufficient to keep the water at a more or less uniform temperature T_w, and that the heat flux into the pool is

$$H_w = k_{H,w} \times (T_w - T) \qquad\qquad (J/(m^2 \cdot s)) \qquad (3.9)$$

where

H_w	=	heat flux by heat transfer from water	$[J/(m^2 \cdot s)]$
$k_{H,w}$	=	heat transfer coefficient on water	$[J/(m^2 \cdot s \cdot K)]$
T	=	liquid pool temperature	$[K]$
T_w	=	water temperature	$[K]$

For boiling on water surface three boiling regimes can be distinguished: nucleate boiling, transition boiling and film-boiling.

The vapour bubble formation at the water liquid interfacing disturbs the heat transfer. The coalescence of bubbles may form an insulation layer between liquid and water, leading to a decrease of heat transfer between water and liquid that results in a decrease of evaporation rate. This type of boiling is called metastable boiling.

The heat transfer coefficient is different for each boiling regime.

If ice formation occured, this would have a considerable effect on the heat transfer from the water body to the liquid pool.

In the past ice formation was considered possible for releases of cryogens on still water surfaces. The underlying references stem from 1975-1978. What is meant by the term 'still waters' in this model remains unclear; for instance, it is unlikely that the depth of the water body would not be relevant.

Zumsteg [1991] reports the formation of small ice particles under experimental conditions, that were dragged by the evolving vapour due to a spill of cryogen onto water. Chang [1982] also reported ice formation on the water surface in experiments on laboratory scale. A survey of experimental spills of cryogenic liquids is given in Prince [1985]; it appears that each cryogen behaves in its own typical way if spilt onto water.

However, there is experimental evidence that ice does not form at the water-cryogen interface because of vigorous boiling. Water droplets may be carried into the evolving vapour, [Melhelm, 1993].

Pool evaporation may be influenced by waves leading to a larger contact surface, and better mixing of the top layer of the water body.

Webber assumes [Webber, 1990], that an ice crust will not be formed if cryogens are spilt on water. His model is intended for analyses of spills on large extents of water and all evidence of ice formation seems to stem from small-scale experiments where a limited amount of water was available as a heat source.

Heat flux from the atmosphere

The convected heat flux from air (H_a) is given by:

$$H_a = k_{H,a} \times (T_a - T) \qquad\qquad (J/(m^2 \cdot s)) \qquad (3.10a)$$

where

$k_{H,a}$	=	heat transfer coefficient to the atmosphere	$[J/(m^2 \cdot s \cdot K)]$
T_a	=	ambient temperature	$[K]$

The heat transfer coefficient $k_{H,a}$ may be estimated by assuming a turbulent flow over a flat plate by the following equations

$$Nu = 0.037 \times Pr_a^{1/3} \times Re^{0.8} \qquad (-) \qquad (3.10b)$$

for turbulent flow $Re > 5 \times 10^5$,

with

$$Nu = k_{H,a} \times (2 \times r_p)/\lambda_a \qquad (-) \qquad (3.10c)$$

$$Re = \rho_a \times u_{w,10} \times (2 \times r_p)/\eta_a \qquad (-) \qquad (3.10d)$$

$$Pr_a = \upsilon_a/D_a \qquad (-) \qquad (3.10e)$$

$$\approx 0.786$$

where
r_p	=	pool radius	[m]
Nu	=	Nusselt's number	[-]
Pr_a	=	Prandtl's number for air	[-]
Re	=	Reynolds' number	[-]
$u_{w,10}$	=	wind speed at 10 metres height	[m/s]
η_a	=	dynamic viscosity air	[N·s/m^2]
λ_a	=	thermal conductivity of air	[J/(K·m·s)]
ρ_a	=	density air	[kg/m^3]
υ_a	=	kinematic viscosity of air	[m^2/s]
D_a	=	diffusion coefficient of air	[m^2/s]

Heat flux from radiation

The rate of long-wave radiation heat exchange (H_{rl}) between the pool surface and the surroundings and the solar radiation (H_{rs}) can be calculated by equations (4.36) and (4.37) of the chapter Vapour cloud dispersion (page 4.62).

Heat transfer in the bulk of the pool

Studer [1988] states that a rigorous way to describe the evaporation of a liquid pool requires an incorporation of all heat and mass transfer components, without ignoring the impact of the intra-pool heat transfer resistance. This latter assumption is considered to be a conservative one, and often made implicitly by assuming a uniform liquid pool temperature.
A deep pool, resulting from a major chemical release, behaves as if it consisted of two separate elements: a thin surface layer and the bulk liquid pool.
Studer shows the effect of intra-pool heat transfer resistance can be ignored in case the initial height of the instantaneous pool is about 4 metres.
It may be expected, however, that the bulk heat transfer resistance will have a substantial effect on spills in bunds with huge barriers, but not in case of unbounded spreading while the liquid height quickly diminishes in time.

3.2.3   Pool spreading

Released liquid will spread onto the subsoil or the water surface in the immediate vicinity of the failing containment.

The spreading will continue unless the pool is contained by a dike or channelled into a sump, or when the liquid has spread to such an extent that its thickness is of the same magnitude as the subsoil roughness, or until the evaporation rate is equal to the release rate so that the amount of liquid in the pool does not increase any more.

The maximum pool diameter of a spreading liquid pool will depend on the topography of the subsoil near the release point. In industrial plants often vessels have been placed in bunds (low walls or dikes). In case the pool is confined to a bund the surface area of the pool is limited. If not, the liquid pool will spread and the surface area of the pool will be a function of time during a large part of the evaporation.

On subsoil most liquid spills at industrial plants will be confined, however not in the case of transportation. Spills onto water will be unbounded, although the width of the water body (channels) may act as a barrier. In practice, very often no barrier is provided around storage tanks for gases liquefied by compression. This means that for the determination of the evaporation of released condensed gases, the spreading of the liquid must be considered. The extent of spreading of an unconfined liquid spill is a key factor that effects the emission rate from the pool surface.

As the liquid spreads, three flow regimes are recognised [Melhelm, 1993]:

1. gravity - inertia regime: gravitational acceleration of the descending liquid mass is counter-balanced by inertia,
2. gravity - viscous regime: in which the gravitational spreading force is opposed by friction at the liquid-subsoil interface,
3. surface tension - viscous regime: in which for very thin liquid films, surface tension replaces gravity as the driving force.

Cryogenic spills rarely reach the gravity-inertia regime because of their rapid evaporation. The surface tension – viscous regime is of importance for heavy hydrocarbons on water.

For the calculation of the evaporation of liquefied gases on subsoil, a distinction should be made between a permeable and a non-permeable subsoil, as the spilt liquid may sink into the ground.

3.2.3.1   Release on land within bunds

The presence of second containments (bunds) reduces the evaporation rate by limiting the pool area, and providing for longer contact times between liquid and subsoil, leading to reduction of heat conduction from the subsoil to the evaporating liquid [World Bank, 1988].

In case the liquid is caught in a bund, the spreading of the spill will be limited. The maximum pool size will be the size of the bund. Of course, this will only be the case when the dimensions of the bund are well designed. If the bund is too small, the released liquid will simply spill over the dike. Furthermore, bund overtopping due to dynamic force may be the cause for secondary containments not to be able to cope with a sudden release of large amounts of liquid [Wilkinson, 1991].

Also in Phelps [1992] a model based on computational fluid dynamics has been presented that is able to predict the behaviour of a running liquid against vertical or inclined walls.

3.2.3.2 Continuous release on land without a bund

The pool will stop spreading when the release of liquid has stopped due to a cut-off or exhaustion. Also when the evaporation rate of the pool equals the release rate on the subsoil the pool will reach its maximum diameter.
In case of a continuous release of liquid, the liquid pool will eventually reach a specific depth, where evaporation through the surface balances the steady discharge into the centre of the pool.

A simple model of viscous effects appears reasonably realistic [Webber, Apr. 1991] and leads to depth of order

$$ h_{c,\infty} = \left(\frac{6 \times \upsilon_L \times q_S}{(\rho_L \times \pi \times g)} \right)^{0.25} \qquad \text{(m)} \qquad (3.11) $$

where

g	=	acceleration due to gravity	$[m/s^2]$
$h_{c,\infty}$	=	minimum depth spreading and vaporising liquid pool under a steady discharge	[m]
q_S	=	liquid source discharge rate	[kg/s]
υ_L	=	kinematic liquid viscosity	$[m^2/s]$
ρ_L	=	liquid density	$[kg/m^3]$

Experimentally, Moorhouse and Carpenter [Webber, Apr. 1991] have studied continuous releases of LNG on smooth concrete, and concluded a spreading depth of around 1 centimetre.

3.2.3.3 Instantaneous release on land without a bund

In practical situations the pool will spread until it reaches some minimum thickness which is related to the surface roughness. As typical values a lower limit of 5 millimetres for very smooth surfaces and for rough surfaces several centimetres were suggested earlier, see table 3.1.
Another suggestion is simply to assume a maximum pool area based on the topography of the surroundings, according to the analyst's judgement.

Table 3.1   Characteristic average roughnesses of some subsoils

Subsoil	Average roughness (m)
Flat sandy soil, concrete, stones, industrial site	0.005
Normal sandy soil, gravel, railroad yard	0.010
Rough sandy soil, farmland, grassland	0.020
Very rough, grown over sandy soil with pot-holes	0.025

The pool area can be estimated conservatively by assuming that all of the released liquid spreads instantaneously to the minimum thickness, and reaches its maximum pool size immediately.
This simplifying assumption leads to overpredictions for the vaporisation rate shortly after the spill. This can be neglected for non-boiling volatile liquids because of the relatively long duration of the evaporation at low evaporation flux q''_v.

Low volatile liquid releases at ambient conditions evaporate at considerable rates only when the pool surface is relatively large, compensating for a relatively low vaporisation mass flux. This may be the case when large amounts of liquid run into a large bund or can spread out to a large extent.

3.2.3.4   Evaporation of chemicals mixed in water [Raj, 1974]

When a soluble chemical water is spilt on water, it rapidly dissolves. Chemicals may not only be readily miscible with water, but may also have high vapour pressures at ambient temperature. When such liquids are spilt, vapour may be generated. When a water-miscible liquid is spilt on a water surface, mixing takes place, thereby diluting the spilt liquid.
The mixing is caused by molecular diffusion in calm water and mass convection (turbulent diffusion) in streaming rivers. In rivers, the main cause for mixing is stream turbulence. Mixing may take place preferentially in one direction. It depends on flow conditions, flow geometry and water density gradients.
In rivers, waves are not important. In general the effects of salinity-driven mixing can be ignored.

3.2.3.5   Evaporation of chemicals that sink in water [Raj, 1974]

There are many liquid chemicals with densities larger than that of water, whose boiling point at atmospheric pressures are less than the water temperature, for instance, chlorine. When such liquids are spilt on water, they may sink and vaporise at the same time because of their low-boiling point.
When a large mass ('blob') of a heavy liquid is spilt on the surface of water in a very short time, the liquid sinks 'en masse' only for a small depth. The increasing sinking velocity of the blob results in a pressure force on the front face. When this pressure force exceeds the internal resistance of the blob, the blob will be broken into small-

sized drops. Due to the break-up of the large blob of heavy liquid into smaller drops, the liquid will evaporate rapidly due to massive heat transfer from the surrounding water.
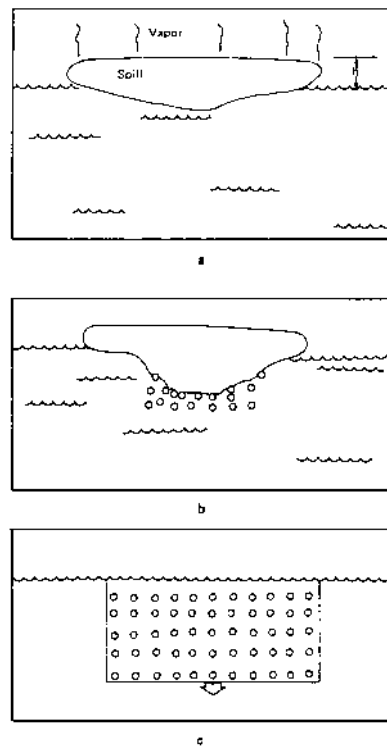
*Figure 3.3   Schematic illustration of the sequence
                of blob break-up into drops [Raj, 1974]*

The parameter which determines the stability of a blob or a drop, or resistance to breaking, is the Weber number, being the ratio of the pressure force to the surface tension force:

$$We = \rho_w \times u_{d,\infty}^2 \times r_d/\sigma \qquad\qquad (-) \qquad\qquad (3.12)$$

We	=	Weber number	[-]
ρ_w	=	density water	[kg/m^3]
$u_{d,\infty}$	=	terminal velocity of deformable drops	[m/s]
r_d	=	drop radius	[m]
σ	=	liquid surface tension	[N/m]

Experimental evidence indicates that most liquids tend to break-up when the Weber number is larger than about 10. It can be shown that the duration over which a large mass, such as occurs in a spill, breaks up into smaller drops, is very short. Experiments indicate that, when a big blob breaks up, drops of various sizes are formed with the drop-size distribution being a function of various physical properties, parameters such as the properties of the liquid and the medium, the agency which causes the break-up, and others.

3.2.4   Mass transfer

For liquids having normal boiling points near or above ambient temperature, mass transfer by diffusion will be the limiting factor. The wind is removing vapour from the pool surface, and due to the resulting concentration gradient mass transfer is induced; liquid will evaporate in order to restore the partial pressure which is in thermodynamic equilibrium to the liquid in the pool at its temperature.
So, the evaporation of a non-boiling liquid depends mainly on the rate at which the vapour can be removed by the air flow above the pool.
In case of boiling liquids with a mass transfer that is very fast, the mass transfer resistance may be neglected as a reasonable first approximation.

When a volatile (non-boiling) soluble liquid is spilt into water, the vaporisation of the chemical takes place only at the water surface, and is caused by the difference in (partial) vapour pressure of the solved chemical at the water surface and in the atmosphere. The evaporation mass flux q''_v depends on the mass transfer coefficient (k_m) and the vapour concentration (c_i) at the liquid pool surface. The vapour concentration is proportional with the saturated vapour pressure of the liquid at the pool surface, depending on its temperature. Applying the ideal gas law results to

$$q''_v = D_v \times dc_i/dz$$

$$= k_m \times c_i(z = 0)$$

$$\approx k_m \times P_v(T_{ps}) \times \mu_i/(R \times T_{ps}) \qquad (kg/(m^2 \cdot s)) \qquad (3.13)$$

where
c_i	=	concentration component i	[kg/m³]
D_v	=	diffusion coefficient vapour in air	[m²/s]
k_m	=	mass transfer coefficient related to concentration	[m/s]
q''_v	=	vaporisation mass flux	[kg/(m²·s)]
$P_v(T)$	=	vapour pressure at temperature T	[N/m²]
R	=	international gas constant	[J/(mol·K)]
T_{ps}	=	liquid temperature at pool surface	[K]
z	=	coordinate in vertical direction	[m]
μ_i	=	molecular weight of substance i	[kg/mol]

Several empirical correlations for estimation of the mass transfer coefficient have been proposed in literature in the following generalised form

$$k_m = f\ (u_{w,10}, r_p, Sc) \qquad (m/s) \qquad (3.14)$$

with

$$Sc = \upsilon_V/D_v \qquad (-) \qquad (3.14a)$$

where
r_p	=	liquid pool radius	[m]
Sc	=	Schmidt number	[-]
D_v	=	diffusion coefficient of vapour into air	[m²/s]

υ_V = kinematic viscosity vapour $\qquad$ [m^2/s]
$u_{w,10}$ = wind speed at standard 10 metres height $\quad$ [m/s]

A model for the mass transfer coefficient k_m based on a more up-to-date understanding of the turbulent atmospheric flow has been developed by [Brighton, 1987]. In this model molecular diffusion is incorporated in the boundary conditions.

Experimental data about mass transfer from evaporating liquid pools as reported in Kawamura and MacKay [1987] are given below. Note that the wind velocity was not made explicit in this publication.
Note that the dimensions of the air temperature and vaporisation mass flux are degrees Celsius ˚C and kg/(m^2·h) respectively.

Table 3.2 $\quad$ *Steady state evaporation rate of liquid pools (after 15 minutes),*
$\qquad\qquad$ <u>*without*</u> *subsoil conduction (insulated pan)*

Chemical		T_{air} (˚C)	q''_v (kg/(m^2·h))
1	Toluene	21	4.49
2	Toluene	29	3.39
3	Cyclohexane	24	5.89
4	Cyclohexane	25	5.89
5	Hexane	-5	5.55
6	Hexane	22	10.88
7	Methanol	7	2.55
8	Dichloromethane	-6	9.49
9	Dichloromethane	1	7.53
10	Dichloromethane	21	16.27
11	Dichloromethane	25	17.98
12	Pentane	1	10.52
13	Pentane	5	6.84
14	Pentane	7	8.13
15	Pentane	9	10.41
16	Freon11	0	33.01
17	Freon11	17	34.93

Table 3.3   *Average evaporation rate of liquid pools during the experiment,*
              <u>*with*</u> *subsoil conduction.*

Chemical		T_{air} (˚C)	q''_v (kg/m²·h)
18	Toluene	25	3.90
19	Cyclohexane	29	9.38
20	Hexane	27	7.28
21	Pentane	23	23.00
22	Pentane	25	27.10
23	Freon11	31	34.88

Note that in conformity with the original publication the vaporisation mass flux has been given in kilogram per square metre per hour, and the temperature in degrees Celsius.

3.3   General overview of existing models

3.3.1   Introduction to section 3.3

The various models for pool evaporation on subsoil or water surface presented in the open literature have a broadly similar structure [Webber, 1991].
All models comprise a heat balance, pool spreading models, and correlations for the local vaporisation flux.
The models differ in:
− the number of heat sources taken into account;
− the collection of selected submodels for spreading and mass transfer;
− the way of approximation by analytical solutions (partially);
− the degree of complexity due to ignoring effects;
− the applied numerical methods to solve the set of equations.
Most models have been based on the same limited number of publications dealing with mass transfer to the atmosphere and pool spreading.

In general the classic models are based on the sharp distinction between boiling and non-boiling liquids, on a non-adequate representation of the expected behaviour of pools of different viscosity on different surfaces [Webber, 1991], and sometimes still on the rather antique mass transfer relation of Sutton. Furthermore, simplifying assumptions were made to describe the spreading of the pool.
These models can be improved from a scientific viewpoint and from the viewpoint of an adequate numerical solution. Advanced and complete but complex models have been found in recent literature. The pool evaporation model GASP has been developed by SRD(AEA)/HSE. Similar models have been found in literature.

In the following section, submodels will be addressed first, dealing separately with the heat balance, mass transfer, or pool spreading.
In this section the following themes are addressed:
− subsection 3.3.2 addresses the submodelling of the heat balance;
− subsection 3.3.3 addresses the submodelling of pool spreading;
− subsection 3.3.4 addresses the submodelling of mass transfer;
− subsection 3.3.5 addresses recent models, which solve the problem integrally.

3.3.2   Heat balance

Simple modelling is based on a sharp distinction between boiling and non-boiling liquids. A sudden switch between models have to be made when describing the transition from boiling to non-boiling. This results in a rather unpleasant discontinuity in the evaporation rate at an arbitrary vapour pressure.
In the modelling of evaporation of boiling liquids, only the heat conduction from the subsoil or from the water surface has been taken into account.

In recent models [Webber, 1990], [Woodward, 1990], [SuperChems 4.0] the complete heat balance is taken into account and thus none of the heat sources are ignored to simplify the model; see paragraph 3.2.2. No principal distinction is made between boiling and non-boiling pools.

3.3.2.1 Film and nucleate boiling on water surfaces

In the previous YellowBook a method has been described to estimate the boiling rate of a cryogen on a water surface, which has been recognised as meta-stable boiling for most industrial commodities [YellowBook, 1988].

In the GASP-model a more simplified approach has been chosen. It is assumed that the spilt chemical boils in the film-boiling regime when the heat flux into the liquid pool exceeds the so-called critical heat flux. If not, the heat flux into the pool is described with a constant heat transfer coefficient.

3.3.3 Pool spreading

3.3.3.1 Pool spreading on land

Simple models for pool spreading on solid surface

Simple spreading models consist of simple mathematical expressions, mostly power expressions, that relate the radius of the spreading liquid pool to the time from the start of the release

$$r(t) = C_s \times t^{Es} \qquad\qquad\qquad (m) \qquad\qquad (3.15)$$

r   = radius of the spreading liquid pool   [m]
t   = time from of the release   [s]

The values for constant C_s and exponent E_s differ for liquids spreading on land and for liquids spreading on water. The constant C_s and exponent E_s depend on the type of release: continuous or instantaneous.
An overview of these simple models can be found in Raj [1981], Raj [1987]. Other models have been given in Shaw [1978], WorldBank [1988], Melhelm [1993] and Frie [1992].
Most remarkable is that the model equations of the three groups differ, regarding which seem qualitatively the same spreading conditions.

Obviously, this varied collection of relations leads to the conclusion that correlations have been made for different situations or have been based on different assumptions. Many previous analyses based on ordinary differential equations, have used the simple assumption that the radial spreading rate (u) of a circular liquid pool is proportional to $\sqrt{(g \cdot h)}$, where (g) is the acceleration due to gravity and (h) is the mean pool depth. For pools spreading on water, this is valid for a restricted time interval after any initial radial acceleration phase and before the pool becomes thin enough for turbulent or viscous effects to become important. In this case (g) must be multiplied by the relative density difference. In other circumstances the spreading behaviour is quite different and generally more complicated [Webber, Jan. 1991].

The sharp distinctions between instantaneous and continuous releases, and between spreading liquid pools and fixed (confined) pools, are made to simplify the spreading model. These rather academic idealisations always shift the problem to the application of the model in practical situations. Consequently, often these ideal assumptions will not hold.

Shallow layer equations governing pool spreading on land

It should be noted that the sharp distinction between continuous and instantaneous releases, which is basically made in the simple spreading models, puts forward the question what to choose in case of semi-continuous or time-dependent releases that appear in reality. In the following a more general approach is made in order to cover the whole range of different spreading regimes for different types of liquid releases.

If the horizontal dimension of the pool is much larger than its depth, the usual fluid equations may be reduced to the approximate form, the so-called 'shallow layer equations', [Webber, 1986]. In case of axial symmetry and instantaneous release, ignoring the vaporisation, the horizontal momentum equation may be expressed as

$$\partial u/\partial t + u \times \partial u/\partial r = -g \times \partial h/\partial r \qquad (m/s^2) \qquad (3.16)$$

and secondly, the conservation of mass:

$$\partial h/\partial t + u \times \partial h/\partial r + h/r \times \partial(r \times u)/\partial r = 0 \qquad (m/s) \qquad (3.17)$$

where
u	=	radial velocity	[m/s]
r	=	radius of the spreading liquid pool	[m]
h	=	liquid pool height	[m]
g	=	gravitational acceleration	[m/s²]

Instead of the gravitational acceleration on subsoil, the reduced acceleration due to gravity will be needed for pools spreading on water.
The process of pool spreading is controlled by the gravitational acceleration of the descending liquid mass and the surface tension, versus the inertia of the liquid mass and the friction due to liquid viscosity.

The solutions that can be derived for the shallow layer equations will not be in the form of one simple power relation for the growth of the pool radius versus time: $r(t) \approx t^n$. However, the solution may be somewhat artificially split up into regimes. These regimes could be approximated by power relations $r(t) \approx t^n$, although these are merely a tangent to the curve, [Webber and Brighton, 1987].
For pools spreading on subsoil, the following approximating power relations could be distinguished:

1a. inviscid or gravity-inertia regime: $r(t) \approx \sqrt{(C_0 + C_1 \times t^2)}$ (m)   (3.18a)

1b. gravity-turbulent regime: $r(t) \approx C_2 \times t^{2/7}$ (m)   (3.18b)

2. gravity-viscous regime: $r(t) \approx C_3 \times t^{1/8}$ (m)   (3.18c)
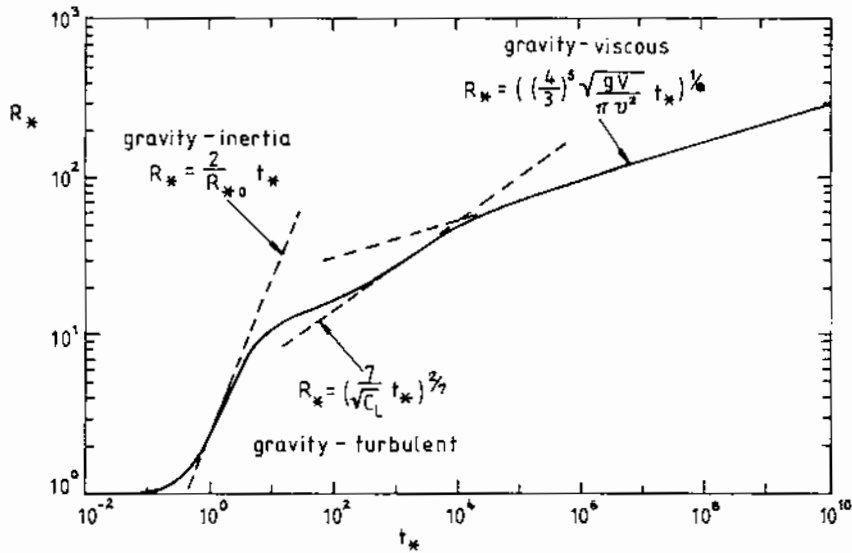
Figure 3.4   A non-volatile pool spreading on subsoil; [Webber and Brighton 1987]

For spills onto water the density difference between water and the floating liquid should be taken into account, and, furthermore, the motion of the water beneath the pool [Webber and Brighton, 1987]:

1a. inviscid or gravity-inertia regime: $r(t) \approx C_4 \times t^{1/2}$ (m)   (3.19a)

1b. gravity-turbulent regime: $r(t) \approx C_2 \times t^{2/7}$ (m)   (3.19b)

2.   gravity-viscous regime: $r(t) \approx C_5 \times t^{1/4}$ (m)   (3.19c)

Obviously one simple power relation between pool radius versus time can not describe the spreading of a pool on a flat surface for all regimes. This may explain why so many spreading relations have been found in literature.

Evaporation of cryogen (boiling liquid) on a permeable subsoil

A spilt cryogen may soak into permeable subsoil. Freezing of water in the soil column may prevent the liquid from penetration into the subsoil.
Obviously, the effect of percolation into the subsoil is more important for small spills than large spills where the liquid pool may be substantially thicker than the penetration depth into the subsoil.

Models for evaporation of cryogens have been given earlier for dry and moist porous subsoil and gravel layers [YellowBook, 1988]. These models are all based on the time-dependent heat penetration theory as has been explained in paragraph 3.2.2.

In Takeno [1994], laboratory experiments have been reported in which cryogenic spills of oxygen on a dry sand layer, liquid oxygen was observed to vaporise while

constantly soaking into and rolling up the upper section of the layer. The leading edge of the rolled-up sand layer was observed to move downwards into the sand layer.

The evaporation rate was determined simply by the velocity of liquid penetration into the dry sand layer, which was nearly independent of the liquid depth. This indicates that the evaporation rate is independent of time and that its rate can be determined by the liquid penetration velocity alone, by

$$H = \rho_{ss} \times C_{p,ss} \times (T_{ss,0} - T_b) \times (1 - \varepsilon_p) \times u_p \qquad (J/(m^2 \cdot s)) \qquad (3.20)$$

H	=	heat flux	$[J/(m^2 \cdot s)]$
ρ_{ss}	=	density of sand	$[kg/m^3]$
$C_{p,ss}$	=	specific heat of sand	$[J/(kg \cdot K)]$
$T_{ss,0}$	=	initial sand temperature	$[K]$
T_b	=	boiling point liquid	$[K]$
ε_p	=	porosity (void fraction) sand	$[-]$
u_p	=	penetration velocity in the sand	$[m/s]$

In the experiments the liquid penetration velocity was merely constant at about 0.0014 m/s, regardless of the liquid depth.
Unfortunately, Takeno [1994] does not supply a model for the calculation of the penetration velocity in the sand u_p, and an additional submodel have to be taken from elsewhere.

The penetration of fluids into soil is a complex phenomen which depends on the type, geometry and resistance properties of the soil, the penetrating material properties and ambient conditions [Melhelm, 1992].
The penetrating fluids into soil is governed by gravitational and capillary forces. In case of low-boiling fluids and cryogens the evolving vapour will cause an opposite vapour flow against the soaking liquid. Apparently the upward force due to the out-blowing vapour due to vaporisation by extracting heat from the sand grains, is in equilibrium with gravitation. When the heat content of the sand at a certain height is exhausted, the liquid will sink deeper into the subsoil.
A rather simplified model presented in Melhelm [1992] assumes liquid penetration to behave as saturated piston flow, influenced by gravitational forces only. So, in this approach all effects of capillary forces, vaporisation of liquid, freezing of the moisture in the subsoil, lateral spreading and heat conduction, have been neglected. In Melhelm [1992] the penetration depth of liquid soaking into porous subsoil is given by

$$z_p = K_0 \times t_z \qquad (m) \qquad (3.21a)$$

$$K_0 = \rho_L \times g \times a_{si}/\eta_L(T_b) \qquad (m/s) \qquad (3.21b)$$

So, that

$$u_p \approx K_0 \qquad\qquad\qquad (m/s) \qquad (3.21c)$$

where

a_{si}	=	intrinsic permeability of the soil	$[m^2]$
g	=	gravitational acceleration	$[m/s^2]$
K_0	=	hydraulic conductivity of the soil at saturated conditions	$[m/s]$
t_z	=	time of penetration	$[s]$
$\rho_L(T_b)$	=	liquid density at boiling point	$[kg/m^3]$
z_p	=	depth of liquid penetration	$[m]$
$\eta_L(T_b)$	=	dynamic viscosity liquid at boiling point	$[N \cdot s/m^2]$

Some values for the intrinsic permeability have been given in Melhelm [1992].

Table 3.4   Intrinsic permeability for some subsoil types

Subsoil type	$a_{si}(m^2)$
coarse sand	10^{-9}
silty sand	10^{-12}
clay till	10^{-15}

The remarkably different outcome of both models in Yellow Book [1988] and Takeno [1994] concerning the time-dependency of the evaporation rate, might be due to a difference in ratio between the initial liquid height and the height of the sand layer.

3.3.3.2   Releases of non-floating chemicals on water

Mixers

HACS-R is an evaporation model for volatile water-soluble chemicals into water, like methanol. It has been developed for U.S. Coast Guard by Raj and is described in a NTIS-report [Raj, 1974]. Dodge reported good model performance in 1982.
It is assumed that the entire liquid spilt goes into solution in water first. After estimating the liquid concentration in the water, the vapour pressure on the water surface of the chemical can be estimated, as well as the vaporisation rate.
The model HACS-R has recently been applied with some modifications [Dharmavaram, 1994].

Sinkers

In a NTIS-report [Raj, 1974] a model has been given describing the evaporation phenomena for liquids heavier than water with boiling temperatures less than ambient.

An evaporative model has been worked out based on the assumption of drop formation when a blob of heavy, low-boiling-point liquid is spilt on a water surface. It has been assumed that the initial blob of liquid breaks up into uniform and equally-sized drops because of pressure forces and instability of the blob.

The details of drag on a deformable drop have been included in the analysis to calculate the terminal velocity of drops. A heat-mass similarity model is used to predict the vaporisation rate. In this model it is assumed that the liquid is immiscible with water.

3.3.4   Mass transfer

The wind is removing vapour from the pool surface, and due to the resulting concentration gradient, mass transfer is induced; liquid will evaporate in order to restore the partial pressure which is in thermodynamic equilibrium to the liquid in the pool at its temperature. Thus, the evaporation of a non-boiling liquid depends mainly on the rate at which the vapour can be removed by the air flow above the pool.

The evaporation mass flux q''_v depends on the mass transfer coefficient (k_m) and the vapour concentration c_i at the liquid pool surface

$$q''_v = k_m \times c_i(z = 0) \qquad\qquad (kg/(m^2{\cdot}s)) \qquad (3.2)$$

where

c_i	=	concentration component i	$[kg/m^3]$
k_m	=	mass transfer coefficient	$[m/s]$
q''_v	=	vaporisation mass flux	$[kg/(m^2{\cdot}s)]$
z	=	coordinate in vertical direction	$[m]$

The dimensionless correlation of Raj & Morris for the mass transfer coefficient k_m, is based on the heat-mass analogy [Raj, 1987], [Studer, 1988]

$$Sh = 0.037 \times (Re^{0.8} - 15500) \times Sc^{1/3} \qquad\qquad (-) \qquad (3.22)$$

with

$$Sh = k_m \times l_p/D_v \qquad\qquad (-) \qquad (3.23a)$$

and

$$Re = \rho_a \times u_{w,10} \times (2 \times r_p)/\eta_a \hspace{3cm} (-) \hspace{2cm} (3.23b)$$

where

Re	=	Reynold's number	[-]
ρ_a	=	density air	[kg/m^3]
$u_{w,10}$	=	wind speed at standard 10 metres height	[m/s]
η_a	=	dynamic viscosity air	[N·s/m^2]
Sh	=	Sherwood's number	[-]
k_m	=	mass transfer coefficient	[m/s]
l_p	=	length pool along-wind direction	[m]
D_v	=	diffusion coefficient vapour in air	[m^2/s]

Note that Sherwood's number Sh for mass transfer is on the analogy of the Nusselt's number Nu for heat transfer.

In the past the correlation of Sutton has been given for the mass transfer coefficient k_m. This relation works well for laboratory experiments but the peculiar dimensionality of the result makes extrapolation suspect [Webber, 1987].

A similar model has been given by MacKay & Matsugu [Kawamura, 1987] which has been validated against a number of experiments

$$k_m = C_{m\&m} \times u_{w,10}{}^{0.78} \times (2 \times r_p)^{-0.11} \times Sc^{-0.67} \hspace{2cm} (m/s) \hspace{1.5cm} (3.24)$$

with

$$Sc = \upsilon_V/D_a \hspace{4cm} (-) \hspace{2cm} (3.25)$$

where

$C_{m\&m}$	=	0.004786	[m$^{0.33}$/s$^{0.22}$]
D_a	=	diffusion coefficient vapour in air	[m^2/s]
k_m	=	mass transfer coefficient	[m/s]
r_p	=	radius of the liquid pool	[m]
$u_{w,10}$	=	wind speed at standard 10 metres height	[m/s]
Sc	=	Schmidt number	[-]
υ_V	=	kinematic viscosity vapour	[m^2/s]

Note that in general for gases and vapours, $Sc \approx 0.8$. The original relation of MacKay & Matsugu was expressed in other dimensions.
The correlations by Sutton, Raj and Kawamura have the Schmidt number in common. In Brighton [1990] it is stated that the exponent is under dispute and is no sound basis for up-scaling the results derived from laboratory experiments only.
The alternative model of Brighton is based on scientific knowledge about atmospheric turbulence [Brighton, 1987]. In this model molecular diffusion is incorporated in the boundary conditions. The model is valid for neutral atmospheric stability. Brighton's theory can be matched with experiments although deviation between predictions and experimental results is large.

3.3.5 Advanced integral models

3.3.5.1 GASP

Quite recently, SRD/HSE developed the model GASP. GASP is an acronym for 'Gas Accumulation over Spreading Pools' [Webber, 1990]. GASP is an evaporation model that has incorporated all of the heat and mass transfer components. GASP solves the set of equations based on a complete heat balance and the shallow water equations (3.16) and (3.17) governing the pool spreading both on subsoil or water surface simultaneously. The mass transfer model is based on the work of Brighton [Brighton, 1987]. The model forces the transition of boiling to non-boiling to be smooth.

The model is able to give correct predictions [Webber, 1990]. The GASP model is only able to cope with (spreading) pools on a subsoil and onto water surface. It is not able to deal with volatile soluble liquids into water, and boiling liquids heavier than water that will sink. The GASP model, and the research and data which it is based upon, have been extensively given attention by several SRD/HSE-publications.
The numerical procedure to solve the equations seems to be robust and does not take too much time on a 486-PC. The computerised model is commercially available.

3.3.5.2 LPOOL

In Woodward [1990] the model LPOOL is given. The model has been developed by Technica Inc. The model is a complete pool evaporation model.

The model makes use of a grid of annular rings to solve the two-dimensional shallow layer equations for radial flow over flat terrain (3.16) and (3.17). It relies on the mass transfer coefficient of MacKay and Matsugu, [Kawamura and MacKay, 1987]. The heat transfer coefficient on water has been correlated to the heat of evaporation (no references)

$$k_{H,w} = C_H \times L_v \hspace{3cm} (J/(m^2 \cdot K \cdot s)) \hspace{1cm} (3.26)$$

with

$$C_H = 0.001$$

where
$k_{H,w}$ = heat transfer coefficient [$J/(m^2 \cdot K \cdot s)$]
L_v = heat of evaporation [J/kg]
C_H = correlation coefficient [$kg/(s \cdot m^2 \cdot K)$]

Also numerical methods have been briefly addressed regarding how to solve the set of equations. The solutions of the set formed by the continuity equation (mass balance) and (momentum balance) and submodels are found by using a Crowley second-order finite difference solution, superimposing the homogeneous and forced solution.

The spreading model has been validated against small-scale, low-release-rate experiments of Belore and McBean who tested pool spread rates with water, and data for crude oil spilt onto frozen arctic ground.

The model has been computerised and is commercially available, though part of a much larger software package [Technica, 1994].

3.3.5.3   SuperChems

The large software package SuperChems of A.D. Little comprises a pool evaporation model that is based on a time-dependent solution of the 'shallow water equations' [Superchems 4.0]. It calculates the liquid regression rate for a spreading pool on different soil types and water. Solubility of the chemical spilt in water is incorporated. The complete heat balance accounts for all possible heat sources. The different spreading regimes are also accounted for. The model accepts time-dependent release rates. The model is commercially available.

3.4 Selection of models

3.4.1 Introduction to section 3.4

In section 3.4 the considerations which have led to the selection of the models that are included in section 3.5, will be explained. In section 3.5 these models will be described in detail.

In general the selection is based on the following considerations:

1. The availability of powerful (personal) computers creates the opportunity to avoid simplified (analytical) solutions, that are only able to cope with idealised situations.
2. Models based on computational fluid dynamics (CFD) can not be used in safety studies and hazard assessment, due to the time-consuming data collection in order to supply the required input and analysis of the results, and due to the large computer power they require.
3. Models should have been validated against unambiguous experimental data.
4. Increased complexity of the model must result in more reliable predictions; unnecessary complications should be avoided.
5. The model should be available in literature; and preferably available in computerised form at minimum cost

3.4.2 Pool evaporation on subsoil and on water surface

In addition the selection of liquid pool evaporation models has been based on the following considerations:

1. The heat balance should take into account all heat source terms;
2. The artificial distinction between boiling and non-boiling liquids should be avoided;
3. The spreading of the liquids should be described by solutions of the shallow layer equations, giving a general solution;
4. The mass transfer should be modelled by a widely applicable model based on experimental data.

Advanced and complete models have been found in recent literature.
The pool evaporation model GASP has been developed by SRD(AEA)/HSE.
Similar models have been found in literature: LPOOL [Woodward, 1990],
SuperChems of A.D. Little [Superchems 4.0].
The recent integral models are really a step forward in supplying a realistic description of the pool evaporation. A major drawback is the relatively high cost of computerised versions commercially available.
Based on the accessibility of the model description in literature, and availability of the computer program, it was preferred to describe the GASP model in more detail in the following section.
The mass transfer model developed by Brighton [Brighton, 1987] is under development and has limited applicability. For practical situations it would be advisable to use the correlation of MacKay and Matsuga, [Kawamura and MacKay, 1987], because it is based on experiments carried out in the open. However, the GASP model uses Brighton's model. For reasons of consistency, the description of the GASP model follows the original publications.

The GASP model is not able to predict evaporation rates of volatile soluble liquids in water. However, the HACS-R model [Raj, 1974] is.

3.4.2.1 Boiling regimes

In literature a lot of attention is given to nucleate boiling and film-boiling. However, metastable boiling is often not taken into consideration, due to its complexity.

Many common industrial liquefied gases will boil in the metastable boiling regime. So, the evaporation should be based on the model for metastable boiling. It must be mentioned however that the selected GASP-model applies a somewhat simplified approach to incorporate the effects of film-boiling.

3.4.2.2 Evaporation of cryogen on sand

Two remarkable different models have been encountered regarding the evaporation of cryogenes on sand.

The approach by Takeno [1994] looks promising, but an adequate model to calculate the penetration velocity of the boiling liquid into the subsoil is lacking and can not easily be developed. Nevertheless, the extended model of Takeno has been addressed in detail in paragraph 3.3.3.1.

While the model for liquid penetration is probably too simple, the TNO-model for evaporation on sand is to be preferred. It must be mentioned however, that the model in YellowBook [1988] concerning evaporation in gravel layers ignores all kind of complications, and may give unrealistically high evaporation rates. Therefore, some additional criteria have to be added.

3.4.3 Evaporation of chemicals mixed in water

In the NTIS-report [Raj, 1974] a model has been given that describs the evaporation phenomena for volatile liquids which are soluble or miscible in water and have a boiling point greater than the water temperature, but less than 100 ˚C. So, the chemical must have a considerable vapour pressure at water temperature. Because it is the only model found in literature to predict evaporation rates the HACS-R model will be described.

In the literature it is reported that the HACS-R model has recently been used for prediction of the evaporation rate of an ammonia spill onto water [Dharmavaram, 1994].

3.4.4 Evaporation of chemicals that sink in water

In the NTIS-report [Raj, 1974] a model has been given that describes the evaporation phenomena for liquids heavier than water with boiling temperatures less than ambient. The use of packed-bed correlation or single-sphere heat transfer

correlations in the model leads to high evaporation rates. In general all of the spilt liquid is predicted to vaporise within a period of about 10 seconds.

No experimental evidence is available to test the results of this theory.

For dispersion predictions purposes, it is acceptable in most cases just to assume a instantaneous release in case of a spill of a boiling liquid heavier than water. It may be valid to use the spill rate itself as the evaporation rate in the case of semi-continuous spills. Therefore the model will not be included in section 3.5.

3.4.5 Application of simple models

The GASP-model is a very complex model and has to be computerised before any prediction can be made.

In case spreading of the liquid pool can be ignored, as may be the case for instantaneous liquid releases in bunds, it is possible to use simple models to guess the magnitude of the evaporation rate, at least with some accuracy.

So, for convenience, simple models will also be presented in section 3.5, though the GASP model is to be preferred from a scientific point of view.

3.5   Description of models

3.5.1   Introduction to section 3.5

Section 3.5 provides descriptions of the recommended models and methods for liquid pool evaporation. It contains all necessary information to perform the calculations. For background of the models the reader should review section 3.3.

Section 3.5 provides detailed descriptions of the models and methods regarding the following topics. Subsection 3.5.2 gives a description of GASP valid for liquid pools (spreading) on subsoil and floating on water.
Subsection 3.5.3 and 3.5.4 treat the evaporation of cryogenes on subsoil and water.
Subsection 3.5.5 provides simple models for pool evaporation in bunds, for which complicated calculations may be avoided without losing too much accuracy.
Subsection 3.5.6 gives a description of HACS-R, valid for volatile (non-boiling) liquid chemicals into water.
In section 3.8 some additional remarks on the limitations of the models presented are given.

3.5.2   GASP [Webber, 1990]

3.5.2.1   Introduction

GASP is an acronym for 'Gas Accumulation over Spreading Pools'. The description of the GASP model has been taken from 'A model for pool spreading and vaporisation and its implementation in the computer code G*A*S*P', by D.M. Webber [Webber, 1990]; courtesy AEA-technology.

The GASP model aims at the description of the spreading and vaporisation of a evaporating liquid pool to predict the evaporation rate and pool size.

The complete specification of the model will be concise and will use results that have been derived by others. References made in the original publication of Webber [Webber, 1990] will not be repeated here.
The model will be defined with reference to the computational methods which are used to solve the equations, and relevant numerical aspects will be touched upon here.

The model is able to predict the vaporisation rate of a circular liquid pool on subsoil or water. The surface onto which the liquid is spilt, is assumed to be flat, horizontal and statistically uniform. Subsoil may be 'rough' so liquid puddles may be formed. Liquid spills onto water are assumed to float on the water surface and not to mix with or to solve into the water.
The pool may be retained within a bund, spread until it meets a bund, or be completely unbunded. The liquid may be released instantaneously, or at a time-

dependent discharge rate. The vaporisation rate is controlled both by the atmospheric dispersion of the vapour and by the heat transfer to the pool.
The model can be applied to any liquid, irrespective of its boiling point.

3.5.2.2   Model structure

The basic structure of the model is a set of coupled ordinary differential equations for the bulk properties of the liquid pool. This scheme has to be solved simultaneously by a numerical method.

The equations are not easily to be solved numerically due to the large variety of time-scales introduced by the several physical phenomena modelled.
Six 'primary' variables have been defined that are expressed by a differential equation as a function of time.

$$dr/dt = ... \qquad\qquad\qquad \text{(3.60SW) and (3.61R)}$$

$$du/dt = ... \qquad\qquad\qquad\qquad\qquad \text{(3.62)}$$

$$dV/dt = ... \qquad\qquad\qquad\qquad\qquad \text{(3.32)}$$

$$d\Phi_r/dt = ... \qquad\qquad\qquad\qquad\qquad \text{(3.79)}$$

$$dV_d/dt = ... \qquad\qquad\qquad\qquad\qquad \text{(3.28)}$$

$$dV_E/dt = ... \qquad\qquad\qquad\qquad\qquad \text{(3.29)}$$

where
r	=	radius of the pool	[m]
u	=	radial liquid velocity at the edge	[m/s]
V	=	volume of liquid in the pool	[m^3]
Φ_r	=	measure of pool temperature (3.27)	[-]
V_d	=	volume of liquid which has been discharged into the pool	[m^3]
V_E	=	volume of vaporised liquid	[m^3]

Scheme 1   Structure of the GASP-model

The model will be specified by defining the right-hand sides of these six equations in terms of so-called 'secondary' variables, such as pool depth, pool area, mean temperature of the pool, vaporisation rate, and various contributions to the heat flux into the pool.

The set of differential equations can be solved by the so-called 'variable-order variable time-step Gear's method'. Within this procedure the values of the six primary variables will be calculated simultaneously for every following time-step.

In general the secondary variables are algebraic functions of the primary variables, except for the heat conducted into the pool from a solid subsoil. This is obtained from a Green's function solution of the Fourier conduction equation in the solid, and is expressed as an integral over time. In case of a spreading pool on the ground this integral has to be solved within every time-step.

The solution of the scheme requires:
1. specification of the initial values of the six primary variables;
2. constants, like ambient conditions;
3. (time-dependent) discharge rate.

Some of the basic quantities have been transformed into functions that match the requirements of the numerical solution procedure.

In the scheme Φ_r is used which is related to the liquid pool temperature T by the definition

$$T = T_b - T_A \times e^{-\Phi_r} \qquad\qquad (K) \qquad\qquad (3.27)$$

where T_b [K] is the boiling point and T_A [K] is a suitable constant temperature scale. Any real value of Φ_r corresponds to a temperature below boiling point. By using quantity Φ_r instead of temperature T, numerical problems can be avoided.

3.5.2.3   Release and Evaporation

First the three primary volume variables, the volume of the liquid in the pool V, the volume of liquid that has been discharged into the pool V_d, and the volume of liquid that has vaporised V_E, are considered.

$$dV_d/dt = q_S/\rho_L \qquad\qquad (m^3/s) \qquad\qquad (3.28)$$

where
V_d	=	liquid volume discharged into the pool	[m^3]
ρ_L	=	density discharged liquid	[kg/m^3]
q_S	=	release rate liquid	[kg/s]
t	=	time from the start of the release	[s]

where q_S is the discharge rate which must be specified. The discharge rate q_S may be zero for an instantaneous release, in which case V_d and V must initially be non-zero and equal. Otherwise q_S is a given function of time. There may or may not be liquid in the pool initially.

$$dV_E/dt = u_{rA} \times A_{top} \qquad\qquad (m^3/s) \qquad (3.29)$$

where
A_{top} = top area of the liquid [m^2]
u_{rA} = averaged liquid surface regression rate over the pool [m/s]
V_E = liquid volume that has vaporised [m^3]

The area A_{top} may differ from the overall pool area A if the pool is not simply connected.

The regression rate u_{rA} is related to the evaporation mass flux density q''_v and the liquid density ρ_L by

$$q''_v = \rho_L \times u_{rA} \qquad\qquad (kg/(m^2 \cdot s)) \qquad (3.30)$$

and V_E is related to the mass Q which has vaporised by

$$Q = \rho_L \times V_E \qquad\qquad (kg) \qquad (3.31)$$

where
ρ_L = liquid density [kg/m^3]

u_{rA} will be used as the standard measure of the vaporisation rate.
The variations in the volume of liquid in the pool V can be described by

$$dV/dt = q_S/\rho_L - u_{rA} \times A_{top} - q_D/\rho_L \qquad\qquad (m^3/s) \qquad (3.32)$$

where
V = liquid volume in the pool [m^3]
q_D = drainage rate [kg/s]

where q_D is a 'drainage' rate which may account for loss of liquid other than by vaporisation seeping into porous subsoil or running into drains. This may also be time-dependent.
Here only problems with no drainage (q_D=0) will be considered, thus

$$V = V_d - V_E \qquad\qquad (m^3) \qquad (3.33)$$

This is a minor limitation of the GASP model, which could easily be overcome by taking q_D into account in the integration procedure.

The remaining features of the model can now split up into spreading phenomena (dr/dt, du/dt, A) and vaporisation phenomena ($d\Phi_r/dt$, T, u_{rA}).

3.5.2.4 Spreading of the liquid pool over a surface

Spreading on three possible surfaces will be considered:

(S):   on smooth subsoil
(R):   on subsoil rough enough to retain liquid in puddles
(W):   on water

The spreading equations will be slightly different for each case.

The reduced acceleration due to gravity for pools spreading on water will be needed, where ρ_w is the density of the water and ρ_L is the density of the pool

$$g_{g/gr} = g \times (\rho_w - \rho_L)/\rho_w \qquad\qquad (m/s^2) \qquad (3.34\ W)$$

For spreading on subsoil the acceleration due to gravity will be

$$g_{g/gr} = g \qquad\qquad (m/s^2) \qquad (3.35\ SR)$$

The depth profile and area of the pool

For spreading on smooth subsoil or on water the area of the pool A is, where r is the radius of the pool

$$A = \pi \times r^2 \qquad\qquad (m^2) \qquad (3.36)$$

and the mean depth is h given by

$$h = V/A \qquad\qquad (m) \qquad (3.37)$$

For spreading on rough, puddle-forming subsoil two layers of liquid can be distinguished: a 'dynamic' region of mean depth h_e over a 'stagnant' region within the depressions of the subsoil.
The mean depth of puddles, averaging over the entire subsoil surface, is defined as h_p.

So for spreading on rough subsoil per definition

$$h_e = V/A - h_p \qquad\qquad (m) \qquad (3.38\ R)$$

$$V_e = V - h_p \times A \qquad\qquad (m^3) \qquad (3.39\ R)$$

and for spreading on smooth subsoil and water

$$h_e = h \qquad\qquad (m) \qquad (3.40\ SW)$$

$$V_e = V \qquad\qquad (m^3) \qquad (3.41\ SW)$$

The depth h_f at the edge of the pool is not in general equal to the mean depth h.

In an integral approach it is necessary to retain some measure of the depth profile in the pool. This can be done by defining a dimensionless shape factor s

$$s = h_f/h \qquad\qquad (-) \qquad\qquad (3.42)$$

Knowing s, the depth h_f at the edge of the pool can be determined.
The value of s will affect gravity spreading. For s < 1 the pool will spread outward on average, for s > 1 inward.
In the following expressions for estimation the dimensionless shape factor s will be presented.

Self-similar solutions of the shallow water equations for an instantaneously released, inviscid, non-volatile pool on subsoil or water can be found in which the pool has a parabolic surface.
Self-similar solutions of the shallow water equations, are solutions described by functions of the same form but with a different scaling parameter.
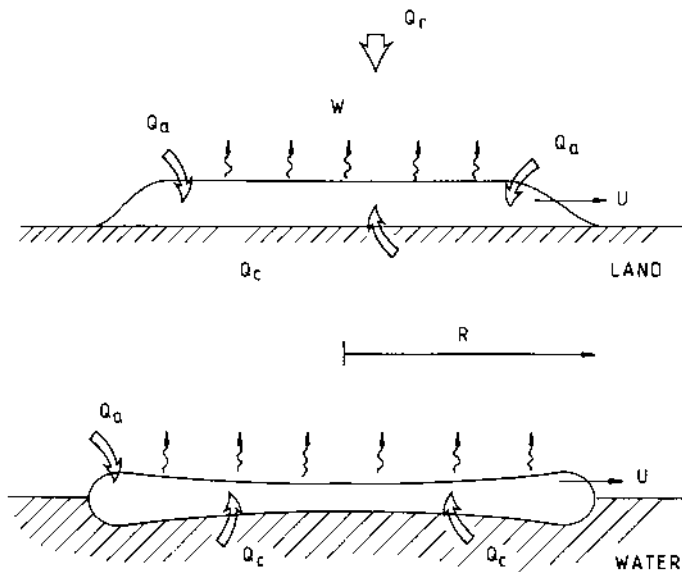
Figure 3.5   Spreading liquid pools on subsoil and on water [Webber, 1990]

On smooth subsoil (see Figure 3.5) the pool has a convex surface and

$$s = 0 \qquad\qquad\qquad (3.43\ S)$$

on water (see Figure 3.5) the front resistance leads to a concave surface (s > 1), and with constant s given by

$$s = u^2/(Fr^2 \times g_{g/gr} \times h) \qquad (-) \qquad (3.44\ W)$$

where
Fr = Froude number [-]
u = radial liquid spreading velocity [m/s]

Here $1/Fr^2$ can be regarded as a frontal drag coefficient and the expression for s can be inferred from the requirement that a front resistance pressure of $\rho_w \times u^2/(2 \times Fr^2)$ is sufficient to provide the hydrostatic pressure at the pool edge.
These expressions for s must be modified to allow for surface tension and other effects.
In this simple paraboloid model, values of s greater than 2 correspond to an annular pool with inner radius r_i given by

$$r_i^2 \quad = r^2 \times (s - 2)/s \quad \text{if } s > 2 \qquad (m^2) \qquad (3.45)$$
$$= 0 \qquad\qquad \text{if } s < 2$$

If solutions are found where s > 2 for part of the flow, this may indicate pool break-up, rather than adherence to a literal interpretation of an annular pool.
The model equations will not in general be analytic at s = 2, and it is convenient to define a function j(s) by

$$j(s) \quad = 1 \qquad\qquad \text{if } s > 2 \qquad (-) \qquad (3.46)$$
$$= 2/s \qquad\qquad \text{if } s < 2$$

For example the top area is given by

$$A_{top} = j(s) \times A \qquad (m^2) \qquad (3.47)$$

The shape factor s depends on a number of factors which are relevant to the frontal depth h_f.
Surface tension is included in the model by setting the frontal depth to a constant value $h_{\sigma,f}$ at which surface tension may hold a pool against gravitational spread

$$h_{\sigma,f} \approx \sqrt{(\sigma/(g \times \rho_L))} \qquad (m) \qquad (3.48)$$

But its precise value will vary with the liquid and the surface on which it is spilt.
Alternatively it has been estimated that viscous effects give rise to a minimum depth $h_{c,\infty}$ during a continuous discharge at (volumetric) rate q_S (see subsection 3.2.3.2)

$$h_{c,\infty} \quad = \left(\frac{6 \times \upsilon_L \times q_S}{(\rho_L \times \pi \times g)} \right)^{0.25} \qquad (m) \qquad (3.11)$$

For whatever effect is the greater, the following definition holds

$$h_{0,max} = \max (h_{\sigma,f}, h_{c,\infty}) \qquad (m) \qquad (3.49)$$

Following the above, discussion on smooth subsoil is set

$$s = h_{0,max}/h \qquad\qquad (-) \qquad\qquad (3.50\ S)$$

and on water

$$s = N + \sqrt{(N^2 + (h_{0,max}/h)^2)} \qquad\qquad (-) \qquad\qquad (3.51\ W)$$

with

$$N\ = u^2/(2 \times Fr^2 \times g_{g/gr} \times h) \qquad \text{if } u > 0 \qquad (-) \qquad\qquad (3.52)$$

$$= 0 \qquad\qquad \text{if } u < 0 \qquad\qquad\qquad\qquad (3.53)$$

The expression for s on water is derived by assuming that surface tension and front resistance forces combine additively to slow the spread of the pool.

In the case where subsoil roughness dominates

$$s = \Phi_1(\varepsilon) \times h_r/(2 \times h) \qquad\qquad (-) \qquad\qquad (3.54\ R)$$

with

$$\varepsilon = 8\ u^2/(g \times h_r) \qquad\qquad (-) \qquad\qquad (3.55)$$

and

$$\Phi_1(\varepsilon) = \sqrt{(1 + \varepsilon)} - 1 \qquad\qquad (-) \qquad\qquad (3.56)$$

where h_r is the roughness scale.

In the model for pool spreading on rough subsoil the functions of ε allow for the removal of mass and momentum from the dynamic part of the pool as it spreads over the depressions.

A trivial example is that in which the pool is confined to a bund. In this case

$$s = 1 \qquad\qquad (-) \qquad\qquad (3.57)$$

For future reference the following functions are defined

$$\Phi_2(\varepsilon) = 1 - 2/\varepsilon \times \Phi_1(\varepsilon) \qquad\qquad (-) \qquad\qquad (3.58)$$

$$\Phi_3(\varepsilon) = \Phi_2(\varepsilon) + 4/\varepsilon \times \Phi_1(\varepsilon) - 2/\sqrt{(1+\varepsilon)} \qquad\qquad (-) \qquad\qquad (3.59)$$

Pool spreading Equations

The radius of the pool for spreading on smooth subsoil or water is given by

$$dr/dt = u \qquad\qquad (m/s) \qquad (3.60\ SW)$$

For spreading on rough subsoil it is modified to (see equation (3.58))

$$dr/dt = u \times \Phi_2(\varepsilon) \qquad\qquad (m/s) \qquad (3.61\ R)$$

The overall force balance on the pool is expressed by

$$du/dt = \Phi(s) \times (4 \times g_{g/gr} \times h_e/r) - C_F \qquad\qquad (m/s) \qquad (3.62)$$

where C_F is a turbulent or viscous resistance term and the coefficient in the first $\Phi(s)$ gravity driving term is given by

$$\Phi(s) = 1 - s \qquad \text{if } s < 2 \qquad\qquad (-) \qquad (3.63)$$
$$\quad = -s^2/4 \qquad \text{if } s > 2$$

In the case of an inviscid ($C_F = 0$), non-volatile pool, these equations summarise the results of the self-similar analysis of the shallow-water equations discussed above.
Note that the gravity driving force is directed outwards for a pool with a convex top surface (s < 1) and inwards for a concave (s > 1) surface.
The resistance forces depend on whether the flow is laminar or turbulent.
The resistance to laminar flow will be modelled as

$$C_{FL} = \beta(s) \times (C \times \upsilon_L \times u/h_e^2) \times (1 - f) \qquad\qquad (m/s^2) \qquad (3.64)$$

where υ_L is the kinematic viscosity of the liquid, h_e is given by (3.38/40), and C is a factor determined by the vertical velocity profile in the pool;
for on land

$$C = 3.0 \qquad\qquad (-) \qquad (3.65a\ SR)$$

and for on water

$$C = 0.66 \qquad\qquad (-) \qquad (3.65b\ W)$$

This has been derived from lubrication theory for spreading on subsoil, but involves empirical knowledge for spreading on water.
The coefficient $\beta(s)$ given by

$$\beta(s) = 2.53 \times j(s)^2 \qquad\qquad (-) \qquad (3.66)$$

is a factor determined by radial profiles, and f is a factor which allows for the radial motion of water under the pool.
Specifically for spreading on subsoil

$$f = 0 \qquad\qquad (-) \qquad (3.67\ LS)$$

whereas for spreading on water f is given by an implicit function

$$\xi \times f^{3/2} = 1 - f \qquad\qquad (3.68\ W)$$

with

$$\xi = \eta_L/\eta_w \times \sqrt{(u \times h^2/(\upsilon_w \times r))} \times (1/j(s)) \qquad (-) \qquad (3.69)$$

where η_L, η_w are the viscosities of the pool and the water beneath, and υ_w is the kinematic viscosity of the water.

The model for the resistance to turbulent flow is

$$C_{FT} = \alpha(s) \times C_f \times u^2/h_e \qquad\qquad (m/s^2) \qquad (3.70)$$

where C_{FT} is a turbulent friction coefficient and

$$\alpha(s) = 4.49 \times j(s) \qquad\qquad (-) \qquad (3.71)$$

is a radial profile factor. The optimum value of C_f is in the region of 0.0015.
The resistance term C_F in (3.62) will be modelled as

$$C_F = \text{sign}(u) \times \max\ (C_{FL}, C_{FT}) \qquad\qquad (m/s^2) \qquad (3.72)$$

The transition from turbulent to laminar now is implicitly controlled by the Reynolds number Re

$$Re = u \times h/\upsilon. \qquad\qquad (-) \qquad (3.73)$$

Constants

The constants which have appeared in the model description comprise:
− well-defined physical properties of liquids;
− factors arising as integrals over profiles of the relevant fields both radially and vertically;
− turbulent friction coefficient C_f;
− puddle depth parameter h_p;
− capillary depth parameter l_σ;
− front resistance parameter Fr for spreading on water.

The constants l_σ and h_p depend on the nature of the surface on which the liquid is spreading and must therefore be estimated for any given application.
Fr can be estimated from empirical observations of liquids spreading on water.

In case of an instantaneous release of a large amount of non-volatile liquid onto water, after the initial radial acceleration, there will be a phase where the resistance terms are negligible compared to inertia and gravity forces.

In this case the spreading equations for a spill on water are solved with constant V, and $u_{rA} = 0$ and $C_F = 0$, to give spreading with pool area proportional to time

$$u = Fr_{rad} \times \sqrt{(g_{g/gr} \times h)} \qquad\qquad \text{(m/s)} \qquad (3.74)$$

where Fr_{rad} is a Froude number given by

$$Fr_{rad} = 4 \times Fr^2/(4 - Fr^2) \qquad\qquad \text{(-)} \qquad (3.75)$$

This spreading regime is well-established and an empirical value

$$Fr_{rad} = 1.64 \qquad\qquad \text{(-)} \qquad (3.76)$$

has been obtained in LNG experiments by Chang and Reid. Therefore the value $Fr = 1.078$ will be adapted. There is however some uncertainty introduced by the existence of other experiments which measure this quantity, and which obtain different values. It is important to emphasise that this spreading regime will be valid only for a limited time until viscous effects become important.

Remarks

The incorporated spreading model is derived from shallow-layer theory and lubrication theory for an instantaneously released, non-volatile pool where V is constant.
In fact it is implicitly assumed that the model is adequate when V is not constant due to vaporisation and release of liquid into the pool.
Vaporisation will only have a significant effect on the spreading behaviour when the radial velocity of the spreading liquid u has decreased to a magnitude comparable with the liquid regression rate u_{rA}.
For continuous releases the different time-scales implicit in the discharge rate and the rate at which the pool wants to spread, make it much more difficult to solve the shallow-layer equations. However, by introducing a minimum pool depth h_0, see before, it is possible to incorporate the limit at which the pool is large enough for vaporisation to balance discharge.

3.5.2.5 Evaporation

Pool Temperature

The pool temperature is described by the average liquid pool temperature T according to the following heat balance

$$\frac{dT}{dt} = \frac{A_{top}}{(C_{p,L} \times \rho_L \times V)} \times (H - \rho_L \times u_{rA} \times L_v) + \left(\frac{q_s}{(\rho_L \times V)}\right) \times (T_{q_s} - T)$$

$$\text{(K/s)} \qquad (3.77)$$

where

A_{top}	=	liquid top area	$[m^2]$
$C_{p,L}$	=	specific heat of the liquid	$[J/(kg \cdot K)]$
H	=	heat flux density from above and below	$[J/(m^2 \cdot s)]$
$L_v(T)$	=	latent heat of vaporisation	$[J/kg]$
q_S	=	liquid source discharge rate	$[kg/s]$
t	=	time from start release	$[s]$
T	=	(average) liquid pool temperature	$[K]$
T_{q_s}	=	liquid source temperature	$[K]$
u_{rA}	=	liquid surface regression rate	$[m/s]$
V	=	volume of liquid in pool	$[m^3]$
ρ_L	=	liquid density	$[kg/m^3]$

Specifically for $\exp(H/\rho_L \times u_{rA} \times L_v) >> 1$ the solutions exhibit an almost instantaneous transition from a regime where temperature increases as heat is supplied, to one where $dT/dt = 0$ very close to the boiling point.
This problem can be overcome by defining

$$\Phi_r = \ln(T_A/(T_b - T)) \qquad\qquad (-) \qquad (3.78)$$

where T_b is the boiling point and T_A a arbitrary temperature scale, taken to be 1 K. So, the following equation can be written

$$\frac{d\Phi_r}{dt} = \omega \times e^{\Phi r} \times \sqrt{(\omega^2 + e^{2\Phi r})} \times \left(\frac{1}{T_A}\right) \times$$

$$\frac{A_{top}}{(C_{p,L} \times \rho_L \times V)} \times (H - \rho_L \times u_{rA} \times L_v) + \left(\frac{q_S}{(\rho_L \times V)}\right) \times (T_{q_s} - T)$$

$$\text{(1/s)} \qquad (3.79)$$

ω = temperature smoothing factor   [-]

For finite ω the transition from boiling to non-boiling is smoothed suitably for numerical computation without otherwise affecting the results. The equation above therefore forms the basic temperature equation of the model.
In practice ω should be chosen small enough to enable the stiffness of the problem to be sufficiently mitigated to avoid numerical problems, but large enough so it does not smooth the solution too much. A value of about 1000 seems to be sufficient.

Note that $\Phi_r \rightarrow \infty$ at the boiling point, which is never actually reached. This is reasonable as the existence of temperature gradients in a real evaporating liquid pool means generally that the average temperature is below the boiling point.

Transport of Vapour

The model for the liquid surface regression rate $u_{rA}(T)$ is that of Brighton, and is given by

$$u_{ra}(T) = -\mu_i \times P_v(T)/(R \times T) \times (u_{*p}/\rho_L) \times (\kappa/Sc_t) \times (1+n) \times G(e^{\chi_{Sc}})/m_{m,v} \times \ln(1-m_{m,v})$$

$$\text{(m/s)} \qquad (3.80)$$

where
μ_i	=	molecular weight liquid	[kg/mol]
$G(e^{\chi_{Sc}})$	=	function given by equation (3.84a)	[-]
$m_{m,v}$	=	mole fraction of vapour above liquid pool surface	[-]
n	=	wind profile index	[-]
$P_v(T)$	=	vapour pressure above the pool	[N/m^2]
R	=	gas constant	[J/(mol·K)]
Sc_t	=	turbulent Schmidt number (≈ 0.85)	[-]
κ	=	von Karman constant (≈ 0.4)	[-]
u_{*p}	=	atmospheric friction velocity above the pool	[m/s]
ρ_L	=	liquid density	[kg/m^3]

The argument χ_{Sc} is given by

$$\chi_{Sc} = 1/n + 2 - \gamma + \ln(2(1+n)^2) - (\kappa/Sc_t) \times (1+n) \times \beta(Sc_L) \quad \text{(-)} \qquad (3.81)$$

where γ is Euler's constant and Sc_L is the (laminar) Schmidt number of the vapour in air, given by

$$\gamma \approx 0.57722 \qquad\qquad\qquad\qquad \text{(-)} \qquad (3.81a)$$

$$Sc_L = \upsilon_L/D_v \qquad\qquad\qquad\qquad \text{(-)} \qquad (3.82)$$

υ_L	=	kinematic vapour viscosity	[m^2/s]
D_v	=	diffusion coefficient vapour in air	[m^2/s]

The function $\beta(Sc_L)$ is given by

$$\beta(Sc_L) = 7.3 \times Re_0^{0.25} \times \sqrt{Sc_L} - 5 \times Sc_t \qquad \text{(-)} \qquad (3.83a)$$

or

$$\beta(Sc_L) = (3.85 \times Sc_L^{1/3} - 1.3)^2 + (Sc_t/\kappa) \times \ln(0.13 \times Sc_L) \quad \text{(-)} \qquad (3.83b)$$

according to whether or not one considers the pool to be aerodynamically rough. Here Re_0 is the roughness Reynolds number $u_* \times z_0/\upsilon_a$ constructed from the friction velocity and the aerodynamic roughness length z_0 of the pool.

The function $G(e^\chi)$ is given by

$$G(e^\chi) = 0.5 - f_0/\pi \times \mathrm{atan}(\chi/\pi) + f_1/(\chi^2 + \pi^2) + f_2 \times \chi/(\chi^2 + \pi^2)^2$$
$$+ f_3 \times (\chi^2 - \pi^2/3)/(\chi^2 + \pi^2)^3 \qquad\qquad (\text{-}) \qquad\qquad (3.84a)$$

with

$$f_0 \;=\; 1 \qquad\qquad\qquad\qquad\qquad (\text{-}) \qquad\qquad (3.84b)$$
$$f_1 \;=\; 1 - \gamma \approx 0.42278 \qquad\qquad (\text{-}) \qquad\qquad (3.84c)$$
$$f_2 \;=\; f(\gamma) \approx 2.824 \qquad\qquad\quad (\text{-}) \qquad\qquad (3.84d)$$
$$f_3 \;=\; f(\gamma) \approx 1.025 \qquad\qquad\quad (\text{-}) \qquad\qquad (3.84e)$$

For the vapour pressure $P_v(T)$ the Antoine correlation is adopted, which may be written

$$m_{m,v} = \exp\left(C_B \times (T - T_b)/((T + C_C) \times (T_b + C_C))\right) \qquad (\text{mol/mol}) \qquad (3.85)$$

with

$$P_v(T) = m_{m,v} \times P_a \qquad\qquad\qquad\qquad (\text{N/m}^2) \qquad\qquad (3.86)$$

where P_a is atmospheric pressure, and $m_{m,v}$ is the mole fraction of the vapour just above the liquid pool surface. Here C_B and C_C are Antoine coefficients and the Antoine A-coefficient (C_A) has been eliminated in favour of the boiling point T_b.
These coefficients can be found by fitting the Antoine correlation for vapour pressures predicted by the equations presented in the annex 'Physical Properties of Chemicals'.

The vaporisation of liquid depends on how fast the atmospheric flow can remove vapour from the surface. The state of the atmosphere is modelled as a function of the friction velocity u_* and an effective wind speed index n.
The latter arises from Brighton's approximation of the wind profile by a power law, which allows the derivation of (3.80). The index n which best approximates a logarithmic profile over the pool is given by

$$1/n = F_N \times (\sqrt{A}/z_{0,p}) \times (\kappa^2/Sc_t) \times (e^{-(1 + \gamma)}) \qquad (\text{-}) \qquad\qquad (3.87)$$

where $F_N(\xi)$ is a function given implicitly by

$$F_N \times e^{F_N} = \xi \qquad\qquad\qquad\qquad\qquad (\text{-}) \qquad\qquad (3.88)$$

The index n depends to a small extent on the pool size.

The friction velocity u_{*p} above the pool may be different from u_{*a} well upwind of the pool, if the pool roughness length $z_{0,p}$ is different from, $z_{0,a}$ of the surroundings. In this case an inner boundary layer grows over the pool and it can be found following Hunt and Simpson.

3.60

$$u_{*p} = u_{*a} \times (\xi/(\xi + \ln (z_{0,a}/z_{0,p}))) \qquad\qquad \text{(m/s)} \qquad (3.89)$$

with

$$\xi = F_N(\kappa^2 \times \sqrt{A}/z_{0,a}) \qquad\qquad\qquad \text{(-)} \qquad (3.90)$$

where $\sqrt{A}$ is a measure of the pool size. Thus the friction velocity u_* also depends on the pool size, as this determines how far the boundary layer over the pool has developed, but only weakly for most cases of interest. The ambient friction velocity is found from the wind speed at standard 10 metres height $u_{w,10}$ and the roughness length $z_{0,a}$ assuming a neutral boundary layer

$$u_{*a} = \kappa \times u_{w,10}/\ln (z_{10}/z_{0,a}) \qquad\qquad \text{(m/s)} \qquad (3.91)$$

with

$$z_{10} = 10 \text{ m}.$$

Alternatively, if one wishes to assume an aerodynamically smooth surface, then an effective $z_{0,a}$ can be found by taking the Reynolds number equal to

$$Re_{0a} = u_{*a} \times z_{0,a}/\upsilon_a \approx 0.13 \qquad\qquad \text{(-)} \qquad (3.92)$$

in which υ_a is the kinematic viscosity of the air.

This gives

$$u_{*a} = 0.13 \times \upsilon_a/z_{10} \times F_N(\kappa \times u_{w,10} \times z_{10}/(0.13 \times \upsilon_a)) \qquad \text{(m/s)} \qquad (3.93)$$

$$z_{0,a} = z_{10}/F_N(\kappa \times u_{w,10} \times z_{10}/(0.13 \times \upsilon_a)) \qquad\qquad \text{(m)} \qquad (3.94)$$

If the pool is considered aerodynamically smooth, then u_* and an effective z_0 are found by solving (3.89) together with

$$u_* \times z_0 = 0.13 \times \upsilon_a \qquad\qquad\qquad \text{(m}^2\text{/s)} \qquad (3.95)$$

This can be done in terms of the function F_N defined above.

The heat flux into the pool

The term heat flux into the pool H in (3.77) is the sum of three contributions
1. heat H_c conducted from the subsoil or convected from the water beneath;
2. heat H_a convected from the air above;
3. heat H_r radiation.

$$H = H_c + H_a + H_r \qquad\qquad\qquad \text{(J/(m}^2\cdot\text{s))} \qquad (3.96)$$

Liquid in contact with the surface beneath

First the heat transfer from below is considered when film-boiling is not taking place.
An approximation which is in many cases quite accurate, is to neglect those components of heat transfer within the subsoil which are parallel to the surface.
A boundary condition can be defined, stating that the subsoil temperature is $T(t)$ under the surface of the spreading pool $A(t)$, and T_a elsewhere. The subsoil is assumed initially to be uniform at temperature T_a, except on the part of the surface in contact with the pool.

In this approximation the mean heat flux density into the pool is given by

$$H_{c1}(t) = -\lambda_s \times \Phi_T(t)/\sqrt{(\pi \times a_s \times t)} - \qquad (J/(m^2 \cdot s)) \qquad (3.97)$$

$$\lambda_s/\sqrt{(4\pi \times a)} \times \int_0^t [(t - \Psi)^{-3/2} \times \{\Phi_T(t) \times A(t) - \Phi(\Psi) \times A(\Psi)\}/A(t)] \times d\Psi$$

with

$$\Phi_T(t) = (T(t) - T_a) \qquad (K) \qquad (3.98)$$

where
λ_s = thermal conductivity of the subsoil $\quad [J/(m \cdot s \cdot K)]$
a_s = thermal diffusivity of the subsoil $\quad [m^2/s]$

This result holds provided only that the pool spreads in such a way that an area of subsoil once covered by liquid, remains covered. The heat flux density is in this model not dependent on the shape of the pool.
In an isothermally-bunded process this reduces to the familiar $1/\sqrt{t}$ law based on the penetration theory, see equation 3.7.

Again neglecting horizontal conductions, at boundary conditions the heat flux density H at the surface is assumed to obey

$$H = k_H \times (T_{p,a} - T_s) \qquad (J/(m^2 \cdot s)) \qquad (3.99)$$

where
T_s = subsoil surface temperature $\quad [K]$
k_H = heat transfer coefficient $\quad [J/(m^2 \cdot s \cdot K)]$
T_a = ambient temperature $\quad [K]$
$T_{p,a}$ = T or T_a $\quad [K]$

Note that $T_{p,a}$ is equal to the pool temperature T where liquid is on the surface and is equal to the ambient temperature T_a elsewhere.
In this case the result corresponding to (3.97) is

$$H_{c1}(t) = -\lambda_s \times \Phi_T(t)/\sqrt{(a_s \times t_0)} \times erfc_*(\sqrt{(t/t_0)}) -$$

$$\lambda s \times \int_0^t [G_*(t - \Psi) \times \{\Phi_T(t) \times A(t) - \Phi(\Psi) \times A(\Psi)\}/A(t)] \times d\Psi \quad (J/(m^2 \cdot s)) \qquad (3.100)$$

where t_0 is the heat transfer time-scale

$$t_0 = \lambda_s{}^2/(a_s \times k_H{}^2) \qquad\qquad (s) \qquad (3.101)$$

and $erfc_*$ is defined in terms of the usual complementary error function $erfc$ by

$$erfc_*(\xi) = \exp(\xi^2).erfc(\xi) \qquad\qquad (-) \qquad (3.102)$$

and G_* is a Green's function

$$G_*(t) = 1/\sqrt{(a_s \times t_0{}^3)} \times \{\sqrt{(t_0/(\pi \times t))} - erfc_*(\sqrt{(t/t_0)})\} \qquad (-) \qquad (3.103)$$

Note that the integral term in the right-hand side of equation (3.100) has to be solved within every time-step. This can be done by the Romberg's integration method.

Note that (3.100) reduces to (3.97) as $t_0 \rightarrow 0$. This means that the two formulae provide comparable results for t larger than the order of t_0. In the computer implementation GASP of this model, both options are available.
Returning to the solution of the full three-dimensional conduction problem. The horizontal conduction time-scale t_H is defined by

$$t_H = A/(4 \times \pi \times a) \qquad\qquad (s) \qquad (3.104)$$

It has been shown that the uni-directional conduction approximation used above, is valid for t smaller than the order of t_H. Whilst this can be shown for constant A, it is expected that this conclusion even holds for time-dependent A.

The solution of the full conduction equation is difficult, even for circular pools.
It has been estimated that for $t \gg t_H$, where three-dimensional conduction effects are most important, and for constant A and T, the heat flux density H_{c3} tends to

$$H_{c3} = -2/\pi \times 1/\sqrt{(a_s \times t_H)} \times \lambda_s \times \Phi_T(t) \qquad ((J/(m^2{\cdot}s)) \qquad (3.105)$$

To improve the accuracy of the uni-directional approximation an ad hoc pragmatic approach is adopted in order to get a smooth transition to the asymptotic value (3.105) which respects the sign of the heat flux, by

$$H_c = (H_{c1}{}^3 + H_{c3}{}^3)^{1/3} \qquad\qquad ((J/(m^2{\cdot}s)) \qquad (3.106)$$

In the case of a cold pool floating on water, the heat transfer into the pool will depend on convection currents within the water. It is assumed that these are sufficient to keep the water at a more or less uniform temperature T_w, and that the heat flux into the pool is given by

$$H_c = k_{H,w} \times (T_w - T) \qquad\qquad ((J/(m^2{\cdot}s)) \qquad (3.107)$$

where
$k_{H,w}$ = heat transfer coefficient on water $\quad [J/(m^2{\cdot}s{\cdot}K)]$

There is some experimental evidence to indicate $k_{H,w}$ is of order 500 J/(m²·s·K) for butane pools, but this may be substance-dependent.

Film-boiling

Concerning film-boiling, the model/correlation of Klimenko will be used which may be summarised briefly as follows.
The length-scale l_c for vapour bubble formation is defined as

$$l_c = 2\pi \times \sqrt{(\sigma/(g \times (\rho_L - \rho_V)))} \qquad \text{(m)} \qquad (3.108)$$

and also a Galileo number

$$Ga = g \times l_c{}^3/\upsilon_v{}^2 \qquad \text{(-)} \qquad (3.109)$$

and an Archimedes number

$$Ar = Ga \times (\rho_L - \rho_V)/\rho_V \qquad \text{(-)} \qquad (3.110)$$

where
σ	=	liquid surface tension	[N/m]
ρ_L	=	liquid density	[kg/m³]
ρ_V	=	vapour density	[kg/m³]
υ_v	=	kinematic viscosity vapour	[m²/s]

Other dimensionless numbers which are required are the Prandtl number of the vapour Pr_v and the dimensionless heat of vaporisation L_{vR} given by

$$L_{vR} = \frac{L_v(T_b)}{(C_{p,v} \times (T_w - T_b))} \qquad \text{(-)} \qquad (3.111)$$

where
$L_v(T_b)$	=	heat of vaporisation at boiling point	[J/kg]
$C_{p,v}$	=	specific heat of the vapour	[J/(kg·K)]
T_w	=	water temperature	[K]
T_b	=	liquid boiling point	[K]

The heat transfer coefficient $k_{H,f}$ for film-boiling is related to a Nusselt number Nu by

$$k_{H,f} = \lambda_v/l_c \times Nu \qquad \text{(J/(m²·s·K))} \qquad (3.112)$$

where
λ_v	=	thermal conductivity of the vapour	[J/(m·s·K)]

Klimenko has correlated the Nusselt number Nu as a function of other dimensionless numbers, the Archimedes number Ar and the dimensionless heat of evaporation L_R

$$Nu = 0.19 \times (Ar \times Pr_v)^{1/3} \times F_1(L_{vR}) \qquad \text{if } Ar < 10^8 \qquad (\text{-}) \qquad (3.113)$$
$$= 0.0086 \times \sqrt{Ar} \times Pr_v^{1/3} \times F_2(L_{vR}) \quad \text{if } Ar > 10^8$$

with

$$F_1(L_{vR}) = 1 \qquad\qquad\qquad \text{if } L_{vR} < 1.4 \qquad (\text{-}) \qquad (3.114)$$
$$= (L_{vR}/1.4)^{1/3} \qquad\qquad \text{if } L_{vR} > 1.4$$

and

$$F_2(L_{vR}) = 1 \qquad\qquad\qquad \text{if } L_{vR} < 2.0 \qquad (\text{-}) \qquad (3.115)$$
$$= \sqrt{(L_{vR}/2)} \qquad\qquad \text{if } L_{vR} > 1.4$$

Film-boiling will take place when exceeding the so-called critical heat flux density. Based on the work of Zuber, as reviewed by Kenning, the critical heat flux density is given by

$$H_{cr} = 0.18 \times \rho_V \times L_v(T_b) \times \left(\sigma \times g \times \frac{(\rho_L - \rho_V)}{(\rho_V \times (\rho_L + \rho_V))} \right)^{1/4} \quad (J/(m^2 \cdot s)) \qquad (3.116)$$

If the heat flux density H_c calculated for a pool on water according to (3.107) appears to be greater than H_{cr}, then H_c is replaced by

$$H_c = k_{H,f} \times (T_w - T) \qquad\qquad\qquad (J/(m^2 \cdot s)) \qquad (3.117)$$

The heat transfer model has been simplified by neglecting the effect of metastable boiling. Webber expects that the approximation should not be too bad within the overall framework of the model.
The computer implementation GASP allows one the option of simply using either $k_{H,f}$ or $k_{H,w}$ in order to test the importance of film-boiling effects.

Heat transfer from the atmosphere

Heat transfer from the air is modelled similarly to the mass transfer model, as formulated by equations (3.80/81). The heat flux density is given by

$$H_a = \rho_a \times C_{p,a} \times u_* \times (T_a - T) \times (\kappa/Sc_t) \times (1+n) \times G(e^{\chi_{Pr}})/m_{m,v} \times (m_{m,v} - 1) \times \ln(1 - m_{m,v})$$
$$(J/(m^2 \cdot s)) \qquad (3.118)$$

where the argument χ_{Pr} is given by

$$\chi_{Pr} = 1/n + 2 - \gamma + \ln(2(1+n)^2) - (\kappa/Sc_t) \times (1 + n) \times \beta(Pr) \quad (\text{-}) \qquad (3.118a)$$

Note that the laminar Schmidt number Sc has been replaced by the (laminar) Prandtl number Pr.

Heat radiation from the atmosphere

The total heat flux H_r radiated from the surroundings into the pool is considered to be constant in the model. The rate of long-wave radiation heat exchange (H_{rl}) between the pool surface and the surroundings and the solar radiation (H_{rs}) can be calculated by equations 4.36 and 4.37 of chapter 'Vapour Cloud Dispersion' (page 4.63).

$$H_r = H_{rl} + H_{rs} \qquad\qquad (J/(m^2{\cdot}s)) \qquad (3.119)$$

3.5.2.6 Numerical methods

The computer implementation GASP uses the 'variable step variable order Gear's numerical method', in order to cope with sudden changes in the solution.
The model of heat transfer to a pool spreading on subsoil implies that the equations being solved are integro-differential equations. Measures have been taken to evaluate the integral H_c efficiently without loss of accuracy, but still requiring substantial computational effort.

3.5.2.7 Remarks

The model described in the previous subsections is based on an improved understanding of spreading phenomena, vaporisation, and by treating transitions between slow evaporation (non-boiling) and vigorous boiling by means of a generalised approach.

The model can still be improved on the following topics:
− incorporating dense gas effects in the vaporisation model, while density effects may not be neglected;
− the effects of waves on the pool surface;
− the effect of sloping or porous subsoil;
− multi-component liquid pools

and
− extended for permeable subsoils;
− including meta-stable boiling regimes.

3.5.3 Evaporation of cryogen (boiling liquid) on a permeable subsoil

A spilt liquid may sink into the subsoil. Freezing of water in the soil column may prevent the liquid from penetration into the subsoil. On the basis of data available in literature, the following cases will be considered:

a. dry porous subsoil   ($m_{w,ms} = 0$);
b. moist porous subsoil ($m_{w,ms} \geq 8$);
c. gravel-bed.

$m_{w,ms}$ = the weight fraction of moist in the subsoil   [kg/kg]

No sufficient data are available in literature to enable a proper description for the range ($0 < m_{w,ms} < 0.08$).

3.5.3.1   Evaporation of a cryogen on a dry porous subsoil

The theoretical evaporation flux for LPG on sand, approximated as a flat solid surface, appears to be a factor 8 smaller than the experimentally determined value for a LPG-spill on sand [YellowBook, 1988].
This can be explained by the influence of the penetration of the evaporating liquid into the subsoil. On the basis of experimental data, it can be expected that this factor will also approximately apply to the evaporation of propane and butane on dry sand. So, a factor of about 8 must be introduced for the calculation of the evaporation on a dry and porous medium [YellowBook, 1988].
Neglecting all other heat sources, the evaporation mass rate q_v at time t of boiling liquid may be estimated as long as it boils, by

$$H_c(t) = 8 \times \lambda_s \times (T_{s,0} - T_b)/\sqrt{(a_s \times \pi \times t)} \qquad \text{(J/(m}^2\text{·s))} \qquad (3.120)$$

with

$$a_s = \lambda_s/(\rho_s \times C_{p,s}) \qquad \text{(m}^2\text{/s)} \qquad (3.121)$$

and

$$q_v(t) = H_c(t)/L_v(T_b) \times A \qquad \text{(kg/s)} \qquad (3.122a)$$

Referring to equation (3.7a), the total amount of vapour evolved from the boiling pool at time t after the release, may be estimated by

$$Q_v(t) = 2 \times q_v(t) \times t \qquad \text{(kg)} \qquad (3.122b)$$

where
a_s	=	thermal diffusivity of subsoil	[m^2/s]
A	=	liquid pool area	
$C_{p,s}$	=	specific heat of subsoil	[J/(kg·K)]
H_c	=	heat flux by conduction	[J/(m^2·s)]
$L_v(T_b)$	=	heat of vaporisation at T_b	[J/kg]
q_v	=	evaporation rate	[kg/s]
t	=	time from the start of the release	[s]
$T_{s,0}$	=	initial subsoil temperature	[K]
T_b	=	(normal) boiling point liquid	[K]
λ_s	=	thermal conductivity of subsoil	[J/(m·s·K)]
ρ_s	=	subsoil density	[kg/m^3]

3.5.3.2 Evaporation of a cryogen on a moist porous subsoil

Evaporation experiments with spilt cryogenes have shown that water in the subsoil freezes when the weight fraction of moist is larger than 8%, preventing the vaporising liquid to penetrate into the capillaries. Then, the evaporation of boiling liquids on the moist porous subsoil can be calculated by modifying the thermal conductivity coefficient of the subsoil, to account for the freezing of the water present in the subsoil. For the calculation of the evaporation of cooled liquefied gases on a moist and permeable soil, i.e $m_{w,ms} > 0.08$, the non-stationary heat conduction theory can still be applied.

The results obtained in this manner appear to be in good agreement with the experimental results. Also in Takeno [1994] reported laboratory tests, when wet sand ($m_{w,ms} = 7\%$) was used, liquid oxygen or hydrogen did not soak into the subsoil, because the frozen layer of water between the liquid and the sand layer acted as a barrier. These experiments showed that for spills of liquid oxygen and hydrogen, the evaporation rates were indeed inversely proportional to the square root of time, except in the early stage just after the start of vaporisation.

Besides variations of the moist content, the heat conductivity of the subsoil can vary substantially due to other factors, e.g.:
− composition of the subsoil (particle size distribution);
− density of the dry soil.

For the calculation of the heat flux from the subsoil into the liquid pool the following relations can be used. The correction term C_R reflects the influence of the freezing of the water in the subsoil

$$H_c(t) = C_R \times \lambda_s \times (T_{s,0} - T_b)/\sqrt{(a_s \times \pi \times t)} \qquad (J/(m^2 \cdot s)) \qquad (3.123)$$

with

$$C_R = 1.0 + 1.4 \times m_{w,ms} - 3.0 \times m_{w,ms}{}^2 \qquad (-) \qquad (3.124)$$

$$\lambda_s = (\beta_1 \times {}^{10}\log(m_{w,ms}) + \beta_2) \times 10^{\beta_3} \qquad (J/(m^2 \cdot s \cdot K)) \qquad (3.125)$$

$$\beta_1 = 0.14 - 0.05 \times j_k \qquad (3.126a)$$

$$\beta_2 = 0.33 - 0.12 \times j_k \qquad (3.126b)$$

$$\beta_3 = 0.0006 \text{ m}^3/\text{kg} \times \rho_{s,dry} \qquad (3.126c)$$

and

$$a_s = C_R \times \lambda_s/(\rho_s \times C_{p,s}) \qquad (m^2/s) \qquad (3.127a)$$

$$\rho_s = (1.0 + m_{w,ms}) \times \rho_{s,dry} \qquad (kg/m^3) \qquad (3.127b)$$

$$C_{p,s} = (C_{p,s,dry} + m_{w,ms} \times C_{p,ice})/(1.0 + m_{w,ms}) \qquad (J/(kg \cdot K)) \qquad (3.127c)$$

So, the vaporisation mass rate can be estimated by

$$q_v(t) = H_c(t)/L_v(T_b) \times A \qquad \text{(kg/s)} \qquad (3.122a)$$

where

C_R	=	correction factor	[-]
j_k	=	clay volume fraction	[m³/m³]
β_1	=	intermediate	[J/(m·s·K)]
β_2	=	intermediate	[J/(m·s·K)]
β_3	=	intermediate	[-]
$m_{w,ms}$	=	weight fraction moist in subsoil	[kg/kg]

This empiric relation applies to LNG. In YellowBook [1989] no validity ranges have been given for the moist weight fraction. Apparently, the conduction coefficient predicted by equation (3.124), increases with increasing moist content, as might be expected, however, until $m_{w,ms} \approx 0.23$. While the free volume of a 'close packing of spheres' is about 26%, and remembering the density of water to be lower than for sand, it is reasonable to conclude that the upper limit for $m_{w,ms}$ is indeed 23%.
The relation for the thermal conductivity for sandy/clay subsoil is also an empiric equation.
The effects of the particle size distribution have implicitly been taken into account by distinguishing the following subsoil types:
1. sand: diameter between 0.002 and 2 millimetres;
2. clay: diameter < 0.002 millimetres.
Particles bigger than 2 millimetres are neglected.

Takeno [1994] reported from experiments with liquid hydrogen, that the liquid did not soak into the dry sand layer, and the evaporation mechanism seemed to be the same as that for the wet layer, because the air contained within the inter-particle cavities in the dry sand layer solidifies at the boiling point of liquid hydrogen.

3.5.3.3 Evaporation of a cryogen in a gravel-bed

In bunds gravel may cover the subsoil. A separate model can be given for the evaporation of cryogens on a gravel-bed. Implicitly assuming a loose stacking of stones and the total outer surface of gravel stones wetted by the evaporating liquid, the evaporation mass flux at time t can be estimated by the heat-penetration theory

$$H_c(t) = 0.89 \times h_{gr}/r_{gr} \times \lambda_{gr} \times (T_{gr,0} - T_b)/\sqrt{(a_{gr} \times t)} \qquad ((J/(m^2 \cdot s)) \qquad (3.128)$$

with

$$q_v(t) = H_c(t)/L_v(T_b) \times A \qquad \text{(kg/s)} \qquad (3.122a)$$

where

a_{gr}	=	thermal diffusivity gravel	[m²/s]
q_v	=	vaporisation mass rate	[kg/s]
h_{gr}	=	height gravel layer	[m]
H_c	=	heat flux	[J/(m²·s)]

L_v	=	heat of evaporation	[J/kg]
r_{gr}	=	average radius gravel stones	[m]
$T_{gr,0}$	=	initial gravel temperature	[K]
T_b	=	normal boiling point spilt liquid	[K]
t	=	time from spill	[s]
λ_{gr}	=	thermal conductivity of gravel	[J/(K·m·s)]

The gravel stones have been regarded as a semi-infinite medium, thus the Fourier solution can only be applied to short durations. With respect to the maximum heat content of the stone, equation (3.128) can be applied for times less than

$$t < 0.085 \times r_{gr}^2 / a_{gr} \qquad\qquad (s) \qquad\qquad (3.129a)$$

In this approach the main problem is the assumption of fully wetted gravel stone surface in the bed. The penetration of liquid into the gravel-bed will be hindered by the generated vapour which may be blown out of the gravel-bed; see subsection 3.3.3.1.

It might be reasonable to expect that equation (3.120) will act as an upper limit for the evaporation rate in gravel-beds, while sand can be regarded as tiny gravel stones. Comparing equation (3.128) with (3.120), based on the thermal conductivity and thermal diffusivity of gravel, this assumption means that equation (3.128) holds if

$$0.89 \times \pi \times \frac{h_{gr}}{r_{gr}} \leq 8$$

thus

$$\frac{h_{gr}}{r_{gr}} < 3 \qquad\qquad\qquad (3.129b)$$

Also the spreading of the liquid in the bund determines the speed by which the gravel stones are wetted. Unrealistic predictions of the evaporation rate, especially for short periods from the start of the spill, might relate to a doubtful approximation of the release being instantaneous.

3.5.3.4   Evaporation of a non-boiling liquid in a gravel-bed

It can be expected that the evaporation of non-boiling liquids in gravel will decrease due to partial coverage of the liquid surface.
No model has been derived for the evaporation of non-boiling liquids in gravel. Few data has been reported about experiments related to this topic.
An investigation has been carried out by TNO, with the purpose of determining the influence of partial coverage of a petrol pool on the evaporation. In this research in a wind tunnel, the surface of the liquid was covered with a layer of polypropylene balls, with a diameter of 10-40 millimetres. The results indicated a reduction of the evaporation rate by 60% to 85% depending on wind velocity [Nievergeld, 1978].
For large spills, where the liquid pool may be substantially thicker than the gravel layer, the effects of the penetration into the layer will be small.

3.5.4   Film and nucleate boiling on water surfaces

Shortly after a cryogen spill onto water the liquid will boil vigorously, due to the relative large temperature difference between water and released liquid.

Pool boiling is defined as boiling from a heated surface submerged in a large volume of stagnant liquid. In general three boiling regimes can be distinguished: nucleate boiling, transition boiling and film-boiling. In Figure 6 a qualitative correlation between these boiling regimes and the temperature difference ΔT between liquid and water is given.
The trajectory from the origin until point 3.1 in Figure 6, is characterised by nucleate boiling. Nucleate boiling is the generation of vapour around nuclei. These noncondensable small gas bubbles or foreign bodies held in suspension in the fluid, together with gas or vapour-filled cracks or cavities in solid surfaces (known as nucleation sites), normally provide ample nuclei to act as centres of vapour formation.

Due to the temperature difference between liquid and water, vapour bubbles are generated around evaporation nuclei at the interfacing surface between liquid and water. These bubbles grow bigger due to evaporation and finally come loose.
This bubble formation will increase with an increasing temperature difference between liquid and water. Beyond the temperature difference ΔT_1 between liquid and water, the bubble formation will accelerate so that it will disturb the heat transfer from the water surface to the liquid. The coalescence of bubbles will form an insulation layer (vapour blanket) between liquid and water, leading to a decrease in heat transfer between water and liquid resulting in a decrease in evaporation rate. This type of boiling is called metastable boiling.
Neglecting the additional thermal resistance between the liquid and subsoil may lead to conservative estimates of the heat flux for spilt cryogens.

At a certain temperature difference the boiling rate has reached a (local) maximum value (point 1), which may be considered the end of the nucleate boiling regime.
Further increase of the temperature difference ΔT between liquid and water will decrease the heat transfer within the metastable boiling regime.
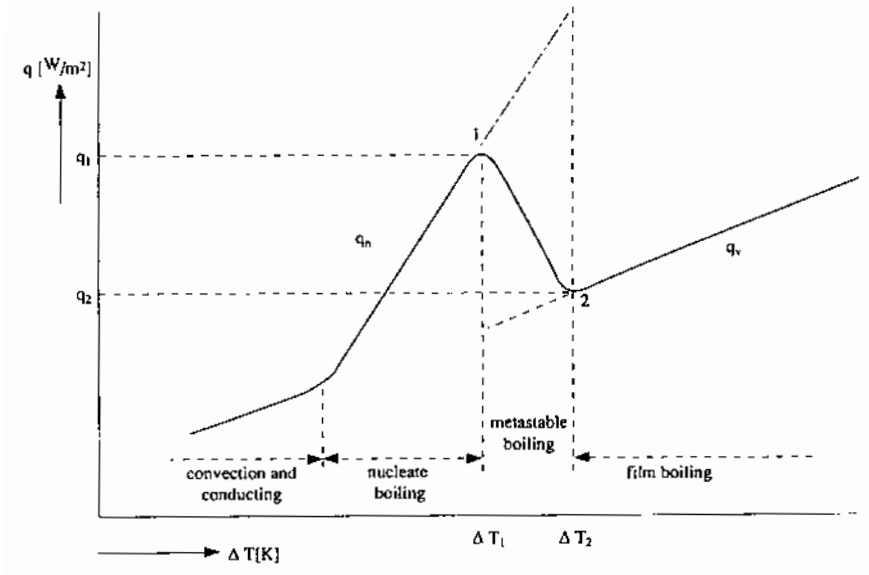
Figure 3.6   Schematic representation of the boiling curve of liquids

At a specific temperature difference between liquid and water ΔT_2, the so-called Leidenfrost temperature, the vaporising liquid becomes completely separated from the water by a vapour film. This regime is called film-boiling.

It appears from the work of Moorhouse and Carpenter that film-boiling can only be achieved on an unheated surface if it is a highly conductive, uncoated metal surface [Webber, 1990]. So, it will be assumed that film-boiling does not take place in the case of a pool on a solid surface. Consideration of film-boiling, then, will be for cryogens floating on water. It must be mentioned however, that in Takeno [1994] it has been reported that liquid oxygen spillt on concrete vaporised above the concrete surface.

As the subsoil surface temperature decreases, the evaporation will become less violent, and so the contact between liquid and subsoil will become better and heat transfer will occur faster in the nucleate boiling regime.

The following method enables the estimation of the boiling rate in the metastable boiling regime [YellowBook, 1988].

The heat flux for nucleate boiling can be estimated by

$$H_{c,n} = 4.1 \times \left(1 + 10 \times \left(\frac{\rho_V}{(\rho_L - \rho_V)}\right)^{2/3}\right)^3 \times \Delta T^3 /$$

$$\left(\sigma \times T_b \times \left(\frac{\sqrt{\upsilon_L}}{\lambda_L} + \frac{10}{\sqrt{(\rho_w \times C_{p,w} \times \lambda_w)}}\right)^2 \times \left(1 + 10 \times \sqrt{\frac{(\rho_L \times C_{p,L} \times \lambda_L)}{(\rho_w \times C_{p,w} \times \lambda_w)}}\right)\right)$$

$$(J/(m^2 \cdot s)) \qquad (3.130)$$

with

3.72

$$\Delta T = (T_w - T_b) \qquad\qquad (K) \qquad (3.130a)$$

where

$C_{p,L}$	=	specific heat liquid	[J/(kg·K)]
$C_{p,w}$	=	specific heat water	[J/(kg·K)]
$H_{c,n}$	=	heat flux in nucleate boiling regime	[J/(m²·s)]
T_w	=	surface temperature water body	[K]
T_b	=	normal boiling point	[K]
ΔT	=	temperature difference	[K]
λ_L	=	thermal conductivity of liquid	[J/(m·s·K)]
λ_w	=	thermal conductivity of water	[J/(m·s·K)]
ρ_L	=	liquid density	[kg/m³]
ρ_V	=	vapour density	[kg/m³]
ρ_w	=	water density	[kg/m³]
υ_L	=	kinematic viscosity liquid	[m²/s]
σ	=	liquid surface tension	[N/m]

The maximum heat flux for nucleate boiling $H_{c,n,max}$ can be estimated by

$$H_{c,n,max} = 0.16 \times L_v \times \sqrt{\rho_V} \times (\sigma \times g \times (\rho_L - \rho_V))^{1/4} \qquad (J/(m^2 \cdot s)) \qquad (3.131)$$

where

g	=	acceleration due to gravity	[m/s²]
L_v	=	heat of vaporisation	[J/kg]
$H_{c,n,max}$	=	maximum heat flux for nucleate boiling	[W/m²]
$\Delta T_{n,max}$	=	$(T_b - T_w)$ corresponding with $H_{c,n,max}$	[K]

From these two equations, the temperature difference $\Delta T_{n,max}$ between the evaporating liquid and the water surface for nucleate boiling, at which the heat flux is at maximum, can be estimated.

For the minimum heat flux for film-boiling, $H_{c,f,min}$ can be estimated by

$$H_{c,f,min} = 0.18 \times \lambda_v \times \Delta T_{f,min} \times \{(g/(\upsilon_v \times a_v)) \times (\rho_L/\rho_{V,av}-1)\}^{1/3}$$

$$(J/(m^2 \cdot s)) \qquad (3.132)$$

with

$$T_{v,av} = (T_b + T_w)/2 \qquad\qquad (K) \qquad (3.133)$$

where

λ_v	=	thermal conductivity vapour	[J/(m·s·K)]
a_v	=	thermal diffusivity vapour	[m²/s]
υ_v	=	kinematic viscosity vapour	[m²/s]
$\rho_{V,av}$	=	vapour density at average temperature	[kg/m³]
$T_{v,av}$	=	average vapour temperature	[K]
$H_{c,f,min}$	=	minimum heat flux for film-boiling	

and the temperature difference $\Delta T_{f,min}$ between the evaporating liquid and the water surface at which film-boiling occurs can be estimated by

$$\Delta T_{f,min} \;=\; (T_c - T_b) \times \left(0.16 + 2.4 \times \frac{(\rho_L \times C_{p,L} \times \lambda_L)}{(\rho_w \times C_{p,w} \times \lambda_w)}\right)^{1/4} \qquad \text{(K)} \qquad\qquad (3.134)$$

where
T_c = critical temperature spilt chemical   [K]
$\Delta T_{f,min}$ = (T_L-T_w) corresponding with $H_{c,f,min}$ [K]

The heat flux during metastable boiling, $H_{c,m}$ can be calculated by means of the following relation

$$H_{c,m} = H_{c,n,max} \times f_T + (1 - f_T) \times H_{c,f,min} \qquad\qquad \text{(J/(m}^2\text{·s))} \qquad (3.135a)$$

with

$$f_T \;=\; \left(1 - \frac{(\Delta T - \Delta T_{n,max})}{(\Delta T_{f,min} - \Delta T_{n,max})}\right)^7 \qquad\qquad\qquad\qquad \text{(-)} \qquad\qquad (3.135b)$$

if

$$\Delta T_{n,max} < \Delta T < \Delta T_{f,min} \qquad\qquad\qquad\qquad \text{(K)} \qquad\qquad (3.136)$$

where
f_T =   function of temperature   [-]
$H_{c,m}$ =   heat flux during metastable boiling   [W/m^2]

The factor f represents an average value which indicates which portion of the heated surface is wetted by the evaporating liquid. For the case f = 1, the water surface is completely wetted by the boiling liquid and nucleate boiling takes place. For f = 0 it is film-boiling. The calculated values for liquids with low-boiling temperatures are in good agreement with some of the scarce experimental results reported in literature.

If $\Delta T < \Delta T_{n,max}$ then use equation (3.130). If $\Delta T > \Delta T_{f,min}$ then use equation (3.107) or (3.117).

For liquids with a boiling temperature close to the water temperature, such as butane and ethylene oxide, the calculated evaporation rates are unrealistically high. For those liquids the following relation has been suggested, assuming heat transfer by convection in the water

$$H_c \;=\; 0.085 \times \lambda_w \times \left(\frac{g \times \alpha_w \times \Delta T^4}{(\upsilon_w \times a_w)}\right)^{1/3} \qquad\qquad \text{(J/(m}^2\text{·s))} \qquad (3.137)$$

with

$$\alpha_w = 1/V \times (\partial V/\partial T)_P \qquad\qquad (1/K) \qquad (3.138a)$$

$$= \frac{1}{\rho} \times (\partial\rho/\partial T)_P \qquad\qquad\qquad (3.138b)$$

and again

$$q_v = H_c/L_v(T_b) \times A \qquad\qquad (kg/s) \qquad (3.122a)$$

where
α_w	=	thermal expansivity of water	[1/K]
λ_w	=	thermal conductivity of water	[J/(m·s·K)]
υ_w	=	kinematic viscosity of water	[m²/s]
a_w	=	thermal diffusivity of water	[m²/s]

Note   The thermal expansivity of water at a temperature of 300 K is equal to $2 \cdot 0 \cdot 10^{-4}$ 1/K [Bolz, 1972].

Note   In Webber [1990] the problem has been simplified by neglecting metastable boiling, with the argument that this approximation should not be too bad within the overall framework of the pool evaporation model; see section 3.5.2.5.

3.5.5   Simple models for evaporation within bunds

3.5.5.1   Boiling liquids

A pool can be considered boiling when the normal boiling point of the spilt chemical is lower than the temperature of the subsoil or the temperature of the water body which it is spilt on. Cryogen will boil off quickly after the release extracting heat mainly from the subsoil. Spilt cryogens boil at a rate mainly controlled by the rate at which heat can get into the liquid from the environment supplying the latent heat of vaporisation. Later on, other heat sources will prevail, like solar heat flux and heat transfer from the atmosphere, but then the liquid pool is not boiling any more.

The simplified approach was based on the following arguments. As long as the liquid pool is boiling, its (average) temperature is remaining constant at normal boiling point, and no latent heat of the pool is withdrawn. Compared to rapid boiling, diffusion of vapour from the liquid into the atmosphere is relatively small. The heat conduction flux from the subsoil at the initial stage is much larger than the heat flux due to other sources. So, by neglecting the small terms in the heat balance, and use of the heat penetration theory, results for instantaneous releases of cryogens onto subsoil in:

$$0 = H_c - q''_v \times L_v \qquad\qquad (J/(m^2 \cdot s)) \qquad (3.139)$$

with

$$H_c(t) = \lambda_s \times (T_{s,0} - T_b)/\sqrt{(a_s \times \pi \times t)} \qquad (J/(m^2 \cdot s)) \qquad (3.140)$$

$T_{s,0}$ = initial subsoil temperature [K]
T_b = normal boiling point spillt liquid [K]

In this simple model the heat balance acts as service-hatch: the evaporation flux from the boiling liquid can directly be related to the time-dependent heat flux from the subsoil.

This one-dimensional model is generally applied. In Webber [1987] it is demonstrated that the implicit assumption of heat transport in the vertical direction is only justified for practical situations.

Note that the effect of spreading, causing the contact between cold liquid and warm subsoil not to be instantaneously established, has been neglected. To avoid an unrealistic high predicted evaporation rate in the initial stages of the spill $t \approx 0$, some delay has to be assumed. It could be a guess how long it will take the liquid to reach the wall of the bund.

When the surface liquid pool A is considered constant, then the evaporation rate at time t can simply be estimated by

$$q_v(t) = qv''(t) \times A = H_c(t)/L_v(T_b) \times A \qquad (kg/s) \qquad (3.122a)$$

Some heat properties of several materials have been given in the table below.

Table 3.5   Heat conduction properties of various materials; note that the italic numbers have been calculated using equation (3.6a): $a = \lambda/(\rho \cdot C_p)$ (3.6a)

Material	λ_s (J/(s·m·K))	ρ_s (kg/m^3)	$C_{p,s}$ (J/(kg·K))	$a_s \times 10^{-7}$ (m^2/s)
Isolation concrete	0.207	900	920	*2.5*
Light concrete	0.418	1800	920	*2.5*
Heavy concrete	1.3	2400	920	*5.9*
Clinkers	0.7	2000	836	*4.2*
Average subsoil 8 wt% moist	0.9	2500	*836*	4.3
Dry sandy subsoil	0.3	1600	799	2.0
Wet sand 8 wt% moist / clay	0.6	*1940*	937	3.3
Wood	0.2	550	2300	*1.6*
Gravel	2.5	2000	1140	11
Carbon steel	46	7840	460	128

3.5.5.2   Non-boiling liquids

After a release of a chemical with a normal boiling point higher than the subsoil temperature or the temperature of the water surface which it is spilt on, the resulting liquid pool will be non-boiling.
The evaporation of (boiling) liquids having normal boiling points near or below ambient temperature, will become non-boiling after the initial boiling stages of the release.
The evaporation of non-boiling liquid pools depends mainly on the rate at which the vapour can be removed by the wind above the pool. Thus, for non-boiling liquids the mass transfer by diffusion will be the limiting factor, especially after the initial stages of the spill.

The simplified approach presented in this paragraph is based on the argument that for relative long duration pool evaporation, the spreading of the liquid pool can be ignored thus assuming the pool reaches its maximum area A immediately. This approach may be a good approximation in case of second containments: bunds.
The heart of the resulting pool evaporation model consists of a relatively simple linear differential equation, which describes the change of the average pool temperature in time.

The vaporisation mass flow rate q_v can be estimated by the equations (3.13), (3.24), and (3.25), i.e. the model by MacKay & Matsugu, [Kawamura and Mackay, 1978]

$$q_v = q''_v \times A \qquad\qquad\qquad (kg/s) \qquad (3.141)$$

with

$$q''_v = k_m \times P_v(T_{ps}) \times \mu_i/(R \times T_{ps}) \qquad (kg/(m^2 \cdot s)) \qquad (3.13)$$

and

$$k_m = C_{m\&m} \times u_{w,10}^{0.78} \times (2 \times r)^{-0.11} \times Sc^{-0.67} \qquad (m/s) \qquad (3.24)$$

with

$$Sc = \upsilon_V/D_a \qquad\qquad\qquad (\text{-}) \qquad (3.25)$$
$$\approx 0.8$$

where
$C_{m\&m}$	=	0.004786	$[m^{0.33}/s^{0.22}]$
D_a	=	diffusion coefficient vapour in air	$[m^2/s]$
k_m	=	mass transfer coefficient related to concentration	$[m/s]$
$P_v(T)$	=	vapour pressure at temperature T	$[N/m^2]$
r	=	liquid pool radius	$[m]$
R	=	international gas constant	$[J/(mol \cdot K)]$
Sc	=	Schmidt number	$[\text{-}]$
T_{ps}	=	liquid temperature at pool surface	$[K]$
$u_{w,10}$	=	wind speed at standard 10 metres height	$[m/s]$
μ_i	=	molecular weight of substance i	$[kg/mol]$
υ_V	=	kinematic viscosity vapour	$[m^2/s]$

It is assumed that the surface temperature of the pool T_{ps} is equal to the temperature of the bulk of the liquid T_p in the pool.

Assuming the specific heat and the liquid density to change little when the liquid pool temperature decreases, the heat balance (3.4) results in

$$\rho_L \times C_{p,L} \times h \times \delta T_p/\delta t \approx \Sigma H - q''_v \times L_v \qquad \text{(J/(m}^2\text{·s))} \qquad \text{(3.142a)}$$

with

$$\Sigma H = H_c + H_a + H_{rl} + H_{rs} \qquad \text{(J/(m}^2\text{·s))} \qquad \text{(3.142b)}$$

so that

$$\delta T_p = (\Sigma H - q''_v \times L_v)/(h \times \rho_L \times C_{p,L}) \times \delta t \qquad \text{(K)} \qquad \text{(3.142c)}$$

Note, that the temperature T_p after a time-step δt, is given by

$$T_p(t + \delta t) = T_p(t) + \delta T_p \qquad \text{(K)} \qquad \text{(3.142d)}$$

where
$C_{p,L}$	=	specific heat liquid	[J/(kg·K)]
h	=	pool depth	[m]
H_c	=	heat flux from subsoil	[J/(m²·s)]
H_a	=	convected heat flux from air	[J/(m²·s)]
H_{rl}	=	long-wave solar radiated heat flux	[J/(m²·s)]
H_{rs}	=	solar radiated heat flux	[J/(m²·s)]
L_v	=	latent heat of vaporisation	[J/kg]
q''_v	=	evaporation flux	[kg/(m²·s)]
t	=	time from the start of the spill	[s]
δt	=	small time-step	[s]
T_p	=	temperature of the liquid pool	[K]
δT_p	=	small temperature step	[K]
ρ_L	=	liquid density	[kg/m³]

While the pool surface area A is constant, application of the mass balance results in

$$\delta h = - q''_v/\rho_L \times \delta t \qquad \text{(m)} \qquad \text{(3.143a)}$$

Note that the pool height h after a time-step δt, is given by

$$h(t + \delta t) = h + \delta h \qquad \text{(m)} \qquad \text{(3.143b)}$$

where
δh = small change in pool depth   [m]

The heat flux from the atmosphere: by convection H_a, and solar radiated heat flux H_{rs}, H_{rl} can be estimated by the methods addressed in paragraph 3.2.2.
The estimation of the instationary heat flux from the ground H_c encounters some difficulties. First, the liquid temperature T_p is not constant.

But, due to the relatively fast (negative) heat penetration into the subsoil, the temperature decrease of the pool may be neglected, so applying equation (3.7) results in

$$H_c(t) = \lambda_s \times (T_s - T_p(t)) / \sqrt{(a_s \times \pi \times t)} \qquad (J/(m^2 \cdot s)) \qquad (3.144)$$

T_s = initial subsoil temperature   [K]
a_s = thermal diffusivity subsoil   [m²/s]
λ_s = thermal conductivity subsoil [J/(m·s·K)]

Equation (3.144) above predicts unrealistically high vaporisation fluxes for times shortly after the start of the release, causing numerical difficulties. Furthermore, the assumption of reaching its final pool diameter instantaneously, is not physically realistic.
A practical solution is to define a time t_{sp} necessary for the liquid to spread, let us say $t_{sp} \approx 20$ s. For times shorter than this spreading time, the heat flux is per definition equal to the heat flux half-way the spreading, so

$$H_c(t) = \lambda_s \times (T_s - T_p(t)) / \sqrt{(a_s \times \pi \times t_{sp}/2)} \quad \text{for } t < t_{sp} \qquad (J/(m^2 \cdot s)) \qquad (3.145a)$$

$$H_c(t) = \lambda_s \times (T_s - T_p(t)) / \sqrt{(a_s \times \pi \times t)} \qquad \text{for } t \geq t_{sp} \qquad (J/(m^2 \cdot s)) \qquad (3.145b)$$

3.5.5.3   Transition boiling to non-boiling

Due to the decreasing temperature of the subsoil the effect of heat conduction from the subsoil will diminish in time. The initially boiling liquid pool will stop boiling eventually. During the transition neither the control by the rate at which heat can get into the liquid from the environment supplying the latent heat of vaporisation, nor the rate at which the vapour can be removed by the air flow above the pool, will be dominant. This is also the case for substances which boil close to ambient temperature like butane.
Both mechanisms for evaporation, controlled by heat transfer and controlled by diffusion, will in fact always be apparent. The first mechanism is dominant in case of a cryogenic spill just after the release, and the second will be dominant in case of a spill of a volatile liquid after quite some time after the release or in case of non-volatile spills.

3.5.6   HACS-R

3.5.6.1   Introduction

When a soluble chemical is spilt on water, it may rapidly dissolve. Chemicals may not only be miscible with water, but may also maintain high vapour pressures at ambient temperature. When such liquids are spillt vapour may be generated from the water surface.

The objective of the model HACS-R is to predict the vaporisation rate, the area and the duration over which the vapour evolvement takes place, if a highly water-soluble, high-vapour-pressure liquid is spillt on a water surface in a non-tidal river.

The description of the model has been taken from the NTIS-report 'Assessment Models in support of the Hazard assessment handbook, by Ph.K. Raj, et al., [1974].

It is assumed that the entire liquid spillt goes into solution in water first. After estimating the liquid concentration in the water, the vapour pressure on the water surface of the chemical can be estimated, as well as the vaporisation rate.
The vaporisation of the chemical takes place only at the water surface, and is caused by the difference in the (partial) vapour pressure of the solved chemical at the water surface and in the atmosphere.

The model is based on the following assumptions:
1. The spill will be considered as an instantaneous point source.
2. The entire mass of the liquid spill goes into solution with water.
3. The chemical spillt reaches the temperature of the water immediately after the spill.
4. Heat transfer, chemical reaction, or phase change effects will not be considered, the total mass of the liquid which is mixing with water remains constant.
5. Settling of liquid due to higher density effects will be ignored

The following data are required to calculate the vapour evolvement rate in a non-tidal river:
1. Mass of liquid spillt.
2. Saturated vapour pressure at water temperature.
3. Vapour pressure as a function of the concentration of liquid data, if Raoult's law (equation 3.166) doesn't hold.
4. River characteristics like depth, width, mean stream velocity and roughness factor.

3.5.6.2 Model description

Introduction

First, a more general model for mixing and dilution in a uniform river is described. It must be mentioned that in general the vapour pressures of solved volatile non-boiling chemicals are so low, that in the far field only very low atmospheric concentrations above the water surface can be expected.
Nevertheless the so-called far field approximation has been given also in order to supply a full description of water dispersion in a river.
Secondly, the model for vapour evolvement from the water surface is described, related to near field approximation.

Mixing and dilution model in a uniform river

The aim of the dispersion submodel is to provide a method for the estimation of liquid concentrations in water in the initial stages after the spill of a water-miscible liquid. The model cannot be applied to lakes, tidal rivers, estuaries, and open sea.

The phenomenon of mixing is generally described theoretically by the classical diffusion equations with one or more dispersion coefficients. The models described are valid for the dispersion of neutrally buoyant liquids that dissolve in water.

Harleman has correlated from experimental data dispersion coefficients for dispersion of pollutants in rivers. These correlations are presented here.

For an instantaneous spill on the surface in the middle of the river at the point (0,b,0), the concentration is given by

$$c_i(x,y,z,t) = \frac{2 \times Q_L}{((4\pi \times t)^{3/2} \times \sqrt{(D_x \times D_y \times D_z)})} \times F_x \times F_y \times F_z \qquad (kg/m^3) \qquad (3.146a)$$

with

$$F_x = \exp\left(-C_{d1} \times t - \frac{(x - u_s \times t)^2}{(4 \times D_x \times t)}\right) \qquad (\text{-}) \qquad (3.146b)$$

$$F_y = \exp\left(-\frac{(y - y_{sp})^2}{(4 \times D_y \times t)}\right) + \exp\left(-\frac{(y - y_{sp} - 2 \times b)^2}{(4 \times D_y \times t)}\right) +$$

$$\exp\left(-\frac{(y + y_{sp} - 2 \times b)^2}{(4 \times D_y \times t)}\right) \qquad (\text{-}) \qquad (3.146c)$$

$$F_z = \exp\left(-\frac{z^2}{(4 \times D_z \times t)}\right) + \exp\left(-\frac{(z - 2 \times h_d)^2}{(4 \times D_z \times t)}\right) \qquad (\text{-}) \qquad (3.146d)$$

where

b	=	half width of the river	[m]
c_i	=	concentration chemical i in water	[kg/m^3]
C_{d1}	=	first order decay coefficient	[1/s]
D_i	=	dispersion coefficient along the i-coordinate	[m^2/s]
Q_L	=	mass spillt chemical	[kg]
u_s	=	mean stream velocity	[m/s]
y_{sp}	=	distance spill centre to river middle	[m]
t	=	time from the instantaneous release	[s]
x	=	coordinate along-stream	[m]
y	=	coordinate across-stream	[m]
z	=	coordinate in depthwise direction	[m]

Equation (3.146a) implicitly assumes that there is no loss of solved chemical through the banks of the river.

For the initial stages of dispersion, this so-called near-field approximation, the following holds. Harleman has given the following turbulent dispersion coefficients for narrow and wide rivers.

Dispersion coefficients for very wide rivers ($2 \times b/h_d > 100$)

$$D_z = 0.067 \times u_* \times h_d \qquad\qquad (m^2/s) \qquad (3.147a)$$

$$D_x = 0.1 \times D_z \qquad\qquad (m^2/s) \qquad (3.147b)$$

$$D_y = 0.1 \times D_z \qquad\qquad (m^2/s) \qquad (3.147c)$$

Dispersion coefficients for narrow rivers ($2 \times b/h_d < 100$)

$$D_z = 0.067 \times u_* \times r_h \qquad\qquad (m^2/s) \qquad (3.148a)$$

$$D_x = 0.1 \times D_z \qquad\qquad (m^2/s) \qquad (3.148b)$$

$$D_y = 0.23 \times u_* \times r_h \qquad\qquad (m^2/s) \qquad (3.148c)$$

with

$$r_h = h_d \times b/(h_d + 2 \times b) \qquad\qquad (m) \qquad (3.148d)$$

where
u_* = shear velocity   [m/s]
r_h = hydraulic radius river   [m]
h_d = river depth   [m]

Note, that the value D_z is the mean of the vertical distribution given by

$$D_z = 0.4\, u_* \times h_d \times (z/h_d) \times (1 - z/h_d) \qquad (m^2/s) \qquad (3.149)$$

The type of river influences the dispersion of a solved chemical. The estimation of dispersion coefficient D_y depends on the shear velocity u_* which is related to the so-called Manning roughness factor C_{MRF}. The shear velocity is by definition equal to

$$u_* = \sqrt{\tau_0/\rho_L} \qquad\qquad (m/s) \qquad (3.150)$$

where
τ_0 = wall shear stress   [N/m^2]
ρ_L = density chemical   [kg/m^3]

and can be calculated by

$$u_* = C_{u*} \times C_{MRF} \times u_s/r_h^{1/6} \qquad\qquad (m/s) \qquad (3.151)$$

with

$$C_{u*} = 3.115 \ m^{1/6} \qquad\qquad (3.151a)$$

where
C_{MRF} = Manning roughness factor   [-]

In the table below some Manning roughness factors are listed.

Table 3.6   *Manning roughness factor for several natural stream channels*

Natural stream channels	C_{MRF}
clean, straight bank, full stage	0.030
winding, some pools and shoals	0.040
same, but with stony sections	0.055
sluggish reaches, very deep pools, very weedy	0.070 - 0.125

It is assumed that the spreading model is valid until a noticeable concentration will be apparent near the river banks. The time t_c for this to happen will be approximately

$$t_c = b^2/D_y \qquad \text{(s)} \qquad (3.152)$$

The 'initial period' t_I is defined as the period up to which equation (3.146a) can be used to predict the concentration

$$t_I = 0.3 \times t_c \qquad \text{(s)} \qquad (3.153)$$

Equation (3.146a) might be used for periods larger than the initial period when terms are included related to the influence of image source terms in the equations, to prevent dispersion through the boundaries.
For periods of time larger than t_I the one-dimensional analysis to describe the mean concentration is used; this is the so-called 'far field approximation'. The concentration is then derived from

$$\partial c_i/\partial t + u_s \times \partial c_i/\partial x = 1/A_s \times \partial(D \times A_s \times \partial c_i/\partial x)/\partial x \qquad \text{(kg/(m}^3\text{·s))} \qquad (3.154)$$

A_s = cross-sectional area river   [m^2]

For an instantaneous spill the local concentration at any time is given by

$$c_i(x,t) = \frac{Q_L}{(A_s \times \sqrt{(4\pi \times D \times t)})} \times \exp\left(-C_{d1} \times t - \frac{(x - u_s \times t)^2}{(4 \times D \times t)}\right)$$
$$\text{(kg/m}^3\text{)} \qquad (3.155)$$

C_{d1} = first order decay coefficient   [1/s]
D = dispersion coefficient   [m^2/s]

For convenience the decay coefficient is introduced in the equation to account for possible unstable or reactive spillt chemicals.
Elder's equation gives the dispersion coefficient D as functions of the river characteristics

$$D = C_{DE} \times n \times u_s \times r_h^{5/6} \qquad \text{for } 2 \times b/h_d > 100 \qquad \text{(m}^2\text{/s)} \qquad (3.156)$$

with

$$C_{DE} = 63 \text{ m}^{1/6} \qquad\qquad (3.156a)$$

and lacking velocity distribution of the river in general, as a first approximation

$$D/(r_h \times u_*) \approx 225 \quad \text{for } 2 \times b/h_d < 100 \qquad\qquad (\text{-}) \qquad\qquad (3.157)$$

Vapour evolvement from the water surface

The calculation procedure is illustrated by the scheme below.

1. Input:
    a. Properties of chemical
    b. Environmental conditions
    c. Spill quantity
2. Calculation mass transfer coefficient
3. Calculation of characteristic parameters
4. Calculation of non-dimensional evaporation rates
5. Integration by Simpson rule

6. Result:
    a. Total mass of vapour evolved
    b. Vaporisation rate
    c. Maximum duration vapour evolvement

Neglecting the contribution from image sources and decay of the spillt chemical, the near field model for dispersion in water can be described by

$$c_i(x,y,z,t) = 2 \times Q_L/((4\pi \times t)^{3/2} \times \sqrt{(D_x \times D_y \times D_z)}) \times$$

$$\exp\left(-\frac{(x - u_s \times t)^2}{(4 \times D_x \times t)} - \frac{y^2}{(4 \times D_y \times t)} - \frac{z^2}{(4 \times D_z \times t)}\right) \qquad (\text{kg/m}^3) \qquad (3.158)$$

where

c_i	=	concentration chemical i in water	[kg/m^3]
D_i	=	dispersion coefficient along the i-coordinate	[m^2/s]
Q_L	=	mass spillt chemical	[kg]
u_s	=	steam velocity	[m/s]
t	=	time from the instantaneous release	[s]
x	=	coordinate along-stream	[m]
y	=	coordinate across-stream	[m]
z	=	coordinate in depthwise direction	[m]

Remark: the origin of the coordinate system lies in middle of the river at the water surface.
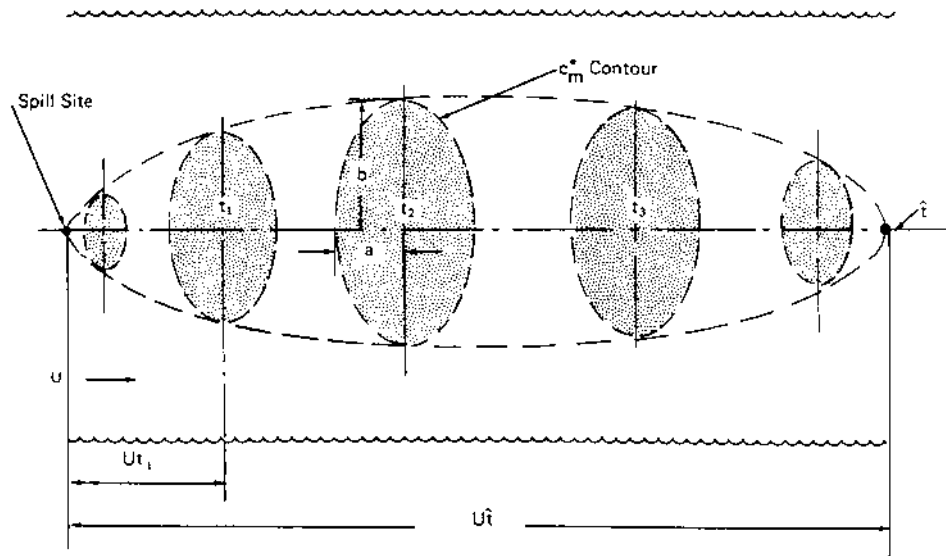
Figure 3.7   Schematic illustration of the evaporation area on water [Raj, 1974]

Equation (3.158) can be used to calculate the concentration of the liquid on the water surface at any position at any time.

The equation above is a solution to the diffusion equation, it predicts finite but exponentially small concentrations at large distances from the point of spill in very shortly after the instantaneous release.

The molar fractional concentration m_m of the spilt chemical in water is given by

$$m_m = 1/(1 + \rho_w/c_i \times (\mu_L/\mu_w)) \qquad (-) \qquad (3.159)$$

ρ_w	=	water density	[kg/m^3]
c_i	=	concentration chemical i in water	[kg/m^3]
μ_L	=	molecular weight of spillt liquid	[kg/mol]
μ_w	=	molecular weight of water	[kg/mol]

A molar concentration m_{m*} may be defined such that the evaporation from water surface having a molar concentration of less than m_{m*}, is negligibly small. The value of m_{m*} is quite arbitrary and may have to be chosen properly for different chemicals. By choosing a value for m_{m*} the area is actually limited from which evaporation can occur. It is estimated that the effect of evaporation is quite small from areas where the vapour pressure is less than 5% of the saturated vapour pressure.

The spill will move downstream with the stream velocity. The regions where the concentrations are greater than m_{m*}, are ellipsoidal. The equation to these ellipses is obtained from equation (3.158). The semi-axes lengths for these elliptical areas are given by

$$r_a(t) = \sqrt{(4 \times D_x \times t \times \ln(c_{max}(t)/c_*))} \qquad (m) \qquad (3.160)$$

$$r_b(t) = \sqrt{(4 \times D_y \times t \times \ln(c_{max}(t)/c_*))} \qquad\qquad \text{(m)} \qquad (3.161)$$

where c_* is the limiting concentration in units of mass/volume, which is a more or less arbitrarily value that may be related to flammability limits or toxicity limits.

At the centre of the elliptical area the concentration is a maximum and is given by

$$c_{i,\,max}(t) \;=\; \frac{2 \times Q_L}{(4 \times \pi \times t)^{3/2} \times \sqrt{(D_x \times D_y \times D_z)}} \qquad\qquad \text{(kg/m}^3\text{)} \qquad (3.162)$$

If now $t_{c\,<\,lim}$ is set equal to the time beyond which the concentration in water of the liquid spilt is below m_{m*} everywhere in the water, then the so-called characteristic time can be calculated by

$$t_{c<lim} = 1/(4 \times \pi) \times (2 \times Q_L/(c_* \times \sqrt{(D_x \times D_y \times D_z)}))^{2/3} \qquad \text{(s)} \qquad (3.163)$$

The rate of evaporation per unit area q''_v may be expressed by

$$q''_v = k_{m,P} \times P_{v,i} \qquad\qquad (3.164)$$

where
$k_{m,p}$ = mass transfer coefficient related to partial pressure [s/m]

note that

$$q''_v = k_m \times c_i \qquad\qquad \text{(kg/(m}^2 \cdot \text{s))}$$

where
k_m = mass transfer coefficient related to concentration   [m/s]

Applying ideal gas law, it can easily be derived that

$$k_{m,P} = k_m \times \mu_i/(R \times T) \qquad\qquad \text{(s/m)} \qquad (3.165)$$

It is assumed that the vapour pressure of the solved chemical follows Raoult's law by which the (partial) vapour concentration is proportional with the molar fraction of the diluted chemical in the water

$$P_i = m_m \times P_v°(T) \qquad\qquad \text{(N/m}^2\text{)} \qquad (3.166)$$

where P_i is the partial pressure of the vapour of the liquid spillt at the water surface, and $P_v°(T)$ is the saturated vapour pressure at temperature T.
Raoult's law is quite close to the actual relationship for most chemicals.

So, that

$$q''_v = k_{m,P} \times m_m \times P_v°(T) \qquad\qquad \text{(kg/(m}^2 \cdot \text{s))} \qquad (3.167)$$

The mass transfer coefficient for surface evaporation is estimated from forced convection boundary layer theory. The heat mass transfer analogy yields the following equations for flow over a flat plate

$$k_m \times L/D_a = 1.328 \times Sc^{1/3} \times Re^{1/2} \quad \text{for laminar flow } (Re < 5 \times 10^5) \qquad (3.168a)$$

$$k_m \times L/D_a = 0.037 \times Sc^{1/3} \times Re^{0.8} \quad \text{for turbulent flow } (Re > 5 \times 10^5) \qquad (3.168b)$$

with

$$Re = \rho_a \times u_{w,10} \times L/\eta_a \qquad (-) \qquad (3.168c)$$

$$Sc = \upsilon_V/D_v \qquad (-) \qquad (3.25)$$
$$\approx 0.8$$

where
c_i = atmospheric vapour concentration just $\quad$ [kg/m^3]
$\quad$ at the evaporating pool surface
D_a = diffusion coefficient chemical in air $\quad$ [m^2/s]
k_m = mass transfer coefficient related to concentration $\quad$ [m/s]
L = characteristic length of the spill $\quad$ [m]
Re = Reynold number $\quad$ [-]
Sc = Schmidt number $\quad$ [-]
υ_V = kinematic vapour viscosity $\quad$ [m^2/s]

The characteristic length used here is the length of spill which is defined by

$$L = V_i^{1/3} \qquad (m) \qquad (3.169)$$

where V_i is the initial spill volume. It is assumed that the mass transfer will not change in spite of the fact that the pool is expanding.

Integrating equation (3.167) over the vaporisation area (3.160/161) results in an expression for the total evaporation rate at any instant

$$q_v = k_{m,P} \times P_v^0 \times \int_0^A m_m \times dA \qquad (kg/s) \qquad (3.170)$$

The integral should be taken over the elliptical area on whose boundary the concentration is m_{m*}. It can be shown that

$$\int_0^A m_m \times dA = \pi \times r_a \times r_b \times m_{m\,mean} \qquad (m^2) \qquad (3.171)$$

with

$$m_{m,mean} = (m_{m,max} - m_m)/\ln(m_{m,max}/m_{m*}) \qquad (-) \qquad (3.172)$$

Note that r_a and r_b, representing the dimensions of the ellipsoidal evaporation area on the water surface, are given by equations (3.160/161).

Combining equations (3.170) and (3.171) yields

$$q_v = \pi \times k_{m,P} \times P_v^\circ \times r_a \times r_b \times m_{m,mean} \qquad \text{(kg/s)} \qquad (3.173)$$

Defining the following characteristic values

$$q_{ch} = 4 \times \pi \times t_{c<lim} \times \sqrt{(D_x \times D_y)} \times k_{m,P} \times P_v^\circ(T) \qquad \text{(kg/s)} \qquad (3.174)$$

$$Q_{ch} = q_{ch} \times t_{c<lim} \qquad \text{(kg)} \qquad (3.175)$$

$$\tau = t/t_{c<lim} \qquad \text{(-)} \qquad (3.176)$$

$$Q_R = Q_v/Q_{ch} \qquad \text{(-)} \qquad (3.177)$$

Q_v = mass of vapour evolved [kg]
Q_{ch} = characteristic vapour mass [kg]
Q_R = dimensionless mass of evolved vapour [-]

and noting that

$$q_R = q_v/q_{ch} \qquad \text{(-)} \qquad (3.178)$$

q_R = dimensionless evaporation rate [-]
q_{ch} = characteristic evaporation rate [kg/s]
q_v = liquid evaporation rate [kg/s]

Using equations (3.173), (3.160/161), and (3.163), results in

$$q_R(\tau) = -3/2 \times \tau \times \ln(\tau) \times m_{m,mean}(\tau) \qquad \text{(-)} \qquad (3.179)$$

The total mass of vapour Q_v evolved up to time $t_{c<lim}$ is given by

$$Q_v = Q_R \times Q_{ch} \qquad \text{(kg)} \qquad (3.180)$$

with

$$Q_R = \int_0^1 q_R \times d\tau = \int_0^1 -3/2 \times \tau \times \ln(\tau) \times m_{m.mean}(\tau) \times d\tau \qquad (3.181)$$

The evaluation of the integral in equation (3.181) has to be done numerically because of the complicated nature of the integral. However, certain observations can be made from the equation.

It is evident that $m_{m,mean} \geq m_{m^*}$, so that replacing the value of $m_{m,mean}$ by m_{m^*} results in a minimum value for m

$$Q_{R,min} = 3/8 \times m_{m^*} \qquad \text{(-)} \qquad (3.182)$$

Similarly, by replacing $m_{m,mean}$ by $m_{m,max}$ corresponding to the maximum molar concentration, the maximum value for Q_R can be shown to be

$$Q_{R,max} = -3/2 \times \int_0^1 \tau \times \ln(\tau)/\{1 + \rho_w \times \mu_L \times \tau^{3/2}/(c_* \times \mu_w)\} \times d\tau \quad (-) \qquad (3.183)$$

If $m_{m,mean}$ is replaced by 1, which would be the absolute maximum value for concentration, then the maximum evaporation m would be equal to 3/8. Then the maximum possible evaporation is set by

$$Q_v = 3/8 \times Q_{ch} \qquad \text{(kg)} \qquad (3.184)$$

The maximum distance where vapour may evolve from the water surface having a concentration larger than the limiting concentration m_{m*}, is given by

$$x_{c<lim} = u \times t_{c<lim} \qquad \text{(m)} \qquad (3.185)$$

3.5.6.3   Remarks

The model given is based on mixing and dilution in water of a spillt liquid and a relatively small amount of evaporation caused by the difference of vapour concentration at the water surface and the atmosphere. It has been assumed that all of the liquid would go into solution. This assumption is valid because it appears that the total vapour generated is a small fraction of the mass spillt.

This is because even though the evaporation is high, in case of a high partial vapour pressure of the spillt chemical, the duration for which vaporisation can occur is primarily determined by the rapidity of mixing of the liquid in water. The more turbulent a stream is, the better the mixing, and the quicker the time in which the concentration everywhere in the water is less than the critical.

In reality the release of chemical takes place in a finite period. Since even in the case of an instantaneous spill, the mass of vapour evolved appears a small fraction of the mass spillt, the predictions can be regarded safely as the worst case for long duration spills. It should be kept in mind that any vaporisation of the spillt liquid during the release process before water contact, has not been taken into account.

3.5.6.4   Releases of ammonia

Ammonia is an industrial commodity soluble in water, but the release of ammonia onto water can not be expected to solve in the water to the full amount of the release.

Ammonia spillt onto water will solve or react to ammonium hydroxide (matter of definition) generating a relatively large amount of heat, by the reaction

$$NH_{3_{(l)}} + H_2O_{(l)} = (NH_4^+)_{aq} + (OH^-)_{aq}$$
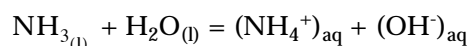
According to Raj and Reid, for an instantaneous ammonia release, about 30% of the spill will evolve from the water surface immediately due to vigorous boiling caused by the reaction heat or mixing heat generated [Melhelm, 1993].

However, this was based on small-scale experiments. But according to Raj in his chapter 'Volatile liquids' in the Hazardous Material Spills Handbook, part 4 'Ammonia', in larger spills approximately 50 percent of the spillt liquid vaporised.

This indicates the effects of the dynamics of a spill on vaporisation.
So, it is advisable to assume that on average about 40% of a spill will evaporate immediately. This fraction has been used in other studies that are not publicly available.
The remaining 60% of the spill will solve into the water, and will evaporate gradually, and model HACS-R may be applied for this part of the ammonia spill. Note that the ammonium hydroxide solution will be warm, and will disperse in the water as a stably stratified fluid. This effect has not been taken into account in the model. Perhaps needless to say, that for short duration releases the flashing of the cryogen ammonia from the water surface has to be taken into account.

Proper estimation of vapour pressures of the components in the solution is critical, since this property has a large and direct effect on the evaporation rate. In multi-component spills the partial vapour pressure depends on the composition of the mixture.
For multi-component liquid pools the evaporation rate will decrease in time also due to the change in composition, while the most volatile components will evaporate first. So, the vapour pressure is dependent on the composition.
For an ammonia-water mixture the following correlations have been derived [Mikesell, 1993]:

$$\ln(P_{v,NH3}/101325.) = 17.17 - 4294/T + 0.1370 \times m_{w,NH3} - 0.00347 \times m_{w,NH3}^2$$
$$+ 23.01 \times m_{w,NH3}/T \qquad (-) \qquad (3.186a)$$

$$\ln(P_{v,H2O}/101325.) = 18.37 - 4552/T + 0.1477 \times m_{w,NH3} - 0.00081 \times w_{w,NH3}^2$$
$$- 43.53 \times m_{w,NH3}/T \qquad (-) \qquad (3.186b)$$

$m_{w,NH3}$	=	mass fraction solved ammonia in water	[kg/kg]
T	=	absolute temperature ammonia-water mixture	[K]
$P_{v,NH3}$	=	partial vapour pressure ammonia	[N/m²]
$P_{v,H2O}$	=	partial vapour pressure water	[N/m²]

Note
1 atm = 101325 N/m².

3.6 Application of the selected models: calculation examples

3.6.1 Introduction to section 3.6

Some models presented in subsection 3.5, HACS-R and especially GASP, are rather complex models. It is practically not possible to perform the calculations by hand or step by step.

Section 3.6 provides examples using the models and methods described in section 3.5. Subsection 3.6.2 provides example calculations with the GASP model for the spreading of liquids on solid subsoil and water, presented in 3.5.2.
Subsection 3.6.3 provides example calculations with the HACS-R model for spills of volatile liquids that solve in water, as presented in 3.5.6.
Subsection 3.6.4 provides example calculations for various supplementary models as has been addressed in section 3.5.

3.6.2 Calculation example GASP

Introduction

GASP models an instantaneous spill of liquid chlorine released from a tank railway wagon onto land. The pool spread is unrestricted.
The initial, cylindrical, pool of chlorine has a radius of 9.16 m (area 263.597 m^2) and volume 65.95 m^3 (implying a depth of 0.250192 m). The rate at which the pool will evaporate is calculated by GASP from knowledge of the ground properties and the atmospheric conditions. The release temperature (239.12 K) is also important. Heat is being transfered from the ground (conductivity 2.5 W/(m·K), diffusivity 11 m^2/s) into the pool. Perfect thermal contact is assumed.
The atmospheric temperature is 15 ˚C and the windspeed is 1.5 m/s.
The net solar radiation can be estimated by equations (4.36) and (4.37) presented in chapter 4 'Vapour cloud dispersion'.
However, for the sake of simplicity a value of 100 kW/m^2 has been chosen.

Initial pool conditions

Initial volume of pool	V	= 65.95	m^3
Initial radius of pool	r	= 9.160	m
Initial depth of pool	h	= 0.2502	m
Initial front velocity	u	= 0.0000	m/s
Initial temperature	T$_0$	= 238.1	K

Atmospheric conditions

Wind speed at 10 metres	u$_{a,10}$	= 1.500	m/s
Ambient temperature	T$_a$	= 288.2	K
Atmospheric friction velocity	u$_*$	= 8.6859E-02	m/s
Roughness length	z$_{0,a}$	= 1.0000E-02	m
The pool has roughness length	z$_{0,p}$	= 2.3000E-04	m

Heat transfer from subsoil to the pool

Thermal conductivity	λ_s	= 2.500	J/(s·m·K)
Thermal diffusivity	a_s	= 11.00	m^2/s

Physical properties of chlorine

Molecular weight	μ_i	= 70.91·10⁻³	kg/mol
Melting point	T_m	= 172.2	K
Boiling point	T_b	= 239.1	K
Critical temperature	T_c	= 417.0	K
Latent heat (at boiling)	$L_v(T_b)$	= 2.8810E+05	J/kg
Latent-heat-index	n	= 0.3800	
Antoine coefft. A	C_A	= 15.96	
Antoine coefft. B	C_B	= 1978.	K
Antoine coefft. C	C_C	= -27.01	K
Specific heat liquid	$C_{p,L}$	= 951.4	J/(kg·K)
Specific heat vapour	$C_{p,V}$	= 465.5	J/(kg·K)
Liquid density	ρ_L	= 1559.	Kg/m^3
Surface tension	σ	= 2.6405E-02	J/m^2
Liquid viscosity	η_L	= 4.9024E-04	N·s/m^2
Vapour viscosity	η_V	= 1.0919E-05	N·s/m^2
Thermal conductivity liquid	λ_L	= 0.1661	J/(m·s·K)
Thermal conductivity vapour	λ_V	= 7.5856E-03	J/(m·s·K)
Molecular diffusivity	D	= 8.0513E-06	m^2/s

Physical properties of air

Density	ρ_a	= 1.225	kg/m^3
Viscosity	η_a	= 1.7894E-05	N·s/m^2
Kinematic viscosity	υ_a	= 1.4607E-05	m^2/s
Prandtl number	Pr_a	= 0.7104	
Molecular weight	μ_a	= 28.96E-03	kg/mol

Constants

Turbulent friction parameter	C_f	= 1.3E-03	
Von Karman's constant	κ	= 0.4	
Turbulent Schmidt number	Sc_t	= 0.85	
Turbulent Prandtl number	Pr_t	= 0.85	
Laminar Schmidt number	Sc_l	= 1.814	

Output

Maximum vaporisation rate	$q_{S,max}$	= 52.71	kg/s
After time	t	= 26.22	s
Pool has evaporated at time	t	= 5638.	s

t (s)	r (m)	Q_v (kg)	h (m)	V_d (m^3)
0.0000	9.160	0.0000	0.2502	65.95
2.8482E-07	9.160	1.9688E-06	0.2502	65.95
5.6965E-07	9.160	3.9377E-06	0.2502	65.95
8.5447E-07	9.160	5.9065E-06	0.2502	65.95
3.5060E-06	9.160	2.4235E-05	0.2502	65.95
6.1575E-06	9.160	4.2563E-05	0.2502	65.95
8.8090E-06	9.160	6.0891E-05	0.2502	65.95
2.4248E-05	9.160	1.6761E-04	0.2502	65.95
3.9687E-05	9.160	2.7433E-04	0.2502	65.95
5.5125E-05	9.160	3.8105E-04	0.2502	65.95
1.1684E-04	9.160	8.0767E-04	0.2502	65.95
1.7856E-04	9.160	1.2343E-03	0.2502	65.95
2.4028E-04	9.160	1.6609E-03	0.2502	65.95
4.2861E-04	9.160	2.9627E-03	0.2502	65.95
6.1694E-04	9.160	4.2645E-03	0.2502	65.95
8.0527E-04	9.160	5.5664E-03	0.2502	65.95
1.2764E-03	9.160	8.8229E-03	0.2502	65.95
1.7475E-03	9.160	1.2079E-02	0.2502	65.95
2.2186E-03	9.160	1.5336E-02	0.2502	65.95
3.2082E-03	9.160	2.2177E-02	0.2502	65.95
4.1979E-03	9.160	2.9017E-02	0.2502	65.95
5.1875E-03	9.160	3.5858E-02	0.2502	65.95
7.0839E-03	9.160	4.8966E-02	0.2502	65.95
8.9802E-03	9.160	6.2074E-02	0.2502	65.95
1.0877E-02	9.160	7.5182E-02	0.2502	65.95
1.2773E-02	9.160	8.8290E-02	0.2502	65.95
1.7217E-02	9.160	0.1190	0.2502	65.95
2.1662E-02	9.160	0.1497	0.2502	65.95
2.6106E-02	9.160	0.1804	0.2502	65.95
3.0551E-02	9.161	0.2112	0.2502	65.95
3.9682E-02	9.161	0.2743	0.2501	65.95
4.8813E-02	9.161	0.3374	0.2501	65.95
5.7944E-02	9.162	0.4005	0.2501	65.95
6.7076E-02	9.162	0.4636	0.2501	65.95
8.2946E-02	9.164	0.5734	0.2500	65.95
9.8816E-02	9.165	0.6831	0.2499	65.95
0.1147	9.167	0.7929	0.2498	65.95
0.1306	9.169	0.9027	0.2497	65.95
0.1594	9.174	1.102	0.2494	65.95
0.1882	9.179	1.302	0.2492	65.95
0.2170	9.185	1.502	0.2488	65.95
0.2458	9.192	1.702	0.2484	65.95
0.2746	9.200	1.902	0.2480	65.95
0.3227	9.216	2.237	0.2472	65.95

t (s)	r (m)	Q_v (kg)	h (m)	V_d (m^3)
0.3708	9.233	2.574	0.2462	65.95
0.4189	9.253	2.911	0.2452	65.95
0.4670	9.276	3.250	0.2440	65.95
0.5150	9.301	3.591	0.2427	65.95
0.5868	9.342	4.103	0.2405	65.95
0.6585	9.389	4.619	0.2381	65.95
0.7302	9.441	5.140	0.2355	65.95
0.8019	9.497	5.667	0.2327	65.95
0.8736	9.559	6.200	0.2297	65.95
0.9453	9.625	6.740	0.2266	65.95
1.047	9.727	7.522	0.2218	65.95
1.150	9.839	8.322	0.2168	65.95
1.252	9.959	9.139	0.2117	65.95
1.354	10.09	9.977	0.2063	65.95
1.456	10.22	10.84	0.2008	65.95
1.558	10.37	11.72	0.1953	65.95
1.676	10.54	12.76	0.1889	65.95
1.794	10.72	13.85	0.1825	65.95
1.911	10.92	14.97	0.1762	65.95
2.029	11.11	16.13	0.1699	65.95
2.147	11.32	17.33	0.1638	65.95
2.265	11.53	18.57	0.1578	65.95
2.382	11.75	19.86	0.1520	65.95
2.559	12.08	21.88	0.1437	65.95
2.735	12.43	24.01	0.1359	65.95
2.881	12.72	25.86	0.1297	65.95
3.027	13.02	27.80	0.1238	65.95
3.173	13.32	29.83	0.1183	65.95
3.319	13.62	31.95	0.1131	65.95
3.465	13.93	34.16	0.1082	65.95
3.612	14.24	36.47	0.1035	65.95
3.758	14.54	38.87	9.9198E-02	65.95
3.976	15.00	42.64	9.3204E-02	65.95
4.194	15.46	46.63	8.7755E-02	65.95
4.412	15.92	50.85	8.2804E-02	65.95
4.631	16.37	55.30	7.8305E-02	65.95
4.849	16.81	59.98	7.4216E-02	65.95
5.067	17.25	64.89	7.0496E-02	65.95
5.285	17.68	70.03	6.7108E-02	65.95
5.543	18.18	76.38	6.3495E-02	65.95
5.800	18.66	83.06	6.0249E-02	65.95
6.058	19.13	90.04	5.7326E-02	65.95
6.315	19.58	97.32	5.4689E-02	65.95
6.572	20.02	104.9	5.2302E-02	65.95
6.830	20.45	112.8	5.0138E-02	65.95

t (s)	r (m)	Q_v (kg)	h (m)	V_d (m^3)
7.087	20.86	120.9	4.8170E-02	65.95
7.344	21.26	129.3	4.6377E-02	65.95
7.602	21.65	138.0	4.4737E-02	65.95
7.859	22.02	146.9	4.3236E-02	65.95
8.117	22.38	156.1	4.1856E-02	65.95
8.374	22.72	165.5	4.0586E-02	65.95
8.631	23.06	175.1	3.9413E-02	65.95
8.889	23.38	184.9	3.8328E-02	65.95
9.146	23.69	194.9	3.7323E-02	65.95
9.403	24.00	205.1	3.6388E-02	65.95
9.661	24.29	215.5	3.5517E-02	65.95
9.965	24.62	228.0	3.4563E-02	65.95
10.27	24.94	240.7	3.3682E-02	65.95
10.57	25.24	253.7	3.2865E-02	65.95
10.88	25.54	266.8	3.2106E-02	65.95
11.18	25.82	280.1	3.1398E-02	65.95
11.48	26.10	293.6	3.0738E-02	65.95
11.79	26.36	307.3	3.0119E-02	65.95
12.16	26.67	324.4	2.9411E-02	65.95
12.53	26.98	341.6	2.8754E-02	65.95
12.91	27.26	359.1	2.8143E-02	65.95
13.28	27.54	376.8	2.7573E-02	65.95
13.65	27.81	394.6	2.7039E-02	65.95
14.03	28.07	412.6	2.6540E-02	65.95
14.40	28.32	430.7	2.6070E-02	65.95
14.91	28.64	455.6	2.5477E-02	65.95
15.41	28.95	480.6	2.4927E-02	65.95
15.92	29.25	505.9	2.4417E-02	65.95
16.43	29.53	531.3	2.3941E-02	65.95
16.93	29.81	556.9	2.3496E-02	65.95
17.44	30.07	582.7	2.3079E-02	65.95
17.95	30.33	608.6	2.2686E-02	65.95
18.57	30.63	640.8	2.2231E-02	65.95
19.20	30.93	673.3	2.1805E-02	65.95
19.83	31.21	705.8	2.1407E-02	65.95
20.46	31.48	738.5	2.1033E-02	65.95
21.09	31.74	771.3	2.0681E-02	65.95
21.71	31.99	804.1	2.0349E-02	65.95
22.34	32.24	837.0	2.0034E-02	65.95
23.12	32.53	877.7	1.9667E-02	65.95
23.89	32.81	918.5	1.9323E-02	65.95
24.67	33.09	959.3	1.8998E-02	65.95
25.44	33.35	1000.	1.8690E-02	65.95
26.22	33.61	1041.	1.8399E-02	65.95
26.99	33.86	1082.	1.8122E-02	65.95

t (s)	r (m)	Q_v (kg)	h (m)	V_d (m^3)
27.77	34.10	1123.	1.7858E-02	65.95
28.73	34.39	1174.	1.7546E-02	65.95
29.70	34.68	1224.	1.7251E-02	65.95
30.66	34.95	1275.	1.6972E-02	65.95
31.63	35.22	1326.	1.6706E-02	65.95
32.59	35.48	1376.	1.6453E-02	65.95
33.56	35.73	1427.	1.6211E-02	65.95
34.53	35.98	1477.	1.5980E-02	65.95
35.68	36.27	1537.	1.5716E-02	65.95
36.84	36.56	1598.	1.5465E-02	65.95
38.00	36.83	1657.	1.5225E-02	65.95
39.16	37.10	1717.	1.4997E-02	65.95
40.32	37.36	1777.	1.4778E-02	65.95
41.48	37.62	1836.	1.4568E-02	65.95
42.63	37.87	1895.	1.4367E-02	65.95
44.24	38.21	1977.	1.4101E-02	65.95
45.84	38.54	2058.	1.3849E-02	65.95
47.45	38.86	2138.	1.3610E-02	65.95
49.05	39.18	2219.	1.3382E-02	65.95
50.66	39.48	2299.	1.3164E-02	65.95
52.26	39.78	2378.	1.2956E-02	65.95
53.86	40.08	2457.	1.2758E-02	65.95
55.94	40.45	2558.	1.2513E-02	65.95
58.01	40.81	2659.	1.2281E-02	65.95
60.08	41.16	2759.	1.2061E-02	65.95
62.15	41.50	2858.	1.1851E-02	65.95
64.23	41.83	2956.	1.1651E-02	65.95
66.30	42.16	3054.	1.1461E-02	65.95
68.37	42.48	3151.	1.1278E-02	65.95
71.12	42.89	3278.	1.1048E-02	65.95
73.87	43.29	3405.	1.0830E-02	65.95
76.61	43.68	3530.	1.0624E-02	65.95
79.36	44.06	3653.	1.0428E-02	65.95
82.11	44.44	3776.	1.0241E-02	65.95
84.86	44.80	3897.	1.0064E-02	65.95
87.60	45.15	4017.	9.8940E-03	65.95
91.17	45.60	4171.	9.6850E-03	65.95
94.73	46.04	4324.	9.4875E-03	65.95
98.29	46.46	4474.	9.3004E-03	65.95
101.9	46.88	4622.	9.1228E-03	65.95
105.4	47.28	4769.	8.9541E-03	65.95
109.0	47.68	4914.	8.7934E-03	65.95
112.6	48.06	5057.	8.6402E-03	65.95
117.2	48.55	5241.	8.4506E-03	65.95
121.9	49.03	5423.	8.2715E-03	65.95

t (s)	r (m)	Q_v (kg)	h (m)	V_d (m³)
126.5	49.50	5601.	8.1023E-03	65.95
131.2	49.95	5777.	7.9418E-03	65.95
135.8	50.39	5950.	7.7896E-03	65.95
140.5	50.82	6121.	7.6448E-03	65.95
145.1	51.24	6290.	7.5069E-03	65.95
151.2	51.77	6505.	7.3369E-03	65.95
157.2	52.29	6716.	7.1768E-03	65.95
163.3	52.79	6924.	7.0254E-03	65.95
169.3	53.28	7128.	6.8822E-03	65.95
175.4	53.76	7329.	6.7464E-03	65.95
181.4	54.22	7526.	6.6174E-03	65.95
187.5	54.68	7720.	6.4946E-03	65.95
195.4	55.26	7968.	6.3430E-03	65.95
203.3	55.82	8211.	6.2002E-03	65.95
211.2	56.36	8450.	6.0655E-03	65.95
211.2	56.36	8451.	6.0648E-03	65.95
211.3	56.37	8452.	6.0641E-03	65.95
211.3	56.37	8454.	6.0633E-03	65.95
211.4	56.37	8455.	6.0626E-03	65.95
211.4	56.38	8456.	6.0619E-03	65.95
211.4	56.38	8458.	6.0612E-03	65.95
211.5	56.38	8459.	6.0605E-03	65.95
211.5	56.38	8460.	6.0597E-03	65.95
211.6	56.39	8462.	6.0590E-03	65.95
211.6	56.39	8463.	6.0583E-03	65.95
212.4	56.45	8487.	6.0448E-03	65.95
212.9	56.48	8502.	6.0366E-03	65.95
213.4	56.51	8517.	6.0284E-03	65.95
213.9	56.55	8532.	6.0202E-03	65.95
214.4	56.58	8547.	6.0120E-03	65.95
215.5	56.65	8577.	5.9955E-03	65.95
216.5	56.72	8608.	5.9790E-03	65.95
217.5	56.79	8638.	5.9628E-03	65.95
218.6	56.86	8668.	5.9466E-03	65.95
220.5	56.99	8726.	5.9158E-03	65.95
222.5	57.11	8784.	5.8855E-03	65.95
224.5	57.24	8842.	5.8558E-03	65.95
226.5	57.37	8899.	5.8266E-03	65.95
228.5	57.49	8956.	5.7980E-03	65.95
230.5	57.61	9013.	5.7700E-03	65.95
232.5	57.73	9069.	5.7425E-03	65.95
234.4	57.85	9126.	5.7155E-03	65.95
236.4	57.97	9182.	5.6891E-03	65.95
238.4	58.08	9237.	5.6632E-03	65.95
240.4	58.20	9293.	5.6379E-03	65.95

t (s)	r (m)	Q_v (kg)	h (m)	V_d (m³)
242.4	58.31	9348.	5.6130E-03	65.95
244.4	58.42	9403.	5.5887E-03	65.95
246.4	58.53	9458.	5.5648E-03	65.95
248.3	58.63	9512.	5.5415E-03	65.95
251.7	58.81	9604.	5.5028E-03	65.95
255.1	58.98	9695.	5.4654E-03	65.95
258.5	59.15	9785.	5.4292E-03	65.95
261.8	59.31	9875.	5.3941E-03	65.95
265.2	59.47	9963.	5.3601E-03	65.95
268.6	59.63	1.0052E+04	5.3272E-03	65.95
274.0	59.87	1.0191E+04	5.2764E-03	65.95
279.4	60.10	1.0329E+04	5.2279E-03	65.95
284.8	60.33	1.0465E+04	5.1815E-03	65.95
290.2	60.54	1.0600E+04	5.1371E-03	65.95
295.6	60.75	1.0732E+04	5.0943E-03	65.95
300.9	60.95	1.0864E+04	5.0533E-03	65.95
308.7	61.23	1.1050E+04	4.9969E-03	65.95
316.4	61.50	1.1233E+04	4.9434E-03	65.95
324.2	61.76	1.1413E+04	4.8924E-03	65.95
331.9	62.01	1.1590E+04	4.8438E-03	65.95
339.7	62.25	1.1764E+04	4.7973E-03	65.95
347.4	62.48	1.1936E+04	4.7528E-03	65.95
356.6	62.75	1.2137E+04	4.7023E-03	65.95
365.8	63.00	1.2334E+04	4.6542E-03	65.95
374.9	63.25	1.2528E+04	4.6082E-03	65.95
384.1	63.49	1.2720E+04	4.5642E-03	65.95
393.3	63.72	1.2908E+04	4.5219E-03	65.95
402.5	63.94	1.3094E+04	4.4813E-03	65.95
411.6	64.15	1.3277E+04	4.4422E-03	65.95
426.4	64.49	1.3568E+04	4.3822E-03	65.95
441.2	64.80	1.3852E+04	4.3255E-03	65.95
455.9	65.11	1.4132E+04	4.2718E-03	65.95
470.7	65.40	1.4406E+04	4.2208E-03	65.95
485.5	65.68	1.4677E+04	4.1722E-03	65.95
500.2	65.95	1.4943E+04	4.1258E-03	65.95
515.0	66.20	1.5205E+04	4.0814E-03	65.95
532.7	66.50	1.5515E+04	4.0306E-03	65.95
550.5	66.79	1.5821E+04	3.9822E-03	65.95
568.2	67.06	1.6123E+04	3.9361E-03	65.95
585.9	67.32	1.6421E+04	3.8919E-03	65.95
603.6	67.58	1.6715E+04	3.8496E-03	65.95
621.4	67.82	1.7007E+04	3.8089E-03	65.95
639.1	68.06	1.7296E+04	3.7698E-03	65.95
653.6	68.25	1.7531E+04	3.7388E-03	65.95
668.2	68.43	1.7765E+04	3.7086E-03	65.95

t (s)	r (m)	Q_v (kg)	h (m)	V_d (m^3)
682.7	68.61	1.7997E+04	3.6794E-03	65.95
697.3	68.78	1.8229E+04	3.6509E-03	65.95
711.8	68.95	1.8459E+04	3.6232E-03	65.95
726.4	69.11	1.8688E+04	3.5962E-03	65.95
743.7	69.30	1.8959E+04	3.5650E-03	65.95
760.9	69.49	1.9228E+04	3.5347E-03	65.95
778.2	69.67	1.9497E+04	3.5052E-03	65.95
795.5	69.84	1.9764E+04	3.4765E-03	65.95
812.7	70.01	2.0031E+04	3.4486E-03	65.95
830.0	70.18	2.0297E+04	3.4213E-03	65.95
859.2	70.45	2.0746E+04	3.3767E-03	65.95
888.4	70.70	2.1193E+04	3.3338E-03	65.95
917.5	70.95	2.1640E+04	3.2925E-03	65.95
946.7	71.19	2.2086E+04	3.2525E-03	65.95
975.9	71.42	2.2532E+04	3.2139E-03	65.95
1005.	71.64	2.2979E+04	3.1764E-03	65.95
1034.	71.85	2.3425E+04	3.1401E-03	65.95
1081.	72.18	2.4148E+04	3.0835E-03	65.95
1128.	72.48	2.4872E+04	3.0293E-03	65.95
1176.	72.77	2.5599E+04	2.9772E-03	65.95
1223.	73.05	2.6329E+04	2.9269E-03	65.95
1270.	73.31	2.7062E+04	2.8784E-03	65.95
1317.	73.55	2.7798E+04	2.8314E-03	65.95
1364.	73.79	2.8537E+04	2.7858E-03	65.95
1420.	74.05	2.9422E+04	2.7330E-03	65.95
1476.	74.30	3.0313E+04	2.6819E-03	65.95
1533.	74.53	3.1208E+04	2.6322E-03	65.95
1589.	74.75	3.2108E+04	2.5839E-03	65.95
1645.	74.96	3.3012E+04	2.5368E-03	65.95
1701.	75.15	3.3921E+04	2.4907E-03	65.95
1757.	75.34	3.4834E+04	2.4457E-03	65.95
1813.	75.51	3.5751E+04	2.4015E-03	65.95
1870.	75.68	3.6672E+04	2.3583E-03	65.95
1926.	75.83	3.7597E+04	2.3157E-03	65.95
1982.	75.98	3.8525E+04	2.2740E-03	65.95
2038.	76.12	3.9456E+04	2.2328E-03	65.95
2094.	76.25	4.0391E+04	2.1923E-03	65.95
2150.	76.38	4.1329E+04	2.1524E-03	65.95
2207.	76.49	4.2270E+04	2.1130E-03	65.95
2263.	76.60	4.3213E+04	2.0740E-03	65.95
2319.	76.71	4.4159E+04	2.0356E-03	65.95
2386.	76.83	4.5288E+04	1.9903E-03	65.95
2452.	76.93	4.6419E+04	1.9457E-03	65.95
2519.	77.04	4.7554E+04	1.9015E-03	65.95
2586.	77.13	4.8692E+04	1.8578E-03	65.95

t (s)	r (m)	Q_v (kg)	h (m)	V_d (m^3)
2653.	77.22	4.9832E+04	1.8145E-03	65.95
2720.	77.30	5.0975E+04	1.7716E-03	65.95
2804.	77.40	5.2426E+04	1.7178E-03	65.95
2889.	77.48	5.3880E+04	1.6645E-03	65.95
2974.	77.56	5.5337E+04	1.6117E-03	65.95
3058.	77.63	5.6796E+04	1.5593E-03	65.95
3143.	77.70	5.8259E+04	1.5072E-03	65.95
3228.	77.76	5.9723E+04	1.4555E-03	65.95
3349.	77.83	6.1836E+04	1.3816E-03	65.95
3471.	77.89	6.3953E+04	1.3081E-03	65.95
3593.	77.95	6.6073E+04	1.2351E-03	65.95
3715.	77.99	6.8195E+04	1.1625E-03	65.95
3837.	78.03	7.0319E+04	1.0902E-03	65.95
3959.	78.06	7.2445E+04	1.0181E-03	65.95
4115.	78.09	7.5172E+04	9.2603E-04	65.95
4271.	78.11	7.7900E+04	8.3422E-04	65.95
4428.	78.13	8.0629E+04	7.4259E-04	65.95
4584.	78.14	8.3359E+04	6.5109E-04	65.95
4740.	78.15	8.6090E+04	5.5968E-04	65.95
4896.	78.15	8.8821E+04	4.6832E-04	65.95
5092.	78.15	9.2247E+04	3.5379E-04	65.95
5288.	78.15	9.5673E+04	2.3928E-04	65.95
5289.	78.15	9.5690E+04	2.3871E-04	65.95
5290.	78.15	9.5707E+04	2.3814E-04	65.95
5291.	78.15	9.5724E+04	2.3757E-04	65.95
5292.	78.15	9.5741E+04	2.3699E-04	65.95
5293.	78.15	9.5758E+04	2.3642E-04	65.95
5294.	78.15	9.5775E+04	2.3585E-04	65.95
5305.	78.15	9.5969E+04	2.2939E-04	65.95
5316.	78.15	9.6162E+04	2.2293E-04	65.95
5327.	78.15	9.6355E+04	2.1646E-04	65.95
5338.	78.15	9.6549E+04	2.1000E-04	65.95
5349.	78.15	9.6742E+04	2.0354E-04	65.95
5380.	78.15	9.7276E+04	1.8569E-04	65.95
5410.	78.15	9.7810E+04	1.6785E-04	65.95
5441.	78.15	9.8344E+04	1.5000E-04	65.95
5471.	78.15	9.8878E+04	1.3215E-04	65.95
5524.	78.15	9.9810E+04	1.0100E-04	65.95
5578.	78.15	1.0074E+05	6.9853E-05	65.95
5631.	78.15	1.0167E+05	3.8704E-05	65.95
5638.	78.15	1.0180E+05	3.4369E-05	65.95

t (s)	H_c J/(m²·s)	H_a J/(m²·s)	T (K)
0.0000	2.9226E+05	24.20	238.1
2.8482E-07	3.9515E+04	24.20	238.1
5.6965E-07	2.8070E+04	24.20	238.1
8.5447E-07	2.2955E+04	24.20	238.1
3.5060E-06	1.1359E+04	24.20	238.1
6.1575E-06	8574.	24.20	238.1
8.8090E-06	7169.	24.20	238.1
2.4248E-05	4322.	24.20	238.1
3.9687E-05	3378.	24.20	238.1
5.5125E-05	2867.	24.20	238.1
1.1684E-04	1969.	24.20	238.1
1.7856E-04	1593.	24.20	238.1
2.4028E-04	1373.	24.20	238.1
4.2861E-04	1028.	24.20	238.1
6.1694E-04	856.9	24.20	238.1
8.0527E-04	750.1	24.20	238.1
1.2764E-03	595.8	24.20	238.1
1.7475E-03	509.2	24.20	238.1
2.2186E-03	451.9	24.20	238.1
3.2082E-03	375.8	24.20	238.1
4.1979E-03	328.5	24.20	238.1
5.1875E-03	295.5	24.20	238.1
7.0839E-03	252.9	24.20	238.1
8.9802E-03	224.6	24.20	238.1
1.0877E-02	204.1	24.20	238.1
1.2773E-02	188.4	24.20	238.1
1.7217E-02	162.3	24.21	238.1
2.1662E-02	144.7	24.21	238.1
2.6106E-02	131.9	24.21	238.1
3.0551E-02	121.9	24.21	238.1
3.9682E-02	107.0	24.21	238.1
4.8813E-02	96.57	24.22	238.1
5.7944E-02	88.71	24.22	238.1
6.7076E-02	82.52	24.22	238.1
8.2946E-02	74.33	24.23	238.1
9.8816E-02	68.22	24.23	238.1
0.1147	63.45	24.24	238.1
0.1306	59.60	24.25	238.1
0.1594	54.19	24.26	238.1
0.1882	50.11	24.27	238.1
0.2170	46.92	24.28	238.1
0.2458	44.34	24.29	238.1
0.2746	42.21	24.30	238.1
0.3227	39.37	24.31	238.1

t (s)	H_c J/(m²·s)	H_a J/(m²·s)	T (K)
0.3708	37.17	24.33	238.1
0.4189	35.41	24.35	238.1
0.4670	33.98	24.36	238.1
0.5150	32.79	24.38	238.1
0.5868	31.37	24.40	238.1
0.6585	30.25	24.43	238.1
0.7302	29.35	24.45	238.1
0.8019	28.61	24.47	238.1
0.8736	28.01	24.50	238.1
0.9453	27.51	24.52	238.1
1.047	26.93	24.56	238.1
1.150	26.47	24.59	238.1
1.252	26.09	24.63	238.1
1.354	25.79	24.66	238.1
1.456	25.53	24.70	238.1
1.558	25.32	24.74	238.1
1.676	25.11	24.78	238.1
1.794	24.92	24.82	238.1
1.911	24.76	24.87	238.1
2.029	24.61	24.92	238.1
2.147	24.47	24.97	238.1
2.265	24.33	25.02	238.0
2.382	24.19	25.07	238.0
2.559	23.99	25.16	238.0
2.735	23.78	25.25	238.0
2.881	23.60	25.33	238.0
3.027	23.42	25.41	238.0
3.173	23.22	25.50	238.0
3.319	23.02	25.59	238.0
3.465	22.82	25.68	238.0
3.612	22.61	25.78	238.0
3.758	22.39	25.89	238.0
3.976	22.05	26.05	238.0
4.194	21.71	26.23	238.0
4.412	21.35	26.41	238.0
4.631	21.00	26.61	237.9
4.849	20.64	26.82	237.9
5.067	20.28	27.04	237.9
5.285	19.92	27.26	237.9
5.543	19.50	27.55	237.9
5.800	19.09	27.84	237.9
6.058	18.69	28.15	237.8
6.315	18.29	28.48	237.8
6.572	17.91	28.81	237.8
6.830	17.53	29.16	237.8

t (s)	H_c J/(m²·s)	H_a J/(m²·s)	T (K)
7.087	17.17	29.52	237.7
7.344	16.82	29.89	237.7
7.602	16.48	30.27	237.7
7.859	16.15	30.66	237.7
8.117	15.84	31.05	237.6
8.374	15.54	31.46	237.6
8.631	15.25	31.87	237.6
8.889	14.97	32.29	237.6
9.146	14.70	32.71	237.5
9.403	14.44	33.15	237.5
9.661	14.20	33.58	237.5
9.965	13.92	34.10	237.4
10.27	13.66	34.63	237.4
10.57	13.40	35.16	237.4
10.88	13.16	35.70	237.3
11.18	12.93	36.24	237.3
11.48	12.72	36.78	237.2
11.79	12.51	37.33	237.2
12.16	12.26	38.00	237.1
12.53	12.04	38.68	237.1
12.91	11.82	39.36	237.0
13.28	11.61	40.04	237.0
13.65	11.42	40.73	236.9
14.03	11.23	41.41	236.9
14.40	11.06	42.09	236.8
14.91	10.84	43.02	236.8
15.41	10.63	43.94	236.7
15.92	10.43	44.86	236.6
16.43	10.25	45.78	236.5
16.93	10.08	46.69	236.5
17.44	9.918	47.60	236.4
17.95	9.766	48.50	236.3
18.57	9.590	49.61	236.2
19.20	9.427	50.72	236.1
19.83	9.274	51.82	236.0
20.46	9.131	52.91	235.9
21.09	8.996	53.98	235.8
21.71	8.871	55.05	235.7
22.34	8.752	56.11	235.6
23.12	8.616	57.41	235.5
23.89	8.489	58.69	235.4
24.67	8.370	59.96	235.3
25.44	8.259	61.21	235.2
26.22	8.155	62.45	235.0
26.99	8.057	63.67	234.9

t (s)	H_c J/(m²·s)	H_a J/(m²·s)	T (K)
27.77	7.965	64.88	234.8
28.73	7.858	66.36	234.6
29.70	7.758	67.83	234.5
30.66	7.665	69.28	234.3
31.63	7.578	70.70	234.2
32.59	7.496	72.11	234.0
33.56	7.419	73.50	233.9
34.53	7.346	74.88	233.7
35.68	7.264	76.50	233.6
36.84	7.188	78.10	233.4
38.00	7.116	79.67	233.2
39.16	7.049	81.22	233.0
40.32	6.986	82.75	232.9
41.48	6.926	84.26	232.7
42.63	6.870	85.74	232.5
44.24	6.796	87.77	232.3
45.84	6.728	89.75	232.0
47.45	6.664	91.70	231.8
49.05	6.604	93.62	231.6
50.66	6.548	95.50	231.3
52.26	6.496	97.35	231.1
53.86	6.446	99.16	230.9
55.94	6.386	101.5	230.6
58.01	6.330	103.7	230.3
60.08	6.278	105.9	230.0
62.15	6.229	108.1	229.7
64.23	6.183	110.2	229.4
66.30	6.140	112.3	229.1
68.37	6.099	114.3	228.8
71.12	6.048	117.0	228.4
73.87	6.001	119.6	228.1
76.61	5.957	122.1	227.7
79.36	5.916	124.6	227.3
82.11	5.877	127.0	227.0
84.86	5.840	129.4	226.6
87.60	5.806	131.7	226.3
91.17	5.764	134.6	225.8
94.73	5.725	137.4	225.4
98.29	5.688	140.2	224.9
101.9	5.654	142.9	224.5
105.4	5.621	145.6	224.1
109.0	5.591	148.1	223.6
112.6	5.562	150.6	223.2
117.2	5.526	153.8	222.7
121.9	5.493	156.9	222.2

t (s)	H_c J/(m²·s)	H_a J/(m²·s)	T (K)
126.5	5.462	159.9	221.7
131.2	5.432	162.8	221.2
135.8	5.404	165.6	220.7
140.5	5.378	168.3	220.2
145.1	5.353	171.0	219.7
151.2	5.322	174.3	219.1
157.2	5.292	177.6	218.5
163.3	5.265	180.7	217.9
169.3	5.238	183.7	217.4
175.4	5.213	186.6	216.8
181.4	5.189	189.4	216.3
187.5	5.166	192.1	215.8
195.4	5.137	195.5	215.1
203.3	5.110	198.8	214.4
211.2	5.083	201.9	213.8
211.2	5.083	201.9	213.8
211.3	5.083	202.0	213.8
211.3	5.083	202.0	213.8
211.4	5.083	202.0	213.8
211.4	5.083	202.0	213.8
211.4	5.082	202.0	213.8
211.5	5.082	202.0	213.8
211.5	5.082	202.1	213.8
211.6	5.082	202.1	213.8
211.6	5.082	202.1	213.8
212.4	5.079	202.4	213.7
212.9	5.078	202.6	213.7
213.4	5.076	202.8	213.6
213.9	5.074	203.0	213.6
214.4	5.073	203.2	213.6
215.5	5.069	203.6	213.5
216.5	5.066	204.0	213.4
217.5	5.063	204.3	213.3
218.6	5.059	204.7	213.3
220.5	5.052	205.5	213.1
222.5	5.045	206.2	213.0
224.5	5.038	206.9	212.8
226.5	5.031	207.6	212.7
228.5	5.024	208.3	212.5
230.5	5.017	209.0	212.4
232.5	5.009	209.7	212.2
234.4	5.002	210.4	212.1
236.4	4.995	211.1	211.9
238.4	4.987	211.8	211.8
240.4	4.980	212.4	211.7

t (s)	H_c J/(m²·s)	H_a J/(m²·s)	T (K)
242.4	4.973	213.1	211.5
244.4	4.965	213.8	211.4
246.4	4.958	214.4	211.3
248.3	4.951	215.0	211.1
251.7	4.939	216.1	210.9
255.1	4.927	217.2	210.7
258.5	4.916	218.2	210.5
261.8	4.904	219.2	210.3
265.2	4.893	220.2	210.0
268.6	4.882	221.2	209.8
274.0	4.866	222.7	209.5
279.4	4.850	224.2	209.2
284.8	4.834	225.7	208.9
290.2	4.820	227.1	208.6
295.6	4.806	228.5	208.3
300.9	4.793	229.8	208.0
308.7	4.775	231.7	207.6
316.4	4.757	233.5	207.2
324.2	4.741	235.2	206.8
331.9	4.726	236.8	206.4
339.7	4.712	238.4	206.1
347.4	4.698	240.0	205.7
356.6	4.683	241.7	205.3
365.8	4.668	243.4	205.0
374.9	4.654	245.0	204.6
384.1	4.641	246.5	204.2
393.3	4.628	248.0	203.9
402.5	4.616	249.4	203.6
411.6	4.605	250.7	203.3
426.4	4.587	252.7	202.8
441.2	4.570	254.6	202.3
455.9	4.554	256.4	201.9
470.7	4.539	258.1	201.5
485.5	4.525	259.7	201.2
500.2	4.511	261.1	200.8
515.0	4.498	262.5	200.5
532.7	4.482	264.0	200.1
550.5	4.467	265.4	199.8
568.2	4.453	266.7	199.5
585.9	4.439	267.9	199.2
603.6	4.426	269.0	198.9
621.4	4.412	270.1	198.6
639.1	4.400	271.0	198.4
653.6	4.389	271.7	198.2
668.2	4.379	272.4	198.0

t (s)	H_c J/(m²·s)	H_a J/(m²·s)	T (K)
682.7	4.370	273.1	197.9
697.3	4.360	273.7	197.7
711.8	4.350	274.2	197.6
726.4	4.341	274.8	197.4
743.7	4.330	275.3	197.3
760.9	4.320	275.9	197.2
778.2	4.309	276.4	197.0
795.5	4.299	276.8	196.9
812.7	4.289	277.3	196.8
830.0	4.279	277.7	196.7
859.2	4.263	278.3	196.5
888.4	4.247	278.8	196.4
917.5	4.232	279.2	196.3
946.7	4.217	279.6	196.2
975.9	4.203	280.0	196.1
1005.	4.189	280.3	196.0
1034.	4.176	280.6	195.9
1081.	4.155	280.9	195.8
1128.	4.135	281.2	195.7
1176.	4.117	281.4	195.7
1223.	4.099	281.5	195.6
1270.	4.082	281.7	195.6
1317.	4.066	281.8	195.6
1364.	4.051	281.8	195.5
1420.	4.034	281.9	195.5
1476.	4.018	281.9	195.5
1533.	4.003	281.9	195.5
1589.	3.989	282.0	195.5
1645.	3.976	282.0	195.5
1701.	3.964	281.9	195.5
1757.	3.952	281.9	195.5
1813.	3.942	281.9	195.5
1870.	3.931	281.9	195.5
1926.	3.922	281.9	195.5
1982.	3.913	281.9	195.4
2038.	3.904	281.9	195.4
2094.	3.896	281.9	195.4
2150.	3.889	281.8	195.4
2207.	3.882	281.8	195.4
2263.	3.875	281.8	195.4
2319.	3.869	281.8	195.4
2386.	3.862	281.8	195.4
2452.	3.856	281.8	195.4
2519.	3.850	281.8	195.4
2586.	3.844	281.8	195.4

t (s)	H_c J/(m²·s)	H_a J/(m²·s)	T (K)
2653.	3.839	281.8	195.4
2720.	3.834	281.7	195.4
2804.	3.828	281.7	195.4
2889.	3.823	281.7	195.4
2974.	3.819	281.7	195.4
3058.	3.814	281.7	195.4
3143.	3.811	281.7	195.4
3228.	3.807	281.7	195.4
3349.	3.803	281.7	195.4
3471.	3.799	281.7	195.4
3593.	3.796	281.7	195.4
3715.	3.793	281.7	195.4
3837.	3.791	281.7	195.4
3959.	3.789	281.7	195.4
4115.	3.787	281.7	195.4
4271.	3.785	281.6	195.4
4428.	3.784	281.6	195.4
4584.	3.783	281.6	195.4
4740.	3.782	281.6	195.4
4896.	3.782	281.6	195.4
5092.	3.781	281.6	195.4
5288.	3.781	281.6	195.4
5289.	3.781	281.6	195.4
5290.	3.781	281.6	195.4
5291.	3.781	281.6	195.4
5292.	3.781	281.6	195.4
5293.	3.781	281.6	195.4
5294.	3.781	281.6	195.4
5305.	3.781	281.6	195.4
5316.	3.781	281.6	195.4
5327.	3.781	281.6	195.4
5338.	3.781	281.6	195.4
5349.	3.781	281.6	195.4
5380.	3.781	281.6	195.4
5410.	3.781	281.6	195.4
5441.	3.780	281.6	195.4
5471.	3.780	281.6	195.4
5524.	3.780	281.6	195.4
5578.	3.780	281.6	195.4
5631.	3.780	281.6	195.4
5638.	3.780	281.6	195.4

3.6.3 Calculation example HACS-R

Properties of the chemical spillt

Chemical spillt		diethylamine (CH$_3$CH$_2$)2NH	
Molecular weight	μ_L	$= 73.14 \cdot 10^{-3}$	kg/mol
Normal boiling point	T_b	$= 56.3$	˚C
Liquid mass spillt	Q_L	$= 10^6$	kg

Environmental Conditions

Width of river	$2 \times b$	$= 31$	m
Depth of river	h_d	$= 10$	m
Mean stream velocity	u_s	$= 1.5$	m/s
Manning roughness factor	C_{MRF}	$= 0.03$	
Water density	ρ_w	$= 1000$	kg/m^3
Limiting concentration	m_{m*}	$= 5$	wt%
Water temperature	T_w	$= 20$	˚C

Calculation of Turbulent Dispersion Coefficients

Mass transfer coefficient	$k_{m,P}$	$= 1.8 \times 10^{-7}$	s/m
Hydraulic radius river	r_h	$= 6.0$	m
Shear velocity	u_*	$= 0.104$	m/s
Width-to-depth ratio	$2 \times b/d_h = 3 \ll 100$		
Classification water body	narrow river		
Longitudinal dispersion coefficient (3.147a)	D_x	$= 0.0042$	m^2/s
Cross-stream dispersion coefficient (3.147b)	D_y	$= 0.1435$	m^2/s
Vertical dispersion coefficient (3.147c)	D_z	$= 0.0418$	m^2/s
Limiting concentration (3.159)	m_{m*}	$= 214$	kg/m^3
Characteristic time (3.163)	$t_{c<lim}$	$= 1205$	s
Saturated vapour pressure at 20˚C	P_v	$= 0.238$	Bar

Results

Characteristic evaporation rate (3.174)	q_{ch}	$= 1{,}591$	kg/s
Characteristic evaporated vapour mass (3.175)	Q_{ch}	$= 1917.1$	kg
The maximum possible evaporation (3.184)	Q_v	$= 719$	kg
Vaporised mass fraction of total spill		$= 0.072$	wt%
Maximum distance where m_{m*} (3.185)	$x_{c<lim}$	$= 1.807$	m

3.6.4 Supplementary models

3.6.4.1 Evaporation of ammonia on a dry sandy subsoil

The model has been explained in paragraph 3.5.3.1.

Input

Chemical spilt	ammonia (NH_3)		
Total liquid mass released in the bund	Q_L	$= 1000$	kg
Bund area	A	$= 100$	m^2
Initial temperature subsoil	$T_{s,0}$	$= 288.15$	K

Physical properties

Normal boiling point	T_b	$= 239.72$	K
Heat of vaporisation at boiling point	$L_v(T_b)$	$= 1.209 \cdot 10^6$	J/kg
table 3.5:			
Thermal diffusivity (dry) sandy subsoil	$a_{s,s}$	$= 2 \cdot 10^{-7}$	m^2/s
Thermal conductivity (dry) sandy subsoil	$\lambda_{s,s}$	$= 0.3$	J/(s·m·K)

Output

Heat flux conducting into the pool after 20 s	H_c	$= 3.28 \cdot 10^3$	J/(m^2·s)
Vaporisation rate after 20 s	q_v	$= 2.71$	kg/s
Total amount of vapour evolved after 20 s	Q_v	$= 108$	kg

Procedure

The heat flux at time t = 20 s, from sandy subsoil can be estimated by equation (3.120). The momentaneous vaporisation rate can be estimated by equation (3.122a).
The total amount of vapour evolved after 20 seconds can be estimated by equation (3.122b), which can not be more than the total mass of liquid ammonia mass released in the bund.

3.6.4.2 Evaporation of a cryogene on a moist sandy subsoil with clay

The model has been explained in paragraph 3.5.3.2.
The only difference with the calculation example presented in paragraph 3.6.4.1 is the estimation of the correction factor C_R in stead of a factor 8. Here only the estimation of the thermal conductivity and thermal diffusivity of moist porous subsoil will be presented.

Input

Moist fraction	$m_{w,ms}$	= 0.08	kg/kg
Clay fraction	j_k	= 0.5	kg/kg

Physical properties

Thermal diffusivity (dry) sandy subsoil	a_s	= $2 \cdot 10^{-7}$	m^2/s
Heat capacity of (dry) sand (and clay)	$C_{p,s,dry}$	= 799	J/(kg·K)
Heat capacity of ice	C_{ice}	= 1930	J/(kg·K)
Thermal conductivity (dry) sandy subsoil	$\lambda_{s,s}$	= 0.3	J/(s·m·K)
Density of dry sand	$\rho_{s,s}$	= 1600	kg/s

Output

Density of subsoil	ρ_s	= 1728	kg/m^3
Heat capacity of subsoil	$C_{p,s}$	= 882.3	J/(kg·K)
Correction factor	C_R	= 1.093	
Thermal conductivity subsoil	λ_s	= 1.312	J/(s·m·K)
Thermal diffusivity subsoil	a_s	= $8.60 \cdot 10^{-7}$	m^2/s

Procedure

The heat flux at time t, from moist sandy subsoil with clay can be estimated by equation (3.123). The correction factor C_R can be estimated by the equations (3.123) until (3.127).

The thermal conductivity of the sand-clay mixture can be calculated by equations (3.125) and (3.126a-c). The thermal diffusivity of the sand-clay mixture can be estimated by equations (3.127a-c), based on averaging the physical properties.

3.6.4.3 Evaporation of propane in a gravel bed

The model has been explained in paragraph 3.5.3.3.

Input

Chemical spilt	propane (C_3H_8)		
Bund area	A	= 1500	m^2
Height gravel layer	h_{gr}	= 0.1	m
Average radius gravel stones	r_{gr}	= 0.05	m
Initial temperature subsoil	$T_{s,0}$	= 288.15	K

Physical properties

Normal boiling point	T_b	= 230.9	K
Heat of vaporisation at boiling point	$L_v(T_b)$	= $4.259 \cdot 10^5$	J/kg
table 3.5:			
Thermal diffusivity gravel	a_s	= $1.1 \cdot 10^{-6}$	m^2/s
Thermal conductivity gravel	λ_s	= 2.5	J/(s·m·K)

Output

Heat flux conducting into the pool after 10 s	H_c	= $153.6 \cdot 10^3$	J/(m^2·s)
Equation valid until	t	= 48.3	s
Check height gravel layer	h_{gr}/r_{gr}	= 2	
Vaporisation rate after 10 s	q_v	= 541.1	kg/s
Total amount of vapour evolved after 10 s	Q_v	= $10.8 \cdot 10^3$	kg

Procedure

The heat flux at time t = 10 s, from sandy subsoil can be estimated by equation (3.128).
However this equation can only be applied for a limited period of time given by equation (3.129). The gravel layer may not be heigher than 3 gravel stones (3.129b). The momentaneous vaporisation rate can be estimated by equation (3.122a).
The total amount of vapour evolved after 10 seconds can be estimated by equation (3.122b), which can not be more than the total mass of liquid propane released in the bund.

3.6.4.4   Film and nucleate boiling on water surfaces

The models has been explained in paragraph 3.5.4.

Liquids with boiling points (much) lower than water

Input

Chemical spilt	propane (C_3H_8)		
Surface temperature waterbody	T_w	= 288.15	K

Physical properties

Normal boiling point propane	T_b	= 230.9	K
Thermal diffusivity vapour at T_b	a_v	= $6.2445 \cdot 10^{-6}$	m^2/s
Specific heat liquid at T_b	$C_{p,L}$	= 2217.15	$J/(kg \cdot K)$
Specific heat water at T_w	$C_{p,w}$	= 4188.67	$J/(kg \cdot K)$
Specific heat of vapour	$C_{p,V}$	= 1037.13	$J/(kg \cdot K)$
Heat of evaporation at T_b	L_v	= $4.259 \cdot 10^6$	J/kg
Normal boiling point	T_b	= 230.9	K
Critical temperature spilled chemical	T_c	= 369.7	K
Thermal conductivity of liquid at T_b	λ_L	= 0.13365	$J/(m \cdot s \cdot K)$
Thermal conductivity of water at T_w	λ_w	= 0.601	$J/(m \cdot s \cdot K)$
Thermal conductivity vapour at T_b	λ_v	= $1.509 \cdot 10^{-2}$	$J/(m \cdot s \cdot K)$
Vapour density at T_b	ρ_V	= 2.33	kg/m^3
Vapour density at T_{av} (259.5 K)	$\rho_{V,av}$	= 2.07	kg/m^3
Liquid density at T_b	ρ_L	= 584.30	kg/m^3
Water density at T_w	ρ_w	= 997.66	kg/m^3
Liquid surface tension at T_b	σ	= $1.588 \cdot 10^{-2}$	N/m
Kinematic viscosity liquid at T_b	υ_L	= $3.361 \cdot 10^{-7}$	m^2/s
Kinematic viscosity vapour at T_b	υ_v	= $2.811 \cdot 10^{-6}$	m^2/s

Physical constant

Acceleration due to gravity	g	= 9.80665	m/s^2

Maximum heat flux for nucleate boiling	$H_{c,n,max} = 3.21 \cdot 10^6$	$J/(m^2 \cdot s)$
(T_L-T_w) corresponding with $H_{c,n,max}$	$\Delta T_{n,max} = 12.9$	K
Minimum heat flux for film boiling	$H_{c,f,min} = 8.21 \cdot 10^3$	$J/(m^2 \cdot s)$
(T_L-T_w) corresponding with $H_{c,f,min}$	$\Delta T_{f,min} = 56.0$	K
Actual heat flux	$H_c = 2.86 \cdot 10^4$	$J/(m^2 \cdot s)$

Procedure

The heat flux for nucleate boiling can be estimated by equation (3.130), and can be expressed as

$$H_{c,n} = 1510 \times \Delta T^3 \qquad (J/(m^2 \cdot s)) \qquad (3.130b)$$

The maximum heat flux for nucleate boiling $H_{c,n,max}$ can be estimated by equation (3.131).
From this two equations the temperature difference $\Delta T_{n,max}$ between the evaporating liquid and the water surface for nucleate boiling, at which the heat flux is at maximum, can be estimated.
The minimum heat flux for film boiling $H_{c,f,min}$ can be estimated by equations (3.132) and (3.133).
The temperature difference $\Delta T_{f,min}$ between the evaporating liquid and the water surface at which film boiling occurs can be estimated by equation (3.134).
The heat flux during metastable boiling $H_{c,m}$ could be calculated by means of equation (3.130a), (3.135) and (3.136) in principle. However, the present temperature difference between water and propane $\Delta T = 57.3$ K is larger than $\Delta T_{c,f,min}$. This means that the propane is fully film boiling. The actual heat flux H_c have been calculated by equation (3.107). The vaporisation mass rate could be calculated by equation (3.122).

Liquids with boiling points close to water

Input

Chemical spilt	n-butane (C_4H_{10})	
Surface temperature waterbody	$T_w = 288.15$	K

Physical properties

Normal boiling point butane	$T_b = 272.7$	K
Heat capacity of water at T_w	$C_{p,w} = 4188.67$	$J/(kg \cdot K)$
Thermal conductivity of water at T_w	$\lambda_w = 0.601$	$J/(m \cdot s \cdot K)$
Kinematic viscosity of water at T_w	$\upsilon_w = 1.1168 \cdot 10^{-6}$	m^2/s
Thermal diffusivity of water at T_w	$a_w = 1.4382 \cdot 10^{-7}$	m^2/s
Thermal expansivity of water at T_w	$\alpha_w = 2.0 \cdot 10^{-4}$	$1/K$

Output

Heat flux	$H_c = 4.53 \cdot 10^3$	$J/(m^2 \cdot s)$

3.114

Procedure

The thermal diffusivity of water a_w can be calculated by equation (3.6a).
The (constant) heat flux can be estimated by equation (3.137).
The vaporisation mass rate could be calculated by equation (3.122a).

3.6.4.5 Simple model non-boiling liquid in bund

The model has been explained in paragraph 3.5.5.2.

Input

Chemical spillt	Gasoline		
Total mass released	Q_L	= 100000	kg
Initial liquid temperature	$T_{L,0}$	= 288.15	K
Fixed pool surface	A	= 1500	m^2
Initial temperature subsoil	$T_{s,0}$	= 288.15	K
Wind velocity	u_w	= 2	m/s
Isolation concrete:			
Thermal conductivity	λ_s	= 0.207	J/(m·s·K)
Thermal diffusity	a_s	= $2.5 \cdot 10^{-7}$	m^2/s
Ambient temperature	T_a	= 288.15	K
Thermal conductivity air	λ_a	= 0.0257	J/(m·s·K)
Prandtl number air	Pr_a	= 0.786	
Viscosity air	η_a	= $1.65 \cdot 10^{-5}$	N·s/m^2

Output

Evaporation rate at 600 sec	q_v	= 10.25	kg/s
Temperature of liquid at 600 sec	T_L	= 273.06	K

Procedure
1. The heat flux from the atmosphere: by convection H_a and solar radiated heat flux H_{rs}, H_{rl} can be estimated by the methods addressed in paragraph 3.2.2.
2. The unstationary heat flux from the ground H_c can be estimated by equations (3.145a) and (3.145b).
3. The vaporisation rate q_v can be estimated by equations (3.141), (3.13), (3.21) and (3.22) on the basis of the conditions of the pool at time t.
4. The changing liquid pool temperature T_p can be determined by the equations (3.142a) to (3.142d) and equation (3.143).
5. The decreasing liquid height h can be determined by the equations (3.143a) and (3.143b).

Note that t is the specified time from the start of the release for which the vaporisation mass rate and pool conditions are required.

The 5 steps have to be repeated for small time-steps $\delta t = t/N_{steps}$ (for instance $N_{steps} = 50$), until one of the following conditions is fulfilled:
1. until specified time t has been reached;
2. all released liquid has vaporised;
3. the pool temperature T_p has decreased below melting point of the spillt chemical

Note that the nett radiation from the surroundings, neglecting direct sun radiation, has been estimated by applying the Stephan-Boltzman law, taking into account the correct emission and absorption factors, by

$$H_s = 4.09 \times 10^{-8} \times (T_a + dT_p)^3 \times (T_a - T_p) \qquad (J/(m^2 \cdot s)) \qquad (3.187)$$

Some particular intermediate results:

Initial pool radius r	:	21.85 m
Reynolds' number Re	:	6.49×10^6
Mass transfer coefficient $k_{H,a}$	:	5.66 m/s

The calculations were carried out with small time-steps $\Delta t = 10$ s.
In the following table intermediate results are presented.

Intermediate results

t (s)	T_p (K)	q_v (kg/s)	h_p (m)	δT_p (K)	H_a (W/m²)	H_c (W/m²)	H_s (W/m²)
0.00	288.15	19.28	0.106	-0.351	0.00	0.00	0.00
10.0	287.80	19.02	0.106	-0.345	1.99	25.95	1.37
20.0	287.45	18.77	0.106	-0.340	3.94	36.37	2.72
30.0	287.11	18.52	0.106	-0.335	5.87	44.20	4.04
40.0	286.78	18.28	0.106	-0.331	7.76	50.66	5.33
50.0	286.45	18.05	0.105	-0.326	9.64	56.24	6.61
60.0	286.12	17.82	0.105	-0.322	11.48	61.18	7.86
70.0	285.80	17.59	0.105	-0.318	13.31	65.63	9.09
80.0	285.48	17.37	0.105	-0.314	15.11	69.69	10.30
90.0	285.17	17.16	0.105	-0.310	16.88	73.44	11.50
100.0	284.86	16.95	0.104	-0.306	18.64	76.91	12.67
110.0	284.55	16.74	0.104	-0.302	20.37	80.14	13.83
120.0	284.25	16.54	0.104	-0.299	22.08	83.18	14.96
130.0	283.95	16.34	0.104	-0.295	23.77	86.03	16.08
140.0	283.66	16.15	0.104	-0.291	25.44	88.72	17.19
150.0	283.36	15.96	0.103	-0.288	27.09	91.27	18.27
160.0	283.08	15.78	0.103	-0.284	28.72	93.69	19.34
170.0	282.79	15.59	0.103	-0.281	30.33	95.99	20.40
180.0	282.51	15.42	0.103	-0.278	31.92	98.18	21.44
190.0	282.23	15.24	0.103	-0.275	33.49	100.27	22.46

Intermediate results (continuation)

t (s)	T_p (K)	q_v (kg/s)	h_p (m)	δT_p (K)	H_a (W/m^2)	H_c (W/m^2)	H_s (W/m^2)
200.0	281.96	15.07	0.103	-0.272	35.05	102.27	23.47
210.0	281.69	14.90	0.102	-0.268	36.58	104.18	24.46
220.0	281.42	14.74	0.102	-0.265	38.10	106.01	25.44
230.0	281.15	14.58	0.102	-0.262	39.60	107.77	26.41
240.0	280.89	14.42	0.102	-0.259	41.09	109.45	27.36
250.0	280.63	14.26	0.102	-0.257	42.56	111.07	28.30
260.0	280.37	14.11	0.102	-0.254	44.01	112.63	29.23
270.0	280.12	13.96	0.101	-0.251	45.45	114.14	30.14
280.0	279.87	13.81	0.101	-0.248	46.87	115.58	31.04
290.0	279.62	13.67	0.101	-0.246	48.27	116.98	31.93
300.0	279.38	13.53	0.101	-0.243	49.66	118.32	32.81
310.0	279.13	13.39	0.101	-0.240	51.04	119.62	33.67
320.0	278.89	13.25	0.101	-0.238	52.40	120.88	34.52
330.0	278.65	13.12	0.101	-0.235	53.75	122.09	35.37
340.0	278.42	12.99	0.100	-0.233	55.08	123.26	36.20
350.0	278.19	12.86	0.100	-0.230	56.40	124.40	37.02
360.0	277.96	12.73	0.100	-0.228	57.70	125.50	37.83
370.0	277.73	12.61	0.100	-0.226	58.99	126.56	38.63
380.0	277.50	12.48	0.100	-0.223	60.27	127.59	39.42
390.0	277.28	12.36	0.100	-0.221	61.53	128.58	40.20
400.0	277.06	12.24	0.100	-0.219	62.79	129.55	40.97
410.0	276.84	12.13	0.099	-0.217	64.03	130.48	41.73
420.0	276.62	12.01	0.099	-0.215	65.25	131.39	42.48
430.0	276.41	11.90	0.099	-0.213	66.47	132.27	43.22
440.0	276.19	11.79	0.099	-0.210	67.67	133.13	43.95
450.0	275.98	11.68	0.099	-0.208	68.86	133.96	44.68
460.0	275.78	11.58	0.099	-0.206	70.04	134.76	45.39
470.0	275.57	11.47	0.099	-0.204	71.21	135.54	46.10
480.0	275.36	11.37	0.099	-0.202	72.37	136.30	46.79
490.0	275.16	11.27	0.098	-0.200	73.51	137.04	47.48
500.0	274.96	11.17	0.098	-0.199	74.65	137.76	48.17
510.0	274.76	11.07	0.098	-0.197	75.77	138.45	48.84
520.0	274.57	10.97	0.098	-0.195	76.88	139.13	49.50
530.0	274.37	10.88	0.098	-0.193	77.99	139.79	50.16
540.0	274.18	10.78	0.098	-0.191	79.08	140.43	50.81
550.0	273.99	10.69	0.098	-0.189	80.16	141.05	51.46
560.0	273.80	10.60	0.098	-0.188	81.23	141.65	52.09
570.0	273.61	10.51	0.098	-0.186	82.29	142.24	52.72
580.0	273.42	10.42	0.097	-0.184	83.35	142.81	53.34
590.0	273.24	10.34	0.097	-0.183	84.39	143.37	53.96
600.0	273.06	10.25	0.097	-0.181	85.42	143.91	54.56

3.7 Interfacing to other models

3.7.1 Introduction to section 3.7

The results from model predictions in this chapter 'Pool Evaporation' may be used for further calculations as input for subsequent physical effect models, described in:

chapter 4 'Vapour Cloud Dispersion', and
chapter 6 'Heat flux from fires'.

The models in this chapter 'Pool Evaporation' may act as a source term model to provide (quantitative) information about:
−   the amount of material entering the atmosphere by evaporation;
−   the dimensions of liquid pool;
−   the thermodynamic state of the evaporating liquids, such as concentrations, temperature, and pressure.

Vapour cloud dispersion will occur when vapours are entering the atmosphere. The pool evaporation models are able to determine the amount of vapour entering the atmosphere and the dimensions of the source.

On the other hand, the results from model predictions in chapter 'Outflow and Spray Release' may provide the required input for pool evaporation models.

Interfacing to the relevant models in chapter 2 'Outflow and Spray Release' and chapter 4 'Vapour Cloud Dispersion' will be addressed in the following paragraphs.

Pool fires may occur after the ignition of a (spreading or shrinking) liquid pool. Models in this chapter 'Pool evaporation' can be addressed to estimate the initial dimensions of the pool before ignition. Interfacing to the relevant models in chapter 6 'Heat flux from fires' will be treated there.

Vapour cloud explosion can only occur after dispersion of flammable material in the atmosphere. After having estimated the characteristics of the evaporating liquid pool, models in chapter 4 'Vapour Cloud Dispersion' have to be addressed first.

3.7.2 Outflow and Spray Release

3.7.2.1 Introduction

There are two ways by which liquid released from its containment can fall onto the ground or onto the water surface:
1. rain out from airborne droplets may occur in case of a two-phase release;
2. the liquid jet flows or falls directly onto the ground in case of a release of a 'non-boiling' liquid.

3.7.2.2 Spray Release

3.7.2.2.1 Interfacing of spray release model for finite duration release of pressurised liquified gases

The mass flow rate of droplets falling onto the ground or onto the water surface can be obtained from equation (2.161) in section 2.5.3.7

$$q_d = q_S - q_{nett,air} \qquad \text{(kg/s)} \qquad (3.188a)$$

q_d = mass rate of spray deposition   [kg/s]
$q_{nett,air}$ = mass flow rate remaining airborne   [kg/s]
q_S = liquid source discharge rate   [kg/s]

The distance from the source where the droplets will fall onto the ground or onto the water surface will be less

$$x(t_0) = u_f \times t_0 \qquad\qquad\qquad (3.188b)$$

where t_0, the time needed by a droplet to fall onto the ground or onto the water surface, following from equation (2.160), and u_f is the jet velocity after flashing, following from equation (2.149) This method provides an upper limit of $x(t_0)$ as in practice the horizontal velocity will decrease due to resistance of the ambient air when the droplets fall.

3.7.2.2.2 Interfacing of spray release model for instantaneous release of pressurised liquified gases

The fraction of the release that will be deposited onto the ground or onto the water surface follows from equation (2.183) in section 2.5.3.8.

$$Q_d = Q - Q_{nett,air} \qquad\qquad \text{(kg)} \qquad (3.189)$$

Q_d = mass deposited spray   [kg]
$Q_{nett,air}$ = mass remaining airborne spray [kg]

The chemical will be deposited onto the ground or onto the water surface in the direct vicinity of the two-phase release.

3.7.2.3 Liquid release

The interfacing of models predicting the (finite) mass flow rate is straightforward. The (time-dependent) mass flow rate predicted by the models in paragraph 2.5.4 can be used without modification.

For instantaneous liquid releases the total mass released provides sufficient information for the pool evaporation models.

3.7.3 Vapour cloud dispersion

3.7.3.1 Introduction

The predicted liquid pool evaporation rate q_v will vary in time. For the atmospheric dispersion models requiring a (semi-)continuous source strength, the same averaging method as described in paragraph 2.7.2.1 can be applied.

Both SLAB and GPM require dimensions of the source. By an integration over time GPM can cope with varying source dimensions in principle. However, for SLAB these dimensions have to be constant.
Note that in general the dimensions of the evaporating pool become less important at a greater distance from the pool, but are important at smaller distances.

For liquid releases within bunds, the dimensions of the bund can be used as source diameter, as the time for the pool to reach its maximum diameter is relatively short.

For durations after the initially spreading pool has reached its maximum diameter, the maximum pool diameter can be used as vapour source diameter for estimating the maximum concentration.

For spreading pools the matter is more complicated.
Using the maximum dimensions of the spreading pool for the predictions of the atmospheric concentration at any time, would lead to underpredictions for neutral gases. Also the average pool diameter would underestimate the concentrations for short durations after the start of the liquid release.
Neglecting the pool dimensions as such, but not the (increasing) evaporation rate, would lead to overpredictions regarding the wind axis.
Physically the concentration at the source can never be higher than the maximum concentration based on the partial vapour pressure at the pool surface

$$c_{i,max} < P°(T_s) \times \mu_i / (R \times T_s) \qquad\qquad (kg/m^3) \qquad (3.190)$$

where

$c_{i,max}$	=	maximum concentration vapour	$[kg/m^3]$
$P°$	=	vapour pressure as function temperature	$[N/m^2]$
R	=	gas constant	$[J/(mol \cdot K)]$
T_s	=	surface tempe rature pool	$[K]$
μ_i	=	mol mass vapour	$[kg/mol]$

The diameter of the source might have an effect on the way heavy gas dispersion models predict the dispersion in the initial stage, where gravity slumping plays a role. Therefore, a smaller source diameter might lead to underpredictions under specific circumstances.

Altogether we suggest to use the time-averaged pool diameter for the prediction of the maximum atmospheric concentrations at the wind axis during the spreading of the pool.

When estimating the concentration as a function of time, the travelling time $t = x/u_a$ of the vapour must be taken into account when switching the diameter of the liquid pool from the time-averaged pool diameter to the maximum (final) pool diameter.

3.7.3.2 Gaussian Plume Model

The Gaussian plume model (GPM, see section 4.5.3) can be applied if the evaporation results in neutrally or positively buoyant cloud.
The input for the Gaussian Plume Model can be limited to the evaporation rate q in (4.51) and the dimensions of the pool b_y and b_x.

3.7.3.3 The dense gas model of Britter and McQuaid

If the density after evaporation $\rho_j > \rho_a$, a dense gas dispersion model is needed. The simplest model is the continuous release model by Britter and McQuaid, see section 4.5.5.1. Input of this model is volume flow rate v_o. The volume flow rate v_o can be calculated by

$$v_o = q_S/\rho_o \qquad\qquad (m^3/s) \qquad (3.191)$$

with

$$\rho_{V,0} = P_a \times \mu_i/(R \times T_s) \qquad\qquad (kg/m^3) \qquad (3.192)$$

where
P_a	=	ambient atmospheric pressure	[N/m^2]
q_S	=	evaporation rate	[kg/s]
v_0	=	volume flow rate	[m/s]
$\rho_{V,0}$	=	vapour density at the source	[kg/m^3]

3.7.3.4 SLAB model

Another dense gas dispersion model, SLAB, is described in section 4.5.5.2. The source conditions are using the SLAB notations (see e.g. Table 4.21):
− Temperature of the source material TS: surface temperature liquid pool T_s.
− Vaporisation flow rate of the source QS: q_S.
− Area of the source AS: appropriate pool area.

For this case the pool evaporation option should be applied, i.e. IDSPL=1

3.8 Discussion

3.8.1 Introduction to section 3.8

In this section some general considerations on the models related to pool evaporation presented in this chapter are given and gaps in the description of pool evaporation are indicated.

3.8.2 General remarks

This chapter presents supplementary models for the evaporation in permeable subsoil and different boiling regimes.
A weakness of this chapter is that the supplementary models were not integrated into the more general GASP model.
To avoid inconsistencies and unforeseen numerical problems, the GASP model has been copied unchanged, and it follows the original publications, although in our opinion some sub-models are not optimal.

Models for pool evaporation from porous media are not well developed or based on limited experimental data.
No sufficient data are available in literature to enable a proper description of moist porous subsoil for the range $(0 < m_{w,ms} < 0.08)$.

The evidence that no substantial ice crust will be formed in case of a spill of cryogen on water, is not too strong.
Limited information could be presented about chemicals that react with water, like ammonia and phosgene. The fraction of instantaneously spilt liquid ammonia on water that is supposed to evolve from the water surface directly, is a rough estimate based on limited evidence.
No model for boiling liquids heavier than water, like chlorine, has been incorporated into this chapter.

3.8.3 Gasp

The GASP model describes pool evaporation of spreading boiling or volatile liquids on land or floating on water.
It is based on improved understanding of spreading phenomena, described by the so-called 'shallow layer equations', and of vaporisation, and the model forces the transition of boiling to non-boiling to be smooth.
The model turned out to be unavoidably complex as the simultaneous spreading, evaporating and (time-dependent) heat transfer, taking all heat sources into account, is a complex problem to solve.

In the model the mass transfer model is based on the theoretical work of Brighton [Brighton,1987]. For practical situations it is advisable to use the correlation Kawamura & MacKay, based on experiments carried out in the open.

The description of the boiling process in GASP has been simplified by neglecting the metastable boiling regime, and by applying a somewhat simplified approach by assuming film boiling or a constant heat transfer coefficient.
In literature a lot of attention is given to nucleate boiling and film boiling. Many common industrial liquefied gases will boil in the metastable boiling regime. So, the evaporation should be based on the model for metastable boiling.

The GASP model can still be approved regarding the following topics: dens gas behaviour of the vapour, effects of pool surface waves, the effects of sloping and porous subsoil and multi-component liquid pools [Webber,1990].

The GASP-model has to be computerised before any prediction can be made. In case the spreading of the liquid pool can be ignored, as may be the case for instantaneous liquid releases in bunds, it is possible to use simple models to guess the order of magnitude of the evaporation rate, at least with some accuracy. These models should be used with care. Some rules of the thumb for their applicability and validity have been given.

3.8.4   HACS-R

The HACS-R model is able to predict the evaporation of soluble volatile chemicals caused by an instantaneous release.
It has been assumed that all of the liquid goes into solution. This assumption is valid because it appears that the total vapour generated is a small fraction of the mass spilt. In reality the release of chemicals takes place over a finite period. Since even in the case of an instantaneous spill, the mass of vapour evolved appears a small fraction of the mass spilt, the predictions can be safely regarded as the worst case for long duration spills.

3.8.5   Epilogue

The gaps in the modelling of pool evaporation indicated here, leave plenty of room for further scientific research.

3.9   References

AIChE (1989)
Chemical Process Quantitative Risk Analysis - guidelines for -, Center for Chemical Process Safety of the American Institute of Chemical Engineers, 1989.

Aloha (1988)
Aloha - Areal Locations of Hazardous Atmospheres Version 4.0 - Technical Appendix, Nat. Oceanic & Atmospheric Administration, USA, 1988.

Beek (1975)
W.J. Beek and K.M.K. Muttzall, Transport Phenomena, J. Wiley and Sons Ltd, 1975.

Blanken (1980)
J.M. Blanken, Behavior of Ammonia in the Event of a Spillage, American Institute of Chemical Engineers, 1980.

Bolz (1972)
R.E. Bolz and G.L.T. Tuve, CRC Handbook of tables for Applied Engineering Science, 2nd Edition, 1972.

Brighton (1987)
P.W.M. Brighton, Evaporation from a Plane Liquid Surface into a Turbulent Boundary Layer, SRD/HSE-report R375, January 1987.

Brighton (1990)
P.W.M. Brighton, Further verification of a theory for mass and heat transfer from evaporating pools, J. of Hazardous Materials, 23 ,1990) 215-234.

Cavanaugh (1994)
T.A. Cavanaugh, J.H. Siegell, K.W. Steinberg, Simulation of vapor emissions from liquid spills, J. of Hazardous Materials, 38 ,1994) 41-63.

Chang (1982)
H.R. Chang and R.C. Reid, Spreading-boiling model for instantaneous spiulls of liquefied petroleum gas (LPG) on water, J. of Hazardous Materials, 25 ,1982) 19-35.

Dharmavaram (1994)
S. Dharmavaram, J.N. Tilton, R.J. Gardner, Fate and transport of ammonia spilt from a barge, J. of Hazardous Materials, 37 ,1994) 475-487.

Frie (1992)
J.L. Frie, G.A. Page, V. Diaz, J.J. Kives, Evaporation of containes and uncontained spills of multicomponent nonideal solutions, 7th Int. Symp. on Loss Prevention and Safety Promotion in the Process Industries, Taormina Italy 4-8 May 1992.

Jones (1992)
D. Jones, Nomenclature for hazard and risk assessment in the process industries, second edition 1992, Institution of chemical Engineeers U.K.

Kawamura and MacKay (1987)
P.I. Kawamura and D. MacKay, The Evaporation of volatile liquids, J. of Hazardous Materials, 15 ,1987) 365-376.

Melhelm (1993)
G.A. Melhelm, and P.A. Croce, Advanced Consequence Modelling Emission, Dispersion, Fires, and Explosions, second draft July, 1993, A.D. Little.

Mikesell (1991)
J.L. Mikesell, A.C. Buckland, V. Diaz and J.J. Kives, Evaporation of Contained Spills of Multicomponent Non-ideal Solutions, presented at Int. Conf. and Workshop on Modelling and Mittigating the Consequences of Accidental Releases of hazardous materials, May 20-24 1991, New Orleans, USA.

Nievergeld (1978)
P. Nievergeld, W.F.Salitatu, Reduction of gasoline evaporation by a partially coverage of the surface of the liquid pool, TNO-CTI-report 78-01601 ,1978).

Phelps (1992)
P.J. Phelps, R. Jureidine, The computer modelling of tank spills and containment overflows, 7th Int. Symp. on Loss Prevention and Safety Promotion in the Process Industries, Taormina Italy 4-8 May 1992.

Prince (1981)
A.J. Prince, A users manual to spill, SRD/HSE-report R210, July 1981.

Prince (1985)
A.J. Prince, Details and results of spill experiments of cryogenic liquids onto land and water, SRD-report R324, April 1985.

Raj (1974)
Ph. K. Raj et al, Assessment models in support of the hazard assessment handbook, NTIS, January 1974.

Raj (1981)
Ph. K. Raj, Models for cryogenic liquid spill behavior on land and water, J. of Hazardous Materials, 5 ,1981) 111-130.

Raj (1987)
Ph. K. Raj and A.J. Morris, Source Characterisation and Heavy Gas Dispersion Models for Reactive Chemicals, Report AFGL-TR-88-0003(I) for the USA Air Force Geophysics Laboratory, Dec. 1987.

Raj (1991)
Ph. K. Raj, Chemical Release/Spill Source Models - A review, presented at Int. Conf. and Workshop on Modelling and Mittigating the Consequences of Accidental Releases of hazardous materials, May 20-24 1991, New Orleans, USA.

Shaw (1978)
P. Shaw and F. Briscoe, Evaporation from spills of hazardous liquids on land and water, SRD/HSE-report R100, May 1978.

Stramigioli (1992)
C. Stramigioli, G. Spadoni, Vaporisation from multicomponent liquid spills,
7th Int. Symp. on Loss Prevention and Safety Promotion in the Process Industries,
Taormina Italy 4-8 May 1992.

Studer (1988)
D.W. Studer, B.A. Cooper and L.C. Doelp, Vaporisation and Dispersion Modelling
of Contained Refrigerated Liquid Spills, Plant/Operations Progress, Vol. 7, No. 2,
April, 1988.

SuperChems 4.0
Superchems - A detailed Consequence Modelling Package -, A.D. Little, Inc,
Cambridge, Massachusetts, USA.

Takeno (1994)
K. Takeno, T. Ichinose, Y. Hyodo, H. Nakamura, Evaporation rates of liquid
hydrogen and liquid oxygen spilt onto the ground, J. Loss Prev. Process Ind, 1994,
Vol 7., Number 5.

Technica (1994)
Personal communications with DNV Technica London.

Webber (1986)
D.M. Webber and P.W.M. Brighton, Similarity solutions for the spreading liquid
pools, SRD/HSE-report R371, July 1986.

Webber and Brighton (1987)
D.M. Webber and P.W.M. Brighton, An integral model of spreading vaporising
pools, SRD/HSE-report R390, August 1987.

Webber (1987)
D.M. Webber, Heat conduction under a spreading pool, SRD/HSE-report R421,
October 1987.

Webber (1988)
D.M. Webber, A model for the evaporation and boiling of liquid pools, SRD/HSE-
report R404, February 1988.

Webber and Jones (1988)
D.M. Webber and S.J. Jones, A model of spreading vaporising pools, paper presented
at the Int. Conference Cloud Modelling 1988.

Webber (1990)
D.M. Webber, Model for Pool Spreading and Vaporisation and its Implementation
in the Computer Code GASP, SRD/HSE-report R507, September 1990.

Webber (Jan. 1991)
D.M. Webber, Source terms, J. Loss Prev. Process Ind, 1991, Vol 4., January.

Webber (Apr. 1991)
D.M. Webber, A model of steady discharge into a vaporising pools, SRD/HSE-report R493, April 1991.

Webster (1981)
Websters' Third New International Dictionary, 1981.

Wilkinson (1991)
A. Wilkinson, Bund overtopping - the consequences following catastrophic failure of large volume liquid storage vessels, SRD/HSE-report R530, October 1991.

Woodward (1990)
J.L. Woodward, A integrated model for discharge rate, pool spread, and dispersion from punctured vessels, J. Loss Prev. Process Ind., 1990, Vol 3, January.

WorldBank (1988)
Technica, Ltd., Techniques for Assessing Industrial Hazards, World Bank technical paper number 55.

YellowBook (1988)
Methods for the calculation of physical effects of the release of dangerous materials (liquids and gases) 2nd ed., 1988), publ. by (Dutch) Directorate General of Labour; English version ,1992).

Zumsteg (1991)
F. Zumsteg anf T.K. Fannalöp, Experiments on the Evaporation of Liquefied Gas over Water, presented at Int. Conf. and Workshop on Modelling and Mittigating the Consequences of Accidental Releases of hazardous materials, May 20-24 1991, New Orleans, USA.

Chapter 4
Vapour cloud dispersion
E.A. Bakkum, N.J. Duijm

Modifications to Chapter 4 (Vapour Cloud Dispersion) with respect to the first print (1997)

Numerous modifications were made concerning typographical errors. A list is given below for the pages on which errors have been corrected.

Some figures in this chapter were poorly printed; viz. figures 4.5, 4.16 and 4.18 as well as the scheme in section 4.5.1. These prints have been improved.

Equation (4.51) on page 4.70 is a general expression for a continuous release.

In section 4.5.3.3 the equations (4.60) and (4.61) describe short duration releases instead of semi-continuous releases.
In equation (4.60b) $\sigma_x(x)$ has been replaced by $\sigma_x(u_a\,t)$.
Below equation (4.61c) a sentence has been added concerning linear interpolation on σ_x for values of x less than 50 m.
In section 4.5.3.6 it has been added that the proposed simplifications will introduce considerable continuity problems in calculating the concentration.

In section 4.5.4.1 describing the free turbulent jet model, equation (4.71) has been replaced and (4.73) has been removed. Hence all subsequent equations in chapter 4 have been renumbered.

The constant in equation (4.79) has been adjusted, as well as the empirical constants C_u and C_c in table 4.10.

The dispersion parameters were changed into the values of the 2nd edition of CPR14E.

In section 4.5.4.2 the equations (4.83) and (4.84) have been adjusted, as well as the constants in equations (4.87) and (4.92).
In equation (4.149) an ending bracket just before the division line has been added.

In section 4.6.3 concerning application of the Gaussian plume model, the examples have been updated.
Now subsection 4.6.3.1 describes the calculation of a plume and subsection 4.6.3.2 shows the calculation of explosive mass of an instantaneous puff.
Hence table 4.14 and figures 4.19 up to and including 4.21 have been replaced.

In subsection 4.6.4.1 the example on the free jet model has been corrected and figure 4.22 has been replaced.

Section 4.6.5 describes example calculations for four source term submodels in the SLAB model. Some errors in the SLAB model have been corrected. All calculations are updated and figures 4.23 up till and including 4.25 are replaced, whereas figure 4.27 has been added. Furthermore the values for the Concentration averaging time and Stability class in table 4.23 have been adjusted.

List of symbols Chapter 4

A	cross-flow area of cloud or plume (4.26)	m^2
b	half-width radius of jet or plume (4.16)	m
b_o	source radius (section 4.3.5.1.)	m
b_{ox}, b_{oy}, b_{oz}	source half dimensions in down-wind, cross-wind and vertical direction, respectively (4.62)	m
b_x, b_y	half-width of cloud in down-wind and cross-wind direction, respectively (4.114)	m
$b_{y,m}$	effective plume half-width including meandering (4.145)	m
b_z	cloud height (4.23)	m
C	general constants, to be defined in the text	
$c(...)$	concentration as a function of the terms between brackets (4.5)	parts per unit volume or $kg\ m^{-3}$
c_o	concentration at source (4.25)	p. p. u. v. or $kg\ m^{-3}$
c_c	concentration at jet, plume or cloud centre-line (4.28)	p. p. u. v. or $kg\ m^{-3}$
c_r, c_g	peak concentration at maximum plume height and plume touch-down, respectively (4.85)	p. p. u. v. or $kg\ m^{-3}$
c_{max}	maximum concentration (Section 4.3.5.1)	p. p. u. v. or $kg\ m^{-3}$
c_{mean}	time-averaged concentration (Section 4.3.5.1)	p. p. u. v. or $kg\ m^{-3}$
c_p	specific heat at constant pressure (4.1)	$J\ kg^{-1}\ K^{-1}$
$c_{p,a}$	ambient specific heat at constant pressure (4.115)	$J\ kg^{-1}\ K^{-1}$
c_{lfl}, c_{ufl}	lower and upper flammability concentration, respectively (4.66)	p. p. u. v. or $kg\ m^{-3}$
d	particle diameter (4.4)	m
e	albedo (4.37)	-
E_{gh}	ground heat (4.115)	$J\ m^{-1}\ s^{-1}$
E_{pc}	phase change energy (4.115)	$J\ m^{-1}\ s^{-1}$
$f\ (\ )$	general function, to be defined in the text, of the terms between brackets	
f	Coriolis parameter (4.8)	s^{-1}
f_x, f_y, f_z	drag term in down-wind, cross-wind and vertical direction, respectively	$kg\ s^{-2}$
F	buoyancy flux factor (4.20)	$m^4\ s^{-3}$
F_o	buoyancy flux factor at source (4.21)	$m^4\ s^{-3}$
F_d	dry deposition flux (4.5)	$kg\ m^{-2}\ s^{-1}$
F_n	wet deposition flux (4.6)	$kg\ m^{-2}\ s^{-1}$

$F_x(..), F_y(..), F_z(..)$

expressions which account for along-wind, lateral,
and vertical dispersion, respectively (4.28) m^{-1}

Fr	Froude number (4.17)	-
g	acceleration of gravity (4.1)	$m\ s^{-2}$
g'	effective gravity $g.(\rho - \rho_a)/\rho_a$ (4.20)	$m\ s^{-2}$
g_o'	effective gravity at source $g.(\rho_o - \rho_a)/\rho_a$ (section 4.3.5.1.)	$m\ s^{-2}$
h	height of plume or cloud centre-line (4.11)	m
h_i	mixing height (4.9)	m
h_s	source height (4.86)	m
Δh_r	final plume rise (4.84)	m
Δh_B	plume rise due to buoyancy (4.88)	m
Δh_M	plume rise due to momentum (4.92)	m
H_0	sensible heat flux (4.1)	$J\ m^{-2}\ s^{-1}$
H_r	net radiation heat flux (4.37)	$J\ m^{-2}\ s^{-1}$
H_{rs}	incoming solar radiation (4.36)	$J\ m^{-2}\ s^{-1}$
H_{ri}	isothermal net radiation heat flux (4.41)	$J\ m^{-2}\ s^{-1}$
H_g	ground heat flux (4.39)	$J\ m^{-2}\ s^{-1}$
H_l	latent heat flux (4.39)	$J\ m^{-2}\ s^{-1}$
ΔH	heat of condensation (4.144b)	$J\ kg^{-1}$
I	rain intensity (4.6)	mm per hour
K	reaction coefficient (4.3)	-
k_s	transfer coefficient (4.45)	-
L	Monin-Obukhov length (stability parameter) (4.1)	m
L_s	constant	m
L_b	buoyancy length-scale (4.101)	m
m	mass fraction of concentration (4.107)	$kg\ kg^{-1}$
M_o	momentum from source (4.17)	$kg\ m\ s^{-2}$
N	cloud cover (4.36)	-
p	(partial) pressure (4.142)	$N\ m^{-2}$
p_a	atmospheric pressure (4.143)	$N\ m^{-2}$
p_s	saturation pressure (4.143)	$N\ m^{-2}$
q	mass flow rate (4.11)	$kg\ s^{-1}$
Q	released mass (4.52)	kg
r	radial distance (4.23)	m

R	gas constant (4.142)	$J\ mol^{-1}\ K^{-1}$
s	coordinate along jet or plume centre-line (4.16)	m
s_l	length-scale parameter (4.71)	m
s_{lfl}	distance to LFL (4.80)	m
s_h	maximum jet height (4.79)	m
s_s	length of potential core (Table 4.10)	m
s_o	distance between real source and virtual source (Table 4.10)	m
t	time (4.12)	s
t_{av}	averaging-time (4.15)	s
t_{min}	minimum averaging-time (4.131)	s
t_L	integral time-scale of atmospheric turbulence (4.13)	s
t_i	integral time-scale of dispersion (4.54)	s
t_r	release duration (4.60)	s
t_{pk}	time to peak concentration (4.155)	s
T	temperature (4.138)	K
T_a	ambient temperature (at screen height, about 2 m) (4.1)	K
T_r	upper level ambient temperature (50 m) (4.41)	K
T_o	ambient temperature at roughness height (4.40)	K
T_s	surface or sea temperature (4.40)	K
T_w	wet bulb temperature (at screen height) (4.45)	K
T_*	turbulent temperature scale (4.34)	K
u	(down-wind) velocity of dispersing material (4.18)	$m\ s^{-1}$
u_a	ambient wind velocity (4.11)	$m\ s^{-1}$
u_c	velocity at jet or plume centre-line (4.73)	$m\ s^{-1}$
u_o	velocity at source (4.17)	$m\ s^{-1}$
u_y, u_z	lateral and vertical velocity of dispersing material, respectively (4.18)	$m\ s^{-1}$
u_*	surface friction velocity (4.1)	$m\ s^{-1}$
v_o	initial volume flow rate (4.100)	$m^3\ s^{-1}$
v_e	entrainment term (4.159)	$m^3\ s^{-1}$
V	cloud volume (4.25)	m^3
V_o	initial volume (4.25)	m^3
w_s	sedimentation velocity (4.4)	$m\ s^{-1}$
w_d	deposition velocity (4.5)	$m\ s^{-1}$
w_e	entrainment velocity (4.16)	$m\ s^{-1}$

$w_{e,t}$	top entrainment velocity (4.23)	m s^{-1}
$w_{e,e}$	edge entrainment velocity (4.23)	m s^{-1}
$w_{e,x}$	down-wind entrainment velocity (4.161)	m s^{-1}
$w_{e,y}$	cross-wind entrainment velocity (4.161)	m s^{-1}
w_H	effective heat transfer velocity (4.136)	m s^{-1}
x	down-wind horizontal coordinate	m
x_b	shape parameter (4.168)	m
x_c	down-wind distance to centre of mass of cloud (4.156)	m
x_{lfl}, x_{ufl}	down-wind distance to lower and upper flammability level, respectively (4.66)	m
x_u	upwind extension of a dense plume (4.101)	m
x_r	distance to maximum plume rise (4.83)	m
x_g	distance to plume touch-down (4.86)	m
x_v, x_{vy}, x_{vz}	virtual distances to account for finite source dimensions during evaluation of plume size (4.68)	m
y	cross-wind horizontal coordinate (4.2)	m
y_{lfl}, y_{ufl}	cross-wind distance to lower and upper flammability limit, respectively (4.65)	m
y_b	shape parameter (4.147)	m
z	vertical (upward) coordinate (4.2)	m
z_b	shape parameter (4.147)	m
z_o	surface roughness length (4.7)	m
z_s	constant (4.47)	m
z_{lfl}	height to lower flammability limit (4.65)	m

Greek symbols

α	moisture availability constant (4.38)	-
α_l	vapour mass fraction coefficient (4.138)	-
γ	ratio of specific heat of air to latent heat of water divided by rate of change (derivative) of saturation specific humidity with temperature (4.38)	-
γ_l	liquid mass fraction coefficient (4.138)	-
Γ_d	dry adiabatic lapse rate (4.33)	0.011 K m^{-1}
κ	von Karman constant (4.1)	0.4
Λ	wash-out coefficient (4.6)	s^{-1} per (mm per hour)
μ_a	molar weight of dry air (4.108)	kg mol^{-1}
μ_s	molar weight of dispersing material (4.108)	kg mol^{-1}

μ_{moist}	molar weight of moist air (4.139)	kg mol^{-1}
ν	kinematic viscosity (4.4)	m^2 s^{-1}
ρ	density (4.2)	kg m^{-3}
ρ_a	ambient density (4.1)	kg m^{-3}
ρ_p	density of particle (4.4)	kg m^{-3}
ρ_s	density of dispersing material (4.141)	kg m^{-3}
σ	Stefan Boltzmann constant (4.37)	5.67.10^{-8} W m^{-2} K^{-4}
σ_x, σ_y, σ_z	down-wind, cross-wind and vertical dispersion parameters of cloud (4.11)	m
σ_{yi}	dispersion parameter of instantaneous plume width (4.56)	m
σ_v, σ_w	standard deviation of turbulent velocities in cross-wind and vertical direction, respectively (4.13)	m s^{-1}
ϕ	conserved quantity (4.18)	arbitrary
φ	earth's latitude (4.8)	˚N
χ	solar elevation (4.36)	˚
ψ	earth's longitude (appendix 1)	˚W
Ψ	stability function (4.32)	-
Ω	earth's rotational speed (4.8)	7.27 . 10^{-5} s^{-1}

Note: the numbers between brackets refer to equations.

Glossary of terms

adiabatic lapse rate	vertical temperature gradient in an atmosphere where the potential temperature gradient is zero
aerodynamic diameter	diameter of a spherical particle that has the same free-fall velocity as the arbitrarily shaped particle
aerosol	airborne particle
albedo	fraction of solar radiation that is reflected into space
ambient	surrounding atmosphere
atmospheric stability	the extent to which vertical temperature (= density) gradients promote or suppress turbulence in the atmosphere
Boussinesq approximation	approximation in the Navier Stokes equation which considers density differences to be relevant for buoyancy only and not for momentum terms
buoyancy	the upward force (Archimedes force) that is caused by a cloud or plume in which the density is lower than the surrounding atmosphere
continuous release	release during a long time with a constant contaminant mass flow rate
dense gas	gas which has a higher specific weight than the surrounding ambient air
density	specific weight
deposition	absorption of gas or particles by the ground or vegetation
dispersion	mixing and spreading of gases in air, which causes clouds to grow
dispersion coefficient	standard deviation of the concentration profile in a cloud in one direction (lateral, i.e. cross-wind, vertical along-wind)
eddy	random vortex motion in turbulence

eddy diffusivity	apparent diffusivity due to turbulence, which acts like a molecular diffusivity in diffusing mass or momentum
ensemble	set of dispersion situations which are described by nominally the same initial and boundary conditions. Differences which occur within an ensemble are due to (turbulent) randomness
entrainment	mixing of (clean) air into a cloud or plume
flammable limits	concentration which is either the LFL or UFL
friction velocity	by definition the cube root from (minus) the shear stress at the surface
gravity spreading	the horizontal spreading of a dense gas cloud on the ground due to the hydrostatic force which is a result of the density difference
integral time-scale	time-scale which can be calculated by integrating (over time lag) the autocorrelation function of a turbulent quantity (i.e. velocity)
instantaneous release	release during which in a (very) short time a (large) amount of gas is released
Karman constant	proportionality constant appearing in the relation between velocity gradient and shear stress for turbulent flow near a rough surface
kinematic viscosity	viscosity divided by fluid density
LFL	lower flammability limit, below this concentration too little flammable gas is present in the air to maintain combustion
mixed layer	layer below the mixing height
mixing height	height of the turbulent boundary layer over the ground
Monin-Obukhov length	length-scale which characterises the atmospheric stability
Navier Stokes equations	momentum balance equations for movements in fluids
neutral atmosphere	atmosphere where potential temperature is constant with height

partial pressure	fraction of total pressure due to the presence of a gas; total pressure is the sum of all partial pressures of the gases present in a mixture
passive dispersion	dispersion solely caused by atmospheric turbulence
phenomenological models	models which present an empirical relation between initial and boundary conditions and observed phenomena, without tempting to describe the physical relationships
precipitation	rain, snow, etc.
pure jet	jet which is only driven by momentum
pure plume	plume which is only driven by buoyancy
plume rise	the ascent of a plume in the air due to vertical momentum at the source or buoyancy
puff	cloud spreading in all directions due to an instantaneous release
regula falsi	method to find a root of a function
roughness length	artificial length-scale appearing in relations describing the wind speed over a surface, and which characterises the roughness of the surface. Note the sizes of the elements causing the roughness can be more than ten times larger than the roughness length
saturation pressure	pressure of a gas at saturated state. It depends on temperature only; above the saturation pressure the gas will condense
saturation specific humidity	specific humidity of air with saturated water vapour, a function of temperature and, to a lesser extent, total pressure
sedimentation	the deposition of particles on the ground due to their free-fall velocity

semi-continuous	release with a constant contaminant mass flow rate during a finite time
shear	vertical velocity gradient
shear stress	stress exerted by the wind on the ground surface due to friction
specific humidity	humidity expressed as mass fraction of water vapour in air
stable	atmosphere where potential temperature increases with height
still air	air without detectable wind speed or direction
turbulence	random motions in a fluid due to instabilities of a large-scale flow
two-phase flow	flow in which two phases are present, e.g. gas and liquid droplets or liquid with gas bubbles
UFL	upper flammability limit, above this concentration too little oxygen is available to maintain combustion
unstable	atmosphere where potential temperature decreases with height
wash-out	absorption of gas or particles in rain-drops falling through a gas cloud or plume

Table of contents Chapter 4

Appendix 4.1   A method for estimating the solar elevation

4 Vapour cloud dispersion

4.1 Introduction

Hazardous material that is released in the atmosphere will be transported and diluted by the wind. This chapter will provide models that enable the prediction of this transportation and dilution process for various release scenarios and conditions. The output of these models are concentrations (as a function of time) at any location surrounding the release (up to several kilometres). Moreover, the total amount of hazardous material in a flammable vapour cloud between the upper and lower flammability limits will be predicted.

Dispersion will be restricted to dispersion within the atmospheric mixed layer in a stationary state. This means that down-wind distances are restricted to typically 10 km.

The input of the models described herein will be the results of the source term model, described in chapters 2 (Outflow and spray release) and 3 (Evaporation). Once the cloud, plume or jet interacts with the ambient air the dispersion processes described in this chapter are to be applied.

The Sections 4.2 through 4.5 in this chapter will each address all of the four main themes of this chapter viz. atmospheric stability; passive dispersion; jets, plumes, and plume rise; and dense gas dispersion. However, each section will treat the topics with a different aim:

Section 4.2 provides the essential and basic understanding of the phenomena of interest. It provides information on atmospheric turbulence in general, and addresses shortly some topics beyond the main themes, viz. deposition, chemical reactions and obstacle effects.

Section 4.3 provides a general overview of the currently available methods and models for the main themes, which enable quantified analysis. It includes some physical/mathematical background to models. The aim of the section is also to position the models selected for detailed description among other existing models.

Section 4.4 presents the considerations which led to the selection of models which are found to be acceptable for use and which are selected for detailed description.

Section 4.5 provides the detailed and complete description of the selected models. Whenever calculations or analyses have to be made, all necessary information can be found in this chapter. It is recommended to read the considerations presented in section 4.7 concerning validity and applicability of the models, before stating the calculations.

Section 4.6 gives examples of the use of the models presented in section 4.5.

Finally, section 4.7 provides some information on general restrictions on the use of models. It includes in some cases suggestions regarding methods to overcome these restrictions or it recommends alternative approaches.

4.2   The phenomenon of dispersion

4.2.1   Introduction to Section 4.2

This section provides the essential and basic understanding of the phenomenon of dispersion.
− Section 4.2.2 introduces atmospheric turbulence and dispersion.
− Section 4.2.3 explains atmospheric stability and the important parameters that describe stability.
− Section 4.2.4 describes the origin and effects of jets and plume rise.
− Section 4.2.6 describes the basic phenomenon of dense gas dispersion.
− Section 4.2.7 discusses some topics related to dispersion, viz. heat transfer, chemical reaction, deposition and effects of obstacles.

4.2.2   Atmospheric turbulence and dispersion

The lower part of the atmosphere in which the releases take place is called the mixed layer. The height of the mixed layer (the mixing height) varies mostly between 200 and 2000 m. The wind flow in this mixed layer is almost always turbulent, i.e. the movement of the air fluctuates continuously in velocity and direction due to the presence of eddies. These turbulent eddies are very effective in dispersing material through the air, a factor of at least 1000 more effective than molecular diffusion.

Turbulent flows are generally described in statistical terms, i.e. by a time-averaged mean velocity and a time-averaged standard deviation of velocity fluctuations around this mean value.

Even for still-air, stable conditions turbulence is present due to temperature differences in the atmosphere which cause movements of air.
According to Hanna [1990], the standard deviations of horizontal turbulent velocities are not lower than 0.5 m/s (with a scatter of ± 0.3 m/s).

Turbulence is generated in two ways viz.:

1. Mechanically through the resistance of the earth's surface on the wind. This causes a decrease of wind speed to the surface (velocity gradient or shear). This shear causes turbulence due to flow instabilities, and a downward turbulent flux of momentum to compensate the resistance force. The wind shear depends mainly on the upper wind speed and the surface roughness.

2. Thermally due to heating of the surface (mainly by the sun). Hot patches of air near the surface start to rise. This causes an upward turbulent flux of heat.

Without any generation of turbulence, turbulence will die due to viscous dissipation. Much more important in the atmosphere is the suppression of turbulence in steadily

stratified layers of air, i.e. in layers in which temperature increases upwards. Vertical movements of air are suppressed.

An important aspect of atmospheric turbulence is the large range of sizes of the turbulent eddies, from several hundreds of metres diameter down to millimetres. The different sizes of eddies act differently in diffusing a puff of gas, see Figure 4.1.
Turbulent eddies smaller than the size of the puff will uniformly disperse material and increase the size of the puff (Figure 4.1a). Turbulent eddies much larger than the size of the puff will only displace the puff without changing its size or geometry (Figure 4.1b). Eddies comparable to the size of the puff will change its geometry and increase its contour (Figure 4.1c). These aspects are also relevant to the understanding of concentration fluctuations. At a certain position one will observe fluctuations of concentrations due to meandering of the whole puff, and due to deformation of the puff. The concentration fluctuations are suppressed by small eddies within the puff.
As the puff grows, it is apparent that the number of eddies contributing to meandering will decrease, whereas 'sub-puff' eddies will contribute more and more to dispersion. The nature of turbulent dispersion changes during the life-time of the puff.
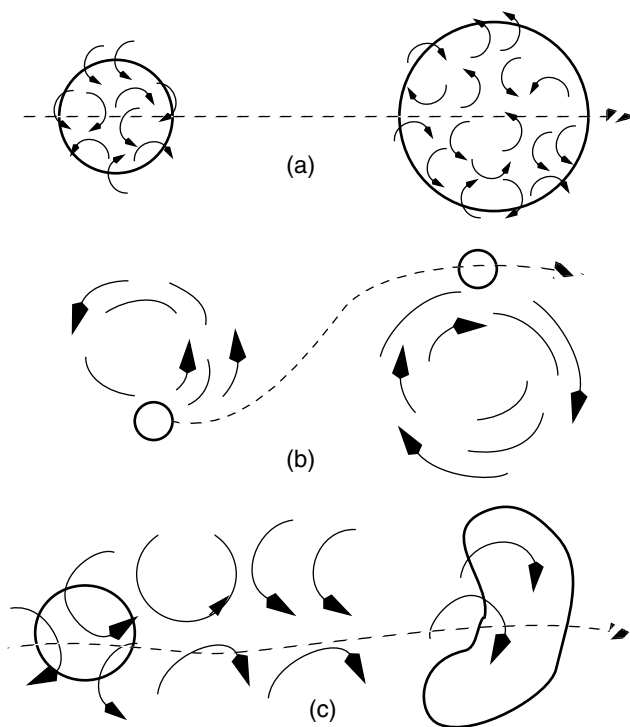
Figure 4.1 Dispersion of a puff of material under three turbulence conditions:
      (a) *Puff embedded in a field in which the turbulent eddies are smaller than the puff.*
      (b) *Puff embedded in a field in which the turbulent eddies are larger than the puff.*
      (c) *Puff embedded in a field in which the turbulent eddies are comparable in size to the puff [Seinfeld, 1986]*

The concepts are also applicable to continuous releases of gas (or aerosol). For continuous releases there is a problem of defining an appropriate averaging-time for determining concentration and plume size. An instantaneous picture of a continuous release will show the effect of individual large eddies displacing the plume centre-line, see Figure 4.2, the instantaneous concentration distribution. If one observes the subsequent action of a number of eddies, the time-averaged concentration distribution will show a Gaussian distribution (Figure 4.2, the 10-min or 1-hour averaged concentration distribution). If there is a maximum size of turbulent eddies, one will be able to define an averaging-time beyond which no change of the averaged concentration distribution can be observed. This is the case for eddies in the vertical plane, as the eddies need to be smaller than the mixing height. However, in the horizontal direction no such limit exists: the wind direction will change continuously. This means that the horizontal cross-wind size of a plume will be ever increasing with increasing averaging-time. This implicates that for any model for prediction of concentration an indication of averaging-time is necessary. The specification of an averaging-time is also relevant from a point of view of consequences: some consequences occur at very small-time-scales, almost instantaneously, (e.g. vapour cloud combustion) at time-scales of human inhalation (toxicity) up to tens of minutes (deposition at ground).
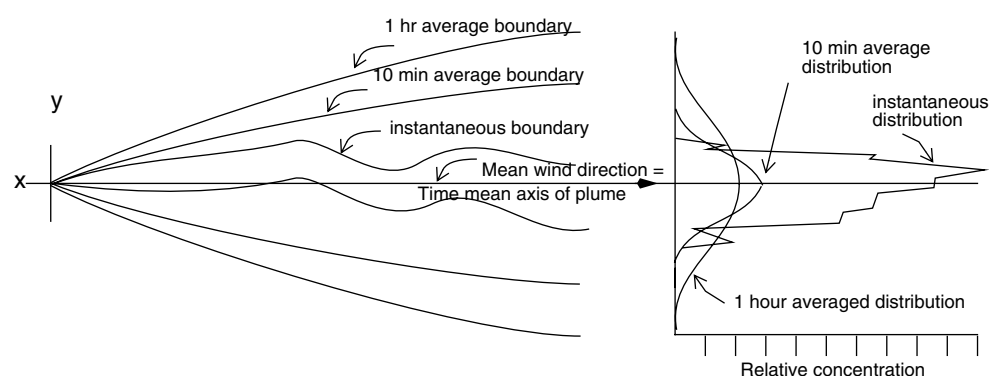
Figure 4.2   Plume boundaries (left) and concentration distributions (right) of a plume at different averaging-times [Seinfeld, 1986]

The inherent variability of turbulence and turbulent diffusion should be kept in mind when assessing model predictions of atmospheric dispersion. In fact, models (try to) predict an ensemble-average puff or plume, i.e. the averaged puff or plume from a large number of releases under nominally similar conditions.

4.2.3   Atmospheric stability

When an airpatch moves from the surface upwards it will expand as pressure decreases. Due to expansion the temperature of the airpatch will decrease. The temperature of a parcel which has been brought adiabatically to ground level is called potential temperature. When the airpatch has the same temperature as its surroundings during its travel upwards, the atmospheric stability is referred to as neutral: no forces due to density differences (originating from temperature

differences) are exerted on the patch. If the temperature of the airpatch becomes lower than its surroundings, the atmosphere is stable; the airpatch is forced downward. If on the contrary the temperature becomes higher than its surroundings, the atmosphere is unstable: the airpatch will accellerate upwards.

The vertical gradients of temperature are illustrated in Figure 4.3. From thermodynamics one calculates the dry adiabatic lapse rate to be -0.01 K/m. For saturated air, the condensation of water vapour reduces the cooling of the air and the decrease of temperature with height is less. This is the wet adiabatic lapse rate. For surface temperatures of about 290 K, the wet adiabatic lapse rate is about -0.005 K/m. (Due to the change of saturation pressure, the difference between the dry and wet adiabatic lapse rate is larger at higher temperatures.) For temperature gradients between the two, the atmosphere is stable for dry air and unstable for saturated air. This regime is called conditionally unstable.
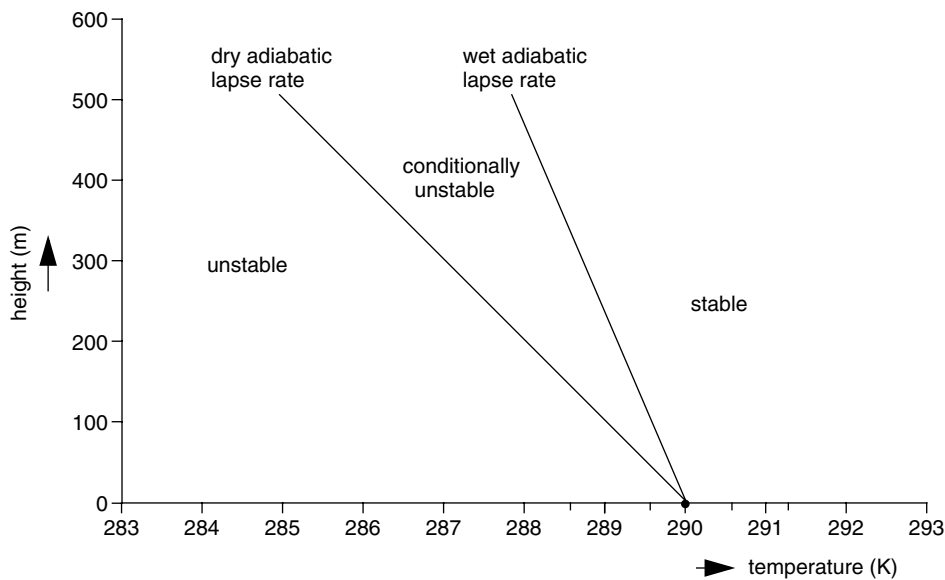
Figure 4.3   Temperature gradients and stability regimes in the atmosphere

During unstable conditions there is a heat flux from the surface upwards (this occurs as the surface is heated by the sun). During stable condition the heat flux is downwards (the surface is cooled at night by heat radiation to the sky). The stability of the mixed layer is determined by the ratio of turbulence generated by the temperature gradient and the turbulence generated mechanically by wind shear at the surface. This ratio can be expressed by a characteristic length-scale, the Monin-Obukhov length, which is defined as:

$$L = -\frac{\rho_a c_p T_a u_*^3}{\kappa g H_o}$$
(m)   (4.1)

The friction velocity u_* is by definition the square root of the shear stress divided by the density of air at the surface. H_o is the sensible heat flux (see Section 4.5.2). In (4.1) ρ_a, c_p, and T are the density, specific heat, and near surface temperature of the air, respectively. κ is the so-called Von Karman constant ($\kappa \approx 0.4$) and g the gravitational acceleration.

The Monin-Obukhov length provides a measure of stability of the mixed layer. L can be interpreted as the height above the ground where turbulence generated by wind shear equals the turbulence dissipated by the heat flux. In unstable conditions there is not such an equilibrium, and this length is negative:

L > 0   stable   (H_o < 0)
L < 0   unstable   (H_o > 0)
L = ∞   neutral   (H_o = 0)

Table 4.1   Interpretation of the Monin-Obukhov length L with respect to atmospheric stability

L		Stability condition
Small negative	- 100 m < L < 0	Very unstable
Large negative	$- 10^5$ m $\leq$ L $\leq$ - 100 m	Unstable
Very large (positive or negative)	$|L| > 10^5$ m	Neutral
Large positive	10 m $\leq$ L $\leq 10^5$ m	Stable
Small positive	0 < L < 10 m	Very stable

Qualitative schemes to characterise stability are often used, e.g. the Pasquill scheme, which rates from class A (unstable) through D (neutral) to F (stable). Methods to determine atmospheric stability and the relation with the Pasquill scheme are described in Section 4.3.2.

4.2.4   Passive dispersion

Situations where the dispersion of a puff or cloud of material is governed solely by the atmospheric turbulence are called passive dispersion. The state of the atmosphere is not changed by the presence of the material in the air.

Assuming homogeneous turbulence and wind speed (i.e. the turbulence and wind speed are the same at all locations in the air) one can derive that the concentration distribution of an initially small puff of material becomes Gaussian in shape. In practice it appears that one observes a Gaussian distribution of concentration in very many occasions. Many dispersion models are based on this Gaussian distribution; these will be discussed in more detail in Section 4.3.3.

4.2.5   Jets and plume rise

4.2.5.1   Jets

Gases which are released with high velocity will cause jets. As long as the velocity inside the jet is high compared to velocities in the ambient air, the extent and mixing in the jet is only affected by the properties of the jet itself.
The velocity difference between the jet and the (assumed quiescent) surrounding air generates fine scale turbulence which causes the jet to spread sideways. The velocity in the jet reduces (about inversely proportional to the distance to the point of release). Finally the velocity will be reduced to such extent that passive dispersion takes over.

Models for free jets in still air and jets in cross-flow (wind) are discussed in Sections 4.3.4.1 and 4.3.4.2 respectively.

4.2.5.2   Plume rise

Material released in the atmosphere may rise because:
1. the material is less dense (buoyant) compared to the surrounding air and/or
2. the material contains upward momentum.

Theoretically, in a neutrally or unstably stratified atmosphere, the material will rise indefinitely. However, due to mixing, the volume over which buoyancy and/or momentum is distributed increases, and this causes the rate of plume rise to decrease rapidly. When vertical motion of the plume is of the same magnitude as the turbulent motion of the plume one assumes the plume or puff to be at its final height.

In case the atmosphere is steadily stratified, there is a height at which the released material, taking into account mixing during plume rise, will be in equilibrium with the density of the air at that height, which then is assumed to present the final plume rise.

After the plume has reached final plume rise, dispersion may be assumed to be passive.
For continuous releases from small source areas (stacks, vent pipes) a large number of models for plume rise exist. These will be discussed in Section 4.3.4.2 to 4.3.4.3.

4.2.6   Dense gas dispersion

Releases of material denser than the ambient air introduce some special effects which affect the dispersion.
The released material will descent to the surface and, once on the ground, spread radially under influence of the gravitational forces. This self-induced flow produces a shallow cloud with increased horizontal extent. At the front of the so-called 'gravity-current' a head will develop with a strong vorticity (see Figure 4.4). This velocity field is deterministic in nature and will replace, for the duration of the gravity spreading,

the random atmospheric turbulence. The self-induced flow will increase mixing, especially just behind the gravity head.

After gravity spreading has finished, the vertical variation of density in the cloud will cause a stable stratification in the cloud which reduces dispersion in vertical direction. Finally the effects of density will be dispersed and negligible and dispersion will become passive.

Dense gas dispersion models will be discussed in Section 4.3.5.
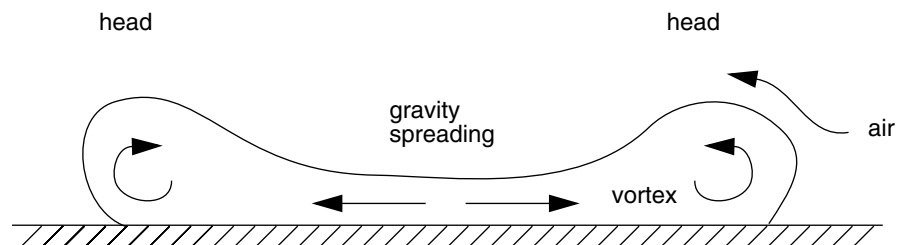
Figure 4.4   Gravity spreading of a dense gas cloud

4.2.7   Some other aspects of dispersion

In this section some aspects of dispersion are discussed that will not be discussed separately or in detail in the remainder of this chapter. These are: heat transfer, chemical reactions, deposition, and obstacle effects.

4.2.7.1   Heat transfer and change of buoyancy

Often the total buoyancy in a cloud, either negative (dense cloud) or positive, remains constant during the dispersion process. This is referred to by saying buoyancy is conserved.
For an instantaneous release this can be expressed as:

$$\iiint_{\text{all space}} \{\rho(x,y,z) - \rho_a(z)\} \; dx \; dy \; dz = \text{constant} \qquad \text{(kg)} \qquad (4.2)$$

Here, $\rho(x,y,z)$ denotes the density in the cloud and $\rho_a(z)$ denotes the density of the ambient air at the same height.

However, some processes in the cloud may change the total buoyancy:
− heat transfer from the surface to the cloud;
− vaporisation of liquid aerosol in the cloud;
− condensation and evaporation of water vapour aerosol in the cloud;
− chemical reactions which change the number of moles and/or which are endothermic or exothermic.

Heat transfer from the surface is relevant to cold plumes, originating e.g. from releases of cryogenic gases. The warm surface heats the cold gas, which can change from negatively buoyant to positively buoyant, causing the cloud to lift from the ground.
Depending on the velocity of the cloud over the surface and the temperature difference, heat transfer is dominated by forced convection or by free convection. For forced convection, the heat flux from the surface is about proportional to the friction velocity and the temperature difference. For free convection, the heat flux is independent of velocity and about proportional to the temperature difference to the power 4/3 rd.

Vaporisation of liquid aerosol, during releases of e.g. pressurised liquified gases, will cool down the air/gas mixture in the cloud, increasing its negative buoyancy.

The ambient air contains always some water vapour. For releases of cold material, the water vapour mixed into the cloud may condensate, thereby increasing the buoyancy. At a later stage, the condensed water may well evaporate again, cooling down the cloud, but these effects often happen at a distance or travel time from the release, where density effects are no longer relevant.

If the released material reacts with components in the air during which the number of molecules change, the total buoyancy is no longer conserved. If the number of molecules decreases, the cloud will become denser and vice versa. The heat produced or required by the chemical reaction will change the total buoyancy as is the case with condensation or evaporation of water.

4.2.7.2   Chemical reactions

Chemical reactions will also convert the initialy released substance into another secondary substance. From a point of view of hazards one might be interested in the primary substance or in the secondary.
In general, a reaction of the form
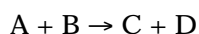
A + B → C + D

is controlled by a reaction constant K which determines equilibrium between the substances A, B, C and D:

$$K = \frac{[A][B]}{[C][D]} \quad \text{(K can be zero or infinite)} \qquad (-) \qquad (4.3)$$

([A], [B], etc, denote concentrations of the substances A, B, etc.)

Local deviations from equilibrium are due to finite reaction rates and, relevant near the release, to concentration fluctuations inside the cloud.

4.2.7.3   Deposition

Material can be removed from the cloud by deposition of material on the ground. One may discriminate the following deposition mechanisms:
− sedimentation of aerosols;
− dry deposition of gases and aerosols at the surface;
− wet deposition by precipitation (rain, snow) of gases and aerosols from the cloud.

All particles in the air have a finite sedimentation velocity. The sedimentation velocity w_s can be approximated by Stokes law:

$$w_s = \frac{1}{18} d^2 g \frac{\rho_p}{\rho_a \nu} \qquad\qquad (m\ s^{-1}) \qquad (4.4)$$

Here d is the (aerodynamic) diameter of the particle and ρ_p the specific density of the particle, ρ_a the density of air, g is gravitational acceleration, and ν is the kinematic viscosity of air.
In practice one may assume that the sedimentation velocity of particles smaller than 10 μm diameter ($w_s < 0.02$ m/s) is negligible, and that dispersion of these particles is similar to dispersion of gas.

Dry deposition of aerosols and gases can be described as a deposition flux F_d which is the product of a deposition velocity w_d and a concentration c at some reference height above the surface.

$$F_d = w_d\, c \qquad\qquad (kg\ m^{-2}\ s^{-1}) \qquad (4.5)$$

The deposition velocity is the inverse of the sum of three resistances; viz. an aerodynamic resistance dominated by turbulence and stability of the atmosphere between the surface and the reference height; a resistance which is caused by the flow around structures at the surface (surface induced resistance), dominated by the friction velocity and surface roughness, and a surface resistance, which depends on the properties of the substance (e.g. solubility in water) and the type of surface (vegetation).
The aerodynamic resistance can change from about 1000 s/m (stable conditions, smooth surface and low wind speed) down to 3 (high-wind speed, rough surface).
Typical values for the surface induced resistance are in the order of 10 s/m. Surface resistances can vary from order of 10 to more than 1000 s/m.

Wet deposition only occurs during precipitation, but it can be much more effective than dry deposition. Wet deposition can be described by a wash-out

coefficient Λ (s^{-1} per mm precipitation per hour)[1] and an intensity of precipitation I (mm/hour)[1]. The wet deposition flux F_n can be written as:

$$F_n = \Lambda I \int_{surface}^{cloudheight} c(z)dz \qquad\qquad \text{(kg m}^{-2}\text{ s}^{-1}) \qquad (4.6)$$

Here, $c(z)$ is the concentration in the cloud. For aerosol ΛI is typically $4 \cdot 10^{-4}$ s^{-1} for a precipitation of 1 mm per hour.

4.2.7.4   Obstacle effects

Dispersion over flat terrain with homogeneous roughness of which the individual roughness elements are smaller than the height of the cloud is rather well understood. The flow and dispersion around individual obstacles or arrays of obstacles is difficult to describe and to quantify in a general way (for a number of specific situations approximate solutions have been found).
Obstacle effects however are important. A rule of thumb to estimate when to account for obstacles is that the smaller value of height or width (in cross-wind direction) is larger than 0.5 to 1. times the local cloud height.
Behind obstacles a so-called recirculation zone exists. This zone may extend to about 10 times the obstacle height [Duijm and Webber, 1993]. Due to increased turbulence in the wake of the obstacle, the maximum groundlevel concentration down-wind of the recirculation is lower than in the absence of the obstacle. Nearer to obstacles no general trend can be indicated: an increase of concentration is possible and increases by a factor of 2 have been reported.

---

[1] Λ and I are usually expressed in these non-SI units.

4.3   General overview of existing models

4.3.1   Introduction to Section 4.3

Section 4.3 provides an overview of methods and models used for dispersion calculations. It presents alternative methods and provides short descriptions of the contents of the main types of models in a general way.
In this section the following themes are discussed:
−   Section 4.3.2 presents atmospheric stability schemes and methods to predict characteristics of the atmosphere.
−   Section 4.3.3 presents passive dispersion models with emphasis on the Gaussian plume models.
−   Section 4.3.4 presents models for jets and plumes in still air and in ambient wind, and simple models for plume rise.
−   Section 4.3.5 presents various types of dense gas dispersion models.

4.3.2   Models to describe atmospheric stability and atmospheric parameters

4.3.2.1   Atmospheric stability classifications

All models used to describe or predict atmospheric dispersion need information about the stability of the atmosphere, mainly to define the rate at which the material is passively dispersed by atmospheric turbulence. This information can be obtained through various methods:
−   Direct measurement of the intensity of wind direction fluctuations in lateral and vertical direction [Erbrink, 1991]. This method requires measurements which are not routinely carried out. The link with alternative schemes (e.g. the Pasquill scheme, see below) is difficult. However, the results can be directly applied to calculate the dispersion parameters (plume widths) for the Gaussian plume model.
−   Classification of horizontal wind direction traces as defined by Singer and Smith 71953], the so-called Brookhaven Gustiness Classes, changing from Class A (unstable) to Class D (stable). It is not clear whether this scheme can represent stability adequately over different types of terrain and different climates.
−   Classification of atmospheric stability from routine meteorological data, such as the well-known Pasquill scheme [Pasquill and Smith, 1983] which is based on observations of wind speed, cloud cover and time of day. The Pasquill scheme is currently the most applied scheme.
−   Direct measurement of friction velocity u_* and Monin-Obukhov lenght L, which provides an unambiguous measure of stability in the lower part of the atmospheric boundary layer (see Section 4.2.2). These measurements are not routinely carried out. The link to e.g. the Pasquill scheme can be made.

- Calculation of friction velocity and Monin-Obukhov length from routine meteorological data and terrain specification as by Holtslag, Nieuwstadt and Van Ulden [Holtslag, 1984; van Ulden and Holtslag, 1985; Holtslag and Nieuwstadt, 1986; Holtslag and de Bruin, 1987; Holtslag, 1987]. The link to the Pasquill scheme can be made.

Most widely-used dispersion models make use of the Pasquill stability categories (A-unstable to F-stable) and parametrisations of the local lateral and vertical plume width (σ_y and σ_z) corresponding to Pasquill-Gifford, Briggs, Smith, etc. (see e.g. Seinfeld [1986], pp 577).

However, better results can be obtained if the qualitative schemes are exchanged in favour of schemes using quantifications of physical parameters of the boundary layer (such as roughness length z_o, heat flux H_o, friction velocity u_*, and Monin-Obukhov length L).
A complete scheme using routinely meteorological data has been developed by Holtslag, Nieuwstad and Van Ulden. The scheme is based on providing an estimate of the surface heat budget, i.e.:

sensible heat flux + latent heat flux + heat flux into the soil =

net radiation =

(1 - albedo) * solar radiation + incoming long wave radiation

- outgoing long wave radiation

The sensible heat flux determines the stability of the atmosphere. Holtslag's scheme provides methods of estimating all terms in the equation above based on routinely available data and information of the local situation (e.g. surface roughness, albedo and solar elevation). Holtslag's scheme is described in Section 4.5.2.

It is possible to link the Pasquill stability scheme to the Monin-Obukhov length depending on local surface roughness by a graph proposed by Golder [1972]. This method is included in Section 4.5.2 (see Figure 4.11).

The stability over extended water surfaces (seas) depends mainly on the temperature differences between the air and the water. From the temperature difference one can compute the sensible heat flux which, together with the friction velocity, determines stability. Hsu [1992] developed a simple scheme (nomogram) to relate the stability in terms of Monin-Obukhov length and Pasquill classes to the temperature difference between the water surface and the air and the wind speed, which are routinely available data, see Section 4.5.2.4 and Figure 4.12.

4.3.2.2   Other atmospheric characteristics

Almost all characteristics of the mixing layer can be expressed in terms of stability parameters (friction velocity u_* and Monin-Obukhov length L). Quantities relevant to dispersion are:
− vertical variation of wind speed;
− vertical variation of standard deviations of turbulent velocities in cross-wind and vertical direction (σ_v and σ_w respectively);
− mixing height.

Variation of wind speed
The vertical variation of wind speed is often approximated by a power law. Alternatively, wind speed u_a can be described by relations which follow from similarity theory in the surface layer:

$$u_a(z) = \frac{u_*}{\kappa} \ f(z/z_o, \ z/L) \hspace{3cm} (\text{m s}^{-1}) \hspace{1cm} (4.7)$$

Here $f(z/z_o, \ z/L)$ is an empirical function, u_* the friction velocity and κ the Von Karman constant. This relation is adequate up to a height of about 100 m above which the vertical variation of wind speed can be neglected. Well-known suggestions for the function f are from Businger and Dyer and Bradley and can be found in the text books Pasquill and Smith [1983], Seinfeld [1986], Panofsky and Dutton [1984], and Stull [1988]. More details can be found in Section 4.5.2.

Turbulence parameters
Values for standard deviations of turbulent velocities in the surface layer are provided by Panofsky and Dutton [1984]. Proposals for formulae describing the vertical variation of these quantities can be found in Gryning et al. [1987], Seinfeld [1986] and Stull [1988]. More information is provided in Sections 4.4.2 and 4.5.2.

Mixing height
The mixing height depends on:
− height of inversion layers;
− surface friction velocity;
− Monin-Obukhov length;
− latitude of position on earth.

The height of inversion layers is very often dominated by advection of large-scale air masses in which these inversion layers are present. These have little relation with the local situation of the mixing layer at any given moment. In The Netherlands the mixing height is dominated by these inversion layers about one third of the time. This situation will be different in other areas, depending on location on earth, proximity to seas and oceans, etc.

If no inversion layers are present, one might estimate the local mixing height from u_*, L and the Coriolis parameter f, which is defined as:

$$f = 2 \ \Omega \ \sin \varphi \hspace{3cm} (\text{s}^{-1}) \hspace{1cm} (4.8)$$

with Ω the earth rotation ($7.27 \cdot 10^{-5}$ s^{-1}) and ϕ the latitude of position on earth (about 51˚ for The Netherlands).

For purely neutral conditions, the mixing height can be calculated as (see e.g. Panofsky and Dutton, [1984]):

$$h_i = 0.2\ u_*/f \qquad\qquad (m) \qquad (4.9)$$

For stable conditions one may write for stationary conditions [Panofsky and Dutton, 1984, Pasquill and Smith, 1983]:

$$h_i = 0.4 \sqrt{\frac{u_*}{f}\ L} \qquad\qquad (m) \qquad (4.10)$$

No stationary solution exists for the mixing height in unstable conditions. The mixing height at a certain time of day can be calculated from the vertical temperature profile at sunrise and the time integrated heat flux since sunrise.

Statistical information about mixing heights can also be estimated from meteorological data. This information accounts for the effects of elevated inversions, but it can not be applied to all positions on earth. For calculations involving unstable conditions without information of time, this is the only applicable method.

Suggestions for mixing height predictions, based on statistical meteorological information and formulae (4.9) and (4.10) above, are presented in Section 4.5.2.

4.3.3 Models to describe passive dispersion

Passive dispersion is governed by atmospheric turbulence. Atmospheric turbulence is determined by the stability of the atmosphere and the height above the surface. Gryning et al. [1987] have defined scaling regions in the atmosphere (Figure 4.5).

Gaussian plume models have been used extensively for all regions mentioned in Figure 4.5. The basic expression for the Gaussian plume model for a continuous release is:

$$c(x,y,z) = \frac{q}{2\pi\ u_a \sigma_y \sigma_z} \cdot \exp\left(-\frac{y^2}{2\sigma_y^2}\right) \cdot \exp\left(-\frac{(h-z)^2}{2\sigma_y^2}\right) \qquad (kg\ m^{-3}) \qquad (4.11)$$
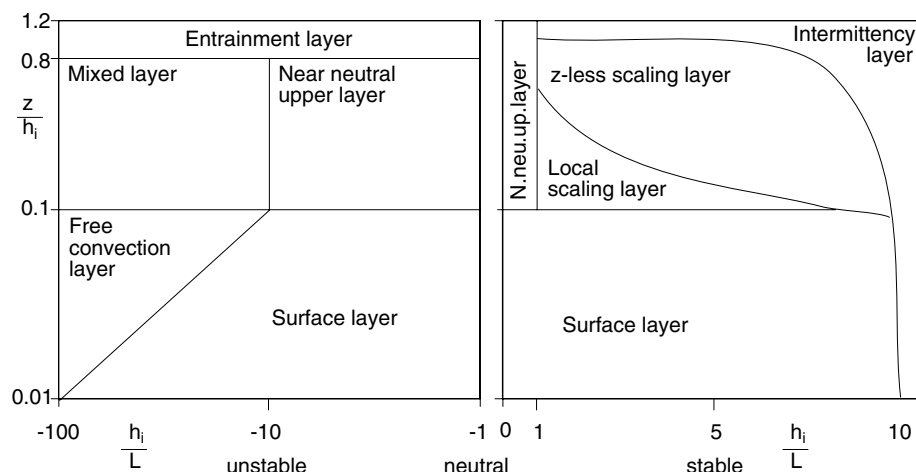
Figure 4.5   The scaling regions of the atmospheric boundary layer shown as function of the dimensionless height z/h$_i$, and the stability parameter h$_i$/L. A detailed discussion can be found in Holtslag and Nieuwstadt [1986]. When used to determine dispersion regions, the dimensionless height is replaced by h/h$_i$ where h is the source height.

The equivalent expression for an instantaneous release is written as:

$$c(x,y,z,t) \; = \; \frac{Q}{(2\pi)^{3/2}\sigma_x\sigma_y\sigma_z} \cdot \exp\left(-\frac{(x-u_a \cdot t)^2}{2\sigma_x^2}\right) \cdot \exp\left(-\frac{y^2}{2\sigma_y^2}\right) \cdot$$

$$\exp\left(-\frac{(h-z)^2}{2\sigma_z^2}\right) \qquad\qquad\qquad \text{(kg m}^{-3}) \qquad (4.12)$$

In (4.11) and (4.12) c(x,y,z) is the concentration at position x,y,z. Q and q are the total released mass and release rate, respectively. u_a is the ambient velocity at which the plume or puff is advected by the wind. σ_x, σ_y, and σ_z are the so-called dispersion parameters in along-wind, cross-wind, and vertical direcion, respectively. The height of the plume centre-line is denoted by h.

For plumes near the ground or near the mixing height additional terms appear in (4.11) and (4.12) to account for 'reflection' of material against the surface or the mixing height.

Within the framework of the Gaussian plume models, differences may appear in:
− the choice of the plume averaged transport velocity u_a: and
− the choice of the dispersion parameters σ_x, σ_y, and σ_z.

In most applications of the Gaussian plume model the transport velocity is taken as the wind speed at plume height h, with a minimum of h for surface releases.

With respect to the dispersion parameters σ_x, σ_y, and σ_z different approaches can be followed, two of which are mentioned here. The fundamentals of the different approaches are discussed in Pasquill and Smith [1983].

The first approach is based on the statistical theory of dispersion in homogeneous turbulence. This leads to expressions in which the spread (i.e. the dispersion parameter) in any direction is proportional to the intensity of velocity fluctuations in that direction times a function of travel time t and some integral time-scale of the turbulence t_L:

$$\sigma_x = \sigma_u \, f\,(t,t_L); \quad \sigma_y = \sigma_v \, f\,(t,t_L); \quad \sigma_z = \sigma_w \, f\,(t,t_L) \qquad \text{(m)} \qquad (4.13)$$

Several proposals for the function $f\,(t,t_L)$ for σ_y and σ_z have been suggested, see e.g. Pasquill and Smith [1983], Panofsky and Dutton [1984], Stern et al. [1984], and Seinfeld [1986]. The function as suggested by Draxler [Stern et al., 1984] for σ_y and σ_z is widely used.

The other approach is to provide fits to experimental data without a link to theoretical considerations. This leads to expressions of the form:

$$\sigma_x = f\,(x); \quad \sigma_y = f\,(x); \quad \sigma_z = f\,(x) \qquad \text{(m)} \qquad (4.14)$$

Widely-used suggestions for the function $f(x)$ for σ_y and σ_z are those of Pasquill-Gifford, M.E. Smith and Briggs [Pasquill and Smith, 1983; Stern et al., 1984; Panofsky and Dutton, 1984]. Seinfeld [1986] also includes the suggestions by Klug as incorporated in German guidelines for stack plume dispersion modelling.

Strictly speaking, the Gaussian plume model can not be used for description of passive dispersion in the surface layer because the vertical variations of wind speed and turbulence intensity in the surface layer cause the vertical concentration distribution to deviate from a normal distribution. Based on similarity theory and the concept of eddy-diffusivity one is able to provide analytical solutions or approximations for the vertical concentration distribution [Pasquill and Smith, 1983; Van Ulden, 1991, Gryning et al., 1987].

Little information is available on the along-wind dispersion parameter σ_x for (near) instantaneous releases. Not only turbulence in along-wind direction contributes to the increase of σ_x, but also the vertical variation of wind speed contributes to an increase of σ_x. Van Ulden [1991] provides a scheme for σ_x which accounts for both effects.

Schemes to estimate the cross-wind dispersion parameter σ_y need to indicate the averaging-time for which they are valid. In order to transfer σ_y-values to other averaging-times a power law expression with an exponent between 0.1 and 0.5 is generally accepted [Guinnup, 1992]. An exponent of 0.2 is widely used [Ermak, 1990];

$$\sigma_{y,t1} \; = \; \sigma_{y,t2}\left(\frac{t_{av,\,1}}{t_{av,\,2}}\right)^{0.2} \qquad \qquad \text{(m)} \qquad (4.15)$$

Here $\sigma_{y,t1}$ and $\sigma_{y,t2}$ refer to a horizontal dispersion parameters for an averaging-time of $t_{av,1}$ and $t_{av,2}$, respectively.

Relations for cross-wind spread of instantaneous releases are provided by Pasquill and Smith [1983], Panofsky and Dutton [1984] and Van Ulden [1991]. These should be used as minimum values for short-term exposure.

The selection of methods for description in the Yellow Book is justified in Section 4.4.3. The description of selected methods is provided in Section 4.5.3.

4.3.4   The modelling of turbulent jets and plumes

4.3.4.1   Jets and plumes in still air

The formalism for the modelling of free turbulent jets has been developed already several decades ago. It is the aim of this section to present the background information of the jet model, which is needed in gas dispersion calculations. The plume model, which is similar in many aspects, is also discussed. The aim of the recent scientific work has not been to make further improvements to the theory, but is concerned mainly with the collection of experimental data to determine the empirical constants in the formalism. The monograph of Chen and Rodi [1980] on the subject contains an outstanding and extensive compilation of the experimental results. Their recommended values of model parameters are discussed in Section 4.5.4.1.

Within the context of the Yellow Book, the definition of a pure jet is: a source of momentum and energy in the atmospheric environment. The fluid motion in a jet release is governed by the inertial forces. When the density of the released compound is different from the density of air, the buoyancy force will compete with the inertial force. The jet is called a positively buoyant jet when the inertial force and the buoyancy force act in the same direction; for a negatively buoyant jet the directions are opposite. Examples of buoyant jet releases are releases of vent stacks, exhausts, safety valves and punctures in pipes and reservoirs. All positively buoyant jets eventually become plumes. The jet momentum is continuously increased by buoyancy, and at some point sufficiently far above the source the momentum of the jet is largely independent of the initial momentum. This represents the fundamental property of a (pure) plume: it is a source of buoyancy. The pure plume can also emerge from a source release without initial momentum. e.g. heat diffusers, cooling towers, chimneys, burners, pool fires and evaporating liquid spills.

The analysis of jets in this section is made under the following simplifying assumptions:
− The release of the chemical compound consists of a turbulent outflow of gases. Two-phase releases are discussed in chapter 2 of this book.
− The source is axially symmetric, with a uniform outflow. These conditions provide a good approximation for the description of a wide class of controlled or accidental gas releases.

- It is assumed that buoyancy can either be neglected, or the buoyancy force is parallel to the inertial forces. In the latter case the release is in vertical direction, since the buoyancy force is caused by gravitation.
- The analysis is only valid when there are no large density differences between the jet and the surrounding atmosphere. This is called the Boussinesq approximation. The restriction is not severe, since jets and plumes which violate the Boussinesq approximation soon mix by entrainment of the surrounding air.
- The atmospheric environment consists of quiescent air at ambient conditions. The environment is neutrally stratified. It does not contain walls or other obstacles.
- Compressibility effects are neglected. In situations where the chemical compound is stored under high pressure a source model must be used to describe the initial expansion of the pressurised release (see Chapter 2), before using the jet model.

A turbulent jet (or plume) consists of 3 regions (see Figure 4.6): an initial region, a transition region, and the fully developed jet. The initial region consists of the core flow and a surrounding shear layer, which forms the boundary with the quiescent air. For a uniform exit velocity the core flow is nearly free of shear. In the transition region, the jet entrains air by the turbulent eddies in the shear layer, and the details of the exit core flow become obliterated. The resultant eddy-dominated flow is called fully developed.
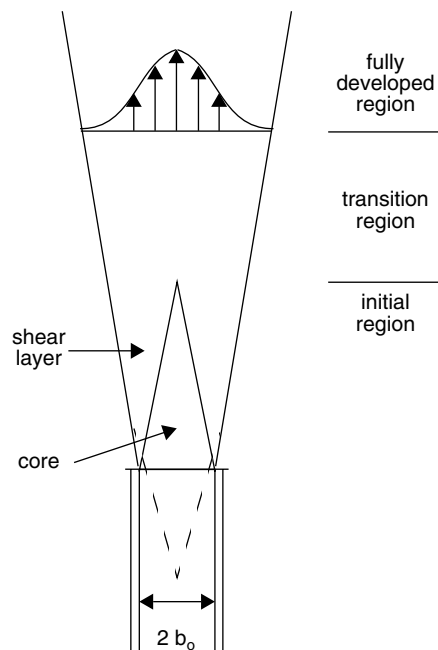
Figure 4.6   The development of a turbulent jet in still air

Non-buoyant jets
The analysis in this section aims to describe the distributions of velocity and concentration in the third region of a fully developed jet. Since the jet develops free of externally applied constraints, the distribution functions are dynamically similar if all quantities are nondimensionalised by local length and time-scales. It is convenient

to relate length and time-scales to the axial distance s from the origin of the jet and to the exit velocity u_o. In this approach it is assumed that the origin of the jet is a virtual point source instead of a finite circular source. In other words, the dimension of the source is neglected. The virtual point source does not necessarily coincide with the real source. However, experimental studies have shown that the separation distance is small, so s is approximately the distance from the real source exit.

The mass flow q(s) in the jet increases with the axial distance:

$$dq/ds = 2 \pi b \rho_a w_e \qquad\qquad (kg\ m^{-1}\ s^{-1}) \quad (4.16).$$

b is an estimate of the radius between the jet centre-line and the boundary surface of the jet; ρ_a is the ambient density. Equation 4.16 defines the entrainment velocity w_e. The physical interpretation is that an air flow passes through the boundary surface of the jet with a velocity w_e. A dimensional analysis shows that w_e is proportional to the jet centre-line velocity u_c. The ratio of these velocities is a measure of the dilution of the jet and is called the entrainment coefficient. The dynamic similarity of the non-buoyant jet in the region of fully developed flow has several other implications for the physical properties:
− The decay of the centre-line velocity u_c and of the centre-line concentration c_c of the chemical compound are both proportional to the inverse of the axial distance s.
− In lateral direction, perpendicular to the jet centre-line, the velocity and the concentration are only a function of the non-dimensional coordinate y/s, where y is the radial distance from the centre-line. Thus, the width b of the jet is proportional to the axial distance s, and the jet shape is conical with the origin, for which b is equal to zero, located at the virtual point source.

Note that the concentration of the compound is defined in parts per unit volume relative to the atmospheric level, i.e. it is the difference between the local value and the value in air.

Buoyant jets
The physical properties of the non-buoyant jet are determined by the cross-section integrated axial momentum M_o and by the ambient density ρ_a. For the pure, non-buoyant jet the density ratio ρ_o/ρ_a of the initial chemical compound and ambient air is unity. In the description of a buoyant jet, the buoyancy flux factor F_o of the chemical compound and ambient air appears as a third parameter. It can be shown [Chen and Rodi, 1980] that dynamic similarity can not exist for buoyant jets, so it is not possible to derive simple relations for the flow quantities, as in the case of the non-buoyant jet. In situations where the buoyant term in the momentum equations of the jet are of minor importance, the non-buoyant relations are approximately valid. The validity depends on the axial distance s, since for large s the buoyant force always becomes competitive with the inertial force. A negatively buoyant jet will rise to a maximum height under its inital momentum and then fall back on itself. A positively buoyant jet will gradually change into a pure plume. The properties of a pure plume are discussed below. Chen and Rodi define in their monograph length-scales that determine the regions of non-buoyant and pure plume behaviour.

Pure plumes

A plume is a buoyant jet whose initial momentum is nearly zero. For convenience it is assumed in this text that:
− The plume weighs less per unit volume than air, so the plume is driven upward under the pressure of the surrounding air.
− Molecular diffusion is negligible compared with turbulent transport.

It can be shown [Chen and Rodi, 1980] that with these assumptions the pure plume is self-preserving, or in other words, dynamically similar. The flow quantities can be derived by performing a dimensional analysis, which begins with the definition of the Froude number:

$$Fr = \frac{\rho_o}{|\rho_a - \rho_o|} \frac{u_o^2}{2b_o g} \qquad\qquad (\text{-}) \qquad\qquad (4.17)$$

Here, u_o is the exit velocity from the source, b_o is the radius of the real axial jet source, ρ_o is the density of the released material and ρ_a is the ambient density. It can be shown that the centre-line velocity u_c and the centre-line concentration c_c of the chemical compound are dependent on the Froude number and decay, respectively, as $s^{-1/3}$ and $s^{-5/3}$. Chen and Rodi have compared the simple relations of non-buoyant jets and pure plumes with experimental data, and determined the values of the model parameters in the equations. This is discussed in section 4.5.4.1.

4.3.4.2   Jets and plumes in cross-wind

The properties of jet and plume releases into a quiescent atmosphere have been discussed in the previous section. In the applications in industry and environmental problems, the release is usually deflected under the action of ambient wind. This configuration, which is called a jet in a cross-flow, is addressed in the present section. The dispersion of the chemical compound in the jet can be calculated with models which solve the full set of conservation equations of the relevant physical quantities. The review of Ooms and Duijm [1984] on the modelling of the dispersion of dense gas stack plumes has not lost its actuality and is used as the basis for the present general discussion of the formalism. A list of the most prominent models is given in this section, and one of these models is treated in detail in Section 4.5.4.2. An easier, although less accurate, way to calculate the plume dispersion is to apply the simple Gaussian plume model. In this case a correction must be made for the initial rise of the released compound due to momentum and density effects. Several mathematical expressions have been derived by Briggs [1969] to model the height of the total plume rise. The present section discusses the mathemathics of the model, and in doing so follows an approach that was originally adopted by Davidson [1989]. Section 4.5.4.3 gives recommendations on the application of Briggs' formulae.

The analysis of jets and plumes in a cross-flow starts from the same simplifying assumptions as given in the introduction of Section 4.3.4.1, with two modifications:
− The atmosphere is not quiescent, but the ambient air is moving as a uniform horizontal turbulent flow.
− In the discussion of integral trajectory models, the Boussinesq approximation is not used.

Section 4.3.4.1 was concerned with free jets and plumes, and their dispersion in an unbounded atmosphere. In practical situations of gas cloud dispersion the important quantity is usually the concentration of the chemical compound at ground level, which can only be determined with a model that accounts for the height of the source with respect to the ground.

The wind imposes a pressure field on the jet, which deflects the jet, deforms the initially circular jet cross-section into a kidney shape and establishes a pair of counter-rotating vortices in the cross-section. Entrainment of the air from the wind into the jet causes further deflection and after some distance the jet movement is approximately horizontal, with a mean velocity approaching the wind velocity (see Figure 4.7).
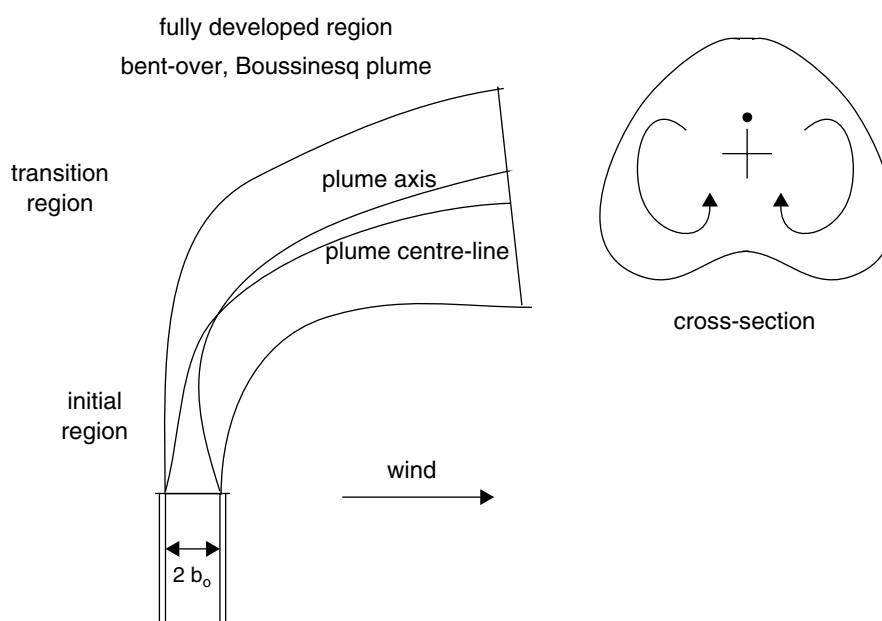
Figure 4.7   The plume trajectory in a cross-flow

One-dimensional integral trajectory models
Integral methods are based on simple profile shapes (mostly tophat or Gaussian) for the velocity, temperature and density distributions in the jet cross-section. Although some models attempt to describe the vortex structures in the jet with an ellipsoid, it is assumed here that the jet cross-section remains circular along its path. The conservation equations for mass, momentum, energy and chemical compound can then be integrated over the jet cross-section to yield ordinary differential equations of some characteristic velocity and density. To close the system of equations, it is

necessary to make further assumptions about the entrainment of air into the jet. The integral equations are of the form:

$$\frac{d}{ds}\left[\int_{o}^{\sqrt{2}b} \rho \ u \ \phi \ 2\pi y \ dy\right] = 2\pi b \ \rho_a \ \phi_a \ w_e(s) + f(s) \qquad (\phi kg m^{-1} s^{-1}) \quad (4.18).$$

In the equation s is the axial coordinate of the jet or plume, and y is the radial coordinate, perpendicular to the axis. ρ is the density and u the flow velocity in the jet, b is the width parameter of the jet and ρ_a is the density of ambient air. The term $w_e(s)$ can be interpreted as the entrainment velocity (cf. equation 4.16) and contains contributions from 3 processes:
− Jet entrainment occurs due to the shear stress with the atmosphere.
− Air is entrained by the velocity component of ambient wind, perpendicular to the jet axis.
− Entrainment due to atmospheric turbulence can be neglected close to the stack, but not at larger distances where it becomes the dominant process.
The functions ϕ and ϕ_a, represent the conserved physical quantity in the jet and in ambient air. It can be equal to 1 (unity), or the horizontal velocity u_x, or the concentration c or the heat content $c_p \cdot \Delta T$, leading to the conservation equations of, respectively, the total mass, the horizontal momentum, the chemical compound mass and the thermal energy. The function f(s) is non-zero only in the momentum equation, where it represents a drag term which takes into account changes in momentum due to the pressure field. It is a point of controversy whether the inclusion of drag forces in the momentum equation is really necessary. The set of equations is completed with the conservation equation for vertical momentum, in which case ϕ equals u_z, and the right-hand side of equation 4.18 includes the influence of the gravitational force.

In the equation the stratification of the atmosphere is not specified. The simplest plume trajectory models introduce two additional assumptions:
− The distributions of physical quantities within the plume are constant (tophat shape) at any given distance from the source.
− The atmosphere is not stratified.
The simplifications allow for an integration of the conservation equations over the whole plume cross-section. The integrated version of equation 4.18 is:

$$\frac{d}{ds}[\rho u \ \phi \ b^2] = 2\pi b \ \rho_a \phi_a w_e(s) + f(s) \qquad (\phi kg m^{-1} s^{-1}) \qquad (4.19)$$

Since by definition $\Delta T_a = 0$ in an unstratified atmosphere, the integrated conservation equation of thermal energy implies that the buoyancy flux factor F is a conserved quantity, see also Section 4.2.7.1 and formula (4.2). It is a measure of the density difference between the jet and ambient air, and defined as:

$$F = g' \ u \ b^2. \qquad (m^4 \ s^{-3}) \qquad (4.20)$$

The density difference is contained in the effective gravity g'.

The conservation equations are usually solved numerically, and yield the averaged density ρ and velocity u of material in the plume, the tilt θ (=arctan(u_z/u_x)) of the plume axis, and the width b of the plume, as a function of the distance s along the plume axis. The tophat profile of the physical quantities in the plume can, if required, afterwards be transformed into a Gaussian shape.

The differences in the assumptions of integral trajectory models become apparent when a comparison is made between the models, which have been implemented in four current dense gas dispersion models, i.e. DEGADIS, HGSYSTEM, PHAST and SLAB. The four implemented plume models are, respectively:
− the Ooms model (1972),
− the HFPLUME model (McFarlane et al. 1990),
− the TECJET model (Havens and Spicer, 1990),
− the model of Hoot, Meroney and Peterka (HMP, 1973).

The HMP differs from the other models in some aspects:
− It consists of analytic expressions for the ground locations of maximal plume rise and touch-down, the maximal height and the centre-line concentrations at these locations. The other models must be solved by means of numerical techniques;
− Entrainment from atmospheric turbulence is not included. Therefore, it does not describe passive gas releases.
In Table 1, information of the models is presented on a number of physical aspects.

Table 4.2   Physical aspects of 1-dimensional integral plume models

	cross section	cross-wind profile	surface roughness	entrainment from atmospheric turbulence	drag force	zone of flow establishment	slumped plume interface
Ooms	ellips	Gaussian	yes	yes	yes	yes	no
HFPLUME	circle	tophat	yes	yes	no	no	yes
TECJET	circle	Gaussian	no	yes	yes	yes	no[1]
HMP	circle	tophat	no	no	no	no	no[1]

[1]   Included in dispersion model.

Plume rise formulae
For many practical problems, it is sufficient to estimate the trajectory of the jet or plume in a cross-flow from empirical correlations. The derivation of the relevant parameters is best done by considering each of the terms in the conservation equations. In this section, the approach of Davidson [1989] is followed. First, the equations are simplified further by application of the Boussinesq approximation ($\rho = \rho_a$ = constant, except in density differences) and the bent-over plume assumption (u = u_a). These assumptions allow to derive an analytical equation for the plume trajectory, which includes the effects of both inertial forces and buoyancy forces.

Since the Boussinesq approximation and the bent-over plume approximation are used in the derivation of the trajectory equation, it is not intended for the calculation of properties close to the source. The plume rise due to initial momentum M_o and initial buoyancy F_o contribute with a down-wind dependency of $x^{1/3}$ and $x^{2/3}$, respectively. This implies that at distances further away from the source, the buoyant plume rise is the dominating term.

The formalism of Davidson is incomplete in the sense that it does not treat the effects of atmospheric stratification and stability. As a consequence, the equations predict an infinite plume rise, whereas in reality it is observed that the plume levels off at a certain height, after which it is influenced almost solely by the atmospheric conditions.

Assuming that the transition to a horizontal plume occurs at a down-wind distance x_r and that the plume rise due to the initial momentum is relatively small, the final plume rise is equal to

$$\Delta h_r = \text{constant } F_o^{1/3} / u_a \qquad \text{(m)} \qquad (4.21).$$

In equation 4.21, F_o is the buoyancy flux factor of the source (defined by 4.20 with u_o, g_o' and b_o). The constant has dimension ($m^{2/3}$). It has been shown by Briggs [1969] that experimental observations of plume rise from tall stacks can be described by equation 4.21, provided that the constant is a function of F and also of the atmospheric stability. Briggs has also derived expressions for momentum-dominated plume rise, of the form

$$\Delta h_r = \text{constant} / u_a^{2/3} \qquad \text{(m)} \qquad (4.22).$$

Here the constant has dimension ($m^{2/3} s^{-2/3}$).
Many models of final plume rise have been proposed by Briggs and by other authors, and most of them assume the functional behaviour which is given in the above equations. They differ mainly in the way that the effects of atmospheric stability are treated. A well-established model is presented in section 4.5.4.3

4.3.5   The modelling of dense gas dispersion

Our interest is in catastrophic releases of a chemical compound, with a large volume or volume flow rate. Many hazardous volatile materials are heavier than air, for one or more of the following reasons:
- The molecular weight of the chemical compound is higher than that of air. Examples are: LPG, cyclohexane, freon and chlorine.
- The chemical compound is released as a cold gas, or cooled due to the evaporation process. Examples are: LNG, ammonia and hydrogen fluoride.
- In case of a flashing release, the cloud is a mixture of aerosols and vapour. This is often seen in ammonia releases.
- Chemical reactions occur which are endothermic or result in the pick-up of atmospheric water vapour. Reactive chemical compounds are ammonia, hydrogen fluoride and nitrogen tetroxide.

The temporal behaviour of the dispersion process is determined by the failure mode:
− In an instantaneous release, a volume of gas is released in a very short time. Examples of instantaneous sources are severely ruptured vessels or rapidly emptying pressurised tanks.
− In a time-varying release the volume flow continues over a long period in an irregular way. An example is a liquid pool which is both spreading and vapourising.
− A continuous release is characterised by a constant volume flow rate with a sufficiently long duration for a steady state to be formed. Examples of this source type are steady-state liquid pools and small ruptures in pipes and vessels.

The instantaneous release type differs from the other two in that along-wind dispersion plays an important role in the dilution of the cloud.

During the dispersion process of a dense (negatively buoyant) gas cloud, 4 consecutive phases are observed:
− The initial phase. The fluid motion is a strong function of the release conditions.
− The gravity spreading phase. The entrainment is mainly due to the turbulence generation by the gravity-induced motion of the cloud.
− An intermediate phase. Entrainment is due to an interplay between the atmospheric turbulence and gravitational forces.
− The passive (neutrally buoyant) dispersion phase.

The gravity spreading phase (see also Section 4.2.6) provides a good illustration of the effects which are typical for dense gas:
− The density gradient induces gravity spreading in the horizontal direction. These gravity currents drive the flow within the cloud, independent of the atmospheric wind.
− Mixing is primarily through the self-generated vortices at the edge of the cloud (also called gravity-front).
− Mixing by atmospheric turbulence at the top of the cloud is suppressed by the density gradient.
− Turbulence within the cloud is reduced due to the stable stratification (i.e. a negative vertical density gradient) of the dense gas layer.

As a consequence, a dense gas cloud remains in the lower part of the atmosphere, with a large spread in the lateral direction. Meandering due to atmospheric turbulence is less than for passive clouds. Attempting to describe dense gases by adapting Gaussian models suitable for passive clouds is inherently inadequate, because the Gaussian models do not account for the momentum and energy effects.

Present dense gas dispersion models can be roughly divided into 3 classes:
− Phenomenological models, in which the dispersion behaviour is described by a series of nomograms.
− Intermediate models, such as box models and grounded plume models.
− Advanced models which solve the Navier-Stokes equations.

Except for models solving the three dimensional Navier-Stokes equations none of the models describe the internal flow in the cloud, such as the vortex in the gravity front. A general description of the models in the 3 classes is given in the Sections 4.3.5.1-4.3.5.3.

4.3.5.1 Empirical relations of dense gas dispersion

Empirical relations between the observed physical quantities in dense gas dispersion experiments originate from laboratory simulations on a small-scale, or from field tests, or from both. Simple formulae based on dimensional arguments can explain many observations of dense gas dispersion. It is, in general, not necessary to specifically model the detailed flows inside the gas cloud, since the gross entrainment integrated over the cloud is important. The starting-point is an inventory of the independent variables that are relevant in dense gas dispersion. They are:

− The mean wind velocity u_a.
− The initial volume V_o of the chemical compound (in case of an instantaneous release), or the volume flow rate v_o (for time-varying releases).
− The dimension b_o of the source.
− The density ρ_o of the chemical compound and ambient density ρ_a.

Other variables, such as the atmospheric stability, the local roughness length and the source geometry, are less important. A dimensional analysis yields the parameters that determine the dispersion process:

x/b_o, y/b_o, z/b_o, $u_a t/b_o$, $u_a^2/(gb_o)$, ρ_o/ρ_a, and either $v_o/(u_a b_o^2)$ or $V_o^{1/3}/b_o$.

Here x is the down-wind distance, y is the lateral coordinate, z is the height, t is the time and g is the gravity constant. The number of parameters can be reduced further by: (1) considering only ground level concentrations, (2) assuming that at any down-wind distance the maximum concentration occurs on the centre-line, and (3) employing the Boussinesq approximation. In the Boussinesq approximation the parameters $u_a^2/(gb_o)$ and ρ_o/ρ_a can be replaced by a single parameter $u_a^2/(g_o'b_o)$, where $g_o' = g(\rho_o-\rho_a)/\rho_a$ is the effective gravity at the source.

In an instantaneous release, the important dependent (output) variable is the concentration of the chemical compound at the time of arrival of the cloud. The concentration attains its maximum value c_{max} at that moment, and subsequently decreases with time as the cloud is advected past the point.

c_{max} is made non-dimensional with the initial concentration c_o expressed as the volume of chemical compound per unit volume. For a source with an approximately spherical or cubic shape, the dimension b_o of the source is proportional to $V_o^{1/3}$, and c_{max}/c_o depends on only 2 parameters: $x/V_o^{1/3}$ and $u_a^2/(g_o'V_o^{1/3})$.

In a time-varying or continuous release, the important dependent variable is the time-averaged concentration c_{mean}.

The source dimension b_o is less important further away from the source, as the plume forgets its past history. Then c_{mean}/c_o again depends on 2 parameters: $x\sqrt{(u_a/v_o)}$ and $u_a^{5/2}/(g_o'\sqrt{v_o})$.

The functional behaviour of the concentration values can be derived from experimental data and the resulting correlations can then be reproduced in nomograms. This approach has been followed by Britter and McQuaid in their Workbook (1988), and also in the VDI Guideline 3783 part 2 (1990).

4.3.5.2 Simple dense gas dispersion models

This section reviews the physical basis and algorithms of models for instantaneous releases (called box models) and models for continuous releases (grounded plume models). The simple dense gas dispersion models describe only the overall behaviour of the cloud. This becomes apparent when one considers the basic assumptions that are made in box and plume models:
− The dispersion moves over flat terrain or water.
− The substrate properties (surface roughness, thermal properties) are uniform over the entire terrain.
− Similarity profiles of velocity and concentration are imposed in all directions of the cloud (usually tophat or Gaussian).
− The cloud spreading is described by gravity intrusion models.
− Local concentration fluctuations are not modelled.

Several extensive publications have appeared on the subject of simple dense gas dispersion models, for instance Wheatley and Webber [1984]; Hanna and Drivas [1987]; and Ermak, Rodean, Lange and Chan [1988].

Box models
Box models have been developed for the description of the dispersion process, which follows after an instantaneous release of dense gas. Typical examples are:
− The work of Cox and Carpenter [1979], which resulted in the computer models CONSEQ, SAFETI and PHAST.
− The work of Eidsvik [1980], and the associated computer model CHARM [Radian Corporation, 1988].
− The work of Fryer and Kaiser [1979], and the associated computer model DENZ.
− The work of Kaiser and Walker [1978], which resulted in the computer models SAFER and TRACE.

All box models assume that the dense gas cloud has the shape of a flat circular cylinder, with a uniform height and radius, and a uniform gas concentration in the entire cloud volume (see Figure 4.8).
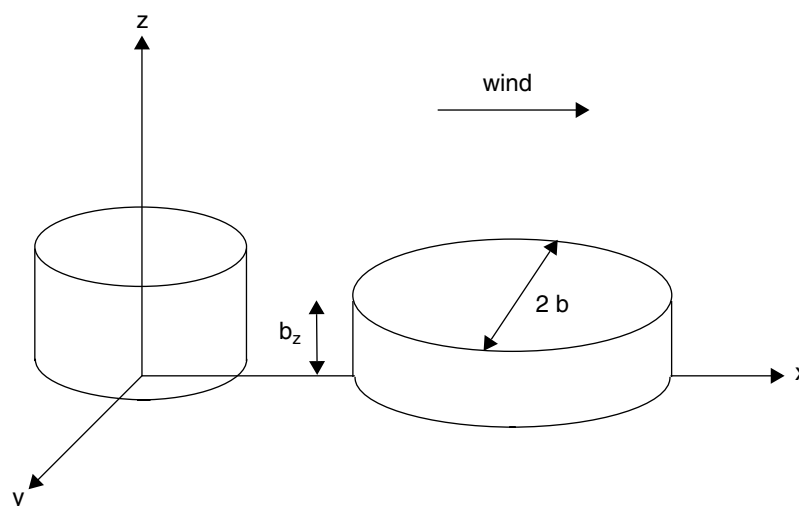
Figure 4.8   The box model of a dense gas cloud

The mean concentration of the cloud is determined by solving the ordinary differential equations for the time-dependent volume (V), radius (r) and position (x) of the cloud. The down-wind position is calculated from the advection velocity of the cloud, which depends on the mean wind speed u_a.

The equation for the evolution of V(t) is

$$dV/dt = \pi\, r^2\, w_{e,t} + 2\, \pi\, r\, b_z\, w_{e,e} \qquad\qquad (m^3\, s^{-1}) \qquad (4.23).$$

In equation 4.23, b_z is the height of the cloud, and $w_{e,t}$ and $w_{e,e}$ are entrainment velocities at the upper surface and at the edge of the cloud. The biggest disagreement between different box models is how these turbulent entrainment velocities are treated.

The equation for the evolution of r(t) is

$$dr/dt = C\sqrt{(g'b_z)} \qquad\qquad (m\, s^{-1}) \qquad (4.24),$$

C is a constant and g' is the effective gravity. Equation 4.24 is called the gravity front equation. It describes the gravity slumping in the initial dispersion phase, i.e. the gravity-induced motion of the cloud. The underlying principle is that the height-averaged pressure drop across the gravity front is in balance with the resistance pressure from the ambient air.
The mean concentration c in the cloud is calculated as a function of down-wind distance x from the relation

$$c(x) / c_o = V_o / V(x) \qquad\qquad (-) \qquad (4.25),$$

where c_o and V_o are, respectively, the initial concentration of the chemical compound and the released volume. Equation 4.25 is valid for a gas cloud that does not exchange heat with its environment (the substrate and the atmosphere) or generate heat internally through latent heat processes (evaporation, condensation) or chemical conversions. These internal heat changes can affect the dispersion of the cloud, and are included in most of the present box models.
At some down-wind distance, the cloud ceases to be influenced by the density perturbation and subsequent dispersion proceeds as if the cloud were neutrally buoyant. At that point the dense gas dispersion formulae can be replaced by the simpler Gaussian puff formalism (see Section 2). Most of the box models have arbitrary assumptions for the transition point, for instance:
− The density perturbation drops below a critical value.
− The Richardson number drops below a critical value.
− The gravity-front velocity reaches a lower level, which is usually some fraction of the ambient wind velocity.

Grounded plume models
The plume models are used for the description of the dispersion process, which follows after a continuous or time-varying release of dense gas. The models assume that the initial momentum of the release is small, so in the Yellow Book they are called grounded plume models in order to distinguish them from the one-dimensional integral trajectory models for lofted plumes (see Section 4.3.4). Steady state plume models describe plumes from a continuous source, and can be developed in

one-to-one correspondence with the already discussed box models, by replacing the time variable t with the down-wind distance x from the source. A typical example is the work of Jagger [1983]. This model employs the entrainment coefficients of Fryer and Kaiser [1979]. A computer model, CRUNCH, was also developed. The more recent computer models (e.g. PHAST [Hanna et al., 1991], DRIFT [Webber et al., 1992], etc.) contain the box module and the plume module within a single package. In grounded plume models, it is assumed that a plume has a rectangular cross-section of height $b_z(x)$ and half-width $b(x)$ (see Figure 4.9).
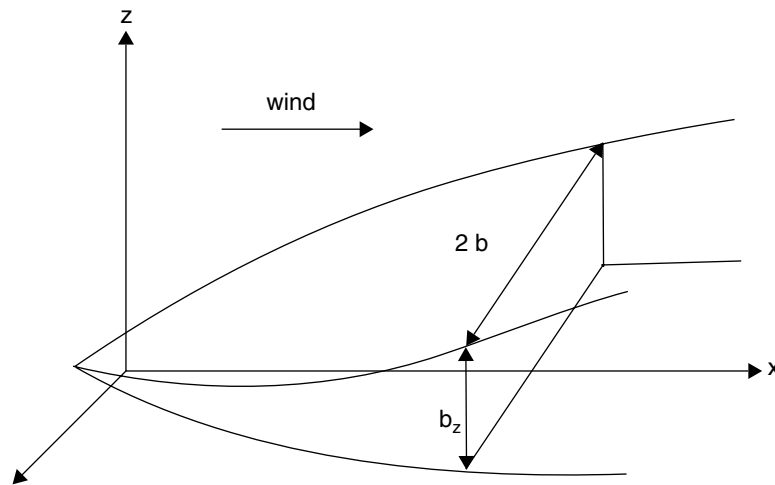
Figure 4.9   The grounded plume model of a continuous dense gas plume

The concentration c of the chemical compound and the advection velocity u are uniform over the entire area $A(x)$ of the cross-section, and in general an empirical relation is assumed between this averaged value of u and the plume height b_z.

The equation for the increase of total mass is

$$d(\rho\, u\, A)/dx = 2\,\rho_a\, b\, w_{e,t} + 2\,\rho_a\, b_z\, w_{e,e} \qquad\qquad \text{(kg m}^{-1}\text{ s}^{-1}) \quad (4.26).$$

ρ and ρ_a are, respectively, the densities of the plume gas and of ambient air. $w_{e,t}$ and $w_{e,e}$ are entrainment velocities at the upper surface and at the edge of the plume. Because of the similarity between the equations 4.23 and 4.26, a plume model equivalent can be built for each box model, by assuming the same closure relations for the entrainment. The equation for the evolution of $b(x)$ is

$$u\, db/dx \;=\; C\sqrt{(g'b_z)} \qquad\qquad \text{(m s}^{-1}) \qquad (4.27),$$

C is a constant, and g' is the effective gravity. It should be noted that gravitational slumping, and also mixing, in the longitudinal direction is neglected in the steady-state plume model. This is justifiable in sufficiently high-wind conditions.
The concentration decay as a function of down-wind distance is obtained by solving the equation of compound species flux simultaneously with the equations 4.26 and

4.27. It is noted that, for simplicity, the internal heat changes have been neglected in the equations, whereas they are incorporated in most of the present steady state plume models.

If the plume material is removed from the source at a lesser rate than the flow rate from the source, then plume material is accumulated at the source. The accumulation is accompanied by horizontal, buoyancy-induced motions providing a much larger plume area near the source. As a result the effective source size can be much larger than the physical source size. Most of the present plume models contain an algorithm to describe the formation of the secondary source blanket.

A different technique to simulate a steady release is to divide the total release into a number of puffs, each of which is considered as a separate release. This technique is used in the CHARM computer model.

Generalised plume models
Generalised steady state plume models give greater structure to the spatial variations of the dense gas concentration than merely assuming a rectangular or Gaussian profile. This enables a greater range of physical processes to be modelled, and certain processes to be more realistically modelled. A well-known example is the model of Colenbrander [1980], where similarity forms for the concentration profiles present the plume as a horizontally homogeneous centre section with Gaussian concentration profile edges (see Figure 4.10).
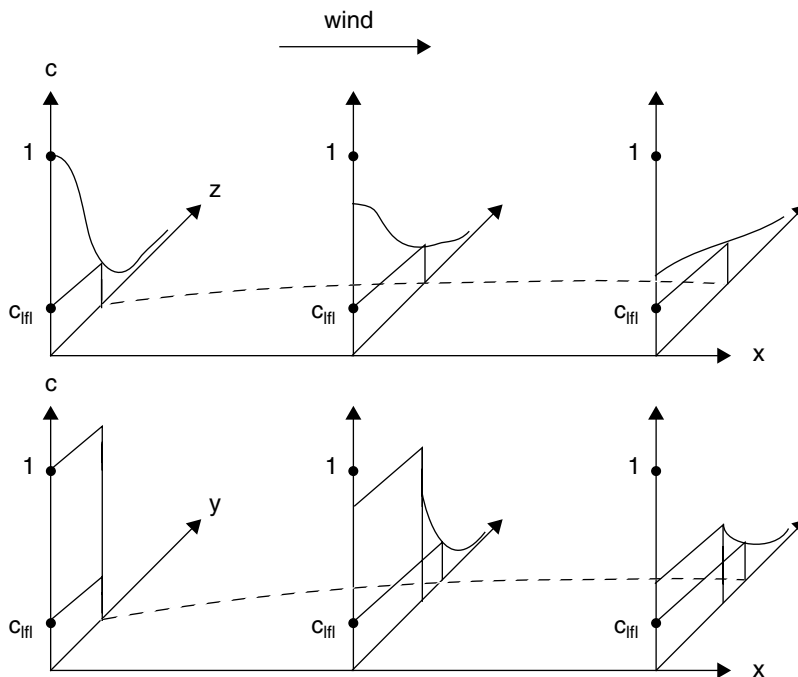
Figure 4.10   The down-wind development of the concentration profiles in vertical and lateral direction, in a generalised plume model. The dashed curve is the LFL isoconcentration contour

In formula:

$$c(x,y,z) = c_c(x) \, F_y(y) \, F_z(z), \qquad\qquad \text{(kg m}^{-3} \text{ or parts per unit volume)}$$

$$\begin{cases} F_y(y) \;=\; 1 & \text{for } |y| \leq b, \\[2mm] F_y(y) \;=\; \exp(-(|y|-b(x))^2 / \sigma_y(x)^2) & \text{for } |y| > b, \end{cases}$$

$$F_z(z) \;=\; \exp(-(z / \sigma_z(x))^2) \qquad\qquad\qquad (4.28).$$

The model is formulated in terms of eddy-diffusivities rather than entrainment velocities. This means that the diffusion equation is solved in the vertical and lateral direction.

This way of formulating the plume model guarantees that the transition to passive behaviour in the edge entrainment and lateral spreading is continuous. The model of Colenbrander has been implemented in computer models such as HEGADAS [McFarlane et al., 1990] and DEGADIS [Havens, 1989].

Time-varying releases
In some cases (e.g. a spreading and vaporising liquid pool) the volume flow rate of the release will show variations with time, and this will also affect the concentration levels in the resulting plume. Colenbrander [1980] has proposed to describe a time-varying release with the concept of travelling observers. The concept consists of 4 steps:
−   Observers travel at a series of times with the wind, starting upwind of the pool.
−   The pool data observed by each observer are determined.
−   For each observer, the concentration is computed via a steady state plume model, adopting the observed pool data. The concentration at time t for a certain down-wind distance is determined by calculating the positions of observers at times t.
−   At time t, the actual concentration is determined from a Gaussian integration with respect to down-wind distance of all observer concentrations. The Gaussian integration involves the longitudinal diffusion by means of a down-wind dispersion coefficient σ_x.
In formula:

$$c_c(x,t) \;=\; \int c_c(u_a t)/(\sqrt{(2\pi)}\sigma_x(u_a t)) \, \exp(-0.5(x - u_a t)^2/\sigma_x(u_a t)^2) \, du_a t \qquad (4.29).$$

$(u_a t)$ is the position at time t of an observer travelling with the wind in the down-wind direction. At this position the observer observes the concentration $c_c(u_a t)$, which is obtained from a steady state plume model. An often used expression for the dispersion coefficient is $\sigma_x(x) = 0.13 \, x$ (see also Sections 4.3.3 and 4.5.3.3 on the Gausian plume model).

4.3.5.3 The conservation equations for a dense gas release

The full equations describing the release of a dense gas are the Navier-Stokes equations for the instantaneous velocity and density fields. The Navier-Stokes equations are partial differential equations expressing the conservation of total mass and the conservation of compound species (the continuity equations), the conservation of enthalpy, and a 3-vector equation of motion. An equation of state is also required. The equations are averaged to obtain equations for the mean fields. In the application of the Navier-Stokes equations to gas dispersion processes, a convenient set of independent fields is formed by the velocity, the temperature, the density and the concentration of the chemical compound. The pressure field is not included, since the mixture of air and dense gas is assumed to be incompressible. A turbulence closure scheme is needed for the description of correlations of fluctuating quantities.

There are dispersion models which attempt to solve, by means of numerical techniques, the Navier-Stokes equations in 3 dimensions, but their development is not at a sufficiently advanced stage that the models can be used routinely. At the moment, the 3-dimensional models can best be viewed as a research tool in the study of the flow field of dispersed clouds. The costs of undertaking a fully 3-dimensional simulation also tend to be significantly greater than the costs of using simple dispersion models. For these reasons the 3-dimensional models are excluded from a discussion in the Yellow Book. An overview of 3-dimensional dense gas dispersion models can be found in the study of Ermak et al. [1988].

The shallow layer theory is related to the 3-dimensional approach. It is based on the full set of conservation equations, but advantage is taken of the simple structure of dense gas clouds in cross-wind planes. The computational effort is greatly reduced by regarding the cross-wind variables as depending only on time and down-wind distance.

Zeman [1982] has developed the formalism to describe the dispersion of a dense gas release in the presence of wind by means of a 1-dimensional shallow layer model. A recent computer implementation based on the formalism is the SLAB model [Ermak, 1990]. The discussion in this section starts with the shallow layer formulation for a continuous grounded plume, and subsequently treats the case of an instantaneous cloud.

The shallow layer plume model
The fields of physical quantities in a plume are regarded as depending only on down-wind distance x, and are averaged in the cross-wind direction. The conservation equations in the shallow layer plume model are equivalent to the equations for a 1-dimensional integral plume model, with additional terms in the former set of equations for the description of the gravitational slumping on the ground. The main difference between the two sets is that the averaging of the fields in the integral plume models is done over the plume cross-sections, and in the shallow layer theory it is done over the cross-wind cross-sections. This implies that the shallow layer equations can be used for lofted plumes in the region where the plume has been bent-over by the wind.
The shallow layer plume model and the steady state grounded plume model, which was discussed in the previous section, differ in their treatment of momentum conservation. In the shallow layer approach, the vector equation of momentum

conservation is solved, whereas the steady state grounded plume model solves the gravity slumping equation (4.27).

The shallow layer cloud model

In the shallow layer model of Zeman [1982], the puff is treated as a grounded cloud with a half-length b_x, a half-width b_y and a height b_z. The independent variable is the down-wind travel time t of the cloud centre-of-mass. The fields of physical quantities in the cloud are averaged over the cloud volume $V = 4b_xb_yb_z$.

Air is entrained in the down-wind and cross-wind sides of the cloud, with different entrainment rates, and at the upper surface of the cloud. The difference between the shallow layer formalism and the box formalism is in the description of gravity slumping. The shallow layer approach solves a vector equation of motion for the gravity spreading, whereas the box models are based on the gravity front equation (4.24).

The shallow layer cloud model can also be applied to releases above ground level. The terms in the conservation equations for gravity spreading must then be replaced by terms which describe a sinking cloud.

4.4 Selection of models

4.4.1 Introduction to Section 4.4

In Section 4.4 the considerations which have led to the selection of models which are included in Section 4.5, are explained. In general the selection is based on considerations with respect to:
− The degree to which a model is able to describe the physical phenomena correctly (validation and verification).
− The general acceptance of a model.
− The degree to which a model is flexible to input and output requirements (applicability and ease of use).
− The transparency and internal consistency of a model (i.e. the consequent use of clear principles and assumptions).

These considerations are presented as follows:
− Section 4.4.2 addresses methods to calculate atmospheric stability and quantities in the mixed layer such as wind speed and turbulence.
− Section 4.4.3 addresses selection of dispersion parameters in Gaussian plume models for passive dispersion.
− Section 4.4.4 addresses mainly the selection of integral models for jets and plumes in ambient wind.
− Section 4.4.5 addresses the selection of dense gas dispersion models.

4.4.2 Schemes for atmospheric stability categories and meteorological data

4.4.2.1 Atmospheric stability catagories

Most widely-used dispersion models make use of the Pasquill-Gifford stability categories (A-unstable to F-stable) and parametrisations of the local lateral and vertical plume width (σ_y and σ_z).
However, already Pasquill and Smith [1983] point out the restrictions of these qualitative schemes in favour of schemes using quantifications of physical parameters of the boundary layer. At the European Workshop 'Objectives for Next Generation of Practical Short-Range Atmospheric Dispersion Models' [Olesen, 1992] it was generally agreed that up-to-date models should use these types of stability schemes. Such a scheme is the scheme developed by Holtslag et. al. (see Section 4.3.2).
This scheme can be coupled directly with calculation of dispersion parameters as a function of Monin-Obukhov length, plume height and down-wind distance or travel time. This approach leads to good agreement with observations [Gryning et. al., 1987].
There is a number of additional advantages of the 'Holtslag'-scheme and the related methodology for calculation of dispersion parameters:
− The scheme is applicable to all climatological zones;
− The calculation of dispersion parameters can be extended to very low wind speed conditions.

However, we have to acknowledge the fact that long-term meteorological data is very often available in terms of Pasquill stability classes. Therefore use will be made of Golder's scheme [1972], see Figure 4.11, to relate Pasquill classes to roughness length and Monin-Obukhov length and vice versa.

For stability over sea the scheme by Hsu [1992], see Figure 4.12, will be adopted.

4.4.2.2   Variation of wind speed

All dispersion models (passive dispersion models and dense gas dispersion models) need information about the vertical variation of wind speed. For wind speeds in the surface layer the use of the Businger-Dyer relations is selected [Panofsky and Dutton, 1984]. These relation use roughness length and Monin-Obukhov length as input.

4.4.2.3   Variation of turbulence

Some application of dispersion parameters for Gaussian plume models require the standard deviation of turbulent velocities in cross-wind and vertical direction. From available suggestions to calculate the variation of these turbulent quantities the expressions by Gryning et. al. [1987] are selected with a change of the proportionality constant in order to make them consistent with the surface-layer data of turbulence provided by Panofsky and Dutton [1984].

4.4.2.4   Determination of mixing height

No selection of mixing height can be made which is valid for all locations. For applications in the Netherlands the expressions for **stable conditions** as presented in Section 4.3.2.2 are selected. For **near neutral conditions** (Pasquill class D) a combination is selected from the expression in Section 4.3.2.2 and a fixed value of 500 m. For **Pasquill class C** a value of 1000 m and for **Pasquill A and B** a value of 1500 m is used.

4.4.3   Selection of models for passive dispersion

4.4.3.1   Selection of model type

For passive dispersion the use of the Gaussian plume model is selected for all scaling regions in the mixing layer (Figure 4.5). For the surface layer and the mixing layer other models provide better agreement with reality, but they are much less flexible with respect to source height, source dimensions and output.

4.4.3.2 Dispersion parameters

Gaussian plume models make use of two (for continuous releases) or three (for instantaneous releases) dispersion parameters σ_x, σ_y, σ_z.

The dispersion parameters σ_x, σ_y, σ_z of the 2nd edition of CPR14E are used (see section 4.5.3.4).

4.4.4 Selection of models for jets and plumes

This section indicates which jet and plume models have been selected from the survey in Section 4.3.4.

Jets and plumes in still air
The theory of jets and plumes is based on similarity principles. The fixation of the empirical constants in the expressions by Chen and Rodi [1980] and their usage of Gaussian profiles for the physical distribution functions in a cross-section have become widely-accepted, and is therefore selected for a more detailed discussion.

One-dimensional integral trajectory models
At present it is not possible to make a conclusive statement which of the various 1-dimensional integral plume models is preferable. However, in many cases the model will be used as a front-end module to a dense gas dispersion model, and the coupling of the models will impose additional model requirements. If the lofted plume model has to be coupled to a grounded steady plume model, which can only treat surface area sources, then the plume touch-down and slumping have to be modelled separately. On the other hand, if the lofted plume model acts as a front-end module to a model that is based on solving the conservation equations, then it is sufficient for the lofted plume model to describe the initial phase of plume rise and down-wind bending of the plume. The dense gas dispersion model, which is discussed in Section 4.5.5, is of the last-mentioned type. The model of Hoot et al. [1973] is easy to couple to this dense gas dispersion model, and it is one of the simplest integral trajectory models, and for these reasons is treated in greater detail.

Plume rise formulae
The selected plume rise formulae are based on an early publication of Briggs [1969], which has become widely-accepted. During the development of the 'Dutch National Model' [Dutch committee on the dispersion of air pollution, 1984] some additions were made in order to extend the validity to tall stacks and to all atmospheric stability conditions. These additions deal 1) with the criterium for final plume rise in neutral atmosphere, and 2) with plume rise in stable atmosphere. The adaptions are incorporated in the set of selected formulae.

4.4.5   Selection of dense gas dispersion models

Criteria for model selection
The criteria for selection of a dense gas dispersion model relate to three aspects, i.e. operational requirements (ease of use), physical plausibility, and educational aspects (transparency of the model).

The operational requirements are:
I   The model is usable in operational conditions. Constraints on cost and time are imposed by the operational environment, and the sophistication and efficiency of the algorithms in the physical model should be compatible with these constraints. It is emphasised that it is not the intention to evaluate the user-friendliness of the software implementations of models. There is a continuous improvement in this area, and available computer models can be adapted to the needs of the user without great effort.
II The model is current. In other words, the model is supported by an organisation, and the model is widely used. Currency of usage can for instance be assessed from the frequency of references in the recent (1983-1993) scientific literature.
III The model allows for coupling of source term models and explosion/fire models.

It is desirable that the model is based on plausible physical assumptions. For dense gas modelling, Wheatley and Webber [1984] have formulated this in terms of 3 objectives:
I   In the model, the transition between the dense gas phase and passive phase of dispersion should be continuous.
II The model should include all turbulent dilution mechanisms (jet entrainment, shear production and enhanced entrainment from gravity spreading, convection).
III The modelling of entrainment should be consistent with results of laboratory experiments on entrainment in stratified flows.
Concerning output requirements, within its range of validity the model should give a fair description of the actual gas dispersion in a realistic release situation. This is formulated by Wheatley and Webber as a 4th objective:
IV The model should realistically describe the ensemble-average spatial concentration distribution in both the dense gas phase and in the passive phase of dispersion.

From an educational point of view, it is preferred to have a few models with wide applicability instead of many models with restricted applicability.

The selection procedure
Dense gas dispersion models for operational use can be divided into 2 classes:
I   Phenomenological models, in which the dispersion behaviour is described by a series of nomograms (see Section 4.3.5.1);
II Intermediate models, such as box models and models based on shallow layer theory (see Sections 4.3.5.2 and 4.3.5.3).
Many of the models are available as computer codes; they often contain source and jet models to describe the initial phase of the dense gas release. The selection of source models is not part of the present chapter; this topic is discussed in the Chapters 2 and 3 of the Yellow Book. The selection of jet models is discussed in Section 4.4.4.

A useful reference document for the assessment of models is the report of Hanna et al. [1991] on an extensive model evaluation project of 14 dispersion models. The project was initiated because there were no standard objective quantitative means of evaluating the dense gas dispersion models.

In the project of Hanna et al. a system has been developed to evaluate the performance of microcomputer-based dispersion models that are applicable to chemical releases into the atmosphere. The study is better than previous dense gas dispersion model evaluation projects because a method was developed which gives conclusive results. Following this work, Hanna and Chang [1992] have reviewed the HGSYSTEM package in the same way as the other 14 models.

The Workbook of Britter and McQuaid [1988] is widely-accepted as a reference text for dense gas dispersion. The nomograms in the book were evaluated by Hanna and turned out to give a good description of experimental data sets.

Therefore, the Workbook is selected in the Yellow Book as a representative of class I models. A detailed discussion of the Britter and McQuaid model is presented in Section 4.5.5.1.

In the reports of Hanna et al. it is concluded that HEGADAS (and also the HGSYSTEM package, which contains HEGADAS as a module) has a good performance for continuous dense gas and passive releases, but it is not intended for modelling instantaneous releases.

The models CHARM, PHAST and SLAB have an acceptable performance for all of the gas releases included in the study of Hanna (i.e. continuous and instantaneous dense gas releases, and continuous passive gas releases). CHARM and PHAST are proprietary models, HEGADAS and SLAB are publicly available.

Since the performances of HEGADAS, CHARM, PHAST and SLAB are all acceptable, the selection of a model for a more detailed discussion was based on educational aspects. The SLAB computer model makes use of shallow layer theory (see Section 4.3.5.3), which has the advantage that the physical processes of dense gas dispersion are formulated in a transparent way. The SLAB model is described extensively in Section 4.5.5.2, as a representative of class II models.

It should be mentioned that, compared with the other 3 acceptable models, SLAB might underpredict concentrations near to the source [Hanna et. al., 1991].

4.5 Description of models

4.5.1 Introduction to Section 4.5

This section provides the description of the recommended models and methods. It contains all necessary information to carry out calculations. No background information on models is provided, for this, the reader should refer to Section 4.3.

However, the reader is advised also to consult section 4.7 with respect to validity and applicability of the models.

The section includes the methods to calculate dispersion from positively, neutrally, and negatively (dense) buoyant releases. The necessary sections for different types of releases are indicated in the scheme below.

Additionally one needs to characterise atmospheric stability. Methods to do so are provided in Section 4.5.2.

```
┌─────────────────────────────┐   ┌─────────────────────────────┐
│   neutral or buoyant release │   │      dense gas release      │
└─────────────────────────────┘   └─────────────────────────────┘
        │                                    │
        ▼                                    ▼
┌────────┐ ┌──────────┐ ┌──────────┐  ┌──────────┐ ┌──────────┐ ┌──────────┐
│free jet│ │area source│ │jet or    │  │vertical  │ │horizontal│ │area      │
│4.5.4.1 │ │/ volume   │ │plume in  │  │jet in    │ │jet       │ │source/   │
│        │ │source     │ │cross-wind?│  │cross-wind?│ │          │ │volume    │
└────────┘ └──────────┘ └──────────┘  └──────────┘ └──────────┘ │source    │
                              │             │                    └──────────┘
                              ▼             ▼
                        ┌──────────┐  ┌────────────┐
                        │plume rise│  │plume       │
                        │4.5.4.2   │  │trajectory  │
                        │          │  │to maximum  │
                        │          │  │plume rise  │
                        │          │  │4.5.4.2     │
                        └──────────┘  └────────────┘
        │           │                       │           │
        ▼           ▼                       ▼           ▼
┌─────────────────────┐        ┌─────────────────────────────┐
│ passive dispersion  │        │ dense gas dispersion including│
│ 4.5.3               │        │ transition to passive         │
│                     │        │ dispersion 4.5.5              │
└─────────────────────┘        └─────────────────────────────┘
```
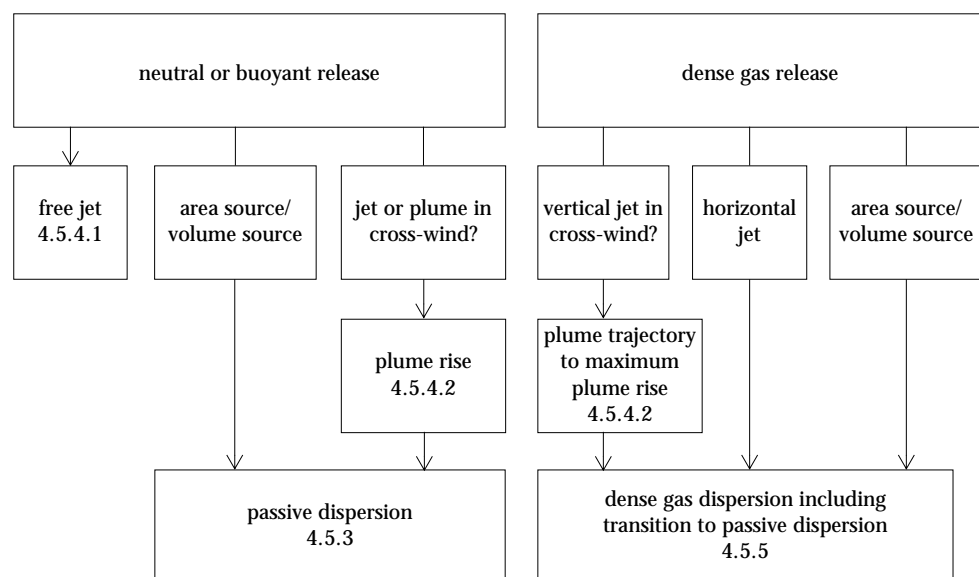
4.5.1.1 Guide to the calculations

Initial conditions for the dispersion are determined by the characteristics of the release (see Chapters 2 and 3), and, except for the free jet model, by the state of the atmosphere (Section 4.5.2). So any calculation starts by selecting the correct calculation procedure according to release type.

Step 1

Has the release a high initial momentum?
− Yes: Use the free jet model in Section 4.5.4.1. Check the validity of the model 1) by applying the conditions provided in formulae (4.71-4.72), and 2) by ensuring cross-wind (for vertical jets) has not bent the plume over in the region of interest (jet velocity should exceed ambient velocity by a factor of 10). If the model is not valid, proceed with steps 2, 3, 4 or 5.
If beyond the jet region atmospheric dispersion is of interest, proceed also with steps 2, 3, 4 or 5.

Step 2

− Determine the roughness length of the area of interest, using Table 4.3, Section 4.5.2.1.

Step 3

− Determine stability of the atmosphere by calculating the Monin Obukhov length and the friction velocity according to Sections 4.5.2.2, 4.5.2.3 and 4.5.2.4. It might be necessary to use the expressions provided in Section 4.5.2.1.

Step 4

Determine whether the release will lead to a cloud denser than the ambient air.
− No: Proceed with step 5.
− Yes: *Step 4.1*
Is the release instantaneous?
    – Yes: Decide whether a fast solution or a complex solution is preferred. For a fast solution, proceed by using the Britter and McQuaid nomogram Figure 4.15 and Diagram 4.1, Section 4.5.5.1. Otherwise, use the SLAB-model, Section 4.5.5.2, Diagram 4.10.
− *Step 4.2*
Is the release continuous?
    – Yes: Step 4.2.1.
        Is the release a vertical jet and this jet be ignored?
        – Yes: Use the HMP-model, Section 4.5.4.2, to determine maximum plume rise and concentration. Thereafter, couple the results with the SLAB-model (formulae 4.107-4.112, Diagram 4.6, Section 4.5.5.2), and proceed the calculation with the continuous SLAB-model (Diagram 4.4).
        – No: Decide whether a fast solution or a complex solution is preferred. For a fast solution, proceed by using the Britter and McQuaid nomogram Figure 4.17 and Diagram 4.2, Section 4.5.5.1. Otherwise, use the SLAB-model, Section 4.5.5.2, Diagram 4.4.

−   *Step 4.3*
Is the release of finite duration?
– Yes: Decide whether a fast solution or a complex solution is preferred. For a fast solution, use the Britter and McQuaid nomograms and follow the instructions at the end of Section 4.5.4.1.
Otherwise, use the SLAB-model, Section 4.5.4.2, and follow the instructions related to Diagram 4.9.

Step 5

The release is non-buoyant or positively buoyant.
− *Step 5.1*
Is the release instantaneous?
– Yes: Apply the Gaussian model as introduced in formula 4.52 and use Sections 4.5.3.1, 4.5.3.2, and 4.5.3.3. If necessary, apply formula 4.65 numerically to calculate flammable mass.
− *Step 5.2*
Is the release continuous?
– Yes: Apply the Gaussian model as introduced by formula 4.51 and use Sections 4.5.3.1, 4.5.3.2, and, if necessary, 4.5.3.4. Apply approximations 4.66-4.70 to calculate flammable mass.
− *Step 5.3*
The release is time-dependent.
–   Apply the Gaussian model as introduced in formulae 4.51 and 4.52. Use Sections 4.5.3.1, 4.5.3.2, and 4.5.3.3, but note the Sections 4.5.3.5 and 4.5.3.6. Use formula 4.65 numerically to calculate the flammable mass.

4.5.2   Models to determine atmospheric stability and vertical variation of wind speed

Atmospheric stability is determined by the Monin-Obukhov length L and/or the Pasquill stability class.
This section provides techniques to calculate Monin-Obukhov length L from routine meteorological data (Section 4.5.2.2), from Pasquill stability class (Section 4.5.2.3), and over sea (Section 4.5.2.4).
First, however, in Section 4.5.2.1, methods to determine vertical variation of velocity and other relevant characteristics will be presented, as these are to be used during the calculation of stability in Section 4.5.2.2 and for application in dispersion models. Additional properties of the atmosphere are presented in Sections 4.5.2.5 through 4.5.2.6.

4.5.2.1   Calculation of vertical variation of velocity and temperature

The necessary data to calculate the vertical variation of wind speed are:
− wind speed at specified height z (e.g. at 10 m height);
− surface roughness length z_o, using Table 4.3;
− an estimate of the Monin-Obukhov length L, from Section 4.5.2.2.

The roughness length should be representative for the whole area over which dispersion calculations are performed. Of course, different values for z_o may be used for different wind directions. It should also be noted that the upwind area has an influence on the turbulence characteristics of the atmosphere. The atmosphere is in equilibrium with the (new) roughness length over a height of approximately one tenth of the down-wind distance from a change in roughness length.

The surface friction velocity u_* can be calculated from velocity $u_a(z)$ at specified height z as follows:

(if z > 100 m; use z = 100 m)

$$u_* = \kappa \cdot \frac{u_a(z)}{f(z/z_o,L)} \qquad\qquad (m\ s^{-1}) \qquad (4.30)$$

(the determination of L and u_* is coupled. Section 4.5.2.2 provides methods to calculate u_* and L iteratively)
and inversely the velocity at an arbitrarily height z from the friction velocity:

$$u_a(z) = \frac{u_*}{\kappa} \cdot f(z/z_o,L) \qquad\qquad (m\ s^{-1}) \qquad (4.31)$$

(if z > 100 m; $u_a(z) = u_a(100\ m)$)

κ is the Von Karman constant; $\kappa = 0.4$. The function $f(z/z_o,L)$ is defined as:

$$
\left\{
\begin{array}{ll}
f(z/z_o,L) = \ln\dfrac{z}{z_o} + 5\dfrac{(z-z_o)}{L} & \text{for } 1/L > 0 \\
 & \qquad\qquad (-) \qquad (4.32) \\
f(z/z_o,L) = \ln\dfrac{z}{z_o} - \Psi\left(\dfrac{z}{L}\right) + \Psi\left(\dfrac{z_o}{L}\right) & \text{for } 1/L \le 0
\end{array}
\right.
$$

Here $\Psi\left(\dfrac{z}{L}\right) = 2\ln\left(\dfrac{1+\Psi'}{2}\right) + \ln\left(\dfrac{1+\Psi'^2}{2}\right) - 2\arctan(\Psi') + \dfrac{\pi}{2}$

$$\Psi' = \left(1 - 16\frac{z}{L}\right)^{1/4}$$

Table 4.3   *Terrain classification in terms of aerodynamical roughness length z_o, by Wieringa, [Holtslag, 1987])*

Class	Short terrain description	z_o (m)
1	Open water, fetch[1] at least 5 km	0.0002
2	Mud flats, snow; no vegetation, no obstacles	0.005
3	Open flat terrain; grass, few isolated obstacles	0.03
4	Low crops; occasional large obstacles, $x/h > 20$[2]	0.10
5	High crops; scattered obstacles, $15 < x/h < 20$[2]	0.25
6	Parkland, bushes; numerous obstacles, $x/h < 15$[2]	0.5
7	Regular large obstacle coverage (suburb, forest)	(1.0)[3]
8	City center with high- and low-rise buildings	(3)[3]

[1]   The upwind length over water should be at least 5 km.
[2]   Here x is a typical upwind obstacle distance and h the height of the corresponding major obstacles.
[3]   These values are rough indications. The presented dispersion models do not account for obstacle effects. The reader should also consult section 4.7.5.

For stable conditions, Section 4.5.2.2, it is necessary to calculate temperature differences in the surface layer. These are calculated as follows (for $1/L > 0$):

$$T_a(z_2) - T_a(z_1) = \frac{T_*}{\kappa}\left\{ \ln\left(\frac{z_2}{z_1}\right) + 5\frac{z_2 - z_1}{L} \right\} - \Gamma_d(z_2 - z_1) \qquad \text{(K)} \qquad (4.33)$$

Γ_d is the dry adiabatic lapse rate (0.011 K m^{-1}). T_* is the turbulent temperature scale, to be calculated from the Monin-Obukhov length-scale L and surface friction velocity:

$$T_* = \frac{u_*^2 \cdot T_a}{\kappa\, g\, L} \qquad \text{(K)} \qquad (4.34)$$

Here T_a is temperature at about 2 m height (K).

Note that these formulae are valid for let say $z > 10 \cdot z_o$, meaning that $u_a > u_*$ in practical situations.

4.5.2.2   Calculation of Monin-Obukhov length from routine meteorological data

The input for calculation of Monin-Obukhov length L requires:
− cloud cover N;
− wind speed at specified height z_u (normally 10 m), $u_a(z_u)$;
− temperature at specified height z_T (normally 2 m) T_a;
− roughness length z_o;
− solar elevation χ (from position, latitude and longitude, date and time, see Appendix 1);
− wet bulb temperature at z_T (only for night-time condition) T_w.

The Monin-Obukhov length can be calculated from the sensible heat flux H_o when the surface friction velocity u_* is known. (Normally, L and u_* need to be calculated iteratively.)

$$\left(L = -\frac{\rho_a c_p \, T_a \, u_*^3}{\kappa \, g \, H_o} \right) p \qquad \text{(m)} \qquad (4.35)$$

The next subsections will provide methods to estimate the sensible heat flux. Alternatively, L can be determined from a Pasquill stability class (Section 4.5.2.3), or temperature difference with sea water (Section 4.5.2.4).

Estimate of sensible heat flux for day-time conditions
During day-time conditions, i.e. between local sunrise and sunset (where sunrise and sunset may be later or earlier, respectively, than the astronomical times due to shading by mountains), the sensible heat flux H_o is dependent on the net radiative heat flux H_r at the surface. Therefore first the incoming solar radiation H_{rs} is to be calculated depending on solar elevation χ and cloud cover N:

$$H_{rs} = (C_1 \cdot \sin \chi - C_2) \cdot (1 - 0.75 \cdot N^{3.4}) \qquad \text{(J m}^{-2}\text{ s}^{-1}\text{)} \qquad (4.36)$$

Here $C_1 = 990$ J m^{-2} s^{-1}, and $C_2 = 30$ J m^{-2} s^{-1}.
Including incoming and outgoing long wave radiation the net radiation H_r is calculated as

$$H_r = \{(1 - e) \cdot H_{rs} + C_3 \, T_a^6 - \sigma \cdot T_a^4 + C_4 \cdot N\}/1.12 \qquad \text{(J m}^{-2}\text{ s}^{-1}\text{)} \qquad (4.37)$$

Here σ is the Stefan-Boltzmann constant ($5.67.10^{-8}$ W m^{-2} K^{-4}), $C_3 = 5.31.10^{-13}$ J K^{-6} m^{-2} s^{-1}, $C_4 = 60$ J m^{-2} s^{-1}, and e the albedo. Values of e are tabulated in Table 4.4.

Table 4.4   Albedo for various surfaces from Byrne et al. [1992]

Surface	Albedo e
Soils (Dark, wet - Light, dry)	0.05 - 0.40
Desert	0.20 - 0.45
Grass (Long [1.0 m] - Short [0.02 m])	0.16 - 0.26
Agricultural crops	0.18 - 0.25
Orchards	0.15 - 0.20
Forests	
Decious (bare-leaved)	0.15 - 0.20
Coniferous	0.05 - 0.15
Water	0.03 - 1.00
Snow (Old - Fresh)	0.40 - 0.95
Ice	
Sea	0.30 - 0.45
Glacier	0.20 - 0.40
Tarmac, Asphalt	0.05
Buildings	0.20 - 0.45

The soil heat flux is estimated to be 10% of the net radiative heat flux; the remaining heat flux is divided between latent heat flux and sensible heat flux.

The sensible heat flux then reads:

$$H_o = \frac{(1-\alpha)+\gamma}{1+\gamma}\,(0.9\,H_r) - C_5\,\alpha \qquad\qquad (J\,m^{-2}\,s^{-1}) \qquad (4.38)$$

Here $C_5 = 20\,J\,m^{-2}\,s^{-1}$, and γ is the ratio of specific heat of air at constant pressure to latent heat of evaporation of water, and to the rate of change of the saturation specific humidity with temperature (values of γ are tabulated in Table 4.5).

Table 4.5   *The dependency of the ratio γ on temperature*
            for standard pressure (= 1000 mbar)

T_a (°C)	γ
-5	2.01
0	1.44
5	1.06
10	0.79
15	0.60
20	0.45
25	0.35
30	0.27
35	0.21

α, the moisture availability constant, depends on the surface moisture condition ($0 \leq \alpha \leq 1$). If sufficient moisture is available for evaporation, like a grass-covered surface in The Netherlands, $\alpha = 1$; for dry bare soil $\alpha = 0$.

When temperature T_a and sensible heat flux H_o are known, L and u_* can be solved by iteration. The iteration starts by calculating u_* for $1/L = 0$ (neutral condition). Normally 3 iterations are sufficient to achieve an accuracy of 5% in L.

Estimate of sensible heat flux for night-time conditions
Estimates of Monin-Obukhov length L and friction velocity u_* for night-time conditions are also based on the surface heat fluxes. In this case the four terms in the heat balance, viz. the net long wave radiation H_r; the sensible heat flux H_o; the latent heat flux H_l; and the ground heat flux H_g, which are all direct or indirect functions of L and/or u_*, are to be calculated. The total sum of heat fluxes needs to be zero, thus:

$$H_o + H_l + H_g - H_r = 0 \qquad\qquad (J\,m^{-2}\,s^{-1}) \qquad (4.39)$$

This can only be obtained by an iterative procedure, e.g. the method of regula falsi, for which $1/L = 0$ (neutral conditions) and $1/L = 1$ (extremely stable) are appropriate starting values.

For each step in the iterative procedure, u_* and T_* need to be calculated by means of formulae (4.30) and (4.34) from Section 4.5.2.1 above, using the current estimate of L and using measured values of wind speed u_a, roughness length z_o, and temperature at so-called screen height (about 2 m).
The scheme requires introduction of temperatures at different levels:
T_a : temperature at 'screen height' (about 2 m).
T_w : wet bulb temperature at 2 m.
T_r : temperature at reference height of 50 m.
T_o : temperature at height of roughness length z_o.
T_s : surface (vegetation) temperature.

T_r and T_o are calculated using the relation (4.33) from Section 4.5.2.1
T_s can be calculated over land from:

$$T_s = T_o - T_* \left(10 + \frac{C_6}{u_*} \right) \qquad\qquad \text{(K)} \qquad\qquad (4.40)$$

Here $C_6 = 4.2$ m s^{-1}.
Now the expressions for the four heat fluxes used in formula (4.39) will be given. It is useful to define an intermediate step, the so-called isothermal net long wave radiation H_{ri}:

$$H_{ri} = -\sigma T_r^4 (1 - C_7 \cdot T_r^2) + C_8 N \qquad\qquad \text{(J m}^{-2}\text{ s}^{-1}) \qquad (4.41)$$

where σ is the Stefan Boltzmann constant, $C_7 = 9.35.10^{-6}$ K^{-2}, $C_8 = 60$ J m^{-2} s^{-1}, and N cloud cover.

The net long wave radiation H_r is then:

$$H_r = H_{ri} + 4\sigma T_r^3 (T_r - T_s) \qquad\qquad \text{(J m}^{-2}\text{ s}^{-1}) \qquad (4.42)$$

The sensible heat flux H_o follows from (4.34) and (4.35):

$$H_o = -\rho_a c_p u_* T_* \qquad\qquad\qquad \text{(J m}^{-2}\text{ s}^{-1}) \qquad (4.43)$$

Here ρ_a is the density and c_p the specific heat of air.

The ground heat flux H_g follows from:

$$H_g = 1.2 \left(\frac{H_{ri}}{3} - \frac{H_o}{4} \right) \qquad\qquad \text{(J m}^{-2}\text{ s}^{-1}) \qquad (4.44)$$

Finally, the latent heat flux is calculated by:

$$H_l = \frac{\frac{1}{1+\gamma}(H_r - H_g) + \rho_a c_p (T_a - T_w) \, K_s \, u_*}{\left(1 + \frac{C_9 \, \gamma}{1 + \gamma} \, k_s \, u_*\right)} \qquad \text{(J m}^{-2}\text{ s}^{-1}\text{)} \qquad (4.45)$$

Here $C_9 = 500$ m^{-1} s, γ follows from Table 4.5 and the transfer coefficient k_s is defined by:

$$k_s = \frac{T_*}{T_a - T_s} \qquad \text{(-)} \qquad (4.46)$$

Now all terms in formula (4.39) are defined.

4.5.2.3 Calculation of Monin-Obukhov length from Pasquill-stability categories

Golder [1972] has developed a scheme to relate Pasquill stability categories A-F to Monin-Obukhov length L, using local surface rougness length. This relation is presented in a graph (Figure 4.11).

Numerically, the Monin-Obukhov length can be calculated from the Pasquill stability categories as follows:

$$1/L = \frac{1}{L_s} \cdot \log_{10}\left(\frac{z_o}{z_s}\right) \qquad \text{(m}^{-1}\text{)} \qquad (4.47)$$

For $0.001 \leq z_o \leq 0.5$ m L_s and z_s are constants, depending on the Pasquill stability class according to Table 4.6. For $z_o > 0.5$ m, the Monin-Obukhov length calculated for $z_o = 0.5$ m should be used. For Pasquill stability class D, formula 4.47 leads to $1/L = 0$.
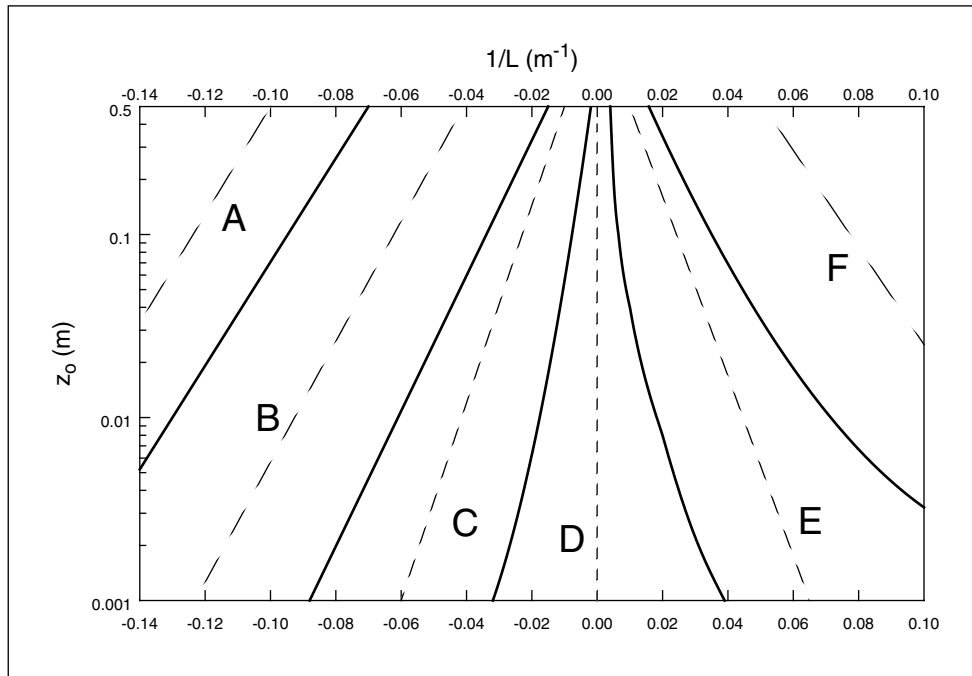
Figure 4.11   Graph proposed by Golder [1972] to relate Pasquill classes to Monin-Obukhov length and surface roughness

Table 4.6   Calculation of Monin-Obukhov length from Pasquill-stability categories

Pasquill stability	L_s (m)	z_s (m)
A	33.162	1117
B	32.258	11.46
C	51.787	1.324
D	∞	(not applicable)
E	-48.330	1.262
F	-31.325	19.36

4.5.2.4   Determination of stability over sea

A stability criterion for wind over sea is provided by Hsu [1992]. 'Sea' is defined as a water surface of a depth of at least 1 m and an upwind distance to the shore of at least 5 km (see also Table 4.3). Stability depends on the wind speed (at 10 m height) and the temperature difference between the air and the sea water, which are routinely observed. The results are obtained graphically (see Figure 4.12).
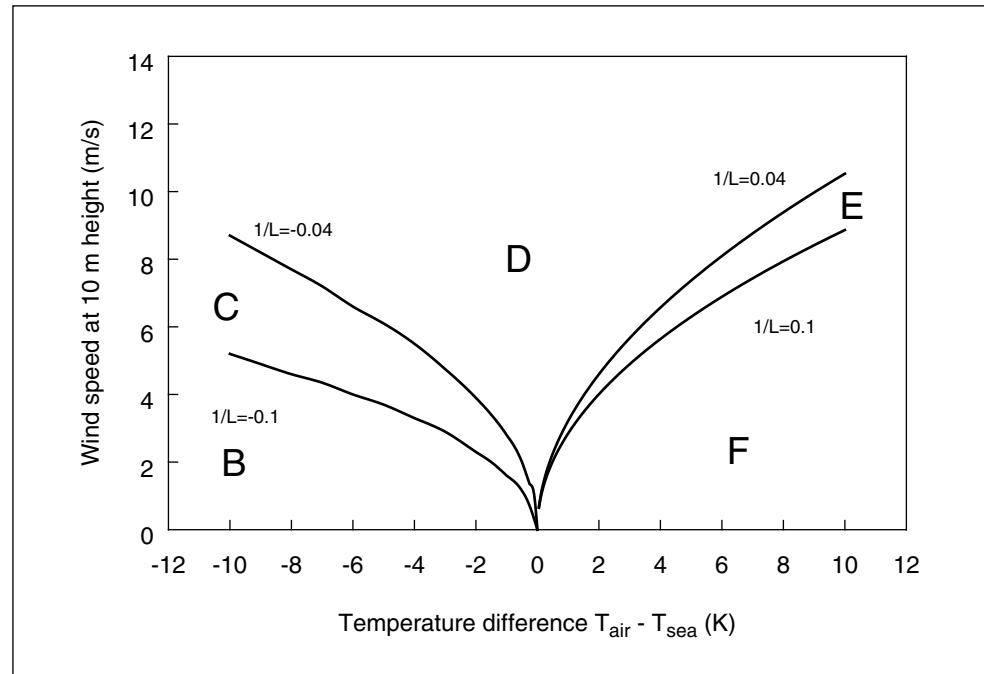
Figure 4.12   *Graph proposed by Hsu [1992] to relate Pasquill stability classes and Monin-Obukhov length over sea to the temperature difference between the air and the sea water*

4.5.2.5   Mixing height

Mixing height h_i depends on stability. The recommendations for mixing height are summarised in Table 4.7. Use needs to be made of the so-called Coriolis parameter f, defined as:

$$f = 2 \, \Omega \, \sin \varphi \qquad\qquad\qquad\qquad (s^{-1}) \qquad\qquad (4.48)$$

with Ω the earth's rotation ($7.27 \cdot 10^{-5} \, s^{-1}$) and φ the latitude of position on earth (about 51˚ for The Netherlands).

Also the friction velocity u_* and Monin-Obukhov length L need to be known. The mixing height is then given by Table 4.7.

Table 4.7

1/L	Pasquill	h_i (m)
> 0	F,E,D	$0.4\sqrt{\dfrac{u_*}{f}L}$
0	D	the smallest value of 0.2 u_*/f or 500 m
< 0	C B A	1000 1500 1500

4.5.2.6   Standard deviation of turbulent velocities

Some of the calculations of dispersion parameters in the Gaussian plume models require the use of the standard deviations of turbulent velocities in vertical direction (σ_w) and cross-wind direction (σ_v). Preferably, use should be made of measured values. Otherwise, use can be made of the following expressions:

$$\begin{cases} \sigma_v = 1.9\,u_*\sqrt{1-\dfrac{h}{h_i}} & \text{for } 1/L > 0 \\[4mm] & \qquad\qquad (\text{m s}^{-1})\quad (4.49) \\[4mm] \sigma_v = u_*\sqrt{0.35\left(\dfrac{h_i}{-\kappa\,L}\right)^{2/3}+\left(3.6-\dfrac{h}{h_i}\right)} & \text{for } 1/L \le 0 \end{cases}$$

The friction velocity u_* follows from stability and wind speed, see Section 4.5.2.1, but a minimum value of u_* of 0.6 / ln (10/z_o) should be used to maintain turbulence during low wind speed conditions. h is plume height and h_i the mixing height (Section 4.5.2.4).

It should be noted that these expressions provide hourly average values of σ_v.

$$\begin{cases} \sigma_w = 1.30\,u_*\left(1-\dfrac{h}{h_i}\right)^{3/4} & \text{for } 1/L > 0 \\[4mm] & \qquad\qquad (\text{m s}^{-1})\quad (4.50) \\[4mm] \sigma_w = u_*\sqrt{1.5\left(\dfrac{h}{-\kappa\,L}\right)^{2/3}\exp\left(\dfrac{-2h}{h_i}\right)+\left(1.7-\dfrac{h}{h_i}\right)} & \text{for } 1/L \le 0 \end{cases}$$

4.68

4.5.3 Passive dispersion

For passive dispersion, use is made of the Gaussian plume model (GPM). The GPM is valid for dispersion calculations over flat, uniform terrain. It can be applied to a short distance from the release down to a distance corresponding to 3 hours of travel time (see section 4.7.2).

The general expression <u>for a continuous release</u> is

$$c(x,y,z) = \frac{q}{u_a} F_y(x, y) F_z(x,z) \qquad (kg \ m^{-3}) \qquad (4.51)$$

where q is the (semi)continuous release rate and u_a the wind velocity at plume height h (if the plume height is less than 10 m, the wind speed at 10 m should be used).

The expression <u>for an instantaneous or short-duration release</u> is:

$$c(x,y,z,t) = Q \ F_x(x,t) \ F_y(t \ u_a,y)F_z(t \ u_a,z) \qquad (kg \ m^{-3}) \qquad (4.52)$$

The functions F_y and F_z in both equations are the same, although the averaging-time applied for F_y will be different in both cases.

In the following sections, the functions F_y, F_z, and F_x will be presented.

4.5.3.1 Lateral dispersion

The expression F_y (x,y) which accounts for lateral (cross-wind) dispersion is calculated as follows:

If lateral dimensions of the source are <u>zero</u>:

$$F_y(x,y) = \frac{1}{\sqrt{2\pi} \ \sigma_y(x)} \cdot \exp\left(-\frac{y^2}{2 \ \sigma_y^2(x)}\right) \qquad (m^{-1}) \qquad (4.53a)^{[1]}$$

If lateral width of the source is $\underline{2b_{oy} > 0}$:

$$F_y(x,y) = \frac{1}{4 \ b_{oy}}\left\{erf\left(\frac{b_{oy} - y}{\sqrt{2}\sigma_y(x)}\right) + erf\left(\frac{b_{oy} + y}{\sqrt{2} \ \sigma_y(x)}\right)\right\} \qquad (m^{-1}) \qquad (4.53b)^{[1]}$$

---

[1] σ_y (x) should be read as: 'σ_y as a function of x'.

The error function erf(x) is defined as erf(x) = $2/\sqrt{\pi}\int_0^x \exp(-t^2)dt$.
Numerical approximate solutions can be found for instance in Press et al. [1986]. An
reasonable analytical approximation is given by

$$\text{erf}(x) \approx \frac{x}{|x|} \cdot \sqrt{1 - e^{-\frac{4x^2}{\pi}}}$$

4.5.3.2   Vertical dispersion

The expression F_z (x,z) which accounts for vertical dispersion is calculated
as follows:

If vertical dimensions of the <u>source are zero</u> and if <u>$\sigma_z(x) \leq 0.6 \cdot h_i\sqrt{1 - h/h_i}$</u> :

$$F_z(x,z) = \frac{1}{\sqrt{2\pi}\,\sigma_z(x)} \cdot \left\{ \exp\left(-\frac{(z-h)^2}{2\,\sigma_z^2(x)} \right) + \exp\left(-\frac{(z+h)^2}{2\,\sigma_z^2(x)} \right) \right\} \quad (\text{m}^{-1}) \qquad (4.57a)[1]$$

If the vertical dimension of the source is <u>$2.b_{oz} > 0$</u> and

<u>$\sigma_z(x) \leq 0.6\,h_i\sqrt{1 - h/h_i}$</u> :

$$F_z(x,z) = \frac{1}{4\,b_{oz}} \left\{ \text{erf}\left(\frac{b_{oz} - z + h}{\sqrt{2}\,\sigma_z(x)} \right) + \text{erf}\left(\frac{b_{oz} + z - h}{\sqrt{2}\,\sigma_z(x)} \right) + \right.$$

$$\left. + \text{erf}\left(\frac{b_{oz} - z - h}{\sqrt{2}\,\sigma_z(x)} \right) + \text{erf}\left(\frac{b_{oz} + z + h}{\sqrt{2}\,\sigma_z(x)} \right) \right\} \qquad (\text{m}^{-1}) \qquad (4.57b)[1]$$

If <u>$0.6\,h_i\sqrt{1 - h/h_i} < \sigma_z(x) \leq 1.6h_i$</u> :

$$F_z(x,z) = \frac{1}{\sqrt{2\pi}\,\sigma_z(x)} \left\{ \exp\left(-\frac{(2h_i - h - z)^2}{2\,\sigma_z^2(x)} \right) + \exp\left(-\frac{(2h_i - h + z)^2}{2\,\sigma_z^2(x)} \right) \right.$$

$$+ \exp\left(-\frac{(z-h)^2}{2\,\sigma_z^2(x)} \right) + \exp\left(-\frac{(z+h)^2}{2\,\sigma_z^2(x)} \right)$$

$$\left. + \exp\left(-\frac{(2h_i + h - z)^2}{2\,\sigma_z^2(x)} \right) + \exp\left(-\frac{(2h_i + h + z)^2}{2\,\sigma_z^2(x)} \right) \right\} \qquad (\text{m}^{-1}) \qquad (4.57c)[1]$$

---

1) σ_z (x) should be read as: 'σ_z as a function of x'.

If $\underline{\sigma_z(x) > 1.6h_i}$:

$$F_z(x,z) = \frac{1}{h_i} \qquad (m^{-1}) \qquad (4.57d)[1]$$

Formula (4.57c) accounts for reflection of plume material at the mixing height, formula (4.57d) assumes the plume material to be uniformly distributed in the mixed layer. In these cases the effects of finite source dimensions are negligible.

4.5.3.3   Along-wind dispersion

For **instantaneous releases** at time $t = 0$, the term F_x which accounts for along-wind dispersion is calculated as follows:

If longitudinal dimensions of the source are <u>zero</u>:

$$F_x(x,t) = \frac{1}{\sqrt{2\pi}\ \sigma_x(u_a t)} \exp\left(-\frac{(x - u_a t)^2}{2\sigma_x^2(u_a t)}\right) \qquad (m^{-1}) \qquad (4.59a)[2]$$

If longitudinal dimension of the source is $\underline{2\ b_{ox} > 0}$:

$$F_x(x,t) = \frac{1}{4b_{ox}}\left\{ erf\left(\frac{b_{ox} - x + u_a t}{\sqrt{2}\ \sigma_x(u_a t)}\right) + erf\left(\frac{b_{ox} + x - u_a t}{\sqrt{2}\ \sigma_x(u_a t)}\right) \right\} \qquad (m^{-1}) \qquad (4.59b)[2]$$

(here, t is time since release)

For **short duration releases** with total emission Q during a release time from $t = 0$ to $t = t_r$, Bianconi and Tamponi [1993] derived the following approximate solution (the solution is exact in case the dispersion parameters are proportional to the square root of diffusion constant times travel time):

for $\underline{0 < t < t_r}$:

$$F_x(x,t) = \frac{1}{2\ u_a t_r}\left\{ erf\left(\frac{x}{\sqrt{2}\ \sigma_x(x)}\right) - \right.$$

$$\left. erf\left(\frac{x - u_a t}{\sqrt{2}\ \sigma_x(x)}\right) \right\} \qquad (m^{-1}) \qquad (4.60a)[3]$$

---

1) σ_z (x) should be read as: 'σ_z as a function of x'.
2)   Here σ_x ($u_a t$) should be read as: 'σ_x as a function of $u_a.t$'
3)   Here σ_x (x) should be read as: 'σ_x as a function of x'

For $t \geq t_r$:

$$F_x(x,t) = \frac{1}{2\,u_a t_r}\left\{ erf\left(\frac{x - u_a(t - t_r)}{\sqrt{2}\,\sigma_x(u_a t)}\right) - \right.$$

$$\left. erf\left(\frac{x - u_a t}{\sqrt{2}\,\sigma_x(u_a t)}\right)\right\} \qquad (m^{-1}) \qquad (4.60b)$$

4.5.3.4 Dispersion parameters

Continuous source

1. Practical formulae for σ_y and σ_z

For practical calculations σ_y and σ_z are approximated as follows [Commissie TNO, 1976]:

$$\sigma_y(x) = a \cdot x^b$$

$$\sigma_z(x) = c \cdot x^d \qquad \text{(adjusted for 100 to } 10^4 \text{ m)}$$

For a,b,c and d the values according to Table 4.8 are applicable:

Table 4.8   Parameters for the calculation of σ_y and σ_z, adjusted according to ref. 1,2,3.

		a	b	c	d
Very unstable	(A)	0.527	0.865	0.28	0.90
Unstable	(B)	0.371	0.866	0.23	0.85
Slightly unstable	(C)	0.209	0.897	0.22	0.80
Neutral	(D)	0.128	0.905	0.20	0.76
Stable	(E)	0.098	0.902	0.15	0.73
Very stable	(F)	0.065	0.902	0.12	0.67

Notes:
1. σ_y to be taken as 10-minutes average
2. σ_z for $z_0 = 0.1$ m and h < 20 m
3.   x, σ_y, σ_z in meters

Nb: If it is necessary to consider distances smaller than 100 meters in the calculation, it is best to interpolate linearly between 0 and the value of σ at 100 meters.

2. Correction for the roughness length z_0

Reference [Pasquill and Smith, 1983] gives a method for taking into account the roughness of the earth's surface and, in particular, the effect of it on the dispersion in the z-direction.

The roughness also includes overgrowth, cultivations and building. In Table 4.9; σ_z is given for $z_0 = 0.1$ m. For other roughness lengths a correction factor according to ref. [Pasquill and Smith, 1983] is used. However, the calculation is made with the aid of a formula according to ref. [Commissie TNO, 1976]:

$$C_{z_0} = (10 \cdot z_0)^{0.53 \cdot x^{-0.22}}$$

$$\sigma_z(x) = C_{z_0} \cdot c \cdot x^d$$

Table 4.9 gives some representative values for z_0.

Flat land	(f.i. polder land with few trees)	z_0 = ca. 0.03 m
Farm land	(f.i. airfield, aqricultural land, polder with many trees)	z_0 = ca. 0.10 m
Cultivated land	(f.i. glass-house land, open area with much overgrowth, scattered houses)	z_0 = ca. 0.30 m
Residential land	(f.i. area with densely located but low buildings, wooded area, industrial area with obstacles which are not to high)	z_0 = ca. 1.0 m
Urban land	(f.i. a big city with high buildings, industrial area with high obstacles)	z_0 = ca. 3.0 m

Since C_{z0} depends on x, it will be easier and even necessary, for most applications, to calculate, for a given value of z_0, new values for c and d, so that with equation:
$\sigma_z(x) = c \cdot x^d$ one can immediately obtain the corrected values of σ_z (see Table 4.9).

Table 4.9   Values of c' and d' for various values of z_0.

		z_0 = 0.03 m		z_0 = 0.1 m		z_0 = 0.3 m		z_0 = 1 m		z_0 = 3 m	
		c'	d'	c'	d'	c'	d'	c'	d'	c'	d'
Very unstable	(A)	0.193	0.932	0.28	0.90	0.383	0.873	0.550	0.842	0.760	0.814
Unstable	(B)	0.160	0.881	0.23	0.85	0.317	0.822	0.455	0.792	0.631	0.763
Slightly unstable	(C)	0.155	0.830	0.22	0.80	0.308	0.771	0.441	0.740	0.612	0.712
Neutral	(D)	0.139	0.791	0.20	0.76	0.276	0.732	0.395	0.701	0.548	0.673
Stable	(E)	0.104	0.761	0.15	0.73	0.207	0.702	0.296	0.671	0.411	0.643
Very stable	(F)	0.083	0.701	0.12	0.67	0.164	0.642	0.236	0.611	0.327	0.583

Nb: All of the values can be approximated by the use of the two equations below:

$$c' = c \cdot 1.98^{\log(10 \cdot z_0)}$$

$$d' = d - 0.059 \cdot \log(10 \cdot z_0)$$

The new values of c and d will be then called c' and d' in the text, whereby the following applies to σ_z:

$$\sigma_z(x) = c' \cdot x^{d'}$$

3. Correction for the mean time of a measurement

If we take a snap shot of a smoke plume we see a band winding erratically (as the hatched part in Figure 4.13). If, however, we were to take an exposure lasting, let us say, 10 minutes, much of the effort of the winding (the 'meandering') would be "averaged out" and we would see a much broader and more regular plume.
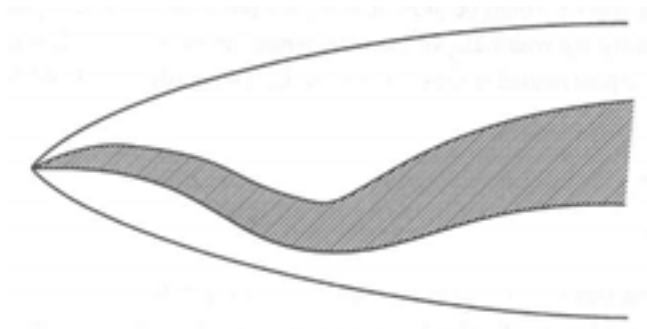
Figure 4.13   Schematic representation of a plume. The hatched part is a snap-shot, the wider contour an average over 10 minutes.

This effort influences measurements and the quantity which a person breathes-in. If a short-duration measurement is taken in an instantaneous position of the plume, a high concentration is registered. If, however, an average value is determined at the same location over a period of, for instance, 10 minutes or an hour, the concentration will be substantially lower. This can be approximately brought into the calculation by introducing a correction factor $C_{t'}$ as follows:

$$C_{t'} = \left(\frac{t'}{600}\right)^{0.2} (t' \text{ in seconds})$$

$$\sigma_y(x) = C_{t'} \cdot a \cdot x^b$$

Nb: This correction is consequently only applicable to σ_y.
σ_y cannot, however, be smaller than the value for an instantaneous source (see next section). The factor $C_{t'}$ has a minimum value of about 0.5.

Instantaneous source

4. Practical formulae for σ_{xI}, σ_{yI} and σ_{zI}

σ_{xI}, σ_{yI} and σ_{zI} are described by the equations:

$$\sigma_{xI}(x) = e_I \cdot x^{f_I}$$

$$\sigma_{yI}(x) = a_I \cdot x^{b_I}$$

$$\sigma_{zI}(x) = c_I \cdot x^{d_I}$$

The data in the literature for these variables are clearly scarcer than those for continuous sources. Values for σ_{xI}, determined partly theoretically, partly experimentally, are given in the references [Beals, 1971], [Drivas and Shair, 1974], [Saffman, 1962], [Tyldesley and Wallington, 1965] and [Chatwin, 1968]. In view of the limited nature of the data, it is all put together by taking the same σ_{xI} for all stability classes (= 0.13·x). The values of σ_{yI} are in the initial stage based on reference [Slade, 1968], with a small adjustment in order to avoid discrepancies with the value for σ_y in case of an continuous source. The value of σ_{zI} is chosen equal to the one of a continuous source, since the correction for the average-time hardly plays a role in this case and because of the fact that close to the ground the vertical "meandering" is repressed by the presence of the ground surface. In reference [Hanna, Briggs and Hosker, 1982] a comparison is made between continuous and instantaneous sources. There it is found that the standard radial deviation of the concentration (σ) of an instantaneous cloud is proportional to the age of the cloud increased by the power of 3/2. For large times σ (instantaneous) approaches the value of σ (continuous), so that the values of the sigmas previously described and practical to apply can be used.

Consequently, we arrive at the following values for the constants:

$e_I = 0.13$	$f_I = 1$
$a_I = a/2$	$b_I = b$
$c_I = c$	$d_I = 1$

The correction factor $C_{t'}$ is obviously hereby not applicable. The correction factor C_{z0} for σ_z is applicable. The values obtained with the help of the above constants are applicable at ground level. For σ_{xI}, in particular, it must be considered that σ_{xI} is strongly dependent on the height of the source since it is primarily influenced by the increase of the wind with the height. Also hereby it is more practical, in most cases, for the z_0 from which we want to initiate our calculations, to determine first the corrected values of c_I and d_I.

4.5.3.5 Sources with finite dimensions

In Sections 4.5.3.1 and 4.5.3.2 solutions are presented for situations in which a continuous source has merely cross-wind or vertical dimensions.

For merely along-wind dimensions 2 b_{ox}, the GPM-solution (Gaussian Plume Model) for a continuous release is:

$$c(x,y,z) = \int\limits_{(x-b_{ox})}^{(x+b_{ox})} \frac{q}{2b_{ox}u_a} \; F_y(x^{'},y) \; F_z(x^{'},z)dx^{'} \qquad \text{(kg m}^{-3}) \qquad (4.62)$$

It appears that already at a short distance the effect of b_{ox} becomes small.

For line sources which are not oblique or parallel to the wind, the line source should be discretised in a large number of point sources.

For area sources with arbitrary shapes, the area can be divided into a number of cross-wind line sources.

4.5.3.6 Sources with time-dependent release rates

A source for which the release rate varies with time can be dealt with by integrating a series of instantaneous releases with a released mass $q(t)dt$ over the time of release:

$$c(x,y,z,t) = \int\limits_{0}^{\infty} q(t^{'})F_x(x,t-t^{'})F_y((t-t^{'})u_a,y) \; F_z((t-t^{'})u_a,z)dt^{'}$$

$$\text{(kg m}^{-3}) \qquad (4.63)$$

4.5.3.7 Considerations with respect to semi-continuous or time-dependent releases

At a short distance from a release which has a constant release rate q over a finite release time t_r, one will observe for a certain time a plume as if it were a continuous release with the same release rate q.
In contrast, at a large distance, even a release over a fairly long period will be observed as a single 'puff'.
Although the expressions (4.60a,b) and (4.63) are correct and applicable to all distances, one may simplify the calculations, as in the former 'Yellow Book', by using the formula (4.51) for continuous sources up to a down-wind distance where

$$\sigma_x(x) < 0.13 \; u_a \; t_r \qquad\qquad \text{(m)} \qquad (4.64a),$$

whereas formula (4.52) for pure instantaneous releases may be used for distances beyond where

$$\sigma_x(x) > 1.3\ u_a\ t_r \qquad\qquad\qquad (m) \qquad (4.64b)$$

These simplifications reduce the complexity and time consumption of the calculations but introduce considerable continuity problems for C (x, y, z, t) in the down-wind axis $(0 < x < \infty)$.

4.5.3.8 Calculation of the total mass of contaminant between Lower and Upper Flammability Limit

In order to assess the impact of delayed ignition of a cloud of inflammable material, it is necessary to calculate the total mass of inflammable material between LFL and UFL.

The general methodology for any type of source or release is as follows:

$$Q_{ex}(t) = \int_0^{x_{lfl}} \int_{-y_{lfl}}^{y_{lfl}} \int_0^{z_{lfl}} f(x,y,z,t)dxdydz\ , \qquad\qquad (kg) \qquad (4.65)$$

where the function f (x,y,z,t) is defined as follows:

$$\begin{cases} f\ (x,y,z,t) &= c\ (x,y,z,t)\ \text{if LFL} < c\ (x,y,z,t) < \text{UFL} \\[2mm] f\ (x,y,z,t) &= 0\ \text{elsewhere.} \end{cases}$$

(For continuous releases, the dependency on time vanishes.)
Here, the concentration has to be calculated by the appropriate representation, depending release mode and source dimensions. For these calculations the lateral dispersion parameter $\sigma_y(x)$ for instantaneous plume cross-sections must be used!

In general, this integral needs to be solved numerically, in discretised form. The evaluation of the integral of (4.65) starts in practice by finding the maximum LFL-distance x_{lfl}, the maximum cloud width to LFL, y_{lfl}, and the maximum cloud height to LFL, z_{lfl}. In order to obtain practical values for these upper boundaries for integration, some methods will be provided to estimate the contour to the LFL, by use of approximate analytical solutions.

For a continuous point source at ground level, the down-wind distance to the LFL can be calculated as:

$$x_{lfl,ground} = \left\{ \frac{q}{\pi\ 0.3\ \sigma_v\ f_{z1}(z_o,\ L)\ c_{lfl}} \right\}^{\frac{1}{f_{z2}(L)\ +\ 1}} \qquad\qquad (m) \qquad (4.66a)$$

Here c_{lfl} denotes the LFL concentration, $f_{z1}(z_o, L)$ and $f_{z2}(L)$ follow from (4.58).

It should be noted that for an elevated plume which has not yet touched the ground, the LFL at centre-line is reached at a shorter distance:

$$x_{lfl,elevated} = x_{lfl,ground}\left(\frac{1}{2}\right)^{\frac{1}{f_{z2}(L)}} \qquad (m) \qquad (4.66b)$$

For plumes which have touched the ground, x_{lfl} will be between $x_{lfl,elevated}$ and $x_{lfl,ground}$.

Note that we consider the plume to touch the ground if $2 \times \sigma_z > h$.

The cross-wind distance to LFL at the ground can be calculated for elevated plumes and plumes at the ground by:

$$y_{lfl}(x) = \sigma_y(x)\sqrt{2 \ln\left(\frac{c(x,0,0)}{c_{lfl}}\right)} \qquad (m) \qquad (4.67)^{[1]}$$

where $c(x,0,0)$ is the concentration at ground level below the plume centre-line.

In the previous approximations of LFL-contours, one may include initial source dimensions by means of a virtual source distance. The virtual source distances x_{vy} and x_{vz} follow from the implicit relations:

$$\sigma_y(x_{vy}) = \frac{b_{oy}}{2.15}, \qquad \sigma_z(x_{vz}) = \frac{b_{oz}}{2.15} \qquad (4.68)$$

A conservative estimate for x_{lfl} can be obtained by substracting the smaller value of x_{vy} or x_{vz} from $x_{lfl,ground}$ or $x_{lfl,elevated}$. $y_{lfl}(x)$ can be obtained by using $\sigma_y(x+x_{vy})$ and $\sigma_z(x+x_{vz})$ instead of $\sigma_y(x)$ and $\sigma_z(x)$ in (4.67) (including in the calculation of $c(x,0,0)$).

For continuous point sources, the mass Q_{ex} between UFL and LFL can be obtained from an approximate analytical solution:

$$\frac{Q_{ex}}{q} = \frac{f_{z2}(L)+1}{f_{z2}(L)+2}\frac{x_{lfl}-x_{ufl}}{u_a} \qquad (s) \qquad (4.69)$$

x_{ufl} can be calculated similar as x_{lfl}.

---

[1] $\sigma_y(x)$ should be read as: 'σ_y as a function of x'.

For sources with initial dimension, but for which $x_{vy} \sim x_{vz} = x_v$, this solution is:

$$
\begin{cases}
\dfrac{Q_{ex}}{q} = \dfrac{1}{u_a} \left\{ \dfrac{(f_{z2}(L) + 1)}{f_{z2}(L) + 2} (x_{lfl} - x_{ufl}) - \dfrac{x_v^{(f_{z2}(L) + 2)}}{f_{z2}(L) + 2} \left(\dfrac{1}{x_{ufl}^{(f_{z2}(L) + 1)}} - \dfrac{1}{x_{lfl}^{(f_{z2}(L) + 1)}} \right) \right\} \\
\hspace{10cm} \text{if } x_{ufl} > 0 \\
\hspace{9cm} \text{(s)} \qquad (4.70) \\[4mm]
\dfrac{Q_{ex}}{q} = \dfrac{1}{u_a} \left\{ \dfrac{(f_{z2}(L) + 1)}{f_{z2}(L) + 2} x_{lfl} - x_v + \dfrac{x_v^{(f_{z2}(L) + 2)}}{(f_{z2}(L) + 2)x_{lfl}^{(f_{z2}(L) + 1)}} \right\} \qquad \text{if } x_{ufl} = 0
\end{cases}
$$

Note that $Q_{ex}/q = 0$ if $x_{lfl} = 0$, which will be the case when the initial concentration is lower than x_{lfl}.

4.5.4   Models for jets, plumes and plume rise

4.5.4.1   The free turbulent jet model

The aim of this section is to explain the jet model of Chen and Rodi [1980], which has been selected for the description of gas releases in a uniform quiescent atmosphere. The source is axially symmetric, with a radius b_o and a uniform outflow velocity u_o in vertical direction. The model is valid for gases which can be approximated to be incompressible, i.e. the release velocity should be less than about one-third of the speed of sound under ambient pressure. In cases where buoyancy can be neglected, the requirement on the initial direction of the release can be omitted. The formulation of flow development is based on the self-preserving properties of jet releases, which is discussed in Section 4.3.4. In a self-preserving flow, simple expressions exist for the centre-line velocity and concentration of the released chemical compound. Chen and Rodi determine common values for the empirical constants in the expressions. They define empirical conditions under which a jet model is applicable, and give expressions for the distribution functions of physical quantities in the lateral cross-sections of the flow (i.e., perpendicular to the mean flow axis).
The dynamical similarity of positively buoyant jets is a good approximation as long as

$$
s < 0.5 \cdot b_o \sqrt{Fr} \ (\rho_o/\rho_a)^{1/4} \qquad \text{(m)} \qquad (4.71),
$$

where Fr is the (densimetric) Froude number, ρ_o and ρ_a are the densities of respectively the initial chemical compound and air, b_o is the radius of the source and s is the axial distance to the hypothetical point source with the same flow characteristics as the real source. The Froude number was already defined in Section 4.3.4 as a measure for the relative importance of initial momentum and weight deficit.

$$
Fr = \frac{\rho_o}{|\rho_a - \rho_o|} \frac{u_o^2}{2b_o g} \qquad \text{(-)} \qquad (4.72).
$$

Here u_o is the exit velocity from the source.

The condition (4.71) implies that the model is only usable in cases in which inertial forces dominate over buoyant forces.
The no wind condition of the free jet model applied to vertical or cross-wind releases is equivalent to assuming that the centre-line velocity is much larger than the ambient wind velocity, typically by a factor of 10. In other situations, simple expressions for the flow quantities do not exist, and calculations have to be done with plume rise formulae (see Section 4.5.4.2), the Gaussian plume model (Section 4.5.3) and integral models like the SLAB computer model (Section 4.5.5.2).

The distribution functions, or profiles, are functions only of the nondimensional cross-flow coordinate y/s. The experimental observations show that the velocity and concentration profiles are approximately Gaussian after the potential core at a distance s_s (see Table 4.10) has disappeared:

$$u(y/s) \, / \, u_c(s) = \exp(-C_{yu} \, (y/s)^2) \qquad\qquad (\text{-}) \qquad\qquad (4.73),$$

$$c(y/s) \, / \, c_c(s) = \exp(-C_{yc} \, (y/s)^2) \qquad\qquad (\text{-}) \qquad\qquad (4.74).$$

$u_c(s)$ and $c_c(s)$ are the centre-line values, and C_{yu} and C_{yc} are empirical constants that determine the profile width. The concentration of the chemical compound is defined in parts per unit volume relative to atmospheric level, i.e. it is the difference between the local value and the value in air. The width constants turn out to be different for jets and plumes.

Non-buoyant jets
Non-buoyant jets are defined as releases of a chemical compound whose density ρ_o is equal to the density ρ_a of ambient air. The collection of experimental data sets in the review of Chen and Rodi consists mainly of this type of release. Some typical aspects were observed in the data sets:
− In most of the experiments, the locations of the real (circular) source and the virtual point source of the model do not coincide, i.e. the real source is located at a distance +(s_o). A good approximation is to take $s_o = 0$.
− In lateral direction, the concentration profiles are broader than the corresponding velocity profiles.
− Close to the source, the potential core is still visible in the jet profile. The distance s_s from the origin to the region of established flow can be derived from the location, where the jet profiles in lateral direction become Gaussian and (4.73) and (4.74) become valid. A good approximation is to take $S_s/b_o = 25$.
The jet flow in the region of established flow is described by the set of equations

$$u_c(s)/u_o = C_u \, b_o/s \qquad\qquad (\text{-}) \qquad\qquad (4.75).$$

$$c_c(s)/c_o = C_c \, b_o/s \qquad\qquad (\text{-}) \qquad\qquad (4.76).$$

c_o is the concentration of the initial chemical compound. A number of empirical constants occur in the model: C_u, C_c, C_{yu}, C_{yc}, s_o and s_s, and their values are given in Table 4.10 for the non-buoyant jet model of Chen and Rodi. The values for C_u, C_c, C_{yu} and C_{yc} are recommendations, whereas for s_o and s_s also the range of observed values is indicated.

Buoyant jets

Buoyant jets have an initial density ρ_o which is different from the density ρ_a of ambient air. The expressions 4.74-4.77 are still valid as long as condition 4.73 is satisfied. The empirical constants C_u, C_c, C_{yu} and C_{yc} can then be obtained from the values for a non-buoyant jet in Table 4.10. Chen and Rodi [1980] suggest in their monograph to correct the constants for density effects:

$$C_c' = \sqrt{\frac{\rho_a}{\rho_o}}\, C_c \qquad\qquad (-) \qquad\qquad (4.78).$$

$$C_u' = \sqrt{\frac{\rho_o}{\rho_a}}\, C_u \qquad\qquad (-) \qquad\qquad (4.77)$$

A vertical negatively buoyant jet rises to a maximum height s_h and then falls back on itself. Chen and Rodi give an equation for the height:

$$s_h = 4.11 \sqrt{Fr}\, b_o \qquad\qquad (m) \qquad\qquad (4.79).$$

Also for negatively buoyant jets the formulae 4.74-4.79 are valid as long as $s \leq s_h$.

Table 4.10   Empirical constants in the non-buoyant
            jet model of Chen and Rodi [1980]

non-buoyant jet		
C_u	6.2	
C_c	5	
C_{yu}	94	
C_{yc}	57	
s_o/b_o	0	(range -6 to 6)
s_s/b_o	25	(range 20 to 30)

Zone limits for ignition and explosive contents

The limiting distances for the ignition of a jet release are determined by the upper and lower flammability level of the chemical compound. A conservative estimate of the safe distance is obtained by equating the concentration on the jet axis to the lower flammability level c_{lfl}. The safe distance s_{lfl} for jets and plumes can then be derived from the equation 4.76, and taking into account (4.79):

$$s_{lfl} = \min\left(b_o C_c'\, \frac{c_o}{c_{lfl}},\, s_h\right) \qquad\qquad (m) \qquad\qquad (4.80)$$

The width of the lower flammability level isocontour can be derived from the equations 4.74, and 4.73. For jets they are given by

$$y_{lfl,jet}(s) = (s/\sqrt{C_{yc}}) \sqrt{\ln\left(\frac{b_o}{s} C_c' \frac{c_o}{c_{lfl}}\right)} \qquad \text{(m)} \qquad (4.81)$$

Note that the equation is invalid in the region of flow establishment, close to the source ($s < s_s$).

The explosive contents of jets and plumes is obtained by integrating over the volume between the upper and lower flammability isocontours. The mathematical formulation for the mass contents of the chemical compound is

$$Q_{ex} = \frac{\pi \rho_o b_o^3 (C_c')^3 c_o}{6C_{yc}} \left[\left(\frac{c_o}{c_{lfl}}\right)^2 - \left(\frac{c_o}{c_{ufl}}\right)^2\right] \qquad \text{(kg)} \qquad (4.82).$$

Note, that in this paragraph c_o, c_{ufl} and c_{lfl} are to be used in parts per unit volume. If $c_o < c_{ufl}$ the last term between the brackets vanishes. If $c_o < c_{lfl}$ then $Q_{ex} = 0$.

4.5.4.2   Models for jets and plumes in ambient wind

This section discusses the model of Hoot, Meroney and Peterka [HMP, 1973] for the dispersion of negatively buoyant plumes, and Briggs formulae [1969] regarding positively buoyant plumes. The models describe the plume trajectory, with emphasis on the development in the region of plume rise. The discussion is based on the one-dimensional integral plume theory, and on the analytical expressions which are derived from simplified versions of this theory. The basic assumptions of the theory are explained in Section 4.3.4. The model is valid for gases which can be approximated to be incompressible, i.e. the release velocity should be less than one-third of the speed of sound under ambient pressure.

The model of Hoot, Meroney and Peterka
Negatively buoyant jets and plumes injected vertically into a cross-wind initially loft to some maximum height, subsequently descend to the ground, impact to the ground with a nearly circular cross-sectional configuration, and then spread laterally as they disperse down-wind (see Figure 4.14).
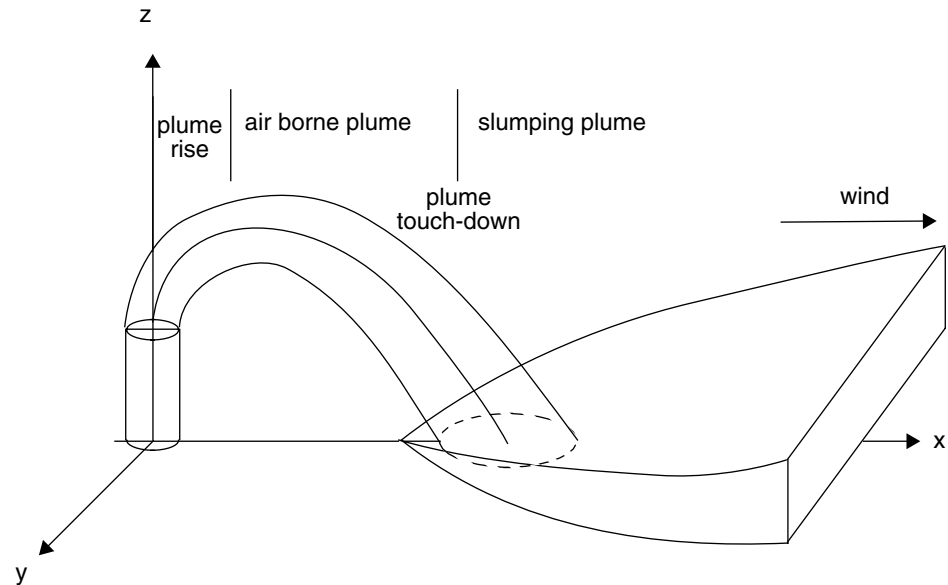
Figure 4.14   *The development phases of lofted plumes for a dense gas: initial plume rise, plume sinking and touch-down, development of a slumped grounded plume*

The integral model of Hoot, Meroney and Peterka [1973] assumes a cross-wind of constant velocity, and tophat profiles for the velocity, the density and the temperature inside the plume. The entrainment due to atmospheric turbulence is not taken into account, so the model is invalid in the far field. Hoot et al. do not solve the equations numerically. Instead they divide the plume path in regions and then obtain in each region analytical solutions of the conservation equations, i.e. sets of equations that describe the plume development. Hoot et al. determined the values of the empirical constants by a comparison of model results with wind-tunnel experiments.

The first set of equations describes the important quantities during plume rise. The down-wind distance to maximum plume rise is estimated in the HMP model as

$$x_r = \min\left(\frac{\rho_o u_o u_a}{g(\rho_o - \rho_a)}, 23.3 b_o \frac{u_o}{u_a} \right) \qquad \text{(m)} \qquad (4.83).$$

g is the gravity constant, u_o and ρ_o are the velocity and the density of the chemical compound at the stack exit, and ρ_a is the density of ambient air. In the HMP model the plume rise Δh_r is given by

$$\Delta h_r / b_o = 2.10 \, (x_r/b_o)^{1/3} \, (u_o/u_a)^{2/3} \qquad \text{(-)} \qquad (4.84).$$

b_o is the radius of the stack exit. Note that a similar dependency on the down-wind distance x and the wind velocity u_a is obtained in Section 4.3.4 for the plume rise of a non-buoyant jet. The peak concentration c_r of the chemical compound at maximum plume rise is

$$c_r / c_o = 6.09 \, (b_o/\Delta h_r)^{1.85} \, (u_o/u_a) \qquad \text{(-)} \qquad (4.85).$$

The second set of equations in the HMP model describes the important quantities during plume touch-down to the ground. The location x_g of the maximal ground concentration is given in the HMP model by

$$x_g - x_r = 0.28(((h_s + 2\Delta h_r)^3 - \Delta h_r^3)/b_o)^{1/2}(\rho_a/\rho_o)^{1/2}(x_r/b_o)^{1/2}(u_a/u_0)$$

$$\text{(m)} \qquad (4.86).$$

h_s is the height of the stack. At touch-down the surface peak concentrations c_g are of the order

$$c_g / c_o = 9.4 \, (b_o/(h_s + 2\Delta h_r))^{1.95} \, (u_o/u_a) \qquad \text{(-)} \qquad (4.87).$$

The surface concentration decreases from the touch-down value as the plume material is transported down-wind and gradually approaches the behaviour of a ground source.

The Briggs formulae for plume rise
In the simplified integral trajectory theory discussed by Davidson [1989] the rise of a positively buoyant plume, neglecting momentum rise, is related to the down-wind distance (x) by a 2/3-power law. Briggs [1969] has derived the empirical constants in the plume rise relations by measuring plume rises from conventional stacks in calm and windy, thermally stratified atmospheres. The equation for the plume trajectory according to Briggs is

$$\Delta h_B(x) = 1.60 \, F_o^{1/3} \, x^{2/3} / u_a \qquad \text{(m)} \qquad (4.88).$$

Here, u_a is the wind speed at release height, with a minimum of 10 m.
F_o is the buoyancy flux factor, defined as

$$F_o = gb_o^2 \, u_o\left(1 - \frac{\rho_o}{\rho_a}\right) \qquad \text{(m}^4 \text{ s}^{-3}) \qquad (4.89),$$

Briggs states that in a neutral or unstable atmosphere (Pasquill-classes A, B, C and D) the plume final rise occurs at

$$x_r = C_1 \cdot F_o^{5/8} \qquad \text{if} \qquad F_o \leq 55 \text{ m}^4/\text{s}^3$$

$$\text{(m)} \qquad (4.90)$$

$$x_r = C_2 \cdot F_o^{2/5} \qquad \text{if} \qquad F_o > 55 \text{ m}^4/\text{s}^3$$

Here, $C_1 = 49 \text{ m}^{-3/2} \text{ s}^{15/8}$, and $C_2 = 119 \text{ m}^{-3/5} \text{ s}^{6/5}$.

The plume final rise is obtained by substitution of the equation 4.90 (x_r) in equation 4.88.

For a release in a stable atmosphere (Pasquill-classes E and F) it is advised to employ a relation from the Dutch National Model. The National Model states that full rise occurs at

$$x_r = C_3 \, u_a \qquad \text{(m)} \qquad (4.91).$$

Here, $C_3 = 87$ s.

Equation 4.91 is valid as long as the vertical temperature gradient at heights between 10 and 200 m in the atmosphere is on average -0.0065 K/m, which corresponds to a temperature gradient as observed under neutral conditions (Pasquill-class D) in The Netherlands.

For low wind velocities in a neutral or unstable atmosphere, the calculation of the plume rise with the equations 4.88-4.90 gives values which are larger than the measured values. Therefore a rule of thumb has been set, stating that in neutral or unstable conditions the calculated plume rise must not exceed the plume rise calculated for stable conditions. In cases where the rule is violated, the equation 4.91 for stable conditions should be applied.

Briggs [1969] has also derived expressions for plume rise dominated by momentum forces, under conditions of neutral atmospheric stability. They are:

$$\Delta h_M = 6 \, b_o \, u_o \, / \, u_a \qquad\qquad\qquad (m) \qquad (4.92).$$

and

$$x_r = 23.3 \, b_o \, u_o \, / \, u_a$$

In cases where both the initial momentum and buoyancy contribute to the final plume rise, it is calculated according to

$$\Delta h_r = \left(\Delta h_B^3 + \Delta h_M^3 \right)^{1/3} \qquad\qquad (m) \qquad (4.93).$$

Trajectory and dilution predictions from simple integral plume theory

The flow diagram in Section 4.5.1 shows that plume rise formulae are used to provide the initial conditions for more complex dispersion models. In some cases it will be necessary to predict the concentration distribution of the release during plume rise. This can be calculated in a 3-step procedure with the simple model discussed by Davidson [1989].

First, the plume trajectory is calculated for all down-wind distances x during plume rise, by means of equation 4.84 for negatively buoyant jets and by means of equations 4.92 (for plume rise Δh_M due to momentum), 4.88 and 4.93 for neutral or positively buoyant jets. The local height $h(x) - h_s$ is obtained from these equations by replacing x_r by x.

The radius at other down-wind distances can be calculated by:

$$b(x) = b_o \sqrt{\frac{\rho_o u_o}{\rho_a u_a} + 0.41(h(x) - h_s)} \qquad\qquad (m) \qquad (4.94).$$

Finally, for a concentration distribution with a tophat shape the cross-sectional averaged concentration can be calculated by:

$$c(x)/c_o = (b_o/b(x))^2 \, (u_o/u_a) \qquad\qquad\qquad (-) \qquad (4.95).$$

(Note the similarity of the model equation 4.95 with the empirical equations 4.85 and 4.88 for the peak concentrations in the HMP model).

The total mass of inflammable material can be calculated by the general expression 4.65.

4.5.5   Dense gas dispersion models

The purpose of this section is 3-fold:
1. To give a scientific description of 2 models for dense gas dispersion, i.e. the Workbook of Britter and McQuaid [1988], and the SLAB computer model [Ermak, 1990]. The description treats the scientific aspects in detail, or refers to the open literature in cases where such a treatment would be too extensive.
2. To indicate the sensitivity, robustness, reliability and restrictions of the algorithms in the 2 models.
3. To provide the user with the same information in order to allow for an effective use of the model, including the preparation of input data and interpretation of the model output.

In other words, the contents of the section is an assessment of the algorithms in the models from a physical point of view, and a discussion of the connection between the in/output parameters of the models and the physical concepts in dense gas atmospheric dispersion.

The 2 models are developed for use in different situations:
− The Britter and McQuaid Workbook contains a set of nomograms which represent the concentration decay in releases from a continuous point source and an instantaneous cubic source, as a function of down-wind distance. It is useful for calculations with an indicative purpose.
− The SLAB computer code should be applied in more advanced dense gas dispersion studies. It describes the concentration in a cloud or plume by solving a 1-dimensional set of conservation equations for mass, chemical compound concentration, energy and the 3 components of momentum. The source can be a horizontal or vertical jet, a steady state surface area source, or an instantaneous release.

4.5.5.1   The Britter and McQuaid model

The model of Britter and McQuaid consists of empirical correlations between a set of independent variables that determine the gross properties of the dense gas dispersion process. The correlations are presented in an extensive Workbook which has been written by Britter and McQuaid [1988] in order to enable non-specialists to prepare estimates of the dispersion of pollutant dense gas emissions. The simplicity of the model imposes restrictions on its applicability. The primary aim of the model is to enable estimates of:
− average concentration levels along the plume axis, for continuous releases, and
− maximum concentration levels along the down-wind cloud path, for instantaneous releases.

In addition, Britter and McQuaid give rules of thumb to estimate isoconcentration contours.

The correlations are based on the method of dimensional analysis which has been presented in Section 4.3.5.1. It is shown there that the dimensional analysis gives the most compact results when the continuous and instantaneous releases are treated separately. This approach is also followed in the Britter and McQuaid (BM) model.

$$\left(\frac{g_o' V_o^{1/3}}{u_a^2}\right)^{1/2} \quad (\text{-})$$
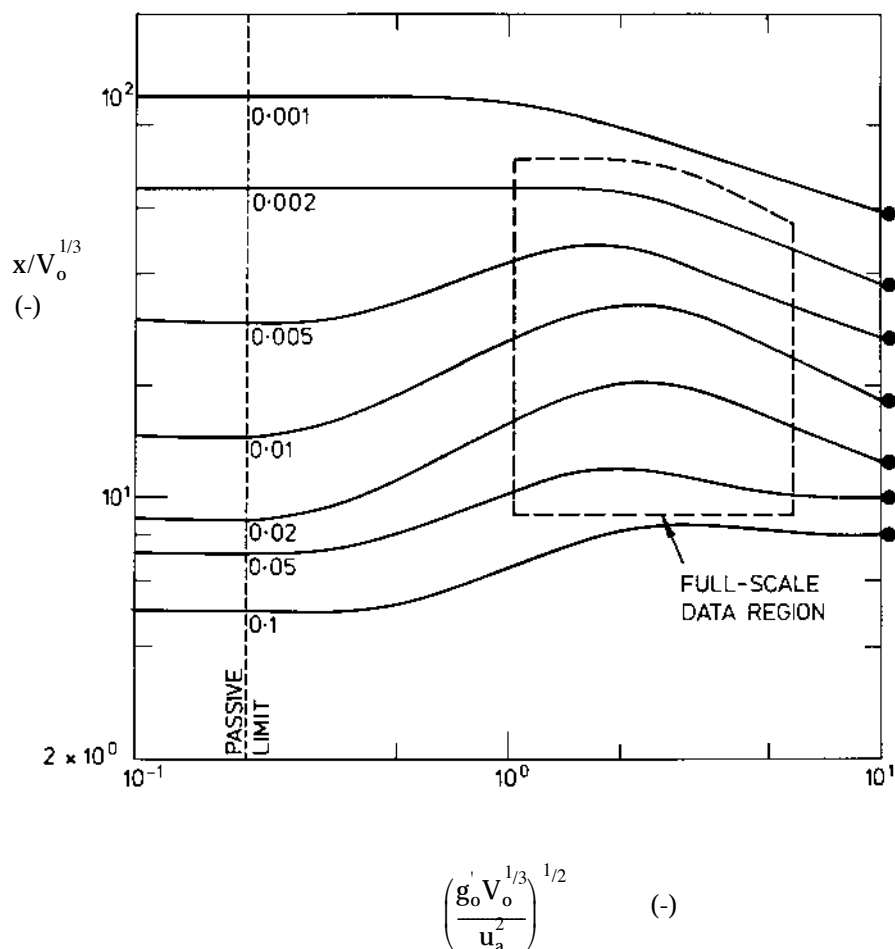
Figure 4.15   Nomograms for instantaneous releases, according to the Workbook of Britter
and McQuaid. Note: the curves correspond to the indicated values of c_{max}/c_o.

Correlations for instantaneous releases
The BM model consists of a collection of curves for down-wind maximum
concentrations c_{max}/c_o in the range between 0.001 and 0.1, which provide the
functional behaviour of $x/V_o^{1/3}$ versus $u_a^2/(g_o' V_o^{1/3})$:

$$x / V_o^{1/3} = f_i[\sqrt{(g_o' V_o^{1/3} / u_a^2)}] \qquad (\text{-}) \qquad (4.96).$$

The symbols in equation 4.96 have already been defined in Section 4.3.5.1.
Figure 4.15 is a graphical presentation of the curves, or nomograms, in the BM
model. The nomograms were derived from widely-accepted field test data (usually
referred to as 'Porton Down' and 'Thorney Island') and from windtunnel data (see
the Workbook of Britter and McQuaid, for more detailed information).

It is noted that the dimensionless parameter $u_a^2/(g_o' V_o^{1/3})$ is transformed in equation 4.96 so that its range of values for the used field and laboratory experimental data is of the order of unity: $0.7 < \sqrt{(g_o' V_o^{1/3}/u_a^2)} < 10$.

The reference wind velocity u_a is taken at a height of 10 m. Concentration values are intended to be valid for the ensemble-average of the maximum of short-time (0.6s) mean concentrations. Here 'ensemble-average' means that the fluctuations, which occur between successive experiments due to changes in the atmospheric conditions and in the in-cloud conditions, are averaged out.

As already mentioned in the introduction, the BM cloud model was developed in order to calculate the down-wind maximum concentration values on the path of the cloud centre. This enables a conservative estimate to be made of the safe distance for ignition or intoxication in all directions. The Workbook of Britter and McQuaid describes another procedure in order to determine the safe distances (in other words, the isocontours) with greater precision. It consists of 3 steps:

$$b(x) = \sqrt{b_o^2 + 3(x/u_a)\sqrt{g_o' V_o}}$$
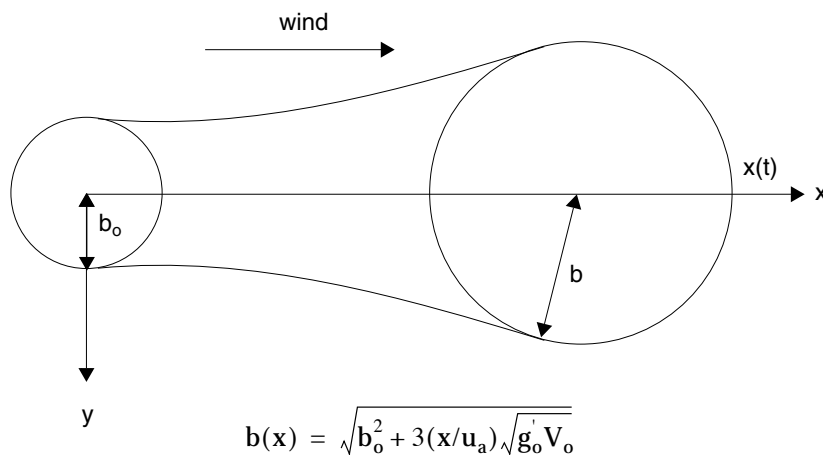
Figure 4.16 Approximations for isoconcentration contours of instantaneous releases, according to the Workbook of Britter and McQuaid

1. Calculate the down-wind distance x to the safe concentration level with the nomograms of the BM cloud model;
2. Calculate the arrival time t of the cloud at x from the relation

$$x = 0.4u_a t + b(t) \qquad \text{(m)} \qquad (4.97),$$

where $0.4u_a$ is an empirical estimate of the advection velocity, and b is the cloud radius. It is given by

$$b(t) = \sqrt{b_o^2 + 1.2t\sqrt{(g_o' V_o)}} \qquad \text{(m)} \qquad (4.98).$$

b_o is the radius of the cloud at the source. Note that the mean height of the cloud follows from:

$$b_z(t) = c_o V_o / (\pi b(t)^2 c_{max}(t)) \qquad\qquad (m) \qquad (4.99).$$

3. The radius $b(t)$ is also the half-width of the cloud at time t. The complete contour of the safe concentration consists of a parabola which encloses the source and is closed off by a circular portion of radius $b(t)$ at the down-wind end (see Figure 4.16).

The 3 steps in the estimation of safe distances are summarised in Flow diagram 4.1.

Diagram 4.1   Estimation of safe distances for an instantaneous release


```
┌─────────────────────────────────┐
│          calculate x            │
└─────────────────────────────────┘

┌─────────────────────────────────┐
│          calculate t            │
└─────────────────────────────────┘

┌───────────────────────────────────────┐
│  draw semi-circle at x - b(t), radius b(t)  │
│  draw semi-circle at origin, radius bo   │
│  draw parabolas to connect semi-circles  │
└───────────────────────────────────────┘
```
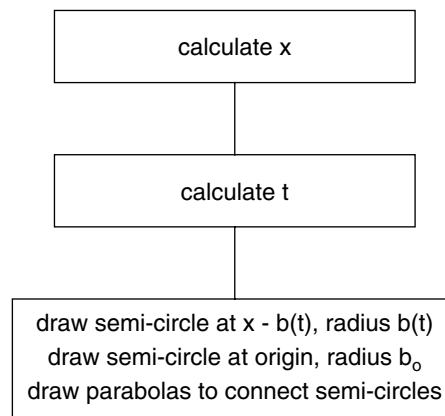
Correlations for continuous releases

The BM model consists of a collection of curves for down-wind mean concentrations c_{mean}/c_o in the range between 0.002 and 0.1, which provide the functional behaviour of $x\sqrt{(u_a/v_o)}$ versus $u_a^{5/2}/(g_o'\sqrt{v_o})$:

$$x / \sqrt{(v_o / u_a)} = f_c[((g_o')^2 v_o / u_a^5)^{1/5}] \qquad\qquad (\text{-}) \qquad (4.100).$$

The symbols in equation 4.108 have already been defined in Section 4.3.5.1. Figure 4.17 is a graphical presentation of the curves, or nomograms, in the BM model. The nomograms have been derived from widely-accepted field test data (usually referred to as 'Thorney Island', 'Maplin Sands' and 'China Lake'; the last one consists of 2 campaigns, named Burro and Coyote) and from windtunnel data (see the Workbook of Britter and McQuaid for more detailed information).
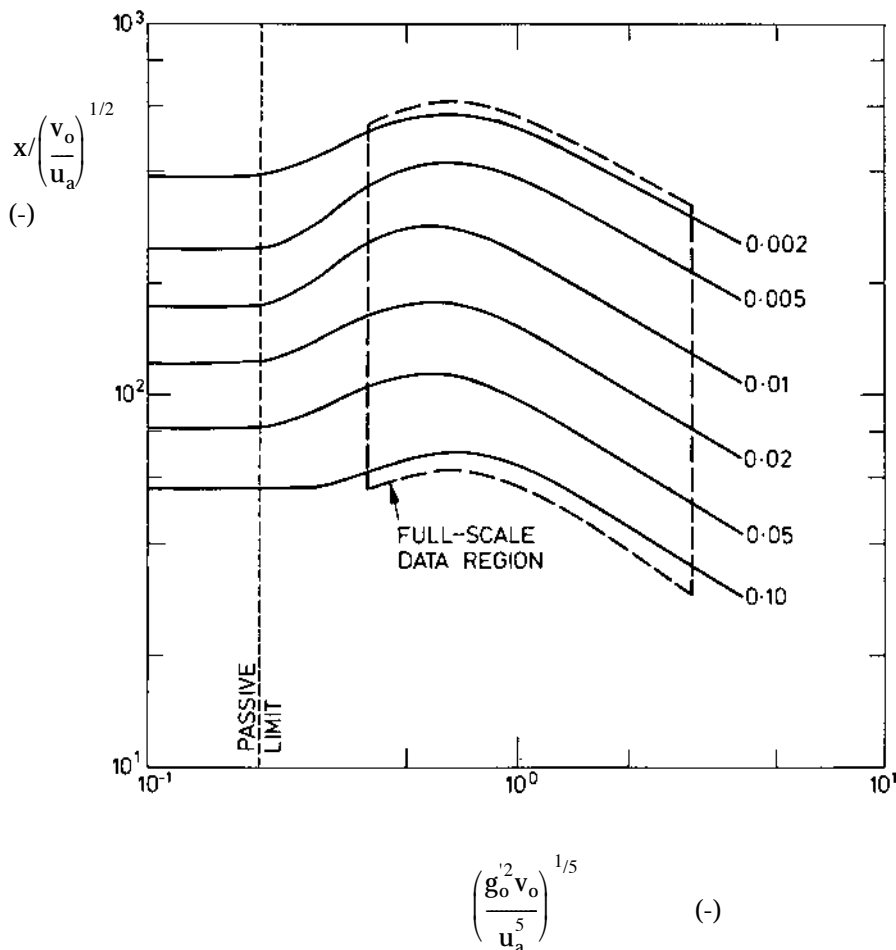
Figure 4.17 Nomograms for continuous releases, according to the Workbook of Britter and McQuaid. Note: the curves correspond to the indicated values of c_{mean}/c_o.

It is noted that the dimensionless parameter $u_a^{5/2}/(g_o'\sqrt{v_o})$ is transformed in equation 4.100 so that its range of values for the used field and laboratory experimental data is of the order of unity: $0 < ((g_o')^2 v_o / u_a^5)^{1/5} < 4$. The reference wind velocity u_a is taken at a height of 10 m. Concentration values are long-time (order of 10 min) averages, so greater concentrations are possible over short times due to fluctuations in concentration. Britter and McQuaid suggest that short-duration averaged concentrations can be a factor 1.6 higher than C_{mean}.

A conservative estimate of the safe distance for ignition or intoxication in all directions is obtained by calculating the down-wind mean concentration values on the plume axis. The Workbook of Britter and McQuaid describes another procedure in order to determine the safe distances with greater precision. It describes the plume by means of empirical expressions for the cross-wind plume area, and consists of 3 steps:
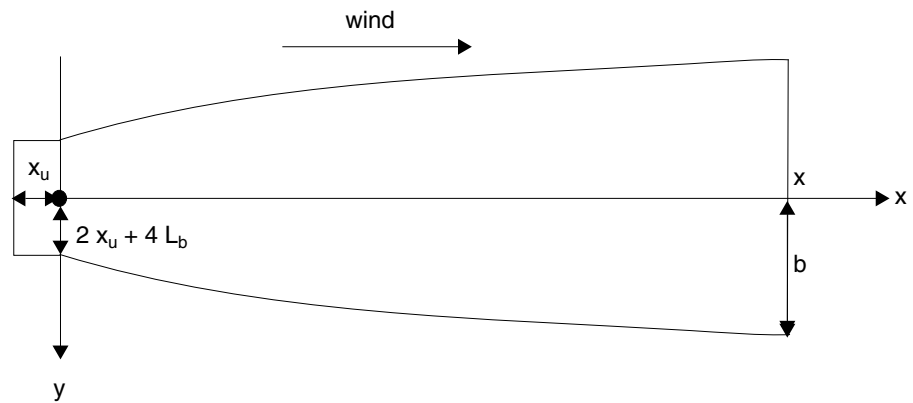
*Figure 4.18   Approximations for isoconcentration contours of continuous releases,
according to the Workbook of Britter and McQuaid*

1. Calculate the down-wind distance x to the safe concentration level with the nomograms of the BM plume model,
2. Calculate the upwind extension x_u of the plume, given by

$$x_u = b_o + 2 L_b \qquad\qquad\qquad \text{(m)} \qquad (4.101).$$

where b_o is the source radius.

$$L_b = v_o g_o' / u_a^3 \qquad\qquad\qquad \text{(m)} \qquad (4.102).$$

3. The down-wind growth of the lateral plume width b(x) is given by

$$b(x) = 2 b_o + 8 L_b + 2.5 L_b^{1/3} x^{2/3} \qquad\qquad \text{(m)} \qquad (4.103).$$

The isocontour can then be calculated from equation 4.103, with an upwind cut-off at x_u, and a down-wind cut-off at x (see Figure 4.18).

The 3 steps in the estimation of safe distances are summarised in flow diagram 4.2.

Diagram 4.2   Estimation of safe distances for a continuous release

```
          ┌─────────────────────────┐
          │      calculate x         │
          └───────────┬─────────────┘
                      │
          ┌───────────┴─────────────┐
          │     calculate L_b        │
          │     calculate x_u        │
          └───────────┬─────────────┘
                      │
  ┌───────────────────┴───────────────────────────┐
  │  draw curves y = ± b(x) between origin and x   │
  │ draw horizontal lines y = ± b(0) between -x_u  │
  │                and origin                       │
  │         close contours at -x_u and x           │
  └─────────────────────────────────────────────────┘
```
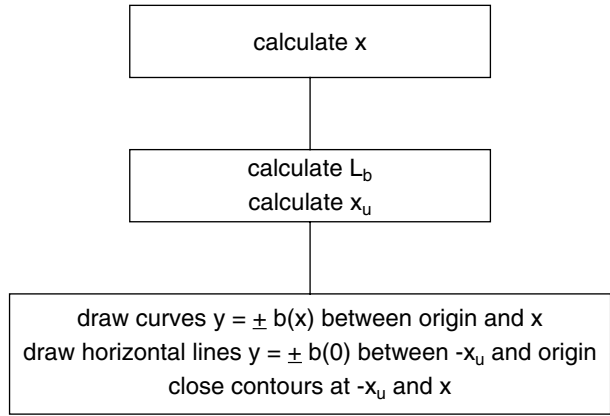
If it is assumed that the down-wind advection velocity is u_a, then the height h of the plume can be calculated from:

$$b_z(x) = v_o / (2\ u_a\ b(x)) \qquad\qquad \text{(m)} \qquad (4.104).$$

Releases of limited duration
In the BM model, a release is considered as effectively steady at a down-wind location x, when the duration t_r is larger than $2.5x/u_a$.

In this case the plume model in Figure 4.17 is applied. The BM cloud model in Figure 4.15 is applicable to releases with a duration less than $0.6x/u_a$.

When t_r is between these boundaries, the nomograms for instantaneous or continuous releases are not directly applicable. In this case the Workbook of Britter and McQuaid recommends the following 3-step procedure for the calculation of the concentration value at a down-wind location x:
1. Assume that the release is instantaneous, with a total volume V_o, and calculate the maximum concentration.
2. Assume that the release is continuous, with a release rate $v_o=V_o/t_r$, and calculate the mean concentration.
3. The smaller of the concentration estimates in the steps 1 and 2 provides the upper bound on the concentration for the finite-duration release.

The 3 steps in the estimation of concentration levels for finite-duration releases are summarised in flow diagram 4.3.

Diagram 4.3   Estimation of concentration levels for finite-duration release

```
┌─────────────────────────────────────────┐
│  calculate c_max for instantaneous release │
└─────────────────────────────────────────┘
                    │
┌─────────────────────────────────────────┐
│  calculate c_mean for continuous release  │
└─────────────────────────────────────────┘
                    │
┌─────────────────────────────────────────┐
│  select minimum of c_max and c_mean       │
└─────────────────────────────────────────┘
```
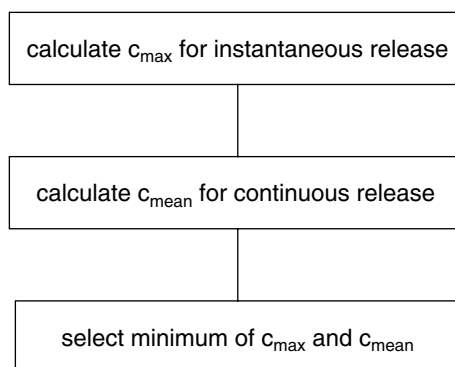
4.5.5.2   The SLAB computer model

The SLAB model is based on the concepts for air entrainment into a dense gas cloud and the subsequent gravity spread of the cloud, which were originally presented by Zeman [1982]. The formalism is an extension of the shallow layer theory, which is described in Section 4.3.5. The implementation into a computer code and the further development of the concepts of Zeman have been carried out by Ermak and Chan [1988, 1990] at Lawrence Livermore National Laboratory, USA. SLAB can treat continuous, finite duration and instantaneous gas releases from ground level area sources and jet flows. Though the model was designed for heavier-than-air releases, it will also simulate cloud dispersion of non-buoyant releases, and even lofting clouds in cases where the cloud becomes lighter than air.
The range of applicability is similar to that of the Gaussian Plume Model (see section 4.5.3).

Continuous releases
When the duration of the release is sufficiently long for the settling of a steady state in the down-wind area, the SLAB model performs a calculation for a continuous release.
This implies that the set of conservation equations, which is solved, is averaged over the cross-wind area A of the plume. As the source release rate q drops to zero, the release changes from a plume into a cloud; the discussion of such finite-duration releases is deferred until later in this section. The calculation for a continuous release consists of 5 steps, which are summarised in the flow diagram 4.4. The initial conditions are defined by the source term parameters. The SLAB model solves the set of governing cross-wind-averaged equations and subsequently performs a correction for the meandering wind (see Section 4.2.3). The concentration distribution $c(x,y,z)$ in 3 dimensions is obtained by means of a transformation, which matches the cross-wind-averaged parameters with realistic lateral and vertical profile functions. Finally the effect of the averaging-time t_{av} can be included in order to estimate toxic doses or to simulate the response of a sensor.

Diagram 4.4   The dispersion calculation for a continuous release in the SLAB model

```
┌─────────────────────────────────────┐
│       define source conditions       │
└─────────────────────────────────────┘
                   │
┌─────────────────────────────────────┐
│  calculate cross-wind-averaged parameters  │
└─────────────────────────────────────┘
                   │
┌─────────────────────────────────────┐
│   calculate the effect of plume meander   │
└─────────────────────────────────────┘
                   │
┌─────────────────────────────────────┐
│           calculate c(x,y,z)          │
└─────────────────────────────────────┘
                   │
┌─────────────────────────────────────┐
│       calculate the effect of $t_{av}$    │
└─────────────────────────────────────┘
```
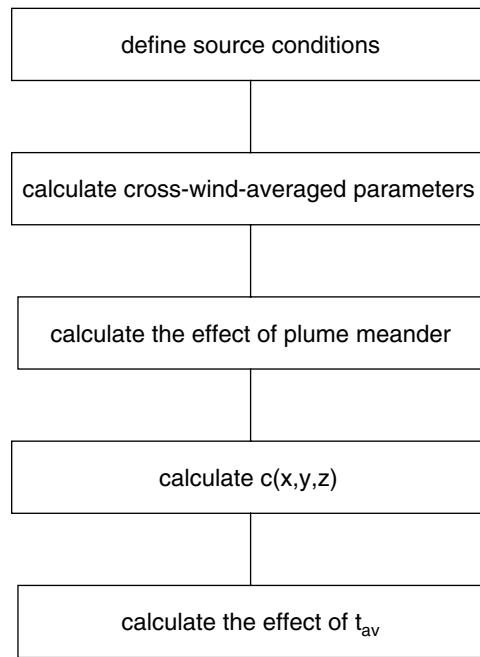
Source terms

The flow diagram 4.5 presents the source terms in the SLAB mode, for continuous releases. Since source modelling is already described in Chapters 2 and 3, the present discussion is only concerned with the aspects which are relevant for the SLAB model.

Diagram 4.5   Source conditions for a continuous release

```
┌──────────┐   ┌──────────┐   ┌──────────┐
│evaporating│   │horizontal│   │ vertical │
│   pool    │   │   jet    │   │   jet    │
└──────────┘   └──────────┘   └──────────┘
     │              │               │
     │              │          ┌──────────┐
     │              │          │  plume   │
     │              │          │   rise   │
     │              │          └──────────┘
     │              │               │
┌─────────────────────────────────────────┐
│   steady state plume dispersion calculations   │
└─────────────────────────────────────────┘
```
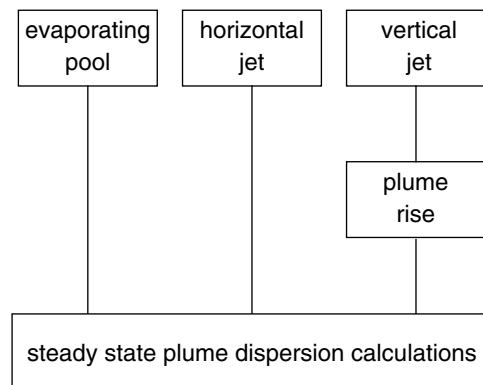
The evaporating pool release: The release is produced by a ground-level area source of finite duration, and its initial form (as long as the source is active) is that of a steady-state plume. The source material consists of pure vapour, with a temperature that is

equal to the boiling point of the chemical compound. In cases where the source area A is not known, it is calculated from the evaporation rate u_o using the equation

$$A = q / (\rho_o u_o) \qquad (m^2) \qquad (4.105).$$

q is the input mass source rate and ρ_o is the vapour density at the boiling point temperature of the chemical compound.

The horizontal jet: The source is an area perpendicular to the ambient wind direction, and its outflow direction is pointing down-wind. The source material consists of a single chemical compound, which may be partially liquid and partially vapour. The vapour fraction is input. The jet temperature is also input, but this may not be below the boiling point of the chemical compared. The height of the source is an input parameter.

The vertical jet: The source is an area source and the source velocity is vertical, in upward direction. The source material consists of a single chemical compound, which may be partially liquid and partially vapour, similar to the horizontal jet. The height of the source is an input parameter. Since the SLAB dispersion model can not handle cross-wind releases, the initial rise and down-wind bending of the jet release is simulated with the 1-dimensional integral model of Hoot, Meroney and Peterka [Hoot, 1973]. The shallow layer dispersion algorithm is used to describe the sinking of the bent-over lofted plume, the touch-down phase, the slumped plume phase and the far field behaviour. The procedure in SLAB to couple the HMP model output results to the input requirements of the shallow layer plume dispersion algorithm is presented below. Note that it is different, and more complex, than the procedure recommended in Section 4.5.4.2, formula (4.95).

The procedure consists of 3 steps:

−   The peak concentration c_r at maximal plume rise is calculated with the HMP model, and then the cross-wind-averaged concentration $c(x_r)$ is obtained from the equation (note here c is to be expressed in parts per unit volume):

$$c(x_r) = (0.524 \ (1-c_r) + c_r) \ c_r \qquad (-) \qquad (4.106)$$

In the derivation of this equation it is assumed that the concentration profile is Gaussian, so that the cross-wind-averaged concentration is 0.524 times the peak value. The additional terms in the equation are needed to ensure that $c \leq 1$ for large values of c_r.

−   The HMP model assumes that the velocity of the bent-over plume is equal to the ambient wind velocity u_a. A correction is applied in SLAB for high density releases, where the down-wind plume velocity can be considerably smaller than u_a. It is:

$$u(x_r) = 0.5u_a \ (1 - m - 2C_f + ((1-m)^2 + 4mC_f)^{1/2}) \ / \ (1-C_f) \qquad (m \ s^{-1}) \qquad (4.107),$$

C_f is a friction coefficient, with a value of 0.02, and m is the mass concentration, defined as:

$$m = \mu_s \ c(x_r) \ / \ (\mu_a + (\mu_s - \mu_a) \ c(x_r)) \qquad (-) \qquad (4.108).$$

μ_s and μ_a are molecular weights of the chemical compound and ambient air respectively. The conversion from volume concentration c (m^3/m^3) to mass

concentration in (kg/kg) is needed because the internal calculations in SLAB are done in 'm'.

– To complete the description of the plume at the point of maximum plume rise, the plume half-width b, the height and centre height h need to be determined. First the area of the plume cross-section at maximum plume rise is obtained from the equation

$$A_r = q / (\rho\, u\, m) \hspace{3cm} (m^2) \hspace{2cm} (4.109).$$

q is the mass flow rate of the source. It is assumed that the half-height is 60% of the half-width:

$$b_y = 1.2\, b \hspace{4cm} (m) \hspace{2cm} (4.110).$$

$$b_y = \max(\sqrt{(A_r / 2.4)}, b_o) \hspace{2.5cm} (m) \hspace{2cm} (4.111).$$

The plume centre height at maximal plume rise is $h(x_r) = h_s + \Delta h_r$.

The procedure is summarised in the Flow diagram 4.6.

In the region of plume rise, the trajectory (x, z_c) of the plume centre is described by the equation of an ellipse:

$$(1 - x/x_r)^2 + (h/\Delta h_r - h_s/\Delta h_r)^2 = 1 \hspace{2.5cm} (-) \hspace{2cm} (4.112).$$

Diagram 4.6   *Coupling of the HMP-model and the SLAB-model*
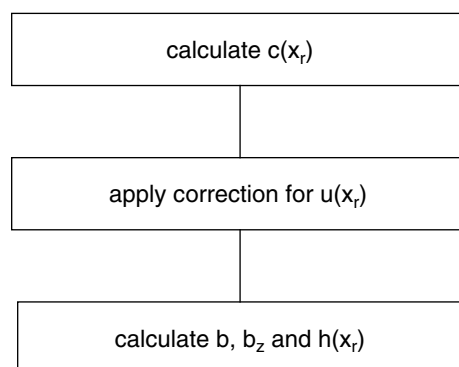
For dispersion calculations of non-buoyant or positively buoyant releases it is preferred to use the simple Gaussian plume model (Section 4.5.3), possibly in combination with Briggs plume rise formulae (Section 4.5.4), instead of the algorithms in the SLAB model.

The equations for a continuous release
The cross-wind-averaged plume properties are calculated in the SLAB model by numerical integration of the governing equations.
The set of equations consists of:
- Cross-wind-averaged conservation equations of the total mass, the mass of the released chemical compound material, the momentum vector and the energy.
- Equations for the width and height of the plume.
- The equation of state, and other thermodynamic equations.

The equations are solved by an integration in discrete steps in the down-wind coordinate. Since the temperature, the density and the vapour/liquid fraction in the plume are highly coupled quantities, the conservation equation of energy and the thermodynamic equations are solved together. This is done using Newton's iteration method for each step of the integration in space. The other conservation equations and the equations for the plume dimensions are ordinary differential equations. They can be solved by numerical integration using the Runge-Kutta method. The evaluation of averaged quantities such as the average wind speed acting on the plume can be done with Simpson's rule.

The cross-wind-averaged conservation equations
For a plume the conservation equations of chemical compound material, total mass and energy are:

$$d\,(m \rho u A)\,/\,dx = 0 \qquad\qquad (\text{kg m}^{-1}\text{s}^{-1})\quad(4.113),$$

$$d\,(\rho u\,A)\,/\,dx = 2\,\rho_a\,(b_y\,w_{e,t} + b_z\,w_{e,e}) \qquad\qquad (\text{kg m}^{-1}\text{s}^{-1})\quad(4.114),$$

$$d\,(\rho u\,A\,c_p\,T)\,/\,dx = 2\,\rho_a\,(b_y\,w_{e,t} + b_z\,w_{e,e})\,c_{p,a}\,T_a + E_{pc} + E_{gh} \qquad (\text{J m}^{-1}\text{s}^{-1})\quad(4.115).$$

The conservation equations of momentum are the equation for the down-wind plume velocity u:

$$d\,(\rho u^2\,A)\,/\,dx = -\,\rho_a\,d(g'\,Ab_z)\,/\,dx + 2\rho_a u_a(b_y\,w_{e,t} + b_z\,w_{e,e}) + f_x \qquad (\text{N m}^{-1})\quad(4.116),$$

and the equation for lateral gravity slumping u_y:

$$d(\rho u\,u_y\,A)\,/\,dx\,=\,2\,g'\,\rho_a\,b_z^2 + f_y \qquad\qquad (\text{N m}^{-1})\quad(4.117),$$

For a lofted plume, the descent of plume height h is described with the momentum equation

$$d(\rho u\,u_z\,A)\,/\,dx\,=\,-\,g'\,\rho_a\,A + f_z \qquad\qquad (\text{N m}^{-1})\quad(4.118),$$

The equation for gravity slumping in the y-direction is not needed in the lofted plume calculation; then $u_y = 0$. A lofted plume becomes grounded when $h \le b_z/2$.
The symbols for physical quantities and expressions used in 4.114-4.119 are summarised in Table 4.11, which also includes the reference to the formulae where the expressions are evaluated.

Table 4.11   Symbols in the conservation equations

		Equation
x, y, z	Spatial coordinates in down-wind direction and the horizontal and vertical cross-wind directions.	
ρ, ρ_a	The densities in the plume and in ambient air.	4.138
T, T_a	The temperatures in the plume and in ambient air.	4.115, 4.136, 4.144b
m	The mass concentration of the chemical compound.	4.113
u	The down-wind plume velocity.	4.116
u_y, u_x[1]	The velocities of plume spreading in the cross-wind directions.	4.117
u_z	Vertical velocity of the lofted plume	4.118
b_y, b_z, A	The half-width, height and area (= $2b_y$ b_z) of the plume.	4.114, 4.117, 4.152
c_p, $c_{p,a}$	The specific heats of the gas in the plume and of ambient air.	
$w_{e,e}$, $w_{e,t}$	The entrainment velocities at the edges and at the upper surface of the plume.	4.124-4.131
E_{pc}	The phase change energy per unit plume length.	4.144b
E_{gh}	The ground heat flux per unit plume length.	4.136-4.137
f_x, f_y, f_z	The friction terms in the 3 spatial directions.	4.132-4.135
g'	The effective gravity g' = g{(ρ_o - ρ_a)/ρ_a}.	

[1] u_x appears in the instantaneous release model (4.163).

Note that for the range of x-values that covers the source area, an additional term, the source flux, must be included on the right-hand side of the mass and energy equations. For a surface source, when the chemical compound is released with a vertical velocity u_o, the surface flux term in the mass equations is given by $2\rho_o u_o b_o$. If the temperature and the specific heat of the chemical compound at the source are denoted by, respectively, T_o and $c_{p,o}$, then the surface flux term in the energy equation is given by $2\rho_o u_o b_o c_{p,o} T_o$.

Ambient wind velocity profile
The entrainment velocities and the flux terms (friction terms, ground heat flux) are functions of the ambient wind. In the SLAB model the ambient wind velocity profile is derived from the gradient:

$$du_a/dz = (u_* / (\kappa z)) \, f_m(z/L) \, f_i(z/h_i) \qquad (s^{-1}) \qquad (4.119),$$

u_a is the ambient wind velocity, u_* is the ambient friction velocity, κ = 0.41 is Von Karman's constant, z is the height, L is the Monin-Obukhov length, h_i is the height of the mixing layer, f_m is the momentum Monin-Obukhov function and $f_i(z/h_i)$ is a mixing layer function. The mixing layer function in SLAB is

$$f_i(z/h_i) = 1 - z / h_i \qquad (-) \qquad (4.120a).$$

$$\begin{cases} f_m(z/L) = 1 + 5\,\dfrac{z}{L} & (L \geq 0) \\[2mm] f_m(z/L) = 1/\left(1 - 16\dfrac{z}{L}\right)^{1/2} & (L < 0) \end{cases} \qquad (-) \qquad (4.120b)$$

The substitution of the expressions for f_m and f_i, followed by an integration of equation 4.119, yields

$$u_a = (u_* / \kappa) \, [\ln(z/z_o) + f(z/z_o, z/L, z/h_i)] \qquad (m\ s^{-1}) \qquad (4.121).$$

f is a complicated function of its parameters. Section 4.5.2.1 provides a detailed description of the variation of u_a with height. The computerised SLAB code uses a somewhat different but more complex function, which leads to only small differences in u_a above 100 m height. Near the ground, equation 4.119 gives meaningless results, so for small heights ($z < 2.72\ z_o$) u_a is approximated by a polynomial:

$$u_a = C_1\,z + C_2\,z^2 \qquad (m\ s^{-1}) \qquad (4.122).$$

The constants C_1 and C_2 are obtained by requiring that u_a and du_a/dz are continuous at the transition point $z = 2.72.z_o$.

The average ambient wind velocity experienced by the dense gas cloud is

$$<u_a> = 1/b_z \int_o^{b_z} u_a(z)\ dz \qquad (m\ s^{-1}) \qquad (4.123).$$

The integral can be calculated with Simpson's rule.

Entrainment rates
While the entrainment concept is essential for the SLAB model, the choice of a particular entrainment (sub)model is not an essential aspect of the model. Different submodels could be used without changing the whole model. In the past years, the entrainment algorithms in SLAB have undergone several improvements. The version which is discussed here [Ermak, 1990], distinguishes between vertical entrainment at the top, and cross-wind and down-wind entrainment at the sides of the cloud (or plume).
The vertical entrainment rate is defined to be

$$w_{e,t} = 1.5\sqrt{3}\ \kappa\ (u_*)_{ic}\ f_i(b_z/h_i) / f_h(b_z/L) \qquad (m\ s^{-1}) \qquad (4.124),$$

$(u_*)_{ic}$ is the in-cloud value of the friction velocity, f_i is the mixing layer function (4.120a) and f_h is a Monin-Obukhov profile function. It is defined likewise as f_m as

$$\begin{cases} f_h \, (b_z/L) = 1 + 5 \, b_z/L & (L \geq 0) \\[2mm] f_h \, (b_z/L) = 1/(1 - 16 \, b_z/L)^{1/2} & (L < 0) \end{cases} \qquad (-) \qquad (4.125)$$

The friction velocity $(u_*)_{ic}$ is calculated from a complicated mathematical expression, which is summarised in Diagram 4.7

Diagram 4.7   Calculation of the incloud friction velocity $(u_*)_{ic}$

calculate $\Delta u = \dfrac{\rho_a}{\rho}(<u_a> - u)$

calculate $(u_*)^2_{mg} = (u_*/<u_a>)^2 \, (u^2 + u_y^2/4) + 1/2 \, u_o u_a$

calculate $(u_*)^2_{mh} = 0.0195 \left(\Delta u^2 + \left(\dfrac{\rho_a}{\rho} u_y \right)^2 \right) / 4$

calculate $(u_*)^3_t = 0.28 \, g \, \dfrac{u_*}{<u_a>} \, b_z \, (u_*)_{mg} \dfrac{T_a - T}{T_a + T}$

calculate $(u_*)^2_{ic} = (u_*)^2_{mg} + (u_*)^2_{mh} + (u_*)^2_t$
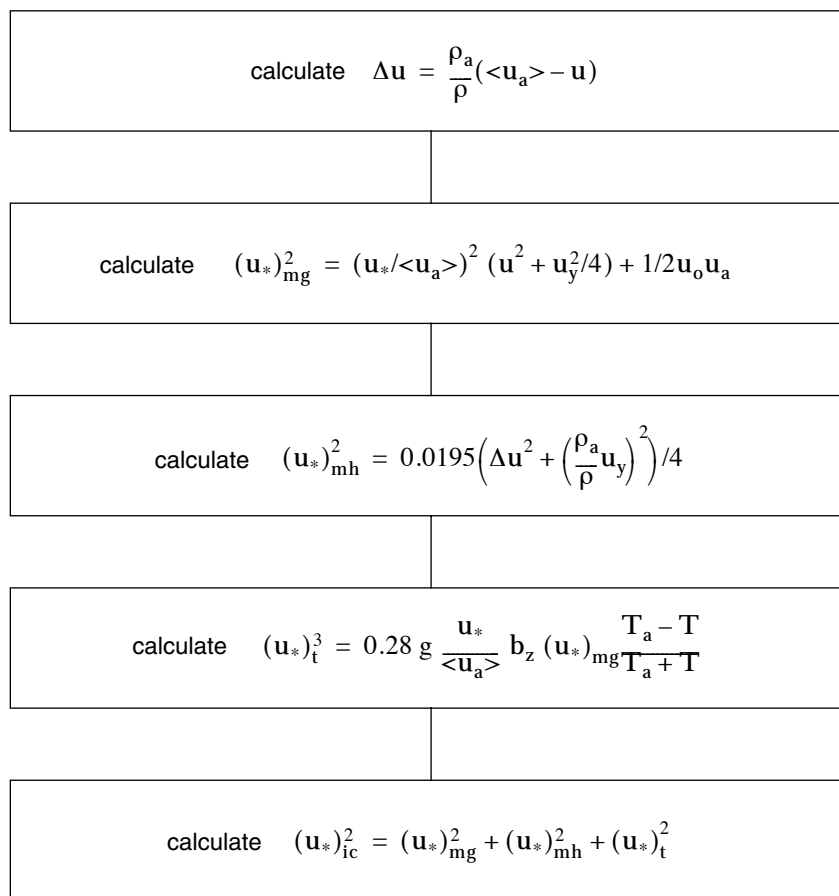
The horizontal cross-wind and down-wind entrainment rates are in the form (for continuous plumes only cross-wind entrainment is needed)

$$w_{e,e} = \left(3 (w^2_{e,e,s} + w^2_{e,e,t}) \right)^{1/2} \qquad (\text{m s}^{-1}) \qquad (4.126).$$

The term $w_{e,e,s}$ is a shear term. For cross-wind entrainment it is due to shear between the cloud and the ambient atmosphere, and given by

$$w_{e,e,s} = 0.209 \, \kappa \, \Delta u \qquad (\text{m s}^{-1}) \qquad (4.127).$$

4.100

Here Δu is the velocity difference between plume and ambient air as defined in Diagram 4.7.

For down-wind entrainment the shear term is due to the increase in ambient velocity with height. It is calculated from a complicated mathematical expression

$$w_{e,e,s} = 0.6 \frac{u_*}{\kappa} f_m\left(\frac{h + 0.5\sigma_z}{L_a}\right) f_i\left(\frac{h + 0.5\sigma_z}{h_i}\right) \qquad (\text{m s}^{-1}) \qquad (4.128).$$

The functions f_m and f_i have been defined in the discussion on the ambient wind profile (4.120a and 4.120b).
The term $w_{e,e,t}$ describes the entrainment due to atmospheric turbulence and is identical for the cross-wind and down-wind direction. It is given by

$$w_{e,e,t} = 0.08 \, u \, (f_s \, (L) \, f_p \, (t_{av}))^2 \, / \, (f_s \, (L) \, f_p \, (t_{av}) + 0.00144 \, b) \qquad (\text{m s}^{-1}) \qquad (4.129).$$

t_{av} is the averaging-time and b is either equal to b_x (down-wind case for time-dependent cloud) or b_y (cross-wind case). The functions are

$$\left\{ \begin{array}{ll} f_s(L) = 1 - \dfrac{C_3}{L}\sqrt{\dfrac{u_*}{<u_a>}} & L < 0 \\[3ex] f_s(L) = 1 / \left(1 + \dfrac{C_3}{L}\sqrt{\dfrac{u_*}{<u_a>}}\right) & L > 0 \end{array} \right. \qquad (-) \qquad (4.130)$$

Here, $C_3 = 34.1$ m.

$$f_p(t_{av}) = ((t_{av} + t_{min}\exp(-t_{av}/t_{min}))/t_i)^{0.2} \qquad (-) \qquad (4.131).$$

The minimum averaging-time t_{min} is 10 seconds. The normalisation time t_i is taken to be 900 seconds, which is the averaging-time that is assumed to apply to the standard dispersion curves for passive gas.

In the limiting case of a passive gas release where all dense gas effects are negligible, SLAB yields a cloud concentration and size that correspond to the values from standard dispersion calculations.

Momentum flux terms
The velocity flux terms (or drag terms) that appear in the momentum equations of the SLAB model are adapted from the work of Zeman [1982]. They are needed in order to determine the velocities and gravity currents u, u_x (in an instantaneous cloud only), u_y and u_z in the dispersing release. The horizontal velocity fluxes f_x and f_y are both composed of a term due to friction with the ground and a drag term at the top of the release. They are calculated from the equations:

$$f_x = -2 \, \rho \, b_y \, ((u_*/<u_a>)^2 \, [(u - \Delta u)^2 - <u_a>^2] + 0.0195 \, \Delta u^2) \qquad (\text{N m}^{-1}) \qquad (4.132)$$

$$f_y = -0.5 \, \rho \, b_y \, u_y{}^2 \, [(u_*/<u_a>)^2 + 0.0195 \, (\rho_a/\rho)^2] \qquad \text{(N m}^{-1}) \qquad (4.133).$$

The use of the equations is slightly different for plumes and clouds. For a plume, the velocity flux term f_x applies to down-wind movement of the dense gas in the plume, and the f_y term determines the horizontal cross-wind gravity spreading. For a cloud, the f_x term determines the average down-wind velocity u of the cloud as a whole, and the f_y term determines the gravity spreading with respect to the moving cloud centre, both in down-wind and cross-wind direction. The term f_z due to vertical movement is not relevant for grounded releases, because the vertical velocity can be calculated directly from other quantities, without solving the vertical momentum equation.
The SLAB model can also be applied to lofted plumes and clouds, but then there is no gravity spreading in the horizontal plane, so u_x (in an instantaneous cloud) and u_y are equal to zero. The movement of the cloud centre is affected only by drag due to shear with the surrounding air, so equation 4.130 applies without the ground friction term:

$$f_x = -0.039 \, \rho \, (2b_y + b_z) \, (u_*/<u_a>)^2 \, \Delta u^2 \qquad \text{(N m}^{-1}) \qquad (4.134).$$

The vertical movement u_z of the lofted plume or cloud is calculated by solving the momentum equation, with a drag term given by

$$f_z = 0.039 \, \rho \, b_z \, u_z{}^2 \qquad \text{(N m}^{-1}) \qquad (4.135).$$

As explained before, f_y is not needed for lofted plumes.

Heat flux term
The heat flux term is also obtained from the work of Zeman [1982]. The heat transfer between the dense gas and the ground is represented in the energy equation by a term

$$E_{gh} = 2 \, \rho \, b_y \, w_H \, c_p \cdot (T_a - T) \qquad \text{(J m}^{-1} \text{ s}^{-1}) \qquad (4.136).$$

The effective heat transfer velocity w_H is an empirical velocity, which also appears in other quantities such as the in-cloud friction velocity $(u_*)_{ic}$. It is given by

$$w_H = \frac{u_*}{<u_a>}(u_*)_{mg} \qquad \text{(m s}^{-1}) \qquad (4.137)$$

$(u_*)_{mg}$ is defined in Diagram 4.7. For a lofted cloud E_{gh} is, of course, equal to zero.

The thermodynamic model
The SLAB computer model contains a submodel for the thermodynamic processes which occur during the dispersion of a mixture of liquids and vapours in the atmosphere. The submodel is restricted in the sense that it allows only phase changes of the released chemical compound and of ambient water vapour that enters the release. The inclusion of moist air effects into the SLAB model requires that additional mass conservation equations are added for dry air and water. The equation of state for the complete system is

$$\rho = \rho_a \, T_a \, / \, (\alpha_l \, T + \gamma_l \, T_a) \qquad \text{(kg m}^{-3}) \qquad (4.138),$$

The coefficients α_l and γ_l are determined by the equations

$$\alpha_l = \mu_{moist} \, (m_a/\mu_a + m_{w,v}/\mu_w + m_{s,v}/\mu_s) \qquad (\text{-}) \qquad (4.139),$$

$$\mu_{moist} = 1 \, / \, ((1 - m_{w,v}{}^a)/\mu_a + m_{w,v}{}^a/\mu_w) \qquad (\text{kg mol}^{-1}) \quad (4.140),$$

$$\gamma_l = (\rho_a/\rho_{w,l})m_{w,l} + (\rho_a/\rho_{s,l})m_{s,l} \qquad (\text{-}) \qquad (4.141).$$

m is the mass concentration and μ is the molecular weight. The quantities are labeled with 2 subscripts. The first subscript is either 'a', 'w' or 's', and indicates whether the material is dry air, water or the chemical compound. The second subscript, separated by the first subscript with a comma, is 'v' or 'l' and indicates the phase of the material, i.e. whether it is a vapour or a liquid. A superscript labels the material of the environment. Example: $m_{w,v}{}^a$ is the mass concentration of water vapour in ambient air. The vapour concentration is calculated separately for the chemical compound and for water by using the condition of local equilibrium. This means that the partial pressure of the vapour phase of each material is equal to the smaller of 2 pressures: (1) the saturation pressure, or (2) the partial pressure when the total mass fraction is in the vapour phase.

For a single material the partial pressure after complete vaporisation ($m_1 = 0$) is

$$p \, = \, \frac{m}{\mu} \, \rho RT \, / \, \left(1 - \frac{\rho}{\rho_a}\gamma_l\right) \qquad (\text{N m}^{-2}) \qquad (4.142).$$

R is the gas constant. The saturation pressure is expressed in the form

$$p_s \, = \, p_a \, \exp\left(C_A - \frac{C_B}{T + C_C}\right) \qquad (\text{N m}^{-2}) \qquad (4.143),$$

p_a is ambient pressure. C_A, C_B and C_C are saturation pressure constants, which are basic properties of the material. The constants C_B and C_C are required as input parameters of the SLAB computer model. Then C_A is calculated from 4.144 and the boiling temperature (input to SLAB).

If the total mass concentration is denoted by m, then the local equilibrium condition expresses the vapour concentration as

$$\begin{cases} m_v = m & (p < p_s) \\[2mm] m_v = m \cdot \dfrac{p_s}{p} & (p > p_s) \qquad (\text{-}) \end{cases} \qquad (4.144).$$

The procedure to evaluate the equation of state is summarised in Diagram 4.8.

Through the dependence of p_s on the cloud temperature T, there is a strong coupling between the energy balance equation (4.115) and the thermodynamic state equations (4.138 - 4.144). The linking term is the phase change energy E_{pc}, which depends on the change of liquid material in the plume per down-wind distance (for the continuous release) or time (for the instantaneous release) integration step. For the continuous release E_{pc} is described by:

$$E_{pc} = \rho uA \; (\Delta H_w \cdot d(m_{w,l})/dx + \Delta H_s \cdot d(m_{s,1})/dx) \qquad (Jm^{-1}s^{-1}) \qquad (4.144b)$$

here ΔH_w and ΔH_s, are the latent heat of water and released material, respectively.

The solution of the thermodynamic state which fulfils both (4.138-4.144) and (4.115 using 4.144b) is performed for each integration time step by Newton's iteration method.

Diagram 4.8   Evaluation of the equation of state

calculate p and p_s for water

calculate $m_{w,v}$

calculate μ_{moist}

calculate p and p_s for the chemical compound

calculate $m_{s,v}$

calculate α_l and γ_l

calculate $\rho(T)$
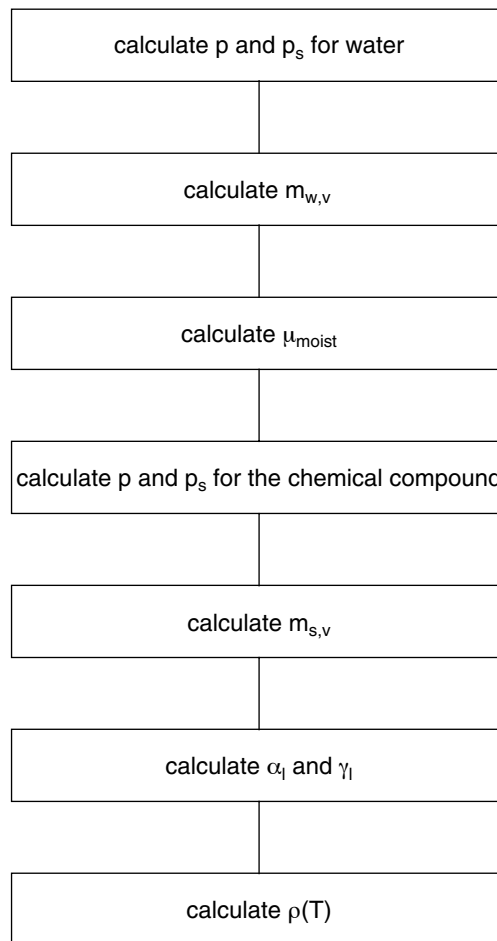
Plume meandering
The random oscillations of the plume centre-line about the mean wind direction are ignored in the numerical solution to the set of conservation equations, plume structure equations and thermodynamic equations.

This effect, called plume meandering, increases the effective half-width $b_{y,m}$ of the plume as t_{av} is increased. The SLAB model corrects for the increase (see also Diagram 4.4).

4.104

$$b_{y,m}{}^2 = b_y{}^2 + 3 \ (r^2(C_{av}) - 1) \ \sigma_y{}^2(t_{av}) \qquad (m^2) \qquad (4.145).$$

σ_y is the standard deviation for a passive gas plume in the absence of plume meandering. The averaging parameter C_{av} is defined as

$$C_{av} = (t_{av} + t_{min} \exp(-t_{av}/t_{min}) \ / \ t_{min})^{0.2} \qquad (-) \qquad (4.146).$$

The exponential function exp is needed in order to guarantee that the averaging parameter becomes unity as t_{av} approaches zero, because in this limit $b_{y,m}$ and b_y should become equal. The exponent k is set equal to 0.2, in accordance with common conventions. The effective minimum averaging-time t_{min} is set equal to 10 seconds, since this has proven to give good results [Ermak, 1990].

The spatial concentration distribution in 3 dimensions
The SLAB plume model calculates only cross-wind-averaged properties, and characterises the shape by the height b_z and the cross-wind half-width b_y. The parameters b_y and b_z do not correspond to a particular concentration level, but describe a surface which encloses the bulk of the dense gas. This means that the user can implement a submodel of the concentration distributions which best fits his purpose. In an early study of steady-state releases, Ermak et al. [1982] have used a quadratic distribution, but exponential or Gaussian distributions are other possibilities. The SLAB version, which is discussed here, assumes that the distribution is Gaussian in the horizontal and vertical cross-sections:

$$c(x,y,z) = 2 \ b_y \ b_z \ c(x) \ F_y(y,y_b,C_y) \ F_z(z,h,\sigma_z) \quad \text{(parts per unit volume)} \quad (4.147),$$

The average volume concentration c(x) is related to the mass concentration by

$$c(x) = \mu_a \ m(x) \ / \ (\mu_s + (\mu_a - \mu_s) \ m(x)) \qquad \text{(parts per unit volume)} \qquad (4.148),$$

μ_s and μ_a are respectively the molecular weights of the chemical compound and ambient air. The function $F_y(y,y_b,C_y)$ is defined as

$$F_y(y,y_b,C_y) = (\mathrm{erf}((y + y_b)/(\sqrt{2}C_y)) - \mathrm{erf}((y - y_b)/(\sqrt{2}C_y)))/(4 \ y_b)$$

$$(m^{-1}) \qquad (4.149),$$

erf denotes the error function, and y_b and C_y are shape parameters. The shape parameters are related: $C_y^2 = \frac{1}{3}(b_y^2 - y_b^2)$. y_b follows from (4.153) below. The function $F_z(z,h,\sigma_z)$ is defined as

$$F_z(z,h,\sigma_z) = (\exp(-(z-h)^2/(2\sigma_z^2)) + \exp(-(z+h)^2/(2\sigma_z^2)))/\sqrt{(2\pi\sigma_z^2)}$$

$$(m^{-1}) \qquad (4.150).$$

h is the height parameter and σ_z is the vertical half-width parameter. The vertical profile function allows for both grounded releases ($h \le 0.5b_z$) and elevated releases ($h > 0.5b_z$), with a width defined as

$$
\left\{
\begin{array}{ll}
\sigma_z = (b_z - h)/\sqrt{3} & \text{(grounded)} \\
\\
\sigma_z = 0.5\ b_z/\sqrt{3} & \text{(lofted)}
\end{array}
\right.
\qquad \text{(m)} \qquad (4.151).
$$

A number of additional cloud structure equations are needed in order to obtain a complete description of the concentration distribution. They are, for a dispersing plume,

$$u\ db_y/dx = (\rho_a/\rho)\ w_{e,e} + u_y \qquad \text{(m s}^{-1}\text{)} \qquad (4.152),$$

$$udy_b/dx = u_y\ y_b/b_y \qquad \text{(m s}^{-1}\text{)} \qquad (4.153),$$

$$u\ dh/dx = -u_y h/b_y \qquad \text{(m s}^{-1}\text{)} \qquad (4.154).$$

The initial conditions of b_y and h follow from the source dimensions b_o and h_s or the plume rise functions ((4.84) and (4.111)). The initial condition for y_b is 0.9 times the initial condition of b_y (to avoid C_y to become zero).

The equations can be solved with the Runge-Kutta method.

The effect of time-averaging
The last step in the Flow diagram 4.4 is to take a time-average at locations (x,y,z) over a duration of time t_{av}. The averaging-time t_{av} is an input parameter, in order to allow the performance of calculations of the average concentration level for different times of exposure. The time-averaged volume concentration c_{av} is determined by averaging the volume concentration c(x,y,z,t) over time:

$$c_{mean}(x,y,z) = 1/t_{av}\int c(x,y,z,t)\ dt \qquad \text{(parts per unit volume)} \qquad (4.155).$$

The integration boundaries are $t_{pk} \pm 0.5t_{av}$, where t_{pk} is the time of peak concentration. For a steady-state calculation, time-averaging has no effect.

This completes the description of the SLAB model in steady-state mode.

Finite-duration sources with a constant emission rate
The released gas of a finite-duration source is eventually advected down-wind as a cloud instead of a plume, and this imposes different requirements on the dispersion algorithms. The most important difference is that the governing equations are spatially averaged over the cloud volume instead of cross-wind-averaged. For a finite-duration release, SLAB starts in the plume submodel, and makes a transition to the puff submodel at the time t_r when the release is terminated. Thus, the calculation is performed in 2 steps:

1. A calculation with the plume model is done, and the location $x_c(t)$ of the corresponding cloud centre-of-mass at a time t is obtained by travelling down-wind until a location x_c is reached where the plume contains half of the total amount of dense gas, released during this time t. The cloud half-length is obtained by a linear interpolation:

$$b_x(t) = b_x(0) + (b_x(t_r)-b_x(0)) \; (x_c(t)-x_c(0)) \; / \; (x_c(t_r)-x_c(0)) \qquad \text{(m)} \qquad (4.156).$$

$x_c(0)$ and $b_x(0)$ are the initial location of the centre-of-mass and the initial cloud half-length, which are determined by the source geometry. The half-width $b_x(t_r)$ at the point of transition is calculated in step 2.

2. At the time t_r the volume-averaged (puff) cloud properties are calculated from the cross-wind-averaged plume properties at the location $x_c(t_r)$. It is assumed that the mass fraction and the density are continuous at the transition, and then the cloud half-length is

$$b_x(t_r) = 0.5 \; u(x_c) \; t_r \qquad \text{(m)} \qquad (4.157),$$

where $u(x_c)$ is the down-wind cloud velocity at location x_c.
The cloud properties (u, T, b_y, b_z etc.) are required to be equal to the plume properties at $x = x_c$.
The procedure is summarised in Flow diagram 4.9. The transformation is needed to start the cloud calculation at $t = t_r$, and it can also be applied to obtain cloud parameters for $t < t_r$.

Diagram 4.9   Transformation of plume parameters to cloud parameters
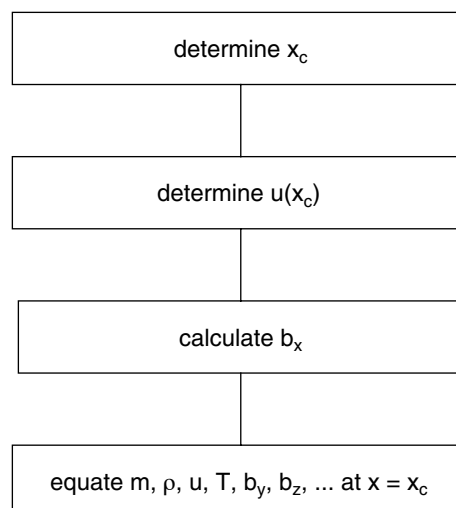
Instantaneous releases
The SLAB model treats sources which inject a dense gas into the atmoshere at a steady rate, but during a finite time, as a cloud. The limiting case is an instantaneous release, for instance due to a tank failure. The calculation is performed with the puff

submodel, using a procedure consisting of 5 steps (see Flow diagram 4.10). The steps differ from the procedure of the plume submodel (see Flow diagram 4.4) in a number of aspects, which are discussed in the remainder of this Section.

Diagram 4.10   The dispersion calculation for an instantaneous release in the SLAB model

```
┌─────────────────────────────────────────────┐
│          define source conditions            │
└─────────────────────────────────────────────┘
                      │
┌─────────────────────────────────────────────┐
│  calculate average parameters for the cloud volume │
└─────────────────────────────────────────────┘
                      │
┌─────────────────────────────────────────────┐
│        calculate the effect of cloud meander  │
└─────────────────────────────────────────────┘
                      │
┌─────────────────────────────────────────────┐
│             calculate c(x,y,z,t)              │
└─────────────────────────────────────────────┘
                      │
┌─────────────────────────────────────────────┐
│          calculate the effect of $t_{av}$     │
└─────────────────────────────────────────────┘
```
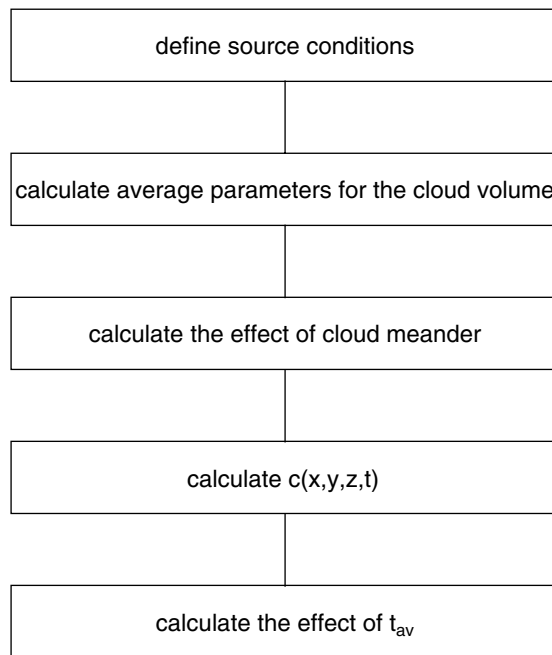
The instantaneous or short-duration evaporating pool: Although the source is of the ground-level area type, it differs from the previous types in that the release occurs instantaneously or in a very short time. The amount of released chemical compound is not characterised by the mass rate q, but by the total mass Q. This type of release is usually accompanied by compressibility effects (see chapter 2), but the source term model in SLAB assumes that the cloud is fully expanded and that the pressure has been reduced to the ambient atmospheric level. The source material consists of pure vapour.

The equations for an instantaneous release
The conservation equations, the cloud structure equations and the thermodynamic equations are solved by an integration in discrete steps in the time coordinate. The numerical techniques which were indicated in the discussion of the plume model, are equally applicable to the puff model.

The volume-averaged conservation equations
For a cloud the conservation equations of species, mass and energy are:

$$d\,(m\rho V) \,/\, dt = 0 \qquad\qquad\qquad (kg\ s^{-1}) \qquad (4.158),$$

$$d\,(\rho V)\,/\,dt = \rho_a\,v_e \qquad\qquad (\text{kg s}^{-1}) \qquad (4.159),$$

$$d\,(\rho V\,c_p\,T)\,/\,dt = \rho_a\,v_e\,c_{pa}\,T_a + 2\,b_x\,(E_{pc} + E_{gh}) \qquad (\text{J s}^{-1}) \qquad (4.160),$$

$$v_e = 4\,(b_y\,b_z\,w_{e,x} + b_x\,b_z\,w_{e,y} + b_x\,b_y\,w_{e,t}) \qquad (\text{m}^3\,\text{s}^{-1}) \qquad (4.161).$$

The down-wind entrainment velocity $w_{e,x}$ and the cross-wind entrainment velocity $w_{e,y}$ are obtained from equation 4.126. The vertical entrainment velocity $w_{e,t}$ is obtained from equation 4.124.

The momentum equation for the centre-of-mass of the cloud is

$$d\,(\rho\,u\,V)\,/\,dt = \rho_a\,v_e\,u_a + 2\,b_x\,f_x \qquad\qquad (\text{N}) \qquad (4.162).$$

The gravity slumping equations for a grounded cloud are

$$d(\rho\,u_x\,V)\,/\,dt = g'\,\rho_a\,b_x\,b_z^2 + 2\,b_x\,f_y \qquad\qquad (\text{N}) \qquad (4.163),$$

$$d(\rho\,u_y\,V)\,/\,dt = g'\,\rho_a\,b_y\,b_z^2 + 2\,b_x\,f_y \qquad\qquad (\text{N}) \qquad (4.164).$$

For a lofted cloud, the equations 4.163-4.164 are replaced by the momentum equation of vertical momentum:

$$d(\rho\,u_z\,V)\,/\,dt = -\,g'\,\rho_a V + 2\,b_x\,f_z \qquad\qquad (\text{N}) \qquad (4.165).$$

The spatial concentration distribution in 3 dimensions
The characterisation of the cloud shape requires a third parameter, the down-wind half-length b_x, in addition to b_y and b_z.
They are obtained by solving the cloud structure equations:

$$db_y/dt = (\rho_a/\rho)\,w_{e,y} + u_y \qquad\qquad (\text{m/s}) \qquad (4.166),$$

$$dy_b/dt = u_y\,y_b\,/\,b_y \qquad\qquad (\text{m/s}) \qquad (4.167).$$

Since a cloud has a finite extension at each location x in the down-wind direction, the term c(x) in the 3-dimensional concentration distribution c(x,y,z,t) contains a down-wind profile function. It is defined as

$$c(x) = 2\,b_x\,c(t)\,F_x(x-x_c,x_b,C_x) \qquad (\text{parts per unit volume}) \qquad (4.168),$$

where the average volume concentration c(t) is related to m(t) through equation 4.148, and the profile function F_x is equal to F_y as defined in equation 4.149, the position of the centre-of-mass of the cloud, x_c is calculated by integrating u from (4.162) to time t. C_x follows from $C_x^2 = \frac{1}{3}(b_x^2 - x_b^2)$. The cloud structure equations for b_x and x_b are

$$db_x/dt = (\rho_a/\rho)\,w_{e,x} + u_x \qquad\qquad (\text{m s}^{-1}) \qquad (4.169),$$

$$dx_b/dt = u_x \, x_b \, / \, b_x \qquad\qquad\qquad\qquad (\text{m s}^{-1}) \qquad (4.170).$$

The equations can be solved with the Runga-Kutta method.
The initial conditions for b_x follow from the source dimensions or equation 4.157.
The initial condition for x_b is 0.9 times the initial condition of b_x.

The effect of time-averaging
The calculation of the time-averaged volume concentration $c_{av}(x,y,z)$ requires the evaluation of the time-integral.
An analytical expression can be derived:

$$c_{av}(x,y,z) = 4 \, b_x b_y b_z \, c(t_{pk}) f_{av}(x_b,C_x,t_{av}) F_y(y,y_b,C_y) F_z(z,h,\sigma_z)$$

$$\text{(parts per unit volume)} \qquad (4.171),$$

$$f_{av}(x_b,C_x,t_{av}) = \frac{C_x}{\sqrt{2} \, x_b \, u \, t_{av}} \left(x_1 \, \text{erf}(x_1) - x_2 \, \text{erf}(x_2) + \frac{1}{\sqrt{\pi}} \left(e^{-x_1^2} - e^{-x_2^2} \right) \right)$$

$$\text{(m}^{-1}) \qquad (4.172),$$

$$x_1 = \left(x_b + \frac{1}{2} u \, t_{av} \right) / (\sqrt{2} \, C_x) \qquad\qquad (\text{-}) \qquad (4.173),$$

$$x_2 = \left(x_b - \frac{1}{2} u \, t_{av} \right) / (\sqrt{2} \, C_x) \qquad\qquad (\text{-}) \qquad (4.174).$$

t_{pk} is the time of peak concentration. The terms F_y and F_z are spatial distribution functions, which were defined in the discussion of continuous releases.

This ends the discussion of instantaneous releases in the SLAB model.

4.6   Application of selected models: calculation examples

4.6.1   Introduction to Section 4.6

Section 4.6 provides examples on the use of models described in Section 4.5.

Section 4.6.2 provides examples on stability calculations using the Holtslag scheme as presented in Section 4.5.2.

Section 4.6.3 considers the use of the Gaussian plume model for continuous and instantaneous releases as described in Section 4.5.3.

Section 4.6.4 provides examples on the calculation of free jets, plume rise and the plume trajectory model (HMP-model) as described in Section 4.5.4.

Section 4.6.5 provides examples on the use of the SLAB model as described in Section 4.5.5.

4.6.2   Examples of stability calculations

This section provides examples on the use of the Holtslag scheme, Section 4.5.2. In Section 4.6.2.1 the application of the day-time scheme and in Section 4.6.2.2 the application of the night-time scheme is presented.

4.6.2.1   Application of the day-time scheme

The site for which the stability is to be established is somewhere in The Netherlands: 51˚ N, -5˚ W.

The day is the 20st of June (in a non-leap year), the time 9.40 UTC locally before noon.

The weather is overcast with broken clouds, N = 6/8, and the air temperature is about 20 ˚C.

The wind speed at 10 m height is 4 m/s. The terrain is flat, grass-covered, without obstacles; the roughness length z_o is estimated to be 0.01 m, see Table 4.3.

The albedo is estimated from Table 4.4 and found to be 0.2; the moisture availability is set at 1.

From Appendix I, we calculate the Julian day to be 171, and the solar elevation 48.6˚; (the solar longitude SL = 7.87, the solar declination SD = 0.409, and α = -0.704). By use of formulae (4.36) to (4.38) the sensible heat flux is calculated to be 72.9 W/m^2.

Iteratively we calculate L and u_*: L = -21.7 m and u_* = 0.260 m/s by use of (4.35).

Observing Golder's graph (Figure 4.11) we find that the unstable situation is to be classified as Pasquill C, so the mixing height is set at 1000 m.

For these calculations we have used $c_{p,a}$ = 1000 W/kg K, ρ_a at 293 K = 1.2 kg/m^3 and γ = 0.45 (Table 4.5).

The input, output and intermediate results are summarised in the following table:

Table 4.12   Day-time stability calculation

Input	position		51˚ N -5˚ W
	day		June 20st
	time		9.40 UTC
	cloud cover	N	6/8
	wind speed	$U_a(10)$	4 m/s
	roughness length	z_o	0.01 m
	albedo	e	0.2
	moisture availability	α	1
Intermediate results	solar radiation	H_{rs}	511.9 W/m^2
	Net radiation	H_r	332.7 W/m^2
Output	sensible heat flux	H_o	72.9 W/m^2
	Monin-Obukhov length	L	-21.7 m
	friction velocity	u_*	0.260 m/s
	Pasquill class		C
	mixing height	h_i	1000 m

4.6.2.2   Application of the night-time scheme

For this example the same site as used in Section 4.6.2.1 is selected.
The sky is clear (N = 0); the wind speed is now 4.5 m/s at 10 m height. The temperature is 20 ˚C (293 K) and the wet bulb temperature is 18 ˚C (291 K).
By use of formulae (4.40) to (4.46) we iteratively find the sum of heat fluxes minimised by using a Monin-Obukhov length L = 17.3 m. The friction velocity $u_* = 0.184$ m/s. For this situation we find the following heat fluxes:

net radiation H_r	=		-51.3 W/m^2
sensible heat flux H_o	=	-23.2 W/m^2	
ground heat flux H_g	=	-25.3 W/m^2	
latent heat flux H_l	=	-2.8 W/m^2	
balance:		-51.3	-51.3 W/m^2

This situation can be classified as Pasquill E, see Figure 4.11.
For the mixing height we need to calculate the Coriolis parameter f for conditions in The Netherlands: latitude 51˚. This leads to f = 1.13 . 10^{-4} s^{-1}. By use of Table 4.7 the mixing height is calculated to be 291 m.
Input and output are summarised in Table 4.13.

Table 4.13   Night-time stability calculation

Input	cloud cover	N	0	
	wind speed	$u_a(10)$	4.5	m/s
	roughness length	z_o	0,01	m
	T_a (2 m)		293	K
	T_w (2m)		291	K
Intermediate results	T_*		0.086	K
	T_r (50 m)		294.4	K
	$T_o (z_o)$		291.8	K
	T_s		289.3	K
	H_{ri}		-80.7	W/m^2
	H_r		-51.3	W/m^2
	H_o		-23.2	W/m^2
	H_g		-25.3	W/m^2
	K_s		0.0236	
	H_l		-2.8	W/m^2
Output	sensible heat flux	H_o	-23.2	W/m^2
	Monin-Obukhov length	L	43	m
	friction velocity	u_*	0.223	m/s
	Pasquill class		E	
	mixing height	h_i	291	m

4.6.3   Application of the Gaussian plume model

In this section two examples are discussed. The concentration below an elevated plume and the LEL contour is calculated for a continuous release and the calculation of the time series and explosive content for an instantaneous release of finite dimensions are shown.

4.6.3.1   Calculations of a plume

In this example the meteorological situation is described using Pasquill stability class, with a neutral atmosphere (class D) and the surroundings of the site can be described as "habitated land".

Natural gas (methane) is released continuously at a release rate of 20 kg/s and we want to know the 10-minute averaged concentration at 1.5m height below the plume centerline and the contour defined by the LEL concentration.

The input is summarized in the following table:

Table 4.14   Passive flammable plume example

Chemical name	Methane	
LEL concentration	33353	mg/m^3
Release type	Continuous	
Mass flow rate of the source	20	kg/s
X-coordinate of release	0	M
Y-coordinate of release	0	M
Z-coordinate (height) of release	4	M
Length source in wind (x) direction	0	M
Length of source in crosswind (y) direction	2.5	M
Length source in vertical (z) direction	2.5	M
Ambient temperature	15	°C
Pasquill stability class	D (Neutral)	
Latitude	51	Deg
Wind speed at 10 m height	3.5	m/s
Roughness length description	Habitated land	
Concentration averaging time	600	s

As atmospheric description is done with pasquill stability class and wind speed at 10 m height, Mounin-Obukhov length (0m^{-1}), σ_V (1.18 m/s), σ_W (0.81 m/s) and mixing height (500m) are obtained using formulae 4.47, 4.49 and 4.50 and table 4.7.

Reflection against the mixing height is to be included as in formulae (4.57a to 4.57d)

The resulting concentrations as function of down-wind distance and contour plot are shown in Figures 4.19 and 4.20.

4.114
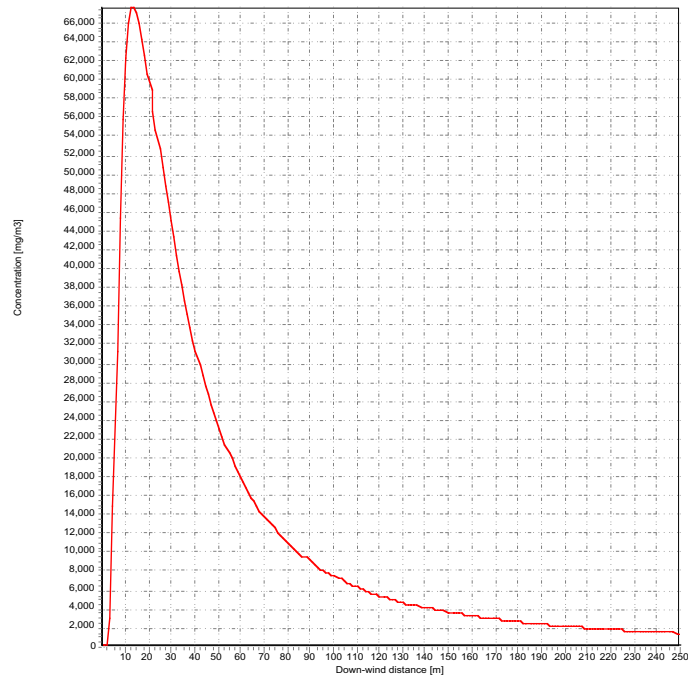
Figure 4.19   Concentration [mg/m³] as function of down-wind distance [m] at
y = 0m and z = 1.5m
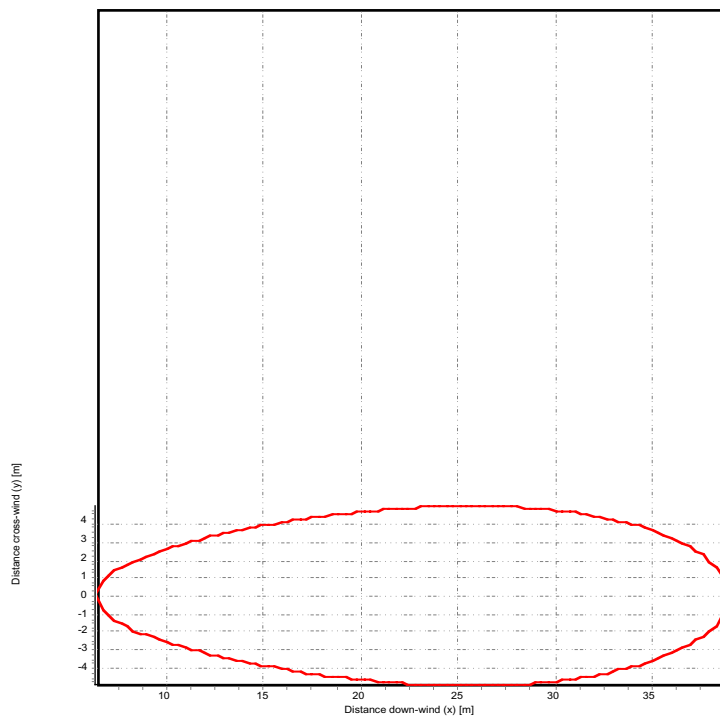
Figure 4.20   Concentration contour plot for LEL [33353 mg/m³] at 1.5m heightt

4.6.3.2 Calculation of explosive mass of an instantaneous puff

For this example use is made of the same meteorological and site conditions as for the previous one: pasquill class D, wind speed of 3.5m/s and habitated land.

The source is assumed to be a cube with sides of 21m, originating from e.g. an initially expanding cloud. This initial cube contains 6000kg of natural gas (methane) at normal ambient conditions (1 atm, 15˚C). For the calculation, the source parameters are represented by $b_{0x} = b_{0y} = b_{0z} = 10.5m$; h = 10.5m.

The input is summarized in Table 4.15

Table 4.15   Input for instantaneous release example

Chemical name	Methane	
Release type	Instantaneous	
Total mass released	6000	Kg
Length source in wind (x) direction	21	M
Length of source in crosswind (y) direction	21	M
Length source in vertical (z) direction	21	M
Ambient temperature	15	°C
Pasquill stability class	D (Neutral)	
Latitude	51	Deg
Wind speed at 10 m height	3.5	m/s
Roughness length description	Habitated land	

The resulting concentration as function of time at a position and explosive mass evolution are shown in Figures 4.21 and 4.22.

The explosive contents are calculated with a numerical 3D integration of one of the halves of the cloud, as this one is symmetric with respect of the xz plane at 0 crosswind distance.
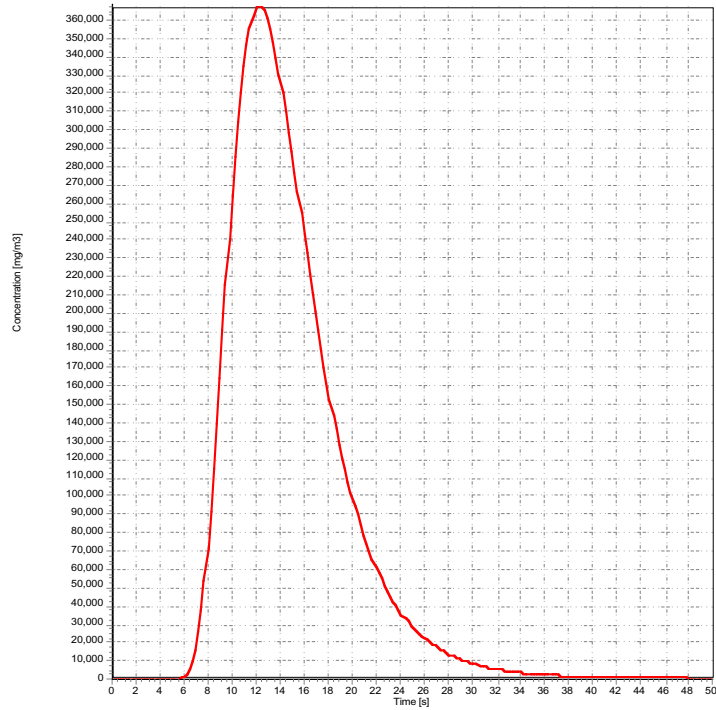
Figure 4.21   Concentration [mg/m^3] time [s] series due to an instantaneous release at (50m, 0m, 1.5m)
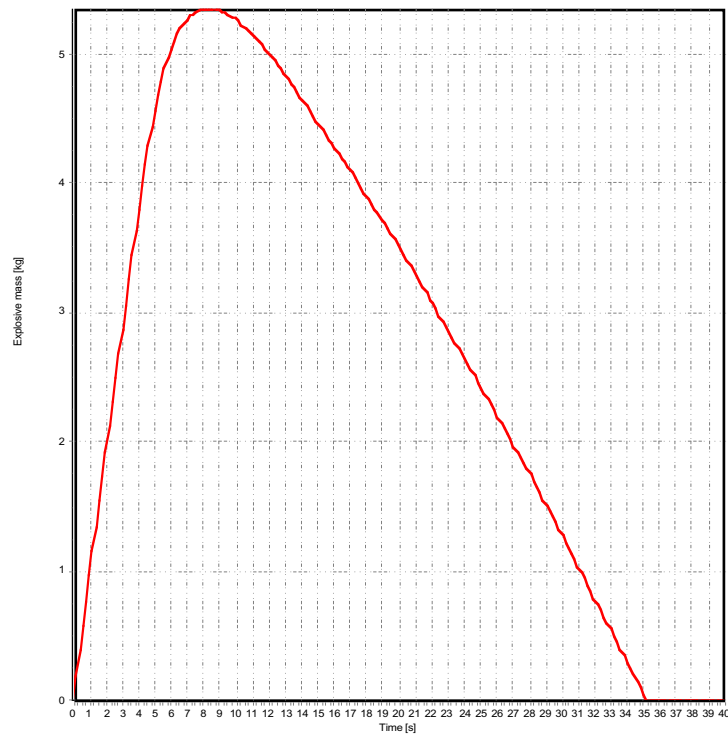
Figure 4.22   Explosive mass [kg] in the surroundings of the release as a function of time [s]

There is a quick dilution of the cloud even in neutral atmospheric conditions due to a relative high wind speed and to the type of land (habitated), which increases the turbulence at ground level; the maximum explosive mass is 5.35kg just 8.35s after the release.

4.6.4 The application of models for jets and plumes

4.6.4.1 The free jet model

The example calculation to illustrate the use of the free jet formalism is a positively buoyant jet in vertical, upward direction, in a homogeneous atmosphere with zero wind speed. A release of this type could occur due to:

− A punctured vessel or a ruptured pipeline, at a small containment overpressure, since the outflow is subsonic.
− A sonic release from a punctured or ruptured container at a high pressure, when the source parameters are derived in the region after the initial expansion to ambient pressure. The procedures which allow to obtain subsonic source parameters from a sonic source configuration are discussed in chapter 2.

The input data for a typical case, a natural gas (NG) jet, are summarised in Table 4.17, although, it must be mentioned that the exit velocity is about one third of the speed of sound. The calculation consists of 3 steps:

− Calculate the Froude number of the source to determine at what range of down-stream distances the jet model can be applied, and where the release should be treated as a plume (4.71-4.72).
− Evaluate the axial concentration decay, and correct for density effects (4.76, 4.78).
− Calculate isocontours and the NG contents in the flammable part (4.81, 4.82).

The numbers in parentheses indicate the relevant equations. The results of the calculations are presented in Figure 4.23. The NG flammable contents is 7.5 kg.
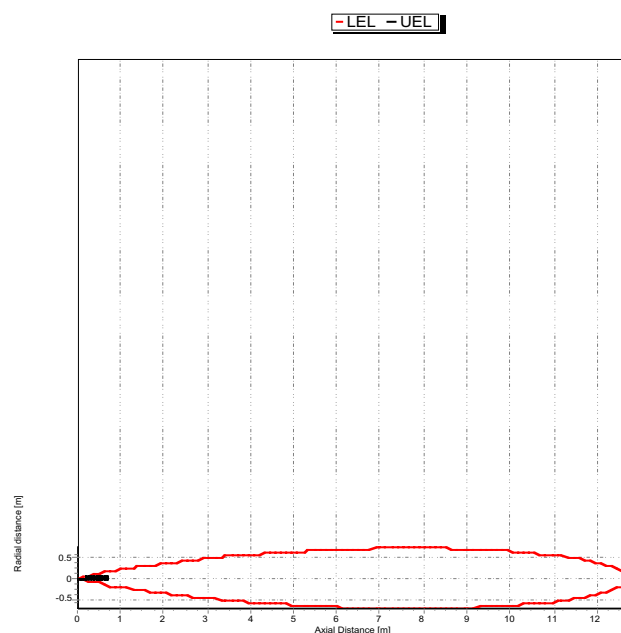
*Figure 4.23   Example of concentration contours (UFL and LFL)
                of a free jet, see Section 4.5.4.1*

Table 4.16   Input data for the free jet model

source diameter	[m]	$2\,b_o$	0.2
exit velocity	[m/s]	u_o	150
NG density	[kg/m^3]	ρ_o	0.78
ambient density	[kg/m^3]	ρ_a	1.21
UFL	[%]	-	15
LFL	[%]	-	5.3

4.6.4.2   The application Briggs plume rise formulae

The Briggs formulae are intended for plume rise predictions of the hot gases, which are emitted from tall stacks. In such cases the temperature difference between the pollutant and the surrounding air is large, and the dispersing plume has a large buoyancy flux factor. Within the framework of the Yellow Book, a possible application of the Briggs formulae is the dispersion of smoke plumes from fires. The example to illustrate the formalism is a vertical upward plume of hot air, which is released from a circular source in a neutral atmosphere.
The input data of the example are summarised in Table 4.18. The calculation consists of 3 steps:
− Calculate the buoyancy flux factor and the distance to final plume rise (4.88-4.91). Note that the plume rise is limited by (4.91).

- Calculate the contributions of initial momentum and buoyancy to the total plume rise (4.88, 4.92).
- Calculate the total plume rise by adding the third powers of the 2 contributions. In general the release of large sources is buoyancy-dominated due to the $x^{2/3}$-dependency, as opposed to the $x^{1/3}$-dependency of the momentum-contribution (4.93).

According to the Briggs formulae the down-wind distance to final plume rise is 348 m. The contributions of initial momentum and buoyancy to the plume rise are, respectively, 30 m and 97 m. So the total plume rise is equal to 98 m.

Table 4.17   Input data for Briggs plume rise formulae

source diameter	[m]	$2\,b_o$	4
exit velocity	[m/s]	u_o	10
density of air (150 ˚C)	[kg/m^3]	ρ_o	0.84
ambient density	[kg/m^3]	ρ_a	1.20
wind velocity	m/s]	u_a	4

4.6.4.3   The integral model of Hoot, Meroney and Peterka

This section contains an example to illustrate the use of the 1-dimensional integral model of Hoot, Meroney and Peterka [HMP, 1973]. The release is a negatively buoyant jet in vertical, upward direction, and the environment is a homogeneous atmosphere. The input data of the example, a release of chlorine at ambient conditions, are summarised in Table 4.19.

Table 4.18   Input data for the HMP model

source diameter	[m]	$2\,b_o$	1
exit velocity	[m/s]	u_o	25
source height	[m]	h_s	20
chlorine density	[kg/m^3]	ρ_o	3.00
ambient density	[kg/m^3]	ρ_a	1.21
wind velocity	m/s]	u_a	4

It can be calculated from the equations in Section 4.5.4 (4.83 and 4.84, using $g = 9.81$ m/s^2) that the plume rise is at its maximum ($\Delta h_r = 11.6$ m) at a down-wind distance x_r of 6.9 m. The peak concentration of chlorine at maximum plume rise is 11.4% (formula 4.86).

The plume starts to descend from the point of maximal plume rise, because the plume material is still heavier than air. The HMP model contains formulae to calculate the down-wind distance of plume touch-down and the approximate concentration at that point (roughly 7% at $x_g = 49$ m), but the user of the Yellow Book is advised to perform the calculations of the plume sinking, touch-down and possiby slumping with the SLAB computer model (see the Section 4.5.5.2), or with the simple

Gaussian plume model. The SLAB model contains the HMP model as a submodel, so the whole calculation, including initial plume rise, can be done with SLAB.

4.6.5 The application of dense gas dispersion models

The SLAB computer model can be applied to dense gas releases from long-duration pool evaporation, from horizontal and vertical two-phase jets, and from short-duration or instantaneous pool releases. The present section contains an example calculation for each of these four source term submodels, in order to illustrate the use of the SLAB model. The examples of the long- and short-duration pool evaporation are also used to illustrate the use of Britter and McQuaid's nomograms.

4.6.5.1 Long-duration pool evaporation

The example to illustrate the pool evaporation source type is a liquid pool of chlorine, caused by a leaking storage drum. The source characteristics were already discussed as an example in Chapter 3. The release disperses as a plume over an area, which is overgrown with low crops. The input data for the SLAB computer model are summarised in Table 4.20. The values for the chlorine source material have been obtained from the table of material properties in the SLAB user manual [Ermak, 1990]. The duration of 200 seconds is sufficient to obtain, for the present range of down-wind distances (1 km), a steady-state solution with the SLAB computer model.

Table 4.19   SLAB input for a long-duration evaporating pool of chlorine

Definition of source term:	evaporating pool, long-duration	IDSPL = 1
Definition of numerical step:	largest step size	NCALC = 1
Molecular weight of source material [kg]:	0.070906 (chlorine)	WMS = 0.070906
Vapor heat capacity of source material at constant pressure [J/kg K]:	498.1 (chlorine)	CPS = 498.1
Boiling point temperature of source gas [K]:	239.1 (chlorine)	TBP = 239.10
Initial liquid mass fraction of source material:	1.0 (liquid)	CMEDO = 1.0
Heat of vaporisation of the source material at the boiling point temperature [J/kg]:	287840.0 (chlorine)	DHE = 287840.
Liquid specific heat of the source material [J/kg K]:	962.35 (chlorine)	CPSL = 962.35
Liquid density of the source material [kg/m^3]:	1574.0 (chlorine)	RHOSL = 1574.0
First saturation constant of source material [-]:	1978.34 (chlorine)	SPB = 1978.34
Second saturation constant of source material [K]:	-27.01 (chlorine)	SPC = -27.01
Temperature of the source material [K]:	239.1	TS = 239.1
Mass flow rate of the source [kg/s]:	5.0	QS = 5.0
Area of the source [m^2]:	100.0	AS = 100.0
Duration of the release, for a finite-duration source [s]:	200.	TSD = 200.
Source mass, for an instantaneous release [kg]:	0	QTIS = 0
Height of the source [m]:	0.	HS = 0
Concentration averaging-time [s]:	60.	TAV = 60
Maximum down-wind distance in the calculation [m]:	1000.	XFFM = 10000
First height where the concentration is calculated [m]:	1.5	ZP(1) = 1.5
Second height where the concentration is calculated (is used only when ZP(1) > 0) [m]:	0.	ZP(2) = 0
Third height where the concentration is calculated (is used only when ZP(1:2) > 0) [m]:	0.	ZP(3) = 0
Fourth height where the concentration is calculated (is used only when ZP(1:3) > 0) [m]:	0.	ZP(4) = 0
Surface roughness height [m]:	0.1 (low crops)	Z0 = 0.1
Measurement height of ambient parameters [m]:	10.	ZA = 10
Ambient wind speed [m/s]:	5.	UA = 5
Temperature of ambient air [K]:	288.15	TA = 288.15
Relative humidity of ambient air [%]:	70.	RH = 70
Stability class:	4 (Pasquill class D)	STAB = 4

An isocontour of the chlorine concentration of 15 g/m^3, corresponding to a molar fraction of 0.5%, at a height of 1.5 m above ground-level (i.e. at inhalation level) at t = 200 s after the start of the evaporation, has been calculated with SLAB, and the results are shown in Figure 4.24.
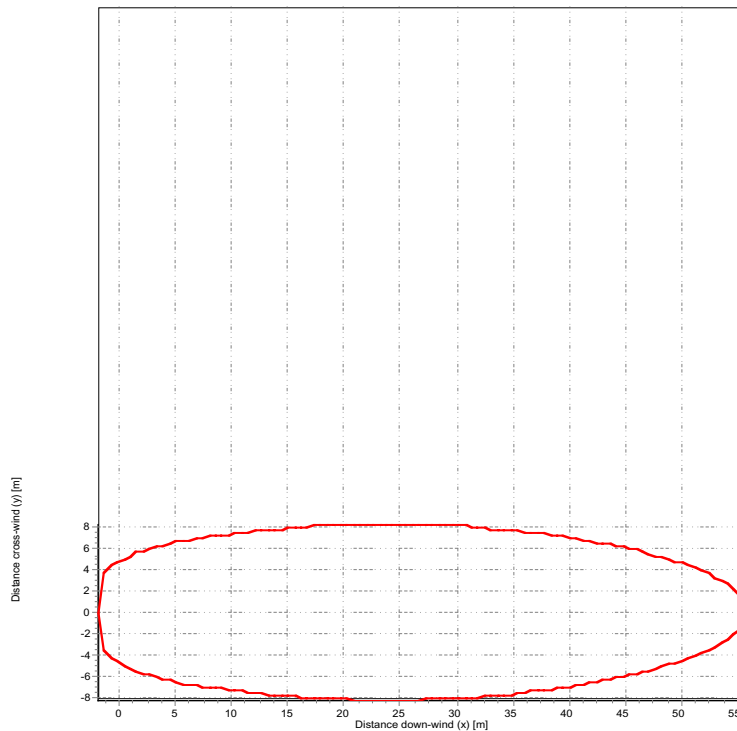
Figure 4.24   Contour of a concentration of 15 g/m³ chlorine due to an evaporating pool

The chlorine concentration was also estimated with the model of Britter and McQuaid. The nomogram for continuous releases should be read with the parameter $((g_o')^2 v_o/u_a^5)^{1/5} = 0.697$ along the horizontal axis, and $x/\sqrt{(v_o/u_a)} = 1.9\ x$ along the vertical axis (see Section 4.5.4.1, the density of chlorine at boiling point is 3.61 kg/m³). The largest distance to c = 0.5% is about 210 m. The difference with SLAB might be due to heat transfer effects.

4.6.5.2   Horizontal jet

The example to illustrate the horizontal jet source type is a jet of propane, of pure vapour, emerging from a ruptured pipeline of a railway tank wagon. The source characteristics were already discussed as an example in Chapter 2. The release disperses as a plume over an area, which is overgrown with low crops. The input data for the SLAB computer model are summarised in Table 4.21. The values for the propane source material have been obtained from the table of material properties in the SLAB user manual.

Table 4.20   SLAB input for a horizontal propane jet

Definition of source term:	horizontal jet	IDSPL = 2
Definition of numerical step:	largest step size	NCALC = 1
Molecular weight of source material [kg/mol]:	0.044097 (propane)	WMS = 0.044097
Vapor heat capacity of source material at constant pressure [J/kg K]:	1678. (propane)	CPS = 1678.
Boiling point temperature of source gas [K]:	231.09 (propane)	TBP = 231.09
Initial liquid mass fraction of source material:	0 (pure vapour)	CMEDO = 0
Heat of vaporisation of the source material at the boiling point temperature [J/kg]:	425740. (propane)	DHE = 425740.
Liquid specific heat of the source material [J/kg K]:	2520. (propane)	CPSL = 2520.
Liquid density of the source material [kg/m^3]:	500.5 (propane)	RHOSL = 500.5
First saturation constant of source material [-]:	1872.46 (propane)	SPB = 1872.46
Second saturation constant of source material [K]:	-25.16 (propane)	SPC = -25.16
Temperature of the source material [K]:	231.1	TS = 231.1
Mass flow rate of the source [kg/s]:	7.85	QS = 7.85
Area of the source [m^2]:	3.14	AS = 3.14
Duration of the release, for a finite-duration source [s]:	1500	TSD = 1500
Source mass, for an instantaneous release [kg]:	0.	QTIS = 0
Height of the source [m]:	3.0	HS = 3
Concentration averaging-time [s]:	0.1	TAV = 0.1
Maximum down-wind distance in the calculation [m]:	500.	XFFM = 1000
First height where the concentration is calculated [m]:	0.	ZP(1) = 0.
Second height where the concentration is calculated (is used only when ZP(1) > 0) [m]:	0.	ZP(2) = 0
Third height where the concentration is calculated (is used only when ZP(1:2) > 0) [m]:	0.	ZP(3) = 0
Fourth height where the concentration is calculated (is used only when ZP(1:3) > 0) [m]:	0.	ZP(4) = 0
Surface roughness height [m]:	0.1 (low crops)	Z0 = 0.1
Measurement height of ambient parameters [m]:	10.	ZA = 10
Ambient wind speed [m/s]:	2.	UA = 2
Temperature of ambient air [K]:	288.15	TA = 288.15
Relative humidity of ambient air [%]:	70.	RH = 70
Stability class:	6 (Pasquill class F)	STAB = 6

The isocontour of the propane concentration of 9.3 g/m^3 (molar fraction 0.5%) at a height of 1.5 m above ground-level at t = 1500 s after the start of the release, has been calculated with SLAB, and the results are shown in Figure 4.25.

4.124
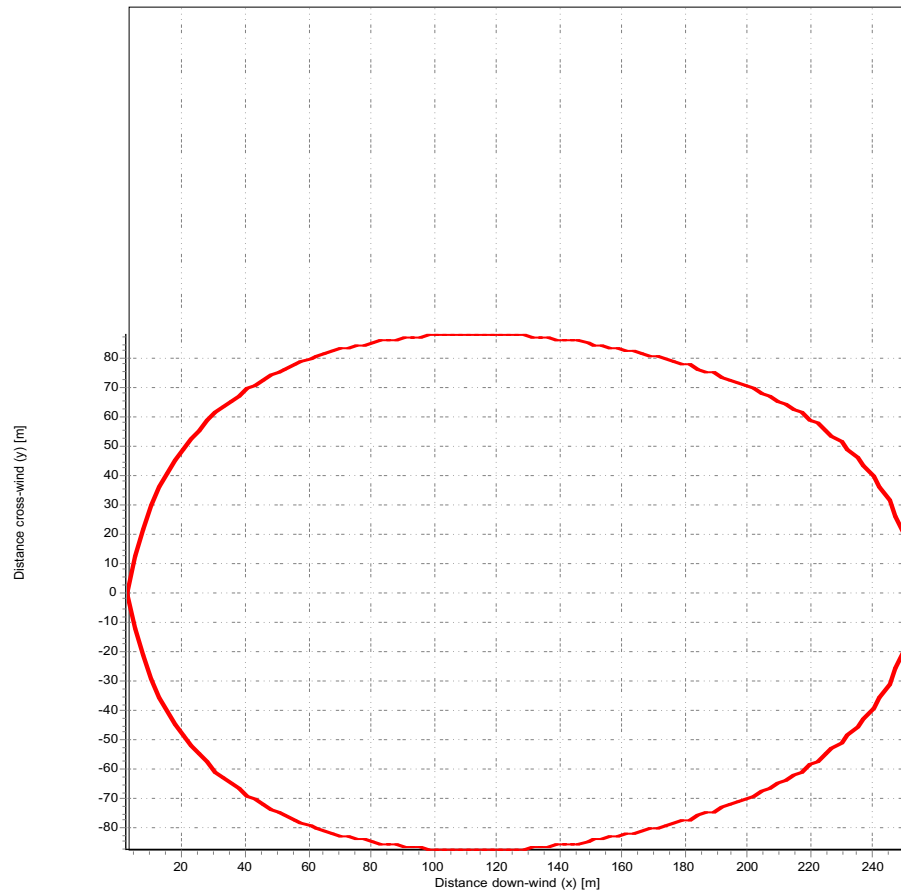
Figure 4.25   Contour of a concentration of 9.3 g/m^3 propane due to a horizontal jet

4.6.5.3   Vertical jet

The example for this case is identical to the example in Section 4.6.3, which illustrates the model of Hoot, Meroney and Peterka. Since SLAB includes the HMP model as a submodel, it gives similar results for the initial plume rise as obtained in Section 4.6.4. It is recalled that the release is a jet of chlorine vapour in vertical, upward direction, and the environment is a homogeneous atmosphere. The input data for the SLAB computer model are summarised in Table 4.22. The input data that describe the physical properties of chlorine are omitted from this table; they are given in Table 4.20. The uniform vertical wind profile in the example is simulated by taking a small surface roughness height in the SLAB model calculation.

Table 4.21   SLAB input for a vertical chlorine jet

Definition of source term:	vertical jet	IDSPL = 3
Definition of numerical step:	largest step size	NCALC = 1
Temperature of the source material [K]:	293.1	TS = 293.1
Mass flow rate of the source [kg/s]:	58.9	QS = 58.9
Area of the source [m^2]:	0.785	AS = 0.785
Duration of the release, for a finite-duration source [s]:	600.	TSD = 600
Source mass, for an instantaneous release [kg]:	0	QTIS = 0
Height of the source [m]:	20.	HS = 20
Concentration averaging-time [s]:	0.1	TAV = 0.1
Maximum down-wind distance in the calculation [m]:	500.	XFFM = 1000
First height where the concentration is calculated [m]:	0.	ZP(1) = 0
Second height where the concentration is calculated (is used only when ZP(1) > 0) [m]:	0.	ZP(2) = 0
Third height where the concentration is calculated (is used only when ZP(1:2) > 0) [m]:	0.	ZP(3) = 0
Fourth height where the concentration is calculated (is used only when ZP(1:3) > 0) [m]:	0.	ZP(4) = 0
Surface roughness height [m]:	0.03 (smooth)	Z0 = 0.03
Measurement height of ambient parameters [m]:	10.	ZA = 10
Ambient wind speed [m/s]:	4.	UA = 4
Temperature of ambient air [K]:	293.1	TA = 293.1
Relative humidity of ambient air [%]:	0.	RH = 0
Stability class:	4 (neutral)	STAB = 4

The output results show that the region of maximal plume rise appears at down-wind distances between 6.1 and 7.6 m, with a final rise of 9.7 m and a cross-wind-averaged concentration of 8.3%. It is noted that these results are slightly different from the calculation in Section 4.6.3, because the surface roughness in SLAB introduces a non-constant vertical wind profile. In the SLAB model simulation, the plume touch-down occurs at a down-wind distance of 43 m, with a cross-wind-averaged concentration of 4.6%. Upon touch-down of the plume, a transition occurs from an airborne plume with a diameter of 8 m to a slumped plume with a height of 2.8 m only. Pressure forces develop during the transition which are converted into horizontal momentum, mainly in the cross-wind direction, resulting in a rapid broadening of the slumped plume. Ultimately differences in velocity between the plume and ambient atmosphere become negligible, and the dispersion process resembles that of a steady plume. Figure 4.26 shows an isocontour of the chlorine concentration (15 g/m^3 corresponding to a molar fraction of 0.5%) at ground level, at t = 600 s after the start of the release calculated with SLAB.

4.126
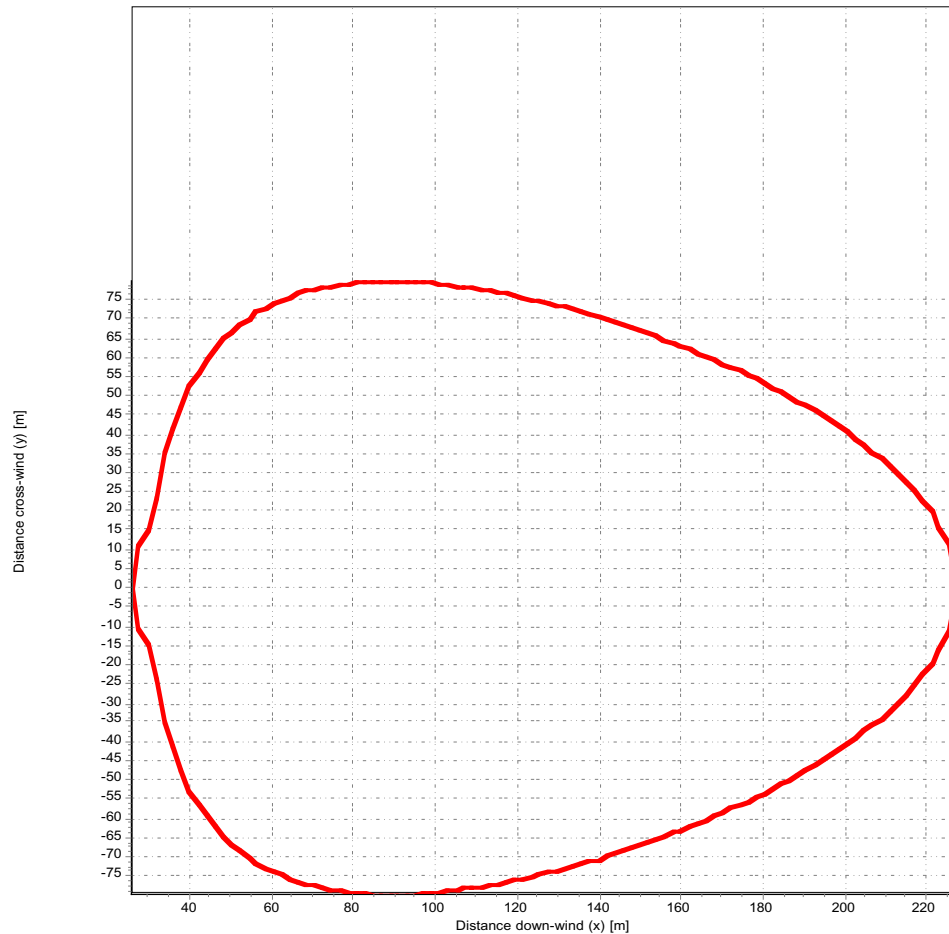
Figure 4.26   Isocontour of 15 g/m³ due to a vertical jet release of chlorine

4.6.5.4   **Short-duration or instantaneous pool release**

The example to illustrate this source type is an instantaneous release of propane, possibly by a BLEVE accident. The release forms a cloud of pure propane gas at ambient conditions. The input data for the SLAB computer model are summarised in Table 4.23, with the exception of the physical properties of propane, which are already given in Table 4.21.

Table 4.22   SLAB input for an instantaneous release

Definition of source term:	instantaneous release	IDSPL = 4
Definition of numerical step:	largest step size	NCALC = 1
Temperature of the source material [K]:	288.15	TS = 230.9
Mass flow rate of the source [kg/s]:	0.	QS = 0.
Area of the source [m^2]:	400.	AS = 652.8
Duration of the release, for a finite-duration source [s]:	0.	TSD = 0
Source mass, for an instantaneous release [kg]:	14.600	QTIS = 14.600
Height of the source [m]:	0.	HS = 9.61
Concentration averaging-time [s]:	3600	TAV = 3600
Maximum down-wind distance in the calculation [m]:	500.	XFFM = 10.000
First height where the concentration is calculated [m]:	0.	ZP(1) = 0
Second height where the concentration is calculated (is used only when ZP(1) > 0) [m]:	0.	ZP(2) = 0
Third height where the concentration is calculated (is used only when ZP(1:2) > 0) [m]:	0.	ZP(3) = 0
Fourth height where the concentration is calculated (is used only when ZP(1:3) > 0) [m]:	0.	ZP(4) = 0
Surface roughness height [m]:	0.03 (grass)	Z0 = 0.03
Measurement height of ambient parameters [m]:	10.	ZA = 10
Ambient wind speed [m/s]:	4.	UA = 4
Temperature of ambient air [K]:	288.15	TA = 288.15
Relative humidity of ambient air [%]:	0.	RH = 0.7
Stability class:	6 (Pasquill class F)	STAB = 6
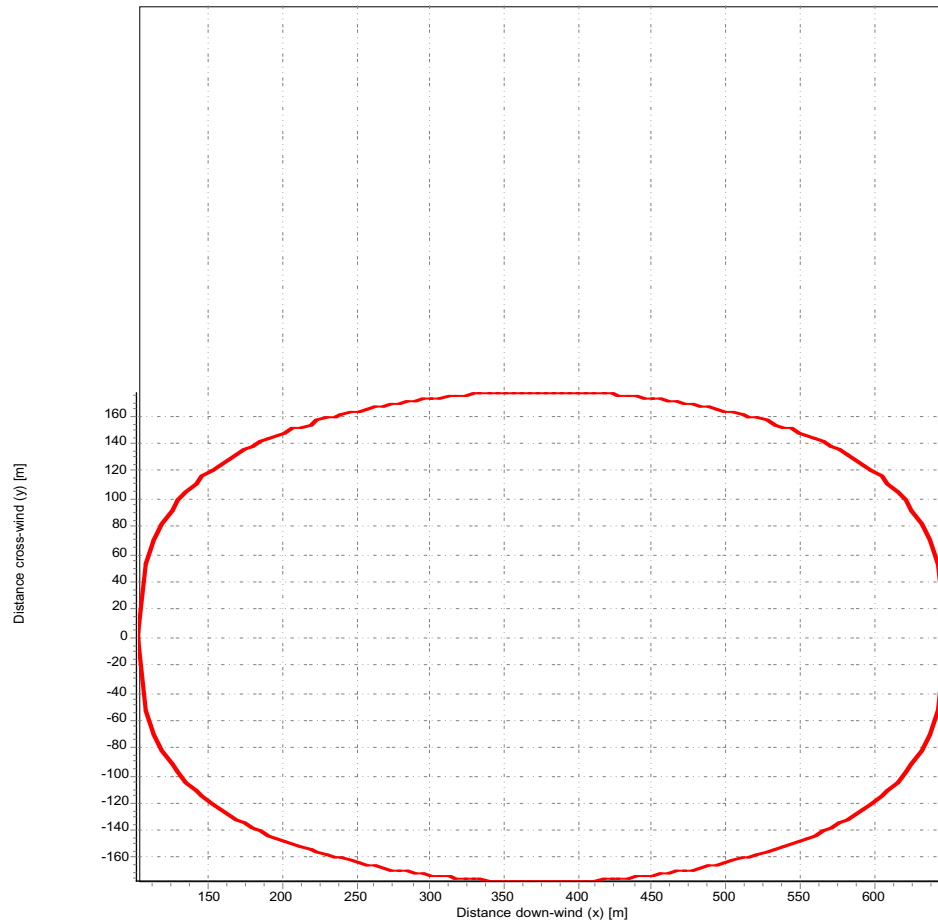
Figure 4.27   Isocontour of 9.3 g/m³ at 240 s after a release of propane.

At 240 s after release the isocontour of 9.3 g/m^3 (molar fraction 0.5%) has been calculated with SLAB at a height of 0 m, and the results are plotted in Figure 4.27.

The largest extent to the 0.5% contour is 913 m at 410 s after release. This distance is also estimated with the model of Britter and McQuaid. The nomogram 4.14 for instantaneous releases should be read with the parameter $\sqrt{(g_o{'}V_o^{1/3}/u_a^2)} = 6.36$ along the horizontal axis, which gives a value for $x/V_o^{1/3}$ of 10 for the 0.05% contour on the horizontal axis, i.e. x = 184 m, which is in reasonable agreement with the result from SLAB, although one should bear in mind that the Britter and McQuaid model leads to the same result irrespective of the atmospheric stability.

4.7   Discussion

4.7.1   Introduction to Section 4.7

This section provides additional information on limitations of selected models, alternative solutions, and gaps of knowledge at present.

4.7.2   Changes in atmospheric conditions

Both the Gaussian plume model as the selected dense gas dispersion model describe dispersion for stationary atmospheric conditions. The models are **not** able to describe phenomena during changes in the boundary layer meteorology, such as passage of fronts, diurnal variation of wind speed and wind direction near coasts, etc. As the meteorological conditions change continuously, the total travel time for which the models are valid needs to be maximised to about 3 hours. The maximum travel distance is thus about 10^4 . u_a m. For larger distances use needs to be made of dedicated long range dispersion models.

4.7.3   Still air

Gaussian plume models are normally excluded for use in still air. By minimising σ_v in formula (4.49) the range of applicability is extended compared to conventional Gaussian plume models. This minimum value of σ_v is probably small, thus conservative from a point of view of maximum concentration.
For continuous releases during very low wind speed for which $u_a < 2$. σ_v, accumulation of plume material at the source will appear (upwind dispersion by wind fluctuations becomes of the same order of magnitude as down-wind convection by wind speed), and the source need to be treated as a series of instantaneous releases where σ_x is calculated (also in the surface layer) by formula (4.61d), and the argument u_a .t in the function F_z (u_a . t, z) is replaced by x for surface layer releases.

4.7.4   Accuracy of the Gaussian plume model

In Figure 4.6 regions of atmospheric conditions are indicated. The use of the Gaussian plume model is well assessed for the 'near neutral upper layer'. As discussed in Section 4.3.2, vertical dispersion in the surface layer, although not strictly Gaussian, is also well understood.
Dispersion in the 'mixed layer' and 'free convection layer' is proven to be not Gaussian in nature. For the 'local scaling layer', 'z-less scaling layer', and 'intermittency layer' no alternative for Gaussian plume modelling has been suggested so far.
The Gaussian plume model will at best have an accuracy of a factor of 2 for the near neutral upper layer [Olesen et al., 1992].

4.7.5 Dispersion over obstacles

Neither the Gaussian plume model, jet and plume models, nor the dense gas models as presented in the previous sections allow predictions to be made which take into account the effects of obstacles. It is not allowed to introduce obstacle effects by increasing the roughness length for the calculation: in effect, the height of the cloud should always exceed (except for very near to the source) the roughness length by an order of magnitude. As discussed in Section 4.2.7, effects of obstacles should be taken into account if the smaller value of height or width of the obstacle(s) is larger than the local cloud height.

Obstacle effects can be treated in a few ways. For passive dispersion some simple models exist for dispersion in the wake of single buildings for which the ratio of width-to-height does not exceed about 5 [Duijm and Webber, 1993]. These models assume a uniform distribution of concentration in the wake of a building. However, differences of a factor 10 are often observed.
Some progress is being made in developing simple models for (dense) gas dispersion over simple obstacle arrays, such as fences perpendicular to the wind, uniformly distributed blocks, and 'street-canyon' like situation [Duijm and Webber, 1993; VDI, 1990].

For situations for which no such specific 'simple' model exists, one needs to use either physical modelling by means of atmospheric boundary-layer wind or water tunnels, or computational fluid dynamic codes (CFD). For passive dispersion in near neutral conditions, for which plume rise or plume descent is not relevant, wind tunnel simulations are as yet unsurpassed for costs and accuracy.
For buoyant or dense releases, additional scaling parameters need to be used in wind tunnels which lead to compromises between viscous effects and density effects. These effects need to be assessed carefully for each case.
CFD-modelling as yet needs approximations with respect to the representation of turbulence. Here again these approximations should be assessed carefully for each case, the situations with stable stratification (either atmospheric or from the dense gas cloud) being the most critical.

4.7.6 Concentration fluctuations

The selected models account for different averaging-times and 'instantaneous' lateral plume widths. These plume widths need to be considered as so-called ensemble-averaged width and these calculations do not exclude fluctuations of plume width and concentrations to occur.
The last decade much attention has been paid to develop general models that describe concentration fluctuations (or at least statistics of concentration fluctuations) in passive and dense gas clouds and plumes.
As yet no generalised model for concentration fluctuations is available. There is evidence that quantities of instantaneous dense and passive releases, such as dose and maximum concentration, are log-normally distributed over the ensemble of realisations. For continuous releases less definite conclusions with respect to distribution functions can be given, partly because here intermittency masks part of the observations.

4.7.7   Removal processes

In Sections 4.2.8 and 4.2.9 some attention is paid to chemical reactions and deposition, respectively. The selected models do not account for these processes. For slow chemical reactions and wet deposition, one may write a first order decrease of material in the plume:

$$\frac{d\,q\,(x)}{dx} = -\,C\,q\,(x) \qquad\qquad\qquad (kg/(m{\cdot}s))\Diamond \qquad (4.175)$$

where q (x) is the source strength to be used in the (Gaussian) plume model at distance x, and C some constant, depending on the chemical reaction or the wash-out rate.

For dry deposition at the ground one may calculate the total flux by integration of (4.5) over the plume width and decrease q (x) in the plume model by this loss of material (source depletion model). However, dry deposition will affect the concentration near the ground, thus changing the vertical distribution of material. A model to describe this phenomenon was developed by Rao [1981]. Although not strictly correct, it provides sufficiently accurate predictions for practical values of deposition velocities and wind speeds [Bakkum, 1993].

4.8 Literature

Bakkum, E.A. (1993),
Een numeriek algoritme voor de berekening van droge depositie en uitwassing van emissies in de atmosfeer (in Dutch),
TNO-IMET report 93-211..

Beals G.A., (1971)
Guide to local diffusion of air pollutants,
tech. report 214 Weather Services USAF, NTIS, AD 726984.

Beljaars, A.C.M., A.A.M. Holtslag (1990),
A software library for the calculation of surface fluxes over land and sea,
Environmental software, **5**, pp 60-68.

Bianconi, R., M. Tamponi (1993),
A mathematical model of diffusion from a steady source of short-duration in a finite mixing layer,
Atmospheric Environment **27A**, pp 781-792,

Blackmore D.R. et al. (1982),
Heavy gas dispersion models,
Journal of Hazardous Materials 6 (1982) 107.

Briggs, G.A. (1969),
Plume rise,
U.S. Atomic Energy Commission Report TID-25075.

Britter, R.E. and McQuaid, J. (1988),
Workshop on the dispersion of dense gases,
HSE Contract Research Report No 17.

A.J. Byrne, S.J. Jones, S.C. Rutherford, G.A. Tickle, D.M. Webber (1992),
Description of ambient atmospheric conditions for the computer code DRIFT, SRD/HSE R553, SRD, Culcheth, U.K.

Chatwin P.C. (1968),
The dispersion of a puff of passive contaminant in the constant stress region,
Quart. J. R. Met. Soc., 94, pp. 350-360.

Chen, C.J. and Rodi, W. (1980),
Vertical turbulent buoyant jets,
Pergamon Press, Oxford.

Colenbrander, G.W. (1980),
A mathematical model for the transient behaviour of dense vapour clouds,
3rd Int. Symp. on Loss Prevention and Safety Promotion in the Process Industry (Basle).

Commissie TNO voor het onderzoek ten dienste van het Milieubeheer (1976)
Modellen voor de berekening van de Verspreiding van Luchtverontreiniging,
Staatsuitgeverij 1976.

Cox, R.A., and Carpenter, R.J. (1979),
Further developments of a dense vapour cloud dispersion model for hazard analysis,
Proceedings of the symposium on heavy gas dispersion, Frankfurt.

Davidson, G.A. (1989),
Simultaneous trajectory and dilution predictions from
a simple integral plume model,
Atmospheric Environment 23, 341.

Deaves, D.M. (1992),
Dense gas dispersion modelling,
Journal of loss prevention in the process industry 4 (1992) 219.

Drivas P.J. and Shair F.H. (1974),
Dispersion of an instantaneous crosswind line source of tracer released from an
Urban highway,
Atm. Env. 8, pp. 475-485.

Duijm, N.J., Webber, D.M (1993 or 1994),
Dispersion in the presence of buildings, Problem Clouds - II, April 15/16, 1993,
Amsterdam, The Netherlands and accepted for publication in J. of Los Prevention in
the Process Industries, 1993 or 1994.

Eidsvik, K.J. (1980),
A model for heavy gas dispersion in the atmosphere,
Atmospheric Environment 14, 769.

Erbrink, J.J. (1991),
A practical model for the calculation of σ_y and σ_z for use in an on-line Gaussian
dispersion model for tall stacks, based on wind fluctuations,
Atm. Env., **25A**, 2, pp 277-283.

Ermak, D.L. et al. (1982),
A comparison of dense gas dispersion model simulations with Burro series LNG spill
test results,
Journal of Hazardous Materials 6 (1982) 129.

Ermak, D.L., Rodean, H.C., Lange, R. and Chan, S.T. (1988),
A survey of denser-than-air atmospheric dispersion models,
LLNL Report under contract W-7405-ENG-48.

Ermak, D.L. (1990),
User's manual for SLAB: an atmospheric dispersion model for denser-than-air
releases, Lawrence Livermore National Laboratory, California 94550.

Fryer, L.S. and Kaiser, G.D. (1979),
DENZ, a computer program for the calculation of the dispersion of dense toxic or
explosive gases in the atmosphere,
Report UKAEA SRD R/52.

Golder, D. (1972),
Relations among stability parameters in the surface layer,
Boundary-Layer Met., **3**, pp 47-58.

Gryning, S.E., A.A.M. Holtslag, J.S. Irwin, B. Sivertsen (1987),
Applied Dispersion modelling based on meteorological scaling parameters,
Atmospheric Environment **21**/1, pp 79-89.

Guinnup, D. (1992),
Non-buoyant Puff and Plume Dispersion Modelling Issues,
Plant/Operations Progress **11**/1, pp 12-15.

Hanna S.R., Briggs G.A. en Hosker Jr. R.P. (1982),
Handbook of Atmospheric Diffusion,
DOE/TIC-11223 (DE 82002045), 1982.

Hanna, S.R. and Drivas, P.J. (1987),
Guidelines for the use of vapor cloud dispersion models,
CCPS American Institute of Chemical Engineers New York.

Hanna, S.R., Strimaitis, D.G., and Chang, J.C. (1991),
Evaluation of commonly-used hazardous gas dispersion models,
Final Report under contract FO8635-89-C-0136,
Sigma Research Corporation, Concord.

Hanna, S.R. (1990),
Lateral Dispersion in Light Wind Stable Conditions, Proceedings of the EURASAP
Meeting and GNFAO/CNR Workshop on Atmospheric Dispersion in Low Wind
speeds and Foggy Conditions, Torino, Sept. 5-7, 1989, ed. D. Anfossi &
A. Longhetto, Il Nuova Cimento della società italiana di fisica vol. 13 C, num. 6,
pp. 889-894.

Hanna, S.R. and Chang, J.C. (1992),
Evaluation of commonly-used hazardous gas dispersion models,
Addition of the HGSYSTEM model,
Final Report A232-300, Sigma Research Corporation, Concord.

Havens, J. (1989),
DEnse GAs DISpersion version 2.1.

Havens, J. and Spicer, T. (1990),
TECJET: An atmospheric dispersion model,
Risk Analysis 10 (1990) 459.

Havens, J. (1992),
Review of dense gas dispersion field experiments,
Journal of loss prevention in the process industry 1 (1992) 28.

Holtslag, A.A.M. (1984),
Estimates of diabatic wind speed profiles from near-surface weather observations,
Boundary-Layer Meteorology **29**, pp 225-250.

Holtslag, A.A.M., and F.T.M. Nieuwstadt (1986),
Scaling the atmospheric boundary layer,
Boundary-Layer Meteorology **36**, pp 201-209.

Holtslag, A.A.M. (1987),
Surface fluxes and boundary layer scaling - model and applications,
KNMI WR-no 87-2, De Bilt.

Holtslag, A.A.M., and H.A.R. de Bruin (1987),
Applied modelling of the night-time surface energy balance over land, submitted to
J. of Climate and Applied Meteor.

Hoot, T.G., Meroney, R.N. and Peterka, J.A. (1973),
Wind tunnel tests of negatively buoyant plumes,
NTIS Report PB-231-590.

Hsu, S.A. (1992),
An overwater stability criterion for the offshore and coastal dispersion model
(research note), Boundary-Layer Met., **60**, pp 397-402.

Jagger, S.F. (1983),
Development of CRUNCH: a dispersion model for continuous releases of
denser-than-air vapour into the atmosphere,
Report UKAEA SRD R 229.

Jones, S.J., Mercer, A., Tickle, G.A., Webber, D.M. and Wren, T. (1991),
Initial verification and validation of DRIFT,
Report SRD/HSE/R580.

Kaiser, G.D. and Walker, B.C. (1978),
Releases of anhydrous ammonia from pressurised containers and the importance of
denser than air mixtures,
Atmospheric Environment 12, 2289.

KNMI (1974),
Luchtverontreiniging en Weer,
Staatsuitgeverij, The Hague.

KNMI (1979),
Luchtverontreiniging en weer, 2e druk,
Staatsuitgeverij, 's Gravenhage.

Li, X., Leijdens, H. and Ooms, G. (1986),
An experimental verification of a theoretical model for the dispersion of a stack plume heavier than air,
Atmospheric Environment 20.

McFarlane, K., Prothero, A., Puttock, J.S., Roberts, P.T. and Witlox, H.W.M. (1990),
Development and validation of atmospheric dispersion models for ideal gases and hydrogen fluoride,
Technical Reference Manual Shell Reseach Report TNER.90.015.

Mercer, A. et al. (1993),
Comparison of heavy gas dispersion models for instantaneous releases,
to be published in Journal of Hazardous Materials (1993).

Olesen, H.R., T. Mikkelsen, eds (1992),
Proceedings of the workshop Objectives for Next Generation of Practical Short-Range Atmospheric Dispersion Models,
NERI, Roskilde, Denmark.

Ooms, G. (1972),
A new method for the calculation of the plume path of gases emitted by a stack,
Atmospheric Environment 6, 899.

Ooms, G. and Duijm, N.J. (1984),
Dispersion of a stack plume heavier than air,
IUTAM Symposium, Springer Verlag.

Panofsky, H.A., and J.A. Dutton (1984),
Atmospheric Turbulence, John Wiley & Sons, New York.

Pasquill F. and Smith F.B., (1983)
Atmospheric Diffusion, Ellis Horwood Ltd., Chichester.

Pasquill, F. and F.B. Smith (1983),
Atmospheric Diffusion, 3rd ed., Ellis Horwood, Chichester.

Peterson, R.L. (1978),
Plume rise and dispersion for varying ambient turbulence, thermal stratification and stack exit conditions,
PhD Thesis, Colorado State University.

Press, W.H. et al. (1986),
Numerical Recipes – The Art of Scientific Computing, Cambridge University Press, Cambridge.

Puttock, J.S. et al. (1991),
Dispersion models and hydrogen fluoride predictions,
Journal of loss prevention in the process industry 4 (1991) 16.

Rao, K.S. (1981),
Analytical solutions of a gradient-transfer model for plume deposition and
sedimentation,
NOAA technical memorandum ERL-ARL-109, NTIS, U.S. Dept. of Commerce.
PB 82-215153.

Radian Corporation (1988),
Description of the Radian complex hazardous air release model.

Saffman P.G. (1962),
The effect of wind shear on horizontal spread from an instantaneous ground source,
Quart. J. R. Met. Soc., 88, pp. 382.

Seinfeld, J.H. (1986),
Atmospheric Chemistry and Physis of Air Pollution,
John Wiley & Sons, New York.

Slade D.H. (1968),
Meteorology and Atomic Energy, U.S. Atomic Energy Commission.

Singer, I.A., Smith, M.E. (1953),
J. Meteorol., **10**, 2, pp 92-114.

Stern, A.C., R.W. Boubel, D.B. Turner, D.L. Fox (1984),
Fundamentals of Air Pollution,
2nd ed., Academic Press, London.

Stull, R.B. (1988),
An Introduction to Boundary Layer Meteorology,
Atmospheric Sciences Library, Kluwer Academic Publishers, Dordrecht.

Tyldesley J.B. and Wallington C.E. (1965),
The effect of wind shear and vertical diffusion on horizontal dispersion,
Quart. J. R. Met. Soc., 91, pp. 158-174 (1965).

Ulden, A.P. van, and A.A.M. Holtslag (1985),
Estimation of Atmospheric Boundary Layer Parameters for Diffusion Applications,
Journal of Climate and Applied Meteorology, **24**, pp 1196-1207.

Ulden, A.P. van (1991),
A surface-layer similarity model for the dispersion of a skewed passive puff near the
ground, Atmospheric Environment **26A**/4, pp 681-692.

VDI Richtlinie 3783 Blatt 2 (1990),
Ausbreitung von storfallbedingten Freisetzungen schwerer
Gase - Sicherheitsanalyse,
Beuth Verlag GmbH, Berlin.

Webber, D.M. et al. (1992),
A model of a dispersing dense gas cloud, and the
computer implementation DRIFT,
UKAEA Report SRD/HSE R586-587.

Werkgroep Verspreiding Luchtverontreiniging (1984),
Parameters in the long-term model of
air pollution Dispersion - New recommendations,
TNO-SCMO, P.O. Box 186, 600 AD Delft, The Netherlands.

Wheatley, C.J. and Webber, D.M. (1984),
Aspects of the dispersion of denser-than-air vapours relevant to
gas cloud explosions,
Final Report SR/007/80/UK/H UK Atomic Energy Authority.

Witlox, H.W.M. et al. (1990),
HGSYSTEM user/technical manuals,
References to chapter 4, Vapour Cloud Dispersion.

Zeman, O. (1982),
The dynamics and modelling of heavier-than-air cold gas releases,
Atmospheric Environment 16, 741.

Appendix 4.1 A method for estimating the solar elevation

A4.1 The Julian day number

The Julian day number, J_n, can be defined as the number of days elapsed since the first of January.

For a date of the form DD-MM-YYYY, YYYY is first examined to see if it is a leap year.

The following table is used for the calculation

MM	1	2	3	4	5	6	7	8	9	10	11	12
	Jan	Feb	Mar	Apr	May	Jun	Jul	Aug	Sep	Oct	Nov	Dec
X	031	059	090	120	151	181	212	243	273	304	334	365

$$J_n = DD + X_{MM-1} \tag{a1.1}$$

in non-leap years, and up to February in all years, and

$$J_n = DD + X_{MM-1} + 1 \tag{a1.2}$$

in leap years after February.

A4.2 The solar elevation

In this section, all arguments of goniometrical functions are in radians. From J_n the solar longitude (SL) can be evaluated by,

$$SL = 4.871 + 0.0175 \, J_n + 0.033 \sin(0.0175 \, J_n) \text{ (rad)} \tag{a1.3}$$

where SL is in radians. The solar declination (SD) follows from

$$SD = \text{arc} \sin(0.398 \sin(SL)) \text{ (rad)} \tag{a1.4}$$

These three quantities are used to compute the smallest angle through which the earth must turn to bring the meridian of the given location directly under the sun

$$\alpha = \psi_w \cdot \frac{\pi}{180} + 0.043 \sin(2 \cdot SL) - 0.033 \sin(0.0175 J_n) + \pi \cdot (t_u/12 - 1) \tag{a1.5}$$

where ψ_w is the western longitude (˚W) of the location and t_u is the universal time in hours.

the solar elevation, χ, is given in radians by:

$$\chi = \arcsin\left\{\sin(\text{SD}) \cdot \sin\left(\varphi\frac{\pi}{180}\right) + \cos(\text{SD}) \cdot \cos\left(\varphi\frac{\pi}{180}\right) \cdot \cos(\alpha)\right\} \qquad (a1.6)$$

where φ is the latitude of the location (˚N). This scheme provides an estimate for χ with an accuracy of within 0.05 rad.

Chapter 5
Vapour cloud explosions
W.P.M. Mercx, A.C. van den Berg

Modifications to Chapter 5 (Vapour cloud explosions) with respect to the first print (1997)

Numerous modifications were made concerning typographical errors. A list is given below for the pages on which errors have been corrected.

At page 5.24: the declaration of variable EmTNT (TNT blast energy) is corrected, and values currently in use for this variable are added.

In the calculation examples of the application of selected methods: calculation examples
A lot of numbers are refined, and values are more accurately read from plots and figures. The values of Tables 5.6, 5.7A, 5.7B have been replaced by refined values.

List of symbols Chapter 5

$A_{f,rainout}$	Jet cross-section after flashing and rainout (5.10)	m^2
a_a	Speed of sound in ambient air (5.4)	$m \cdot s^{-1}$
$b_{f,rainout}$	Jet radius after flashing and rainout (5.10)	m
b_i	Dimension of a box	m
c_p	Specific heat at constant pressure	$J \cdot kg^{-1} \cdot K^{-1}$
c_s	Stoichiometric concentration (5.7)	%
D_1	Smallest dimension of obstacle perpendicular to flame propagation direction	m
D_2	Dimension of obstacle parallel to flame propagation direction	m
d_c	Diameter of a cylinder	m
d_s	Diameter of a sphere	m
E	Total combustion energy (5.2)	J
E_m	Combustion energy per unit mass (5.1)	$J \cdot kg^{-1}$
E_{mf}	Combustion energy of fuel per unit mass (5.1)	$J \cdot kg^{-1}$
E_{mTNT}	Combustion energy of TNT per unit mass (5.1)	$J \cdot kg^{-1}$
E_v	Combustion energy per unit volume (5.9)	$J \cdot m^3$
i_s	Positive side-on impulse of blast-wave (5.6)	$Pa \cdot s$
P_{sc}	Overpressure in vapour cloud	Pa
P_s	Peak side-on overpressure of blast-wave (5.3)	Pa
P_s'	Scaled peak side-on overpressure of blast-wave (5.3)	-
p_a	Ambient pressure (5.2)	Pa
p_{dyn}	Peak dynamic pressure in blast-wave (5.5)	Pa
p_{dyn}'	Scaled dynamic pressure in blast-wave (5.5)	-
p_{CJ}	'Chapman-Jouguet' peak detonation pressure	Pa
p_{vN}	'Von Neumann' peak detonation pressure	Pa
Q_{ex}	Mass quantity of flammable part of the cloud (5.7)	kg
Q_f	Mass of fuel involved (5.1)	kg
Q_{TNT}	Equivalent mass of TNT (5.1)	kg
r	Distance to explosion centre (5.2)	m
r'	Scaled distance (5.2)	-
r_o	Radius of flammable cloud (5.9)	m
r_o'	Scaled radius of flammable cloud	-
T_e	Temperature of combustion products	K
T_i	Temperature at start of combustion	K
T_a	Ambient temperature	K
t_p	Positive phase duration of blast-wave (5.4)	s
t_p'	Scaled positive phase duration of blast-wave (5.4)	-
V	Volume	m^3
V_c	Volume of vapour cloud at stoichiometric concentration (5.8)	m^3
V_{gr}	Volume of vapour within obstructed region (5.8)	m^3
V_o	Volume of unobstructed part of the cloud (5.8)	m^3
V_r	Free volume of the obstructed region	m^3
α_e	TNT equivalency based on energy (5.1)	-
α_m	TNT equivalency based on mass (5.1)	-
ρ	Density (5.7)	kg/m^3

Note: the numbers between brackets refer to equations.

Glossary of terms

blast (wave)	a rapidly propagating pressure or shock-wave in atmosphere with high pressure, high density and high particle velocity
burning velocity	the velocity of a propagating flame, measured relative to the unburnt gases immediately ahead of the flame front
deflagration	a propagating chemical reaction of a substance in which the propagation of the reaction front is determined by conduction and molecular diffusion
detonation	a propagating chemical reaction of a substance in which the propagation of the reaction front is determined by compression beyond the auto-ignition temperature
explosion	a sudden release of energy that causes a blast
flammable limits	the upper and lower concentration limit of combustible material in a homogeneous mixture with a gaseous oxidiser that will propagate a flame
impulse	a measure used to quantify the consequences of a short duration pressure pulse. It is calculated by integration of the pressure-time history
laminar flame propagation	propagation of a flame in a laminar flow, characterised by a very thin flamefront with a smooth surface that can be curved
pressure wave	rapidly propagating wave in atmosphere causing a gradual change in gas-dynamic-state: high density, pressure and particle velocity
separation distance	the minimal distance between two congested areas at which the areas can be considered as two separate explosion sources
shock-wave	rapidly propagating wave in atmosphere causing a instantaneous change in gas-dynamic-state: high density, pressure and particle velocity
side-on overpressure	the pressure experienced by an object as a blast-wave passes by

stoichiometric ratio	the ratio characterised by, or being, a proportion of chemicals exactly right for a combustion with no excess of flammable material or oxygen
TNT-equivalence	the amount of TNT (trinitrotoluene) that would produce observed damage levels similar to those of the explosion under consideration
turbulent flame propagation	propagation of a flame in a turbulent flow, characterised by a rough combustion zone rather than by a thin and smooth flame front
vapour cloud explosion	the explosion resulting from an ignition of a premixed cloud of flammable vapour, gas or spray with air, in which flames accelerate to sufficiently high velocities to produce significant overpressure
volume blockage fraction	the ratio of the volume of the obstructed area occupied by obstacles to the total volume of the obstructed area itself

Table of contents Chapter 5

5   Vapour cloud explosions

5.1   Introduction

One of the physical phenomena that may occur after the accidental release of dangerous goods is a vapour cloud explosion. A vapour cloud can be created by either the release of a gas from a containment or by the evaporation of a liquid that was released from a containment. A 'Source Term' calculation, in most cases followed by a 'Dispersion' calculation, will be performed usually prior to a 'Vapour Cloud Explosion' calculation.

Not all gases or vapours are flammable and if they are, they are not flammable under all circumstances. If however, the vapour cloud is flammable, or part of the cloud is flammable, a vapour cloud explosion may occur. At least, the cloud will burn after it is ignited. Other conditions described in this chapter are required to turn the burn of a cloud into a devastating explosion.

The phenomenon of a 'Vapour Cloud Explosion' (VCE) is described in this chapter. An 'effect' model for the determination of the 'blast' resulting from a VCE is selected, described and elucidated with some examples. Results of this vapour cloud explosion blast model can be used as input to subsequent consequence models for the determination of damage to structures and injury to people. These models can be found in CPR-16E [1990].

The phenomenon of a vapour cloud explosion is presented in section 5.2. There, also basic features of vapour cloud explosions are explained.
Knowledge of the basic features and the explosion phenomenon is necessary to select a model for blast prediction.

Section 5.3 describes the existing models for vapour cloud explosion blast prediction and a discussion is presented regarding advantages and disadvantages of groups of models. After having motivated the preference for a specific group of models, one model out of this group is selected in section 5.4.

The model is presented by discussing the underlying physical features in section 5.5. There, also model deficiencies and available guidance to cover these deficiencies are discussed. Recommendations are made to cover deficiencies in a safe and conservative approach. Two procedures are presented, one for the determination of obstructed regions and one for the application of the Multi-Energy method.

The concept of the Multi-Energy method is generally accepted as the practical model representing best the mechanics of an unconfined vapour cloud explosion. The application in practice though is hampered due to the lack of appropriate guidance for application as some aspects are still not yet fully described due to the lack of experimental data.
Current internationally performed research aims at, amongst other things, improving practical prediction models and derivation of guidance for application. Additional information will become available from the EU sponsored projects MERGE (Modelling and Experimental Research into Gas Explosions) and EMERGE

(Extended MERGE). The project GAME (Guidance for the Application of the Multi-Energy method) and its successor GAMES (GAME Second phase) will provide valuable information for estimating the class of the source strength. Additional research should however be initiated to obtain knowledge on separation distances between obstructed regions.

As this information is not available presently it is advised to choose a source strength class number 10. The result will be conservative as the class number is lower in almost all cases. The result will be better in comparison with the TNT equivalency method as the basic mechanism of a gas explosion is recognised, to wit: pressure is generated only in those areas where the flame is accelerated by turbulence generated by the interaction of the expansion flow ahead of the flame and obstacles present in the flame path.

Examples for becoming familiarised with the procedures are presented in section 5.6.

The last section deals with interfacing to other models (section 5.7).

5.2 The phenomenon of a vapour cloud explosion

5.2.1 Introduction to vapour cloud explosions

Major industrial accidents like the explosion at the caprolactam plant of Nypro Ltd in Flixborough (United Kingdom) on June 1, 1974 and the explosion at the naphtha cracking unit of DSM in Beek (The Netherlands) on September 15, 1975 demonstrate the enormous impact VCE's can have.

These two examples are often quoted to give an impression of a typical VCE as they are well-known and well-documented. Although these two major accidents occurred several years ago, this does not imply that VCE's are ruled out due to the enormous amount of safety precautions that have been developed and implemented since then. More recent accidents include Celanese (1987), Shell (1988), Phillips (1989) and Exxon (1989) in the USA and Total (1991) near Marseille in France. The last causing window pane breakage at a distance of more than four kilometres.

All VCE's result from the ignition of a flammable cloud which was formed due to the release of a large quantity of flammable vaporising liquid or gas from a storage tank, a process or transport vessel, or a pipeline.

However, not all of these releases will necessarily lead to a VCE.

Generally speaking, several conditions need to be present for a vapour cloud explosion with damaging overpressure to occur.

First, the released material must be flammable and at suitable conditions of pressure or temperature. Examples of suitable materials are liquefied gases under pressure (propane, butane), ordinary flammable liquids particularly at high temperatures and/ or pressures (cyclohexane, naphtha), and non-liquefied flammable gases (methane, ethene, acetylene).

Secondly, a cloud must be formed prior to ignition (dispersion phase). Should ignition occur instantly at the release, a flare - in itself causing extensive localised heat radiation damage - will occur. However, significant blast pressures causing widespread damage are not likely to occur. Should the cloud be allowed to form over a period of time within a process area and subsequently ignite, blast pressures propagating away from the cloud centre can result in extensive damage over a wide area. Ignition delays from one to five minutes are considered the most probable of generating a vapour cloud explosion, although major incidents with ignition delays as low as a few seconds and higher than 30 minutes have been documented.

Thirdly, a part of the cloud must be within the flammable range of the material. A vapour cloud will generally have three regions - a rich region near the point of release, a lean region at the edge of the cloud and a region in between that is within the flammable range. The percentage of the vapour cloud in each region varies, depending on a great deal of different factors, including type and amount of the material released, pressure at release, size of release opening (all of them source terms), degree of confinement of the cloud, and wind, humidity and other environmental effects [Hanna and Drivas, 1987].

Fourthly, the blast effects produced by vapour cloud explosions are determined by the speed of flame propagation. The faster the flame propagates through the flammable

cloud, the higher the overpressure in the cloud will be, which will increase the blast effects outside the cloud. This implies that the mode of flame propagation is very important. In general, the mode of flame propagation will be a deflagration. Under extraordinary conditions a detonation might occur.
Section 5.2.2 discusses the modes of combustion in more detail.

When ignition occurs in a flammable cloud at rest, the flame will start to propagate away from the ignition point. The combustion products expand causing flow ahead of the flame. Initially this flow will be laminar. Under laminar or near-laminar conditions the flame speeds for normal hydrocarbons are in the order of 5 to 30 m/s which is too low to produce any significant blast overpressure. Under these conditions, that is, should the combustion rate not be intensified, the vapour cloud will simply burn and the event is described as a large flash fire.

Therefore, an additional condition is necessary for vapour cloud explosions with pressure development: the presence of turbulence. Research testing has shown that turbulence will significantly enhance the combustion rate in deflagrations.

Turbulence may arise in a vapour cloud explosion accident scenario in various ways, namely:
- by the release of flammable material itself, for instance a jet release or a catastrophic failure of a vessel resulting in a explosively dispersed cloud,
- by the interaction of the expansion flow ahead of the flame with obstacles present in a congested area, for instance, in industrial installations.

Both mechanisms may cause very high flame speeds and, as a result, strong blast pressures.
The generation of high combustion rates is limited to the release area or to congested areas respectively. As soon as the flame enters an area without turbulence due to the release, or enters an area without obstruction, the combustion rate will drop as well as the pressure generation.
Of course, both mechanisms may also occur simultaneously, as with a jet release within a congested area.

In the extreme, the turbulence can cause the flame propagation mode to change suddenly from deflagration into detonation. This mode of flame propagation is attended by propagation speeds in excess of the speed of sound (twice to 5 times the speed of sound) and maximum overpressures of about 18 bar (18×10^5 Pa). To maintain its speed of propagation, turbulence is no longer necessary, which means that unobstructed and/or quiescent flammable parts of a cloud may also participate in the production of blast. It should, however, be emphasised that for a detonation to propagate, experimental indications suggest that the flammable part of the cloud must be rather homogeneously mixed. For this reason a vapour cloud detonation of the cloud as a whole, is a most unlikely phenomenon to occur.

The likelihood of occurrence of deflagration and a detonation is also influenced by the ignition process. Hydrocarbon-air mixtures need a high-explosive charge as the ignition source for direct initiation of a detonation. Therefore, deflagrations are the most common combustion mode and detonations arise from a Deflagration to Detonation Transition (DDT).

Historically, the phenomenon described in this chapter was referred to as 'Unconfined Vapour Cloud Explosions' (UVCE), but with respect to the extent of influence of (partial) confinement and obstructions, the term 'unconfined' is a misnomer in general. It is more accurate to call this type of explosion a 'Vapour Cloud Explosion'.

The various aspects of ignition, deflagration, detonation, explosion mechanism and the subsequent blast will be described in greater detail in the following sections.

5.2.2   Combustion modes

The overpressure in a VCE is directly coupled to the speed at which the combustion front runs through the flammable cloud. Higher overpressures result from higher flame speeds. There are two basic mechanisms of flame propagation: a deflagration and a detonation. Both mechanisms are explained next.

Deflagration

The mechanism of flame propagation in a deflagration is determined largely by heat conduction and molecular diffusion of heat and species. For deflagrations, laminar and turbulent combustion can be distinguished.
Figure 5.1 shows the change in temperature across a laminar flame, whose thickness is approximately of one millimetre.
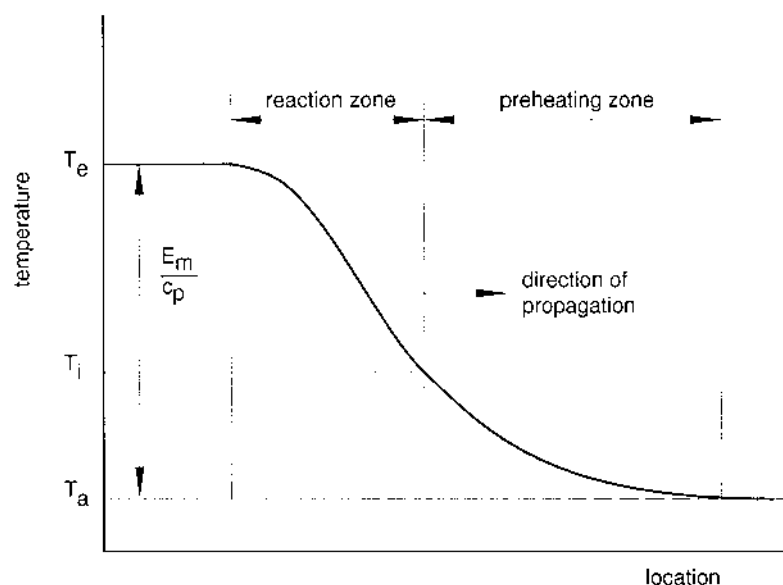
Figure 5.1   Temperature distribution across a laminar flame

Heat is produced by chemical reaction in a reaction zone. The heat is transported ahead of the reaction zone into a preheating zone in which the mixture is heated, that is to say, preheated for reaction. Since molecular diffusion is a relatively slow process,

laminar flame propagation is slow. Table 5.1 gives an overview of laminar burning velocities and other basic properties of some of the most common hydrocarbons and hydrogen.

The laminar burning velocity is the velocity at which a laminar flame propagates relative to the reactive mixture.
In general, the velocity of the mixture is not zero. The hot combustion products expand, thereby creating a flow field ahead of the flame. The flame speed is the velocity of the flame relative to the combustion products. The ratio between the densities of the unburnt mixture and the combustion products is called the expansion ratio.

Table 5.1   Explosion properties of flammable gases and vapours in air at atmospheric conditions

gas or vapour	flammability limits[1] (vol.%)	auto-ignition temperature (C)	maximum laminar burning velocity (m/s)	heat of combustion[2] (MJ/m^3)
methane	5.0-(9.5)-15.0	595	0.448	3.23
ethane	3.0-(5.6)-15.5	515	0.476	3.39
propane	2.1-(4.0)- 9.5	470	0.464	3.46
ethene	2.8-(6.5)-28.6	425	0.735	3.64
butane	1.3-(3.1)- 8.5	365	0.449	3.48
propene	2.0-(4.4)-11.0	455	0.512	3.59
hydrogen	4.0-(29.5)-75.6	560	3.25	3.01
cyclohexane	1.2-(2.3)- 8.3	260	0.440	3.85

[1]   between brackets: the stoichiometric concentration with air
[2]   for stoichiometrically mixtures with air

The difference between burning velocity and flame speed can be elucidated by regarding the propagation of a flame in a tube open at one end and closed at the other. In case ignition occurs in the open end, the flame burns into the stagnant reactive mixture. The combustion products vent directly through the open end. In this situation the velocity of the mixture is zero and the flame propagates at the laminar burning velocity.
If ignition occurs at the closed end, the expanding combustion products create a flow field in the reactive mixture. Consequently, the actual flame speed equals the expansion ratio times the laminar burning velocity.
For stoichiometric hydrocarbon-air mixtures this ratio is about eight.

The expansion induced flow velocity of the unburnt mixture can be such that the flow is turbulent. No thin and smooth flame front can be recognised in that case. Conversion of reactants into combustion burnt products now occurs in a combustion zone. At the geometrical level of the turbulence eddies, the concept of a thin combustion zone propagating at a (laminar) burning velocity is still valid and determines, together with the total flame area, the combustion rate. This combustion rate determines the speed of the combustion zone.

5.16

Without change in the basic mechanism of a deflagration, flame speeds can have all values between very low (a few metres per second) and high (more than 1000 metres per second) with accompanying increasing overpressures from a few to more than a thousand kiloPascals.

Detonation

In detonative combustion the reaction front is propagated by a shock-wave which compresses the mixture beyond its auto-ignition temperature. At the same time, the shock is maintained by the heat released from the combustion reaction.

Some basic features must be understood to understand the behaviour of a detonation. Surprisingly accurate values of overall properties of a detonation, including wave speed and pressure, may be computed from the Chapman-Jouguet (CJ) model [Nettleton, 1987]. In this model, a detonation wave is simplified as a reactive shock in which instantaneous shock compression and the instantaneous reaction at the combustion front coincide. For stoichiometric hydrocarbon-air mixtures, the detonation wave speed is in the range of 1700-2100 m/s and corresponding detonation wave overpressures are in the range of 18-22 bars (18×10^5 - 22×10^5 Pa). A slightly more realistic concept from the point of view that it reflects more than what is actually occurring in the detonation, is the Zel'dovich-Von Neumann-Döhring (ZND) model. In this model, the fuel-air mixture does not react on shock compression beyond auto-ignition conditions before a certain induction period has elapsed (Figure 5.2).
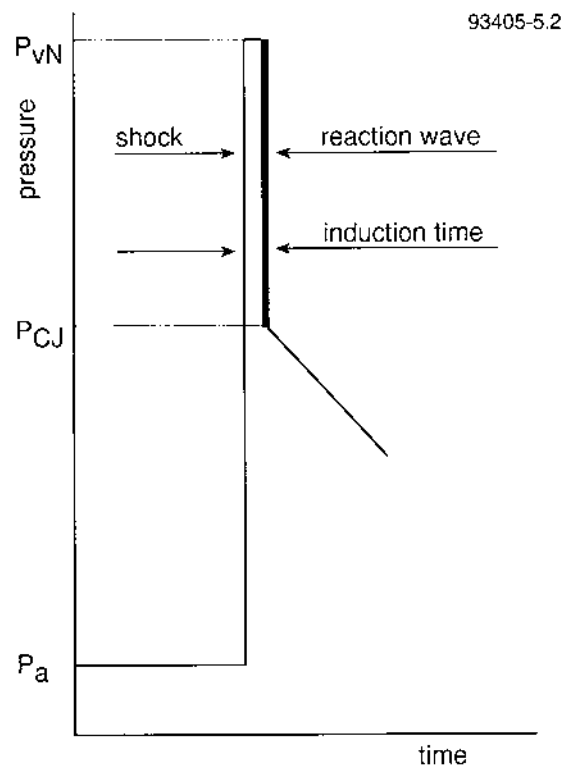
Figure 5.2   The ZND model for a detonation

The pressure behind the non-reactive shock is much higher than the CJ detonation pressure. The CJ pressure is attained on reaction after the induction time. The induction period lasts only some microseconds and, as a consequence, the 'Van Neumann spike' (p_{vN}) is difficult to detect experimentally.

The one-dimensional representation described above is too simple to describe the behaviour of a detonation in response to boundary conditions. Denisov et al. [1962] showed that a detonation is not a stable process, but a highly fluctuating one. Figure 5.3 shows how a plane configuration of a shock and a reaction front breaks up into a cellular structure. At a smaller scale, a multi-dimensional cyclic character is determined by a process of continuous decay and reinitiation. The collision of transverse waves plays a key role in the structure of a detonation wave.

The cellular structure can be visualised in experiments. A characteristic dimension of the structure or cell size can then be distinguished. The cell size depends strongly on the fuel and mixture composition; more reactive mixtures result in smaller cell sizes. The cell size is also a measure for the minimal dimensions of a geometry for sustaining the detonation. Therefore, the cell size reflects the susceptibility of a fuel-air mixture to detonation. Table 5.2 shows that a stoichiometric mixture of methane and air has a low susceptibility to detonation compared to other hydrocarbon-air mixtures.

93405-5.3
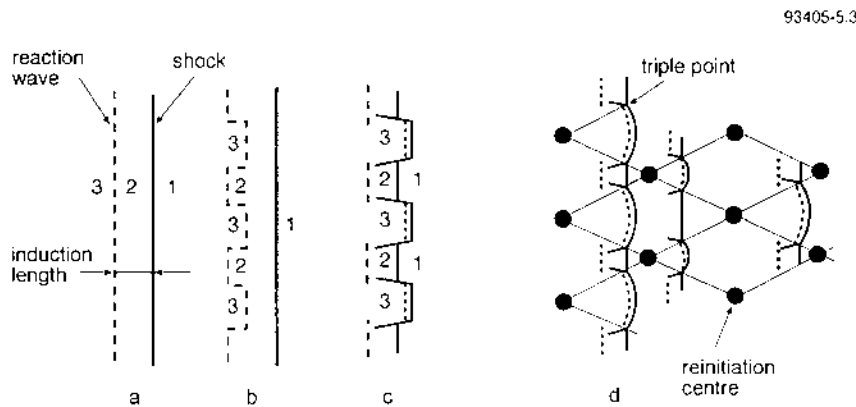
Figure 5.3   Instability of ZND-concept of a detonation wave
              1: non-reacted zone
              2: induction zone
              3: reacted zone

The obvious difference between detonations and deflagrations is that flame speed and overpressure are higher in a detonation. A characteristic difference is that flame speed and overpressure in a detonation are typical for a given mixture whilst flame speed and overpressure in a deflagration can have a wide range of values depending on the geometrical boundary conditions.

5.2.3 Ignition

Ignition can lead to either of the two combustion modes, deflagration or detonation, depending on source properties. Ignition energies leading to deflagrations are in the order of 10^{-4} J, whereas direct initiation of detonation requires an energy of approximately 10^6 J. Table 5.2 gives minimum ignition energies for deflagration and detonation for some fuel-air mixtures. Considering the high energy required for detonation, a direct initiation of a detonation is a very unlikely occurrence.

In practice, vapour cloud ignition can be the result of a sparking electric apparatus or hot surfaces present in a chemical plant, such as extruders, hot steam lines or friction between moving parts of a machine. Another common source of ignition is open fire and flame, for instance, in furnaces and heaters. Mechanical sparks, for example, from the friction from moving parts of a machine and falling objects, are also frequent sources of ignition. Many metal-to-metal combinations result in mechanical sparks that are capable of igniting gas or vapour-air mixtures.

In general, ignition sources must be assumed to be present in industrial installations.

Table 5.2   Characteristic detonation cell size and ignition energies for deflagration and detonation for some stoichiometric fuel-air mixtures

fuel	cell size	minimum ignition energy for	
		deflagration	detonation
	(mm)	(mJ)	(mJ)
methane	300	0.28	2.3×10^{11}
propane	55	0.25	2.5×10^9
propene	55	0.28	7.6×10^8
ethene	25	0.07	1.2×10^8
acetylene	10	0.007	1.29×10^5

5.2.4 Gas explosion mechanism

Research during the last twenty-five years has revealed the mechanism by which a slow-burning flame is transformed into an intense blast generating process like a vapour cloud explosion.

When a flammable vapour cloud is ignited, initially a thin laminar flame with a smooth surface will start to propagate away from the ignition location. Due to the intrinsic unstable nature of a flame, flame instabilities will wrinkle the flame surface, thereby enlarging the flame surface and thus the combustion rate. This results in an increased expansion which pushes the flame to a larger speed. Effective burning velocities are not much higher than the laminar burning velocity, and overpressures generated are in the order of some hundreds of Pascals.

Due to the expansion of the reacted products, a flow field is created ahead of the flame. If this field is disturbed, for instance due to shear layers occurring in the flow at solid boundaries or, more important, if the flow pattern is changed by the presence

of obstacles, the shape of the flame is changed. The flame will be stretched and wrinkled, as a result its surface is enlarged and the combustion rate is increased.

As more fuel is converted into combustion products per unit of volume and time, expansion flow becomes stronger. Again, the flame surface area is enlarged and the whole process is accelerated. At a certain velocity the flow becomes turbulent and the combustion front breaks up in a combustion zone. In a turbulent mixture combustion takes place in an extended zone in which combustion products and unreacted mixture are intensely mixed. High combustion rates can result because, within the combustion zone, the reacting interface between combustion products and reactants can become very large.

Higher combustion rates produce stronger expansion, i.e. higher flow velocities with an increased level of turbulence. This process feeds on itself, a positive feedback coupling comes into action (Figure 5.4).
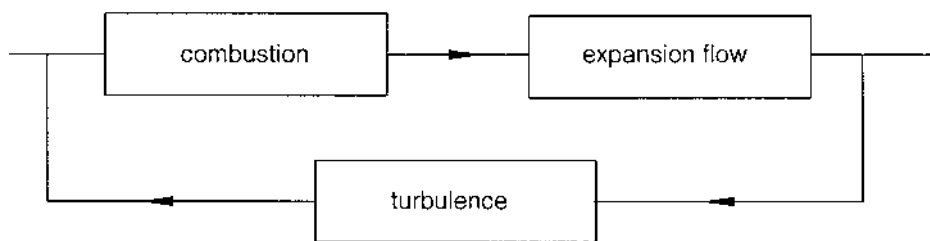
Figure 5.4   Positive feedback, the basic mechanism of a gas explosion

The obstacles and structures present in the vapour cloud, acting as turbulence generators, play a very important role in the development of the process. A change of the obstacle configuration in the flow path changes the acceleration process. An absence of turbulence generators will lead to a reduction in flow speed and will decelerate the flame. Acceleration of the flame is influenced also by the measure of obstruction and confinement of the expansion flow. Due to the restricted expansion possibilities of the combustion products a one-dimensional flow (in a pipe) causes more acceleration than a two-dimensional (between parallel plates) or a three-dimensional flow with no confinement at all.

5.2.5   Deflagration to detonation transition (DDT)

If the positive feedback process described in the previous paragraph continues to accelerate the flame, the combustion mode may suddenly change drastically. The reactive mixture just in front of the turbulent combustion zone is preconditioned for reaction by a combination of compression and heating by turbulent mixing with combustion products. If turbulent mixing becomes too intense, the combustion reaction may quench locally as the chemical process of combustion can not cope with the physical process of turbulence. A very local, non-reacting but highly reactive mixture of reactants and hot products is the result. The intensity of

heating by compression can raise temperatures of fractions of the mixture to levels above the auto-ignition temperature. These highly reactive 'hot spots' react very rapidly, resulting in localised, constant volume sub-explosions [Urtiew and Oppenheim, 1966, Lee and Moen, 1980]. If the surrounding mixture is sufficiently close to auto-ignition (as a result of blast compression from one of these sub-explosions), a detonation wave results. This wave engulfs the entire process of flame propagation.

Although continuous research revealed much of the DDT process, the exact conditions are still hard to predict and it is very difficult to make quantitative predictions in general. Much research has studied DDT in gas explosions in pipes. This has resulted in values for the so-called run-up distances expressed in a number of pipe diameters for the flame to travel before DDT occurs. Internals and obstructions reduce these run-up distances considerably.
DDT in unconfined three-dimensional obstructed geometries with hydro-carbon-air mixtures have seldom been reported. An example of the onset of a DDT was reported recently [Mercx et al., 1994].

5.2.6   Blast

A characteristic feature of explosions is blast. Vapour cloud explosions are characterised by rapid combustion in which high-temperature combustion products expand and affect the surroundings. In this fashion, the heat of combustion of a fuel-air mixture (chemical energy) is partially converted into expansion (mechanical energy). Mechanical energy is transmitted into the surrounding atmosphere in the form of a blast-wave. This process of energy conversion is very similar to that occurring in internal combustion engines. Such a process can be characterised by its thermodynamic efficiency. At atmospheric conditions, the theoretical maximum thermodynamic efficiency for conversion of chemical energy into mechanical energy in gas explosions is approximately 40%. Thus, less than half of the total heat of combustion produced in explosive combustion can be transmitted as blast-wave energy.

A blast-wave is experienced in the surrounding atmosphere as a transient change in the gas-dynamic-state parameters: pressure, density and particle velocity. In a blast-wave, these parameters increase rapidly, then decrease less rapidly to sub-ambient values (i.e. develop a negative phase). Subsequently parameters slowly return to atmospheric values (Figure 5.5).
The shape of the blast-wave is highly dependent on the nature of the explosion process. If the combustion process within a gas explosion is relatively slow, then expansion is slow and the blast consists of a low-amplitude pressure wave characterised by a gradual increase in gas-dynamic-state variables (Figure 5.5A). If, on the other hand, combustion is rapid, the blast is characterised by a sudden increase in gas-dynamic-state variables and a shock-wave results (Figure 5.5B).
The shape of the blast-wave changes during propagation. In a two- or three-dimensional expansion the magnitude of the peak overpressure will decrease with increasing distance from the origin. Initial pressure waves tend to steepen to shock-waves during propagation and wave 'durations' tend to increase during propagation because the gas velocity is related to the overpressure.
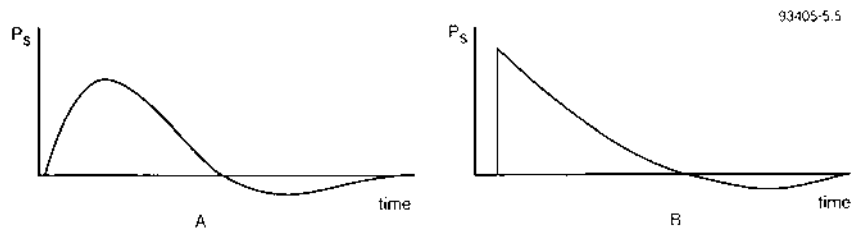
Figure 5.5   Blast-waves overpressure histories
              A: pressure wave
              B: shock-wave

The loading of a structure due to blast depends on the interaction between the blast-wave and the structure itself as the interaction changes the blast-wave parameters. This phenomenon of explosion blast is not the subject of this chapter but is described in detail in, for instance, CPR-16E [1990].

5.3 General overview of existing vapour cloud explosion blast models

5.3.1 Introduction to section 5.3

Basically there are two groups of models for describing explosion blast. The first group of models quantifies the source as an equivalent quantity of high explosives, generally TNT, in order to be able to apply known TNT blast characteristics. Historically, these types of models are widely-used and well-accepted. During the last decade, the process of pressure development in a vapour cloud explosion has been the subject of intense international research after discovering the impossibility to describe some major vapour cloud explosion incidents with available methods at that time. This research effort resulted in methods which take into account the different behaviour of a vapour cloud explosion with respect to a high-explosives detonation. This second group of models will be referred to as fuel-air charge blast models. This type of models is being applied more and more, although some lack of data hinders a general acceptation.
The differences between the models in a group result from the differences in guidance in the application the concept and from differences in the used blast distance relations.

The two groups of models are discussed in the next two sections.

5.3.2 Methods based on TNT charge blast

The military have always been interested in the destructive potential of high-explosives. Consequently, the relationship between damage and high-explosives has been available for many years [e.g. Robinson 1944, Schardin 1954, Glasstone and Dolan 1977 and Jarrett 1968]. Therefore, it is an understandable approach to relate the explosive power of an accidental explosion to an equivalent TNT-charge. In this way, damage patterns observed in many major vapour cloud explosion incidents were related to equivalent TNT-charge weights.
Because the need to quantify the potential explosive power of fuels arose long before the mechanisms of blast generation in vapour cloud explosions were fully understood, the TNT-equivalency concept was also utilised to make predictive estimates, i.e. to assess the potential damage effects from a given amount of fuel. Basically, the use of TNT-equivalency methods for blast predictive purposes is very simple. The available combustion energy in a vapour cloud is converted into an equivalent charge weight of TNT according to:

$$Q_{TNT} = \alpha_e \times \frac{Q_f \times E_{mf}}{E_{mTNT}} = \alpha_m \times Q_f \qquad \text{(kg)} \qquad (5.1)$$

in which:

α_e =   TNT equivalency based on energy   [-]
α_m =   TNT equivalency based on mass   [-]
E_{mf} =   Combustion energy of fuel per unit mass $[J \cdot kg^{-1}]$
E_{mTNT} =   TNT blast energy per unit mass $[J \cdot kg^{-1}]$
Q_f =   Mass of fuel involved   [kg]
Q_{TNT} =   Equivalent mass of TNT   [kg]
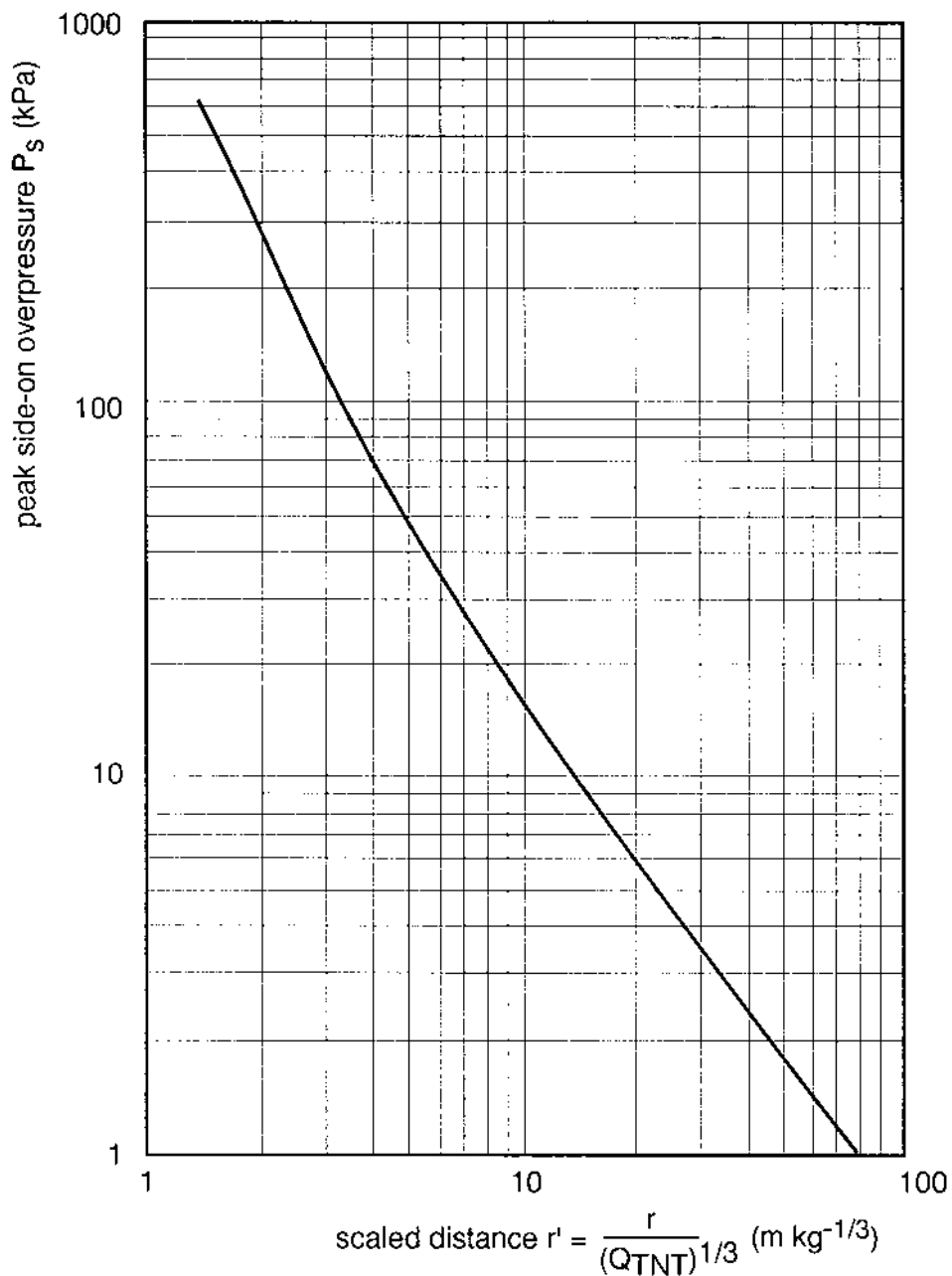
Figure 5.6   *Peak side-on overpressure due to a surface TNT explosion according to Marshall [1976]*

Values of E_{mTNT} currently in use range from 4.19 to 4.65 MJ/kg [Brasie and Simpson, 1968].

The TNT-equivalency is also indicated in literature as the equivalency factor, yield factor, efficiency factor or efficiency.

Knowing the TNT-charge weight, the blast characteristics in terms of the peak side-on overpressure of the blast-wave dependent on the distance to the charge and the corresponding damage pattern, are known. They can be read from a chart containing a scaled graphical representation of experimental data. For this purpose various data sets are available, Figure 5.6 gives an example.

Strictly speaking, TNT-equivalency methods reduce the problem of vapour cloud explosion blast modelling to the determination of an appropriate value for the TNT-equivalency.

Reported values for the TNT-equivalency, deduced from the damage observed in many vapour cloud explosion incidents, range from a fraction of one per cent up to some tens of per cent. This is reflected in the TNT-equivalence factors adopted in TNT blast charge methods.

A brief overview of these methods is given next. It should to be kept in mind that TNT-equivalence factors given have to be used with particular methods to quantify the amount of fuel involved and with particularly mentioned TNT blast charts.

All TNT-equivalence factors given are based on energy.

Brasie and Simpson [1968] and Brasie [1976]

They recommend TNT equivalencies of 2% for near-field and 5% for far-field effects in combination with a method to quantify the amount of fuel released.

Eichler and Napadensky [1977]

Because of the distance dependency of the TNT-equivalence factor they recommend 20% for the 1 psi (6.9 kPa) overpressure level only.

Health Safety Executive [1979 and 1986]

They recommend a value of 3% for gases with average reactivity (methane), 6% for above average gases (propene oxide) and 10% for very reactive gases (ethene oxide). The mass of fuel in the cloud is taken as twice the theoretical flash of the amount released, in order to account for spray and aerosol formation.

The maximum overpressure in the cloud is taken as 1 bar (100 kPa). The duration of the blast-wave should be chosen between 100 and 300 ms.

Exxon [CCPS, 1994]

Exxon provides guidance to determining the quantity of material in the cloud and advises TNT-equivalencies of 3% for a vapour cloud covering an open terrain and 10% for a vapour cloud that is partially confined or obstructed.

Industrial Risk Insurers [1990]

IRI present two credible incidents to determine the quantity of fuel in the cloud and uses a TNT-equivalence factor of 2%.

Factory Mutual Research [1990]

FMR notes that history shows TNT-equivalence factors as high as 50% but most fall in a range between 10%. Like HSE they recommend factors depending on the reactivity of the fuel involved. Factors are assigned to three classes: low-reactive 5%, average-reactive 10% and high-reactive 15%.

CPR-14E [1988]

One of the two models given in this version of the 'Yellow Book' relates the available explosion energy directly to damage circles (correlation model). In fact, this is a TNT-equivalence model. A 'yield' (TNT-equivalence factor) of 10% is used.

British Gas [Harris and Wickens, 1989]

Their method is intended for a non-detonating cloud of natural gas (mostly methane). Their approach is not based on the total amount of fuel released but on the mass of the material which can be contained in stoichiometric proportions in any severely congested region in the cloud. An overpressure of four bars ($4 \cdot 10^6$ Pa) is assumed within the confined part. A TNT-equivalence factor of 20% should be used for the total congested mass. They state that the method predicts significantly lower far-field overpressures in cases where there is little obstruction and that in many circumstances the possibility of VCE's with significant overpressures can be discounted.

Direction des etudes et Recherches, France [Van den Berg and Lannoy, 1993]

The value of the TNT equivalence factor [Van den Berg and Lannoy, 1993] has been discussed by Lannoy. He refers to a statistical analysis of 120 damage points of 23 accidents showing a wide distribution of TNT equivalencies (0.02%-15.9%) with a medium of 3%. Of the cases 97% was covered by a TNT equivalence lower than or equal to 10% while the mean value observed was an equivalency of 4% covering 60% of the cases. He states that TNT equivalence methods for VCEs should only be used for the assessment of far-field blast effects where the levels are less than 30 kPa. Otherwise the methods lead to overdesigned structures. Attention is drawn to the French situation where the French Authority Safety Rule [1982] recommends the 10% equivalency for safety factors and that the French Chemical Industry [1986] recommends the 4% equivalency, both based on the full amount of fuel released.

5.3.3 Methods based on fuel-air charge blast

So far, vapour cloud explosion blast has been modelled without considering a major feature of gas and vapour explosions, namely, that their strength is a variable. In addition, TNT blast characteristics do not correspond properly to vapour cloud explosion blast characteristics. This is demonstrated by the distance dependent TNT-equivalency observed in vapour cloud explosion blast. In particular, the blast

from relatively mild (low strength) vapour cloud explosions can not be represented by TNT-blast in a satisfactory way. Therefore, the need for a blast model which reflects more basic gas explosion blast characteristics, was felt.

Munday [1976] developed a method to match the gas dynamics produced by spherical flame propagation to far-field TNT-blast characteristics.
Baker et al. [1983] recommended the use of computational data on gas explosion blast for vapour cloud explosion blast modelling. The data were generated with the CLOUD-code. Spherical steady flame speed gas explosions were numerically simulated [Luckritz, 1977 and Strehlow et al. 1979]. The blast effects were condensed in a graphical representation of the distribution of the most important blast parameters in the vicinity of a spherical fuel-air charge. The above references, however, did not give suggestions for using these tools for a predictive estimate of a vapour cloud's explosive potential. Vapour cloud explosion blast prediction methods, using fuel-air blast data, are presented next.

Wiekema [1980]

Wiekema [1980] used the gas dynamics induced by a spherical expanding piston as a model for vapour cloud explosion blast [CPR-14E, 1988]. A piston blast model offers the possibility to introduce a variable initial strength of the blast.
This approach enables modelling vapour cloud explosion blast by considering the two major characteristics of gas explosion blast:
−   the scale, determined by the combustion energy of the total cloud inventory, and
−   the initial strength, determined largely by the combustion rate in the explosion process for which three reactivity classes are defined. Some influence of obstruction is taken into account.

Output parameters are peak overpressure and positive phase duration.

The Multi-Energy method [Van den Berg, 1985]

Experimental research during the last decade showed clearly that deflagrative combustion generates blast only in those parts of a quiescent vapour cloud which are sufficiently obstructed and/or partially confined [Zeeuwen et al., 1983, Harrison and Eyre, 1987, Harris and Wickens, 1989 and Van Wingerden, 1989].
This feature is the basis of the Multi-Energy method and underlies the method of blast modelling.
Contrary to the TNT-blast models (except the one from Harris and Wickens) and the model of Wiekema [1980], in which the contributing energy is based on the total energy content of the cloud, the Multi-Energy method takes into account the total combustion energy of those parts of the cloud that are located in obstructed and/or partly confined areas. An obstructed area is an area where obstacles are present in a configuration suited to accelerate a flame if the area is engulfed by a flammable gas mixture. Each obstructed area should be treated separately as a blast source in case their relative separation distance is large enough. Otherwise, all the individual source energies should be added and the explosion manifests itself as a single event.

An idealised gas explosion blast model was generated by computation and presented in three non-dimensionalised graphs from which the most important parameters can be determined (peak overpressure, positive phase duration, shape of the blast-wave and dynamic peak pressure). Steady flame speed gas explosions were numerically

simulated with the BLAST-code [Van den Berg, 1980] and their blast effects were registered.

These blast charts should be used for calculating the blast from each explosion source.

Although in the Multi-Energy method a fuel-air charge blast model is recommended for the representation of blast effects, a TNT-blast model may be used as well. It can be demonstrated that the blast resulting from a TNT explosion with a 20% TNT equivalency of the energy will correspond closely to the blast as predicted with the Multi-Energy severest blast curve in the overpressure range of 10 to 100 kPa. Overpressure according to the Multi-Energy method will be higher in the far field due to the specific nature of a VCE.

This TNT-equivalency approach within the Multi-Energy framework, however, lacks the basic possibilities for a further refinement in the specification of an initial blast strength.

Shell [Cates, 1991]

Cates [1991] has proposed a methodology comparable with the Multi-Energy method.

He claims that, due to the pressure decay law used, in the Multi-Energy method, overpressures in the far-field are underpredicted by the Multi-Energy used, although still higher predictions are made compared to the TNT equivalence methods. He also claims that, from a comparison with experiments, the Multi-Energy method overestimates the near field overpressure, even if the overpressure measured in the cloud is used.

As a number of questions are still unanswered a simple acoustic law is preferred to determine peak overpressure.

Another adaptation is that the volume of the cloud to be taken into account should be extended to 2 m outside the obstructed region. The reason is that due to venting of unburnt gases out of the obstructed area during combustion, part of the unobstructed volume near to the obstructed part will be very turbulent and thus contribute to overpressure generation.

A decision tree is presented to estimate a source overpressure.

Mobil Research/Baker Engineering [Baker et al., 1994]

The method of Baker et al. [1994] consists of a combination of the Multi-Energy method and the blast curves of Strehlow [1979], with peak overpressures and impulse as output parameters. The blast curves of Strehlow were appreciated more than those of the Multi-Energy method because Strehlow gives a graph with curves for the impulse. A more basic reason to choose for the Strehlow curves is that each curve is based on a certain flame speed reached in the VCE.

Based on an extensive survey of all available experimental investigations on VCE, guidance has been derived for a proper choice of the maximum flame speed to be expected.

Although a method is given to determine the source strength in terms of flame speed, still judgements and assumptions have to be made to determine the obstacle density, reactivity and flame diversion.

Baker et al. [1994] provide some guidance.

5.4 Selection of a model

TNT charge blast models

The basic assumption in TNT charge blast models, a proportional relation between the amount of fuel available in the cloud and the TNT-charge weight expressing the cloud's explosive potential, is most questionable. This is reflected by the wide range of equivalencies found if a large number of vapour cloud explosion incidents, involving only fuels whose heats of combustion are of the same magnitude as those of hydrocarbons, is analysed.

Nevertheless, the TNT-equivalency concept makes it possible to model the blast effects of a vapour cloud explosion in a very simple and practical way. The attractiveness of these methods is the very direct, empirical relation between a charge weight of TNT and the resulting structural damage. Therefore, the TNT-equivalency seems to be a useful tool if the property damage potential of vapour cloud explosion is the major concern.

Values for the TNT-equivalency are deduced by statistical analysis from the damage observed in a limited number of major vapour cloud explosion incidents. For the wide range of equivalencies observed, characteristic values such as an average (4%) and an approximate upper limit (10%) were recommended to be used for predictive purposes. The average value is very near the TNT equivalency in the distribution where the majority of cases are found, i.e. an equivalency of 4% corresponds to 'an average major incident'. Undoubtedly, 'an average major incident' represents a situation in which an accidental release of fuel is most likely such as, for instance, the site of a refinery or chemical plant or the site of a crowded marshalling yard during operations. Strictly speaking, by using an average value of the TNT-equivalency, 'average major incident conditions' are extrapolated to an actual situation. Therefore, TNT-equivalency methods give a reasonable estimate of far-field blast effects only if the actual conditions correspond more or less to 'average major incident conditions'.

TNT blast is a poor model for vapour cloud explosion blast. While a TNT charge produces a shock-wave of a very high amplitude and a short duration, a vapour cloud explosion produces a blast-wave, often shocks, of lower amplitude and longer duration. If the blast modelling is the starting point for the computation of structural response, for instance, the design of blast resistant structures like control rooms, TNT blast will be a less satisfactorily model. Then, the shape and the positive phase duration of the blast-wave are important parameters which should be considered and the use of a more appropriate blast model is recommended.

A practical value for TNT-equivalency is an average, based on a wide statistical distribution found in practice. As a consequence, a predictive estimate with TNT-equivalency on the basis of an average value has a very limited statistical reliability. A more deterministic estimate of blast effects is possible if a parameter could be found which correlates with the process of blast generation in vapour cloud explosions.

In the alternative group of models, the fuel-air charge blast models, such a parameter is introduced.

In summary, TNT equivalency models:
- state a proportional relationship between charge weight and cloud energy content,
- use a TNT equivalence factor(proportionality) based on incident statistics which shows very wide and flat distribution. This bad correlation contradicts the basic assumption of proportionality,
- have therefore a poor statistical reliability,
- do not take into account the variability of explosion strengths,
- do not match with vapour cloud explosion blast characteristics (distance dependant efficiency factor),
- overpredict near-by pressure effects,
- predict only overpressures (not duration and blast-wave shape),
- are simple and easy to apply,
- are commonly used although there is common dissatisfaction.

Fuel-air charge blast models

The fuel-air charge blast model in CPR-14E [1988] takes reactivity of the cloud as the parameter determining overpressure in the cloud. Furthermore the model bases the combustion energy on the total inventory of the cloud. A large amount of experimental data became available after the release of the model and proved this concept wrong. Reactivity plays a role, certainly, but turbulence is the key parameter determining overpressure generation. As the interaction of the expanding flow ahead of the flame with obstacles is a very effective turbulence generator, overpressure is mainly produced in partially confined and obstructed regions in the vapour cloud. This basic mechanism is underlying the Multi-Energy concept.

The blast characteristics, peak overpressure, duration, impulse and wave shape depend on the 'source strength' of each explosion centre. The blast charts of the Multi-Energy method as well as the blast charts of Strehlow (Mobil/Baker method) cover this basic feature of a vapour cloud explosion.
Selection of the 'source strength' is based on overpressure with the Multi-Energy method and on flame speed with the Mobil/Baker method. As both parameters can be coupled there is no reason to select between both models regarding this aspect. Preference could be given to the Multi-Energy blast charts as the curves are smoothed for practical application and extend to larger scaled distances than the Strehlow blast curves. Furthermore, the Multi-Energy blast charts provide the shape of the blast-wave, which is important when the results are coupled to consequence models for calculation of damage to structures and injury to people [CPR-16E, 1990].

Conservative application of both models in a sense that always the most severe overpressure is selected will result in overpressure distance relations comparable to those predicted with TNT-equivalence models, with equivalence factors as high as 20%, for the intermediate field, if the combustion energy of the partially confined areas is taken into account.
In fact, this is exactly the concept of the TNT charge blast method of Harris and Wickens [1989].
Even in these cases, the set blast parameters of the fuel charge blast models will be in better compliance with actual vapour cloud explosion blast.
From a comparison with experiments it appeared that even if the measured overpressure in the cloud is taken as the source strength, the blast overpressures resulting from the appropriate curve results in overpredictions of the actual measured values for most cases.

Guidance to selecting less conservative estimates for the source strength is increasing [Kinsella, 1993, Baker et al., 1994, Cates, 1991] but is still incomplete, and still user judgement is required. Furthermore, validation with experimental data is acknowledged but not published. This guidance should therefore be applied with care.

In summary, fuel-air charge blast models:
− acknowledge the basic gas explosion mechanism,
− are based on boundary conditions rather than on cloud volume,
− are deterministic, not statistical,
− do not use statistics but actual conditions to determine blast,
− take into account a variety of explosion strengths,
− all combinations of overpressure, duration and blast-wave shapes are possible,
− give all input variables requested by 'Green Book' damage models,
− are rather easy to apply if used in a conservative manner,
− are widely accepted as a better alternative,
− application in a less conservative manner is hindered by lack of guidance,
− available guidance is not properly supported,
− have all possibilities for further refinement.

It will be obvious from the discussion of the various models that preference is given to fuel-air charge blast models.

Within the group of fuel-air charge blast models the Multi-Energy method is preferred because:
− the fuel-air charge blast model of CPR 14-E [1988] is not acceptable as it uses reactivity as the basic parameter rather than boundary conditions,
− the Mobil/Baker method is even more a concept and less worked out than the Multi-Energy method.

5.5 Description of model

5.5.1 Introduction to the Multi-Energy concept

Experimental research during the last decade showed clearly that deflagrative combustion generates blast only in those parts of a quiescent vapour cloud which are sufficiently obstructed and/or partially confined [Zeeuwen et al., 1983, Harrison and Eyre, 1987, Harris and Wickens, 1989 and Van Wingerden, 1989]. The conclusion that a partially confined and/or obstructed environment offers appropriate conditions for deflagrative explosive combustion has found general acceptance today [Tweeddale, 1989]. However, other parts of the cloud - parts which are already in turbulent motion at the moment of ignition - may develop explosive, blast generating combustion as well. Therefore, high-velocity intensely turbulent jets, for instance, which may be the result of fuel release from under high pressure, should be considered as possible sources of blast in a flammable vapour cloud. The remaining parts of the flammable vapour-air mixture in the cloud burn out slowly, without significant contribution to the blast. This idea is called the Multi-Energy concept and underlies the method of blast modelling.

Contradictory to conventional modelling methods in which a vapour cloud explosion is regarded as an entity, in this concept a vapour cloud explosion is rather defined as a number of sub-explosions corresponding to the various sources of blast in the cloud. This concept is illustrated in Figure 5.7.

93405-5.7
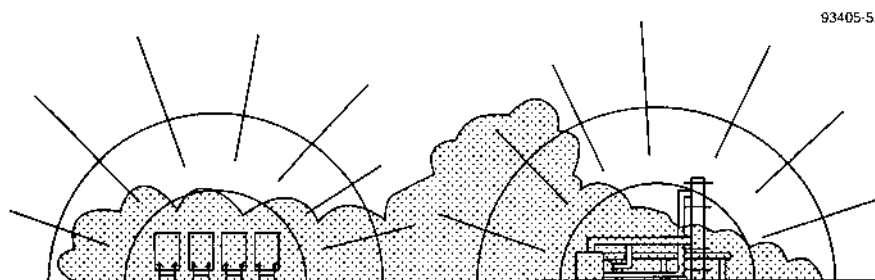
Figure 5.7   Vapour cloud containing two blast generating obstructed regions

Here, two of the most notorious blast generators from the vapour cloud explosion record [Baker et al., 1983] are blanketed in a large vapour cloud. Their blast effects should be considered separately.

Blast effects are represented by using a blast model. Generally, blast effects from vapour cloud explosions are directional. Such an effect, however, cannot be modelled without a detailed numerical simulation of phenomena.
An easy-to-apply method, on the other hand, requires a simplified approach according to which blast effects are represented in an idealised, symmetric way. An

idealised gas explosion blast model was generated by computation and is represented in Figures 5.8 A, B and C. Steady flame speed gas explosions were numerically simulated with the BLAST-code [Van den Berg, 1980] and their blast effects were registered.

The blast charts were composed for vapour cloud explosions having a combustion energy E_v of 3.5 MJ/m^3 which is the combustion energy for most hydrocarbon mixtures at stoichiometric concentration with air.

Only the most significant blast-wave parameters such as the side-on peak overpressure, peak dynamic pressure and positive phase duration of the blast-wave, are represented dependent on the distance to the blast centre for a hemi-spherical fuel-air charge of radius r_o on the earth's surface. The data are reproduced in a fully non-dimensional (Sach's-scaled) representation so that the blast parameters can be read off in any consistent set of units.

The initial strength of the blast is indicated by a number ranging from 1, for very low, up to 10, for detonative strength. The initial blast strength is defined as a corresponding set of blast-wave parameters at the location of the charge radius r_o. In addition, a rough indication for the shape of the blast-wave is given. Detonative blast consists of a shock-wave which is represented by solid lines. Pressure waves of low initial strength are indicated by dotted lines. Pressure waves may steepen to shock-waves in the far-field. In between, there is a state of transition indicated by dashed lines. The pictures show the characteristic behaviour of gas explosion blast. Pressure waves, produced by a fuel-air charge of low strength, show an acoustic overpressure decay behaviour and a constant duration in the positive phase. A much faster decay of the overpressure and a substantial increase of the positive phase duration is observed for shock-waves in the vicinity of a charge of high initial strength. Eventually, the high-strength blast develops a more or less acoustic decay in the far field.

Before the Multi-Energy method can be applied, the volume and the location of the flammable vapour cloud must be known or assumed. For this, source term models and dispersion models may be applied. Furthermore, the lay-out, or at least a rough impression of the build-up area where the cloud is located, must be available in order to determine the location, the number and the volume of the obstructed regions within the cloud. Then, the blast charts belonging to the Multi-Energy method can be applied to obtain values for the most important blast parameters.

93405-5.8a
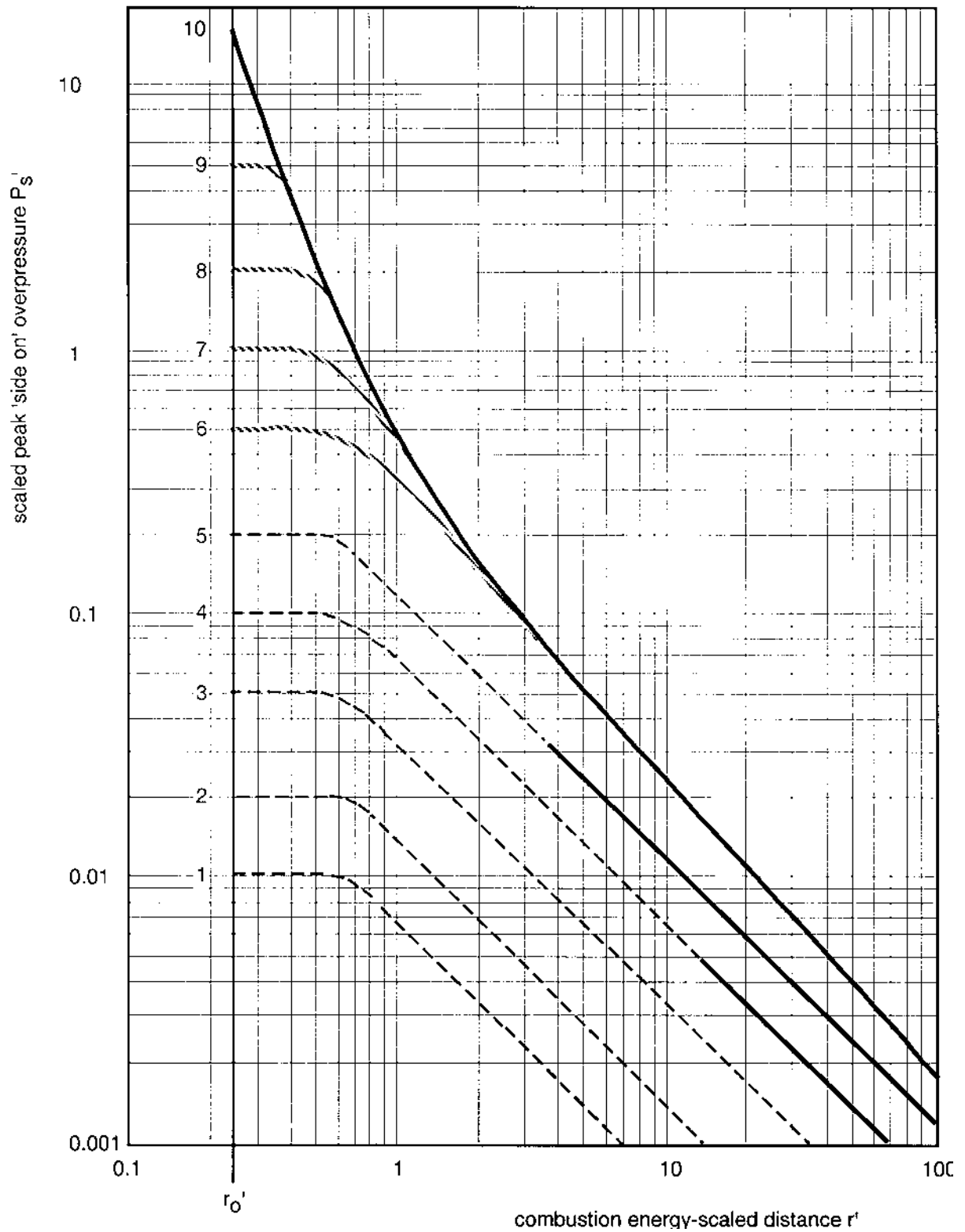
Figure 5.8A   Multi-Energy method blast chart: peak side-on overpressure
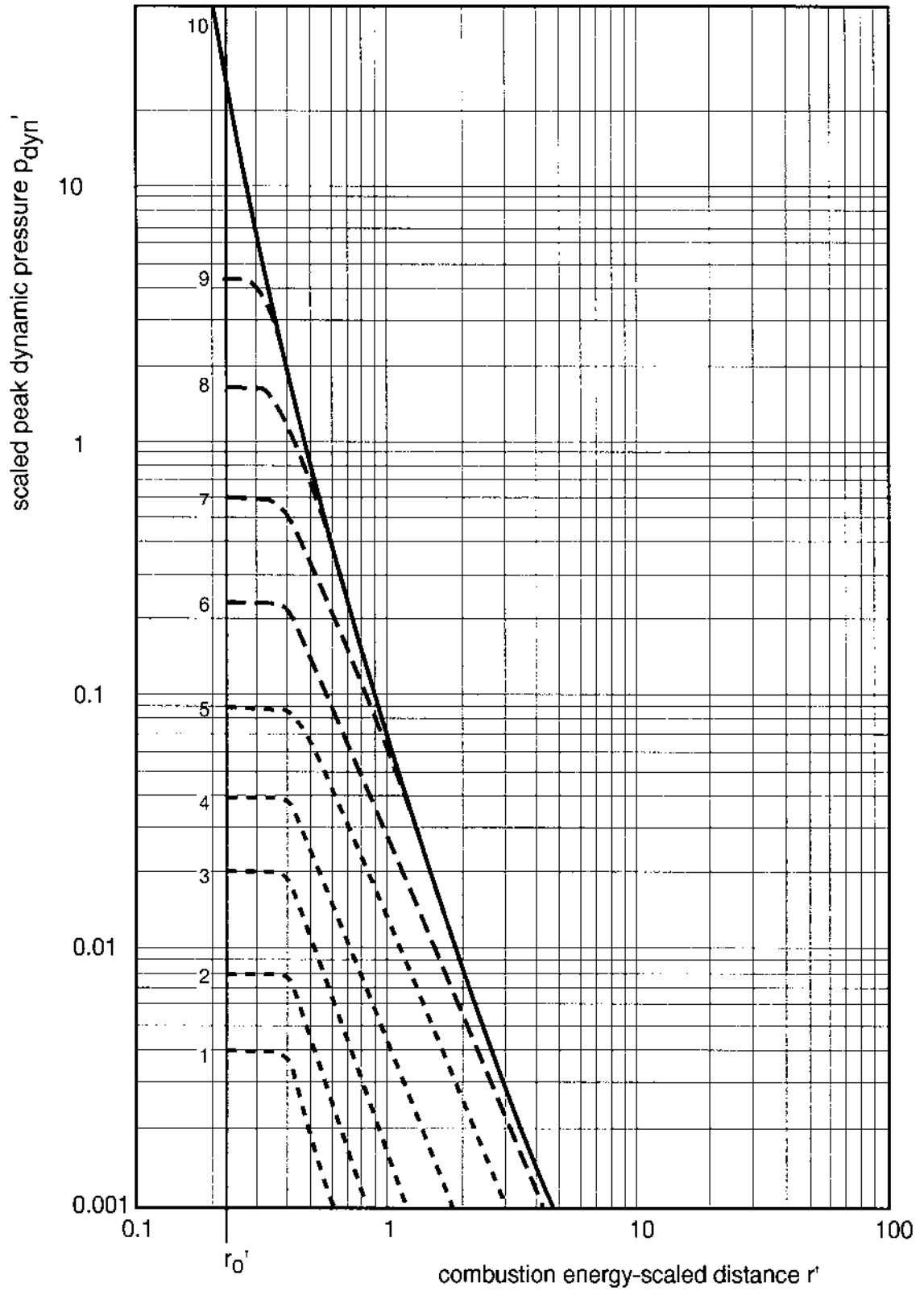
Figure 5.8B   Multi-Energy method blast chart: peak dynamic pressure
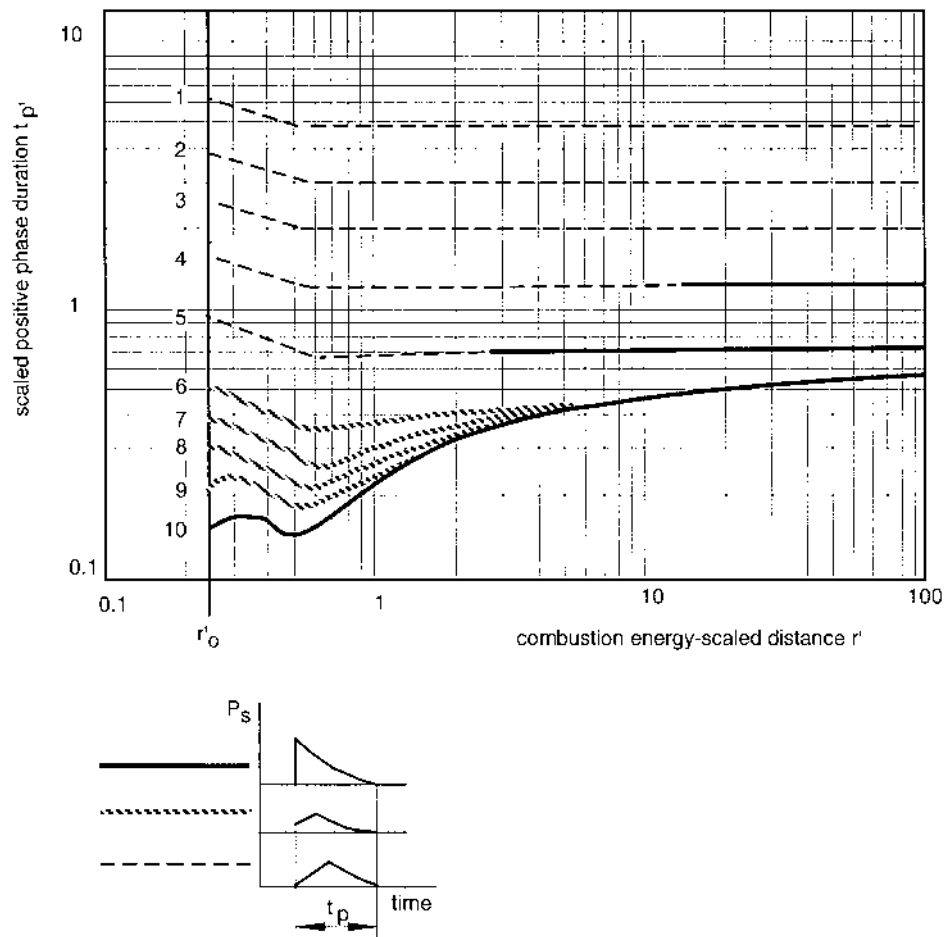
Figure 5.8C   Multi-Energy method blast chart: positive phase duration and blast-wave shape

The blast parameters are read off the blast charts (Figures 5.8):

−   calculate the scaled distance r' which is the distance r of the location under consideration to the centre of the explosion divided by the energy available E and the ambient pressure p_a:

$$r' = r/(E/p_a)^{1/3} \qquad\qquad (-) \qquad (5.2)$$

−   assume an explosion strength (class 1 to 10) and read off the charts the scaled peak side-on overpressure P_s', the scaled peak dynamic pressure p_{dyn}' and the scaled positive phase duration t_p'

−   calculate the peak overpressure P_s from:

$$P_s = P_s' \times p_a \qquad\qquad (Pa) \qquad (5.3)$$

− calculate the positive phase duration t_p from:

$$t_p = t_p' \times (E/p_a)^{1/3}/a_a \qquad\qquad \text{(s)} \qquad (5.4)$$

− calculate the peak dynamic pressure p_{dyn} from:

$$p_{dyn} = p_{dyn}' \times p_a \qquad\qquad \text{(Pa)} \qquad (5.5)$$

− determine the shape of the blast-wave from Figure 5.8C

− calculate the positive impulse i_s by integrating the overpressure variation during the positive phase resulting in multiplying the side-on overpressure with the positive phase duration and with a factor 1/2:

$$i_s = 1/2 \times P_s \times t_p \qquad\qquad \text{(Pa·s)} \qquad (5.6)$$

An interesting feature is that at a distance larger than about 10 charge radii from the centre, the blast is independent on whether the explosion was a strong deflagration (higher than, or equal to, number 6) or a detonation (see Figure 5.8). Using this hemi-spherical fuel-air charge blast model, the blast produced by the various sources in the cloud can be modelled.

Contrary to more conventional methods, in the Multi-Energy concept the explosion hazard is not primarily determined by the fuel-air mixture itself, but above all by the environment in which the vapour disperses - the boundary conditions to the combustion process. If somewhere a release of fuel is anticipated, the explosion hazard assessment can be limited to an investigation of the environment on potential blast generative capabilities.

Today, it is recognised more and more that it is very unlikely to have a detonation in a fuel-air cloud originating from an accidental release in the open. The point is that the inhomogeneity of the fuel-air mixture in the cloud, which is inherent to the process of atmospheric turbulent dispersion, generally prevents a possible detonation from propagating [Van den Berg et al., 1987]. The heavy explosion on December 7, 1970 at Port Hudson, MO., where almost all of a large unconfined vapour cloud detonated, should be blamed on an exceptional coincidence of circumstances. Lingering in a shallow valley under calm atmospheric conditions, a dense propane-air cloud had the opportunity to homogenise sufficiently by molecular diffusion during an exceptionally long ignition delay [NTSB, 1972 and Burgess and Zabetakis, 1973]. This incident is unprecedented, to our knowledge.
Therefore, in a vast majority of cases the assumption of deflagrative combustion is a sufficiently safe approach in a vapour cloud explosion hazard assessment. Deflagrative overpressures in a confined area, however, can lead to blast comparable to blast from a detonation.

5.5.2   Discussion

Deficiencies of the model

The Multi-Energy method is expected to reasonably match reality, wearing the ability to predict high, respectively low, overpressures in cases where they may be expected. Nevertheless, some deficiencies still exist and these should be covered before a solid procedure for the application method is possible.
These deficiencies concern:
−   the overpressure in an obstructed region (the 'source strength' or 'class number'),
−   the definition of an obstructed region,
−   the minimal distances between potential explosion sources for which these sources can be assumed to act independently (the 'separation distance').

Available guidance on the choice for the source strength

Since the introduction of the Multi-Energy method [Van den Berg, 1985], especially the lack of guidance in the choice of the source strength has been recognised and since then some guidance has become available. This is summarised next.

SRD, AEA Technology [Kinsella, 1993]

Kinsella [1993] provides guidance, based on a review of major accidents, to how to account, in the Multi-Energy method, for the influence of:
−   degree of obstruction by obstacles inside the vapour cloud,
−   ignition energy,
−   degree of confinement.

These three blast source strength factors are defined as follows.

−   Obstruction:
    –   High
        Closely packed obstacles within gas cloud giving an overall volume blockage fraction (i.e. the ratio of the volume of the obstructed area occupied by the obstacles and the total volume of the obstructed area itself) in excess of 30% and with spacing between obstacles less than 3 m.
    –   Low
        Obstacles in gas cloud but with overall blockage fraction less than 30% and/or spacing between obstacles larger than 3 m.
    –   None
        No obstacles within gas cloud.

−   Parallel plane confinement:
    –   Yes
        Gas clouds, or parts of it, are confined by walls/barriers on two or three sides.
    –   No
        Gas cloud is not confined, other than by the ground.

- Ignition strength
  - High
    The ignition source is, for instance, a confined vented explosion. This may be due to the ignition of part of the cloud by a low energy source, for example, inside a building.
  - Low
    The ignition source is a spark, flame, hot surface, etc.

The results of categorising are expressed in a matrix in Table 5.3 which gives the Multi-Energy method strength class numbers corresponding to the various combinations of the boundary and initial conditions.

Table 5.3   Initial blast strength index

Blast strength category	Ignition energy		Obstruction			Parallel plane confinement	Multi-Energy Unconfined	Class
	Low	High	High	Low	No			
	(L)	(H)	(H)	(L)	(N)	(C)	(U)	
1		H	H			C		7-10
2		H	H				U	7-10
3	L		H			C		5-7
4		H		L		C		5-7
5		H		L			U	4-6
6		H			N	C		4-6
7	L		H				U	4-5
8		H			N			4-5
9	L			L		C		3-5
10	L			L			U	2-3
11	L				N	C		1-2
12	L				N		U	1

Shell [Cates, 1991]

Although Cates [1991] does not apply the Multi-Energy blast charts, the decision tree presented can be used to estimate a source overpressure i.e. a Multi-Energy source strength class.
The decision tree is given in Table 5.4.

Table 5.4   Decision tree for determination of 'source strength' overpressure P_{sc}

START:		Is the hazard area, or any part of the hazard area more than 60% enclosed by walls, roof, obstacles etc.?
	YES:	Seek specialist advice on venting and blow-out panels
	NO:	Is the fuel which may leak, more reactive than ethene?
	YES:	Seek specialist advice or assume $P_{sc} = 800$ kPa.
	NO:	Are there any obstacles at all in the hazard area (No means all area is completely open)?
	NO:	Assume $P_{sc} = 10$ kPa.
	YES:	Are there any small, nearly enclosed areas where ignition may take place?
	YES:	There may be a risk of bang-box ignition (jet or high energy ignition)
	NO:	Is there any place from where the easiest route for gas to reach an unconfined area involves passing four or more successive obstacles?
	NO:	Assume $P_{sc} = 20$ kPa.
	YES:	Characterise successive obstacles by how much gap (for the gas to pass through) there is between them and how far successive obstacles are apart. Write down both these distances as a number of obstacle diameters and multiply them. Is the product more than 30?
	YES:	If there are less than 6 successive obstacles: $P_{sc} = 30$ kPa, for 6-7 successive obstacles $P_{sc} = 70$ kPa, for more than 7: $P_{sc} = 100$ kPa.
	NO:	Overpressures may be severe; if less than six obstacle layers, take $P_{sc} = 70$ kPa, if six or more, take $P_{sc} = 100$ kPa or get specialist assessment.

Mobil Research/Baker Engineering [Baker et al., 1994]

Based on an extensive survey of all available experimental investigations on VCE, guidance has been derived to a proper choice of the maximum flame speed to be expected. The guidance has been condensed in a table with three variables: obstacle density, flame expansion and reactivity. Three levels for each variable are available: high, medium and low obstacle density and reactivity and one-, two and three-

dimensional flame expansion. The table given by Baker et al. is presented here in Table 5.5. The flame speeds have been replaced by source overpressures according to the blast charts used by Baker et al.

Table 5.5   *Source overpressures P_{sc} for soft ignition sources*

1-dimensional flame expansion				
		Obstacle density		
		high (kPa)	medium (kPa)	low (kPa)
reactivity	high	>1000	>1000	>1000
	medium	800	400	200
	low	800	200	40
2-dimensional flame expansion				
		Obstacle density		
		high (kPa)	medium (kPa)	low (kPa)
reactivity	high	400	200	100
	medium	300	120	7
	low	120	70	4
3-dimensional flame expansion				
		Obstacle density		
		high (kPa)	low (kPa)	low (kPa)
reactivity	high	100	15	4
	medium	20	7	1
	low	15	7	1

The reactivity is chosen according to the 'Yellow Book', edition 1988, procedure [CPR-14E, 1988]. Methane and carbon monoxide have low reactivity. The laminar burning velocities of high reactivity fuels are, in excess of 0.8 m/s: hydrogen, acetylene, ethene oxide and propene oxide. All other fuels have medium reactivity.

Obstacle density is the most difficult to quantify. Low obstacle density is defined for situations in which there are few obstacles in the flame path, or the obstacles are widely spaced (less than 10% blockage ratio, i.e. the ratio of the area perpendicular to the flame direction occupied by obstacles to the total area itself) and there are only one or two layers of obstacles. High obstacle density situations have three or more fairly closely spaced obstacle layers of obstacles with a blockage ratio of 40% or more, per layer.

Discussion and recommendation

The information presented in the various publications gives some guidance to how to choose a source strength. The influence of the most important parameters

obstruction and confinement is shown. Kinsella [1993] takes into account the ignition strength while Baker [1994], and to some extent Cates [1991], adds reactivity.

Obstruction is characterised by either an obstacle volume blockage or an obstacle area blockage. Furthermore, the distance between obstacles for flame acceleration is maximised. This guidance demonstrates the influence of the most important parameters involved.

It should be emphasised though that application of this guidance is highly questionable. Still large uncertainties exist (as mentioned by the authors of these articles also) and absolute values for parameters should be distrusted. Results from experiments show that the actual overpressure can easily be underestimated by a factor 10 (or even up to a factor 30) when using this guidance [Mercx et. al., 1994].

It is therefore recommended to be conservative in the choice of a source strength for the initial blast and not to use this guidance at all.

The problems to quantify the influence of obstruction do not exist for the quantification of the reactivity. Based on scaling laws it is possible to predict the influence on the explosion effect if the type of gas is changed [Mercx et. al., 1994]. It is possible to obtain a relative rating with these laws. However, a reference is required for an absolute quantification and for that the influence of obstruction should be quantified too. One could decide on the maximum overpressure of methane for instance. British Gas assumes a maximum overpressure of four bars ($4 \cdot 10^5$ Pa) [Harris and Wickens, 1989], (see 5.3.2). This value complies with an explosion class of almost nine. Starting with this reference excludes the possibility of reactivity classification as most gases are more reactive than methane. This would lead to explosion class nine and ten only.

Therefore, the lack of knowledge of how to classify obstructions prohibits the classification for reactivity.

As a result, a proper choice for the initial strength of the blast-wave from an obstructed region cannot be motivated presently. It is recommended:
− to differentiate between obstructed and non-obstructed regions,
− to choose a high initial blast strength for each obstructed region: number 10,
− to choose a low initial blast strength for the remaining unobstructed region: number 1. In case initial low turbulence motion is expected in non-obstructed regions, for instance, due to the momentum of the fuel release, a number of 3 is advised,
− not to differentiate between reactivities.

If such a safe and conservative approach results in unacceptably high overpressures, a more accurate estimate for the initial blast strength may be found by consulting the growing body of experimental data on gas explosions, or by performing an experiment tailored to the situation in question.

Another possibility is numerical simulation with advanced computational fluid dynamic codes such as FLACS [Hjertager, 1982 and 1989], PHOENIX [Kjäldman and Huhtanen, 1985] or REAGAS [Van den Berg, 1989]. A way in which such codes could be utilised for vapour cloud explosion blast modelling has been demonstrated by Van den Berg et al. [1991].

The initial strength of the blast, however, is still a major issue of research.

It should be noted that applying the Multi-Energy method with an explosion class number 10, the overpressures will be similar to those obtained by applying the TNT-equivalence method with an efficiency factor of 20% to the **obstructed part** of the cloud (and not to the whole cloud).

5.5.3 Procedure for the division of an area into obstructed and unobstructed regions

A procedure to subdivide a region into obstructed and unobstructed parts is presented next.

The procedure given is thought to be safe and conservative in the sense that always too large a volume of the obstructed region will be selected. The procedure offers a possibility for optimisation, i.e. reduction, of the obstructed volume. This optimisation procedure can be followed but obviously requires more time. The optimisation procedure in itself will not lead to unsafe situations.

The procedure to build-up an obstructed region is based on the effect obstacles have on the generation of turbulence in the expansion flow ahead of the flame. A zone with obstacle induced turbulence will exist behind an obstacle. The length of this zone is related to a characteristic dimension of the obstacle. However, if the scale of an obstacle becomes larger, it is assumed that the length of the influenced zone is bounded by an upper value.

The procedure is as follows.

Step 1: break-down structures into basic geometrical structural shapes

Structures in a potential hazardous area like an industrial site may be considered as being composed of (or fairly well bounded by) basic geometrical shapes:
- cylinders with length l_c and diameter d_c
- boxes with dimensions b_1, b_2, b_3
- spheres with diameter d_s

Step 2: assume an ignition location

After ignition of a flammable cloud in a congested area the flame will travel outward so the orientation with respect to the flame propagation direction of each obstacle is known.

Step 3: determine obstacle orientation

Take the **smallest** dimension oriented in a plane perpendicular to the flame propagation direction to be D_1, then:
$D_1 = l_c$ or d_c for a cylinder
$D_1 =$ smallest of b_1 and b_2, b_2 and b_3, or b_1 and b_3 for a box
$D_1 = d_s$ for a sphere

Take the obstacle dimension parallel to the flame propagation direction to be D_2.

Step 4: build-up of obstructed region

An obstacle belongs to an obstructed region if the distance from its centre to the centre of any obstacle in the obstructed region is smaller than 10 times D_1 or 1.5 times D_2 of the obstacle under consideration in the obstructed region (D_1 and D_2 belonging to any obstacle in the obstructed region).
If the distance between the outer boundary of the obstructed region and the outer boundary of the obstacle is larger than 25 m, then the obstacle does not belong to that obstructed region.

Note there are values given to three factors. These are a factor times D_1 and a factor times D_2 (respectively 10 and 1.5) for obstacle distances, and a value (25 m) for the distance between obstructed region and obstacle to determine if the obstacle is part of that obstructed region. It is not yet possible to quantify these values accurately. The values given are thought to be safe though.

Step 5: defining a box containing the obstructed region

The obstructed region is defined as a box that contains all the obstacles in the obstructed region,
including: the space between a confining surface and an obstructed region in case the distance between that surface and any obstacle in the obstructed region is less than 10 times D_1 or 1.5 times D_2 (for instance the earth's surface)
excluding: parts of cylinders or boxes that clearly do not belong to the obstructed region, such as upper parts of chimneys, distillation columns (vertically oriented cylinders) or pipes (horizontally oriented cylinders) connecting, for instance, chemical units, each potentially being an obstructed region, at a chemical plant.
The excluded parts may form an obstructed region in themselves.

The free volume of the obstructed region V_r is de volume of the box minus the space occupied by the obstacles. In case it is not possible to calculate or estimate the volume occupied by the obstacles, assume V_r equals the total volume of the box.

Step 6: subdivision into multiple boxes

The box containing the obstructed region smooths the outer boundary of the actual obstacle boundaries, thereby including additional space free of obstacles. In case this free space is not included in the obstructed region by the procedure for building-up the obstructed region but by drawing the box around the obstructed region, sub-division into multiple directly adjacent boxes is acceptable for reducing the volume of the obstructed region.

Step 7: define additional obstructed regions if appropriate

In case not all obstacles present are inside the obstructed region, possibly more obstructed regions within the cloud can be defined.
In that case, the region where ignition occurs is called the 'donor' region, the other regions are 'acceptor' regions.

The direction of flame propagation, required for the orientation of the obstacles in the acceptor region, depends on the orientation of the acceptor region with respect to the donor region.

If separate obstructed regions are located close to each other, they may be initiated more or less at the same time. The coincidence of their blasts in the far-field may not be ruled out and the respective blasts should be superposed.
Presently there is no guidance to the minimum distance between donor and acceptor regions at which they can be assumed to be separate explosions. Due to this lack, a great possibility of reducing the hazards of a vapour cloud explosion can not be realised. The procedure for applying the Multi-Energy method described in the next section contains a safe and conservative approach to cover this deficiency.

Remarks

Due to the choice of having a high initial blast strength for an obstructed region, the need for having a clear definition of an obstructed region grows.
The exact boundaries of an obstructed region are in fact not very important to the determination of blast. According to the blast charts (Figure 5.8), the energy E has to be raised to the power of 1/3.

The subdivision of a hazardous site into obstructed and unobstructed regions and the attribution of a source strength to each region is a major issue in ongoing research. As a simplified Multi-Energy method is applied here, a simplified procedure for the subdivision into obstructed and unobstructed regions is adapted.

In order to obtain a rather straightforward, easy to apply and fully closed procedure, a number of influences which lead to reduction of the explosion severity, have been neglected. This indicates that further optimisation is possible but that this should be obtained through consultation of experts.

5.5.4   Procedure for the application of the Multi-Energy method

The procedure of vapour cloud explosion blast modelling according to the Multi-Energy concept can be subdivided into a number of steps. Figure 5.9 shows these successive steps.

Apply constraints

↓

Determine cloud size

↓

Recognise potential blast sources

↓

Define obstructed regions

↓

Estimate boundaries of obstructed regions or use procedure of section 5.5.3 → section 5.5.3

Break down structures into basic geometric structural shapes

↓

Assume an ignition location

↓

Determine obstacle orientation

↓

Build up obstructed region

↓

Define a box containing the obstructed region

↓

Subdivide into multiple boxes

↓

Define additional obstructed regions if appropriate

Estimate the source strength or class number for each region

↓

Combine obstructed regions

↓

Locate unobstructed part of vapour cloud

↓

Calculate radius

↓

Calculate blast parameters

↓

Handle multiple obstructed regions

↓

Construct blast history at specific location

Figure 5.9   Flow diagram for application of the method

Step 1: application constraints

- Realise that the Multi-Energy method is used for determination of the blast parameters from 'unconfined' vapour cloud explosions. Blast from vented vapour cloud explosions and from internal explosions should be assessed using other methods. These methods can be either semi-emperical like the methods of Bradley and Mitcheson [Harris, 1983] or deterministic like the computational fluid dynamics (CFD) codes AutoReaGas, FLACS, EXSIM and others.
- Realise that the Multi-Energy method is a simplification of reality. It does not take into account directional blast effects due to the inhomogeneous distribution of confinement and obstruction of the vapour cloud or due to the non-point-symmetrical shape of the vapour cloud. Use more sophisticated models, like the CFD codes mentioned above, to assess these aspects.
- Assume that blast modelling on the basis of deflagrative combustion is a sufficiently safe and conservative approach. Keep in mind that unconfined vapour cloud detonation is extremely unlikely and has only a single precedent, to our present knowledge.

Step 2: determination of cloud size

- Determine the mass quantity after an accidental release that can contribute to the formation of a flammable cloud.

In general, a dispersion calculation will preceed the explosion calculation. See section 5.7 on how to calculate the flammable mass quantity within a cloud.
In case no dispersion calculation is made, the mass quantity has to be estimated. In a safe approach one could assume that the whole mass inventory contained within the process unit under consideration, contributes to the formation of a flammable cloud. In case of pool evaporation one could multiply the evaporation rate by a certain time period to come up with a mass quantity.

- Calculate the volume V_c of a cloud with a density ρ containing the flammable mass quantity Q_{ex} at stoichiometric concentration c_s (c_s in vol.%) with:

$$V_c = Q_{ex}/(\rho \times c_s) \hspace{3cm} (m^3) \hspace{1cm} (5.7)$$

Step 3: recognition of potential blast sources

- Identify potential sources of blast in the vicinity of a postulated location of the centre of the cloud.

Potential sources of strong blast are, for example:
- extended spatial configuration of objects, e.g. process equipment at chemical plants or refineries piles of crates,
- the space between extended parallel planes, e.g.
    - underneath groups of closely parked cars on parking lots or marshalling yards,
    - open buildings, e.g. multi-story parking garages,
- the space in tubelike structures, e.g.
    - tunnels, bridges, corridors,
    - sewage systems, culverts,
- an intensely turbulent fuel-air mixture in a jet due to release at high pressure.

Step 4: define obstructed regions

− Define obstructed regions using the procedure given in the previous section or estimate boundaries of obstructed regions and determine the free volume V_r of each obstructed region.
− Determine the maximum part of the cloud V_{gr} that can be inside the obstructed regions.
− Calculate the volume V_o of the unobstructed part of the vapour cloud with:

$$V_o = V_c - V_{gr} \qquad\qquad (m^3) \quad (5.8)$$

− Calculate the energy E of each region, obstructed as well as unobstructed, by multiplying V_{gr} and V_o by the combustion energy per unit volume.

Step 5: estimate the source strength or class number for each region

As has been explained before, a conservative approach would be to choose a class number of 10 for each obstructed region. Other numbers may be chosen based on additionally obtained information if required. Choose a low initial blast strength for the remaining unobstructed regions: number 1. In case initial low turbulence motion is expected in unobstructed regions, for instance, due to the momentum of the fuel release, a number of 3 is advised.

Step 6: combination of obstructed regions

In case more than one obstructed region has to be considered:
− Define an additional blast source (obstructed region) by adding all energies of the separate blast sources together and by assuming a centre for the additional blast source. This centre can be determined by considering the centres of the separate blast sources and their respective energies.

Step 7: location of unobstructed part of vapour cloud

− Determine a centre for the unobstructed vapour cloud volume. This centre can be determined by considering the centres of the separate unobstructed regions and their respective energies.

Now, a certain number of explosion centres and their respective energies E have been determined. For each centre the blast parameters as a function of distance to its centre can be calculated using the blast charts given in Figure 5.8.

Step 8: calculate radius

− Model the blast from each source by the blast from an equivalent hemi-spherical fuel-air charge of volume E/E_v m^3 ($E_v = 3.5$ MJ/m^3 is an average value for most hydrocarbons at stoichiometric concentration). Form an impression of the scale by calculation the radius r_o for each blast source from:

$$r_o = (3/2 \times E/(E_v \times \pi))^{1/3} \qquad\qquad (m) \quad (5.9)$$

Step 9: calculate blast parameters

The blast parameters at a specific distance r from a blast source can be read off Figure 5.8 A, B and C after calculating the scaled distance r'.

− Calculate the scaled distance r' with:

$$r' = r/(E/p_a)^{1/3} \qquad\qquad (\text{-}) \qquad (5.2)$$

− Depending on the class number 1, 3 or 10, read the scaled peak side-on overpressure P_s', the scaled dynamic peak pressure p_{dyn}' and the scaled positive phase duration t_p' off the respective blast charts in Figure 5.8.

− Calculate the peak side-on overpressure P_s, the peak dynamic pressure p_{dyn} and the positive phase duration t_p with:

$$P_s = P_s' \times p_a \qquad\qquad (\text{Pa}) \qquad (5.3)$$

$$p_{dyn} = p_{dyn}' \times p_a \qquad\qquad (\text{Pa}) \qquad (5.5)$$

$$t_p = t_p' \times (E/p_a)^{1/3}/a_a \qquad\qquad (\text{s}) \qquad (5.4)$$

− Determine the shape of the blast-wave from the Figure 5.8.

− Calculate the positive impulse i_s by integrating the overpressure variation over the positive phase which can be approximated by multiplying the side-on overpressure with the positive phase duration and with a factor 1/2:

$$i_s = 1/2 \times P_s \times t_p \qquad\qquad (\text{Pa·s}) \qquad (5.6)$$

Step 10: handling of multiple obstructed regions

If separate blast sources are located close to each other, they may be initiated more or less at the same time. The coincidence of their blasts in the far-field may not be ruled out and the respective blasts should be superposed. This should be accomplished by taking the respective quantities of combustion energy of the sources in question together.
To determine the parameters in the blast-wave at a specific distance, one should use the blast source as defined in step 6.

Step 11: construct the blast history at a specific location

Combustion in the unobstructed region is considerably different from combustion in an obstructed region. Blast from an obstructed region will result in sharp and relatively short peaks (shock-waves). The relatively slow combustion in an unobstructed region will result in pressure waves of long duration. Due to the influence of the respective energies, however, either of the blast-waves can be of importance at a specific location.

5.51

It may be assumed that the blast history at a specific location consists of the blast parameters and blast shape resulting from the obstructed region on which the blast parameters of the unobstructed region are superposed.

5.6   Application of selected models: calculation examples

5.6.1   Introduction to section 5.6

Examples are given to show how the procedures described in this chapter work.
In section 5.6.2 the procedure of defining and refining of an obstructed region is elucidated for a specific hazardous site.
In section 5.6.3 ignition of a specific vapour cloud located in the hazardous site of section 5.6.2 is postulated and the blast parameters are determined.
Two situations are considered in section 5.6.3. One in which the obstructed region is larger and one in which the obstructed region is smaller than the vapour cloud volume (respectively 5.6.3.1 and 5.6.3.2).
Section 5.6.4 gives the determination of the obstructed region for a more complex lay-out.

5.6.2   Definition of an obstructed region

The boundaries of obstructed regions can be chosen by carefully considering the lay-out of a hazardous site. In case of doubt or in case a more precise definition is required, the more time consuming procedure of section 5.5.3 can be followed. This procedure will be followed here.

As an example for the build-up of obstructed regions on a hazardous site, an LPG storage and distribution centre is chosen. The picture in Figure 5.10 shows an overview. Figure 5.11 gives a map from which it becomes clear that the LPG installation at San Juan Ixhuatepec near Mexico City was the basis for this example [Pietersen, 1985].

The facility comprises 6 spherical storage tanks, 4 with a volume of 1600 m^3 and 2 with a volume of 2400 m^3. An additional 48 horizontal cylindrical bullet tanks are situated near the large spheres.
The total storage capacity of about 16000 m^3.
The storage is subdivided into 6 zones, see Figure 5.12.
Horizontal distances are given in Figure 5.13.

Additional dimensions are:
− the minimum height underneath the bullet tanks is 2 m;
− the minimum height underneath the spheres is 2 m;
− additional pipework on top of cylinders and spheres has a height of 0.5 m;
− the storage area is surrounded by an open corridor of 30 m width;
− alongside the length of the outer cylinders, stairs with a width of 1.5 m are situated.

Figure 5.10   Picture of LPG storage facility

From the first glance it will be clear that any of the groups of cylinders or spheres are an obstructed region.

Step 1: break-down of structures into basic geometrical structural shapes

The structures exist of big spheres and cylinders. Other structures like stairs, walkways, supports, pipes will not be considered here. This is a valid approach: the dimensions of the large obstacles will dominate the process of building an obstructed region: 10 times D_1 of a big obstacle will override 10 times D_1 of a small obstacle located near the larger one (step 4). Figure 5.12 shows all major basic geometrical structural shapes.

Step 2: assume an ignition location

Assume ignition in the centre of the southern group of cylinders in zone 4 (figure 5.13).

The build-up of the obstructed region is started by taking the cylinder west of the ignition location as a start (marked as 1).
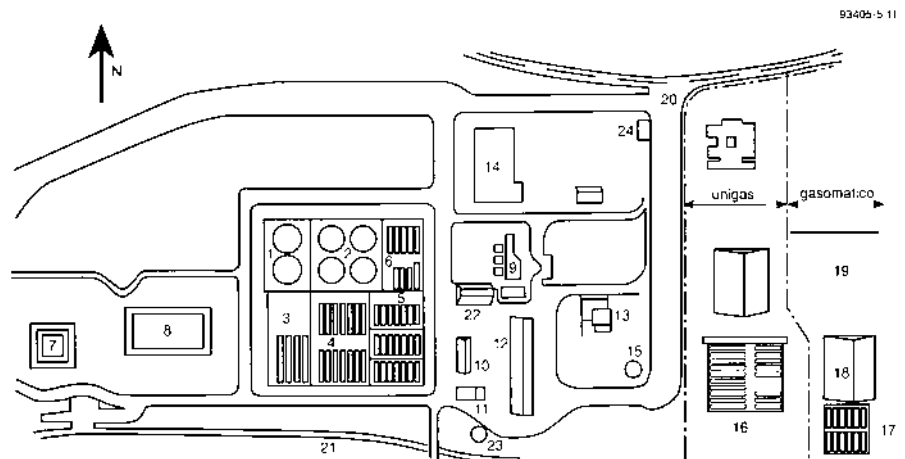
Figure 5.11   Plan of LPG installation

Legenda:

1	2 spheres of 2400 m³, ds = 16.5 m	12	car loading
2	4 spheres of 1600 m³, ds = 14.5 m	13	gas boille store
3	4 cylinders of 270 m³, dc = 3.5 m, length = 32 m	14	pipe/valve manifold
4	14 cylinders of 180 m³, dc = 3.5 m, length = 21 m	15	waterlower
5	21 cylinders of 36 m³, dc = 2 m, length = 13m	16	LPG storage Unigas
6	6 cylinders of 54 m³, dc = 2 m, length = 19 m	17	Storage Gasomatico
	3 cylinders of 45 m³, dc = 2 m, length = 16 m	18	battling terminal
		19	depot cars with boilles
7	flare pit	20	entrance
8	pond	21	rail car loading
9	control room	22	store
10	pumphouse	23	watertank
11	fire pumps	24	garrison
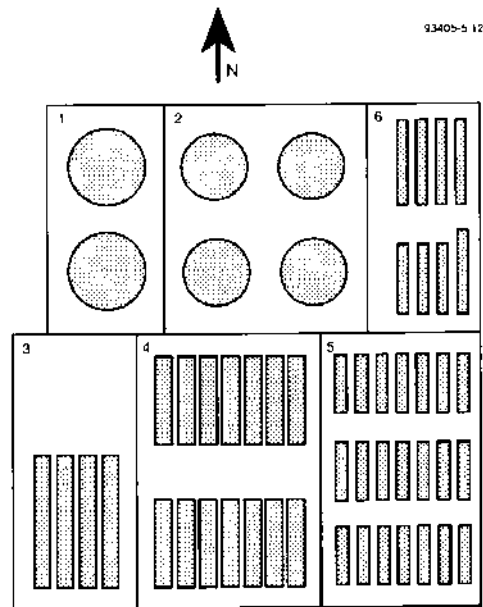
Figure 5.12   Division into zones
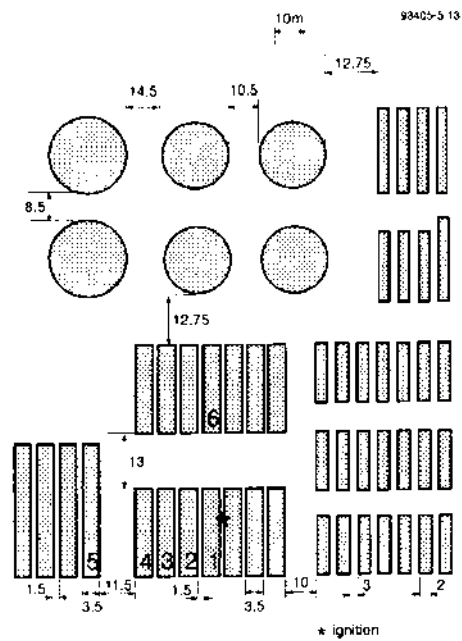
Figure 5.13   Build-up of obstructed region

Step 3: determine obstacle orientation

In order to decide whether cylinder 2 is part of the obstructed region, values for D_1 and D_2 have to be determined. Following the direction of flame propagation from the ignition location, via cylinder 1 towards cylinder 2, the orientation of the axis of cylinder 1 is perpendicular to the direction of flame propagation. Therefore both D_1 and D_2 equal the diameter 3.5 m in this case.

Step 4: build-up of obstructed region

The distance between cylinder 1 and the adjacent, cylinder 2 is 1.5 m. This distance is smaller than 10 times D_1 and also smaller than 1.5 times D_2. Thus, cylinder 2 is part of the obstructed region.

The obstructed region is enlarged to include now cylinder 1 and 2.

It is obvious that all seven cylinders of the southern group in zone 4 are within one obstructed region.

The distance between the east cylinder in zone 3 (number 5) and the west cylinder of the obstructed region (number 4) is 11.5 m. D_1 and D_2 both equal still 3.5 m. Thus cylinder 5 belongs to the obstructed region too.
It is can be easily derived that all 4 cylinders of zone 3 belong to the obstructed region also.

The distance between the northern and southern group of cylinders in zone 4 is 13 m. In this case $D_1 = 3.5$ m and $D_2 = 21$ m. The distance of 13 m is smaller than 10 times D_1 and 1.5 times D_2. Thus, cylinder 6 and all other cylinders in that group are part of the obstructed region.

Repeating the procedure for the other cylinder groups as well as the spheres, results in one obstructed region covering all cylinders and spheres.
Additional pipework and stairs located within a distance of D_1 or D_2 from a sphere or cylinder belongs to the obstructed region too.

Step 5: define box containing the obstructed region

A box containing all obstacles in the obstructed region has the following dimensions length: 108.5 m, width 110 m, and height 19.5 m (Figure 5.14, 19.5m is the height of the highest cylinder including pipework on top).
The space underneath the obstacles is part of the obstructed region too, the distance of 2m to a confining surface (the earth) is smaller than 10 times D_1 or 1.5 D_2, or all big obstacles.

A single big box in this case includes large volumes of free space, due to the large variation in height between cylinders and spheres. A sub-division into multiple directly adjacent boxes is therefore beneficial.
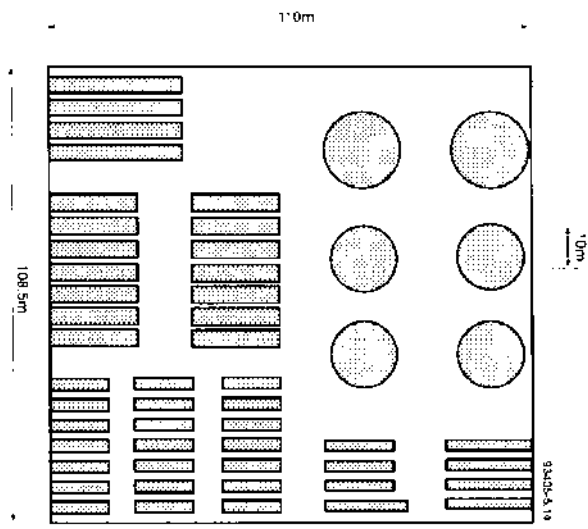
Figure 5.14   Single box
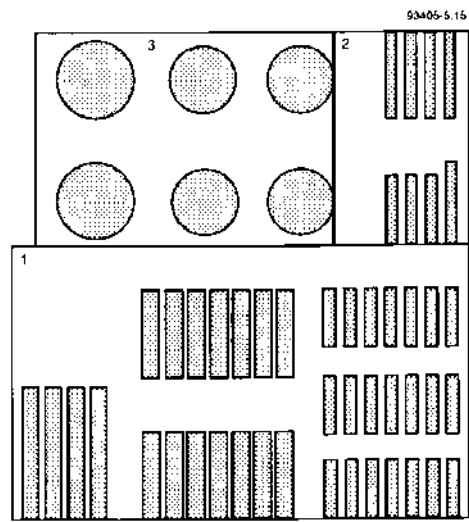
Figure 5.15   Three boxes

Step 6: subdivision in multiple boxes

A first subdivision into 3 boxes is shown in Figure 5.15
Box 1:   contains the cylinders in zones 3,4 and 5;
         dimensions: length 108.5 m, width 65 m and height 6 m.
Box 2:   contains the cylinders in zone 6;
         dimensions: length 45 m, width 31.25 m and height 4.5 m.
Box 3:   contains all spheres in zone 1 and 2;
         dimensions: length 65.5 m, width 45 m, height 19.5 m.

A second further subdivision is possible as the free space in box 1 north of zone 3 does not belong to the obstructed region. All other free space between groups of cylinders are part of the obstructed region and can therefore not be excluded by further subdivision into multiple boxes.
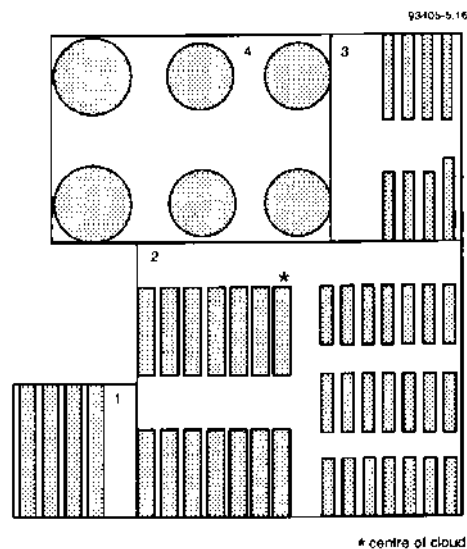
Figure 5.16   Four boxes

We now have four boxes (Figure 5.16):
Box 1:   contains the cylinders in zone 3 and the space between zones 3 and 4;
         dimensions: length 32 m, width 31.5 m, height 6 m.
Box 2:   contains the cylinders in zones 4 and 5 and the space between zones 4 and 2, and 5 and 6;
         dimensions: length 77 m, width 65 m and height 6 m.
Box 3:   contains the cylinders in zone 6;
         dimensions length 45 m, width 31.25 m and height 4.5 m.
Box 4:   contains all spheres in zone 1 and 2;
         dimensions: length 65.5 m, width 45 m, height 19.5 m.

The volume of the obstructed region is the sum of the volumes of the four boxes minus the space occupied by the obstacles:

Box 1: $32 \times 31.5 \times 6$ = 6048 m^3
Box 2: $77 \times 65 \times 6$ = 30030 m^3
Box 3: $45 \times 31.25 \times 4.5$ = 6328 m^3
Box 4: $65.5 \times 45 \times 19.5$ = $\underline{57476}$ m^3
         Total volume   = 99882 m^3

The volume of the cloud inside the obstructed region is determined by deduction of the volume of the cylinders and spheres of the volume of the obstructed region.

The storage capacity is 16000 m^3 which is assumed to equal the volume of the storage vessels.

So: V_{gr} = 99882 - 16000 = 83882 m^3

Obviously, further subdivision is possible and acceptable as long as the rules for subdivision are followed. One has to balance the benefit from further subdivision (which can be rather small) with the required time to perform the subdivision (which can be rather long) in order to decide to which level of detail subdivision is carried out.

Step 7: define additional obstructed regions if appropriate

As all obstacles present are inside the one obstructed region defined, no additional obstructed regions are requested.

5.6.3   Vapour cloud explosion

Vapour cloud smaller than obstructed region

The blast parameters resulting from a vapour cloud explosion located in the LPG storage facility of the example in section 5.6.2 will be determined. A table will be composed showing at what distances a specific side-on overpressure is expected to occur. The other blast parameters are calculated at these distances.

Step 1: application constraints

The incident of an accidental release of flammable material will probably have a number of effects with a number of consequences. Due to the explosion, domino effects are expected. Pressurised vessels may be shifted and damage and even fail, creating physical explosions, BLEVES, fires and missiles.
The Multi-Energy method is to be used for the determination of the blast parameters as a result of a relatively large and initially non-turbulent flammable fuel-air cloud. Determination of blast as a result of bursting vessels is treated in chapter 7 'Rupture of Vessels'.

Step 2: determination of cloud size

Due to a failure of a feed pipe to one of the cylindrical vessels, a certain amount of liquid propane is spilt in the bunt underneath the vessels. The spill starts to evaporate and a fuel-air cloud is generated which fills the space between the storage tanks. It is assumed that at the moment of ignition 4750 kg liquid propane has evaporated.

It is assumed that the evaporated propane has mixed with air stoichiometrically (4%) and that the temperature of the mixture is 15 ˚C.
The density of propane vapour at 15 ˚C is 1.86 kg/m^3 so the volume of the cloud equals

$V_c = 100/4 \times 4750/1.86 = 63844$ m^3

Step 3: recognition of potential blast sources

Here, only blast sources relating to a vapour cloud explosion are at issue.
According to the guidance given in section 5.5.4, potential blast sources are underneath all cylinders and spheres.

Step 4: define obstructed regions

The example in section 5.6.2 defines a single obstructed region comprising four boxes. It is calculated there that

$V_{gr} = 83882$ m^3

The volume of the vapour that can be contained in the obstructed region is larger than the volume of the assumed cloud. Therefore V_{gr} is reduced to V_c:

$V_{gr} = V_c = 63844$ m^3

The centre of the vapour cloud is taken as the approximate centre of the obstructed region: the north end of the most eastern cylinder in the northern cylinder group of zone 4 see Figure 5.16.

The volume of the unobstructed part of the cloud is zero:

$V_o = 0$ m^3

The heat of combustion of a stoichiometric propane air mixture is 3.46 MJ/m^3 so the energy E of the blast source is:

$E = 3.46 \times 10^6 \times 63844 = 221$ GJ

Step 5: estimate the source strength

A strength number 10 is selected.

Step 6: combination of obstructed regions

Not applicable.

Step 7: location of unobstructed part of the cloud

Not applicable.

Step 8: calculate radius

From equation (5.9):

$$r_o = \left(\frac{3}{2 \times \pi} \times 63844 \right)^{1/3}$$

follows: $r_o = 31$ m

Step 9: calculate blast parameters

In case one wants to know at which distance a specific overpressure occurs (for instance $P_s = 10$ kPa):

The dimensionless peak side-on overpressure is:

$P_s' = P_s/p_a = 10/100 = 0.1$

Select on the vertical axis of Figure 5.8C the value 0.1 and pick the point where the pressure decay line belonging to a class strength of 10 crosses this value. Select on the horizontal axis the value of the scaled distance that belongs to the scaled pressure of 0.1 and the class 10 line.

It is found that:

$r' = 3$

The actual distance equals:

$r = r' \times (E/p_a)^{1/3} = 3 \times (221 \times 10^9/1 \times 10^5)^{1/3} = 3 \times 128 = 385$ m

The other blast parameters at that distance are calculated as follows:

The positive phase duration t_p at a distance of 390 m is:

$r' = 3$

From Figure 5.8C:

$t_p' = 0.38$ (class 10)

$t_p = t_p' \times (E/p_a)^{1/3} /a_a = 0.38 \times (221 \times 10^9/1 \times 10^5)^{1/3} / 340 = 0.146$ s $= 146$ ms

The positive impulse:

$$i_s = 1/2 \times P_s \times t_p = 1/2 \times 10^4 \times 0.146 = 730 \text{ Pa·s}$$

The peak dynamic pressure, use figure 5.8B:

at r' = 3:

$$p_{dyn}' = 0.003 \text{ (class 10)}$$

$$p_{dyn} = p_{dyn}' \times p_a = 0.003 \times 1 \times 10^5 = 300 \text{ Pa}$$

The shape of the blast-wave:

The pressure decay line belonging to class 10 is solid, which means the shape of the blast is that of a shock-wave.

To get an impression of distances and blast parameters, Table 5.6 shows the result of some calculations.

Table 5.6   Distances for specific blast overpressures and remaining blast parameters

P_s (kPa)	r' (-)	r (m)	t_p' (-)	t_p (ms)	p_{dyn} (kPa)	i_s (Pa*s)	shape
100	0.7	92	0.18	68	23	3403	shock-wave
50	1	131	0.23	87	7.1	2184	shock-wave
20	1.8	229	0.32	122	1.3	1210	shock-wave
10	3	385	0.38	146	0.3	730	shock-wave
5	5.2	682	0.44	168	< 0.01	419	shock-wave

Vapour cloud larger than obstructed region

The hazardous location is now assumed to consists only of the cylindrical vessels of zone 4 (Figure 5.12). All other data remains similar to that in section 5.6.2.

A table will be composed similar to Table 5.6 in order to get an impression of the reduction in distance at which a specific side-on overpressure is expected to occur. Also, the effect of the unobstructed part of the cloud is demonstrated.

Only the appropriate steps are addressed here:

Step 2:

$$V_c = 63844 \text{ m}^3$$

Step 4:

The obstructed area is now a box enclosing all vessels, stairs and pipework in zone 4. The box has dimensions: length 37.5 m, width 55 m and height 6 m.

$V_r = 37.5 \times 55 \times 6 = 12375 \text{ m}^3$

$V_{gr} = 37.5 \times 55 \times 6 - 14 \times 180 = 9855 \text{ m}^3$

$V_{gr} < V_c$

$V_o = V_c - V_{gr} = 63844 - 9855 = 53989 \text{ m}^3$

Obstructed region:　　　　$E = 9855 \times 3.46 \times 10^6 = 34 \text{ GJ}$.
Unobstructed region:　　　$E = 53989 \times 3.46 \times 10^6 = 187 \text{ GJ}$.

Step 5:

Class number for obstructed region is taken to be 10.
Class number for unobstructed region is taken to be 3.

Step 7:

The location of the centre of both the obstructed and unobstructed region is taken to be the centre of zone 4.

Step 8:

Obstructed region:　　　　$r_o = 16.8$ m.
Unobstructed region:　　　$r_o = 29.5$ m.

Step 9:

The blast parameters for the obstructed and unobstructed region are determined for specific values of the peak side-on overpressure (Table 5.7A).
For the distances r belonging to specific peak side-on overpressures, the blast parameters for the unobstructed region have been determined (Table 5.7B)

Table 5.7A Distances for specific blast overpressures and remaining blast parameters (obstructed region, class 10)

P_s (kPa)	r' (-)	r (m)	t_p' (-)	t_p (ms)	p_{dyn} (kPa)	i_s (Pa*s)	shape
100	0.7	50	0.18	37	22	1800	shock-wave
50	1	70	0.23	47	7.2	1173	shock-wave
20	1.7	122	0.32	65	1.3	653	shock-wave
10	2.9	206	0.38	78	0.3	390	shock-wave
5	5.2	365	0.44	90	< 0.01	225	shock-wave

Table 5.7B Distances for specific blast overpressures and remaining blast parameters (unobstructed region, class 3)

P_s (kPa)	r' (-)	r (m)	t_p' (-)	t_p (ms)	p_{dyn} (kPa)	i_s (Pa*s)	shape
5	0.58	72	2	734	0.73	1834	pressure wave
4	0.81	100	2	734	0.3	1467	pressure wave
3	1.1	136	2	734	0.12	1100	pressure wave
2	1.7	204	2	734	< 0.1	733	pressure wave
1	3.4	415	2	734	< 0.1	367	pressure wave

5.6.4   Determination of obstructed region

The lay-out of the previous example, the LPG storage and distribution centre, was quit straightforward. Therefore, another example is given regarding determination of the obstructed region for a more complicated case.

Description of the site

Figure 5.17A shows a three-dimensional view of the chemical unit under consideration. There only equipment is shown. Supporting structures and some buildings were omitted for visuality. Figure 5.17B shows the floor plan at ground level. The unit is located on a rectangular site of 120 x 50 m.
In order to get a better impression of the unit, additional Figures (5.17C through G) are added showing side-views from various locations. These locations are indicated in Figure 5.17A by C through G.
The area is sub-divided into two small and two large sections by two perpendicular pipebridges (Figure 5.17H), both having a width of 8m, a height of 10m and lengths of 100 and 50 m respectively. The main items within each sector are given next:

The two smaller sections consist of:
- I: a storage area with the tanks AD16 and AD26, diameter 8m, height 12m. total area 25 x 21 m^2 (Figure 5.17 C);

- II: substation #92, height 10m, total area 25 x 21 m^2.

The two larger sections consist of vertical columns and installations on multi-level supporting structures:
- III: columns AT3 diameter 5m, height 40m, with adjacent support structure height 16m (Figure 5.17E);
   AT8 diameter 2.5m, height 12m (Figure 5.17E);
   AT4 diameter 5.8m, height 50m (Figure 5.17D);
   AD-433 diameter 4m, height 6m (Figure 5.17D);
   multi-level structure 25 x 15 m^2 of variable height 16.5, 33 and 45m (Figure 5.17D);
   total area 87 x 21 m^2;
- IV: columns AF1 average diameter 6m, height 40m (Figure 5.17G);
   AT5 diameter 5m, height 30m (Figure 5.17F);
   AT6 diameter 2.5m, height 15m (Figure 5.17F);
   multi-level structure 20 x 15 m^2, with columns AR2A and AR2B diameter 5m, height 20m (Figure 5.17F);
   total area 87 x 21 m^2.

Determination of obstructed region

The flow diagram of section 5.5.4 gives the possibility to determine the volume of the congested regions in two ways: by rough estimation or by the procedure of section 5.5.3 in case such a procedure may be required.

Estimation of volume:

The average height of the site is assumed to be 15m. Together with outer dimensions of 120 x 50 m, this leads to a volume of the obstructed region of 90000 m^3.

Application of procedure:

Step 1: break-down structures into basic geometrical shapes

The installation consists of a combination of horizontally and vertically orientated cylinders supported by elements such as beams and columns. There are some box-type shapes the largest of which is sub-station#92 in section I. The open multi-level supporting structures should be considered as composed of a number of smaller geometrical shapes, rather than one big shape. There are no spheres.
The dimensions of the bigger obstacles are given next as it will appear (step 4) that only those are decisive for the build-up of the obstructed region:

- Cylinder AD16, d_c: 8   m, l_c: 12 m;
- Cylinder AD26, d_c: 8   m, l_c: 12 m;
- Box #92, b_1: 20   m, b_2: 15 m, b_3: 10 m;
- Cylinder AT3, d_c: 5   m, l_c: 40 m;
- Cylinder AT8, d_c: 2.5 m, l_c: 12 m;
- Cylinder AT4, d_c: 5.8 m, l_c: 50 m;
- Cylinder AF1, d_c: 6   m, l_c: 40 m;
- Cylinder AD-433, d_c: 4   m, l_c: 6 m;
- Cylinder AT5, d_c: 5   m, l_c: 30 m;
- Cylinder AT6, d_c: 2.5 m, l_c: 15 m;
- Cylinders AR-2A and B, d_c: 4   m, l_c: 20 m.

Step 2: assume ignition location

Ignition is assumed to occur in between the multi-level structure and AT3 in section III. It is not expected that variation of the ignition location will result in variable dimensions of the congested region. The location has to be chosen for starting the build-up of the obstructed region in step 4.

Step 3: determine obstacle orientation

The flame will mainly propagate horizontally. Horizontal dimensions of the site are larger than the vertical ones. The flame will pass more obstacles in the horizontal plane.
For all vertical cylinders: $D_1 = d_c$ and $D_2 = l_c$.

Step 4: build-up of obstructed region

The nearest large obstacle to the ignition location is AT3. It forms a congested region with all obstacles within a distance smaller than 10 x D1 or 25m. The latter value is decisive in this case. This implies that the whole multi-level support structure in section III, the long pipebridge separating section III and IV, the multi-level support structure in sector IV and the area around AT8 is part of the obstructed region.

A big cylinder located in the multi-level structure in sector III is AD-433. Within 10 x D_1 (40m) or 25m of this cylinder, AT4 is located. So AT4 is also part of the obstructed region. Sector I and II as well as the shorter pipebridge are located within 10 x D_1 (58m) or 25m of AT4, so they are part of the obstructed region too.

AT6 is within 25m of AR-2B and AT5 is close to AT6, so these are included as well as is AF1 which is located about 20m from AR-2A.

Some smaller horizontal oriented cylinders located along the long edges of the site (Figure 5.17A and B) are also within the obstructed region.

The procedure leads to the result that the whole site is part of the obstructed region.

The volume of the vapour cloud inside the obstructed region V_{gr} is to be determined from the comparison of the free volume in the obstructed region V_r (step 5 from paragraph 5.5.3) and the volume of a cloud with stoichiometric concentration V_c (step 2 of paragraph 5.5.4).

Step 5: defining a box containing the obstructed region

Step 6: subdivision into multiple boxes

A box containing the obstructed region has the dimensions of the site: 120 x 50m with a height equal to the highest vertical cylinder (50m, AT4).
Subdivision into multiple boxes is done by reducing the height where possible, i.e. where the distance between obstacles is larger than 25m.
A result is shown in Figure 5.17I. This figure shows the subdivision of the obstructed region into multiple boxes. The height as well as the volume of each particular box is given. The boundary of the obstructed region is also indicated in Figures 5.17C through G. Further subdivision is possible but will require considerable effort.

The total volume of the obstructed region equals 82421 m^3.
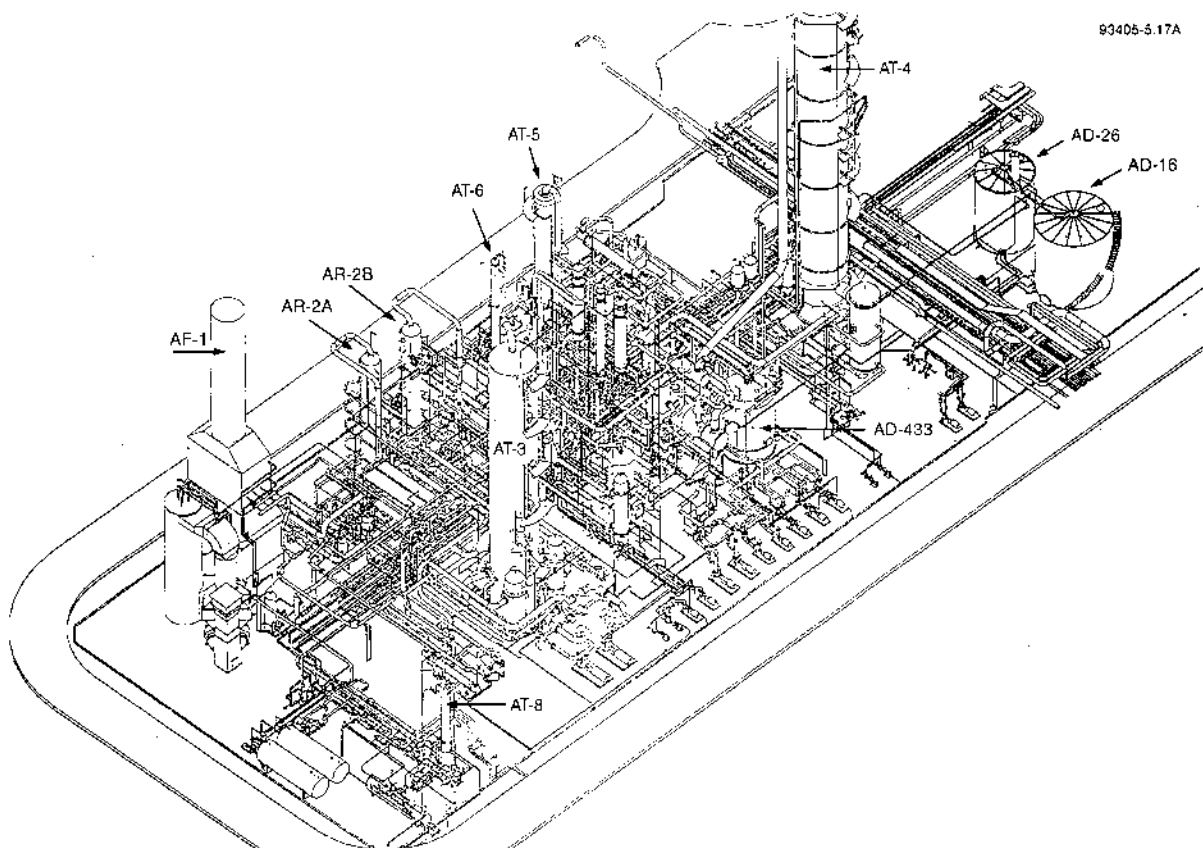
Figure 5.17A   Three-dimensional view of plant
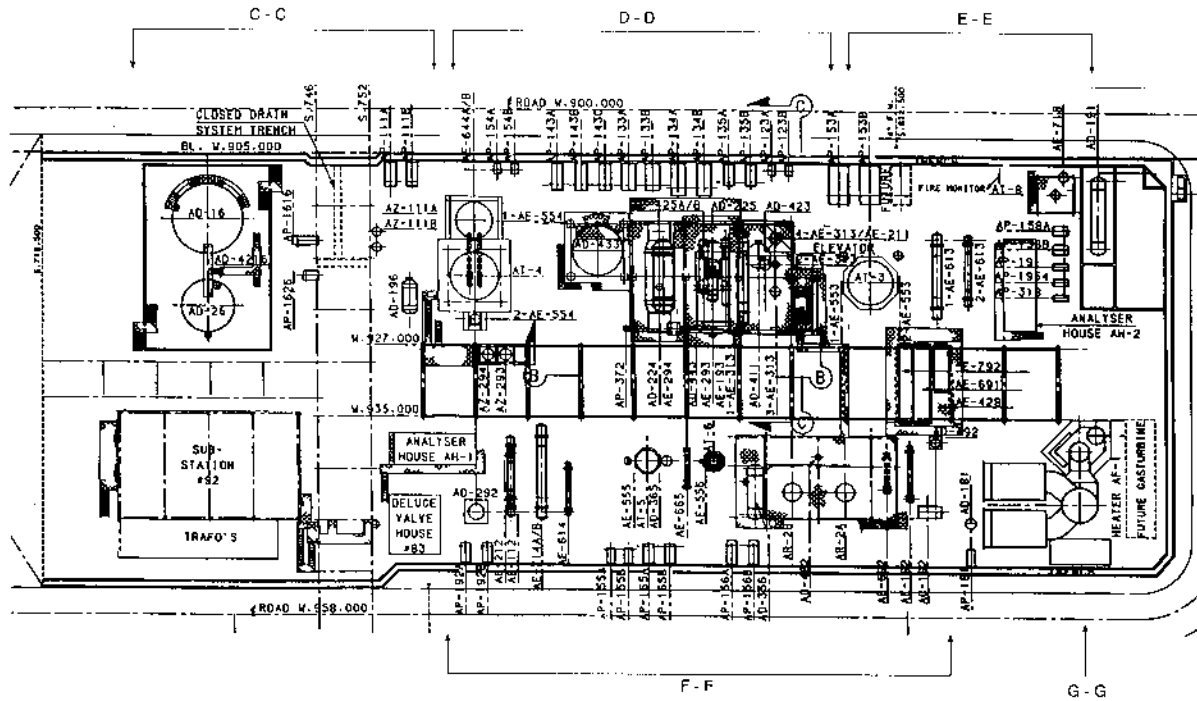
Figure 5.17B   Horizontal cross-section
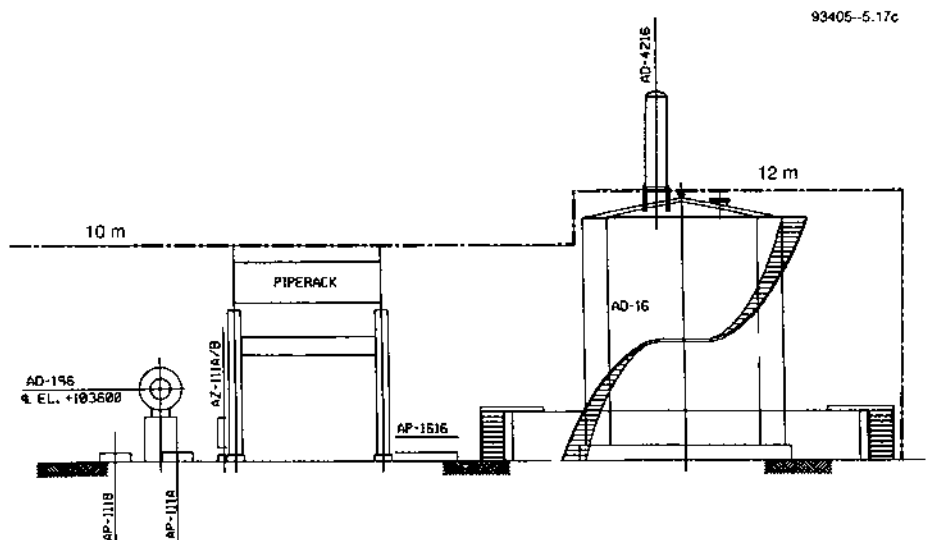
Figure 5.17C   View from location C-C
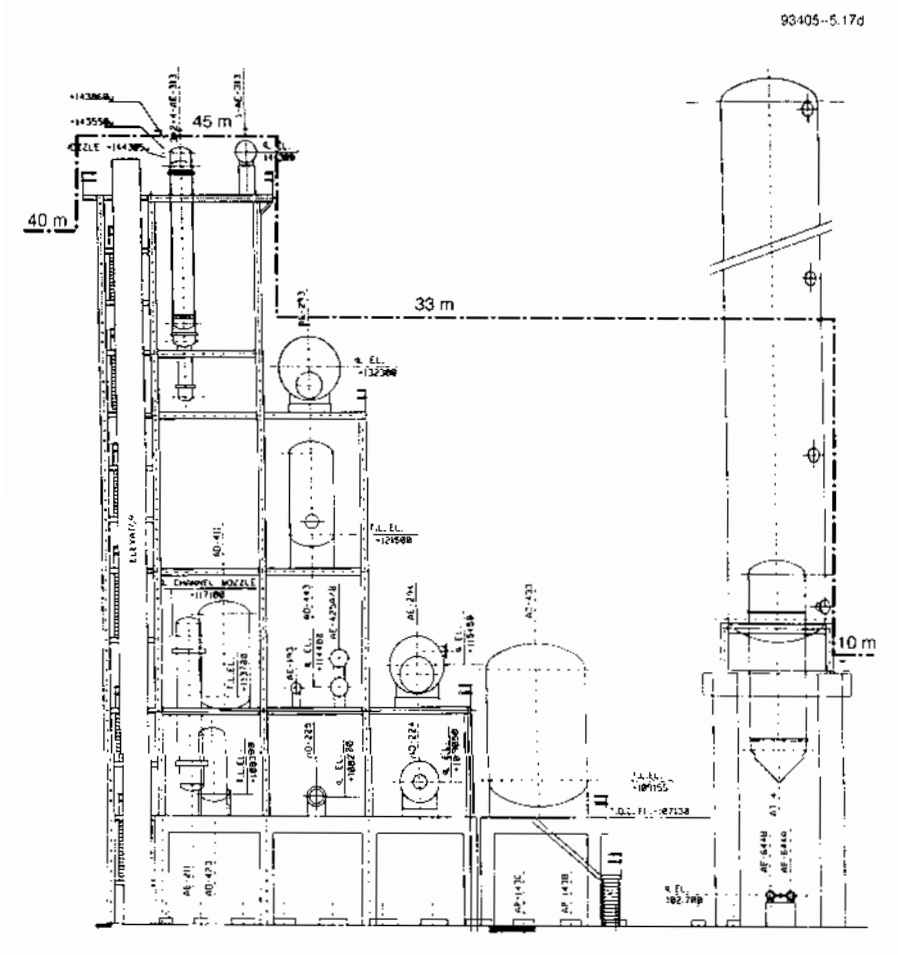
Figure 5.17D   View from location D-D

Figure 5.17E   *View from location E-E*
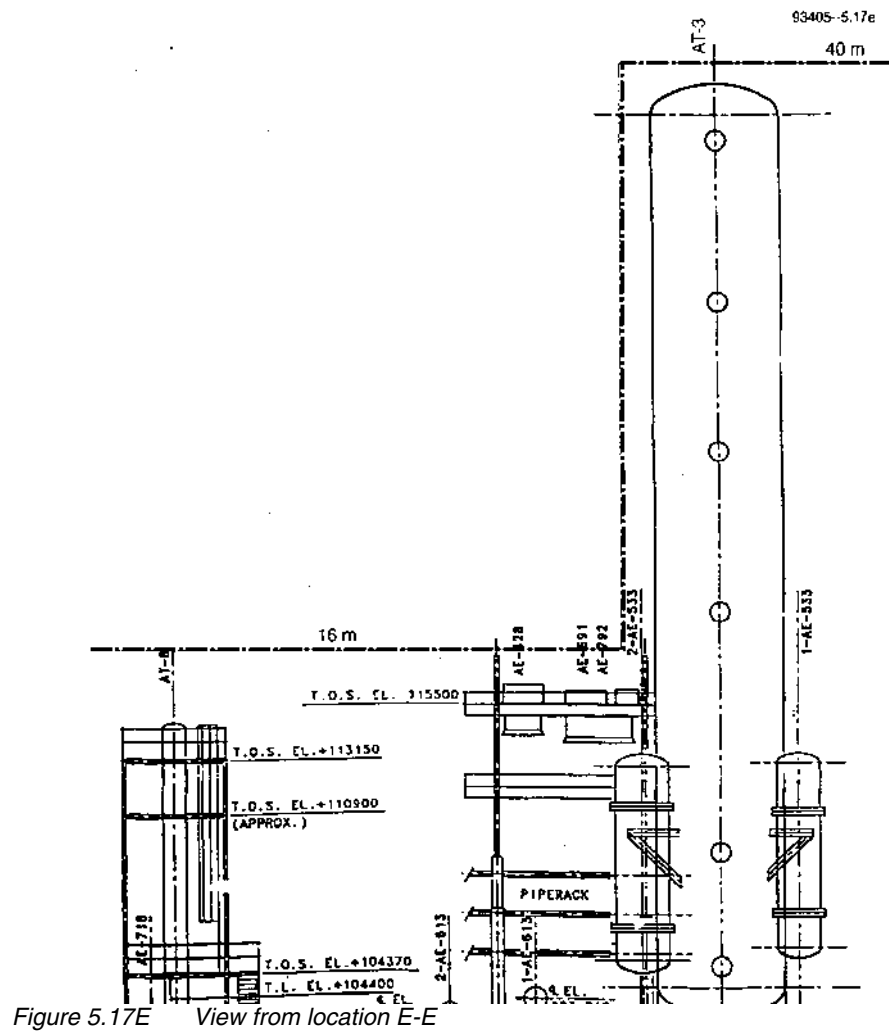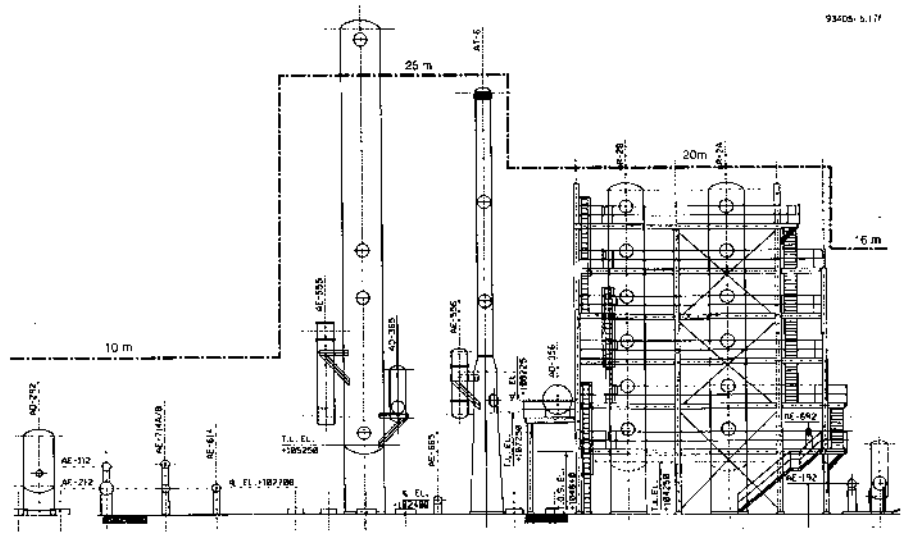
Figure 5.17F   View from location F-F
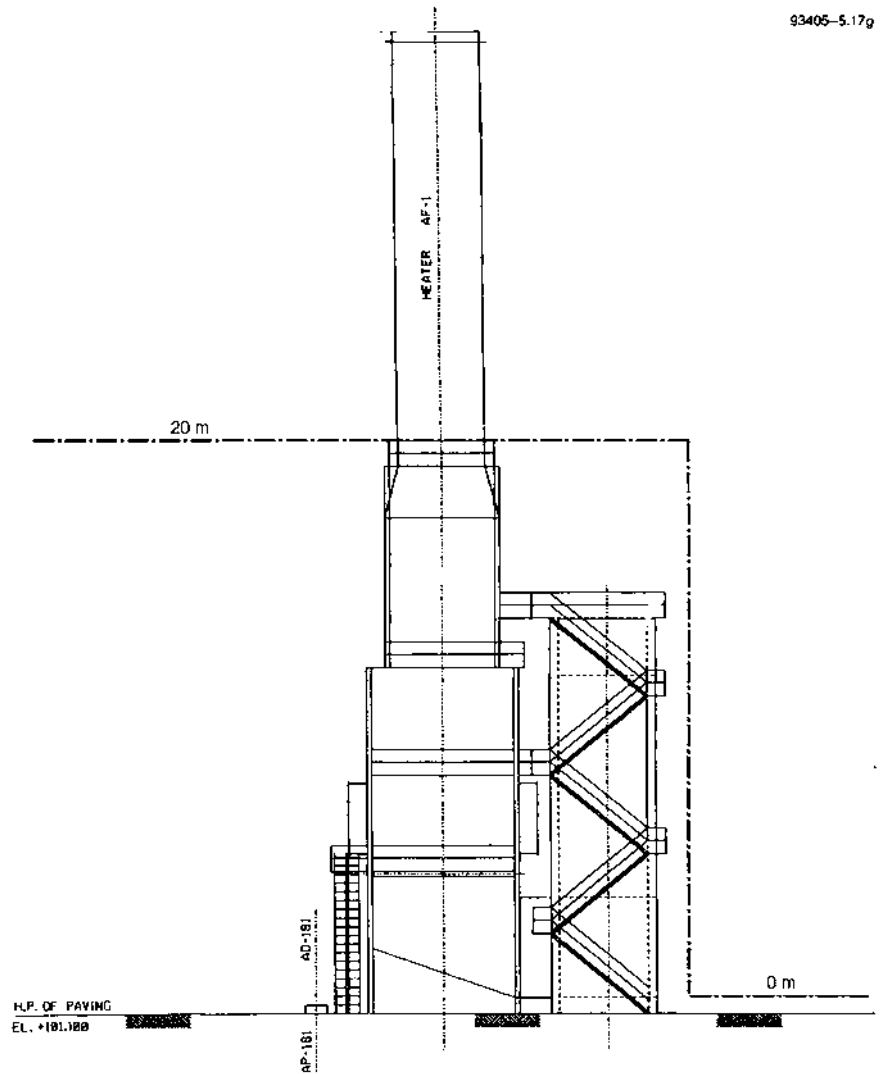
Figure 5.17G   View from location G-G
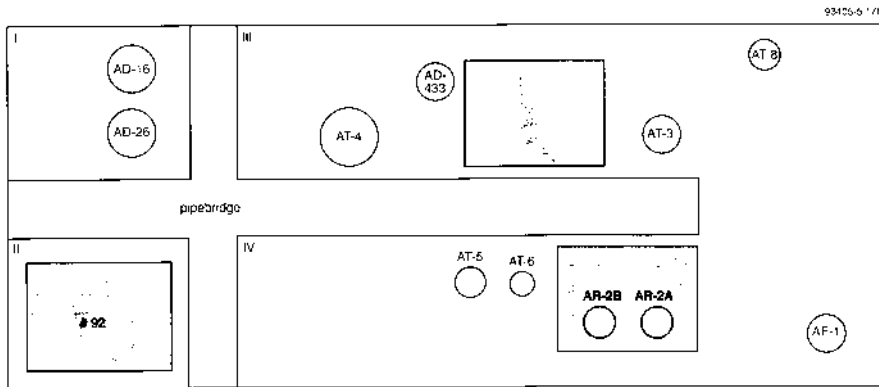
Figure 5.17H   Subdivision into sections and most important obstacles
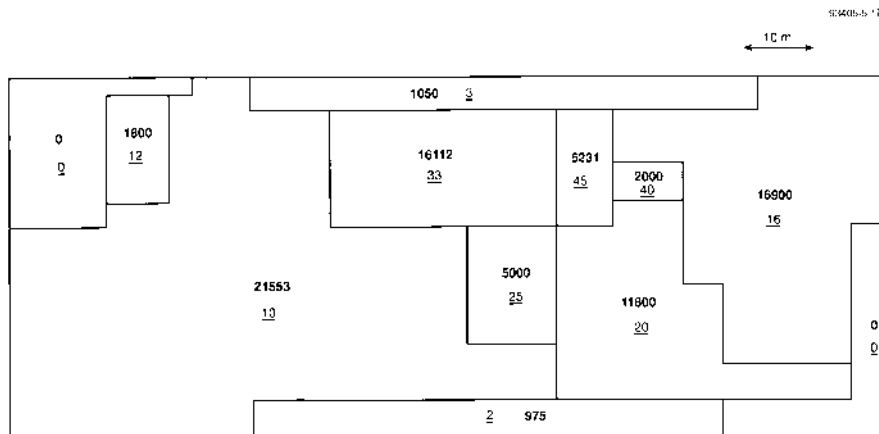
Figure 5.17I   Subdivision into multiple boxes
Bold: volume in m³
Underlined: height in m

5.7 Interfacing to other models

Input variables

The vapour cloud explosion blast model presented in this chapter describes the physical effect of an explosion that may occur after ignition of a flammable vapour cloud. What is needed as input is:
− the combustion energy involved in the explosion,
− the location of the cloud at the moment of the explosion.

According to the Multi-Energy method, the combustion energy involved in the explosion is the combustion energy of the confined fraction of the cloud. In order to determine this fraction one has to determine the flammable mass quantity of the cloud.

Equations with which the flammable mass quantity of the cloud can be calculated are given in chapter 2 'Outfow and Spray Release' and chapter 4 'Vapour cloud dispersion'.

Entrainment with air is necessary to create a flammable cloud. Entrainment with air is calculated for:
− a free jet (section 4.5.4.1),
− a finite duration spray release (section 2.5.3.7),
− an instantaneous release (section 2.5.3.8),
− passive dispersion (section 4.5.3).

The flammable contents of the cloud created by the free jet is calculated using equation (4.83).

The condition of the cloud for the finite duration spray release after flashing including the effects of rain-out are described by step 2 of the procedure given in section 2.5.3.7. Equation (2.164) provides a value for $A_{f,rain-out}$. $A_{f,rain-out}$ together with:

$$b_{f,rain-out} = (A_{f,rain-out}/\pi)^{1/2} \qquad\qquad\qquad (m) \qquad (5.10)$$

is the input for equations (4.81) and (4.82). The explosive content, including droplets not rained out, then follows from equation (4.83).

Instantaneous release is described in section 2.5.3.8. The concentration in the cloud is homogeneously distributed. The cloud is therefore flammable when this concentration is in between the lower and upper flammability limit. The explosive mass of the cloud can be calculated using equation (2.183).

Both the combustion energy involved and the cloud location can be determined following a dispersion calculation (chapter 4, section 4.5.3.7). Equation (4.65) of that section provides the mass of the flammable part of the cloud.

The flammable mass calculated using either of the above equations, is to be multiplied by the combustion energy per unit volume. Table 5.1 gives this property for some gases.

Output variables

The output of the model consists of the most important parameters to characterise the blast-wave at a specific distance from the explosion centre for free field conditions. In order to gain knowledge about damage to structures and injury to people, additional models should be applied using the blast parameters as input. Models that can be used are described in CPR-16E [1990] chapters 2 and 3.

5.8   Literature

Baker W.E., Cox P.A., Westine P.S., Kulesz J.J. and Strehlow R.A. (1983),
Explosion hazards and evaluation,
Fundamental studies in engineering, Vol.5, Elsevier Scientific Publishing Company,
Amsterdam.

Baker Q.A., M.J. Tang and E Scheier (1994),
Vapor cloud explosion analysis,
AIChE 28th Loss Prevention Symposium, Atlanta, Georgia, USA, April 1994.

Brasie W.C. and Simpson D.W. (1968),
Guidelines for estimating explosion damage,
63rd National AIChE meeting, St Louis (MO), USA.

Brasie W.C. (1976),
The hazard potential of chemicals,
AIChE Loss Prevention, Vol.10, pp.135-140.

Burgess D.S. and Zabetakis M.G. (1973),
Detonation of a flammable cloud following a propane pipeline break:
the December 9, 1970, explosion in Port Hudson (MO),
Bureau of Mines Report of Investigations No. 7752, United States Department of the
Interior.

Cates A.T (1991),
Fuel Gas explosion guidelines,
Conference on fire and explosion hazards, Moreton-in-Marsh, April 1991.

CCPS (1994),
Guidelines for evaluating the characteristics of vapor cloud explosions, flash fires and
bleves,
Center for Chemical Pocess Safety of the American Institute of Chemical Engineers.

CPR-14E (1988),
Methods for the calculation of physical effects of the escape of dangerous materials,
Ministry of Social Affairs and Employment, The Netherlands.

CPR-16E (1990),
Methods for the calculation of possible damage to people and goods due to the
physical effects of the escape of dangerous materials,
Ministry of Social Affairs and Emplyoment, Voorburg, The Netherlands.

Desinov Yu. N., Shchelkin K.I. and TroshinYa.K. (1962),
Some questions of analogy between combustion in a thrust chamber and a detonation
wave,
8th Int. Symp. on Combustion, Pittsburgh, PA, pp 1152-1159.

Eichler T.V. and Napadensky H.S. (1977),
Accidental vapor phase explosions on transportation routes near nuclear power
plants,
IIT Research Institute final report no. J6405, Chicago (IL), USA.

Factory Mutual Research (1990),
Private Communication.

French Authority Safety Rule (1982),
Regle fondamentele de Surete I.2.d Prise en compte des risques lies a
l'environnement industriel et aux voies de communication,
Ministere de l'industrie, Paris.

French Chemical Industry (1986),
Cahier de securite: Explosion de gaz en milieu confine,
Union des Industries Chimiques.

Glasstone S. and Dolan P.J. Ed. (1977),
The effects of nuclear weapons,
US Dept.of Defence and US Dept.of Energy.

Gugan K. (1979),
Unconfined vapour cloud explosions,
The Institution of Chemical Engineers, UK.

Hanna S.R. and Drivas P.J. (1987),
Guidelines for Use of Vapour Cloud Dispersion Models,
AIChE, CCPS, New. York.

Harris R.J. (1983),
The investigation and control of gas explosions in buildings and heating plant,
E & F Spon Ltd, London, UK, 1983.

Harris R.J. and Wickens M.J. (1989),
Understanding vapour cloud explosions - an experimental study,
55th Autumn Meeting of the Institution of Gas Engineers, Kensington, UK.

Harrison A.J. and Eyre J.A. (1987),
The effect of obstacle arrays on the combustion of large premixed gas/air clouds,
Combustion Science and Technology, Vol.52, pp 121-137.

Hjertager B.H. (1982),
Simulation of transient compressible turbulent flows,
Combustion Science and Technology, Vol.27, pp 159-170.

Hjertager B.H. (1989),
Simulation of gas explosions,
Modeling, Identification and Control , Vol.10, No.4, pp 227-247.

Health and Safety Executive (1979),
Second Report Advisory Committee Major Hazards,
U.K. Health and Safety Commission.

Health and Safety Executive (1986),
The effect of explosions in the process industries,
Loss Prevention Bulletin, No.68, pp 37-47.

Hopkinson B. (1915),
British Ordnance Board Minutes 13565.

Industrial Risk Insurers (1990),
Oil and Chemical Properties Loss Potential Estimation Guide,
IRI-Information February 1.

IChemE (1994),
Explosions in the Process Industries,
Rugby, UK.

Jarrett D.E. (1968),
Derivation of the British explosives safety distances,
Anuals of the New York Academy of Sciences, Vol.152.

Kinsella K.G. (1993),
A rapid assessment methodology for the prdiction of vapour cloud explosion
overpressure,
proceedings of the International Conference and Exhibition on Safety, Health and
Loss Prevention in the Oil, Chemical and Process Industries, Singapore.

Kjäldman L. and R. Huhtanen (1985),
Simulation of flame acceleration in unconfined vapour cloud explosions, Research
report No 357, Technical Research Centre of Finland.

Lee J.H.S and Moen I.O. (1980),
The mechanism of transition from deflagration to detonation in vapor cloud
explosions,
Prog. Energy Combustion Science, vol. 6 pp 359-389.

Luckritz R.T. (1977),
An investigation of blast-waves generated by constant velocity flames, Aeronautical
and Astronautical Engineering Department, University of Illinois, Urbana,Il ,USA,
Technical report no. AAE 77-2.

Marshall V.C. (1976),
The siting and construction of control buildings - a strategic approach,
I.Chem.E.Symp.Series, No.47.

Mercx W.P.M., Johnson D.M. and Puttock J. (1994),
Validation of scaling techniques for experimental vapour cloud explosion
investigations,
AIChE Loss Prevention Symposium, Atlanta, Georgia, USA, April 1994.

Munday G. (1976),
Unconfined vapour-cloud explosions: A reappraisal of TNT equivalence, Inst.
Chem. Eng. Symposium Series No.47, pp 19-38.

Nettleton M.A. (1987),
Gaseous detonations, their nature, effects an control,
Chapman and Hall, New York.

NTSB (1972),
Pipeline Accident Report, Phillips Pipe Line Company propane gas
explosion, Franklin County (MO), December 9, 1970,
National Transportation Safety Board, Washington (DC), report no. NTSB-PAR-
72-1.

Pietersen C.M. and Cendejas Huerta S. (1985),
Analysis of the LPG incident in San Juan Ixhuatepec, Mexico City, 19 November
1984,
TNO report ref. 85-0222, May 1985, The Netherlands.

Robinson C.S. (1944),
Explosions, their anatomy and destructiveness,
McGraw-Hill, New York.

Sachs R.G. (1944),
The dependence of blast on ambient pressure and temperature,
BRL report No. 466, Aberdeen Proving Ground, Maryland, USA.

Schardin H. (1954),
Ziviler Luftschutz,
No.12, pp 291-293.

Strehlow R.A., Luckritz R.T., Adamczyk A.A. and Shimpi S.A. (1979),
The blast-wave generated by spherical flames,
Combustion and Flame, Vol.35, pp 297-310.

Tweeddale M. (1989),
Conference report on the 6th Int.Symp. on Loss Prevention and Safety Promotion in
the Process Industries,
Journal of Loss Prevention in the Process Industries, Vol.2, No.4, pp 241.

Urtiew P.A. and Oppenheim A.K. (1966),
Experimental observations of the transition to detonation in an explosive gas,
Proceedings Royal Society London, A295:13-28.

Van den Berg A.C. (1980),
BLAST - a 1-D variable flame speed blast simulation code using a 'Flux-Corrected
Transport' algorithm,
Prins Maurits Laboratory TNO report no.PML 1980-162, The Netherlands.

Van den Berg A.C. (1985),
The Multi-Energy method - A framework for vapour cloud explosion blast
prediction,
Journal of Hazardous Materials, Vol.12, pp 1-10.

Van den Berg A.C., Van Wingerden C.J.M., Zeeuwen J.P. and Pasman H.J. (1987),
Current research at TNO on vapor cloud explosion modeling,
Int.Conf.on Vapor Cloud Modeling, Cambridge (MA), USA, pp 687-711, AIChE,
New York.

Van den Berg A.C. (1989),
REAGAS - a code for numerical simulation of 2-D reactive gas dynamics in gas
explosions,
TNO Prins Maurits Laboratory report no. PML1989-IN48, The Netherlands.

Van den Berg A.C., Van Wingerden C.J.M. and The H.G. (1991),
Vapor cloud explosion blast modeling,
International Conference and Workshop on Modeling and Mitigation the
Consequences of Accidental Releases of Hazardous materials, May 21-24, New
Orleans, USA.

Van den Berg A.C. and A. Lannoy (1993),
Methods for vapour cloud explosion blast modelling,
Journal of Hazardous Materials, Vol 34, pp 151-171.

Van Wingerden C.J.M. (1989),
Experimental investigation into the strength of blast-waves generated by vapour cloud
explosions in congested areas,
6th Int. Symp. on Loss Prevention and Safety Promotion in the Process Industries,
Oslo, Norway, pp 26-1,26-16.

Wiekema B.J. (1980),
Vapour cloud explosion model,
Journal of Hazardus Materials, Vol.3, pp 221-232.

Zeeuwen J.P. Van Wingerden C.J.M. and Dauwe R.M. (1983),
Experimental investigation into the blast effect produced by unconfined vapour cloud
explosions,
4th Int. Symp. on Loss Prevention and Safety Promotion in the Process Industries,
Harrogate, UK, ChemE Symp.Series No.80, pp D20-D29.

Chapter 6
Heat flux from fires
W.F.J.M. Engelhard

Modifications to Chapter 6 (Heat Flux from Fires) with respect to the first print (1997)

Numerous modifications were made concerning typographical errors. A list is given below for the pages on which errors have been corrected.

Page 6.19:	Corrected the sentence that in the appendix formulae a given to calculate the view factor for all types of fires.
Page 6.29:	Corrected the sentence above equation 6.5. The equations 6.5 and 6.6 have been extended for readability in a more scientific way.
Page 6.33:	Corrected the symbol a', b', c' and d' in the text.
Page 6.34:	Updated the symbols below equation 6.14. Corrected the last sentence on the page wrt. the reference to the equations.
Page 6.38:	Updated the explanation of the symbols below equation 6.21.
Page 6.47:	Updated the equations 6.25 and 6.26.
Page 6.53:	Equation 6.35 for M_j for choked flow has been written down in a more scientific way. The equation for M_j in case of unchoked flow has been added and also an explanation of the used symbols in these equations.
Page 6.55:	Included a note wrt. the constant 2.85 in the value for C_c. The equation 6.44 has been updated and also the explanation of the symbol Θ_{jv}.
Page 6.56:	Updated equation 6.46 and 6.47 and the explanation of the symbols below equation 6.47.
Page 6.57:	Inserted the correct formulae for the calculation of the lift-off of the flame (b) in equation 6.49. Added below equation 6.49 the equation to calculate the value of (K) in equation 6.49. Corrected the equation 6.54
Page 6.65:	Included a list of symbol explanations below equation 6.67. Noted below equation 6.13 that according to Mudan [84] $u^* < 1 \rightarrow u^* = 1$. In equation 6.12 the scaled wind velocity should be raised to the power of -0.21.
Page 6.87:	In table 6.11, the values for LNG on water and land were interchanged.
Page 6.97 – 6.121:	The calculation examples have been fully corrected for according to the above changes.
Appendix 6.1-7:	Equation 6.14 has been updated for the typographical error !
Appendix 6.1-9:	The Figure 6.A.7 is for an elevated flame wrt. the target.
Appendix 6.1-11:	Below equation 6.A.30 an equation for B has been inserted.
Appendix 6.1-12:	The numerical values in Table 6.A.2 have been corrected and updated.
Appendix 6.1-13:	Figure 6.A.11 has been updated wrt the values in Table 6.A.2.

List of symbols Chapter 6

a	Acceleration (6.76)	m/s^2
a	Constant in Appendix (6.A.15)	-
a'	Constant (6.16)	-
A	Surface area of the flame (6.2)	m^2
A	Constant in Appendix (6.A.8)	-
A_0	Surface area of the leak (6.76)	m^2
A_p	Surface area of the pool (6.7)	m^2
A_t	Cross-sectional area of the tank (6.76)	m^2
dA_1	Infinitesimal surface area (6.A.13)	m^2
dA_2	Infinitesimal surface area (6.A.13)	m^2
b	Frustum lift-off height (6.49)	m
b	Constant in Appendix (6.A.15)	-
b	In Appendix, the width of a flat radiator (6.A.28)	m
b'	Constant (6.16)	-
B	Constant in Appendix (6.A.9)	-
B_c	'Spalding' convection mass transfer number (6.88)	
c	Variable $\tan\Theta/\cos\Theta$ (6.70)	-
c'	Constant (6.16)	-
c_1	Constant (6.6)	$(m^{1.22} \cdot s^{0.61})/kg^{0.61}$
c_2	Constant (6.10)	s
c_3	Constant (6.19)	$J/(m^2 \cdot s)$
c_4	Constant (6.19)	$J/(m^2 \cdot s)$
c_5	Constant (6.19)	m^{-1}
c_6	Constant (6.21)	$(N/m^2)^{-0.32}$
c_7	Constant (6.29)	$(N/m^2)^{0.09} \cdot m^{0.09}$
c_8	Constant (6.67)	$kg/(m^2 \cdot s)$
c_9	Constant (6.90)	$m/kg^{0.325}$
c_{10}	Constant (6.91)	$s/kg^{0.26}$
C	Constant in Appendix (6.A.15)	-
C'	Factor (6.53)	-
C_a	Constant (6.42)	-
C_b	Constant (6.42)	-
C_c	Constant (6.42)	-
C_p	Specific heat capacity at constant pressure (6.9)	$J/(kg \cdot K)$
C_v	Specific heat capacity at constant volume (6.32)	$J/(kg \cdot K)$
C_0	Flow coefficient for fluids through a circular hole (6.75)	-
d'	Constant (6.17)	-
d_h	Diameter of the hole of the release point (6.83)	m
d_j	Diameter of the jet at the exit hole (6.41)	m
D	Pool diameter (6.6)	m
D	Constant in Appendix (6.A.15)	-
D'	Actual elongated flame base diameter (6.18)	m
D_{max}	Maximum diameter of pool fire (6.78)	m
D_s	Effective hole diameter (6.39)	m
D_w	The maximum pool dimension in the direction of the wind (6.18)	m
e'	Constant (6.17)	-
E	Constant in Appendix (6.A.15)	-

f	Fraction of the volume of the pressure tank, filled with the flammable liquefied pressurised gas (6.89)	-
f'	Constant (6.17)	-
F	Constant in Appendix (6.A.15)	-
F_h	Geometrical view factor for the horizontal plane of the radiated object (6.A.18)	-
F_{max}	Maximum geometrical view factor of the radiated object (6.A.18)	-
F_s	Fraction of the generated heat radiated from the flame surface (6.3)	-
F_v	Geometrical view factor for the vertical plane of the radiated object (6.A.18)	-
F_{view}	Geometric view factor (6.4)	-
Fr	Froude number $U^2/(g \times D)$ (6.15)	-
Fr_{10}	Froude number for wind velocity at a height of 10 metres (6.68)	-
g	Gravitational acceleration 9.81 (6.14)	m/s^2
g'	Constant (6.18)	-
G	Constant in Appendix (6.A.17)	-
h	Heat transfer coefficient (6.88)	$J/(m^2 \cdot s \cdot K)$
h'	Constant (6.18)	-
h_i	Initial height of the liquid above the release point (6.75)	m
h_r	Ratio between the flame length L (or L_b or L_f) and the radius of the flame R (6.A.6)	-
H	Constant in Appendix (6.A.17)	-
H_{bleve}	Height from the centre of the fire ball to the ground under the fire ball (6.22)	m
i'	Constant (6.18)	-
I	Constant in Appendix (6.A.17)	-
k	Absorption extinction coefficient of the flame (6.8)	m^{-1}
L	Average flame height (6.6)	m
L_1	Lift-off height of the fire (6.A.20)	m
L_2	Flame length (6.A.21)	m
L_b	Flame length, flame tip to centre of exit plane (6.44)	m
L_{b0}	Flame length, in still air (6.43)	m
L_f	Frustum (flame) length	m
m	Mass of the flammable material (6.89)	kg
m'	Mass flow rate (6.39)	kg/s
m_h'	Burning rate at still weather conditions (6.5)	kg/s
m"	Burning flux at still weather conditions (6.6)	$kg/(m^2 \cdot s)$
$m"_{wind}$	Burning flux under windy weather conditions (6.10)	$kg/(m^2 \cdot s)$
$m_\infty"$	see m", for $D \to \infty$ (6.66)	$kg/(m^2 \cdot s)$
M_j	Mach number of the expanding jet (6.35)	-
n_1	Normal vector on the receiving surface area (6.A. fig. 6)	-
n_2	Normal vector at a certain point on the radiating (6.A. fig. 6) surface area	-
p_c	Vapour pressure of carbon-dioxide (6.26)	N/m^2
p_w	Partial vapour pressure of water in air at a relative humidity of RH (6.25)	N/m^2
p_w^o	Saturated vapour pressure of water in air (6.73)	N/m^2
P_{air}	Atmospheric pressure (6.33)	N/m^2
P_c	Static pressure at the hole exit plane (6.34)	N/m^2

P_c^*	Reduced pressure of carbon-dioxide (6.25)	N/m^2
P_{init}	Initial pressure (6.33)	N/m^2
P_{sv}	Vapour pressure of flammable material inside the vessel (6.21)	N/m^2
P_w^*	Reduced vapour pressure of water (6.25)	N/m^2
q''	Heat flux (6.4)	$J/(m^2 \cdot s)$
q_{rw}''	Radiant heat flux to the pool burning surface	$J/(m^2 \cdot s)$
Q'	Combustion energy per second (6.2)	J/s
r_{fb}	Radius of the fire ball (6.22)	m
R	Radius of the pool or flame (6.73)	m
R_c	Gas constant (6.32)	$J/(mol \cdot K)$
R_l	Length of the frustum (6.45)	m
R_{max}	Maximum radius of the pool fire (6.78)	m
R_w	Ratio of wind speed to the jet speed (6.38)	-
Re	Reynolds number (6.15)	-
RH	Relative Humidity (6.72)	-
$Ri(D_s)$	Richardson number based on D_s (6.52)	-
$Ri(L_{b0})$	Richardson number based on L_{b0} (6.45)	-
S_p	Pool perimeter (6.7)	m
SEP	Surface emissive power (6.1)	$J/(m^2 \cdot s)$
SEP_{act}	Actual surface emissive power, SEP, which is the average radiation emittance (emissive power) of the flame surface (6.4)	$J/(m^2 \cdot s)$
SEP_{max}	Maximum surface emissive power (6.3)	$J/(m^2 \cdot s)$
SEP_{soot}	The surface emissive power of soot, which is about $20 \cdot 10^3$ (6.20)	$J/(m^2 \cdot s)$
SEP_{theor}	Theoretical Surface Emissive Power (6.2)	$J/(m^2 \cdot s)$
t	Time (6.73)	s
t_{max}	Time at which the pool (fire) reaches its maximum diameter (6.77)	s
t_{rel}	Total release time (6.87)	s
t_{tot}	Total duration of the fire (6.87)	s
t_D	Time at which a tank has been released	s
T	Temperature	K
T_a	Ambient temperature (6.1)	K
T_{air}	Air temperature (6.38)	K
T_b	The liquid boiling temperature (6.9)	K
T_f	Temperature of the radiator surface of the flame (6.1)	K
T_j	Temperature of the gas in the jet (6.33)	K
T_l	Ambient combustion temperature	K
T_s	Initial gas temperature (6.33)	K
u_w	Wind velocity (6.10)	m/s
u^*	Scaled wind velocity (6.12)	-
u_c	Characteristic wind velocity (6.13)	m/s
u_j	Jet velocity (6.36)	m/s
v_0	Initial outflow velocity (6.74)	m/s
v_f	Discharge velocity of the liquid from a tank (6.73)	m/s
V	Tank volume	m^3
V_{rel}	Amount of LPG which will be released in case of complete tank failure (6.89)	m^3
W	Stoichiometric mass fraction (6.30)	-
W_1	Width of frustum base (6.54)	m
W_2	Width of frustum tip (6.55)	m

W_{air}	Molecular weight air (6.38)	kg/mol
W_g	Molecular weight of gas (6.30)	kg/mol
x	Distance from the surface area of the flame to the object (6.30)	m
x_1	The projection of the elongated centreline of an elevated flame and the flame length, or Distance between the centre of the flame and the object at a certain elevation in a plane (at that elevation) parallel to the ground (6.A.19)	m
x_{bleve}	Distance measured over the ground from the projected centre of the fire ball on the ground under the fire ball, and the object (6.92)	m
x_r	Ratio between the distance from the centre of the flame to radiated object X and the radius of the flame R (6.A.5)	-
X	Distance from the centre of the flame (fireball) to the radiated object (6.5)	m
X'	Distance from the centre of the bottom plane of a lifted-off flame and the object (6.61)	m
X_m	The projected distance from the elongated centreline to the ground of an elevated flame and the flame length (A.6. fig. 7)	m
Y	Variable (6.42)	-
z	Elevation of the flame base in Appendix (6.A.19)	m
α	Angle between hole axis and flame axis (6.46)	°
α_c	Absorption factor for carbon dioxide (6.24)	-
α_w	Absorption for water vapour (6.24)	-
β	Mean-beam-length corrector (6.8)	-
β_1	Angle between the normal vector of the receiving surface area and a line directed from the receiving area to a certain point on the radiating surface area (6.A.13)	rad
β_2	Angle between the normal vector of the radiating surface area at a certain point and a line directed from the radiating surface area to the receiving surface area (6.A.13)	rad
β'	Inverse of the non-dimensional time	-
γ	Ratio of specific heats, Poisson constant (6.32)	-
δ	Pool thickness (6.65)	m
ΔH	Net available heat (6.94)	J/kg
ΔH_c	Combustion heat of the flammable material at its boiling point (6.5)	J/kg
ΔH_v	Vaporisation heat of the flammable material at its boiling point (6.9)	J/kg
ΔT	Temperature difference between flame and ambient temperature	K

Greek symbols

ε	Emittance factor (emissivity) (6.1)	-
ε_w	Emission factor for the water reduced vapour pressure (6.28)	-

ε_c	Emission factor for the reduced carbondioxide pressure (6.27)	-
ς	The fraction of the surface that is covered by soot (6.20)	-
Θ	Tilt angle of the flame, which is the angle between the centre line of the flame and the normal vector perpendiculum to the horizontal plane (6.15)	°
θ	Orientation angle in Appendix (6.A.1)	rad
Θ'	Angle between the centreline of a lifted-off flame and the plane between the centre of the bottom of the lifted-off flame and the object (6.62)	°
Θ_j	Angle between hole axis and the horizontal in the vertical plane (6.44)	°
Θ_{jv}	Angle between hole axis and the horizontal in the direction of the wind (6.64)	°
υ	Kinematic viscosity of air (6.69)	m^2/s
ρ	Density of liquid (6.73)	kg/m^3
ρ_{air}	Density of air (6.11)	kg/m^3
ρ_j	Density of gas in the jet (6.40)	kg/m^3
ρ_{lpg}	Density of lpg (6.89)	kg/m^3
ρ_{mat}	Density of the flammable material in the pressure tank (6.89)	kg/m^3
ρ_v	Vapour density flammable material (6.15)	kg/m^3
σ	Constant of Stefan-Boltzmann, which is $5.6703 \cdot 10^{-8}$ (6.1)	$J/(m^2 \cdot s \cdot K^4)$
τ	Dimensionless time (6.77)	-
τ_a	Atmospheric transmissivity (6.4)	-
τ_D	Dimensionless time at which a tank has been released (6.83)	-
τ_i	Dimensionless time at the moment of ignition (6.82)	-
τ_{max}	Dimensionless time at a maximum pool diameter (6.84)	-
Φ	Normalised pool area (6.79)	-
ϕ	Half of the view angle, in Appendix (6.A.1)	rad
Φ_i	Normalised pool area at ignition (6.81)	-
Φ_{max}	Maximum normalised pool area at τ_{max} (6.82)	-
Ω	Angle between the wind direction and normal vector perpendicular to the pipeline in the horizontal plane (6.47)	°

Note: the numbers between brackets refer to equations.

Glossary of terms

Absorptivity	The ratio of the radiant energy absorbed by any surface or substance, to that absorbed under the same conditions by a black body.
BLEVE	<u>B</u>oiling <u>L</u>iquid <u>E</u>xpanding <u>V</u>apour <u>E</u>xplosion; results from the sudden failure of a vessel containing a pressurized liquid at a temperature well above its normal (atmospheric) boiling point.
Burning rate	The linear rate of evaporation of material from a liquid pool during a fire, or the mass rate of combustion of a gas or solid. The context in which the term is used should be specified.
Emissivity	The ratio of the radiation emitted by any surface or substance to that emitted by a black body at the same temperature.
Field model	A field model is a mathematical model that uses as its framework the solution of the Navier-Stokes equations for time-averaged fluid flow. Additional sub-models are necessary to describe turbulence and combustion. There is nothing necessarily fundamental about field modelling. The sub-models can range from being completely empirical and very limited 'fits' through to rigorous and soundly based approaches capable of further development. A field model used for fire prediction is only as strong as its sub-models.
Fire	A process of combustion characterized by heat or smoke or flame or any combination of these.
Fireball	A fire, burning sufficiently rapidly for the burning mass to rise into the air as a cloud or ball.
Fire prevention	Measures taken to prevent outbreaks of fire at a given location.
Fire protection	Design features, systems or equipment intended to reduce the damage from a fire at a given location.

Fire storm	An extremely large area fire resulting in a tremendous inrush of air which may reach hurricane force.
Fire temperature	A term best avoided wherever possible. Fire temperature only has a conventional meaning for an idealised, isotropic, isothermal, hot gas and soot mixture that is optically thick at all wavelengths. In this report the term is used only in this sense as far as possible. Other uses are qualified.
Flame front	The boundary between the burning and unburnt portions of a flammable vapour and air mixture, or other combusting system.
Flash fire	The combustion of a flammable vapour and air mixture in which flame passes through that mixture at less than sonic velocity, such that negligible damaging overpressure is generated.
Flow	Transport of a fluid (gas or liquid or gas/liquid-mixture) in a system (pipes, vessels, other equipment).
Flow coefficient	The flow coefficient is the product of a contraction and a friction factor. For a sharp-edged orifice the friction factor is nearly 1 and the value of the flow coefficient is fully determined by the contraction factor. In general the value of the flow coefficient is between 0.6 and 0.8.
Fluid	Material of any kind that can flow, which may extend to gases to highly viscous substances, like gases and liquids and gas/liquid-mixtures; meaning not fixed or rigid, like solids.
Frustum	The part of a cone-shaped solid next to the base and formed by cutting off the top by a plan-parallel to the base.
Gas	State of aggregation of chemical or mixture of chemicals that is fully in the gaseous state under the present pressure and temperature; gases neither have independent shape nor volume.

Integral model	An integral model is a mathematical model formulated in exactly the same way as a field model. It solves equations that describe the conservation of mass, momentum and scalar quantities within a flow, and contains sub-models of the turbulence structure and combustion and heat transfer processes.
	In integral models however, the cross-stream variation of the flow and scalar variables is assumed to be self similar so that the partial differential equations used in the field models can be reduced to form ordinary differential equations. Entrainment laws are required to describe how air gets into the flame. These models demand far less computer time than field models.
Jet flame	The combustion of material emerging with significant momentum from an orifice.
LFL (LEL)	The Lower Flammability Limit (Lower Explosion Limit) is the concentration in air of a flammable material below which combustion will not propagate.
Mass burning rate	The mass burning rate of a pool fire is the mass of fuel supplied to the flame per unit time, per unit area of the pool.
Multi-component rate	For the purposes of this report, a multi-component fuel has been made of a number of different hydrocarbons which have different boiling points. Thus, when heated, a multi-component fuel can fractionate and the vapour driven off can have a different composition of hydrocarbons.
Optical thickness	A gas/soot layer is optically thick when any further increase in the layer thickness does not produce an increase in emitted radiation.
Physical effects	Physical phenomena that occur during or after a release of hazardous chemicals.
Physical effects models	Models that provide (quantitative) information about physical effects, mostly in terms of heat fluxes (thermal radiation), blast due to explosions, and environmental (atmospheric) concentrations.

Pool fire	The combustion of material evaporating from a layer of liquid at the base of the fire.
Pressurised liquefied gas	Gas that has been compressed to a pressure equal to saturated vapour pressure at storage temperature, so that the larger part has condensed to the liquid state.
Semi-empirical model	A semi-empirical model is a mathematical model that uses as its framework simple physical arguments and empirical correlations fitted to data from experiments which are very similar, in terms of scale, fuel type, etc., to the situation which is to be modelled.
SEP	The SEP or Surface Emissive Power of a flame is the heat radiated outwards per unit surface area of the flame. There is considerable confusion in the literature about the meaning of these empirical parameters characterising flame radiation.
Surface flux	The radiation power emanating from a flame or other source per unit surface, also known as surface emissive power (SEP).
Transmissivity	The fraction of incident thermal radiation passing unabsorbed through a path of unit length of a medium.
UFL (UEL)	The Upper Flammability Limit (Upper Explosion Limit) is the concentration in air of a flammable material above which combustion will not propagate; UEL ≡ UFL.
Vapour	Chemical in the gaseous state which is in thermodynamic equilibrium with its own liquid under the present saturation pressure at a given temperature.

| View factor | The view factor quantifies the geometric relationship between the emitting and receiving surfaces; it describes how much of the field of view of the receiving surface is filled by the flame. The view factor is equal to unity if the flame completely fills the field of view of the receiving surface, otherwise it is a fraction of unity. The view factor depends on the dimensions, shape of the flame, the distance and the orientation of the receiving object. |

Note: Some definitions have been taken from Jones [1992], AIChE [1989] and Webster [1993].

Table of contents Chapter 6

Appendix 6.1   View factors for some radiation configurations

6   Heat flux from fires

6.1   Introduction

If flammable liquids and gases are released, there is the possibility of a fire after ignition. Heat transfer from a fire causes a heat flux with the potential to cause damage to objects in the surrounding area.
This heat flux can be estimated with the formulae presented in this chapter.
Before the heat flux can be determined it is necessary to estimate the released amount. For gas and liquid the release rate can be calculated with models from chapter 2. For liquids the release duration is an important parameter for the pool size. Calculations to determine the pool size can be found in chapter 3.

In chapter 6 the following types of fire will be discussed:
− jet flames
− impinging fires
− pool fires on land
− pool fires on water
− fire balls
Except for impinging fires, heat radiation is the most important phenomenon in heat transfer. In case of an impinging fire also heat convection and heat conduction through the vessel wall have to be taken into account.

The heat radiated to objects in the surroundings of a fire is determined by the dimensions and shape of the surface area of the fire, the heat generated due to combustion, the fraction of heat which is emitted as heat radiation, produced soot which screens the luminous parts of the flame, water vapour and carbon-dioxyde in the air which absorbs the radiation, and the position of the object.

Chapter 6 has been structured in such a way that in chapter 6.2 first a general overview of all important physical phenomena with respect to heat radiation has been given.
In chapter 6.3 an overview of all existing and available models has been presented, based on literature search.
Because much literature has been published about models for each type of fire, a selection has been made, which is presented in chapter 6.4.
In chapter 6.5 the selected models are described. In some cases the whole recipe had to be followed to make clear what is in the model. Where possible a calculation schedule is given.
In chapter 6.6 calculation examples are given for the selected models. The calculations have been made in steps, in order to show which formulae have to be used with the correct figures and dimensions.
In chapter 6.7 the interface between models, used in chapter 6, and models in the other chapters of the Yellow Book, are given.
Ultimately the limitations of the selected models, described in Chapter 6, are discussed in chapter 6.8. Literature references can be found in chapter 6.9.
The Appendix gives formulae to calculate the view factors for all types of fires. Because the formulae for the cylinder and the flat plate are rather complicated, calculation results are presented in tables which can be used if the shape of the model has been determined.

6.2 Phenomenon of heat transfer from a fire

6.2.1 Introduction

The flames of a hydrocarbon fire consist of high-temperature combustion products with a radiation temperature between 800 and 1600 K. Flame temperature and radiation spectrum of the flame are important for the determination of the heat flux. Because of the temperature difference between the hot gases of the flame and objects in the surroundings, heat will be transferred.
In general the combustion energy in the flames can be transferred by heat radiation, heat convection and heat conduction.
At some metres distance from the fire, heat radiation is predominant in heat transfer. If objects are engulfed by a fire, heat convection and heat conduction have to be taken into account.
Heat conduction is only a relevant heat transport phenomenon in the material itself.

6.2.2 Surface emissive power

The Surface Emissive Power is the heat flux due to heat radiation at the surface area of the flame in W/m^2.
In principle the heat rate from a radiating surface of a flame can be calculated with the Stefan-Bolzmann equation, which, for a so-called grey radiator (with $0 < \varepsilon < 1$) is:

$$SEP = \varepsilon \times \sigma \times (T_f^4 - T_a^4) \qquad (J/(m^2 \cdot s)) \qquad (6.1)$$

in which:

SEP = Surface Emissive Power, in $J/(m^2 \cdot s)$
ε = Emittance factor (emissivity)
σ = Constant of Stefan-Boltzmann, which is $5.6703 \cdot 10^{-8}$ $J/(m^2 \cdot s \cdot T^4)$
T_f = Temperature of the radiator surface of the flame, in K
T_a = Ambient temperature, in K

If $\varepsilon = 1$, the radiator is called a 'black radiator'. The SEP calculated is the theoretically maximum heat flux which can be achieved. However, the flame temperature is difficult to determine because the flame temperature over the flame surface is not homogeneous and the flame in general is not a black radiator. In practice, the Stefan-Bolzmann equation is of limited use for calculation of the surface emissive power of flames.
Therefore the so-called 'solid flame' approach is used, which means that part of the combustion heat is radiated through the visible flame surface area of the flame. However, flames do not really emit radiation from their surface area only. The emitted heat flux varies with the distance over which emission occurs. Thus the use of SEPs is a two-dimensional simplification of a very complex three-dimensional heat radiation phenomenon [Cowley, 1991].
The heat which passes through the visible 'surface' of the flame comes from the gaseous combustion products, hot fuel vapour and incandescent soot deep within the flame.

SEP_{theor}, can be estimated from the combustion energy generated per second, which can be determined from the combustion burning-rate, the heat of combustion of the material and the surface area of the flame.

$$SEP_{theor} = Q'/A \qquad\qquad J/(m^2{\cdot}s) \qquad (6.2)$$

in which:
SEP_{theor} = Theoretical Surface Emissive Power, in $J/(m^2{\cdot}s)$
Q' = Combustion energy per second, in J/s
A = Surface area of the flame, in m^2

SEP_{max} can be calculated from SEP_{theor} and the fraction of the generated heat radiated from the flame surface. Hereby it is necessary to select a value of the radiation fraction F_s (some values of F_s are given in table 6.6 and in formulae (6.21) and (6.59)):

$$SEP_{max} = F_s \times SEP_{theor} \qquad\qquad J/(m^2{\cdot}s) \qquad (6.3)$$

in which:
SEP_{max} = The maximum Surface Emissive Power from a flame without soot production, in $J/(m^2{\cdot}s)$
F_s = Fraction of the combustion energy radiated from the flame surface

The F_s factor, in formula (6.3), gives the fraction of the generated heat in the fire which is emitted by the flame surface in the form of heat radiation. This fraction differs per type of fire, such as jet flame, pool fire and fire ball, but also depends on the type of combustible material.
Black smoke or soot produced in the flame can absorb a large part of the radiation. So the actual value of SEP_{act} has to be introduced which can be calculated from SEP_{max} and SEP_{soot}.

6.2.3 Heat flux at a distance from the fire

The heat flux q" at a certain distance from the fire, which is experienced by the receiver per unit area, can be calculated by:

$$q'' = SEP_{act} \times F_{view} \times \tau_a \qquad\qquad J/(m^2{\cdot}s) \qquad (6.4)$$

in which:
q'' = Heat flux at a certain distance, in $J/(m^2{\cdot}s)$
SEP_{act} = Actual surface emissive power, in $J/(m^2{\cdot}s)$
F_{view} = View factor
τ_a = Atmospheric transmissivity

Formula (6.4) shows the relationship between the heat flux and the surface emissive power, view factor and the heat transmissivity, which are discussed in chapter 6.5.
For an impinging fire calculation the heat flux on the surface subjected to the fire is complicated, because it includes terms such as heat conduction in the vessel wall and heat transfer inside and outside the vessel.

6.3 General overview of existing models for heat radiation and heat transfer

6.3.1 Introduction

The objective of this section is to give an overview of all existing models found in literature about jet flames, pool fires on land, pool fires on water, impinging jets and fire balls. In some occasions only the results of experiments are given without analytical correlations in order to check the order of magnitude of the calculated results, because in some cases the calculations are inaccurate.

In this section the principles of the models will be explained. If more models exist to describe the same phenomenon, similarities and differences will be explained.

The mathematical tools for predicting the heat flux at a distance, associated with jet flames, in subsections 6.3.2, and pool fires on land, in subsection 6.3.4, can be divided broadly into three classes:

1. Semi-empirical models
2. Field models
3. Integral models

1. Semi-empirical

Semi-empirical modelling is a relatively simple technique for providing models for predicting the heat flux at a distance, associated with jet flames and pool fires. Because of their simplicity, semi-empirical models are usually designed only to predict quantities such as flame shape and radiative, rather than to provide a detailed description of the fire itself.

Most semi-empirical modelling of jet flames and pool fires has focused on the prediction of flame shapes and heat fluxes to external objects. There are two types of models:

1. Point source models, which do not attempt any shape prediction and assume that the source of the heat radiation is a point;

2. Surface emitter models, which assume that heat is radiated from the surface of a solid object (usually tilted cone or cylinder).

By their nature, semi-empirical models depend heavily on experimental data. Correlations may describe the gross features of the fire. For example, to represent the location of a fire in space, correlations for the flame length and the trajectory of the centre line of the fire may be derived. Alternatively the fire may be represented by coupling the fire geometry obtained from such correlations with secondary correlations for surface emissive power or the fraction of combustion energy input to the flame that is emitted as radiation.

Semi-empirical models are ideally suitable for routine hazard assessment purposes because they are mathematically simple, and hence easily understood. A prerequisite of any semi-empirical model is that it provides reliable prediction. Moreover it may be important that models are readily embodied in simple computer programs with

short run times. Thus, they can only be applied to the specific type of fire examined in the experiments which form the basis of the model. Also, although dimensional analysis may have been used in deriving the correlations within the model, the range over which those correlations apply will be limited (e.g. in terms of flammable material, mass flow rate, etc.).

2. Field models

Field models are based on solutions of the time-averaged Navier-Stokes- equations of fluid flow. These are equations that describe, in partial differential form, the conservation of mass, momentum and scalar quantities in flowing fluid. In general most field models are good at predicting fluid flow when no combustion is involved. Combustion problems are much more difficult to model. Additional sub-models must be included to describe the important physical and chemical processes which occur in such flows. Field models are mathematically complex, embodied in large computer programs and have significant run times on large computer systems.

3. Integral models

Integral models are a compromise between semi-empirical models and field models. The models that incorporate a more rigorous description of the physics permit them to be used over a wider range of circumstances than semi-empirical models. Integral models are formulated mathematically in the same way as field models. They solve equations that describe the conservation of mass, momentum and scalar quantities within a flow, and can in principle contain sub-models of the turbulence structure and combustion and heat transfer process. These equations are, expressed in a simplified form, namely in integral models, such that their solution is demanding far less computer time than for field models.

In the integral approach, the partial differential equations, used in the field models, can be integrated (hence the name) and reduced to form ordinary differential equations with the downstream coordinate being the independent variable. Therefore, in formulating such a model it is essential to identify the flow properties which are self-similar and to choose an appropriate cross-stream profile to represent them.

Some of the models require advanced computer programs for the calculations. It is not the intention to describe these models. Only the general approach, if possible, will be touched. These models will be mentioned just to inform the reader.
Although the overview of types of models has to be as complete as possible in this chapter, the semi-emperical models suit the purpose of the Yellow Book best.
Therefore most of the attention will be given to the semi-empirical models.

For pool fires on land and water a lot of experimental data is available. However, in some cases models have not been developed. More information can be found in chapter 6.5.

6.3.2   Jet flames

6.3.2.1   Introduction

Jet flames can fully develop in an unconfined environment. At first, the influence of wind is disregarded to estimate its shape in idealised conditions. The flame shape is usually defined as the envelope of the visible flame.
The characteristic flame shapes can be determined by the jet length and diameter. If there is a curvature in the flame, calculation of the heat flux at a certain distance has to be done numerically.
When jet flames can be approximated by a cone or a cylinder shape, the view factor can be determined analytically.

In the past the turbulent free jet was mentioned as a valid model to estimate the dimensions of a jet flame by using the lean-limit-approach of Brzustowski, which means that the contours of the flame are similar to the contours of the lower explosion limit. The turbulent free jet is a very simple model which does not take into account lift-off of a flame, the influence of the wind and the effect of the increasing temperature due to the heat of combustion. Furthermore no description was given how the model should be used to estimate the view factor.

6.3.2.2   Semi-empirical models for jet flames

The most important consideration when assessing the relevance and applicability of any such model, is the range of the experimental data used in its derivation.

There are three types of models which can be distinguished:

1. Point source models, which do not attempt any shape prediction and assume that the source of the heat radiation is a point;

    The only single point source model identified was the API-model which was originally developed for designing vertical flare stacks producing subsonic flares.

2. Multiple point source models, which attempt to model the effect of flame shape on the radiated heat flux by distributing radiating point sources along a modelled flame centre line trajectory.

    Some multiple point source models attempt to take into account the flame geometry by employing multiple radiation sources, for example, a number of points along a predicted flame axis. Some of the models assume a number of equidistant point sources along the flame axis. In the model it is also assumed that each of the points represent an equal part of the total radiation.

3. Surface emitter models, which assume that heat is radiated from the surface of a solid object (usually a tilted frustum of a cone or a cylinder) modelling the flame.

   All the surface emitter models with the conical frustum flame shape are based on Chamberlain [1987], explained in subsection 6.5.2.

A list of semi-empirical models from Cowley [1991], has been shown in table 6.1.

Table 6.1   Semi-emperical models of Jet Flames

Model name	Organisation	Type
API 521	American Petroleum Institute	Single Point Source
WHAZAN	Technica	Multiple Point Source
FLARESIM	Simulation Engineering	Multiple Point Source
	Cremer & Warner	Multiple Point Source
THORIN	British Gas Midland Research Station	Multiple Point Source
FLARE	Technica	Conical frustum
TORCH	AEA Technology SRD	Conical frustum
	W.S. Atkins Engineering Sciences Ltd	Conical frustum
MAJESTIC SHELF2 PIPEFIRE MAJ3D	HSE Major Hazard Assessment Unit, Bootle	Conical frustum

6.3.2.3   Field models for jet flames

The following field models are available: Jasmin, Harwell-Flow3D, Kameleon Fire [Cowley, 1991]. Furthermore there are research organisations which have specialised models. Field models consist of several sub-models such as:

− **Turbulence models** which produce realistic flow fields in the geometry being considered. Standard k-ε turbulence models have been shown to predict flow field incorrectly when the flow has significant swirl.

− **Combustion of gaseous species models**, based on the instantaneous chemical properties, and which are capable of predicting the concentration of partial products of combustion such as CO and have the facility to test the effect of turbulent fluctuations on the reactions.

- **Soot production and oxidation models**, based on instantaneous species concentrations derived from the gaseous combustion model, hence the requirement to predict partial products of combustion such as OH, which plays a major role in soot oxidation. Since the timescales of soot reactions are much longer than the timescale of gas reactions, the effect of residence time should be included in the soot model. Finally, the effects of turbulent fluctuations should be tested.

- **Radiative heat transfer models**, capable of handling non-isothermal, non-homogeneous species distributions, reabsorption of radiation within the flame and the effect of turbulent fluctuations which are tested.

The requirements for these models are:
- The boundary conditions on surfaces and openings should be defined for all the variables.
- Boundary conditions, such as pressure conditions, at openings should not produce unphysical behaviour in the flow variables.
- In most combustion problems, it is necessary to extend the computational grid well outside the area of interest because of ventilation flows and flame extensions.
- Numerical methods should be tested for convergence of computational solutions and numerical accuracy.

6.3.2.4   Integral models

Earlier integral models ignore the unmixedness of turbulent jet diffusion flames, [Cowley, 1991]. At a given axial position both the flammable material and the air can coexist at the same time in separate turbulent eddies without reacting until they are mixed together. The key sub-models in jet fire integral models are similar to the sub-models for field models of jet fires.
Integral models of jet fires from Cowley [1991] are: UPMFIR, TORCIA, THRAIN and Cook's model.
Of the integral models only Cook's model has been validated against large scale flames. However, even Cook's integral model does not have its sub-models' validation against data from large-scale experiments because no such data exists.

6.3.3   Impinging fires

6.3.3.1   Introduction

The past 5 to 10 years much attention has been paid to heat impact of impinging flames. Two types of impinging jet flames are recognised in literature, viz. the situation in which the object does not perturb the flame, and the situation in which the object causes a strong distortion of the flame.

In the literature an overview of appraised work on jet flame impingement up to 1986 could be found. Much of the work has been conducted on laboratory flames, burners and furnaces.

Cowley (1991) states that soundly based information on heat transfer from large jet fires to engulf objects is lacking. Whilst theoretical models are now beginning to address these problems, currently the only reliable method for obtaining impingement heat flux is direct measurement in flames of adequate size.

6.3.3.2   Fire engulfment of tanks

In the publications Ramskill [1988] and Ramskill [1989] a description of the 'Engulf-II' is given. In Ramskill [1989] the description was detailed containing all the mathematical formulae. The models described show that differential equations have to be solved simultaneously. In the ENGULF-code a fourth order Runge-Kutta algorithm is used to calculate the wall temperatures and the bulk vapour and liquid temperatures.
The present code 'Engulf-II', can model either total or partial fire engulfment of a LPG-tank, including jet flame impingement. Other features available within the code are the treatment of safety relief vent valves, bulk boiling of liquid contents, external tank wall thermal insulation by water spray cooling, tank failure prediction and the modelling of a gas or petrol filled tank. According to Ramskill (1988) the code predictions have to be in agreement with available experimental data.
No field tests were performed but the basics of the models presented are useful.

Computational Fluid Dynamics (CFD) field modelling approaches are particularly under development. It is possible that this method is capable of predicting a wide range of impingement conditions. CFD is a sophisticated and powerful technique in which the basic physics and chemistry of a flowing fluid can be solved in space and time. However, there are a large number of unknowns that can only be solved with the aid of practical data. Run times of these models are in the order of hours. CFD methods must be regarded as useful adjuncts to the experimental work.

6.3.4   Pool fires on land

6.3.4.1   Introduction

A pool fire can be defined as a turbulent diffusion fire burning above a horizontal pool vaporising flammable material under conditions where the flammable material has zero or very low initial momentum, Cowley [1991].

A key feature of these fires is that there is a degree of feedback between the fire and the flammable material. To a greater or lesser extent, there is a heat transfer back from the fire to the pool that influences or even controls the rate of evaporation and hence the fire size and other characteristics.
The pool with flammable material is not necessarily static. It may be spreading or contracting. Additional flammable material could be coming from a leak. Depletion of the local flammable material supply can occur via drainage or overflow to other areas - perhaps giving tide to running liquid fires.
The most important parameters for a burning pool which determine the flame shape are the flame length, flame tilt and the flame drag. The aspect of influence of the wind

on the flame shape and burning rate can be considered as an addition to the previous edition of the Yellow Book and will be discussed in this section.

6.3.4.2 Semi-empirical models for pool fires

Point source model
In the point source model it is assumed that the heat radiation of the flame is radiated from a point which equally disperses in radial direction from the emission point as a sphere.
The heat flux q" versus the distance from the emission point decreases with the inverse square of the distance.

$$q'' = F_s \times m_h' \times \Delta H_c/(4 \times \pi \times X^2) = F_s \times m_h' \times \frac{\Delta H_c}{4 \times \pi \times X^2} \qquad (J/(m^2 \cdot s)) \qquad (6.5)$$

in which:
q'' = Heat flux, in $J/(m^2 \cdot s)$
F_s = Fraction of the combustion heat radiated from the flame surface
m_h' = Burning rate, in kg/s
ΔH_c = Net heat of combustion at the boiling point of the flammable material, in J/kg
X = The distance from the source to the receiver, in m

These models can be accurate for distances greater than 5 pool diameters from the centre of the flame. The key parameters which affect the prediction from the point source models are the location of the assumed point source, whether maximum fluxes or fluxes to an oriented receiving surface are required, and the fraction of combustion energy released as radiation.
The source can be located at the geometrical centre of the flame, which is determined by empirical correlations for the flame length and tilt, or it can be located at the centre of the pool.

In the commercially available package WHAZAN another point source model has been used, derived from formulae from Yellow Book [1992] and Thomas [1963].

$$q'' = \frac{\left(\pi \times D \times L + \pi \times \frac{D^2}{4}\right) \times m'' \times F_s \times \Delta H_c}{(c_1 \times m''^{0.61} + 1) \times (4 \times \pi \times X^2)} \qquad (J/(m^2 \cdot s)) \qquad (6.6)$$

in which:
D = Pool diameter, in m
L = Average flame height, in m
m'' = Burning flux at still weather conditions, in $kg/(m^2 \cdot s)$
ΔH_c = The heat of combustion of the flammable material at its boiling point, in J/kg
F_s = Fraction of the generated heat radiated from the flame surface
X = Distance from the point source, in m
c_1 = 72 $(m^{1.22} \cdot s^{0.61})/kg^{0.61}$

Surface emitter models
In principle these models can give an accurate predicted radiation perpendicular to
the flame length, so formula (6.4) can be used; see also subsections 6.5.3 and 6.6.2.

The atmospheric absorption can be calculated as described in chapter 6.5; the view
factor can be calculated with the formulae in the Appendix for a cylinder or tilted
cylinder and the average surface emissive power assigned to a given flame shape. The
surface emissive power is constant over the flame surface or has two separate values -
one for strongly emitting clear flames at the base of the flames and one for dark sooty
flames above. It can also be given by statistical description of the bright flame and the
dark sooty areas.

6.3.4.3   Field models for pool fires

Field models are mathematically complex, embodied in flare computer
programs and have significant run times on large computer systems.

6.3.4.4   Integral model for pool fires

At present there are no integral models for pool fires which could be used
for the prediction of large-scale pool fire hazard consequences.

6.3.4.5   Dimensions of the pool fire

Pool diameter

The equivalent pool diameter of a confined pool can be estimated from the estimated
surface area and the pool perimeter, with:

$$D = 4 \times A_p / S_p \qquad\qquad \text{(m)} \qquad\qquad (6.7)$$

in which:
A_p =   Surface area of the pool, in m²
S_p =   Pool perimeter, in m.

In practice it is rather difficult to calculate the pool perimeter with an irregular shape.
Therefore the pool diameter can be better determined with an equivalent circular
pool or, if the pool is rather square, with an equivalent square. This means that the
dimensions of the pool are determined using the surface area of the original pool.

The only literature which could be found about a fire of an unconfined pool is
described in Cline [1983].

This model describes a pool fire on land which was fed from a storage tank. A maximum pool diameter was ultimately obtained if the burning rate and the spill rate from the tank are equal.

In this model the thickness of the pool has to be taken arbitrarily.

Burning rate

In Babrauskas [1983] equations are given for the simulation of the burning rate in large pool fires, based on large scale experiments.

For most flammable liquids, reliable measurements exist only for m" as a function of D and not for k, T_f, k or β separately. In table 6.5 values of k × β are listed. The data can be presented in the mathematical function as:

$$m" = f(m_\infty", k, \beta, D) \qquad (kg/(m^2 \cdot s)) \qquad (6.8)$$

in which:
$m_\infty"$ = Burning flux, in kg/(m²·s) and for large pool diameter
k = Absorption extinction coefficient of the flame, in m⁻¹
β = Mean-beam-length corrector
D = Pool diameter, in m

If the mass burning rate is not tabulated, the best correlation to use for predicting the mass burning rate is that of Burgess, Hertzberg [1974]; applicable for single component liquids under ambient conditions. It shows the burning rate as function of:

$$m" = f(\Delta H_c, \Delta H_v, C_p, T_b, T_a) \qquad (kg/(m^2 \cdot s)) \qquad (6.9)$$

in which:
ΔH_c = The heat of combustion of the flammable material at its boiling point, in J/kg
ΔH_v = The heat of vaporisation of the flammable material at its boiling point, in J/kg
C_p = The heat capacity, in J/(kg·K)
T_a = Ambient temperature, in K
T_b = The liquid boiling temperature, in K

The influence of wind on the burning rate has been demonstrated experimentally. For, e.g., a burning hexane pool a doubling of the burning rate was observed. Babrauskas [1983] has derived the following relationship between the burning rate of a pool and the wind velocity:

$$m"_{wind}/m" = 1 + c_2 \times u_w/D \qquad (-) \qquad (6.10)$$

in which:
m" = Burning flux at still weather conditions, in kg/(m²·s)
$m"_{wind}$ = Burning flux under windy weather conditions, in kg/(m²·s)
c_2 = 0.15 s
u_w = Wind velocity, in m/s
D = Pool diameter, in m

According to Babrauskas [1983] this is the best available formula, with the restriction that it is not applicable for alcohols, nor for conditions under which a fire is blown out (wind velocity > approximately 5 m/s).

Babrauskas [1983] made some remarks on the experimental data which show a slight decrease in burning rate of very large pools with diameters larger than 5 to 10 metres. It seems that not enough systematic and precise data exist to provide a numerical model here, assuming independence of m" on D in this regime. Qualitatively this is presumed to be due to poorer mixing, leading to a larger cool vapour zone, lower flame temperatures, and cooler smoke (which can act to shield a fire base from its flames). In any case, this effect is likely to be larger than about 20%.

Flame length

Many models are proposed in literature. In general for visible flame, length without any influence of wind is estimated by the equation from Thomas (1963):

$$L/D = f(m", \rho_{air}, D) \qquad\qquad (-) \qquad\qquad (6.11)$$

in which:
m"   =   Burning rate at still weather conditions, in kg/(m²·s)
ρ_{air} =   Density of air, in kg/m³
D   =   Pool diameter, in m

Under wind blow conditions formula (6.11) becomes a function of u^*:

$$L/D = f(m", \rho_{air}, D, u^*) \qquad\qquad (-) \qquad\qquad (6.12)$$

with

$$u^* = u_w/u_c \qquad\qquad (-) \qquad\qquad (6.13)$$

$$u_c = (g \times m" \times D/\rho_{air})^{1/3} \qquad\qquad (m/s) \qquad\qquad (6.14)$$

in which:
D   =   pool diameter, in m
g   =   Gravitational acceleration, in m/s².
m"   =   Burning rate at still weather conditions, in kg/(m²·s)
ρ_{air} =   Density of air, in kg/m³
u_w =   Wind velocity, in m/s
u_c =   Characteristic wind velocity, in m/s
u^* =   Scaled wind velocity

If u_w is less than u_c then u^* is assigned the value of unity. For wind velocities up to the characteristic value, the flame length therefore remains constant whilst at higher values flame shortening occurs.

It seems that the influence of the wind velocity on the burning rate, as indicated in Babrauskas (1983) has already been incorporated in the Thomas equations. So in the Thomas equations the burning rate in still air (u_w = 0 m/s) has to be used.

Flame tilt

Under wind conditions the flame is tilted in the wind direction with a certain angle Θ. Many small scale experiments have shown relationship with the Froude number Fr and the Reynolds number Re in [Sliepcevich, 1966]. A more simple relationship derived for large scale LNG-fire has also be found in [Atallah, 1973].

From Sliepcevich [1966] the following equations are found, showing the relationship:

$$\Theta = f(Fr, Re, \rho_v, \rho_{air}) \qquad\qquad (°) \qquad\qquad (6.15)$$

with

$$Re = D \times u_w/\upsilon$$

$$Fr = u_w^2/(g \times D)$$

in which:
Re = Reynolds number
Fr = Froude number

In the Reynolds equation 'υ' is the kinematic viscosity of air.

Although the equation for a tilted flame in [Sliepcevich, 1966] was initially derived from small scale fires, the equations for a conical and cylindrical representation were obtained from data from large LNG-pool fires, which were correlated.

The parameters a', b', c' and d' of the equation developed by Welker and Sliepcevich [Sliepcevich, 1966], are presented as follows:

$$\tan\Theta/\cos\Theta = a' \times (Fr)^{b'} \times (Re)^{c'} \times (\rho_v/\rho_{air})^{d'} \qquad\qquad (-) \qquad\qquad (6.16)$$

In table 6.2 values for the required parameters are given.

Table 6.2   Values of parameters of formula (6.16)

Equation		a'	b'	c'	d'
6.16-1	Conical flame	3.0	0.422	0.011	0
6.16-2	Cylindrical flame	1.9	0.399	0.050	0
6.16-3 Sliepcevich [1966]		3.3	0.8	0.07	0
6.16-4 Binding [1992]		0.666	0.333	0.117	-0.6

In the two equations for the conical and cylindrical flame, the density terms have been incorporated into a constant since the data is only applicable to one kind of flammable material.

The relationship given by Binding [1992] was determined by curve fitting with experimental data. The data does not indicate a relationship between the flame tilt and fuel type and therefore the correlation does not incorporate the term for gas vapour density used by Sliepcevich [1966]. The tilt is only applied to the lower half of the flames. Based on the experimental data, the model uses an angle of $\Theta/2$ applied to the upper half of the flame.

Due to the influence of wind the Thomas equation becomes:

$$\cos\Theta = e' \times (u^*)^f \qquad\qquad (-) \qquad\qquad (6.17)$$

In table 6.3 values for the required parameters are given.

Table 6.3   Values of parameters for formula (6.17)

Equation		e'	f'
6.17-1	Conical flame	0.87	-0.272
6.17-2	Cylindrical flame	0.86	-0.250
6.17-3 American Gas Association [1974]		1	-0.5

In most cases the vapour pressure is relatively low, so $\rho_v \approx \rho_{air}$, which means that:

$$u_c = (g \times m'' \times D/\rho_v)^{1/3} \approx (g \times m'' \times D/\rho_{air})^{1/3} \qquad\qquad (m/s) \qquad\qquad (6.14)$$

In which:

m'' = Burning flux at still weather conditions, in kg/(m^2·s)
g = Gravitational acceleration, in m/s^2
D = Pool diameter, in m
ρ_v = Vapour density of the flammable material, in kg/m^3

In the Thomas equations for a tilted flame, wind velocities at 10 m above the ground have to be used.

All the formulae developed for the determination of the tilted flame angle Θ have their limitations because the experiments were often carried out on a small scale or on a large scale with LNG pools (equations 6.17-1, 6.17-2 and 6.17-3).

Flame drag correlation

Due to wind the flame tilts and spills over the edge of a pool or storage tank. Consequently, the flame surface approaches any nearby object on the leeward of the pool, increasing the heat flux of thermal radiation. If wind is hard enough, the flame may impinge on, for instance, an adjacent tank.

Figure 6.1 shows a schematic representation of the pool diameter D, the flame height L, and the flame base D' which is elongated due to the effect of wind.
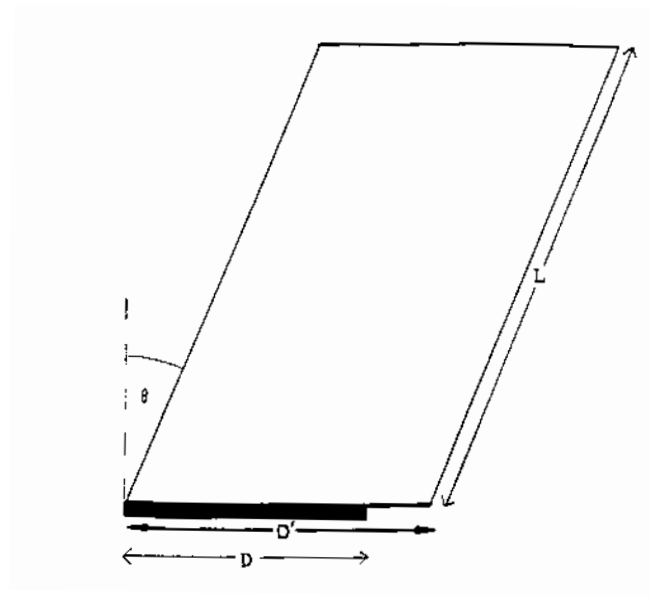
Figure 6.1

Correlation resulting for flames with a conical representation from Moorhouse (1982):

$$D'/D_w = g' \times (Fr)^{h'} \times (\rho_v/\rho_{air})^{i'} \qquad\qquad (-) \qquad\qquad (6.18)$$

In table 6.4 values for the required parameters are given.

Table 6.4   Values of parameters of formula (6.18)

Equation		g'	h'	i'
6.18-1	Conical flame	1.6	0.061	0
6.18-2	Cylindrical flame	1.5	0.069	0
6.18-3 Sliepcevich [1966]		2.1	0.21	0.48

The large scale LNG pool fires reported here are for square and rectangular pools and the extent of flame drag was expressed as D'/D_w. D_w is the maximum pool dimension in the direction of the wind. For circular pools it can be assumed that $D = D_w$.

A detailed study was performed in Sliepcevich [1966] which includes the flame drag for small circular fires in a wind tunnel using different fuels. The data resulted in equation (6.18-3) in table 6.4, in which D' is the actual elongated flame base dimension and D is the circular pool diameter.

The wind velocity at 10 m above the ground should be used in the Fr number.

6.3.4.6 Surface emissive power of pool fires

A method to assume the surface emissive power of pool fires is that the model flame has one uniform SEP over the whole of its surface. This approach was adopted in Mudan [1984] in which a derivation of the following correlation was given, using data from gasoline, kerosene and JP-5.

The SEP in W/m^2 is given by:

$$SEP = c_3 \times e^{-c5 \times D} + c_4 \times (1 - e^{-c5 \times D}) \qquad (J/(m^2 \cdot s)) \qquad (6.19)$$

$$
\begin{aligned}
c_3 &= 140 \times 10^3 \ J/(m^2 \cdot s) \\
c_4 &= 20 \times 10^3 \ J/(m^2 \cdot s) \\
c_5 &= 0.12 \ m^{-1} \\
D &= \text{Pool diameter, in m}
\end{aligned}
$$

where D is the pool diameter. Alternatives are presented in other literature and their approach for the flame shape is divided in lower and upper zones. The emissive power of the lower zone is taken as the SEP of clear flame multiplied by a factor which is the fraction of unobscured flame in the upper region.

The general approach for this type of flame is given in the following formula:

$$SEP_{act} = SEP_{max} \times (1 - \varsigma) + SEP_{soot} \times \varsigma \qquad (J/(m^2 \cdot s)) \qquad (6.20)$$

in which:
ς = the fraction of the surface of the flame covered by soot

Next to models, also literature presented many measurement results. This information will be described in chapter 6.5.

6.3.5 Pool fires on water

6.3.5.1 Introduction

Studies to model the effects of pool fires on water have, in the first place, been undertaken to evaluate the safety associated with transportation and storage of flammable materials, such as LNG and LPG. More recent studies have been directed towards the evaluation of combustion of spills of crude and fuel oils on water.

Many additional studies have been undertaken concerning specific topics, such as ignition, rate of flame spreading, burning rate and external factors which affect burning rate, effect of weathering and evaporation, heat transfer mechanisms and modelling. All these studies have generated qualitative results.
One model could be found to calculate the burning rate of hydrocarbons on water.

6.3.5.2 Burning rate

Extensive testing was carried out on water to determine the effect of the pool diameter on the burning rate of several crude oils. A compromise was that the oil was burnt in a pan floating in water, so the effect of spreading was neglected.
For all fuels tested, the burning rate initially decreased reaching a minimum point and finally rose to a constant value with an increasing test pan diameter. A constant burning rate was observed for pan diameters > 1 m.

In Petty [1983] seven different crude oils were combusted. The average burning rate in a 2 metre-diameter pans was determined at $5.8 \cdot 10^{-2}$ kg/(m²·s). The average burning rates between crude oils do not appear to be a function of a crude oil's overall specific gravity.

From the test results, a formula was derived to calculate the burning rate; this formula is given in chapter 6.5.

The wind influence on the burning rate was also determined in one of the experiments and resulted in an increase of the burning rate with a factor 2.

6.3.5.3 Pool diameter

This model of Cline [1983] as mentioned in subsection 6.3.4.5 is intended for unconfined pool fires on land.
It is assumed that the burning rate in kg/(m²·s) is constant; normally the burning rate is a function of the pool diameter.
No other models were found in literature, all data describe result of experiments.

6.3.5.4 Flame height

In Aravamudan [1979] an analytical expression was given to calculate the flame height. However, this equation does not correspond well with the figures presented.

6.3.5.5 Surface emissive power

For the surface emissive power for pool fires only test results were given. This data was not correlated with formulae.

6.3.6 Fire balls

6.3.6.1 Introduction

In Bagster [1989] an overview was given of the available models for the BLEVE's with a fireball. The models are exponential relationships to determine the fireball's diameter and duration. The TNO-model showed the best overall curve fit of the results.

The exponent of the relationships seems not to differ too much and is more or less dependent on the scale of the experiments. A graphical comparison between a number of models was made with results of accidents and experiments. In some cases, the quantity involved may be overestimated because of prior combustion or leakage.

A new development for the calculation of the fraction of generated heat which is radiated is given in subsection 6.3.6.2.

6.3.6.2 Fraction of the generated heat which is radiated

In [Roberts, 1982] the thermal radiation output from a fireball was characterised in terms of the fraction of combustion energy released through radiation, and its dependence on the release pressure. The following relation was obtained:

$$F_s = c_6 \times (P_{sv})^{0.32} \qquad\qquad (-) \qquad\qquad (6.21)$$

in which:

F_s = Fraction of the generated heat radiated from the flame surface
c_6 = 0.00325 $(N/m^2)^{0.32}$
P_{sv} = Saturated vapour pressure before the release, in N/m^2

6.3.6.3 Lift height of the fire ball

In Cowley [1991] and Bagster [1989] the fireball models have been evaluated in order to find the best available model. The TNO-model showed the best overall curve fit of the results. The formulae include the maximum diameter, duration and the centre height of the fire ball.

6.4   Selection of models

6.4.1   Introduction

In chapter 6.3 all models for the different fire types are addressed. Sometimes a number of different models were found for the same fire type or for the calculation of different aspects or parameters; in some cases the model is completely new to the previous edition of the Yellow Book and in other cases it is only an addition or extension.
In this chapter 6.4 the selection is made for those models mentioned in chapter 6.3. A choice between models means that criteria have to be used. These criteria are:
− degree of validation of the model against experimental data;
− complexity of the model.

6.4.2   Jet flames

For jet flames two models were considered because both were validated with large scale experiments.
One of the models is a centreline trajectory model which is fully described in [Cook, 1987]. The model uses difference equations in order to calculate the size and shape of the flame in small steps. Therefore a computer is necessary to calculate the heat radiation numerically; an analytical solution does not exist for flame models with the centre line trajectory. This computer model is commercially available as 'Thorin'.

The other model is a geometric solid flame shape from [Chamberlain, 1987] which is also validated with large scale experiments, however, it can be programmed more easily than the centre line trajectory model. In principle the heat radiation model for a frustum can be calculated analytically. In order to simplify calculations for the view factor, the shape of the frustum can even be approximated by a cylinder, by using the average diameter of the frustum.

Although the centre line trajectory models may approach the real flame shape better than the geometric models, the difference in heat radiation results at a distance seems to be minor.
Both models were validated for a wide range of natural gas experiments, so arguments of non- or limited validation cannot be used for the selection. Because the calculation of the geometric solid flame model can be made with less computational effort, this model has been chosen.

6.4.3   Heat impact of impinging fires

Until now no simple models were available for impinging fires to determine the heat flux and the temperature rise in steel walls and surfaces exposed to fire.

A thorough description of the heat impact of impinging and engulfing flames has been presented in [Ramskill, 1988]. At this moment 'ENGULF' can be considered as the

best attempt to model impingement and engulfment of tanks and vessels. However, other literature sources indicate that there are a large number of unknowns that can only be clarified by experimental data.

The current results of the tests show until now that the current knowledge and understanding in combusting flows is essentially qualitative.
At this moment there are no validated predictive tools available that can accurately describe the extent of engulfment and the heat flux distribution over fire impinged objects.

The model 'ENGULF' has not been incorporated, because it is a 3-D model and because it has not been validated until now.

6.4.4   Pool fires on land

For heat radiation calculations of a stationary flame shape, the 'Thomas'-equation (6.11) and the equation (6.9) of Burgess, Hertzberg [1974] can still be used. The 'Thomas'-equation appears to be adequate for predicting the flame length of pool fires with a diameter of up to 20 m. The relations which take the influence of wind into account can be added.

As indicated in Yellow Book [1992] the equivalent diameter of an irregular pool shape can be determined with the surface area of the pool and the perimeter. It is difficult to estimate the perimeter and therefore it is proposed to calculate the pool diameter, by assuming a circular pool with the same surface area as the original pool. If the shape of the irregular pool can be better compared with a square, then the length of one side can be calculated.

The equations to calculate Θ (angle of tilting of the flame) are different. The Thomas-equations (6.17-1) and (6.17-2) consistently underpredicts the experimentally obtained flame tilt angle while equation (6.17-3) tends to overpredict. The equations (6.17-1) and (6.17-2) in table 6.3 are for small scale experiments and equation (6.17-3) is only applicable to large scale LNG fires.

The equations (6.16-1), (6.16-2) and (6.16-3) in table 6.2 for conical and cylindrical flames are based on small scale experiments with different types of flammable materials, whereas equation (6.16-4) is determined by fitting of experimental data. The data does not incorporate the term for the gas vapour density used by Sliepcevich (1966).
In general, equation (6.16-4) is preferred for calculations because it fits experimental data.

With equation (6.19) the surface emissive power SEP can be calculated. This formula takes into account the influence of soot. It has been validated for gasoline, kerosene and JP-5 pool fires. The SEP seems only dependent of the pool diameter.

The view factor for conical and cylindrical flames can be analytically described. In the Appendix the graphical representation as well as the analytical equation are presented.

Furthermore, some experimental results were found in literature and are given in chapter 6.5.

Unconfined pool
The only model for pool fires on land [Cline, 1983], could also be applicable to pool fires on water. With the models the maximum diameter of spreading pool fires can be calculated. The model has not been validated for large scale situations on land. However, it seems to match the small scale measurements well.
Some equations (6.78), (6.80) and (6.82) will be given, despite limited validation.

6.4.5 Pool fires on water

No data could be found on the calculation of the flame height. Formulae (6.11) and (6.12) for pool fires on land will be used for pool fires on water. Furthermore, some experimental results were found in literature and are given in chapter 6.5.

6.4.6 Fire balls

In Cowley [1991] and Bagster [1989] fireball models have been evaluated in order to find the best available model. It can be concluded that (6.90) shows the best prediction for the whole range of data available from small scale fireballs to large ones. Equations (6.90) and (6.91) which are required for calculation of the fireball diameter and duration respectively, seem to match the available accidental data of fireballs well. The centre height of the fire ball, which belongs to these selected formulae, is

$$H_{bleve} = 2 \times r_{fb} \tag{6.22}$$

according to Bagster [1989].

Equation (6.21) for the calculation of the fraction of the generated heat which is related to the saturated vapour pressure, is a useful extension to this model.

6.5   Description of selected models

6.5.1   Introduction

In this chapter, for all fire types a description of the selected models is given. The objective of the selected models is to estimate the heat flux onto an object at a certain distance.
The formulae are presented in steps and where necessary an explanation has been given. If required, experimental data in tables and figures is given.

6.5.2   Surface emissive power

The important parameters for heat radiation which contribute to the heat load of an object, are:

−   Surface Emissive Power (SEP) is the heat radiated outwards per surface area of the flame, including the influence of the soot formation (subsection 6.5.2.2).
−   View factor F_{view} (subsection 6.5.2.3) which takes into account:
   –   The shape of the fire, including the influence of wind
   –   Distance of receptor to the outside surface of the fire,
   –   Orientation of the receiving surface (horizontal, vertical and maximum value).
−   Atmospheric transmissivity τ_a (subsection 6.5.2.4).

6.5.2.1   Released heat from combustion

The heat which is generated in a fire depends on the burning rate and the heat of combustion of the flammable material.
For modelling a static situation, the shape and the dimensions of the fire are taken constant, which implies that the supply rate of flammable material is equal to the combustion rate. The burning rate differs for the various fire types, for instance:

Jet flame: the burning rate under stationary conditions is equal to the release rate in kg/s of the flammable material.
Pool fire: the evaporation rate from the pool is equal to the burning rate.
Fire ball: the burning rate is equal to the total amount of flammable material divided by the duration of the fire ball (which is in fact also the supply rate).

6.5.2.2   Fraction of the heat radiated

The radiation emittance of materials for which SEP_{max} has not been measured can be estimated from the combustion energy generated per second, which can be determined from the combustion burning-rate and the heat of combustion of the material, the surface area of the flame and a fraction of the generated heat which

is radiated. Hereby it is necessary to select a value of the radiation fraction F_s. A careful estimation departs from the maximum value found in literature for F_s (see for some values of F_s in table 6.6 and formulae (6.21) and (6.59)):

$$SEP_{max} = F_s \times SEP_{theor} \qquad (J/(m^2 \cdot s)) \qquad (6.3)$$

$$SEP_{max} = F_s \times Q'/A \qquad (J/(m^2 \cdot s)) \qquad (6.23)$$

in which:
SEP_{max} = Maximum Surface Emissive Power from a flame without soot production, in $J/(m^2 \cdot s)$
Q' = Combustion energy per second, in J/s
F_s = Fraction of the combustion energy radiated from the flame surface
A = Surface area of the flame, in m^2

The F_s factor, in formula (6.3), gives the fraction of the generated heat in the fire emitted by the flame surface in the form of heat radiation. This fraction differs per type of fire, such as jet flame, pool fire and fire ball, but also depends on the type of combustible material.

In contrast to formula (6.3), however, it appears from experiments that the emissivity decreases with an increase of the flame diameter. Mudan [1984] attributes this to an increasing formation of black smoke at the flame boundary, such as has been established by hydrocarbons with a molecular ration of carbon: hydrogen bigger than 0.3. This black smoke or soot can absorb a great part of the radiation. So the actual value of SEP_{act} is less than SEP_{theor} and SEP_{max}.

The following formula can be used:

$$SEP_{act} = SEP_{max} \times (1 - \varsigma) + SEP_{soot} \times \varsigma \qquad (J/(m^2 \cdot s)) \qquad (6.20)$$

in which:
ς = Fraction of the surface of the flame covered by soot

Hägglund [1976] has found for smoke $SEP_{soot} \approx 20 \times 10^3 \ J/(m^2 \cdot s)$ (in agreement with $T \approx 800 \ K$). Only when such a smoke is not present, the value of SEP calculated from the flame temperature must be approximated with formula (6.1).

Mudan [1984] proposes to estimate the emittance of sooting flame surface, assuming that the major part of the flame (for instance 80%) is enveloped by black smoke and that there are only certain spots (20%) in which the emittance is maximal.

6.5.2.3 View factor

The geometrical view factor is the ratio between the received and the emitted radiation energy per unit area.
The factor is determined by the flame dimensions and shape, and by the relative position and orientation of the receiving object.

In general, simple flame shapes are taken for the calculations such as sphere, cylinder and flat plate.

The view factor of a cylinder can be used for a circular pool fire and a flat plate for a square or rectangular pool fire. The view factor of a sphere can be used for a fire ball. Practical data and theoretical background of these view factor are given in Appendix. The formula of the view factor becomes more complicated for e.g. a tilted flame, due to wind influence. For this type of fire a rather complicated analytical solution exists.

6.5.2.4   Atmospheric transmissivity

The atmospheric transmissivity (τ_a) accounts for the fact that the emitted radiation is partly absorbed by the air present between the radiator and the radiated object. The factor is equal to 1 minus the absorption factor, the value which depends on the absorbing properties of the components of the air in relationship to the emission spectrum of the fire. Since water vapour and carbon-dioxide are the main absorbing components within the wave length area of the heat radiation, the following approximating expression can be given:

$$\tau_a = 1 - \alpha_w - \alpha_c \qquad\qquad (\text{-}) \qquad\qquad (6.24)$$

Both factors depend on the partial vapour pressure, length L covered by the radiation, the radiator temperature and the ambient temperature. The partial vapour pressure of carbon-dioxide in the atmosphere is normally 30 N/m^2, however, the partial vapour pressure of water depends always on the temperature and the relative humidity.

The absorption takes place in some absorption bands of which the major ones are:

water: 1.8 μm, 2.7 μm, 6.3 μm
carbon-dioxide: 2.7 μm, 4.3 μm, 14.4 - 20 μm

Since the energy distribution of the radiation depends on the radiator temperature, the absorption will also be dependent on it. An exact calculation of τ_a is complicated.

An approximation method on the basis of emission factors given by Hottel [1967] and summarized by Mudan [1984] is only outlined here:

a.   determine the partial vapour pressure of water p_w and the length x to be covered by the radiation in the flame.

b.   calculate the reduced vapour pressures.

$$P_w{}^* = p_w \times \left(\frac{T_f}{T_a}\right) \qquad\qquad (\text{N/m}^2) \qquad (6.25)$$

$$P_c{}^* = p_c \times \left(\frac{T_f}{T_a}\right) \qquad\qquad (\text{N/m}^2) \qquad (6.26)$$

in which T_f is the flame or radiator surface temperature and T_a the ambient temperature.

c. Determine the emission factors ε_w (for water vapour) and ε_c (for carbon-dioxide) for these reduced vapour pressures from the graphs from Hottel [1967], not included in this paragraph.

d. Calculate the absorption factors α_w (for water vapour) and α_c (for carbon-dioxide) from the preceding, in accordance with Welker [1982]:

$$\alpha_w = \varepsilon_w \times (T_a/T_f)^{0.45} \qquad\qquad\qquad (-) \qquad\qquad (6.27)$$

$$\alpha_c = \varepsilon_c \times (T_a/T_f)^{0.65} \qquad\qquad\qquad (-) \qquad\qquad (6.28)$$

From equations (6.25) and (6.27) we obtain α_w as function of $P_w{}^* \times x$, in which x is the distance from the surface area of the flame to the object, in m; from equations (6.26) and (6.28) we obtain α_c, as function of $P_c{}^* \times x$. In order to be able to convert these functions into values of: α_w, as function of $p_w \times x$, and α_c, as function of $p_c \times x$, the temperature T_f must be known.
In table 6.5 a number of typical flame temperatures can be found. These values vary between 800 and 1600 K.
If no data is available an average temperature of 1200 K is recommended.

However, for temperatures T_f α_w and α_c can be estimated directly using the graphs from Hottel [1967] which are given in Figures 6.2 and 6.3.
The transmissivity τ_a can be calculated as a function of x, the distance between radiator surface and object.

For relative humidities (RH) of 0.4 and 1 and an 'average' radiation temperature of 1200 K, the transmissivity in Figure 6.4 (in this subsection) has been calculated.

It can be seen from this that differences in relative humidity have little influence on τ_a provided τ_a is expressed as a function of $p_w \times x$. The relationship shown is in relatively good agreement with the graphs given by Raj [1977], which in turn are derived for a radiator temperature of 1150 °C, disregarding the carbon-dioxide absorption.
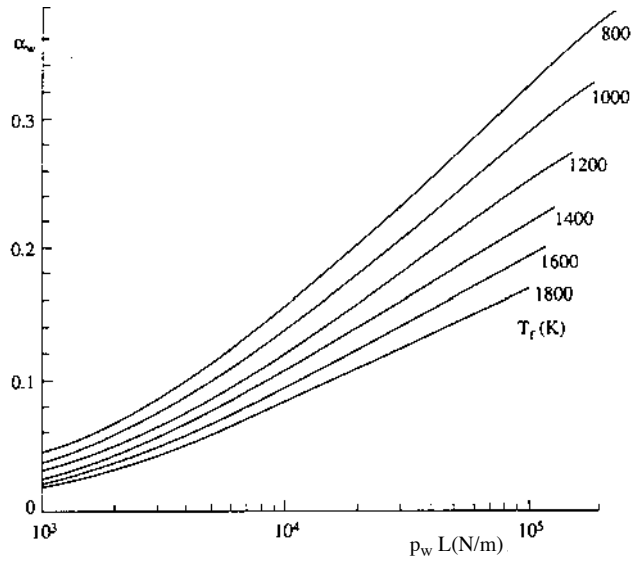
Figure 6.2   Absorption factors for water vapour
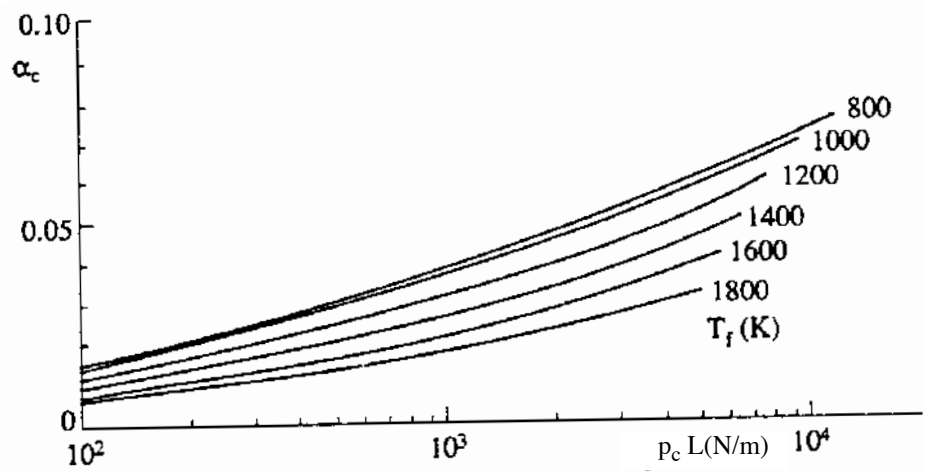
Figure 6.3   Absorption factors for carbon-dioxide
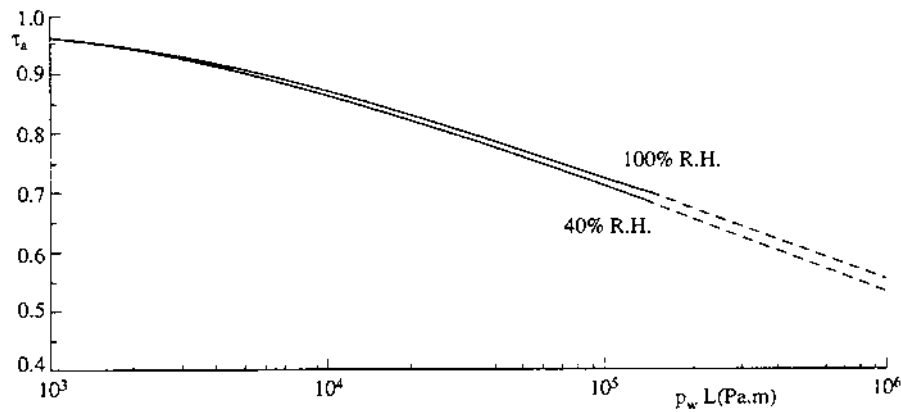
Figure 6.4   *Transmissivity as a function of the product water vapour pressure p_w and length x (radiator temperature 1200 K)*

A simple formula was produced [Bagster, 1989], based on data of Figure 6.4, to calculate the atmospheric transmissivity for all types of fire.

$$\tau_a = c_7 \times (p_w \times x)^{-0.09} \qquad\qquad (\text{-}) \qquad\qquad (6.29)$$

in which:

c_7 =   2.02 $(N/m^2)^{0.09} \cdot m^{0.09}$

p_w =   Partial water vapour pressure of water in air at a relative humidity RH, in N/m^2

x   =   Distance from the surface area of the flame to the object, in m

This formula can only be used for calculations in the range between:

   $10^4 < p_w \times x < 10^5$ N/m.

In all other cases it is not advised to use (6.29).

6.5.3   Jet flames

In this subsection the model from Chamberlain [1987] has been described. This model, also called 'Thornton-model', predicts the flame shape and radiation field of flares from flare stacks and flare booms. This model has been developed in several years of research and has been validated with wind tunnel experiments and field tests both onshore and offshore. The model represents the flame as a frustum of a cone, radiating as a solid body with a uniform surface emissive power. Correlation describing the variation of flame shape and surface emissive power under a wide range of ambient and flow conditions. By increasing the gas exit velocity, the fraction of heat released as radiation and the levels of received radiation are reduced. Correlation of laboratory data and field experience has shown that flames are fully stable under a

6.50

much wider range of ambient and flow conditions than indicated in API RP 521. Figure 6.5, which is given below, shows the sequence of steps:

```
┌──────────────────────────────────┐
│ Calculate effective source       │
│ diameter                         │
│ (Subsection 6.5.3.1 and 6.5.3.2, │
│ steps 1-9)                       │
└──────────────────────────────────┘
              │
┌──────────────────────────────────┐
│ Calculate lenght of the jet flame│
│ (Subsection 6.5.3.2, steps 10-12)│
└──────────────────────────────────┘
              │
┌──────────────────────────────────┐
│ Calculate surface area of the    │
│ jet flame                        │
│ (Subsection 6.5.3.2, steps 13-20)│
└──────────────────────────────────┘
              │
┌──────────────────────────────────┐
│ Calculate heat generated due     │
│ to combustion                    │
│ (Subsection 6.5.3.3, step 21)    │
└──────────────────────────────────┘
              │
┌──────────────────────────────────┐
│ Calculate surface emissive       │
│ power (SEP)                      │
│ (Subsection 6.5.3.3, steps 22-23)│
└──────────────────────────────────┘
              │
┌──────────────────────────────────┐
│ Calculate view factor            │
│ (Subsection 6.5.3.4, steps 24-25)│
└──────────────────────────────────┘
              │
┌──────────────────────────────────┐
│ Calculate transmissivity         │
│ (Subsection 6.5.2.4)             │
└──────────────────────────────────┘
              │
┌──────────────────────────────────┐
│ Calculate heat flux at a certain │
│ distance                         │
│ (Subsection 6.5.3.5)             │
└──────────────────────────────────┘
```

Figure 6.5   Sequence for the calculation of the heat flux of a jet flame at a certain distance

The flow diagram for the calculation of the heat flux at a certain distance of a jet flame can be divided into five parts, viz.:

− Calculation of the exit velocity of the expanding jet;
− Calculation of the dimension of the flame;
− Calculation of the surface emissive power (SEP);
− Calculation of the view factor;
− Calculation of the heat flux at a certain distance.

6.5.3.1   Calculation of the exit velocity of the expanding jet

Step 1 to 6 show the calculation of the exit velocity of an expanding jet. This exit velocity is an important parameter for the calculation of the flame length, lift-off and the widths of the frustum. First the properties of the flammable material are required for the calculation of the exit velocity of the gas, i.e.: molecular weight, the Poisson constant and the storage conditions of the gas, such as temperature and pressure.

Step 1
Determine the mass fraction of flammable material in a stoichiometric mixture with air:

$$W = W_g/(15.816 \times W_g + 0.0395) \qquad\qquad (\text{-}) \qquad\qquad (6.30)$$

in which:
W_g =   Molecular weight of gas, in kg/mol

Step 2
Calculate Poisson constant γ

$$\gamma = C_p/C_v \qquad\qquad\qquad (\text{-}) \qquad\qquad (6.31)$$

For a so-called 'ideal gas'

$$C_v = C_p - R_c/W_g \qquad\qquad\qquad (\text{J/(kg·K)}) \qquad (6.32)$$

in which:
C_p =   Specific heat capacity at constant pressure, in J/(kg·K)
C_v =   Specific heat capacity at constant volume, in J/(kg·K)
R_c =   Gas constant 8.314 J/(mol·K)

However, for high pressure gas, it is necessary to calculate γ more accurately by using equation (6.31).

Step 3
Determine the temperature of the expanding jet:

$$T_j = T_s \times (P_{air}/P_{init})^{((\gamma - 1)/\gamma)} \qquad (K) \qquad (6.33)$$

in which:
T_s =   Initial temperature of the gas, in K
P_{air} =   Atmospheric pressure, in N/m^2
P_{init} =   Initial pressure, in N/m^2
γ =   Ratio of specific heats, Poisson constant

Step 4
Determine the static pressure at the hole exit plane:

$$P_c = P_{init} \times (2/(\gamma + 1))^{(\gamma/(\gamma - 1))} \qquad (N/m^2) \qquad (6.34)$$

Step 5
Determine the Mach-number for choked flow of an expanding jet:

$$M_j = \sqrt{\frac{(\gamma + 1) \times \left(\left(\dfrac{P_c}{P_{air}} \right)^{\left(\frac{\gamma - 1}{\gamma} \right)} - 2 \right)}{\gamma - 1}} \qquad (-) \qquad (6.35)$$

in which:
P_c =   Static pressure at the hole exit plane, in N/m^2

or in case of unchoked flow

$$M_j = \sqrt{\frac{\sqrt{1 + 2(\gamma - 1)F^2} - 1}{\gamma - 1}}$$

in which:
F = $3.6233 \cdot 10^{-5} \times \dfrac{m^1}{d_o^2} \sqrt{\dfrac{T_j}{\gamma W_g}}$
m' =   Mass Flow Rate, in kg/s
d_o =   Diameter of hole, in m
T_j =   Temperature of the gas in the jet, in K
W_g =   Molecular weight of gas, in kg/mol

Step 6
Determine the exit velocity of the expanding jet

$$u_j = M_j \times (\gamma \times R_c \times T_j/W_g)^{1/2} \qquad (m/s) \qquad (6.36)$$

in which:
R_c =   Gas constant 8.314 J/(mol·K)
T_j =   Temperature of the gas in the jet, in K
W_g =   Molecular weight of gas, in kg/mol

Background of this model can be found in chapter 2.

6.5.3.2 Calculation of the flame dimensions

In step 7 to 20 position and dimensions of the flames are determined. These position parameters are required to calculate the lift-off and the angle of the flame with respect to the object. This is important for the calculation of the view factor. The flame dimensions are used to calculate the surface area of the flame.

Step 7
Determine the ratio of wind speed to jet velocity

$$R_w = u_w/u_j \qquad\qquad (-) \qquad\qquad (6.37)$$

in which:
u_w = Wind velocity, in m/s
u_j = Velocity of the jet, in m/s

Step 8
Determine the density of air:

$$\rho_{air} = P_{air} \times W_{air}/(R_c \times T_{air}) \qquad\qquad (kg/m^3) \qquad\qquad (6.38)$$

in which:
P_{air} = Atmospheric pressure, in N/m^2
W_{air} = Molecular weight air, in kg/mol
R_c = Gas constant 8.314 J/(mol·K)
T_{air} = Air temperature, in K

Step 9
Determine combustion effective source diameter:

In combustion modelling the effective source diameter D_s is a widely used concept, representing the throat diameter of an imaginary nozzle releasing air of density ρ_{air} at a mass flow rate m'.

$$D_s = (4 \times m'/(\pi \times \rho_{air} \times u_j))^{1/2} \qquad\qquad (m) \qquad\qquad (6.39)$$

in which:
D_s = Effective hole diameter, in m
m'   = mass flow rate, in kg/s
ρ_{air} = Density of air, in kg/m^3
u_j = Velocity of the jet, in m/s

If the hole size is given, the mass flow rate at the exit hole has then to be calculated with the models from chapter 2 for the calculation of the release rate of gas.

The effective hole diameter in case of a choked flow can be calculated as follows:

$$\rho_j = P_c \times W_g/(R_c \times T_j) \qquad\qquad (kg/m^3) \qquad (6.40)$$

$$D_s = d_j \times (\rho_j/\rho_{air})^{1/2} \qquad\qquad (m) \qquad (6.41)$$

in which:
P_c = Static pressure at the hole exit plane, in N/m^2
W_g = Molecular weight of gas, in kg/mol
R_c = Gas constant 8.314 J/(mol·K)
T_j = Temperature of the gas in the jet, in K
d_j = Diameter of the jet at the exit hole, in m
ρ_j = Density of gas in the jet, in kg/m^3
ρ_{air} = Density of air, in kg/m^3

It can be assumed that the diameter of the jet is about equal to the hole diameter.

Step 10
Calculate first auxiliary variable Y by iteration with equation

$$C_a \times Y^{5/3} + C_b \times Y^{2/3} - C_c = 0 \qquad\qquad (-) \qquad (6.42)$$

in which:
Y = Dimensionless variable

This equation includes the following coefficients:

$$C_a = 0.024 \times (g \times D_s/u_j^2)^{1/3}$$

$$C_b = 0.2$$

$$C_c = (2.85/W)^{2/3}$$

Note, that the constant 2.85 (β in Chamberlain [1987] is valid for parafins only.

Step 11
Determine the length of the jet flame in still air:

$$L_{b0} = Y \times D_s \qquad\qquad (m) \qquad (6.43)$$

L_{b0} = Flame length, in still air, m

Step 12
Determine the length of the jet flame measured from the tip of the flame to the centre of the exit plane:

$$L_b = L_{b0} \times ((0.51 \times e^{(-0.4 \times u_w)} + 0.49)) \times$$
$$(1.0 - 6.07 \cdot 10^{-3} \times (\Theta_{jv} - 90°)) \qquad \text{(m)} \qquad (6.44)$$

in which:

Θ_{jv} = Angle between hole axis and the horizontal in the direction of the wind

Figure 6.6 shows a diagram with the cone frustum parameters of the 'Thornton-model'. Note that point P is always at the intersection of the hole and frustum axes. The 5 basic parameters that are used to correlate flame shape with flaring conditions, are R_l, W_1, W_2, α and b.

Figure 6.6   Diagram showing the cone frustum parameters used in the Thornton model. Note that point P is always at the intersection of the hole and the frustum axes. The 5 basic parameters used to corrolate flame shape with flaring conditions are R_l, W_1, W_2, α and b

Step 13
Determine the Richardson number of the flame in still air:

$$Ri(L_{b0}) = (g/(D_s^2 \times u_j^2))^{1/3} \times L_{b0} \qquad \text{(-)} \qquad (6.45)$$

If $R_w \leq 0.05$ (see (6.37)), then the flame is jet dominated. The tilt angle α is given by:

$$\alpha = (\Theta_{jv} - 90°) \times (1 - e^{(-25.6 \times Rw)}) + (8000 \times R_w)/Ri(L_{b0}) \qquad \text{(°)} \qquad (6.46)$$

in which:

Θ_{jv} = Angle between hole axis and the horizontal in the direction of the wind
$Ri(L_{b0})$ = Richardson number based on L_{b0}

If $R_w > 0.05$, then the flame tilt becomes increasingly dominated by wind forces:

$$\alpha = \begin{aligned}&(\Theta_{jv} - 90°) \times (1 - e^{(-25.6 \times Rw)}) + \\ &(134 + 1726 \times (R_w - 0.026)^{1/2})/Ri(L_{b0}))\end{aligned} \qquad (°) \qquad (6.48)$$

Step 14
Determine the lift-off of the flame by the following emperical relation:

$$b = L_b \times \frac{\sin K\alpha}{\sin \alpha} \qquad\qquad (m) \quad (6.49)$$

in which:
L_b = Flame length, flame tip to centre of exit plane, in m
K = $0.185 \times e^{-20Rw} + 0.015$

In still air ($\alpha = 0°$), b is equal to $0.2 \times L_b$. For 'lazy' flames pointing directly into high winds ($\alpha = 180°$), $b = 0.015 \times L_b$.

Step 15
Determine length of frustum (flame):

$$R_l = (L_b^2 - b^2 \times \sin^2(\alpha))^{1/2} - b \times \cos(\alpha) \qquad (m) \quad (6.50)$$

in which:
R_l = Length of frustum, in m

Step 16
Determine the ratio between air and jet density:

$$\rho_{air}/\rho_j = T_j \times W_{air}/(T_{air} \times W_g) \qquad\qquad (-) \quad (6.51)$$

Step 17
Determine the Richardson number based on the combustion source diameter and factor C', used for the calculation of the frustum base width:

$$Ri(D_s) = (g/(D_s^2 \times u_j^2))^{1/3} \times D_s \qquad\qquad (-) \quad (6.52)$$

$$C' = 1000 \times e^{(-100 \times Rw)} + 0.8 \qquad\qquad (-) \quad (6.53)$$

Step 18
Determine the frustum base width:

$$W_1 = D_s \times (13.5 \times e^{-6Rw} + 1.5) \times 1 - \left[1 - \frac{1}{15} \times \sqrt{\frac{P_{air}}{P_j}}\right] \times e^{-70Ri(Ds)^{C'Rw}} \quad (m) \quad (6.54)$$

in which:
W_1 = Width of frustum base, in m

Step 19
Determine the frustum tip width:

$$W_2 = L_b \times (0.18 \times e^{(-1.5 \times Rw)} + 0.31) \times (1 - 0.47 \times e^{(-25 \times Rw)}) \quad \text{(m)} \qquad (6.55)$$

in which:
W_2 = Width of frustum tip, in m

Step 20
Determine the surface area of frustum, including end discs:

$$A = \pi/4 \times (W_1^2 + W_2^2) + \pi/2 \times (W_1 + W_2) \times \\ ((R_1^2 + ((W_2 - W_1)/2)^2)^{1/2} \qquad \text{(m}^2\text{)} \qquad (6.56)$$

in which:
A = Surface area of frustum including end discs, in m^2

As an alternative for the calculation of the frustum surface area, the surface area for a cylinder with an average width can be applied, so calculations in Appendix can be applied.

$$A = \pi/2 \times ((W_1 + W_2)/2)^2 + \pi \times R_1 \times (W_1 + W_2)/2 \qquad \text{(m}^2\text{)} \qquad (6.57)$$

in which:
A = Surface area of a cylinder including end discs, in m^2

6.5.3.3 Calculation of the surface emissive power

The surface emissive power can be calculated with the net heat released from combustion of the flammable gas, the fraction of that part of the heat radiated and the surface area of the frustum.

Step 21
Determine the net heat per unit time released:

$$Q' = m' \times \Delta H_c \qquad \text{(J/s)} \qquad (6.58)$$

in which:
Q' = Combustion energy per second, in J/s
m' = Mass flow rate, in kg/s
ΔH_c = Heat of combustion, in J/kg

Step 22
Determine the fraction of heat radiated from the surface of the flame:

$$F_s = 0.21 \times e^{(-0.00323 \times uj)} + 0.11 \qquad \text{(-)} \qquad (6.59)$$

6.58

in which:

F_s =   Fraction of the generated heat radiated from the flame surface

Step 23
Determine the surface emissive power:

$$SEP_{max} = F_s \times Q'/A \qquad\qquad (J/(m^2{\cdot}s)) \qquad (6.60)$$

in which:
SEP_{max} =   Maximum surface emissive power, in $J/(m^2{\cdot}s)$

This is the final result of the 'Thornton-model'.

6.5.3.4   Calculation of the view factor

Coordinate transformation to X',Θ' is required before a model for the calculation of the view factors can be used.

Step 24
In Figure 6.7, this transformation takes into account the lift-off of the flame, change in distance to the object due to lift-off and the change of the angle under which the object observes the flame. This transformation is only correct if $\Theta_j = \Theta_{jv}$.

$$X' = ((b \times \sin\Theta_j)^2 + (X - b \times \cos\Theta_j)^2)^{1/2} \qquad (m) \qquad (6.61)$$

$$\Theta' = 90° - \Theta_j + \alpha - \arctan(b \times \sin\Theta_j /(X - b \times \cos\Theta_j)) \qquad (°) \qquad (6.62)$$

$$x = X' - (W_1 + W_2)/4 \qquad (m) \qquad (6.63)$$

In which:
X'   =   Distance from the centre of the bottom plane of a lifted-off flame to the object, in m
X   =   Distance from the centre of the flame without lift-off to the object, in m
x   =   Distance from the surface area of the flame to the object, in m
Θ'   =   Angle between the centreline of a lifted-off flame and the plane between the centre of bottom of the lifted-off flame and the object, in degrees
b   =   Frustum lift-off height, m
Θ_j =   Angle between hole axis and the horizontal in the vertical plane, in degrees
α =   Angle between hole axis and the flame axis, in degrees
W_1 =   Width of frustum base, in m
W_2 =   Width of frustum tip, in m
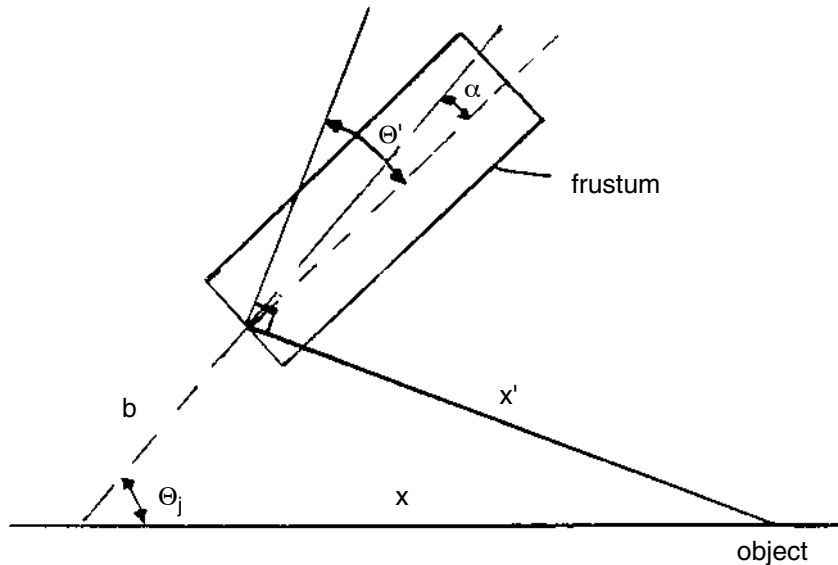
Figure 6.7   Distances, lengths and angles required for the calculation of a lifted-off flame

Step 25

Atallah et.al. [1990] show the mathematical formula to calculate the maximum view factor of a tilted cylinder at a lift in the direction of the cylinder's central axis. The frustum can be approximated by a cylinder, using the average diameter of the frustum. In the formulae of the Appendix the value of Θ' and X' can be used in Θ and X to calculate the view factor of a tilted cylinder with the formulae in the Appendix. If the tilt angle of the flame, the radius of the pool/flame, the flame length and the distance from the flame centre to the object are known, the maximum view factor can be calculated.

It is not allowed to position the object above or under the lifted cylinder, so the distance of the object from the centre of the flame should be greater than the radius of the cylinder.

6.5.3.5   Calculation of the heat flux at a certain distance

With the dimensions of the flame and the view factor the thermal heat flux at a certain distance x from the heat source can be calculated, with:

$$q''(x) = SEP_{act} \times F_{view} \times \tau_a \qquad\qquad (J/(m^2 \cdot s)) \qquad (6.4)$$

The SEP_{act} is the result of the calculations executed in step 23 in this chapter. The value of the view factor of a tilted cylinder can be calculated with the formulae in Appendix.

Both the transmissivity factor τ_a and the view factor F_{view} are distance dependent.

6.5.4   Pool fires on land

For pool fires on land a number of calculation steps can be distinguished, as is shown in Figure 6.8.

In the heat radiation calculations for pool fire the following main steps can be distinguished:
− Calculation of the liquid pool diameter;
− Calculation of the burning rate;
− Calculation of the flame dimensions of a pool fire;
− Calculation of the surface emissive power;
− Calculation of the heat flux at a certain distance.

These steps have been shown in fig. 6.8.
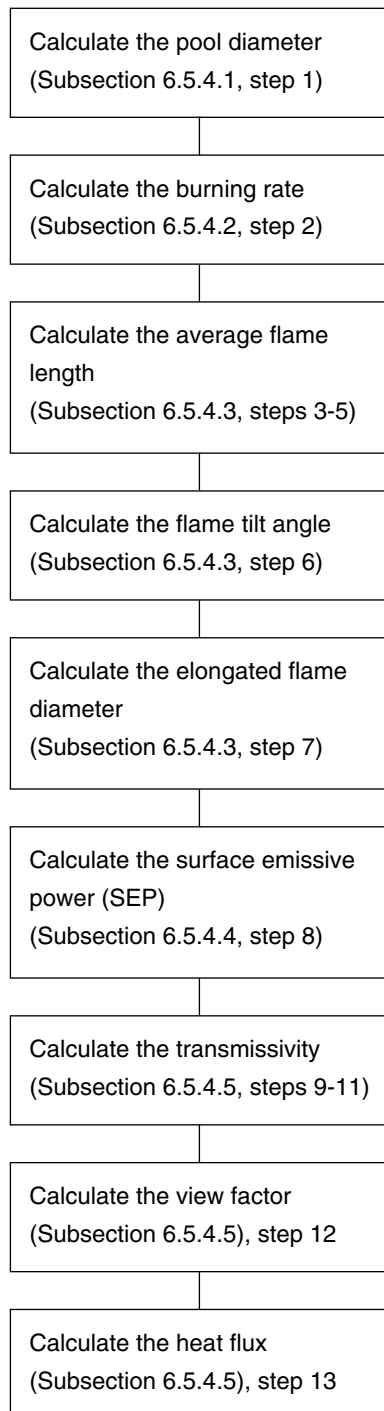
Figure 6.8   *Calculation diagram of the heat flux from a pool fire of a confined pool on land at a certain distance*

6.5.4.1   Calculation of the liquid pool diameter

In reality liquid pools will have an irregular shape. In this section the method is given for transferring this shape into a circular or rectangular pool, which is required for the calculation of the view factor.

Step 1
Determine the pool diameter

For circular pools the heat source can be considered to be cylindrical. In case of a rectangular or a nearly rectangular pool, for a ratio length/width smaller than 2, an equivalent or effective pool diameter D can be calculated, which is defined as follows:

Pools with an irregular shape from which the surface area can be determined, can be transformed into a circular pool. The pool diameter can then be calculated with:

$$D = (4 \times A_p/\pi)^{1/2} \qquad\qquad \text{(m)} \qquad\qquad (6.64)$$

in which:
D   = Pool diameter, in m
A_p = Surface area of the pool, in m^2

For a length/width ratio larger than 2 (a gutter), an equivalent diameter has to be calculated. The pool fire can thereafter be considered as a flat radiator. The Appendix includes formulae, numeric values and graphs of the geometric view factor for some radiator configurations.
If the released volume and the thickness of the pool can be determined, the circular pool diameter can also be calculated with:

$$D = (4 \times V/(\pi \times \delta))^{1/2} \qquad\qquad \text{(m)} \qquad\qquad (6.65)$$

in which:
V   = Volume of the released liquid, in m^3
δ = Thickness of the pool, in m

If the pool is confined in a bund, surface area, length and width are known. This can be used for calculation of the equivalent pool diameter or the side of an equivalent square.

6.5.4.2   Calculation of the burning rate

The burning rate is a function of the pool diameter. However, the influence of the diameter is only relevant for pools with a diameter smaller than 1 metre. Furthermore the flammable component will have an influence on the amount of absorption.
Table 6.5 shows burning rates of particular flammable components for large poolfires. The burning rate of single component liquid flammable material can be calculated with formula (6.9) in step 2a.

Step 2
Determine the pool burning rate m"

$$m'' = m_\infty'' \times (1 - e^{-k \times \beta \times D}) \qquad\qquad (kg/(m^2 \cdot s)) \qquad (6.66)$$

in which:
m" = Burning rate at still weather conditions, in kg/(m²·s)
m_∞'' = see m" for D → ∞ (see also table 6.5)
k = Absorption extinction coefficient of the flame, in m⁻¹
β = Mean beam length corrector

This form was first recommended by Burgess, Zabetakis [1961], in which (1- $e^{-k \times \beta \times D}$) represents the effective flame volume emissivity. The difference between m" and m_∞'' becomes less than 10% if the pool diameter is more than 2 metres.

In general the value of the factor (1 - $e^{-k \times \beta \times D}$) is above 0.95 if the pool diameter is more than 1 metre, so m" ≈ m_∞''.
There will be an influence of wind on the burning rate, which has been accounted for in the calculations for the flame length and diameter of the pool fire.

Table 6.5 shows data for Large Pool Burning Rate Estimates, [Babrauskas, 1983].

Table 6.5

Flammable material	m_∞'' (kg/(m².s))	k × ß (m⁻¹)	k (m⁻¹)	T_f (K)
Liq. H$_2$	0.169	6.1	-	1600
LNG	0.078	1.1	0.5	1500
LPG	0.099	1.4	0.4	-
Butane	0.078	2.7	-	-
Hexane	0.074	1.9	-	-
Heptane	0.101	1.1	-	-
Benzene	0.085	2.7	4.0	1490
Xylene	0.090	1.4	-	-
Gasoline	0.055	2.1	2.0	1450
Kerosene	0.039	3.5	2.6	1480
JP-5	0.054	1.6	0.5	1250
Methanol	0.015	1)	-	1300
Ethanol	0.015	1)	0.4	1490

1) Value independent of diameter in turbulent regime

Step 2a Alternative
If the mass burning rate has not been tabulated, the best correlation for predicting the mass burning rate of single component liquid flammable materials under ambient conditions is from Burgess [1974]:

$$m'' = c_8 \times \Delta H_c / (\Delta H_v + C_p \times (T_b - T_a)) \qquad (kg/(m^2 \cdot s)) \qquad (6.67)$$

in which:
c_8 = $0.001 \ kg/(m^2 \cdot s)$
ΔH_c =   The heat of combustion of the flammable material and its boiling point in J/kg
ΔH_v =   The heat of vaporisation of the flammable material and its boiling point, in J/kg
C_p =   The heat capacity in J/(kg·K)
T_b =   The liquid boiling temperature, in K
T_a =   Ambient temperature in K

6.5.4.3   Calculation of the flame dimensions of a pool fire (confined)

The diameter of a pool, which is in first approximation equal to the diameter of the fire, has been calculated in subsection 6.5.4.1. The other dimensions of a flame will be calculated in this subsection. The influence of wind on flame dimensions will also be considered here. A number of equations have been introduced in this chapter which take that influence into account, so length of the tilted cylinder, the tilt angle of the cylinder and the change of the flame basis are calculated here. In step 3 to 7 the formulae are given to calculate the dimensions. In step 7 there are two possibilities given to calculate the flame basis, viz. for a conical and a cylindrical flame.

Step 3
Determine the characteristic wind velocity u_c

$$u_c = (g \times m'' \times D / \rho_{air})^{1/3} \qquad (m/s) \qquad (6.14)$$

in which:
u_c =   Characteristic wind velocity, in m/s
g =   Gravitational acceleration 9.81 m/s²
m'' =   Burning flux in still weather conditions, in kg/(m²·s)
D =   Pool diameter, in m

Step 4
Determine the scaled wind velocity u^*

$$u^* = u_w / u_c \qquad (-) \qquad (6.13)$$

in which:
u_w =   Wind velocity at height of 10 metres, in m/s

Step 5
Determine the mean length L of the fire

$$L/D = 55 \times (m''/(\rho_{air} \times (g \times D)^{1/2}))^{0.67} \times (u^*)^{-0.21} \qquad (-) \qquad (6.12)$$

in which:
L   = Average flame height, in m

Step 6
Determine the flame tilt angle Θ, using the Froude and Reynolds numbers:

$$Fr_{10} = u_w^2/(g \times D) \qquad (-) \qquad (6.68)$$

in which:
Fr_{10} = Froude number for wind velocity at a height of 10 metres

$$Re = u_w \times D/\upsilon \qquad (-) \qquad (6.69)$$

in which:
υ   = Kinematic viscosity of air, in m^2/s

$$\tan\Theta/\cos\Theta = 0.666 \times (Fr_{10})^{0.333} \times (Re)^{0.117} \qquad (-)$$

in which:
Θ   = Tilt angle of the flame, in degrees

In general, if tanΘ/cosΘ = c, than Θ can analytically be calculated by:

$$\Theta = \arcsin(((4 \times c^2 + 1)^{1/2} -1)/(2 \times c)) \qquad (°) \qquad (6.70)$$

Step 7
Due to influence of wind the flame will elongate and the flame basis will have a kind of elliptical shape, Lautkaski [1992].

The elongated diameter of the flame basis can increase the surface area of the flame on one side. Moreover, the distance between the outer flame surface and the radiated object may decrease.

In Figure 6.9 is shown how the shape of the pool fire may change due to the influence of the wind.
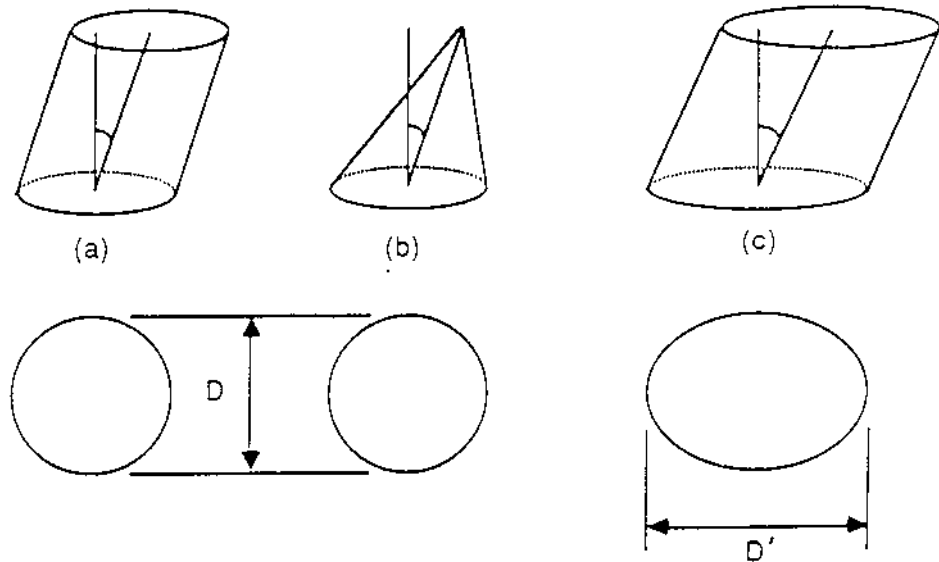
Figure 6.9   Three common pool geometries with a
(a) cylindrical flame, (b) conical flame,
(c) cylindrical flame with elongated flame base diameter

Step 7a)

$$D'/D = 1.6 \times (Fr_{10})^{0.061} \qquad (\text{-}) \qquad (6.18\text{-}1)$$

for a conical flame presentation

Step 7b)

$$D'/D = 1.5 \times (Fr_{10})^{0.069} \qquad (\text{-}) \qquad (6.18\text{-}2)$$

for a cylindrical flame presentation

in which:
D   = Pool diameter, in m
D'   = Actual elongated flame base diameter, in m

6.5.4.4   Calculation of the surface emissive power

If the flame dimensions have been determined as well as the heat generated in the flame due to combustion, the surface emissive power can be calculated. Formula (6.19) is an empirical relationship between the diameter and the surface emissive power. In tables 6.7 and 6.8 the surface emissive power has been shown for liquid pools of different components, as well as the ratio of the flame height and the pool diameter. Also the influence of the pool diameter on the surface emissive power is shown.

Experimental results of pool fires with references are collected in table 6.9, which may be used to check whether the calculated results are realistic.

At the end of step 8, additional information about the surface emissive power from literature is given.

Step 8

The calculation of the Surface Emissive Power SEP for a tilted cylindrical flame, according to the approach of the Yellow Book [1992]:

$$SEP_{max} = F_s \times m'' \times \Delta H_c / (1 + 4 \times L/D) \qquad (J/(m^2 \cdot s)) \qquad (6.71)$$

in which:

SEP_{max} = Maximum Surface Emissive Power, in $J/(m^2 \cdot s)$
F_s = Fraction of the generated heat radiated from the flame surface
m'' = Burning rate, in $kg/(m^2 \cdot s)$
ΔH_c = Heat of combustion, in J/kg
L = Average height of flame, in m
D = Pool diameter, in m

In Balluff [1985] results of experimental data are presented from fires of different types of fuel, showing the share of heat radiation in relation to the tank diameter, see Figure 6.10.
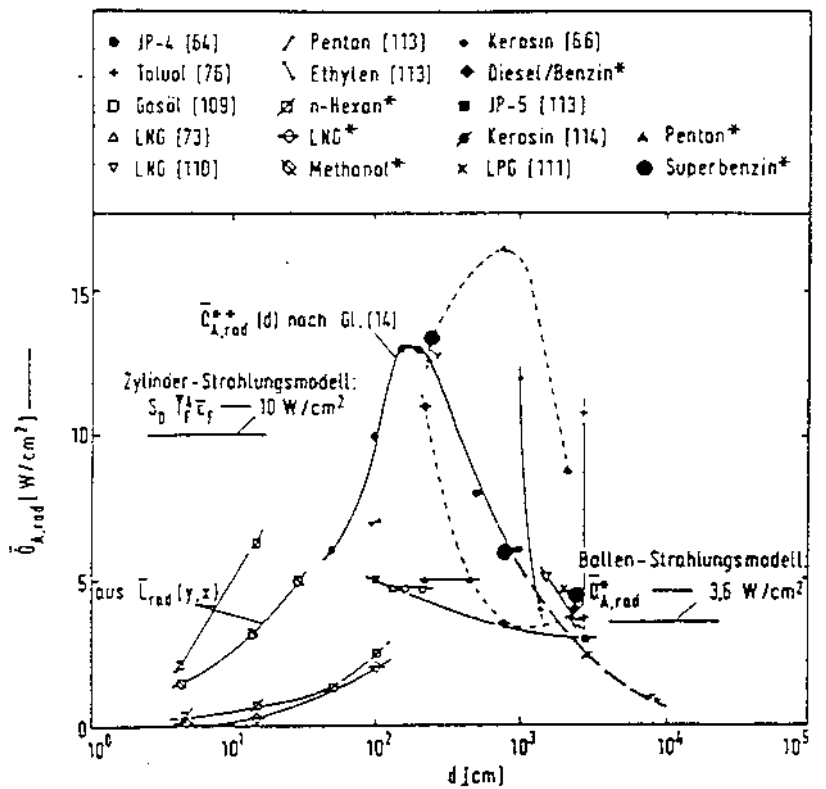
Figure 6.10 Experimental data from fires of different types of fuel, showing the share of heat radiation

There are, however, two effects which have an impact on the fraction of the generated combustion heat, F_s, which is radiated:

a. for small diameters, F_s is clearly smaller than 1,
b. for large diameters, soot formation is possible in case of a limited air supply.

In both these cases the SEP will be smaller. It is, therefore rather remarkable that the combustible substances investigated by Burgess, Hertzberg [1974] (table 6.6): methanol, methane and benzene have a radiation fraction which is practically independent of the pool diameter.

In table 6.6 some experimental values of the fraction of the radiated heat are given.

Table 6.6   Radiation fraction F_s for various poolfires, Burgess, Hertzberg [1974]

Substance	Pool diameter (m)	Radiation fraction F_s (-)
methanol	0.076 0.152 1.22	0.162 0.165 0.177
methane	0.305 0.76 1.53 3.05 6.10	0.21 0.23 0.15-0.24 0.24-0.34 0.20-0.27
butane	0.305 0.457 0.76	0.199 0.205 0.269
gasoline	1.22 1.53 3.05	0.30-0.40 0.16-0.27 0.13-0.14
benzene	0.076 0.457 0.76 1.22	0.350 0.345 0.350 0.360

The radiation fraction is a factor which generally can only be given with little certainty. Its value appears to range between 0.1 and 0.4.

In literature $\varsigma = 80\%$ has been found as a representative figure for pool fires of oil products

$$SEP_{act} = SEP_{max} \times (1 - \varsigma) + SEP_{soot} \times \varsigma \qquad (J/(m^2 \cdot s)) \qquad (6.20)$$

in which:

SEP_{act} = Actual surface emissive power, in $J/(m^2 \cdot s)$

SEP_{soot} = The surface emissive power of soot, which is about $20 \cdot 10^3 \ J/(m^2 \cdot s)$

Another approach with the following empirical formula assumes one uniform SEP over the whole of the flame surface. This approach was adopted by Mudan who derived the following correlation using data from gasoil, kerosene and JP-5.
In order to calculate the worst case, the larger diameter has to be taken.

$$SEP_{act} = 140 \cdot 10^3 \times e^{-0.12 \times D} + 20 \cdot 10^3 \times (1 - e^{-0.12 \times D}) \qquad (J/(m^2 \cdot s)) \qquad (6.19)$$

in which:

D = Pool diameter, in m

In tables 6.7, 6.8 and 6.9 the flame dimensions are shown in relation to the surface emissive power.

Table 6.7   Relative flame height (L/D) and actual surface emissive power (SEP$_{act}$) of the flame surface of boiling pools (T$_b$ < 20˚C), Yellow Book [1992]

	D = 1 m		D = 10 m	
Substance	**L/D** (-)	**SEP$_{act}$** ($10^3 \ J/(m^2 \cdot s)$)	**L/D** (-)	**SEP$_{act}$** ($10^3 \ J/(m^2 \cdot s)$)
Acetaldehyde	2.88	35	1.43	64
Ammonia	1.57	17	0.78	30
Butane	4.84	86	2.40	165
Butadiene	4.88	87	2.42	168
I-Butane	5.02	87	2.49	168
Dimethylamine	3.59	59	1.78	112
Ethane	4.76	96	2.36	185
Ethene	4.52	90	2.24	173
Ethylchloride	3.01	28	1.49	52
Ethylene oxide	2.79	37	1.38	68
Carbon monoxide	2.71	13	1.34	24
Methane	4.59	100	2.29	193
Methyl bromide	2.25	9	1.11	16
Methyl chloride	4.90	15	2.43	27
Propane	5.08	98	2.52	188
Propylene	4.90	92	2.43	178
Vinylchloride	2.68	26	1.41	46
Hydrogen sulphide	2.20	18	1.09	32

Table 6.8 Relative flame height (L/D) and actual surface emissive power (SEP$_{act}$) of the flame surface of non-boiling pools ($T_b \geq 20$ °C), Yellow Book [1992]

	D = 1 m		D = 10 m	
Substance	**L/D** **(-)**	**SEP$_{act}$** **(10^3 J/(m²·s))**	**L/D** **(-)**	**SEP$_{act}$** **(10^3 J/(m²·s))**
Acetone	3.06	42	1.52	79
Acetonitrile	2.27	34	1.13	62
Acrylonitrile	2.64	36	1.31	67
Allyl Alcohol	2.45	37	1.21	68
Benzene	4.16	71	2.06	135
Diethylamine	4.29	71	2.12	135
Ethylene Diamine	2.37	36	1.18	66
Ethyl Formate	2.86	29	1.42	54
Ethyl Mercaptan	3.44	45	1.71	84
Hexane	4.53	87	2.24	166
Methanol	1.59	19	0.79	34
Methyl Acetate	2.59	26	1.28	48
Methyl Formate	2.31	18	1.14	33
Vinyl Acetate	2.89	32	1.43	59
Carbon Disulphide	2.37	15	1.18	28

Table 6.9 gives a summary of measured emittance and radiation temperatures for recent experiments conducted with large poolfires of hydrocarbons. It seems from this table that, depending on absorption by smoke, the emittances can vary between maximum values and a small fraction of these values. Previously conducted experiments with large LNG pool fires, American Gas Association [1974], Burgess, Zabetakis [1971], Carne [1971], Maezawa [1973] have shown a maximum emittance of $142 \cdot 10^3$ J/(m²·s).

In table 6.9 the radiation emittances and temperatures for pool fire experiments are shown.

*Table 6.9   Radiation emittances and temperatures for pool fire experiments
[Yellow Book 1992]*

Reference	Flammable material	Pool diameter D (m)	SEP$_{act}$ (10^3 W/m^3)	Radiation temperature (K)	Remarks
Raj [1977]	LNG (on water)	8,5-15	210-280	1500	(a)
Minzer [1982]	LNG (on land)	20	150-220		(a)+(b)
May [1973]	LNG (on land)	15 and 24	52 and 36		
Minzer [1982]	LPG (on land)	20	48		(d)
Welker [1982]	LPG (on land)	2-17	60-160		
Hägglund, Persson [1976]	Aviation fuel (JetB)	1-10	60-130	1240	(c)
NASA [1979]	Aviation (JP-4)	5.8	1200		(e)
Fu [1971]	(JP-4;JP-5)	2.4	40-80		
Modak [1978]	(JP-5)	1-30	30-50		(f)
Alger [1979]	(JP-5)	3	110		
TNO [1978]	(kerosine)	10 and 14	120		
JISE [1982]	(kerosine)	30-80 (average)	10-25		(b)+(c)
Alger [1979]	methanol	3	70		
Modak [1978]	pentane	1.0	61		
Modak [1978]	ethene	2.5	130		

(a) determined with a narrow angle radiometer

(b) determined with a wide angle radiometer

(c) large fires radiate less than small fires

(d) high smoke production

(e) flame surface covered by smoke

(f) SEP = 30·10^3 W/m^2 by D =30 m

Additional information on Surface emissive power

It is clear that the SEP is not uniform on the surface of the flame. Apart from having temperature variations throughout, the flame is actually a volumetric rather than a surface emitter and is therefore less emissive near its edges where the path length through the flame is shorter. The use of the solid flame model with the assumption of a surface emitter is a convenient concept to aid calculation techniques.
The flame surface consists of more-emissive parts, the so-called 'hot-spots', and less-emissive parts affected by the quantity of black soot produced. This depends on the size of the fire and the proportion of heavier hydrocarbons in the LNG.

When the diameter of a soot producing hydrocarbon pool fire increases, the soot escapes from the flame due to incomplete combustion. This soot cools rapidly and instead of radiating heat, absorbs heat radiation strongly and reduces the radiation considerably. Thus the average SEP will at first increase with the pool diameter and then decrease because the flame surface becomes more and more obscured by soot. This can be explained, because the entrained oxygen in the air will be consumed on its way to the centre of the flame, causing incomplete combustion in the central part of the flame.
For large diameter open flames, almost the entire flame surface becomes partially obscured by dark soot, except for a very narrow region at the base of the fire where air entrainment keeps the soot away. Bright flame only appears in blooms and puffs as large scale vortices bring radiating regions to the surface.

For LPG the average surface emissive power from the present fire was $48 \cdot 10^3$ J/(m$^2 \cdot$s), only a third of that from the LNG fire. This low average value was entirely attributable to the soot-masking of the luminous flame. The larger value of about $80 \cdot 10^3$ J/(m$^2 \cdot$s) was previously obtained from a 1.8 m diameter LPG fire. This suggests that the maximum average surface flux for LPG fires occurs close to the pool diameter at which black soot formation starts to be significant. Further increases in pool diameter will then produce more soot and hence lower average surface fluxes. This was demonstrated more clearly for kerosine. In experiments it was demonstrated that the SEP of a small kerosine fire of 2 m diameter was about $130 \cdot 10^3$ J/(m$^2 \cdot$s) while the soot produced in a 10 m pool reduced the SEP to $60 \cdot 10^3$ J/(m$^2 \cdot$s). More recent research showed for a 20 m pool fire that the SEP reduced to $35 \cdot 10^3$ J/(m$^2 \cdot$s), Minzer [1982].

The clear flame length is assumed to be 30% of the total flame length for the pool diameters larger than 5 m. For pools larger that 25 m in diameter the whole of the flame is assumed to be partially obscured by soot, Cowley [1991].

6.5.4.5 Calculation of the heat flux at a certain distance

For the calculation of the heat flux the transmissivity in the air has to be determined. This can be done with the formulae given in subsection 6.5.2.4. First the relative humidity has to be determined. Also formula (6.29) can be used to estimate the decrease in heat radiation at a certain distance. This is shown in step 11.

Step 9
Determine absorption factor for water vapour α_w for an average flame temperature from Figure 6.2 (subsection 6.5.2.4), at a certain distance x, between the flame surface and the object.

Calculate the partial vapour pressure of water p_w at T_a and a relative humidity RH.

$$p_w = RH \times p_w^o \qquad \text{(N/m}^2) \qquad (6.72)$$

in which:
RH   = Relative humidity, fraction between 0 and 1
p_w^o = Saturated vapour pressure of water in air, in N/m^2

Calculate $p_w \times x$

From Figure 6.2 α_w in relation to $p_w \times x$ can be found

Step 10
Determine the absorption coefficient for carbon-dioxide α_c for an average flame temperature from Figure 6.3 (subsection 6.5.2.4) and a distance x, between the flame surface and target.

Calculate $p_c \times x$

From Figure 6.3 α_c in relation to $p_c \times x$ can be found

Step 11
Determine the atmospheric transmissivity

$$\tau_a = 1 - \alpha_w - \alpha_c \qquad\qquad (\text{-}) \qquad\qquad (6.24)$$

or τ_a can directly be read from Figure 6.4 in subsection 6.5.2.4, or can be calculated with:

$$\tau_a = 2.02 \times (p_w \times x)^{-0.09} \qquad\qquad (\text{-}) \qquad\qquad (6.29)$$

Because p_c is constant in air, this can be eliminated in the formula (6.29) as a variable and is included in the constants of the formula.

Step 12
Calculate the view factor with the formulae in Appendix. Use the calculated flame dimensions and the distance from the flame to the radiated object as input.

Step 13
Calculate the maximum heat flux at a certain distance.

$$q'' = SEP_{act} \times F_{view} \times \tau_a \qquad\qquad (J/(m^2 \cdot s)) \qquad\qquad (6.4)$$

6.5.5   Pool fire on land (unconfined)

For unconfined pool fires on land a number of calculations steps can be distinguished, as shown in Figure 6.11.

In the heat radiation calculations for pool fire the following main steps can be distinguished:

− Calculation of the liquid pool diameter;
− Calculation of the burning rate;
− Calculation of the flame dimensions of a pool fire;
− Calculation of the surface emissive power;
− Calculation of the heat flux at a certain distance.

6.75

```
┌─────────────────────────────────┐
│ Calculate the pool diameter      │
│ (Subsection 6.5.5.2, steps 1-10) │
└─────────────────────────────────┘
              │
┌─────────────────────────────────┐
│ Calculate the total release time │
│ and duration of the fire         │
│ (Subsection 6.5.5.2, step 11)    │
└─────────────────────────────────┘
              │
┌─────────────────────────────────┐
│ Calculate the burning rate       │
│ (Subsection 6.5.5.3, steps 12 or │
│ 12a)                             │
└─────────────────────────────────┘
              │
┌─────────────────────────────────┐
│ Calculate the average flame      │
│ length                           │
│ (Subsection 6.5.5.3, steps 13-15)│
└─────────────────────────────────┘
              │
┌─────────────────────────────────┐
│ Calculate the flame tilt angle   │
│ (Subsection 6.5.3.3, step 16)    │
└─────────────────────────────────┘
              │
┌─────────────────────────────────┐
│ Calculate the elongated flame    │
│ diameter                         │
│ (Subsection 6.5.5.3, step 17)    │
└─────────────────────────────────┘
              │
┌─────────────────────────────────┐
│ Calculate the surface emissive   │
│ power (SEP)                      │
│ (Subsection 6.5.5.4, step 18)    │
└─────────────────────────────────┘
              │
┌─────────────────────────────────┐
│ Calculate the transmissivity     │
│ (Subsection 6.5.5.5, steps 19-21)│
└─────────────────────────────────┘
              │
┌─────────────────────────────────┐
│ Calculate the view factor        │
│ (Subsection 6.5.5.5, step 22)    │
└─────────────────────────────────┘
              │
┌─────────────────────────────────┐
│ Calculate the heat flux          │
│ (Subsection 6.5.5.5, step 23)    │
└─────────────────────────────────┘
```
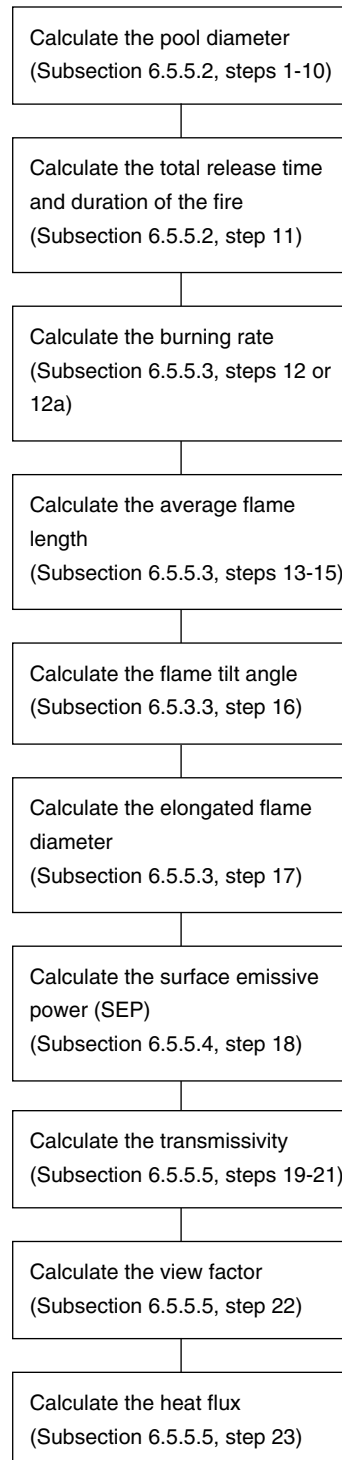
Figure 6.11   Calculation diagram of the heat flux from a pool fire of an unconfined pool on land at a certain distance

6.5.5.1   Description of the model

In Cline [1983] the pool diameter can be calculated for a burning pool which is fed from a storage tank. In the first instance pool diameter and surface area will increase. The burning rate will also increase with the surface area. At a certain moment the burning rate is equal to the release rate from the tank, which also determines the maximum pool diameter.
This maximum pool diameter can be used for the calculation of the flame height.

The model in its general form is:

$$2 \times \pi \times R \times \delta \times \rho \times dR/dt = \rho \times A \times v_f - \pi \times m'' \times R^2 \qquad \text{(kg/s)} \qquad (6.73)$$

The discharge velocity v_f is controlled by the hydrostatic pressure of the fluid level in the tank. Assuming the fuel tank to discharge through an orifice permits the time-dependent flow velocity to be described by the following relationship:

$$v_f = v_0 - a \times t \qquad \text{(m/s)} \qquad (6.74)$$

for: $0 \leq t \leq t_D$,

with

$$v_0 = C_0 \times (2 \times g \times h_i)^{1/2} \qquad \text{(m/s)} \qquad (6.75)$$

where

$$a = (C_0 \times A_0/A_t)^2 \times g \qquad \text{(m/s}^2) \qquad (6.76)$$

In this expression A_t denotes the cross-sectional area of the tank while h_i is the level of the fluid in the tank in relation to the location of the release area. The burning rate of the liquid m'' can be calculated by using the formulae in subsection 6.5.4.2. The equation above was made dimensionless, using the non-dimensional time τ defined as:

$$\tau = m'' \times t/(\rho \times \delta) \qquad \text{(-)} \qquad (6.77)$$

The dependent variable R can be similarly expressed in a dimensional form as follows:

$$\Phi = m'' \times \pi \times R^2/(\rho \times A_0 \times v_0) \qquad \text{(-)} \qquad (6.78)$$

The non-dimensional form of the pool spread differential equation is:

$$d\Phi/d\tau + \Phi = 1 - \beta' \times \tau \qquad \text{(-)} \qquad (6.79)$$

The non-dimensional parameter, β', is given by the following relationship:

$$\beta' = (a \times \delta \times \rho/(v_0 \times m'')) \qquad \text{(-)} \qquad (6.80)$$

Physically, β' represents the inverse of the non-dimensional time required to discharge the available fuel load in the tank, i.e., $\beta' = 1/\tau_D$.

It is important to note that the non-dimensional equation is valid only for the time interval in which the fuel pool is burning and the tank is releasing fuel, that is $\tau_i \leq \tau \leq \tau_D$. The lower bound of the time domain, τ_i, represents an initial condition on the spill at the onset of ignition. The initial condition on the non-dimensional equation is taken as:

$$\Phi(\tau_i) = \Phi_i \qquad\qquad (-) \qquad\qquad (6.81)$$

where Φ_i is the normalsed pool area at ignition. Solving the non-dimensional equation in conjunction with this condition, leads to the following solution for the transient growth of the burning pool fire:

$$\Phi(\tau) = 1 + \beta' \times (1 - \tau) - [1 - \Phi_i + \beta' \times (1 - \tau_i)] \times e^{-(\tau - \tau_i)} \qquad (-) \qquad (6.82)$$

for: $\tau_i \leq \tau \leq \tau_D$

Two situations can be distinguished:
1. a fuel pool initially burning, $\Phi(\tau_i = 0) = 0$
2. a fuel pool with a delayed ignition.

For both situations a solution has been given. In case of a fuel pool initially burning, the size of the pool initially increases and after having reached a maximum it will decrease in size owing to the continually decreasing fuel discharge from the source tank. The interior sections of the fuel pool are 're-supplied' with fuel whereas the outermost edges of the pool become depleted. To satisfy mass conservation the edges of the pool turn back, resulting in a decrease in pool size. This is presented in Figure 6.12.
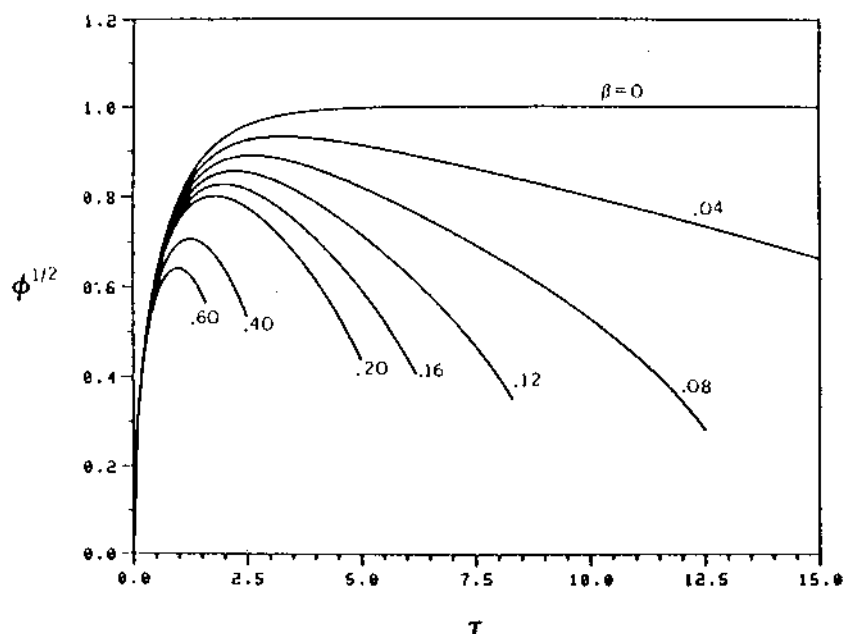
Figure 6.12   Normalised Radial Pool Fire Growth - Initially Ignited Pool Fire

Figure 6.13 shows the analytical solution of the ignited pool fire.
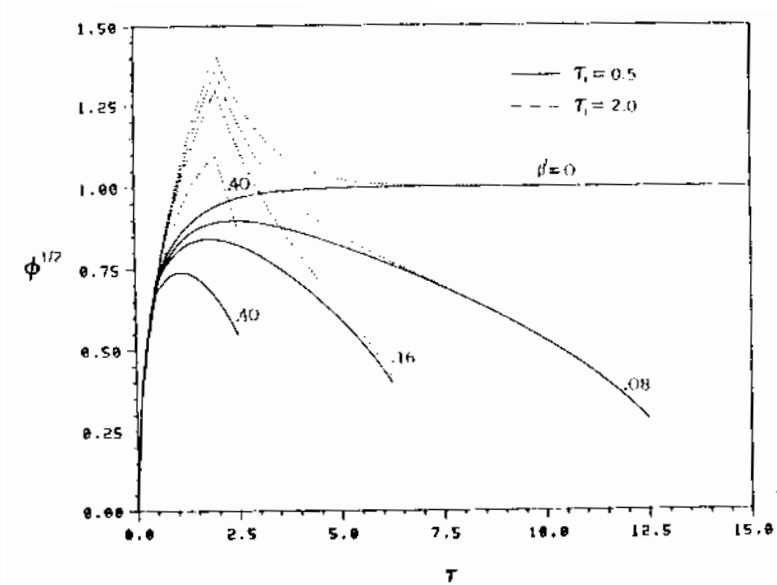
Figure 6.13   Normalised Radial Pool Fire Growth - Delayed Ignited Pool Fire

Experiments were carried out to demonstrate the relationship between fuel discharge and fire size suggested by the present theory. A series of experiments were conducted to measure the time-dependent growth of an unconfined spill fire. Although the experiments were carried out on a small scale using JP-4 as a fuel, the experiments showed that the model described the situation well.
No large scale experiments were carried out to validate the model.

6.5.5.2   Calculation of the pool diameter of a pool fire

The following input has been used for the calculation example:

A_t = the cross-sectional area of the tank, in m²
h_i = the initial height of the liquid above the release point, in m
g = gravitational constant is 9.81 m/s²
C_0 = flow coefficient of fluids through a circular hole
d_h = hole diameter of the release point, in m
δ = a thickness of the petrol layer on the ground
m'' = the mass burning flux m'' of the petrol at still weather conditions, in kg/(m²·s)
ρ = density of petrol, in kg/m³
$\Phi(\tau_i = 0)$ = 0, which means that the ignition took place at the beginning of the release while no liquid pool was present before the release.

Step 1
Calculate the surface area A_0 of the hole:

$$A_0 = \pi/4 \times d_h^2 \qquad\qquad (m^2) \qquad (6.83)$$

in which:
d_h = hole diameter of the release point, in m

Step 2
Calculate the initial outflow velocity v_0:

$$v_0 = C_0 \times (2 \times g \times h_i)^{1/2} \qquad\qquad (m/s) \qquad (6.75)$$

in which:
C_0 = flow coefficient of fluids through a circular hole
g = gravitational constant is 9.81 m/s²
h_i = the initial height of the liquid above the release point, in m

The flow coefficient C_0 is the product of a contraction and a friction factor. For a sharp-edged orifice the friction factor is nearly 1 and the value of the flow coefficient is fully determined by the contraction factor. In general the value of the flow coefficient is between 0.6 and 0.8

Step 3
Calculate the acceleration constant a:

$$a = (C_0 \times A_0/A_t)^2 \times g \qquad\qquad (m/s^2) \qquad (6.76)$$

in which:
A_t = the cross-sectional area of the tank

Step 4
The mass burning rate m" in kg/(m²·s) at still weather conditions can be taken from table 6.5, or can be calculated with formula (6.66) in subsection 6.5.4.2.

Step 5
Calculate the dimensionless parameter τ with:

$$\tau = m'' \times t/(\rho \times \delta) \qquad\qquad (-) \qquad (6.77)$$

in which t remains a variable.

Step 6
Calculate the dimensionless parameter Φ with:

$$\Phi = m'' \times \pi \times R^2/(\rho \times A_0 \times v_0) \qquad\qquad (-) \qquad (6.78)$$

in which R remains a variable.

Step 7
Calculate the dimensionless parameter β' with:

$$\beta' = (a \times \delta \times \rho/(v_0 \times m''))\ \ \ \ \ \ \ \ \ \ \ \ \ \ \ \ \text{(-)}\ \ \ \ \ \ \ \ \ \ \ \ \text{(6.80)}$$

in which:
δ =   pool thickness, in m
ρ =   liquid density, in kg/m^3

Step 8
Use the non-dimensional form of the pool spread differential equation, which is applicable for $\tau_i \leq \tau \leq \tau_D$; it is assumed that there is a fire when the release has started, thus $\Phi(\tau_i = 0) = 0$ or Figure 6.12 can be used:

$$\Phi(\tau) = 1 + \beta'(1 - \tau) - [1 - \Phi_i + \beta'\ (1 - \tau_i)]\ e^{-(\tau - \tau i)}\ \ \ \ \ \ \ \text{(-)}\ \ \ \ \ \ \ \ \ \ \ \ \text{(6.82)}$$

Step 9
Determine the time at which the pool diameter will be maximal.
This can be derived from formula (6.82), if $d\Phi/d\tau = 0$ is taken. This results in:

$$\tau_{max} = \ln((1+\beta')/\beta')\ \ \ \ \ \ \ \ \ \ \ \ \ \ \ \ \text{(-)}\ \ \ \ \ \ \ \ \ \ \ \ \text{(6.84)}$$

Furthermore

$$\tau = m'' \times t/(\rho \times \delta)\ \ \ \ \ \ \ \ \ \ \ \ \ \ \ \ \text{(-)}\ \ \ \ \ \ \ \ \ \ \ \ \text{(6.77)}$$

in which t remains a variable.

Rearranging formula (6.77) gives:

$$t_{max} = \tau_{max} \times \rho \times \delta/m''\ \ \ \ \ \ \ \ \ \ \ \ \ \ \ \ \text{(s)}$$

Step 10
Determine the maximum pool diameter at $\tau_i = 0$ and $\Phi_i = 0$ and using formula (6.82).

$$\Phi_{max} = 1 + \beta' \times (1 - \tau_{max}) - (1 + \beta') \times e^{-\tau max}\ \ \ \ \ \ \ \text{(-)}\ \ \ \ \ \ \ \ \ \ \ \ \text{(6.82)}$$

With formula (6.82) the maximum pool radius can be calculated, with:

$$\Phi_{max} = m'' \times \pi \times R_{max}^2/(\rho \times A_0 \times v_0)\ \ \ \ \ \ \ \text{(m)}\ \ \ \ \ \ \ \ \ \ \ \ \text{(6.78)}$$

and

$$D_{max} = 2 \times R_{max}\ \ \ \ \ \ \ \ \ \ \ \ \ \ \ \ \text{(m)}$$

Now the same calculations can be applied from subsection 6.5.4 to calculate the flame height and the heat flux at a certain distance from the tank.

Step 11

Determination of the total release time t_{rel} and duration of the fire t_{tot}.

The total time of the petrol release from the tank will be:

$$t_{rel} = (A_t/(C_0 \times A_0)) \times (2 \times h_i/g)^{1/2} \qquad \text{(s)} \qquad (6.85)$$

which can be solved from the differential equation:

$$A_t \times dh/dt = - C_0 \times A_0 \times (2 \times g \times h)^{1/2} \qquad \text{(m}^3\text{/s)}$$

with $h = h_i$ at time $t = 0$.

The total duration of the fire will be the release time plus the time to burn the petrol in the pool completely.

The time to burn the pool completely after the release has stopped can be derived from:

$$\pi \times R^2 \times m'' \times t = \pi \times R^2 \times \delta \times \rho \qquad \text{(kg)}$$

which results in

$$t = \delta \times \rho/m'' \qquad \text{(s)} \qquad (6.86)$$

$$t_{tot} = t_{rel} + t$$

$$t_{tot} = t_{rel} + \delta \times \rho/m'' \qquad \text{(s)} \qquad (6.87)$$

6.5.5.3   Calculation of the flame dimensions of a pool fire

The flame dimension can be calculated in the following steps.

Step 12

Determine the pool burning rate m'' at still weather conditions

$$m'' = m_\infty'' \times (1 - e^{-k \times \beta \times D}) \qquad \text{(kg/(m}^2\text{·s))} \qquad (6.66)$$

In general the value of the factor $(1 - e^{-k \times \beta \times D})$ is above 0.95 if the pool diameter is more than 1 metre, so $m'' \approx m_\infty''$.

Step 12a

If the mass burning rate was not tabulated, the best correlation to use for predicting the mass burning rate of single component fuels which are liquids under ambient conditions is that of Burgess, Hertzberg [1974]:

$$m'' = 0.001 \times \Delta H_c/(\Delta H_v + C_p \times (T_b - T_a)) \qquad \text{(kg/(m}^2\text{·s))} \qquad (6.67)$$

Step 13
Determine the characteristic wind velocity u_c

$\quad$ $U_c = (g \times m'' \times D/\rho_{air})^{1/3}$ $\qquad\qquad\qquad\qquad$ (m/s) $\qquad$ (6.14)

Step 14
Determine the dimensionless wind velocity u^*

$\quad$ $u^* = u_w/u_c$ $\qquad\qquad\qquad\qquad\qquad\qquad\qquad\quad$ (-) $\qquad$ (6.13)

Step 15
Determine the mean fire length

$\quad$ $L/D = 55 \times (m''/(\rho_{air} \times (g \times D)^{1/2}))^{0.67} \times (u^*)^{0.21}$ $\qquad$ (-) $\qquad$ (6.12)

The flame length can now be calculated because D is known.

Step 16
Determine the flame tilt angle Θ:

$\quad$ $Fr_{10} = u_w^2/(g \times D)$ $\qquad\qquad\qquad\qquad\qquad\qquad$ (-) $\qquad$ (6.68)

$\quad$ $Re = u_w \times D/\upsilon$ $\qquad\qquad\qquad\qquad\qquad\qquad\quad$ (-) $\qquad$ (6.69)

$\quad$ $\tan\Theta/\cos\Theta = 0.666 \times (Fr_{10})^{0.333} \times (Re)^{0.117}$ $\qquad$ (-) $\qquad$ (6.16)

In general, if $\tan\Theta/\cos\Theta = c$, then Θ can analytically be calculated by:

$\quad$ $\Theta = \arcsin(((4 \times c^2 + 1)^{1/2} - 1)/(2 \times c))$ $\qquad\qquad$ (°) $\qquad$ (6.70)

Step 17
Determine the actual elongated flame base dimension

Step 17a)

$\quad$ $D'/D = 1.6 \times (Fr_{10})^{0.061}$ $\qquad\qquad\qquad\qquad\qquad$ (-) $\qquad$ (6.18-1)

for a conical flame presentation.

D' can now be calculated, because D is known.

Step 17b)

$\quad$ $D'/D = 1.5 \times (Fr_{10})^{0.069}$ $\qquad\qquad\qquad\qquad\qquad$ (-) $\qquad$ (6.18-2)

for a cylindrical flame presentation.

6.5.5.4   Calculation of the surface emissive power

Step 18
Calculate the Surface Emissive Power SEP_{theor} for a tilted cylindrical flame

$$SEP = 140 \cdot 10^3 \times e^{-0.12 \times D} + 20 \cdot 10^3 \times (1 - e^{-0.12 \times D}) \qquad (J/(m^2 \cdot s)) \qquad (6.19)$$

Table 6.6 can be used to estimate F_s.

$$SEP_{max} = F_s \times m'' \times \Delta H_c / (1 + 4 \times L/D) \qquad (J/(m^2 \cdot s)) \qquad (6.71)$$

$$SEP_{act} = SEP_{max} \times (1 - \varsigma) + SEP_{soot} \times \varsigma \qquad (J/(m^2 \cdot s)) \qquad (6.20)$$

6.5.5.5   Calculation of the heat flux at a certain distance

Step 19
Determine absorption factor for water vapour α_w for an average flame temperature of T_f from Figure 6.2 and for a distance x from the flame surface.

Calculate the partial vapour pressure of water p_w at 15 ˚C and a relative humidity RH.

$$p_w = RH \times p_w^o \qquad (N/m^2) \qquad (6.72)$$

Now $p_w \times x$ can be calculated.

Figure 6.2 has to be used to find α_w.

Step 20
Determine the absorption coefficient for carbon-dioxide α_c for an average flame temperature of T_f K from Figure 6.3. and a distance x from the flame surface.

Now $p_c \times x$ can be calculated.

Figure 6.3 has to be used to find α_c.

Step 21
The calculation with formula (6.24) is generally much more accurate. If the value of $p_w \times x$ is between 10^4 and 10^5 N/m, formula (6.29) can be used.

Determine the atmospheric transmissivity.

$$\tau_a = 1 - \alpha_w - \alpha_c \qquad (-) \qquad (6.24)$$

Step 22
Calculate the view factor with the formulae, shown in Appendix, section 3

a $= L/R$ (-)

b $= X/R$ (-)

$A = \sqrt{(a^2 + (b + 1)^2 - 2 \times a \times (b + 1) \times \sin\theta)}$

$B = \sqrt{(a^2 + (b - 1)^2 - 2 \times a \times (b - 1) \times \sin\theta)}$

$C = \sqrt{(1 + (b^2 - 1) \times \cos^2\theta)}$

$D = \sqrt{((b - 1)/(b + 1))}$

$E = (a \times \cos\theta)/(b - a \times \sin\theta)$

$F = \sqrt{(b^2 - 1)}$

The maximum view factors F_h and F_v can now be calculated with formulae (6.A.14) and (6.A.15), respectively.
The maximum view factor can be calculated with formula (6.A.18).

$$F_{max} = \sqrt{(F_v^2 + F_h^2)}$$ (-)   (6.A.18)

Step 23
Calculate the maximum heat flux at a certain distance x

$$q'' = SEP_{act} \times F_{view} \times \tau_a$$ (J/(m^2·s))   (6.4)

6.5.6   Pool fires on water

For pool fires on water a number of calculation steps can be distinguished, as shown in Figure 6.14.

6.84

```
┌─────────────────────────────┐
│ Calculate the pool diameter  │
│ (Subsection 6.5.6.1)         │
└─────────────────────────────┘
              │
┌─────────────────────────────┐
│ Calculate the burning rate   │
│ (Subsection 6.5.6.2)         │
└─────────────────────────────┘
              │
┌─────────────────────────────┐
│ Calculate the average flame  │
│ lenght                       │
│ (Subsection 6.5.6.3)         │
└─────────────────────────────┘
              │
┌─────────────────────────────┐
│ Calculate the flame tilt angle│
│ (Subsection 6.5.6.3)         │
└─────────────────────────────┘
              │
┌─────────────────────────────┐
│ Calculate the elongated flame│
│ diameter                     │
│ (Subsection 6.5.6.3)         │
└─────────────────────────────┘
              │
┌─────────────────────────────┐
│ Calculate the surface emissive│
│ power (SEP)                  │
│ (Subsection 6.5.6.4)         │
└─────────────────────────────┘
              │
┌─────────────────────────────┐
│ Calculate the transmissivity │
│ (Subsection 6.5.6.4)         │
└─────────────────────────────┘
              │
┌─────────────────────────────┐
│ Calculate the view factor    │
│ (Subsection 6.5.6.4)         │
└─────────────────────────────┘
              │
┌─────────────────────────────┐
│ Calculate heat flux at a certain│
│ distance                     │
│ (Subsection 6.5.6.4)         │
└─────────────────────────────┘
```

Figure 6.14   Calculation diagram for the heat flux from a pool fire on water at a certain distance

In the heat radiation calculations for pool fire the following steps can be distinguished:

- Calculation of the liquid pool fire diameter;
- Calculation of the burning rate;
- Calculation of the flame dimensions of the pool fire;
- Calculation of the surface emissive power;
- Calculation of the heat flux at a certain distance.

6.5.6.1 Calculation of the liquid pool fire diameter

No models could be found about calculation of the diameter of the liquid pool fire. If the pool on water is confined the equivalent diameter can be calculated with equation (6.64). A confined pool can be formed if the perimeter and the surface area of the pool do not change in time. This will occur in e.g. harbours when the spill is enclosed by oil booms.

6.5.6.2 Burning rate

In general liquid pools will spread. However, measurements on burning rate are made in controlled conditions with fixed pool diameters.

From literature Petty [1983] the following experimental data have been published in table 6.10.

Table 6.10   Mass burning fluxes of flammable materials on water from experiments

Flammable material on water	Pool diameter (m)	Mass burning flux (kg/(m²·s))	Temperature of the flammable material (˚C)
LPG	10.4	0.629	
	12.9	0.240	
	16.9	0.175	
LNG	16.8	0.255	
Gasoline	28.2	0.054	
Crude oil:			
- Saharan	2	0.056	30
	2	0.047	5
- Attaka	2	0.057	30
- El Sider	2	0.048	30
- Labuan	2	0.043	30
	2	0.043	5
- Ekofisk	2	0.065	30
- Isthmus/mayan	2	0.073	30
	2	0.047	5
- North Slope	2	0.069	30
	2	0.061	5
- Diesel	2	0.051	5
- Bunker C fuel oil	2	0.031	5

Few models can be found in literature about the burning flux of pool fires in water. Most of the available literature is about experimental data.
A comparison between the burning flux of crude oils and gasoline in pool fires on land and water does not show much difference.
For LPG on water the burning flux is about twice as high as for LPG on land and for LNG this is about three times higher. The differences between the burning flux for the water and land situation are presented in the following table 6.11.

Table 6.11   Mass burning fluxes for several flammable materials vs. pool diameter and water and land

Flammable material in water	Pool diameter (m)	Mass burning flux (kg/(m²·s))
LPG on land	20.0	0.13
	12.2	0.136
LPG on water	10.4	0.629
	12.9	0.24
	14.9	0.295
	16.9	0.175
LNG on land	up to 16.8	0.255
LNG on water	up to 13.7	0.094
	20.0	0.106
	35.0	0.14

For the calculation of the burning flux on water the following equation can be used from Petty [1983]:

$$m'' = [q_{rw}''/(Q \times \ln[B_c + 1])] + [(h/C_p) \times \ln(B_c + 1)] \qquad (kg/(m^2 \cdot s)) \qquad (6.88)$$

in which:
m" = burning flux in kg/(m²·s)
q_{rw}"= radiant heat flux to the pool burning surface in J/(m²·s).
Q   = heat of vaporisation in J/kg
B_c = 'Spalding' convection mass transfer number
h   = heat transfer coefficient in W/(m²·K)
C_p = heat capacity in J/(kg·K)

The value of B_c ranged from 10.17 to 15.12, so the term $\ln(B_c+1)$ varies between 2.41 to 2.78, which is a variation of 13%. In general 2.6 can be taken for calculations.

6.5.6.3   Calculation of the flame dimension

The formulae for the calculation of the flame height of a confined pool fire on land, as described in subsection 6.5.4, can be used.

6.5.6.4   Calculation of the heat flux at a certain distance

The heat flux can be calculated in a similar way as for pool fires on land. In literature only experimental data could be found with respect to the surface emissive power. This showed much scatter in the measured SEP's. No significant difference in SEP between the land and the water situation could be found.
The calculations for heat flux at a distance, as described in subsection 6.5.5, can be used.

6.5.7   Fire balls

The calculation steps for the heat flux of a fire ball caused by a BLEVE can be carried out in four steps, starting from the estimation of the amount of LPG which would be involved in a BLEVE.

For the calculation of a fire ball from a BLEVE the following calculation steps are required, see Figure 6.15.

Calculate the amount of LPG
involved in BLEVE
(Subsection 6.5.7.1, step 1)

Calculate the radius of the fire
ball
(Subsection 6.5.7.1, step 2)

Calculate the duration time of
the fire ball
(Subsection 6.5.7.1, step 3)

Calculate the lift-off height of
the fire ball
(Subsection 6.5.7.1, step 4)

Calculate the distance from the
surface area of the fire ball to
the object
(Subsection 6.5.7.2, step 5)

Calculate the view factor
(Subsection 6.5.7.2, step 6)

Calculate the fraction of the
generated heat radiated by the
fire ball
(Subsection 6.5.7.2, step 7)

Calculate the available heat for
combustion
(Subsection 6.5.7.2, step 8)

```
                    │
      ┌─────────────┴──────────────┐
      │ Calculate the surface emissive │
      │ power (SEP)                 │
      │ (Subsection 6.5.7.2, step 9)│
      └─────────────┬──────────────┘
                    │
      ┌─────────────┴──────────────┐
      │ Calculate the distance from the │
      │ centre of the fire ball to the │
      │ object                      │
      │ (Subsection 6.5.7.2, step 10)│
      └─────────────┬──────────────┘
                    │
      ┌─────────────┴──────────────┐
      │ Calculate the transmissivity │
      │ (Subsection 6.5.7.2, steps 11-13)│
      └─────────────┬──────────────┘
                    │
      ┌─────────────┴──────────────┐
      │ Calculate the heat flux at a │
      │ certain distance            │
      │ (Subsection 6.5.7.2, step 14)│
      └────────────────────────────┘
```

Figure 6.15   Calculation diagram for the heat flux from a fire ball at a certain distance from
               the fire ball

6.5.7.1   Calculation of the dimensions, duration and lift-off height

The formulae used for the calculation are given below. In step 2 the released amount is ignited and the radius of the fireball can be determined with (6.90); in step 3 the duration of a fireball with (6.91) can be calculated and step 4 the centre height is calculated with equation (6.22). All equations are from TNO [1983].

Step 1
Calculate the amount of LPG release in case of a complete failure of the tank

$$m = V_{rel} \times \rho_{mat} = f \times V \times \rho_{mat} \qquad (kg) \qquad (6.89)$$

m = Mass of the flammable material, in kg
f = Fraction of the volume of the pressure tank, filled with the flammable liquefied pressurised gas
V = Volume of the tank, in m³
V_{rel} = Amount of e.g. LPG which will be released in case of a complete tank failure
ρ_{mat} = Density of the flammable material in the pressure tank, in kg/m³

Step 2
The radius of the fireball can be calculated from the quantity of combusting material:

$$r_{fb} = c_9 \times m^{0.325} \qquad\qquad (m) \qquad (6.90)$$

In which:
c_9 = 3.24 m/kg$^{0.325}$
r_{fb} = Radius of the fireball, in m
m = Mass of the flammable material, in kg

Step 3
The duration of the fireball is:

$$t = c_{10} \times m^{0.26} \qquad\qquad (s) \qquad (6.91)$$

in which:
c_{10} = 0.852 s/kg$^{0.26}$
t = Duration of the fireball, in s
m = Mass of the flammable material, in kg

Step 4
The lift-off height of the fire ball:

$$H_{bleve} = 2 \times r_{fb} \qquad\qquad (m) \qquad (6.22)$$

in which:
H_{bleve} = Height from the centre of the fire ball to the ground under the fire ball, in m

6.5.7.2   Calculation of the heat flux at a certain distance

In most literature a uniform heat radiation is assumed. In reality the radiative emission from a fireball varies over its surface. It was found that peak emissions came from areas at the top of the expanding fireball whereas the emission was lower from lower portions of the fireball because of increased soot shielding and poorer mixing with ambient air. They also noted a time dependence of the surface emissive power. After an initial period of intense emission there was a gradual decrease in the SEP. The SEP also varies with fuel type.

For the calculation of the heat flux at a certain distance, parameters such as view factor, fraction of the radiated heat and the surface emissive power, are required. In the view factor the effects of the distance from the object to the centre of the flame are taken into account.
In step 6 the view factor, in step 7 the fraction of the generated heat and in steps 9 the emissive power of the fire ball can be calculated.
The heat flux at a certain distance as a result of the calculations can be obtained in step 14.

Step 5
Calculate the distance X from the centre of the fire ball to the object.

$$X = (x_{bleve}^2 + H_{bleve}^2)^{1/2} \qquad \text{(m)} \qquad (6.92)$$

In which:
x_{bleve} = Distance measured over the ground from the projected centre of the fire ball on the ground under the fire ball, and the object, in m
H_{bleve} = Height from the centre of the fire ball to the ground under the fire ball, in m
X = Distance from the centre of the fire ball to the radiated object, in m

Figure 6.16 shows the distances from the fire ball to the radiated object, required for calculations.
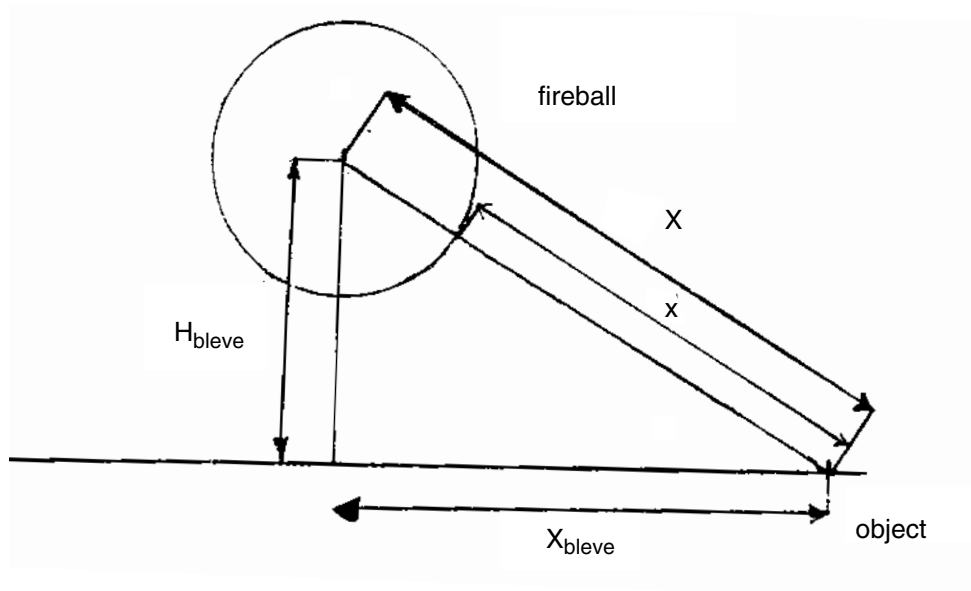
Figure 6.16   Distances from the centre of the fire ball to the object after lift-off.

Step 6
Calculate maximum value of the view factor at a distance X with:

$$F_{view} = (r_{fb}/X)^2 \qquad \text{(-)} \qquad (6.93)$$

in which:
F_{view} = Geometric view factor, dimensionless
r_{fb} = Radius of the fire ball, in m
X = Distance from the centre of the fire ball to the radiated object, in m

Step 7
Calculate the fraction F_s of the generated heat radiated by a fire ball

$$F_s = c_6 \times (P_{sv})^{0.32} \qquad \text{(-)} \qquad (6.21)$$

in which:
c_6 = 0.00325 $(N/m^2)^{0.32}$
P_{sv} = Vapour pressure of flammable material inside the vessel, in N/m^2

Step 8
Calculate the nett available heat for radiation

$$\Delta H = \Delta H_c - \Delta H_v - C_p \times \Delta T \qquad\qquad (J/kg) \qquad (6.94)$$

in which:
ΔH = Nett available heat, in J/kg
ΔH_c = Combustion heat of the flammable material at its boiling point, in J/kg
ΔH_v = Vaporisation heat of the flammable material at its boiling point, in J/kg
C_p = Specific heat capacity at constant pressure, $J/(kg \cdot K)$
ΔT = Temperature difference between flame and ambient temperature, in K

Assume ΔT = 1700 K

Step 9
Calculate the Surface Emissive Power SEP_{act}

If it is assumed that there is no soot formation, then $SEP_{act} = SEP_{max}$

$$SEP_{act} = \Delta H \times m \times F_s/(4 \times \pi \times r_{fb}^2 \times t) \qquad (J/(m^2 \cdot s)) \qquad (6.95)$$

in which:
SEP_{act} = Actual Surface Emissive Power, SEP, in $J/(m^2 \cdot s)$, which is the average radiation emittance (emissive power) of the flame surface.
SEP_{max} = Maximum Surface Emissive Power, in $J/(m^2 \cdot s)$.

From the few measurements of the surface emissive powers of fireballs it is reported that butane fireballs typically have average SEP values of the visible flame between $300 \cdot 10^3$ and $350 \cdot 10^3$ $J/(m^2 \cdot s)$. Spot SEPs from highly emissive areas at the top of the fireballs are up to $500 \cdot 10^3$ $J/(m^2 \cdot s)$.

Step 10
Calculate the actual path length between the surface area of the fire ball and the object.

The actual path length x of radiation from a fire ball is the difference from the centre of the fire ball of the radiated object and distance minus the BLEVE-radius.

$$x = X - r_{fb} \qquad\qquad (m) \qquad (6.96)$$

in which:
x = Distance from the surface area of the flame to the object, in m

Step 11
Determine absorption factor for water vapour α_w for an average flame temperature of T_f in K from Figure 6.2, in subsection 6.5.2.4, and for a distance x from the flame surface.

Calculate the partial vapour pressure of water p_w at t ˚C and a relative humidity RH.

$$p_w = RH \times p_w^o \qquad\qquad (N/m^2) \qquad (6.72)$$

Now $p_w \times x$ can be calculated.

Figure 6.2 has to be used to find α_w.

Step 12
Determine the absorption coefficient for carbon-dioxide α_c for an average flame temperature of T_f in K from Figure 6.3, in subsection 6.5.2.4, and a distance x from the flame surface.

Now $p_c \times x$ can be calculated.

Figure 6.3 has to be used to find α_c.

Step 13
The calculation with formula (6.24) in general is much more accurate. If the value of $p_w \times x$ is between 10^4 and 10^5 N/m, formula (6.29) can be used.

Determine the atmospheric transmissivity with

$$\tau_a = 1 - \alpha_w - \alpha_c \qquad\qquad (-) \qquad (6.24)$$

or use Figure 6.4 in subsection 6.5.2.4

Step 13a
Calculate the partial vapour pressure of water p_w at t ˚C and a relative humidity RH.

$$p_w = RH \times p_w^o \qquad\qquad (N/m^2) \qquad (6.72)$$

An alternative for the calculation of the atmospheric transmissivity τ_a is formula (6.29)

$$\tau_a = c_7 \times (p_w \times x)^{-0.09} \qquad\qquad (-) \qquad (6.29)$$

in which:
c_7 = 2.02 $(N/m^2)^{0.09} \cdot m^{0.09}$
p_w = Partial vapour pressure of water in air at a relative humidity RH, in N/m^2
x = Distance from the surface area of the flame to the object in m

This formula can only be used for calculations in the range between:

$10^4 < p_w \times x < 10^5$ N/m.

Step 14
Calculate the heat flux at a certain distance from the centre of fire ball

$$q'' = SEP_{act} \times F_{view} \times \tau_a \qquad\qquad (J/(m^2 \cdot s)) \qquad (6.4)$$

in which:
q'' = Heat flux at a certain distance, in $J/(m^2 \cdot s)$
τ_a = Atmospheric transmissivity

For the calculation of the F_{view} the distance X from the centre of the fire ball to the object should be used and for the calculation τ_a the distance x, calculated with (6.96) from the surface area of the fire ball should be used.

6.6 Application of selected models: calculation example

6.6.1 Introduction

In this chapter examples are given of the selected models described in chapter 6.5 of the jet flame, pool fire on land and on water and for the fire ball.
The examples are chosen in such a way that these reflect as much as possible the actual situation.
The examples are presented in steps in a logical order so the approach can easily be translated to a computer program.

6.6.2 Jet flames

In this calculation example the heat flux is calculated in 30 steps for an object at a certain distance from a jet flame.
The following input data has been used for the calculation example of a high pressure pipeline (Hole Diameter 100 mm, choked flow) with methane gas:

W_g = 16.042 kg/kmol = 0.016042 kg/mol
W_{air} = 0.02896 kg/mol
T_s = 15 ˚C = 288.15 K
T_f = 1200 K = 926.15 °C
P_{air} = $1.01325 \cdot 10^5$ N/m^2 (1 Bar)
P_{init} = 10^7 N/m^2 = Pa = 100 Bar
C_p = 2201.6 J/kg·K
R_c = 8.31451 J/mol·K
g   = 9.80665 m/g
u_W = 5 m/s
m'   = 30 kg/s
Θ_j = 85˚
Θ_{jv} = [$\Theta_j \leq \Theta_{jv} \leq 90$˚], assumption Θ_{jv} = 85˚ and wind ⊥ pipe
ΔH_c = $50 \cdot 10^6$ J/kg
RH   = 0.7
p_w = 1705 N/m^2 at 15 ˚C
p_c = 30.3975 N/m^2 in air (0.03% CO_2 in atmosphere)
T_a = Ambient temperature 15 ˚C = 288 K
ς   = 0 (it is assumed that there is no soot formation)
X   =150 m (Distance release point to receiver)

First the flame dimensions will be calculated and the Surface Emmisive Power (SEP). With this data the maximum heat load at a certain distance of the flame can be determined.

Step 1
Determine the mass fraction of fuel in a stoichiometric mixture with air:

$$W = W_g/(15.816 \times W_g + 0.0395) \qquad (6.30)$$
$$= 0.0186/(15.816 \times 0.016042 + 0.0395)$$
$$= 0.05471$$

Step 2
Calculate the Poisson constant γ

Combining formulae (6.31) and (6.32) γ can be calculated with:

$$\gamma = (1 - R_c/(C_p \times W_g))^{-1}$$
$$= (1 - 8.31451/(2201.6 \times 0.016042))^{-1}$$
$$= 1.30788$$

(this number will be used in the calculations).

Step 3
Determine the temperature of the expanding jet:

$$T_j = T_s \times (P_{air}/P_{init})^{((\gamma - 1)/\gamma)} \qquad (6.33)$$
$$= 288.15 \times (1.01325 \cdot 10^5/10^7)^{((1.30788 - 1)/1.30788)}$$
$$= 97.758 \text{ K}$$

Step 4
Determine the static pressure at the hole exit plane:

$$P_c = P_{init} \times (2/(\gamma + 1))^{(\gamma/(\gamma - 1))} \qquad (6.34)$$
$$= 10^7 \times (2/(1.30788 + 1))^{(1.30788/(1.30788 - 1))}$$
$$= 5.443070 \cdot 10^6 \text{ N/m}^2$$

Step 5
Determine the Mach-number of the expanding jet:

$$M_j = (((\gamma + 1) \times (P_c/P_{air})^{((\gamma - 1)/\gamma)} - 2)/(\gamma - 1))^{1/2} \qquad (6.35)$$
$$= (((1.30788 + 1) \times$$
$$(5.443 \cdot 10^6 \text{ N/m}^2/1.01325 \cdot 10^5)^{((1.30788 - 1)/1.30788)} - 2)/(1.30788 - 1))^{1/2}$$
$$= 3.55688$$

Step 6
Determine the exit velocity of the expanding jet

$$u_j = M_j \times (\gamma \times R_c \times T_j/W_g)^{1/2} \qquad (6.36)$$
$$= 3.55688 \times (1.30788 \times 8.31451 \times 97.758/0.016042)^{1/2}$$
$$= 915.60648 \text{ m/s}$$

Step 7
Determine the ratio of wind speed to jet velocity

$$R_w \quad = u_w/u_j \qquad\qquad\qquad (6.37)$$
$$= 5/915.60648$$
$$= 0.00546$$

Step 8
Determine the density of air:

$$\rho_{air} \quad = (P_{air} \times W_{air})/(R_c \times T_{air}) \qquad\qquad (6.38)$$
$$= (1.01325 \cdot 10^5 \times 0.02896)/(8.31451 \times 288.15)$$
$$= 1.224785 \text{ kg/m}^3$$

Calculate the density in the jet:

$$P_j \quad = P_c \times W_g/(R_c \times T_j) \qquad\qquad (6.40)$$
$$= 5.443070 \cdot 10^6 \times 0.016042/(8.31451 \times 97.758)$$
$$= 107.43 \text{ kg/m}^3$$

Step 9
Determine combustion source diameter (choked):

$$D_s \quad = d_j \times \sqrt{\frac{P_j}{\rho_{air}}}$$

$$= 0.1 \ (= 100 \text{ mm}) \text{ - } \sqrt{\frac{107.43}{1.224785}}$$

$$= 0.93656 \text{ m}$$

Step 10
Calculate first Y by iteration with the equation

$$C_a \times Y^{5/3} + C_b \times Y^{2/3} - C_c = 0 \qquad\qquad (6.42)$$

This involves the following coefficients:

$$C_a \quad = 0.024 \times (g \times D_s/u_j^2)^{1/3}$$
$$= 0.024 \times (9.80665 \times 0.93656/(915.60648^2))^{1/3}$$
$$= 5.33 \cdot 10^{-4}$$

$$C_b \quad = 0.2$$

$$C_c \quad = (2.85/W)^{2/3}$$
$$= (2.85/0.05471)^{2/3}$$
$$= 13.9482$$

$$5.33 \cdot 10^{-4} \times Y^{5/3} + 0.2 \times Y^{2/3} - 13.9482 = 0$$

as a result of an iteration, becomes Y = 262.716

Step 11
Determine the length of the jet flame in still air:

$$L_{b0} = Y \times D_s \qquad\qquad (6.43)$$
$$= 262.716 \times 0.93656$$
$$= 246.05056 \text{ m}$$

Step 12
Determine the length of the jet flame measured from the tip of the flame to the centre of the exit plane:

$$L_b = L_{b0} \times ((0.51 \times e^{(-0.4 \times u_w)} + 0.49)) \times (1.0 - 6.07 \cdot 10^{-3} \times (\Theta_j - 90°))$$
$$= 246.05056 \times ((0.51 \times e^{(-0.4 \times 5)} + 0.49)) \times (1.0 - 6.07 \cdot 10^{-3} \times (85° - 90°))$$
$$= 141.72199 \text{ m} \qquad\qquad (6.44)$$

Step 13
Determine the Richardson number on the flame in still air:

$$Ri(L_{b0}) = (g/(D_s^2 \times u_j^2))^{1/3} \times L_{b0} \qquad\qquad (6.45)$$
$$Ri(246.05056) = (9.80665/(0.93656)^2 \times (915.60648)^2))^{1/3} \times 246.05056$$
$$= 5.8349$$

Because $R_w \leq 0.05$, the flame is jet dominated, and the tilt angle α is given by:

$$\alpha = (\Theta_{jv} - 90°) \times (1 - e^{(-25.6 \times Rw)}) + 8000 \times R_w/Ri(L_{b0}) \qquad\qquad (6.46)$$
$$= (85° - 90°) \times (1 - e^{(-25.6 \times 0.00546)}) + 8000 \times 0.00546/5.8349)$$
$$= 6.8348$$

Step 14
Determine the lift-off of the flame (b):

$$K = 0.185 \times e^{-20\ Rw} + 0.015$$
$$= 0.185 \times e^{-20 \times 0.0546} + 0.015 = 0.180859$$

$$b = L_b \times \frac{\sin K\alpha}{\sin \alpha} \qquad\qquad (6.49)$$
$$= 141.72199 \times \frac{\sin(0.180859 \times 6.8348)}{\sin 6.8348} =$$
$$= 25.69$$

for $\alpha = 0°$ or $180°$ than b is equal to $0.2 \times L_b$ in still air ($\alpha = 0°$),
or $b = 0.015$ for 'lazy' flames pointing directly into high winds ($\alpha = 0°$)

Step 15
Determine length of frustum (flame):

$$R_l = (L_b^2 - b^2 \times \sin^2(\alpha))^{1/2} - b \times \cos(\alpha) \qquad\qquad (6.50)$$
$$= \sqrt{(141.72199)^2 - (25.69)^2 \times \sin^2(6.8348)} - 25.69 \times \cos(6.8348) =$$
$$= 116.18097 \text{ m}$$

6.100

Step 16

Determine the ratio between air and jet density:

$$\rho_{air}/\rho_j = T_j \times W_{air}/(T_{air} \times W_g) \qquad (6.51)$$
$$= 97.758 \times 0.02896/288.15 \times 0.0160428$$
$$= 0.612424$$

Step 17

Determine the Richardson number based on the combustion source diameter and factor C', used in calculating the frustum base width:

$$Ri(D_s) \quad = (g/(D_s^2 \times u_j^2))^{1/3} \times D_s \qquad (6.52)$$
$$Ri(0.1958) = (9.80665/(0.93656)^2 \times (915.60648)^2)^{1/3} \times 0.93656$$
$$= 0.0222$$

$$C' = 1000 \times e^{(-100 \times Rw)} + 0.8 = 1000 \times e^{-100 \times 0.0062} + 0.8 = 580.0123431 \qquad (6.53)$$

Step 18

Determine frustum base width:

$$W_1 \quad = \quad D_s \times (13.5 \times e^{(-6 \times Rw)} + 1.5) \times (1 - (1 - (\rho_{air}/\rho_j)^{1/2}/15) \times e^{-70 \times Ri(Ds)^{C' \times Rw}})$$
$$= \quad 0.93656 \times (13.5 \times e^{(-6 \times 0.00546)} + 1.5) \times (1 - (1 - (0.6124)^{1/2}/15)$$
$$\times e^{(-70 \times 0.0222)^{580.01 \times 0.00546}})$$
$$= \quad 0.71691 \text{ m} \qquad (6.54)$$

Step 19

Determine frustum tip width:

$$W_2 \quad = L_b \times (0.18 \times e^{(-1.5 \times Rw)} + 0.31) \times (1 - 0.47 \times e^{(-25 \times Rw)})$$
$$= 141.72199 \times (0.18 \times e^{(-1.5 \times 0.00546)} + 0.31) \times (1 - 0.47 \times e^{(-25 \times 0.00546)})$$
$$= 40.84751 \text{ m} \qquad (6.55)$$

Step 20

Determine the surface area of the frustum, including end discs:

$$A \quad = \quad \pi/4 \times (W_1^2 + W_2^2) + \pi/2 \times (W_1 + W_2) \times (R_1^2 + ((W_2 - W_1)/2)^2)^{1/2}$$
$$= \quad 3.1416/4 \times (0.71691^2 + 40.84751^2) + 3.1416/2 \times$$
$$(0.71691 + 40.84751) \times (116.18097)^2 + ((40.84751 - 0.71691)/2)^2)^{1/2}$$
$$= \quad 9008.52 \text{ m}^2 \qquad (6.56)$$

Step 20 a

Determine the surface area of a cylinder with the average of the widths

$$A \quad = \pi/2 \times ((W_1 + W_2)/2)^2 + \pi \times R_1 \times (W_1 + W_2)/2 \qquad (6.57)$$
$$= 3.1416/2 \times ((0.71691 + 40.84751)/2)^2 + 3.1416 \times 116.18097 \times$$
$$(0.71691 + 40.84751)/2$$
$$= 8263.79 \text{ m}^2$$

Step 21
Determine the net heat released:

$$Q' = m' \times \Delta H_c \tag{6.58}$$
$$= 30 \times 50{\cdot}10^6$$
$$= 1.5{\cdot}10^9 \text{ J}$$

Step 22
Determine the fraction of heat radiated from the flame surface:

$$F_s = 0.21 \times e^{(-0.00323 \times u_j)} + 0.11 \tag{6.59}$$
$$= 0.21 \times e^{(-0.00323 \times 915.6064)} + 0.11$$
$$= 0.12091$$

Step 23
Determine the theoretical Surface Emissive Power SEP_{act}:

$$SEP_{act} = F_s \times Q'/A \tag{6.60}$$
$$= 0.12091 \times \frac{1.5 \cdot 10^9}{8263.79}$$
$$\approx 21.951{\cdot}10^3 \text{ J/m}^2{\cdot}\text{s}$$
$$= 21.951 \text{ kW/m}^2$$

Step 24
Calculate the transformation parameters X', Θ' and x

$$X' = ((b \times \sin\Theta_j)^2 + (X - b \times \cos\Theta_j)^2)^{1/2} \tag{6.61}$$
$$= ((25.69 \times \sin(85°))^2 + (150 - 25.69 \times \cos(85°))^2)^{1/2}$$
$$= 149.96 \text{ m}$$

$$\Theta' = 90° - \Theta_j + \alpha - \arctan(b \times \sin\Theta_j /(X - b \times \cos\Theta_j)) \tag{6.62}$$
$$= 90° - 85 + 6.8348 - \arctan(25.69 \times \sin 85°/(150 - 25.69 \times \cos 85°))$$
$$= 2.00843$$

$$x = X' - (W_1 + W_2)/4 \tag{6.63}$$
$$= 149.96 - \frac{(0.71691 + 40.84751)}{4}$$
$$= 139.5698 \text{ m}$$

Step 25
Calculate the value of the view factor with the formulae presented in Appendix, Section 3, for a tilted cylinder. A tilted cylinder matches the shape of the flame.

At a distance of 46.7 metres from the flame and Θ' of 8.7°, a view factor of 0.0672 can be calculated with the formulae from Appendix (see also step 29).

Step 26
Calculate the actual Surface Emissive Power SEP_{act}, assuming for a methane flame hardly any soot formation. This means that $\varsigma = 0$, then

$$SEP_{act} = SEP_{max} \times (1 - \varsigma) + SEP_{soot} \times \varsigma \qquad (6.20)$$

becomes

$$
\begin{aligned}
SEP_{act} &= SEP_{max} \\
&= 21.951 \ J/m^2{\cdot}s
\end{aligned}
$$

Step 27
Determine absorption factor for water vapour α_w for an average flame temperature of 1200 K from Figure 6.2 and a distance x of 46.7 metres.

Calculate the partial vapour pressure of water p_w at 15 °C and a relative humidity RH of 0.7

$$
\begin{aligned}
p_w &= RH \times p_w^o \\
&= 0.7 \times 1705 \\
&= 1193.5
\end{aligned}
\qquad (6.72)
$$

$$p_w \times x = 1193.5 \times 139.5698 = 16.6576{\cdot}10^4 \ N/m$$

From Figure 6.2, subsection 6.5.2.4, it can be found that $\alpha_w = 0.2776$

Step 28
Determine the absorption coefficient for carbon-dioxide α_c for an average flame temperature of 1200 K from Figure 6.3 and a distance x of 46.7 metres

$$p_c \times x = 30.3975 \times 139.5698 = 4.242{\cdot}10^3 \ N/m$$

From Figure 6.3, subsection 6.5.2.4, it can be found that $\alpha_c = 0.04941$

Step 28a
Determine the atmospheric transmissivity

$$\tau_a = 1 - \alpha_w - \alpha_c \qquad (6.24)$$

$$\tau_a = 1 - 0.2776 - 0.04941 = 0.67302$$

or Figure 6.4, in subsection 6.5.2.4 can be used

Step 28b
An alternative way of calculating the atmospheric transmissivity

$$
\begin{aligned}
\tau_a &= 2.02 \times (p_w \times x)^{-0.08} \\
&= 2.02 \times (16.6576{\cdot}10^4)^{-0.08} \\
&= 0.772
\end{aligned}
\qquad (6.29)
$$

There is some difference with the calculated atmospheric transmissivity in step 28b. It is decided that the result of step 28 will be taken for the calculation of the maximum heat flux in step 30.

Step 29
Calculate the view factor F_{view} with the formulae in Appendix, section 3.1

R = $(W_1 + W_2)/4$ = (0.71691 + 40.84751)/4 = 10.3911 m
X = X' = 149.96 m
L = R_l = 116.18097 m
Θ = Θ' = 2.00843˚

a = L/R
= 116.18097/10.3911 = 11.18

b = X/R
= 149.96/10.3911 = 14.43166

A = $\sqrt{(a^2 + (b+1)^2 - 2 \times a \times (b+1) \times \sin\theta)}$

= $\sqrt{(11.18^2 + (14.43166 + 1)^2 - 2 \times 11.18 \times (14.43166 + 1) \times \sin(2.00843°))}$

= 18.736

B = $\sqrt{(a^2 + (b-1)^2 - 2 \times a \times (b-1) \times \sin\theta)}$

= $\sqrt{(11.18^2 + (14.43166 - 1)^2 - 2 \times 11.18 \times (14.43166 - 1) \times \sin(200843°))}$

= 17.1724

C = $\sqrt{(1 + (b^2 - 1) \times \cos^2\theta)}$

= $\sqrt{(1 + (14.43166^2 - 1) \times \cos^2(2.00843°))}$

= 14.4228

D = $\sqrt{((b-1)/(b+1))}$

= $\sqrt{((14.43166 - 1))/(14.43166 + 1))}$

= 0.93295

E = $(a \times \cos\theta)/(b - a \times \sin\theta)$
= $(11.18 \times \cos(2.00843˚))/(14.43166 - 11.18 \times \sin(2.00843˚))$
= 0.79587

6.104

$$F \quad = \sqrt{(b^2 - 1)}$$

$$= \sqrt{(14.43166^2 - 1)}$$

$$= 14.3969$$

The maximum view factors F_h and F_v can now be calculated with formulae (6.A.14) and (6.A.15), respectively.

$$F_v \quad = 0.02665$$

$$F_h \quad = 0.00934$$

The maximum view factor can be calculated with formula (6.A.18).

$$F_{max} \quad = \sqrt{(F_v^2 + F_h^2)} \tag{6.A.18}$$

$$= \sqrt{(0.02665^2 + 0.00934^2)}$$

$$= 0.0282$$

Step 30
Calculate the maximum heat flux at a distance of 49.8 metres from the centre of the flame to the radiated object.

$$q'' \quad = SEP_{act} \times F_{view} \times \tau_a \tag{6.4}$$
$$= 2.1951 \cdot 10^4 \times 0.0282 \times 0.673$$
$$= 417.236 \text{ J/m}^2\text{s} = 0.417 \text{ kW/m}^2$$

6.6.3   Pool fires on land (confined)

In this calculation example the heat flux is calculated in 13 steps for an object at a certain distance from a confined pool fire on land.

In this example we consider a pool caused by a release of 28.3 m³ of benzeen with a thickness of about 0.02 m.

The following input has been used for the calculation example:

V = 28.3 m³ $\quad A = 1415 \text{ m}^2$
δ = 0.02 m
m = $\rho \cdot V = 882 \times 28.3 = 24960$ kg
u_w = 5 m/s
m_∞'' = 0.085 kg/m²·s (from table 6.2)
$k \times \beta$ = 2.7 m⁻¹
υ = kinematic viscosity of air at 15 ˚C, 7.5133·10⁻⁶ m²/s (from Annex 1)
g = 9.80665 m/s

RH = 0.7 = 70%
p_w^o = 1705 N/m^2 (RH = 1) at 15 ˚C
p_c = 30.3975 N/m^2 in air (0.03% CO_2 in atmosphere)
T_a = Ambient temperature 15 ˚C = 288.15 K
ς = 0.8 = 80%
ΔH_c = 4.015·10^7 J/kg
T_b = 80.056 ˚C (= 353.206 K)
ρ_{air} = 1.2243 kg/m^3
x = 100 m (from centre of pool)
SEP_{soot} = 20·10^3 J/m^2·s

Step 1
Determine the circular pool diameter:

$$D = (4 \times V/(\pi \times \delta))^{1/2} \tag{6.64}$$
$$= (4 \times 28.3/(3.1416 \times 0.02))^{1/2}$$
$$= 42.445 \text{ m}$$

Step 2
Determine the pool burning rate m" at still weather conditions

$$m" = m_\infty" \times (1 - e^{-k \times \beta \times D}) \tag{6.66}$$
$$= 0.085 \times (1 - e^{-2.7 \times 42.445})$$
$$= 0.085 \text{ kg/(m}^2\text{·s)}$$

In general the value of the factor $(1 - e^{-k \times \beta \times D})$ is above 0.95 if the pool diameter is more than 1 metre, so m" ≈ m_∞".
In Annex 1 data can be found to calculate the burning rate of some single components, which can be used in the calculation of step 2a.

Step 3
Determine the characteristic wind velocity u_c

$$u_c = (g \times m" \times D/\rho_{air})^{1/3} \tag{6.14}$$
$$= (9.80665 \times 0.085 \times 42.445/1.2243)^{1/3}$$
$$= 3.06866 \text{ m/s}$$

Step 4
Determine the dimensionless wind velocity u^*

$$u^* = u_w/u_c \tag{6.13}$$
$$= 5/3.06866$$
$$= 1.62937$$

Step 5
Determine the mean length of the fire

$$L/D = 55 \times (m"/(\rho_{air} \times (g \times D)^{1/2}))^{0.67} \times (u^*)^{-0.21} \tag{6.12}$$
$$= 55 \times (0.085/(1.2243 \times (9.80665 \times 42.445)^{1/2}))^{0.67} \times 1.62937^{-0.21}$$
$$= 1.101938$$

6.106

$$L = 1.101938 \times D$$
$$= 1.101938 \times 42.445$$
$$= 46.7725 \text{ m}$$

Step 6
Determine the flame tilt angle Θ:

$$Fr_{10} = u_w^2/(g \times D) \tag{6.68}$$
$$= 5^2/(9.80665 \times 42.445)$$
$$= 0.0545$$

$$Re = u_w \times D/\upsilon \tag{6.69}$$
$$= 5 \times 42.445/7.5133 \cdot 10^{-6}$$
$$= 2.824 \cdot 10^7$$

$$\tan\Theta/\cos\Theta = 0.666 \times (Fr_{10})^{0.333} \times (Re)^{0.117} \tag{6.16}$$
$$= 0.666 \times (0.0545)^{0.333} \times (2.824 \cdot 10^7)^{0.117}$$
$$= 1.94315$$

In general, if $\tan\Theta/\cos\Theta = c$, then Θ can analytically be calculated by:

$$\Theta = \arcsin(((4 \times c^2 + 1)^{1/2} - 1)/(2 \times c)) \tag{6.70}$$
$$= \arcsin(((4 \times 1.94315^2 + 1)^{1/2} - 1)/(2 \times 1.94315))$$
$$= 50.8286°$$

Step 7
Determine the actual elongated flame base dimension

Step 7a)

$$D'/D = 1.6 \times (Fr_{10})^{0.061} \text{ for a conical flame presentation} \tag{6.18-1}$$
$$= 1.6 \times (0.0545)^{0.061}$$
$$= 1.3398$$

$$D' = 1.3398 \times 42.445$$
$$= 56.867 \text{ m}$$

Step 7b)

$$D'/D = 1.5 \times (Fr_{10})^{0.069} \text{ for a cylindrical flame presentation} \tag{6.18-2}$$
$$= 1.5 \times (0.0545)^{0.069}$$
$$= 1.2272$$

$$D' = 1.2272 \times 42.445$$
$$= 52.0869 \text{ m}$$

Step 8

Calculate the Surface Emissive Power SEP_{theor} for a tilted cylindrical flame

$$\begin{aligned} SEP &= 140 \cdot 10^3 \times e^{-0.12 \times D} + 20 \cdot 10^3 \times (1 - e^{-0.12 \times D}) \\ &= 140 \cdot 10^3 \times e^{-0.12 \times 42.445} + 20 \cdot 10^3 \times (1 - e^{-0.12 \times 42.445}) \\ &= 21 \cdot 10^3 \ W/m^2 \end{aligned} \qquad (6.19)$$

From table 6.6, F_s has been estimated at 0.40

$$\begin{aligned} SEP_{max} &= F_s \times m'' \times \Delta H_c/(1 + 4 \times L/D) \\ &= 0.40 \times 0.085 \times 4.015 \cdot 10^7/(1 + 4 \times 1.101938) \\ &= 25.24 \cdot 10^4 \ J/m^2 \cdot s \end{aligned} \qquad (6.71)$$

In literature $\varsigma = 80\%$ has been found

$$\begin{aligned} SEP_{act} &= SEP_{max} \times (1 - \varsigma) + SEP_{soot} \times \varsigma \\ &= 25.24 \cdot 10^4 \times (1 - 0.8) + 20 \cdot 10^3 \times 0.8 \\ &= 6.6 \cdot 10^4 \ J/m^2 \cdot s \end{aligned} \qquad (6.20)$$

Step 9

Determine absorption factor for water vapour α_w for an average flame temperature of 1200 K from Figure 6.2, in subsection 6.5.2.4, and for a distance x of 50 m from the flame surface.

Calculate the partial vapour pressure of water p_w at 15 ˚C and a relative humidity RH of 0.7.

$$\begin{aligned} p_w &= RH \times p_w^o \\ &= 0.7 \times 1705 \\ &= 1193.5 \ N/m^2 \end{aligned} \qquad (6.72)$$

$$\begin{aligned} p_w \times x &= 1193.5 \times 100 \\ &= 11.93 \cdot 10^4 \ N/m \end{aligned}$$

From Figure 6.2 it can be found that $\alpha_w = 0.24513$

Step 10

Determine the absorption coefficient for carbon-dioxide α_c for an average flame temperature of 1200 K from Figure 6.3, subsection 6.5.2.4, and a distance x of 50 metres

$$\begin{aligned} p_c \times x &= 30.3975 \times 100 \\ &= 3.03975 \cdot 10^3 \ N/m \end{aligned}$$

From Figure 6.3 it can be found that $\alpha_c = 0.0401285$

Step 11

The calculation with formula (6.24) is generally much more accurate. If the value of $p_w \times x$ is between 10^4 and 10^5 N/m, formula (6.29) can be used.

Determine the atmospheric transmissivity

$$
\begin{aligned}
\tau_a &= 1 - \alpha_w - \alpha_c \\
&= 1 - 0.24513 - 0.0401285 \\
&= 0.71474
\end{aligned}
\tag{6.24}
$$

or use Figure 6.4 in subsection 6.5.2.4.

Step 12

Calculate the view factor with the formulae from Appendix, section 3

$$
\begin{aligned}
a &= L/R \\
&= 46.7725/21.222 \\
&= 2.20396
\end{aligned}
$$

$$
\begin{aligned}
b &= X/R \\
&= 100/21.222 \\
&= 4.712
\end{aligned}
$$

$$
\begin{aligned}
A &= \sqrt{(a^2 + (b+1)^2 - 2 \times a \times (b+1) \times \sin\theta)} \\
&= \sqrt{(2.20396^2 + (4.712+1)^2 - 2 \cdot 2.20396 \times (4.712+1) \times \sin(50.8286°))} \\
&= 4.2384
\end{aligned}
$$

$$
\begin{aligned}
B &= \sqrt{(a^2 + (b-1)^2 - 2 \times a \times (b-1) \times \sin\theta)} \\
&= \sqrt{(2.20396^2 + (4.712-1)^2 - 2 \times 2.20396 \times (4.712-1) \times \sin(50.8286°))} \\
&= 2.439498
\end{aligned}
$$

$$
\begin{aligned}
C &= \sqrt{(1 + (b^2 - 1) \times \cos^2\theta)} \\
&= \sqrt{(1 + (4.712^2 - 1) \times \cos^2(50.8286°))} \\
&= 3.07555
\end{aligned}
$$

$$
\begin{aligned}
D &= \sqrt{((b-1)/(b+1))} \\
&= \sqrt{((4.712-1)/(4.712+1))} \\
&= 0.806135
\end{aligned}
$$

$$E \quad = (a \times \cos \theta)/(b - a \times \sin \theta)$$
$$= (2.20396 \times \cos(50.8286°))/(4.712 - 2.20396 \times \sin(50.828°))$$
$$= 0.4635$$

$$F \quad = \sqrt{(b^2 - 1)}$$

$$= \sqrt{(4.712^2 - 1)}$$

$$= 4.60457$$

The maximum view factors F_h and F_v can now be calculated with formulae (6.A.14) and (6.A.15), respectively.

$$F_v \quad = 0.091915$$

$$F_h \quad = 0.029146$$

The maximum view factor can be calculated with formula (6.A.18).

$$F_{max} \quad = \sqrt{(F_v^2 + F_h^2)} \qquad\qquad (6.A.18)$$

$$= \sqrt{(0.091915^2 + 0.029146)^2}$$

$$= 0.0964$$

Step 13
Calculate the maximum heat flux at a distance of 50 metres

$$q'' \quad = SEP_{act} \times F_{view} \times \tau_a \qquad\qquad (6.4)$$
$$= 6.6 \cdot 10^4 \times 0.0964 \times 0.71474$$
$$= 4.581 \cdot 10^3 \ J/m^2 \cdot s$$

6.6.4 Pool fires on land (unconfined)

In this calculation example the heat flux is calculated in 22 steps for an object at a certain distance from an unconfined pool fire on land.

In this calculation example, we consider a pool caused by an open 4" valve which is connected with a 196 m³ benzeen storage tank.
At some distance of the tank the benzeen is released at ground level. It is assumed that the flow resistance in the pipe can be neglected.

The following input has been used for the calculation example:

A_t = 19.63 m² (diameter of the tank is 5 metres) =

$$\pi \cdot r^2 = \pi \times \left(\frac{d}{2}\right)^2 = \pi \cdot \left(\frac{5}{2}\right)^2$$

m = $\rho \cdot V$ = 882 × 196 = 172872 kg
h_i = 196 m³/19.6 m² = 9.98 m
g = 9.80665 m/s²
C_0 = 0.7
d_h = 0.1 m = 100 mm
$m'' = m''_\infty$ = 0.085 kg/m²·s
$k \times \beta$ = 2.7 m⁻¹
ρ = 882 kg/m³
δ = 0.02 m (assumed thickness) = 20 mm
$\Phi(\tau_i = 0)$ = 0, which means that the ignition took place at the beginning of the release while no liquid pool was present before the release.
υ = 7.513·10⁻⁶ m²/s)
u_w = 5 m/s
T_f = 1200 K
P_{air} = 1.0133·10⁵ N/m²
P_{init} = 10⁷ N/m²
γ = 1.4
RH = 0.7 = 70%
p_w^o = 1705 N/m² (RH = 1) at 15 ˚C
p_c = 30.3975 N/m² (0.03% CO_2 in atmosphere)
T_a = Ambient temperature 15 ˚C = 288.15 K
T_b = 80.056 °C (= 353.206 K)
ς = 0.8 = 80%
ΔH_c = 4.015·10⁷ J/kg
ρ_{air} = 1.2243 kg/m³
x = 100 m (from centre of pool)
SEP_{soot} = 20·10³ J/m².s

Step 1
Calculate the surface area A_0 of the hole:

$$A_0 = \pi/4 \times d_h^2$$
$$= 3.1416/4 \times 0.1^2 = \pi/4 \times 0.1^2$$
$$= 0.0079 \text{ m}^2$$

Step 2
Calculate the initial outflow velocity v_0:

$$v_0 = C_0 \times (2 \times g \times h_i)^{1/2} \tag{6.75}$$
$$= 0.7 \times (2 \times 9.80665 \times 9.98)^{1/2}$$
$$= 9.7935 \text{ m/s}$$

Step 3
Calculate the acceleration constant a:

$$a \quad = (C_0 \times A_0/A_t)^2 \times g \qquad\qquad (6.76)$$
$$= (0.7 \times 0.0079/19.63)^2 \times 9.80665$$
$$= 7.827 \cdot 10^{-7} \text{ m/s}^2$$

Step 4
The mass burning rate m" of the petrol at still weather conditions is taken from table 6.5.

$$m" \quad = 0.085 \text{ kg/m}^2 \cdot \text{s}$$

Step 5
Calculate τ

$$\tau \quad = m" \times t/(\rho \times \delta) \qquad\qquad (6.77)$$
$$= 0.085 \times t/(882 \times 0.02)$$
$$= 4.8185 \cdot 10^{-3} \times t$$

Step 6
Calculate Φ

$$\Phi \quad = m" \times \pi \times R^2/(\rho \times A_0 \times v_0) \qquad\qquad (6.78)$$
$$= 0.085 \times 3.1416 \times R^2/(882 \times 0.0079 \times 9.7935)$$
$$= 3.913 \cdot 10^{-3} \times R^2$$

Step 7
Calculate β'

$$\beta' \quad = (a \times \delta \times \rho/(v_0 \times m")) \qquad\qquad (6.80)$$
$$= (7.7827 \cdot 10^{-7} \times 0.02 \times 882/(9.7935 \times 0.085))$$
$$= 1.649 \cdot 10^{-5}$$

Step 8
Use the non-dimensional form of the pool spread differential equation, which is applicable for $\tau_i \leq \tau \leq \tau_D$; it is assumed that there is a fire when the release has started, thus $\Phi(\tau_i = 0) = 0$:

$$\Phi(\tau) \quad = 1 + \beta'(1 - \tau) - [1 - \Phi_i + \beta'(1 - \tau_i)] \, e^{-(\tau - \tau i)} \qquad (6.82)$$
$$= 1 + 1.649 \cdot 10^{-5} \times (1 - \tau) - (1 + 1.649 \cdot 10^{-5}) \times e^{-\tau}$$

Step 9
Determine the time at which the pool diameter will be maximal.
This will be obtained, if $d\Phi/d\tau = 0$ and means that:

$$\tau_{max} \quad = \ln((1+\beta')/\beta') \qquad\qquad (6.84)$$
$$= \ln((1 + 1.649 \cdot 10^{-5})/1.649 \cdot 10^{-5})$$
$$= 11.0128$$

Furthermore

$$\tau \quad = 4.8185 \cdot 10^{-3} \times t \tag{6.77}$$

$$t_{max} \quad = 11.0128/4.8185 \cdot 10^{-3}$$
$$= 2285 \ s$$
$$= 0.63 \ h$$

Step 10
Determine the maximum pool diameter.

$$\Phi_{max} \quad = 1 + (1.649 \cdot 10^{-5} \times (1 - 11.0128)) - (1 + 1.649 \cdot 10^{-5}) \times e^{-11.0128} \tag{6.82}$$
$$= 1 - 1.6511 \cdot 10^{-4} - 1.6489 \cdot 10^{-5}$$
$$= 0.9998$$

$$R_{max} \quad = (\Phi/3.913 \cdot 10^{-3})^{1/2} \tag{6.78}$$
$$= (0.9998/3.913 \cdot 10^{-3})^{1/2}$$
$$= 15.985 \ m$$

$$D_{max} \quad = 2 \times R_{max} = 2 \times 15.985$$
$$= 31.97 \ m$$

Now the same calculations from subsection 6.6.3 can be applied to calculate the flame height and the heat flux at a certain distance from the tank.

Step 11
Determine of the total release time t_{rel} and duration of the fire t_{tot}.

The total time of the benzene release from the tank will be:

$$t_{rel} \quad = (A_t/(C_0 \times A_0)) \times (2 \times h_i/g)^{1/2} \tag{6.85}$$
$$= (19.63/(0.7 \times 0.0079)) \times (2 \times 9.98/9.80665)^{1/2}$$
$$= 5064 \ s$$
$$= 1.41 \ h$$

This means that:

$$\tau \quad = 4.8185 \cdot 10^{-3} \times t \tag{6.77}$$
$$= 4.8185 \cdot 10^{-3} \times 5064$$
$$= 24.40$$

Formula 6.82 can now be filled in, giving the following result:

$$\Phi \quad = 1 + (1.649 \cdot 10^{-5} \cdot (1-24.4)) - (1 + 1.649 \cdot 10^{-5})e^{-24.4}$$
$$= 1 - 3.85866 \cdot 10^{-4} - 2.53 \cdot 10^{-11} = 0.9996$$

Because $R = (\Phi/3.913 \cdot 10^{-3})^{1/2}$ it means that the pool diameter will not decrease significantly between 0.63 and 1.41 h.

The total duration of the fire will be the release time plus the time to burn the benzene in the pool completely.

$$t_{tot} = t_{rel} + \delta \times \rho/m'' \qquad (6.87)$$
$$= 5064 + 0.02 \times (882/0.085)$$
$$= 5271.5 \text{ s}$$
$$= 1.46 \text{ h}$$

Step 12
Determine the characteristic wind velocity u_c

$$u_c = (g \times m'' \times D/\rho_{air})^{1/3} \qquad (6.14)$$
$$= (9.80665 \times 0.085 \times 31.97/1.2243)^{1/3}$$
$$= 2.792 \text{ m/s}$$

Step 13
Determine the dimensionless wind velocity u^*

$$u^* = u_w/u_c \qquad (6.13)$$
$$= 5/2.792$$
$$= 1.79$$

Step 14
Determine the mean length of the fire

$$L/D = 55 \times (m''/(\rho_{air} \times (g \times D)^{1/2}))^{0.67} \times (u^*)^{-0.21} \qquad (6.12)$$
$$= 55 \times (0.085/(1.2243 \times (9.80665 \times 31.97)^{1/2}))^{0.67} \times (1.79)^{-0.21}$$
$$= 1.1857$$

$$L = 1.1857 \times D$$
$$= 1.1857 \times 31.97$$
$$= 37.91 \text{ m}$$

Step 15
Determine the flame tilt angle Θ:

$$Fr_{10} = u_w^2/(g \times D) \qquad (6.68)$$
$$= 5^2/(9.80665 \times 37.91)$$
$$= 0.00799$$

$$Re = u_w \times D/\upsilon \qquad (6.69)$$
$$= 5 \times 37.91/7.513 \cdot 10^{-6}$$
$$= 2.12 \cdot 10^7$$

$$\tan\Theta/\cos\Theta = 0.666 \times (Fr_{10})^{0.333} \times (Re)^{0.117} \qquad (6.16)$$
$$= 0.666 \times (0.0799)^{0.333} \times (2.12 \cdot 10^7)^{0.117}$$
$$= 2.0669$$

In general, if $\tan\Theta/\cos\Theta = c$, then Θ can analytically be calculated by:

$$\begin{aligned}\Theta\ &= \arcsin(((4 \times c^2 + 1)^{1/2} - 1)/(2 \times c)) & (6.70)\\ &= \arcsin(((4 \times 2.0669^2 + 1)^{1/2} - 1)/(2 \times 2.0669))\\ &= 51.9°\end{aligned}$$

Step 16
Determine the actual elongated flame base dimension

Step 16a)

$$\begin{aligned}D'/D\ &= 1.6 \times (Fr_{10})^{0.061} \text{ for a conical flame presentation} & (6.18\text{-}1)\\ &= 1.6 \times (0.0799)^{0.061}\\ &= 1.371\end{aligned}$$

$$\begin{aligned}D'\ &= 1.371 \times 31.97\\ &= 43.84 \text{ m}\end{aligned}$$

Step 16b)

$$\begin{aligned}D'/D\ &= 1.5 \times (Fr_{10})^{0.069} \text{ for a cylindrical flame presentation} & (6.18\text{-}2)\\ &= 1.5 \times (0.0799)^{0.069}\\ &= 1.2599\end{aligned}$$

$$\begin{aligned}D'\ &= 1.2599 \times 31.97\\ &= 40.28 \text{ m}\end{aligned}$$

Step 17
Calculate the Surface Emissive Power SEP_{max} for a tilted cylindrical flame

$$\begin{aligned}SEP_{act}\ &= 140 \cdot 10^3 \times e^{-0.12 \times D} + 20 \cdot 10^3 \times (1 - e^{-0.12 \times D}) & (6.19)\\ &= 140 \cdot 10^3 \times e^{-0.12 \times 31.97} + 20 \cdot 10^3 \times (1 - e^{-0.12 \times 31.97})\\ &= 3019.96 + 19568.6 = 22.59 \cdot 10^3 \text{ J/m}^2 \cdot \text{s}\end{aligned}$$

From table 6.6, F_s has been estimated at 0.40

$$\begin{aligned}SEP_{max}\ &= F_s \times m'' \times \Delta H_c/(1 + 4 \times L/D) & (6.71)\\ &= 0.4 \times 0.085 \times 4.0185 \cdot 10^7/(1 + 4 \times 1.1857)\\ &= 23.72 \cdot 10^4 \text{ J/m}^2 \cdot \text{s}\end{aligned}$$

In literature $\varsigma = 80\%$ has been found

$$SEP_{act} = SEP_{max} \times (1 - \varsigma) + SEP_{soot} \times \varsigma \qquad (6.20)$$

becomes

$$= 23.72 \cdot 10^4 \times (1 - 0.8) + 20 \cdot 10^3 \times 0.8$$

$$= 6.34 \cdot 10^4 \text{ J/m}^2 \cdot \text{s}$$

Step 18
Determine absorption factor for water vapour α_w for an average flame temperature of 1200 K from Figure 6.2, subsection 6.5.2.4, and for a distance x of 100 m from the flame surface.
Calculate the partial vapour pressure of water p_w at 15 ˚C and a relative humidity RH of 0.7.

$$p_w \quad = RH \times p_w^o \qquad\qquad\qquad\qquad (6.72)$$
$$= 0.7 \times 1705$$
$$= 1193.5 \text{ N/m}^2$$

$$p_w \times x \quad = 1193.5 \times 100$$
$$= 119350 \text{ N/m}$$

From Figure 6.2 it can be found that $\alpha_w = 0.2497$

Step 19
Determine the absorption coefficient for carbon-dioxide α_c for an average flame temperature of 1200 K from Figure 6.3, in subsection 6.5.2.4, and a distance x of 100 metres

$$p_c \times x \quad = 3039.75 \text{ N/m}$$

From Figure 6.3 it can be found that $\alpha_c = 0.04$

Step 20
The calculation with formula (6.24) is generally much more accurate. If the value of $p_w \times x$ is between 10^4 and 10^5 N/m, formula (6.29) can be used.

Determine the atmospheric transmissivity

$$\tau_a \quad = 1 - \alpha_w - \alpha_c \qquad\qquad\qquad\qquad (6.24)$$
$$= 1 - 0.2497 - 0.04$$
$$= 0.71$$

or Figure 6.4 in subsection 6.5.2.4 can be used.

Step 21
Calculate the view factor with the formulae from Appendix, section 3

$$a \quad = L/R$$
$$= 37.91/15.985$$
$$= 2.377$$

$$b \quad = X/R$$
$$= 100/15.985$$
$$= 6.271$$

A $\quad = \sqrt{(a^2 + (b+1)^2 - 2 \times a \times (b+1) \times \sin\theta)}$

$\quad = \sqrt{(2.377^2 + (6.271+1)^2 - 2 \times 2.377(6.271+1) \times \sin(51.9°))}$

$\quad = 5.595$

B $\quad = \sqrt{(a^2 + (b-1)^2 - 2 \times a \times (b-1) \times \sin\theta)}$

$\quad = \sqrt{(2.377^2 + (6.271-1)^2 - 2 \times 2.377(6.271-1) \times \sin(51.9°))}$

$\quad = 3.703$

C $\quad = \sqrt{(1 + (b^2-1) \times \cos^2\theta)}$

$\quad = \sqrt{(1 + (6.271^2-1) \times \cos^2(51.9°))}$

$\quad = 3.949$

D $\quad = \sqrt{((b-1)/(b+1))}$

$\quad = \sqrt{((6.271-1)/(6.271-1+1))}$

$\quad = 0.851$

E $\quad = (a \times \cos\theta)/(b - a \times \sin\theta)$
$\quad = (2.377 \times \cos(51.9°))/(6.271 - 2.377 \times \sin(51.9°))$
$\quad = 0.333$

F $\quad = \sqrt{(b^2-1)}$

$\quad = \sqrt{(6.271^2-1)}$

$\quad = 6.191$

The maximum view factors F_h and F_v can now be calculated with formulae (6.A.14) and (6.A.15), respectively.

$F_v \quad = 0.0466$

$F_h \quad = 0.00977$

The maximum view factor can be calculated with formula (6.A.18).

$$F_{max} = \sqrt{(F_v^2 + F_h^2)} \qquad\qquad (6.A.18)$$

$$= \sqrt{(0.0466^2 + 0.00977^2)}$$

$$= 0.0476$$

Step 22
Calculate the maximum heat flux at a distance of 25 metres from the flame surface.

$$q'' = SEP_{act} \times F_{view} \times \tau_a \qquad\qquad (6.4)$$
$$= 6.34 \cdot 10^4 \times 0.0476 \times 0.71$$
$$= 2.141 \cdot 10^3 \text{ J/m}^2 \cdot \text{s}$$

6.6.5 Fire balls

In this calculation example the heat flux is calculated in 14 steps for an object at a certain distance from a fire ball.

Calculate the heat flux of a fire ball after a BLEVE of a road tanker with a capacity of 45 m³, at a distance of 200 m. Tank is filled for 85% with propane.

The following input is required for the calculation:
V = Capacity of the tank, is 45 m³
f = Filling degree, is 0.85 = 85%
ρ_{lpg} = Density of LPG is 517 kg/m³ (propane) (±9 °C)
P_{sv} = $16 \cdot 10^5$ N/m² = Pa = 16 Bar
ΔH_c = $46.013 \cdot 10^6$ J/kg
ΔH_v = $0.426134 \cdot 10^6$ J/kg
C_p = $2.582 \cdot 10^3$ J/kg·K (±9 °C)
ΔT = 1717 K (assumed T_f = 2000 K; $T_{ambient}$ = 10 °C
x_{bleve} = 200 m
P_w° = 17.05 N/m²
P_c = 30.3975 N/m² (0.03% CO_2 in atmosphere)
T_{boil} = 230 K = -43 °C

Step 1
Calculate the amount of LPG release in case of a complete failure of the tank

$$V_{rel} = f \times V$$
$$= 0.85 \times 45$$
$$= 38.25 \text{ m}^3$$

$$m = f \times V \times \rho_{lpg} \qquad\qquad (6.89)$$
$$= V_{rel} \times \rho_{lpg}$$
$$= 38.25 \times 517$$
$$= 19775 \text{ kg}$$

Step 2

The radius of the fireball can be calculated from the quantity of combusting material:

$$r_{fb} = 3.24 \times m^{0.325} \tag{6.90}$$
$$= 3.24 \times 19775^{0.325}$$
$$= 80.68 \text{ m}$$

Step 3
The duration of the fireball is:

$$t = 0.852 \times m^{0.26} \tag{6.91}$$
$$= 0.852 \times 19775^{0.26}$$
$$= 11.15 \text{ s}$$

Step 4
The lift-off height of the fire ball, measured from the centre of the fire ball to the ground underneath the fire ball.

$$H_{bleve} = 2 \times r_{fb} \tag{6.22}$$
$$= 2 \times 80.68$$
$$= 161.366 \text{ m}$$

Step 5
Calculate the distance X from the centre of the fire ball to the object.

$$X = (x_{bleve}^2 + H_{bleve}^2)^{1/2} \tag{6.92}$$
$$= \sqrt{200^2 + 161.366^2}$$
$$= 256.98 \text{ m}$$

Step 6
Calculate maximum F_{view} at a distance X.

$$F_{view} = (r_{fb}/X)^2 \tag{6.93}$$
$$= (80.68/256.98)^2$$
$$= 0.09856$$

Step 7
Calculate the fraction F_s of the generated heat radiated by a fire ball.

$$F_s = 0.00325 \times (P_{sv})^{0.32} \tag{6.21}$$
$$= 0.00325 \times (16 \cdot 10^5)^{0.32}$$
$$= 0.314$$

Step 8
Calculate the heat available for combustion and radiation.

$$\Delta H = \Delta H_c - \Delta H_v - C_p \times \Delta T \quad\quad (6.94)$$
$$= 4.6013 \cdot 10^7 - 0.426134 \cdot 10^6 - 2.582 \cdot 10^3 \times 1717$$
$$= 41.153 \cdot 10^6 \text{ J/kg}$$

Step 9
Calculate the Surface Emissive Power SEP_{act}

Assume that there is no soot formation, so $SEP_{act} = SEP_{max}$

$$SEP_{act} = \Delta H_c \times m \times F_s/(4 \times \pi \times r_{fb}^2 \times t) \quad\quad (6.95)$$
$$= 41.153 \cdot 10^6 \times 19775 \times 0.314/(4 \times \pi \times 80.68^2 \times 11.15)$$
$$= 28.02 \cdot 10^4 \text{ J/m}^2 \cdot s$$

Step 10
Calculate the actual path length between the surface area of the fire ball and the object.

The actual path length x of radiation from a fire ball surface is the hypothenuse minus the BLEVE-radius.

$$x = X - r_{fb} \quad\quad (6.96)$$
$$= 256.98 - 80.68$$
$$= 176.296 \text{ m}$$

This is the distance between the surface area of the fire ball and the object and has to be used in the calculation of τ_a.

Step 11
Calculate the partial vapour pressure of water p_w at 15 ˚C and a relative humidity RH of 0.7.

$$p_w = RH \times p_w^o \quad\quad (6.72)$$
$$= 0.7 \times 1705$$
$$= 1193.5 \text{ N/m}^2$$

$$p_w \times x = 1193.5 \times 176.296$$
$$= 21.04 \cdot 10^4 \text{ N/m}$$

From Figure 6.2, $\alpha_w = 0.223$ can be found.

Step 12
Determine the absorption coefficient for carbon-dioxide α_c for an average flame temperature of T_f in 1200 K from Figure 6.3 and a distance x from the flame surface.

Now $p_c \times x$ can be calculated.

$$p_c \times x = 30.3976 \times 176.296 = 5.358 \cdot 10^3 \text{ N/m}$$

6.120

From Figure 6.3, $\alpha_c = 0.0435$ can be found.

Step 13
Determine the atmospheric transmissivity

$$
\begin{aligned}
\tau_a \quad &= 1 - \alpha_w - \alpha_c \qquad\qquad\qquad\qquad\qquad (6.24)\\
&= 1 - 0.223 - 0.0435\\
&= 0.7335
\end{aligned}
$$

The calculation with formula (6.24) is generally much more accurate. If the value of $p_w \times x$ is between 10^4 and 10^5 N/m, formula (6.29) can be used.

Step 13a
An alternative for the calculation of the atmospheric transmissivity τ_a

$$
\tau_a \quad = c_7 \times (p_w \times x)^{-0.09} \qquad\qquad\qquad\qquad\qquad (6.29)
$$

This formula can only be used for calculations in the range between:

$$
10^4 < p_w \times x < 10^5 \text{ N/m.}
$$

$$
\begin{aligned}
\tau_a \quad &= 2.02 \times (p_w \times x)^{-0.09}\\
&= 2.02 \times (21.04 \cdot 10^4)^{-0.09}\\
&= 0.67
\end{aligned}
$$

Step 14
Calculate the heat flux at 200 metres from the road tanker

$$
\begin{aligned}
q'' \quad &= SEP_{act} \times F_{view} \times \tau_a \qquad\qquad\qquad\qquad (6.4)\\
&= 28.02 \cdot 10^4 \times 0.09856 \times 0.7335\\
&= 20.361 \cdot 10^3 \text{ J/m}^2 \cdot \text{s}
\end{aligned}
$$

6.7 Interface with the other models

6.7.1 Introduction

In this chapter the interface between other models in the Revised Yellow Book is given. A chapter has been dedicated to each model.

6.7.2 Jet flames

In the jet flame model of Chamberlain the released amount has been calculated with the models that can be found in chapter 2, subsection 2.5.2, about gas releases through orifices and piping.
These formulae are all added to this chapter to be able to render a complete model, as presented in Chamberlain [1987].

6.7.3 Pool fires on land

For pool fires on land, confined and unconfined pool can be distinguished. In chapter 2, subsection 2.5.4, attention has been paid to outflow and in chapter 3, subsection 3.3.3, to the increase in size of an unconfined pool. However, spreading of an unconfined burning pool as presented in this chapter, also includes the parameter burning rate. So the models about spreading pools presented in this chapter 6, subsection 6.5.5, differ from models presented in chapter 3, subsection 3.3.3.1.

6.7.4 Pool fires on water

No models could be found for pool fires on water.

6.7.5 Fire balls

For the fire balls an instantaneous release has been assumed. No input from other chapters is required.

6.8   Discussion

6.8.1   Introduction

In this chapter strengths and, limitations of the models are given, as well as unknown areas, which need to be investigated. If possible, it is indicated whether research or development is required.

6.8.2   Jet flames

The model from Chamberlain [1987] for a fire jet of gas has been validated for a great number of experiments. The model is only applicable to gas. The experiments where carried out for natural gas flares and cover a range of gas velocities from Mach 0.006 to Mach 1.53.

When the flow becomes choked, the expansion beyond the exit hole is idealised as if it takes place in a convergent-divergent nozzle, using standard orifice equations for isentropic flow. This idealisation is probably a weakness in the theoretical model because this assumption can only be made under certain conditions, such as regards a Laval-tube. On the basis of this assumption all results of the measurements were matched, and will not have an impact on the end results.

The lift-off of a flame, due to the hot flame and a density of the flame tip lower than air has been incorporated in the model.

6.8.3   Pool fires on land

Confined pool
For confined pool fires many experiments were carried out with all types of hydrocarbons, including crude oil and liquefied gases.

All relevant parameters are determined for the calculation of the shape. Phenomena such as flame drag and flame tilt, as well as different flame shapes, are described in literature. However, little attention has been given how to use these parameters in the calculation of the view factor, and in heat radiation calculations in general.

Unconfined pool
For unconfined pool fires on land many experiments were carried out to measure flame dimensions, the burning rate of the released material, and the influence of wind. Only one theoretical model was found in literature to determine the variation of the diameter of a circular burning pool versus time. The pool was fed from a storage tank. Small-scale measurements were carried out to validate the model but showed incorrect results in the curves, so conclusions drawn should be considered with care. No further measurements were carried out to determine the flame height, flame shape and influence of wind in relation to this type of pool fire. In the model the pool thickness is taken as input parameter, though nothing is said about a good choice of value.

The situation of an unconfined pool described in the model can only occur in case the distance to the tank and the circular pool is large enough, so the pool can fully develop. Also the effect of resistance of the pipe on the flow rate should be taken into account for the feed rate to the pool.

In the study no attention has been paid to the maximum diameter and thickness of the pool. More measurements are required to determine the effects of an unconfined pool. The experiments should be carried out for larger-scale experiments in order to obtain more data about this subject.

6.8.4 Pool fires on water

Publications about measurements regarding pool fire on water have not paid attention to e.g. growth of the pool; only stationary situations were considered. In reality pool fires on water will show more or less the characteristics of unconfined pool fires on land. It should be further investigated whether models proposed for pool fires for an unconfined pool on land can be used for water, since the burning rate of crude oil and other hydrocarbons on water seems to be equal to the burning rate on land. The remarks made for an unconfined pool fire in subsection 6.8.2 are also applicable to this type of fire.

6.8.5 Fire balls

No new developments in modelling the dimension of a fireball were found in literature.

6.9   Literature

AIChE (1989),
Chemical Process Quantitative Risk Analysis - guidelines for -, Center for Chemical
Process Safety of the American Institute of Chemical Engineers, 1989.

Alger (1979),
Alger, R.S., Corlett, R.C., Gorden, A.S., Williams, F.A.,
Some aspects of turbulent pool fires,
Fire Tech. <u>15</u> (2), 142-146 (1979).

American Gas Association (1974),
LNG Safety Program - Interim Report on Phase II Work
Report no. IS-3-1 (July 1974).

Aravamudan (1979),
Aravamudan, Krishna, Moussa, A.N., Raj, P.P.K.,
Experiments involving pool and vapor fires from spills if liquefied natural gas on
water,
US Department of Transportation, Report No. C6-D-55-79, March 1979.

Atallah (1973),
Atallah, R.,
LNG Safety Program Phase II - Consequences of LNG spills on land,
American Gas Association, November 1973, Project 1S-3-1.

Atallah (1990),
Atallah, S. and Shah., J.N.,
LNG Fire
A thermal radiation model for LNG fires,
Topical report GRI-89/0176, GRI, 1990.

Babrauskas, (1983)
Babrauskas, V.,
Estimating Large Pool Fire Burning Rates,
Fire Technology, 1983, pp. 251-261.

Bagster (1989),
Bagster, D.G. and Pittblado, R.M.,
Thermal Hazards in the Process Industry,
Chemical Engineering Progress, July 1989, pp. 69-75.

Balluff (1985),
Balluff, C., Brötz, W., Göck, D., Schieß, N., Schönbucher, A.,
Erforschung von Schadefeuern flüssiger Kohlenwasserstoffe als Beitrage zur
sicherheit von Chemieanlagen,
Chem. -Ing.-Tech. 57 (1985) nr. 10, S. 823-834.

Binding (1992),
Binding, T.M. and Pritchard, M.J.,
Fire 2: A new Approach for predicting Thermal Radiation Levels from Hydrocarbon Pool Fires,
I.Chem E Symposium Series No. 130., Volume 3, 1992.

Brzustowski (1973),
Brzustowski, T.A. and Sommer, E.C.,
Predicting Radiant Heating from Flares,
Proceedings API Division of Refining, 1973, 53, pp. 865-893.

Burgess (1974),
Burgess, D.S. and Herzberg, M.,
Advances in thermal engineering,
J. Wiley and Sons, Chichester, UK,
Chapter 27, p 413, 1974.

Burgess, Hertzberg (1974),
Burgess, D., Hertzberg, M.,
Radiation from pool flames
Chapter 27 from: Heat Transfer in Flames (N.H. Afgan and J.M. Beer ed.)(1974)

Burgess, Zabetakis (1961),
Burgess, D.S. and Zabetakis, M.G.,
Research on the Hazards Associated with the Production and Handling of liquid Hydrogen,
R.I. 5707, Bureau of Mine, Pittsburgh (1961).

Burgess, Zabetakis (1971),
Burgess, D.S. and Zabetakis, M.G.,
Fire and explosion hazards associated with liquefied natural gas
Bureau of Mines, Report no. 6099, U.S. Department Division, London (December 1971)

Buschman Jr. (1961),
Buschman Jr., A.J. and Pittman, C.M.,
Configuration factors for exchange of radiant energy between antisymmetrical sections of cylinders, cones, and hemispheres and their bases, NASA, Technical Note D 944 (Oct. 1961).

Carne (1971),
Carne, M.,
Buxton-Bund Fire Tests
Report by the Gas Council, Research and Development Division, London (December 1971)

Chamberlain (1987),
Chamberlain, G.A.,
Development in design methods for predicting thermal radiation from flares,
Chem. Eng. Res. Des. Vol. 65. July 1987, pp. 299-309.

Cline (1983),
Cline, D.D. and Koenig, L.N.,
The transient Growth of an Unconfined Pool Fire,
Fire Technology, Pool fire, pp. 149-162, 1983.

Cowley (1991),
Cowley, L.T. and Johnson, A.D.,
Blast and Fire Engineering Project for Topside Structures,
Fl1 Oil and gas Fires: Characteristics and Impact.

Cook (1987),
Cook, D.K., Fairweather, M., Hammonds, J., Hughes, D.J.,
Size and radiative Characteristics of Natural Gas Flares,
Part 2: Empirical Model,
Chem. Eng. Res. Des. Vol. 65. July 1987, pp. 318-325.

Cunningham (1961),
Cunningham, F.G.,
Power input to a small flat plate from a diffusively radiating sphere, with application
to earth satellites NASA,
Technical Note D-710 (Aug. 1961).

Fu (1971),
Fu, T.T.,
Heat radiation from fires of aviation fuels,
Fire Technology, $\underline{7}$ (1), 47-56 (1971).

Hägglund (1976),
Hägglund, B. and Persson, L.E.,
The heat radiation from petroleum fires,
FOA Rapport C201126-D6 (July 1976).

Hottel (1967),
Hottel, H.C., Saforim, A.F.,
Radiative transfer
McGraw Hill, New York (1967)

JISE (1982),
Japan Institute for Safety Engineering,
Report on burning of petroleum fires,
1982, (in Japans).

Jones (1992),
Jones, D.,
Nomenclature for hazard and risk assessment in the process industry
Institute of Chemical Engineers, second edition, 1992.

Lautkaski (1992),
Lautkaski, R.,
Validation of flame drag correlations with data from large pool fires,
J. Loss Prev. Process Ind., 1992, Vol 5, no 3, pp. 175-180.

Love (1968),
Love, T.J.,
Radiative Heat Transfer,
C.E. Merrill Publishing Company, Columbus, Ohio (1968).

Maezawa (1973),
Maezawa, M.,
Experiments onfire hazards of liquefied flammable gases
Japan Society of Safety Engineering (May 1973)

May (1973),
May, W.G. and McQueen, W.,
Radiation from large LNG fires,
Combustion Science Technology, $\underline{7}$ (2), 51-56 (1973).

Minzer (1982),
Minzer, G.A. and Eyre, J.A.,
Large - scale LNG and LPG pool fires,
I. Chem. Eng. Symposium Series, $\underline{71}$, 147-163 (1982).

Modak (1978),
Modak, A.,
Radiation from products of combustion,
Tech. Rep. OAOE6, BU-1, Factory Mutual Research Corp.,
Nordwood, Mass., USA (1978).

Moorhouse (1982),
Moorhouse, J.,
Scaling Criteria for pool fires derived from large scale experiments,
I. Chem. E. Symposium Series No. 71, (1982), pp. 165-179.

Mudan (1984),
Mudan, K.S.,
Thermal Radiation Hazards from Hydrocarbon Pool Fires,
Prog. Energy Comb. Science $\underline{10}$,pp. 59-80, 1984.

Mudan (1987),
Mudan, K.S.,
Geometric view factors for thermal radiation hazard assessment,
Fire Safety Journal, 12:89-96, 1987.

NASA (1979),
NASA,
On the experiments with 7.5 m and 15 m JP-4 fuel pool fire measurements, to be published by Dr. Mansfield,
NASA Ames Research Centre, Moffet Field, California, USA (1979).

Petty (1983),
Petty, S.E.,
Combustion of Crude Oil on water,
Fire Safety Journal, 5 (1983) pp. 123-134.

Raj (1977),
Raj, P.K.,
Calculations of thermal radiation hazards from LNG fires, a review of the state of the art,
A.G.A. Transmission Conference, T135-148 (May 1977).

Ramskill (1988),
Ramskill, P.K.,
A description of the 'Engulf' computer codes - codes to model the thermal response of an LPG tank either fully or partially engulfed by fire,
Journal of Hazardous Materials, 20 (1988) pp. 177-196.

Ramskill (1989),
Ramskill, P.K.,
Engulf-II - A Computer Code to the thermal response of a tank partially or totally engulfed in fire,
SRD/HSE/R480, July 1989.

Roberts (1982),
Roberts, A.F.,
Thermal radiation hazard from releases of LPG from pressurised storage,
Fire Safety Journal, 4, pp. 197-212, 1982.

Sliepcevich (1966),
Sliepcevich, C.M. and Welker, J.R.,
Bending of wind-blow flames from liquid pools,
Fire Technology 2, 1966, pp. 127-135.

Sparrow (1970),
Sparrow, M.E. and Cess, R.D.,
Radiation Heat Transfer,
Brooks/Cole Publishing Company, Belmont, California (1970).

Thomas (1963),
Thomas, P.H.
The size of flames of natural fires.
Nineth Symposium on Combustion, Academic Press, New York, p 844-859 (1963).

TNO (1978),
TNO-meting,
TNO, Hoofdafdeling Maatschappelijke Technologie, memo 78-04889, (juni 1978).

TNO (1983),
LPG, A study
Comparative risk analysis for the storage, handling, transport and use of LPG and Petrol,
Subreport 1112, 1983.

Yellow Book (1992),
Methods for the calculation of physical effects
resulting from releases of hazardous materials (liquids and gases)
Second Edition 1992, CPR 14 E

Webster (1993),
Webster Third New International Dictionary of the English Language Unabridged
Merriam-Webster Inc., Publishers
Springfield, Massachusetts, USA

Welker (1982),
Welker, J.R.,
Radiation from LPG fires,
Western States Section, Combustion Institute Spring Meeting, (1982).

Appendix 6.1 View factors for some radiator configurations

In this appendix the view factors are given for the following radiator configurations:

1. A spherical radiator;
2. A vertical cylindrical radiator;
3. A vertical flat radiator.

Reference is made to Love [1968] and Sparrow [1970] for other configurations. The view factors are dependent on the position and on the orientation of the receiver with respect to the radiator. With regard to the orientation, it will simply be assumed that the receiver:

a. is flat and with dimensions negligible versus the dimensions of the radiator and the distance to it;
b. is located at ground level;
c. has a specific orientation (to be established at a later stage) with respect to the shortest distance between radiator and receiver.

1. The view factor for a spherical radiator (in particular a fireball), Cunningham [1961]
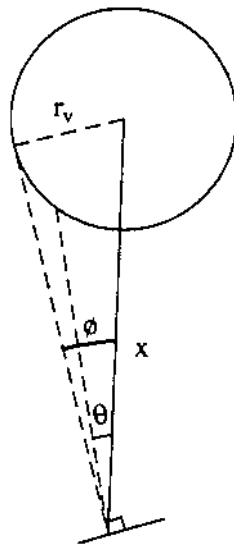
Figure 6.A.1

When the centre of the sphere is located at a distance X from the receiver and the orientation angle θ (see Figure 6.A.1) meets the requirement:

$$\theta \le (\pi/2) - \phi \qquad \text{(rad)} \qquad (6.A.1)$$

in which φ is half the view angle, the view factor is simply given by:

$$F_{view} = (r_{fb}/X)^2 \times \cos \theta \qquad (-) \qquad (6.A.2)$$

The sphere, in this case, is completely visible.

When the orientation angle is so wide that the sphere is not completely visible, which is the case if:

$$\theta > \pi/2 - \phi \qquad (Rad) \qquad (6.A.3)$$

the view factor is then given by:

$$F_{view} = \frac{1}{2} - \frac{1}{\pi} \sin^{-1}\left[\frac{(x_r^2 - 1)^{1/2}}{x_r \sin \theta}\right] + \frac{1}{\pi x_r^2} \cos \theta \cos^{-1}[-(x_r^2 - 1)^{1/2} \cot \theta]$$
$$-\frac{1}{\pi x_r^2}(x_r^2 - 1)^{1/2}(1 - x_r^2 \cos^2 \theta)^{1/2} \qquad (6.A.4)$$

in which:

$$x_r = X/r_{fb} \qquad (-) \qquad (6.A.5)$$

In Figure 6.A.2 the view factors, in accordance to (6.A.4) are given for some orientation angles θ.
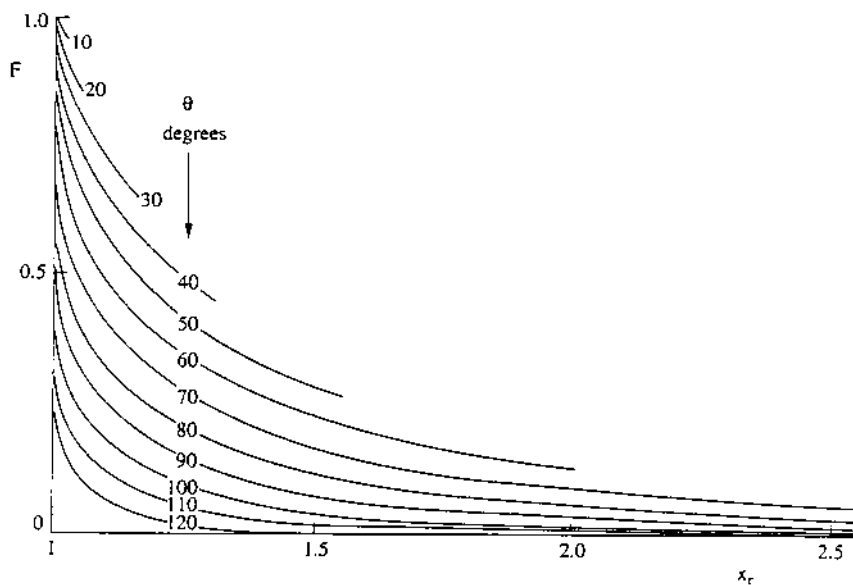
Figure 6.A.2   View factors for a spherical radiator as function of the ratio distance/radius
(incomplete view)

2. The view factor for a vertical cylindrical radiator [Raj, 1977]:

Assume that the plane of the receiver is oriented in such a manner that the normal vector to this plane and the centre line of the cylinder are located in one (vertical) plane (see Figure 6.A.3). The view factor is then dependent (besides L and X) on the orientation angle θ.
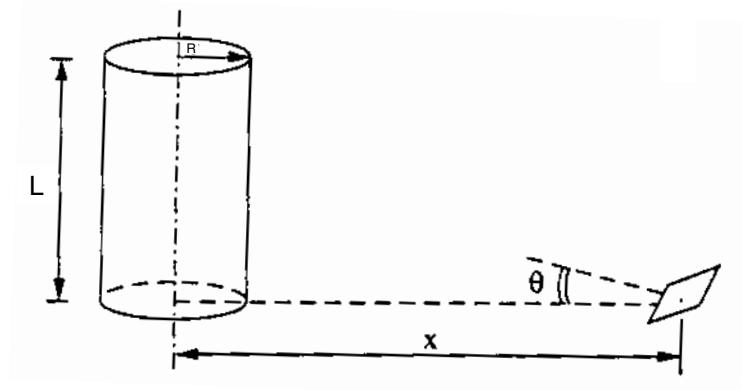
Figure 6.A.3

We define:

$$h_r = L/R \qquad\qquad (-) \qquad\qquad (6.A.6)$$

$$x_r = X/R \qquad\qquad (-) \qquad\qquad (6.A.7)$$

$$A = (x_r + 1)^2 + h_r^2 \qquad\qquad (-) \qquad\qquad (6.A.8)$$

$$B = (x_r - 1)^2 + h_r^2 \qquad\qquad (-) \qquad\qquad (6.A.9)$$

then, for a horizontal plane at ground level ($\theta = \pi/2$):

$$F_h = \frac{1}{\pi}\left\{ \tan^{-1}\sqrt{\frac{x_r + 1}{x_r - 1}} - \left(\frac{x_r^2 - 1 + h_r^2}{\sqrt{AB}}\right)\tan^{-1}\sqrt{\frac{(x_r - 1)A}{(x_r + 1)B}} \right\} \qquad (6.A.10)$$

and for a vertical plane at ground- level ($\theta = 0$):

$$F_v = \frac{1}{\pi}\left\{ \frac{1}{x_r}\tan^{-1}\left(\frac{h_r}{\sqrt{x_r^2 - 1}}\right) + \left(\frac{h_r(A - 2x_r)}{x_r\sqrt{AB}}\right)\tan^{-1}\sqrt{\frac{(x_r - 1)A}{(x_r + 1)B}} - \frac{h_r}{x_r}\tan^{-1}\sqrt{\frac{x_r - 1}{x_r + 1}} \right\}$$
$$(6.A.11)$$

The maximum view factor is: $F_{max} = \sqrt{(F_h^2 + F_v^2)}$ $\qquad\qquad (-) \qquad\qquad (6.A.12)$

For the view factor of an inclined cylindrical radiator see reference Raj [1977] of this chapter. The geometric view factors follow from (6.A.10) and (6.A.11) and are presented numerically in table 6.A.1 and graphically in Figure 6.A.4.

Table 6.A.1   View factors for a vertical cylindrical radiator $h_r = L/R$; $x_r = X/R$

1) horizontal plane ($10^3 \times F_h$)

x_r	h_r									
	0.1	0.2	0.5	1.0	2.0	3.0	5.0	6.0	10.0	20.0
1.1	132	242	332	354	360	362	362	362	363	363
1.2	44	120	243	291	307	310	312	312	313	314
1.3	20	65	178	242	268	274	277	278	278	279
1.4	11	38	130	203	238	246	250	251	252	253
1.5	6	24	97	170	212	222	228	229	231	232
2.0	1	5	27	73	126	145	158	160	164	166
3.0	-	-	5	19	50	71	91	95	103	107
4.0	-	-	1	7	22	38	57	62	73	78
5.0	-	-	-	3	11	21	37	43	54	61
10.0	-	-	-	-	1	3	7	9	17	26
20.0	-	-	-	-	-	-	1	1	3	8

2) vertical plane ($10^3 \times F_v$)

x_r	h_r									
	0.1	0.2	0.5	1.0	2.0	3.0	5.0	6.0	10.0	20.0
1.1	330	415	449	453	454	454	454	454	454	455
1.2	196	308	397	413	416	416	416	416	416	417
1.3	130	227	344	376	383	384	384	384	384	385
1.4	94	173	296	342	354	356	356	357	357	357
1.5	71	135	253	312	329	332	333	333	333	333
2.0	28	56	126	194	236	245	248	249	249	250
3.0	9	19	47	86	132	150	161	163	165	167
4.0	5	10	24	47	80	100	115	119	123	125
5.0	3	6	15	29	53	69	86	91	97	100
10.0	-	1	3	6	13	19	29	32	42	48
20.0	-	-	-	1	3	4	7	9	14	21

3) maximum value ($10^3 \times F_{max}$)

x_r	h_r									
	0.1	**0.2**	**0.5**	**1.0**	**2.0**	**3.0**	**5.0**	**6.0**	**10.0**	**20.0**
1.1	356	481	559	575	580	581	581	581	581	581
1.2	210	331	466	505	517	519	520	521	521	521
1.3	132	236	387	448	468	472	474	474	475	475
1.4	94	117	323	398	427	433	436	436	437	437
1.5	72	138	271	355	392	400	404	404	405	406
2.0	28	56	129	208	267	285	294	296	299	300
3.0	9	19	48	88	141	166	185	189	195	197
4.0	5	10	24	47	83	106	129	134	143	147
5.0	3	6	15	29	54	73	94	100	111	117
10.0	-	1	3	6	13	19	30	34	45	55
20.0	-	-	-	1	3	4	7	9	14	22
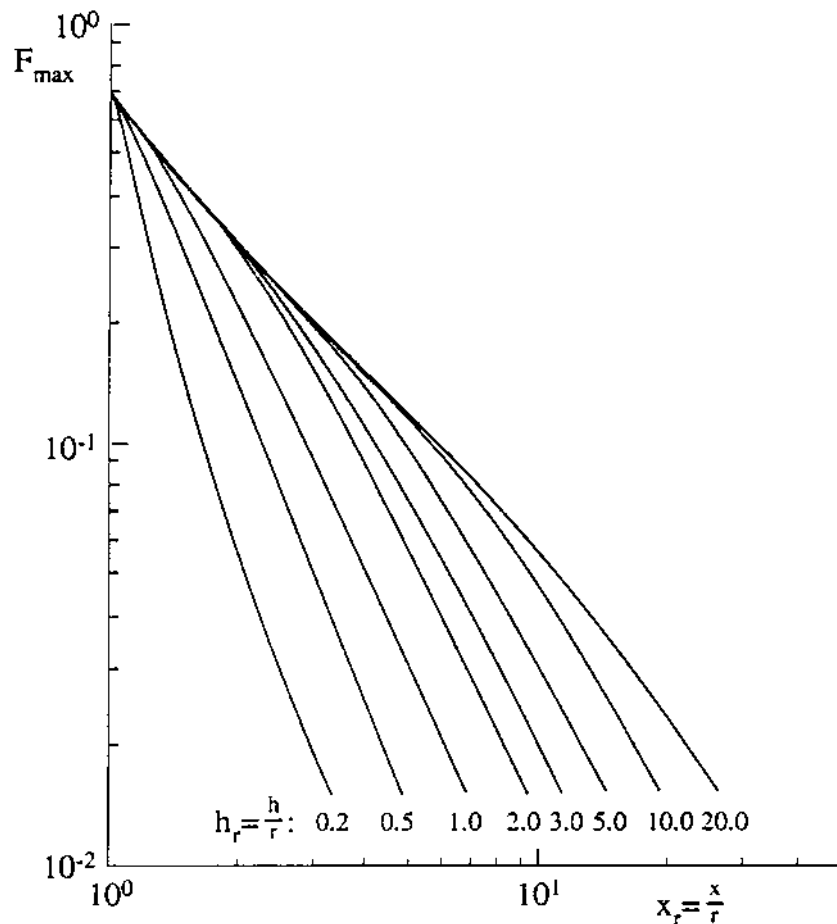
Figure 6.A.4 Maximum view factors for cylindrical radiators as a function of the relative distance to the axis

3. Geometric view factor of the tilted cylindrical flame

We define the geometric view factor F_{view} as the fraction of total thermal energy emitted by a source which is received or intercepted by a given target or observer. The value of F_{view} depends on the relative distance between the source and the target, the geometrical shape of the source and the angular orientation of the source and the target.
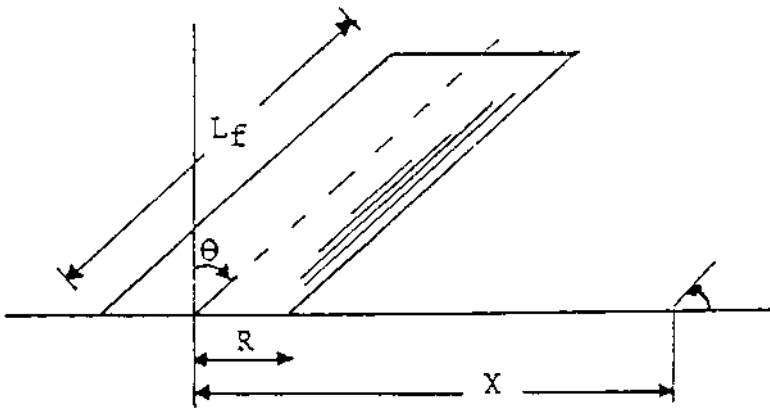
Figure 6.A.5   Target and flame geometry for a tilted cylindrical flame

The geometrical view factor F_{view} is defined as follows:

$$F_{\substack{dA_1, A_2 \\ view}} = \frac{1}{\pi} \iint_{A_2} \left(\frac{\cos \beta_1 \cos \beta_2}{x^2} \right) dA_2 \qquad (6.A.13)$$

where x is the distance between the centres of dA_1 and dA_2, β_1 is the angle of the normal vector to plane dA_1 and the line connecting dA_1 and dA_2 and β_2 is the angle of the normal vector to plane dA_2 and the line connecting dA_1 and dA_2. In Figure A.6 the parameters are shown for the infinisimal surfaces dA_1 and A_2.
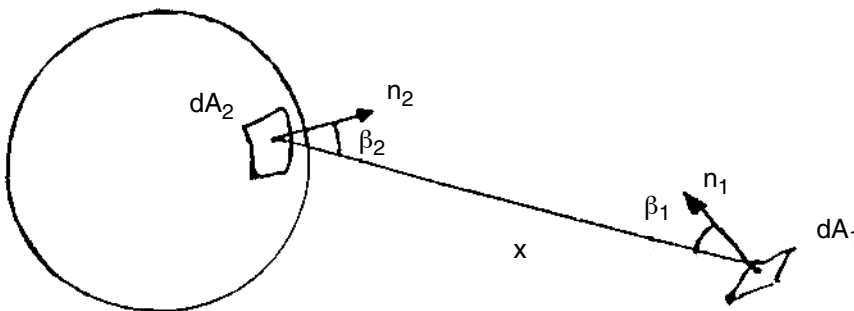
Figure 6.A.6

Mudan [1987] derived analytical geometrical view factor expressions for horizontal and vertical receiving targets for simple fire geometries including cylinder and rectangular parallelepiped.

3.1 Cylindrical flames

Consider a cylindrical approximation to the tilted flame as shown by Figure 6.A.5. The vertical and horizontal area view factors are given by the following expressions (also see Atallah [1990]):

$$\pi F_v = -E \tan^{-1} D + E\left[\frac{a^2 + (b+1)^2 - 2b(1 + a \sin \theta)}{AB}\right]\tan^{-1}\left(\frac{AD}{B}\right)$$

$$\frac{\cos \theta}{C} + \left[\tan^{-1}\left(\frac{ab - F^2 \sin \theta}{FC}\right) + \tan^{-1}\left(\frac{F^2 \sin \theta}{FC}\right)\right]$$

(6.A.14)

$$\pi F_h = \tan^{-1}\left(\frac{1}{D}\right) + \frac{\sin \theta}{C}\left[\tan^{-1}\left(\frac{ab - F^2 \sin \theta}{FC}\right) + \tan^{-1}\left(\frac{F^2 \sin \theta}{FC}\right)\right]$$

$$\left[\frac{a^2 + (b+1)^2 - 2(b+1+ab \sin \theta)}{AB}\right]\tan^{-1}\left(\frac{AD}{B}\right)$$

6.A.15)

a	$= L/R$ (L_b/R or L_f/R)	(-)	
b	$= X/R$	(-)	
A	$= \sqrt{(a^2 + (b+1)^2 - 2 \times a \times (b+1) \times \sin\theta)}$	(-)	
B	$= \sqrt{(a^2 + (b-1)^2 - 2 \times a \times (b-1) \times \sin\theta)}$	(-)	
C	$= \sqrt{(1 + (b^2 - 1) \times \cos^2\theta)}$	(-)	
D	$= \sqrt{((b-1)/(b+1))}$	(-)	
E	$= (a \times \cos \theta)/(b - a \times \sin \theta)$	(-)	
F	$= \sqrt{(b^2 - 1)}$	(-)	

L_f is the tilted flame length. The angle of tilt θ is measured with respect to the vertical and is positive for targets located downwind from the source and negative for targets located upwind from the source.

Additional forms are derived from calculating the view factors for a target in the crosswind direction, i.e. whose direction is perpendicular to the tilt angle:

$$2\pi F_h = 2\tan^{-1} D$$

$$+\left(\frac{F\ \sin\ \theta}{I}\right)\left[\tan^{-1}\left(\frac{\frac{ab}{F}+\sin\ \theta}{I}\right)-\tan^{-1}\left(\frac{\frac{ab}{F}-\sin\ \theta}{I}\right)-2\tan^{-1}\left(\frac{\sin\ \theta}{I}\right)\right]$$

$$-\left(\frac{a^2+b^2-1}{G}\right)\left[\tan^{-1}\left(\frac{HD-2a\ \sin\ \theta}{G}\right)+\tan^{-1}\left(\frac{HD+2a\ \sin\ \theta}{G}\right)\right] \qquad (6.A.16)$$

$$2\pi F_v = -\left(\frac{a^2\ \sin\ \theta\ \cos\ \theta}{2(a^2\ \sin^2\ \theta+b^2)}\right)\ln\left[\frac{a^2+b^2-1-2a\ \frac{F}{b}\ \sin\ \theta}{a^2+b^2-1+2a\frac{F}{b}\ \sin\ \theta}\right]$$

$$+\left(\frac{\cos\ \theta}{I}\right)\left[\tan^{-1}\left(\frac{\frac{ab}{F}+\sin\ \theta}{I}\right)+\tan^{-1}\left(\frac{\frac{ab}{F}-\sin\ \theta}{I}\right)\right]$$

$$+\left(\frac{ab\ \cos\ \theta}{b^2+a^2\ \sin^2\ \theta}\right)\left(\frac{a^2+b^2+1}{G}\right)\left[\tan^{-1}\left(\frac{HD-2a\ \sin\ \theta}{G}\right)+\tan^{-1}\left(\frac{HD+2a\ \sin\ \theta}{G}\right)\right]$$

$$-\left(\frac{2ab\ \cos\ \theta}{b^2+a^2\ \sin^2\ \theta}\right)\tan^{-1} D \qquad (6.A.17)$$

where

$$G = \sqrt{\left((a^2+b^2+1)^2-4\times(b^2+a^2\times\sin^2\theta)\right)} \qquad (-)$$

$$H = a^2+(b+1)^2 \qquad (-)$$

$$I = \sqrt{(b^2-\sin^2\theta)} \qquad (-)$$

The maximum view factor is estimated from the vector sum of F_h and F_v:

$$F_{max} = \sqrt{(F_v^2+F_h^2)} \qquad (-) \qquad (6.A.18)$$

With minor modifications, Equations (6.A.14) and (6.A.15) can be used to estimate the view factors when the flame base is elevated with respect to the target as shown in Figure 6.A.7, when the target is elevated with respect to the flame base as shown in Figure 6.A.8 and when the target is in the shadow of the flame as shown in Figure 6.A.9.
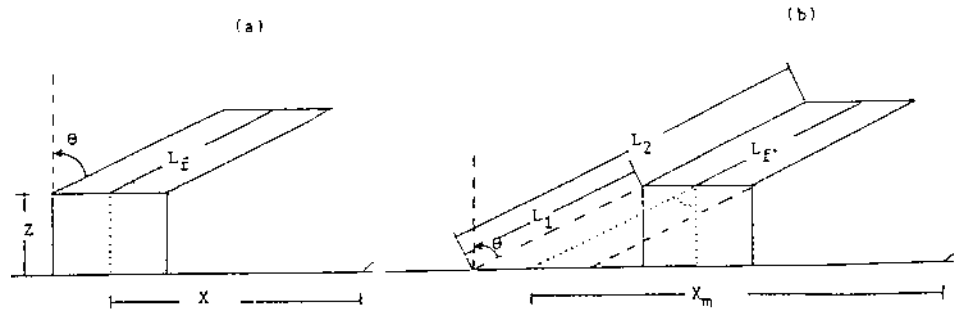
Figure 6.A.7   Elevated flame with respect to target
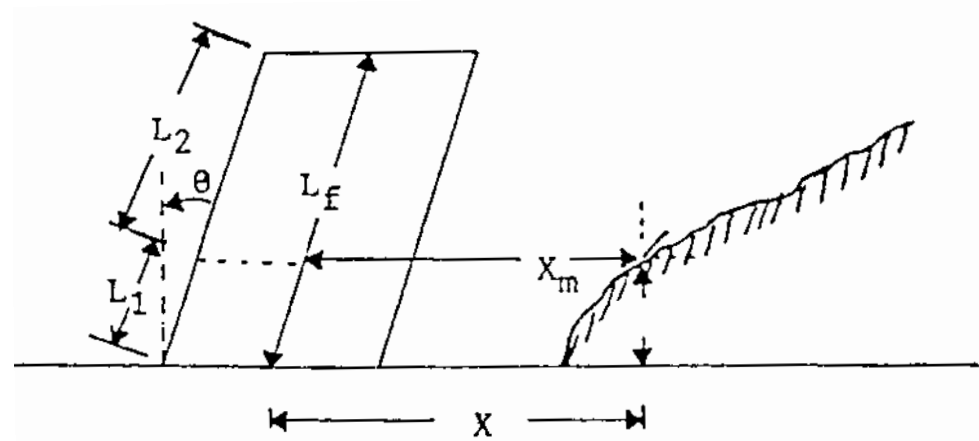
Figure 6.A.8   Elevated target with respect to flame
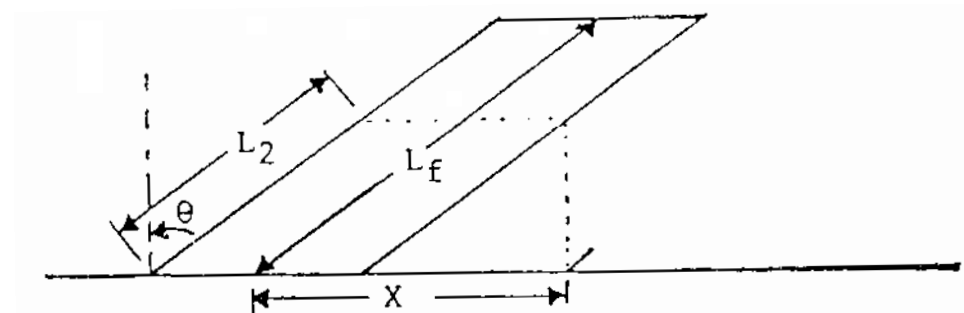
Figure 6.A.9   Target in flame shadow

For an elevated flame base we modify the flame length and the target location:

$$x_1 = X + z \times \tan \theta \qquad\qquad\qquad \text{(m)} \qquad\qquad (6.A.19)$$

$$L_1 = z/\cos \theta \qquad\qquad\qquad\qquad\qquad \text{(m)} \qquad \text{(6.A.20)}$$

$$L_2 = L + L_1 \qquad\qquad\qquad\qquad\qquad \text{(m)} \qquad \text{(6.A.21)}$$

The view factors are then calculated as follows:

$$F_v = F_v(L_2) - F_v(L_1) \qquad\qquad\qquad\qquad \text{(-)} \qquad \text{(6.A.22)}$$

$$F_h = F_h(L_2) - F_h(L_1) \qquad\qquad\qquad\qquad \text{(-)} \qquad \text{(6.A.23)}$$

The view factors are calculated in a similar fashion when the target is elevated with respect to the flame base:

$$x_1 = X - z \times \tan \theta \qquad\qquad\qquad\qquad \text{(m)} \qquad \text{(6.A.24)}$$

$$L_1 = z/\cos \theta \qquad\qquad\qquad\qquad\qquad \text{(m)} \qquad \text{(6.A.25)}$$

$$L_2 = L - L_1 \qquad\qquad\qquad\qquad\qquad \text{(m)} \qquad \text{(6.A.26)}$$

When the observer is in the flame shadow, the vertical view factor must be calculated with a truncated flame length:

$$L_1 = X/\sin \theta \qquad\qquad\qquad\qquad\qquad \text{(m)} \qquad \text{(6.A.27)}$$

The horizontal view factor is unchanged.

4. The view factor for a vertical flat radiator, Raj [1977], Love [1968], Sparrow [1970]

It will be assumed here that the crossing lines of, respectively, the radiator with the ground and the receiver with the ground, are parallel. The view factor will then be calculated as the sum of the factors for plane part I and plane part II (see Figure 6.A.10). For each of these parts the following is defined:
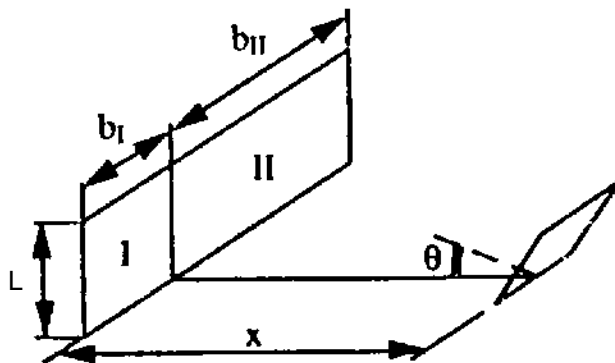
Figure 6.A.10

$$h_r = L/b \qquad\qquad (-) \qquad (6.A.28)$$

$$x_r = X/b \qquad\qquad (-) \qquad (6.A.29)$$

$$A = 1/\sqrt{(h_r^2 + x_r^2)} \qquad\qquad (-) \qquad (6.A.30)$$

$$B = h_r/\sqrt{1 + x_r^2} \qquad\qquad (-) \qquad (6.A.31)$$

We have for horizontal plane at ground level ($\theta = \pi/2$):

$$F_h = \frac{1}{2\pi}\left\{\tan^{-1}\left(\frac{1}{x_r}\right) - A\ x_r\tan^{-1}A\right\} \qquad (6.A.32)$$

For a vertical plane at ground level ($\theta = 0$):

$$F_v = \frac{1}{2\pi}\left\{h_r A\ \tan^{-1}A + \left(\frac{B}{h_r}\right)\ \tan^{-1}B\right\} \qquad (6.A.33)$$

The maximum view factor is given by:

$$F_{max} = \sqrt{(F_h^2 + F_v^2)} \qquad\qquad (-) \qquad (6.A.34)$$

It should be noted (except if $b_I = b_{II}$) that this is not the maximum view factor of a plane at a distance X from the radiator; this because of the restriction which is made with respect to the orientation of the receiver. The view factors F_h, F_v and F_{max} of the radiator can now be obtained simply by adding the values for plane part I and plane part II. Numerical values are given in table 6.A.2, and, F_{max} versus x_r is represented graphically in Figure 6.A.10.

Table 6.A.2   View factors for a vertical flat radiator ($h_r = L/b$, $x_r = X/b$, see Figure 6.A.9)

1) horizontal plane ($10^3 \times F_h$)

x_r	h_r								
	0.1	0.2	0.3	0.5	1.0	1.5	2.0	3.0	5.0
0,1	93	176	218	258	294	306	311	315	317
0,2	34	94	143	206	271	294	304	311	316
0,3	17	55	96	164	250	282	296	307	314
0,4	10	36	69	132	228	267	286	301	309
0,5	7	25	51	107	205	251	272	290	301
1	2	7	16	39	105	153	183	212	230
2	0	1	3	8	28	50	71	99	125
3	0	0	1	3	10	20	31	50	75
5	0	0	0	1	2	5	9	16	31

2) vertical plane ($10^3 \times F_v$)

x_r	h_r								
	0.1	0.2	0.3	0.5	1.0	1.5	2.0	3.0	5.0
0,1	256	347	393	446	481	471	452	417	380
0,2	173	285	352	423	470	463	446	412	375
0,3	129	233	306	392	453	451	436	404	367
0,4	103	193	264	356	431	436	423	394	358
0,5	85	163	228	319	406	417	408	382	347
1	40	79	115	178	274	310	319	311	285
2	14	27	41	66	119	156	178	196	193
3	7	13	20	32	62	86	104	126	139
5	2	5	7	12	24	35	45	61	79

3) maximum value ($10^3 \times F_{max}$)

x_r	h_r								
	0.1	0.2	0.3	0.5	1.0	1.5	2.0	3.0	5.0
0,1	273	389	449	515	564	562	549	523	495
0,2	176	300	380	471	543	549	539	517	490
0,3	130	239	321	425	517	532	527	508	483
0,4	104	197	273	379	488	511	511	496	473
0,5	86	165	234	337	455	487	491	480	459
1	40	79	116	182	294	346	368	376	367
2	14	27	41	67	123	164	192	220	230
3	7	13	20	33	62	88	109	136	158
5	2	5	7	12	24	36	46	63	85
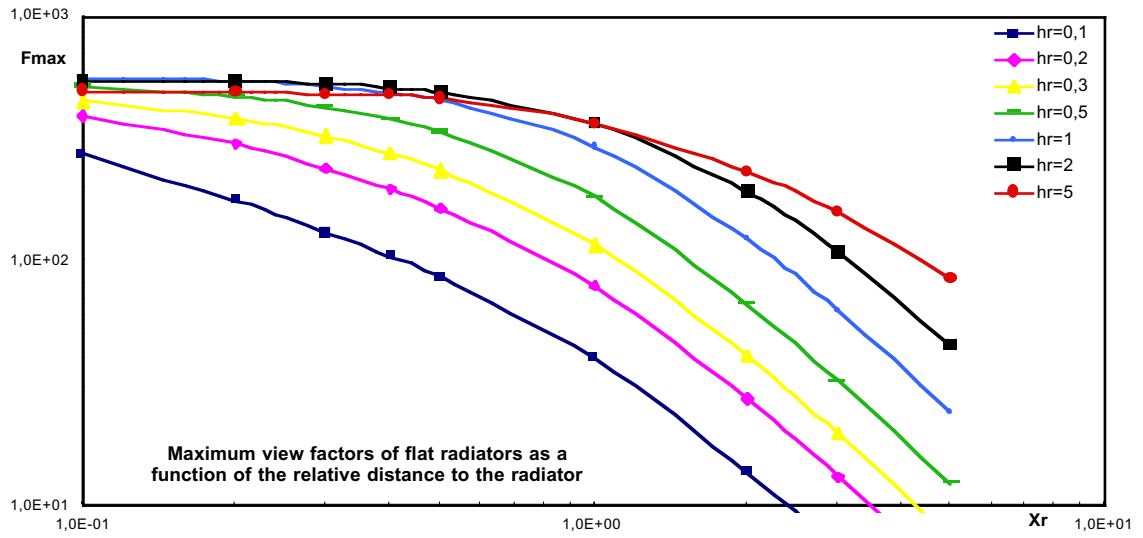
Figure 6.A.11   Maximum view factors of flat radiators as a function of the relative distance to the radiator

Chapter 7
Rupture of vessels

J.C.A.M. van Doormaal, R.M.M. van Wees

Modifications to Chapter 7 (Rupture of Vessels) with respect to the first print (1997)

Numerous modifications were made concerning typographical errors. A list is given below for the pages on which errors have been corrected.

In the section on initial fragment velocity calculations a scaled velocity correction factor graph is added.

Correction of Formula 7.19

Application of selected methods: calculation examples
A lot of numbers are refined, for example the ambient pressure of $0.1*10^6$ is replaced by $1.01325*10^5$, and values are more accurately read from plots and figures.

A large adjustment is made in step 12 in the calculation examples, in the 3rd edition it was accounted for that the vessel was slightly elevated using values of table 7.4, in the fourth edition this has been removed.

List of symbols of chapter 7

a_a	speed of sound in ambient air (7.9)	m/s
a_l	speed of sound in compressed gas (section 7.5.3, step 3b1)	m/s
A_D	exposed area in plane perpendicular to trajectory (7.22)	m^2
A_L	exposed area in plane parallel to trajectory (7.22)	m^2
A_{plate}	area of plate-like fragment (Table 7.8)	m^2
A_{sb}	constant for surface burst (7.7)	-
A_{ke}	fraction of available energy that goes into kinetic energy of the fragments (7.15)	-
A_M	constant for Moore's method (7.19)	-
C_D	drag coefficient (7.22)	-
C_L	lift coefficient (7.22)	-
d_v	vessel diameter (section 7.5.3, step 3b3)	m
e_{av}	specific liberated energy (7.4)	J/kg
E_{av}	liberated or available energy (7.1)	J
E_{ex}	explosion energy or blast wave energy (7.7)	J
g	acceleration of gravity (7.22)	m/s^2
h	specific enthalpy (enthalpy per unit mass) (7.2)	J/kg
h_1	specific enthalpy in initial state (= at failure) (section 7.5.2, step 4b)	J/kg
h_2	specific enthalpy in final state (section 7.5.2, step 4c)	J/kg
h_f	specific enthalpy of saturated liquid (7.3)	J/kg
h_g	specific enthalpy of saturated vapour (7.3)	J/kg
i_s	positive impulse of blast wave (7.14)	Pa.s
$\bar{I}$	non-dimensional impulse of blast wave (7.14)	-
L_v	vessel length (section 7.5.3, step 3b3)	m
M_v	mass of empty vessel (7.15)	kg
M_c	total mass of vessel contents (7.6)	kg
M_{fl}	mass of released phase or component of the fluid (7.5)	kg
M_{cap}	mass of end cap of cylindrical vessel (Table 7.6)	kg
M_f	fragment mass (Table 7.6)	kg
n_f	number of fragments (section 7.5.3, step 2)	-
p	absolute pressure (7.2)	Pa
p_a	ambient pressure (7.1)	Pa
p_1	vessel's internal pressure (absolute) at failure (7.1)	Pa
$\bar{P}_1$	scaled pressure (7.16)	-
p_s	peak side-on pressure (absolute) of blast wave (7.13)	Pa
p_{so}	peak shock pressure directly after burst (7.12)	Pa

$\overline{P}_s$	non-dimensional peak side-on overpressure of the blast wave (7.13)	-
$\overline{P}_{so}$	non-dimensional peak shock overpressure directly after burst (7.12)	-
r_t	distance from the centre of the vessel to the target (7.8)	m
r_0	equivalent bursting radius (7.10)	m
R	gas constant (section 7.5.3, step 3b1)	J/(mol·K)
$\overline{R}$	non-dimensional distance to target (7.8)	-
R_f	maximal flying range of fragment (7.21)	m
$\overline{R}_f$	scaled maximal flying range of fragment (7.21)	-
$\overline{R}_0$	non-dimensional equivalent bursting radius (7.11)	-
s	specific entropy (entropy per unit mass) (7.3)	J/(kg·K)
s_1	specific entropy in initial state (= at failure) (7.3)	J/(kg·K)
s_2	specific entropy in final state (section 7.5.2, step 4c)	J/(kg·K)
s_f	specific entropy of saturated liquid (7.3)	J/(kg·K)
s_g	specific entropy of saturated vapour (7.3)	J/(kg·K)
T_a	absolute temperature of ambient air (7.9)	K
T_b	boiling temperature at atmospheric pressure (section 7.5.2, step 3)	K
T_c	critical temperature (section 7.5.2, step 3)	K
T_g	absolute temperature of compressed gas (7.9)	K
T_l	temperature of liquid (section 7.5.2, step 1)	K
T_{sl}	superheat limit temperature at atmospheric pressure (section 7.5.2, step 3)	K
u	specific internal energy (7.2)	J/kg
u_1	specific internal energy in initial state (section 7.5.2, step 4b)	J/kg
u_2	specific internal energy in final state (7.3)	J/kg
u_f	maximum laminar burning velocity (7.17)	m/s
v	specific volume (7.2)	m³/kg
v_1	specific volume in initial state (= at failure) (section 7.5.2, step 4b)	m³/kg
v_2	specific volume in final state (section 7.5.2, step 4c)	m³/kg
v_f	specific volume of saturated liquid (7.3)	m³/kg
v_g	specific volume of saturated vapour (7.3)	m³/kg
V_g	volume of gas-filled part of vessel (7.1)	m³
V_{fl}	volume of released phase or component of the fluid (7.5)	m³
$\underline{v}_i$	initial velocity of fragment (7.15)	m/s
$\overline{v}_i$	scaled initial velocity of fragment (7.22)	-
X	vapour ratio (7.3)	-
γ_a	ratio of specific heats of ambient air (7.9)	-
γ_1	ratio of specific heats of the gas (7.1)	-
μ_a	molar mass of ambient air (7.9)	kg/mol
μ_1	molar mass of compressed gas (7.9)	kg/mol

7.6

Φ	dimensionless parameter that characterises the energy release (7.17)	-
ρ_a	density of ambient air (7.21)	kg/m^3
ΔH_f	heat of reaction per kg product (7.6)	J/kg

Note: the numbers betwen brackets refer to equations.

7.9

Glossary of terms

blast	Rapidly propagating pressure or shock wave in atmosphere with high pressure, high density and high particle velocity.
BLEVE	Boiling Liquid Expanding Vapour Explosion: At vessel rupture the liquefied contents of the vessel boil and flash instantaneously, causing a considerable blast. When the contents are flammable a large fireball can be formed.
explosion	A sudden release of energy that causes a blast.
fragment range	Distance a fragment can fly.
impulse	A measure used to quantify the consequences of a short duration pressure pulse. It is calculated by the integration of the pressure-time curve.
pressure vessel burst	Vessel burst of a pressurised container (not necessarily a true pressure vessel).
pressure wave	Rapidly propagating wave in atmosphere causing a gradual change in gas-dynamic-state: high pressure, high density and high particle velocity.
primary effects	Effects that occur in the first instance and that originate from the source itself: blast wave, fragments of vessel.
secondary effects	Effects that occur in the second instance and/or that originate from other sources: e.g. fireball, debris picked up by blast wave.
shock wave	Rapidly propagating wave in atmosphere causing an instantaneous change in gas-dynamic-state: high pressure, high density and high particle velocity.
side-on pressure or impulse	The pressure or impulse experienced by an object as a blast wave passes by.

Table of contents of chapter 7

7 Rupture of vessels

7.1 Introduction

A vessel rupture is coupled with the release of the contents and the release of the internal energy. Depending on the characteristics of the material in the vessel, the released contents can cause a buoyant fireball, a vapour cloud explosion, a flash fire or toxic gases. The sudden release of energy can give rise to damaging blast waves and high velocity fragments.

This chapter presents methods that enable the prediction of the blast waves, vessel fragmentation and fragment velocities. The other effects mentioned are treated in other chapters, see section 7.7.

A basic understanding of the phenomena of vessel burst is necessary before one can start with any calculations. One must be able to identify the problem under consideration. All types of vessel bursts can be divided into five categories: pressure vessel bursts with non-reactive contents, BLEVEs, runaway reactions, decomposition of energetic materials and internal explosions. For each category the approach to calculate the effects is different.

Section 7.2 provides the essential and basic understanding of the phenomena. Anyone who is not familiar with the subject is advised to start by reading this section.

Section 7.3 provides a general overview of the currently available methods for a quantified analysis. It includes some background to the methods. The aim of the section is also to position the methods selected for detailed description among other existing methods.

Section 7.4 presents the considerations which led to the selection of methods described in this chapter.

Section 7.5 provides the detailed and complete description of the selected methods.

Section 7.6 presents examples of the use of the methods presented in section 7.5.

Section 7.7 directs the user to other chapters for effects of vessel rupture other than blast waves and fragmentation.

Finally section 7.8 provides some information on general restrictions regarding application of the methods.

7.2 The phenomenon of vessel rupture

7.2.1 Effects

A vessel can rupture due to several causes, but in all situations the effects are similar. Vessel rupture produces three primary effects:
1. release of vessel contents,
2. fragmentation of the vessel coupled with missile effects, and
3. blast due to the expansion of the pressurised contents.

The release of the vessel contents can cause so-called secondary effects, such as a buoyant fireball with heat radiation, a vapour cloud explosion, a flash fire or dispersion of a toxic substance. Whether these secondary effects will occur depends among others on the flammability and toxicity of the contents. The above-mentioned secondary effects are the subject of other chapters and hence not considered here.

The fragments of the vessel can become missiles with high velocities that will be propelled for a long distance and that will hit anything they find on their way. The internal energy of the vessel's contents is partly converted into kinetic energy of the fragments.

Another part of the internal energy is converted into expansion of the contents of the vessel. This form of mechanical energy is transmitted to the surrounding atmosphere in the form of a blast wave.

In the surrounding atmosphere, a blast wave is experienced as a transient change in gas-dynamic-state parameters: pressure, density and particle velocity. This means that a blast wave has the potential to crush objects due to the overpressure or to blow them over due to wind force. Generally the parameters increase rapidly or instantaneously after which they decrease gradually to sub-ambient values, i.e. a negative phase is developed. Subsequently, the parameters slowly return to atmospheric values. Rapid and slow are relative terms here. Generally, a blast wave lasts a fraction of a second.

Figure 7.1 shows two examples of very common shapes of a blast wave. The shape highly depends on the nature of the expansion process. In case of a slow expansion process, the blast consists of a low-amplitude pressure wave that is characterised by a gradual increase in pressure (Figure 7.1a). If, on the other hand, expansion is rapid, the blast is characterised by a steep increase, the so-called shock (Figure 7.1b). The most important shock wave parameters are the peak overpressure p_S and the positive impulse i_S, which is calculated by integration of the pressure-time curve.

a)   b)
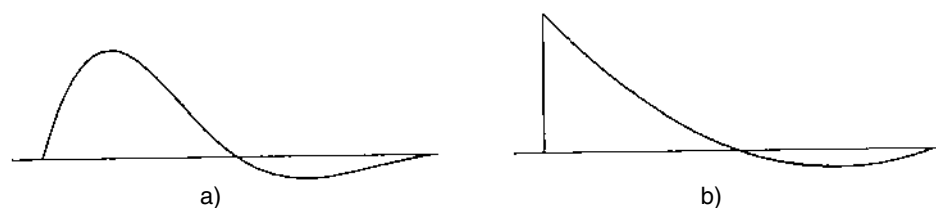
Figure 7.1   Blast wave shapes

The shape and power of a blast wave changes during propagation. Pressure waves tend to steepen to shock waves in the far field, and the duration tends to increase. The peak pressure decreases rapidly during propagation.

Characteristic for the blast wave from a vessel burst is the large negative phase, usually followed by a second shock (see Figure 7.2).
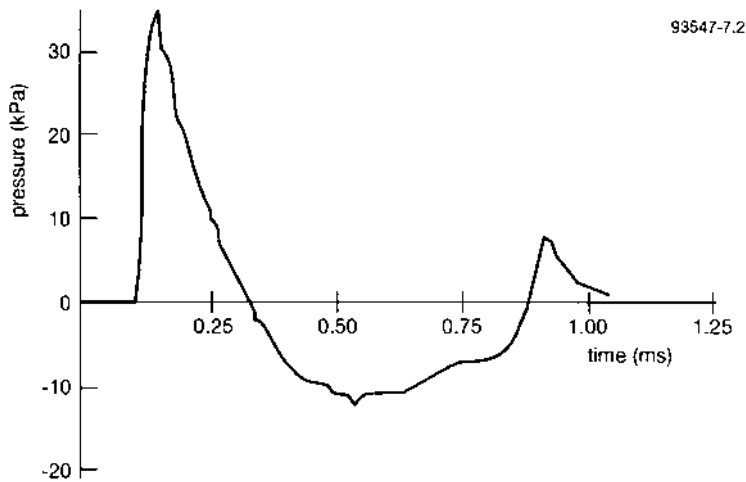
Figure 7.2   Pressure-time history of a blast wave from a pressure vessel burst, Esparza and Baker [1977]

7.2.2   Causes of vessel ruptures

Fundamentally, there are two reasons why a vessel fails. Either the pressure inside the vessel rises above the design pressure or the strength of the vessel decreases below the working pressure. Too high a pressure can arise as a consequence of overfilling, overheating, overheating due to an external fire, a failing pressure control system, a runaway reaction inside the vessel or an internal explosion. A reduction in vessel strength might be caused by corrosion, erosion, overheating, fatigue, a material defect from which a crack starts to grow or an external impact.

A common cause of vessel burst is filling with a blocked vent line or overfilling. This usually happens with vessels that are meant for atmospheric storage. These vessels are often weak and the damage is usually limited to the vessel itself, except in cases where the vessel is located indoors. Other common causes are a runaway reaction in a reaction vessel and overheating due to an external fire. These are much more violent and cause much damage, especially when the contents are flammable.

Blast and fragmentation effects originate from the transformation of internal energy into mechanical energy. Therefore the blast and fragmentation effects directly depend on the available internal energy. This internal energy is a function of the thermodynamic properties and mass of the vessel contents and is practically determined by two parameters:
− the condition of the vessel at the moment of rupture,
− the condition of the vessel contents.

The condition of vessel and contents relate to the cause of container failure. In case of a fire near/below vessels filled with pressurised liquefied gases for instance, direct flame impingement will weaken the container walls. The pressure at which the container fails will usually be about equal to the pressure at which the safety valve operates. The temperature of the contents will usually be considerably higher than the ambient temperature.

If a vessel ruptures as a result of excessive internal pressure, its bursting overpressure may be several times higher than its design overpressure. However, if the rupture is due to corrosion or mechanical impact, bursting pressure is approximately equal to the working pressure. The temperature in these situations will depend on process conditions.

7.2.3   Types of bursts

The calculation of blast and fragmentation effects of vessel bursts can roughly be divided into two steps. In the first step the available energy is calculated, in the second step the effects are based on the energy resulting from the first step. This second step is principally the same for all types of vessel bursts. In the first step however, distinction must be made between various types of vessel bursts. Different methods must be used for each way in which the internal energy can be liberated for transformation into mechanical energy. In relation to the liberation of the internal energy all types of vessel bursts can be subdivided into the following six groups:
− pressure vessel bursts with ideal gas,
− pressure vessel bursts with non-ideal gas or vapour,
− BLEVEs,
− (exothermic) runaway reaction,
− decomposition of energetic materials,
− internal explosion.

Pressure vessel bursts concern vessels containing a pressurised gas or vapour. The only source of energy for blast and fragmentation is the expansion of the gas or vapour. The liquid does not or only slowly flash, so that it will not supply a significant amount of energy. There is no fundamental difference in behaviour between vessels filled with ideal or non-ideal gases. Only the calculation methods that are to be used for the energy differ.

A BLEVE is an explosion resulting from the failure of a vessel containing a liquid at a temperature significantly above its boiling point at normal atmospheric pressure, e.g. pressure liquefied gases. The fluid in the vessel is usually a combination of liquid and vapour. Before rupture, the liquid contained is more or less in equilibrium with the saturated vapour. If the vessel ruptures, vapour is vented and the pressure in the liquid drops sharply. Upon loss of equilibrium, liquid flashes at the liquid-vapour interface, the liquid-container-wall interface, and, depending on temperature, throughout the liquid.

Instantaneous boiling throughout the liquid will occur whenever the temperature of the liquid is higher than the superheat temperature (nucleation temperature). Microscopic vapour bubbles begin to form and grow, generally at submicron nucleation sites such as impurities, crystals or ions. Through this process, a large fraction of the liquid can vaporise within milliseconds. The liberated energy in such cases is very high, causing high blast pressures and generation of fragments with high

initial velocities, and resulting in propulsion of fragments over long distances. No boiling occurs if the temperature is below the boiling temperature. Between these temperatures, the liquid may boil instantaneously under certain conditions, Venart et al. [1992].

Runaway reactions can occur in a vessel if the heat of reaction or decomposition exceeds the cooling capacity of the vessel. The runaway itself is characterised by an exponential increase of temperature with time. The pressure increases due to the formation of non-condensable gases and/or an increasing vapour pressure of the liquid components. This process can only be controlled by a properly dimensioned pressure relief device, like a rupture disc or pressure relief valve. If these devices malfunction or if the reaction is faster than foreseen, the pressure may continue to rise until the vessel fails.

Materials can decompose so fast and release so much energy that a transition from a runaway reaction to a deflagration or even a detonation can occur. These materials are called energetic materials. The contents of the vessel may decompose within milliseconds and the reaction of the entire contents may even be completed before the vessel bursts open. The explosions they cause are more like explosions from high explosives than like pressure vessel bursts. In fact, many of these energetic materials can also be made to detonate outside a vessel.

Internal explosions typically occur in storage or transport tanks when a flammable vapour-air or dust-air mixture is ignited, e.g. by a spark. This mixture burns in a few tenths of a second. Since many of these explosions occur during filling or cleaning, they often cause no more than a jet fire through the opened hatch, but sometimes the vessel ruptures.

For the pressure vessel burst and the BLEVE, the vessel rupture can be due to an excessive pressure or a weakening of the vessel. A runaway reaction and an internal explosion on the other hand, are due to an excessive pressure. In these two situations, energy is not only released by the expansion of the contents of the vessel. An additional source of energy can be respectively the chemical reaction or the combustion, which may continue after failure of the vessel.

7.3 General overview of existing methods

7.3.1 Introduction to section 7.3

The scope of this section is to give an overview of the existing methods for predicting the blast fragmentation effects of a vessel burst.
Little research has been carried out to bursting vessels. The number of methods for calculating the effects is therefore limited. Most of the research deals with pressure vessels with ideal gases. Just a few studies have been devoted to vessels filled with non-ideal gases and liquids. Little has been done in the field of vessel ruptures due to a runaway reaction or an internal explosion.

7.3.2 Methods for blast effects

Methods for calculating blast effects of pressure vessel bursts can roughly be divided into two categories:
1. Methods solving the set of differential equations of fluid mechanics by which the shock wave can be described.
2. Generalised methods based on thermodynamic terms and the available energy for blast generation.

Methods to solve the equations of fluid mechanics

The differential equations that describe the shock wave are non-steady and non-linear. Numerical integration techniques are necessary to solve the equations unless many simplifications are allowed. With these simplifications it may be possible to solve the equations analytically.

Analytical work is scarce. A valuable study is the analytical analysis of a bursting membrane in a shock tube with a one-dimensional technique by Liepmann and Roshko [1967]. As a result of this analysis, a relationship for the initial overpressure at the shock front has been obtained, which is valid for all types of pressure vessel bursts. The initial overpressure depends on the pressure in the sphere, the speed of sound and the ratio of specific heats. The equation of Liepmann and Roshko is an implicit equation which can be solved by iteration.

Many numerical methods have been proposed for solving the differential equations and calculating the blast effects, most of them finite-difference methods. Most work in this area reported in open literature concerns ideal gas. See for instance Baker et al. [1977], Boyer et al. [1958], Huang and Chou [1968] and Guirao et al. [1979], who used several types of methods.
Specialised commercial computer programs for numerical calculation of blast effects from a vessel burst are not available. Some general purpose Eulerian-Lagrangian codes, like Autodyn or MSC Pisces, may be used to predict blast and fragment velocities. Within these codes one has to set up the problem oneself. For that purpose one needs to have knowledge of the chosen code and also of vessel bursts.

Methods based on thermodynamics

In the second category of the generalised methods, based on thermodynamics, the different states of the vessel contents before the start and after the completion of the explosion process are compared. The explosion energy can thus be calculated. This explosion energy is an appropriate quantity for comparing the vessel burst with well-known and well-defined explosions, so that the characteristics of the blast wave can be estimated.

There are two methods that belong to this category. These are the TNT-equivalence method and a method developed by Baker et al. [1977].
The TNT-equivalence method is often-used for blast calculations, since the blast effects from TNT have been well studied and are well-known. Therefore, this approach gives the user access to a large body of blast field, blast-structure interaction and structural response data. Based on the available energy an equivalent amount of TNT, for which the blast effects are known, can be calculated.
One should be well aware of the fact that compared to a TNT-explosion, the shock wave produced by bursting vessels has lower initial overpressures, a slower decay of the overpressure with distance, longer positive phase durations, much larger negative phases and strong secondary shocks. Therefore, the TNT-equivalence method gives only reasonable results for far range, which definition is related to the explosion energy. Usually, one can speak of far range at a distance of 10 to 20 times the vessel diameter or more.

Pressure vessel bursts

The method proposed by Baker et al. [1977] has been developed for pressure vessel bursts with an ideal gas and was later extended for vessels with non-ideal gases. The method differs from the TNT-equivalence method in the distinction between far and close range for vessels. For far range, the method makes use of the similarity with high explosives, in this case Pentolite. For close range, the method is based on results from numerical calculations on vessel bursts with an ideal gas. These numerical calculations were verified by experiments. The close range modification is only applicable to vessels with ideal gases.

In addition to the blast calculation method, Baker gives a simple correction method for including the influence of a nearby surface and a correction method for a cylindrical vessel instead of a spherical one.
The correction method for a nearby surface is based on experimental results with free-air explosions of a high explosive. It was not experimentally validated for pressure vessel bursts by Baker. Later Cain et al. [1992] showed the validity of the method with a limited number of tests. Other methods are not found in literature. The influence of a nearby surface appeared to have received little attention. Pittmann [1976] did study the influence of a nearby surface using a two-dimensional code. His results, however, were inconclusive because of the small number of cases studied and the coarse grid used in the code.
The correction method for cylindrical vessels is based on knowledge of non-spherical explosions of high explosives and on qualitative knowledge of cylindrical vessel bursts only. Although several researchers studied the effects of cylindrical vessel bursts, this did not result in methods for calculating the effects. Only qualitative knowledge has

been gained, for instance that the shock wave along the axis of the vessel is initially considerably weaker than the wave normal to the axis.

BLEVEs

The work done in the field of BLEVEs is much more limited. Most studies only produced qualitative knowledge about BLEVEs.
There is the theoretical work of Reid [1976] and some experimental work by Venart et al. [1992], which increases the understanding of the phenomenon of a BLEVE and which gives a method to predict whether a BLEVE will occur or not, but the effects of a BLEVE have not been considered. This theory is in most cases applicable.
The only method for blast predictions for these situations is given by Baker et al. [1977]. Baker's method includes a modification for vessels with flashing liquids, similar to the method for non-ideal gases.

Runaway reactions

Heemskerk [1995] conducted a study into the blast effects of runaway reactions. He concluded that reaction rates are too low to raise the pressure inside the vessel above the failure pressure during the failure process of the vessel. The energy of the ongoing reaction after the moment the vessel ruptures hardly contributes to the blast effects. For blast calculations a vessel burst due to a runaway reaction can therefore be treated similar to a pressure vessel burst with ideal or non-ideal gases.

Internal explosions

The same is likely to be true for internal explosions, but this has not been studied. A conservative approach is to assume that the combustion is complete and use Baker's method.

Decomposition of energetic materials

The decomposition of energetic materials is always approached with TNT-equivalency methods. A main point of discussion is the fraction of energy which contributes to the blast, because often a part of the contents of the vessel does not decompose or decomposes too slowly to be able to fully contribute to the blast. The research effort on energetic materials focuses on the question of explosiveness of materials, Yoshida [1987], Heemskerk [1995]. This is outside the scope of this chapter.

7.3.3   Methods for fragmentation effects

The fragmentation of the vessel is coupled with missile effects. These so-called primary missile effects (= missiles that originate from the source itself) are determined by number, mass, shape, velocity and trajectory of the fragments. Secondary missiles, objects in the environment of the vessel that are picked up by the blast wave, are not considered.

Methods for calculating fragment velocity

The methods available for calculating the initial fragment velocity can be divided into three groups:
1. kinetic energy methods,
2. methods based on theoretical considerations,
3. empirical formulae.

The first group of methods is based on the assumption that a particular fraction of the energy will be transferred into kinetic energy of the fragments. The difference between the various methods in this group lies in the difference in definition of the fragment energy. As for blast effects, it is not known which measure for the kinetic energy is most suitable. Some definitions prescribe all or almost all internal energy for the calculation. It may be obvious that an upper limit will be found. Other definitions prescribe a part of all internal energy, based on experimental observations. In cases similar to the experiments these definitions may give a very good result. In other cases they may over- or underestimate the kinetic energy.

Theoretically, these methods are applicable to all types of vessel bursts, except to vessels filled with energetic materials, but it is not always simple to define the kinetic energy.

The second group of methods for estimating the fragment velocity is based on theoretical considerations.

A method for pressure vessels filled with ideal gas was introduced by Grodzovskii and Kukanov [1965] and improved by various researchers. This method takes into account gas flow through the ever-increasing gaps between fragments. Baker et al. [1983] used such a theoretical method to perform a parameter study and to compose with the results a diagram which can be used to determine initial fragment velocity for bursting pressurised vessels filled with ideal gas. The diagram is only applicable to spherical vessels or cylindrical vessels with a length-to-diameter ratio of 10, that have a uniform thickness and contain ideal gases. Furthermore, the diagram has been obtained for vessels bursting into equal fragments. Therefore, one must be careful to apply the diagram for unequal fragments.

A second method belonging to the group of methods based on theoretical considerations is given by Gel'fand et al. [1989]. Gel'fand et al. composed some dimensionless diagrams which can be used to determine the velocity of fragments in the rupture of spherical and cylindrical vessels containing an inert or a reactive gas mixture. For the reactive mixture two situations are considered: a runaway reaction and a combustion.

The diagrams are based upon a set of differential equations describing the motion of the fragments, the gas state, the energy of the mixture and the kinetics of the chemical reaction. The flow of gas through gaps between the fragments is taken into account. The set has been solved by applying the Runge-Kutta numerical integration method. The method of Gel'fand is based on, first, the assumption that non-uniform distribution of parameters with regard to the fragmentation effects may be ignored and, secondly, on the assumption of isentropic flow. These assumptions are allowed in case of large fragments.

Only the results for the inert mixture were compared with a limited number of experimental results and did correspond well. Gel'fand et al. state that the velocity estimate in case of a reactive mixture is conservative, whereas the velocity in case of an inert mixture is underestimated by no more than 5%.

The third group contains empirical relations for the initial velocity for vessels filled with ideal gases. Moore [1967] presents an empirical relation which distinguishes spherical and cylindrical vessels. The relation is derived for fragments accelerated from high explosives packed in a casing. Therefore, this equation predicts velocities higher than actual, especially for low vessel pressures and few fragments.

Baum [1987] gives a set of empirical relations to calculate an upper value for the initial fragment velocity from a spherical or cylindrical vessel burst, filled with an ideal gas or a flashing liquid (BLEVEs), into a small or large number of fragments. Some of the equations are based on a very small number of experiments.

For internal explosions and runaway reactions, only Gel'fand et al. [1989] present a method (see above).

The method of Gurney [Brown, 1985], and its adaptation by Moore (see above) could be considered for vessels filled with energetic materials. Gurney's method was derived for cased high explosives.

Methods to calculate fragment ranges

For the methods to calculate the fragment ranges (= flying distance), it is not required to distinguish between the four types of vessel bursts. The fragment range is calculated given the initial velocity and the mass of the fragment.

The forces that act upon fragments during their flight are gravity and dynamic fluid forces. The latter can be subdivided into drag and lift components, i.e. friction and uplift.

The simplest method to calculate the fragment range is by neglecting the dynamic fluid forces. Then the range only depends on the initial velocity and the initial trajectory angle. With this method the fragment range is usually considerably overestimated, but when lift forces are high it can also be underestimated.

Baker et al. [1983] solved a set of differential equations for the fragment range which included the fluid-dynamic forces by assuming that the orientation of a fragment during its flight remains the same with respect to its trajectory. They plotted the results in a diagram for practical use. The curves were generated by maximisation of range through variation of the initial trajectory angle. The curves concern similar lift-to-drag ratios which are not always easy to determine, because these ratios vary with the angle of attack and during the flight. A method to calculate the ratios is also given.

In some accidents rocketing effects are developed. Large fragments are propulsed for unexpectedly long distances. Baker et al. [1978] provided (1) equations for a simplified rocketing problem and (2) a computer program for a rocketing problem, but they stated that the method was not yet ready to be used for range prediction.

Ranges for rocketing fragments can also be calculated from guide-lines by Baum [1987]. The difference between this approach and Baker's approach appear to be small.

Mass and range distributions of fragments

The methods presented previously give no information on distributions of mass, velocity and range of fragments, and no information on the number of fragments to be expected. There are no methods that consider these parameters.

Some information might be found in the analysis of results of accidental explosions. Vital information is, however, lacking for most of such events. A pragmatic approach, based on the small amount of information available, is proposed by us to overcome this problem.

Baker et al. [1978] analysed 25 accidental vessel explosions for mass and range distribution, number of fragments and fragment shape, divided into six groups of like events. With statistical analyses estimates of range distributions for the six groups and fragment-mass distributions for three of the six groups were obtained and plotted in diagrams. With these figures it is possible to estimate the percentage of all the fragments which would have a range or mass smaller than, or equal to, a certain value. This is only valid for cases exactly the same as studied. The quantitative information cannot be generalised because of lacking data.

7.4 Selection of methods

7.4.1 Introduction to section 7.4

In the field of vessel bursts sometimes only one method is available or even none. When there are more methods, in this section the considerations will be explained for the selection of the methods which will be included in section 7.5.

In general the selection is based on the following criteria:
1. The method should give accurate results.
2. The method should be based on plausible physical assumptions.
3. The method should be easy to apply, also for someone not familiar with the field.
4. The method should preferably be widely applicable.
5. The limits for the applicability of the method should be well defined.

The considerations will be presented as follows:
1. Section 7.4.2 addresses the methods for predicting the blast effects.
2. Section 7.4.3 addresses the methods for predicting the fragment velocity and other fragmentation effects.

7.4.2 Methods for blast effects

For the description in section 7.5 a method based on thermodynamics has been chosen. The limitation of methods of this category, that the energy available for blast is not well-known and that therefore the method is not very accurate, is outreached by the simpleness of the method and its broad applicability. For these reasons these methods have been used widely. No specialist knowledge of vessel bursts is necessary to use the method, the opposite of which is true when solving the differential equations of fluid mechanics. Moreover, although the blast energy is not well-known, it is possible to define a conservative approach.

In this category there are only two methods which are more or less generally applicable. These two methods are:
− TNT-equivalence method;
− Baker's method.

Both methods are comparable, except that Baker's method distinguishes between close and far range for pressure vessel bursts with ideal gas. For these scenarios Baker's method is more accurate. Therefore, Baker's method is described in section 7.5.

The method can be used for all six types of vessel bursts with a different definition for the available energy for each type of burst.

7.4.3 Methods for fragment velocity and range

In section 7.5 the kinetic energy method is described because it provides a very simple method to obtain a rough estimate of the fragment velocity. The method is always applicable, to each type of vessel burst and regardless of the number of fragments.

Other, more accurate, methods are: (1) Baker's method for rupture of vessels with inert gases into many fragments, (2) Baker's and Gel'fand's method for rupture of vessels with inert gases into a few fragments, (3) Baum's empirical relation for BLEVEs, (4) Gel'fand's method for runaway reactions and internal explosions.

For pressure vessel ruptures into many fragments, Baker's method and Baum's empirical relation give similar results. The same holds for Baker's and Gel'fand's method for rupture of vessels into a few fragments. For BLEVEs, runaway reactions and internal explosions there is no choice. One can only dispose of Baum's empirical relation, Baker's method and Gel'fand's method.

To be able to calculate the fragment velocity for any situation (except for BLEVEs) it is necessary to describe at least two methods. No method covers all possible situations. There are two possibilities: Gel'fand's and Baker's method, or Gel'fand's and Baum's method. The first option has been chosen because these two methods are similar which makes the application simple for the user. Baum's empirical relations do not give extra information.

Moore's method is included as a check to guarantee that the previous methods are not applied beyond their limits. Furthermore, it is the most appropriate method for vessels filled with very high pressure gas and for vessels filled with energetic materials.

For calculating fragment ranges, the method of Baker has been included. For chunky fragments the method is very easy to use. For plate-like fragments, for which the lift coefficient is very important, it takes some additional effort to use the method, but there is no acceptable alternative.

Only qualitative remarks can be made about other fragmentation effects, such as the number of fragments and the distribution of mass and range, by way of a pragmatic approach and for a few special situations with use of Bakers statistical analysis.

It is no use describing Baker's statistical approach here. It can scarcely be used. It is only applicable to the same situations, same vessels with same contents, as in the cases studied. The pragmatic approach, proposed by us, is more widely applicable. It is also based on the qualitative data from Baker's statistical analysis. This approach is therefore described in section 7.5.

7.5 Description of selected methods

7.5.1 Introduction to section 7.5

In this section the recommended methods to calculate the blast effects and the fragmentation effects are described. It contains all necessary information to perform calculations. No background information on the methods is provided. For this, the reader should refer to section 7.3, whereas the limitations of the methods are discussed in section 7.8.

The reader should have a little basic understanding of the phenomena of a vessel burst. Therefore, anyone who is unfamiliar with the subject is advised to read section 7.2 first.

The methods to calculate the blast effects are described in section 7.5.2. Methods to calculate the fragmentation effects are given in section 7.5.3.

7.5.2 Methods for calculating the blast effects

The blast effects can be calculated with the procedure described below. First, information on the problem must be gathered. With the data the blast energy must be calculated. Finally the properties of the blast wave at the location of interest are determined.

Step 1   Collect data

Collect the following data:
a. vessel contents: ideal or non-ideal gas, vapour or liquid,
b. type of possible vessel burst: pressure vessel burst, BLEVE, runaway reaction, internal explosion or decomposition of energetic material,
c. the vessel's internal pressure (absolute) at failure, p_1,
d. the ambient pressure, p_a,
e. the volume of gas-filled part of vessel, V_g,
f. the ratio of specific heats of the gas, γ_1,
g. the distance from the centre of the vessel to the so-called target, r_t,
h. the shape of the vessel: spherical or cylindrical,
i. the temperature of the liquid at failure, T_l, its boiling temperature at ambient conditions, T_b, and its critical temperature, T_c.

Ad c and i.

The following table provides guidance regarding pressure and temperature at failure to be assumed for several situations. It is not possible to give an unequivocal advice for decomposition of energetic materials. Here the approach must be different.
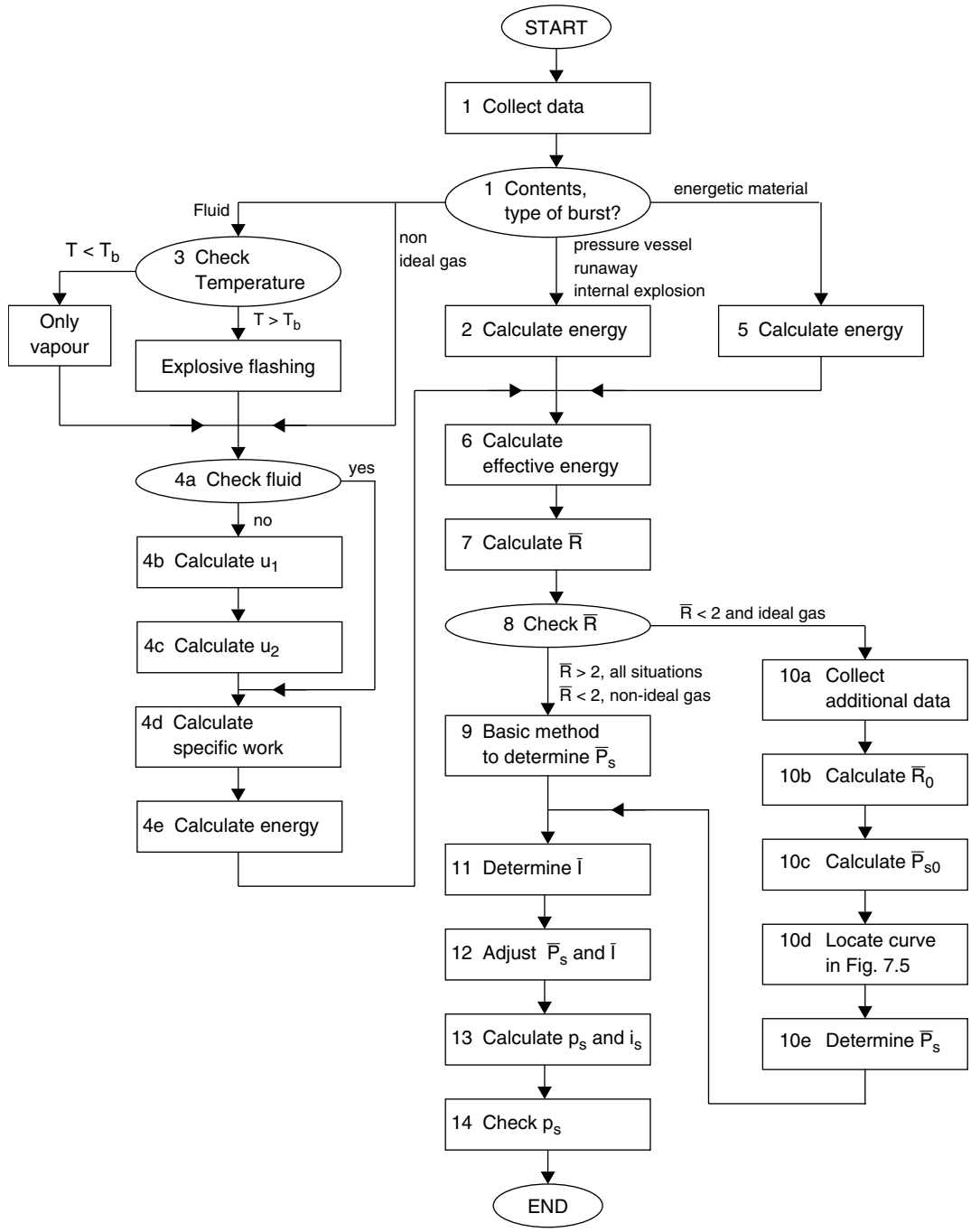
Table 7.1   Characteristic pressure and temperature at failure

Situation	Pressure at failure	Temperature at failure
Corrosion of vessel, Erosion of vessel, Material defect, External impact, Fatigue of vessel	Storage or working pressure	Storage or process temperature
External fire	1.21 × opening pressure of safety valve	Determine with use of thermodynamics tables
Overfilling (in combination with failing safety valve)	Design pressure × safety factor (= usually 2.5)	Storage or process temperature
Overheating (in combination with failing safety valve)	Design pressure × safety factor (= usually 2.5)	Determine with use of thermodynamic tables
Runaway reaction	Design pressure × safety factor (= usually 2.5)	Calculate with ideal gas law for that pressure
Decomposition of energetic materials	See step 5	See step 5
Internal explosion	3-4 × initial pressure for gas mixtures close to the explosion limits, 8-10 × initial pressure for stoichiometric gas or vapour mixtures, Rombouts [1988]	Liquid: storage or process temperatures Gas: adiabatic flame temperature

Ad b

The method for calculating the internal energy depends on the type of vessel burst. That is why one has to identify the problem as one of the following types of vessel bursts, which are described in section 7.2. For each type of vessel burst it is stated which step one has to continue with:

− Pressure vessel burst with ideal gas	go to step 2
− Pressure vessel burst with non-ideal gas or vapour	go to step 4
− BLEVE (vessel with liquid)	go to step 3
− Runaway reaction, ideal gases	go to step 2
non-ideal gases/vapour	go to step 4
− Decomposition of energetic materials	go to step 5
− Internal explosion	go to step 2

*Step 2   Calculation of the liberated energy of a pressure vessel burst or runaway reaction
           with an ideal gas, or an internal explosion*

The liberated energy E_{av} of a compressed gas as it expands to atmospheric pressure
is calculated as follows:

$$E_{av} = \frac{(p_1 - p_a) \times V_g}{\gamma_1 - 1} \qquad\qquad (J) \qquad\qquad (7.1)$$

where

E_{av} = liberated/expansion energy of compressed gas   [J]
p_1 = absolute pressure of gas   [Pa]
p_a = absolute pressure of ambient air   [Pa]
V_g = volume of gas-filled space of vessel   [m³]
γ_1 = ratio of specific heats of gas in system   [-]

Next: go to step 6.

Step 3   Check temperature of liquid

The temperature determines whether or not the liquid in a vessel will boil when
depressurised:

$T_l < T_b$: the liquid will not boil, only the vapour in the vessel will
contribute to a blast wave (= pressure vessel burst with
vapour)

$T_b < T_l < T_{sl}$: the liquid will boil, possibly BLEVE

$T_l > T_{sl}$: the liquid will boil explosively, BLEVE

where:

T_b = boiling temperature at atmospheric pressure   [K]
T_c = critical temperature (i.e. temperature above which
a gas cannot be liquefied by pressure alone)   [K]
T_{sl} = superheat limit temperature at atmospheric pressure,
approximately equal to $0.89 \times T_c$ for many fluids   [K]

If the liquid is a mixture of fluids, consider each fluid separately.
Continue with step 4.

*Step 4   Calculation of the liberated energy in case of a vessel burst or runaway reaction with
           a non-ideal gas or vapour or liquid (BLEVE)*

Step 4a   Determine if the fluid is given in Table 7.2 or Figure 7.3

The work performed by a fluid as it expands has been calculated for the following
seven common fluids:
− ammonia
− carbon dioxide
− ethane
− isobutane
− nitrogen

  − oxygen
  − propane

If the fluid of interest is listed, go to step 4d. If not, go to step 4b.

Step 4b Determine internal energy in initial state, u_1

The work done by an expanding fluid (i.e., a liquid or a vapour) is defined as the difference in internal energy u between the fluid's initial and final states. Most thermodynamic tables and graphs do not present u but only the enthalpy h, absolute pressure p, specific volume v, absolute temperature T and the specific entropy s. Therefore, u must be calculated with the following equation:

$$u = h - pv \qquad\qquad\qquad\qquad \text{(J/kg)} \qquad\qquad (7.2)$$

where
u	=	specific internal energy	[J/kg]
h	=	specific enthalpy (enthalpy per unit mass)	[J/kg]
p	=	absolute pressure	[Pa]
v	=	specific volume	[m^3/kg]

To use a thermodynamic graph, locate the fluid's initial state on the graph. (For a saturated fluid, this point lies either on the saturated liquid or on the saturated vapour curve, at a pressure p_1.) Read the enthalpy h_1, volume v_1, and entropy s_1 from the graph. If thermodynamic tables are used, interpolate these values from the tables. Calculate the specific internal energy in the initial state u_1 with equation (7.2), both for the vapour phase and the liquid phase.
The thermodynamic properties of mixtures of fluids are usually not known. A crude estimate of a mixture's internal energy can be made by summing up the internal energy of each component.
Continue with step 4c.

Step 4c Determine internal energy in expanded state, u_2

The specific internal energy of the fluid in the expanded state u_2 can be determined as follows: If a thermodynamic graph is used, assume an isentropic expansion (entropy s is constant) to atmospheric pressure p_a. Therefore, follow the constant-entropy line from the initial state to p_a. Read h_2 and v_2 at this point, and calculate the specific internal energy u_2 by using of equation (7.2). This is illustrated in example 1 in section 7.6.2.
If thermodynamic tables are used, read the enthalpy h_f, volume v_f, and entropy s_f of the saturated liquid at ambient pressure, p_a, interpolating if necessary. In the same way, read these values (h_g, v_g, s_g) for the saturated vapour state at ambient pressure. Then, use the following equation to calculate the specific internal energy u_2:

$$u_2 = (1 - X)h_f + Xh_g - (1 - X)p_av_f - Xp_av_g \qquad\qquad \text{(J/kg)} \qquad\qquad (7.3)$$

where
X	=	vapour ratio $(s_1 - s_f)/(s_g - s_f)$	[-]
s	=	specific entropy	[J/(kg·K)]

Subscript 1 refers to initial state
Subscript 2 refers to the expanded state
Subscript f refers to state of saturated liquid at ambient pressure
Subscript g refers to state of saturated vapour at ambient pressure

Equation (7.3) is only valid if X is between 0 and 1. If not, use a thermodynamic graph, as demonstrated in section 7.6.
Continue with step 4d.

Step 4d Calculate the specific liberated energy

The specific work done by an expanding fluid is

$$e_{av} = u_1 - u_2 \qquad \text{(J/kg)} \qquad (7.4)$$

where e_{av} is the specific work or specific liberated energy. The results of these calculations are given for seven common gases in Table 7.2 and Figures 7.3 and 7.4. Table 7.2 gives superheat limit temperature T_{sl}, initial conditions and specific work done in expansion based upon isentropic expansion of either saturated liquid or saturated vapour until atmospheric pressure is reached.
Figures 7.3 and 7.4 present the same information for saturated hydrocarbons. Note that a liquid has much more energy per unit volume than a vapour.

Table 7.2   Expansion work of ammonia, carbon dioxide, nitrogen and oxygen

Fluid	T_1 (K)	p_1 (10^5 Pa)	Liquid		Vapour	
			e_{av} (kJ/kg)	e_{av}/v_f (MJ/m³)	e_{av} (kJ/kg)	e_{av}/v_g (MJ/m³)
Ammonia, T_{sl} = 361.0 K	324.8	21.2	82.5	46.2	297.0	4.89
	360.0	48.0	152.5	74.7	365.0	14.80
	400.0	102.8	278.5	95.7	344.0	47.00
Carbon dioxide, T_{sl} = 270.8 K	244.3	14.8	54.4	58.2	98.0	3.77
	255.4	21.1	60.9	62.1	109.0	6.00
	266.5	29.1	68.1	65.6	117.0	9.17
Nitrogen, T_{sl} = 112.3 K	104.0	10.0	13.2	8.78	41.9	1.75
	110.0	14.5	18.2	11.3	47.7	2.98
	120.0	24.8	28.6	15.0	53.5	6.66
Oxygen, T_{sl} = 137.7 K	120.0	10.1	12.8	12.5	43.9	1.73
	130.0	17.3	18.7	16.8	53.4	3.65
	140.0	27.5	27.2	22.1	60.0	7.00
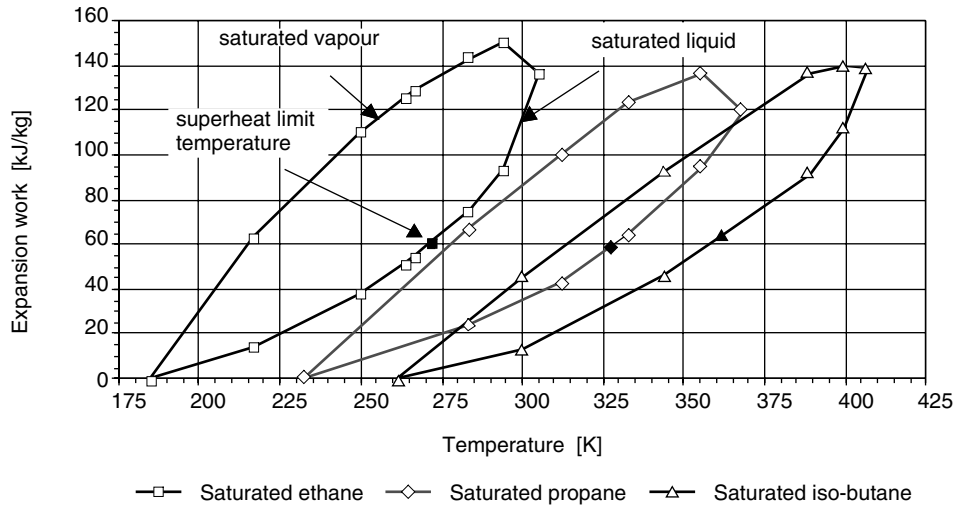
Figure 7.3   Expansion work per unit mass of saturated ethane, propane, and isobutane. The saturated liquid state is on the lower part of the curves. The solid marker indicates the superheat limit temperature
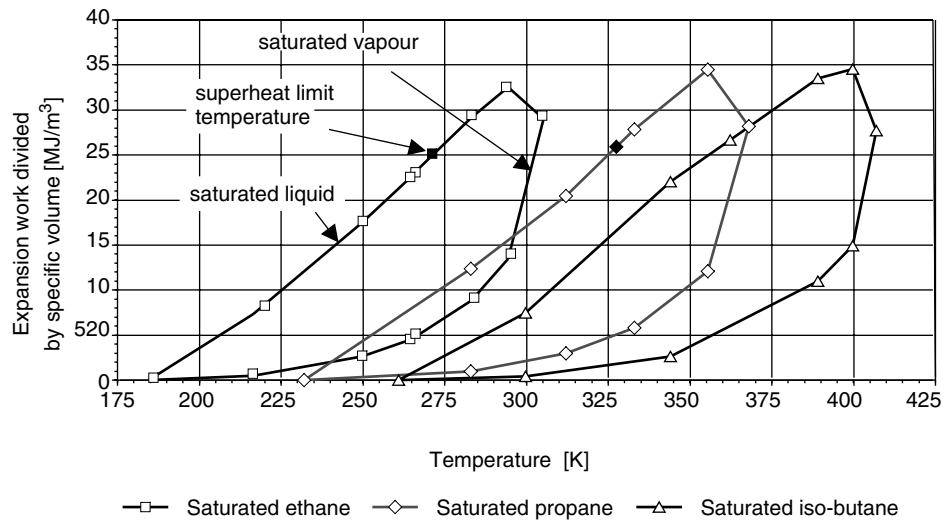
Figure 7.4   Expansion work divided by specific volume of saturated ethane, propane, and isobutane. The saturated liquid state is on the upper part of the curves. The solid marker indicates the superheat limit temperature

Calculate the specific work done by the fluid for the vapour phase and the liquid phase, and in case of a mixture of fluids, for all components.
Continue with step 4e.

Step 4e   Calculate total liberated energy

To calculate the available energy, multiply the specific expansion work by the mass of the phase or component of the fluid released or else, if energy per unit volume is used, multiply by the volume of the phase or component of the fluid released.

$$E_{av} = e_{av} \times M_{fl} \qquad\qquad (J) \qquad\qquad (7.5a)$$

$$E_{av} = (e_{av}/v) \times V_{fl} \qquad\qquad (J) \qquad\qquad (7.5b)$$

where
M_{fl} = mass of released phase or component of the fluid   [kg]
V_{fl} = volume of released phase or component of the fluid   [m^3]

Repeat steps 4b to 4e for each phase and component present in the vessel, and add the energies to find the total liberated energy E_{av}. When this total energy has been found, go to step 6.

Step 5   Determine the available energy for a decomposition of an energetic material

For a decomposition of an energetic material it is not possible to give an unequivocal advice on the failure pressure. A different approach to calculate the liberated energy is therefore necessary.
The upper limit for the liberated energy is given by the total amount of chemical energy of the decomposition. This is shown by an example.

The heat of reaction can be found from the difference between the heat of formation of the reactants and that of the reaction products. Yoshida [1987] gives an example for the detonative decomposition of nitromethane. The heats of formation of the reactants and reaction products, in kJ/mol, are given below the stoichiometic equation.

$$CH_3NO_2 \text{ (l)} \rightarrow (3/2)\ H_2O \text{ (l)} + (1/4)\ CO_2 \text{ (g)} + (1/2)\ N_2 \text{ (g)} + (3/4)\ C \text{ (s)}$$

-ΔH_f 113.4   287.3   395.2   0   0
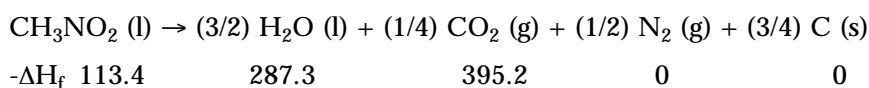
The heat of reaction ΔH_f is: $(3/2) \times 287.3 + (1/4) \times 395.2 - 113.4 = 416.4$ kJ/mol, or 6.8 MJ/kg nitromethane. For more information see Yoshida [1987].
The total chemical energy can now be found by multiplying the heat of reaction with the total mass of product:

$$E_{av} = M_c\ \Delta H_f \qquad\qquad (J) \qquad\qquad (7.6)$$

where
ΔH_f = the heat of reaction per kg product   [J/kg]
M_c = the total mass of contents of the vessel   [kg]

7.34

This method will considerably overestimate the explosion effects in most cases, because often only part of the vessel's contents decomposes or does not decompose quickly enough to contribute to the blast.
Continue with step 6.

Step 6   Determine the effective blast wave energy, E_{ex}

The effective blast wave energy is given by

$$E_{ex} = A_{sb} \times E_{av} \hspace{2cm} \text{(J)} \hspace{2cm} (7.7)$$

In this equation it is assumed that all available energy will be converted into blast wave energy. With the factor A_{sb}, the presence of a reflecting ground surface can be taken into account. $A_{sb} = 1$, when the vessel is high in the air, $A_{sb} = 2$ when the vessel is less than 15 degrees above the horizon, as seen from the target.
Note that this method only predicts the peak overpressure of the incident shock wave. The target may receive additional loadings from reflected shock waves. This is especially the case when the vessel is high in the air. To find the total load in these cases, use the methods described in TM 5-1300 [1990] or consult an expert.
Continue with step 7.

Step 7   Calculate $\overline{R}$ of the target

The non-dimensional distance of the so-called 'target', $\overline{R}$, is defined as

$$\overline{R} = r_t \left[\frac{p_a}{E_{ex}} \right]^{1/3} \hspace{2cm} \text{(-)} \hspace{2cm} (7.8)$$

where r_t is the distance in metres at which blast parameters are to be determined.
Continue with step 8.

Step 8: Check the value of $\overline{R}$

For $\overline{R} \geq 2$ the basic method gives good results. For $\overline{R} < 2$ however, the basic method gives too high a value. A refined method is available for pressure vessel bursts or runaway reactions with ideal gas.
Therefore, continue according to the following list:

$\overline{R} \geq 2$,	continue with step 9.
$\overline{R} < 2$, ideal gas	go to step 10.
$\overline{R} < 2$, other vessel bursts	continue with step 9 and realise that the results will be conservative.

Step 9   Determine $\overline{P}_s$ for all types of vessel bursts except for a pressure vessel burst with an ideal gas at close range ($\overline{R} < 2$)

$\overline{P}_s$ is the non-dimensional side-on overpressure of the blast wave. This non-dimensional overpressure can be read from Figure 7.5 or 7.6 for the appropriate $\overline{R}$. Use the curve labelled 'high explosive' if Figure 7.5 is used.
Next: go to step 11.
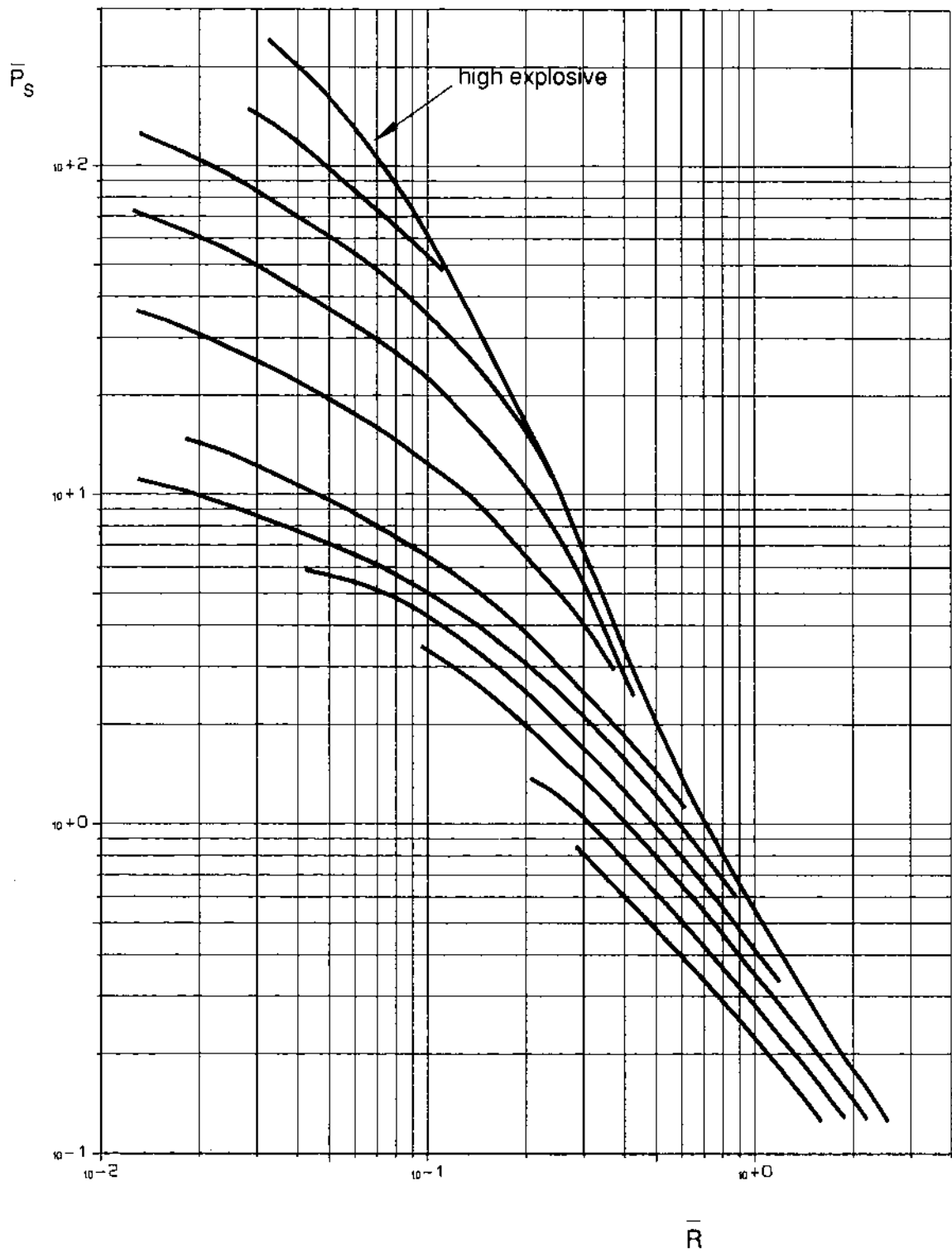
Figure 7.5   Non-dimensional overpressure versus non-dimensional distance for
             overpressure calculations, Baker et al. [1977].
             $\overline{R} = r_t (p_a / E_{ex})^{1/3}$ and $\overline{P}_s = p_s / p_a - 1$
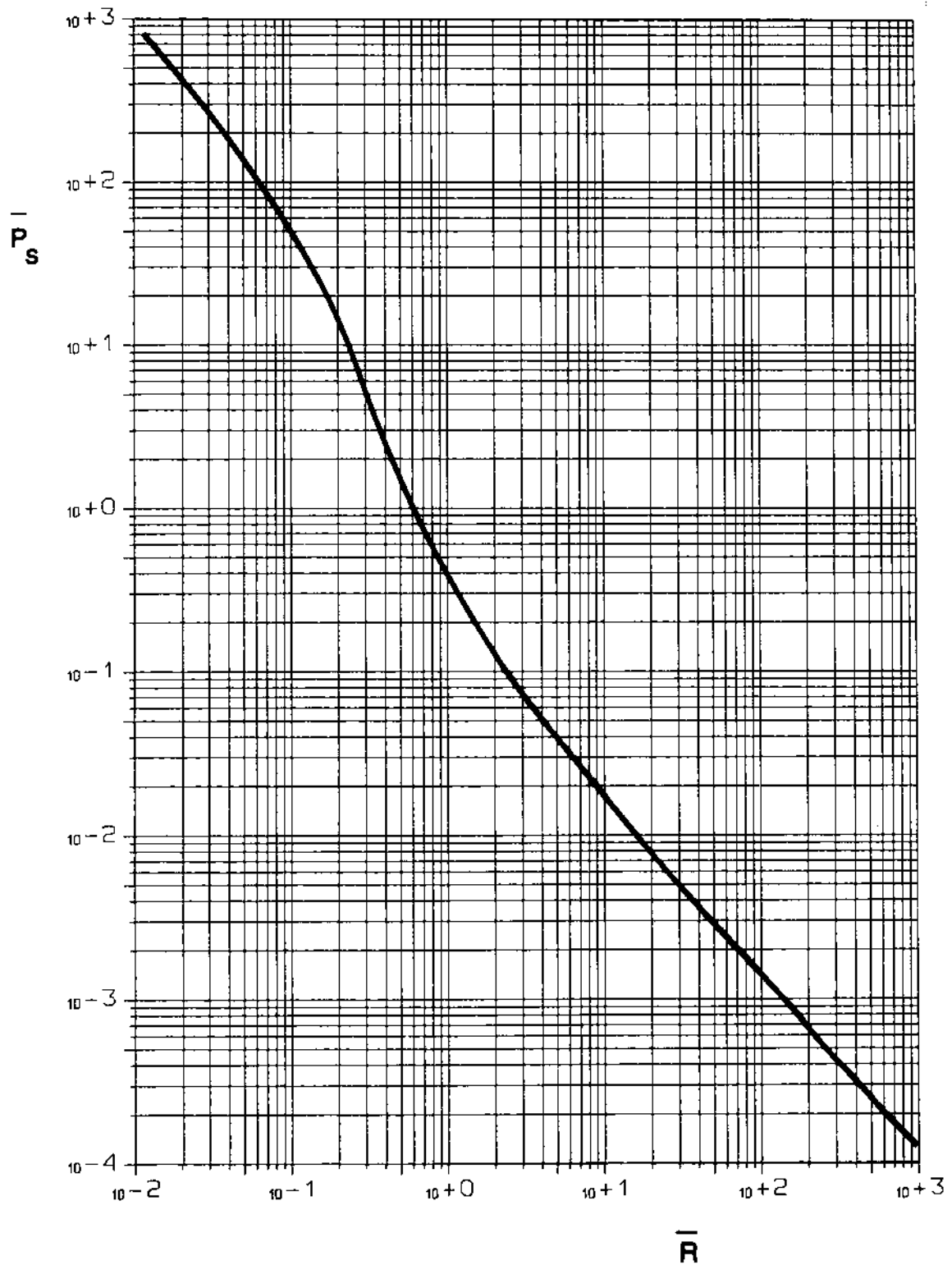
Figure 7.6 $\overline{P}_s$ *versus* $\overline{R}$ *for pentolite, Baker et al. [1977].*
$\overline{R} = r_t \, (p_a / E_{ex})^{1/3}, \ \overline{P}_s = p_s / p_a - 1$

Step 10   Determine $\overline{P}_s$ for a pressure vessel burst with an ideal gas and $\overline{R} < 2$
(Refined method for the near field)

Because the similarity of the blast waves of vessel bursts and high explosives does not hold for the near field, a refined method is necessary to predict the blast pressures.

Step 10a   Collect additional data

In addition to the data collected in step 1 of the basic method, the following data is needed:
−   the ratio of the speed of sound in the compressed gas to its speed in ambient air, a_1/a_a;
−   the ratio of specific heats of ambient air, $\gamma_a = 1.40$, the molar mass is 0.0290 kg/mol.

For an ideal gas $(a_1/a_a)^2$ is

$$\left[\frac{a_1}{a_a}\right]^2 = \frac{\gamma_1 T_g \mu_a}{\gamma_a T_a \mu_1} \qquad\qquad (-) \qquad\qquad (7.9)$$

where

T_a	=	absolute temperature of ambient air	[K]
T_g	=	absolute temperature of compressed gas	[K]
μ_1	=	molar mass of compressed gas	[kg/mol]
μ_a	=	molar mass of ambient air	[kg/mol]
γ_a and γ_1 are specific heat ratios			[-]

Continue with step 10b.

Step 10b   Calculate the initial distance

This refined method assumes the blast wave to be completely symmetrical. Such a shape would result from the explosion of a hemispherical vessel placed directly on the ground. Therefore, a hemispherical vessel is used instead of the actual vessel for calculation purposes.
Calculate the hemispherical vessel's radius r_0 from the volume of the gas-filled part of the actual vessel V_g:

$$r_0 = \left[\frac{3V_g}{2\pi}\right]^{1/3} = 0.782 \times V_g^{1/3} \qquad\qquad (m) \qquad\qquad (7.10)$$

This is the starting distance on the overpressure versus distance curve. It must be transformed into the non-dimensional starting distance, $\overline{R}_0$, with:

$$\overline{R}_0 = r_0 \left[\frac{p_a}{E_{ex}}\right]^{1/3} \qquad\qquad (-) \qquad\qquad (7.11)$$

Continue with step 10c.

Step 10c   Calculate the initial peak overpressure $\overline{P}_{so}$

The peak shock pressure directly after the burst, p_{so}, is much lower than the initial gas pressure in the vessel p_1. The non-dimensional peak shock overpressure directly after the burst, $\overline{P}_{so}$, is defined as $(p_{so}/p_a) - 1$. It is given by the following expression:

$$\frac{p_1}{p_a} = (\overline{P}_{so} + 1)\left[1 - \frac{(\gamma_1 - 1)(a_a/a_1)\overline{P}_{so}}{[2\gamma_a(2\gamma_a + (\gamma_a + 1)\overline{P}_{so})]^{1/2}}\right]^{\left(\frac{-2\gamma_1}{\gamma_1 - 1}\right)}$$

$$(-) \qquad\qquad (7.12)$$

where

p_1	=	initial absolute pressure of compressed gas	[Pa]
p_a	=	ambient pressure	[Pa]
$\overline{P}_{so}$	=	non-dimensional peak shock overpressure directly after burst:	
		$\overline{P}_{so} = (p_{so} / p_a) - 1$	[-]
p_{so}	=	peak shock pressure directly after burst	[Pa]
γ_a	=	ratio of specific heats of ambient air	[-]
γ_1	=	ratio of specific heats of compressed gas	[-]
a_a	=	speed of sound in ambient air	[m/s]
a_1	=	speed of sound in compressed gas	[m/s]

This is an implicit equation which can only be solved by iteration. One might use a spreadsheet to solve $\overline{P}_{so}$. An alternative is to read $\overline{P}_{so}$ from Figure 7.7 or 7.8.
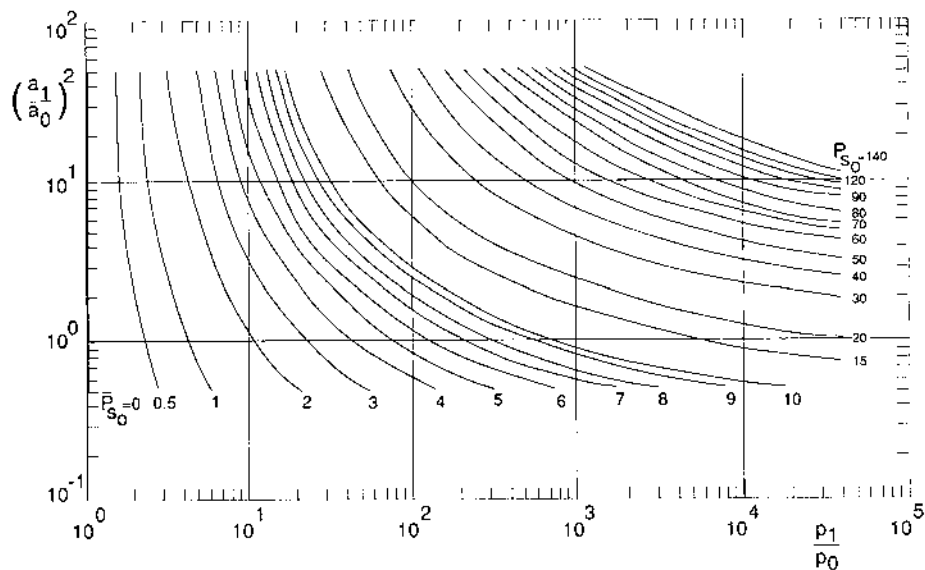
Figure 7.7   Gas temperature versus pressure for constant $\overline{P}_{so}$ for $\gamma_1 = 1.4$, Baker et al. [1977]
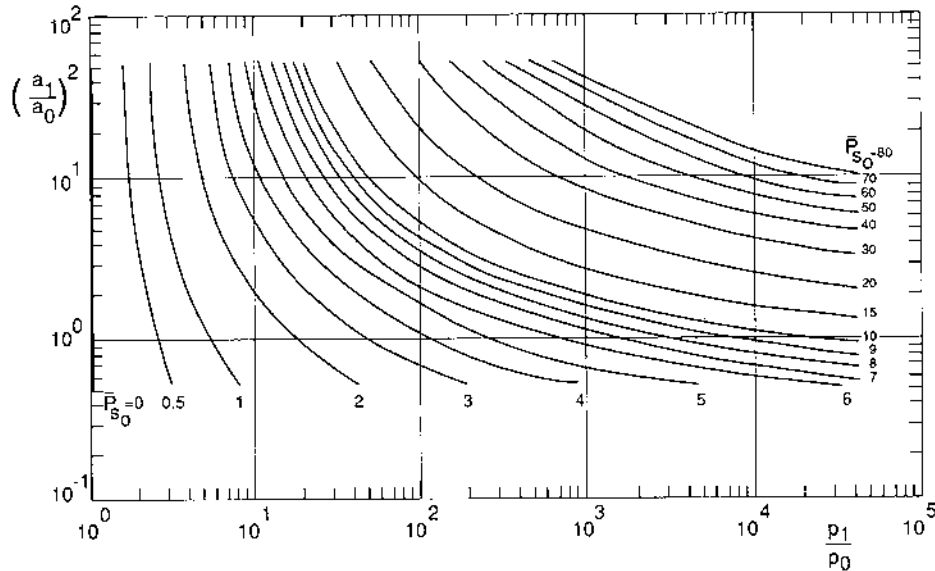
Figure 7.8   Gas temperature versus pressure for constant $\overline{P}_{so}$ for $\gamma_1 = 1.66$, Baker et al. [1977]

Continue with step 10d.

Step 10d   Locate the starting point of Figure 7.5

In steps 10b and 10c, the vessel's non-dimensional radius and the blast wave's non-dimensional peak pressure at that radius were calculated. As a blast wave travels outward, its pressure decreases rapidly. The relationship between the peak pressure $\overline{P}_s$ and the distance $\overline{R}$ depends upon the initial conditions. Accordingly, Figure 7.5 contains several curves. Locate the correct curve by plotting $(\overline{R}, \overline{P}_{so})$ in the figure. Continue with step 10e.

Step 10e   Determine $\overline{P}_s$

To determine the non-dimensional side-on overpressure $\overline{P}_s$, read $\overline{P}_s$ from Figure 7.5 for the appropriate $\overline{R}$ (calculated in step 7). Use the curve which goes through the starting point, or else draw a curve through the starting point parallel to the nearest curve.
Continue with step 11.

Step 11   Determine $\overline{I}$

To determine the non-dimensional side-on impulse $\overline{I}$, read $\overline{I}$ from Figure 7.9 or 7.10 for the appropriate $\overline{R}$. Use the curve labelled as 'vessel burst'. For $\overline{R}$ in the range of 0.1 to 1.0, the $\overline{I}$ versus $\overline{R}$ curve of Figure 7.10 is more convenient.
Continue with step 12.
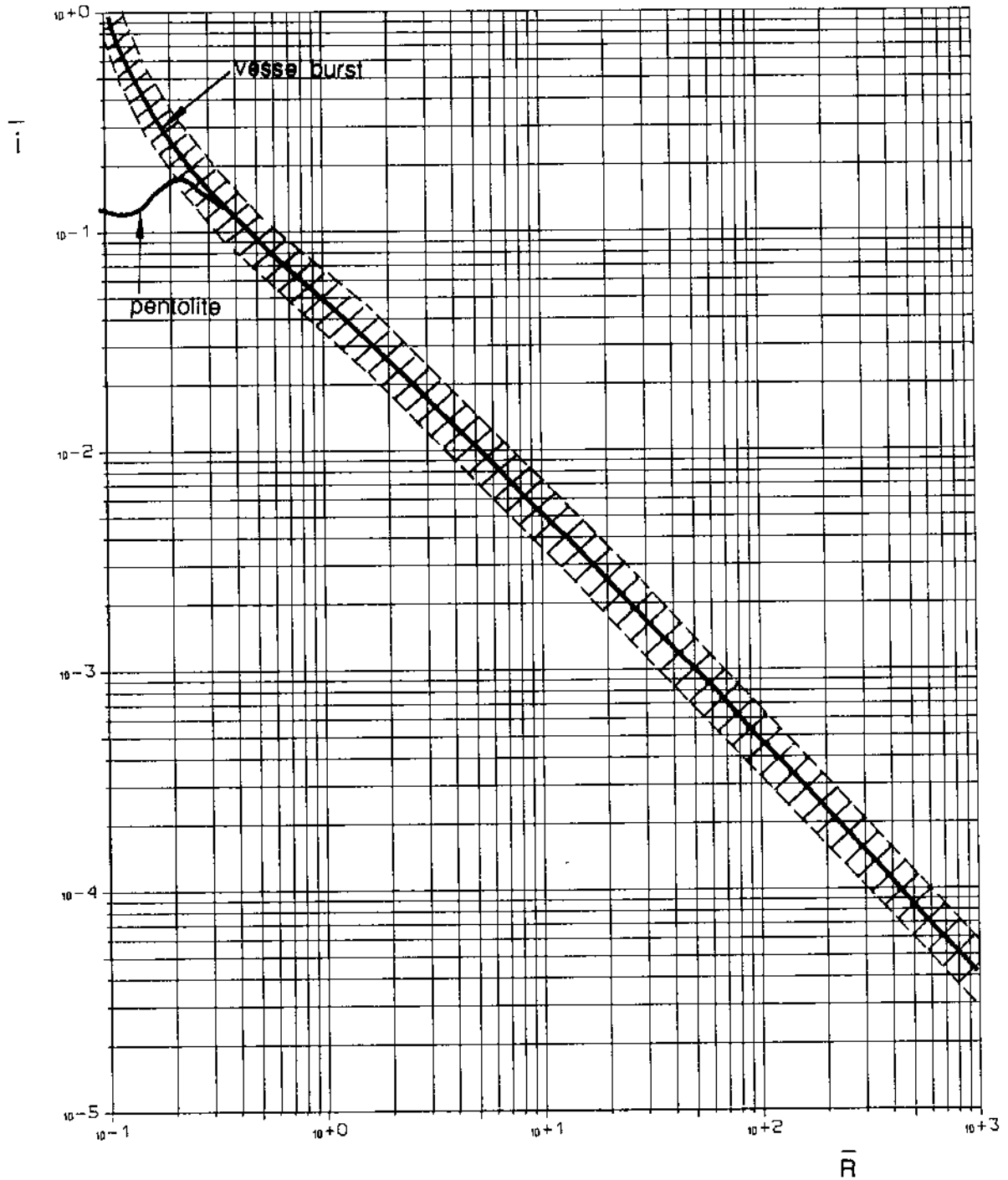
Figure 7.9 $\bar{I}$ versus $\bar{R}$ for pentolite and gas vessel bursts, Baker et al. [1977],
$\bar{R} = r_t (p_a / E_{ex})^{1/3}$, $\bar{I} = (i_s a_a) / (p_a^{2/3} E_{ex}^{1/3})$
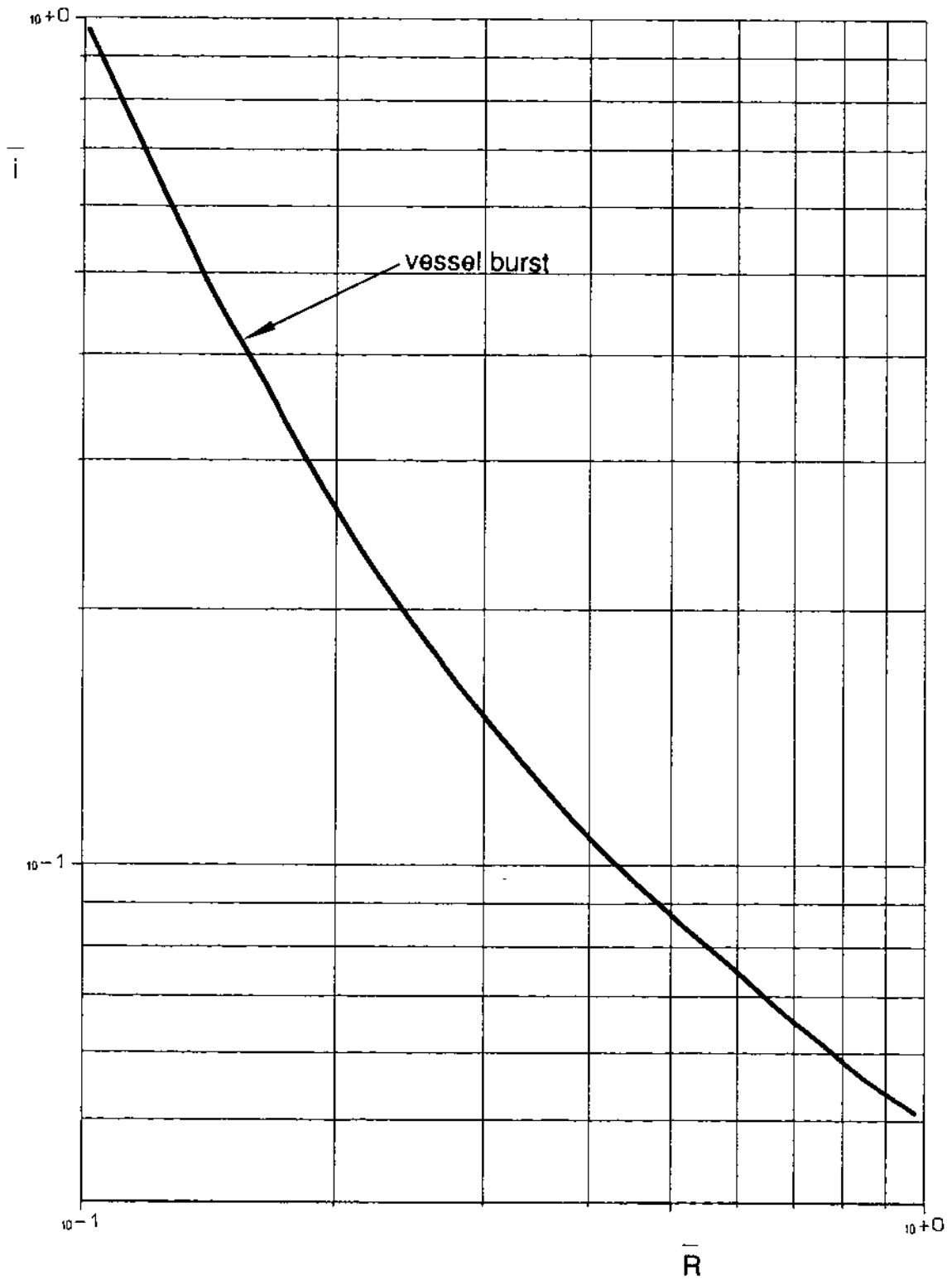
Figure 7.10 $\bar{I}$ versus $\bar{R}$ for gas vessel bursts, Baker et al. [1977],
$\bar{R} = r_t\,(p_a\,/\,E_{ex})^{1/3}$, $\bar{I} = (i_s a_a)\,/\,(p_a^{2/3} E_{ex}^{1/3})$

7.42

Step 12   Adjust $\overline{P}_s$ and $\overline{I}$ for geometry effects

The above procedure gives blast parameters applicable to a completely symmetrical blast wave, such as would result from the expansion of a hemispherical vessel above the ground or a spherical vessel in free air. In practice, vessels are either spherical or cylindrical, and placed at some height above the ground. This influences blast parameters. To adjust for these geometry effects, $\overline{P}_s$ and $\overline{I}$ must be multiplied by some adjustment factors. Table 7.3 and 7.4 give multiplication factors for adjusting the scaled values for cylindrical vessels of various $\overline{R}$ and for vessels elevated slightly above the ground, respectively.

It must be mentioned that for cylindrical vessels the blast field is asymmetrical when placed horizontally. The blast wave is weakest along the axis. The correction method will only provide the maximum values for a horizontal tank.

Continue with step 13.

Table 7.3   Adjustment factors for $\overline{P}_s$ and $\overline{I}$ for cylindrical vessels for various $\overline{R}$

$\overline{R}$	Multiplier for	
	$\overline{P}_s$	$\overline{I}$
< 0.3	4	2
≥ 0.3 and ≤ 1.6	1.6	1.1
>1.6 and ≤ 3.5	1.6	1
>3.5	1.4	1

Table 7.4   Adjustment factors for $\overline{P}_s$ and $\overline{I}$ for vessels slightly elevated above the ground

$\overline{R}$	Multiplier for	
	$\overline{P}_s$	$\overline{I}$
< 1	2	1.6
≥ 1	1.1	1

Step 13   Calculate p_s, i_s

Use the following equations to calculate the side-on peak overpressure p_s - p_a and the side-on impulse i_s from the non-dimensional side-on peak overpressure $\overline{P}_s$ and the non-dimensional side-on impulse $\overline{I}$:

$$p_s - p_a = \overline{P}_s \times p_a \qquad \text{(Pa)} \qquad (7.13)$$

$$i_s = \frac{\overline{I} \times p_a^{2/3} \times E_{ex}^{1/3}}{a_a} \qquad \text{(Pa·s)} \qquad (7.14)$$

where a_a is the speed of sound in ambient air in metres per second. For sea-level average conditions, p_a is approximately 101.3 kPa and a_a is 340 m/s.
Continue with step 14.

Step 14   Check p_s

This method has only a limited accuracy, especially in the near field. Under some circumstances, the calculated p_s might be higher than the initial pressure in the vessel p_1, which is physically impossible. If this should happen, take p_1 as the peak pressure instead of the calculated p_s.

Note that the methods presented above give upper estimates of blast parameters. In practice, overpressures in one case might very well be much lower than predicted by the method, and in another case they might be close to the predicted value.
The method is therefore not suitable for analysis of accidents. It is just a tool to predict safe upper values for plant layout etc.

7.5.3   Methods for fragmentation effects

The risk from fragments at a particular location is related to the number of fragments that may fall on or fly through that location and their potential to do damage, i.e. their mass and velocity.

```
                                    ┌──────────┐
                                    │  START   │
                                    └────┬─────┘
                                         ▼
                              ┌────────────────────┐
                              │ 1  Estimate number │
                              │    of fragments    │
                              └─────────┬──────────┘
                                        ▼
                              ┌────────────────────┐
                              │ 2  Estimate        │
                              │    fragment mass   │
                              └─────────┬──────────┘
                                        ▼
  kinetic energy method        ╭──────────────────╮        Gel' fand's or Baker's
  for all types        ────────│ 3  Choose method │────────  for all but BLEVE
  Baum's for BLEVE             ╰──────────────────╯
```

Kinetic energy method

- 3a1 Collect data
- 3a2 Calculate energy
- 3a3 Calculate initial velocity

Gel' fand's or Baker's method

- 3b1 Collect data
- 3b2 Calculate $\overline{P}_1$ and if ness Φ
- 3b3 Determine initial velocity

If $\overline{P}_1$ too high

Calculate with Moore's

Check with Moore's   Check with Moore's

Moore's method

- 3c1 Collect additional data
- 3c2 Calculate energy
- 3c3 Calculate initial velocity
- 3c4 Adjust v_i if necessary

4c1 Collect additonal data to determine flying range

4c2 Calculate $\overline{v}_i$

4c3 Determine $\overline{R}_f$

4c4 Determine R_f

END

Step 1   Estimate number of fragments

There are no methods to predict the number of fragments. An estimate of the number of fragments can only be made by using a pragmatic approach which is based on analyses of accidental explosions.

A pragmatic approach to estimate the number of fragments to be expected is summarised in Table 7.5. It means that in case of a local weakening of the vessel it is most probable that it will break into two pieces, whereas in case of overpressure the vessel will break into more pieces, usually along the welds. A cylinder usually has only a few welds whereas a sphere has much more welds.

Table 7.5   Pragmatic approach to estimate number of fragments

Situation	Number of fragments
Local weakening	2 pieces
Overpressure	
Cylinder	2 or 3 pieces
Sphere	10 to 20 pieces

Continue with step 2.

Step 2   Estimate fragment mass, M_f

As is the case for the number of fragments, there is no method available to estimate the mass of the fragment. Only a pragmatic approach can be used.

This pragmatic approach is related to the pragmatic approach for the determination of the number of fragments. Knowing this number n_f, it is easy to calculate the average mass of the fragments, being equal to M_v/n_f.

This estimate of the average fragment mass can be considered as reasonable in case of rupture into many fragments or in case of rupture into a few equal fragments. This is the case for spheres.

Cylinders, however, usually do not break into equal parts. They usually break at the end caps. The vessel often projects its end caps along the axis of the vessel and the unfolded shell perpendicular to the vessel's axis.

A survey of possible fragments is given in Table 7.6.

Table 7.6   Fragment mass and shape, pragmatic approach

Type of vessel	Fragment mass M_f	Fragment shape
Sphere, 2 fragments	$M_v/2$	hemisphere
Sphere, many fragments	M_v/n_f	plates
Cylinder, 2 equal pieces	$M_v/2$	half of tank
Cylinder, 2 unequal pieces	1 piece: M_{cap} other piece: M_v-M_{cap}	cap/hemisphere tank with one cap missing
Cylinder, 3 unequal pieces	2 pieces: M_{cap} other: (M_v-2M_{cap})	cap/hemisphere plate
Cylinder, many pieces	2 pieces: M_{cap} rest: $(M_v-2M_{cap})/(n_f-2)$	cap/hemisphere strip

Continue with step 3.

Step 3   Calculate fragment velocity

Calculate the fragment velocity according to one of the methods in Table 7.7.

Table 7.7   Selection of methods for fragmentation effects, depending on the type of burst

Type of burst	Method	Go to step
Rough estimate for all types of vessel bursts, except decomposition of energetic materials	Kinetic energy method	3a
Pressure vessel burst	Baker's and/or Gel'fand's method	3b
Runaway reaction, internal explosion	Gel'fand's method	3b
BLEVE	Baum's empirical formula	3a
For high scaled pressures and decomposition of energetic materials	Moore's empirical relation	3c

Check the results of the other methods (step 3a and 3b) with the empirical relation of Moore (3c).

Step 3a   Kinetic energy method to roughly predict the initial fragment velocity and Baum's empirical formula for BLEVEs

The theoretical upper limit and a rough estimate of the initial fragment velocity can be calculated as follows.

Step 3a1   Collect data

Collect the same data as collected in step 1 of the method for calculating the blast effects, see paragraph 7.5.2. Determine also the total mass of the empty vessel, M_v.

Step 3a2   Calculate the liberated energy, E_{av}

Calculate the liberated energy in accordance with the method for blast effects, see paragraph 7.5.2.

Step 3a3   Calculate initial velocity, v_i

This initial velocity of a fragment can be calculated by using of the following equation:

$$v_i = \sqrt{\frac{2 \times A_{ke} \times E_{av}}{M_v}} \qquad\qquad \text{(m/s)} \qquad (7.15)$$

where
E_{av} = liberated energy   [J]
M_v = total mass of empty vessel   [kg]
A_{ke} is the fraction of the liberated energy that goes into kinetic energy of the fragments. It depends on the situation.
Upper limit $A_{ke} = 0.6$
Rough estimate $A_{ke} = 0.2$
BLEVE $A_{ke} = 0.04$

Note that with the rough estimate the initial velocity can sometimes be underestimated considerably.
Next: go to step 3c.

Step 3b   Baker's and/or Gel'fand's method to estimate initial fragment velocity

Step 3b1   Collect data

Collect the following data:
− absolute pressure of gas at failure, p_1
− ambient pressure, p_a
− volume of gas-filled part of the vessel, V_g
− specific heat ratio of gases in vessel, γ_1
− speed of sound in gas at failure, a_1, $a_1^2 = T_g \gamma_1 R / \mu_1$
  where
  R   = 8.314 J/(mol·K)
  T_g = absolute temperature inside vessel at failure   [K]
  μ_1 = molecular mass   [kg/mol]
− mass of vessel, M_v
− shape of vessel.

In case of a runaway reaction or internal explosion collect also the following data:
- maximum laminar burning velocity of reaction, u_f. For a few gases u_f is given in Table 5.1 in chapter 'Vapour Cloud Explosions'.
- heat of reaction per kg of the product, ΔH_f, which follows from the stoichiometric equation for the reaction, see section 7.5.2, step 5.

Step 3b2   Calculate the dimensionless scaled overpressure $\overline{P}_1$

Calculate the scaled overpressure according to:

$$\overline{P}_1 = (p_1 - p_a) \times V_g/(M_v a_1^2) \qquad\qquad (\text{-}) \qquad\qquad (7.16)$$

In case of a runaway reaction or internal explosion also calculate the dimensionless parameter Φ, which characterises the rate of energy release. Φ is given by:

$$\Phi = \frac{\Delta H_f \times u_f}{a_1^3} \qquad\qquad (\text{-}) \qquad\qquad (7.17)$$

Step 3b3   Read v_i from Figure 7.11

Choose the proper chart from Figures 7.11. Choose the proper line in this chart and read v_i/a_1 for $\overline{P}_1$, as determined in the previous step. If one can choose between Baker's solution and the solution of Gel'fand, it is best to choose the most conservative solution. Since a_1 has been determined in step 3b1, the initial velocity v_i is now known.
In case of a runaway reaction the proper line in the chart is determined by the dimensionless parameter Φ as calculated in step 3b2 and by the specific heat ratio γ_1. The lines in the chart for a certain γ_1 are in the same order as in the legend.
In case of a cylinder with a different length-diameter ratio than in the figures, one should determine v_i/a_1 by interpolating between the values for the two closest vessels. Continue with step 3c.
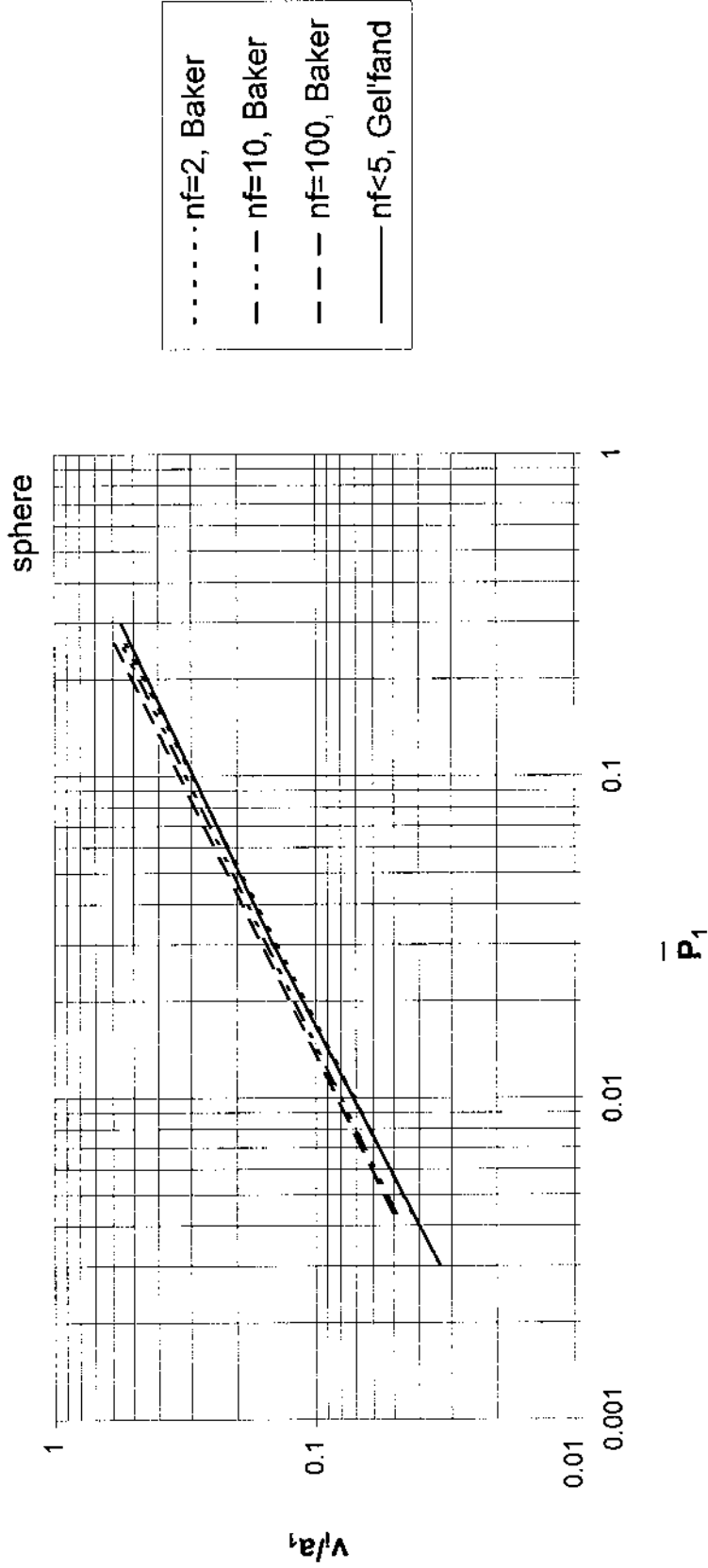
Figure 7.11a Fragment velocity versus scaled pressure for a sphere with ideal gas (n_f is number of fragments)
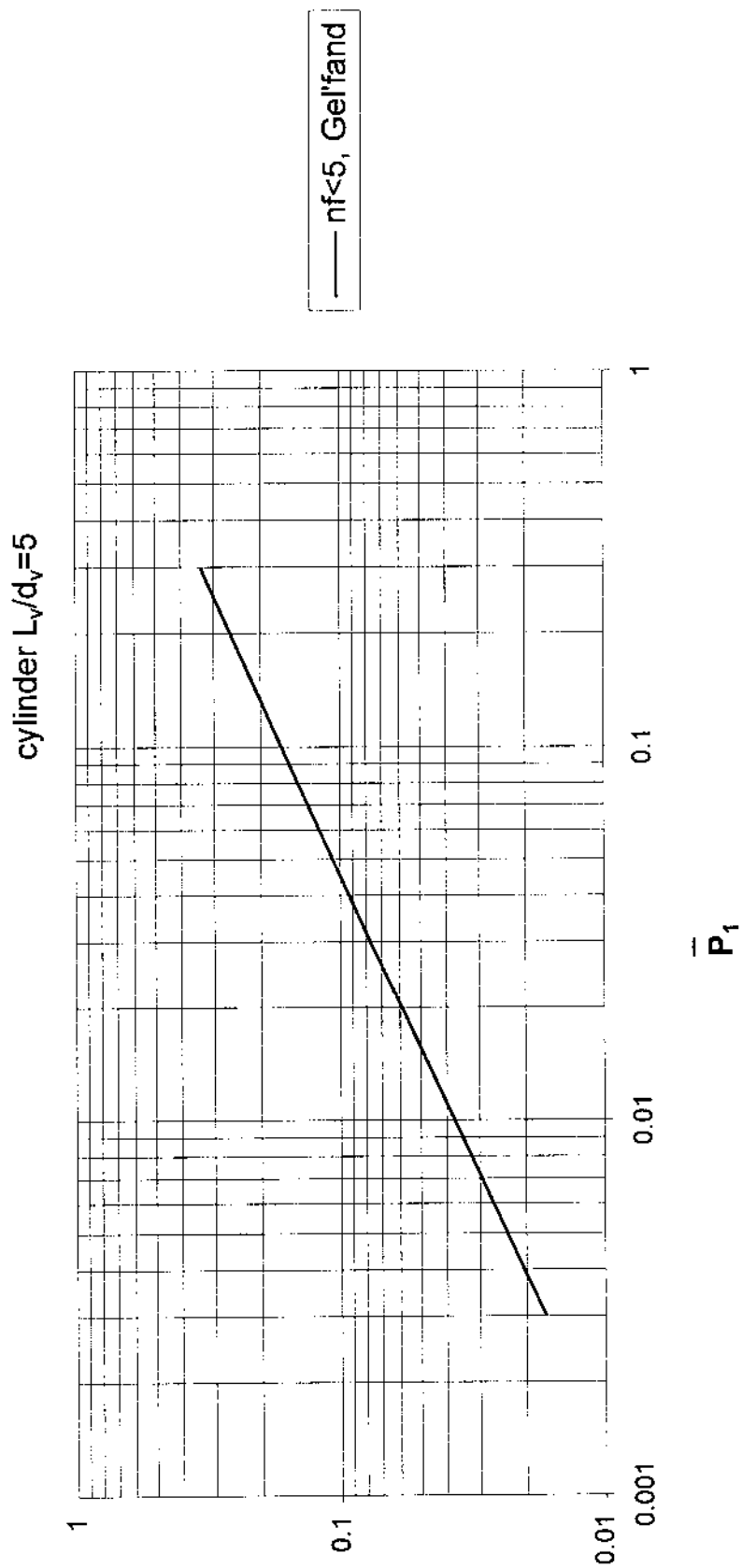
Figure 7.11b Fragment velocity versus scaled pressure for a cylinder with a length-diameter ratio of 5, filled with an ideal gas (n_f is number of fragments)
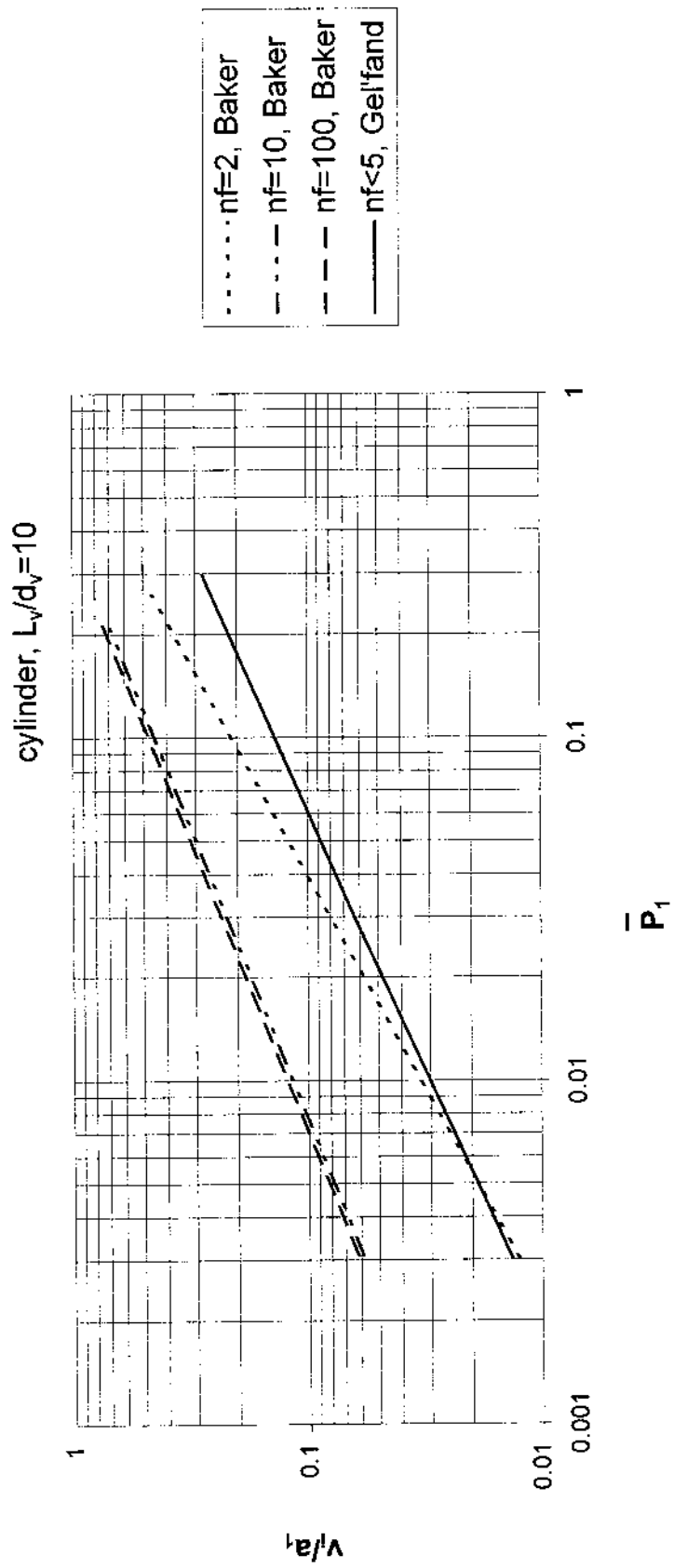
Figure 7.11c Fragment velocity versus scaled pressure for a cylinder with a length-diameter ratio of 10, filled with an ideal gas (n_f is number of fragments)
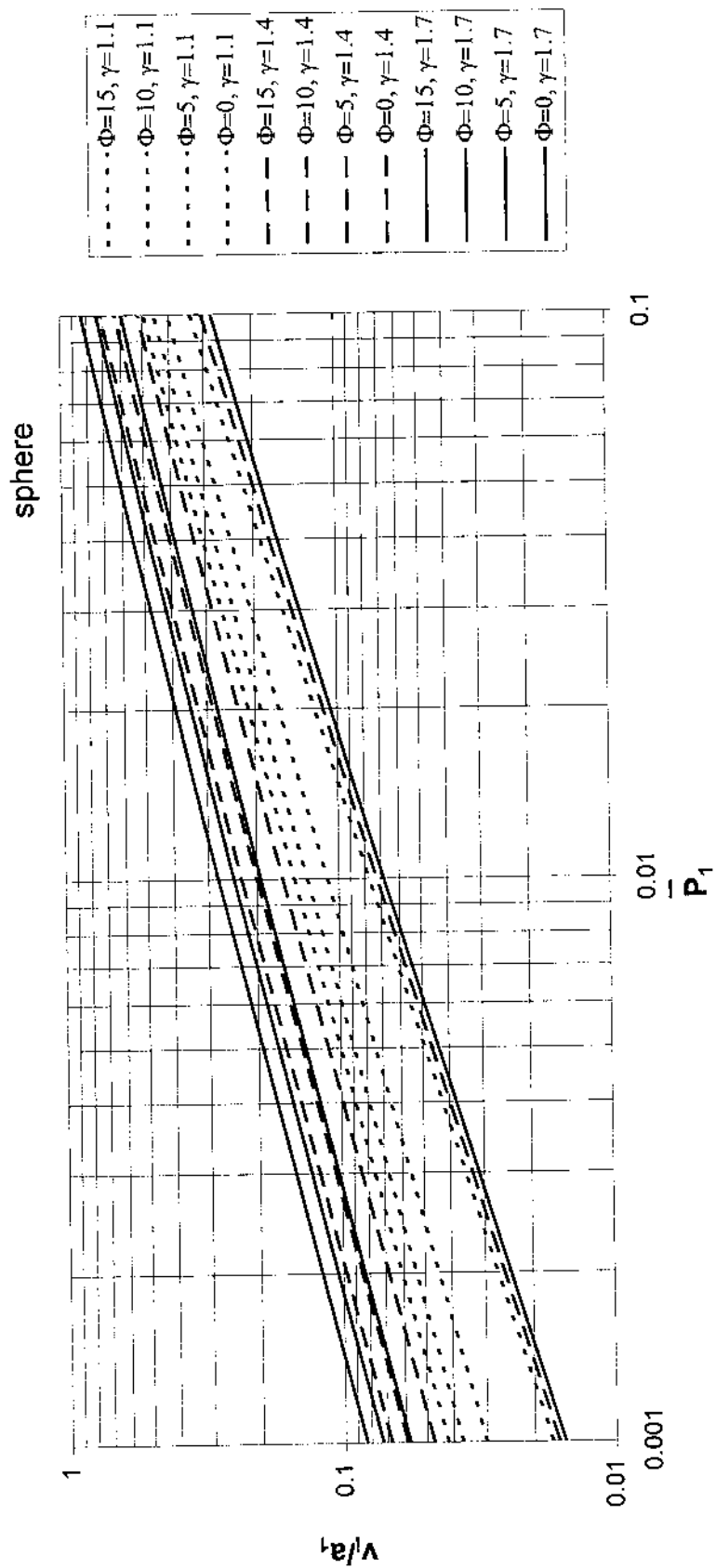
Figure 7.11d Fragment velocity versus scaled pressure for a sphere, ruptured because of a runaway reaction (lines are in the same order as in the legend).
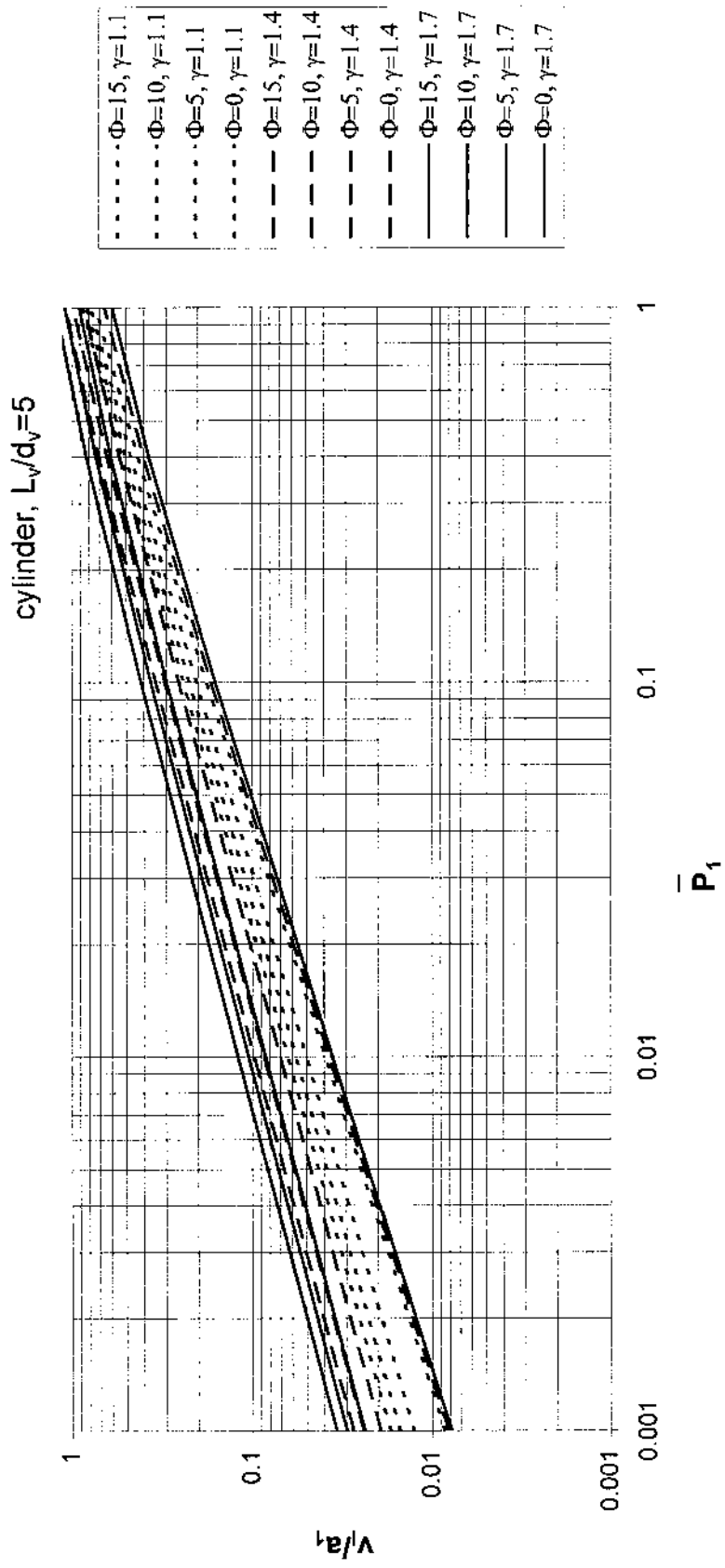
Figure 7.11e Fragment velocity versus scaled pressure for a cylinder with a length-diameter ratio of 5, ruptured because of a runaway reaction (lines are in the same order as in the legend).
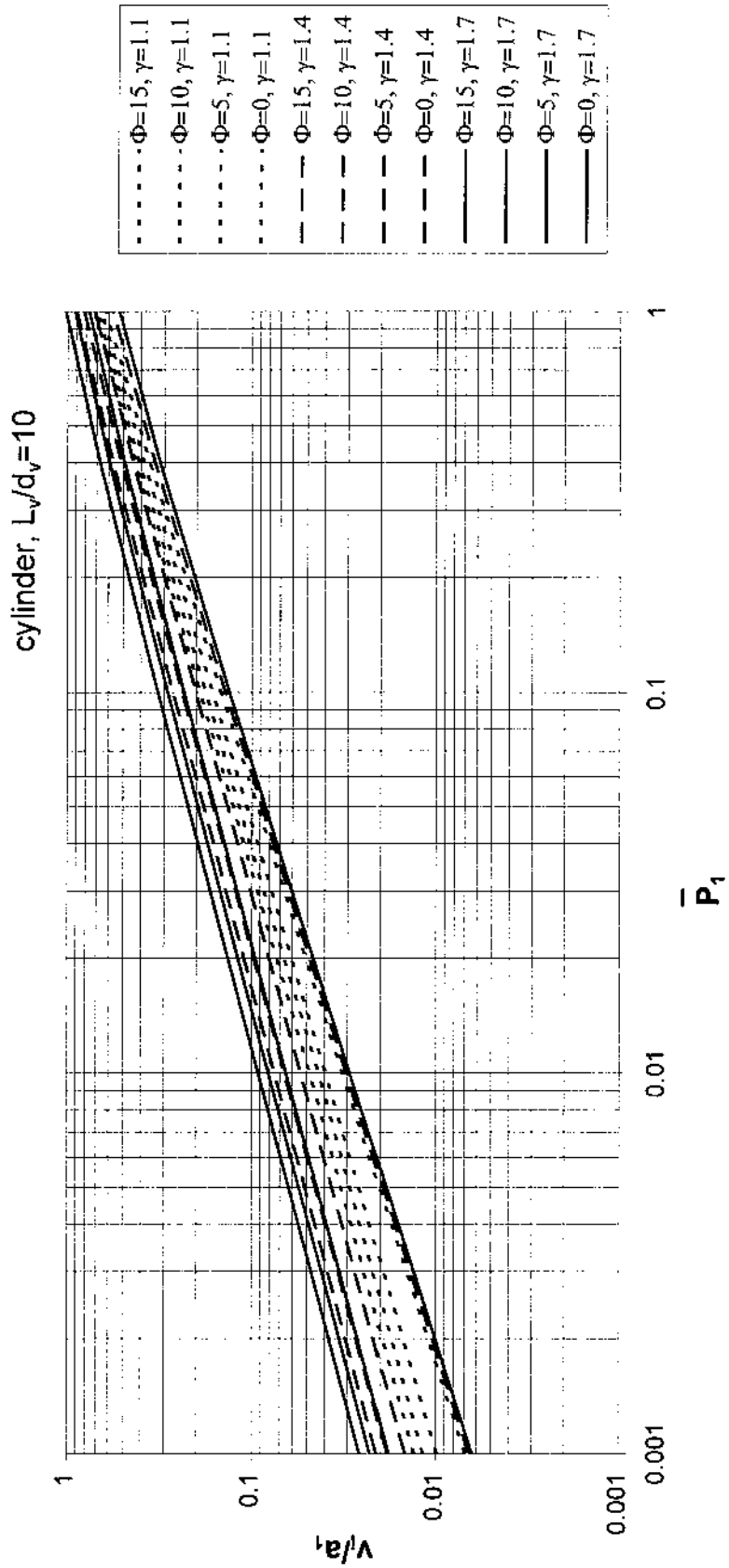
Figure 7.11f Fragment velocity versus scaled pressure for a cylinder with a length-diameter ratio of 10, ruptured because of a runaway reaction (lines are in the same order as in the legend).

Step 3c   Moore's empirical formula for the initial fragment velocity in case of a high scaled pressure $\overline{P}_1$, decomposition of energetic materials, or to check the calculated v_i.

Step 3c1   Collect data

Collect the same data as collected in step 1 of the method for calculating the blast effects, see paragraph 7.5.2. Determine also the total mass of the empty vessel M_v and the mass of the gas inside the vessel M_c.

Step 3c2   Calculate the liberated energy, E_{av}

Calculate the liberated energy in accordance with the method for blast effects, see paragraph 7.5.2.

Step 3c3 Calculate initial velocity, v_i

This initial velocity can be calculated by using of the following equation:

$$v_i = 1.092\left[\frac{E_{av}A_M}{M_v}\right]^{0.5} \qquad\qquad \text{(m/s)} \qquad (7.18)$$

$$\text{where for spherical vessels } A_M = \frac{1}{1 + 3M_c/5M_v} \qquad\qquad \text{(-)} \qquad (7.19)$$

$$\text{and for cylindrical vessels } A_M = \frac{1}{1 + M_c/2M_v} \qquad\qquad \text{(-)} \qquad (7.20)$$

Step 3c4   Check v_i, calculated according to other method

If the initial velocity calculated before is higher than according to Moore's empirical relation, then this velocity is too high. Use the value found with Moore's equation. Continue with step 4.

Step 4   Calculate range of flying fragments

After a fragment is accelerated to a certain initial velocity, the forces acting upon it during flight are those of gravity and fluid dynamics (lift and drag). These forces determine the distance a fragment can fly.

Figure 7.12 plots scaled maximum range $\overline{R}_f$ and scaled initial velocity $\overline{v}_i$ as a function of the lift-to-drag ratio C_LA_L/C_DA_D. This figure is based on the assumption that fragment orientation remains constant with respect to the trajectory (constant angle of attack). The scaled parameters are defined by

$$\overline{R}_f = \frac{\rho_a C_D A_D R_f}{M_f} \qquad (-) \qquad (7.21)$$

$$\overline{v}_i = \frac{\rho_a C_D A_D v_i^2}{M_f g} \qquad (-) \qquad (7.22)$$

where

$\overline{R}_f$	=	scaled maximal range	[-]
R_f	=	maximal range	[m]
$\overline{v}_i$	=	scaled initial velocity	[-]
v_i	=	initial velocity	[m/s]
ρ_a	=	density of ambient atmosphere	[kg/m^3]
C_D	=	drag coefficient	[-]
C_L	=	lift coefficient	[-]
A_D	=	exposed area in plane perpendicular to trajectory	[m^2]
A_L	=	exposed area in plane parallel to trajectory	[m^2]
g	=	gravitational acceleration	[m/s^2]
M_f	=	mass of fragment	[kg]
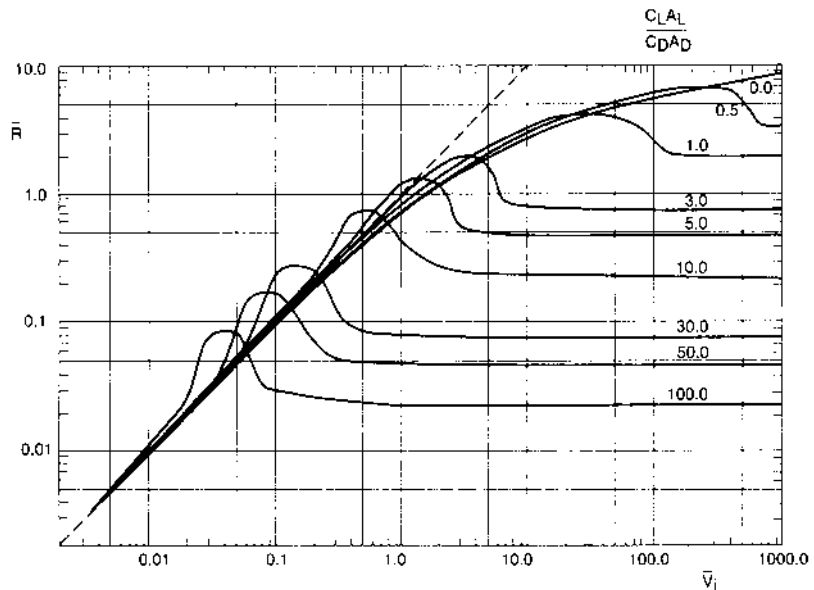
Figure 7.12   Scaled curves for fragment range predictions. ----: solution for no wind resistance, $R_f = v_i^2/g$

Using Figure 7.12 the maximum fragment range can be predicted as follows.

Step 4a   Determine the following parameters
- ρ_a, density of ambient atmosphere (kg/m^3)
- the (average) value for $C_D A_D$ (m^2), by using Table 7.8. The average value is needed in case of tumbling, which often occurs.
- the value for the lift-to-drag ratio $C_L A_L / C_D A_D$, with use of Table 7.8. For blunt and tumbling objects the lift equals zero.

Table 7.8   Drag and lift of fragments

Shape	C_DA_D	C_LA_L/C_DA_D
Plate (tumbling)	$0.585 \times A_{plate}$	0
Plate (no tumbling, face on)	$1.17 \times A_{plate}$	0
Plate (no tumbling, edge on)	$0.1 \times A_{plate}$	0 to 10[1)]
Hemisphere (tumbling)	$0.615 \times \pi/4 \times d_v^2$	0
Hemisphere (no tumbling)	$0.47 \times \pi/4 \times d_v^2$	0
Half a tank (rocketing)	$0.47 \times \pi/4 \times d_v^2$	0
Cylinder (edge on)	$1.20 \times d_v \times L_v$	0
Strips (tumbling)	$0.99 \times A_{strip}$	0

[1)]   The value depends on the plate's angle. Use the value which gives
       the maximum fragment range, or calculate a number of possible
       ranges.

Step 4b   Calculate the scaled initial velocity

The scaled initial velocity is given by equation (7.22).

$$\bar{v}_i \;=\; \frac{\rho_a C_D A_D v_i^2}{M_f g} \qquad\qquad (\text{-}) \qquad\qquad (7.22)$$

Step 4c   Read scaled maximal range from Figure 7.12

Step 4d   Calculate R_f

By using of equation (7.21) the maximal range R_f can be calculated.

$$\bar{R}_f \;=\; \frac{\rho_a C_D A_D R_f}{M_f} \qquad\qquad (\text{-}) \qquad\qquad (7.21)$$

7.6 Application of selected methods: calculation examples

7.6.1 Introduction to section 7.6

Bursting vessels can generate blast and propel fragments to several hundred metres distance. In this section calculation methods to predict the hazards of vessel bursts are demonstrated. The calculation methods have been described in section 7.5.

Section 7.6.2 and 7.6.3 respectively provide examples of blast effects and of fragmentation effects. In all these examples, one tank is considered with its environment. Different types of vessel bursts are studied by assuming different contents for the tank.

In the examples, data are just listed and equations are used without repeating them. The numbers of the equations are given, so that the reader can easily retrace them in section 7.5. Decision points are explained in accordance with the flow charts.

Like the description of the test method, the examples are also presented stepwise. The numbers of each step in the examples correspond to those in the description of the methods and in the chart flows.

7.6.2 Example 1: blast effects

Consider a cylindrical vessel, used for the storage of propane, which has been repaired. After the repair, the vessel is pressure tested with nitrogen gas at a pressure 25% above the design pressure. If the vessel bursts during the test, a large storage tank, located 15 m from the vessel, and a control building, located 100 m from the vessel, might be endangered. What would be the side-on overpressure and impulse at these points?

After a successful pressure test, the vessel is re-entered into service. The safety valve is set at 1.5 MPa (15 bar) overpressure. What might happen if the vessel was exposed to a fire? Consider the vessel being filled for 80% with propane.

Solution for gas-filled vessel

Step 1   Collect data

a. Nitrogen at ambient temperature can be regarded as an ideal gas.
b. Since the vessel contains an ideal gas, we are dealing with a pressure vessel burst.
c. The design overpressure of the vessel is 1.92 MPa, the test pressure is 25% higher. Therefore, the absolute internal pressure p_1 is:

$$p_1 = 1.25 \times 1.92 \times 10^6 + 0.1 \times 10^6 = 2.5 \text{ MPa (25 bar)}$$

d. The ambient pressure p_a is 101325 Pa.
e. The volume of the vessel is 25 m^3.
f. The ratio of specific heats of nitrogen, γ_1, is 1.40.
g. The distance from the centre of the vessel to the 'target', r_t, is 100 m for the control building and 15 m for the large storage tank.
h. The shape of the vessel is cylindrical. It is placed horizontally, on the ground.

Step 2   Energy calculation

The energy of the compressed gas is calculated using equation (7.1).
Substitution gives:

$$E_{av} = \frac{(2.5 \times 10^6 - 0.1 \times 10^6) \times 25}{1.4 - 1} = 150 \text{ MJ}$$

Step 6   Effective blast energy

Assuming that all energy is available for blast energy and using the fact that the vessel is placed on the ground, the calculated liberated energy must be multiplied by a factor 2 in order to obtain the effective blast energy. So, E_{ex} = 300 MJ.

Step 7   Calculate the non-dimensional distance $\overline{R}$ of the acceptor.

The non-dimensional range $\overline{R}$ is calculated using equation (7.8).
Substitution gives for the control building:

$$\overline{R} = 100 \times \left(\frac{0.1 \times 10^6}{300 \times 10^6}\right)^{1/3} = 6.97$$

And for the large storage tank: $\overline{R}$ = 1.05

Step 8   Check $\overline{R}$

The non-dimensional range $\overline{R}$ is checked to see whether the basic method can be followed or the refined method must be used. The control building lies at a non-dimensional range of 6.9, so the basic method can be followed. The range of the large storage tank is less than 2, so the refined method must be used to obtain an accurate result.

First, the blast parameters at the control building will be determined.

Step 9   Determine $\overline{P}_s$

The non-dimensional side-on peak overpressure $\overline{P}_s$ at the control building is read from Figure 7.6. For $\overline{R}$ = 6.9, $\overline{P}_s$ = 0.028.

Step 11   Determine $\overline{I}$

The non-dimensional side-on impulse $\overline{I}$ at the control building is read from Figure 7.10. For $\overline{R}$ = 6.9, $\overline{I}$ = 0.0075.

Step 12   Adjust $\overline{P}_s$ and $\overline{I}$ for geometry effects

To account for the fact that the blast wave from the vessel will not be perfectly symmetrical, $\overline{P}_s$ and $\overline{I}$ are adjusted, depending on $\overline{R}$. To account for a cylindrical vessel, $\overline{P}_s$ is multiplied by 1.4. Thus, $\overline{P}_s$ becomes:

$$\overline{P}_s = 1.4 \times 0.028 = 0.0391$$

No adjustment of $\overline{I}$ is necessary at this range.

Step 13   Calculate p_s and i_s

To calculate the side-on peak overpressure p_s - p_a and the side-on impulse i_s from the non-dimensional side-on peak overpressure $\overline{P}_s$ and the non-dimensional side-on impulse $\overline{I}$, equations (7.13) and (7.14) are used.
The ambient speed of sound a_a is approximately 340 m/s. Substitution gives:

$$p_s - p_a = 0.0391 \times 101325 = 3.97 \text{ kPa}$$

$$i_s = (0.0075 \times (101325)^{2/3} \times (300 \times 10^6)^{1/3}) / 340 = 32 \text{ Pa·s}$$

Step 14   Check p_s

Because the accuracy of this method is limited, p_s needs to be checked against p_1. In this case, p_s is much smaller than p_1, so no corrections have to be made.
Thus, the calculated blast parameters at the control building are: a side-on peak overpressure of 3.97 kPa and a side-on impulse of 32 Pa·s.

As shown above, the distance to the large storage tank is too small to use the basic method with good results. Therefore, the refined method is used to calculate the blast parameters at the large storage tank.

Step 10a   Collect additional data

− The ratio of the speed of sound in the compressed nitrogen and the speed of sound in the ambient air, a_1/a_a, is approximately 1.
− The ratio of specific heats of the ambient air is 1.40.

Step 10b   Calculate the starting distance

The starting distance is computed with equation (7.10). Substitution gives:

$$r_0 = 0.782 \times 25^{1/3} = 2.29 \text{ m}$$

r_0 must be transformed into the non-dimensional starting distance $\overline{R}_0$ with equation 7.11. Substitution gives:

$$\overline{R}_0 = 2.29 \times (0.1 \times 10^6 / 300 \times 10^6)^{1/3} = 0.16$$

Step 10c   Calculate the initial peak overpressure $\overline{P}_{so}$

The non-dimensional peak overpressure of the shock wave directly after the burst of the vessel, $\overline{P}_{so}$, can be read from Figure 7.7. The result is: $\overline{P}_{so} = 3.05$, eight times less than the initial pressure in the vessel.

Step 10d   Locate the starting point on Figure 7.5

To select the proper curve in Figure 7.5, the starting point $\overline{R}_0$, $\overline{P}_{so}$ is drawn in the figure.

Step 10e   Determine $\overline{P}_s$

To determine the non-dimensional side-on peak overpressure $\overline{P}_s$ at the large storage tank, $\overline{P}_s$ is read from Figure 7.5. The non-dimensional distance was computed before as $\overline{R} = 1.05$. Following the curve from the starting point, a $\overline{P}_s$ of 0.36 is found. The procedure is continued with step 11.

Step 11   Determine $\overline{I}$

The non-dimensional side-on impulse $\overline{I}$ at the tank is read from Figure 7.9. For $\overline{R} = 1.05$, $\overline{I} = 0.048$.

Step 12   Adjust $\overline{P}_s$ and $\overline{I}$ for geometry effects

To account for the fact that the blast wave from the vessel will not be perfectly symmetrical, $\overline{P}_s$ and $\overline{I}$ are adjusted, depending on $\overline{R}$. To account for the vessel's placement slightly above ground level, $\overline{P}_s$ is multiplied by 1.1. To account for the cylindrical shape of the vessel, $\overline{P}_s$ is multiplied by 1.6 and $\overline{I}$ is multiplied by 1.1. Thus, $\overline{P}_s$ and $\overline{I}$ become:

$$\overline{P}_s = 1.6 \times 0.36 = 0.576$$

$$\overline{I} = 1.1 \times 0.048 = 0.053$$

Step 13   Calculate p_s and i_s

To calculate side-on peak overpressure p_s - p_a and side-on impulse i_s from the non-dimensional side-on peak overpressure $\overline{P}_s$ and the non-dimensional side-on impulse $\overline{I}$, equation (7.13) and (7.14) are used.

The ambient speed of sound a_a is approximately 340 m/s. Substitution gives:

$$p_s - p_a = 0.576 \times 101325 = 58 \text{ kPa}$$

$$i_s = 0.053 \times (101325)^{2/3} \times (300 \times 10^6)^{1/3}) / 340 = 225 \text{ Pa·s}$$

Step 14   Check p_s

Because the accuracy of this method is limited, p_s needs to be checked against p_1. In this case, p_s is much smaller than p_1, so no corrections have to be made.
Thus, the calculated blast parameters at the large storage vessel are: a side-on peak overpressure of 63 kPa and a side-on impulse of 230 Pa.s.

Solution for liquid-filled vessel

Step 1   Collect data

a. The vessel contains pressure liquefied propane.
b. The possible type of vessel burst is a BLEVE.
c. The failure overpressure is assumed to be 1.21 times the opening pressure of the safety valve. Thus, p_1 is:

$$p_1 = 1.21 \times 1.5 + 0.1 = 1.9 \text{ MPa (19 bar)}$$

d. The ambient pressure p_a is assumed to be 101325 Pa.
e. The volume of the vessel is 25 m^3.
f. The distance from the centre of the vessel to the receptor is 100 m for the control building and 15 m for the large storage tank.
g. The shape of the vessel is cylindrical. It is placed horizontally, on saddles.
h. The ambient temperature is 293 K. The temperature of saturated propane at a vapour pressure of 1.9 MPa is 327.7 K.

Step 3   Check temperature of liquid

The boiling temperature and superheat limit temperature are given in Perry and Green [1984]: T_b = 231 K, T_{sl} = 326 K. The temperature of the propane is above superheat limit temperature. So, a BLEVE may occur.

Step 4a   Check if the fluid is in Table 7.2 or Figure 7.3

Although the specific expansion energy of propane is included in the list of fluids in Figure 7.3, steps 4b to 4d are followed for this demonstration. It will be demonstrated both by using a thermodynamic graph and a thermodynamic table.

Step 4b and 4c using a thermodynamic table

Step 4b   Determine u_1

Thermodynamic data for propane can be found in e.g. Perry and Green [1984]. These are presented in Table 7.9.

Table 7.9   Thermodynamic data for propane

T_1 (K)	p_1 (MPa)	h_f (kJ/kg)	h_g (kJ/kg)	v_f (m³/kg)	v_g (m³/kg)	s_f (kJ/kgK)	s_g (kJ/kgK)
327.7	1.90	674.31	948.32	2.278×10^{-3}	0.0232	4.7685	5.6051
230.9	0.10	421.27	849.19	1.722×10^{-3}	0.419	3.8721	5.7256

The vessel is assumed to be filled with saturated liquid and vapour. The specific internal energy of the saturated liquid can be computed by substituting the appropriate thermodynamic data of Table 7.9 in equation (7.2):

$$u_1 = 674.31 \times 10^3 - 1.90 \times 10^6 \times 2.278 \times 10^{-3}$$

It follows that: $u_1 = 669.98$ kJ/kg.
The specific internal energy of the saturated vapour can be computed in the same way:

$$u_1 = 948.32 \times 10^3 - 1.90 \times 10^6 \times 0.0232 = 904.24 \text{ kJ/kg}$$

Step 4c   Determine u_2

The specific internal energy of the fluid after expansion to the ambient pressure, u_2, is calculated using equation (7.3).
For the saturated liquid, the vapour ratio X is:

$$X = (4.7685 - 3.8721) / (5.7256 - 3.8721) = 0.484$$

and u_2 is:

$$u_2 = (1 - 0.484) \times 421.27 \times 10^3 + 0.484 \times 849.19 \times 10^3 -$$

$$(1 - 0.484) \times 0.1 \times 10^6 \times 1.722 \times 10^{-3} - 0.484 \times 0.1 \times 10^6 \times 0.419$$

$$= 608.01 \text{ kJ/kg}$$

For the saturated vapour, X = 0.935 and $u_2 = 782.19$ kJ/kg

Step 4b and 4c using a thermodynamic graph

Step 4b   Determine u_1

Figure 7.13 gives an schematic view of the enthalpy-pressure graph of propane. Clearly visible is the curve indicating the saturated state. The top of this curve is the critical point. On the left of this point is the liquid state, and on the right the vapour state. The graph also shows lines of constant temperature T, constant specific volume v, constant entropy s and constant vapour ratio X. The thermodynamic data can also be drawn in other types of graphs, e.g. an enthalpy-entropy graph.
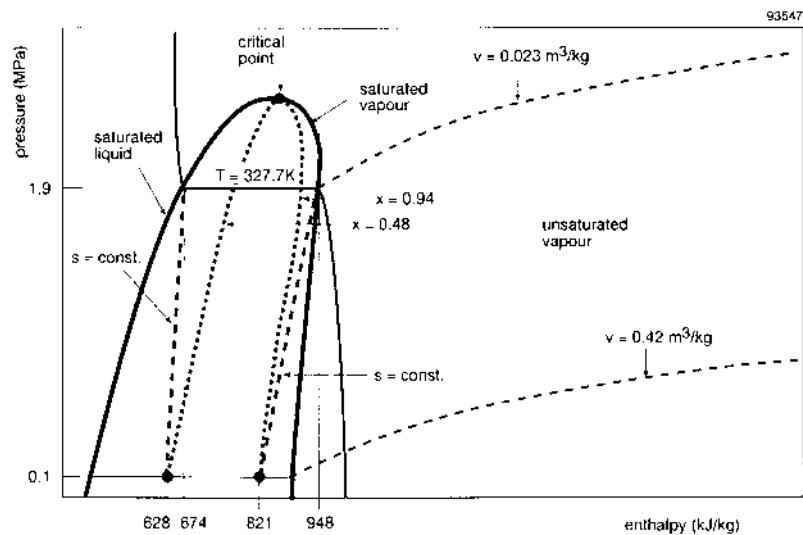
Figure 7.13   Enthalpy-pressure graph of propane (schematic)

The vessel is assumed to be filled with saturated liquid and saturated vapour. The specific internal energy of the saturated liquid can be computed with equation (7.2). The initial state can be found on the graph by locating the point on the saturated liquid curve which has a pressure of 1.9 MPa. The specific enthalpy of that state is 674 kJ/kg. The specific volume of this state cannot be read from the graph. It can be assumed that it is negligible. This gives for the specific internal energy:

$$u_1 = 674 \times 10^3 - 1.90 \times 10^6 \times 0.0$$

It follows that: $u_1 = 674$ kJ/kg.
The specific internal energy of the saturated vapour can be computed the same way. In this case, the specific volume is not negligible.

$$u_1 = 948 \times 10^3 - 1.90 \times 10^6 \times 0.023 = 904.3 \text{ kJ/kg}$$

Step 4c   Determine u_2

The state of the fluid after expansion can be found by following the constant entropy curve from the initial state to the state with atmospheric pressure. The final state is a mixture of liquid and vapour if the initial state is saturated liquid or vapour. The specific enthalpy of the final state can be read directly from the graph: $h_2 = 6.28 \cdot 10^3$ J/kg. The specific volume must be computed from the vapour ratio X in the final state and the specific volume v of the saturated liquid and vapour at atmospheric pressure.

$$v_2 = (1 - X)v_f + Xv_g \qquad\qquad (m^3/kg) \qquad\qquad (7.23)$$

In practice, the specific volume of the saturated liquid is negligible, so the specific volume after expansion from the saturated liquid state becomes:

$$v_2 = 0.48 \times 0.42 = 0.20 \ m^3/kg$$

This results in:

$$u_2 = 628 \times 10^3 - 0.1 \times 10^6 \times 0.20 = 608 \ kJ/kg$$

for the specific internal energy after expansion from the saturated liquid state.

Similarly, for expansion from the saturated vapour state the specific volume in the final state is 0.395 m^3/kg and $u_2 = 782$ kJ/kg

Step 4d   Calculate the specific work

The specific work done by the fluid in expansion is calculated using equation 7.4. Substitution of the values for the saturated liquid gives:

$$e_{av} = 669.98 \times 10^3 - 608.01 \times 10^3 = 61.97 \ kJ/kg$$

and for the saturated vapour:

$$e_{av} = 904.24 \times 10^3 - 782.19 \times 10^3 = 122.05 \ kJ/kg$$

Note that these values could also have been read from Figure 7.3.

Step 4e   Calculate the energy of the explosion

The energy of the explosion is calculated using equation (7.5). In this equation the mass of the released liquid is given by dividing the volume of the released liquid by its specific volume.
When the vessel is full, 80% of the volume is occupied by liquid. The mass of the liquid is approximately:

$$M_{fl} = 0.80 \times 25 / 2.278 \times 10^{-3} = 8780 \ kg$$

In fact, the specific volume of propane at ambient temperature should have been used, but that makes little difference in the result.

The mass of the vapour is:

$M_{fl} = 0.20 \times 25 / 0.0232 = 215.5$ kg

For the explosion energy for the saturated liquid, this results in:

$E_{av} = 61.97 \times 10^3 \times 8780 = 544.1$ MJ

and for the saturated vapour:

$E_{av} = 122.05 \times 10^3 \times 215.5 = 26.3$ MJ

Assuming that the blast of the expansion of the vapour is synchronous with the blast from the flashing of the liquid, the total energy of the surface explosion is:

$E_{av} = 544.1 \times 10^6 + 26.3 \times 10^6 = 570.4$ MJ

Step 6   *Determine the effective blast wave energy*

The available energy must be multiplied by 2 because it is a surface explosion. So,

$E_{ex} = 2 \times 570.4 = 1140.8$ MJ

Step 7   *Calculate $\overline{R}$ of receptor*

The non-dimensional range of the 'target' is calculated using equation (7.8). This results for the large storage vessel in:

$\overline{R} = 15 \times (101325 / 1140.8 \times 10^6)^{1/3} = 0.67$

and for the control building:

$\overline{R} = 100 \times (101325 / 1140.8 \times 10^6)^{1/3} = 4.5$

Computations are continued with step 9.

Step 9   *Determine $\overline{P}_s$*

The non-dimensional side-on peak overpressure $\overline{P}_s$ at the large storage tank is read from Figure 7.5. The non-dimensional distance $\overline{R} = 0.67$. Reading from the curve labelled 'high explosive', a $\overline{P}_s$ of 1.12 is found.
The procedure is continued with step 11.

Step 11   Determine $\bar{I}$

The non-dimensional side-on impulse $\bar{I}$ at the tank is read from Figure 7.10. For $\bar{R} = 0.67$, $\bar{I} = 0.068$.

Step 12   Adjust $\bar{P}_s$ and $\bar{I}$ for geometry effects

To account for the fact that the blast wave from the vessel will not be perfectly symmetrical, $\bar{P}_s$ and $\bar{I}$ are adjusted, depending on $\bar{R}$. The multiplication factors to account for the cylindrical shape are taken from Tables 7.3 and 7.4.
Thus $\bar{P}_s$ and $\bar{I}$ become:

$$\bar{P}_s = 1.6 \times 1.12 = 1.79$$

$$\bar{I} = 1.1 \times 0.068 = 0.075$$

Step 13   Calculate p_s and i_s

To calculate the side-on peak overpressure $p_s - p_a$ and the side-on impulse i_s from the non-dimensional side-on peak overpressure $\bar{P}_s$ and the non-dimensional side-on impulse $\bar{I}$, equation (7.13) and (7.14) are used. The ambient speed of sound a_a is approximately 340 m/s. Substitution gives:

$$p_s - p_a = 1.79 \times 101325 = 181.7 \text{ kPa (1.82 bar)}$$

$$i_s = (0.075 \times (101325)^{2/3} \times (1140.8 \times 10^6)^{1/3}) / 340 = 501 \text{ Pa·s}$$

Step 14   Check p_s

Because the accuracy of this method is limited, p_s needs to be checked against p_1. In this case, p_s is smaller than p_1, so no corrections are necessary.
Thus, the calculated blast parameters at the large storage vessel are: a side-on peak overpressure of 182 kPa and a side-on impulse of 501 Pa.s.

The same procedure must be followed to calculate the pressure and impulse at the control building. A side-on peak overpressure of 6.6 kPa and a side-on impulse of 79 Pa.s can be found.

Note the following points:
− The explosion of the propane filled vessel has much more energy than the gas-filled vessel, and therefore causes a much more severe blast.
− This calculation takes into account only the blast from the expansion of the contents of the vessel. In fact, this blast may be followed by a blast from a vapour cloud explosion or heat radiation from the fireball of the BLEVE. These possibilities must be considered separately, with the methods presented in other chapters, see section 7.7.

7.6.3   Example 2: fragments

As an example to demonstrate the use of the theoretically and empirically derived equations for fragmentation effects, the vessel of example 1 is considered again. As additional information it is given that the vessel has hemispherical end caps with a mass of 193 kg, a mass of 3859 kg and a length-to-diameter ratio of 10.
Two different situations will be examined for maximum fragment range: failure during testing, and failure due to an external fire.

Case 1: Failure during testing

Step 1   Estimate number of fragments

Since we have to do with a cylindrical vessel, it is most probable that it will break into two or three parts.

Step 2   Estimate fragment mass

It is most probable that the vessel will break at the end caps. Each end cap has a mass of 193 kg. The cylinder has a mass of 3859 - 2 × 193 = 3473 kg.

Step 3   Calculate initial fragment velocity

Step 3a   Calculate a rough estimate for the initial fragment velocity using the kinetic energy method

In example 1 an energy of 150 MJ has been calculated.
The following initial velocity is found:

$$v_i = \left(\frac{2 \times 0.2 \times 150 \times 10^6}{3859}\right)^{0.5} = 125 \text{ m/s}$$

Step 3b   Calculate initial fragment velocity using Baker's or Gel'fand's method

The speed of sound in the gas at failure is:

$$a_i = \left(\frac{293 \times 1.40 \times 8314.51}{28.01}\right)^{0.5} = 349.2 \text{ m/s}$$

The value of the scaled pressure equals (equation 7.16):

$$\bar{P}_1 = \frac{(2.5 \times 10^6 - 101325) \times 25}{3859 \times 349.2^2} = 0.133$$

The proper chart for the present example is given in Figure 7.11c. From this chart it can be read that v_i/a_1 equals 0.16 according to Gel'fand's method. So,

$$v_i = 0.16 \times a_1 = 0.16 \times 349.2 = 55.6 \text{ m/s}$$

Or with Baker's method, $\bar{v}_i = 0.296$. So,

$$v_i = 0.296 \times a_1 = 0.296 \times 349.2 = 103.3 \text{ m/s}$$

Note that Baker's method is more conservative. Note that by applying the rough method in the present example, the velocity is overestimated.

Step 3c   Check with Moore's equation

The total mass of nitrogen in the vessels follows from the ideal gas law

$$M_c = \frac{p_1 V_g}{T_g R} \times \mu_i = \frac{2.5 \times 10^6 \times 25}{293 \times 8.31} \times 28.013 \times 10^{-3} = 720 \text{ kg}$$

Equation (7.20) gives

$$A_M = \frac{1}{1 + 720/(2 \times 3859)} = 0.915$$

Substitution in equation (7.18) gives

$$v_i = 1.092 \times \left[\frac{150 \times 10^6 \times 0.915}{3859}\right]^{0.5} = 206 \text{ m/s}$$

This value is much higher than the initial velocity according to Gel'fand's method or Baker's method. No correction is necessary, $v_i = 103.3$ m/s according to Baker's method.

Step 4   Calculate maximal range

The maximal range is calculated here for the end cap. For the range of the rest of the cylinder the calculation is similar.

Step 4a   Collect data

- $\rho_a = 1.20 \text{ kg/m}^3$
- The end cup will probably be tumbling. Therefore the drag and lift coefficients for a tumbling hemisphere are used. The vessel diameter is 1.50 m.
- $C_D A_D = 0.615 \times \pi/4 \times 1.50^2 = 1.087 \text{ m}^2$
- $C_L A_L / C_D A_D = 0$

Step 4b   Calculated scaled initial velocity with equation (7.22)

$$\bar{v}_i = \frac{1.2 \times 1.087 \times 103.3^2}{193 \times 9.81} = 7.35$$

Step 4c   Read $\overline{R}_f$ from Figure 7.12

$\overline{R}_f \approx 2.38$

Step 4d   Calculate R_f with equation (7.21)

$$R_f = \frac{\overline{R}_f M_f}{\rho_a C_D A_D} = \frac{2.38 \times 193}{1.2 \times 1.087} = 352 \text{ m}$$

It can be concluded that both the storage tank and the control building may be hit by the end cap.

Case 2: Failure due to external fire

Step 1   Estimate number of fragments

Due to the external fire the vessel is locally weakened. Therefore, it is most probable that it will break into two parts.

Step 2   Estimate fragment mass

The fragment mass depends on the location of impingement of the fire. We assume that the vessel will break into two equal parts with a mass of 3859/2 = 1930 kg.

Step 3   Calculate initial fragment velocity

Step 3a   Calculate the initial fragment velocity for a BLEVE

In example 1 an energy of 570.4 MJ has been calculated.
The following initial velocity is found:

$$v_i = \left(\frac{2 \times 0.04 \times 570.4 \times 10^6}{3859} \right)^{0.5} = 108.7 \text{ m/s}$$

Step 3c   Check with Moore's equation

The mass of vapour in the vessel has been calculated in step 4e of example 1: $M_{fl} = 215.5$ kg.

Equation (7.20) gives

$$A_M = \frac{1}{1 + 215.5 / (2 \times 3859)} = 0.97$$

Substitution in equation (7.18) gives

$$v_i = 1.092 \times \left[\frac{570.4 \times 10^6 \times 0.97}{3859} \right]^{0.5} = 414 \text{ m/s}$$

This value is much higher than the initial velocity according to Baum's method. No correction is necessary. $v_i = 108.7$ m/s.

Step 4   Calculate maximal range

We assume that each half of the vessel will travel parallel to its original axis.

Step 4a   Collect data

− $\rho_a = 1.20$ kg/m^3
− $C_D A_D = 0.47 \times \pi/4 \times 1.50^2 = 0.831$ m^2
− $C_L A_L/C_D A_D = 0$

Step 4b   Calculated scaled initial velocity with equation (7.22)

$$\bar{v}_i = \frac{1.2 \times 0.831 \times 108.7^2}{1930 \times 9.81} = 0.62$$

Step 4c   Read $\overline{R}_f$ from Figure 7.12.

$$\overline{R}_f \approx 0.495$$

Step 4d   Calculate R with equation (7.21)

$$R_f = \frac{\overline{R}_f M_f}{\rho_a C_D A_D} = \frac{0.495 \times 1930}{1.2 \times 0.831} = 958 \text{ m}$$

It can be seen that such a rocketing fragment can travel large distances.

7.7 Interfacing with other models

Vessel rupture is an initial event. Therefore, there are no links from other models to the methods for vessel rupture.

The (total) rupture of a vessel causes several physical effects at the same time:
1. pressure effects,
2. fragments,
3. instantaneous release of chemicals in case of no ignition, and
4. buoyant fireballs in case of ignition of flammable chemicals.

The modelling of these simultaneous physical effects has been carried out fully independently.
Complete models for coping with pressure effects and fragments are described in this chapter. The results of these models are not required by any other model in this Yellow Book.

The modelling of the instantaneous release of chemicals in case of no ignition has been described in Chapter 2 'Outflow and Spray release'. Subsequently, vapour cloud dispersion and vapour cloud explosion have been described in Chapter 4 and 5 respectively.
The modelling of the heat load caused by a buoyant fireball in case of ignition has been described in Chapter 6 'Heat load from fires'.

7.8   Discussion

The aim of this section is to discuss the applicability of the presented methods and to mention their limitations.

In this chapter the phenomena of vessel bursts have been described. Methods to predict blast and fragment effects have been presented and selected.
From the description of the phenomena has emerged that the result of a vessel burst, e.g. blast and fragments, strongly depends on the cause of the failure. Because of the complexity of the failure process and the number of variables, the research has not yet resulted in accurate prediction methods to quantify blast and fragment effects.
Based on the current knowledge of the phenomena methods have been selected which are generally applicable. With the selected and presented methods one can predict the blast effects and also the velocities and flight distances of fragments in a conservative way.
Because of lack of detailed knowledge of several aspects of the phenomena, the currently available methods have their limitations. In order to guide the user, the main limitations of the presented methods are listed below.

With respect to blast:
− A choice has to be made on which measure of explosion energy is responsible for the generation of blast. In the method presented in Section 7.5 the energy of a gas-filled pressure vessel and an internal explosion is calculated with Brode's formula (7.1), the energy for vessels filled with vapour by use of the formula for work done in expansion and for a chemical reaction by use of the chemical energy. Scientifically, this is annoying, because there is no good motivation for the choice of one measure of energy over another. In practice this is less of a problem, because the results of all formulae do not differ much. All these formulae give conservative results for the blast energy.
− In order to take the influence of the earth surface into account for the blast parameters, the results for high explosives have to be used, because insufficient data is available on vessel bursts. Because of the differences in the short range between the blast effects due to a vessel burst and an explosion of high explosives, the given procedure is conservative, as has been shown by a few experiments.
− More or less the same holds for the influence of non-spherical releases on blast parameters. Also for this situation the data from high explosives is used to take the effect into account.
− For BLEVEs, non-ideal gases, runaway reactions and internal explosions, no specific models have been developed. Therefore, an adaptation of the method for pressure vessel bursts with ideal gases is used. The necessary approximations for the non-ideal situations have been chosen in such a way that the presented method is conservative.

With respect to fragment generation:
− There is a lack of a solid experimental or theoretical basis to choose the fraction of explosion energy that contributes to fragment generation.
− The failure mode depends on parameters such as material, wall thickness and initial pressure. The number of fragments is not known in advance. Therefore, methods have been presented for predicting the effect of failure into two parts or failure into a large number of fragments.

In summary, the presented methods enable the user to predict the phenomena of blasts and fragments in a conservative way. Worst case scenarios can be predicted, but one should be well aware of the feature of conservatism if the methods are used for accident analysis.

7.9 Literature

Baker, W.E., Kulesz, J.J., Ricker, R.E., Bessey, R.L., Westine, P.S., Parr, V.B., Oldham, G.A. (1977),
Workbook for predicting pressure wave and fragment effects of exploding propellant tanks and gas storage vessels,
NASA CR-134906, NASA Scientific and Technical Information Office, Washington, D.C.

Baker, W.E., Kulesz, J.J. et al. (1978),
Workbook for estimating the effects of accidental explosions in propellant handling systems,
NASA Contractor report no. 3023, NASA Scientific and Technical Information Office, Washington, D.C.

Baker, W.E., Cox, P.A., Westine, P.S., Kulesz, J.J, Strewlow R.A. (1983),
Explosion Hazards and Evaluation,
Elsevier Publishing Company, Amsterdam.

Baum M.R. (1987),
Disruptive failure of pressure vessels: preliminary design guide lines for fragment velocity and the extent of the hazard zone,
Advances in Impact, Blast Ballistics and Dynamic Analysis of Structures, ASME PVP, Vol. 124., pp. 175-181.

Boyer, D.W., Brode, H.L., Glass, I.I., Hall, J.G. (1958),
Blast from a pressurized sphere,
UTIA Report No. 48, January 1958.

Brown, S.J. (1985),
Energy release protection for pressurized systems,
Part I. Review of studies into blast and fragmentation,
Appl. Mech. Rev., Vol. 38, No. 12, pp. 1625-1651, Dec. 1985.

Cain M.R, Sharp D.E., Coleman, M.D. (1992),
Pressure vessel burst test program / Progress report No. 3,
AIAA Paper 92-3608 920725, Presented at the 28th AIAA/SAE/ASME/ASEE Joint Propulsion Conference and Exhibit, Nashville, TN, 6-8 July 1992.

Esparza, and Baker, W.E. (1977),
Measurement of Blast Waves from Bursting Pressurized Frangible Spheres,
NASA CR-2843, National Aeronautics and Space Administration, Washington DC.

Gel'fand, B.E., Frolov, S.M., and Bartenev, A.M. (1989),
Calculation of the rupture of a high-pressure reactor vessel,
Combustion, Explosion and Shock Waves, Vol. 24, No. 4, pp. 488-496.

Grodzovskii, G.L. and Kukanov, F.A. (1965),
Motions of fragments of a vessel bursting in a vacuum,
Inzhenemyi Zhumal, Vol. 5, No. 2, pp. 352-355.

Guirao, C.M. et al. (1979),
On the Scaling of Blast Waveshock waves from Fuel-Air Explosives,
Proceedings of 6th Symposium on Blast Simulation, Cahors, France.

Heemskerk, A.H. (Ed.) (1995),
Guidelines for Chemical Reactivity Evaluation and Application to Process Design,
AIChE, Center for Chemical Process Safety, New York, 1995.

Huang, S.L., and Chou, P.C. (1968),
Calculations of Expanding Shock Waves and Late-Stage Equivalence,
Drexel Institute of Technology Report 125-12, April 1968.

Liepmann, H.W., and Roshko, A. (1967),
Elements of Gasdynamics,
John Wiley and Sons, Inc. New York.

Moore, C.V. (1967),
Nuclear Engineering and Design, Vol. 5, pp 81-97.

Perry, R.H., Green D. (1984),
Perry's Chemical Engineers' Handbook,
6th New York, McGraw-Hill.

Pittmann, J.F. (1976),
Blast and Fragments from Superpressure Vessel Rupture,
NSWC/WOL/TR 75-87, Naval Surface Weapons Center, White Oak, Silver Spring,
Maryland.

Reid, R.C. (1976),
Superheated Liquids,
Liquids in the superheated state, far from being a laboratory curiosity, occur more
often than thought and may cause industrial accidents,
American Scientist, Volume 64, March-April 1976, pp 146-156.

Rombouts, E. (1988),
Methoden voor het berekenen van physische effekten,
CPR-14, Tweede druk, 1988.

TM 5-1300 (1990),
Structures to resist the effects of accidental explosions,
Deparments of the Army, the Navy, and the Air Force, TM 5-1300, NAVFAC
P-397, AFR 88-22, Washington, DC, November 1990.

Venart, J.E.S., Rutledge, G.A., Sumathipala, K., Sollows, K. (1992),
To BLEVE or not to BLEVE: Anatomy of a Boiling Liquid Expanding Vapour
Explosion,
7th Loss Prevention Symposium, 1992, Taormina.

Yoshida, T. (1987),
Safety of Reactive Chemicals,
Elsevier, Amsterdam, 1987.

Chapter 8
Interfacing of models
C.J.H. van den Bosch

Glossary of terms

consequences or damage	A measure of the expected loss due to injury of people, loss of property or harm to the environment, or a combination of these.
hazard	A chemical or physical condition that has the potential of causing damage.
hazardous chemical	A chemical which, by virtue of its chemical properties, constitutes a hazard.
instantaneous release	The escape of a particular quantity of hazardous chemical over a relatively short time-span, typically a few seconds
interfacing of models	Translation, conversion and transfer of the results of a previous model (output data) in order to supply the required information for a subsequent model (input data). Translation of data means that calculated physical quantities (results, output data) are expressed in other appropriate physical quantities. Conversion of data means that the output data are reformulated to form another representation (format) that can be processed by the subsequent model. Transfer of data means getting the output of the previous model and putting this forward to the subsequent model.
physical effects models	Models that provide (quantitative) information about physical effects, mostly in terms of heat fluxes (thermal radiation), blast due to explosions, and environmental (atmospheric) concentrations.
risk	A measure of (economic) losses in terms of both the incident likelihood and the magnitude of damage.
scenario	A(n) (accident) scenario is a qualitative description of a particular route by which a (released) hazardous material can lead to one type of physical effect having consequences for human beings and or properties.

source term

Physical phenomena that take place at a release of a chemical from its containment before entering the environment of the failing containment, determining:
- the amount of chemical entering the surroundings in the vicinity of the containment,
- the dimensions of the area or space in which this process takes place,
- the thermodynamic state of the released chemical, such as concentration, temperature, and pressure,
- velocities of the outflowing chemical at the boundaries of the source region.

source term model

Models that provide (quantitative) information about the source term, to be input into a subsequent dispersion or other physical effect model.

Table of contents of chapter 8

8.1 Introduction of chapter 8

Safety and risk assessment studies are used to evaluate the risk of activities involving hazardous materials. The assessment of the hazards requires knowledge of the danger each hazardous material could present to human beings and to properties, qualitatively and quantitatively, due to explosion, intoxication, and fires.

In the previous chapters the physical effects related to hazardous materials have been addressed independently. Due to the way scientific research is organised most models have been developed to describe an isolated specific physical and/or chemical phenomenon. Where in reality transitions go fluently from one stage to the following stage of the event that starts with the release of hazardous material and ends with the exposure to people and properties, the modelling of the complete process takes often place stepwise.
Most of the time more than one model is needed. These models have to be 'coupled', meaning that their results, i.e. the predictions of the models (output data) have to be adapted and transferred to serve as input to other subsequent models.
Thus, a particular scenario is represented by a chain of models.
The procedure of adaptation and transfer of data is usually addressed by 'interfacing'.

In this final chapter the interfacing of models will be treated in a general way, and the interfacing will be put into perspective of so-called scenarios.

The line between the physical effect models to vulnerability or consequence models that estimate the damage to people and properties, will be drawn.

This chapter of the Yellow Book will comprise the following. First, a systematic approach will be explained regarding how to compile a list with accident scenarios in principle. Secondly, 'interfacing methods' between similar effect models will be addressed in general. Next, representative scenarios will be given, that will be worked out numerically as calculation examples.

8.1.1 Relation with previous chapters

Chapter 4 'Vapour Cloud Dispersion' is more or less the central chapter of the Yellow Book. This chapter has no special paragraph about interfacing. Interfacing of models into dispersion models are treated in the chapters: Outflow & Spray Release, Pool Evaporation, Vapour Cloud Explosions.

For the description of other interfacing to models, logical backward chaining has been followed: one has to find required input data from models in prior chapters.

Release of hazardous material, spray release, due to rupture of containments, pipe breaks or cracks in vessels or pipe walls, are initiating events. Therefore, no links of the models described in chapter 2 'Outflow and Spray Release' to prior models exist.
Vessel rupture is also an initiating event. Therefore no links to prior models exist.
The description of the resulting blast effects and fragmentation in chapter 7 'Rupture of Vessels' is sufficient.

8.2   Factors that determine scenarios

The way in which a hazardous material can lead to consequences varies enormously.

The processes involved depend on the properties of hazardous material, the process or system conditions, the way in which the accidental decontainment takes place, and possible subsequent reactions with the environment. A hazardous material can be toxic, flammable or both. The containment may be slightly damaged or totally ruptured by some kind of mechanical impact, or by being set on fire.

Released into the atmosphere, the hazardous material may:

−   cause fire and/or explosions,
−   lead to atmospheric concentrations of toxic materials to which humans can be exposed, causing immediate toxic effects,
−   lead to pollution of the environment.

In order to cope with the wide variety of possible accident developments, the concept of '(accident) scenario' is used.

In the following a rather restricted definition of scenario is used:

A (n) (accident) scenario is a qualitative description of a particular route by which a (released) hazardous material can lead to one type of physical effect having consequences for human beings and or properties.

In order to identify possible scenarios involving hazardous materials, a formal and somewhat schematic but systematic approach has been chosen: first, the factors are identified that determine a scenario, secondly, possible realistic scenarios are identified by combining the possible 'values' of these factors.

In general, a scenario is determined by the following factors:

A1. Chemical composition   : single compound, mixture
A2. Initial process condition : pressure, temperature
B.   Release type   : small opening, total rupture
C.   Immediate surroundings : mechanical/chemical interaction
D.   Dispersion   : atmospheric dispersion, dispersion in water bodies or in the ground
E.   Physical effect   : heat flux, blast, atmospheric concentrations of hazardous materials

These factors will be elucidated in the following sections.

8.2.1   Initial conditions

Given the chemical composition of the hazardous material, (partial) pressure and temperature determine the aggregation state of the compound. The Yellow Book deals with gases or vapours and liquids only, thus, the following process conditions are considered:
1. compressed gas,
2. refrigerated (liquefied) gases,
3. non-boiling liquids,
4. pressurised liquefied gases

These process conditions determine to a large extend the physical phenomena that will occur during the release of the material. An overview is given in the table below. These topics have been addressed in detail in chapters 2 and 3.

Table 8.1   Overview of physical phenomena during the release of material

Process condition	Pre-dispersion effects
Compressed gas	(sub-)Sonic release into the atmosphere
Refrigerated gases	Pool formation, initially boiling and later on non-boiling evaporating
Non-boiling liquids	Pool formation, evaporating but non-boiling
Pressurised liquefied gases	Flash off, possibly followed by (immediate) evaporation of a liquid spray due to entrainment of atmospheric air; (partial) rain-out may lead to pool formation and subsequent pool evaporation

8.2.2   Release types

The following release types are considered:
1. finite duration release,
2. instantaneous release.

Ad 1.
The containment may be damaged partially, resulting in an opening to the environment which is relatively small compared to the total amount of hazardous material in the process. This opening could be a hole in the wall of the containment, or a rupture of a pipe: relatively short piping in installations or relatively long transport pipelines.

Ad 2.
A containment can rupture totally. This causes the content, at least the larger part of the inventory, to be released into the environment in a relatively short time.

These topics have been addressed in detail in chapter 2.

8.2.3   Immediate surroundings

Depending on the process conditions, the released gas or liquid will interact with the immediate surroundings. These interactions have a direct effect on the (thermodynamic) state of the hazardous material entraining into the atmosphere. Near the source the dispersion is often still dominated by the effects of the release itself.

Liquids may spread over land or water (floating) or sink or solve into the subsoil or into water.

The *mechanical interactions* influencing the way the entrainment into the atmosphere (atmosphere, water body, or subsoil) takes place, are:
1. free entrainment: outflow, jet, spreading,...,
2. restricted entrainment: collision with obstacles, bund,... .

Physical-chemical interactions may take place due to a reaction of the hazardous material with the atmosphere (combustion), or with water or subsoil (chemical reaction).

It is also conceivable that a sudden change in physical conditions of released chemicals results in auto-reactions such as decomposition or polymerisation.

Many topics mentioned here have been addressed in chapters 3 and 6.

Table 8.2   Possible interactions with the environmental of the containment of the material released

Environmental compartment	Possible physical-chemical interaction
1. Interaction with atmosphere	1.1. no chemical reaction 1.2. combustion 1.3. auto-reaction
2. Interaction with water	2.1. floating 2.2. solving 2.3. sinking 2.4. reaction 2.5. auto-reaction
3. Interaction with subsoil	3.1. no chemical reaction 3.2. absorption 3.3. reaction 3.4. auto-reaction

8.2.4   Dispersion into the (far) atmosphere

In the 'Yellow Book' only atmospheric dispersion is considered.

Gases, vapours and liquid sprays may disperse into the atmosphere.

8.2.5 Physical effects directly causing damage

The following physical effects can cause damage to people and properties:
1. heat flux,
2. blast,
3. atmospheric concentrations of hazardous material.

Ad 1.
Heat flux is associated with fire. Combustion can occur in all thermodynamic states: solids, liquids and gases, after ignition. Pressurised gas releases may lead to flares or to local fires. Liquid pools may lead to pool fires. Totally ruptured vessels with pressurised flammable gas can lead to fire balls in case of an ignited BLEVE. These topics have been addressed in detail in chapter 6.

Ad 2.
Two types of explosions can be distinguished: physical and chemical explosions. A physical explosion is a catastrophic rupture of a pressurised gas-filled vessel; the sudden failure of the vessel causes blast in its immediate environment. These topics have been addressed in detail in chapter 7.

In a chemical explosion a chemical reaction is generating the energy of the resulting blast. Chemical explosions may be subdivided into two classes.
First, gases/vapours, liquids and solids may be explosive by themselves: a rapid auto-reaction causes the blast.
Secondly, gases/vapours and liquid sprays may form a flammable mixture with air.
After ignition a blast may occur if the flammable gas mixture is (partly) confined by obstacles. These topics have been addressed in detail in chapter 5.

Ad 3.
If a released toxic hazardous material is dispersed into the atmosphere, damaging effects may only be expected due to some kind of physical contact: exposure to the skin, swallowing, inhalation, etc.
In the end a release may also result in low concentration pollution of the environment. The topic of atmospheric dispersion has been addressed in detail in chapter 4.

To be able to estimate the expected consequences (damage), besides the characteristics of potential targets or receptors (people, properties) the consequence models require (basic) input from the physical effect models.

For safety and risk assessment studies this input is the main physical effect parameter of interest!

The required input depends on the type of consequence, as has been illustrated below.

Table 8.3   Physical effects required for estimation of consequences (damage)

Mechanism	Determining factor	Basic physical effects
1. Intoxication	Dose (Toxic load) $D_c = \int c\,(x, y, z, t)^n \times dt$	Atmospheric concentration as a function of time
2. Explosions	Blast	Maximum overpressure and positive phase duration
3. Fires	Heat load $D_H = \int q''_H\,(x, y, z, t)^m \times dt$	Heat flux as a function of time

8.3 Interfacing of models in general

Having identified the five factors that determine a scenario, all combinations of the possible 'values' of the factors can be constructed, resulting in a list of possible scenarios. Afterwards, a screening has to be carried out to sort out all combinations that are physically unrealistic.

In this final chapter we will treat the interfacing of models in a general way, and the interfacing is put into the perspective of so-called scenarios.

In order to avoid duplications, the interfacing in the perspective of the scenarios is presented here on a higher abstraction level.
The scheme below shows *all possible links* between the steps within a scenario on a higher level: links between groups of models.

Table 8.4   Possible steps between groups of models within a scenario

gases or spray release	– dispersion	– (VCE) blast
gas release	– heat flux from fire	
liquid release or spray release	– evaporation – dispersion	– (explosion) blast
liquid release	– heat flux from fire	

Note that for intoxication the prediction of the concentrations by an atmospheric dispersion model suffices.

This means that the interfacing between the following group of models has to be addressed.

Table 8.5   Interfacing between groups of models

Model type 1	Model type 2	Phenomenon	Explaining paragraph
1. gas release	dispersion	atmospheric dispersion of heavy gas or neutral gas or jet release	2.7.2.2
2. spray release	dispersion	atmospheric dispersion of heavy gas/spray mixture	2.7.2.3
3. spray release	pool evaporation	liquid rain-out of a spray	3.7.2.2
4. dispersion	blast	vapour cloud explosion	5.7
5. gas release	heat flux from fire	flares	6.7.2
6. liquid release	evaporation	pool formation	3.7.2.3
7. evaporation	dispersion	pool evaporation	3.7.3
8. liquid release	heat flux from fire	pool fires	6.7.3

This interfacing of models has already been described in the individual chapters and will not be repeated here.
Table 8.5 indicates in which chapter and paragraph a particular interfacing of models has been described.

8.4 Interfacing of models: calculation examples

8.4.1 Introduction of the scenario examples

The following scenarios are more or less illustrative and will be worked out as calculation examples in the following paragraphs.

The scenario descriptions below are expressed as much as possible in terms of combinations of 'values' of the scenario factors presented previously:

1. The hazardous material is a compressed gas, a hole in its containment permits release to the atmosphere freely, the flammable gas jet is immediately ignited and forms a flare, causing heat flux at some distance;
2. The hazardous material is a refrigerated gas stored under atmospheric pressure, and through a leak in the container liquid is being released freely, so a spreading boiling floating pool on water will be formed, and evaporation leads to atmospheric concentrations of hazardous material;
3. The hazardous material is a pressurized liquefied gas; a full bore pipe rupture permits release to the atmosphere, followed by evaporation of a liquid spray due to mixing with atmospheric air; between obstacles the flammable gas is ignited after a delay and an explosion or deflagration may occur;

The physical phenomena related to a BLEVE have been treated in different chapters. In order to give an overall picture of the BLEVE, an integral calculation example will be given here, so:

4. A BLEVE (Boiling Liquid Expanding Vapour Explosion) shows the following physical effects able to cause damage: heat radiation, pressure waves and fragmentation.

No intermediate results of the models will be presented in this chapter, except for the GASP model. Here we merely take the opportunity to demonstrate the capabilities of this model.

8.4.2 Calculation example: Scenario 1

Concise scenario description

Compressed methane (CH_4) is released from a vessel through a pipe and after ignition a flare results.
The (maximum) heat load at maximum outflow rate of methane, and the heat load at average outflow rate of methane gas will be estimated at several distances to the vessel.

Required models and methods

The time-varying methane gas out flow can be estimated by the models given in paragraph 2.5.2.

The heat load and the dimensions of the flare can be estimated by the Chamberlain model given in paragraph 6.5.3.

According to table 8.5 methods about interfacing of gas release models to fire models have been given paragraph 6.7.2. However, the outflow of methane is estimated by models presented in chapter 2.

Numerical elaboration

Outflow

Input:

Initial pressure	P_0	= 60.0E+05	N/m²
Initial temperature	T_0	= 288.15	K
Vessel volume	V	= 100	m³
Pipe length	l_p	= 100	m
Pipe diameter	d_p	= 0.2	m
Internal roughness pipe	ε	= 4.5E-05	m
Leak size	d_h	= 0.1	m
Discharge coefficient	C_d	= 1	

Output:

Mass flow at 0 s	q_S	= 46.29	kg/s
Mass flow at 50 s	q_S	= 24.40	kg/s
Gas pressure at 50 s	P	= 28.66E+05	N/m²
Gas temperature at 50 s	T	= 243.13	K

Note, that the symbols are according to chapter 2 'Outflow and Spray Release'.

Jet flame

Input (t=0s):

Mass flow rate	m'	= 46.29	kg/s
Initial gas pressure	P_{init}	= 60.00E+05	N/m²
Initial temperature	T_s	= 288.15	K
Height source	$b \cdot \sin\Theta_j$	= 5	m
Tilt of hole axis	Θ_j	= 0	°
Wind velocity at 10 m height	u_w	= 2	m/s
Ambient temperature	T_a	= 288.15	K
Relative humidity	RH	= 0.7	
Fraction CO_2 atmosphere	p_c	= 30	N/m²
Horizontal distance (X-coordinate)	X	= 50	m

Output (t=0s):

Heat radiation flux	q"	= 3.10E+03	W/m²
Safe distance (q"=1.0E+03 W/m²)	X	= 123.12	m
Surface Emissive Power flare	SEP_{act}	= 170.67+03	W/m²
Angle between hole axis and flame axis	α	= 3.89	°
Frustum lift-off height	b	= 9.69	m
Width of frustum base	W_1	= 2.57	m
Width of frustum tip	W_2	= 13.61	m
Length of frustum (flame)	R_l	= 56.98	m
Tilt central axis flare	$\Theta_j - \alpha$	= 3.89	°
View factor	F_{view}	= 0.02	
Atmospheric transmissitivity	τ_a	= 0.78	

Jet flame

Input (t=50s):

Mass flow rate	m'	= 24.40	kg/s
Initial gas pressure	P_{init}	= 28.66E+05	N/m²
Initial temperature	T_s	= 243.13	K
Height source	$b \cdot \sin\Theta_j$	= 5	m
Tilt of hole axis	Θ_j	= 0	°
Wind velocity at 10 m height	u_w	= 2	m/s
Ambient temperature	T_a	= 288.15	K
Relative humidity	RH	= 0.7	
Fraction CO_2 atmosphere	p_c	= 30	N/m²
Horizontal distance (X-coordinate)	X	= 50	m

Output (t=50s):

Heat radiation flux	q"	= 2.38E+03	W/m²
Safe distance (q"=1.0E+03 W/m²)	X	= 92.63	m
Surface Emissive Power flare	SEP_{act}	= 166.0E+03	W/m²
Angle between hole axis and flame axis	α	= 4.29	°
Frustum lift-off height	b	= 7.52	m
Width of frustum base	W_1	= 2.14	m
Width of frustum tip	W_2	= 10.70	m
Length of frustum (flame)	R_l	= 40.20	m
Tilt central axis flare	Θ_j-α	= 4.49	°
View factor	F_{view}	= 0.02	
Atmospheric transmissitivity	τ_a	= 0.78	

Note, that the symbols are according to chapter 6 'Heat fluxes from fires'.

8.4.3 Calculation example: Scenario 2

Concise scenario description

Refrigerated ammonia (NH_3), stored in a vertical cylinder, is incidentally released through a leak in the container wall into the surroundings. A crack occurs in the wall of a pipeline connected to the storage. The cross-sectional area of the crack is about 10% of the cross-sectional area of the pipeline.
After three hours the release of ammonia can be stopped.
An ammonia liquid pool will spread on the ground and evaporate.
Some atmospheric concentrations of ammonia, toxic to humans, will be estimated at several distances from the source.

Required models and methods

The time-varying outflow of initially non-boiling ammonia liquid from a vessel can be estimated by the models given in paragraph 2.5.4 of chapter 'Outflow and Spray release'.

The evaporation of a initially boiling and later on non-boiling ammonia pool on land can be calculated by the GASP model presented in paragraph 3.5.2 of chapter 'Pool evaporation'.

Atmospheric concentrations of the toxic (heavy) ammonia gas can be estimated by the SLAB model presented in paragraph 4.5.5.2 of chapter 'Vapour cloud dispersion'.

According to table 8.5 methods about interfacing of liquid release models to pool evaporation models have been given in paragraph 3.7.2.3, and about interfacing of pool evaporation models to dispersion models in paragraph 3.7.3.

Numerical elaboration

Outflow

Input:

Vessel volume	V	= 30000	m³
Length cylinder	h_v	= 30	m
Filling degree	ϕ	= 0.75	
Pressure above liquid	P	= 101325	N/m²
Pipe length	l_p	= 1	m
Pipe diameter	d_p	= 0.4	m
Internal roughness pipe	ε	= 4.5·10⁻⁵	m
Leak size	d_h	= 0.1265	m
Height leak	h_h	= 0 m	
Initial temperature	T_0	= 237.3	K
Discharge coefficient	C_d	= 1	
Time after start release	t	= 10800	s

Output:

Outflow rate liquid	at t=0 s	q_S	= 180.59	kg/s
	at t=3600 s	q_S	= 176.70	kg/s
	at t=7200 s	q_S	= 172.81	kg/s
	at t=10800 s	q_S	= 168.92	kg/s
Average outflow rate until t=10800 s		$q_{S,av}$	= 174.8	kg/s (0.255 m³/s)
Liquid density		ρ_L	= 684.4	kg/m³
Filling degree at 10800 s		ϕ	= 0.66	
Height of liquid at 10800 s		h_L	= 19.69	m
Total mass released at 10800 s		Q	= 0.1926·10⁷	kg

Note that the symbols are according to chapter 2 'Outflow and Spray release'.

Pool evaporation

GASP models a semi-continuous release of refrigerated ammonia onto land. Ammonia is spilt at a rate of 0.255 m³/s through an aperture of 0.0126 m². The implied discharge velocity is 20.3 m/s.
The temperature at the discharge point is 239.72 K.
The pool spread is unrestricted. Heat is being transferred from light concrete subsoil, with conductivity 0.418 J(m·s·K) and diffusivity 2.5 m²/s, into the pool. Perfect thermal contact is assumed. The capillary depth has been set equal to the average roughness of the light concrete subsoil.
The atmospheric temperature is 15 ˚C (288.15 K) and the windspeed is 4.5 m/s.
The net solar radiation can be estimated by equations (4.36) and (4.37) presented in chapter 4 'Vapour cloud dispersion'. However, for the sake of simplicity a value of 100 J/(m²·s) for the net solar radiation has been used.

Initial liquid release conditions

Discharge aperture	A_h	= 1.2568E-02	m²
Discharge velocity	u_d	= 20.32	m/s

Initial pool conditions

Initial volume of pool	V	= 2.0313E-02	m³
Initial radius of pool	r	= 6.3250E-02	m
Initial depth of pool	h	= 1.616	m
Initial front velocity	u	= 0.3976	m/s
Initial temperature	T_0	= 239.7	K
Capillary depth	l_h	= 5.0000E-03	m

Atmospheric conditions

Wind speed at 10 metres	$u_{a,10}$	= 4.500	m/s
Atmospheric temperature	T_a	= 288.15	K
Atmospheric friction velocity	u_*	= 0.2368	m/s
Roughness length	$z_{0,a}$	= 5.0000E-03	m
Roughness length pool	$z_{0,p}$	= 2.3000E-04	m

Heat transfer to the pool

Thermal conductivity	λ_s	= 0.4180	J/(m·s·k)
Thermal diffusivity	a_s	= 2.500	m²/s

Physical properties of ammonia at T=239.7 K

Molecular weight	μ_i	= 17.03·10⁻³	kg/mol
Melting point	T_m	= 195.5	K
Boiling point	T_b	= 239.7	K
Critical temperature	T_c	= 405.6	K
Heat of vaporisation	$L_v(T_b)$	= 1.3715E+06	J/kg
Latent-heat-index	n	= 0.3800	
Antoine coefficient A	C_A	= 16.95	
Antoine coefficient B	C_B	= 2133.	K
Antoine coefficient C	C_C	= -32.98	K
Specific heat liquid	$C_{p,L}$	= 4416.	J/(kg·K)
Specific heat vapour	$C_{p,V}$	= 1987.	J/(kg·K)
Liquid density	ρ_L	= 682.7	Kg/m³
Surface tension	σ	= 3.5385E-02	N/m
Liquid viscosity	η_L	= 2.5032E-04	N·s/m²
Vapour viscosity	η_V	= 8.1553E-06	N·s/m²
Thermal conductivity liquid	λ_L	= 0.6194	J/(m·s·K)
Thermal conductivity vapour	λ_V	= 1.9841E-02	J/(m·s·K)
Molecular diffusivity	D	= 1.4622E-05	m²/s

Properties of air

Density	ρ_a	= 1.225	kg/m^3
Viscosity	η_a	= 1.7894E-05	N·s/m^2
Kinematic viscosity	υ_a	= 1.4607E-05	m^2/s
Prandtl number	Pr_a	= 0.7104	
Effective molecular weight	μ_a	= 28.96·10^{-3}	kg/mol

Constants

Turbulent friction parameter	C_f	= 1.3000E-03
Von Karman's constant	κ	= 0.4000
Turbulent Schmidt number	Sc_t	= 0.8500
Turbulent Prandtl number	Pr_t	= 0.85
Laminar Schmidt number	Sc_l	= 0.9990

Output

Maximum vaporisation rate	$q_{S,max}$	= 174.2	k/s
after time	t	= 1.0800E+04	s
Pool has evaporated at time	t	= 1.1342E+04	s

Intermediate results of SLAB can be found at the end of this paragraph.

Note that the symbols are according to chapter 3 'Pool evaporation'.

Heavy gas dispersion

From table 8.6 it appears that the pool reaches its maximum radius 31.66 m, at t=1377 after the start of the release. After t=11342 s the pool has evaporated. After t=10800 s (3 hours) the liquid pool surface will keep its maximum size, but the pool will partially dry up.

While the pool will have its maximum size for about 87.9% of the time, the source dimension for the dispersion model SLAB will be assumed to be equal to maximum size of the pool, thus:

$$A_S = \pi \cdot r_{p,max}^2$$

$$= 3150 \text{ m}^2$$

After t=10800 s (3 hours) about $Q_v \approx 1.86+06$ kg of ammonia has evaporated. This implies an average evaporation rate:

$$q_{s,av} = 172.2 \text{ kg/s}$$

For a conservative estimation, the duration of the source, as input for the SLAB dispersion model, will be set equal to the time the liquid pool has evaporated, thus:

$$t_S = 11342 \text{ s}$$

Input:

Mass flow rate of the source	q	= 172.2	kg/s
Duration of release	t_r	= 11342	s
Source radius	b_0	= 31.66	m
Temperature after release	T	= 239.72	K
Wind velocity at 10 m height	u_a	= 4.5	m/s
Pasquill stability class	D		
Relative humidity	$p_w/p_{s,w}$	= 70 %	
Ambient temperature	T_a	= 288.15	K
Roughness length	$z_{0,p}$	= 1	
Concentration averaging time	t_{av}	= 60	s
Time t after start release	t	= 1800	s
Height receptor	z	= 1.5	m

Threshold 1% lethality after 30 minutes exposure $c_{1\%,30}$ = 1,871   mg/m³
Threshold 50% lethality after 30 minutes exposure $c_{50\%,30}$ = 5,999   mg/m³
Threshold 99% lethality after 30 minutes exposure $c_{99\%,30}$ = 19,233   mg/m³

Output:

Distance to threshold $c_{1\%}$	$x_{1\%}$	= 41.5	m
Distance to threshold $c_{50\%}$	$x_{50\%}$	= 40.3	m
Distance to threshold $c_{99\%}$	$x_{99\%}$	= 39.0	m

Clearly, the relative light ammonia-air-mixture will rise from the pool.

Note that the source area is 3150 m².
Note that the symbols are according to chapter 4 'Vapour cloud dispersion'.

Table 8.6

t (s)	r (m)	Qv (kg)	h (m)	Vd (m³)
0.0000	6.3250E-02	0.0000	1.616	2.0313E-02
5.0338E-04	6.3469E-02	4.3812E-07	1.615	2.0442E-02
2.4550E-03	6.4676E-02	2.1707E-06	1.593	2.0940E-02
6.1352E-03	6.8472E-02	5.6723E-06	1.485	2.1880E-02
1.1777E-02	7.7885E-02	1.2071E-05	1.224	2.3321E-02
1.8536E-02	9.3989E-02	2.2489E-05	0.9025	2.5047E-02
2.7798E-02	0.1223	4.4693E-05	0.5831	2.7413E-02
3.8736E-02	0.1619	8.9195E-05	0.3669	3.0206E-02
5.5937E-02	0.2315	2.2189E-04	0.2054	3.4599E-02
7.6240E-02	0.3198	5.2831E-04	0.1238	3.9784E-02
9.9749E-02	0.4256	1.1731E-03	8.0461E-02	4.5788E-02
0.1308	0.5676	2.6759E-03	5.3077E-02	5.3721E-02
0.1718	0.7545	6.1692E-03	3.5888E-02	6.4191E-02
0.2273	1.001	1.4464E-02	2.4887E-02	7.8371E-02
0.3085	1.339	3.5931E-02	1.7585E-02	9.9111E-02
0.4319	1.789	9.4027E-02	1.2974E-02	0.1306
0.5909	2.261	0.2186	1.0643E-02	0.1712
0.7524	2.641	0.4025	9.6679E-03	0.2125
0.9425	2.999	0.6879	9.2016E-03	0.2610
1.202	3.384	1.186	9.0513E-03	0.3273
1.526	3.758	1.961	9.1793E-03	0.4101
1.875	4.079	2.962	9.4702E-03	0.4993
2.331	4.417	4.496	9.9360E-03	0.6157
2.897	4.758	6.708	1.0549E-02	0.7601
3.615	5.112	9.952	1.1315E-02	0.9435
4.539	5.488	14.76	1.2237E-02	1.180
5.743	5.900	21.96	1.3302E-02	1.487
7.382	6.386	33.36	1.4494E-02	1.906
9.578	6.977	51.35	1.5637E-02	2.466
12.56	7.752	80.99	1.6476E-02	3.229
16.67	8.816	132.3	1.6727E-02	4.278
21.87	10.13	217.1	1.6396E-02	5.605
28.14	11.60	351.3	1.5832E-02	7.207
37.08	13.42	603.9	1.5198E-02	9.489
48.64	15.41	1036.	1.4650E-02	12.44
64.42	17.65	1807.	1.4127E-02	16.47
77.84	19.27	2620.	1.3768E-02	19.90
97.99	21.35	4094.	1.3305E-02	25.05
130.4	24.02	7049.	1.2697E-02	33.33
179.2	26.86	1.2632E+04	1.2039E-02	45.79
194.2	27.51	1.4568E+04	1.1894E-02	49.61
197.8	27.65	1.5050E+04	1.1863E-02	50.54
213.6	28.21	1.7207E+04	1.1752E-02	54.58
239.2	28.87	2.0852E+04	1.1673E-02	61.11

t (s)	r (m)	Q_v (kg)	h (m)	V_d (m^3)
277.9	29.48	2.6614E+04	1.1728E-02	71.00
328.0	30.04	3.4352E+04	1.1809E-02	83.79
390.5	30.72	4.4411E+04	1.1703E-02	99.75
453.0	31.13	5.4840E+04	1.1628E-02	115.7
515.5	31.28	6.5440E+04	1.1655E-02	131.7
590.3	31.44	7.8235E+04	1.1648E-02	150.8
665.0	31.56	9.1149E+04	1.1621E-02	169.9
752.9	31.59	1.0640E+05	1.1628E-02	192.3
842.7	31.63	1.2201E+05	1.1623E-02	215.2
947.4	31.64	1.4025E+05	1.1621E-02	242.0
1070.	31.65	1.6158E+05	1.1621E-02	273.2
1213.	31.65	1.8654E+05	1.1621E-02	309.8
1377.	31.66	2.1517E+05	1.1621E-02	351.7
1568.	31.66	2.4853E+05	1.1621E-02	400.6
1794.	31.66	2.8788E+05	1.1621E-02	458.2
2077.	31.66	3.3712E+05	1.1621E-02	530.4
2376.	31.66	3.8931E+05	1.1621E-02	606.8
2617.	31.66	4.3142E+05	1.1621E-02	668.5
2820.	31.66	4.6668E+05	1.1621E-02	720.1
3022.	31.66	5.0194E+05	1.1621E-02	771.8
3224.	31.66	5.3720E+05	1.1621E-02	823.4
3426.	31.66	5.7247E+05	1.1621E-02	875.1
3652.	31.66	6.1179E+05	1.1621E-02	932.7
3901.	31.66	6.5518E+05	1.1621E-02	996.2
4149.	31.66	6.9856E+05	1.1621E-02	1060.
4393.	31.66	7.4104E+05	1.1621E-02	1122.
4608.	31.66	7.7847E+05	1.1621E-02	1177.
4844.	31.66	8.1975E+05	1.1621E-02	1237.
5081.	31.66	8.6103E+05	1.1621E-02	1298.
5318.	31.66	9.0231E+05	1.1621E-02	1358.
5555.	31.66	9.4359E+05	1.1621E-02	1419.
5791.	31.66	9.8487E+05	1.1621E-02	1479.
6028.	31.66	1.0262E+06	1.1621E-02	1540.
6265.	31.66	1.0674E+06	1.1621E-02	1600.
6502.	31.66	1.1087E+06	1.1621E-02	1660.
6738.	31.66	1.1500E+06	1.1621E-02	1721.
7002.	31.66	1.1960E+06	1.1621E-02	1788.
7275.	31.66	1.2436E+06	1.1621E-02	1858.
7499.	31.66	1.2827E+06	1.1621E-02	1915.
7723.	31.66	1.3217E+06	1.1621E-02	1972.
7947.	31.66	1.3608E+06	1.1621E-02	2030.
8190.	31.66	1.4031E+06	1.1621E-02	2092.
8440.	31.66	1.4467E+06	1.1621E-02	2155.
8671.	31.66	1.4870E+06	1.1621E-02	2215.
8872.	31.66	1.5221E+06	1.1621E-02	2266.

t (s)	r (m)	Q_v (kg)	h (m)	V_d (m³)
9083.	31.66	1.5589E+06	1.1621E-02	2320.
9339.	31.66	1.6035E+06	1.1621E-02	2385.
9623.	31.66	1.6530E+06	1.1621E-02	2458.
9907.	31.66	1.7025E+06	1.1621E-02	2530.
1.0163E+04	31.66	1.7472E+06	1.1621E-02	2596.
1.0393E+04	31.66	1.7872E+06	1.1621E-02	2654.
1.0600E+04	31.66	1.8234E+06	1.1621E-02	2707.
1.0800E+04	31.66	1.8582E+06	1.1621E-02	2758.
1.0803E+04	31.66	1.8587E+06	1.1403E-02	2758.
1.0811E+04	31.63	1.8602E+06	1.0711E-02	2758.
1.0825E+04	31.42	1.8625E+06	9.7747E-03	2758.
1.0839E+04	30.84	1.8650E+06	8.9467E-03	2758.
1.0839E+04	30.84	1.8650E+06	8.9429E-03	2758.
1.0841E+04	30.73	1.8653E+06	8.8424E-03	2758.
1.0850E+04	30.19	1.8667E+06	8.4520E-03	2758.
1.0865E+04	28.95	1.8691E+06	7.8567E-03	2758.
1.0889E+04	26.56	1.8723E+06	7.1861E-03	2758.
1.0915E+04	23.58	1.8752E+06	6.7325E-03	2758.
1.0948E+04	19.25	1.8779E+06	6.7530E-03	2758.
1.0970E+04	15.75	1.8791E+06	7.8008E-03	2758.
1.0986E+04	12.86	1.8796E+06	1.0058E-02	2758.
1.0997E+04	10.93	1.8799E+06	1.2839E-02	2758.
1.1006E+04	9.915	1.8801E+06	1.4751E-02	2758.
1.1008E+04	9.830	1.8801E+06	1.4841E-02	2758.
1.1009E+04	9.812	1.8802E+06	1.4839E-02	2758.
1.1011E+04	9.793	1.8802E+06	1.4728E-02	2758.
1.1012E+04	9.807	1.8802E+06	1.4574E-02	2758.
1.1014E+04	9.844	1.8802E+06	1.4343E-02	2758.
1.1014E+04	9.855	1.8802E+06	1.4284E-02	2758.
1.1016E+04	9.937	1.8803E+06	1.3897E-02	2758.
1.1019E+04	10.15	1.8803E+06	1.3055E-02	2758.
1.1024E+04	10.50	1.8804E+06	1.1797E-02	2758.
1.1030E+04	10.89	1.8806E+06	1.0446E-02	2758.
1.1030E+04	10.90	1.8806E+06	1.0440E-02	2758.
1.1031E+04	10.93	1.8806E+06	1.0317E-02	2758.
1.1033E+04	11.01	1.8806E+06	9.9856E-03	2758.
1.1037E+04	11.07	1.8807E+06	9.5285E-03	2758.
1.1037E+04	11.08	1.8807E+06	9.5045E-03	2758.
1.1038E+04	11.07	1.8807E+06	9.4333E-03	2758.
1.1041E+04	11.02	1.8808E+06	9.2768E-03	2758.
1.1044E+04	10.89	1.8809E+06	9.2343E-03	2758.
1.1046E+04	10.78	1.8809E+06	9.2639E-03	2758.
1.1051E+04	10.41	1.8810E+06	9.5232E-03	2758.
1.1059E+04	9.597	1.8811E+06	1.0499E-02	2758.
1.1066E+04	8.700	1.8813E+06	1.2057E-02	2758.

t (s)	r (m)	Q_v (kg)	h (m)	V_d (m³)
1.1072E+04	8.139	1.8813E+06	1.3224E-02	2758.
1.1076E+04	7.948	1.8814E+06	1.3552E-02	2758.
1.1076E+04	7.938	1.8814E+06	1.3562E-02	2758.
1.1078E+04	7.892	1.8814E+06	1.3546E-02	2758.
1.1080E+04	7.883	1.8814E+06	1.3453E-02	2758.
1.1080E+04	7.884	1.8814E+06	1.3410E-02	2758.
1.1082E+04	7.913	1.8815E+06	1.3129E-02	2758.
1.1085E+04	7.998	1.8815E+06	1.2614E-02	2758.
1.1085E+04	7.999	1.8815E+06	1.2608E-02	2758.
1.1086E+04	8.041	1.8815E+06	1.2385E-02	2758.
1.1089E+04	8.165	1.8815E+06	1.1776E-02	2758.
1.1091E+04	8.258	1.8816E+06	1.1331E-02	2758.
1.1092E+04	8.275	1.8816E+06	1.1251E-02	2758.
1.1094E+04	8.353	1.8816E+06	1.0865E-02	2758.
1.1098E+04	8.451	1.8816E+06	1.0246E-02	2758.
1.1100E+04	8.458	1.8817E+06	1.0105E-02	2758.
1.1100E+04	8.457	1.8817E+06	1.0055E-02	2758.
1.1103E+04	8.419	1.8817E+06	9.9210E-03	2758.
1.1106E+04	8.297	1.8818E+06	9.9233E-03	2758.
1.1106E+04	8.291	1.8818E+06	9.9271E-03	2758.
1.1108E+04	8.199	1.8818E+06	1.0005E-02	2758.
1.1112E+04	7.916	1.8818E+06	1.0376E-02	2758.
1.1118E+04	7.363	1.8819E+06	1.1413E-02	2758.
1.1125E+04	6.855	1.8819E+06	1.2598E-02	2758.
1.1129E+04	6.652	1.8820E+06	1.3038E-02	2758.
1.1129E+04	6.651	1.8820E+06	1.3039E-02	2758.
1.1130E+04	6.602	1.8820E+06	1.3086E-02	2758.
1.1133E+04	6.575	1.8820E+06	1.2972E-02	2758.
1.1133E+04	6.575	1.8820E+06	1.2963E-02	2758.
1.1134E+04	6.582	1.8820E+06	1.2834E-02	2758.
1.1137E+04	6.631	1.8820E+06	1.2415E-02	2758.
1.1142E+04	6.770	1.8821E+06	1.1525E-02	2758.
1.1147E+04	6.902	1.8821E+06	1.0588E-02	2758.
1.1150E+04	6.907	1.8822E+06	1.0397E-02	2758.
1.1152E+04	6.883	1.8822E+06	1.0294E-02	2758.
1.1155E+04	6.756	1.8822E+06	1.0345E-02	2758.
1.1157E+04	6.681	1.8822E+06	1.0448E-02	2758.
1.1160E+04	6.477	1.8822E+06	1.0823E-02	2758.
1.1166E+04	6.060	1.8823E+06	1.1833E-02	2758.
1.1172E+04	5.733	1.8823E+06	1.2695E-02	2758.
1.1172E+04	5.728	1.8823E+06	1.2706E-02	2758.
1.1173E+04	5.694	1.8823E+06	1.2768E-02	2758.
1.1176E+04	5.649	1.8823E+06	1.2761E-02	2758.
1.1177E+04	5.643	1.8824E+06	1.2692E-02	2758.
1.1177E+04	5.644	1.8824E+06	1.2657E-02	2758.

t (s)	r (m)	Q_v (kg)	h (m)	V_d (m³)
1.1178E+04	5.654	1.8824E+06	1.2487E-02	2758.
1.1182E+04	5.714	1.8824E+06	1.1946E-02	2758.
1.1187E+04	5.825	1.8824E+06	1.1087E-02	2758.
1.1190E+04	5.856	1.8824E+06	1.0681E-02	2758.
1.1190E+04	5.856	1.8824E+06	1.0660E-02	2758.
1.1192E+04	5.846	1.8824E+06	1.0561E-02	2758.
1.1195E+04	5.775	1.8825E+06	1.0547E-02	2758.
1.1197E+04	5.698	1.8825E+06	1.0662E-02	2758.
1.1197E+04	5.682	1.8825E+06	1.0693E-02	2758.
1.1199E+04	5.587	1.8825E+06	1.0895E-02	2758.
1.1203E+04	5.360	1.8825E+06	1.1494E-02	2758.
1.1207E+04	5.108	1.8825E+06	1.2254E-02	2758.
1.1209E+04	5.041	1.8825E+06	1.2446E-02	2758.
1.1209E+04	5.025	1.8825E+06	1.2486E-02	2758.
1.1211E+04	4.972	1.8826E+06	1.2589E-02	2758.
1.1214E+04	4.943	1.8826E+06	1.2489E-02	2758.
1.1214E+04	4.943	1.8826E+06	1.2477E-02	2758.
1.1215E+04	4.947	1.8826E+06	1.2364E-02	2758.
1.1218E+04	4.977	1.8826E+06	1.2016E-02	2758.
1.1222E+04	5.049	1.8826E+06	1.1347E-02	2758.
1.1226E+04	5.088	1.8826E+06	1.0832E-02	2758.
1.1226E+04	5.088	1.8826E+06	1.0821E-02	2758.
1.1227E+04	5.083	1.8826E+06	1.0743E-02	2758.
1.1229E+04	5.043	1.8826E+06	1.0701E-02	2758.
1.1233E+04	4.926	1.8827E+06	1.0916E-02	2758.
1.1233E+04	4.920	1.8827E+06	1.0932E-02	2758.
1.1234E+04	4.869	1.8827E+06	1.1066E-02	2758.
1.1237E+04	4.730	1.8827E+06	1.1483E-02	2758.
1.1241E+04	4.537	1.8827E+06	1.2130E-02	2758.
1.1241E+04	4.514	1.8827E+06	1.2204E-02	2758.
1.1242E+04	4.494	1.8827E+06	1.2268E-02	2758.
1.1243E+04	4.444	1.8827E+06	1.2407E-02	2758.
1.1247E+04	4.396	1.8827E+06	1.2381E-02	2758.
1.1247E+04	4.396	1.8827E+06	1.2342E-02	2758.
1.1248E+04	4.397	1.8827E+06	1.2278E-02	2758.
1.1250E+04	4.415	1.8827E+06	1.2019E-02	2758.
1.1253E+04	4.464	1.8827E+06	1.1477E-02	2758.
1.1257E+04	4.501	1.8827E+06	1.0941E-02	2758.
1.1259E+04	4.493	1.8827E+06	1.0846E-02	2758.
1.1261E+04	4.443	1.8828E+06	1.0854E-02	2758.
1.1265E+04	4.305	1.8828E+06	1.1224E-02	2758.
1.1267E+04	4.213	1.8828E+06	1.1543E-02	2758.
1.1270E+04	4.085	1.8828E+06	1.2015E-02	2758.
1.1270E+04	4.085	1.8828E+06	1.2018E-02	2758.
1.1271E+04	4.048	1.8828E+06	1.2148E-02	2758.

t (s)	r (m)	Q_v (kg)	h (m)	V_d (m^3)
1.1273E+04	3.988	1.8828E+06	1.2330E-02	2758.
1.1276E+04	3.956	1.8828E+06	1.2263E-02	2758.
1.1276E+04	3.956	1.8828E+06	1.2261E-02	2758.
1.1277E+04	3.957	1.8828E+06	1.2179E-02	2758.
1.1279E+04	3.974	1.8828E+06	1.1907E-02	2758.
1.1282E+04	4.018	1.8828E+06	1.1365E-02	2758.
1.1286E+04	4.035	1.8828E+06	1.0985E-02	2758.
1.1287E+04	4.020	1.8828E+06	1.0914E-02	2758.
1.1291E+04	3.936	1.8829E+06	1.1082E-02	2758.
1.1295E+04	3.768	1.8829E+06	1.1704E-02	2758.
1.1295E+04	3.767	1.8829E+06	1.1709E-02	2758.
1.1296E+04	3.739	1.8829E+06	1.1826E-02	2758.
1.1298E+04	3.672	1.8829E+06	1.2093E-02	2758.
1.1301E+04	3.603	1.8829E+06	1.2279E-02	2758.
1.1303E+04	3.594	1.8829E+06	1.2185E-02	2758.
1.1303E+04	3.594	1.8829E+06	1.2160E-02	2758.
1.1304E+04	3.601	1.8829E+06	1.2003E-02	2758.
1.1307E+04	3.627	1.8829E+06	1.1621E-02	2758.
1.1310E+04	3.658	1.8829E+06	1.1136E-02	2758.
1.1310E+04	3.658	1.8829E+06	1.1084E-02	2758.
1.1311E+04	3.658	1.8829E+06	1.1041E-02	2758.
1.1313E+04	3.642	1.8829E+06	1.0980E-02	2758.
1.1316E+04	3.569	1.8829E+06	1.1161E-02	2758.
1.1320E+04	3.415	1.8829E+06	1.1805E-02	2758.
1.1325E+04	3.298	1.8829E+06	1.2229E-02	2758.
1.1326E+04	3.291	1.8829E+06	1.2143E-02	2758.
1.1327E+04	3.291	1.8829E+06	1.2118E-02	2758.
1.1328E+04	3.298	1.8829E+06	1.1947E-02	2758.
1.1330E+04	3.323	1.8829E+06	1.1565E-02	2758.
1.1334E+04	3.346	1.8830E+06	1.1125E-02	2758.
1.1334E+04	3.346	1.8830E+06	1.1124E-02	2758.
1.1334E+04	3.345	1.8830E+06	1.1077E-02	2758.
1.1336E+04	3.333	1.8830E+06	1.1027E-02	2758.
1.1339E+04	3.263	1.8830E+06	1.1227E-02	2758.
1.1342E+04	3.146	1.8830E+06	1.1763E-02	2758.

Table 8.8

t (s)	H_c (J(m²·s))	H_a (J/(m²·s))	T (K)
0.0000	1.9457E+05	0.4159	239.7
5.0338E-04	465.8	0.4161	239.7
2.4550E-03	406.0	0.4172	239.7
6.1352E-03	379.6	0.4205	239.7
1.1777E-02	334.0	0.4272	239.7
1.8536E-02	278.6	0.4358	239.7
2.7798E-02	217.4	0.4455	239.7
3.8736E-02	168.6	0.4534	239.7
5.5937E-02	124.0	0.4655	239.7
7.6240E-02	95.87	0.4742	239.7
9.9749E-02	77.57	0.4778	239.7
0.1308	63.51	0.4794	239.7
0.1718	52.57	0.4796	239.7
0.2273	43.64	0.4788	239.7
0.3085	35.70	0.4771	239.7
0.4319	28.47	0.4747	239.7
0.5909	22.91	0.4735	239.7
0.7524	19.34	0.4724	239.7
0.9425	16.56	0.4714	239.7
1.202	14.07	0.4703	239.7
1.526	12.08	0.4690	239.7
1.875	10.66	0.4679	239.7
2.331	9.404	0.4668	239.7
2.897	8.355	0.4658	239.7
3.615	7.456	0.4648	239.7
4.539	6.681	0.4637	239.7
5.743	6.011	0.4626	239.7
7.382	5.415	0.4614	239.7
9.578	4.900	0.4601	239.7
12.56	4.440	0.4584	239.7
16.67	4.002	0.4563	239.7
21.87	3.581	0.4540	239.7
28.14	3.181	0.4518	239.7
37.08	2.761	0.4493	239.7
48.64	2.389	0.4469	239.7
64.42	2.059	0.4445	239.7
77.84	1.864	0.4431	239.7
97.99	1.652	0.4414	239.7
130.4	1.421	0.4395	239.7
179.2	1.202	0.4376	239.7
194.2	1.153	0.4372	239.7
197.8	1.143	0.4371	239.7
213.6	1.098	0.4368	239.7
239.2	1.037	0.4364	239.7

t (s)	H_c (J(m²·s))	H_a (J/(m²·s))	T (K)
277.9	0.9751	0.4361	239.7
328.0	0.9327	0.4357	239.7
390.5	0.8970	0.4354	239.7
453.0	0.8690	0.4351	239.7
515.5	0.8535	0.4351	239.7
590.3	0.8427	0.4350	239.7
665.0	0.8346	0.4349	239.7
752.9	0.8293	0.4349	239.7
842.7	0.8259	0.4349	239.7
947.4	0.8232	0.4349	239.7
1070.	0.8213	0.4349	239.7
1213.	0.8198	0.4349	239.7
1377.	0.8187	0.4349	239.7
1568.	0.8178	0.4349	239.7
1794.	0.8171	0.4349	239.7
2077.	0.8165	0.4349	239.7
2376.	0.8160	0.4349	239.7
2617.	0.8158	0.4349	239.7
2820.	0.8156	0.4349	239.7
3022.	0.8154	0.4349	239.7
3224.	0.8153	0.4349	239.7
3426.	0.8152	0.4349	239.7
3652.	0.8151	0.4349	239.7
3901.	0.8150	0.4349	239.7
4149.	0.8150	0.4349	239.7
4393.	0.8149	0.4349	239.7
4608.	0.8148	0.4349	239.7
4844.	0.8148	0.4349	239.7
5081.	0.8148	0.4349	239.7
5318.	0.8147	0.4349	239.7
5555.	0.8147	0.4349	239.7
5791.	0.8147	0.4349	239.7
6028.	0.8146	0.4349	239.7
6265.	0.8146	0.4349	239.7
6502.	0.8146	0.4349	239.7
6738.	0.8146	0.4349	239.7
7002.	0.8145	0.4349	239.7
7275.	0.8145	0.4349	239.7
7499.	0.8145	0.4349	239.7
7723.	0.8145	0.4349	239.7
7947.	0.8145	0.4349	239.7
8190.	0.8145	0.4349	239.7
8440.	0.8145	0.4349	239.7
8671.	0.8145	0.4349	239.7
8872.	0.8144	0.4349	239.7

t (s)	H_c (J(m²·s))	H_a (J/(m²·s))	T (K)
9083.	0.8144	0.4349	239.7
9339.	0.8144	0.4349	239.7
9623.	0.8144	0.4349	239.7
9907.	0.8144	0.4349	239.7
1.0163E+04	0.8144	0.4349	239.7
1.0393E+04	0.8144	0.4349	239.7
1.0600E+04	0.8144	0.4349	239.7
1.0800E+04	0.8144	0.4349	239.7
1.0803E+04	0.8144	0.4349	239.7
1.0811E+04	0.8150	0.4349	239.7
1.0825E+04	0.8203	0.4350	239.7
1.0839E+04	0.8351	0.4353	239.7
1.0839E+04	0.8352	0.4353	239.7
1.0841E+04	0.8378	0.4354	239.7
1.0850E+04	0.8491	0.4357	239.7
1.0865E+04	0.8636	0.4364	239.7
1.0889E+04	0.8096	0.4378	239.7
1.0915E+04	-.7068	0.4398	239.7
1.0948E+04	-1.944	0.4431	239.7
1.0970E+04	-3.357	0.4465	239.7
1.0986E+04	-5.304	0.4500	239.7
1.0997E+04	-7.162	0.4528	239.7
1.1006E+04	-7.883	0.4544	239.7
1.1008E+04	-7.769	0.4545	239.7
1.1009E+04	-7.708	0.4546	239.7
1.1011E+04	-7.450	0.4546	239.7
1.1012E+04	-7.233	0.4546	239.7
1.1014E+04	-6.962	0.4545	239.7
1.1014E+04	-6.899	0.4545	239.7
1.1016E+04	-6.518	0.4544	239.7
1.1019E+04	-5.801	0.4540	239.7
1.1024E+04	-4.907	0.4534	239.7
1.1030E+04	-4.166	0.4528	239.7
1.1030E+04	-4.164	0.4528	239.7
1.1031E+04	-4.112	0.4528	239.7
1.1033E+04	-3.994	0.4527	239.7
1.1037E+04	-3.928	0.4526	239.7
1.1037E+04	-3.931	0.4526	239.7
1.1038E+04	-3.945	0.4526	239.7
1.1041E+04	-4.056	0.4526	239.7
1.1044E+04	-4.270	0.4528	239.7
1.1046E+04	-4.435	0.4530	239.7
1.1051E+04	-4.992	0.4536	239.7
1.1059E+04	-6.257	0.4549	239.7
1.1066E+04	-7.792	0.4565	239.7

t (s)	H_c (J/(m²·s))	H_a (J/(m²·s))	T (K)
1.1072E+04	-8.693	0.4576	239.7
1.1076E+04	-8.817	0.4580	239.7
1.1076E+04	-8.810	0.4580	239.7
1.1078E+04	-8.696	0.4581	239.7
1.1080E+04	-8.546	0.4581	239.7
1.1080E+04	-8.488	0.4581	239.7
1.1082E+04	-8.161	0.4581	239.7
1.1085E+04	-7.651	0.4579	239.7
1.1085E+04	-7.645	0.4579	239.7
1.1086E+04	-7.444	0.4578	239.7
1.1089E+04	-6.941	0.4576	239.7
1.1091E+04	-6.615	0.4574	239.7
1.1092E+04	-6.561	0.4574	239.7
1.1094E+04	-6.322	0.4572	239.7
1.1098E+04	-6.066	0.4570	239.7
1.1100E+04	-6.059	0.4570	239.7
1.1100E+04	-6.068	0.4570	239.7
1.1103E+04	-6.182	0.4571	239.7
1.1106E+04	-6.507	0.4573	239.7
1.1106E+04	-6.523	0.4573	239.7
1.1108E+04	-6.759	0.4575	239.7
1.1112E+04	-7.482	0.4581	239.7
1.1118E+04	-8.950	0.4592	239.7
1.1125E+04	-10.31	0.4603	239.7
1.1129E+04	-10.70	0.4608	239.7
1.1129E+04	-10.70	0.4608	239.7
1.1130E+04	-10.70	0.4609	239.7
1.1133E+04	-10.51	0.4610	239.7
1.1133E+04	-10.49	0.4610	239.7
1.1134E+04	-10.33	0.4610	239.7
1.1137E+04	-9.853	0.4609	239.7
1.1142E+04	-9.000	0.4605	239.7
1.1147E+04	-8.391	0.4602	239.7
1.1150E+04	-8.380	0.4602	239.7
1.1152E+04	-8.482	0.4603	239.7
1.1155E+04	-8.978	0.4606	239.7
1.1157E+04	-9.263	0.4607	239.7
1.1160E+04	-10.05	0.4612	239.7
1.1166E+04	-11.70	0.4622	239.7
1.1172E+04	-12.89	0.4631	239.7
1.1172E+04	-12.90	0.4631	239.7
1.1173E+04	-12.97	0.4632	239.7
1.1176E+04	-12.93	0.4633	239.7
1.1177E+04	-12.83	0.4633	239.7
1.1177E+04	-12.78	0.4633	239.7

t (s)	H_c (J/(m²·s))	H_a (J/(m²·s))	T (K)
1.1178E+04	-12.56	0.4633	239.7
1.1182E+04	-11.92	0.4631	239.7
1.1187E+04	-11.09	0.4628	239.7
1.1190E+04	-10.89	0.4627	239.7
1.1190E+04	-10.90	0.4627	239.7
1.1192E+04	-10.95	0.4628	239.7
1.1195E+04	-11.34	0.4630	239.7
1.1197E+04	-11.76	0.4632	239.7
1.1197E+04	-11.84	0.4632	239.7
1.1199E+04	-12.36	0.4634	239.7
1.1203E+04	-13.61	0.4641	239.7
1.1207E+04	-14.99	0.4648	239.7
1.1209E+04	-15.32	0.4650	239.7
1.1209E+04	-15.38	0.4650	239.7
1.1211E+04	-15.55	0.4651	239.7
1.1214E+04	-15.42	0.4652	239.7
1.1214E+04	-15.40	0.4652	239.7
1.1215E+04	-15.24	0.4652	239.7
1.1218E+04	-14.78	0.4651	239.7
1.1222E+04	-14.00	0.4649	239.7
1.1226E+04	-13.64	0.4648	239.7
1.1226E+04	-13.64	0.4648	239.7
1.1227E+04	-13.64	0.4648	239.7
1.1229E+04	-13.93	0.4649	239.7
1.1233E+04	-14.78	0.4653	239.7
1.1233E+04	-14.83	0.4653	239.7
1.1234E+04	-15.20	0.4655	239.7
1.1237E+04	-16.23	0.4659	239.7
1.1241E+04	-17.66	0.4664	239.7
1.1241E+04	-17.82	0.4665	239.7
1.1242E+04	-17.95	0.4666	239.7
1.1243E+04	-18.25	0.4667	239.7
1.1247E+04	-18.29	0.4669	239.7
1.1247E+04	-18.23	0.4669	239.7
1.1248E+04	-18.13	0.4669	239.7
1.1250E+04	-17.75	0.4668	239.7
1.1253E+04	-17.02	0.4667	239.7
1.1257E+04	-16.56	0.4666	239.7
1.1259E+04	-16.62	0.4666	239.7
1.1261E+04	-17.09	0.4667	239.7
1.1265E+04	-18.42	0.4672	239.7
1.1267E+04	-19.32	0.4675	239.7
1.1270E+04	-20.56	0.4679	239.7
1.1270E+04	-20.57	0.4679	239.7
1.1271E+04	-20.90	0.4680	239.7

t (s)	H_c (J(m²·s))	H_a (J/(m²·s))	T (K)
1.1273E+04	-21.39	0.4682	239.7
1.1276E+04	-21.38	0.4683	239.7
1.1276E+04	-21.38	0.4683	239.7
1.1277E+04	-21.25	0.4683	239.7
1.1279E+04	-20.82	0.4682	239.7
1.1282E+04	-20.04	0.4681	239.7
1.1286E+04	-19.75	0.4680	239.7
1.1287E+04	-19.92	0.4681	239.7
1.1291E+04	-20.94	0.4684	239.7
1.1295E+04	-23.02	0.4689	239.7
1.1295E+04	-23.05	0.4689	239.7
1.1296E+04	-23.40	0.4690	239.7
1.1298E+04	-24.21	0.4693	239.7
1.1301E+04	-24.87	0.4695	239.7
1.1303E+04	-24.76	0.4696	239.7
1.1303E+04	-24.72	0.4696	239.7
1.1304E+04	-24.45	0.4695	239.7
1.1307E+04	-23.79	0.4694	239.7
1.1310E+04	-23.16	0.4693	239.7
1.1310E+04	-23.14	0.4693	239.7
1.1311E+04	-23.15	0.4693	239.7
1.1313E+04	-23.37	0.4694	239.7
1.1316E+04	-24.49	0.4696	239.7
1.1320E+04	-26.90	0.4702	239.7
1.1325E+04	-28.50	0.4706	239.7
1.1326E+04	-28.43	0.4706	239.7
1.1327E+04	-28.38	0.4706	239.7
1.1328E+04	-28.05	0.4706	239.7
1.1330E+04	-27.33	0.4705	239.7
1.1334E+04	-26.75	0.4704	239.7
1.1334E+04	-26.75	0.4704	239.7
1.1334E+04	-26.76	0.4705	239.7
1.1336E+04	-26.98	0.4705	239.7
1.1339E+04	-28.31	0.4707	239.7
1.1342E+04	-30.56		

8.4.4   Calculation example: Scenario 3

Concise scenario description

In an industrial installation, propane (C_3H_8) has been stored as a pressurized liquified gas in a vertical cylinder, and propane is transported from the vessel through piping. Due to a full bore rupture of the piping propane is released. In the resulting horizontal two-phase jet, the liquid spray vaporises due to mixing with atmospheric air. After a vapour cloud has developed in the industrial plant, delayed ignition occurs, followed by an explosion. Blast overpressures and positive phase durations will be estimated for a few distances from the centre of the explosion.

Procedure

The two-phase release of propane through an pipe can be estimated by models, including TPDIS, presented in paragraph 2.5.3. The subsequent spray release results into a two-phase jet which dimensions can be estimated by the model presented in paragraph 2.5.3.7.

Atmospheric concentrations of flammable (heavy) propane gas can be estimated by the SLAB model presented in paragraph 4.5.5.2. The concentration of the resulting cloud has to be integrated between the iso-concentration contour for which c=lfl, and the iso-concentration contour for which c=ufl.

The confined flammable propane gas within the obstructed area and the characteristics of the resulting blast after ignition can be estimated by the Multi-Energy-Model presented in paragraph 5.5.

According to table 8.5, methods about interfacing spray release models to dispersion models have been given paragraph 2.7.2.3, and about interfacing dispersion models to (explosion) blast models in paragraph 5.7.

Two-phase propane release from vessel through a pipe

Input:

Pipe length	l_p	=	10	m
Pipe diameter	d_p	=	0.154	m
Internal roughness pipe	ε	=	$4.5 \cdot 10^{-5}$	m
Initial upstream temperature	T_0	=	300	K
Leak size	d_h	=	0.154	m
Contraction factor	C_d	=	0.62	

Output:

Mass flow	q_S	=	80.0	kg/s
Vapour mass fraction at exit	$\Phi_{m,e}$	=	0.079	kg/kg
Exit temperature	T_e	=	289.7	K
Upstream pressure	P	=	$730.9 \cdot 10^3$	N/m^2

Note that the symbols used are conform chapter 2 'Outflow and Spray release'.

Spray release

Input:

(Average) mass flow rate	q_S	=	80	kg/s
Exit temperature	T_e	=	289.7	K
Exit vapour mass fraction	$\Phi_{m,e}$	=	0.079	kg/kg
Source exit height	h_s	=	1	m
Leak size	d_h	=	0.154	m
Discharge coefficient	C_d	=	0.62	
Ambient temperature	T_a	=	300	K
Relative humidity	RH	=	70	%

Output:

Nett air-borne mass flow rate	$q_{S,nett,air}$	=	80.00	kg/s
Jet diameter after rain-out	$b_{f,rainout}$	=	0.37	m
Temperature after rain-out	$T_{f,rainout}$	=	230.9	K
Vapour mass fraction after rain-out	$\Phi_{m,f,rainout}$	=	0.46	kg/kg
Jet diameter after air entrainment	b_j	=	1.47	m
Temperature of air/vapour mixture	T_j	=	191.42	K
Vapour mass fraction in air/vapour mixture	$\Phi_{m,j}$	=	0.46	kg/kg
Concentration in air/vapour mixture	c_j	=	0.115	m³/m³
Concentration in air/vapour mixture	c_j'	=	0.317	kg/m³

Note that the symbols used are conform chapter 2 'Outflow and Spray release.

Heavy gas dispersion

Input:

Mass flow rate of the source	q_S	=	80.0	kg/s
Duration of release	t_r	=	100	s
Maximum diameter of expanded jet	b_0	=	0.37	m
Height of source	h	=	1.0	m
Vapour temperature after expansion	T	=	230.9	K
Wind velocity at 10 m height	u_a	=	2	m/s
Pasquill stability class	F			
Relative humidity	RH	=	70	%
Ambient temperature	T_a	=	300	K
Roughness length	z_0	=	1.0	m

Output (t=10 s):

Maximum explosive mass lfl<c<ufl	$Q_{ex,max}$	=	741	kg
... at time	t	=	40	s
Maximum explosive distance	$x_{lfl,max}$	=	164	m
... at time	t	=	213	s

Note that the symbols used are conform chapter 4 'Vapour cloud dispersion'.

Vapour cloud explosion

Input:

Total flammable mass	Q_{ex}	=	741	kg
Ambient temperature	T_a	=	300	K
Stoichiometric concentration	c_s	=	0.0706	kg/m³
Cloud volume at stoichiometric concentration	V_c	=	$105 \cdot 10^4$	m³
Fraction of flammable cloud confined	V_{gr}/V_c	=	1.0	m³/m³
Strength number	10			

Output:

Heat of combustion in the confined cloud	E	=	$37.3 \cdot 10^9$	J
Side-on peak overpressure at 100 m	P_s	=	$0.265 \cdot 10^5$	N/m²
Positive phase duration at 100 m	t_p	=	0.053	s
Side-on peak overpressure at 200 m	P_s	=	$0.111 \cdot 10^5$	N/m²
Positive phase duration at 200 m	t_p	=	0.074	s
Side-on peak overpressure at 500 m	P_s	=	$0.0378 \cdot 10^5$	N/m²
Positive phase duration at 500 m	t_p	=	0.089	s

Note that the symbols used are conform chapter 5 'Vapour cloud explosion'.

8.4.5   BLEVE

Concise scenario description

A horizontal cylindrical vessel with pressurized liquefied propane (C_3H_8) stands within a large fire. The volume of the vessel is 25.0 m^3 and the vessel is filled to 80% with liquefied propane. After some time the vessel ruptures totally and the two-phase mixture, instantaneously released, is ignited immediately.
Due to the external fire the vessel is locally weakened. Therefore it is most probable that it will break into two equal parts.
A large storage tank, located 15 m from the vessel, and a control building at 100 m from the vessel, may be hit.

Required models and methods

The model for the estimation of the pressure waves and fragmentation is described in chapter 7.
The model for the estimation of the fireball characteristics is described in chapter 6.

Note that both models are independent of each other.

Pressure effects and fragments

Input:

Mass of liquid propane	M_f	=	8780	kg
Mass of propane vapour	M_g	=	215.5	kg
Failure overpressure	p_1	=	$19.0 \cdot 10^5$	N/m^2
Ambient pressure	p_a	=	$1.0 \cdot 10^5$	N/m^2
Ambient temperature	T_a	=	293	K
Mass vessel	M_v	=	3859	kg
Vessel diameter	d_v	=	1.5	m
Length-to-diameter ratio	l_v/d_v	=	10.0	

Output:

The total energy released	E_{av}	=	$570 \cdot 10^6$	J
Side-on peak pressure at 15 m	P_s	=	468000	N/m^2
Side-on impulse at 15 m	i_s	=	795	$N \cdot s/m^2$
Side-on peak pressure at 100 m	P_s	=	107700	N/m^2
Side-on impulse at 100 m	i_s	=	86	$N \cdot s/m^2$
Number of fragments	n_f	=	2	
Fragment mass	M_f	=	1930	kg
Initial velocity fragments	v_i	=	109	m/s
Possible travel distance	R_f	=	900	m

Procedure

Here the short-cut method has been followed. The total energy, E_{av} that is released by the expansion of the vapour and the flashing of the liquid can be calculated by equation (7.4), figure 7.3, and equation (7.5a). This explosive energy release produces a blast wave. Estimates of the blast parameters at the large storage vessel can be estimated by equations (7.7) and (7.8), and figures 7.5 and 7.6.

The initial velocity of the vessel parts and the potential travel distance can be estimated by equation (7.15) and (7.22), together with figure 7.12 and equation (7.21).

The complete calculation of the blast and fragmentation effects is presented in section 7.6.

Note that the symbols used are according to chapter 7 'Rupture of vessels'.

Fire ball

Input:

Total mass propane released	m	=	8996	kg
Vapour pressure at burst vessel	P_{sv}	=	$19.0 \cdot 10^5$	N/m²
Ambient pressure	P_{air}	=	$1.013 \cdot 10^5$	N/m²
Ambient temperature	T_a	=	293	K
Partial H_2O pressure (humidity 70 %)	p_w	=	1623	N/m²
Assumed flame temperature	T_f	=	1200	K

Output:

Maximum heat radiation flux at X_{bleve} = 100 m	q"	=	$33.9 \cdot 10^3$	J/(m²·s)
View factor X_{bleve} = 100 m	F_{view}	=	0.15	
Atmospheric transmissitivity X_{bleve} = 100 m	ρ_a	=	0.72	
Maximum heat radiation flux at X_{bleve} = 839 m	q"	=	$100 \cdot 10^3$	J/(m²·s)
View factor X_{bleve} = 839 m	F_{view}	=	0.0054	
Atmospheric transmissitivity X_{bleve} = 839 m	ρ_a	=	0.60	
Surface Emissive Power fireball	SEP_{act} =		$308 \cdot 10^3$	J/(m²·s)
Duration of the fireball	t	=	9.09	s
Radius of the fireball	r_{fb}	=	62.5	m
Height centre fireball	H_{bleve} =		125	m

Procedure

The radius, duration and lift-off height of the fire ball can be calculated by equations (6.90), (6.91) and (6.22), respectively.

The straight distance between the centre of the fire ball to the receptor can be calculated by equation (6.92) based on the horizontal distance to the vessel and the lift-off height of the fire ball.

The view factor, depending on the radius of the fire ball and the distance to the centre of the fireball, can be calculated by equation (6.93). The surface emissive power of the fire ball can be estimated by equations (6.21) and (6.95). The heat flux the receptor is receiving, depends on the surface emissive power, atmospheric transmissitivity and the view factor, and can be estimated by equation (6.4).

The complete calculation of heat flux due to a fire ball, caused by an ignition of a BLEVE, is presented in section 6.6.5.

Note that the symbols used are according to chapter 6 'Heat fluxes from fires'.

8.5　　Discussion and conclusions

Interfacing of models deals with the transfer of data from a previous model to a subsequent model in the chain representing a scenario.

The chain of models necessary to quantify the physical effects is depending on the availability of existing (computerised) models. Models vary in degree of complexity and detail, and have a common tendency to describe highly idealised laboratory situations in which one single phenomenon is under study. Consequently, the detailed predictions of the prior model have to be simplified in order to serve as input for the next model. This simplification always results in a loss of information and thus final predictions deteriorate to some extent.

In theory, integral models should be able to preserve all information about prior physical phenomena, taking into account variations in time and magnitude.
However, improved predictions are not necessary for all types of (safety-) studies.
The description of such integral models is much more complicated because of the fact that more details have to be taken into account and a special dedicated numerical procedure must be applied. The large numerical integral procedure this approach would require, would further enlarge the required computational capacity.
For the present, the maximum degree of model complexity has been reached by models such as GASP in chapter 3 'Pool Evaporation', that are still reasonably manageable in safety and risk assessment studies.

Several types of physical effects are possible for a given set of accident conditions. Furthermore, hazardous materials may follow more than one route leading to particular consequences.
Thus, more than one scenario may be required to fully access all possible physical effects causing damage. These scenarios differ from each other by a different kind of spill of hazardous material under particular process and meteorological conditions.

In case the released hazardous material will react and form toxic reaction products, the list of scenarios can easily be extended to follow-up scenarios. The best way to avoid endless repetitions of very similar scenarios is to consider the reaction products of the primary hazardous material released, and look for the most fitting scenario.

Always the possibility of so-called domino-effects is apparent, i.e. triggering of secondary events by a primary event such that the result is an increase in consequences or area of an effect zone. These domino effects are generally only considered if they result in a significant escalation of the original incident.

8.6   References

AIChE (1989),
Chemical Process Quantitative Risk Analysis – guidelines for –,
Center for Chemical Process Safety of the American Institute of Chemical Engineers,
1989.

Bosch (1992),
C.J.H.van den Bosch, H. Bekkering,
System description IRIS: Effect Module, TNO-report 92-054, for the Netherlands
Ministry for Home Affairs, 11-2-92.

Potts (1981),
Hazard Assessment Computer System -Users' operation manual vol.1-,
R.G. Potts, A.D. LITTLE for US Coast Guard, 30-09-81.

Annex
Physical properties of chemicals
C.J.H. van den Bosch

List of symbols Annex

c_{lfl}	Concentration at lower flammability limit	kg/m³
c_{ufl}	Concentration at upper flammability limit	kg/m³
c_S	Maximum solubility in water	kg/m³
$C_{p,g}$	Specific heat gas/vapour	J/(mol·K)
$C_{p,L}$	Specific heat liquid	J/(kg·K)
$C_{X,...}$	Coefficient 'X' of temperature relation	-
LFL	Lower flammability limit	vol%
UFL	Upper flammability limit	vol%
$P°$	Vapour pressure	N/m²
P_c	Critical pressure	N/m²
T_b	Boiling point	K
T_c	Critical temperature	K
T_{fl}	Flash point	K
T_m	Melting point	K

Greek symbols

γ	Poisson ratio $C_{p,g}/C_{v,g}$	-
ΔH_c	Heat of combustion	J/kg
L_v	Heat of vaporisation	J/kg
η_g	Dynamic viscosity gas/vapour	N·s/m²
η_L	Dynamic viscosity liquid	N·s/m²
μ	Molecular weight	kg/mol
ρ_g	Gas/vapour density	kg/m³
ρ_L	Liquid density	kg/m³
σ	Surface tension	N/m

Table of contents of Annex

A.1   Introduction

For several chemicals physical properties are given as physical constants or as coefficients of relations expressing properties' temperature dependency.
Data has been collected from various sources. Most individual sources do not provide all physical properties required. All sources referred to have been used to compile a data set of physical constants and coefficients, as complete as possible.

Physical constants are given for each chemical.
The chemical specific coefficients of the temperature relations are given for each chemical. Using these equations the physical properties can be calculated for any temperature, within the valid range.

Values for the temperature-dependent physical properties are given for T = 288.15 K (15 ˚C).

Physical properties given as physical constant:

Molecular weight	μ
Melting point	T_m
Boiling point	T_b
Critical temperature	T_c
Critical pressure	P_c
Flash point	T_{fl}
Heat of combustion	ΔH_c
Lower flammability limit	LFL
Upper flammability limit	UFL
Solubility in water	c_S

Physical properties given as a function of absolute temperature:

Specific heat gas/vapour	$C_{p,g}$
Poisson ratio $C_{p,g}/C_{v,g}$	γ
Gas/vapour density	ρ_g
Gas/vapour viscosity	η_g
Vapour pressure	$P°$
Heat of vaporisation	L_v
Specific heat liquid	$C_{p,L}$
Liquid density	ρ_L
Liquid viscosity	η_L
Surface tension	σ

A.1.1 Yaws' concept

The following equations, according to the concept of Yaws [1977] express the temperature dependency of the physical properties:

$$C_{p,g}(T) = C_{A,Cpg} + C_{B,Cpg} \times T + C_{C,Cpg} \times T^2 + C_{D,Cpg} \times T^3 \quad \text{(cal/(mol·K))}$$

$$C_{p,L}(T) = C_{A,CpL} + C_{B,CpL} \times T + C_{C,CpL} \times T^2 \quad \text{(cal/(g·K))}$$

$$\Delta H_v(T) = \Delta H_v(T_0) \times ((T_c\text{-}T)/(T_c\text{-}T_{Hv,0}))^{C\Delta Hv} \quad \text{(cal/g)}$$

$$\eta_g(T) = C_{A,\eta g} + C_{B,\eta g} \times T + C_{C,\eta g} \times T^2 \quad \text{(μP)}$$

$$^{10}\log(\eta_L(T)) = C_{A,\eta L} + C_{B,\eta L}/T + C_{C,\eta L} \times T + C_{D,\eta L} \times T^2 \quad \text{(cP)}$$

$$^{10}\log(P^°(T)) = C_{A,P^·} + C_{B,P^·}/T + C_{C,P^·} \times {}^{10}\text{Log}(T) + C_{D,P^·} \times T + C_{E,P^·} \times T^2$$
$$\text{(mm Hg)}$$

$$\sigma(T) = \sigma(T_{\sigma,0}) \times ((T_c\text{-}T)/(T_c\text{-}T_{\sigma,0}))^{C\sigma} \quad \text{(dyne/cm)}$$

$$\rho_L(T) = C_{A,\rho L} \times C_{B,\rho L}^{-(1-(T/Tc))^{(2/7)}} \quad \text{(g/cm}^3)$$

Note that the following relations are also applied in this chapter:

$$C_{v,g} = C_{p,g} - R$$

$$\gamma = C_{p,g}/C_{v,g}$$

$$\rho_g = P \times \mu/(R \cdot T)$$

It must be stressed that the coefficients presented are valid only for relations that correspond to those given by Yaws [1977]. Note that these quantities have to be converted into S.I.-units. In table A.1.1 conversion factors have been given.

Table A.1.1   Conversion factors

From unit	To unit	Multiply by
cal/(mol·K)	J/(mol·K)	4,184.0
cal/(g·K)	J/(kg·K)	4,184.0
cal/g	J/kg	4,184.0
μP	N·s/m^2	10^{-7}
cP	N·s/m^2	10^{-3}
mm Hg	N/m^2	101325/760.0
dyne/cm	N/m	10^{-3}
g/cm^3	kg/m^3	10^3

All calculation examples presented in this Yellow Book are based on these relations. Other databases exist, based on other mathematical equations. There is no reason whatsoever to presume that these other (private) databases could not also be applied to perform the calculations by the models presented in this book.

The calculated temperature-dependent physical properties may differ a few per cent from those calculated using the equations presented here, hence the predictions by the models will also slightly differ, if other databases are used.

A.1.2   Concept according to DIPPR

In the DIPPR database the following functions of (absolute) temperature are used:

$$f_0(T) = A + B \times T + C \times T^2 + D \times T^3 + E \times T^4$$

$$f_1(T) = Exp(A + B/T + C \times Ln(T) + D \times T^E)$$

$$f_2(T) = (A \times T^B) / (1 + C/T + D/T^2)$$

$$f_3(T) = A + B \times Exp(-C/T^D)$$

$$f_4(T) = A + B/T + C/T^3 + D/T^8 + E/T^9$$

$$f_5(T) = A/ B^{(1 + (1 - T/C)^D)}$$

$$f_6(T) = A \times \ (1 - T/Tc)^{(B + C \times T/Tc + D \times (T/Tc) + E \times (T/Tc)^3)}$$

$$f_7(T) = A + B \times (C/T/Sinh\ (C/T))^2 + D \times (E/T/Cosh(E/T))^2$$

It must be mentioned that in DIPPR the most appropriate equation for a physical property is used for a particular chemical. This means that for the same physical property several equations are applied.
For example for propane the following equations have been used

$$C_{p,g}(T) = f_7(T) \qquad C_{p,L}(T) = f_0(T) \qquad \Delta H_v(T) = f_6(T)$$

$$\eta_g(T) = f_2(T) \qquad \eta_L(T) = f_1(T) \qquad P°(T) = f_1(T)$$

$$\sigma(T) = f_6(T) \qquad \rho_L(T) = f_5(T)$$

A.2   References

Chem (1995),
Chemiekaarten - Gegevens voor het veilig werken met chemicaliën,
NIA/VNCI/Samsom H.D. Tjeenk Willink, 10e editie, Alphen a/d Rijn 1994-95.

CRC (1995),
Handbook of Chemistry and Physics, CRC Press, 75th ed., 1995

DIPPR (1990),
Th. B. Selover, Use of DIPPr data in reactive chemical hazard assessment,
Plant/Operations Progress,9(4),207-212,October 1990.

Landolt
Landolt-Börnstein, Zahlenwerte und Funktionen, Springer-Verlag.

Yaws (1977),
C.L. Yaws, Physical Properties, McGraw-Hill, New York, 1977.

A.3   Data physical properties

Physical properties are listed for the following chemicals:

1.   ACROLEIN

```
Material_Name                     = ACROLEIN
Molecular formula                 = CH2CHCHO
UN number                         =         1092
Molecular weight                  =        56.060000 kg/kmol
Critical temperature              =       506.000000 K (232.85 °C)
Melting point                     =       185.450000 K (-87.70 °C)
Triplepoint temperature           =       185.450000 K (-87.70 °C)
Normal boiling point              =       325.840000 K (52.69 °C)
Standard net heat of combustion   = 2.771000E+0007 J/kg ( 1.553423E+0009 J/kmol)
Flash point                       =       247.150000 K (-26.00 °C)
Lower flammability limit          =         2.800000 vol% in air
Upper flammability limit          =       100.000000 vol% in air
Solubility in water               =       206.000000 kg/m3


Temperature dependent data (calculated at 288.15 K  (15.00 °C)
Liquid density                    = 8.440330E+0002    kg/m3 (844.03 kg/m3 )
Vapor pressure                    = 2.399542E+0004    N/m2 (0.24 Bar   )
Heat of vaporization              = 5.478413E+0005    J/kg (547841.26 J/kg  )
Liquid heatcapacity               = 2.151910E+0003    J/kg*K (2151.91 J/kg*K)
Gas heatcapacity (ideal gas)      = 1.130799E+0003    J/kg*K (1130.80 J/kg*K)
Liquid viscosity                  = 3.649874E-0004    Pa*s
Vapor viscosity                   = 8.227617E-0006    Pa*s
Surface tension                   = 2.456317E-0002     N/m
Poisson ratio                     = 1.151


Functions (calculated at 288.15 K  (15.00 °C) and 1.000000E+05 N/m2  (1.000 Bar)
Gas density (ideal gas law) :          2.340 kg/m3
Mass of 1 m3 gas/vapour     :          2.340 kg
Volume of 1 kg gas/vapour   :          0.427 m3
Mass of 1 m3 liquid         :        844.033 kg
Volume of 1000 kg liquid    :          1.185 m3


Probit constants (Toxicity)
A =        5.621200 SI units(Kg*s/m3)
B =        1.000000 SI units(Kg*s/m3)
N =        1.000000 SI units(Kg*s/m3)

A =       -3.251597 (ppm*min)
B =        1.000000 (ppm*min)
N =        1.000000 (ppm*min)

A =       -4.099966 (mg*min/m3)
B =        1.000000 (mg*min/m3)
N =        1.000000 (mg*min/m3)


Temperature dependent data (Parameters):

Liquid density
Formula Nr.   1    rho = A * B^-((1-T/C)^2/7)  (where C=Tc) [g/cm3] [g/cm3]
Minimum temperature               =       185.450000 [K]
Maximum temperature               =       506.000000 [K]
Parameter 1                       = 3.228800E-0001
Parameter 2                       = 2.944900E-0001
Parameter 3                       = 5.060000E+0002
Parameter 4                       = 0.000000E+0000
Parameter 5                       = 0.000000E+0000
```

```
Vapor pressure
Formula Nr.   2    Log(P) = A + B/T + C*Log(T) + D*T + E*T^2  [mm Hg] [mm Hg]
Minimum temperature                 =       185.450000 [K]
Maximum temperature                 =       506.000000 [K]
Parameter 1                         =     3.900860E+0001
Parameter 2                         =    -2.746400E+0003
Parameter 3                         =    -1.117600E+0001
Parameter 4                         =    -1.054000E-0003
Parameter 5                         =     6.868000E-0006

Heat of vaporization
Formula Nr.   3    Hv = A * ((C-T)/(C-B)^D  (A=Hv1, B=T1, C=Tc)  [cal/g] [cal/g]
Minimum temperature                 =       185.450000 [K]
Maximum temperature                 =       506.000000 [K]
Parameter 1                         =     1.195000E+0002
Parameter 2                         =     3.457000E+0002
Parameter 3                         =     5.060000E+0002
Parameter 4                         =     2.964000E-0001
Parameter 5                         =     0.000000E+0000

Liquid heatcapacity
Formula Nr.   4    Cpl = A + B*T + C*T^2 + D*T^3  [cal/g/K] [cal/g/K]
Minimum temperature                 =       275.000000 [K]
Maximum temperature                 =       350.000000 [K]
Parameter 1                         =     3.669900E-0001
Parameter 2                         =     4.970900E-0004
Parameter 3                         =     6.687800E-0008
Parameter 4                         =    -7.132000E-0011
Parameter 5                         =     0.000000E+0000

IG heatcapacity
Formula Nr.   5    Cp = A + B*T + C*T^2 + D*T^3  [cal/mol] [cal/mol]
Minimum temperature                 =       298.150000 [K]
Maximum temperature                 =      1000.100000 [K]
Parameter 1                         =     4.864400E+0000
Parameter 2                         =     2.794800E-0002
Parameter 3                         =     2.931600E-0005
Parameter 4                         =    -2.487000E-0008
Parameter 5                         =     0.000000E+0000

Liquid viscosity
Formula Nr.   6    Log(Visc) = Ea + Eb/T + Ec*Log (T) + Ed*T + Ee*T*T  (where Ec=0!) [centiPoise]
[centiPoise]
Minimum temperature                 =       222.890000 [K]
Maximum temperature                 =       353.220000 [K]
Parameter 1                         =    -1.791500E+0000
Parameter 2                         =     3.689500E+0002
Parameter 3                         =     0.000000E+0000
Parameter 4                         =     3.078400E-0004
Parameter 5                         =    -1.847000E-0007

Vapor viscosity
Formula Nr.   7    Visc = A + B*T + C*T^2  [microPoise] [microPoise]
Minimum temperature                 =       325.840000 [K]
Maximum temperature                 =       995.840000 [K]
Parameter 1                         =    -1.718200E+0001
Parameter 2                         =     3.226100E-0001
Parameter 3                         =    -5.332000E-0005
Parameter 4                         =     0.000000E+0000
Parameter 5                         =     0.000000E+0000

Surface Tension
Formula Nr.   8    Sigma = A * ((C-T)/(C-B))^D  (A=Sigma1, B=T1, C=Tc)  [dynes/cm] [dynes/cm]
Minimum temperature                 =       185.450000 [K]
Maximum temperature                 =       506.000000 [K]
Parameter 1                         =     1.658000E+0001
Parameter 2                         =     3.457000E+0002
Parameter 3                         =     5.060000E+0002
Parameter 4                         =     1.281300E+0000
Parameter 5                         =     0.000000E+0000
```

Annex-10

2.   ACRYLONITRILE

```
Material_Name                     = ACRYLONITRILE
Molecular formula                 = CH2CHCN
UN number                         =         1093
Molecular weight                  =        53.060000 kg/kmol
Critical temperature              =       535.000000 K (261.85 °C)
Melting point                     =       189.630000 K (-83.52 °C)
Triplepoint temperature           =       189.630000 K (-83.52 °C)
Normal boiling point              =       350.500000 K (77.35 °C)
Standard net heat of combustion   = 3.184800E+0007 J/kg ( 1.689855E+0009 J/kmol)
Flash point                       =       273.150000 K (-0.00 °C)
Lower flammability limit          =         2.420000 vol% in air
Upper flammability limit          =       100.000000 vol% in air
Solubility in water               =        73.000000 kg/m3


Temperature dependent data (calculated at 288.15 K  (15.00 °C)
Liquid density                    = 8.124973E+0002    kg/m3 (812.50 kg/m3 )
Vapor pressure                    = 9.106335E+0003    N/m2 (0.09 Bar   )
Heat of vaporization              = 6.336796E+0005    J/kg (633679.62 J/kg  )
Liquid heatcapacity               = 2.029729E+0003    J/kg*K (2029.73 J/kg*K)
Gas heatcapacity (ideal gas)      = 1.187232E+0003    J/kg*K (1187.23 J/kg*K)
Liquid viscosity                  = 3.683722E-0004    Pa*s
Vapor viscosity                   = 6.674399E-0006    Pa*s
Surface tension                   = 2.790906E-0002     N/m
Poisson ratio                     = 1.152


Functions (calculated at 288.15 K  (15.00 °C) and 1.000000E+05 N/m2  (1.000 Bar)
Gas density (ideal gas law) :         2.215 kg/m3
Mass of 1 m3 gas/vapour     :         2.215 kg
Volume of 1 kg gas/vapour   :         0.452 m3
Mass of 1 m3 liquid         :       812.497 kg
Volume of 1000 kg liquid    :         1.231 m3


Probit constants (Toxicity)
A =        5.265800 SI units(Kg*s/m3)
B =        1.000000 SI units(Kg*s/m3)
N =        1.300000 SI units(Kg*s/m3)

A =       -7.568639 (ppm*min)
B =        1.000000 (ppm*min)
N =        1.300000 (ppm*min)

A =       -8.600019 (mg*min/m3)
B =        1.000000 (mg*min/m3)
N =        1.300000 (mg*min/m3)


Temperature dependent data (Parameters):

Liquid density
Formula Nr.   1    rho = A * B^-((1-T/C)^2/7)  (where C=Tc) [g/cm3] [g/cm3]
Minimum temperature               =       189.630000 [K]
Maximum temperature               =       535.000000 [K]
Parameter 1                       = 2.470400E-0001
Parameter 2                       = 2.265000E-0001
Parameter 3                       = 5.350000E+0002
Parameter 4                       = 0.000000E+0000
Parameter 5                       = 0.000000E+0000
```

```
Vapor pressure
Formula Nr.    2     Log(P) = A + B/T + C*Log(T) + D*T + E*T^2  [mm Hg] [mm Hg]
Minimum temperature                   =       189.630000 [K]
Maximum temperature                   =       535.000000 [K]
Parameter 1                           =     3.448330E+0001
Parameter 2                           =    -2.749000E+0003
Parameter 3                           =    -9.465400E+0000
Parameter 4                           =    -8.991000E-0004
Parameter 5                           =     5.199700E-0006

Heat of vaporization
Formula Nr.    3     Hv = A * ((C-T)/(C-B)^D  (A=Hv1, B=T1, C=Tc)  [cal/g] [cal/g]
Minimum temperature                   =       189.630000 [K]
Maximum temperature                   =       535.000000 [K]
Parameter 1                           =     1.373000E+0002
Parameter 2                           =     3.623000E+0002
Parameter 3                           =     5.350000E+0002
Parameter 4                           =     2.733000E-0001
Parameter 5                           =     0.000000E+0000

Liquid heatcapacity
Formula Nr.    4     Cpl = A + B*T + C*T^2 + D*T^3  [cal/g/K] [cal/g/K]
Minimum temperature                   =       189.630000 [K]
Maximum temperature                   =       400.000000 [K]
Parameter 1                           =     4.947600E-0001
Parameter 2                           =    -4.940000E-0004
Parameter 3                           =     1.595400E-0006
Parameter 4                           =     1.850800E-0013
Parameter 5                           =     0.000000E+0000

IG heatcapacity
Formula Nr.    5     Cp = A + B*T + C*T^2 + D*T^3  [cal/mol] [cal/mol]
Minimum temperature                   =       200.000000 [K]
Maximum temperature                   =      1500.000000 [K]
Parameter 1                           =     3.897900E+0000
Parameter 2                           =     4.600500E-0002
Parameter 3                           =    -2.709000E-0005
Parameter 4                           =     6.015100E-0009
Parameter 5                           =     0.000000E+0000

Liquid viscosity
Formula Nr.    6     Log(Visc) = Ea + Eb/T + Ec*Log (T) + Ed*T + Ee*T*T  (where Ec=0!) [centiPoise]
[centiPoise]
Minimum temperature                   =       240.000000 [K]
Maximum temperature                   =       390.000000 [K]
Parameter 1                           =    -9.171000E-0001
Parameter 2                           =     2.560100E+0002
Parameter 3                           =     0.000000E+0000
Parameter 4                           =    -1.668000E-0003
Parameter 5                           =     9.100300E-0007

Vapor viscosity
Formula Nr.    7     Visc = A + B*T + C*T^2  [microPoise] [microPoise]
Minimum temperature                   =       303.150000 [K]
Maximum temperature                   =      1000.000000 [K]
Parameter 1                           =    -5.005000E+0000
Parameter 2                           =     2.412800E-0001
Parameter 3                           =    -1.518000E-0005
Parameter 4                           =     0.000000E+0000
Parameter 5                           =     0.000000E+0000

Surface Tension
Formula Nr.    8     Sigma = A * ((C-T)/(C-B))^D  (A=Sigma1, B=T1, C=Tc)  [dynes/cm] [dynes/cm]
Minimum temperature                   =       189.630000 [K]
Maximum temperature                   =       535.000000 [K]
Parameter 1                           =     1.904000E+0001
Parameter 2                           =     3.623000E+0002
Parameter 3                           =     5.350000E+0002
Parameter 4                           =     1.070500E+0000
Parameter 5                           =     0.000000E+0000
```

Annex-12

3.   AIR

```
Material_Name                    = AIR
Molecular formula                = --
UN number                        =            1003
Molecular weight                 =       28.960000 kg/kmol
Critical temperature             =      143.000000 K (-130.15 °C)
Melting point                    =       60.000000 K (-213.15 °C)
Triplepoint temperature          =       60.000000 K (-213.15 °C)
Normal boiling point             =       80.000000 K (-193.15 °C)
Standard net heat of combustion  =  0.000000E+0000 J/kg ( 0.000000E+0000 J/kmol)
Flash point                      =        0.000000 K (-273.15 °C)
Lower flammability limit         =        0.000000 vol% in air
Upper flammability limit         =        0.000000 vol% in air
Solubility in water              =        0.200000 kg/m3


Temperature dependent data (calculated at 288.15 K  (15.00 °C)
Liquid density                   =       Undefined
Vapor pressure                   =       Undefined
Heat of vaporization             =       Undefined
Liquid heatcapacity              =       Undefined
Gas heatcapacity (ideal gas)     =  1.003217E+0003   J/kg*K (1003.22 J/kg*K)
Liquid viscosity                 =       Undefined
Vapor viscosity                  =  1.668360E-0005     Pa*s
Surface tension                  =       Undefined
Poisson ratio                    =  1.401


Functions (calculated at 288.15 K  (15.00 °C) and 1.000000E+05 N/m2  (1.000 Bar)
Gas density (ideal gas law) :         1.209 kg/m3
Mass of 1 m3 gas/vapour     :         1.209 kg
Volume of 1 kg gas/vapour   :         0.827 m3
Mass of 1 m3 liquid         :      Undefined
Volume of 1000 kg liquid    :      Undefined


Probit constants (Toxicity)
A =        0.000000 SI units(Kg*s/m3)
B =        0.000000 SI units(Kg*s/m3)
N =        0.000000 SI units(Kg*s/m3)

A =        0.000000 (ppm*min)
B =        0.000000 (ppm*min)
N =        0.000000 (ppm*min)

A =        0.000000 (mg*min/m3)
B =        0.000000 (mg*min/m3)
N =        0.000000 (mg*min/m3)


Temperature dependent data (Parameters):

Liquid density
Formula Nr.   1    rho = A * B^-((1-T/C)^2/7)  (where C=Tc)  [g/cm3] [g/cm3]
Minimum temperature              =       63.150000 [K]
Maximum temperature              =      126.100000 [K]
Parameter 1                      = 3.063500E-0001
Parameter 2                      = 2.802100E-0001
Parameter 3                      = 1.430000E+0002
Parameter 4                      = 0.000000E+0000
Parameter 5                      = 0.000000E+0000
```

```
Vapor pressure
Formula Nr.    2     Log(P) = A + B/T + C*Log(T) + D*T + E*T^2  [mm Hg] [mm Hg]
Minimum temperature                   =        63.150000 [K]
Maximum temperature                   =       126.100000 [K]
Parameter 1                           =     2.208250E+0001
Parameter 2                           =    -4.636600E+0002
Parameter 3                           =    -7.642500E+0000
Parameter 4                           =     1.512500E-0002
Parameter 5                           =     9.202400E-0006

Heat of vaporization
Formula Nr.    3     Hv = A * ((C-T)/(C-B)^D  (A=Hv1, B=T1, C=Tc)  [cal/g] [cal/g]
Minimum temperature                   =        63.150000 [K]
Maximum temperature                   =       126.100000 [K]
Parameter 1                           =     4.082000E+0001
Parameter 2                           =     9.463000E+0001
Parameter 3                           =     1.430000E+0002
Parameter 4                           =     3.875700E-0001
Parameter 5                           =     0.000000E+0000

Liquid heatcapacity
Formula Nr.    4     Cpl = A + B*T + C*T^2 + D*T^3  [cal/g/K] [cal/g/K]
Minimum temperature                   =        64.000000 [K]
Maximum temperature                   =       120.000000 [K]
Parameter 1                           =     9.990900E-0001
Parameter 2                           =    -1.390000E-0002
Parameter 3                           =     9.090500E-0005
Parameter 4                           =     2.520200E-0008
Parameter 5                           =     0.000000E+0000

IG heatcapacity
Formula Nr.    5     Cp = A + B*T + C*T^2 + D*T^3  [cal/mol] [cal/mol]
Minimum temperature                   =       250.000000 [K]
Maximum temperature                   =      1500.000000 [K]
Parameter 1                           =     7.064000E+0000
Parameter 2                           =    -1.256000E-0003
Parameter 3                           =     3.227700E-0006
Parameter 4                           =    -1.234000E-0009
Parameter 5                           =     0.000000E+0000

Liquid viscosity
Formula Nr.    6     Log(Visc) = Ea + Eb/T + Ec*Log (T) + Ed*T + Ee*T*T  (where Ec=0!)  [centiPoise]
[centiPoise]
Minimum temperature                   =        63.150000 [K]
Maximum temperature                   =       125.000000 [K]
Parameter 1                           =    -7.685000E-0001
Parameter 2                           =     4.193500E+0001
Parameter 3                           =     0.000000E+0000
Parameter 4                           =    -7.046000E-0003
Parameter 5                           =    -1.886000E-0006

Vapor viscosity
Formula Nr.    7     Visc = A + B*T + C*T^2  [microPoise] [microPoise]
Minimum temperature                   =        80.000000 [K]
Maximum temperature                   =      1500.000000 [K]
Parameter 1                           =     2.202900E+0001
Parameter 2                           =     5.434000E-0001
Parameter 3                           =    -1.418000E-0004
Parameter 4                           =     0.000000E+0000
Parameter 5                           =     0.000000E+0000

Surface Tension
Formula Nr.    8     Sigma = A * ((C-T)/(C-B))^D  (A=Sigma1, B=T1, C=Tc)  [dynes/cm] [dynes/cm]
Minimum temperature                   =        63.150000 [K]
Maximum temperature                   =       126.100000 [K]
Parameter 1                           =     5.143000E+0000
Parameter 2                           =     9.463000E+0001
Parameter 3                           =     1.430000E+0002
Parameter 4                           =     1.245700E+0000
Parameter 5                           =     0.000000E+0000
```

4.   AMMONIA

```
Material_Name                     = AMMONIA
Molecular formula                 = NH3
UN number                         =         1005
Molecular weight                  =       17.030000 kg/kmol
Critical temperature              =      405.650000 K (132.50 °C)
Melting point                     =      195.410000 K (-77.74 °C)
Triplepoint temperature           =      195.410000 K (-77.74 °C)
Normal boiling point              =      239.720000 K (-33.43 °C)
Standard net heat of combustion   = 1.860300E+0007 J/kg ( 3.168091E+0008 J/kmol)
Flash point                       =      208.400000 K (-64.75 °C)
Lower flammability limit          =       16.000000 vol% in air
Upper flammability limit          =      100.000000 vol% in air
Solubility in water               =      530.000000 kg/m3


Temperature dependent data (calculated at 288.15 K  (15.00 °C)
Liquid density                    = 6.165555E+0002    kg/m3 (616.56 kg/m3 )
Vapor pressure                    = 7.275728E+0005    N/m2 (7.28 Bar   )
Heat of vaporization              = 1.209099E+0006    J/kg (1209099.14 J/kg  )
Liquid heatcapacity               = 4.593142E+0003    J/kg*K (4593.14 J/kg*K)
Gas heatcapacity (ideal gas)      = 2.111294E+0003    J/kg*K (2111.29 J/kg*K)
Liquid viscosity                  = 1.457633E-0004    Pa*s
Vapor viscosity                   = 9.763079E-0006    Pa*s
Surface tension                   = 2.324988E-0002     N/m
Poisson ratio                     = 1.301


Functions (calculated at 288.15 K  (15.00 °C) and 1.000000E+05 N/m2  (1.000 Bar)
Gas density (ideal gas law) :         0.711 kg/m3
Mass of 1 m3 gas/vapour     :         0.711 kg
Volume of 1 kg gas/vapour   :         1.407 m3
Mass of 1 m3 liquid         :       616.555 kg
Volume of 1000 kg liquid    :         1.622 m3


Probit constants (Toxicity)
A =        7.936700 SI units(Kg*s/m3)
B =        1.000000 SI units(Kg*s/m3)
N =        2.000000 SI units(Kg*s/m3)

A =      -16.286131 (ppm*min)
B =        1.000000 (ppm*min)
N =        2.000000 (ppm*min)

A =      -15.599977 (mg*min/m3)
B =        1.000000 (mg*min/m3)
N =        2.000000 (mg*min/m3)


Temperature dependent data (Parameters):

Liquid density
Formula Nr.   1    rho = A * B^-((1-T/C)^2/7)  (where C=Tc) [g/cm3] [g/cm3]
Minimum temperature               =      195.410000 [K]
Maximum temperature               =      405.650000 [K]
Parameter 1                       = 2.348500E-0001
Parameter 2                       = 2.527900E-0001
Parameter 3                       = 4.056500E+0002
Parameter 4                       = 0.000000E+0000
Parameter 5                       = 0.000000E+0000
```

```
Vapor pressure
Formula Nr.   2     Log(P) = A + B/T + C*Log(T) + D*T + E*T^2  [mm Hg] [mm Hg]
Minimum temperature                =        195.410000 [K]
Maximum temperature                =        405.650000 [K]
Parameter 1                        =      2.724560E+0001
Parameter 2                        =     -1.850300E+0003
Parameter 3                        =     -7.149700E+0000
Parameter 4                        =      5.716300E-0004
Parameter 5                        =      4.017500E-0006

Heat of vaporization
Formula Nr.   3     Hv = A * ((C-T)/(C-B)^D  (A=Hv1, B=T1, C=Tc)  [cal/g] [cal/g]
Minimum temperature                =        195.410000 [K]
Maximum temperature                =        405.650000 [K]
Parameter 1                        =      2.762000E+0002
Parameter 2                        =      3.005000E+0002
Parameter 3                        =      4.056500E+0002
Parameter 4                        =      4.030600E-0001
Parameter 5                        =      0.000000E+0000

Liquid heatcapacity
Formula Nr.   4     Cpl = A + B*T + C*T^2 + D*T^3  [cal/g/K] [cal/g/K]
Minimum temperature                =        195.410000 [K]
Maximum temperature                =        385.150000 [K]
Parameter 1                        =     -4.109200E+0000
Parameter 2                        =      6.139300E-0002
Parameter 3                        =     -2.427000E-0004
Parameter 4                        =      3.204800E-0007
Parameter 5                        =      0.000000E+0000

IG heatcapacity
Formula Nr.   5     Cp = A + B*T + C*T^2 + D*T^3  [cal/mol] [cal/mol]
Minimum temperature                =        100.000000 [K]
Maximum temperature                =       1500.000000 [K]
Parameter 1                        =      7.264000E+0000
Parameter 2                        =      3.012700E-0003
Parameter 3                        =      6.415500E-0006
Parameter 4                        =     -3.150000E-0009
Parameter 5                        =      0.000000E+0000

Liquid viscosity
Formula Nr.   6     Log(Visc) = Ea + Eb/T + Ec*Log (T) + Ed*T + Ee*T*T  (where Ec=0!) [centiPoise]
[centiPoise]
Minimum temperature                =        195.410000 [K]
Maximum temperature                =        393.150000 [K]
Parameter 1                        =     -4.221200E+0000
Parameter 2                        =      5.021700E+0002
Parameter 3                        =      0.000000E+0000
Parameter 4                        =      9.842400E-0003
Parameter 5                        =     -1.438000E-0005

Vapor viscosity
Formula Nr.   7     Visc = A + B*T + C*T^2  [microPoise] [microPoise]
Minimum temperature                =        195.410000 [K]
Maximum temperature                =       1000.000000 [K]
Parameter 1                        =     -7.893800E+0000
Parameter 2                        =      3.675200E-0001
Parameter 3                        =     -4.532000E-0006
Parameter 4                        =      0.000000E+0000
Parameter 5                        =      0.000000E+0000

Surface Tension
Formula Nr.   8     Sigma = A * ((C-T)/(C-B))^D  (A=Sigma1, B=T1, C=Tc)  [dynes/cm] [dynes/cm]
Minimum temperature                =        195.410000 [K]
Maximum temperature                =        405.650000 [K]
Parameter 1                        =      2.057000E+0001
Parameter 2                        =      3.005000E+0002
Parameter 3                        =      4.056500E+0002
Parameter 4                        =      1.102800E+0000
Parameter 5                        =      0.000000E+0000
```

Annex-16

5. BUTANE (n-)

```
Material_Name                   = BUTANE (n-)
Molecular formula               = C4H10
UN number                       =           1011
Molecular weight                =      58.100000 kg/kmol
Critical temperature            =     425.200000 K (152.05 °C)
Melting point                   =     135.000000 K (-138.15 °C)
Triplepoint temperature         =     134.860000 K (-138.29 °C)
Normal boiling point            =     272.700000 K (-0.45 °C)
Standard net heat of combustion = 4.586000E+0007 J/kg ( 2.664466E+0009 J/kmol)
Flash point                     =     195.400000 K (-77.75 °C)
Lower flammability limit        =       1.900000 vol% in air
Upper flammability limit        =     100.000000 vol% in air
Solubility in water             =       0.000000 kg/m3


Temperature dependent data (calculated at 288.15 K  (15.00 °C)
Liquid density                  = 5.844904E+0002    kg/m3 (584.49 kg/m3 )
Vapor pressure                  = 1.821095E+0005    N/m2 (1.82 Bar   )
Heat of vaporization            = 3.621405E+0005    J/kg (362140.53 J/kg  )
Liquid heatcapacity             = 2.457016E+0003    J/kg*K (2457.02 J/kg*K)
Gas heatcapacity (ideal gas)    = 1.643666E+0003    J/kg*K (1643.67 J/kg*K)
Liquid viscosity                = 1.649110E-0004    Pa*s
Vapor viscosity                 = 7.297645E-0006    Pa*s
Surface tension                 = 1.397065E-0002     N/m
Poisson ratio                   = 1.095


Functions (calculated at 288.15 K  (15.00 °C) and 1.000000E+05 N/m2  (1.000 Bar)
Gas density (ideal gas law) :          2.425 kg/m3
Mass of 1 m3 gas/vapour     :          2.425 kg
Volume of 1 kg gas/vapour   :          0.412 m3
Mass of 1 m3 liquid         :        584.490 kg
Volume of 1000 kg liquid    :          1.711 m3


Probit constants (Toxicity)
A =       0.000000 SI units(Kg*s/m3)
B =       0.000000 SI units(Kg*s/m3)
N =       0.000000 SI units(Kg*s/m3)

A =       0.000000 (ppm*min)
B =       0.000000 (ppm*min)
N =       0.000000 (ppm*min)

A =       0.000000 (mg*min/m3)
B =       0.000000 (mg*min/m3)
N =       0.000000 (mg*min/m3)


Temperature dependent data (Parameters):

Liquid density
Formula Nr.   1    rho = A * B^-((1-T/C)^2/7)  (where C=Tc) [g/cm3] [g/cm3]
Minimum temperature             =     120.000000 [K]
Maximum temperature             =     400.000000 [K]
Parameter 1                     = 2.415000E-0001
Parameter 2                     = 2.948000E-0001
Parameter 3                     = 4.252000E+0002
Parameter 4                     = 0.000000E+0000
Parameter 5                     = 0.000000E+0000
```

```
Vapor pressure
Formula Nr.    2    Log(P) = A + B/T + C*Log(T) + D*T + E*T^2  [mm Hg] [mm Hg]
Minimum temperature                =       195.000000 [K]
Maximum temperature                =       400.000000 [K]
Parameter 1                        =    7.300000E+0000
Parameter 2                        =   -1.200000E+0003
Parameter 3                        =    1.000000E-0020
Parameter 4                        =    1.000000E-0020
Parameter 5                        =    1.000000E-0020


Heat of vaporization
Formula Nr.    3    Hv = A * ((C-T)/(C-B)^D  (A=Hv1, B=T1, C=Tc)  [cal/g] [cal/g]
Minimum temperature                =       200.000000 [K]
Maximum temperature                =       500.000000 [K]
Parameter 1                        =    9.000000E+0001
Parameter 2                        =    2.727000E+0002
Parameter 3                        =    4.252000E+0002
Parameter 4                        =    3.700000E-0001
Parameter 5                        =    0.000000E+0000


Liquid heatcapacity
Formula Nr.    4    Cpl = A + B*T + C*T^2 + D*T^3  [cal/g/K] [cal/g/K]
Minimum temperature                =       120.000000 [K]
Maximum temperature                =       400.000000 [K]
Parameter 1                        =    3.000000E-0001
Parameter 2                        =    2.500000E-0003
Parameter 3                        =   -1.300000E-0005
Parameter 4                        =    2.700000E-0008
Parameter 5                        =    0.000000E+0000


IG heatcapacity
Formula Nr.    5    Cp = A + B*T + C*T^2 + D*T^3  [cal/mol] [cal/mol]
Minimum temperature                =       200.000000 [K]
Maximum temperature                =      1500.000000 [K]
Parameter 1                        =    2.266000E+0000
Parameter 2                        =    7.900000E-0002
Parameter 3                        =   -2.650000E-0005
Parameter 4                        =   -6.740000E-0010
Parameter 5                        =    0.000000E+0000


Liquid viscosity
Formula Nr.    6    Log(Visc) = Ea + Eb/T + Ec*Log (T) + Ed*T + Ee*T*T  (where Ec=0!) [centiPoise]
[centiPoise]
Minimum temperature                =       120.000000 [K]
Maximum temperature                =       400.000000 [K]
Parameter 1                        =   -3.168000E+0000
Parameter 2                        =    3.135000E+0002
Parameter 3                        =    0.000000E+0000
Parameter 4                        =    1.034000E-0002
Parameter 5                        =   -2.026000E-0005


Vapor viscosity
Formula Nr.    7    Visc = A + B*T + C*T^2  [microPoise] [microPoise]
Minimum temperature                =       200.000000 [K]
Maximum temperature                =       800.000000 [K]
Parameter 1                        =    3.762000E-0001
Parameter 2                        =    2.491000E-0001
Parameter 3                        =    9.901000E-0006
Parameter 4                        =    0.000000E+0000
Parameter 5                        =    0.000000E+0000


Surface Tension
Formula Nr.    8    Sigma = A * ((C-T)/(C-B))^D  (A=Sigma1, B=T1, C=Tc)  [dynes/cm] [dynes/cm]
Minimum temperature                =       120.000000 [K]
Maximum temperature                =       400.000000 [K]
Parameter 1                        =    2.200000E+0001
Parameter 2                        =    2.250000E+0002
Parameter 3                        =    4.252000E+0002
Parameter 4                        =    1.198200E+0000
Parameter 5                        =    0.000000E+0000
```

Annex-18

6.   CARBON MONOXIDE

```
Material_Name                   = CARBON MONOXIDE
Molecular formula               = CO
UN number                       =        1016
Molecular weight                =       28.010000 kg/kmol
Critical temperature            =      132.920000 K (-140.23 °C)
Melting point                   =       68.150000 K (-205.00 °C)
Triplepoint temperature         =       68.150000 K (-205.00 °C)
Normal boiling point            =       81.700000 K (-191.45 °C)
Standard net heat of combustion = 1.010400E+0007 J/kg ( 2.830130E+0008 J/kmol)
Flash point                     =       67.050000 K (-206.10 °C)
Lower flammability limit        =       12.500000 vol% in air
Upper flammability limit        =      100.000000 vol% in air
Solubility in water             =        0.000000 kg/m3


Temperature dependent data (calculated at 288.15 K  (15.00 °C)
Liquid density                  =        Undefined
Vapor pressure                  =        Undefined
Heat of vaporization            =        Undefined
Liquid heatcapacity             =        Undefined
Gas heatcapacity (ideal gas)    = 1.039527E+0003   J/kg*K (1039.53 J/kg*K)
Liquid viscosity                =        Undefined
Vapor viscosity                 = 1.668827E-0005     Pa*s
Surface tension                 =        Undefined
Poisson ratio                   = 1.400


Functions (calculated at 288.15 K  (15.00 °C) and 1.000000E+05 N/m2  (1.000 Bar)
Gas density (ideal gas law) :         1.169 kg/m3
Mass of 1 m3 gas/vapour     :         1.169 kg
Volume of 1 kg gas/vapour   :         0.855 m3
Mass of 1 m3 liquid         :      Undefined
Volume of 1000 kg liquid    :      Undefined


Probit constants (Toxicity)
A =        2.321166 SI units(Kg*s/m3)
B =        1.000000 SI units(Kg*s/m3)
N =        1.000000 SI units(Kg*s/m3)

A =       -7.245492 (ppm*min)
B =        1.000000 (ppm*min)
N =        1.000000 (ppm*min)

A =       -7.400000 (mg*min/m3)
B =        1.000000 (mg*min/m3)
N =        1.000000 (mg*min/m3)


Temperature dependent data (Parameters):

Liquid density
Formula Nr.   1    rho = A * B^-((1-T/C)^2/7)  (where C=Tc) [g/cm3] [g/cm3]
Minimum temperature             =       68.150000 [K]
Maximum temperature             =      132.920000 [K]
Parameter 1                     = 2.942500E-0001
Parameter 2                     = 2.733800E-0001
Parameter 3                     = 1.329200E+0002
Parameter 4                     = 0.000000E+0000
Parameter 5                     = 0.000000E+0000
```

```
Vapor pressure
Formula Nr.   2    Log(P) = A + B/T + C*Log(T) + D*T + E*T^2  [mm Hg] [mm Hg]
Minimum temperature              =         68.150000 [K]
Maximum temperature              =        132.920000 [K]
Parameter 1                      =     4.611950E+0001
Parameter 2                      =    -7.443300E+0002
Parameter 3                      =    -1.949400E+0001
Parameter 4                      =     3.642400E-0002
Parameter 5                      =     2.554400E-0005


Heat of vaporization
Formula Nr.   3    Hv = A * ((C-T)/(C-B)^D  (A=Hv1, B=T1, C=Tc)  [cal/g] [cal/g]
Minimum temperature              =         68.150000 [K]
Maximum temperature              =        132.920000 [K]
Parameter 1                      =     4.356000E+0001
Parameter 2                      =     1.005000E+0002
Parameter 3                      =     1.329200E+0002
Parameter 4                      =     3.180000E-0001
Parameter 5                      =     0.000000E+0000


Liquid heatcapacity
Formula Nr.   4    Cpl = A + B*T + C*T^2 + D*T^3  [cal/g/K] [cal/g/K]
Minimum temperature              =         68.150000 [K]
Maximum temperature              =         90.000000 [K]
Parameter 1                      =     4.702800E-0001
Parameter 2                      =     6.002600E-0004
Parameter 3                      =     2.323900E-0009
Parameter 4                      =    -1.043000E-0011
Parameter 5                      =     0.000000E+0000


IG heatcapacity
Formula Nr.   5    Cp = A + B*T + C*T^2 + D*T^3  [cal/mol] [cal/mol]
Minimum temperature              =        170.000000 [K]
Maximum temperature              =       1100.000000 [K]
Parameter 1                      =     7.045700E+0000
Parameter 2                      =    -1.196000E-0003
Parameter 3                      =     3.472100E-0006
Parameter 4                      =    -1.401000E-0009
Parameter 5                      =     0.000000E+0000


Liquid viscosity
Formula Nr.   6    Log(Visc) = Ea + Eb/T + Ec*Log (T) + Ed*T + Ee*T*T  (where Ec=0!) [centiPoise]
[centiPoise]
Minimum temperature              =         68.550000 [K]
Maximum temperature              =        131.370000 [K]
Parameter 1                      =    -1.366300E+0000
Parameter 2                      =     6.540800E+0001
Parameter 3                      =     0.000000E+0000
Parameter 4                      =    -2.344000E-0003
Parameter 5                      =    -6.416000E-0007


Vapor viscosity
Formula Nr.   7    Visc = A + B*T + C*T^2  [microPoise] [microPoise]
Minimum temperature              =         68.150000 [K]
Maximum temperature              =       1250.000000 [K]
Parameter 1                      =     1.283800E+0001
Parameter 2                      =     5.909900E-0001
Parameter 3                      =    -1.957000E-0004
Parameter 4                      =     0.000000E+0000
Parameter 5                      =     0.000000E+0000


Surface Tension
Formula Nr.   8    Sigma = A * ((C-T)/(C-B))^D  (A=Sigma1, B=T1, C=Tc)  [dynes/cm] [dynes/cm]
Minimum temperature              =         68.150000 [K]
Maximum temperature              =        132.920000 [K]
Parameter 1                      =     5.646000E+0000
Parameter 2                      =     1.005000E+0002
Parameter 3                      =     1.329200E+0002
Parameter 4                      =     1.133000E+0000
Parameter 5                      =     0.000000E+0000
```

Annex-20

7.   CARBONDISULFIDE

```
Material_Name                     = CARBONDISULFIDE
Molecular formula                 = CS2
UN number                         =            1131
Molecular weight                  =        76.140000 kg/kmol
Critical temperature              =       552.000000 K (278.85 °C)
Melting point                     =       161.580000 K (-111.57 °C)
Triplepoint temperature           =       161.110000 K (-112.04 °C)
Normal boiling point              =       319.380000 K (46.23 °C)
Standard net heat of combustion   = 1.450200E+0007 J/kg ( 1.104182E+0009 J/kmol)
Flash point                       =       243.150000 K (-30.00 °C)
Lower flammability limit          =         1.300000 vol% in air
Upper flammability limit          =       100.000000 vol% in air
Solubility in water               =         2.000000 kg/m3


Temperature dependent data (calculated at 288.15 K  (15.00 °C)
Liquid density                    = 1.267902E+0003    kg/m3 (1267.90 kg/m3 )
Vapor pressure                    = 3.226504E+0004    N/m2 (0.32 Bar   )
Heat of vaporization              = 3.685778E+0005    J/kg (368577.84 J/kg  )
Liquid heatcapacity               = 9.993362E+0002    J/kg*K (999.34 J/kg*K)
Gas heatcapacity (ideal gas)      = 5.806365E+0002    J/kg*K (580.64 J/kg*K)
Liquid viscosity                  = 3.794892E-0004    Pa*s
Vapor viscosity                   = 9.563160E-0006    Pa*s
Surface tension                   = 3.304700E-0002     N/m
Poisson ratio                     = 1.232


Functions (calculated at 288.15 K  (15.00 °C) and 1.000000E+05 N/m2  (1.000 Bar)
Gas density (ideal gas law) :          3.178 kg/m3
Mass of 1 m3 gas/vapour     :          3.178 kg
Volume of 1 kg gas/vapour   :          0.315 m3
Mass of 1 m3 liquid         :       1267.902 kg
Volume of 1000 kg liquid    :          0.789 m3


Probit constants (Toxicity)
A =       0.000000 SI units(Kg*s/m3)
B =       0.000000 SI units(Kg*s/m3)
N =       0.000000 SI units(Kg*s/m3)

A =       0.000000 (ppm*min)
B =       0.000000 (ppm*min)
N =       0.000000 (ppm*min)

A =       0.000000 (mg*min/m3)
B =       0.000000 (mg*min/m3)
N =       0.000000 (mg*min/m3)


Temperature dependent data (Parameters):

Liquid density
Formula Nr.   1    rho = A * B^-((1-T/C)^2/7)  (where C=Tc) [g/cm3] [g/cm3]
Minimum temperature               =       161.110000 [K]
Maximum temperature               =       552.000000 [K]
Parameter 1                       = 4.302000E-0001
Parameter 2                       = 2.632500E-0001
Parameter 3                       = 5.520000E+0002
Parameter 4                       = 0.000000E+0000
Parameter 5                       = 0.000000E+0000
```

```
Vapor pressure
Formula Nr.    2    Log(P) = A + B/T + C*Log(T) + D*T + E*T^2  [mm Hg] [mm Hg]
Minimum temperature                 =        161.110000 [K]
Maximum temperature                 =        552.000000 [K]
Parameter 1                         =     2.097620E+0001
Parameter 2                         =    -1.969200E+0003
Parameter 3                         =    -4.912400E+0000
Parameter 4                         =     6.857900E-0004
Parameter 5                         =     1.525500E-0006


Heat of vaporization
Formula Nr.    3    Hv = A * ((C-T)/(C-B)^D  (A=Hv1, B=T1, C=Tc)  [cal/g] [cal/g]
Minimum temperature                 =        161.110000 [K]
Maximum temperature                 =        552.000000 [K]
Parameter 1                         =     8.050000E+0001
Parameter 2                         =     3.566000E+0002
Parameter 3                         =     5.520000E+0002
Parameter 4                         =     2.985000E-0001
Parameter 5                         =     0.000000E+0000


Liquid heatcapacity
Formula Nr.    4    Cpl = A + B*T + C*T^2 + D*T^3  [cal/g/K] [cal/g/K]
Minimum temperature                 =        163.930000 [K]
Maximum temperature                 =        552.000000 [K]
Parameter 1                         =     1.944500E-0001
Parameter 2                         =     5.827900E-0004
Parameter 3                         =    -2.731000E-0006
Parameter 4                         =     4.309600E-0009
Parameter 5                         =     0.000000E+0000


IG heatcapacity
Formula Nr.    5    Cp = A + B*T + C*T^2 + D*T^3  [cal/mol] [cal/mol]
Minimum temperature                 =        100.000000 [K]
Maximum temperature                 =        773.000000 [K]
Parameter 1                         =     5.595400E+0000
Parameter 2                         =     2.258400E-0002
Parameter 3                         =    -2.040000E-0005
Parameter 4                         =     6.359600E-0009
Parameter 5                         =     0.000000E+0000


Liquid viscosity
Formula Nr.    6    Log(Visc) = Ea + Eb/T + Ec*Log (T) + Ed*T + Ee*T*T  (where Ec=0!) [centiPoise]
[centiPoise]
Minimum temperature                 =        235.000000 [K]
Maximum temperature                 =        320.000000 [K]
Parameter 1                         =    -3.665800E+0000
Parameter 2                         =     6.549200E+0002
Parameter 3                         =     0.000000E+0000
Parameter 4                         =     2.539300E-0003
Parameter 5                         =     2.896000E-0006


Vapor viscosity
Formula Nr.    7    Visc = A + B*T + C*T^2  [microPoise] [microPoise]
Minimum temperature                 =        273.150000 [K]
Maximum temperature                 =        582.950000 [K]
Parameter 1                         =    -7.759100E+0000
Parameter 2                         =     3.662400E-0001
Parameter 3                         =    -2.579000E-0005
Parameter 4                         =     0.000000E+0000
Parameter 5                         =     0.000000E+0000


Surface Tension
Formula Nr.    8    Sigma = A * ((C-T)/(C-B))^D  (A=Sigma1, B=T1, C=Tc)  [dynes/cm] [dynes/cm]
Minimum temperature                 =        161.110000 [K]
Maximum temperature                 =        552.000000 [K]
Parameter 1                         =     2.311000E+0001
Parameter 2                         =     3.566000E+0002
Parameter 3                         =     5.520000E+0002
Parameter 4                         =     1.190900E+0000
Parameter 5                         =     0.000000E+0000
```

Annex-22

8.   CHLORINE

```
Material_Name                      = CHLORINE
Molecular formula                  = Cl2
UN number                          =             1017
Molecular weight                   =        70.910000 kg/kmol
Critical temperature               =       417.150000 K (144.00 °C)
Melting point                      =       172.120000 K (-101.03 °C)
Triplepoint temperature            =       172.120000 K (-101.03 °C)
Normal boiling point               =       239.120000 K (-34.03 °C)
Standard net heat of combustion    =  0.000000E+0000 J/kg ( 0.000000E+0000 J/kmol)
Flash point                        =        0.000000 K (-273.15 °C)
Lower flammability limit           =        0.000000 vol% in air
Upper flammability limit           =        0.000000 vol% in air
Solubility in water                =        7.000000 kg/m3


Temperature dependent data (calculated at 288.15 K  (15.00 °C)
Liquid density                     = 1.427436E+0003    kg/m3 (1427.44 kg/m3 )
Vapor pressure                     = 5.889504E+0005    N/m2 (5.89 Bar   )
Heat of vaporization               = 2.565440E+0005    J/kg (256544.02 J/kg  )
Liquid heatcapacity                = 8.994889E+0002    J/kg*K (899.49 J/kg*K)
Gas heatcapacity (ideal gas)       = 4.714603E+0002    J/kg*K (471.46 J/kg*K)
Liquid viscosity                   = 3.405445E-0004    Pa*s
Vapor viscosity                    = 1.295505E-0005    Pa*s
Surface tension                    = 1.890329E-0002     N/m
Poisson ratio                      = 1.331


Functions (calculated at 288.15 K  (15.00 °C) and 1.000000E+05 N/m2  (1.000 Bar)
Gas density (ideal gas law) :          2.960 kg/m3
Mass of 1 m3 gas/vapour     :          2.960 kg
Volume of 1 kg gas/vapour   :          0.338 m3
Mass of 1 m3 liquid         :       1427.436 kg
Volume of 1000 kg liquid    :          0.701 m3


Probit constants (Toxicity)
A =       10.599000 SI units(Kg*s/m3)
B =        0.500000 SI units(Kg*s/m3)
N =        2.750000 SI units(Kg*s/m3)

A =       -4.860538 (ppm*min)
B =        0.500000 (ppm*min)
N =        2.750000 (ppm*min)

A =       -6.350155 (mg*min/m3)
B =        0.500000 (mg*min/m3)
N =        2.750000 (mg*min/m3)


Temperature dependent data (Parameters):

Liquid density
Formula Nr.   1    rho = A * B^-((1-T/C)^2/7)  (where C=Tc) [g/cm3] [g/cm3]
Minimum temperature                =       172.120000 [K]
Maximum temperature                =       417.150000 [K]
Parameter 1                        = 5.624400E-0001
Parameter 2                        = 2.718800E-0001
Parameter 3                        = 4.171500E+0002
Parameter 4                        = 0.000000E+0000
Parameter 5                        = 0.000000E+0000
```

```
Vapor pressure
Formula Nr.   2    Log(P) = A + B/T + C*Log(T) + D*T + E*T^2  [mm Hg] [mm Hg]
Minimum temperature              =       172.120000 [K]
Maximum temperature              =       417.150000 [K]
Parameter 1                      =   2.275110E+0001
Parameter 2                      =  -1.570600E+0003
Parameter 3                      =  -5.743400E+0000
Parameter 4                      =   8.377100E-0004
Parameter 5                      =   2.769700E-0006


Heat of vaporization
Formula Nr.   3    Hv = A * ((C-T)/(C-B)^D  (A=Hv1, B=T1, C=Tc)  [cal/g] [cal/g]
Minimum temperature              =       172.120000 [K]
Maximum temperature              =       417.150000 [K]
Parameter 1                      =   6.010000E+0001
Parameter 2                      =   2.946000E+0002
Parameter 3                      =   4.171500E+0002
Parameter 4                      =   3.810400E-0001
Parameter 5                      =   0.000000E+0000


Liquid heatcapacity
Formula Nr.   4    Cpl = A + B*T + C*T^2 + D*T^3  [cal/g/K] [cal/g/K]
Minimum temperature              =       172.000000 [K]
Maximum temperature              =       353.000000 [K]
Parameter 1                      =   2.175900E-0001
Parameter 2                      =   1.240400E-0004
Parameter 3                      =  -3.898000E-0007
Parameter 4                      =  -2.544000E-0010
Parameter 5                      =   0.000000E+0000


IG heatcapacity
Formula Nr.   5    Cp = A + B*T + C*T^2 + D*T^3  [cal/mol] [cal/mol]
Minimum temperature              =       100.000000 [K]
Maximum temperature              =       773.000000 [K]
Parameter 1                      =   6.351200E+0000
Parameter 2                      =   7.605900E-0003
Parameter 3                      =  -7.389000E-0006
Parameter 4                      =   2.387200E-0009
Parameter 5                      =   0.000000E+0000


Liquid viscosity
Formula Nr.   6    Log(Visc) = Ea + Eb/T + Ec*Log (T) + Ed*T + Ee*T*T  (where Ec=0!) [centiPoise]
[centiPoise]
Minimum temperature              =       190.000000 [K]
Maximum temperature              =       300.000000 [K]
Parameter 1                      =  -7.674200E+0000
Parameter 2                      =   6.904900E+0002
Parameter 3                      =   0.000000E+0000
Parameter 4                      =   2.860800E-0002
Parameter 5                      =  -4.135000E-0005


Vapor viscosity
Formula Nr.   7    Visc = A + B*T + C*T^2  [microPoise] [microPoise]
Minimum temperature              =       200.000000 [K]
Maximum temperature              =      1000.000000 [K]
Parameter 1                      =  -5.394300E+0000
Parameter 2                      =   4.949800E-0001
Parameter 3                      =  -9.254000E-0005
Parameter 4                      =   0.000000E+0000
Parameter 5                      =   0.000000E+0000


Surface Tension
Formula Nr.   8    Sigma = A * ((C-T)/(C-B))^D  (A=Sigma1, B=T1, C=Tc)  [dynes/cm] [dynes/cm]
Minimum temperature              =       172.120000 [K]
Maximum temperature              =       417.150000 [K]
Parameter 1                      =   1.788000E+0001
Parameter 2                      =   2.946000E+0002
Parameter 3                      =   4.171500E+0002
Parameter 4                      =   1.085000E+0000
Parameter 5                      =   0.000000E+0000
```

Annex-24

9. ETHENE

```
Material_Name                     = ETHENE
Molecular formula                 = CH2=CH2
UN number                         =        1962
Molecular weight                  =       28.052000 kg/kmol
Critical temperature              =      282.900000 K (9.75 °C)
Melting point                     =      104.000000 K (-169.15 °C)
Triplepoint temperature           =      104.000000 K (-169.15 °C)
Normal boiling point              =      169.300000 K (-103.85 °C)
Standard net heat of combustion   = 4.719400E+0007 J/kg ( 1.323886E+0009 J/kmol)
Flash point                       =      125.700000 K (-147.45 °C)
Lower flammability limit          =        2.750000 vol% in air
Upper flammability limit          =      100.000000 vol% in air
Solubility in water               =        0.100000 kg/m3


Temperature dependent data (calculated at 288.15 K  (15.00 °C)
Liquid density                    =        Undefined
Vapor pressure                    =        Undefined
Heat of vaporization              =        Undefined
Liquid heatcapacity               =        Undefined
Gas heatcapacity (ideal gas)      = 1.540338E+0003   J/kg*K (1540.34 J/kg*K)
Liquid viscosity                  =        Undefined
Vapor viscosity                   = 9.812499E-0006     Pa*s
Surface tension                   =        Undefined
Poisson ratio                     = 1.238


Functions (calculated at 288.15 K  (15.00 °C) and 1.000000E+05 N/m2  (1.000 Bar)
Gas density (ideal gas law) :          1.171 kg/m3
Mass of 1 m3 gas/vapour     :          1.171 kg
Volume of 1 kg gas/vapour   :          0.854 m3
Mass of 1 m3 liquid         :       Undefined
Volume of 1000 kg liquid    :       Undefined


Probit constants (Toxicity)
A =        0.000000 SI units(Kg*s/m3)
B =        0.000000 SI units(Kg*s/m3)
N =        0.000000 SI units(Kg*s/m3)

A =        0.000000 (ppm*min)
B =        0.000000 (ppm*min)
N =        0.000000 (ppm*min)

A =        0.000000 (mg*min/m3)
B =        0.000000 (mg*min/m3)
N =        0.000000 (mg*min/m3)


Temperature dependent data (Parameters):

Liquid density
Formula Nr.   1    rho = A * B^-((1-T/C)^2/7)  (where C=Tc)  [g/cm3] [g/cm3]
Minimum temperature               =      103.800000 [K]
Maximum temperature               =      282.900000 [K]
Parameter 1                       = 2.118000E-0001
Parameter 2                       = 2.784000E-0001
Parameter 3                       = 2.829000E+0002
Parameter 4                       = 0.000000E+0000
Parameter 5                       = 0.000000E+0000
```

```
Vapor pressure
Formula Nr.   2    Log(P) = A + B/T + C*Log(T) + D*T + E*T^2  [mm Hg] [mm Hg]
Minimum temperature              =       104.000000 [K]
Maximum temperature              =       283.100000 [K]
Parameter 1                      =    3.089500E+0001
Parameter 2                      =   -1.196800E+0003
Parameter 3                      =   -1.015300E+0001
Parameter 4                      =    9.935100E-0003
Parameter 5                      =    0.000000E+0000

Heat of vaporization
Formula Nr.   3    Hv = A * ((C-T)/(C-B)^D  (A=Hv1, B=T1, C=Tc)  [cal/g] [cal/g]
Minimum temperature              =       103.800000 [K]
Maximum temperature              =       282.900000 [K]
Parameter 1                      =    1.154000E+0002
Parameter 2                      =    1.693000E+0002
Parameter 3                      =    2.829000E+0002
Parameter 4                      =    3.800000E-0001
Parameter 5                      =    0.000000E+0000

Liquid heatcapacity
Formula Nr.   4    Cpl = A + B*T + C*T^2 + D*T^3  [cal/g/K] [cal/g/K]
Minimum temperature              =       104.000000 [K]
Maximum temperature              =       233.000000 [K]
Parameter 1                      =    3.402000E-0001
Parameter 2                      =    6.218000E-0003
Parameter 3                      =   -5.012000E-0005
Parameter 4                      =    1.263000E-0007
Parameter 5                      =    0.000000E+0000

IG heatcapacity
Formula Nr.   5    Cp = A + B*T + C*T^2 + D*T^3  [cal/mol] [cal/mol]
Minimum temperature              =       298.000000 [K]
Maximum temperature              =      1500.000000 [K]
Parameter 1                      =    9.340000E-0001
Parameter 2                      =    3.690000E-0002
Parameter 3                      =   -1.930000E-0005
Parameter 4                      =    4.010000E-0009
Parameter 5                      =    0.000000E+0000

Liquid viscosity
Formula Nr.   6    Log(Visc) = Ea + Eb/T + Ec*Log (T) + Ed*T + Ee*T*T  (where Ec=0!) [centiPoise]
[centiPoise]
Minimum temperature              =       103.800000 [K]
Maximum temperature              =       282.900000 [K]
Parameter 1                      =   -7.706000E+0000
Parameter 2                      =    4.681000E+0002
Parameter 3                      =    0.000000E+0000
Parameter 4                      =    3.725000E-0002
Parameter 5                      =   -7.633000E-0005

Vapor viscosity
Formula Nr.   7    Visc = A + B*T + C*T^2  [microPoise] [microPoise]
Minimum temperature              =       173.000000 [K]
Maximum temperature              =      1073.000000 [K]
Parameter 1                      =    3.586000E+0000
Parameter 2                      =    3.513000E-0001
Parameter 3                      =   -8.055000E-0005
Parameter 4                      =    0.000000E+0000
Parameter 5                      =    0.000000E+0000

Surface Tension
Formula Nr.   8    Sigma = A * ((C-T)/(C-B))^D  (A=Sigma1, B=T1, C=Tc)  [dynes/cm] [dynes/cm]
Minimum temperature              =       103.800000 [K]
Maximum temperature              =       282.900000 [K]
Parameter 1                      =    1.952000E+0001
Parameter 2                      =    1.530000E+0002
Parameter 3                      =    2.829000E+0002
Parameter 4                      =    1.276000E+0000
Parameter 5                      =    0.000000E+0000
```

Annex-26

10.   GASOLINE

```
Material_Name                       = GASOLINE
Molecular formula                   = C4-C12
UN number                           =             1203
Molecular weight                    =        115.000000 kg/kmol
Critical temperature                =        469.700000 K (196.55 °C)
Melting point                       =        253.000000 K (-20.15 °C)
Triplepoint temperature             =        253.000000 K (-20.15 °C)
Normal boiling point                =        333.000000 K (59.85 °C)
Standard net heat of combustion     = 4.500000E+0007 J/kg ( 5.175000E+0009 J/kmol)
Flash point                         =        227.500000 K (-45.65 °C)
Lower flammability limit            =          1.400000 vol% in air
Upper flammability limit            =        100.000000 vol% in air
Solubility in water                 =          0.000000 kg/m3


Temperature dependent data (calculated at 288.15 K  (15.00 °C)
Liquid density                      = 7.403767E+0002    kg/m3 (740.38 kg/m3 )
Vapor pressure                      = 4.277501E+0004    N/m2 (0.43 Bar   )
Heat of vaporization                = 3.701350E+0005    J/kg (370135.03 J/kg  )
Liquid heatcapacity                 = 2.195435E+0003    J/kg*K (2195.44 J/kg*K)
Gas heatcapacity (ideal gas)        = 1.039853E+0003    J/kg*K (1039.85 J/kg*K)
Liquid viscosity                    = 4.421504E-0004    Pa*s
Vapor viscosity                     = 6.591885E-0006    Pa*s
Surface tension                     = 1.962751E-0002     N/m
Poisson ratio                       = 1.075


Functions (calculated at 288.15 K  (15.00 °C) and 1.000000E+05 N/m2  (1.000 Bar)
Gas density (ideal gas law) :           4.800 kg/m3
Mass of 1 m3 gas/vapour     :           4.800 kg
Volume of 1 kg gas/vapour   :           0.208 m3
Mass of 1 m3 liquid         :         740.377 kg
Volume of 1000 kg liquid    :           1.351 m3


Probit constants (Toxicity)
A =        0.000000 SI units(Kg*s/m3)
B =        0.000000 SI units(Kg*s/m3)
N =        0.000000 SI units(Kg*s/m3)

A =        0.000000 (ppm*min)
B =        0.000000 (ppm*min)
N =        0.000000 (ppm*min)

A =        0.000000 (mg*min/m3)
B =        0.000000 (mg*min/m3)
N =        0.000000 (mg*min/m3)


Temperature dependent data (Parameters):

Liquid density
Formula Nr.   1    rho = A * B^-((1-T/C)^2/7)  (where C=Tc) [g/cm3] [g/cm3]
Minimum temperature                 =        273.000000 [K]
Maximum temperature                 =        330.000000 [K]
Parameter 1                         = 3.010000E-0001
Parameter 2                         = 3.070000E-0001
Parameter 3                         = 4.697000E+0002
Parameter 4                         = 0.000000E+0000
Parameter 5                         = 0.000000E+0000
```

```
Vapor pressure
Formula Nr.   2     Log(P) = A + B/T + C*Log(T) + D*T + E*T^2  [mm Hg] [mm Hg]
Minimum temperature             =       263.000000 [K]
Maximum temperature             =       343.000000 [K]
Parameter 1                     = -1.137520E+0001
Parameter 2                     =  0.000000E+0000
Parameter 3                     =  0.000000E+0000
Parameter 4                     =  7.820000E-0002
Parameter 5                     = -1.042000E-0004

Heat of vaporization
Formula Nr.   3     Hv = A * ((C-T)/(C-B)^D  (A=Hv1, B=T1, C=Tc)  [cal/g] [cal/g]
Minimum temperature             =       260.000000 [K]
Maximum temperature             =       470.000000 [K]
Parameter 1                     =  8.361200E+0001
Parameter 2                     =  3.130000E+0002
Parameter 3                     =  4.697000E+0002
Parameter 4                     =  3.800000E-0001
Parameter 5                     =  0.000000E+0000

Liquid heatcapacity
Formula Nr.   4     Cpl = A + B*T + C*T^2 + D*T^3  [cal/g/K] [cal/g/K]
Minimum temperature             =       240.000000 [K]
Maximum temperature             =       330.000000 [K]
Parameter 1                     =  2.713000E-0001
Parameter 2                     =  1.000000E-0003
Parameter 3                     = -4.212800E-0007
Parameter 4                     =  0.000000E+0000
Parameter 5                     =  0.000000E+0000

IG heatcapacity
Formula Nr.   5     Cp = A + B*T + C*T^2 + D*T^3  [cal/mol] [cal/mol]
Minimum temperature             =       200.000000 [K]
Maximum temperature             =      1500.000000 [K]
Parameter 1                     =  3.077910E+0000
Parameter 2                     =  9.977430E-0002
Parameter 3                     = -4.079680E-0005
Parameter 4                     =  5.303310E-0009
Parameter 5                     =  0.000000E+0000

Liquid viscosity
Formula Nr.   6     Log(Visc) = Ea + Eb/T + Ec*Log (T) + Ed*T + Ee*T*T  (where Ec=0!) [centiPoise]
[centiPoise]
Minimum temperature             =       273.000000 [K]
Maximum temperature             =       330.000000 [K]
Parameter 1                     =  2.233000E+0000
Parameter 2                     =  0.000000E+0000
Parameter 3                     =  0.000000E+0000
Parameter 4                     = -1.310000E-0002
Parameter 5                     =  1.430000E-0005

Vapor viscosity
Formula Nr.   7     Visc = A + B*T + C*T^2  [microPoise] [microPoise]
Minimum temperature             =       250.000000 [K]
Maximum temperature             =       600.000000 [K]
Parameter 1                     = -8.111910E+0000
Parameter 2                     =  2.729870E-0001
Parameter 3                     = -5.576810E-0005
Parameter 4                     =  0.000000E+0000
Parameter 5                     =  0.000000E+0000

Surface Tension
Formula Nr.   8     Sigma = A * ((C-T)/(C-B))^D  (A=Sigma1, B=T1, C=Tc)  [dynes/cm] [dynes/cm]
Minimum temperature             =       273.000000 [K]
Maximum temperature             =       330.000000 [K]
Parameter 1                     =  1.900000E+0001
Parameter 2                     =  2.930000E+0002
Parameter 3                     =  4.697000E+0002
Parameter 4                     =  1.200000E+0000
Parameter 5                     =  0.000000E+0000
```

11.   HYDROGEN

```
Material_Name                    = HYDROGEN
Molecular formula                = H2
UN number                        =         1049
Molecular weight                 =     2.016000 kg/kmol
Critical temperature             =    32.800000 K (-240.35 °C)
Melting point                    =    14.000000 K (-259.15 °C)
Triplepoint temperature          =    13.947000 K (-259.20 °C)
Normal boiling point             =    19.200000 K (-253.95 °C)
Standard net heat of combustion  = 1.419000E+0008 J/kg ( 2.860704E+0008 J/kmol)
Flash point                      =    12.900000 K (-260.25 °C)
Lower flammability limit         =     4.000000 vol% in air
Upper flammability limit         =   100.000000 vol% in air
Solubility in water              =     0.000000 kg/m3


Temperature dependent data (calculated at 288.15 K  (15.00 °C)
Liquid density                   =       Undefined
Vapor pressure                   =       Undefined
Heat of vaporization             =       Undefined
Liquid heatcapacity              =       Undefined
Gas heatcapacity (ideal gas)     = 1.431780E+0004   J/kg*K (14317.81 J/kg*K)
Liquid viscosity                 =       Undefined
Vapor viscosity                  = 8.272483E-0006     Pa*s
Surface tension                  =       Undefined
Poisson ratio                    = 1.405


Functions (calculated at 288.15 K  (15.00 °C) and 1.000000E+05 N/m2  (1.000 Bar)
Gas density (ideal gas law) :       0.084 kg/m3
Mass of 1 m3 gas/vapour     :       0.084 kg
Volume of 1 kg gas/vapour   :      11.884 m3
Mass of 1 m3 liquid         :     Undefined
Volume of 1000 kg liquid    :     Undefined


Probit constants (Toxicity)
A =       0.000000 SI units(Kg*s/m3)
B =       0.000000 SI units(Kg*s/m3)
N =       0.000000 SI units(Kg*s/m3)

A =       0.000000 (ppm*min)
B =       0.000000 (ppm*min)
N =       0.000000 (ppm*min)

A =       0.000000 (mg*min/m3)
B =       0.000000 (mg*min/m3)
N =       0.000000 (mg*min/m3)


Temperature dependent data (Parameters):

Liquid density
Formula Nr.   1    rho = A * B^-((1-T/C)^2/7)  (where C=Tc)  [g/cm3] [g/cm3]
Minimum temperature              =    13.600000 [K]
Maximum temperature              =    32.800000 [K]
Parameter 1                      = 3.150000E-0002
Parameter 2                      = 3.473000E-0001
Parameter 3                      = 3.280000E+0001
Parameter 4                      = 0.000000E+0000
Parameter 5                      = 0.000000E+0000
```

```
Vapor pressure
Formula Nr.   2    Log(P) = A + B/T + C*Log(T) + D*T + E*T^2  [mm Hg] [mm Hg]
Minimum temperature             =        13.600000 [K]
Maximum temperature             =        32.800000 [K]
Parameter 1                     =    5.236600E+0000
Parameter 2                     =   -4.628000E+0001
Parameter 3                     =   -4.480900E-0001
Parameter 4                     =    2.529000E-0002
Parameter 5                     =    0.000000E+0000


Heat of vaporization
Formula Nr.   3    Hv = A * ((C-T)/(C-B)^D  (A=Hv1, B=T1, C=Tc)  [cal/g] [cal/g]
Minimum temperature             =        13.600000 [K]
Maximum temperature             =        32.800000 [K]
Parameter 1                     =    1.070000E+0002
Parameter 2                     =    2.020000E+0001
Parameter 3                     =    3.280000E+0001
Parameter 4                     =    2.370000E-0001
Parameter 5                     =    0.000000E+0000


Liquid heatcapacity
Formula Nr.   4    Cpl = A + B*T + C*T^2 + D*T^3  [cal/g/K] [cal/g/K]
Minimum temperature             =        13.600000 [K]
Maximum temperature             =        28.000000 [K]
Parameter 1                     =    3.790000E+0000
Parameter 2                     =   -3.298000E-0001
Parameter 3                     =    1.217090E-0002
Parameter 4                     =   -2.434800E-0006
Parameter 5                     =    0.000000E+0000


IG heatcapacity
Formula Nr.   5    Cp = A + B*T + C*T^2 + D*T^3  [cal/mol] [cal/mol]
Minimum temperature             =       298.000000 [K]
Maximum temperature             =      1500.000000 [K]
Parameter 1                     =    6.880000E+0000
Parameter 2                     =   -2.200000E-0005
Parameter 3                     =    2.100000E-0007
Parameter 4                     =    1.300000E-0010
Parameter 5                     =    0.000000E+0000


Liquid viscosity
Formula Nr.   6    Log(Visc) = Ea + Eb/T + Ec*Log (T) + Ed*T + Ee*T*T  (where Ec=0!) [centiPoise]
[centiPoise]
Minimum temperature             =        13.600000 [K]
Maximum temperature             =        32.800000 [K]
Parameter 1                     =   -4.857000E+0000
Parameter 2                     =    2.513000E+0001
Parameter 3                     =    0.000000E+0000
Parameter 4                     =    1.409000E-0001
Parameter 5                     =   -2.773000E-0003


Vapor viscosity
Formula Nr.   7    Visc = A + B*T + C*T^2  [microPoise] [microPoise]
Minimum temperature             =       113.000000 [K]
Maximum temperature             =      1473.000000 [K]
Parameter 1                     =    2.187000E+0001
Parameter 2                     =    2.220000E-0001
Parameter 3                     =   -3.751000E-0005
Parameter 4                     =    0.000000E+0000
Parameter 5                     =    0.000000E+0000


Surface Tension
Formula Nr.   8    Sigma = A * ((C-T)/(C-B))^D  (A=Sigma1, B=T1, C=Tc)  [dynes/cm] [dynes/cm]
Minimum temperature             =        13.600000 [K]
Maximum temperature             =        32.800000 [K]
Parameter 1                     =    2.410000E+0000
Parameter 2                     =    1.700000E+0001
Parameter 3                     =    3.280000E+0001
Parameter 4                     =    1.101200E+0000
Parameter 5                     =    0.000000E+0000
```

12.   HYDROGEN CHLORIDE

```
Material_Name                      = HYDROGEN CHLORIDE
Molecular formula                  = HCl
UN number                          =          1050
Molecular weight                   =      36.460000 kg/kmol
Critical temperature               =     324.650000 K (51.50 °C)
Melting point                      =     158.970000 K (-114.18 °C)
Triplepoint temperature            =     158.970000 K (-114.18 °C)
Normal boiling point               =     188.150000 K (-85.00 °C)
Standard net heat of combustion    = 7.844600E+0005 J/kg ( 2.860141E+0007 J/kmol)
Flash point                        =       0.000000 K (-273.15 °C)
Lower flammability limit           =       0.000000 vol% in air
Upper flammability limit           =       0.000000 vol% in air
Solubility in water                =     720.000000 kg/m3


Temperature dependent data (calculated at 288.15 K  (15.00 °C)
Liquid density                     = 8.469085E+0002    kg/m3 (846.91 kg/m3 )
Vapor pressure                     = 3.728652E+0006    N/m2 (37.29 Bar   )
Heat of vaporization               = 2.757109E+0005    J/kg (275710.86 J/kg  )
Liquid heatcapacity                = 1.753942E+0003    J/kg*K (1753.94 J/kg*K)
Gas heatcapacity (ideal gas)       = 7.957981E+0002    J/kg*K (795.80 J/kg*K)
Liquid viscosity                   = 9.022553E-0005    Pa*s
Vapor viscosity                    = 1.413966E-0005    Pa*s
Surface tension                    = 5.004225E-0003     N/m
Poisson ratio                      = 1.402


Functions (calculated at 288.15 K  (15.00 °C) and 1.000000E+05 N/m2  (1.000 Bar)
Gas density (ideal gas law) :          1.522 kg/m3
Mass of 1 m3 gas/vapour     :          1.522 kg
Volume of 1 kg gas/vapour   :          0.657 m3
Mass of 1 m3 liquid         :        846.909 kg
Volume of 1000 kg liquid    :          1.181 m3


Probit constants (Toxicity)
A =       -1.428900 SI units(Kg*s/m3)
B =        3.690000 SI units(Kg*s/m3)
N =        1.000000 SI units(Kg*s/m3)

A =      -35.756985 (ppm*min)
B =        3.690000 (ppm*min)
N =        1.000000 (ppm*min)

A =      -37.300003 (mg*min/m3)
B =        3.690000 (mg*min/m3)
N =        1.000000 (mg*min/m3)


Temperature dependent data (Parameters):

Liquid density
Formula Nr.   1   rho = A * B^-((1-T/C)^2/7)  (where C=Tc)  [g/cm3] [g/cm3]
Minimum temperature                =     158.970000 [K]
Maximum temperature                =     324.650000 [K]
Parameter 1                        = 4.023500E-0001
Parameter 2                        = 2.491600E-0001
Parameter 3                        = 3.246500E+0002
Parameter 4                        = 0.000000E+0000
Parameter 5                        = 0.000000E+0000
```

```
Vapor pressure
Formula Nr.   2     Log(P) = A + B/T + C*Log(T) + D*T + E*T^2  [mm Hg] [mm Hg]
Minimum temperature              =        158.970000 [K]
Maximum temperature              =        324.650000 [K]
Parameter 1                      =        3.085270E+0001
Parameter 2                      =       -1.435900E+0003
Parameter 3                      =       -9.269400E+0000
Parameter 4                      =        2.414900E-0003
Parameter 5                      =        8.196100E-0006

Heat of vaporization
Formula Nr.   3     Hv = A * ((C-T)/(C-B)^D  (A=Hv1, B=T1, C=Tc)  [cal/g] [cal/g]
Minimum temperature              =        158.970000 [K]
Maximum temperature              =        324.650000 [K]
Parameter 1                      =        9.041000E+0001
Parameter 2                      =        2.418000E+0002
Parameter 3                      =        3.246500E+0002
Parameter 4                      =        3.864100E-0001
Parameter 5                      =        0.000000E+0000

Liquid heatcapacity
Formula Nr.   4     Cpl = A + B*T + C*T^2 + D*T^3  [cal/g/K] [cal/g/K]
Minimum temperature              =        165.000000 [K]
Maximum temperature              =        185.000000 [K]
Parameter 1                      =        3.101300E-0001
Parameter 2                      =        5.859200E-0004
Parameter 3                      =        2.148400E-0008
Parameter 4                      =       -4.085000E-0011
Parameter 5                      =        0.000000E+0000

IG heatcapacity
Formula Nr.   5     Cp = A + B*T + C*T^2 + D*T^3  [cal/mol] [cal/mol]
Minimum temperature              =        273.000000 [K]
Maximum temperature              =       1500.000000 [K]
Parameter 1                      =        7.075800E+0000
Parameter 2                      =       -1.102000E-0003
Parameter 3                      =        2.292800E-0006
Parameter 4                      =       -7.206000E-0010
Parameter 5                      =        0.000000E+0000

Liquid viscosity
Formula Nr.   6     Log(Visc) = Ea + Eb/T + Ec*Log (T) + Ed*T + Ee*T*T  (where Ec=0!) [centiPoise]
[centiPoise]
Minimum temperature              =        233.150000 [K]
Maximum temperature              =        313.150000 [K]
Parameter 1                      =        2.002600E+0000
Parameter 2                      =       -2.604000E+0002
Parameter 3                      =        0.000000E+0000
Parameter 4                      =       -5.924000E-0003
Parameter 5                      =       -5.258000E-0006

Vapor viscosity
Formula Nr.   7     Visc = A + B*T + C*T^2  [microPoise] [microPoise]
Minimum temperature              =        200.000000 [K]
Maximum temperature              =       1000.000000 [K]
Parameter 1                      =       -1.125000E+0001
Parameter 2                      =        5.642100E-0001
Parameter 3                      =       -1.196000E-0004
Parameter 4                      =        0.000000E+0000
Parameter 5                      =        0.000000E+0000

Surface Tension
Formula Nr.   8     Sigma = A * ((C-T)/(C-B))^D  (A=Sigma1, B=T1, C=Tc)  [dynes/cm] [dynes/cm]
Minimum temperature              =        158.970000 [K]
Maximum temperature              =        324.650000 [K]
Parameter 1                      =        1.449000E+0001
Parameter 2                      =        2.418000E+0002
Parameter 3                      =        3.246500E+0002
Parameter 4                      =        1.297000E+0000
Parameter 5                      =        0.000000E+0000
```

Annex-32

13.   HYDROGEN CYANIDE

```
Material_Name                     = HYDROGEN CYANIDE
Molecular formula                 = HCN
UN number                         =        1051
Molecular weight                  =      27.030000 kg/kmol
Critical temperature              =     456.650000 K (183.50 °C)
Melting point                     =     259.910000 K (-13.24 °C)
Triplepoint temperature           =     259.830000 K (-13.32 °C)
Normal boiling point              =     298.850000 K (25.70 °C)
Standard net heat of combustion   = 2.306300E+0007 J/kg ( 6.233929E+0008 J/kmol)
Flash point                       =     255.370000 K (-17.78 °C)
Lower flammability limit          =       6.000000 vol% in air
Upper flammability limit          =     100.000000 vol% in air
Solubility in water               =     100.000000 kg/m3


Temperature dependent data (calculated at 288.15 K  (15.00 °C)
Liquid density                    = 6.945373E+0002    kg/m3 (694.54 kg/m3 )
Vapor pressure                    = 6.700760E+0004    N/m2 (0.67 Bar   )
Heat of vaporization              = 1.048359E+0006    J/kg (1048359.52 J/kg  )
Liquid heatcapacity               = 2.616330E+0003    J/kg*K (2616.33 J/kg*K)
Gas heatcapacity (ideal gas)      = 1.311660E+0003    J/kg*K (1311.66 J/kg*K)
Liquid viscosity                  = 2.011130E-0004    Pa*s
Vapor viscosity                   = 2.574882E-0006    Pa*s
Surface tension                   = 1.888982E-0002     N/m
Poisson ratio                     = 1.306


Functions (calculated at 288.15 K  (15.00 °C) and 1.000000E+05 N/m2  (1.000 Bar)
Gas density (ideal gas law) :          1.128 kg/m3
Mass of 1 m3 gas/vapour     :          1.128 kg
Volume of 1 kg gas/vapour   :          0.886 m3
Mass of 1 m3 liquid         :        694.537 kg
Volume of 1000 kg liquid    :          1.440 m3


Probit constants (Toxicity)
A =      19.262881 SI units(Kg*s/m3)
B =       1.000000 SI units(Kg*s/m3)
N =       2.400000 SI units(Kg*s/m3)

A =      -9.514656 (ppm*min)
B =       1.000000 (ppm*min)
N =       2.400000 (ppm*min)

A =      -9.800000 (mg*min/m3)
B =       1.000000 (mg*min/m3)
N =       2.400000 (mg*min/m3)


Temperature dependent data (Parameters):

Liquid density
Formula Nr.   1    rho = A * B^-((1-T/C)^2/7)  (where C=Tc) [g/cm3] [g/cm3]
Minimum temperature               =     259.830000 [K]
Maximum temperature               =     456.650000 [K]
Parameter 1                       = 1.974900E-0001
Parameter 2                       = 1.878700E-0001
Parameter 3                       = 4.566500E+0002
Parameter 4                       = 0.000000E+0000
Parameter 5                       = 0.000000E+0000
```

```
Vapor pressure
Formula Nr.   2    Log(P) = A + B/T + C*Log(T) + D*T + E*T^2  [mm Hg] [mm Hg]
Minimum temperature              =        259.830000 [K]
Maximum temperature              =        456.650000 [K]
Parameter 1                      =    2.928310E+0001
Parameter 2                      =   -2.196200E+0003
Parameter 3                      =   -7.854800E+0000
Parameter 4                      =   -4.266000E-0004
Parameter 5                      =    5.813000E-0006

Heat of vaporization
Formula Nr.   3    Hv = A * ((C-T)/(C-B)^D  (A=Hv1, B=T1, C=Tc)  [cal/g] [cal/g]
Minimum temperature              =        259.830000 [K]
Maximum temperature              =        456.650000 [K]
Parameter 1                      =    2.177000E+0002
Parameter 2                      =    3.582000E+0002
Parameter 3                      =    4.566500E+0002
Parameter 4                      =    2.607400E-0001
Parameter 5                      =    0.000000E+0000

Liquid heatcapacity
Formula Nr.   4    Cpl = A + B*T + C*T^2 + D*T^3  [cal/g/K] [cal/g/K]
Minimum temperature              =        259.830000 [K]
Maximum temperature              =        298.850000 [K]
Parameter 1                      =    8.024300E-0001
Parameter 2                      =   -1.307000E-0003
Parameter 3                      =    1.857500E-0006
Parameter 4                      =    1.879700E-0009
Parameter 5                      =    0.000000E+0000

IG heatcapacity
Formula Nr.   5    Cp = A + B*T + C*T^2 + D*T^3  [cal/mol] [cal/mol]
Minimum temperature              =        100.000000 [K]
Maximum temperature              =       1500.000000 [K]
Parameter 1                      =    5.683800E+0000
Parameter 2                      =    1.154300E-0002
Parameter 3                      =   -7.027000E-0006
Parameter 4                      =    1.807300E-0009
Parameter 5                      =    0.000000E+0000

Liquid viscosity
Formula Nr.   6    Log(Visc) = Ea + Eb/T + Ec*Log (T) + Ed*T + Ee*T*T  (where Ec=0!) [centiPoise]
[centiPoise]
Minimum temperature              =        259.850000 [K]
Maximum temperature              =        298.150000 [K]
Parameter 1                      =   -2.410000E+0000
Parameter 2                      =    4.335200E+0002
Parameter 3                      =    0.000000E+0000
Parameter 4                      =    4.523200E-0004
Parameter 5                      =    9.467600E-0007

Vapor viscosity
Formula Nr.   7    Visc = A + B*T + C*T^2  [microPoise] [microPoise]
Minimum temperature              =        300.000000 [K]
Maximum temperature              =        425.000000 [K]
Parameter 1                      =   -8.391300E+0000
Parameter 2                      =    8.982500E-0002
Parameter 3                      =    7.991800E-0005
Parameter 4                      =    0.000000E+0000
Parameter 5                      =    0.000000E+0000

Surface Tension
Formula Nr.   8    Sigma = A * ((C-T)/(C-B))^D  (A=Sigma1, B=T1, C=Tc)  [dynes/cm] [dynes/cm]
Minimum temperature              =        259.830000 [K]
Maximum temperature              =        456.650000 [K]
Parameter 1                      =    1.092000E+0001
Parameter 2                      =    3.582000E+0002
Parameter 3                      =    4.566500E+0002
Parameter 4                      =    1.019800E+0000
Parameter 5                      =    0.000000E+0000
```

Annex-34

14. HYDROGEN FLUORIDE

```
Material_Name                    = HYDROGEN FLUORIDE
Molecular formula                = HF
UN number                        =            1052
Molecular weight                 =       20.010000 kg/kmol
Critical temperature             =      461.150000 K (188.00 °C)
Melting point                    =      189.790000 K (-83.36 °C)
Triplepoint temperature          =      189.790000 K (-83.36 °C)
Normal boiling point             =      292.670000 K (19.52 °C)
Standard net heat of combustion  = 1.811600E+0003 J/kg ( 3.625012E+0004 J/kmol)
Flash point                      =        0.000000 K (-273.15 °C)
Lower flammability limit         =        0.000000 vol% in air
Upper flammability limit         =        0.000000 vol% in air
Solubility in water              =     1000.000000 kg/m3


Temperature dependent data (calculated at 288.15 K  (15.00 °C)
Liquid density                   = 9.672703E+0002    kg/m3 (967.27 kg/m3 )
Vapor pressure                   = 8.575827E+0004    N/m2 (0.86 Bar   )
Heat of vaporization             = 3.783930E+0005    J/kg (378393.05 J/kg  )
Liquid heatcapacity              = 2.489282E+0003    J/kg*K (2489.28 J/kg*K)
Gas heatcapacity (ideal gas)     = 1.453429E+0003    J/kg*K (1453.43 J/kg*K)
Liquid viscosity                 = 2.225353E-0004    Pa*s
Vapor viscosity                  = 1.071795E-0005    Pa*s
Surface tension                  = 9.138491E-0003     N/m
Poisson ratio                    = 1.400


Functions (calculated at 288.15 K  (15.00 °C) and 1.000000E+05 N/m2  (1.000 Bar)
Gas density (ideal gas law) :        0.835 kg/m3
Mass of 1 m3 gas/vapour     :        0.835 kg
Volume of 1 kg gas/vapour   :        1.197 m3
Mass of 1 m3 liquid         :      967.270 kg
Volume of 1000 kg liquid    :        1.034 m3


Probit constants (Toxicity)
A =       8.228900 SI units(Kg*s/m3)
B =       1.000000 SI units(Kg*s/m3)
N =       1.500000 SI units(Kg*s/m3)

A =      -8.672754 (ppm*min)
B =       1.000000 (ppm*min)
N =       1.500000 (ppm*min)

A =      -8.400021 (mg*min/m3)
B =       1.000000 (mg*min/m3)
N =       1.500000 (mg*min/m3)


Temperature dependent data (Parameters):

Liquid density
Formula Nr.   1    rho = A * B^-((1-T/C)^2/7)  (where C=Tc) [g/cm3] [g/cm3]
Minimum temperature              =      189.790000 [K]
Maximum temperature              =      461.150000 [K]
Parameter 1                      = 2.067800E-0001
Parameter 2                      = 1.298200E-0001
Parameter 3                      = 4.611500E+0002
Parameter 4                      = 0.000000E+0000
Parameter 5                      = 0.000000E+0000
```

```
Vapor pressure
Formula Nr.   2     Log(P) = A + B/T + C*Log(T) + D*T + E*T^2  [mm Hg] [mm Hg]
Minimum temperature                =        189.790000 [K]
Maximum temperature                =        461.150000 [K]
Parameter 1                        =    2.515930E+0001
Parameter 2                        =   -1.825500E+0003
Parameter 3                        =   -6.813000E+0000
Parameter 4                        =    9.564300E-0004
Parameter 5                        =    5.614500E-0006

Heat of vaporization
Formula Nr.   3     Hv = A * ((C-T)/(C-B)^D  (A=Hv1, B=T1, C=Tc)  [cal/g] [cal/g]
Minimum temperature                =        181.000000 [K]
Maximum temperature                =        461.000000 [K]
Parameter 1                        =    8.948400E+0001
Parameter 2                        =    2.927000E+0002
Parameter 3                        =    4.611500E+0002
Parameter 4                        =    3.800000E-0001
Parameter 5                        =    0.000000E+0000

Liquid heatcapacity
Formula Nr.   4     Cpl = A + B*T + C*T^2 + D*T^3  [cal/g/K] [cal/g/K]
Minimum temperature                =        189.790000 [K]
Maximum temperature                =        292.670000 [K]
Parameter 1                        =    3.073600E-0001
Parameter 2                        =    9.971000E-0004
Parameter 3                        =   -1.234000E-0010
Parameter 4                        =    1.820400E-0013
Parameter 5                        =    0.000000E+0000

IG heatcapacity
Formula Nr.   5     Cp = A + B*T + C*T^2 + D*T^3  [cal/mol] [cal/mol]
Minimum temperature                =         50.000000 [K]
Maximum temperature                =       1500.000000 [K]
Parameter 1                        =    7.007700E+0000
Parameter 2                        =   -3.707000E-0004
Parameter 3                        =    5.620500E-0007
Parameter 4                        =    6.758700E-0012
Parameter 5                        =    0.000000E+0000

Liquid viscosity
Formula Nr.   6     Log(Visc) = Ea + Eb/T + Ec*Log (T) + Ed*T + Ee*T*T  (where Ec=0!)  [centiPoise]
[centiPoise]
Minimum temperature                =        204.000000 [K]
Maximum temperature                =        292.670000 [K]
Parameter 1                        =   -4.619600E+0000
Parameter 2                        =    7.528000E+0002
Parameter 3                        =    0.000000E+0000
Parameter 4                        =    3.704700E-0003
Parameter 5                        =    3.456100E-0006

Vapor viscosity
Formula Nr.   7     Visc = A + B*T + C*T^2  [microPoise] [microPoise]
Minimum temperature                =        285.500000 [K]
Maximum temperature                =        472.680000 [K]
Parameter 1                        =   -2.158700E+0002
Parameter 2                        =    1.513000E+0000
Parameter 3                        =   -1.360000E-0003
Parameter 4                        =    0.000000E+0000
Parameter 5                        =    0.000000E+0000

Surface Tension
Formula Nr.   8     Sigma = A * ((C-T)/(C-B))^D  (A=Sigma1, B=T1, C=Tc)  [dynes/cm] [dynes/cm]
Minimum temperature                =        189.790000 [K]
Maximum temperature                =        461.150000 [K]
Parameter 1                        =    6.482000E+0000
Parameter 2                        =    3.255000E+0002
Parameter 3                        =    4.611500E+0002
Parameter 4                        =    1.412200E+0000
Parameter 5                        =    0.000000E+0000
```

Annex-36

15. HYDROGEN SULFIDE

```
Material_Name                     = HYDROGEN SULFIDE
Molecular formula                 = H2S
UN number                         =          1053
Molecular weight                  =      34.080000 kg/kmol
Critical temperature              =     373.530000 K (100.38 °C)
Melting point                     =     187.680000 K (-85.47 °C)
Triplepoint temperature           =     187.450000 K (-85.70 °C)
Normal boiling point              =     212.800000 K (-60.35 °C)
Standard net heat of combustion   = 1.810300E+0007 J/kg ( 6.169502E+0008 J/kmol)
Flash point                       =     166.400000 K (-106.75 °C)
Lower flammability limit          =       4.300000 vol% in air
Upper flammability limit          =     100.000000 vol% in air
Solubility in water               =       6.000000 kg/m3


Temperature dependent data (calculated at 288.15 K  (15.00 °C)
Liquid density                    = 7.998392E+0002    kg/m3 (799.84 kg/m3 )
Vapor pressure                    = 1.617544E+0006    N/m2 (16.18 Bar   )
Heat of vaporization              = 4.372398E+0005    J/kg (437239.84 J/kg  )
Liquid heatcapacity               = 2.012115E+0003    J/kg*K (2012.11 J/kg*K)
Gas heatcapacity (ideal gas)      = 1.006428E+0003    J/kg*K (1006.43 J/kg*K)
Liquid viscosity                  = 4.036770E-0004    Pa*s
Vapor viscosity                   = 1.216139E-0005    Pa*s
Surface tension                   = 1.071192E-0002     N/m
Poisson ratio                     = 1.320


Functions (calculated at 288.15 K  (15.00 °C) and 1.000000E+05 N/m2  (1.000 Bar)
Gas density (ideal gas law) :          1.422 kg/m3
Mass of 1 m3 gas/vapour     :          1.422 kg
Volume of 1 kg gas/vapour   :          0.703 m3
Mass of 1 m3 liquid         :        799.839 kg
Volume of 1000 kg liquid    :          1.250 m3


Probit constants (Toxicity)
A =      10.655125 SI units(Kg*s/m3)
B =       1.000000 SI units(Kg*s/m3)
N =       1.900000 SI units(Kg*s/m3)

A =     -10.833752 (ppm*min)
B =       1.000000 (ppm*min)
N =       1.900000 (ppm*min)

A =     -11.500000 (mg*min/m3)
B =       1.000000 (mg*min/m3)
N =       1.900000 (mg*min/m3)


Temperature dependent data (Parameters):

Liquid density
Formula Nr.   1    rho = A * B^-((1-T/C)^2/7)  (where C=Tc)  [g/cm3] [g/cm3]
Minimum temperature               =     187.680000 [K]
Maximum temperature               =     373.530000 [K]
Parameter 1                       = 3.483400E-0001
Parameter 2                       = 2.816100E-0001
Parameter 3                       = 3.735300E+0002
Parameter 4                       = 0.000000E+0000
Parameter 5                       = 0.000000E+0000
```

```
Vapor pressure
Formula Nr.   2    Log(P) = A + B/T + C*Log(T) + D*T + E*T^2  [mm Hg] [mm Hg]
Minimum temperature                =        187.680000 [K]
Maximum temperature                =        373.530000 [K]
Parameter 1                        =    2.003420E+0001
Parameter 2                        =   -1.368500E+0003
Parameter 3                        =   -4.737200E+0000
Parameter 4                        =    1.039000E-0003
Parameter 5                        =    1.823500E-0006

Heat of vaporization
Formula Nr.   3    Hv = A * ((C-T)/(C-B)^D  (A=Hv1, B=T1, C=Tc)  [cal/g] [cal/g]
Minimum temperature                =        187.680000 [K]
Maximum temperature                =        373.530000 [K]
Parameter 1                        =    1.079000E+0002
Parameter 2                        =    2.806000E+0002
Parameter 3                        =    3.735300E+0002
Parameter 4                        =    3.831800E-0001
Parameter 5                        =    0.000000E+0000

Liquid heatcapacity
Formula Nr.   4    Cpl = A + B*T + C*T^2 + D*T^3  [cal/g/K] [cal/g/K]
Minimum temperature                =        191.480000 [K]
Maximum temperature                =        208.150000 [K]
Parameter 1                        =    4.097300E-0001
Parameter 2                        =    2.715900E-0004
Parameter 3                        =    3.012300E-0007
Parameter 4                        =    1.513100E-0010
Parameter 5                        =    0.000000E+0000

IG heatcapacity
Formula Nr.   5    Cp = A + B*T + C*T^2 + D*T^3  [cal/mol] [cal/mol]
Minimum temperature                =        100.000000 [K]
Maximum temperature                =       1500.000000 [K]
Parameter 1                        =    7.757300E+0000
Parameter 2                        =    1.405700E-0004
Parameter 3                        =    5.461200E-0006
Parameter 4                        =   -2.403000E-0009
Parameter 5                        =    0.000000E+0000

Liquid viscosity
Formula Nr.   6    Log(Visc) = Ea + Eb/T + Ec*Log (T) + Ed*T + Ee*T*T  (where Ec=0!) [centiPoise]
[centiPoise]
Minimum temperature                =        190.120000 [K]
Maximum temperature                =        223.180000 [K]
Parameter 1                        =   -4.638800E+0000
Parameter 2                        =    5.337700E+0002
Parameter 3                        =    0.000000E+0000
Parameter 4                        =    7.180400E-0003
Parameter 5                        =    5.032300E-0006

Vapor viscosity
Formula Nr.   7    Visc = A + B*T + C*T^2  [microPoise] [microPoise]
Minimum temperature                =        230.000000 [K]
Maximum temperature                =        570.000000 [K]
Parameter 1                        =   -1.511200E+0001
Parameter 2                        =    5.113500E-0001
Parameter 3                        =   -1.279000E-0004
Parameter 4                        =    0.000000E+0000
Parameter 5                        =    0.000000E+0000

Surface Tension
Formula Nr.   8    Sigma = A * ((C-T)/(C-B))^D  (A=Sigma1, B=T1, C=Tc)  [dynes/cm] [dynes/cm]
Minimum temperature                =        187.680000 [K]
Maximum temperature                =        373.530000 [K]
Parameter 1                        =    1.194000E+0001
Parameter 2                        =    2.806000E+0002
Parameter 3                        =    3.735300E+0002
Parameter 4                        =    1.280900E+0000
Parameter 5                        =    0.000000E+0000
```

Annex-38

16.   METHANE

```
Material_Name                     = METHANE
Molecular formula                 = CH4
UN number                         =         1971
Molecular weight                  =        16.043000 kg/kmol
Critical temperature              =       190.400000 K (-82.75 °C)
Melting point                     =        91.000000 K (-182.15 °C)
Triplepoint temperature           =        90.670000 K (-182.48 °C)
Normal boiling point              =       111.500000 K (-161.65 °C)
Standard net heat of combustion   = 5.002000E+0007 J/kg ( 8.024709E+0008 J/kmol)
Flash point                       =        84.650000 K (-188.50 °C)
Lower flammability limit          =         5.000000 vol% in air
Upper flammability limit          =       100.000000 vol% in air
Solubility in water               =         0.000000 kg/m3


Temperature dependent data (calculated at 288.15 K  (15.00 °C)
Liquid density                    =         Undefined
Vapor pressure                    =         Undefined
Heat of vaporization              =         Undefined
Liquid heatcapacity               =         Undefined
Gas heatcapacity (ideal gas)      = 2.208183E+0003   J/kg*K (2208.18 J/kg*K)
Liquid viscosity                  =         Undefined
Vapor viscosity                   = 1.082961E-0005     Pa*s
Surface tension                   =         Undefined
Poisson ratio                     = 1.307


Functions (calculated at 288.15 K  (15.00 °C) and 1.000000E+05 N/m2  (1.000 Bar)
Gas density (ideal gas law) :        0.670 kg/m3
Mass of 1 m3 gas/vapour     :        0.670 kg
Volume of 1 kg gas/vapour   :        1.493 m3
Mass of 1 m3 liquid         :     Undefined
Volume of 1000 kg liquid    :     Undefined


Probit constants (Toxicity)
A =       0.000000 SI units(Kg*s/m3)
B =       0.000000 SI units(Kg*s/m3)
N =       0.000000 SI units(Kg*s/m3)

A =       0.000000 (ppm*min)
B =       0.000000 (ppm*min)
N =       0.000000 (ppm*min)

A =       0.000000 (mg*min/m3)
B =       0.000000 (mg*min/m3)
N =       0.000000 (mg*min/m3)


Temperature dependent data (Parameters):

Liquid density
Formula Nr.   1    rho = A * B^-((1-T/C)^2/7)  (where C=Tc)  [g/cm3] [g/cm3]
Minimum temperature               =        90.400000 [K]
Maximum temperature               =       190.400000 [K]
Parameter 1                       = 1.611000E-0001
Parameter 2                       = 2.877000E-0001
Parameter 3                       = 1.904000E+0002
Parameter 4                       = 0.000000E+0000
Parameter 5                       = 0.000000E+0000
```

```
Vapor pressure
Formula Nr.    2     Log(P) = A + B/T + C*Log(T) + D*T + E*T^2  [mm Hg] [mm Hg]
Minimum temperature                     =        90.800000 [K]
Maximum temperature                     =       191.100000 [K]
Parameter 1                             =     2.257300E+0001
Parameter 2                             =    -6.562400E+0002
Parameter 3                             =    -7.394200E+0000
Parameter 4                             =     1.189600E-0002
Parameter 5                             =     0.000000E+0000

Heat of vaporization
Formula Nr.    3     Hv = A * ((C-T)/(C-B)^D  (A=Hv1, B=T1, C=Tc)  [cal/g] [cal/g]
Minimum temperature                     =        90.400000 [K]
Maximum temperature                     =       190.400000 [K]
Parameter 1                             =     1.217000E+0002
Parameter 2                             =     1.115000E+0002
Parameter 3                             =     1.904000E+0002
Parameter 4                             =     3.800000E-0001
Parameter 5                             =     0.000000E+0000

Liquid heatcapacity
Formula Nr.    4     Cpl = A + B*T + C*T^2 + D*T^3  [cal/g/K] [cal/g/K]
Minimum temperature                     =        90.400000 [K]
Maximum temperature                     =       163.000000 [K]
Parameter 1                             =     1.230000E+0000
Parameter 2                             =    -1.033000E-0002
Parameter 3                             =     7.200000E-0005
Parameter 4                             =    -1.073000E-0007
Parameter 5                             =     0.000000E+0000

IG heatcapacity
Formula Nr.    5     Cp = A + B*T + C*T^2 + D*T^3  [cal/mol] [cal/mol]
Minimum temperature                     =       298.000000 [K]
Maximum temperature                     =      1500.000000 [K]
Parameter 1                             =     5.040000E+0000
Parameter 2                             =     9.320000E-0003
Parameter 3                             =     8.870000E-0006
Parameter 4                             =    -5.370000E-0009
Parameter 5                             =     0.000000E+0000

Liquid viscosity
Formula Nr.    6     Log(Visc) = Ea + Eb/T + Ec*Log (T) + Ed*T + Ee*T*T  (where Ec=0!) [centiPoise]
[centiPoise]
Minimum temperature                     =        90.400000 [K]
Maximum temperature                     =       190.400000 [K]
Parameter 1                             =    -1.167000E+0001
Parameter 2                             =     4.993000E+0002
Parameter 3                             =     0.000000E+0000
Parameter 4                             =     8.125000E-0002
Parameter 5                             =    -2.263000E-0004

Vapor viscosity
Formula Nr.    7     Visc = A + B*T + C*T^2  [microPoise] [microPoise]
Minimum temperature                     =       193.000000 [K]
Maximum temperature                     =      1273.000000 [K]
Parameter 1                             =     1.596000E+0001
Parameter 2                             =     3.439000E-0001
Parameter 3                             =    -8.140000E-0005
Parameter 4                             =     0.000000E+0000
Parameter 5                             =     0.000000E+0000

Surface Tension
Formula Nr.    8     Sigma = A * ((C-T)/(C-B))^D  (A=Sigma1, B=T1, C=Tc)  [dynes/cm] [dynes/cm]
Minimum temperature                     =        90.400000 [K]
Maximum temperature                     =       190.400000 [K]
Parameter 1                             =     1.502600E+0001
Parameter 2                             =     1.048400E+0002
Parameter 3                             =     1.904000E+0002
Parameter 4                             =     1.394100E+0000
Parameter 5                             =     0.000000E+0000
```

Annex-40

17.   METHANOL

```
Material_Name                    = METHANOL
Molecular formula                = CH3OH
UN number                        =          1230
Molecular weight                 =       32.040000 kg/kmol
Critical temperature             =      512.550000 K (239.40 °C)
Melting point                    =      175.550000 K (-97.60 °C)
Triplepoint temperature          =      175.550000 K (-97.60 °C)
Normal boiling point             =      337.850000 K (64.70 °C)
Standard net heat of combustion  = 1.958000E+0007 J/kg ( 6.273432E+0008 J/kmol)
Flash point                      =      284.000000 K (10.85 °C)
Lower flammability limit         =        6.000000 vol% in air
Upper flammability limit         =      100.000000 vol% in air
Solubility in water              =     1000.000000 kg/m3
```

```
Temperature dependent data (calculated at 288.15 K  (15.00 °C)
Liquid density                   = 8.093461E+0002    kg/m3 (809.35 kg/m3 )
Vapor pressure                   = 9.712178E+0003    N/m2 (0.10 Bar   )
Heat of vaporization             = 1.203047E+0006    J/kg (1203046.63 J/kg  )
Liquid heatcapacity              = 2.477973E+0003    J/kg*K (2477.97 J/kg*K)
Gas heatcapacity (ideal gas)     = 1.360598E+0003    J/kg*K (1360.60 J/kg*K)
Liquid viscosity                 = 5.940974E-0004    Pa*s
Vapor viscosity                  = 9.335405E-0006    Pa*s
Surface tension                  = 2.300430E-0002     N/m
Poisson ratio                    = 1.236
```

```
Functions (calculated at 288.15 K  (15.00 °C) and 1.000000E+05 N/m2  (1.000 Bar)
Gas density (ideal gas law) :          1.337 kg/m3
Mass of 1 m3 gas/vapour     :          1.337 kg
Volume of 1 kg gas/vapour   :          0.748 m3
Mass of 1 m3 liquid         :        809.346 kg
Volume of 1000 kg liquid    :          1.236 m3
```

```
Probit constants (Toxicity)
A =        0.000000 SI units(Kg*s/m3)
B =        0.000000 SI units(Kg*s/m3)
N =        0.000000 SI units(Kg*s/m3)

A =        0.000000 (ppm*min)
B =        0.000000 (ppm*min)
N =        0.000000 (ppm*min)

A =        0.000000 (mg*min/m3)
B =        0.000000 (mg*min/m3)
N =        0.000000 (mg*min/m3)
```

```
Temperature dependent data (Parameters):

Liquid density
Formula Nr.   1    rho = A * B^-((1-T/C)^2/7)  (where C=Tc) [g/cm3] [g/cm3]
Minimum temperature              =      175.550000 [K]
Maximum temperature              =      512.550000 [K]
Parameter 1                      = 2.928000E-0001
Parameter 2                      = 2.760000E-0001
Parameter 3                      = 5.125500E+0002
Parameter 4                      = 0.000000E+0000
Parameter 5                      = 0.000000E+0000
```

```
Vapor pressure
Formula Nr.    2    Log(P) = A + B/T + C*Log(T) + D*T + E*T^2  [mm Hg] [mm Hg]
Minimum temperature                =        205.750000 [K]
Maximum temperature                =        513.150000 [K]
Parameter 1                        = -4.262900E+0001
Parameter 2                        = -1.186200E+0003
Parameter 3                        =  2.327900E+0001
Parameter 4                        = -3.508200E-0002
Parameter 5                        =  1.757800E-0005

Heat of vaporization
Formula Nr.    3    Hv = A * ((C-T)/(C-B)^D  (A=Hv1, B=T1, C=Tc)  [cal/g] [cal/g]
Minimum temperature                =        175.500000 [K]
Maximum temperature                =        512.400000 [K]
Parameter 1                        =  2.601000E+0002
Parameter 2                        =  3.377000E+0002
Parameter 3                        =  5.125500E+0002
Parameter 4                        =  4.000000E-0001
Parameter 5                        =  0.000000E+0000

Liquid heatcapacity
Formula Nr.    4    Cpl = A + B*T + C*T^2 + D*T^3  [cal/g/K] [cal/g/K]
Minimum temperature                =        175.400000 [K]
Maximum temperature                =        493.000000 [K]
Parameter 1                        =  8.382000E-0001
Parameter 2                        = -3.231000E-0003
Parameter 3                        =  8.296000E-0006
Parameter 4                        = -1.689000E-0010
Parameter 5                        =  0.000000E+0000

IG heatcapacity
Formula Nr.    5    Cp = A + B*T + C*T^2 + D*T^3  [cal/mol] [cal/mol]
Minimum temperature                =        298.000000 [K]
Maximum temperature                =       1000.000000 [K]
Parameter 1                        =  3.620000E+0000
Parameter 2                        =  2.490000E-0002
Parameter 3                        = -7.050000E-0006
Parameter 4                        =  0.000000E+0000
Parameter 5                        =  0.000000E+0000

Liquid viscosity
Formula Nr.    6    Log(Visc) = Ea + Eb/T + Ec*Log (T) + Ed*T + Ee*T*T  (where Ec=0!) [centiPoise]
[centiPoise]
Minimum temperature                =        233.000000 [K]
Maximum temperature                =        512.400000 [K]
Parameter 1                        = -1.709000E+0001
Parameter 2                        =  2.096000E+0003
Parameter 3                        =  0.000000E+0000
Parameter 4                        =  4.738000E-0002
Parameter 5                        = -4.893000E-0005

Vapor viscosity
Formula Nr.    7    Visc = A + B*T + C*T^2  [microPoise] [microPoise]
Minimum temperature                =        273.000000 [K]
Maximum temperature                =       1173.000000 [K]
Parameter 1                        = -5.636300E+0000
Parameter 2                        =  3.445000E-0001
Parameter 3                        = -3.340000E-0006
Parameter 4                        =  0.000000E+0000
Parameter 5                        =  0.000000E+0000

Surface Tension
Formula Nr.    8    Sigma = A * ((C-T)/(C-B))^D  (A=Sigma1, B=T1, C=Tc)  [dynes/cm] [dynes/cm]
Minimum temperature                =        175.400000 [K]
Maximum temperature                =        512.400000 [K]
Parameter 1                        =  2.260000E+0001
Parameter 2                        =  2.930000E+0002
Parameter 3                        =  5.125500E+0002
Parameter 4                        =  8.115000E-0001
Parameter 5                        =  0.000000E+0000
```

18.   METHYL MERCAPTAN

```
Material_Name                      = METHYL MERCAPTAN
Molecular formula                  = CH3SH
UN number                          =         1064
Molecular weight                   =       48.100000 kg/kmol
Critical temperature               =      469.950000 K (196.80 °C)
Melting point                      =      150.180000 K (-122.97 °C)
Triplepoint temperature            =      150.180000 K (-122.97 °C)
Normal boiling point               =      279.110000 K (5.96 °C)
Standard net heat of combustion    = 2.394000E+0007 J/kg ( 1.151514E+0009 J/kmol)
Flash point                        =      220.000000 K (-53.15 °C)
Lower flammability limit           =        3.900000 vol% in air
Upper flammability limit           =      100.000000 vol% in air
Solubility in water                =       23.000000 kg/m3


Temperature dependent data (calculated at 288.15 K  (15.00 °C)
Liquid density                     = 8.755845E+0002    kg/m3 (875.58 kg/m3 )
Vapor pressure                     = 1.488974E+0005    N/m2 (1.49 Bar   )
Heat of vaporization               = 5.014725E+0005    J/kg (501472.47 J/kg  )
Liquid heatcapacity                = 1.850550E+0003    J/kg*K (1850.55 J/kg*K)
Gas heatcapacity (ideal gas)       = 1.062031E+0003    J/kg*K (1062.03 J/kg*K)
Liquid viscosity                   = 3.049121E-0004    Pa*s
Vapor viscosity                    = 9.002020E-0006    Pa*s
Surface tension                    = 2.556052E-0002     N/m
Poisson ratio                      = 1.194


Functions (calculated at 288.15 K  (15.00 °C) and 1.000000E+05 N/m2  (1.000 Bar)
Gas density (ideal gas law) :        2.008 kg/m3
Mass of 1 m3 gas/vapour     :        2.008 kg
Volume of 1 kg gas/vapour   :        0.498 m3
Mass of 1 m3 liquid         :      875.585 kg
Volume of 1000 kg liquid    :        1.142 m3


Probit constants (Toxicity)
A =       0.000000 SI units(Kg*s/m3)
B =       0.000000 SI units(Kg*s/m3)
N =       0.000000 SI units(Kg*s/m3)

A =       0.000000 (ppm*min)
B =       0.000000 (ppm*min)
N =       0.000000 (ppm*min)

A =       0.000000 (mg*min/m3)
B =       0.000000 (mg*min/m3)
N =       0.000000 (mg*min/m3)


Temperature dependent data (Parameters):

Liquid density
Formula Nr.   1   rho = A * B^-((1-T/C)^2/7)  (where C=Tc) [g/cm3] [g/cm3]
Minimum temperature                =      150.180000 [K]
Maximum temperature                =      469.950000 [K]
Parameter 1                        = 3.323400E-0001
Parameter 2                        = 2.806300E-0001
Parameter 3                        = 4.699500E+0002
Parameter 4                        = 0.000000E+0000
Parameter 5                        = 0.000000E+0000
```

```
Vapor pressure
Formula Nr.   2    Log(P) = A + B/T + C*Log(T) + D*T + E*T^2  [mm Hg] [mm Hg]
Minimum temperature                    =        150.180000 [K]
Maximum temperature                    =        469.950000 [K]
Parameter 1                            =    2.025240E+0001
Parameter 2                            =   -1.949900E+0003
Parameter 3                            =   -4.227100E+0000
Parameter 4                            =    2.582700E-0004
Parameter 5                            =   -1.382000E-0006


Heat of vaporization
Formula Nr.   3    Hv = A * ((C-T)/(C-B)^D  (A=Hv1, B=T1, C=Tc)  [cal/g] [cal/g]
Minimum temperature                    =        150.180000 [K]
Maximum temperature                    =        469.950000 [K]
Parameter 1                            =    1.141000E+0002
Parameter 2                            =    3.101000E+0002
Parameter 3                            =    4.699500E+0002
Parameter 4                            =    3.787000E-0001
Parameter 5                            =    0.000000E+0000


Liquid heatcapacity
Formula Nr.   4    Cpl = A + B*T + C*T^2 + D*T^3  [cal/g/K] [cal/g/K]
Minimum temperature                    =        233.000000 [K]
Maximum temperature                    =        280.000000 [K]
Parameter 1                            =    5.336200E-0001
Parameter 2                            =   -7.525000E-0004
Parameter 3                            =    4.104900E-0007
Parameter 4                            =    3.962200E-0009
Parameter 5                            =    0.000000E+0000


IG heatcapacity
Formula Nr.   5    Cp = A + B*T + C*T^2 + D*T^3  [cal/mol] [cal/mol]
Minimum temperature                    =        100.000000 [K]
Maximum temperature                    =       1500.000000 [K]
Parameter 1                            =    7.606200E+0000
Parameter 2                            =    1.500800E-0002
Parameter 3                            =    4.590600E-0006
Parameter 4                            =   -4.533000E-0009
Parameter 5                            =    0.000000E+0000


Liquid viscosity
Formula Nr.   6    Log(Visc) = Ea + Eb/T + Ec*Log (T) + Ed*T + Ee*T*T  (where Ec=0!)  [centiPoise]
[centiPoise]
Minimum temperature                    =        150.180000 [K]
Maximum temperature                    =        270.180000 [K]
Parameter 1                            =   -1.538600E+0000
Parameter 2                            =    2.778600E+0002
Parameter 3                            =    0.000000E+0000
Parameter 4                            =   -6.108000E-0005
Parameter 5                            =    1.486600E-0007


Vapor viscosity
Formula Nr.   7    Visc = A + B*T + C*T^2  [microPoise] [microPoise]
Minimum temperature                    =        273.150000 [K]
Maximum temperature                    =        473.150000 [K]
Parameter 1                            =   -3.694300E+0001
Parameter 2                            =    4.530400E-0001
Parameter 3                            =   -4.312000E-0005
Parameter 4                            =    0.000000E+0000
Parameter 5                            =    0.000000E+0000


Surface Tension
Formula Nr.   8    Sigma = A * ((C-T)/(C-B))^D  (A=Sigma1, B=T1, C=Tc)  [dynes/cm] [dynes/cm]
Minimum temperature                    =        150.180000 [K]
Maximum temperature                    =        469.950000 [K]
Parameter 1                            =    2.183000E+0001
Parameter 2                            =    3.101000E+0002
Parameter 3                            =    4.699500E+0002
Parameter 4                            =    1.226100E+0000
Parameter 5                            =    0.000000E+0000
```

Annex-44

19. NITROGEN DIOXIDE


```
Material_Name                     = NITROGEN DIOXIDE
Molecular formula                 = NO2
UN number                         =           1067
Molecular weight                  =        46.010000 kg/kmol
Critical temperature              =       431.350000 K (158.20 °C)
Melting point                     =       261.950000 K (-11.20 °C)
Triplepoint temperature           =       261.950000 K (-11.20 °C)
Normal boiling point              =       294.000000 K (20.85 °C)
Standard net heat of combustion   = 7.193600E+0007 J/kg ( 3.309775E+0009 J/kmol)
Flash point                       =         0.000000 K (-273.15 °C)
Lower flammability limit          =         0.000000 vol% in air
Upper flammability limit          =         0.000000 vol% in air
Solubility in water               =      1000.000000 kg/m3


Temperature dependent data (calculated at 288.15 K  (15.00 °C)
Liquid density                    = 1.466996E+0003    kg/m3 (1467.00 kg/m3 )
Vapor pressure                    = 7.555354E+0004    N/m2 (0.76 Bar   )
Heat of vaporization              = 8.288280E+0005    J/kg (828828.00 J/kg  )
Liquid heatcapacity               = 3.097803E+0003    J/kg*K (3097.80 J/kg*K)
Gas heatcapacity (ideal gas)      = 8.256559E+0002    J/kg*K (825.66 J/kg*K)
Liquid viscosity                  = 4.409570E-0004    Pa*s
Vapor viscosity                   = 1.275916E-0005    Pa*s
Surface tension                   = 2.823386E-0002     N/m
Poisson ratio                     = 1.280


Functions (calculated at 288.15 K  (15.00 °C) and 1.000000E+05 N/m2  (1.000 Bar)
Gas density (ideal gas law) :           1.920 kg/m3
Mass of 1 m3 gas/vapour     :           1.920 kg
Volume of 1 kg gas/vapour   :           0.521 m3
Mass of 1 m3 liquid         :        1466.996 kg
Volume of 1000 kg liquid    :           0.682 m3


Probit constants (Toxicity)
A =      28.423045 SI units(Kg*s/m3)
B =       1.000000 SI units(Kg*s/m3)
N =       3.700000 SI units(Kg*s/m3)

A =     -16.192022 (ppm*min)
B =       1.000000 (ppm*min)
N =       3.700000 (ppm*min)

A =     -18.600000 (mg*min/m3)
B =       1.000000 (mg*min/m3)
N =       3.700000 (mg*min/m3)


Temperature dependent data (Parameters):

Liquid density
Formula Nr.   1    rho = A * B^-((1-T/C)^2/7)  (where C=Tc) [g/cm3] [g/cm3]
Minimum temperature               =       293.150000 [K]
Maximum temperature               =       431.350000 [K]
Parameter 1                       = 6.014800E-0001
Parameter 2                       = 2.910600E-0001
Parameter 3                       = 4.313500E+0002
Parameter 4                       = 0.000000E+0000
Parameter 5                       = 0.000000E+0000
```

```
Vapor pressure
Formula Nr.    2     Log(P) = A + B/T + C*Log(T) + D*T + E*T^2   [mm Hg] [mm Hg]
Minimum temperature                     =        261.950000 [K]
Maximum temperature                     =        431.350000 [K]
Parameter 1                             =     1.976430E+0001
Parameter 2                             =    -1.998700E+0003
Parameter 3                             =    -4.411800E+0000
Parameter 4                             =     1.708200E-0003
Parameter 5                             =     3.427300E-0006

Heat of vaporization
Formula Nr.    3     Hv = A * ((C-T)/(C-B)^D   (A=Hv1, B=T1, C=Tc)   [cal/g] [cal/g]
Minimum temperature                     =        294.300000 [K]
Maximum temperature                     =        294.300000 [K]
Parameter 1                             =     1.980000E+0002
Parameter 2                             =     0.000000E+0000
Parameter 3                             =     4.313500E+0002
Parameter 4                             =     0.000000E+0000
Parameter 5                             =     0.000000E+0000

Liquid heatcapacity
Formula Nr.    4     Cpl = A + B*T + C*T^2 + D*T^3   [cal/g/K] [cal/g/K]
Minimum temperature                     =        298.000000 [K]
Maximum temperature                     =        400.000000 [K]
Parameter 1                             =     4.812200E-0001
Parameter 2                             =     8.684500E-0004
Parameter 3                             =     3.060700E-0010
Parameter 4                             =    -2.423000E-0013
Parameter 5                             =     0.000000E+0000

IG heatcapacity
Formula Nr.    5     Cp = A + B*T + C*T^2 + D*T^3   [cal/mol] [cal/mol]
Minimum temperature                     =         50.000000 [K]
Maximum temperature                     =        920.000000 [K]
Parameter 1                             =     7.089700E+0000
Parameter 2                             =     6.667900E-0003
Parameter 3                             =     1.301700E-0006
Parameter 4                             =    -1.840000E-0009
Parameter 5                             =     0.000000E+0000

Liquid viscosity
Formula Nr.    6     Log(Visc) = Ea + Eb/T + Ec*Log (T) + Ed*T + Ee*T*T   (where Ec=0!) [centiPoise]
[centiPoise]
Minimum temperature                     =        273.150000 [K]
Maximum temperature                     =        313.150000 [K]
Parameter 1                             =     3.182900E+0000
Parameter 2                             =    -3.515200E+0002
Parameter 3                             =     0.000000E+0000
Parameter 4                             =    -6.236000E-0003
Parameter 5                             =    -6.283000E-0006

Vapor viscosity
Formula Nr.    7     Visc = A + B*T + C*T^2   [microPoise] [microPoise]
Minimum temperature                     =        295.000000 [K]
Maximum temperature                     =        460.000000 [K]
Parameter 1                             =    -3.679700E+0002
Parameter 2                             =     2.303500E+0000
Parameter 3                             =    -2.114000E-0003
Parameter 4                             =     0.000000E+0000
Parameter 5                             =     0.000000E+0000

Surface Tension
Formula Nr.    8     Sigma = A * ((C-T)/(C-B))^D   (A=Sigma1, B=T1, C=Tc)   [dynes/cm] [dynes/cm]
Minimum temperature                     =        261.950000 [K]
Maximum temperature                     =        431.350000 [K]
Parameter 1                             =     1.675000E+0001
Parameter 2                             =     3.466000E+0002
Parameter 3                             =     4.313500E+0002
Parameter 4                             =     9.954000E-0001
Parameter 5                             =     0.000000E+0000
```

Annex-46

20. PROPANE

```
Material_Name                    = PROPANE
Molecular formula                = C3H8
UN number                        =           1978
Molecular weight                 =       44.096000 kg/kmol
Critical temperature             =      369.700000 K (96.55 °C)
Melting point                    =       86.000000 K (-187.15 °C)
Triplepoint temperature          =       85.470000 K (-187.68 °C)
Normal boiling point             =      230.900000 K (-42.25 °C)
Standard net heat of combustion  = 4.601300E+0007 J/kg ( 2.028989E+0009 J/kmol)
Flash point                      =      169.500000 K (-103.65 °C)
Lower flammability limit         =        2.100000 vol% in air
Upper flammability limit         =      100.000000 vol% in air
Solubility in water              =        0.000000 kg/m3
```

```
Temperature dependent data (calculated at 288.15 K  (15.00 °C)
Liquid density                   = 5.092712E+0002    kg/m3 (509.27 kg/m3 )
Vapor pressure                   = 7.307659E+0005    N/m2 (7.31 Bar   )
Heat of vaporization             = 3.481610E+0005    J/kg (348160.99 J/kg  )
Liquid heatcapacity              = 2.582192E+0003    J/kg*K (2582.19 J/kg*K)
Gas heatcapacity (ideal gas)     = 1.661416E+0003    J/kg*K (1661.42 J/kg*K)
Liquid viscosity                 = 1.030978E-0004    Pa*s
Vapor viscosity                  = 7.989814E-0006    Pa*s
Surface tension                  = 8.154658E-0003     N/m
Poisson ratio                    = 1.128
```

```
Functions (calculated at 288.15 K  (15.00 °C) and 1.000000E+05 N/m2  (1.000 Bar)
Gas density (ideal gas law) :         1.841 kg/m3
Mass of 1 m3 gas/vapour     :         1.841 kg
Volume of 1 kg gas/vapour   :         0.543 m3
Mass of 1 m3 liquid         :       509.271 kg
Volume of 1000 kg liquid    :         1.964 m3
```

```
Probit constants (Toxicity)
A =      0.000000 SI units(Kg*s/m3)
B =      0.000000 SI units(Kg*s/m3)
N =      0.000000 SI units(Kg*s/m3)

A =      0.000000 (ppm*min)
B =      0.000000 (ppm*min)
N =      0.000000 (ppm*min)

A =      0.000000 (mg*min/m3)
B =      0.000000 (mg*min/m3)
N =      0.000000 (mg*min/m3)
```

```
Temperature dependent data (Parameters):

Liquid density
Formula Nr.   1    rho = A * B^-((1-T/C)^2/7)  (where C=Tc) [g/cm3] [g/cm3]
Minimum temperature              =       85.300000 [K]
Maximum temperature              =      369.700000 [K]
Parameter 1                      = 2.204000E-0001
Parameter 2                      = 2.753000E-0001
Parameter 3                      = 3.697000E+0002
Parameter 4                      = 0.000000E+0000
Parameter 5                      = 0.000000E+0000
```

```
Vapor pressure
Formula Nr.   2     Log(P) = A + B/T + C*Log(T) + D*T + E*T^2  [mm Hg] [mm Hg]
Minimum temperature              =        144.100000 [K]
Maximum temperature              =        323.000000 [K]
Parameter 1                      =     3.600700E+0001
Parameter 2                      =    -1.737200E+0003
Parameter 3                      =    -1.166600E+0001
Parameter 4                      =     8.518700E-0003
Parameter 5                      =     0.000000E+0000

Heat of vaporization
Formula Nr.   3     Hv = A * ((C-T)/(C-B)^D  (A=Hv1, B=T1, C=Tc)  [cal/g] [cal/g]
Minimum temperature              =         85.300000 [K]
Maximum temperature              =        369.700000 [K]
Parameter 1                      =     1.018000E+0002
Parameter 2                      =     2.309000E+0002
Parameter 3                      =     3.697000E+0002
Parameter 4                      =     3.800000E-0001
Parameter 5                      =     0.000000E+0000

Liquid heatcapacity
Formula Nr.   4     Cpl = A + B*T + C*T^2 + D*T^3  [cal/g/K] [cal/g/K]
Minimum temperature              =         85.300000 [K]
Maximum temperature              =        353.000000 [K]
Parameter 1                      =     3.326000E-0001
Parameter 2                      =     2.332000E-0003
Parameter 3                      =    -1.336000E-0005
Parameter 4                      =     3.016000E-0008
Parameter 5                      =     0.000000E+0000

IG heatcapacity
Formula Nr.   5     Cp = A + B*T + C*T^2 + D*T^3  [cal/mol] [cal/mol]
Minimum temperature              =        298.000000 [K]
Maximum temperature              =       1500.000000 [K]
Parameter 1                      =    -5.800000E-0001
Parameter 2                      =     6.990000E-0002
Parameter 3                      =    -3.290000E-0005
Parameter 4                      =     6.540000E-0009
Parameter 5                      =     0.000000E+0000

Liquid viscosity
Formula Nr.   6     Log(Visc) = Ea + Eb/T + Ec*Log (T) + Ed*T + Ee*T*T  (where Ec=0!) [centiPoise]
[centiPoise]
Minimum temperature              =         85.300000 [K]
Maximum temperature              =        369.700000 [K]
Parameter 1                      =    -3.372000E+0000
Parameter 2                      =     3.135000E+0002
Parameter 3                      =     0.000000E+0000
Parameter 4                      =     1.034000E-0002
Parameter 5                      =    -2.026000E-0005

Vapor viscosity
Formula Nr.   7     Visc = A + B*T + C*T^2  [microPoise] [microPoise]
Minimum temperature              =        193.000000 [K]
Maximum temperature              =       1273.000000 [K]
Parameter 1                      =     4.912000E+0000
Parameter 2                      =     2.712000E-0001
Parameter 3                      =    -3.806000E-0005
Parameter 4                      =     0.000000E+0000
Parameter 5                      =     0.000000E+0000

Surface Tension
Formula Nr.   8     Sigma = A * ((C-T)/(C-B))^D  (A=Sigma1, B=T1, C=Tc)  [dynes/cm] [dynes/cm]
Minimum temperature              =         85.300000 [K]
Maximum temperature              =        369.700000 [K]
Parameter 1                      =     2.200000E+0001
Parameter 2                      =     1.830000E+0002
Parameter 3                      =     3.697000E+0002
Parameter 4                      =     1.198200E+0000
Parameter 5                      =     0.000000E+0000
```

Annex-48

21. PROPENE


```
Material_Name                     = PROPENE
Molecular formula                 = CH3CH=CH2
UN number                         =            1077
Molecular weight                  =        42.080000 kg/kmol
Critical temperature              =       364.900000 K (91.75 °C)
Melting point                     =        88.000000 K (-185.15 °C)
Triplepoint temperature           =        87.890000 K (-185.26 °C)
Normal boiling point              =       225.300000 K (-47.85 °C)
Standard net heat of combustion   = 4.580400E+0007 J/kg ( 1.927432E+0009 J/kmol)
Flash point                       =       165.000000 K (-108.15 °C)
Lower flammability limit          =         2.000000 vol% in air
Upper flammability limit          =       100.000000 vol% in air
Solubility in water               =         0.000000 kg/m3
```


```
Temperature dependent data (calculated at 288.15 K  (15.00 °C)
Liquid density                    = 5.226934E+0002    kg/m3 (522.69 kg/m3 )
Vapor pressure                    = 8.909625E+0005    N/m2 (8.91 Bar    )
Heat of vaporization              = 3.488223E+0005    J/kg (348822.30 J/kg  )
Liquid heatcapacity               = 2.567563E+0003    J/kg*K (2567.56 J/kg*K)
Gas heatcapacity (ideal gas)      = 1.513526E+0003    J/kg*K (1513.53 J/kg*K)
Liquid viscosity                  = 9.137159E-0005    Pa*s
Vapor viscosity                   = 8.103778E-0006    Pa*s
Surface tension                   = 8.282738E-0003     N/m
Poisson ratio                     = 1.150
```


```
Functions (calculated at 288.15 K  (15.00 °C) and 1.000000E+05 N/m2  (1.000 Bar)
Gas density (ideal gas law) :          1.756 kg/m3
Mass of 1 m3 gas/vapour     :          1.756 kg
Volume of 1 kg gas/vapour   :          0.569 m3
Mass of 1 m3 liquid         :        522.693 kg
Volume of 1000 kg liquid    :          1.913 m3
```


```
Probit constants (Toxicity)
A =        0.000000 SI units(Kg*s/m3)
B =        0.000000 SI units(Kg*s/m3)
N =        0.000000 SI units(Kg*s/m3)

A =        0.000000 (ppm*min)
B =        0.000000 (ppm*min)
N =        0.000000 (ppm*min)

A =        0.000000 (mg*min/m3)
B =        0.000000 (mg*min/m3)
N =        0.000000 (mg*min/m3)
```


```
Temperature dependent data (Parameters):

Liquid density
Formula Nr.   1    rho = A * B^-((1-T/C)^2/7)  (where C=Tc)  [g/cm3] [g/cm3]
Minimum temperature               =        87.700000 [K]
Maximum temperature               =       364.900000 [K]
Parameter 1                       = 2.252000E-0001
Parameter 2                       = 2.686000E-0001
Parameter 3                       = 3.649000E+0002
Parameter 4                       = 0.000000E+0000
Parameter 5                       = 0.000000E+0000
```

```
Vapor pressure
Formula Nr.   2    Log(P) = A + B/T + C*Log(T) + D*T + E*T^2  [mm Hg] [mm Hg]
Minimum temperature               =        123.000000 [K]
Maximum temperature               =        365.100000 [K]
Parameter 1                       =    3.687700E+0001
Parameter 2                       =   -1.725500E+0003
Parameter 3                       =   -1.205700E+0001
Parameter 4                       =    8.994800E-0003
Parameter 5                       =    0.000000E+0000


Heat of vaporization
Formula Nr.   3    Hv = A * ((C-T)/(C-B)^D  (A=Hv1, B=T1, C=Tc)  [cal/g] [cal/g]
Minimum temperature               =         87.700000 [K]
Maximum temperature               =        364.900000 [K]
Parameter 1                       =    1.046000E+0002
Parameter 2                       =    2.253000E+0002
Parameter 3                       =    3.649000E+0002
Parameter 4                       =    3.800000E-0001
Parameter 5                       =    0.000000E+0000


Liquid heatcapacity
Formula Nr.   4    Cpl = A + B*T + C*T^2 + D*T^3  [cal/g/K] [cal/g/K]
Minimum temperature               =         87.700000 [K]
Maximum temperature               =        313.000000 [K]
Parameter 1                       =    4.706000E-0001
Parameter 2                       =    1.683000E-0003
Parameter 3                       =   -1.682000E-0005
Parameter 4                       =    4.407000E-0008
Parameter 5                       =    0.000000E+0000


IG heatcapacity
Formula Nr.   5    Cp = A + B*T + C*T^2 + D*T^3  [cal/mol] [cal/mol]
Minimum temperature               =        298.000000 [K]
Maximum temperature               =       1500.000000 [K]
Parameter 1                       =    6.800000E-0001
Parameter 2                       =    5.680000E-0002
Parameter 3                       =   -2.860000E-0005
Parameter 4                       =    5.600000E-0009
Parameter 5                       =    0.000000E+0000


Liquid viscosity
Formula Nr.   6    Log(Visc) = Ea + Eb/T + Ec*Log (T) + Ed*T + Ee*T*T  (where Ec=0!) [centiPoise]
[centiPoise]
Minimum temperature               =        113.000000 [K]
Maximum temperature               =        364.900000 [K]
Parameter 1                       =   -5.009000E+0000
Parameter 2                       =    4.132000E+0002
Parameter 3                       =    0.000000E+0000
Parameter 4                       =    1.771000E-0002
Parameter 5                       =   -3.092000E-0005


Vapor viscosity
Formula Nr.   7    Visc = A + B*T + C*T^2  [microPoise] [microPoise]
Minimum temperature               =        173.000000 [K]
Maximum temperature               =       1273.000000 [K]
Parameter 1                       =   -5.601000E+0000
Parameter 2                       =    3.188000E-0001
Parameter 3                       =   -6.291000E-0005
Parameter 4                       =    0.000000E+0000
Parameter 5                       =    0.000000E+0000


Surface Tension
Formula Nr.   8    Sigma = A * ((C-T)/(C-B))^D  (A=Sigma1, B=T1, C=Tc)  [dynes/cm] [dynes/cm]
Minimum temperature               =         87.700000 [K]
Maximum temperature               =        364.900000 [K]
Parameter 1                       =    1.998000E+0001
Parameter 2                       =    2.030000E+0002
Parameter 3                       =    3.649000E+0002
Parameter 4                       =    1.179700E+0000
Parameter 5                       =    0.000000E+0000
```

22. SULPHUR DIOXIDE

```
Material_Name                    = SULPHUR DIOXIDE
Molecular formula                = SO2
UN number                        =        1079
Molecular weight                 =        64.060000 kg/kmol
Critical temperature             =       430.750000 K (157.60 °C)
Melting point                    =       200.000000 K (-73.15 °C)
Triplepoint temperature          =       197.670000 K (-75.48 °C)
Normal boiling point             =       263.130000 K (-10.02 °C)
Standard net heat of combustion  = 0.000000E+0000 J/kg ( 0.000000E+0000 J/kmol)
Flash point                      =         0.000000 K (-273.15 °C)
Lower flammability limit         =         0.000000 vol% in air
Upper flammability limit         =         0.000000 vol% in air
Solubility in water              =       105.000000 kg/m3


Temperature dependent data (calculated at 288.15 K  (15.00 °C)
Liquid density                   = 1.394521E+0003    kg/m3 (1394.52 kg/m3 )
Vapor pressure                   = 2.803136E+0005    N/m2 (2.80 Bar   )
Heat of vaporization             = 3.629193E+0005    J/kg (362919.33 J/kg  )
Liquid heatcapacity              = 1.350315E+0003    J/kg*K (1350.31 J/kg*K)
Gas heatcapacity (ideal gas)     = 6.222876E+0002    J/kg*K (622.29 J/kg*K)
Liquid viscosity                 = 3.621724E-0004    Pa*s
Vapor viscosity                  = 1.245779E-0005    Pa*s
Surface tension                  = 2.362892E-0002     N/m
Poisson ratio                    = 1.264


Functions (calculated at 288.15 K  (15.00 °C) and 1.000000E+05 N/m2  (1.000 Bar)
Gas density (ideal gas law) :         2.674 kg/m3
Mass of 1 m3 gas/vapour     :         2.674 kg
Volume of 1 kg gas/vapour   :         0.374 m3
Mass of 1 m3 liquid         :      1394.521 kg
Volume of 1000 kg liquid    :         0.717 m3


Probit constants (Toxicity)
A =        9.862881 SI units(Kg*s/m3)
B =        1.000000 SI units(Kg*s/m3)
N =        2.400000 SI units(Kg*s/m3)

A =      -16.843761 (ppm*min)
B =        1.000000 (ppm*min)
N =        2.400000 (ppm*min)

A =      -19.200000 (mg*min/m3)
B =        1.000000 (mg*min/m3)
N =        2.400000 (mg*min/m3)


Temperature dependent data (Parameters):

Liquid density
Formula Nr.   1    rho = A * B^-((1-T/C)^2/7)  (where C=Tc) [g/cm3] [g/cm3]
Minimum temperature              =       197.670000 [K]
Maximum temperature              =       430.750000 [K]
Parameter 1                      = 5.123900E-0001
Parameter 2                      = 2.533200E-0001
Parameter 3                      = 4.307500E+0002
Parameter 4                      = 0.000000E+0000
Parameter 5                      = 0.000000E+0000
```

```
Vapor pressure
Formula Nr.   2     Log(P) = A + B/T + C*Log(T) + D*T + E*T^2  [mm Hg] [mm Hg]
Minimum temperature                 =       197.670000 [K]
Maximum temperature                 =       430.750000 [K]
Parameter 1                         =    2.075270E+0001
Parameter 2                         =   -1.831700E+0003
Parameter 3                         =   -4.597200E+0000
Parameter 4                         =    6.785100E-0004
Parameter 5                         =    4.663200E-0007

Heat of vaporization
Formula Nr.   3     Hv = A * ((C-T)/(C-B)^D  (A=Hv1, B=T1, C=Tc)  [cal/g] [cal/g]
Minimum temperature                 =       197.670000 [K]
Maximum temperature                 =       430.750000 [K]
Parameter 1                         =    7.977000E+0001
Parameter 2                         =    3.142000E+0002
Parameter 3                         =    4.307500E+0002
Parameter 4                         =    4.128800E-0001
Parameter 5                         =    0.000000E+0000

Liquid heatcapacity
Formula Nr.   4     Cpl = A + B*T + C*T^2 + D*T^3  [cal/g/K] [cal/g/K]
Minimum temperature                 =       197.670000 [K]
Maximum temperature                 =       263.130000 [K]
Parameter 1                         =    3.495600E-0001
Parameter 2                         =   -1.321000E-0004
Parameter 3                         =    8.943900E-0008
Parameter 4                         =    8.704000E-0011
Parameter 5                         =    0.000000E+0000

IG heatcapacity
Formula Nr.   5     Cp = A + B*T + C*T^2 + D*T^3  [cal/mol] [cal/mol]
Minimum temperature                 =       100.000000 [K]
Maximum temperature                 =      1500.000000 [K]
Parameter 1                         =    6.487700E+0000
Parameter 2                         =    1.258100E-0002
Parameter 3                         =   -7.544000E-0006
Parameter 4                         =    1.528800E-0009
Parameter 5                         =    0.000000E+0000

Liquid viscosity
Formula Nr.   6     Log(Visc) = Ea + Eb/T + Ec*Log (T) + Ed*T + Ee*T*T  (where Ec=0!) [centiPoise]
[centiPoise]
Minimum temperature                 =       239.650000 [K]
Maximum temperature                 =       323.150000 [K]
Parameter 1                         =   -8.538000E-0001
Parameter 2                         =    1.861800E+0002
Parameter 3                         =    0.000000E+0000
Parameter 4                         =   -6.998000E-0004
Parameter 5                         =   -3.825000E-0007

Vapor viscosity
Formula Nr.   7     Visc = A + B*T + C*T^2  [microPoise] [microPoise]
Minimum temperature                 =       200.000000 [K]
Maximum temperature                 =      1000.000000 [K]
Parameter 1                         =   -1.294600E+0001
Parameter 2                         =    5.104600E-0001
Parameter 3                         =   -1.152000E-0004
Parameter 4                         =    0.000000E+0000
Parameter 5                         =    0.000000E+0000

Surface Tension
Formula Nr.   8     Sigma = A * ((C-T)/(C-B))^D  (A=Sigma1, B=T1, C=Tc)  [dynes/cm] [dynes/cm]
Minimum temperature                 =       197.670000 [K]
Maximum temperature                 =       430.750000 [K]
Parameter 1                         =    1.862000E+0001
Parameter 2                         =    3.142000E+0002
Parameter 3                         =    4.307500E+0002
Parameter 4                         =    1.181000E+0000
Parameter 5                         =    0.000000E+0000
```

Annex-52

23.   TOLUENE

```
Material_Name                     = TOLUENE
Molecular formula                 = C6H5CH3
UN number                         =         1294
Molecular weight                  =       92.100000 kg/kmol
Critical temperature              =      591.800000 K (318.65 °C)
Melting point                     =      178.000000 K (-95.15 °C)
Triplepoint temperature           =      178.180000 K (-94.97 °C)
Normal boiling point              =      383.600000 K (110.45 °C)
Standard net heat of combustion   = 4.055000E+0007 J/kg ( 3.734655E+0009 J/kmol)
Flash point                       =      277.000000 K (3.85 °C)
Lower flammability limit          =        1.270000 vol% in air
Upper flammability limit          =      100.000000 vol% in air
Solubility in water               =        0.500000 kg/m3


Temperature dependent data (calculated at 288.15 K  (15.00 °C)
Liquid density                    = 8.710100E+0002    kg/m3 (871.01 kg/m3 )
Vapor pressure                    = 2.196688E+0003    N/m2 (0.02 Bar   )
Heat of vaporization              = 4.159887E+0005    J/kg (415988.71 J/kg  )
Liquid heatcapacity               = 1.666549E+0003    J/kg*K (1666.55 J/kg*K)
Gas heatcapacity (ideal gas)      = 1.124195E+0003    J/kg*K (1124.20 J/kg*K)
Liquid viscosity                  = 6.275112E-0004    Pa*s
Vapor viscosity                   = 6.636030E-0006    Pa*s
Surface tension                   = 2.909345E-0002     N/m
Poisson ratio                     = 1.087


Functions (calculated at 288.15 K  (15.00 °C) and 1.000000E+05 N/m2  (1.000 Bar)
Gas density (ideal gas law) :         3.844 kg/m3
Mass of 1 m3 gas/vapour     :         3.844 kg
Volume of 1 kg gas/vapour   :         0.260 m3
Mass of 1 m3 liquid         :       871.010 kg
Volume of 1000 kg liquid    :         1.148 m3


Probit constants (Toxicity)
A =        0.000000 SI units(Kg*s/m3)
B =        0.000000 SI units(Kg*s/m3)
N =        0.000000 SI units(Kg*s/m3)

A =        0.000000 (ppm*min)
B =        0.000000 (ppm*min)
N =        0.000000 (ppm*min)

A =        0.000000 (mg*min/m3)
B =        0.000000 (mg*min/m3)
N =        0.000000 (mg*min/m3)


Temperature dependent data (Parameters):

Liquid density
Formula Nr.   1    rho = A * B^-((1-T/C)^2/7)  (where C=Tc) [g/cm3] [g/cm3]
Minimum temperature               =      178.000000 [K]
Maximum temperature               =      591.800000 [K]
Parameter 1                       = 2.883000E-0001
Parameter 2                       = 2.624000E-0001
Parameter 3                       = 5.918000E+0002
Parameter 4                       = 0.000000E+0000
Parameter 5                       = 0.000000E+0000
```

```
Vapor pressure
Formula Nr.   2    Log(P) = A + B/T + C*Log(T) + D*T + E*T^2  [mm Hg] [mm Hg]
Minimum temperature            =      213.000000 [K]
Maximum temperature            =      593.600000 [K]
Parameter 1                    =    1.152100E+0002
Parameter 2                    =   -4.918100E+0003
Parameter 3                    =   -4.346700E+0001
Parameter 4                    =    3.854800E-0002
Parameter 5                    =   -1.349600E-0005

Heat of vaporization
Formula Nr.   3    Hv = A * ((C-T)/(C-B)^D  (A=Hv1, B=T1, C=Tc)  [cal/g] [cal/g]
Minimum temperature            =      178.000000 [K]
Maximum temperature            =      591.800000 [K]
Parameter 1                    =    8.610000E+0001
Parameter 2                    =    3.836000E+0002
Parameter 3                    =    5.918000E+0002
Parameter 4                    =    3.800000E-0001
Parameter 5                    =    0.000000E+0000

Liquid heatcapacity
Formula Nr.   4    Cpl = A + B*T + C*T^2 + D*T^3  [cal/g/K] [cal/g/K]
Minimum temperature            =      178.000000 [K]
Maximum temperature            =      583.000000 [K]
Parameter 1                    =   -1.461000E-0001
Parameter 2                    =    4.584000E-0003
Parameter 3                    =   -1.346000E-0005
Parameter 4                    =    1.425000E-0008
Parameter 5                    =    0.000000E+0000

IG heatcapacity
Formula Nr.   5    Cp = A + B*T + C*T^2 + D*T^3  [cal/mol] [cal/mol]
Minimum temperature            =      298.000000 [K]
Maximum temperature            =     1500.000000 [K]
Parameter 1                    =   -9.340000E+0000
Parameter 2                    =    1.385000E-0001
Parameter 3                    =   -8.720000E-0005
Parameter 4                    =    2.060000E-0008
Parameter 5                    =    0.000000E+0000

Liquid viscosity
Formula Nr.   6    Log(Visc) = Ea + Eb/T + Ec*Log (T) + Ed*T + Ee*T*T  (where Ec=0!) [centiPoise]
[centiPoise]
Minimum temperature            =      233.000000 [K]
Maximum temperature            =      591.800000 [K]
Parameter 1                    =   -2.553000E+0000
Parameter 2                    =    5.591000E+0002
Parameter 3                    =    0.000000E+0000
Parameter 4                    =    1.987000E-0003
Parameter 5                    =   -1.954000E-0006

Vapor viscosity
Formula Nr.   7    Visc = A + B*T + C*T^2  [microPoise] [microPoise]
Minimum temperature            =      273.000000 [K]
Maximum temperature            =     1273.000000 [K]
Parameter 1                    =   -8.421000E+0000
Parameter 2                    =    2.711000E-0001
Parameter 3                    =   -4.018000E-0005
Parameter 4                    =    0.000000E+0000
Parameter 5                    =    0.000000E+0000

Surface Tension
Formula Nr.   8    Sigma = A * ((C-T)/(C-B))^D  (A=Sigma1, B=T1, C=Tc)  [dynes/cm] [dynes/cm]
Minimum temperature            =      178.000000 [K]
Maximum temperature            =      591.800000 [K]
Parameter 1                    =    2.852000E+0001
Parameter 2                    =    2.930000E+0002
Parameter 3                    =    5.918000E+0002
Parameter 4                    =    1.236400E+0000
Parameter 5                    =    0.000000E+0000
```

24. WATER

```
Material_Name                   = WATER
Molecular formula               = H2O
UN number                       =            100
Molecular weight                =       18.016000 kg/kmol
Critical temperature            =      648.000000 K (374.85 °C)
Melting point                   =      273.150000 K (-0.00 °C)
Triplepoint temperature         =      273.160000 K (0.01 °C)
Normal boiling point            =      373.150000 K (100.00 °C)
Standard net heat of combustion = 0.000000E+0000 J/kg ( 0.000000E+0000 J/kmol)
Flash point                     =        0.000000 K (-273.15 °C)
Lower flammability limit        =        0.000000 vol% in air
Upper flammability limit        =        0.000000 vol% in air
Solubility in water             =     1000.000000 kg/m3
```

```
Temperature dependent data (calculated at 288.15 K  (15.00 °C)
Liquid density                  = 1.036876E+0003    kg/m3 (1036.88 kg/m3 )
Vapor pressure                  = 1.705909E+0003    N/m2 (0.02 Bar   )
Heat of vaporization            = 2.545846E+0006    J/kg (2545846.12 J/kg  )
Liquid heatcapacity             = 4.190668E+0003    J/kg*K (4190.67 J/kg*K)
Gas heatcapacity (ideal gas)    = 1.868251E+0003    J/kg*K (1868.25 J/kg*K)
Liquid viscosity                = 1.165873E-0003    Pa*s
Vapor viscosity                 = 1.212163E-0005    Pa*s
Surface tension                 = 8.806352E-0002     N/m
Poisson ratio                   = 1.328
```

```
Functions (calculated at 288.15 K  (15.00 °C) and 1.000000E+05 N/m2  (1.000 Bar)
Gas density (ideal gas law) :        0.752 kg/m3
Mass of 1 m3 gas/vapour     :        0.752 kg
Volume of 1 kg gas/vapour   :        1.330 m3
Mass of 1 m3 liquid         :     1036.876 kg
Volume of 1000 kg liquid    :        0.964 m3
```

```
Probit constants (Toxicity)
A =       0.000000 SI units(Kg*s/m3)
B =       0.000000 SI units(Kg*s/m3)
N =       0.000000 SI units(Kg*s/m3)

A =       0.000000 (ppm*min)
B =       0.000000 (ppm*min)
N =       0.000000 (ppm*min)

A =       0.000000 (mg*min/m3)
B =       0.000000 (mg*min/m3)
N =       0.000000 (mg*min/m3)
```

```
Temperature dependent data (Parameters):

Liquid density
Formula Nr.   1   rho = A * B^-((1-T/C)^2/7)  (where C=Tc)  [g/cm3] [g/cm3]
Minimum temperature             =      273.160000 [K]
Maximum temperature             =      647.350000 [K]
Parameter 1                     = 3.471000E-0001
Parameter 2                     = 2.740000E-0001
Parameter 3                     = 6.480000E+0002
Parameter 4                     = 0.000000E+0000
Parameter 5                     = 0.000000E+0000
```

```
Vapor pressure
Formula Nr.   2      Log(P) = A + B/T + C*Log(T) + D*T + E*T^2  [mm Hg] [mm Hg]
Minimum temperature                =        273.160000 [K]
Maximum temperature                =        647.130000 [K]
Parameter 1                        =     2.988850E+0001
Parameter 2                        =    -3.152900E+0003
Parameter 3                        =    -7.315200E+0000
Parameter 4                        =     1.126200E-0005
Parameter 5                        =     1.804800E-0006


Heat of vaporization
Formula Nr.   3      Hv = A * ((C-T)/(C-B)^D   (A=Hv1, B=T1, C=Tc)  [cal/g] [cal/g]
Minimum temperature                =        273.160000 [K]
Maximum temperature                =        647.130000 [K]
Parameter 1                        =     4.759000E+0002
Parameter 2                        =     4.601000E+0002
Parameter 3                        =     6.480000E+0002
Parameter 4                        =     3.774600E-0001
Parameter 5                        =     0.000000E+0000


Liquid heatcapacity
Formula Nr.   4      Cpl = A + B*T + C*T^2 + D*T^3  [cal/g/K] [cal/g/K]
Minimum temperature                =        273.150000 [K]
Maximum temperature                =        533.150000 [K]
Parameter 1                        =     6.933800E-0001
Parameter 2                        =     3.194400E-0003
Parameter 3                        =    -1.101000E-0005
Parameter 4                        =     1.259900E-0008
Parameter 5                        =     0.000000E+0000


IG heatcapacity
Formula Nr.   5      Cp = A + B*T + C*T^2 + D*T^3  [cal/mol] [cal/mol]
Minimum temperature                =        100.000000 [K]
Maximum temperature                =       1500.000000 [K]
Parameter 1                        =     7.981000E+0000
Parameter 2                        =    -9.050000E-0004
Parameter 3                        =     4.294100E-0006
Parameter 4                        =    -1.507000E-0009
Parameter 5                        =     0.000000E+0000


Liquid viscosity
Formula Nr.   6      Log(Visc) = Ea + Eb/T + Ec*Log (T) + Ed*T + Ee*T*T  (where Ec=0!)  [centiPoise]
[centiPoise]
Minimum temperature                =        273.150000 [K]
Maximum temperature                =        643.150000 [K]
Parameter 1                        =    -8.426800E+0000
Parameter 2                        =     1.559300E+0003
Parameter 3                        =     0.000000E+0000
Parameter 4                        =     1.334000E-0002
Parameter 5                        =    -9.176000E-0006


Vapor viscosity
Formula Nr.   7      Visc = A + B*T + C*T^2  [microPoise] [microPoise]
Minimum temperature                =        373.150000 [K]
Maximum temperature                =       1073.100000 [K]
Parameter 1                        =    -3.536800E+0001
Parameter 2                        =     4.243600E-0001
Parameter 3                        =    -1.268000E-0005
Parameter 4                        =     0.000000E+0000
Parameter 5                        =     0.000000E+0000


Surface Tension
Formula Nr.   8      Sigma = A * ((C-T)/(C-B))^D  (A=Sigma1, B=T1, C=Tc)  [dynes/cm] [dynes/cm]
Minimum temperature                =        273.160000 [K]
Maximum temperature                =        647.130000 [K]
Parameter 1                        =     4.054000E+0001
Parameter 2                        =     4.601000E+0002
Parameter 3                        =     6.480000E+0002
Parameter 4                        =     1.193900E+0000
Parameter 5                        =     0.000000E+0000
```

Annex-56